The international journal of science / 16 February 2023

nature



GONE TO EARTH

Bioinspired seed carriers drill their own holes to boost sowing success

Pre-emptive strikes
The diabetes drug that could change how autoimmunity is treated

Friend or foe?
Assessing the effects of social media on teen mental health

The gentle touch
Looser receptor grip can boost effectiveness of certain antibodies

VISIT…

LANZAROTE Caliente.COM

Nature.2023.02.18

[Sat, 18 Feb 2023]

- **This Week**
- **News in Focus**
- **Books & Arts**
- **Opinion**
- **Work**
- **Research**
- **Amendments & Corrections**

This Week

- **Our efforts to diversify Nature’s journalism are progressing, but work remains** [15 Feb 2023]
  • Two years ago, this journal pledged to report on the diversity of sources in our journalistic content. The first results are now in.
- **UK, please drop the rhetoric and fight for collaboration with Europe** [14 Feb 2023]
  • Now is not the time to undermine positive moves over the future of EU–UK science collaboration.
- **Solar geoengineering is scary — that’s why we should research it** [14 Feb 2023]
  • Research on blocking sunlight needs a dose of realpolitik.

- EDITORIAL
- 15 February 2023

Our efforts to diversify *Nature*'s journalism are progressing, but work remains

Two years ago, this journal pledged to report on the diversity of sources in our journalistic content. The first results are now in.



Credit: Ilnur Khisamutdinov/Alamy

In June 2021, researchers at the University of Colorado School of Medicine in Aurora turned a magnifying glass on *Nature*'s written journalism.

Computational biologists Natalie Davidson and Casey Greene reported that most of the individuals we quoted were male.

Using automated methods, the authors found that 69% of the people quoted directly in *Nature*'s written journalism in 2020 were male (N. R. Davidson and C. S. Greene Preprint at bioRxiv https://doi.org/gkscd5; 2021). This figure had been falling — the authors' analysis of some 16,000 articles published between 2005 and 2020 found that the number was 87% in 2005 — but 69% was still unacceptably high.

The journal's editorial teams collectively pledged to work harder to improve the diversity of those whose words or voices are quoted or paraphrased in our reporting (see *Nature* **594**, 473–474; 2021). In April 2021, we began a pilot project to track aspects of diversity in some of *Nature*'s journalism more systematically. That September, we began tracking diversity in journalistic content across all relevant teams. This week, we're reporting data for 1,118 written articles and 123 podcasts and videos published between 1 April 2021 and 31 January 2023. In the written pieces, *Nature* directly quoted or paraphrased the words of 5,252 people. The podcasts and videos featured the voices of a total of 240 people.

As part of our tracking efforts, members of *Nature*'s editorial teams recorded the preferred pronouns of those who were quoted or paraphrased, as well as their geographical location and career stage. We did not collect data on race or ethnicity for this phase of our project, but are working to widen the racial and ethnic diversity of our sources to make our reporting more representative of global science.

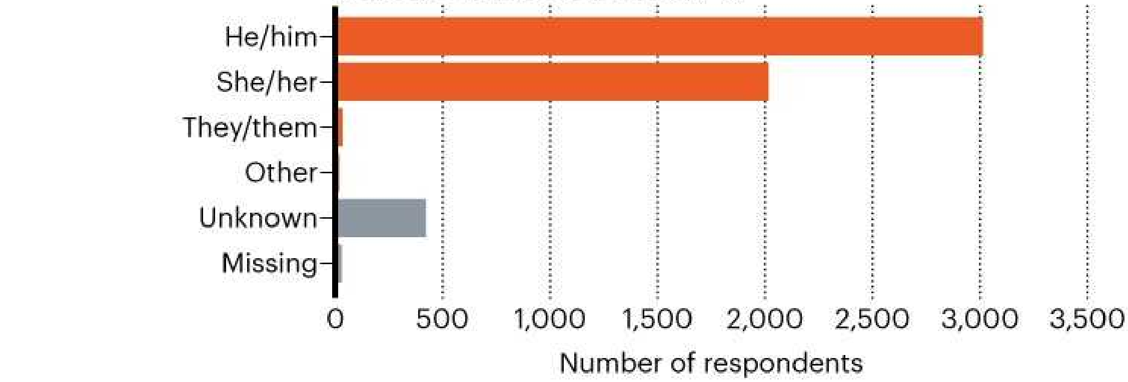
Our data show that people using he/him pronouns comprised around 55% of those quoted or paraphrased in written articles published since April 2021, with about 36% using she/her pronouns. There were 24 people with they/them pronouns, and 5 who used other pronouns (see '*Nature*'s journalism in charts'). The preferred pronouns of most of the remaining 9% are not known, meaning that of those who did disclose their preference, around 60% used he/him pronouns and some 40% used she/her.

NATURE'S JOURNALISM IN CHARTS

Breakdown of 5,492 people quoted or paraphrased in *Nature*'s journalism (written, audio and video) published between April 2021 and January 2023.

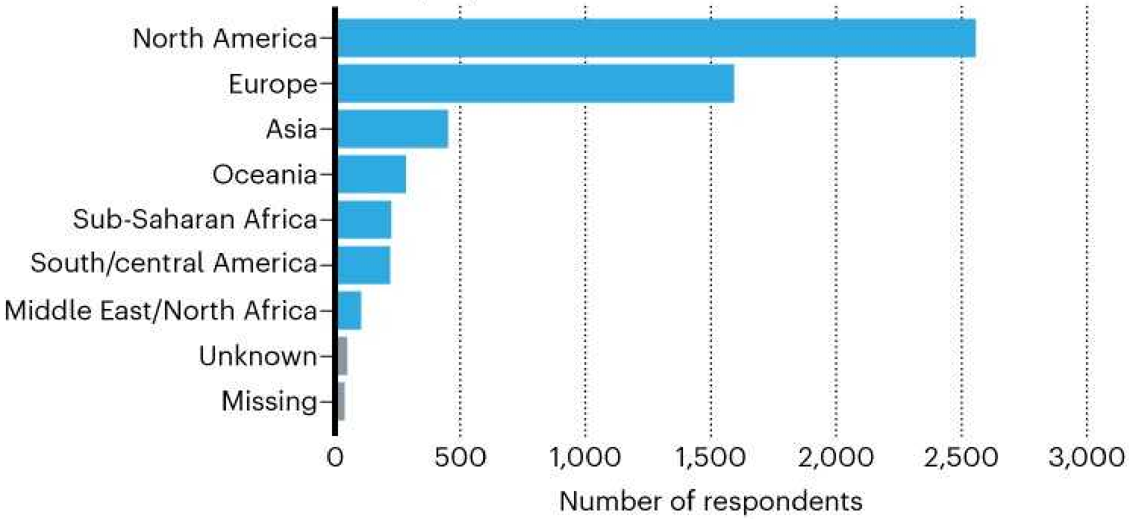
Breakdown of people quoted by gender

Pronouns that people identify by



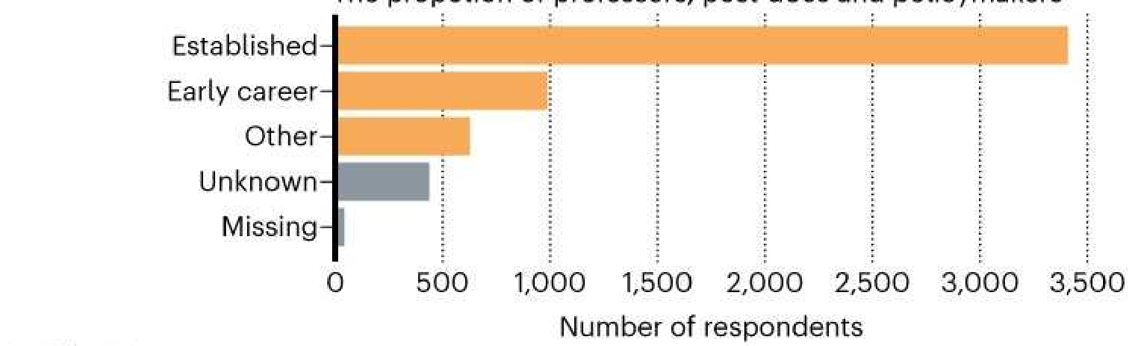
Geographic location

Where people are based



Career stage

The propotion of professors, post-docs and policymakers



©nature

Slightly more than 60% of those quoted or paraphrased in *Nature's* written journalism were 'established' in their careers, meaning that they were professors or had tenure or another senior role. By contrast, 18% fell into the 'early career' category, which included graduate students, postdoctoral researchers and non-tenured faculty members. The 'other' category, which encompassed 11% of people, includes those in non-academic settings, such as campaigning organizations, industry and policymaking. Some 75% of all of those quoted were based in North America or Europe.

Of the 240 people quoted or featured in our podcast and video content, 48% used he/him pronouns (amounting to 52% of those who disclosed their pronouns). Some 60% of those featured were established in their careers, and 81% were based in North America or Europe.

These data show that we are continuing to make progress on gender diversity. But there is clearly still work to do, particularly when it comes to improving the global representation of voices in our pages, as well as the proportion of researchers at earlier career stages.

We will continue to record our data, and we aim to improve on these figures, proactively seeking out and trying to better represent voices from historically less-represented peoples and parts of the world. The result, we hope, will be better journalism derived from a more accurate representation of the diverse scientific community of which *Nature* is a part.

Nature **614**, 389 (2023)

doi: https://doi.org/10.1038/d41586-023-00399-1

This article was downloaded by **calibre** from https://www.nature.com/articles/d41586-023-00399-1

| Section menu | Main menu |

- EDITORIAL
- 14 February 2023

UK, please drop the rhetoric and fight for collaboration with Europe

Now is not the time to undermine positive moves over the future of EU–UK science collaboration.



Riski Sunak’s government has brought a seriousness to UK relations with the EU.Credit: Jack Hill/AFP/Getty

“We are more than ready to go it alone.” One of the first public statements made by Michelle Donelan, the United Kingdom’s new secretary of state for science, was to declare that the country’s scientific community can live without European Union funding schemes. That might be true in the literal

sense. But her sentiment, contained in an article for *The Sunday Telegraph* newspaper on 12 February, was not the headline message that researchers were hoping for from their new, cabinet-level, minister. It was also not the message of a government that is serious about its aspirations to make the United Kingdom a 'science superpower', as ministers have frequently claimed.

Science leaders had broadly welcomed Donelan's appointment, and the elevation of science to a cabinet-level department. But there has been dismay at the 'go-it-alone' rhetoric.

UK science ministers often attend the top table of decision-making, but the science ministerial position is not usually a cabinet-level one. The new Department for Science, Innovation and Technology now brings together research funding, research strategy and digital technologies, which were previously in three separate departments. Crucially, Donelan reports to Prime Minister Rishi Sunak, and will focus on harnessing science and innovation for economic growth, in which the United Kingdom lags behind most of its peer-group countries.



UK government announces new science department and minister

But building research for any purpose (whether for discovery science, the science needed in environmental protection, or science for industrial

development) is not like heating an oven-ready microwave meal. Results are not a matter of plucking something off the shelf, pressing some buttons and getting an outcome in record time.

As Robin Grimes, former chief science adviser to the UK defence ministry, told members of the UK Parliament last year, the collaborative relationships that are leading to advances in research have, in some cases, been decades in the making. If these are severed, new ones can't be formed instantly.

Research in the United Kingdom is already suffering from the loss of European relationships. Formerly UK-based holders of prestigious European Research Council grants have had to relocate to an EU country to keep these grants. And, in future, there are likely to be fewer European researchers in the United Kingdom following a collapse in the number of EU students coming to the country to study. Many of these students would have stayed to pursue further studies and research, making the country their home in the process.



UK universities report sharp post-Brexit drop in EU students

A sensible science policy is impossible, therefore, unless the question of EU research collaboration and funding is addressed. And on that point the UK government seems to be giving out mixed messages.

At the heart of this dispute is UK membership of Horizon Europe, the EU's flagship research and innovation programme for 2021–27, with a budget of

€95.5 billion (US$102.4 billion). Before Brexit, UK-based scientists were automatically eligible to apply for EU funds — and had among the bloc's highest success rates. Now the United Kingdom must apply for what is called associate membership, a category in which the country must pay separately to access the fund.

The EU says that the United Kingdom can participate in Horizon Europe, but it has imposed a political condition: participation will be allowed only once there is resolution in a dispute over trading arrangements between the United Kingdom and the EU on the UK border with Ireland — a problem that has been rumbling on since the United Kingdom formally left the bloc in January 2020.

Seriousness meets urgency

There is some rare good news here. Sunak's government, in contrast to the administration of former prime minister Boris Johnson, has brought seriousness and urgency to these talks — so much so that there are reports of a (possibly) imminent deal. An agreement, whenever it happens, would be a substantial step towards UK and EU researchers being able to work together again as they did for nearly five decades.

In another rare move, politicians of the major UK political parties, along with experts and business leaders, met last week to discuss, among other things, how to move forwards constructively with EU partners in a post-Brexit world. This, too, is welcome, because it suggests that there's a real desire for a national consensus on new beginnings with the EU.

This journal hopes that Donelan will adopt such a spirit when dealing with researchers and with the EU. The minister mentioned in her *Sunday Telegraph* article that the United Kingdom would establish its own replacement fund for collaborations with research-intensive non-EU nations, including Japan, Switzerland and the United States, if association to Horizon Europe did not materialize.

Any such collaborations are to be welcomed. But where's the logic in comparing them to — or using them to downplay — the United Kingdom's

existing science relationships? If the country really aspires to harness science in the service of society and the economy, multiple collaborative projects, on many levels, will be required: within and between disciplines, globally and regionally, including with the United Kingdom's nearest neighbours.

Nature **614**, 390 (2023)

doi: https://doi.org/10.1038/d41586-023-00398-2

This article was downloaded by **calibre** from https://www.nature.com/articles/d41586-023-00398-2

| Section menu | Main menu |

- WORLD VIEW
- 14 February 2023

Solar geoengineering is scary — that's why we should research it



Research on blocking sunlight needs a dose of realpolitik.

- Katharine Ricke

In April 2022, the start-up company Make Sunsets launched balloons into the stratosphere to release sulfur dioxide to make the atmosphere more reflective. This and other solar-geoengineering techniques aim to bounce solar radiation into space to partially counteract climate change. Make Sunsets's experiments were not public knowledge until *MIT Technology Review* published a piece on them last December (see go.nature.com/3xvcb).

Make Sunsets's release was commercially driven: the aim was to grab attention for the technique, to sell 'cooling credits' for future balloon

flights. The amount of sulfur dioxide involved was environmentally negligible. But this publicity stunt shows why it's a dangerous moment for solar-geoengineering science.

Solar geoengineering is a frightening yet tantalizing prospect. Techniques such as creating sulfuric acid aerosols in the stratosphere or spraying seawater into marine clouds seem relatively cheap, fast-acting and easy. Computer modelling studies have found that reflecting sunlight could greatly reduce regional temperature and precipitation changes caused by greenhouse gases (S. Tilmes *et al. Earth Syst. Dynam.* **11**, 579–601; 2020). But we have very little evidence on how this would affect weather, agriculture, human health or other living things.

As a climate scientist who studies the regional effects and policy implications of solar geoengineering, I find these facts disconcerting. If we start geoengineering instead of mitigating emissions, other effects of carbon dioxide in the atmosphere — notably ocean acidification — would still happen. And without appropriate governance, elite interests could control the technique's use and ignore the consequences for vulnerable people.



Developing countries must lead on solar geoengineering research

Many climate scientists think that solar-geoengineering research comes with unacceptable risks, but I disagree: shunning this research is riskier than

studying it.

This is an area in which climate scientists can still make a fundamental difference in decision-making: large uncertainties remain, and there are presently no massive financial interests invested in geoengineering in the way that fossil-fuel companies are invested in blocking emissions reductions. But solar-geoengineering research needs to change in at least three ways.

First, real-world field testing is needed. Current research is too idealistic and based almost entirely on computer modelling. Problems with solar geoengineering are much more likely to emerge when theories meet physical realities. The story of ocean iron fertilization is instructive. In the 1990s and 2000s, 13 field experiments tested the outcomes of adding iron to nutrient-poor areas of the ocean's surface. The researchers confirmed that they could stimulate phytoplankton blooms that sucked carbon dioxide out of the atmosphere, but found that most of the carbon was not stored in the deep ocean and was re-released. Much better for comparable problems with solar geoengineering to emerge during research — not publicity stunts or last-ditch measures to save treasured ecosystems.

Second, we must diversify the field to avoid bias. For example, women are, on average, more risk averse than men, so a field dominated by men will have overly optimistic framings. Researchers from powerful, well-resourced countries might be more optimistic about agency in global decision-making than those from poorer places.

Without diversity, research won't be seen as legitimate by the full range of global stakeholders. If you are a scientist working on solar geoengineering in Europe or North America, where most of the research has been done, you should work to broaden participation in the field, geographically and demographically.



[Should we fertilize oceans or seed clouds? No one knows]

Finally, model-based research should reflect geopolitical realities. Current models tend to assume there will be global cooperation, which is difficult to achieve in the real world. Models should instead reflect the likelihood that, without governance, schemes will be uncoordinated and regional.

A few studies have modelled regional approaches — one by my group found that reversing a drought in northern Africa causes one in East Africa (K. Ricke *et al. Geophys. Res. Lett.* **48**, e2021GL093129; 2021). More are needed, and different research groups should tackle regional possibilities in their own ways. The patterns that emerge can inform policy.

This approach has resonated with decision-makers, such as a group of diplomats and civil servants in Latin America and the Caribbean that I met with last summer. In turn, these interactions help to generate salient research questions.

Scientists working on solar geoengineering should welcome — indeed, demand — governance. A 2021 US National Academies committee report (see go.nature.com/3ykj7) that I helped to write laid out how to govern this type of science. The American Geophysical Union is beginning to establish protocols for self-governance of solar-geoengineering research, but as others have pointed out, scientific governance on solar geoengineering

should not be led by the United States. Governance should be international, facilitated by the United Nations.

Sometimes, when I make these arguments, colleagues misinterpret me as saying that solar geoengineering is a good idea. We have insufficient scientific evidence to say whether it is or isn't. But inaction won't change the incentives for blocking sunlight or sap wishful thinking: only publicly accumulating evidence will.

Nature **614**, 391 (2023)

doi: https://doi.org/10.1038/d41586-023-00413-6

This article was downloaded by **calibre** from https://www.nature.com/articles/d41586-023-00413-6

News in Focus

- **How quickly does COVID immunity fade? What scientists know** [02 Feb 2023]
  • Vaccination, infection with SARS-CoV-2 and a combination of both provide varying degrees of protection.
- **Scientists made a new kind of ice that might exist on distant moons** [02 Feb 2023]
  • The 'amorphous' solid is denser and could be water ‘frozen in time’.
- **Antibiotic use in farming set to soar despite drug-resistance fears** [06 Feb 2023]
  • Analysis finds antimicrobial drug use in agriculture is much higher than reported.
- **Turkey–Syria earthquake: what scientists know** [06 Feb 2023]
  • Turkey and Syria’s buildings have always been vulnerable to earthquakes, but war has made things worse.
- **COVID drug drives viral mutations — and now some want to halt its use** [07 Feb 2023]
  • Analysis reveals the signature of the antiviral drug molnupiravir in SARS-CoV-2 sequences riddled with mutations.
- **Underdog technologies gain ground in quantum-computing race** [06 Feb 2023]
  • Individual atoms trapped by optical ‘tweezers’ are emerging as a promising computational platform.
- **Dogma-defying bacteria package DNA in unusual ways** [03 Feb 2023]
  • Some bacteria appear to encase their genomes in proteins called histones — which weren’t thought to exist in bacterial cells.
- **What it would take to bring back the dodo** [10 Feb 2023]
  • An audacious plan to ‘de-extinct’ dodos depends on huge leaps in biotechnology and resurrecting a lost habitat.

- **[How a pioneering diabetes drug offers hope for preventing autoimmune disorders]** [15 Feb 2023]
  • The approval of an antibody therapy that pauses the progression of type 1 diabetes is a first in the field, and some say a model for other drug developers.

- NEWS
- 02 February 2023

How quickly does COVID immunity fade? What scientists know

Vaccination, infection with SARS-CoV-2 and a combination of both provide varying degrees of protection.

- Cassandra Willyard



A kiosk in Shanghai, China, offers free SARS-CoV-2 testing.Credit: CFOTO/Future Publishing via Getty

Three years into the pandemic, the immune systems of the vast majority of humans have learnt to recognize SARS-CoV-2 through vaccination, infection or, in many cases, both. But just how quickly do these types of immunity fade?

New evidence suggests that 'hybrid' immunity, the result of both vaccination and a bout of COVID-19, can provide partial protection against reinfection for at least eight months[1]. It also offers greater than 95% protection against severe disease or hospitalization for between six months and a year after an infection or vaccination, according to estimates from a meta-analysis[2]. Immunity acquired by booster vaccination alone seems to fade somewhat faster.

But the durability of immunity is much more complex than the numbers suggest. How long the immune system can fend off SARS-CoV-2 infection depends not only on how much immunity wanes over time but also on how well immune cells recognize their target. "And that has more to do with the virus and how much it mutates," says Deepta Bhattacharya, an immunologist at the University of Arizona College of Medicine in Tucson. If a new variant finds ways to escape the existing immune response, then even a recent infection might not guarantee protection.

Omicron era

Omicron has presented just such a scenario. In late 2021 and early 2022, the main Omicron subvariants that were causing infections were BA.1 and BA.2. By mid-2022, the BA.5 wave was gathering strength in some countries, raising the prospect that those who'd already had one round of Omicron could soon be exposed to another. Data are now providing a sense of the risk of reinfection over time.

In one study[1], researchers looking at Portugal's national database of infections studied vaccinated people who became infected during the BA.1/BA.2 wave. Analysis showed that 90 days after an infection, this population had high immune protection — their risk of becoming infected with BA.5 was just one-sixteenth that of people who had been vaccinated but never infected. After that, hybrid immunity against infection declined

steeply for a few months and then stabilized, ultimately providing protection for eight months after infection, the duration of the study.



What the Omicron wave is revealing about human immunity

Another study[3] looked at 338 vaccinated health-care workers in Sweden, some of whom had had a previous SARS-CoV-2 infection. The authors found that workers with hybrid immunity had some level of protection against infection with BA.1, BA.2 and BA.5 for at least eight months. Swabbing of these workers' noses revealed high levels of 'mucosal' antibodies, which are thought to be a better shield against infection than antibodies that circulate in the blood.

A study[4] in Qatar compared the infection risks of people who had never caught SARS-CoV-2 with those of people who'd had a previous infection with Omicron or an earlier variant. Both groups included vaccinated and unvaccinated individuals. The results show that more recent infections provide greater protection than older ones in all cases. But because the virus kept evolving, the authors couldn't untangle whether those differences were because of waning immunity, the virus's growing ability to evade the immune response or, more likely, a combination of the two.

Infection reprieve

Taken together, the studies suggest that hybrid immunity provides some protection against infection for at least seven or eight months, and probably longer. “That’s pretty good,” says Charlotte Thålin, an immunologist at the Karolinska Institute in Stockholm and an author of the Swedish study.

Other data suggest that in people whose immunity arises only from vaccination, a booster dose provides relatively short-lived protection against infection. Researchers in Israel studied more than 10,000 health-care workers who had not previously been infected; all received either three or four doses of the vaccine made by Pfizer and BioNTech[5]. The authors found that the fourth dose’s efficacy against infection fell rapidly. In fact, after four months, the fourth dose was no better than three doses at preventing infection.



Immunity against Omicron from breakthrough infection could be a matter of timing

However, “we are talking just about what we call relatively mild disease”, says study co-author Gili Regev-Yochay, an epidemiologist at Sheba Medical Center Tel Hashomer in Ramat Gan, Israel. None of the people in the study developed severe COVID-19.

What about those who haven’t been vaccinated? Another study[6] in Qatar suggests that if the virus doesn’t change, infection-based immunity against

reinfection can last up to three years. But that immunity can fade faster if the virus mutates. The authors studied data from unvaccinated people who were infected with a pre-Omicron variant. Fifteen months later, those infections were less than 10% effective at protecting against Omicron infection. And it is much riskier to rely on immunity from infection than to get immunized.

But it's nearly impossible to apply the study results to predict an individual's risk of becoming infected in future. Immunity depends on a variety of factors, including genetics, age and sex. And past risk of infection isn't necessarily a good predictor of the risk of future infection, because new variants are continually arising.

Booster break

How growing global hybrid immunity will affect the timing and frequency of infection surges isn't yet clear. Neither is it clear how this will influence health officials' decisions about when to offer future booster doses.

For people who are at high risk of developing severe COVID-19, it might make sense to get boosters frequently. Younger individuals without any risk factors who live in regions where the virus has been circulating freely "may already have very significant protection that may not require as frequent boosters", says Luís Graça, an immunologist in the Faculty of Medicine at the University of Lisbon and a co-author of the Portuguese study. Another option might be to give a booster when antibody levels fall below a certain threshold, says Regev-Yochay.

Thålin understands how frustrating the caveats and uncertainty can be, but says that researchers aren't likely to pin down an answer anytime soon. "The virus is evolving so fast," she says. "What's true today might not be true tomorrow."

Nature **614**, 395-396 (2023)

doi: https://doi.org/10.1038/d41586-023-00124-y

References

1. Malato, J. *et al. Lancet Infect. Dis.* **23**, 148–150 (2023).
2. Bobrovitz, N. *et al. Lancet Infect. Dis*. https://doi.org/10.1016/S1473-3099(22)00801-5 (2023).
3. Marking, U. *et al. Lancet Infect. Dis.* **23**, 150–152 (2023).
4. Chemaitelly, H. *et al. N. Engl. J. Med*. https://doi.org/10.1056/NEJMc2214114 (2023).
5. Canetti, M. *et al. N. Engl. J. Med.* **387**, 2092–2094 (2022).
6. Chemaitelly, H. *et al. J. Travel Med.* **29**, taac109 (2022).

This article was downloaded by **calibre** from https://www.nature.com/articles/d41586-023-00124-y

| Section menu | Main menu |

- NEWS
- 02 February 2023

Scientists made a new kind of ice that might exist on distant moons

The 'amorphous' solid is denser and could be water ‘frozen in time’.

- Jonathan O'Callaghan



Milling ordinary ice with steel balls disrupted its crystalline structure and led to a novel, denser version of solid water.Credit: Alexander Rosu-Finsen, Christoph Salzmann

Scientists have created a new type of ice that matches the density and structure of water, perhaps opening a door to studying water's mysterious properties.

"It might be liquid water frozen in time," says Martin Chaplin, a specialist in water structure at London South Bank University, who was not involved in the work. "It could be very important."

The ice is called medium-density amorphous ice. The team that created it, led by Alexander Rosu-Finsen at University College London (UCL), shook regular ice in a small container with centimetre-wide stainless-steel balls at temperatures of –200 ˚C to produce the variant, which has never been seen before. The ice appeared as a white granular powder that stuck to the metal balls. The findings were published today in *Science*[1].

Haphazard molecules

Normally, when water freezes, it crystallizes and its molecules are arranged into the familiar hexagonal, solid structure that we call ice. Ice is less dense than its liquid form — an unusual property for a crystal. Depending on conditions such as pressure and the speed of freezing, water can also solidify in any of two dozen other regular arrangements. Amorphous ice is different: it has no such order. “You have lots of molecules joining on haphazardly,” says Chaplin.

Two types of amorphous ice have been previously discovered, both in the twentieth century. ‘Low-density’ amorphous ice is the result of water vapour freezing onto a very cold surface, at a temperature lower than –150 ˚C; ‘high-density’ amorphous ice forms by compressing ordinary ice at similar temperatures under high pressure. Although neither type is common on Earth, both are plentiful in space. “Comets are big chunks of low-density amorphous ice,” says Christoph Salzmann, a chemist at UCL and a co-author of the latest work.

The team used a ball mill, a tool normally used to grind or blend materials in mineral processing, to grind down crystallized ice. Using a container with metal balls inside, they shook a small amount of ice about 20 times per second. The metal balls produced a ‘shear force’ on the ice, says Salzmann, breaking it down into a white powder.

Firing X-rays at the powder and measuring them as they bounced off — a process known as X-ray diffraction — allowed the team to work out its structure. The ice had a molecular density similar to that of liquid water, with no apparent ordered structure to the molecules — meaning that

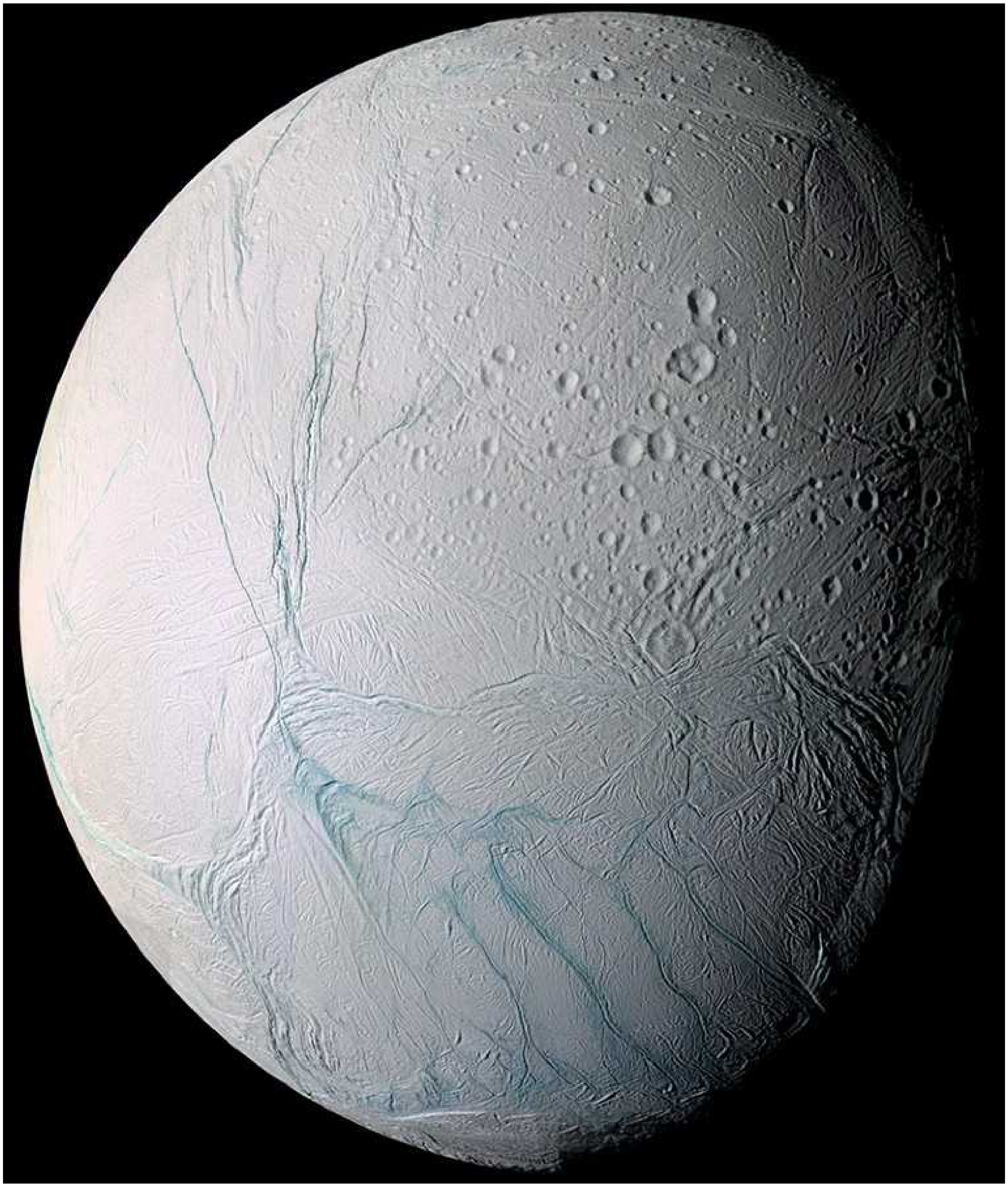
crystallinity was “destroyed”, says Salzmann. “You’re looking at a very disordered material.”

The results are “pretty convincing”, says Marius Millot, a physicist at the Lawrence Livermore National Laboratory in California. “This is a great example of how we still have things to understand with water.”

The results matched models produced by scientists on the team at the University of Cambridge, UK, predicting what would happen if regular ice was broken down in this manner. It’s unclear, however, whether the resultant powder truly matches the properties of liquid water, given that it was previously frozen as crystallized ice. Investigating that will require further work.

Big implications

If confirmed, the new form of ice could enable studies of water in a manner that was not possible before. “Liquid water is a strange material,” says Chaplin. “We still don’t know as much about it as we’d like.” For example, it is commonly thought that water is composed of two forms, low-density and high-density water, matching the previously known variants of amorphous ice. The discovery of a medium-density amorphous ice could challenge that idea.



The ice plates on the surface of Enceladus rub against one another under tidal forces as the moon orbits Saturn. Denser, 'amorphous' ice could form at their boundaries.Credit: NASA/JPL/Space Science Institute

“If medium-density amorphous ice is really connected to liquid water, it would imply that this model is incorrect,” says Salzmann. “It could open up

a new chapter in ice research.”

There are implications, too, for understanding other worlds. Some moons in our Solar System, such as Jupiter’s moon Europa and Saturn’s moon Enceladus, have icy surfaces. If two icy areas on such a moon were to rub together because of tidal forces, they could produce medium-density amorphous ice between them through the same shearing process that the researchers used.

The increase in density could create gaps in the surface, producing disruptions on the moons as the ice cracks together. “There would be a massive collapse of the ice,” says Salzmann. “It could have severe implications for the geophysics of the icy moons.”

That could, in turn, have implications for the potential habitability of liquid-water oceans that lie under the ice surfaces on these moons. “One of the key things about those moons is whether you can have an interface between liquid water and the rocks — this is where life could emerge,” says Millot. “Amorphous ice could have a role that we need to understand.”

Nature **614**, 396-397 (2023)

doi: https://doi.org/10.1038/d41586-023-00293-w

References

1. Rosu-Finsen, A. *et al. Science* **379**, 474–478 (2023).

This article was downloaded by **calibre** from https://www.nature.com/articles/d41586-023-00293-w

- NEWS
- 06 February 2023

Antibiotic use in farming set to soar despite drug-resistance fears

Analysis finds antimicrobial drug use in agriculture is much higher than reported.

- Sara Reardon



Researchers have struggled to calculate the amount of antibiotics used in agriculture in many countries.Credit: Edwin Remsberg/The Image Bank/Getty

The use of antibiotics in animal farming — a major contributor to antimicrobial resistance — is expected to grow by 8% between 2020 and 2030 despite ongoing efforts to curtail their use, according to an analysis[1].

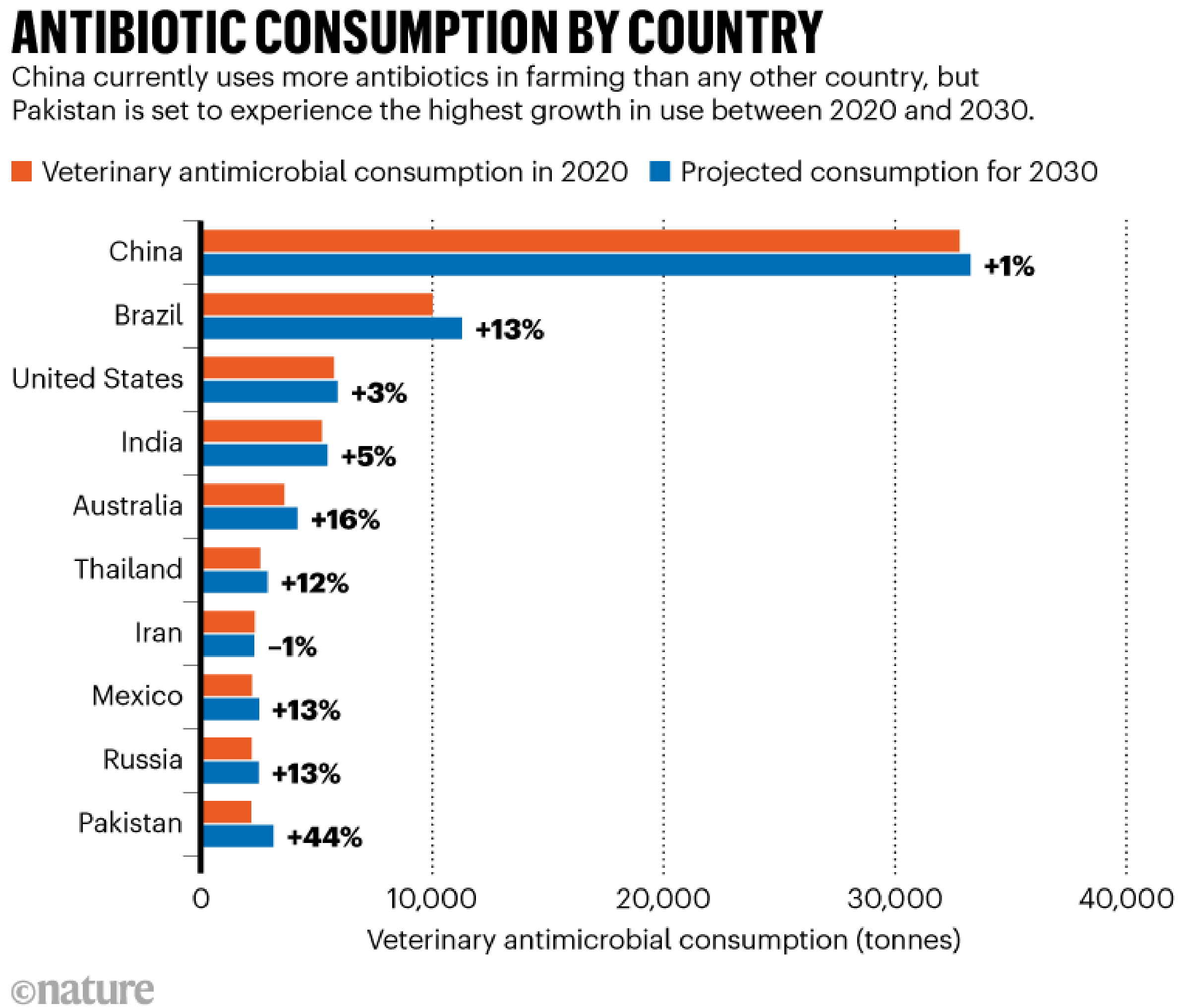
Overuse of antibiotics in agriculture is thought to be a major driver of the rise in humans of bacterial infections that cannot be treated with antibiotics. Although antibiotics can be necessary to treat infections in livestock, they are often used to speed up animal growth and prevent diseases among animals in crowded, unsanitary conditions.

Many governments have struggled to make or enforce rules to decrease antibiotic usage. For instance, although a number of countries, including the United States and much of Europe, ban the use of antibiotics that promote growth, manufacturers can just say they are marketing the drugs to prevent disease.

Researchers have also struggled to calculate the amount of antibiotics used in particular countries because most do not release their agricultural-antibiotic usage data publicly, says study co-author Thomas Van Boeckel, a spatial epidemiologist at the Swiss Federal Institute of Technology in Zurich (ETH Zurich). Instead, many release the data to the World Organization for Animal Health (WOAH), which groups country's antibiotics data into continents, so that is all that researchers can see. And around 40% of countries do not report their antibiotic use to WOAH at all. "The majority of data on antibiotic use in the world is unusable," van Boeckel says.

Country estimates

To estimate antibiotic usage in 229 countries, Van Boeckel worked with Ranya Mulchandani, an epidemiologist at ETH Zurich, and other colleagues to collect data from individual governments, farm surveys and scientific articles that reported veterinary use of antibiotics. They cross-referenced these with data on farm-animal populations worldwide, as well as on antibiotic sales from the 42 countries that reported those data publicly. From there, they extrapolated trends for the remaining 187 countries.



Source: R. Mulchandani *et al. PLOS Glob. Public Health* **3**, e0001305 (2023)

The team calculated that antibiotic use in Africa is probably twice what WOAH reports, and use in Asia is 50% higher than reported. The authors attribute this to the fact that many countries in these regions do not respond to WOAH surveys. Accounting for these in their calculations, the authors estimate that by 2030, the world will use around 107,500 tonnes of antibiotics in livestock per year, compared with just under 100,000 tonnes in 2020. Antibiotic use is highest in Asia, and China in particular (see 'Antibiotic consumption by country') — a trend that is expected to continue until 2030. The researchers also estimate that antibiotic use will grow the fastest in Africa, rising by 25% between 2020 and 2030 owing to increased demand for meat products.

However, Mulchandani cautions that most of the 42 data-sharing countries were high-income, meaning that the types of antibiotic they use, and the purpose, might not represent all nations.

At a ministerial conference on antimicrobial resistance in Muscat, Oman, last November, 39 countries — including major agricultural producers Russia and India — pledged to reduce their agricultural use of antimicrobials by 30–50% by 2030. Even if that goal isn't met, says Steven Roach, programmes director at the non-profit organization Keep Antibiotics Working, who is based in Iowa City, the agreement means that the countries are more likely to begin releasing baseline data on their antibiotic usage. "It suggests there is potential for real reduction if there's global will," he says. In the meantime, he adds, the types of method used in the latest study are the only way to get a global picture of antibiotic use.

In the future, Van Boeckel says, his team will model scenarios such as what would happen if more countries adopted stricter antibiotic distribution approaches similar to that taken by Sweden, which requires a veterinarian's prescription for antibiotics to be used on animals. Making usage data more publicly accessible, he adds, could lead to increased accountability for countries — and agricultural producers — that do not use antibiotics responsibly.

Nature **614**, 397 (2023)

doi: https://doi.org/10.1038/d41586-023-00284-x

References

1. Mulchandani, R., Wang, Y., Gilbert, M. & Van Boeckel, T. P. *PLOS Glob. Public Health* **3**, e0001305 (2023).

This article was downloaded by **calibre** from https://www.nature.com/articles/d41586-023-00284-x

- NEWS EXPLAINER
- 06 February 2023
- Update 07 February 2023
- Update 09 February 2023

Turkey–Syria earthquake: what scientists know

Turkey and Syria's buildings have always been vulnerable to earthquakes, but war has made things worse.

- Miryam Naddaf



The earthquake destroyed buildings in the town of Jandaris, near Afrin, Syria.Credit: Rami al-Sayed/AFP/Getty

A magnitude-7.8 earthquake hit southeastern Turkey and parts of Syria in the early hours of the morning of 6 February. At least 17,000 people are known to have lost their lives, with thousands more injured. The quake was followed by a magnitude-7.5 event some 9 hours later, as well as more than 200 aftershocks.

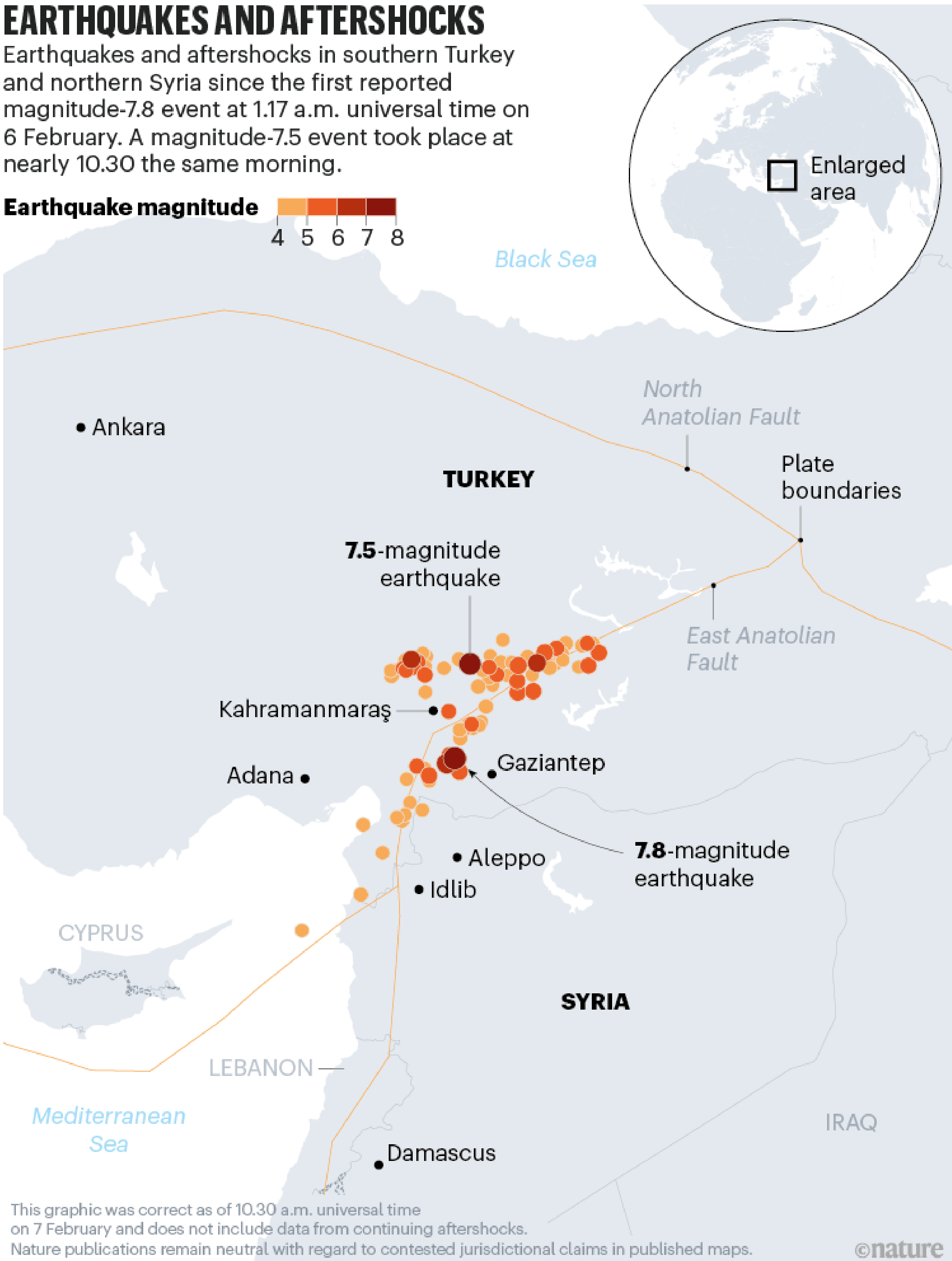
The earthquake and its aftershocks have flattened buildings and sent rescuers digging through concrete debris to find survivors, with the death toll expected to increase further. *Nature* spoke to four researchers about the seismic activity in the region and what the next few days will bring.

Turkey is in an active earthquake zone

Most of Turkey sits on the Anatolian plate between two major faults: the North Anatolian Fault and the East Anatolian Fault. The tectonic plate that carries Arabia, including Syria, is moving northwards and colliding with the southern rim of Eurasia, which is squeezing Turkey out towards the west, says David Rothery, a geoscientist at the Open University in Milton Keynes, UK. "Turkey is moving west about 2 centimetres per year along the East Anatolian Fault," he adds. "Half the length of this fault is lit up now with earthquakes."

Seyhun Puskulcu, a seismologist and coordinator of the Turkish Earthquake Foundation, based in Istanbul, says people in Turkey are well aware of their vulnerability to earthquakes. "This wasn't a surprise," says Puskulcu, who last week was touring the cities of Adana, Tarsus and Mersin, and areas of western Turkey, delivering workshops on earthquake awareness.

The epicentre of the main earthquake was 26 kilometres east of the city of Nurdaği in Turkey's Gaziantep province, at a depth of 17.9 kilometres. The magnitude-7.5 event occurred around 4 kilometres southeast of Ekinözü in the Kahramanmaraş province (see 'Earthquakes and aftershocks').



US Geological Survey Earthquake Hazards Program

War has destabilized already-vulnerable buildings

Deaths in earthquakes are often caused by falling bricks and masonry. According to the US Geological Survey, many people in Turkey who were affected by the earthquake live in structures that are extremely likely to be damaged by shaking, with unreinforced brick masonry and low-rise concrete frames.

In a study[1] published last March in *Soil Dynamics and Earthquake Engineering*, Arzu Arslan Kelam at the Middle East Technical University, Ankara, and her colleagues suggested that the centre of the city of Gaziantep would experience medium-to-severe damage from a magnitude-6.5 earthquake. This is because most existing buildings are low-rise brick structures that are constructed very close to each other.

In 1999, a magnitude-7.4 earthquake hit 11 kilometres southeast of Izmit, Turkey, killing more than 17,000 people and leaving more than 250,000 homeless. After this tragedy, the Turkish government introduced new building codes and a compulsory earthquake insurance system. However, many of the buildings affected by this week's quake were built before 2000, says Mustafa Erdik, a civil engineer at Boğaziçi University, Turkey.

Things are worse in Syria, where more than 11 years of conflict have made building standards impossible to enforce. The earthquake struck Syria's northwestern regions, with buildings collapsing in Aleppo and Idlib. Some war-damaged buildings in Syria have been rebuilt using low-quality materials or "whatever materials are available", says Rothery. "They might have fallen down more readily than things that were built at somewhat greater expense. We've yet to find out," he adds.

What's next?

Researchers say people need to brace themselves for yet more quakes and aftershocks, as well as deteriorating weather. "The possibility for major aftershocks causing even more damage will continue for weeks and months," says Ilan Kelman, who studies disasters and health at University College London.

“The weather forecast for the region for tonight is dropping below freezing. That means that people who are trapped in the rubble, who might be rescued, could well freeze to death. So these hazards continue,” he adds.

Nature **614**, 398-399 (2023)

doi: https://doi.org/10.1038/d41586-023-00364-y

Updates & Corrections

- **Update 07 February 2023**: This story has been updated with the latest death toll.

- **Update 09 February 2023**: This story has been updated again with the latest death toll at the time of publishing.

References

1. Kelam, A. A. *et al. Soil Dyn. Earthq. Eng.* **154**, 107129 (2022).

This article was downloaded by **calibre** from https://www.nature.com/articles/d41586-023-00364-y

- NEWS
- 07 February 2023

COVID drug drives viral mutations — and now some want to halt its use

Analysis reveals the signature of the antiviral drug molnupiravir in SARS-CoV-2 sequences riddled with mutations.

- Ewen Callaway



Genomic analysis has linked the antiviral drug molnupiravir to highly mutated lineages of SARS-CoV-2.Credit: Ziad Ahmed/NurPhoto/Getty

A drug widely used to treat COVID-19 might be spurring the evolution of new SARS-CoV-2 variants.

The drug, molnupiravir, works by introducing a flurry of mutations to the viral genome; this helps to clear infections. But a study[1] of more than 13 million SARS-CoV-2 sequences has uncovered sequences that bear molnupiravir's fingerprints. The study's authors say the results suggest that molnupiravir treatment has sparked the evolution of viral lineages carrying numerous mutations that, in at least some cases, have the capacity to spread to other individuals.

The study was posted on the medRxiv preprint server in January. It has not yet been peer reviewed.

"Whether this should be of concern — that is an open question," says Jesse Bloom, an evolutionary virologist at the Fred Hutchinson Cancer Research Center in Seattle, Washington. Mutations to the SARS-CoV-2 genome can help the virus to evade immunity and become more transmissible, but most mutations are likely to harm it.

Molecular mimic

Molnupiravir was developed by the pharmaceutical giant Merck, based in Rahway, New Jersey, and was authorized by regulators in the United States and United Kingdom in late 2021, and in Australia in early 2022. A company-sponsored clinical trial found that the drug — a pill taken for five days — reduced hospitalizations and deaths in people at risk of severe COVID-19.

Molnupiravir mimics some of the building blocks of RNA, the genetic material in SARS-CoV-2. The drug peppers the viral genome with mutations, which add up to make SARS-CoV-2 worse at replicating. This results in a marked reduction in SARS-CoV-2 levels in infected human cells and hamsters[2].

But scientists have raised the possibility that, in rare cases, molnupiravir treatment might not entirely eliminate SARS-CoV-2, allowing some individuals who have taken the drug to continue to transmit the virus.



[How your first brush with COVID warps your immunity]

Those concerns were largely theoretical until Ryan Hisner, a US schoolteacher who is part of a loose-knit community of SARS-CoV-2 variant spotters, started noticing peculiar patterns in sequencing data from around the world: a number of lineages carried many more mutations than their nearest relatives. Most of the genetic changes were of the type induced by molnupiravir.

The researchers’ analysis of global sequences showed that the prevalence of the suspect lineages rose substantially in 2022, the first year molnupiravir was widely used. The lineages were also much more likely to show up in sequencing data from countries where the drug was used — the United States, the United Kingdom and Australia — than in data from countries that hadn’t approved it, such as France and Canada.

Where SARS-CoV-2 sequence data include the age of the individual sampled, the telltale lineages tended to have come from older people, who are more likely to take molnupiravir. And in Australia, where molnupiravir was pre-placed in care homes, the researchers identified a viral lineage carrying 25 mutations that had infected at least 20 people, mostly in their eighties and nineties.

Among the lineages that showed molnupiravir's influence, a few — including the one from Australia — were represented by multiple sequences, indicating that they were capable of spreading. "I would say that our work closes down the possibility that these viruses can never be transmitted," says team member Theo Sanderson, a computational biologist at the Francis Crick Institute in London.

Evolutionary dead ends?

Evidence linking molnupiravir to the mutation-heavy sequences is "circumstantial", Merck said in a statement. "The authors assume these mutations were associated with molnupiravir treatment without evidence the viral sequences were isolated from treated patients."

Bloom thinks the researchers make a good case that molnupiravir treatment is yielding some highly mutated viruses with the capacity to spread. But it's not clear whether this could contribute to new coronavirus variants, or whether it is simply creating weakling viruses that are unlikely to spread very far. "SARS-CoV-2 is already generating plenty of mutations even in the absence of drug treatment," he adds.

Rustem Ismagilov, a quantitative bioscientist at the California Institute of Technology in Pasadena, says the study underscores the need to quickly measure any risk that molnupiravir poses in terms of sparking new variants, and to weigh them against the drug's benefits. "If we are playing Russian roulette, we'd better know our odds."

Sarah Otto, an evolutionary biologist at the University of British Columbia in Vancouver, Canada, says the paper is another blow to the continued use of molnupiravir. She notes that a large-scale UK study found that the drug had no effect on hospitalizations or deaths[3]. "Given the large-scale risks of this mutagen producing new variants faster, including variants that are immune evasive, I encourage public-health leaders to call for a global halt to its use," Otto says.

Nature **614**, 399 (2023)

doi: https://doi.org/10.1038/d41586-023-00347-z

References

1. Sanderson, T., Hisner, R., Donovan-Banfield, I., Peacock, T. & Ruis, C. Preprint at medRxiv https://doi.org/10.1101/2023.01.26.23284998 (2023).
2. Rosenke, K. *et al. Nature Commun.* **12**, 2295 (2021).
3. Butler, C. C. *et al. Lancet* **401**, 281–293 (2023).

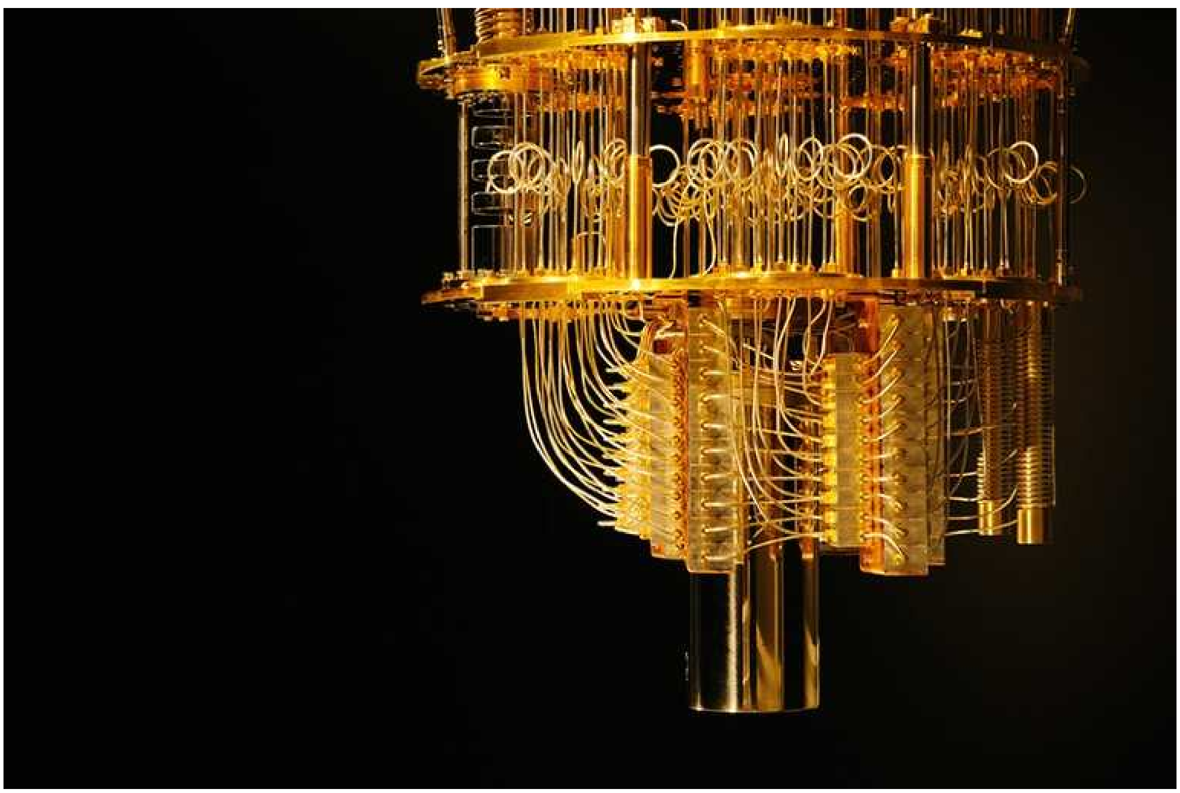
This article was downloaded by **calibre** from https://www.nature.com/articles/d41586-023-00347-z

- NEWS
- 06 February 2023

Underdog technologies gain ground in quantum-computing race

Individual atoms trapped by optical ‘tweezers’ are emerging as a promising computational platform.

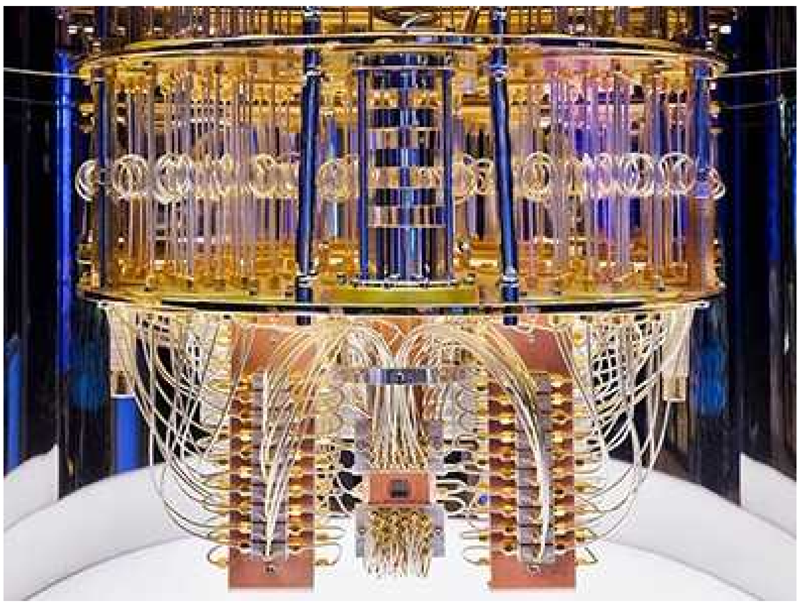
- Davide Castelvecchi



IBM’s quantum-computing system has a cryostat at its centre to cool the quantum chip.Credit: IBM

The race to build practical quantum computers might be entering a new phase. Some of the front-runner technologies are now facing size constraints, and others are rapidly coming up from behind.

For years, two leading approaches have enabled physicists to make progress partly by cramming devices with more and more qubits, the quantum equivalent of a computer's memory bits. One of those methods encodes qubits as currents running on superconducting loops. The other uses excited states of individual ions trapped in a vacuum by electromagnetic fields.



First quantum computer to pack 100 qubits enters crowded race

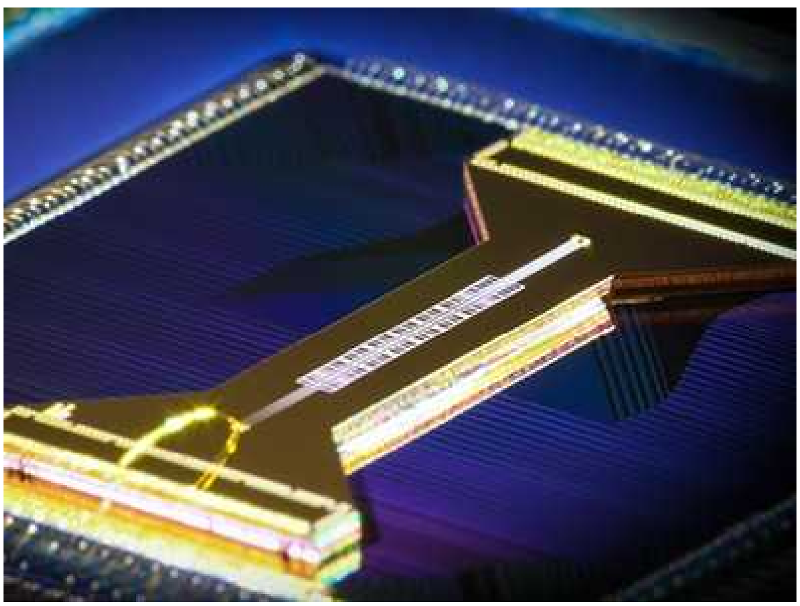
But in the past two years, qubits that consist of single neutral atoms — as opposed to ions — and are held with 'tweezers' made of laser light have suddenly become competitive. And other techniques that are at an even earlier stage of development could yet catch up.

"Superconducting qubits and trapped-ion qubits have done the most-advanced experiments, with the most qubits under control," says Barbara Terhal, a theoretical physicist at QuTech, a quantum-research institute at the Delft University of Technology in the Netherlands. "However, this is no guarantee that these platforms will stay in the lead."

The quest for qubits

Quantum computers promise to solve problems that are out of reach for classical machines by harnessing phenomena such as quantum superposition, in which an object can exist in two simultaneous states — spinning both clockwise and anticlockwise, for example. Physicists call such states qubits to distinguish them from ordinary bits, which can be only ‘0’ or ‘1’.

Quantum states are notoriously fragile. In a quantum computer, the information they carry — which can extend across several qubits to form ‘entangled’ states — tends to degrade or get lost as a calculation progresses. To preserve the states for as long as possible, qubits must be kept isolated from the environment. But they cannot be too isolated from one another because they must interact to perform calculations.



Quantum computer race intensifies as alternative technology gains steam

This — among other factors — makes building a useful quantum computer challenging. But the field has come further than QuTech director of research Lieven Vandersypen would have expected ten years ago. “The progress is actually impressive.”

Google made headlines in 2019 when it claimed that a machine made of 54 superconducting qubits had performed the first quantum computation that would have taken impossibly long on a classical computer, an achievement

that researchers call quantum advantage. The technology company IBM, which has invested heavily in superconducting qubits, expects to reach a milestone in the next few months, when it will unveil a quantum chip named Condor, the first to breach the 1,000-qubit barrier.

Last November, the company announced its previous chip, the 433-qubit Osprey — a follow-up to the 127-qubit Eagle, which set a record in 2021. "We really wanted to lay a road map like you would expect from the semiconductor industry," says Jerry Chow, who leads the quantum-computer programme at the IBM Thomas J. Watson Research Center in Yorktown Heights, New York.

Quality and quantity

Chow says that IBM's aim is not only to scale up the number of qubits, but also to improve their quality. Some of the company's superconducting elements can hold their quantum states for more than 300 microseconds, he says — a record for the technology. In another crucial measure, 99.9% of operations involving two qubits are now error-free.



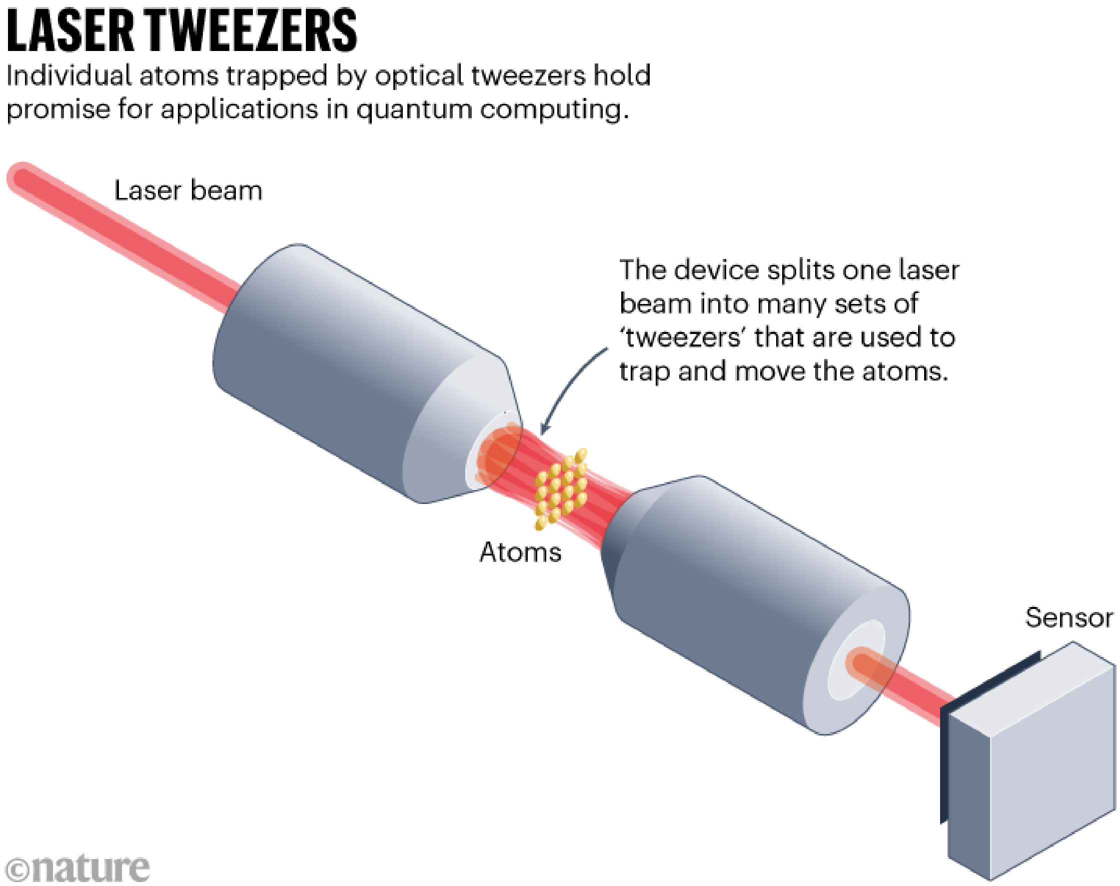
Beyond quantum supremacy: the hunt for useful quantum computers

Scaling up becomes impractical once the number of superconducting qubits on a chip goes much beyond 1,000, because each qubit needs to be individually wired to external circuits for control and readout. IBM will therefore take a modular approach. Starting in 2024, each further step on its road map will aim not to increase the number of qubits on a chip, but to link multiple chips into one machine — something that is not straightforward if the connection has to carry the quantum states unharmed or help to entangle qubits on separate chips. The chips are at the hearts of massive contraptions encased in cryogenic systems that keep the chips close to 0 kelvin.

Trapped-ion computers could have even more-stringent size constraints than superconducting ones, partly because they require a separate laser device to control each ion. Typically, that has meant limiting the traps to rows of around 32 ions per chip. But IonQ, a start-up company spun off from the University of Maryland in College Park, says its approach enables it to pack multiple rows of ions into a single chip, perhaps reaching as many as 1,024 qubits. To go beyond that, IonQ also plans to move to a modular approach, connecting multiple chips. In laboratory experiments, trapped ions have reached fidelities as high as 99.99%, according to a spokesperson for the company.

Tweezer tech

Another technique — which, until a few years ago, was barely on the radar — might soon break the 1,000-qubit barrier as well. It traps neutral atoms using tightly focused laser beams, called optical tweezers, and encodes qubits in the electronic states of the atoms or in the spins of atoms' nuclei (see 'Laser tweezers'). The approach has been developing gradually for more than a decade, but now it's "booming", says Giulia Semeghini, a physicist at Harvard University in Cambridge, Massachusetts.



Source: Ref. 1

To assemble multiple qubits, physicists split a single laser beam into many, for example by passing it through a screen made of liquid crystals. This can create arrays of hundreds of tweezers, each trapping their own atom. The atoms are typically a few micrometres away from their neighbours, where they can persist in a quantum state for several seconds or more. To make the atoms interact, physicists point a separate laser at one of them to tickle it into an excited state, in which an outer electron orbits much farther away from the nucleus than normal. This boosts the atom's electrostatic interactions with a neighbour.

Using tweezers, researchers have built arrays of more than 200 neutral atoms, and they are rapidly combining new and existing techniques to turn these into fully working quantum computers.

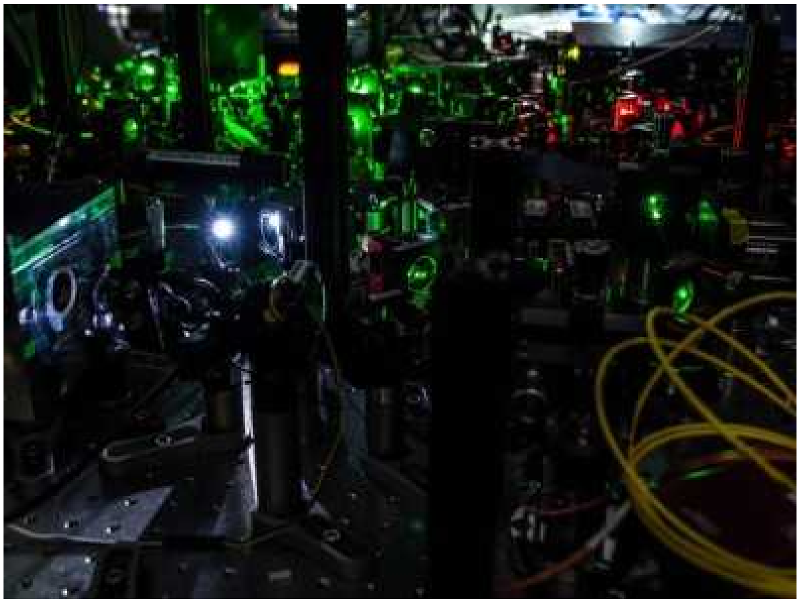
One major advantage of the technique is that physicists can combine multiple types of tweezers, some of which can move around quickly — with the atoms they carry. “Every time you want two of them to interact, you bring them together,” says Harvard physicist Dolev Bluvstein. This makes the technique more flexible than other platforms such as superconductors, in which each qubit can interact only with its direct neighbours on the chip. A team including Semeghini and Bluvstein demonstrated this flexibility in an April 2022 paper[1].

The tweezer-based qubits should soon be 99% error-free, although further improvements will take substantial work, Semeghini says.

The pace of improvement in neutral atoms has surprised the quantum-computing community. “The path to scale to thousands of atomic qubits is clear and will likely happen within two years,” says physicist Chao-Yang Lu at the University of Science and Technology of China (USTC) in Hefei.

Spin control

Other qubit technologies are still in their infancy, but advancing steadily. One method encodes information in the spin of individual electrons trapped by electric fields inside conventional semiconductors such as silicon. Last year, Vandersypen and his collaborators demonstrated a fully working six-qubit machine of this kind[2]. As in the case of optical tweezers, the electron spins can be shuttled around the device to bring them next to others on demand. But just like other types of qubit, a major difficulty is keeping the spins from influencing each other when they are not supposed to, in what physicists call crosstalk.



[Quantum network is step towards ultrasecure internet]

The benefit of semiconductor-based qubits would be the ability to make chips in the same type of factory where current computer chips are produced, although a team led by physicist Michelle Simmons at the University of New South Wales in Sydney, Australia, assembles the devices atom by atom using the tip of an automated scanning tunnelling microscope. “Everything is patterned with sub-nanometre precision,” she says.

Yet another approach is still at the conceptual stage, but it has received substantial investment, by Microsoft in particular. The technique aims to exploit ‘topological states’ to make qubits robust to degradation, just like a knotted string that can be twisted and pulled but not untied. In 2020, researchers observed the basic physical mechanism for one kind of topological protection, and they are now working on demonstrating the first topological qubits.

“Every platform that is pursued today has some promise, but developing it can require really novel ideas that you can’t predict,” says Vandersypen. Pan Jian-Wei, a physicist who works on multiple quantum-computing approaches at USTC, agrees. When it comes to the race to develop quantum computers, “it is still too early to say which candidate will win”.

Nature **614**, 400-401 (2023)

doi: https://doi.org/10.1038/d41586-023-00278-9

References

1. Bluvstein, D. *et al. Nature* **604**, 451–456 (2022).

2. Philips, S. G. J. *et al. Nature* **609**, 919–924 (2022).

This article was downloaded by **calibre** from https://www.nature.com/articles/d41586-023-00278-9

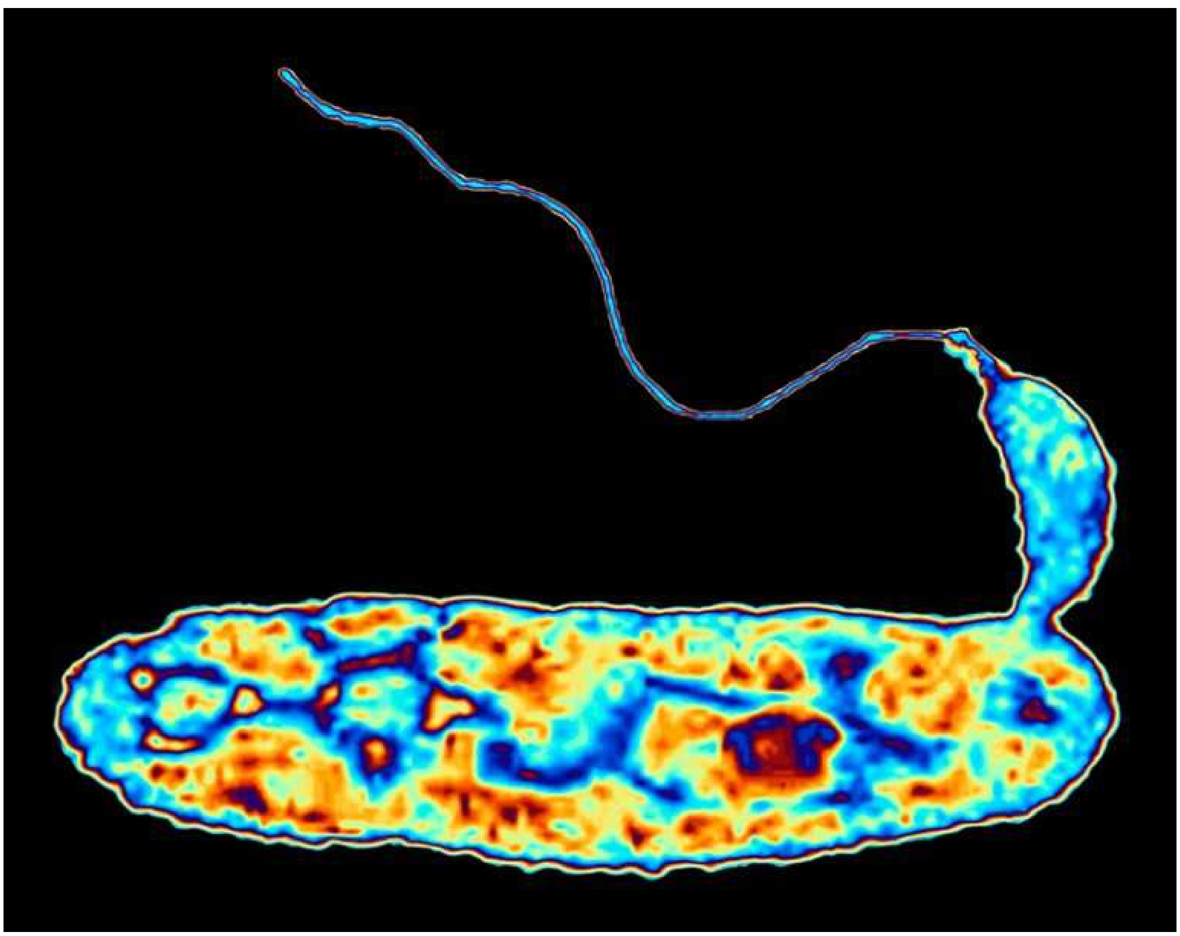
| Section menu | Main menu |

- NEWS
- 03 February 2023

Dogma-defying bacteria package DNA in unusual ways

Some bacteria appear to encase their genomes in proteins called histones — which weren’t thought to exist in bacterial cells.

- Heidi Ledford



The predatory bacterium *Bdellovibrio bacteriovorus* infiltrates larger bacteria and digests them from within.Credit: Alfred Pasieka/Science Photo Library

A startling discovery in bacteria suggests that some species have a bizarre way of packaging chromosomes and regulating gene expression — using proteins that, until recently, weren't thought to exist in bacteria at all.

In a preprint posted on bioRxiv on 26 January, researchers report the characterization of proteins called histones that, in two bacterial species, seem to bind together to coat regions of the bacterial chromosome[1]. This is completely different from the arrangement of histones seen in other organisms. For example, in organisms called eukaryotes, whose cells have a membrane-bounded nucleus, DNA winds around histones, rather than being encased by them.

Although histones are vital tools for maintaining chromosome structure and controlling gene activity in eukaryotes and microorganisms called archaea, for years it was widely assumed that they did not exist in bacteria.

As more bacterial genome sequences became available, the discovery of sequences characteristic of histones challenged that assumption[2]. "But nobody had ever characterized them or done functional studies," says Remus Dame, a biochemist and microbiologist at Leiden University in the Netherlands. "This is definitely something new and interesting."

Uniform structure

Eukaryotic histones are remarkably uniform in their structure and function — a consistency that can be frustrating for researchers who want to study histone evolution, says biochemist Karolin Luger at the University of Colorado Boulder. "If you want to get at the evolutionary origin, you can't go to a 'primitive' eukaryote," she says. "It already has everything."

The lack of diversity also raises questions for synthetic biologists in search of new ways to control gene expression, says Tobias Warnecke, a molecular evolutionary biologist at Imperial College London. "The fundamental

composition of the chromatin and how gene expression works is very similar across eukaryotes and then you start wondering, ‘is that a frozen accident?’” he says. “Is there something special about histones that makes them unique, or can we build systems in a different way?”

Recent explorations of archaeal histones have yielded more diverse systems, and Warnecke and Antoine Hocher, a systems biologist also at Imperial College, decided to see what surprises bacterial histone-like proteins might hold. Together with Luger and other collaborators, they studied the proteins from two species that can be readily grown in the laboratory: the pathogen *Leptospira interrogans* and a predatory bacterium called *Bdellovibrio bacteriovorus*. This infiltrates larger bacteria and digests them from within, chopping up its prey’s DNA and proteins for use as building blocks to replicate itself.

When the researchers isolated the histone protein from *B. bacteriovorus* and analysed its structure, both on its own and while it was interacting with DNA, they were surprised to find that it did not behave like any known histones from archaea or eukaryotes. The bacterial histones came together in pairs that surrounded the DNA strand. Long chains of these could act as a shield around the DNA, a marked difference from their function in eukaryotes, in which histones group together to form a spool around which the DNA winds. “I was blown away,” says Luger.

Protective proteins

It’s a striking finding, but it still isn’t clear whether that structure reflects how histones and DNA interact in the bacterial cells, or whether it’s an artefact of working with the isolated proteins in the laboratory, says Dame.

For now, researchers can only speculate as to what the histones might be doing, and how their unusual mode of action might help the bacteria survive. For *B. bacteriovorus*, the histones could be protecting the DNA from picking up stray pieces of the fragmented genomes of its prey, says Warnecke.

The bacterium is also known for having tightly packed DNA during its free-swimming phase, before it infects its prey, notes Géraldine Laloux, a microbiologist at the Catholic University of Louvain in Belgium. “We have been wondering what drives this very strong compaction and how it de-compacts,” says Laloux. “This unique way of binding the DNA could bring new insights into this.”

As part of their study, the researchers surveyed thousands of bacterial genomes. They found histone-like proteins in about 2% of the genomes, which suggests that there will be many other systems to study. “People got excited and said ‘oh, bacteria weren’t supposed to have histones’,” says Warnecke. “But if you work on microbial evolution, you know that if you look hard enough, you’ll find some.”

Nature **614**, 401 (2023)

doi: https://doi.org/10.1038/d41586-023-00334-4

References

1. Hocher, A. *et al.* Preprint at bioRxiv https://doi.org/10.1101/2023.01.26.525422 (2023).

2. Alva, V. & Lupas, A. N. *Bioinformatics* **35**, 2349–2353 (2018).

This article was downloaded by **calibre** from https://www.nature.com/articles/d41586-023-00334-4

- NEWS EXPLAINER
- 10 February 2023

What it would take to bring back the dodo

An audacious plan to ‘de-extinct’ dodos depends on huge leaps in biotechnology and resurrecting a lost habitat.

- Ewen Callaway



The flightless dodo went extinct in the seventeenth century. Biotech company Colossal Biosciences plans to resurrect it.Credit: Hart, F/Bridgeman Images

A biotech company announced a bold effort to ‘de-extinct’ the dodo last week. The flightless birds vanished from the island of Mauritius — in the

Indian Ocean — in the late seventeenth century, and became emblematic of humanity's negative impacts on the natural world. Could the plan actually work?

Colossal Biosciences, based in Dallas, Texas, has landed US$225 million in investment (including funds from the celebrity Paris Hilton) — having previously announced plans to de-extinct thylacines, an Australian marsupial, and create elephants with woolly mammoth traits. But Colossal's plans depend on huge advances in genome editing, stem-cell biology and animal husbandry, making success far from certain.

"It's incredibly exciting that there's that kind of money available," says Thomas Jensen, a cell and molecular reproductive physiologist at Wells College in Aurora, New York. "I'm not sure that the end goal they're going for is something that's super feasible in the near future."

Iridescent pigeons

Colossal's plan starts with the dodo's closest living relative, the iridescent-feathered Nicobar pigeon (*Caloenas nicobarica*). The company plans to isolate and culture specialized primordial germ cells (PGCs) — which make sperm and egg-producing cells — from developing Nicobars. Colossal's scientists would edit DNA sequences in the PGCs to match those of dodos using tools such as CRISPR. These gene-edited PGCs would then be inserted into embryos from a surrogate bird species to generate chimeric animals — those with DNA from both species — that make dodo-like eggs and sperm. These could potentially produce something resembling a dodo (*Raphus cucullatus*).

To gene edit Nicobar pigeon PGCs, scientists first need to identify the conditions that allow these cells to flourish in the laboratory, says Jae Yong Han, an avian-reproduction scientist at Seoul National University. Researchers have done this with chickens, but it will take time to identify the appropriate culture conditions that suit other birds' PGCs.

A greater challenge will be determining the genetic changes that could transform Nicobar pigeons into Dodos. A team including Beth Shapiro, a

palaeogeneticist at the University of California, Santa Cruz, who is advising Colossal on the dodo project, has sequenced the dodo genome but has not yet published the results. Dodos and Nicobar pigeons shared a common ancestor that lived around 30 million to 50 million years ago, Shapiro's team reported in 2016[1]. By comparing the nuclear genomes of the two birds, the researchers hope to identify most of the DNA changes that distinguish between them.

Insights from rats

Tom Gilbert, an evolutionary biologist at the University of Copenhagen who also advises Colossal, expects the dodo genome to be of high quality — it comes from a museum sample he provided to Shapiro. But he says that finding all the DNA differences between the two birds is not possible. Ancient genomes are cobbled together from short sequences of degraded DNA, and so are filled with unavoidable gaps and errors. And research he published last year comparing the genome of the extinct Christmas Island rat (*Rattus macleari*) with that of the Norwegian brown rat (*Rattus norvegicus*)[2] suggests that gaps in the dodo genome could lie in the very DNA regions that have changed the most since its lineage split from that of Nicobar pigeons.

Even if researchers could identify every genetic difference, introducing the thousands of changes to PGCs would not be simple. "I'm not sure it's feasible in the near future," says Jensen, whose team is encountering difficulties making a single genetic change to the genomes of quail.

Focusing on only a subset of DNA changes, such as those that alter protein sequences, could slash the number of edits needed. But it's still not clear that this would yield anything resembling a wild dodo, says Gilbert. "My worry is that Paris Hilton thinks she's going to get a dodo that looks like a dodo," he says.

A further problem will be the need to find a large bird, such as an emu (*Dromaius novaehollandiae*), that can act as the surrogate, says Jensen. "Dodo eggs are much, much larger than Nicobar pigeon eggs, you couldn't grow a dodo inside of a Nicobar egg."

Chicken embryos are fairly receptive to PGCs from other birds, and Jensen's team has created chimeric chickens that can produce quail sperm — efforts to generate eggs have failed so far. But he thinks it will be far more challenging to transfer PGCs — particularly heavily gene-edited ones — from one wild bird into another.

Conservation boon?

Colossal chief executive Ben Lamm acknowledges these hurdles, but argues that they aren't deal-breakers. Work towards dodo de-extinction will help with conservation efforts for other birds, he adds. "It will bring a lot of new technologies to the field of bird conservation," agrees Jensen.

Vikash Tatayah, conservation director at the Mauritian Wildlife Foundation in Vacoas-Phoenix, is also enthusiastic about the attention dodo de-extinction could bring to conservation. "It's something we would like to embrace," he says.

But he points out that the predators that threatened the dodo in the seventeenth century haven't gone away, whereas most of its habitat has. "You do have to ask," he says, "if we could have such money, wouldn't it be better spent on restoring habitat on Mauritius and preventing species from going extinct?"

Nature **614**, 402 (2023)

doi: https://doi.org/10.1038/d41586-023-00379-5

References

1. Soares, A. E. R. *et al. BMC Evol. Biol.* **16**, 230 (2016).

2. Lin, J. *et al. Curr. Biol.* **32**, 1650–1656 (2022).

This article was downloaded by **calibre** from https://www.nature.com/articles/d41586-023-00379-5

- NEWS FEATURE
- 15 February 2023

How a pioneering diabetes drug offers hope for preventing autoimmune disorders

The approval of an antibody therapy that pauses the progression of type 1 diabetes is a first in the field, and some say a model for other drug developers.

- Elie Dolgin



Student Mikayla Olsten received the antibody therapy teplizumab in 2016, which has kept her from developing symptoms of type 1 diabetes. Credit: Natalie Behring for *Nature*

Her sister's life-threatening experience with diabetes was a wake-up call for Mikayla Olsten.

In 2016, when Olsten was 14 years old, her youngest sibling Mia landed in intensive care with failing kidneys and fluid in her lungs. It was ketoacidosis, a complication of type 1 diabetes (T1D) that is often the first sign that the body is not making enough of the sugar-regulating hormone insulin. Blood glucose levels spike, as do toxic waste products, throwing organ function into disarray.

Although she is healthy today, Mia is one of the estimated 9 million people worldwide who must deal with the daily grind of T1D, carefully managing their blood sugar and insulin levels.

And the scare prompted the Olsten family to test Mikayla for signs of diabetes that often precede disease symptoms. There was no previous history of T1D in the family, but siblings of those affected are at a greatly elevated risk.

The results came back positive for four of the five T1D markers that physicians look for, each a type of 'autoantibody' that tells the immune system to attack insulin-producing cells in the pancreas. Mikayla also had abnormal sugar metabolism — the disease process was already under way. Her odds of making it through secondary school without progressing to a diabetes diagnosis were about one in three, clinicians estimated.

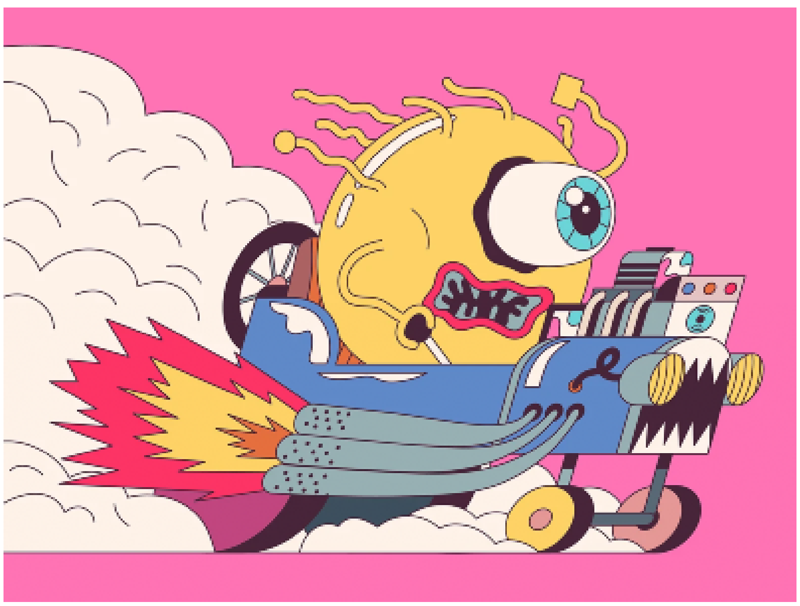
Yet Mikayla, now 21 and studying exercise physiology at Brigham Young University–Idaho in Rexburg, continues to live diabetes-free — probably thanks to a drug called teplizumab.

Teplizumab is a type of antibody therapy. It blocks T cells, the 'attack dogs' of the immune system, stopping them destroying insulin-producing islet cells in the pancreas. Mikayla received a two-week course of treatment in

July 2016, as part of a clinical trial to test whether the therapy could help to keep T1D at bay.

The 76-person study[1,2] — which ran from 2011 to 2018 — found that people who received the treatment developed diabetes symptoms after about five years, on average. That's three years longer than the average delay for those who received the placebo.

Mikayla has remained diabetes-free for 6.5 years so far; others in the study have gone a decade or longer without needing to begin insulin therapy, which is currently the only effective way to manage the disease. Last November, drug authorities in the United States approved teplizumab for people 8 years and older who meet certain risk criteria.



The race to supercharge cancer-fighting T cells

"This is a huge, huge step forward for the field," says Aaron Kowalski, president and chief executive of JDRF, a non-profit research organization in New York City that focuses on T1D. "It's the first disease-modifying therapy in type 1 diabetes — ever."

It's also the first drug proven to delay the onset of an autoimmune disorder. And its development provides a roadmap for the discovery of

pharmaceuticals to stall or prevent other conditions, including rheumatoid arthritis and multiple sclerosis.

But identifying people who might benefit from such therapies remains a challenge: optimal screening strategies have yet to be established, and presymptomatic signs of disease are not well defined for each condition. Furthermore, because teplizumab offers only a temporary reprieve from T1D, researchers will need to find better approaches.

So, even as the field is "celebrating that we have teplizumab approved, it doesn't mean we're done", says Jay Skyler, an endocrinologist at the University of Miami in Florida. "It means we're just beginning."

From treatment to prevention

Teplizumab traces its roots to a New Jersey drug company called Ortho Pharmaceutical. There, scientists generated an early version of the antibody, dubbed OKT3. Originally sourced from mice, the molecule was able to bind to the surface of T cells and limit their cell-killing potential[3]. In 1986, it was approved to help prevent organ rejection after kidney transplants, making it the first therapeutic antibody allowed for human use.

But OKT3 was problematic: at high doses, it triggered a life-threatening complication known as cytokine release syndrome. And because it originated in mice, the human immune system would react against it, diminishing the drug's potency over time. Researchers outside the company tweaked the formula to avoid these issues, and teplizumab was born.

The therapy initially entered clinical trials in 1999 as a treatment for people who had been newly diagnosed with T1D. A small study[4], led by Kevan Herold, an immunologist now at the Yale School of Medicine in New Haven, Connecticut, found that a single course of the therapy could help people to maintain or even boost their insulin activity for years.

But a larger, follow-up trial ended in failure. Teplizumab proved no better than a placebo at reducing insulin usage and managing blood-sugar levels[5].

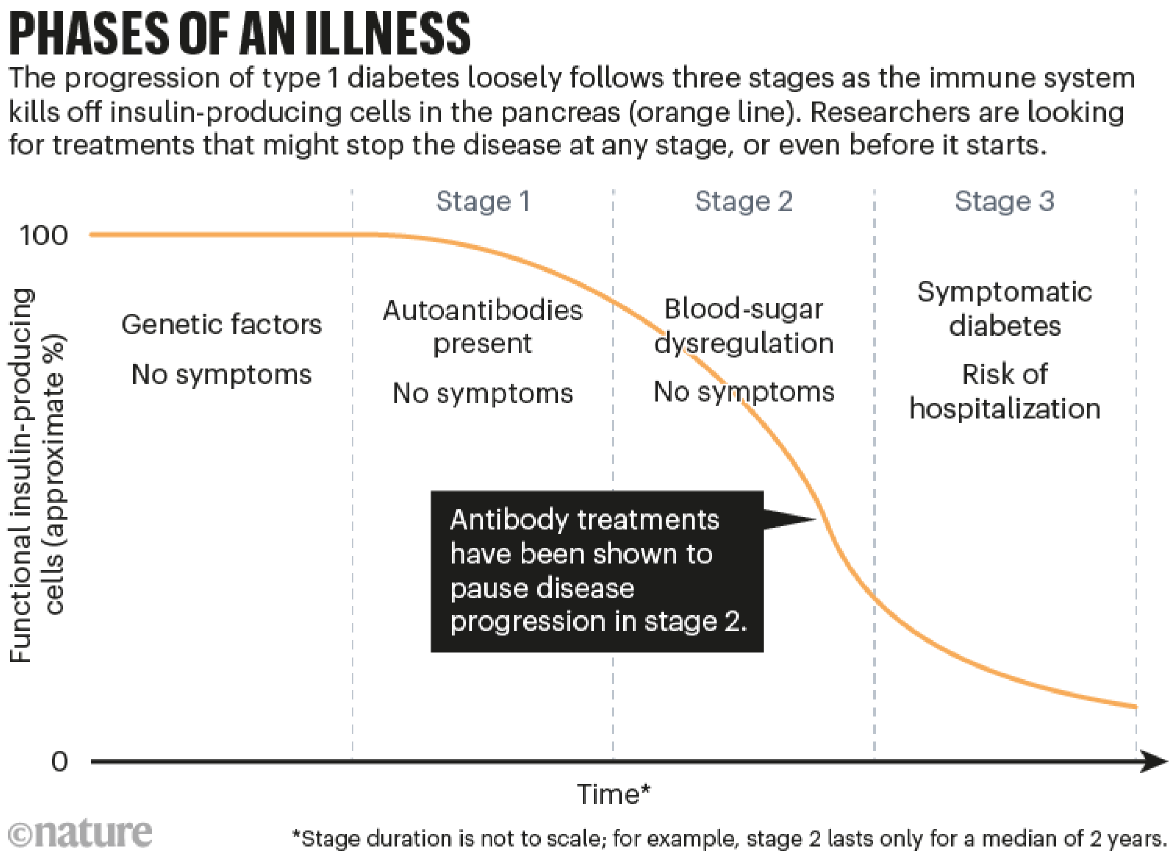
A similar drug called otelixizumab performed just as poorly[6]. Both therapies were abandoned.

It was a let-down for the diabetes field. But Herold wasn't ready to give up.

Further analyses by Herold and his colleagues showed that the drug wore down the islet-targeted T cells[7], and sent them into a state of partial exhaustion that helped to safeguard the pancreas against further assault. What's more, many people seemed to benefit from the therapy, especially those who were younger or with less-advanced disease.

If the drug works best in those patients, reasoned Herold, then it might really shine if given before symptoms appear. So, in 2011 Herold spearheaded the launch of the Teplizumab Prevention Study, the one through which Mikayla and other at-risk individuals received their treatment.

Those trial results underpinned the US Food and Drug Administration's decision last year to approve teplizumab for people with stage 2 disease — those who do not yet have a T1D diagnosis, but who have two or more autoantibodies against islet cells and signs of altered sugar metabolism (see 'Phases of an illness').



Source: R. A. Insel *et al. Diab. Care* **38**, 1964–1974 (2015)

A temporary reprieve

Since taking teplizumab in the clinical trial, Claire Wirt, a 16-year-old from Rochester, New York, has lived T1D-free for 7 years and counting. “It gets you so many childhood experiences without having to deal with diabetes 24/7,” she says. And biologically, that delay could reduce the stress that high blood-sugar levels can put on blood vessels, nerves and other organ systems, which add up over time.

But the reprieve isn’t cheap. The one-time treatment costs around US$194,000 — and that doesn’t include the expense of giving infusions or screening to find people who might benefit from the therapy.

Some researchers have questioned the therapy's cost-effectiveness. But Ashleigh Palmer, co-founder and chief executive of drug firm Provention Bio in Red Bank, New Jersey, which acquired the rights to teplizumab in 2018, defends the pricing decision. "What we're doing with our therapeutic here is game-changing," Palmer says. "And I don't see any reason why we shouldn't price the product appropriately."



Will pigs solve the organ crisis? The future of animal-to-human transplants

Analysts predict that global annual sales of teplizumab could exceed $250 million as a preventive therapy — plus a possible $1.5 billion or so if the drug is approved for people who have stage 3 disease. To that end, the company is running a 300-person trial to test the drug's efficacy in children and teenagers who have been newly diagnosed with T1D.

In the pharmaceutical industry, all eyes are now on those sales in the United States. If Provention Bio and its marketing partner, the French drug giant Sanofi, can profit, then many more companies could begin exploring prophylactic therapies. But developing trials for autoimmunity remains risky, time-consuming and costly, says Jessica Dunne, a T1D scientist who previously led screening and prevention research at JDRF and Janssen in Raritan, New Jersey.

“So, what happens with teplizumab will be a little bit of a bellwether,” she says.

Janssen, which launched an ambitious ‘disease interception’ unit in 2015, shut its entire T1D division late last year, citing a “change in scientific strategy”, according to Janssen spokesperson Brian Kenney. But other big-name drug makers are planning to test their experimental diabetes agents as preventive medicines — and they credit teplizumab with setting the standard for regulatory and clinical success.

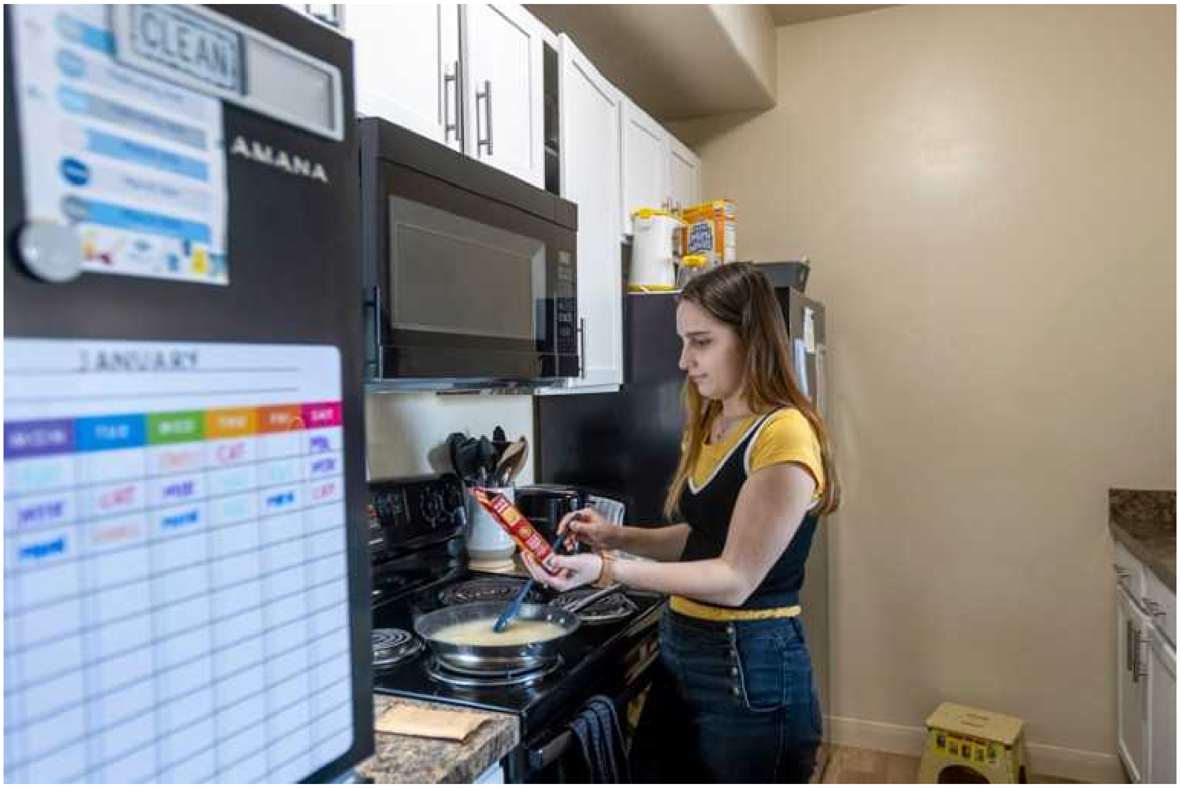
“It has shown drug developers that it is possible to modify the disease for a length of time that is meaningful to people,” says Johnna Wesley, head of T1D and chronic kidney disease research at Novo Nordisk, which is headquartered in Bagsværd, Denmark.

A long road

The company’s lead product for preventing T1D is a DNA-encoded therapeutic designed to stop the immune system attacking pancreatic cells[8]. Compared with teplizumab, which targets all T cells regardless of their function, Novo Nordisk’s drug is more narrowly tailored to T cells that attack the insulin-producing cells of the pancreas — which, according to Wesley, could offer safety and efficacy benefits.

Once the company has determined a reasonable dose level for people with established T1D, further development could include a prevention trial for people with stage 2 disease, Wesley says.

Academic groups are also evaluating several other drugs in that setting. Among them are other T-cell-targeted therapies — such as anti-thymocyte globulin, which is currently used to prevent organ rejection — as well as drugs that promote and preserve pancreatic capabilities directly.



Mikayla Olsten was screened for diabetes-related autoantibodies after her younger sister was hospitalized with complications from type 1 diabetes.Credit: Natalie Behring for *Nature*

But intervening at stage 2 might be too late, and do little more than delay the inevitable. As Richard Insel, former chief scientific officer at JDRF, points out: “The earlier you can get in there, the more likely you’ll be able to stop the disease in its tracks.” Some trials are testing drugs in people who have stage 1 disease — when diabetes-related autoantibodies are present but blood-sugar metabolism remains normal.

Other trials are looking even earlier than stage 1, searching for treatments that can be given in infancy to children who are at risk of T1D. Researchers have been exploring dietary changes for infants; introducing probiotic bacteria; and vaccinating against viruses, such as coxsackievirus B, that seem to trigger T1D symptoms. But giving children powdered insulin, which helps to train the immune system not to attack its own insulin-producing cells, has shown the greatest promise so far.

In early testing, children who received oral insulin alongside their breakfast developed a special type of immune cell, known as a regulatory T cell, that provides a layer of protection against future autoimmune attack[9]. A larger confirmatory trial is ongoing.

Auto focus

The T1D community is not alone in its quest to prevent autoimmunity. Those seeking to treat autoimmune diseases such as rheumatoid arthritis (RA) and multiple sclerosis (MS) have long followed the T1D prevention playbook in their own pursuit of disease-stalling agents.

“Type 1 diabetes has been our model,” says Paul Emery, a rheumatologist at the University of Leeds, UK.

The heart of the strategy for RA and MS is developing clearer definitions of what it means to be in a pre-disease state, and determining the various stages and diagnostics that could allow for rigorous prevention studies.



The ‘breakthrough’ obesity drugs that have stunned researchers

Rheumatologists have had some success with preventing disease using a T-cell-blocking agent called abatacept, with a preliminary study[10] showing that

the drug reduces joint inflammation and delays the development of RA in at-risk individuals. And for MS, clinicians have identified a drug that, in preliminary testing, wards off neurological symptoms in people who have early signs of nerve damage in the brain[11].

Late last year, a team led by Darin Okuda, a neurologist at the University of Texas Southwestern Medical Center in Dallas, reported results for an anti-inflammatory drug called dimethyl fumarate. When given to people with a distinct type of anomalous brain scan, the drug helped to reduce the risk of MS by more than 80% compared with a placebo[11]. Over the course of 22 months, 3 of 44 people who received the drug progressed to MS, compared with 14 of 43 placebo-treated individuals.

“The results were the best that I could have wished for,” Okuda says.

One of the challenges of developing such drugs is the complexity of the clinical trials. First, researchers have to find appropriate trial participants, either by testing for early indicators of disease or for genetic risk factors. Then, they have to wait for years after the treatment to see who progresses.

“These studies take so dang long,” says Michael Haller, a paediatric endocrinologist at the University of Florida in Gainesville.

But the success with T1D could help. “Because of teplizumab,” Haller says, “I think a lot more people will get screened, and we’ll have a lot more folks interested.”

Screening for diabetes-related autoantibodies and other risk factors is unusual in most health-care systems, so many of the outreach and screening efforts are centred on families affected by T1D. That’s why Mikayla and Wirt had their blood tested — and it is this group of people that Provention Bio and Sanofi will target in their initial marketing of teplizumab.

But only around 15% of all people diagnosed with T1D have a previous family history of the disease, so researchers are studying ways of expanding the reach of screening.

Ahead of the problem

Some favour testing everyone for diabetes-related autoantibodies. This could be done at two time points in early childhood — say, at ages 2 and 6 — when the immune markers are most likely to appear. Clinicians in Israel have begun implementing this approach, blanket-testing thousands of toddlers.



[Diabetes risk rises after COVID, massive study finds]

Teplizumab is not yet available in Israel, so the efforts are focused on protecting against severe complications, explains Moshe Phillip, an endocrinologist at the Schneider Children's Medical Center of Israel in Petach Tikvah, who is leading the effort. Studies show that children who are screened and tracked have around one-tenth the risk of ketoacidosis after T1D starts (see, for example, ref. 12). "That alone is a good reason to screen," Phillip says.

Others think that DNA testing of blood spots collected at birth might be a better way to go. "With the genetics, you're a step before the autoantibodies," says Kristina Casteels, a paediatric endocrinologist at University Hospitals Leuven (UZ Leuven) in Belgium.

Across Europe, Casteels and her colleagues have genetically screened more than 100,000 newborns in this way, looking for gene variants that raise the chances of T1D. The parents of babies at greatest risk were then offered the

chance for their child to participate in early-prevention trials — with probiotics or oral insulin. In other countries, newborns with high-risk genes are followed using regular autoantibody tests.

These approaches have strengths and weaknesses. Autoantibody tests aren't standardized, so can vary in their accuracy, says Kimber Simmons, a paediatric endocrinologist at the University of Colorado's Barbara Davis Center for Diabetes in Aurora. And with few resources available to counsel people, including physicians, about what it means to be at risk for T1D, such mass-screening efforts could lead to undue stress and clinical mismanagement, at least in the near term, says Carla Greenbaum, a diabetes investigator at the Benaroya Research Institute in Seattle, Washington.

Add in the costs of screening and of the drug therapies themselves, and it's unclear whether health-care systems are prepared for wide-scale T1D prevention.

None of that is at the front of Mikayla's mind, however. "At this point, I'm just grateful that I don't have diabetes yet," she says. "I know that I'm going to eventually have it, and I'm prepared for that. But right now, I'm more just loving my life."

Nature **614**, 404-406 (2023)

doi: https://doi.org/10.1038/d41586-023-00400-x

References

1. Sims, E. K. *et al. Sci. Transl. Med.* **13**, eabc8980 (2021).
2. Herold, K. C. *et al. N. Engl. J. Med.* **381**, 603–613 (2019).
3. Kung, P. C., Goldstein, G., Reinherz, E. L. & Schlossman, S. F. *Science* **206**, 347–379 (1979).
4. Herold, K. C. *et al. Clin. Immunol.* **132**, 166–173 (2009).
5. Sherry, N. *et al. Lancet* **378**, 487–497 (2011).

6. Aronson, R. *et al. Diab. Care* **37**, 2746–2754 (2014).

7. Long, A. S. *et al. Sci. Immunol.* **1**, eaai7793 (2016).

8. Pagni, P. P. *et al. Diabetes* **71**, 157–169 (2022).

9. Bonifacio, E. *et al. JAMA* **313**, 1541–1549 (2015).

10. Rech, J. *et al. Ann. Rheum. Dis.* **81** (Suppl. 1), 526-527 (2022).

11. Okuda, D. T. *et al. Ann. Neurol*. https://doi.org/10.1002/ana.26555 (2022).

12. Ziegler, A.-G. *et al. JAMA* **323**, 339–351 (2020).

This article was downloaded by **calibre** from https://www.nature.com/articles/d41586-023-00400-x

| Section menu | Main menu |

Books & Arts

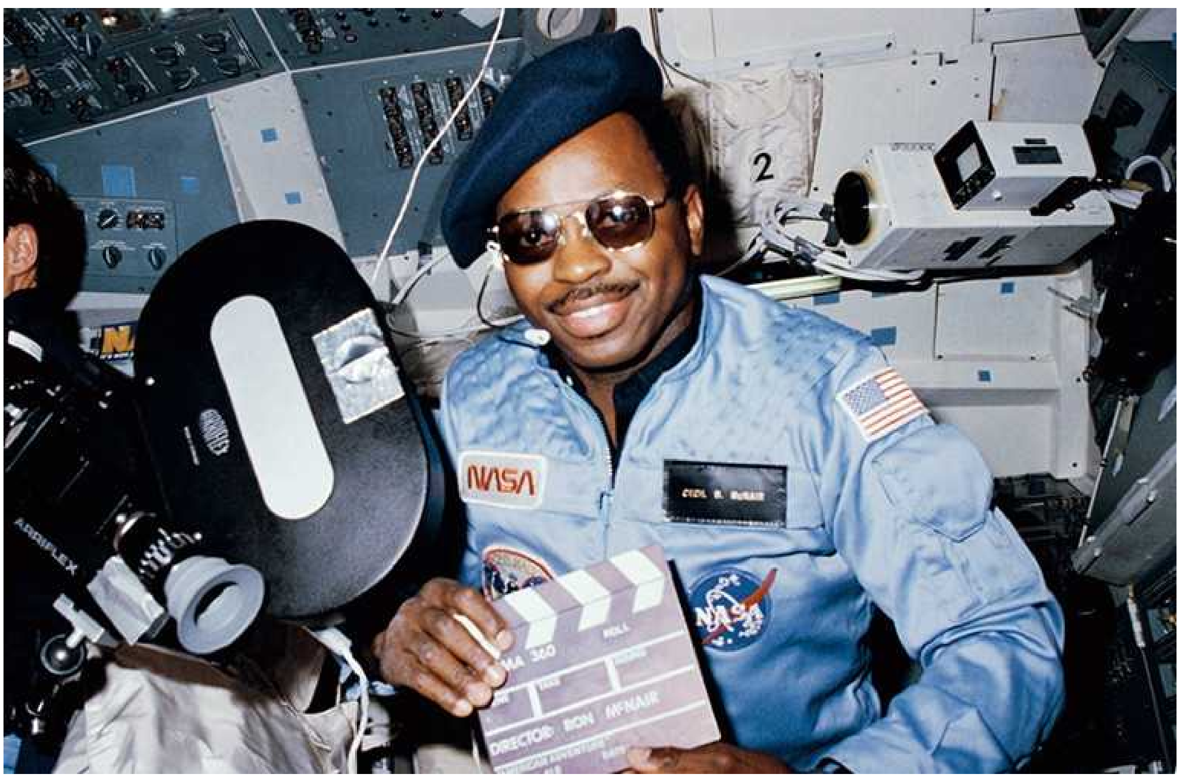
- **How NASA’s breakthrough ‘class of ’78’ changed the face of space travel** [13 Feb 2023]
  • The inclusion of women and people of colour in NASA’s astronaut cadet programme was unprecedented — and met sometimes fierce resistance.
- **The next pandemic, and why time is money: Books in brief** [13 Jan 2023]
  • Andrew Robinson reviews five of the best science picks.

- BOOK REVIEW
- 13 February 2023

How NASA’s breakthrough ‘class of ’78’ changed the face of space travel

The inclusion of women and people of colour in NASA’s astronaut cadet programme was unprecedented — and met sometimes fierce resistance.

- Alexandra Witze

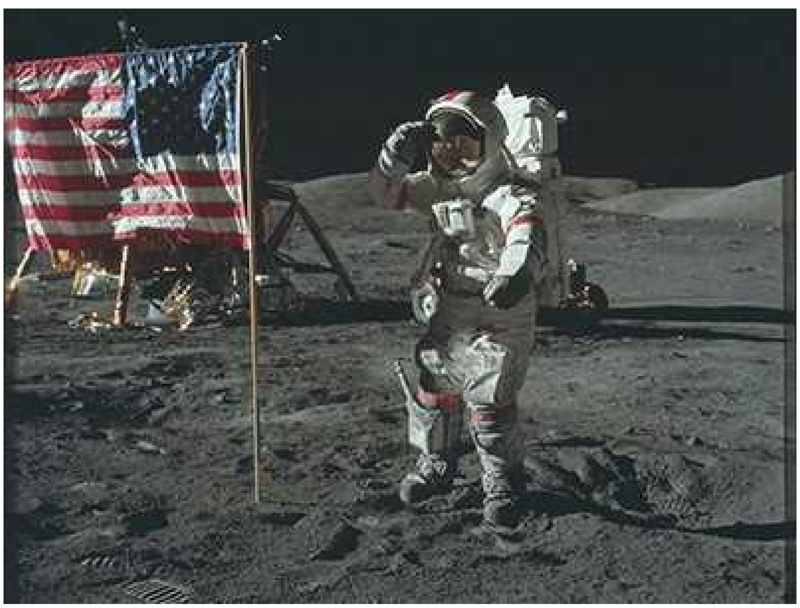


Ronald McNair, part of the class of 1978, died in the space shuttle *Challenger* in 1986.Credit: NASA

The New Guys: The Historic Class of Astronauts That Broke Barriers and Changed the Face of Space Travel *Meredith Bagby* William Morrow (2023)

Growing up in racially segregated South Carolina in the 1950s, Ronald McNair saw door after door slammed in his face. The public pool was for white people only, so he could not learn to swim. When he was nine years old, a librarian called the police on him for trying to borrow calculus books.

McNair fought the racism and went on to study physics at the North Carolina Agricultural and Technical State University in Greensboro — a historically Black institution — and at the Massachusetts Institute of Technology in Cambridge. In 1978, NASA chose him as a finalist to be an astronaut, in the first such group to contain women, people of colour and scientists. His pioneering class included Sally Ride, who would become the first US woman in space; Ellison Onizuka, the first Asian American in space; and Guion Bluford, the first African American in space.



Fifty years after astronauts left the Moon, they are going back. Why?

With *The New Guys*, Meredith Bagby, a film producer and former journalist, has produced a broad and easily readable narrative about this group of US astronauts. She does not break new ground in outlining their experiences and the team's role in space history. But she does illuminate the historic nature of

their selection — and, significantly, how they helped to shape NASA’s space shuttle programme, from its first flight in 1981 until its end in 2011.

NASA’s first astronaut class, chosen in 1959, was the iconic Mercury Seven that included John Glenn, Alan Shepard and Gus Grissom. The next six groups were in the same vein: all white, male military pilots lionized for having “the right stuff”. Then came the class of 1978. Of the 35 new astronauts, 14 were civilians, 6 were women and 4 were men of colour.

It was a time of huge change for NASA. The Apollo Moon programme had wound down, and NASA had set its sights on developing a reusable space plane that would launch like a rocket and land like an aeroplane. Astronauts on this vehicle would deploy military and scientific satellites into space. It was time for a new type of astronaut for a new type of spaceship.

Breaking through prejudice

Bagby views the shuttle era through the experiences of its astronauts, with a focus on women moving into new roles. They include Ride, a gay woman who remained in the closet while at NASA because the agency would not hire her otherwise; geologist Kathryn Sullivan; physicians Rhea Seddon and Anna Fisher; biochemist Shannon Lucid; and engineer Judith Resnik.

In the late 1970s, the view in much of NASA’s ranks was that the agency had lowered its standards to admit a more diverse class, and the class acquired the soubriquet “Those Fucking New Guys”. John Glenn and Chuck Yeager, the quintessential “right stuff” pilots, were among those who fought against hiring women as astronauts. Opposition from Yeager had probably helped to keep Ed Dwight, a Black test pilot, from joining a previous class.



Sally Ride, the first US woman in space, works on the flight deck of the space shuttle *Challenger* in 1983.Credit: NASA

Bagby's narrative shines as she explores the early years of the space shuttle as NASA focused on deploying large satellites. In 1990, for instance, Sullivan helped to launch the Hubble Space Telescope, an observatory too large to get into orbit on any other vehicle.

It is easy to forget that shuttle astronauts performed the first on-orbit satellite repair back in 1984, on the Solar Maximum Mission observatory, and deployed important scientific spacecraft such as the Galileo mission to Jupiter and the Ulysses mission to study the Sun. But the pressure to fly as often as possible to meet the needs of customers quickly caught up with NASA. From 1983 onwards, cost-cutting meant fewer engineers, fewer inspections and less time and attention to spend on thorny mechanical issues.

On separate flights in January 1985 and April 1985, Onizuka and fellow class member Frederick Gregory came close to death without knowing it, when the O-rings that helped to seal the shuttle's solid rocket boosters nearly failed. Facing a long list of planned launches, NASA managers overrode

concerns aired by contractors. In January 1986, four members of the group — McNair, Onizuka, Resnik and Richard Scobee — were on board with three other astronauts when the space shuttle *Challenger*'s O-rings failed just after lift-off, causing an explosion that killed them all.



[The $93-billion plan to put astronauts back on the Moon]

Ride served on the panel that investigated those deaths, and helped to bring the O-ring cover-up to public light. The disaster led to the end of the shuttle's role in deploying satellites and in partnering with the military.

And yet Ride found herself on an investigation panel again in 2003 — this time concerning the fatal accident of the shuttle *Columbia*, which disintegrated just before landing because a piece of foam that had detached from the fuel tank during launch had damaged the craft's thermal-protection tiles. As with *Challenger*, NASA culture was to blame. Mission control did not even inform the *Columbia* crew about the foam strike until a week into the nearly 16-day mission, when it said: "This item is not even worth mentioning other than wanting to make sure that you are not surprised by it in a question from a reporter."

NASA retired the shuttle fleet in 2011, after astronauts finished construction on the International Space Station — an abrupt ending to the programme and to the story of the 1978 astronaut class.

Much of the information in *The New Guys* can be found elsewhere. David Shayler and Colin Burgess's 2020 book *NASA's First Space Shuttle Astronaut Selection* contains more technical detail on the class of 1978. Sociologist Diane Vaughan's *The Challenger Launch Decision* (1996) is the definitive account of the circumstances of that disaster. The many popular histories of the shuttle programme include journalist Pat Duggins's 2007 book *Final Countdown*. But *The New Guys* succeeds as a comprehensive and engaging overview of this period in space-exploration history.

Today, NASA's astronaut corps is much more diverse; last year, the European Space Agency even announced the world's first physically disabled astronaut candidate, former paralympic athlete John McFall. And for that, we can all thank the Fucking New Guys.

Nature **614**, 407-408 (2023)

doi: https://doi.org/10.1038/d41586-023-00401-w

This article was downloaded by **calibre** from https://www.nature.com/articles/d41586-023-00401-w

- BOOK REVIEW
- 13 January 2023

The next pandemic, and why time is money: Books in brief

Andrew Robinson reviews five of the best science picks.

- Andrew Robinson

BREATHLESS

THE SCIENTIFIC RACE TO DEFEAT A DEADLY VIRUS

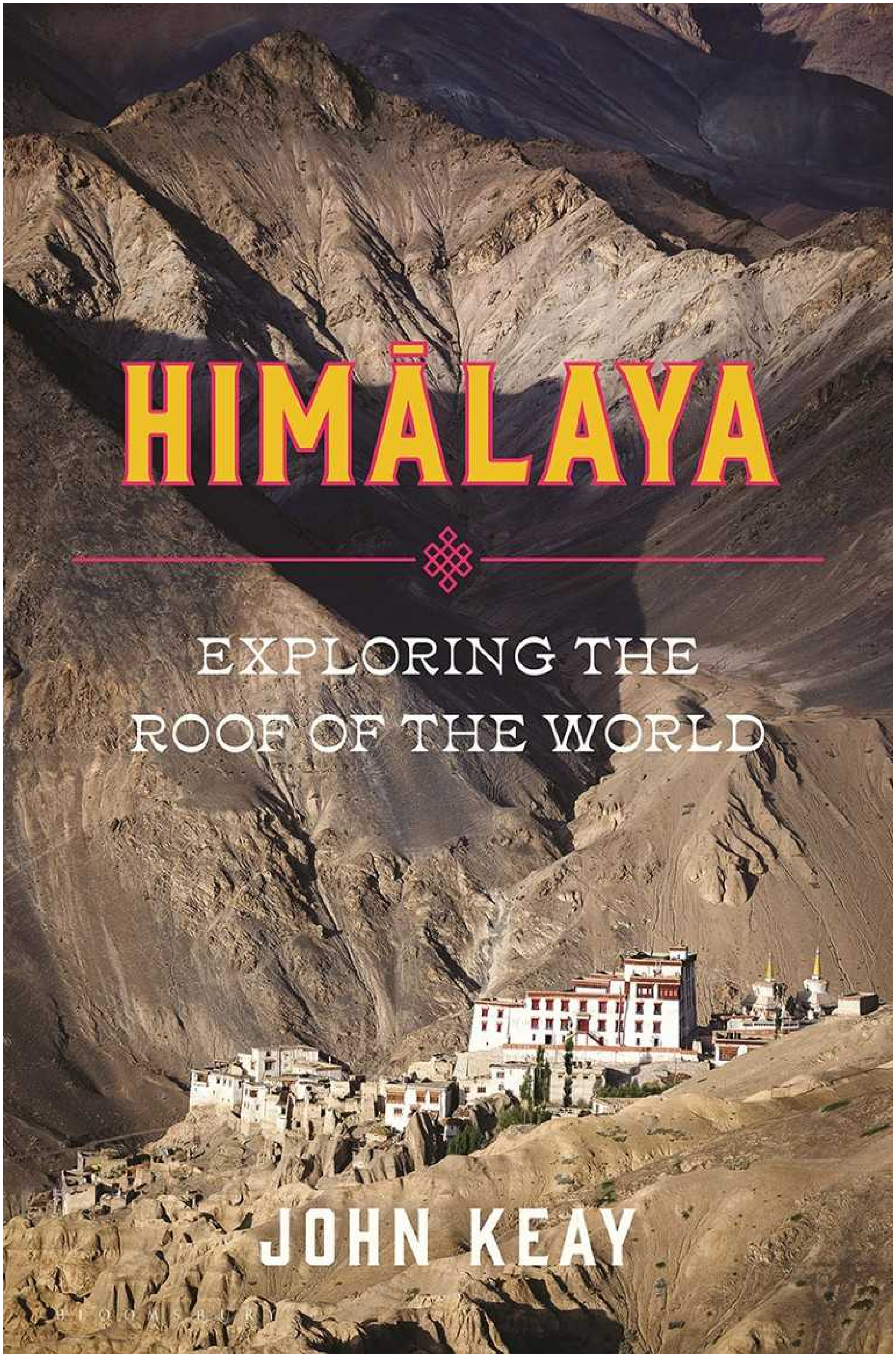
DAVID QUAMMEN

NEW YORK TIMES BESTSELLING AUTHOR OF *SPILLOVER* AND *THE TANGLED TREE*

Breathless

David Quammen *Simon & Schuster* (2022)

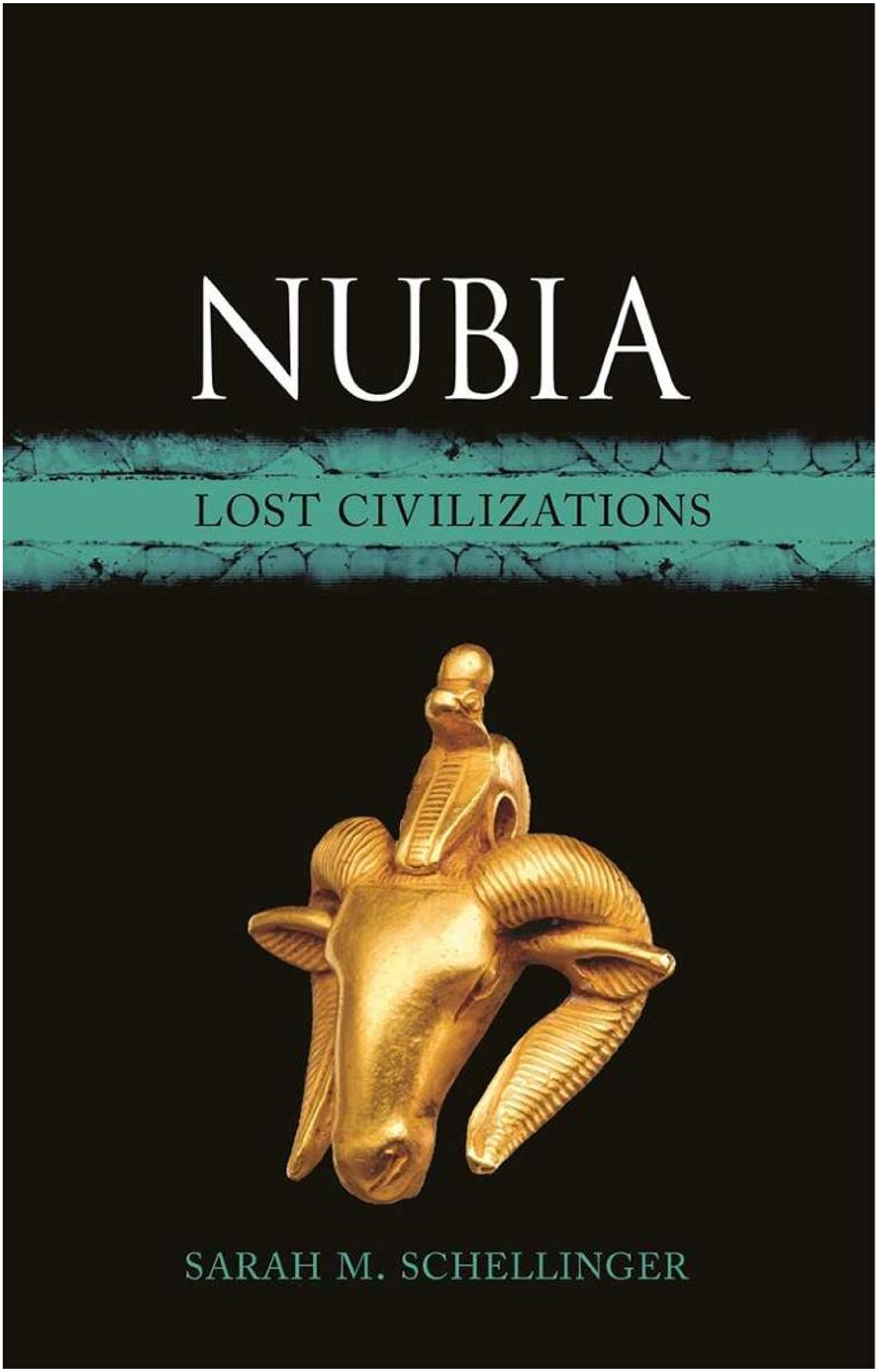
“There are many more fearsome viruses where SARS-CoV-2 came from, wherever that was,” concludes science, nature and travel writer David Quammen. He foresees worse pandemics this century. His engrossing, at times breathless, scientific narrative of the COVID-19 pandemic involves interviews with almost 100 virologists and other scientists, in China and elsewhere. Some had spent more than two decades predicting a global outbreak caused by a new virus, but were ignored because of politics or for economic reasons.


HIMĀLAYA
EXPLORING THE ROOF OF THE WORLD
JOHN KEAY
BLOOMSBURY

Himalaya

John Keay *Bloomsbury Circus* (2022)

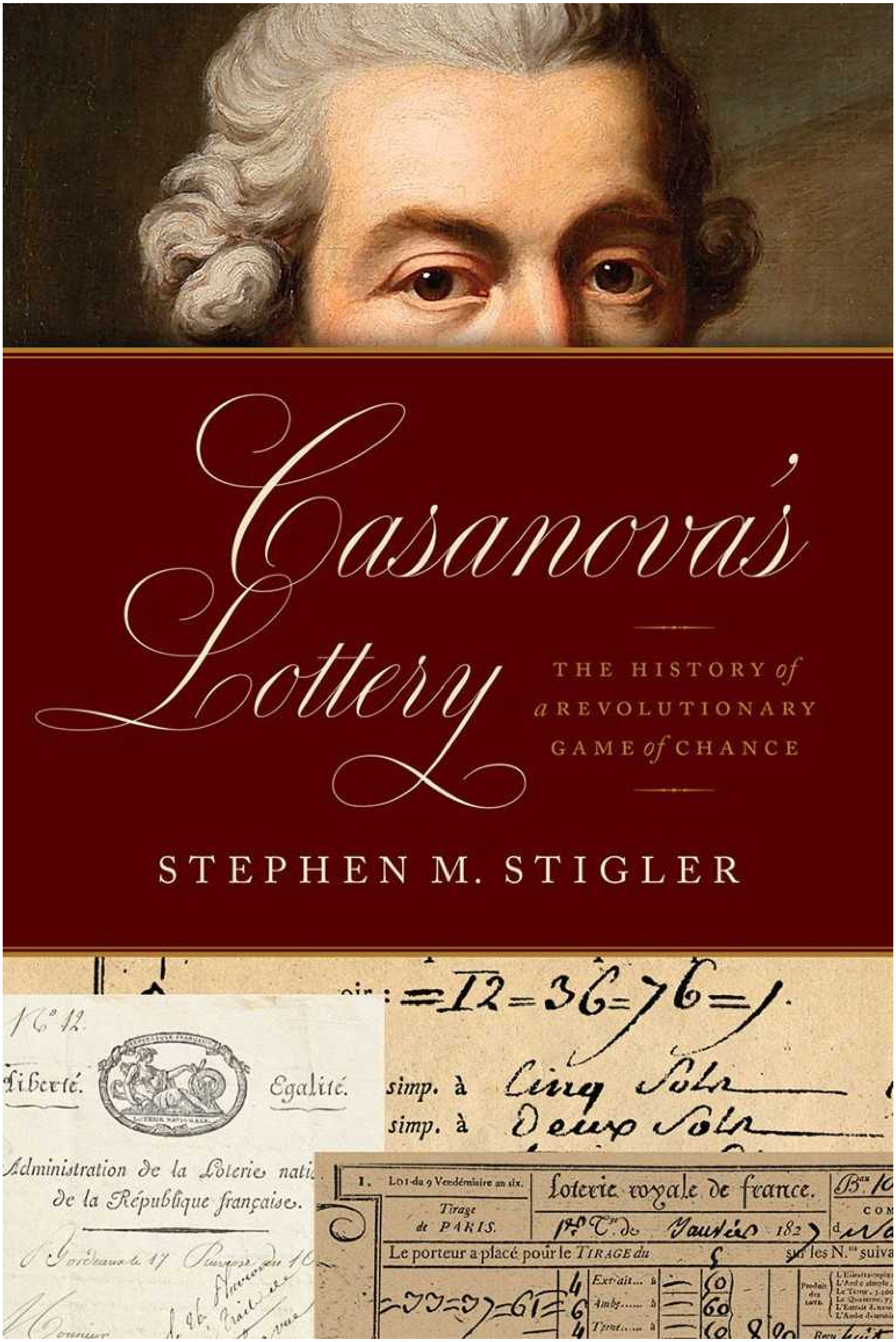
Historian John Keay has written passionately about the Himalayas since his first book in the 1970s. His latest embraces archaeology, ethnology, geology and palaeontology, along with imperialism, mysticism and mountaineering. The synthesis is always engaging but sometimes, as Keay admits, “as disjointed as the Himalayan skyline”. This “orogenous zone” — a region characterized by mountain building — is now, of course, threatened by global warming, but its militarized history will complicate any attempts to rescue it.


NUBIA
LOST CIVILIZATIONS
SARAH M. SCHELLINGER

Nubia

Sarah M. Schellinger *Reaktion* (2022)

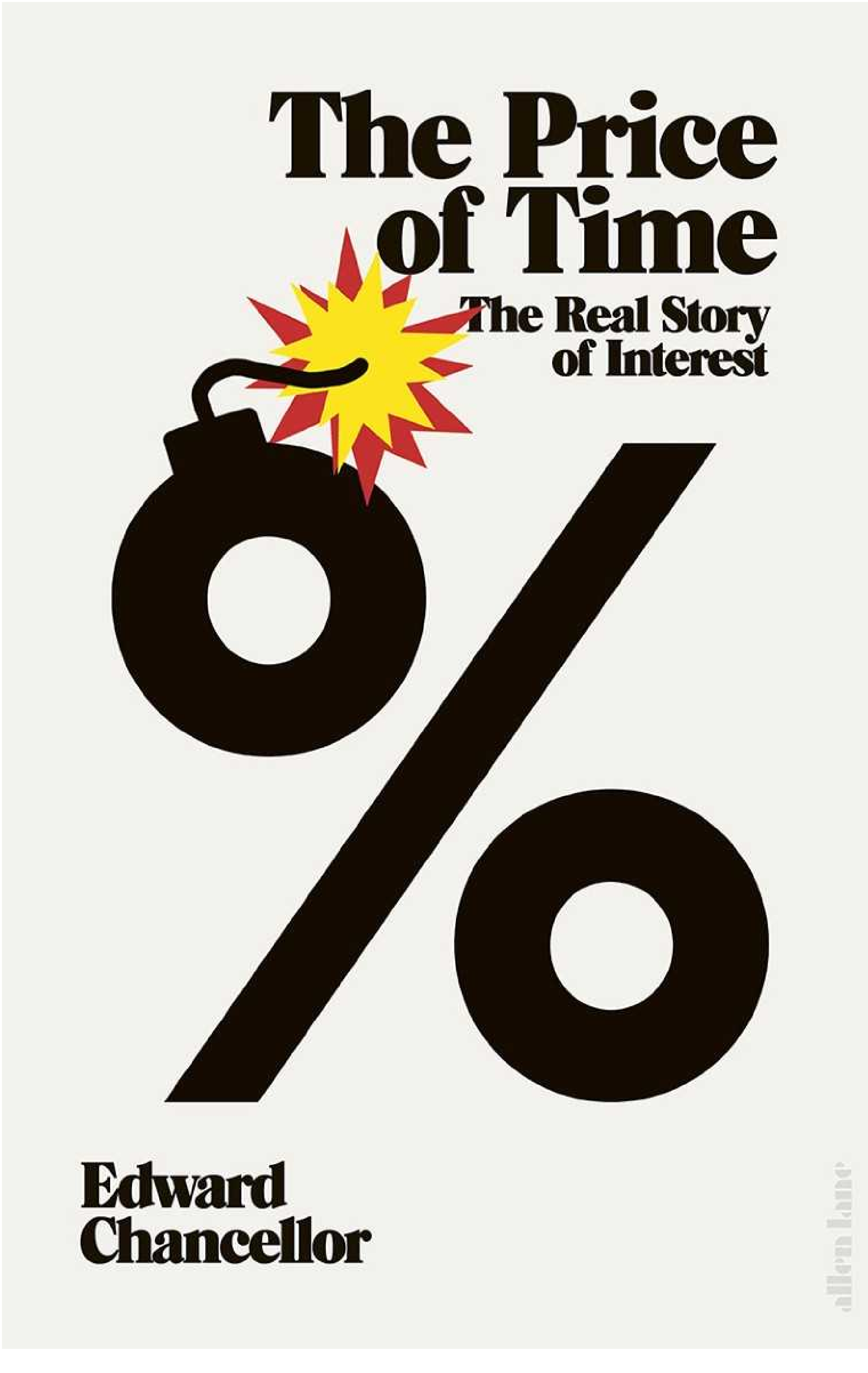
The River Nile flows in two great bends through Sudan, forming six cataracts from Khartoum to Lake Nasser on the Egyptian border. The ancient history of this vast area, known to archaeologists as Nubia, is the complex subject of art historian Sarah Schellinger's wide-ranging addition to the series Lost Civilizations. She brings Nubia "out of the shadow of Egypt" and reveals it as an ancient world power, entangled with Egyptian culture as "frenemies" for three millennia. Nubians even ruled Egypt from roughly 712 to 664 bc.


Casanova's Lottery
THE HISTORY of a REVOLUTIONARY GAME of CHANCE
STEPHEN M. STIGLER
Liberté.
Egalité.
Administration de la Loterie nati
de la République française.
simp. à
simp. à
Loterie royale de france.
Tirage de PARIS.
Le porteur a placé pour le TIRAGE du

Casanova's Lottery

Stephen M. Stigler *Univ. Chicago Press* (2022)

In 1758, the French state launched an unusual lottery suggested by famed Italian gambler Giacomo Casanova. It lasted until 1836, with a three-year gap during the French Revolution, providing 4% of national income at its peak. However, every time it was drawn, the state was at risk of losing a large amount, with "little more than a mathematical theory to protect it", writes statistician Stephen Stigler as he tells the lottery's story for the first time. The scheme was eventually suppressed for moral, cultural and economic reasons.


The Price of Time
The Real Story of Interest
Edward Chancellor
allen lane

The Price of Time

Edward Chancellor *Allen Lane* (2022)

In 1748, statesman and scientist Benjamin Franklin remarked: “Time is money — time is the stuff of which life is made.” Investment strategist turned financial historian and journalist Edward Chancellor reflects on this remark’s implications by tracing the history of financial interest from its ancient Mesopotamian origins to this century’s global credit booms. His well-informed, readable, topical account reminds us that very low interest rates often benefit rich people, who have access to credit, more than poor people.

Nature **614**, 408 (2023)

doi: https://doi.org/10.1038/d41586-023-00060-x

This article was downloaded by **calibre** from https://www.nature.com/articles/d41586-023-00060-x

Opinion

- **C. David Allis (1951–2023)** [03 Feb 2023]
  • Biologist who revolutionized the chromatin and gene-expression field.
- **How social media affects teen mental health: a missing link** [14 Feb 2023]
  • Researchers investigating the impacts of social media on mental health must consider where exactly adolescents are in their cognitive and social development.

- OBITUARY
- 03 February 2023

C. David Allis (1951–2023)

Biologist who revolutionized the chromatin and gene-expression field.

- Sharon Dent &
- Shiv Grewal



Credit: Koji Sasahara/AP/Shutterstock

David (Dave) Allis was a pioneer in the biology of chromatin, the complex of protein and nucleic acid that makes up chromosomes. He revealed how modifications to it, specifically chemical changes to the histone proteins around which DNA wraps, affect gene expression and many other fundamental aspects of cellular function. His ‘histone code’ hypothesis suggested that other proteins read histone modifications, which are important for almost every process in eukaryotic cells that uses DNA as a template. Allis played a major part in elucidating how epigenetic changes — those beyond the genome — can affect human health and disease,

suggesting entirely new avenues for therapy development. He has died aged 71.

Histone modifications were first reported by Vincent Allfrey in 1966, but before Allis's work, their significance and associated enzyme activities remained unclear. Allis showed that they had a direct link with the regulation of DNA's transcription into RNA and hence into expressed proteins. His work illuminated how the cell establishes and maintains patterns of gene expression, and laid the groundwork for understanding how a single genome can generate cells of many types. He received the Canada Gairdner International Award, the Breakthrough Prize in Life Sciences and the Albert Lasker Award for Basic Medical Research (with Michael Grunstein).

Allis was born in Cincinnati, Ohio, in 1951, and earned a PhD in biology from Indiana University Bloomington. During postdoctoral training with Martin Gorovsky at the University of Rochester, New York, he studied the freshwater protozoan *Tetrahymena*, a model organism that he carried into his independent research at Baylor College of Medicine in Houston, Texas. Allis set out to identify enzymes that add acetyl groups to histones (histone acetyltransferases, or HATs), reasoning that *Tetrahymena*, which has many acetylated histones, would be an excellent source of them. This decision demonstrated his knack for pursuing a unique line of inquiry with deliberation and commitment, which would prove pivotal in making significant advances.

His major breakthrough came in 1996, with his discovery of the enzyme GCN5, which acts to promote transcription, as a HAT (J. E. Brownell *et al. Cell* **84**, 843–851; 1996). No histone-modifying enzymatic activity had yet been identified, and no data indicated that transcription machinery might include such activity. The impact of Allis's discovery was immediate and immense, leading to an explosion in papers on HATs. The importance of histone acetylation in transcriptional regulation is now unquestioned.

Allis also had a pivotal role in defining the cause-and-effect relationship between specific modifications and gene expression. His work, more than that of any other, sparked a renaissance in the study of gene regulation through chromatin structure.

Allis settled at the Rockefeller University in New York City in 2003, after appointments at Syracuse University in New York, the University of Rochester and the University of Virginia in Charlottesville. He went on to describe the role of histone modifications beyond acetylation, including a connection between histone phosphorylation and the segregation of chromosomes during cell division. He and his collaborators uncovered a link between histone mutations and chromatin changes associated with malignant cancers. He was quick to recognize the clinical significance of this, and to note that similar mutations might alter global chromatin states in other illnesses. His work will prove essential in unravelling complex aspects of many diseases and providing new treatments.

Allis had an infectious enthusiasm for science, and he influenced the course of discovery well beyond his own laboratory. He welcomed new ideas and shared tools and expertise that fostered major discoveries by others, such as the identification of histone methyltransferase enzymes and the discovery that site-specific histone methylation patterns define chromatin domains as ‘open’ (accessible to gene transcription machinery) and ‘closed’ (relatively inaccessible). For example, histone H3 turned out to perform two opposite functions depending on the methylation states of two lysine residues only a few amino acids apart, which are read by specific protein ligands. This provided crucial evidence for the existence of the histone code (B. D. Strahl and C. D. Allis *Nature* **403**, 41–45; 2000). Allis’s paper on this hypothesis has now been cited more than 6,000 times.

Allis was known for his warmth, creativity and humour. In accepting his many honours, he showed huge appreciation for his lab members and the community of colleagues and collaborators, citing them as the inspiring force behind his own success. He cherished his family, crediting the support of his wife Barb with his accomplishments, and proudly sharing pictures of his children and grandchildren.

He celebrated colleagues around the globe by sending them quirky, treasured mementos to honour their findings, among them hats decorated with HAT modifications, or cartoons such as one that invoked iconic cereal box-covers featuring Olympians, tweaked to celebrate the discovery of differential histone methylation patterns specifying distinct gene expression states. We

end by saying to him what he often said to others to recognize major achievements: “Good show!” We miss you, Dave.

Nature **614**, 409 (2023)

doi: https://doi.org/10.1038/d41586-023-00346-0

This article was downloaded by **calibre** from https://www.nature.com/articles/d41586-023-00346-0

- COMMENT
- 14 February 2023

How social media affects teen mental health: a missing link

Researchers investigating the impacts of social media on mental health must consider where exactly adolescents are in their cognitive and social development.

- Amy Orben &
- Sarah-Jayne Blakemore



Teenagers are now spending more time on social media than ever before — coinciding with a rise in mental-health problems in this age group.Credit:

Leon Neal/Getty

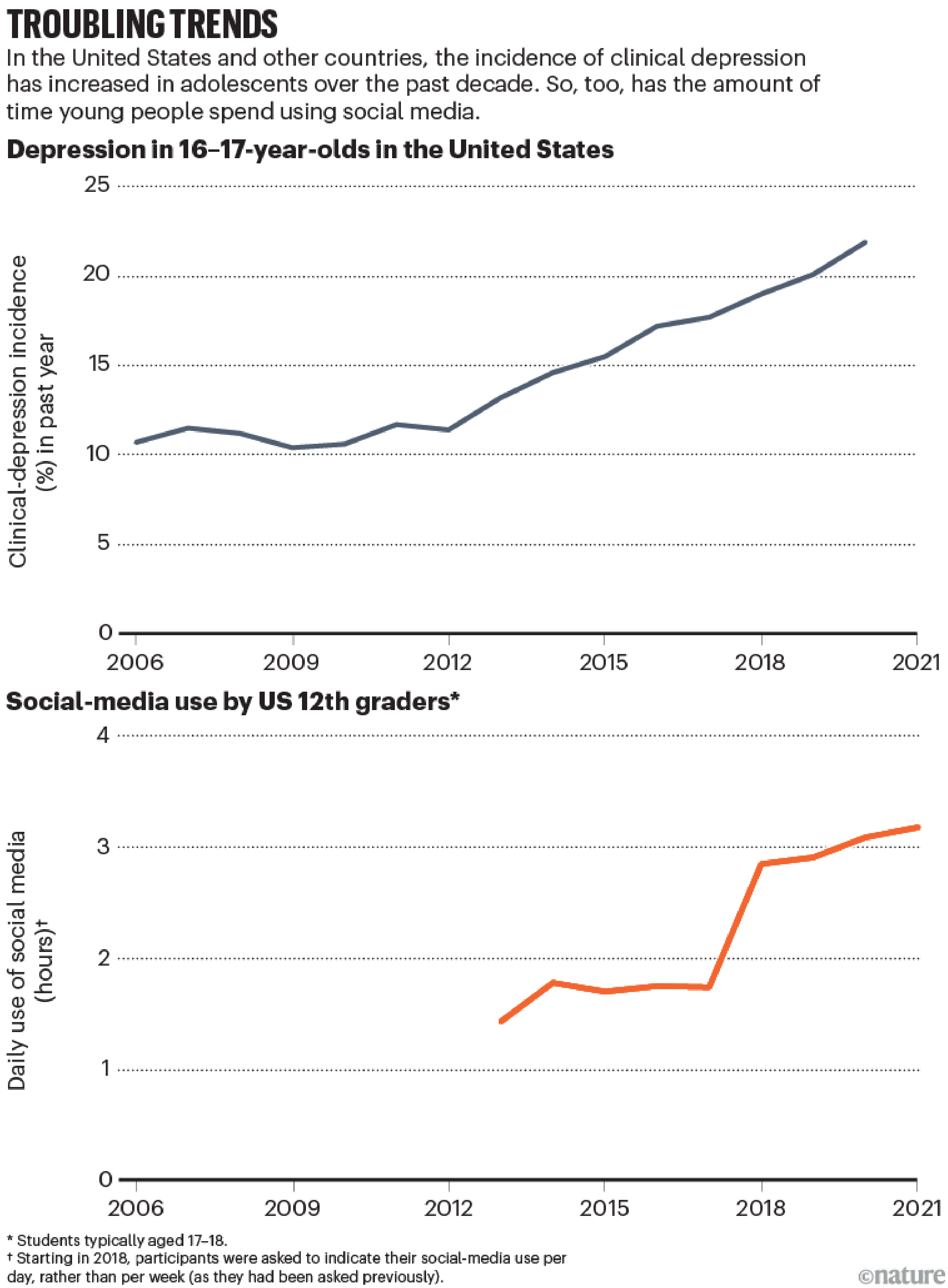
Depression, anxiety and suicidality have all sharply increased in adolescents over the past decade[1]. So, too, has the amount of time that young people spend online (see 'Troubling trends'). Partly because of fears that there's a link between these trends, governments around the world are under pressure to do more to regulate technology companies.

In the United Kingdom, the Online Safety Bill, currently being debated by Parliament, seeks to protect children from harmful content online. Last year, the European Union approved the Digital Services Act — which, among other things, has introduced tougher mandates requiring companies to remove illegal content from their websites. And in 2021, the US surgeon-general called for social-media companies to prioritize adolescent health and well-being at "all stages of product development"[1].

A difficulty facing policymakers, however, is that most of the scientific evidence on the impact of social media and other online activities on adolescent mental health is inconsistent[2]. Some studies might report similar effects, such as small negative correlations between time spent on social media and measures of well-being, but researchers differ in how important they think such findings are[3].

There might be many reasons why psychologists, psychiatrists, computational scientists and others have failed to obtain a clearer picture of what is going on[2]. Many have called for more detailed, objective assessments of what activities users engage in during their time online — an issue being addressed in part by smartphone apps that track the amount of time people spend on certain platforms[4]. Others say that what makes any one person vulnerable to the negative impacts of social media needs to be better understood[5].

All these arguments make sense. But in our view, there is another gap: researchers have not systematically interrogated, using large-scale data sets or experiments, how the relationship between social-media use and mental health changes with developmental stage.



Source: US National Survey on Drug Use and Health; Monitoring the Future

Developmental stage matters

To explore this, in 2020 and 2021, we analysed longitudinal data from two UK data sets[6]. The data had been collected every year between 2011 and 2018: 17,409 participants had been asked about their social-media use and life satisfaction, either in interviews or in online questionnaires, once per year for up to seven years. At the time of the first surveys, the participants' ages had ranged from 10 to 21.

To establish how social-media use and level of life satisfaction relate to each other over time, we looked for a connection between participants' estimates of their time spent on social media at ages 10, 11, 12 and so on until age 20, and the level of life satisfaction that they reported a year later. In other words, we used age as a proxy for developmental stage.

The effect sizes were small, but we found that social-media use (the participants' estimates of how much time they spent each weekday, on average, interacting with friends through a social website or app) did predict levels of life satisfaction a year later — but this was true only for participants at certain developmental stages.



Time for the Human Screenome Project

In participants who self-reported as female, increased social-media use (meaning an increase in a participant's use compared with their own average across the data-collection period) at 11, 12 or 13 years old predicted decreased life satisfaction (compared with their average) a year later. The same pattern occurred in participants who self-reported as male when they were 14 or 15 years old. These age ranges align with when young people go through puberty; on average, girls enter puberty earlier than boys[7].

For both female and male participants, increased social-media use at 19 years old — which is soon after most young people first leave home and gain independence — again predicted lower levels of life satisfaction a year later.

There are several reasons to be cautious when interpreting these results. First, the study needs to be replicated, and more sophisticated measures used to track both social-media use and what developmental stage a person is at. Also, this study and others indicate that social media's effects on mental health vary substantially between individuals[8]. Finally, the impact of social media seems to be bidirectional and complex: for male and female participants of all ages, reporting a life-satisfaction level in any one year that was lower than their personal average predicted a small increase in social-media use a year later.

Still, the idea that people's sensitivity to online social environments might be linked to certain developmental changes fits with what we know about adolescence from neurocognitive studies and other research.

A time of change

Early adolescence is characterized by wide-reaching hormonal changes, as well as physiological changes throughout the body. At the same time, all sorts of neural, cognitive and social shifts are happening. These changes could make social-media environments, such as those provided by Snapchat or TikTok, particularly alluring, but also especially impactful on mental health[9–11].

Several developmental-psychology studies have shown, for instance, that adolescents — particularly those in early to mid-adolescence — place increased importance on being able to interact with their peers, and on what their peers think of them[12]. Other studies suggest that although young children tend to view themselves positively, as they become adolescents, their ideas about themselves come to more closely align with what they perceive others to think of them[13,14]. Still more work has shown that being rejected or not being included has a greater impact on mood for those in early to mid-adolescence than for people older than 25[15].



Cognitive changes during puberty might make social media particularly alluring.Credit: Eddie Linssen/Alamy

Social media provides new ways for adolescents to quantify social approval — for instance, through the number of 'likes' that they receive after posting something online, or by how many seconds, minutes or hours they have to wait before receiving feedback. For some people, being able to constantly track feedback from peers could heighten anxieties about self-worth or amplify the impact of judgements from peers. Some researchers have

proposed that digital innovations, such as games or social-media platforms including TikTok, might even impact adolescents' development of a sense of self, how they perceive others' opinions of them or what habits they develop around social-media use[14,16,17].

Adolescents' social environments tend to undergo particularly dramatic changes at certain stages, too.

In the United Kingdom and elsewhere, most young people move from primary schools to secondary schools, where social networks are larger and more unstable, when they are 11[18]. Being able to access peers through communication pathways on social media — many of which are eminently available, highly public, permanent, asynchronous and lacking social cues, such as facial expressions and body language — could be especially impactful at this time[9]. The same is true when young people leave school for work or college. In both early and later adolescence, young people become more independent, and social pressures might increase.

Plugging the gap

We urge more psychologists, psychiatrists and other behavioural-science researchers to examine the effects of social-media use at specific developmental stages. In many studies, the effects of using social media are averaged over a broad age range. This means that potential fluctuations in the impacts of social media as adolescents age might be missed. Some investigators have collected data from smaller age ranges, or from participants who are all the same age, but they often generalize their results to the entire adolescent age range.



Smartphones are bad for some teens, not all

To try to pinpoint how exactly developmental stage affects how young people interact with and experience online spaces, researchers could use methodologies from fields such as developmental neuroscience or developmental psychology. In some psychology studies, for instance, researchers give participants feedback from fictional participants, and assess changes to people's sense of self-worth over time[19]. Other studies measure whether participants' opinions or actions (such as how much they donate to charity) are influenced by their peers' opinions or actions, or how much participants' self-judgements are affected by how they perceive others to judge them. In principle, such experimental paradigms could be used in combination with digital data sources to investigate how the use of social media and development interact to affect the fragility of young people's sense of self and their self-worth.

Likewise, measures of pubertal hormones collected through saliva samples or estimates of puberty stage in self-reported questionnaires in major data-collection efforts, such as the Adolescent Brain Cognitive Development (ABCD) study, could be used to establish whether people's age or pubertal stage is most important when it comes to determining sensitivity to social media. (The ABCD study is the largest long-term study of brain development and child health in the United States.)

So far, investigating the role of online environments in the rise in mental-health problems in young people has been challenging and frustrating — not least because social-media companies are generally reluctant to share their data with researchers. But mental-health difficulties experienced in adolescence can affect someone through every life stage: around 48% of people with a mental-health disorder, such as depression, first experience symptoms before they are 18 years old[20]. What's more, new digital technologies will keep emerging.

It is therefore crucial that psychologists, neuroscientists and other researchers keep refining their approaches to better understand what kind of online experiences prime some young people for depression, anxiety, self-harm and a suite of other mental-health problems.

Nature **614**, 410-412 (2023)

doi: https://doi.org/10.1038/d41586-023-00402-9

References

1. Office of the Surgeon General. *Protecting Youth Mental Heath: The US Surgeon General's Advisory* (US Department of Health and Human Services, 2021).

2. Odgers, C. L. & Jensen, M. R. *J. Child Psychol. Psychiatry* **61**, 336–348 (2020).

3. Valkenburg, P. M., Meier, A. & Beyens, I. *Curr. Opin. Psychol.* **44**, 58–68 (2022).

4. Ellis, D. A. *Comput. Human Behav.* **97**, 60–66 (2019).

5. Valkenburg, P. M. & Peter, J. *J. Commun.* **63**, 221–243 (2013).

6. Orben, A., Przybylski, A. K., Blakemore, S.-J. & Kievit, R. A. *Nature Commun.* **13**, 1649 (2022).

7. Pfeifer, J. H. & Allen, N. B. *Biol. Psychiatry* **89**, 99–108 (2021).

8. Beyens, I., Pouwels, J. L., van Driel, I. I., Keijsers, L. & Valkenburg, P. M. *Sci. Rep.* **10**, 10763 (2020).

9. Nesi, J., Choukas-Bradley, S. & Prinstein, M. J. *Clin. Child Fam. Psychol. Rev.* **21**, 267–294 (2018).

10. Weinstein, E. & James, C. *Behind Their Screens: What Teens are Facing (and Adults Are Missing)* (Blackstone, 2022).

11. Crone, E. A. & Konijn, E. A. *Nature Commun.* **9**, 588 (2018).

12. Blakemore, S.-J. & Mills, K. L. *Annu. Rev. Psychol.* **65**, 187–207 (2014).

13. Rodman, A. M., Powers, K. E. & Somerville, L. H. *Proc. Natl Acad. Sci. USA* **114**, 13158–13163 (2017).

14. Peters, S. *et al. Dev. Cogn. Neurosci.* **48**, 100921 (2021).

15. Sebastian, C., Viding, E., Williams, K. D. & Blakemore, S.-J. *Brain Cogn.* **72**, 134–145 (2010).

16. Granic, I., Morita, H. & Scholten, H. *Psychol. Inquiry* **31**, 195–223 (2020).

17. Maza, M. T. *et al. JAMA Pediatr.* **177**, 160–167 (2023).

18. Burnett Heyes, S. *et al. Child Dev.* **86**, 1489–1506 (2015).

19. Will, G.-J., Rutledge, R. B., Moutoussis, M. & Dolan, R. J. *eLife* **6**, e28098 (2017).

20. Solmi, M. *et al. Mol. Psychiatry* **27**, 281–295 (2022).

This article was downloaded by **calibre** from https://www.nature.com/articles/d41586-023-00402-9

Work

- **Stop the peer-review treadmill. I want to get off** [13 Feb 2023]
  • Faced with a deluge of papers, journal editors are struggling to find willing peer reviewers.
- **Searching the ocean for secrets to help fight climate change** [13 Feb 2023]
  • By sampling prehistoric sediments in the ocean floor, geologist Hartmut Schulz hopes to identify ancient analogues of today’s warming world.

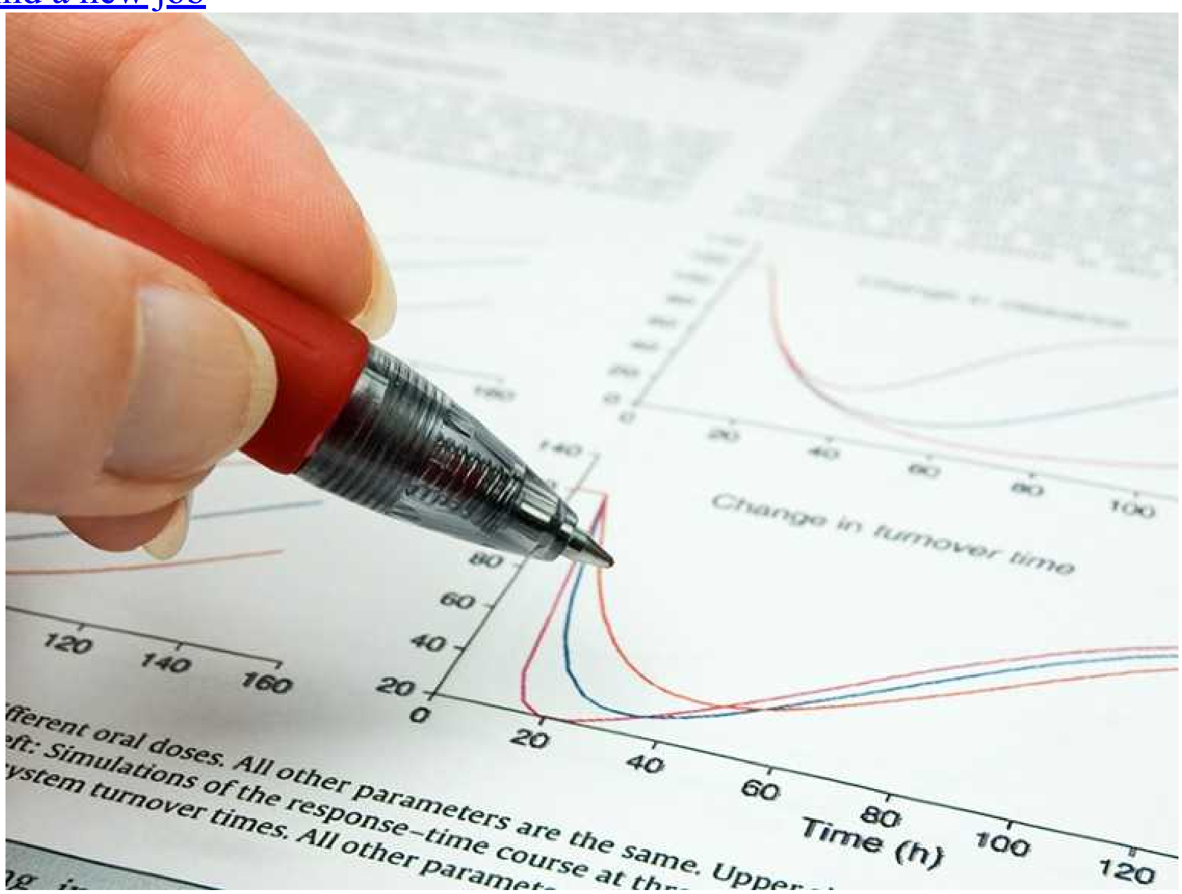
- CAREER FEATURE
- 13 February 2023

Stop the peer-review treadmill. I want to get off

Faced with a deluge of papers, journal editors are struggling to find willing peer reviewers.

- Amber Dance

Find a new job



Downwards curve: many researchers see reviewing as a burden that lowers their productivity.Credit: Getty

In November 2022, health economist Chris Sampson found himself in desperate need of a hero. As associate editor for *Frontiers in Health Services*, he'd been trying to get a paper reviewed since April. He'd sent out about 150 invitations to potential reviewers and received four reviews, but only one of sufficient quality to be useful. Sampson, who works at the Office of Health Economics, a research and consultancy company based in London, needed two more good reviews, so he tweeted: "I need a #peerreview hero … Heroes, DM me."

Sampson's plight is a problem faced by editors the world over in the face of uncontrolled growth in the number of journals and papers. The tally of articles indexed by the citation database Web of Science tripled from about one million in 1990 to nearly three million in 2016, according to the website Publons[1], which tracks peer-review contributions and is now part Web of Science under the analytics company Clarivate. But the size and composition of the reviewer pool has not kept pace, say editors, because journals often favour well-known scientists from countries with established science infrastructures, rather than early-career researchers or scientists from emerging science nations.

Balazs Aczel is a psychologist at Eötvös Loránd University in Budapest who studies the processes of science. Using a data set covering more than 87,000 scholarly journals, Aczel and his colleagues estimated that researchers globally, in aggregate, spent the equivalent of more than 15,000 years on peer review in 2020 alone[2]. And many scientists are declining to review more frequently. On Clarivate's ScholarOne, a manuscript-tracking platform that helps to organize reviews for more than 8,000 academic journals, the average rate at which scientists accept a review dropped from 37.5% in 2020 to 32.3% in 2022.



Balazs Aczel found that global researchers collectively spent more than 15,000 years on peer review in 2020.Credit: Gabor Z. Horvath

Pandemic burnout seems to have exacerbated the problem. A poll of *Nature* readers last November (the results of which will be reported later this month) found that about one-third had reduced their reviewing activity since March 2020. Senior and mid-career researchers, who perform the bulk of peer reviews, were most likely to cut back.

“It is unrewarded work,” says Donna Yates, a criminologist at Maastricht University in the Netherlands. “One gets nothing from peer review, other than being taken away from work that helps your research or teaching.” In addition, the scant evidence available suggests that peer review adds only marginally to publications’ quality, says Olavo Amaral, who studies the

reproducibility of science at the Federal University of Rio de Janeiro in Brazil.

Many scientists are increasingly frustrated with journals — *Nature* among them — that benefit from the unpaid work of reviewing while charging high fees to publish in them or read their content. A spokesperson for Springer Nature says: “We’re always looking to find new and better ways of recognizing peer reviewers for their valuable and essential work.” They also pointed to a 2017 survey of more than 1,200 *Nature* reviewers, in which 87% of respondents said they considered reviewing to be their academic duty, 77% viewed it as safeguarding the quality of published research and 71% expected no reward or recognition for reviewing (see go.nature.com/3dnzpgr). But now, amid post-pandemic challenges, many reviewers find that duty overly burdensome.

Yates and others suggest that cash payments would solve the problem, but others say such a system would be unethical and unsustainable. A better solution might be to share the load more widely — with early-career scientists, for instance, or those in less well resourced countries, who are not yet heavily involved — or even to let computer algorithms bear some of the burden.

“I think the notion that we have to review every paper might be a bit utopic,” says Amaral. “I think the system itself might be untenable.”

Expectation and reward

The current peer-review system can be traced back to the eighteenth century, when the United Kingdom’s Royal Societies distributed reports to expert members. The goal was to veto anything that might damage publishers’ reputations. A more formal system, using anonymous experts as publishing gatekeepers, emerged in Britain and United States during the nineteenth century, when papers supplanted pamphlets and lectures as the main means of disseminating scientific results. An influx of public funding for US science in the mid-twentieth century created further pressure for quality control as the volume of published papers increased. Thus, peer review arose in English-speaking nations when science was an elite pursuit — unlike

today's global enterprise, which also includes the preprint option to get information out without gatekeeping by reviewers or journals.



Olavo Amaral says that journals can create better systems for controlling research quality.Credit: Patrícia Bado

Journals typically require two or three reviewers per paper, and scientists do four to five reviews a year on average[1], although some perform many more, according to Publons. They're generally expected to fold reviewing into their academic workloads. It's rarely an explicit duty or rewarded with money or credit, although it can be rewarding: scientists not only get to see the latest research before anyone else, but also gain insight into the review process that can help with their own submissions.

Jesse Cook, a graduate student in clinical psychology at the University of Wisconsin–Madison, considers reviewing an important act of altruism for the scientific community. In 2019, a couple of years into his PhD studies on sleep, he began consulting for companies — who asked him how much he'd like to be paid. He now makes between US$150 and $200 an hour for that work — throwing into sharp relief the fact that journals rely on similar levels of expertise in their peer-review processes, but pay nothing.

The COVID-19 pandemic made him consider his time more carefully. "I think we all had a perspective adjustment," says Cook. "And obviously family time became a priority for many." Cook still does about one review per month — but he also declines more often than he used to, preserving time for his family and dissertation research. Others are also being more selective in the invitations they accept. "Reviewing for free for a for-profit company is kind of a scam," says Amaral, who prefers to review for non-profit journals.

Rebeccah Lijek, a molecular biologist and peer-review scholar at Mount Holyoke College in South Hadley, Massachusetts, directs her reviewing energies to preprints, posted on servers such as bioRxiv and open to comments from anyone. She loves being able to consider the science just on its merits, without judging whether a study is original enough to deserve publication by a specific journal. She finds the process more collegial and has made new connections and friends through it. "It's just a little bit more fun," says Lijek.



Rebeccah Lijek reviews mostly preprints.Credit: Mount Holyoke College staff photography

Preprints can help to spread scientific findings quickly, as happened during the COVID-19 pandemic. But they don't replace the publications that scientists need to populate their CVs. And the publication process is getting slower, says Detlef Weigel, a plant geneticist at the Max Planck Institute for Biology in Tübingen, Germany. Forty years ago, reviews came back in about three weeks, he recalls — now, he doesn't expect a reply for six weeks at the earliest.

By the time papers come out, studies might be months or even years old, which can have serious policy implications, says Sandersan Onie, a psychology researcher at the Black Dog Institute, a non-profit mental-health

research facility in Sydney, Australia. For example, he cites a study that he's submitting on suicide rates in Indonesia. "We need to get this information out to help shape policy," says Onie, who is also president of the Indonesian Association for Suicide Prevention in Jakarta.



Sandersan Onie says that delays in peer review can be a matter of life and death when it comes to psychology studies.Credit: Aphrodite Delaguiado

The never-ending publication cycle creates more work for researchers, says Firdaus Hafidz, a public-health researcher at Gadjah Mada University in Yogyakarta, Indonesia, who is still trying to publish work from his PhD, earned in 2018. If a review takes months or years, he adds, he might have to update the literature review or redo analyses.

The glacial pace of peer review can cause some young researchers to leave academia altogether, says Pradeep Kumar, a biomaterials scientist at the University of the Witwatersrand in Johannesburg, South Africa. To move from the master's degree programme to PhD candidacy there, students must

publish a paper. When delays occur, students often head off to work in industry for the interim — but some never return. Kumar has lost three students, all women, that way. “Publication delayed is publication denied,” he says.

In search of incentives

To combat delays, the centuries-old peer-review system needs a redesign, says Onie. “If you want people to do something, it just needs to be incentivized.”

Some journals do pay reviewers or waive their article fees or subscription costs. For example, submitting three or more reviews per year for a Nature Research journal entitles reviewers to a free, online subscription to the journal they choose from Nature Research’s offerings. The Springer Nature spokesperson says that the publisher’s reviewers appreciate recognition in the form of these subscriptions, and having their names included in the published papers.

Other journals give reviewers public credit by posting the reviews or crediting scientists’ profiles on Clarivate’s Web of Science Reviewer Recognition Service. But Yates says that such online credit is worthless. She reviews three papers for every one she submits, but would like to be paid for her efforts, as she is for applying her criminology expertise as a consultant in government projects, or for giving expert testimony in courts. “Peer review should be flat-out paid,” she says.



Why early-career researchers should step up to the peer-review plate

Other scientists argue that paying reviewers would be unaffordable for many journals unless they raised subscription fees. Aczel and his colleagues estimated the monetary value of the time that scientists in three nations devote to reviewing, and came up with upwards of US$1.5 billion a year in the United States, more than $600 million in China, and nearly $400 million in the United Kingdom[2]. Non-profit journals might not be able to compete for reviewers if commercial rivals paid. And researchers eager for an easy pay cheque might churn out lower-quality reviews.

Pablo Manavella, a plant molecular biologist at the Coastal Agrobiotechnology Institute in Santa Fe, Argentina, worries that journals would just pass the extra costs of reviewer fees onto authors — something that those in lower-income nations could ill afford. Extra fees, in the form of article-processing charges, would come out of Manavella's scant government grants and be funnelled to reviewers, who are more likely to reside in wealthier nations. "I don't think that this is right," he says.

Nor is a cheque what most reviewers desire. In a 2019 report about grant peer review by Publons, the authors asked scientists what would motivate them to take on reviews. Cash ranked sixth, behind such incentives as more-explicit recognition by employers and online records of review efforts[3].

“A lot of people respond quite well to having some kind of credibility or prestige,” such as being listed on an editorial board in exchange for review, says Sampson. “I think that’s a much more generalizable and fairer basis for rewarding peer review.”

Expanding evaluation

But none of these incentives gives researchers what they truly need — time. To get thoughtful reviews, without sucking reviewers dry, journals might need a far-reaching overhaul.

One simpler solution is to enlarge the pool of reviewers, seeking out a more diverse group. “We’re not using enough early-career researchers,” says Bernd Pulverer, head of scientific publications at EMBO Press in Heidelberg, Germany, and formerly chief editor of *Nature Cell Biology*. “We’re using too many men, too many white people.” EMBO is tracking reviewers by gender and country and inviting more early-career researchers, Pulverer says.

To find reviewers, editors often turn to software. But these computer-generated lists aren’t as diverse as they could be, says Regine Paul, a political scientist at the University of Bergen in Norway and co-editor of *Critical Policy Studies*. Her system gives her 30 suggestions for each paper. “Among those there will usually be one or two scholars not from the United States or Europe or Australia,” she laments. She does her best to find a wider range of reviewers herself, but doesn’t always have enough time.



Computer-generated lists of reviewers aren't diverse enough, says Regine Paul.Credit: Eivind Senneset

Onie notes that some potential reviewers in lower-income nations might decline to review because they lack confidence. In Indonesia, he says, "we have professors who have never published a paper because academia is so new." A handful of programmes now offer training, and even certification, in peer review for early-career or inexperienced researchers.

Seeking reviews from members of under-represented groups could add to the 'minority tax' that they face already through being routinely asked to spend unpaid time on issues such as diversity, equity and inclusion. Moreover, in some nations in the global south, reviewing could eat into a researcher's income or laboratory funding, because some governments and universities tie funding to publications. Kumar says that Witwatersrand, for example, grants investigators a proportion of government subsidies to run their labs, and that proportion is based on their publishing rate. Hafidz and Onie, both based in Indonesia, say they can receive cash payments of

hundreds or even thousands of US dollars for publishing in a top-tier journal. But reviews don't garner any bonuses, so any time spent reviewing, rather than on getting papers published, could be money down the drain.

Another solution could be to reduce the amount of reviewing that journals require. Some journals are screening papers more heavily before sending them out for review, and are rejecting papers or asking for improvements before inviting reviewers to weigh in, says Josh Dahl, senior director of product management at Clarivate. Other researchers say that some types of paper, such as those introducing databases or ideas without new data, could go through with less extensive review.



[To fix peer review, break it into stages]

Computers could help, too. Journals already rely on algorithms to identify plagiarism or altered images. And although tools such as artificial intelligence aren't poised to take over peer review just yet, software could check statistical analyses or run a checklist on basic methods[4] — functions that, according to data collected by Amaral, human reviewers perform only modestly well anyway[5].

Journals could also recycle reviews, so that not every resubmission would require three new reviewers. Aczel estimated that this would save 28 million reviewer-hours per year[2]. For example, scientists whose studies are rejected

by one Springer Nature or PLOS journal can resubmit to other journals in the same family, with the same reviews attached. At the end of January, the journal *eLife* instituted a model whereby all peer-reviewed papers are published on its platform as 'reviewed preprints' alongside an assessment from the journal and public reviews. Authors have the option to respond, and can then choose whether to revise, complete publication with *eLife* or send the study and reviews to another publication.

Other organizations offer reviews before authors commit to a particular journal. Peer Community in, a non-profit initiative, offers peer review, after which authors can publish freely in one of the organization's partner journals or submit their study, with accompanying reviews, to other publications. Another programme, Review Commons, provides authors with reviews, which they can then include in submissions to several affiliate journals, including those from EMBO Press. The programme, launched at the end of 2019, is "working very well", Pulverer says. "The information is sufficient for editors to make informed decisions." Reviewers are eager to participate, because they're able to focus on the science in the study, rather than its suitability for a specific journal.

Serge Horbach, a postdoc in the sociology of science at Aarhus University in Denmark, thinks that science is heading for a 'publish–review–curate' model. Instead of acting as gatekeepers, journals would come in at the end, to archive the version of record and index papers in databases. "The journal gives it a stamp of approval and says, now we accept this as certified knowledge," Horbach explains.

Amaral, who sees the current peer-review system as insupportable, says it doesn't have to stay that way. "I think we can rebuild better quality control, in better ways." Doing so might keep reviewers from cracking under the pressure of the ever-growing scientific enterprise.

Nature **614**, 581-583 (2023)

doi: https://doi.org/10.1038/d41586-023-00403-8

References

1. Publons. *2018 Global State of Peer Review* (Publons, 2018).

2. Aczel, B., Szaszi, B. & Holcombe, A. O. *Res. Integrity Peer Review* **6**, 14 (2021).

3. Hayes, M. & Hardcastle, J. *Grant Review in Focus*. (Publons, 2019).

4. Schulz, R. *et al. BMC Res. Notes* **15**, 203 (2022).

5. Carneiro, C. F. D. *et al. BMC Res. Integrity Peer Rev.* **5**, 16 (2020).

This article was downloaded by **calibre** from https://www.nature.com/articles/d41586-023-00403-8

- WHERE I WORK
- 13 February 2023

Searching the ocean for secrets to help fight climate change

By sampling prehistoric sediments in the ocean floor, geologist Hartmut Schulz hopes to identify ancient analogues of today's warming world.

- James Mitchell Crow



Hartmut Schulz is a marine geologist at the University of Tübingen, Germany. Credit: Volker Diekamp/Marum, University of Bremen

I am a marine geologist, interested in the study of deep time. In my field, we collect long sediment cores from the ocean floor, to reconstruct the oceans

and climates of the past, looking for analogues of the current warming climate.

This picture was taken on a cold evening in September 2022 during a research cruise to Baffin Bay, off the Greenland coast. Today, in the Arctic, ice is melting rapidly. We know there was also a very warm period around 400,000 years ago, when large parts of the Greenland ice sheet could have melted and contributed to sea-level rise.

On this cruise, we tried to reach sediments from that time, to analyse them for climate proxies such as pollen, which indicate how much of the ice sheet had melted and been replaced by vegetation.

In this photo, I am separating a newly collected core into sections for storage in the ship's hold. We obtain the cores using iron tubing that is usually 10–20 metres long and which we drive into the sediment using a 2-tonne weight.

Then we winch the tube out to see what we've got. The ideal core is long and straight, but we sometimes get a 'banana' — when the tube has struck a buried rock and become bent.

Although it looks as if I am working alone, there are people all around me. At sea, you always work in a team. I like that very much. In total, I have spent close to 2 years on the open ocean, including an 11-week cruise in the Antarctic Ocean. The Southern Ocean was the most impressive: so vast, so harsh.

The Baffin Bay cruise finished in St John's, Newfoundland, Canada, on 4 October last year. The cores have now been shipped to Bremen, Germany, where the cruise's lead scientist is based. We will gather there this year to decide which cores to study first.

You can't sample the whole ocean when you're collecting cores; you must be selective. We think we found a good position for reaching 400,000-year-old sediments, but it is tricky. We will see.

Nature **614**, 586 (2023)

doi: https://doi.org/10.1038/d41586-023-00404-7

This article was downloaded by **calibre** from https://www.nature.com/articles/d41586-023-00404-7

Research

- **Heterogeneous melting near the Thwaites Glacier grounding line** [15 Feb 2023]
  • Thwaites Eastern Ice Shelf observations from a new underwater vehicle show that high melt rates occur where ice is sharply sloped at the ocean interface, with lower melt where the ice is comparatively flat.
- **Suppressed basal melting in the eastern Thwaites Glacier grounding zone** [15 Feb 2023]
  • Despite observations from a hot-water-drilled access hole showing warm ocean waters beneath Thwaites Glacier Eastern Ice Shelf, the basal melt rate is strongly suppressed due to the low current speeds and strong density stratification.
- **Imprinted SARS-CoV-2 humoral immunity induces convergent Omicron RBD evolution** [19 Dec 2022]
  • Convergent mutations in hotspots of the SARS-CoV-2 Omicron receptor-binding domain can cause immune evasion and maintain sufficient ACE2-binding capability.
- **Neonatal imprinting of alveolar macrophages via neutrophil-derived 12-HETE** [04 Jan 2023]
  • The production of eicosanoids by neutrophils during the neonatal period is necessary for the self-renewal and maintenance of alveolar macrophages during lung development.
- **Single-cell spatial landscapes of the lung tumour immune microenvironment** [01 Feb 2023]
  • Using imaging mass cytometry, the tumour and immunological spatial landscapes of 416 lung adenocarcinomas are characterized, which, when combined with deep learning, can predict clinical outcomes with high accuracy.
- **Single-cell spatial immune landscapes of primary and metastatic brain tumours** [01 Feb 2023]
  • Imaging mass cytometry of human brain tumours provides spatial information that, combined with existing transcriptomic data, reveals the existence of a cellular neighbourhood containing a rare macrophage population associated with prolonged survival.
- **Aberrant phase separation and nucleolar dysfunction in rare genetic diseases** [08 Feb 2023]
  • Frameshift mutations that create arginine-rich basic tails in transcription factors and other proteins can lead to altered phase separation in the nucleolus, which in turn leads to syndromes

such as brachyphalangy, polydactyly and tibial aplasia.

- **Structure of the lysosomal mTORC1–TFEB–Rag–Ragulator megacomplex** [25 Jan 2023]
  • Cryogenic-electron microscopy is used to determine the structure of TFEB as presented to mTORC1 for phosphorylation and an explanation is found for the strong dependence of TFEB phosphorylation on FLCN and the RagC GDP state.
- **The case for standardizing gene nomenclature in vertebrates** [15 Feb 2023]
  •
- **Reply to: The case for standardizing gene nomenclature in vertebrates** [15 Feb 2023]
  •

- Article
- Open Access
- Published: 15 February 2023

Heterogeneous melting near the Thwaites Glacier grounding line

- B. E. Schmidt ,
- P. Washam,
- P. E. D. Davis,
- K. W. Nicholls,
- D. M. Holland,
- J. D. Lawrence,
- K. L. Riverman,
- J. A. Smith,
- A. Spears,
- D. J. G. Dichek,
- A. D. Mullen,
- E. Clyne,
- B. Yeager,
- P. Anker,
- M. R. Meister,
- B. C. Hurwitz,
- E. S. Quartini,
- F. E. Bryson,
- A. Basinski-Ferris,
- C. Thomas,
- J. Wake,
- D. G. Vaughan,
- S. Anandakrishnan,
- E. Rignot,
- J. Paden &
- …

- K. Makinson

Show authors

Nature **volume 614**, pages 471–478 (2023)

- 4121 Accesses
- 804 Altmetric
- Metrics details

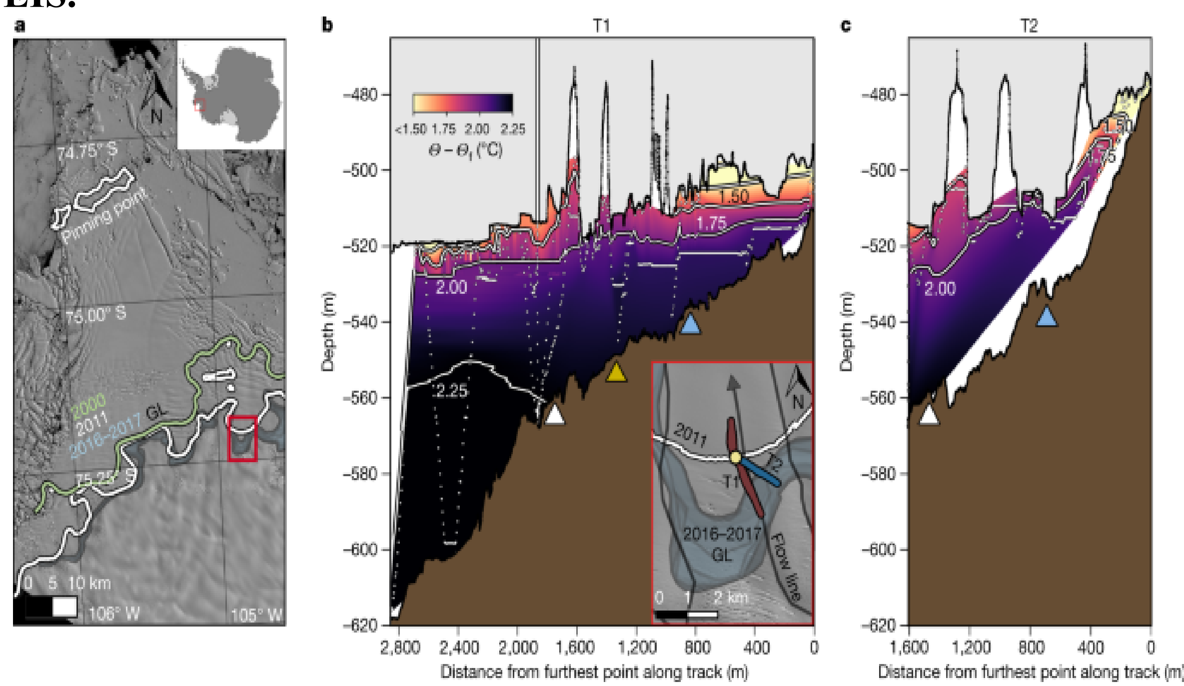
Abstract

Thwaites Glacier represents 15% of the ice discharge from the West Antarctic Ice Sheet and influences a wider catchment[1,2,3]. Because it is grounded below sea level[4,5], Thwaites Glacier is thought to be susceptible to runaway retreat triggered at the grounding line (GL) at which the glacier reaches the ocean[6,7]. Recent ice-flow acceleration[2,8] and retreat of the ice front[8,9,10] and GL[11,12] indicate that ice loss will continue. The relative impacts of mechanisms underlying recent retreat are however uncertain. Here we show sustained GL retreat from at least 2011 to 2020 and resolve mechanisms of ice-shelf melt at the submetre scale. Our conclusions are based on observations of the Thwaites Eastern Ice Shelf (TEIS) from an underwater vehicle, extending from the GL to 3 km oceanward and from the ice–ocean interface to the sea floor. These observations show a rough ice base above a sea floor sloping upward towards the GL and an ocean cavity in which the warmest water exceeds 2 °C above freezing. Data closest to the ice base show that enhanced melting occurs along sloped surfaces that initiate near the GL and evolve into steep-sided terraces. This pronounced melting along steep ice faces, including in crevasses, produces stratification that suppresses melt along flat interfaces. These data imply that slope-dependent melting sculpts the ice base and acts as an important response to ocean warming.

Main

Offshore ocean and atmospheric conditions force warm circumpolar deep water (CDW) onto the Amundsen Sea continental shelf[13,14], where it contributes to ice loss and GL retreat of glaciers draining this sector of the West Antarctic Ice Sheet, including Thwaites Glacier[11]. Thwaites Glacier extends seaward from the Walgreen Coast, forming the Thwaites Glacier Tongue (TGT) to the west and the TEIS that rests on a prominent sea-floor pinning point (Fig. 1a). Warm CDW flows towards the glacier along the coastline and through sea-floor channels[15,16,17], where it drives melting. The bed underneath the upstream grounded ice deepens to a maximum of 2,300 m below sea level[4,5], making it susceptible to large-scale retreat from ocean-driven melting[7]. Collapse of Thwaites Glacier, which itself represents more than half a metre of global sea-level-rise potential, could also destabilize neighbouring glaciers that account for a further 3 m of future sea level rise[4].

Fig. 1: Warm water reaches near the ice base and retreating GL of the TEIS.



a, Historical GL positions (coloured lines/zones after ref. [12]) demonstrate notable GL retreat over the past two decades (QGIS map: Landsat 8, 15 m pixel^{-1}, band 8 image LC08_L1GT_003113_20200131_20200211_01_T2_B8, 31 January 2020; the red box denotes the study region). **b**,**c**, Warm water is delivered close to

the ice base (upper grey regions), shown by contours of thermal driving (degrees above in situ freezing point). The ice (black line) and seabed (brown regions) elevation profiles are measured by up and down altimetry from Icefin, which compare with bathymetry from mapping and forward sonar (Fig. 2). The small circles denote the Icefin track, along two transects approaching the GL, T1 (red) and T2 (blue) shown in the lower inset (red box from **a**). The yellow circle in the inset and vertical line through the ice denote the location of the borehole. The T1 track is oriented 5–10° oblique to the flow direction of the glacier and T2 approximately 50° oblique to flow; Icefin reached the grounded point of the glacier at the end of T2. Triangles in **b** and **c** mark historic GL locations estimated from satellite interferometry for 2011 (white), and the furthest downstream estimate in 2016 (blue)[12]. In **b**, the yellow triangle denotes the potential GL wedge detected by Icefin (Fig. 2). Nearest to the GL, although temperatures are colder than the deep water, the ocean water holds more than one degree of thermal driving. The ice base transitions from rough near the GL to terraced (progressively steeper-sided step-like features) near and downstream of the borehole, suggestive of progressive melting. Crevasses also contain terraces, especially clear in **c**.

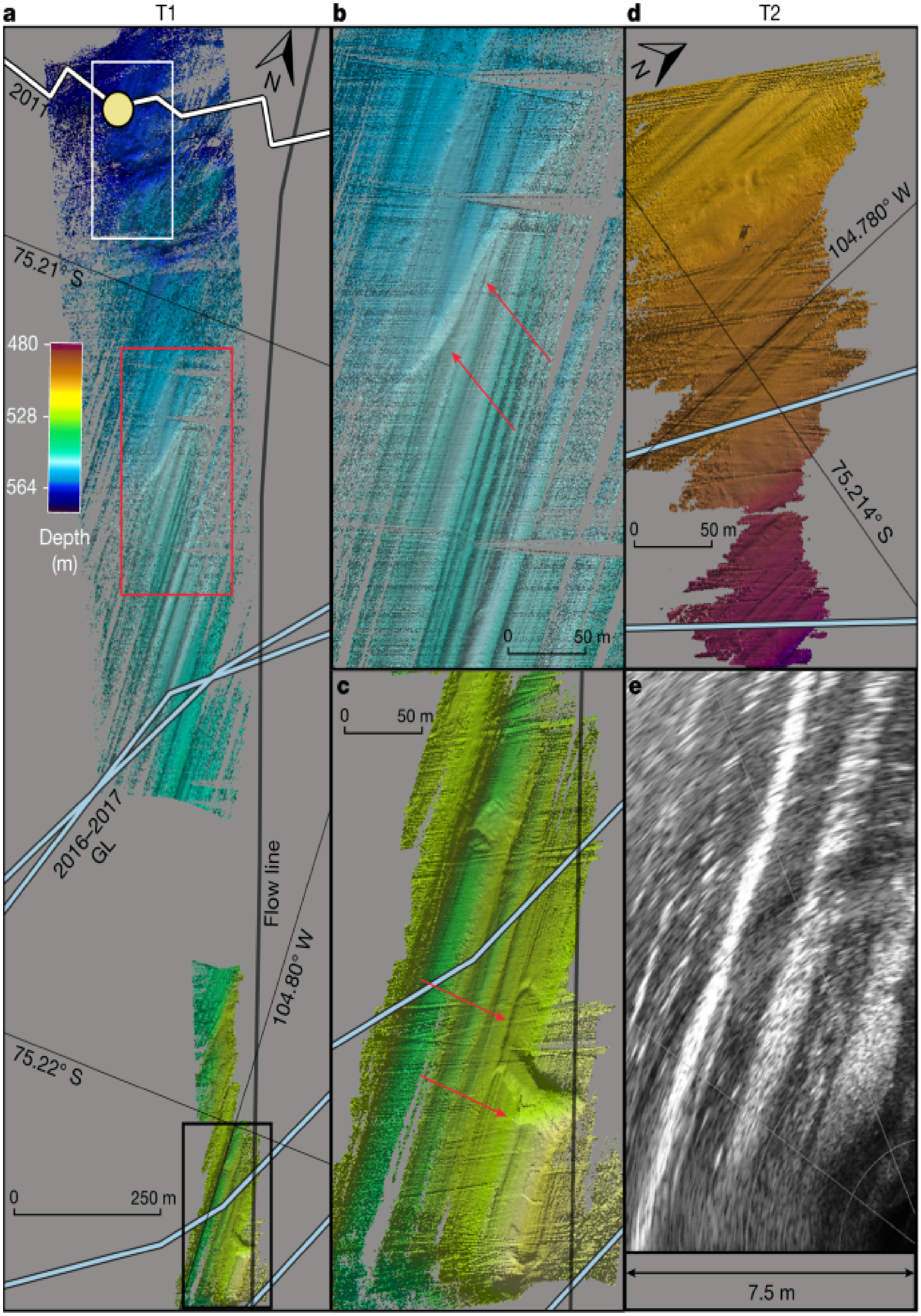
Changes in the Thwaites system have accelerated over the past 20 years (refs. [8,9,10]), resulting in breakup of the TGT and propagation of rifts across the TEIS[10]. Recent GL retreat has varied from 0.6 to 1.2 km year^{-1} (ref. [12]). Ocean melting, dynamic thinning and ice-flow rates influence this retreat[12], but exactly how these factors operate is difficult to constrain with generally poor observations below the ice. Satellite observations, which measure the surface elevation of the glacier, suggest that the TEIS is thinning on average 25 metres per decade[10,12], whereas airborne ice-penetrating radar that directly measures ice thickness estimates rates up to 45 metres per decade[18].

Although ocean-driven melting directly influences the stability of ice around Antarctica[19,20], little data resolve the interaction between the ice and ocean directly[21,22,23,24,25,26,27,28,29,30]. Models of ocean forcing are often limited by resolution or available parameterizations. Generally, models represent ice shelves simplistically as wedges of ice with flat or curved interfaces and an inferred sea-floor geometry as a function of distance from the presumed GL. Usually a zero-melt condition is imposed at the GL[31], which is inconsistent

with evidence of thinning and GL retreat. Although retrograde bed slopes facilitate positive feedback in grounded ice loss from ocean-forced melt[6,7], glaciers resting on prograde slopes still face influence from warm water undercutting the ice. Temperature and salinity variations influence circulation and heat exchange between the ice and ocean. These variations occur at scales much smaller than those resolved by remote sensing or captured in ice-shelf-wide models of ice–ocean interactions. Furthermore, few direct measurements have been made near the ice base[24,25,26,27,28,29,30], and none at the GL of a considerable glacier, that would help models at large and small scales better represent melting. Therefore, how melting occurs under ice shelves and particularly at the GL, influencing ice loss, remains largely unresolved.

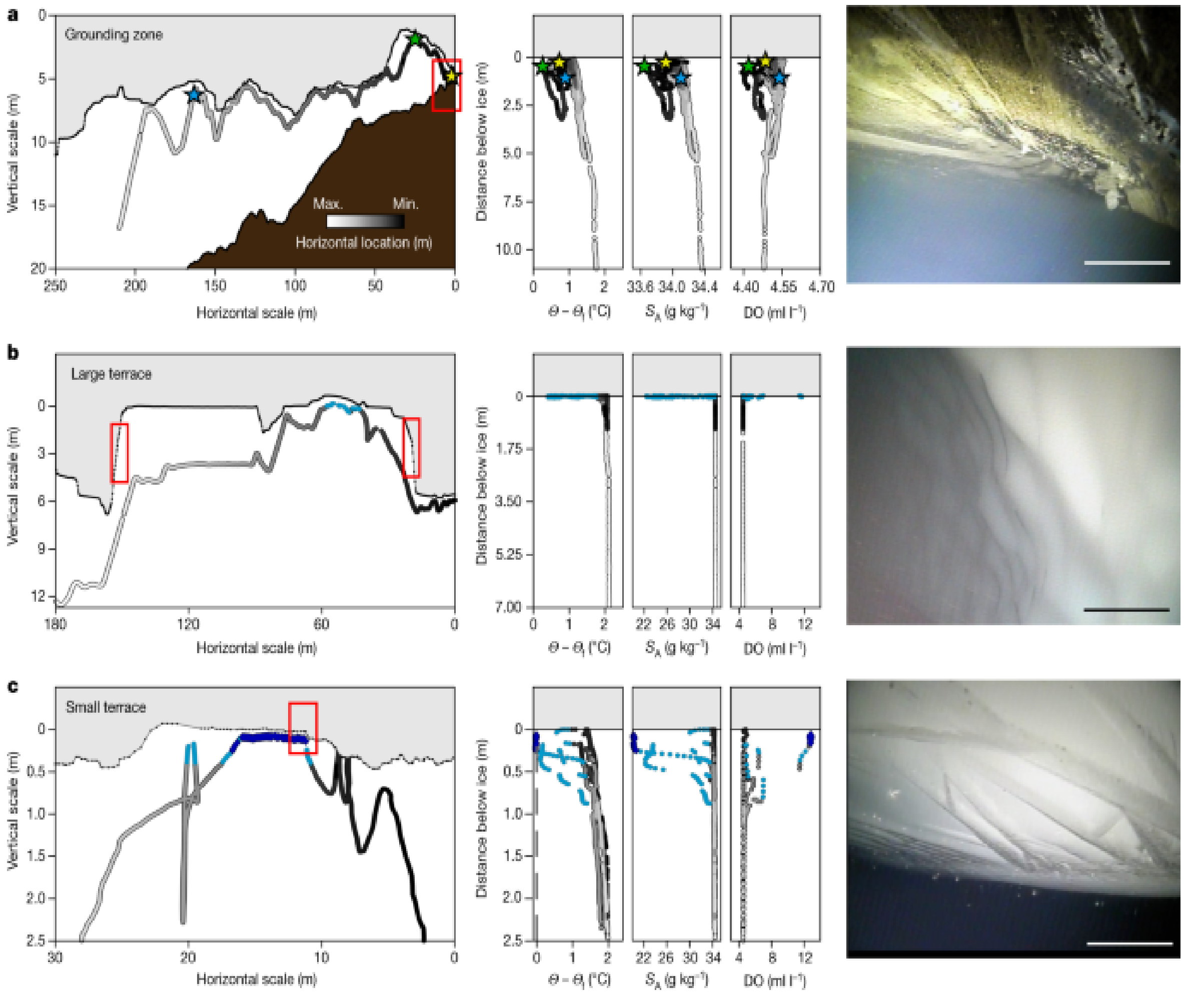
As part of the National Science Foundation (NSF)-Natural Environment Research Council (NERC) International Thwaites Glacier Collaboration (ITGC), a comprehensive field campaign was carried out over two austral summers, with an ice-shelf-drilling campaign in 2019–2020 to access the ocean cavity[28] and sediments below the TEIS to observe the changing system directly. We conducted detailed in situ hydrographic measurements in an area of the TEIS referred to as the ‘butterfly’[12]. The ice in this region is grounded at about 500 m below sea level (Figs. 1 and 2), typical of most of the Thwaites system outside the western trunk. We deployed the new underwater vehicle Icefin (Extended Data Fig. 1) through the borehole over five under-ice missions spanning 9–11 January 2020. The vehicle measured ocean temperature, salinity, dissolved oxygen and current velocities (Fig. 1 and Extended Data Fig. 2), mapped the sea floor and ice base in three dimensions (Figs. 1 and 2) and imaged the ice and sea floor (Fig. 3).

Fig. 2: Sea-floor bathymetry shows smooth retreat and ice–bed interactions near the TEIS GL.


a
T1
b
d
T2
2011
N
75.21° S
480
528
564
Depth
(m)
2016–2017
GL
Flow line
104.80° W
75.22° S
0
250 m
0
50 m
c
0
50 m
104.780° W
75.214° S
0
50 m
e
7.5 m

The sea-floor bathymetry near the TEIS GL is characterized by along-flow ridged bedforms having several different wavelengths, as well as evidence for two possible former GL positions (white and red boxes) and channelized subglacial outflow (black box). Data in **a**–**d** are from downward-facing bathymetric sonar and **e** from forward sonar on Icefin. Reworked sediments (white box) are observed near the borehole (yellow circle). **b**, A single sinuous 2–3-m-tall slope consistent with a GL sediment wedge is found about 200 m north of the 2016 GL estimated from remote sensing (red boxed region from **a**; red arrows denote wedge). The wedge crosscuts the 2–5-m wavelength along-flow bedforms (Extended Data Figs. 5 and 6). **c**, An isolated 4-m-deep channel cut into the sea floor makes two sharp turns and includes a segment that cuts perpendicular to most bedforms, suggesting that this feature formed from rerouting of subglacial water as the GL retreated (Extended Data Fig. 5). **d**, The bedform topography near the GL of T2 shows evidence of linear ridges striking north (Extended Data Fig. 4). **e**, Forward-looking sonar data of the ice base near the GL shows that the ice has the same 2–5-m-wavelength ridges as the shortest-wavelength features on the sea floor. These data together suggest that GL retreat has been largely continuous over the observable period, since at least 2011 based on remote sensing. Moreover, the similarities between the bed and ice morphology at the GL suggest that the ice–bed interactions set up slopes that are then progressively melted by the intruding seawater. Bathymetric sonar, **a**–**d**, was processed in Qimera and projected using QGIS. Forward sonar are projected using the Oculus ViewPoint software.

Fig. 3: Ocean conditions influence ice base morphology, which varies with distance from the GL.



The Icefin vehicle track is shaded by relative along-track distance from downstream (white) to upstream (black). Light-blue data denote regions with cooling and freshening in terraces and dark blue denotes the coldest/freshest data observed. **a**, Conditions in the near-GL water cavity show the influence of melting (freshening) close to the GL along T2 (left). Coloured stars denote close passes to the ice that also have distinct signatures of mixing and melting. Vertical profiles of thermal driving ($\Theta - \Theta_f$), absolute salinity (S_A) and dissolved oxygen (DO) binned with distance from the ice base show complex signatures that vary with location (Extended Data Fig. 3), suggesting the influence of both melting and SGW outflow (centre). Imagery near the GL (red box) shows ridged ice topography and sediment-laden clear basal ice at the GL (yellow star) (right). Scale bar, approximately 0.5 m. **b**, Ocean conditions in a large terrace formed in the ice base imply melting near the sidewalls (red boxes, 800 m from the GL along T2) (left). Warm, salty water (black, grey) is found along the sidewalls, whereas much

fresher and more oxygenated water with low thermal driving (cold relative to in situ freezing) collects in the terrace roof (centre). Imagery of terrace sidewalls across the TEIS uniformly show scalloped surfaces reflecting turbulent melting (Extended Data Fig. 8 and Supplementary Video 1) (right). Scale bar, approximately 0.5 m. **c**, As in **b** but for a small terrace at 2,400 m downstream along T1 that contains cold, fresh and oxygen-rich water along its roof. Here the water becomes supercooled, with ice crystals forming laterally (right) across the heavily stratified interface (red box) between this 0.1 m upper boundary layer and the warm, saline and more oxygen-poor lower ocean waters. Scale bar, approximately 0.1 m.

Conditions under the ice shelf

The ice base deepened with distance from the GL, ranging from about 500 m to 520 m below sea level over the nearly 3 km T1 survey (Fig. 1b) and sloping downward more steeply along T2 from a minimum of 475 m depth at the GL (Fig. 1c). The sea floor (prograde) also sloped downward away from the GL (Figs. 1 and 2). The temperature, salinity and dissolved oxygen content of ocean water reflects mixing of different reservoirs, including ocean, melted glacial ice (glacial meltwater (GMW)) and subglacial water (SGW) from beneath the grounded ice. Warm water occupied much of the ocean under the TEIS, with maximum thermal driving of 2.25 °C (ocean temperatures 2.25 °C above the in situ freezing point), decreasing only slightly to 2 °C within about 5–10 m of the ice base and 400 m of the GL (Fig. 1b,c). This decrease in thermal driving resulted from pressure release, a cooling of the water from 0 °C to −0.25 °C and a freshening from 34.50 g kg^{-1} to 34.40 g kg^{-1} (Extended Data Fig. 2). Dissolved oxygen, which reflects both exchange with the atmosphere before submerging below the ice and that released from melting ice, increased in concentration over this region from 4.47 ml l^{-1} to 4.50 ml l^{-1}; the coupled change in hydrographic conditions indicates a slight increase in GMW closer to the ice (Extended Data Fig. 3). The relatively well-mixed water column was overlain by a stratified upper layer, generally 5–10 m thick, at which the ocean cooled, freshened and increased in oxygen owing to local ice melt producing a greater admixture of GMW.

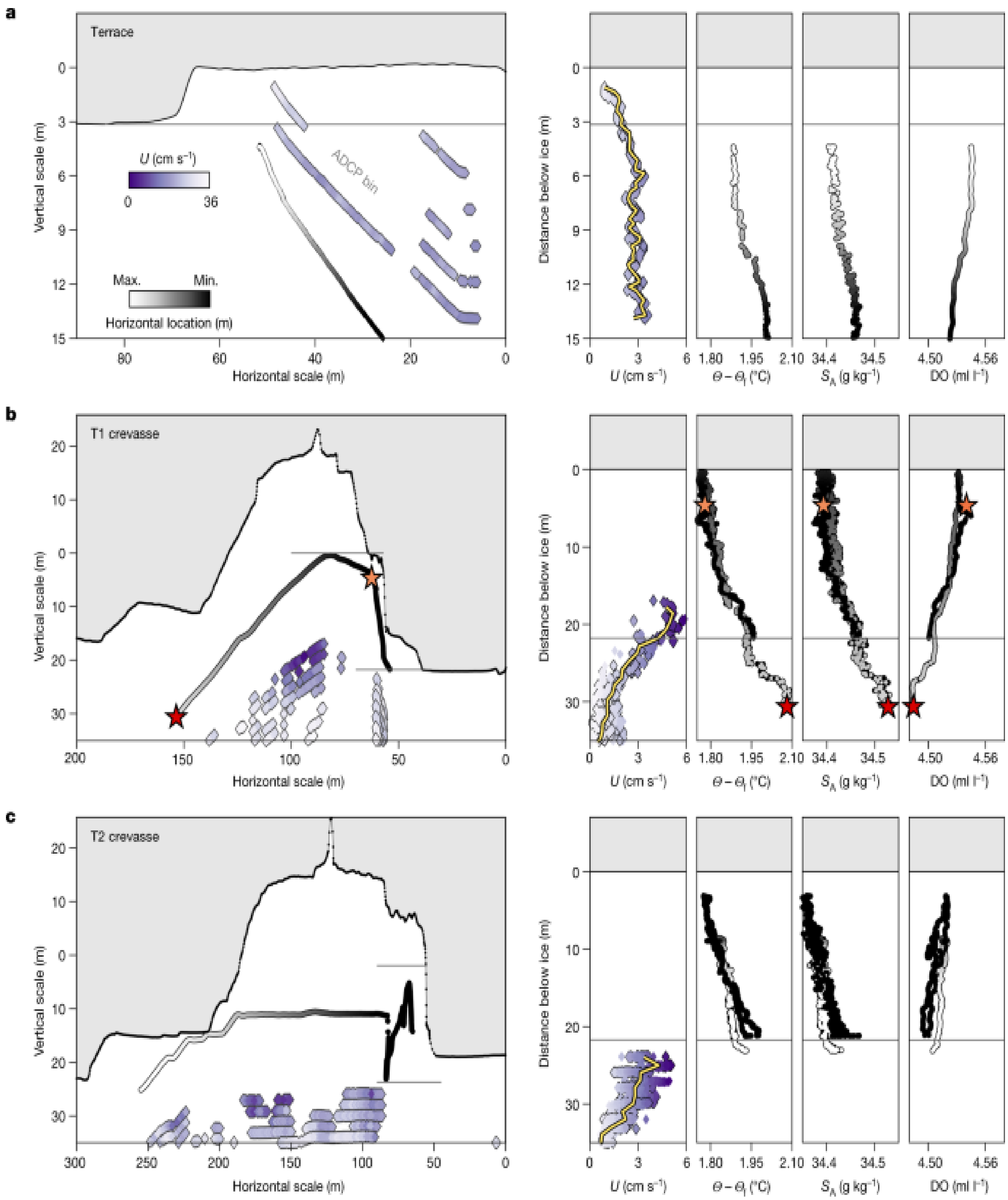
The sea floor was primarily characterized by bedform ridges oriented north–south parallel to glacier flow (Fig. 2). Sea-floor ridge–crest spacing varies by an order of magnitude from 3–25 m and tens of centimetres to 10 m heights; most ridges have 0.5–2 m heights (Extended Data Figs. 4–6). Sporadic boulders and drop stones are visible through the sediment (Fig. 3 and Supplementary Video 1). Near the borehole, troughs crosscutting the ridges suggest reworking of the sediment, which could occur if the glacier was pinned near this location that coincides with the estimated 2011 GL position[12] (Fig. 2a). Upstream of the borehole, a single semi-linear feature cuts across the along-flow ridges and crests, with a sharp step in depth of 2–3 m height (Fig. 2b); this is downstream of all estimated GL positions for 2016–2017 (ref. [12]). We interpret this feature as the sediment wedge produced when the ice shelf was grounded at this position, approximately 1,250 m from the end of the T1 survey and 1,500 m from the furthest upstream 2017 GL location. We observe no other clear evidence of GL wedges in this region. Thus, the bathymetry suggests that the GL retreated smoothly up the prograde sea floor, with only one stable location since at least 2011.

Local variations in ice-shelf basal slope (topography) influence melting through modulation of near-ice ocean-density gradients (stratification) and small-scale turbulence that control ocean heat and salt fluxes[32,33,34,35,36,37,38]. Nearest the GL, the ice base comprises a system of short-wavelength ridges (Fig. 2e) that have similar shape and 2–5-m spacing of small-amplitude (0.1–0.5 m) ridges in the sea floor (Fig. 2b–d and Extended Data Fig. 4) that overlay broad (about 50 m) topographic undulations. Within a kilometre of the GL, the ice surface is very rough, about 30% consisting of high slopes. Relatively clear ice laden with sediment, called basal ice, is found consistently in this region and in patches downstream, interrupting white, bubble-rich meteoric ice. The fine-grained (sand to mud) debris (Fig. 3a, right and Supplementary Video 1) and interspersed angular clasts ranging in size from a few to tens of centimetres comprises strong laminated layers in the basal ice at centimetre-scale spacing. Visible melting was observed throughout the region, with grains and small drop stones steadily falling out of basal ice, adding to the turbidity of the water column (Supplementary Video 1). Small terraces and scalloped morphology carved into the ice appear within 200 m of the GL, indicating

that melting rapidly erodes these sloping ice faces. The steep faces grow in vertical scale with distance from the GL, showing progressive evolution of the shape of the ice from melting the longer it is exposed to the warm ocean.

The rough ice base observed at the GL erodes downstream, giving way to steep-sided, flat-roofed terraces (Figs. 1 and 3). The walls of these features form up to 90° angles to their flat roofs and keels, rising tens of centimetres to more than 6 m in height (Fig. 1b,c) and uniformly exhibiting scalloped surface textures (Fig. 3b, right), indicative of turbulent ocean-driven melting[33]. Terraces are also observed in crevasses. Conversely, the downstream ice under the TEIS is extremely flat, with surface slopes less than 5° (Figs. 1, 4 and 5). Ice-shelf basal topography carved by melt has been observed elsewhere, such as keels and channels[29,39,40,41,42], including terraces at nearby Pine Island Glacier[29] associated with steep slopes along marginal and channel features that were argued to form by means of feedback between slopes and melting. We observed terraces distributed across the TEIS, in many different orientations and across a range of horizontal and vertical scales, both associated with and independent of other basal features. Our observations argue that terraces are widespread basal features of ice shelves that overlay warm ocean cavities; these are not yet represented in most ice-shelf models.

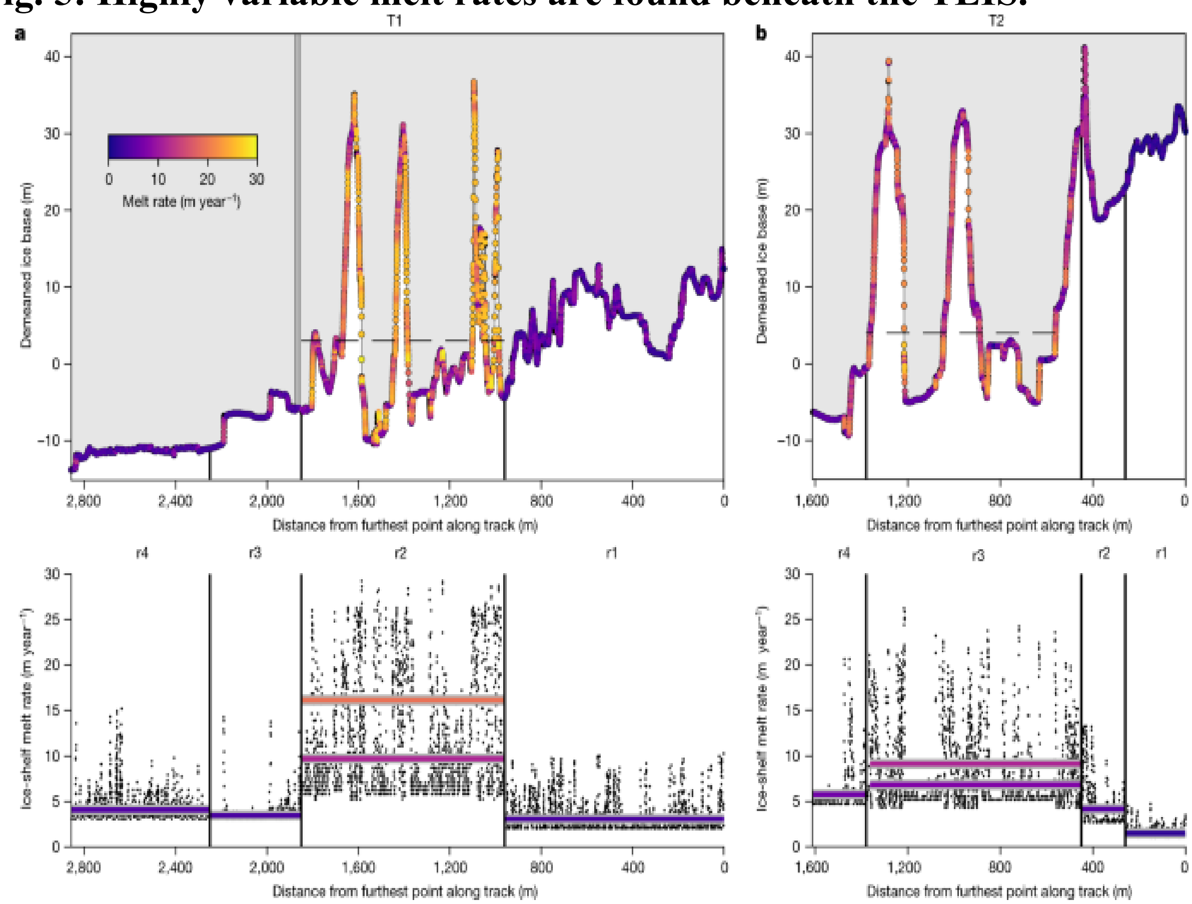
Fig. 4: Ocean currents and ice topography contribute to variable melting in terraces and crevasses.



Here the Icefin vehicle track is shaded by relative along-track distance from downstream (white) to upstream (black) and current velocities are shaded from slowest (white) to fastest (purple). **a**, Horizontal and vertical trends near a corner of a wide terrace (1,900 m downstream in T1 near the borehole) show freshening and cooling water inside the terrace and slowing currents as the water feels the influence of the ice interface. The grey lines

denote the bottom of the terrace. Vertical profiles of ocean-current speed (U), thermal driving ($\Theta - \Theta_f$), absolute salinity (S_A) and dissolved oxygen (DO) binned with distance from the ice base show that, although the water is warm close to the interface, the current velocity slows in the boundary layer, suggesting breaking from friction at the interface[28]. **b**,**c**, As in **a** for the furthest crevasse from the GL, observed along both T1 (**b**) and T2 (**c**). The panels on the right are binned with distance from the top of a step in the crevasse sidewall along T1 marked with the upper grey line. The lower grey line indicates the elevation of the bottom of the crevasse in T1. Stars in **b** relate to the location in the left panel. These panels show warm water with thermal driving of nearly 1.8 °C ($\Theta - \Theta_f$) reaching the crevasse walls accompanied by very slight freshening and oxygen increase that indicate melting (S_A and DO) that would then rise into the crevasse.

Fig. 5: Highly variable melt rates are found beneath the TEIS.



a,**b**, Estimates of the spatially varying ice-shelf melt rate are shown for each of four subregions along T1 (**a**) and T2 (**b**) (r1–r4 are the same regions as in

Extended Data Table 2). The ice surface is coloured by melt rate calculated along each slope (top panels) from the three-equation parameterization (Methods) under regionally averaged ocean conditions, demonstrating the increased melt rate along steep slopes. Horizontal coloured lines (bottom panels) correspond to the mean melt rates in each region. For regions r2 in T1 and r3 in T2, two means are presented, as conditions were observed to change with height in the crevasses, in which the water higher in the crevasses was colder and fresher than the water lower in these features. The lower bar indicates the melt rate determined by variable ocean forcing in the upper crevasse above the dashed lines in the top panels; the upper bar represents the mean melt rate below the dashed line in the crevasses. The means for each of these regions are as follows: T1: r1: 3.07 m year^{-1}; r2: 16.16 m year^{-1} (below dashes), 9.72 m year^{-1} (above dashes); r3: 3.48 m year^{-1}; r4: 4.11 m year^{-1}; T2: r1: 1.47 m year^{-1}; r2: 4.18 m year^{-1}; r3: 9.12 m year^{-1} (below dashes), 6.82 m year^{-1} (above dashes); r4: 5.76 m year^{-1}.

Ice–ocean interactions

In situ observations of the undisturbed ice–ocean boundary layer beneath ice shelves are inherently difficult to make through boreholes owing to contamination from the heated freshwater used to drill the access hole. Before this work, no in situ measurements existed that could constrain behaviour at the GL. To make these observations, we drove Icefin along the base of the ice to capture the boundary layer along flat interfaces, at an angle towards and then contacting the ice to measure gradients up to the ice, and straight into vertical sidewalls, in some cases measuring within about 5 cm of the interface.

Throughout the region, thermal driving was about 1.75 °C within 1 m of the ice base, providing ample heat to drive melting (Methods). Generally, the near-ice water column under the TEIS closely fits the well-defined mixing lines between GMW and a source water mass, and observations imply fully developed turbulent mixing[35,37] (Methods and Extended Data Fig. 3), although data nearest the ice reflect increased melt. Our observations show strong vertical stratification approaching flat portions of the ice–ocean interface containing GMW formed from melting along neighbouring slopes rising to the ice base (Figs. 3 and 4). Ocean currents weaken within 5 m of

the ice from a background speed near 3 cm s^{-1} (ref. [28]) to near zero close to the interface (Fig. 4a). By contrast, currents increased in crevasses to a measured maximum of 5.90 cm s^{-1} (Fig. 4b,c).

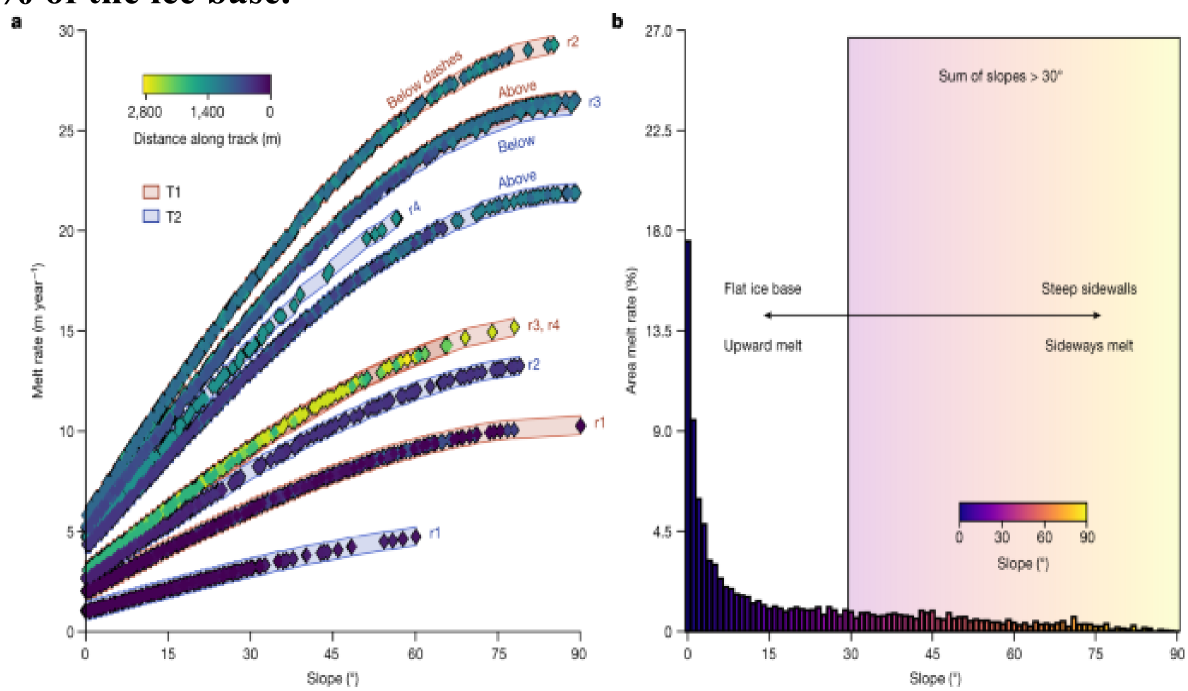
In the terraces, dissolved oxygen increases with decreasing temperature and salinity, consistent with input from melting ice. Some of the strongest stratification we observed was in a shallow terrace formed along the roof of another large terrace, at which the salinity of the boundary layer was 20 g kg^{-1}, or roughly one-third fresher than the surrounding ocean water. Extremely fresh layers (36–42% freshwater) in recesses along terrace roofs are not fully turbulent, as salinity and dissolved oxygen exhibit much larger signatures than temperature, suggesting a regime in which diffusive processes control heat and salt flux[43]. The thicknesses of these fresher layers are on the order of tens of centimetres and probably reflect the transition between the fully turbulent outer and viscous inner portions of the ice–ocean boundary layer[44].

The water closest to the GL is cooler and fresher than the surrounding ocean (excluding freshwater in terrace roofs), with a dissolved oxygen signature distinct from elsewhere in the region. These data have a shallower temperature–salinity (*T*–*S*) slope of 2.05 °C (g kg^{-1})$^{-1}$ than the melt mixing line (roughly 2.5 °C (g kg^{-1})$^{-1}$) and decrease in dissolved oxygen with freshening (Extended Data Fig. 3). This admixture of fresh, oxygen-poor water suggests the presence of discharged SGW from upstream of the GL[45]. Although no SGW source is observed directly, bathymetry near the GL along T1 suggests a recent subglacial channel (Fig. 2c), and SGW outflow measured downstream varies over time[28]. Estimates of SGW concentration calculated from *T*–*S* and DO–*S* properties indicate maximum values of 7 ml l^{-1} and 24 ml l^{-1}, respectively. The much higher SGW estimate implied from DO–*S* suggests that the debris-laden basal ice prevalent near the GL is also low in oxygen (such as ref. [45]) and originated as SGW that was accreted in the overdeepened basin further upstream (Extended Data Fig. 7).

To test the impact of melting in the region, we calculated melt rates assuming shear-driven turbulent mixing, according to local-ice base slope and using current speeds and hydrographic conditions that were averaged over regions with similar conditions (denoted in Fig. 5). We compared these

to results from three autonomous phase-sensitive radio echo sounders (ApRES) and the oceanographic mooring at the borehole[28] (Fig. 5 and Methods). This approach using regionally averaged ocean conditions (Methods) yields average upward melt rates of 5 m $year^{-1}$, but melt in the region is highly variable (Figs. 5 and 6). The stratification suppresses melting along flat interfaces, whereas estimated melt rates along vertical faces approach 30 m $year^{-1}$.

Fig. 6: The ice-shelf melt rate is strongly slope-dependent and steep slopes contribute up to 27% of the ice loss under the TEIS along only 9% of the ice base.



a, Estimated spatially varying ice-shelf melt rates along T1 and T2 show the strong influence of local slope. Here each curve consists of individual melt-rate data points that have been calculated using the regionally averaged ocean conditions (Methods) corresponding to the regions labelled in Fig. 5. Red curves are from T1 and blue curves are from T2. **b**, Sideways melting along slopes greater than 30° contributes an estimated 27% of the melting under the TEIS, whereas these slopes account for only 9% of the ice base. Upward melting along low slopes is still the most notable source of melting, in which slopes less than 30° account for 73% of melting, while representing 91% of the ice.

Although stratification suppresses melting upward (moderate vertical melt or thinning), higher lateral turbulent mixing[46] and destabilizing rising GMW[36,47,48] allows warm water to reach sloped surfaces and promote melting (high sideways melt; Figs. 5 and 6). The scalloped ice surfaces observed only on steep faces is consistent with high sideways melting (Fig. 3b and Extended Data Fig. 8). Melting is strongest along the near-vertical walls of crevasses, at which water 1.8 °C above freezing was observed reaching within 1 m of the vertical crevasse wall (Fig. 4b). Water cools with height in the middle of the crevasses, freshens and becomes more oxygenated, suggesting a local accumulation of meltwater exceeding 3 ml l^{-1} from the erosion of the crevasse walls. Currents were faster in the crevasses by up to a factor of two compared with the background[28], with flow speeds reaching about 6 cm s^{-1}. These observations imply melt rates along the crevasse sidewalls of up to 43 m $year^{-1}$ in one crevasse at the location of these observations (Methods), whereas melting elsewhere is more suppressed (Fig. 6; ref. [28]).

Topographic controls on ice-shelf evolution

These results indicate that ice–ocean interactions under the TEIS are influenced by even small-scale ice topography, which would extend to other warm-based ice shelves in which low to moderate current speeds allow high levels of near-ice ocean stratification to persist. We calculate moderate average upward melting along flat surfaces at 5 m $year^{-1}$, which matches measured melt rates on similar interfaces from three long-term ApRES and mooring data[28] and are consistent with the historical estimates from ice-penetrating radar[18]. Nearest to the GL along each survey line, melt rates average 2 m $year^{-1}$ but range from 1 to 10 m $year^{-1}$ (Figs. 5 and 6). Our observations show that the feedback between ice slope and melting is relevant to the entire base of ice shelves, including near the GL. The varied topography of the ice base at the GL, carved as it flowed over the bed before reaching the ocean, becomes a broadly distributed network of sloped ice surfaces along which melting is promoted.

Our observations suggest that melting along sloped ice is an important factor in the total ice loss near the GL of Thwaites Glacier. In the region surveyed,

27% of the total melting occurs along slopes that are greater than 30° (Fig. 6). Because crevasses funnel water through them[28] at rates that can efficiently transfer heat and salt into the steep crevasse walls (Fig. 4), these locally high melt rates should widen both crevasses and basal rifts across the glacier, including the TGT and the TEIS, and could contribute to increased calving of the glacier[8,10]. The rough topography near the GL may enable melting to persist in this region despite low current speeds. Our work implies that basal melting of warm-based ice shelves is heterogeneous and exploits ice topography inherited from interactions with the bed and formed by crevassing. Such effects are challenging to observe, not yet captured in models of GL retreat and probably contribute to the loss of ice elsewhere along the Antarctic coast.

Methods

Icefin vehicle

The Icefin vehicle[49] is a modular, hybrid, remotely operated vehicle with autonomous capabilities that was designed for use through holes bored or melted in ice (Extended Data Fig. 1). For this work, Icefin was fitted with sensors for scientific analysis of the ice–ocean system and navigation (Extended Data Table 1). Most water-column sensors are located in the vehicle nose to provide undisturbed water flow. Forward cameras, lights and sonar provide perception for science and navigation, and bathymetric sonar maps sea-floor geometry. A high-definition camera and Doppler velocity logger (DVL) with acoustic Doppler current profiler (ADCP) point in the same sense, and altimeter in the opposite sense, in the navigation module that can be oriented down (sea-floor facing) or up (ice facing). A rear-facing camera monitors the tether/tail. Guidance, navigation and control of Icefin allow for geolocated scientific data through the fusion of an advanced fibre-optic gyroscope inertial measurement unit, compass, DVL, altimeter and pressure sensor providing low-level motion control and high-level localization. The five thrusters provide five degrees of freedom movement, control pitch, yaw, heave and sway without protruding surfaces, and permit hovering. Icefin is rated to 1.5 km depth, weighs 120 kg in air, is 23 cm wide and 4.5 m long. At the TEIS, Icefin was deployed vertically from an articulating launch and recovery system, lowered through the borehole by

means of a 3.5-km-long 4-mm-diameter Kevlar-reinforced (1,800 lb breaking strength; Linden) fibre optic attached to a strength-enforced termination at the vehicle, enabling control, communication and data retrieval.

Icefin was deployed for five 6–8-h missions during 11–14 January 2020 to map environmental gradients in cross-section extending seaward from the GL, overlapping surface, airborne and ApRES surveys. The Icefin data are grouped into two composite profiles, transect 1 (T1) and transect 2 (T2); T1 consists of missions 1 (about 1.2 km south), 2 (about 1.9 km south) and 3 (about 1 km north) and T2 is mission 4 (about 1.6 km southeast). Missions 1-4 were conducted with the navigation module down and mission 5 with the navigation module up. Multipath in the clear basal ice reduced vehicle positioning accuracy in mission 5. T2 intersected the GL at 104.780° W, 75.214° S. For missions 1 and 3, the vehicle conducted survey segments alternating between pitching up towards the ice and down towards the sea floor at about 20–30° to acquire hydrographic profiles while making forward progress, similar to ocean gliders.

Post-processing of hydrographic data

Hydrographic data come from three sensors on Icefin: conductivity–temperature (*C*–*T*), pressure (*P*) and DO sensors. All sensors were factory calibrated before the fieldwork. *C*–*T* and DO sensors were field calibrated. Pressure measurements (1 Hz) were interpolated to match the 5-Hz *C*–*T* data to derive hydrographic variables. DO measurements (1 Hz) were not interpolated.

Data post-processing

1. 1.

   Remove background atmospheric pressure,

2. 2.

Remove outliers ±2 standard deviations from mean for *C*–*T* and DO (excluding borehole data),

3. 3.

Apply three-point weighted mean filter to *C*–*T*, *P* and DO,

4. 4.

Align *C* and *T* measurements with time lag (0 s lag produced the best results),

5. 5.

Remove *C*, *T* and DO data for vehicle speeds <5 cm s^{-1},

6. 6.

Derive hydrographic variables (conservative temperature, absolute salinity, density and so on) using TEOS-10 (ref. [50]),

7. 7.

Remove pressure/salinity effects on DO[51].

Post-processing ocean-current speeds

Ocean-current speeds are derived from the onboard DVL/ADCP, which calculates the *X*, *Y* and *Z* vehicle velocities (major, minor and vertical axes) and retrieves water-column velocities in 2-m bins at a variable start distance from the vehicle. The minimum altitude from an interface for current profiling to occur is 10 m; gradients in vehicle pitch, roll, heading and speed dictate the distance of the first bin from the vehicle and sampling frequency (maximum 5 Hz). We subsample velocities to 1 Hz. Water-column *X* velocities are differenced from the vehicle velocity, resulting in an uncertainty of ≤1 cm s^{-1}. Vehicle *Y* and *Z* velocities are substantially lower than *X*, so *Y* and *Z* velocity uncertainties are likewise lower. Here we only analyse *X* and *Y* velocities.

Data post-processing:

1. 1.

   Remove data in out-of-range bins (for example, below sea floor, above ice base),

2. 2.

   Remove spurious data: exactly 0 m s^{-1} or 32,767 m s^{-1},

3. 3.

   Remove measurements when vehicle pitch or roll >+/−30°,

4. 4.

   Convert from vehicle reference frame to geographic reference frame,

5. 5.

   Apply 30 s mean filter,

6. 6.

   Filter for gradients <1 standard deviation from mean vehicle speed, pitch, roll and individual bin velocity,

7. 7.

   Collate bins by each up/down vehicle swoop into 1-m vertical bins, removing data >1 standard deviation of the mean for that range.

Post-processing of ice and sea-floor elevations

Ice-base and sea-floor elevations are derived from DVL and altimeter data and bathymetric sonar data. The DVL takes into account pitch, roll and heading when producing ranges and the altimeter and sonar data are

corrected for these attitudes. Bathymetric sonar was processed in Qimera, in which obvious outliers were filtered or cleaned by hand.

Data post-processing (DVL, altimeter):

1. 1.

   Remove data >2 standard deviations of the mean gradient in interface elevation (ice base or sea floor),

2. 2.

   Manually remove outliers.

After post-processing, 94% of ice-base measurements had horizontal resolution 26 ± 14 cm, with minimum and maximum spacings of 1.4 mm and 3.38 m, respectively. Ninety-three percent of sea-floor data had horizontal resolution 29 ± 20 cm and minimum and maximum spacings of 2.3 mm and 4.72 m, respectively.

Water-mass partition

We use a three-point endmember partition[35] to estimate concentrations of water masses below the shelf, which assumes that hydrographic properties (Θ, S_A and DO) reflect a mixture of three water masses:

1. 1.

   A source water mass (SRC) responsible for driving melt: $\Theta = -0.21$ °C, $S_A = 34.50$ g kg^{-1}, DO = 4.48 ml l^{-1},

2. 2.

   GMW from local ice-shelf melt: $\Theta = -92.50$ °C, $S_A = 0$ g kg^{-1}, DO = 25.20 ml l^{-1},

3. 3.

SGW discharged from upstream beneath the grounded glacier[52]: $\Theta = -0.34$ °C, $S_A = 0$ g kg^{-1}, DO = 1.61 ml l^{-1}.

This partition uses conservative tracers that only vary as a result of a physical mixture of water masses and mix under fully turbulent conditions[35,37]. Subsets of the data not in a fully turbulent mixing regime are excluded from the partition. These data are easily identified by double-diffusive characteristics—large changes in S_A (and DO) relative to Θ that result from faster molecular diffusion of heat than salt[43,44].

The source water mass (SRC, red star in Extended Data Fig. 3 and Fig. 4b) is the warmest, saltiest and most oxygen-depleted point in the *T*–*S* and DO–*S* space that fits the GMW mixing line on which our data lie: *T*–*S* and DO–*S* slopes of −2.49 °C (g kg^{-1})$^{-1}$ and 0.60 ml l^{-1} (g kg^{-1})$^{-1}$, respectively. SRC generally resides 10 m below the ice base (outside crevasses). Warmer, saltier and more oxygen-depleted data (red data in Extended Data Fig. 3) further down in the water column exhibit a different slope in the *T*–*S* (−2.74 °C (g kg^{-1})$^{-1}$) and DO–*S* (0.35 ml l^{-1} (g kg^{-1})$^{-1}$) space, suggestive of mixing processes not derived from local glacial modification. Thus, SRC hydrographic properties represent the local water mass melting the ice shelf, referred to as a composite tracer[35]. SRC is a derivative mixture of modified CDW and winter water that resides around the depth of the highly variable pycnocline separating these water masses in Pine Island Bay. Relatively weak inflow of about 3 cm s^{-1} into our study region and at a distance of about 75 km from Pine Island Bay[28] results in a ventilation period of around one month for SRC. During this time Θ, S_A and DO properties could be altered through interaction with the ice base along other sections of the TEIS, consumption by organisms or mixture with other water masses. We forgo choosing hydrographic properties for the absolute source water mass to ensure that the properties used in our three-point water-mass partition are conservative for local ice–ocean interactions.

The Θ and S_A values for GMW consider the latent heat loss associated with phase change from solid to liquid freshwater. An extrapolation of the Gade or GMW mixing line[35,37] for our data to 0 g kg^{-1} results in an effective temperature of −86.46 °C. GMW is high in DO because of air bubbles in

meteoric ice that dissolve into solution when melted. An extrapolation of the DO–S mixing line to 0 g kg^{-1} for our data results in a DO concentration of 25.20 ml l^{-1}.

The Θ and S_A values for SGW represent freshwater at the pressure-depressed freezing point at GL depth of 480 m in T2 (Fig. 1c). We use in situ DO measurements from Lake Whillans, West Antarctica[45] for the SGW endmember, as active subglacial lakes exist upstream of the TEIS[53,54,55]. Thus, we expect that basal ice here should carry similarly low DO.

Three-equation melt parameterization

We estimate ice-shelf melt rates along T1 and T2 using the three-equation boundary layer (BL) parameterization for heat and salt transfer between the ocean and ice[56], which assumes that shear-driven turbulence controls ice melt as the dominant mechanism conveying heat and salt to the viscous sublayer (VSL), beyond which molecular diffusion operates[57]. Near-ice ocean-current measurements exhibit shear (Fig. 4a), which agrees with the physics governing Ekman layers[28] and is consistent with shear-driven turbulence.

This assumption does not hold for regions with low current speeds, at which molecular processes and diffusive convection dictate heat and salt fluxes at distances greater than the typical VSL[44,58], order several millimetres[56]. We only observed such conditions in two small regions along the roofs of two terraces with extremely fresh layers ($S \approx 20$ psu) tens of centimetres thick (Fig. 3b,c) that did not hold fully turbulent mixing lines and exhibited larger salinity gradients than temperature. Other near-ice ocean data did not exhibit these thick, fresh layers but instead gradually cooled and freshened towards the ice throughout the surveyed area. This density change stabilizes the BL beneath regions of the ice base, reducing vertical shear-driven turbulent mixing[59]. Therefore, although shear-driven turbulence dominates heat and salt fluxes, turbulent fluxes are modified by stratification[47,60]. We account for stratification in our melt rates.

The three-equation BL parameterization is as follows:

$${T}_{{\rm{B}}}=a{S}_{{\rm{B}}}+b+c{p}_{{\rm{B}}}$$
(1)

$${Q}_{{\rm{O}}}^{{\rm{T}}}-{Q}_{{\rm{I}}}^{{\rm{T}}}={Q}_{{\rm{Latent}}}^{{\rm{T}}}$$
(2)

$${Q}_{{\rm{O}}}^{{\rm{S}}}-{Q}_{{\rm{I}}}^{{\rm{S}}}={Q}_{{\rm{Fresh}}}^{{\rm{S}}}$$
(3)

Equation (1) represents temperature, practical salinity and pressure at the ice–ocean interface, in which $a = -5.73 \times 10^{-2}$ °C (g kg^{-1})$^{-1}$, $b = 9.39 \times 10^{-2}$ and $c = -7.53 \times 10^{-8}$ °C Pa^{-1} are constants and $T_{\rm B}$ is always at the freezing point. $T_{\rm B}$ and $S_{\rm B}$ are not directly observed and are estimated below.

Equation (2) represents the heat flux balance and equation (3) represents the salt flux balance, in which ${Q}_{{\rm{O}}}^{{\rm{S}}}$ is the ocean salt flux towards the ice, ${Q}_{{\rm{I}}}^{{\rm{S}}}$ is the diffusive salt flux through the ice (0 here) and ${Q}_{{\rm{Fresh}}}^{{\rm{S}}}$ is the freshwater flux from melting. ${Q}_{{\rm{O}}}^{{\rm{T}}}$ is the ocean sensible heat flux into the ice base, ${Q}_{{\rm{I}}}^{{\rm{T}}}$ is the conductive heat flux through the ice shelf and ${Q}_{{\rm{Latent}}}^{{\rm{T}}}$ is the latent heat removed during melting:

$${Q}_{{\rm{O}}}^{{\rm{T}}}={\rho }_{{\rm{w}}}{c}_{{\rm{p}}}{u}_{* }{\varGamma }_{{\rm{T}}}(T-{T}_{{\rm{B}}})$$
(4)

$${Q}_{{\rm{Latent}}}^{{\rm{T}}}={\rho }_{{\rm{i}}}{L}_{{\rm{F}}}\dot{m}$$
(5)

In equation (4), $\rho_{\rm w}$ and T represent the density and temperature, respectively, of seawater outside the BL/VSL. For seawater, $c_{\rm p} = 3{,}974$ J kg^{-1} °C^{-1}, the friction velocity u_* is the kinematic stress at the ice–ocean interface and the heat transfer coefficient $\varGamma_{\rm T}$ describes turbulent mixing of heat across the BL. The density of ice is $\rho_{\rm i} = 918$ kg m^{-3}, $L_{\rm F} = 3.34 \times 10^5$ J kg^{-1} is latent heat of

fusion and $\dot{m}$ is the ice-shelf melt rate (m year^{-1}), in which $\dot{m}$ is positive for melting. We use the quadratic stress formula to relate u_* to near-ice current speeds[61]:

$${u}_{* }^{2}={C}_{{\rm{D}}}{U}^{2}$$
(6)

in which $C_D = 2.2 \times 10^{-3}$ is a dimensionless drag coefficient assumed to be constant[27] and U is the current speed. Without a vertical-ice-column temperature profile, we vary ${Q}_{{\rm{I}}}^{{\rm{T}}}$ as 0.12–0.2 of the magnitude of ${Q}_{{\rm{O}}}^{{\rm{T}}}$ (refs. [42,62]).

$${Q}_{{\rm{O}}}^{{\rm{S}}}={\rho }_{{\rm{w}}}{u}_{* }{\varGamma }_{{\rm{S}}}(S-{S}_{{\rm{B}}})$$
(7)

$${Q}_{{\rm{Fresh}}}^{{\rm{S}}}={\rho }_{{\rm{i}}}\dot{m}({S}_{{\rm{B}}}-\,{S}_{{\rm{I}}})$$
(8)

Equations (7) and (8) resemble equations (4) and (5), in which S is salinity outside the BL/VSL, S_B is the ice–ocean interface salinity and S_I is the salinity of the ice shelf (considered 0 here). The salt transfer coefficient $\varGamma_S$ is much smaller than $\varGamma_T$, owing to slower molecular diffusion of salt than heat in the VSL[63]. We consider a range of published values for $\varGamma_S$ between $\frac{1}{70}$ and $\frac{1}{25}$ of $\varGamma_T$ (refs. [23,57,59]) and choose the ratio that produces optimal agreement between melt rates derived by the heat flux and salt flux equations.

We estimated melt rates in five subregions based on ice-base characteristics and near-ice ocean conditions T, S and U (Fig. 5). We compiled integrated probability density functions of the ocean conditions in each subregion, then consider the 25th, 50th and 75th percentiles of T and S within 5 m of the ice base and the 50th, 75th and 100th percentiles of U within 10 m of the ice base for each subregion. We select higher percentiles (and therefore speeds) for U because observed ocean currents increased towards the ice (ref. [28]; Fig. 4) before slowing from friction (ref. [28]; Fig. 4) and because less current data

were collected near the ice base. Extended Data Table 2 provides ocean properties entered into equations (4), (7) and (8). We then consider an array of ten values for the ice–ocean interface properties (T_B, S_B) by varying S_B from the minimum observed salinity to the 75th percentile of S for each subregion and then converted to T_B using equation (1) for the ice-base mean pressure.

We estimate $\varGamma_T$ by dividing the published range of the thermal Stanton number (${{C}_{{\rm{D}}}^{1/2}\varGamma }_{{\rm{T}}} = 2.18 \times 10^{-4} – 1.10 \times 10^{-3}$) from observations beneath ice shelves[24,55] by C_D, yielding $\varGamma_T = 4.60 \times 10^{-3}–2.35 \times 10^{-2}$, then considering that $\varGamma_S$ ranges between $\frac{1}{70}$ and $\frac{1}{25}$ of $\varGamma_T$. We vary $\varGamma_T$ and $\varGamma_S$ from their minimum to maximum values based on the sine of the ice-base slope, from 0° to 90°, because slope/roughness of the ice interacts with stratification to produce variable melting[36,48,63,64,65], and rising buoyant GMW also destabilizes stratification along steep ice slopes. The equations by which we calculated this are as follows:

$${\varGamma }_{{\rm{T}}}={\varGamma }_{{{\rm{T}}}_{\min }}+\left({\varGamma }_{{{\rm{T}}}_{\max }}-{\varGamma }_{{{\rm{T}}}_{\min }}\right)\sin \phi \tag{9}$$

$${\varGamma }_{{\rm{S}}}={\varGamma }_{{{\rm{S}}}_{\min }}+\left({\varGamma }_{{{\rm{S}}}_{\max }}-{\varGamma }_{{{\rm{S}}}_{\min }}\right)\sin \phi \tag{10}$$

We compared calculated melt rates to ApRES data at three locations[38]: T1 distance 2,250–2,857 m; region 2: T1 distance 1,810–1,904 m and T2 distance 1,480–1,608 m; and region 3: T1 distance 0–960 m. The set of conditions that produced the best fit to the observed melt rates along the flat (slope <5°) ice base were the 75th percentile of T and S, the 100th percentile of U and nearly the freshest S_B and warmest T_B, with heat conduction ${Q}_{{\rm{I}}}^{{\rm{T}}}=0.12{Q}_{{\rm{I}}}^{{\rm{T}}}$ and salt transfer coefficient $\varGamma_S = \frac{1}{45}\varGamma_T = 1.03 \times 10^{-4}–5.21 \times 10^{-4}$. The best-fit melt-rate estimates are: region 1: 3.41 m year^{-1} versus 3 m

year^{-1} observed; region 2: 4.80 m year^{-1} (T1) and 4.65 m year^{-1} (T2) versus 5 m year^{-1} observed; region 3: 2.37 m year^{-1} versus 2 m year^{-1} observed.

We compared stratified, shear-driven turbulent estimates to those for an assumed diffusive-convective melt rate[47], considering $Q_{\rm I}^{\rm T}=0.12 Q_{\rm O}^{\rm T}$:

$$\dot{m}=\frac{1}{L_{\rm F}\rho_{\rm i}}\left[\rho_{\rm w}c_{\rm p}k_{\rm T}\left(\frac{0.5\left(T-T_{\rm B}\right)}{3\sqrt{4k_{\rm s}t}}\right)-0.12\left(\rho_{\rm w}c_{\rm p}k_{\rm T}\left(\frac{0.5\left(T-T_{\rm B}\right)}{3\sqrt{4k_{\rm s}t}}\right)\right)\right] \quad (11)$$

in which $k_{\rm T} = 1.40 \times 10^{-7}$ m^2 s^{-1} is the molecular diffusion (conduction) of heat, $k_{\rm s} = 1.30 \times 10^{-9}$ m^2 s^{-1} is the molecular diffusion of salt and t is the amount of time that diffusive convection has driven melting. For $t = 1$ h, the diffusive-convective melt rate gives 2.26 m year^{-1} for region 1, 2.35 m year^{-1} for region 2 and 2.06 m year^{-1} for region 3. At $t = 1$ day, the melt rate decreases to 0.46 m year^{-1} for region 1, 0.48 m year^{-1} for region 2 and 0.42 m year^{-1} for region 3. At $t = 1$ week, the melt estimate decreases to 0.17 m year^{-1} for region 1, 0.18 m year^{-1} for region 2 and 0.16 m year^{-1} for region 3. Although diffusive convection melt rates initially resemble those observed, they abate to <10% of the observations within a week as the BL grows. The ApRES melt rate time series do not exhibit this decrease, showing that, although stratification inhibits turbulence, current shear still determines the melt rate along flat and low-sloped regions of the survey area.

Tuning the melt rate uniformly over the survey region overestimates melt along portions of the ice base that are in diffusive regimes and possibly in the unmapped tops of crevasses; however, this is a small fraction of the region surveyed. Ocean properties will cool/freshen with height in the crevasses and current speeds may change compared with the lower 10% surveyed (ref. [28]; Fig. 4). This approach however underestimates melt rates along steep ice slopes below the upper crevasse sections, because low $S_{\rm B}$

(22.14 psu) and therefore high T_B reduces assumed thermal forcing ($T - T_B$): the ApRES at the borehole measured lateral melt rates of 70 m year^{-1} on the terrace wall (mean slope 79°) at 1,800 m along T1, compared with 26.35 m year^{-1} estimated. Changing to a salinity of 34.28 psu (75th percentile for T1 subregion 3) obtains a melt rate of 45.97 m year^{-1}, closer to observed.

We also compared shear-driven melt rates to those from a buoyancy-driven turbulent melt-rate parameterization[36]:

$$\dot{m}=7.8{(T-{T}_{{\rm{f}}})}^{1.34}{\sin }^{\frac{2}{3}}\phi $$
(12)

in which φ is the ice slope and $T - T_f$ is thermal driving outside the BL/VSL. For slope $\varphi = 79°$, $S = 34.28$ psu and $T = -0.34$ °C (75th percentile for T1 subregion 3), the buoyancy-driven melt-rate estimate is 18.43 m year^{-1}, considerably lower than that observed and 45.97 m year^{-1} estimated from shear-driven turbulence, and does not account for \({Q}_{{\rm{I}}}^{{\rm{T}}}=0.12{Q}_{{\rm{O}}}^{{\rm{T}}}\). Ocean conditions at the opposing crevasse wall are warmer (−0.33 to −0.28 °C) and saltier (34.26–34.27 psu) than what we use to estimate melt on the terrace wall, suggesting that conditions are warmer near the ice or vertical velocities increase turbulence, increasing melt.

Statistics

All statistics were performed in MATLAB. The above sections provide the details of these statistical analyses, with the underlying mean and standard deviation functions being native to MATLAB.

Data availability

The datasets generated and/or analysed during the present study have been submitted to https://www.usap-dc.org/ and are available at https://doi.org/10.15784/601618. The processing and figure-plotting scripts are available at https://doi.org/10.5281/zenodo.7278005.

References

1. Rignot, E. et al. Recent Antarctic ice mass loss from radar interferometry and regional climate modelling. *Nat. Geosci.* **1**, 106–110 (2008).

2. Mouginot, J., Rignot, E. & Scheuchl, B. Sustained increase in ice discharge from the Amundsen Sea Embayment, West Antarctica, from 1973 to 2013. *Geophys. Res. Lett.* **41**, 1576–1584 (2014).

3. Rignot, E. et al. Four decades of Antarctic Ice Sheet mass balance from 1979–2017. *Proc. Natl Acad. Sci.* **116**, 1095–1103 (2019).

4. Scambos, T. A. et al. How much, how fast?: A science review and outlook for research on the instability of Antarctica's Thwaites Glacier in the 21st century. *Global Planet. Change* **153**, 16–34 (2017).

5. Morlighem, M. et al. Deep glacial troughs and stabilizing ridges unveiled beneath the margins of the Antarctic ice sheet. *Nat. Geosci.* **13**, 132–137 (2020).

6. Joughin, I., Smith, B. E. & Medley, B. Marine ice sheet collapse potentially under way for the Thwaites Glacier Basin, West Antarctica. *Science* **344**, 735–738 (2014).

7. Schoof, C. Ice sheet grounding line dynamics: steady states, stability, and hysteresis. *J. Geophys. Res. Earth Surf.* **112**, F03S28 (2007).

8. Miles, B. W. J. et al. Intermittent structural weakening and acceleration of the Thwaites Glacier Tongue between 2000 and 2018. *J. Glaciol.* **66**, 485–495 (2020).

9. Bevan, S. L., Luckman, A. J., Benn, D. I., Adusumilli, S. & Crawford, A. Brief communication: Thwaites Glacier cavity evolution. *Cryosphere* **15**, 3317–3328 (2021).

10. Alley, K. E. et al. Two decades of dynamic change and progressive destabilization on the Thwaites Eastern Ice Shelf. *Cryosphere* **15**,

5187–5203 (2021).

11. Rignot, E., Mouginot, J., Morlighem, M., Seroussi, H. & Scheuchl, B. Widespread, rapid grounding line retreat of Pine Island, Thwaites, Smith, and Kohler glaciers, West Antarctica, from 1992 to 2011. *Geophys. Res. Lett.* **41**, 3502–3509 (2014).

12. Milillo, P. et al. Heterogeneous retreat and ice melt of Thwaites Glacier, West Antarctica. *Sci. Adv.* **5**, eaau3433 (2019).

13. Thoma, M., Jenkins, A., Holland, D. & Jacobs, S. Modelling circumpolar deep water intrusions on the Amundsen Sea continental shelf, Antarctica. *Geophys. Res. Lett.* **35**, L18602 (2008).

14. Jacobs, S. S., Hellmer, H. H. & Jenkins, A. Antarctic ice sheet melting in the Southeast Pacific. *Geophys. Res. Lett.* **23**, 957–960 (1996).

15. Jacobs, S. S., Jenkins, A., Giulivi, C. F. & Dutrieux, P. Stronger ocean circulation and increased melting under Pine Island Glacier ice shelf. *Nat. Geosci.* **4**, 519–523 (2011).

16. Webber, B. G. et al. Mechanisms driving variability in the ocean forcing of Pine Island Glacier. *Nat. Commun.* **8**, 14507 (2017).

17. Wåhlin, A. K. et al. Pathways and modification of warm water flowing beneath Thwaites Ice Shelf, West Antarctica. *Sci. Adv.* **7**, eabd7254 (2021).

18. Schroeder, D. M. et al. Multidecadal observations of the Antarctic ice sheet from restored analog radar records. *Proc. Natl Acad. Sci.* **116**, 18867–18873 (2019).

19. Rignot, E., Jacobs, S., Mouginot, J. & Scheuchl, B. Ice-shelf melting around Antarctica. *Science* **341**, 266–270 (2013).

20. Pritchard, H. et al. Antarctic ice-sheet loss driven by basal melting of ice shelves. *Nature* **484**, 502–505 (2012).

21. Nicholls, K. W. et al. Measurements beneath an Antarctic ice shelf using an autonomous underwater vehicle. *Geophys. Res. Lett.* **33**, L08612 (2006).

22. Jenkins, A., Nicholls, K. W. & Corr, H. F. Observation and parameterization of ablation at the base of Ronne Ice Shelf, Antarctica. *J. Phys. Oceanogr.* **40**, 2298–2312 (2010).

23. Jenkins, A. et al. Observations beneath Pine Island Glacier in West Antarctica and implications for its retreat. *Nat. Geosci.* **3**, 468–472 (2010).

24. Stanton, T. P. et al. Channelized ice melting in the ocean boundary layer beneath Pine Island Glacier, Antarctica. *Science* **341**, 1236–1239 (2013).

25. Begeman, C. B. et al. Ocean stratification and low melt rates at the Ross Ice Shelf grounding zone. *J. Geophys. Res. Oceans* **123**, 7438–7452 (2018).

26. Stewart, C. L. et al. Basal melting of Ross Ice Shelf from solar heat absorption in an ice-front polynya. *Nat. Geosci.* **12**, 435–440 (2019).

27. Davis, P. E. & Nicholls, K. W. Turbulence observations beneath Larsen C ice shelf, Antarctica. *J. Geophys. Res. Oceans* **124**, 5529–5550 (2019).

28. Davis, P. E. D. et al. Suppressed basal melting in the eastern Thwaites Glacier grounding zone. *Nature* **614**, 479–485 (2023).

29. Dutrieux, P. et al. Basal terraces on melting ice shelves. *Geophys. Res. Lett.* **41**, 5506–5513 (2014).

30. Washam, P., Nicholls, K. W., Münchow, A. & Padman, L. Summer surface melt thins Petermann Gletscher Ice Shelf by enhancing channelized basal melt. *J. Glaciol.* **65**, 662–674 (2019).

31. Seroussi, H. et al. Continued retreat of Thwaites Glacier, West Antarctica, controlled by bed topography and ocean circulation.

Geophys. Res. Lett. **44**, 6191–6199 (2017).

32. Bushuk, M., Holland, D. M., Stanton, T. P., Stern, A. & Gray, C. Ice scallops: a laboratory investigation of the ice–water interface. *J. Fluid Mech.* **873**, 942–976 (2019).

33. Couston, L. A. et al. Topography generation by melting and freezing in a turbulent shear flow. *J. Fluid Mech.* **911**, A44 (2021).

34. Gwyther, D. E., Galton-Fenzi, B. K., Dinniman, M. S., Roberts, J. L. & Hunter, J. R. The effect of basal friction on melting and freezing in ice shelf–ocean models. *Ocean Model.* **95**, 38–52 (2015).

35. Jenkins, A. The impact of melting ice on ocean waters. *J. Phys. Oceanogr.* **29**, 2370–2381 (1999).

36. McConnochie, C. D. & Kerr, R. C. Dissolution of a sloping solid surface by turbulent compositional convection. *J. Fluid Mech.* **846**, 563–577 (2018).

37. Gade, H. G. Melting of ice in sea water: a primitive model with application to the Antarctic ice shelf and icebergs. *J. Phys. Oceanogr.* **9**, 189–198 (1979).

38. Malyarenko, A. et al. A synthesis of thermodynamic ablation at ice–ocean interfaces from theory, observations and models. *Ocean Model.* **154**, 101692 (2020).

39. Rignot, E. & Steffen, K. Channelized bottom melting and stability of floating ice shelves. *Geophys. Res. Lett.* **35**, L02503 (2008).

40. Alley, K. E., Scambos, T. A., Siegfried, M. R. & Fricker, H. A. Impacts of warm water on Antarctic ice shelf stability through basal channel formation. *Nat. Geosci.* **9**, 290–293 (2016).

41. Marsh, O. J. et al. High basal melting forming a channel at the grounding line of Ross Ice Shelf, Antarctica. *Geophys. Res. Lett.* **43**, 250–255 (2016).

42. Washam, P., Nicholls, K. W., Münchow, A. & Padman, L. Tidal modulation of buoyant flow and basal melt beneath Petermann Gletscher Ice Shelf, Greenland. *J. Geophys. Res. Oceans* **125**, e2020JC016427 (2020).

43. Kimura, S., Nicholls, K. W. & Venables, E. Estimation of ice shelf melt rate in the presence of a thermohaline staircase. *J. Phys. Oceanogr.* **45**, 133–148 (2015).

44. McPhee, M. G., Maykut, G. A. & Morison, J. H. Dynamics and thermodynamics of the ice/upper ocean system in the marginal ice zone of the Greenland Sea. *J. Geophys. Res. Oceans* **92**, 7017–7031 (1987).

45. Christner, B. C. et al. A microbial ecosystem beneath the West Antarctic ice sheet. *Nature* **512**, 310–313 (2014).

46. Gregg, M. C. Diapycnal mixing in the thermocline: a review. *J. Geophys. Res. Oceans* **92**, 5249–5286 (1987).

47. Rosevear, M. G., Gayen, B. & Galton-Fenzi, B. K. Regimes and transitions in the basal melting of Antarctic ice shelves. *J. Phys. Oceanogr.* **52**, 2589–2608 (2022).

48. Kerr, R. C. & McConnochie, C. D. Dissolution of a vertical solid surface by turbulent compositional convection. *J. Fluid Mech.* **765**, 211–228 (2015).

49. Meister, M. R., et al. Icefin: redesign and 2017 Antarctic field deployment. https://doi.org/10.1109/OCEANS.2018.8604725 (2019).

50. McDougall, T. J. & Barker, P. M. Getting started with TEOS-10 and the Gibbs Seawater (GSW) Oceanographic Toolbox. SCOR/IAPSO WG 127, 28 pp (2011).

51. Uchida, H., Johnson, G. C., & McTaggart, K. E. CTD oxygen sensor calibration procedures. https://doi.org/10.25607/OBP-1344 (2010).

52. Joughin, I. R., Tulaczyk, S. & Engelhardt, H. F. Basal melt beneath Whillans ice stream and ice streams A and C, West Antarctica. *Ann.*

Glaciol. **36**, 257–262 (2003).

53. Smith, B. E., Gourmelen, N., Huth, A. & Joughin, I. Connected subglacial lake drainage beneath Thwaites Glacier, West Antarctica. *Cryosphere* **11**, 451–467 (2017).

54. Malczyk, G., Gourmelen, N., Goldberg, D., Wuite, J. & Nagler, T. Repeat subglacial lake drainage and filling beneath Thwaites Glacier. *Geophys. Res. Lett.* **47**, e2020GL089658 (2020).

55. Hoffman, A. O., Christianson, K., Shapero, D., Smith, B. E. & Joughin, I. Brief communication: Heterogenous thinning and subglacial lake activity on Thwaites Glacier, West Antarctica. *Cryosphere* **14**, 4603–4609 (2020).

56. Holland, D. M. & Jenkins, A. Modeling thermodynamic ice–ocean interactions at the base of an ice shelf. *J. Phys. Oceanogr.* **29**, 1787–1800 (1999).

57. Jenkins, A. A one-dimensional model of ice shelf-ocean interaction. *J. Geophys. Res. Oceans* **96**, 20671–20677 (1991).

58. Rosevear, M. G., Gayen, B. & Galton-Fenzi, B. K. The role of double-diffusive convection in basal melting of Antarctic ice shelves. *Proc. Natl Acad. Sci.* **118**, e2007541118 (2021).

59. McPhee, M. G., Morison, J. H. & Nilsen, F. Revisiting heat and salt exchange at the ice-ocean interface: ocean flux and modeling considerations. *J. Geophys. Res. Oceans* **113**, C06014 (2008).

60. Vreugdenhil, C. A. & Taylor, J. R. Stratification effects in the turbulent boundary layer beneath a melting ice shelf: insights from resolved large-eddy simulations. *J. Phys. Oceanogr.* **49**, 1905–1925 (2019).

61. McPhee, M. G. The effect of the oceanic boundary layer on the mean drift of pack ice: application of a simple model. *J. Phys. Oceanogr.* **9**, 388–400 (1979).

62. Arzeno, I. B. et al. Ocean variability contributing to basal melt rate near the ice front of Ross Ice Shelf, Antarctica. *J. Geophys. Res. Oceans* **119**, 4214–4233 (2014).

63. Steele, M., Mellor, G. L. & Mcphee, M. G. Role of the molecular sublayer in the melting or freezing of sea ice. *J. Phys. Oceanogr.* **19**, 139–147 (1989).

64. Morlighem, M. et al. BedMachine v3: complete bed topography and ocean bathymetry mapping of Greenland from multibeam echo sounding combined with mass conservation. *Geophys. Res. Lett.* **44**, 11,051–11,061 (2017).

65. Mondal, M., Gayen, B., Griffiths, R. W., & Kerr, R. C. Ablation of sloping ice faces into polar seawater. *J. Fluid Mech.* **863**, 545–571 (2019).

66. Gardner, A. S., Fahnestock, M. A. & Scambos, T. A. MEaSUREs ITS_LIVE regional glacier and ice sheet surface velocities, version 1. Data archived at NASA National Snow and Ice Data Center Distributed Active Archive Center. https://doi.org/10.5067/6II6VW8LLWJ7 (2021).

Acknowledgements

We thank the personnel from the United States Antarctic Program and the British Antarctic Survey, without whom these data could not be collected. Fieldwork and support for analysis was provided by the NSF-NERC International Thwaites Glacier Collaboration (ITGC), financed by NSF OPP grant 1739003 (US), NERC NE/S006656/1, NERC NE/S006761/1 and NERC NE/S006427/1 (UK). We recognize the support of the ITGC staff and scientists in the execution of this ambitious field campaign. The Icefin team acknowledges past Georgia Tech team members who helped develop and field the vehicle: J. Lutz, M. 'Kit' Philleo, C. Ramey, C. Walker, J. Buffo, T. Hobbs and School of Earth and Atmospheric Sciences (EAS) chair G. Huey and the EAS staff who supported this work. The Icefin vehicle was initially developed with funding from Georgia Institute of Technology and startup

funds for B.E.S. Now in its third version, Icefin was redesigned under NASA grant NNX16AL07G, principal investigator B.E.S. The Icefin project is now located at Cornell University.

Author information

Authors and Affiliations

1. Department of Astronomy, Cornell University, Ithaca, NY, USA

   B. E. Schmidt, P. Washam, D. J. G. Dichek, A. D. Mullen, M. R. Meister, E. S. Quartini & F. E. Bryson

2. Department of Earth and Atmospheric Sciences, Cornell University, Ithaca, NY, USA

   B. E. Schmidt, P. Washam, D. J. G. Dichek, A. D. Mullen, M. R. Meister, E. S. Quartini & F. E. Bryson

3. British Antarctic Survey, Cambridge, UK

   P. E. D. Davis, K. W. Nicholls, J. A. Smith, P. Anker, C. Thomas, J. Wake, D. G. Vaughan & K. Makinson

4. Courant Institute of Mathematical Sciences, New York University, New York, NY, USA

   D. M. Holland & A. Basinski-Ferris

5. Center for Global Sea Level Change, New York University Abu Dhabi, Abu Dhabi, United Arab Emirates

   D. M. Holland & B. Yeager

6. School of Earth and Atmospheric Sciences, Georgia Institute of Technology, Atlanta, GA, USA

   J. D. Lawrence, A. Spears, B. C. Hurwitz & F. E. Bryson

7. Department of Environmental Studies, University of Portland, Portland, OR, USA

K. L. Riverman

8. Department of Geosciences, Pennsylvania State University, State College, PA, USA

E. Clyne & S. Anandakrishnan

9. Environmental Studies, Lewis & Clark College, Portland, OR, USA

E. Clyne

10. Department of Earth System Science, University of California, Irvine, Irvine, CA, USA

E. Rignot

11. Center for Remote Sensing and Integrated Systems, University of Kansas, Lawrence, KS, USA

J. Paden

Contributions

B.E.S. led the Icefin vehicle development and field team, drove the vehicle, drafted the paper and processed imaging and sonar data. P.W. participated in early-season fieldwork near McMurdo Station, analysed hydrographic data, produced figures and helped write the paper. P.E.D.D., K.W.N., D.M.H., K.L.R. and J.A.S. participated in the ITGC field campaign, helped formulate ideas and discussed analyses, J.D.L. and A.S. helped develop Icefin and the data analysis pipeline, participated in the early season field work, and discussion, E.C. participated in the field campaign and data discussion, D.J.G.D. and A.D.M. helped develop Icefin, operated the vehicle and participated in the ITGC field campaign, B.Y. participated in data discussions, P.A. developed the hot water drill and drilled the access hole, M.R.M., was lead engineer for Icefin and B.C.H., E.S.Q. and F.E.B. helped

develop and field Icefin, C.T., J.W., A.B.-F. and D.G.V. participated in the field campaign and S.A., E.R., J.P. and K.M. helped obtain funding for the project and discussed the paper.

Corresponding author

Correspondence to B. E. Schmidt.

Ethics declarations

Competing interests

The authors declare no competing interests.

Peer review

Peer review information

Nature thanks Susheel Adusumilli, Craig Lee, Craig McConnochie and the other, anonymous, reviewer(s) for their contribution to the peer review of this work.

Additional information

Publisher's note Springer Nature remains neutral with regard to jurisdictional claims in published maps and institutional affiliations.

Extended data figures and tables

Extended Data Fig. 1 The Icefin vehicle is a modular underwater vehicle designed to deploy through boreholes in the ice (diagram produced using SolidWorks).

The vehicle consists of a total of seven modules: forward science including oceanographic sensors (CTD, DO), forward-looking sonar, cameras and

lighting; forward directional thrusters; customizable science payload, shown here as configured for the Thwaites missions with a bathymetric sonar; electronics module; aft science and navigation module with DVL/ADCP, altimeter, high-definition camera and light; aft directional thruster; and rear thruster with rear camera. The fibre-optic tether mounts to a bridle at the tail of the vehicle and connects through the rear bulkhead of the electronics module, delivering live data feeds to the surface.

Extended Data Fig. 2 Salinity and dissolved oxygen generally track with temperature near the retreating GL of the TEIS.

a, As in Fig. 1, image of the TEIS, with historical GL positions in coloured lines showing notable retreat over the past two decades (QGIS map: Landsat 8, 15 m pixel^{-1}, band 8 image LC08_L1GT_003113_20200131_20200211_01_T2_B8, 31 January 2020; the red box denotes the study region); inset denotes the geographic location of the TEIS in relation to Antarctica. **b**–**g**, Hydrography of the ocean under the ice shows that absolute salinity (**d**,**e**) and dissolved oxygen (**f**,**g**) track with temperature (Fig. 1b,c) under the TEIS. The inset in **b** provides a focused view of the study region: the yellow circle denotes the location of the hot-water-drilled access hole, the red line represents T1 (5–10° oblique to the flow direction of the glacier) and the blue line represents T2 (50° oblique to flow). Triangles in **b**–**g** mark historic GL locations estimated from satellite data[12] (white, 2011; blue, 2016–2017) and shown by the Icefin bathymetric sonar data (yellow).

Extended Data Fig. 3 Salinity, temperature and dissolved oxygen profiles show signatures of melting and mixing below the TEIS.

T–*S* (**a**) and DO–*S* (**b**) diagrams compare hydrographic data from T1 and T2. Data are colourized after the data shown in Figs. 3 and 4 (with distance along track and for which blue colours denote extremely fresh section) and stars denote locations also called out with stars in Figs. 3 and 4. The warm, salty and oxygen-poor data in red are not shown in Figs. 3 or 4 but come from the outermost data from Extended Data Fig. 2 at distances greater than

10 m from the ice base. This water does not interact with the ice base in the surveyed region. Heavy lines show linear mixing lines between the source water mass responsible for melting the ice base locally (red star) and a pure mixture of GMW or SGW under fully turbulent mixing conditions[35,37,42]. These may not fully describe sheltered environments along terrace roofs, in which diffusive processes may dominate[43,44].

Extended Data Fig. 4 The bathymetry near the GL of the TEIS along the T2 survey is characterized by ridged bedforms of varying wavelengths.

a, Sonar-derived bathymetry from nearest the GL, coloured by depth, showing examples of linear ridges (after Fig. 2, bathymetry and profiles produced with Qimera and projected in QGIS). White lines denote the position of profiles found in **c** and **d**. **b**, Forward-looking sonar shows that the ice-shelf basal topography near the GL (after Fig. 2) is characterized by similar ridges, having an approximately 2.5 m ridge-crest spacing and sloped faces. Forward-looking sonar is projected in Oculus ViewPoint. **c**,**d**, Linear profiles of the bed topography across the region show evidence for ridges with approximately 1-m, 2–2.5-m and 5-m wavelengths. These data show that the shape of the ice surface at the GL is inherited from scraping over the bedforms and is later modified into terraces.

Extended Data Fig. 5 Ridged bedforms with pronounced ridge-crest amplitudes are found along the T1 survey.

a, Sonar-derived bathymetry from the borehole to the nearest approach made to the GL, coloured by depth (after Fig. 2, bathymetry and profiles produced with Qimera and projected in QGIS), in which boxes denote the sections shown in **b** and **c**. **b**,**c**, Close-up views showing details of two regions of the survey. Red (**b**) and white (**c**) lines denote the position of profiles found in **d** and **e**. **d**,**e**, Linear profiles of the bed topography showing that small-scale ridges formed across larger, longer-wavelength topography. **f**,**g**, Nearest the GL, 1-m, 5-m and 10-m wavelength along-flow ridges are observed.

Extended Data Fig. 6 Sea-floor topography suggests past dynamics influencing the retreat of Thwaites Glacier.

a, Sonar-derived bathymetry from the borehole to the nearest approach made to the GL, coloured by depth, with callouts for panels **b** and **c** (after Fig. 2, bathymetry and profiles produced with Qimera and projected in QGIS). **b**,**c**, Close-up views showing details of two regions of the survey, after Fig. 2. Red and white lines indicate the position of profiles found in **d**–**g**. **d**,**e**, Linear profiles of a crosscutting approximately 3-m-tall sinuous ridge are consistent with a past grounding event allowing enhanced sediment deposition in this area. This is the only such feature in the survey data. **f**,**g**, Linear profiles across a possible former subglacial channel near the GL. In **f**, a 5-m-deep U-shaped trough in the sediment begins parallel to ice flow but then cuts perpendicular to ice flow across lineated bed features and then turns sharply, which could be consistent with a channel incised by subglacial outflow into the sediment. In **g**, the upstream extent of the trough is less conspicuous, suggesting either modification as the ice ungrounded or that the SGW was not routed discretely through this area.

Extended Data Fig. 7 Bed elevation and ice speed for the TEIS show a changing system susceptible to GL retreat.

a, Colourized bed elevation from BedMachine v3 (ref. [64]) for the TEIS is overlaid on a Landsat 8 image with the historical GL positions (coloured lines/zones after ref. [12] are identical to Fig. 1a and Extended Data Fig. 2a, in which green is 2000, white is 2011 and blue is 2016–2017). QGIS map: Landsat 8, 15 m pixel^{-1}, band 8 image LC08_L1GT_003113_20200131_20200211_01_T2_B8, 31 January 2020; the red box denotes the study region. Note that the regions upstream of the present GL are grounded more than 800 m below sea level. **b**, As in **a** except coloured by the average 2019 seaward ice-flow speeds for this region from the 120 m pixel^{-1} ITS_LIVE remote-sensing product[66]. Note that the flow speeds increase as the ice crosses the GL and decrease near the pinning point.

Extended Data Fig. 8 Topography of terraces under the TEIS demonstrates strongly asymmetric melting and melt processes.

a–**d**, Images of a terrace upstream of the borehole along T1 show a steep, curved sidewall (**a**), flat roof (**b**), sharp transition from the wall to the flat base (**c**) and close-up of scallops in the wall show differences between modes of melting upward along the roof and base with sideways turbulent melting along the sidewall. Upward-looking views of the base (**e**) and sidewall (**f**) of another terrace downstream of the borehole show similar features. Small terraces near the GL along T1 show the initiation of scallops along smaller features in the basal ice (**g**), in which asymmetric ice melting is clear from the shape and streams of particulates (**h**,**i**).

Extended Data Table 1 The Icefin vehicle carried 11 science sensors for hydrography and ice and sea-floor measurements during the Thwaites Glacier missions
Extended Data Table 2 Regionally averaged ocean properties were used to estimate melt rates along T1 and T2

Supplementary information

Supplementary Video 1

Forward-looking video of Icefin's approach to the GL of the TEIS shows visual evidence of melting and ice–bed interactions. Clear basal ice with embedded pebbles and stones and laminated sediments is observed through the region (video clips from Icefin top forward camera over the last 200 m towards the GL of the TEIS). Variable melting causes particles and pebbles to fall from the ice. The rough, ridged ice base shows topography inherited from scraping along the sea floor as well as the initiation of small, sinuous terraces with scalloped interfaces. At the end of the video, the water column was less than 50 cm thick and the ice is observed resting on the bed in the distance in front of the vehicle.

Rights and permissions

Open Access This article is licensed under a Creative Commons Attribution 4.0 International License, which permits use, sharing, adaptation, distribution and reproduction in any medium or format, as long as you give appropriate credit to the original author(s) and the source, provide a link to the Creative Commons licence, and indicate if changes were made. The images or other third party material in this article are included in the article's Creative Commons licence, unless indicated otherwise in a credit line to the material. If material is not included in the article's Creative Commons licence and your intended use is not permitted by statutory regulation or exceeds the permitted use, you will need to obtain permission directly from the copyright holder. To view a copy of this licence, visit http://creativecommons.org/licenses/by/4.0/.

Reprints and Permissions

About this article

Cite this article

Schmidt, B.E., Washam, P., Davis, P.E.D. *et al.* Heterogeneous melting near the Thwaites Glacier grounding line. *Nature* **614**, 471–478 (2023). https://doi.org/10.1038/s41586-022-05691-0

- Received: 27 April 2022
- Accepted: 22 December 2022
- Published: 15 February 2023
- Issue Date: 16 February 2023
- DOI: https://doi.org/10.1038/s41586-022-05691-0

Share this article

Anyone you share the following link with will be able to read this content:

Get shareable link

Sorry, a shareable link is not currently available for this article.

Copy to clipboard

Provided by the Springer Nature SharedIt content-sharing initiative

Suppressed basal melting in the eastern Thwaites Glacier grounding zone

- Peter E. D. Davis
- Keith W. Nicholls
- Keith Makinson

Nature Article Open Access 15 Feb 2023

High variability reveals complexity under Thwaites Glacier

- Craig McConnochie

Nature News & Views 15 Feb 2023

This article was downloaded by **calibre** from https://www.nature.com/articles/s41586-022-05691-0

- Article
- Open Access
- Published: 15 February 2023

Suppressed basal melting in the eastern Thwaites Glacier grounding zone

- Peter E. D. Davis ,
- Keith W. Nicholls,
- David M. Holland,
- Britney E. Schmidt,
- Peter Washam,
- Kiya L. Riverman,
- Robert J. Arthern,
- Irena Vaňková,
- Clare Eayrs,
- James A. Smith,
- Paul G. D. Anker,
- Andrew D. Mullen,
- Daniel Dichek,
- Justin D. Lawrence,
- Matthew M. Meister,
- Elisabeth Clyne,
- Aurora Basinski-Ferris,
- Eric Rignot,
- Bastien Y. Queste,
- Lars Boehme,
- Karen J. Heywood,
- Sridhar Anandakrishnan &
- …
- Keith Makinson

Show authors

Nature **volume 614**, pages 479–485 (2023)

- 8039 Accesses
- 823 Altmetric
- Metrics details

Abstract

Thwaites Glacier is one of the fastest-changing ice–ocean systems in Antarctica[1,2,3]. Much of the ice sheet within the catchment of Thwaites Glacier is grounded below sea level on bedrock that deepens inland[4], making it susceptible to rapid and irreversible ice loss that could raise the global sea level by more than half a metre[2,3,5]. The rate and extent of ice loss, and whether it proceeds irreversibly, are set by the ocean conditions and basal melting within the grounding-zone region where Thwaites Glacier first goes afloat[3,6], both of which are largely unknown. Here we show—using observations from a hot-water-drilled access hole—that the grounding zone of Thwaites Eastern Ice Shelf (TEIS) is characterized by a warm and highly stable water column with temperatures substantially higher than the in situ freezing point. Despite these warm conditions, low current speeds and strong density stratification in the ice–ocean boundary layer actively restrict the vertical mixing of heat towards the ice base[7,8], resulting in strongly suppressed basal melting. Our results demonstrate that the canonical model of ice-shelf basal melting used to generate sea-level projections cannot reproduce observed melt rates beneath this critically important glacier, and that rapid and possibly unstable grounding-line retreat may be associated with relatively modest basal melt rates.

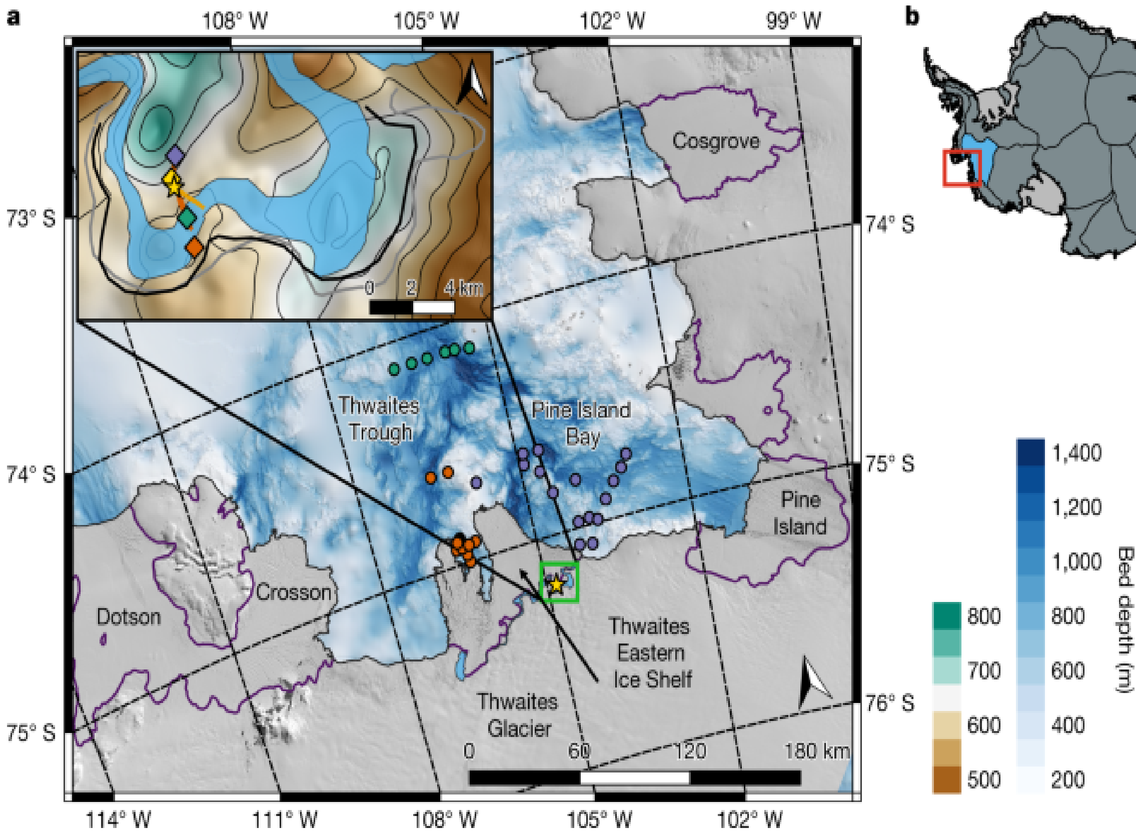
Main

The response of the marine-based West Antarctic Ice Sheet (WAIS) to a warming climate contributes substantial uncertainty to twenty-first century

sea-level projections[9]. The evolution of the ice sheet is dynamically linked to the fate of the floating ice shelves found at its seaward margin[10]. By exerting a resistive force at the grounding line where the ice sheet first goes afloat, ice-shelf buttressing helps control the flow of grounded ice into the ocean[11]. Over recent decades, elevated ocean-driven basal melting has triggered rapid thinning of many West Antarctic ice shelves[12], reducing the strength of ice-shelf buttressing[11]. The rate of ice-shelf mass loss has increased by 70% between 1994 and 2012 (ref. 12), precipitating a shift towards faster drainage of grounded ice into the ocean[13]. Several major grounding lines in the Amundsen Sea sector have retreated rapidly inland[14], raising the possibility of an unstable collapse of the WAIS[15].

Nowhere are these processes more apparent and potentially serious than at Thwaites Glacier, which drains about 10% of the WAIS[1,16] (Fig. 1). Thwaites is largely grounded below sea level on a retrograde bed[4] (that is, a bed that deepens inland) and is particularly susceptible to marine ice-sheet instabilities[2,3]. Its grounding line has retreated 14 km inland since the late 1990s[17] and, in some regions, is retreating by up to 1.2 km per year at present (ref. 18). Thwaites may have already entered a state of rapid and irreversible ice loss[3], and its complete collapse within centuries would contribute 65 cm to the global sea level[5]. A full destabilization of the main glaciers in the Amundsen Sea sector would contribute 3 m to the global sea level over thousands of years[19]. The rate and extent of ice loss from Thwaites Glacier, and whether it proceeds irreversibly, is highly sensitive to the poorly understood ocean conditions and basal melt rate in the constantly evolving grounding-zone region[6].

Fig. 1: Map of Thwaites Glacier and location of the observations used in this study.



a, Landsat 8 satellite image of Thwaites Glacier and the location of the hot-water-drilled access hole (yellow star; 75.207° S, 104.825° W) in the grounding-zone 'butterfly' region of TEIS (inset map). Blue-coloured contours with hillshade show bed depth in the Amundsen Sea from ship-based survey[49] and BedMachine[5]. The lilac, green and orange dots show the location of 2019–2020 ship-based CTD profiles from the International Thwaites Glacier Collaboration TARSAN project. The coastline (black) and grounding line (purple) are from the SCAR Antarctic Digital Database[50]. The inset map shows the detail of the grounding-zone butterfly region. Green–brown-coloured contours with hillshade show bed depth from BedMachine[5]. The blue-shaded area shows the location of the 2016–2017 grounding-zone region[18], whereas the solid black and grey lines show the position of the grounding line in 2019 and 2021, respectively. Green, purple, orange and yellow diamonds show the location of ApRES instruments measuring the basal melt rate, in addition to the ApRES located at the hot-water-drilled access hole (yellow star). The red (T1) and orange (T2) lines show the transects taken by the Icefin remotely operated underwater vehicle. **b**, Overview of Antarctica using data from MEaSUREs Antarctic

Boundaries[51] with the location of Thwaites Glacier shown by the red box. Thin black lines delineate the main ice-sheet drainage basins[52], with the Thwaites drainage basin highlighted in blue. Figure 1 was created with the QGIS Geographic Information System.

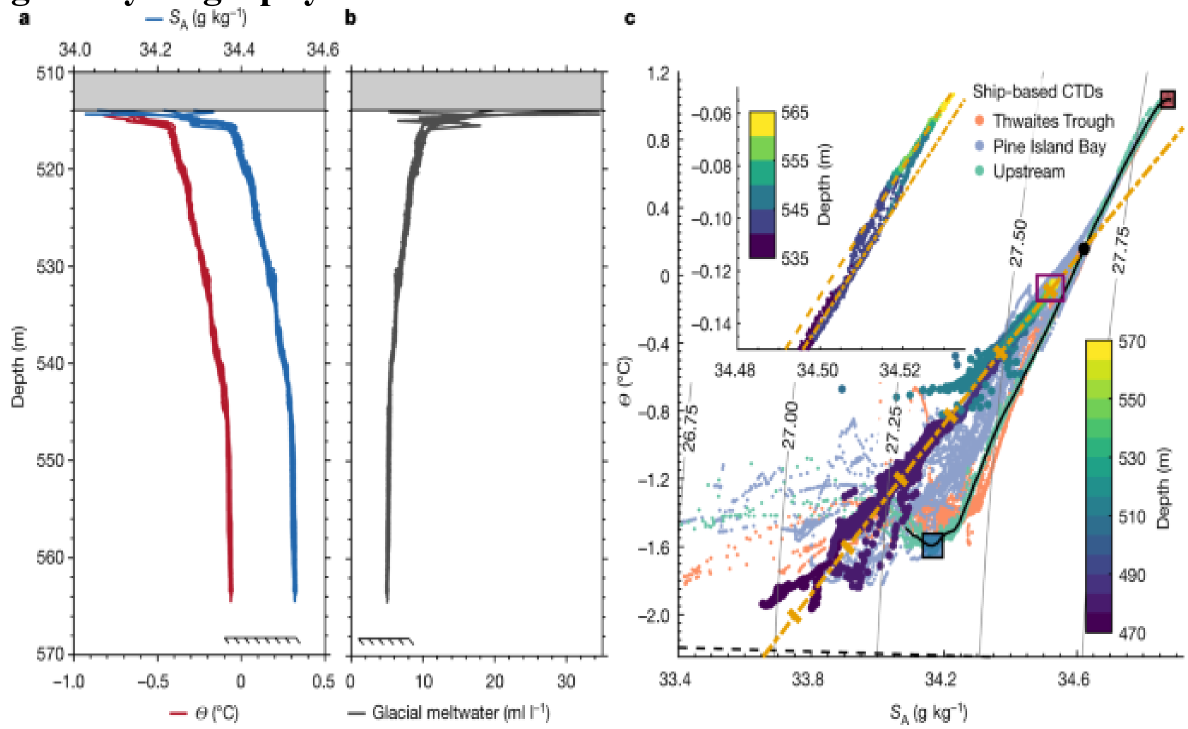
Here, to our knowledge, we present the first observations from the Thwaites Glacier grounding zone. A hot-water-drilled access hole was made through 587 m of ice approximately 1.5–2.0 km downstream of the present-day grounding line (Fig. 1) in the relatively accessible 'butterfly' region of TEIS. A borehole-deployable conductivity, temperature and depth (CTD) profiler was used to sample the hydrographic structure of the 54-m-deep water column, while the Icefin remotely operated underwater vehicle measured the spatial variability in ocean conditions all the way to the grounding line[20]. Long-term basal melt rates at five different sites (Fig. 1) were measured using Autonomous phase-sensitive Radio-Echo-Sounder[21] (ApRES) and an oceanographic mooring consisting of a current meter and a temperature–conductivity sensor was deployed 1.5 m beneath the ice-shelf base to monitor the temporal evolution of ocean properties. Wider oceanographic context is provided by ship-based CTD profiles from 2019 and 2020 (ref. [22]) (Fig. 1).

Water-column structure and hydrography

The grounding zone is characterized by warm and salty water at depth, with cooler and fresher water at the ice base (Fig. 2a). Thermal driving near the ice–ocean interface (a key parameter for controlling basal melting; see Methods) reaches 1.54 °C, similar to beneath the Pine Island Ice Shelf[23]. A highly salt-stratified basal boundary layer is seen within 2 m of the ice–ocean boundary, where the sharp gradient in absolute salinity (S_A) creates a strong barrier to vertical mixing (Extended Data Fig. 1a). Although density in the polar regions is set by salinity and thus the grounding-zone water column is stably stratified (Fig. 2c), the vertical gradient of conservative temperature (Θ) is unstable with respect to density (that is, cold water lies above warm water) and the water column might be susceptible to diffusive convection. Although this double-diffusive process could provide a limited source of energy for vertical mixing[24,25,26], with an average density ratio of

only 0.2 and a Turner angle of −57°, the temperature gradient is too weak to sustain a thermohaline staircase (Extended Data Fig. 1b; see Methods). Low variability between CTD casts indicates that lateral gradients in temperature and salinity are weak (see Methods).

Fig. 2: Hydrography and meltwater content beneath TEIS.



a,**b**, Vertical profiles of conservative temperature (Θ; red) and absolute salinity (S_A; blue) (**a**) and glacial meltwater content (grey) (**b**) collected over 4 days (9 to 12 January 2020) in the grounding-zone region of Thwaites Glacier (yellow star in Fig. 1). The ice base is indicated by the shaded grey box and the seabed is indicated by the slash-backed line. **c**, Θ–S_A diagram with σ_0 (density) contours for the grounding-zone CTD and Icefin data (large dots coloured by depth) and the ship-based CTD data from the International Thwaites Glacier Collaboration TARSAN project (small dots coloured by location: orange for Thwaites Trough, purple for Pine Island Bay and green for upstream that match the colours used to indicate their location in Fig. 1). The solid black line indicates the ambient mCDW–WW thermocline. The dot-dashed orange line indicates the meltwater mixing line that characterizes the grounding-zone data. The large black dot indicates where this meltwater mixing line intersects the ambient mCDW–WW

thermocline. The thick orange dashes on the meltwater mixing line indicate 5 ml l^{-1} intervals in glacial meltwater content, starting at 0 ml l^{-1} at the large black dot. The dashed black line indicates the in situ freezing temperature as a function of salinity at the grounding line. The red and blue boxes with black outline indicate the range of Θ and S_A values of the mCDW and WW endmembers. The inset axes in **c** show the Θ–S_A relationship coloured by depth (note the different colour scale) for the CTD data from the well-mixed benthic boundary layer (purple box in the main plot). The dashed orange line indicates the slightly warmer meltwater mixing line that characterizes the data from this region of the water column.

Basal melting is forced by a single source water mass: modified Circumpolar Deep Water (mCDW)[22]. The Icefin and borehole-based CTD data lie predominantly on a straight line in Θ–S_A space with a gradient of 2.40 ± 0.01 °C (g $kg^{-1})^{-1}$ (Fig. 2c). The gradient is consistent with that expected when glacial meltwater from ocean-driven basal melting mixes with ambient seawater[27]. The properties of the source mCDW can be determined by tracing the meltwater mixing line back to its intersection with the main mCDW–Winter Water (WW) thermocline outside the ice-shelf cavity (Fig. 2c). The source mCDW has a Θ value of 0.16 °C and an S_A value of 34.62 g kg^{-1}, with a potential density of 1,027.66 kg m^{-3}. mCDW with such density is found at a depth of around 528 m outside the ice-shelf cavity. The mCDW that feeds the grounding zone probably originates from Pine Island Bay; however, we cannot rule out a more northerly source from Thwaites Trough[22,28] (Fig. 1). In the well-mixed lower layer, the CTD data shift onto a slightly warmer meltwater mixing line (source water Θ = 0.18 °C; Fig. 2c, inset), indicating that the lower cavity is fed by a slightly warmer mCDW.

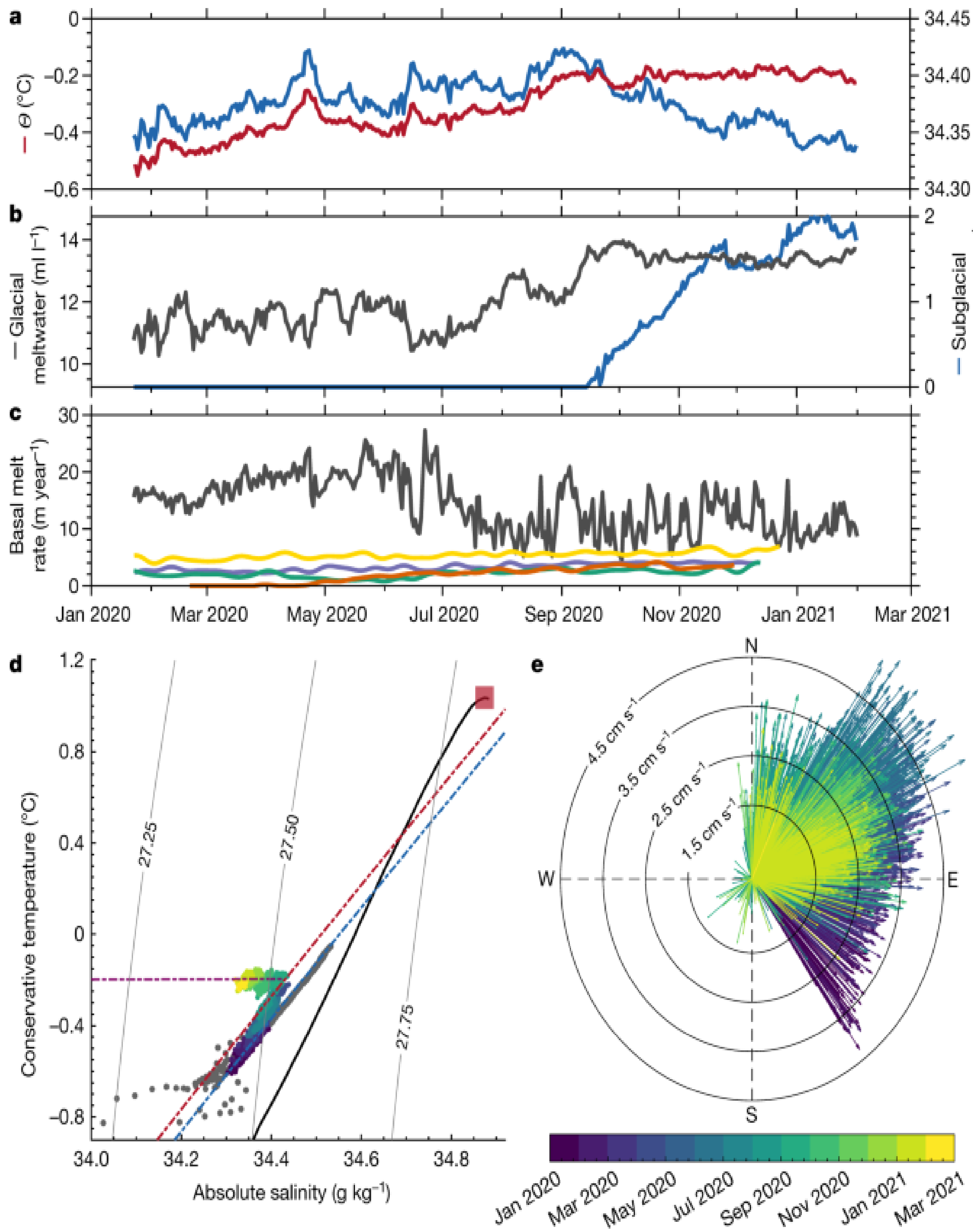
Glacial meltwater plays a central role in controlling ocean circulation around Antarctica[29]. At the borehole, glacial meltwater is found throughout the water column, with the concentration exceeding 10 ± 2 ml l^{-1} at the ice base (Fig. 2b; see Methods). The meltwater distribution indicates that ocean water at all depths has interacted with an ice-shelf base, consistent with the narrow water column and proximity to the grounding line. At the grounding line itself, the glacial meltwater concentration observed by Icefin reaches a

maximum value of approximately 31 ml l^{-1} (Fig. 2c). This is close to the saturation value of approximately 35 ml l^{-1}, at which point Θ is at the in situ freezing point and no further basal melting can occur.

Temporal variability in ocean conditions

Ocean conditions in the Amundsen Sea vary across a wide range of timescales and affect the ocean properties and basal melt rate beneath the fringing ice shelves[30,31,32]. Between January and September 2020, the grounding zone became warmer and saltier (Fig. 3a). In Θ–S_A space, the hydrographic properties evolved along a trajectory that lies at an angle to the meltwater mixing line from the CTD profile (Fig. 3d). This trajectory can only be explained by a change in the source water mass. By September 2020, the Θ and S_A values of the mCDW feeding the grounding zone increased to 0.43 °C and 34.69 g kg^{-1}, respectively, with a potential density of 1,027.70 kg m^{-3}. mCDW with this density is found at a depth of around 584 m outside the ice-shelf cavity. The depth of the seabed and the prograde bedrock slope at the borehole (Fig. 4a) prevents this denser mCDW from reaching the grounding zone directly. Instead, the mCDW–WW thermocline outside the ice-shelf cavity must have shoaled, flooding the grounding zone with increasingly warmer mCDW. Long-timescale variability in thermocline depth is largely controlled by slowly evolving trends in remote wind forcing at the Amundsen Sea continental shelf break[32]. Superimposed on the warming trend are short pulses of warming and cooling (for example, April and June 2020; Fig. 3a), which are probably driven by local wind and sea-ice forcing that modifies the ocean density and temperature structure[30,33] and generates eddies and internal waves that propagate into the TEIS cavity. During this period, thermal driving increased by 0.36 °C (Extended Data Fig. 2a), although a large proportion can be associated with the ever-increasing distance between the ocean mooring and the ice–ocean interface that results from basal melting (see Methods). At the same time, glacial meltwater concentration increased from about 11.0 ml l^{-1} to about 13.4 ml l^{-1} (Fig. 3b).

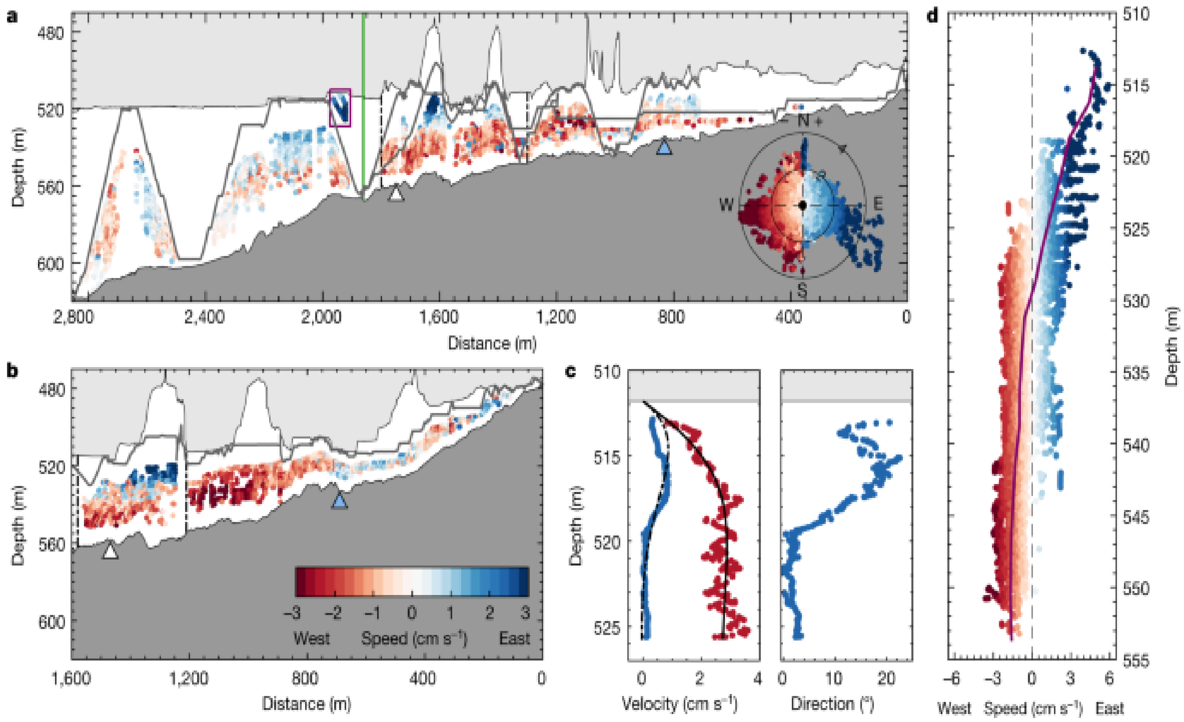
Fig. 3: Temporal evolution of hydrographic conditions, meltwater content and basal melt rate.



a, Daily averaged time series of conservative temperature (Θ; red) and absolute salinity (S_A; blue) from the ocean mooring deployed 1.5 m beneath the ice base. **b**, Glacial meltwater (grey) and subglacial runoff (blue) derived from observations of Θ and S_A. **c**, Observed ApRES basal melt rate (green, purple, yellow and orange lines) low-pass-filtered with a 15-day cutoff

plotted against the basal melt rate estimated from the three-equation melt-rate model (grey line; see Methods). The line colours for the ApRES basal melt-rate time series in **c** match their locations in Fig. 1. **d**, Θ–S_A diagram with σ_0 contours for the time series data in **a** coloured as a function of time. The blue and red dot-dashed lines are meltwater mixing lines that fit the observed data for January 2020 (blue) and August 2020 (red). The purple dot-dashed line is a mixing line between the grounding-zone Θ and S_A values in August 2020 and fresh subglacial runoff. The solid black line indicates the ambient mCDW–WW thermocline from ship-based CTD data (Fig. 2c), whereas the red-shaded box indicates the range of Θ and S_A values of the mCDW endmember. The grey dots show the CTD data from the borehole. **e**, Velocity vectors from the sub-ice current meter coloured as a function of time. Radial contours indicate flow speed in cm s^{-1}.

Fig. 4: Cross-sections and vertical profiles of current speed and direction.



a,**b**, Flow speed and direction in the grounding-zone region from an ADCP mounted on the Icefin remotely operated underwater vehicle for transect T1 (**a**) and transect T2 (**b**) (see inset panel in Fig. 1). Individual data points are coloured by flow speed, with blue colours indicating flow to the east (into

the page) and red colours indicating flow to the west (out of the page). The vehicle track is indicated by the grey line, with the ice shelf and seabed indicated by the light grey and dark grey patches, respectively. The green line in **a** marks the location of the borehole, and the purple box indicates the region of the water column plotted in **c**. Inset in **a** is geographic velocity vectors coloured by flow speed for the combined data from T1 and T2. Radial contours indicate flow speed in cm s^{-1}. Triangles in **a** and **b** mark the location of historic grounding-line locations estimated from satellite interferometry in 2011 (white) and the furthest downstream estimate in 2016 (blue)[18]. **c**, *u* eastward velocity (blue), *v* northward velocity (red) and geographic flow direction within 14 m of the ice base about 2,000 m from the grounding zone along T1 (purple box in panel **a**). The dot-dashed and solid black lines show the *u* (dot-dashed) and *v* (solid) velocity profiles from an analytical model of an under-ice Ekman boundary layer. **d**, Average velocity profile coloured by flow speed for all velocity data between 1,300 m and 1,800 m from the grounding zone along transect T1 (black dot-dashed lines in panel **a**) and between 1,210 m and 1,580 m from the grounding zone along transect T2 (black dot-dashed lines in panel **b**).

From September 2020, S_A begins to fall, whereas Θ remains constant at −0.2 °C (Fig. 3a). In Θ–S_A space, the hydrographic properties evolve along a horizontal trajectory, which cannot be explained by a change in source water mass (as meltwater mixing lines no longer intersect with the mCDW–WW thermocline). Instead, this trajectory is indicative of freshwater sourced from subglacial discharge at the grounding line (Fig. 3b,d). Subglacial waters beneath Thwaites come from basal melting of grounded ice that results from fast ice flow and large basal shear stress[34]. A persistent hydrological system exists upstream of Thwaites' grounding line[35] (Extended Data Fig. 3), along with subglacial lakes that exhibit episodic draining and filling events[36,37]. This hydrological system constantly reconfigures as a result of changes in the volume of meltwater production and glacier dynamics, and facilitates a flow of meltwater towards the grounding line in a channelized network, where it is discharged at the pressure-dependent freezing point[38,39] (Extended Data Fig. 3). Although we cannot explain the mechanisms responsible for controlling discharge events, sedimentary evidence indicates that subglacial discharge beneath TEIS tends to occur in pulses[35], consistent with the sudden onset we observe (Fig. 3b). Possible mechanisms include a

shift in the drainage network to favour discharge beneath TEIS or the onset of a subglacial lake drainage event[36,37]. Subglacial discharge is linked to changes in basal friction and ice-stream velocity, and thus has the potential to modulate ice flow into the ocean[35,38]. In addition, subglacial freshwater input will drive a complex interplay between the density-driven enhancement in sub-ice-shelf circulation that should drive stronger basal melting and strengthening boundary-layer stratification that should suppress basal melting.

Ice base current speeds are key to setting basal melt rates. At our site, flow speeds are weak, averaging 2.4 cm s^{-1} (Fig. 4a,b and Extended Data Fig. 4a). Tidal variability is limited and is dominated by diurnal constituents (Extended Data Fig. 4c and Extended Data Table 1). Flow is oriented parallel to the grounding line (Fig. 4), with cooler and fresher meltwater-laden waters flowing towards the east in the upper layer, whereas warmer and saltier mCDW-derived waters flow to the west in the lower layer. The flow direction in the butterfly region is heavily steered by topography and is not necessarily representative of the westwards flow generally expected beneath TEIS[22,28].

The magnitude of velocity, heat and salt mixing in the ice shelf–ocean boundary layer is challenging to measure and contributes substantial uncertainty when modelling the future behaviour of the Antarctic ice sheet[6]. Here we can indirectly derive the first estimate of the eddy viscosity beneath TEIS by examining the Ekman boundary layer that forms at the ice base (see Methods). Under the influence of rotation and frictional stresses, the flow direction observed by Icefin turns progressively clockwise as the boundary is approached, generating a transverse flow at the ice base (Fig. 4c). Fitting an analytical model for an under-ice Ekman boundary layer to the acoustic Doppler current profiler (ADCP) data yields an eddy viscosity of around $9 \times 10^{-4} \pm 5 \times 10^{-4}$ m^2 s^{-1}, with an Ekman depth of about 3.6 m (Fig. 4c). This same Ekman behaviour is observed by the borehole current meter but it emerges as a function of time as the distance between the ice base and the instrument increases as the basal ice melts. The flow direction persistently swings anticlockwise from southeast in January 2020 to northeast in August 2020 (Fig. 3e and Extended Data Fig. 4b), after which

the depth of the instrument exceeds the Ekman depth and the flow direction is no longer set primarily by distance from the boundary.

Ice-shelf basal melting

Despite the high thermal driving (Extended Data Fig. 2a), basal melt rates average no more than 2.0–5.4 m year^{-1} (Fig. 3c; see Methods). Low rates of basal melting have been observed since at least 2019 (Extended Data Fig. 5) and have probably persisted for much longer based on likely trends in ocean conditions (discussed in more detail later). The basal melt rate varies between sites and gradually increases with time; it is also no higher at the grounding line itself, as evidenced by an ApRES instrument that crossed from grounded to floating ice in April 2020 (orange curve in Fig. 3c). Spatial variations in the melt rate are probably associated with local flow patterns and variability in ice-shelf basal topography, as well as proximity to the grounding line, where the thinner, frictionally controlled water column with lower current speeds (Fig. 4) and weaker thermal driving[20] (Fig. 2c) restricts basal melting.

Basal melting, controlled by the rate at which turbulent ocean mixing transports heat and salt vertically to the ice-shelf base through the ice shelf–ocean boundary layer[40], is highly suppressed beneath TEIS by the strong stratification and quiescent ocean environment. Different boundary-layer turbulence regimes have been identified depending on the relative strength of the vertical current shear and buoyancy forcing: well-mixed shear controlled, stratified buoyancy controlled and diffusive-convective[8,41]. As the boundary layer beneath TEIS is characterized by weak current speeds (Fig. 4) and strong stratification (Fig. 2a), the well-mixed shear-controlled regime is precluded[42]. The temperature gradient is too weak to sustain strong diffusive-convective turbulence[26] (Extended Data Fig. 1b) and thus the transport of heat through the boundary layer is predominantly controlled by stratified turbulence dynamics[7,8]. In this regime, weak flow speeds cannot generate sufficient shear-driven turbulence to overcome the highly stable ice-base stratification, strongly suppressing the vertical heat (and salt) transport to the ice base and, ultimately, the basal melt rate, despite strong thermal forcing[7] (Fig. 2a). In the buoyancy-controlled regime beneath TEIS,

basal melting is largely rate-limited by the density stratification and current speed, which control heat transport to the ice base, rather than by the amount of heat available. TEIS already exhibits excess levels of thermal driving (that is, there is more ocean heat available than that required to maintain basal melting) and the temperature increase required to drive substantially higher basal melt rates is probably unfeasible. Instead, order-of-magnitude increases in basal melting will only be driven by a large-scale acceleration in ocean circulation or a marked weakening of the ice-base stratification.

The canonical three-equation model for ice-shelf basal melting (see Methods) is widely used to generate sea-level projections, yet it is formulated exclusively for the well-mixed turbulence regime, in which the melt rate depends solely on the product of the thermal driving and flow velocity[40]. This formulation is not appropriate for TEIS. When forced with observed current speeds and thermal driving, it predicts melt rates upward of 14 m year^{-1}, with a maximum of 32 m year^{-1}, often exceeding observed values by more than an order of magnitude (Fig. 3c). This discrepancy arises as the model approximates the turbulent transfer of heat and salt through the ice shelf–ocean boundary layer using transfer coefficients that assume no influence of stratification (see Methods). Therefore, in the stratified regime, it substantially overestimates the efficiency of heat and salt transport through the boundary layer, and thus over-predicts the magnitude of the basal melt rate[7] (Fig. 3c). Furthermore, this incorrect dependence on thermal driving and flow velocity means that the three-equation model as conventionally formulated cannot simulate the observed variability, predicting a fall in basal melt rates from May 2020 onwards owing to weaker current speeds, in contrast to the observations (Fig. 3c and Extended Data Fig. 4a). Although the transfer coefficients in the three-equation model could be reformulated to include some functional dependence on stratification, ultimately, knowledge of the vertical structure of density and velocity through the ice shelf–ocean boundary layer, knowledge that is widely lacking at present, must be incorporated into more sophisticated parameterizations to accurately predict melt rates under stratified conditions[7,8].

Much of the present-day grounding line beneath TEIS sits on a bedrock ridge that runs northeast to southwest beneath the ice shelf (Extended Data Fig. 6a). Bed depth along the grounding line is relatively constant and

generally no deeper than that in the butterfly region (Extended Data Fig. 6b). Basal melt rates throughout much of the TEIS grounding zone are therefore unlikely to be substantially higher than our observed value. The weak basal melt conditions observed here contrast with numerical models[28,43], which suggest that TEIS grounding-zone basal melt rates are an order of magnitude higher. We note that the modest melt rates we observe are not representative of the main trunk of Thwaites Glacier, which is characterized by much steeper basal slope angles and is grounded on bedrock >1,000 m below sea level (Extended Data Fig. 6b). As such, basal melting of the main trunk would be expected to be very much higher[18,44].

Despite weak basal melting throughout the TEIS grounding zone, the grounding line has retreated rapidly at a rate of 0.6–1.2 km year^{-1} between 2011 and 2017 (ref. [18]). Although the retreat rate is spatially variable, the grounding line has continued to retreat over the period covered by our melt rate observations (2019–2021), widely reaching 0.4 km year^{-1} throughout the butterfly region, with a maximum >1.5 km year^{-1} (Fig 1). Thus our observations suggest that the rapid grounding-line retreat beneath TEIS since 2011 has probably been associated with relatively modest basal melt rates. Indeed, neither the increase in thermal forcing associated with the deeper 2011 grounding line (about 0.7 °C higher; Extended Data Fig. 6c) nor the interannual variability in thermocline depth in Pine Island Bay[30,31] are sufficient to drive order-of-magnitude changes in basal melting, consistent with the stratified turbulence regime. The strong stratification observed at the ice base that is responsible for suppressing the basal melt rate is probably highly persistent, maintained by the input of glacial meltwater and subglacial discharge (Fig. 3b). At the same time, there is little oceanographic evidence to suggest that current speeds would have been much higher in the past to erode this stratification, as the region is subject to weak tidal forcing, and narrow, frictionally controlled water columns close to grounding lines with a flat ice base are not conducive to rapid flow. However, coupled with melting in the vicinity of the seaward pinning point of TEIS[14,22], even relatively modest basal melting in the grounding zone can still force notable change to grounded ice. A small increase in basal melting can create a large melt imbalance that triggers melt-induced thinning of TEIS and drives a reduction in basal drag at the grounding line[6,45]. The reduction in basal drag weakens the back stress imposed by the ice shelf[46], resulting in a loss of

buttressing and dynamic thinning of grounded ice upstream[47,48]. As this thinner ice goes afloat, the grounding line can retreat rapidly inland and up the prograde bedrock slope characteristic of the butterfly region. Although ice–ocean models suggest that high rates of basal melting beneath newly floating ice can provide a strong positive feedback to continuing retreat[6], our results indicate that this feedback is weak. Nevertheless, sustained grounding-zone basal melting, weaker ice-shelf buttressing and the advection of increasingly thinner ice over the grounding line will continue to condition TEIS to persistent retreat in the future, even without a strong positive feedback from elevated basal melting[6].

Methods

Borehole observations

A Sea-Bird Scientific SBE 49 FastCAT CTD profiler was used to observe the water-column structure between 9 January and 12 January 2020. A total of 15 individual CTD casts were completed, sampling at a rate of 16 Hz. Before each deployment, the CTD was stored in a warm bath (approximately 5 °C) to minimize icing in the conductivity cell during the profiler's traverse of the approximately 90-m air-filled portion of the borehole. The CTD data were processed using standard routines in the Sea-Bird data-processing software version 7.26.7.129 and each profile was averaged into 0.1-m vertical bins. Absolute salinity and conservative temperature were computed using the Gibbs SeaWater (GSW) Oceanographic Toolbox for TEOS-10 (refs. [53,54]). The temperature and conductivity sensors were manufacturer-calibrated before deployment and the stated accuracy of the sensors are ±0.002 °C and ±0.0003 S m^{-1}, respectively.

A moored turbulence instrument cluster was deployed about 1.5 m beneath the ice base to observe the small-scale turbulent fluctuations in the ice shelf–ocean boundary layer[42]. Consisting of a Nobska Modular Acoustic Velocity Sensor (MAVS) differential acoustic travel-time 3D velocity sensor, an RBRcoda fast-response temperature sensor and an RBRconcerto inductive conductivity sensor, the turbulence instrument cluster was scheduled to operate in burst mode, sampling at 5 Hz for 15 min every 2 h. For each 15-

min burst, the average temperature, conductivity and velocity values were received over an Iridium satellite link. In this study we use the mean values from 4,459 individual bursts collected between 23 January 2020 and 1 February 2021. An analysis of the full 5-Hz turbulence data awaits a future study. The stated uncertainty in the velocity components is 3 mm s^{-1}, whereas the stated uncertainty in the temperature and conductivity data are ±0.002 °C and ±0.0003 S m^{-1}, respectively. A small offset in the conductivity data caused by proximity effects associated with the inductive sensor was removed through regression against the CTD conductivity data.

Lateral gradients in temperature and salinity

CTD profiling beneath TEIS was largely carried out in three separate sessions with approximately 19 h between the first and second sessions and 47 h between the second and third sessions. Dividing the mean absolute difference in temperature and salinity between each session pair by the lateral advective distance over the time separating each pair (assuming a mean flow speed of 3 cm s^{-1} during the CTD deployment period; Extended Data Fig. 4a) gives a mean lateral gradient of $2.7 \times 10^{-3} \pm 10^{-4}$ °C km^{-1} for temperature and $1.1 \times 10^{-3} \pm 10^{-5}$ g kg^{-1} km^{-1} for salinity. The effect of tidal flow has been ignored in these calculations, as the tidal flow speeds are an order of magnitude weaker.

ApRES

An ApRES was established within 10 m of the borehole on 23 January 2020 and set to record a burst of 20 measurements once every 2 h. The data were recovered from the instrument on 27 December 2020. Data from four further ApRES deployments are also presented in this study (Fig. 1): a 5-month record from the first half of 2019 from an instrument deployed 360 m downstream of the borehole and data from three sites from 2020, contemporaneous with the borehole dataset. One of the 2020 sites was 1,310 m downstream of the borehole, another 1,340 m upstream of the borehole and, finally, one instrument was deployed on grounded ice 2,600 m upstream of the borehole, which tracked across the grounding line during 2020 and recorded every 3 h.

ApRES uses frequency-modulated continuous-wave modulation, with a chirp that scans from 200 to 400 MHz over a 1-s period. The measurements in each burst were checked for quality and then averaged. Each averaged burst was processed[55] to generate a radar return that preserves the signal phase.

By using both amplitude and phase, ApRES can monitor the changing distance between the antennas and the ice-shelf base with millimetre-scale precision. This raw Lagrangian ice-shelf thinning includes both the basal melt signal and the ice-column vertical strain that results from ice flow and snow compaction[21]. As well as the range to the ice base, the range to reflecting horizons within the ice column can be monitored and used to estimate the vertical strain within the ice as follows. The motion of internal reflecting horizons in any given depth interval can be found by cross-correlating the complex return for sequential (two-hourly) measurements for the entire time series. The vertical motion of the ice within the layer from one return to the next was derived from the phase of the cross-correlation and the reliability of that estimate was indicated by its amplitude. As all displacements are measured with respect to the antennas, the vertical displacement of any individual layer is the effect of the integrated strain in the ice above. The ice-shelf thinning rate, as measured from the antennas, is obtained by using a depth interval that tracks the return from the ice base.

For tracking the ice base to obtain the total thinning rate, an assumption in ApRES data processing is that, over the period of the time series, the topography of the ice base local to the radar does not change at length scales at or longer than the wavelength of the radar waves in ice, in this case, at length scales greater than about 0.5 m. This requirement was not met at the borehole site nor at various periods of the time series from the upstream sites. However, it was possible to use the first multiple echo, which is the result of the radar signal travelling from the transmit antenna to the ice base, back to the ice surface and then back to the ice base, before finally returning to the receive antenna. The range to the multiple is largely immune to local topographic evolution in the ice base, presumably because of the much larger effective footprint. The multiple is very much weaker than the first basal return, but its phase can be reliably tracked. For the downstream ApRES deployment, and those sections of the other deployments when the first basal return was not changing its form, the melt-rate time series from

the first and second returns yielded a satisfactory match. Short-term variations in derived melt rate (3 to 5 days) were much stronger from the multiple, possibly resulting from snow-accumulation events.

Vertical profiles of vertical ice velocities, averaged across the entire time series, were calculated by dividing the return into 4-m layers, cross-correlating as described above and calculating the mean vertical velocity for each layer. From these profiles a depth interval was selected from the lower part of the ice column from which to calculate the integrated non-melt contribution to the thinning rate. The selection of the depth interval was based on the strength of the time-averaged correlations and, for the downstream site, the borehole site and the first upstream site, was 300–472 m, 304–436 m and 300–550 m, respectively. The strain from one measurement to the next was averaged across the depth interval and the time series differentiated and low-pass-filtered to provide a time series of vertical velocity variability at timescales of 5 days and longer. Although the strain rate in the ice column was expected to evolve slowly as the ice moved downstream, we assumed that non-tidal short-term variations would not be present. The vertical profiles of vertical velocity showed an approximately linear gradient through the selected depth intervals and an offset vertical velocity was determined by extrapolating that variation to the depth of the basal reflector. That offset was then added to the vertical velocities to yield the final non-melt contribution to the time series of ice-shelf thinning rate. The 2019 site, and the initially grounded site, were processed slightly differently. The internal reflections from near the ice base were good enough to allow a deep depth interval to be selected and cross-correlated to yield an integrated vertical strain directly. Intervals from 520 to 580 m and from 515 to 550 m were used for the 2019 and initially grounded sites, respectively, with a minor correction to accommodate a small, approximately linearly increasing strain rate near the base.

The final melt-rate time series was calculated by subtracting the non-melt contribution from the thinning rate and then low-pass-filtering at a cutoff of 15 days.

Icefin remotely operated underwater vehicle

Icefin was equipped with a Neil Brown Ocean Sensors conductivity–temperature (CT) sensor and a Valeport ultraP pressure sensor. The stated manufacturer accuracies are ±0.001 S m^{-1}, ±0.005 °C and 0.1 dbar for conductivity, temperature and pressure, respectively, which translate into uncertainties of ±0.008 g kg^{-1} for S_A and ±0.018 °C for Θ. All sensors were factory calibrated before deployment and then cross-compared with the SBE 49 CTD profiler to remove offsets in conductivity and temperature of 0.0286 S m^{-1} and 0.0236 °C. The CT sensor recorded at a frequency of 5 Hz, whereas the pressure sensor recorded at 1 Hz. Pressure measurements were interpolated to match the 5-Hz CT data. Hydrographic data were post-processed by removing outliers that exceeded more than two standard deviations from the mean, as well as data points collected when the vehicle speed was lower than 5 cm s^{-1}. A three-point weighted-mean filter was also applied to the conductivity and temperature data.

Ocean current speeds were measured using a LinkQuest NavQuest 600 Micro Doppler Velocity Log, which doubles as an ADCP. The ADCP provides measurements of the current speed in 2-m bins at a variable distance from the vehicle, controlled by gradients in the pitch, roll, heading and speed of the vehicle. Uncertainty in the current velocity is typically 1% of the vehicle's velocity in its direction of travel. As Icefin travels at speeds ≤50 cm s^{-1}, the uncertainty in velocity recorded by the ADCP in the direction of travel is ≤5 mm s^{-1}. The uncertainty in velocities perpendicular to the direction of travel is typically much lower. The velocity data were recorded at a rate of 1 Hz and were post-processed by removing data points when the vehicle pitch or roll is greater than 30°. A 30-s running mean filter was applied to all data points and measurements were filtered for gradients greater than one standard deviation from the mean in vehicle speed, pitch, roll and individual bin velocity. Finally velocities were bin-averaged into 1-m depth bins and velocities were excluded if they exceeded one standard deviation of the mean for each bin.

Ship-based CTD profiles

A dual-sensors system based on a Sea-Bird 911 CTD was used for conductivity, temperature and pressure measurements outside the ice-shelf cavity from the RVIB Nathaniel B. Palmer in 2019 and 2020. Standard Sea-

Bird software Seasave version 7.26.1.8 was used for data collection and conductivity cell thermal mass correction in 2019 and Seasave version 7.26.7.121 in 2020. Manufacturer-recommended values for cell thermal mass correction were used as follows: thermal anomaly amplitude, $\alpha = 0.03$ and thermal anomaly time constant $1/\beta = 7.0$. Water samples were taken from the CTD rosette and analysed using a Guildline Portasal salinometer to calibrate the primary and secondary conductivity sensors on the CTD profiler.

Density ratio and Turner angle

Double-diffusive convection occurs as a result of the difference in molecular diffusivities between salt and heat[56]. Under Antarctic ice shelves, the presence of cold and fresh meltwater-laden waters above warm and salty modified Circumpolar Deep Water drives a double-diffusive process known as diffusive convection. Strong diffusive convection can lead to the formation of ‘diffusive staircases’, where well-mixed layers in temperature and salinity are separated by sharp interfaces[57,58]. Diffusive convection can still occur without staircase formation however. Diffusive convection can exert a first-order control on the rate of ice-shelf basal melting[59,60].

The susceptibility of a water column to diffusive convection can be characterized through the density ratio

$${R}_{{\rho }}={\alpha }\frac{\partial \varTheta }{\partial {\rm{z}}}/{\beta }\frac{\partial {S}_{{\rm{A}}}}{\partial {\rm{z}}},$$ (1)

which measures the degree of compensation between temperature and salinity gradients in terms of their effect on density stratification. α is the thermal expansion coefficient, β the haline contraction coefficient, $\frac{\partial \varTheta }{\partial {\rm{z}}}$ the vertical gradient of conservative temperature and $\frac{\partial {S}_{{\rm{A}}}}{\partial \text{z}}$ is the vertical gradient of absolute salinity. A water column is susceptible to diffusive convection when R_ρ is between 0 and 1, with the strength of diffusive convection increasing as R_ρ approaches 1. The Turner angle

$${\rm{Tu}}=\arctan 2\left({\alpha }\frac{\partial \varTheta }{\partial {\rm{z}}}+{\beta }\frac{\partial {S}_{{\rm{A}}}}{\partial {\rm{z}}},{\alpha }\frac{\partial \varTheta }{\partial {\rm{z}}}-{\beta }\frac{\partial {S}_{{\rm{A}}}}{\partial {\rm{z}}}\right)$$
(2)

is related to the density ratio, in which arctan2 is the four-quadrant inverse tangent ($\tan^{-1}$) and the water column is susceptible to diffusive convection when Tu is between −45° and −90°.

Glacial meltwater and subglacial discharge fractions

Meltwater fractions are calculated using the composite tracer method[27] and water-mass endmembers derived from the ship-based CTD profiles. In the absence of glacial meltwater or subglacial discharge, it is assumed that the ambient water column beneath TEIS would be composed exclusively of mCDW and WW that mix along a straight line between their corresponding endmembers[61] (Fig. 2c and Extended Data Fig. 7). For each conservative temperature and absolute salinity observation, a composite tracer can be constructed

$${\psi }_{{{\rm{o}}{\rm{b}}}_{{\rm{W}}{\rm{W}}}}=({\Theta }_{{\rm{m}}{\rm{C}}{\rm{D}}{\rm{W}}}-{\Theta }_{{\rm{o}}{\rm{b}}})-({S}_{{{\rm{A}}}_{{\rm{m}}{\rm{C}}{\rm{D}}{\rm{W}}}}-{S}_{{{\rm{A}}}_{{\rm{o}}{\rm{b}}}})\left(\frac{{\Theta }_{{\rm{m}}{\rm{C}}{\rm{D}}{\rm{W}}}-{\Theta }_{{\rm{W}}{\rm{W}}}}{{S}_{{{\rm{A}}}_{{\rm{m}}{\rm{C}}{\rm{D}}{\rm{W}}}}-{S}_{{{\rm{A}}}_{{\rm{W}}{\rm{W}}}}}\right),$$
(3)

in which $\Theta_{\rm mCDW}$ and ${S}_{{{\rm{A}}}_{{\rm{mCDW}}}}$ are the conservative temperature and absolute salinity of the mCDW endmember, respectively, $\Theta_{\rm WW}$ and ${S}_{{{\rm{A}}}_{{\rm{WW}}}}$ are the conservative temperature and absolute salinity of the WW endmember, respectively, and $\Theta_{\rm ob}$ and $\,{S}_{{{\rm{A}}}_{{\rm{ob}}}}$ are observed values of conservative temperature and absolute salinity, respectively. If a data point lies on the ambient mCDW–WW mixing line, \

${\psi }_{{{\rm{o}}{\rm{b}}}_{{\rm{W}}{\rm{W}}}}$ is equal to zero. The value of ${\psi }_{{{\rm{o}}{\rm{b}}}_{{\rm{W}}{\rm{W}}}}$ will become non-zero, however, if glacial meltwater (MW) causes a data point to move off the ambient mixing line. The value of the composite tracer in pure MW is

$${\psi }_{{{\rm{M}}{\rm{W}}}_{{\rm{W}}{\rm{W}}}}=({\Theta }_{{\rm{m}}{\rm{C}}{\rm{D}}{\rm{W}}}-{\Theta }_{{\rm{M}}{\rm{W}}})-({S}_{{{\rm{A}}}_{{\rm{m}}{\rm{C}}{\rm{D}}{\rm{W}}}}-{S}_{{{\rm{A}}}_{{\rm{M}}{\rm{W}}}})\left(\frac{{\Theta }_{{\rm{m}}{\rm{C}}{\rm{D}}{\rm{W}}}-{\Theta }_{{\rm{W}}{\rm{W}}}}{{S}_{{{\rm{A}}}_{{\rm{m}}{\rm{C}}{\rm{D}}{\rm{W}}}}-{S}_{{{\rm{A}}}_{{\rm{W}}{\rm{W}}}}}\right),$$
(4)

in which Θ_{MW} and ${S}_{{{\rm{A}}}_{{\rm{MW}}}}$ are the conservative temperature and absolute salinity of the MW endmember, respectively. The fraction of glacial meltwater (x_{MW}) present in the water column can then be calculated from

$${x}_{{\rm{M}}{\rm{W}}}=\frac{{\psi }_{{{\rm{o}}{\rm{b}}}_{{\rm{W}}{\rm{W}}}}}{{\psi }_{{{\rm{M}}{\rm{W}}}_{{\rm{W}}{\rm{W}}}}}.$$
(5)

To quantify the variability in x_{MW} caused by uncertainty in the water-mass endmembers, 1,000 independent estimates of the meltwater fraction were made using a set of random endmember properties derived from the normal distribution described by the mean and standard deviation of each endmember property (Extended Data Table 2). The observed meltwater fraction is given by the mean of the 1,000 independent estimates, and the uncertainty is given by the standard error of the mean. In general, the uncertainty is two orders of magnitude smaller than the mean.

The conservative temperature and absolute salinity of the mCDW and WW endmembers were extracted from the ship-based CTD casts collected in front of TEIS (Fig. 2c). The properties of the WW endmember (Extended

Data Table 2) are set to those found at the depth of the temperature minimum below the surface layer, whereas the mCDW endmember properties are set to those found at the depth of the temperature maximum. The MW endmember has an effective conservative temperature of −90.8 °C (ref. [27]) and an absolute salinity of 0 g kg^{-1}, whereas the conservative temperature of the subglacial discharge endmember is set to the pressure-dependent in situ freezing temperature for freshwater at the depth of the grounding line (−0.36 °C) with an absolute salinity of 0 g kg^{-1}. The endmember values are consistent with those used in previous studies[61,62].

Starting in September 2020, a persistent signal of fresh subglacial discharge (SD) appears in the hydrographic data. In $\varTheta$–S_A space, individual data points fall above the mCDW–MW mixing line, indicative of the presence of this fourth water mass (Extended Data Fig. 7). With only $\varTheta$ and S_A available as tracers, it is not possible to solve for all water-mass fractions simultaneously, as the system is underdetermined. Instead, we have to make a necessary assumption that the influence of WW is negligible and that the water column is composed solely of a mix of mCDW, MW and SD. Although this practical assumption cannot be fully justified, WW is typically found above a depth of 400 m in the Amundsen Sea[61,63,64] and is therefore mostly excluded from the grounding-zone region owing to the depth of the ice base (Fig. 4). As a result, the impact of this assumption on the water-mass fractions is probably small. To determine the SD faction for data points that lie outside the mCDW–WW–MW mixing triangle, a composite tracer is constructed that is equal to zero for data points that lie along the mCDW–MW mixing line:

$${\psi }_{{{\rm{ob}}}_{{\rm{MW}}}}=\left({\varTheta }_{{\rm{mCDW}}}-{\varTheta }_{{\rm{ob}}}\right)-\left({S}_{{{\rm{A}}}_{{\rm{mCDW}}}}-{S}_{{{\rm{A}}}_{{\rm{ob}}}}\right)\left(\frac{{\varTheta }_{{\rm{mCDW}}}-{\varTheta }_{{\rm{MW}}}}{{S}_{{{\rm{A}}}_{{\rm{mCDW}}}}-{S}_{{{\rm{A}}}_{{\rm{MW}}}}}\right).$$
(6)

The value of this composite tracer in pure SD is

$${\psi }_{{\rm{SD}}}=\left({\varTheta }_{{\rm{mCDW}}}-{\varTheta }_{{\rm{SD}}}\right)-\left({S}_{{{\rm{A}}}_{{\rm{mCDW}}}}-{S}_{{{\rm{A}}}_{{\rm{SD}}}}\right)\left(\frac{{\varTheta }_{{\rm{mCDW}}}-{\varTheta }_{{\rm{MW}}}}{{S}_{{{\rm{A}}}_{{\rm{mCDW}}}}-{S}_{{{\rm{A}}}_{{\rm{MW}}}}}\right),$$
(7)

in which $\Theta_{\rm SD}$ and \({S}_{{{\rm{A}}}_{{\rm{SD}}}}\) are the conservative temperature and absolute salinity of the SD endmember, respectively, and the SD fraction can be calculated from

$${x}_{{\rm{SD}}}=\frac{{\psi }_{{{\rm{ob}}}_{{\rm{MW}}}}}{{\psi }_{{\rm{SD}}}}.$$
(8)

Similarly, the MW fraction for data points that lie outside the mCDW–WW–MW mixing triangle can be derived by constructing a composite tracer that is equal to zero for data points that lie along the mCDW–SD mixing line:

$${\psi }_{{{\rm{ob}}}_{{\rm{SD}}}}=\left({\varTheta }_{{\rm{mCDW}}}-{\varTheta }_{{\rm{ob}}}\right)-\left({S}_{{{\rm{A}}}_{{\rm{mCDW}}}}-{S}_{{{\rm{A}}}_{{\rm{ob}}}}\right)\left(\frac{{\varTheta }_{{\rm{mCDW}}}-{\varTheta }_{{\rm{SD}}}}{{S}_{{{\rm{A}}}_{{\rm{mCDW}}}}-{S}_{{{\rm{A}}}_{{\rm{SD}}}}}\right).$$
(9)

Taking the value of this composite tracer in pure MW as

$${\psi }_{{{\rm{M}}{\rm{W}}}_{{\rm{S}}{\rm{D}}}}=({\Theta }_{{\rm{m}}{\rm{C}}{\rm{D}}{\rm{W}}}-{\Theta }_{{\rm{M}}{\rm{W}}})-({S}_{{{\rm{A}}}_{{\rm{m}}{\rm{C}}{\rm{D}}{\rm{W}}}}-{S}_{{{\rm{A}}}_{{\rm{M}}{\rm{W}}}})\left(\frac{{\Theta }_{{\rm{m}}{\rm{C}}{\rm{D}}{\rm{W}}}-{\Theta }_{{\rm{S}}{\rm{D}}}}

{{S}_{{{\rm{A}}}_{{\rm{m}}{\rm{C}}{\rm{D}}{\rm{W}}}}-{S}_{{{\rm{A}}}_{{\rm{S}}{\rm{D}}}}}\right),$$
(10)

the MW fraction can be calculated as

$${x}_{{\rm{M}}{\rm{W}}}=\frac{{\psi }_{{{\rm{o}}{\rm{b}}}_{{\rm{S}}{\rm{D}}}}}{{\psi }_{{{\rm{M}}{\rm{W}}}_{{\rm{S}}{\rm{D}}}}}.$$
(11)

Ice base Ekman boundary layer

Assuming a momentum balance between a steady, uniform, geostrophic flow beneath a flat ice base and the frictional stress exerted by the ice base against this flow[65,66]:

$$-fv=-\frac{1}{{\rho }_{0}}\frac{\partial p}{\partial x}+\nu \frac{{\partial }^{2}u}{\partial {z}^{2}}$$
(12)
$$+fu=-\frac{1}{{\rho }_{0}}\frac{\partial p}{\partial y}+\nu \frac{{\partial }^{2}v}{\partial {z}^{2}}$$
(13)
$$0=-\frac{1}{{\rho }_{0}}\frac{\partial p}{\partial z},$$
(14)

in which f is the Coriolis parameter, ρ_0 is the fluid density, p is pressure, ν is the kinematic eddy viscosity and u and v are the horizontal velocity components, then the vertical structure of the horizontal velocity components through the boundary layer are given by the canonical Ekman solution[66]

$$u={u}_{{\rm{g}}}\left(1-{{\rm{e}}}^{-z/d}\cos \frac{z}{d}\right)$$
(15)
$$v={u}_{{\rm{g}}}{{\rm{e}}}^{-z/d}\sin \frac{z}{d},$$
(16)

in which u_g is the magnitude of the far-field geostrophic flow, z is boundary layer depth and d is the Ekman depth:

$$d=\sqrt{\frac{2\nu }{f}}.$$
(17)

Using the root mean square error as a cost function, we fit equations (15) and (16) to the u and v boundary-layer velocity profiles from Icefin to determine the value of the eddy viscosity and the Ekman depth beneath TEIS.

Thermal driving and the three-equation model for basal melting

The rate of ice-shelf basal melting is controlled by the divergence of the sensible heat flux at the phase change interface[40]

$${\rho }_{{\rm{i}}}{a}_{{\rm{b}}}{L}_{{\rm{i}}}={{\rho }_{{\rm{i}}}{c}_{{\rm{i}}}{\kappa }_{{\rm{i}}}\frac{{\rm{\partial }}{T}_{{\rm{i}}}}{{\rm{\partial }}z}|}_{{\rm{b}}}+{\rho }_{{\rm{w}}}{c}_{{\rm{w}}}\langle {W}^{{\prime} }{T}_{w}^{{\prime} }\rangle ,$$
(18)

in which ρ is density, a_b the basal melt rate, L_i the latent heat of fusion of ice, c the specific heat capacity, κ_i the thermal diffusivity of ice, T the temperature and W is the vertical ocean velocity. The subscripts i, b and w refer to ice, ice–ocean boundary and ocean, respectively. The primes refer to turbulent fluctuations and the angled brackets to the time average. The first term on the right-hand side is the conductive heat flux into the ice, whereas the second term represents the vertical turbulent heat flux through the oceanic boundary layer. In the absence of direct turbulence measurements, or in regional or global models that do not resolve the vertical scales of the ice shelf–ocean boundary layer, the second term is quantified through a simple turbulence closure scheme that models the heat flux, $\langle {W}^{{\prime} }{T}_{w}^{{\prime} }\rangle$, as a product of the drag coefficient (C_d), a non-dimensional turbulent transfer coefficient for temperature (Γ_T), the horizontal ocean velocity (U), and the thermal driving (T_d), that is given as the difference between the in situ ocean temperature

some distance from the ice–ocean boundary (T_w; in this case, the temperature at the ocean mooring deployed 1.5 m beneath the ice shelf) and the temperature at the ice–ocean boundary (T_b) that is assumed to be at the in situ freezing point at salinity S_b and pressure P_b:

$${\rho }_{{\rm{w}}}{c}_{{\rm{w}}}\langle {W}^{{\prime} }{T}_{w}^{{\prime} }\rangle ={\rho }_{{\rm{w}}}{c}_{{\rm{w}}}{C}_{{\rm{d}}}^{1/2}{\varGamma }_{{\rm{T}}}U[{T}_{{\rm{w}}}-\,{T}_{{\rm{b}}}({S}_{{\rm{b}}},{P}_{{\rm{b}}})].$$
(19)

The in situ freezing point at the ice–ocean boundary is given by the liquidus condition

$${T}_{{\rm{b}}}={\lambda }_{1}{S}_{{\rm{b}}}+{\lambda }_{2}+{\lambda }_{3}{P}_{{\rm{b}}},$$
(20)

in which λ_1, λ_2 and λ_3 are constants and the boundary salinity (S_b) is given by the salt balance at the phase-change interface:

$${\rho }_{{\rm{i}}}{a}_{{\rm{b}}}\left({S}_{{\rm{b}}}-{S}_{{\rm{i}}}\right)={\rho }_{{\rm{w}}}{C}_{{\rm{d}}}^{1/2}{\varGamma }_{{\rm{S}}}U\left[{S}_{{\rm{w}}}-{S}_{{\rm{b}}}\right],$$
(21)

in which Γ_S is the turbulent transfer coefficient for salt and the salinity of ice (*Si*) is taken to be zero for ice shelves. The turbulent transfer coefficients, Γ_T and Γ_S, assume that the thermal and saline diffusive sublayers (diffusive regions next to the ice base that are dominated by molecular-scale processes) are controlled exclusively by current shear and thin with increasing current velocity; however, there are known to be many ice shelf–ocean environments where this is not the case[8]. The system of equations described by equations (18)–(21) represents the canonical three-equation model for ice-shelf basal melting[40,67]. It can be solved for the basal melt rate given

observed ocean temperature, salinity and flow speed and physical constants in Extended Data Table 3 (refs. [40,42]).

Because thermal driving is defined as the difference between the ocean temperature recorded by the mooring and the freezing temperature at the ice–ocean boundary, its magnitude is sensitive to the distance between the ocean mooring and the ice base. Basal melting increases the distance between the ocean mooring and the ice base as a function of time, and this drives an apparent increase in thermal driving without a change in the source water mass as the mooring effectively descends into warmer water. If we assume that the temperature profile through the boundary layer is fixed with respect to time, we can use the observed CTD profiles to estimate that the apparent change in thermal driving owing to ice-base recession is about 0.2 °C, or roughly 57% of the observed change (Extended Data Fig. 2a).

Although the rate of basal melting beneath TEIS predicted by the three-equation melt-rate model is linearly related to the magnitude of the thermal driving, it is relatively insensitive to the apparent change in thermal driving owing to ice-base recession. Indeed, the mean predicted melt rate only falls by 8% when thermal driving is corrected for ice-base recession (Extended Data Fig. 2b) and the predicted melt rate remains an order of magnitude higher than the observed values. The small reduction in predicted melt rate is consistent with our assertion that basal melting beneath TEIS is limited by the strong stratification, weak flow speeds and the lack of shear-driven turbulence, rather than the amount of heat available in the boundary layer. Irrespective of ice-base recession, thermal driving continues to exceed 1.8 °C by the beginning of 2021 (Extended Data Fig. 2a), highlighting the substantial amount of heat that is available in the grounding-zone region to drive basal melting. The apparent increase in thermal driving owing to ice-base recession therefore has no impact on our conclusion that the three-equation melt-rate model is unable to accurately predict the melt rate beneath TEIS.

Data availability

The CTD data are available from the UK Polar Data Centre (https://doi.org/10.5285/97204415-683f-4d55-8b38-a2700fa94efe). The

mooring data are available from the UK Polar Data Centre (https://doi.org/10.5285/4ffad557-1c3c-4ea7-a73d-6d782331b08a). The ApRES basal melt-rate data are available from the UK Polar Data Centre (https://doi.org/10.5285/B81BFF87-3429-4754-B4B5-C6B58198E744). The Icefin data are available from the United States Antarctic Program Data Center (https://doi.org/10.15784/601618).

Code availability

The MATLAB Gibbs-SeaWater (GSW) Oceanographic Toolbox for TEOS-10 (v3.06) is available at: https://www.teos-10.org/software.htm. The custom MATLAB (R2021a) code and additional materials and libraries required to process the data and generate the figures in the article are available on request from the corresponding author.

References

1. Scambos, T. A. et al. How much, how fast?: A science review and outlook for research on the instability of Antarctica's Thwaites Glacier in the 21st century. *Glob. Planet. Change* **153**, 16–34 (2017).

2. Yu, H. et al. Impact of iceberg calving on the retreat of Thwaites Glacier, West Antarctica over the next century with different calving laws and ocean thermal forcing. *Geophys. Res. Lett.* **46**, 14539–14547 (2019).

3. Joughin, I. et al. Marine ice sheet collapse potentially under way for the Thwaites Glacier Basin, West Antarctica. *Science* **344**, 735–738 (2014).

4. Fretwell, P. et al. Bedmap2: improved ice bed, surface and thickness datasets for Antarctica. *Cryosphere* **7**, 375–393 (2013).

5. Morlighem, M. et al. Deep glacial troughs and stabilizing ridges unveiled beneath the margins of the Antarctic ice sheet. *Nat. Geosci.* **13**, 132–137 (2020).

6. Arthern, R. J. et al. The sensitivity of West Antarctica to the submarine melting feedback. *Geophys. Res. Lett.* **44**, 2352–2359 (2017).

7. Vreugdenhil, C. A. et al. Stratification effects in the turbulent boundary layer beneath a melting ice shelf: insights from resolved large-eddy simulations. *J. Phys. Oceanogr.* **49**, 1905–1925 (2019).

8. Rosevear, M. G. et al. Regimes and transitions in the basal melting of Antarctic ice shelves. *J. Phys. Oceanogr.* **52**, 2589–2608 (2022).

9. IPCC. *Climate Change 2021: The Physical Science Basis. Contribution of Working Group I to the Sixth Assessment Report of the Intergovernmental Panel on Climate Change* (Cambridge Univ. Press, 2021).

10. Fürst, J. J. et al. The safety band of Antarctic ice shelves. *Nat. Clim. Change* **6**, 479–482 (2016).

11. Dupont, T. K., & Alley, R. B. Assessment of the importance of ice-shelf buttressing to ice-sheet flow. *Geophys. Res. Lett.* **32**, L04503 (2005).

12. Paolo, F. S. et al. Volume loss from Antarctic ice shelves is accelerating. *Science* **348**, 327–331 (2015).

13. Mouginot, J. et al. Sustained increase in ice discharge from the Amundsen Sea Embayment, West Antarctica, from 1973 to 2013. *Geophys. Res. Lett.* **41**, 1576–1584 (2014).

14. Rignot, E. et al. Widespread, rapid grounding line retreat of Pine Island, Thwaites, Smith, and Kohler glaciers, West Antarctica, from 1992 to 2011. *Geophys. Res. Lett.* **41**, 3502–3509 (2014).

15. Bamber, J. L. et al. Reassessment of the potential sea-level rise from a collapse of the West Antarctic Ice Sheet. *Science* **324**, 901–903 (2009).

16. Rignot, E. et al. Four decades of Antarctic Ice Sheet mass balance from 1979–2017. *Proc. Natl Acad. Sci.* **116**, 1095–1103 (2019).

17. Scheuchl, B. et al. Grounding line retreat of Pope, Smith, and Kohler Glaciers, West Antarctica, measured with Sentinel-1a radar interferometry data. *Geophys. Res. Lett.* **43**, 8572–8579 (2016).

18. Milillo, P. et al. Heterogeneous retreat and ice melt of Thwaites Glacier, West Antarctica. *Sci. Adv.* **5**, eaau3433 (2019).

19. Feldmann, J. et al. Collapse of the West Antarctic Ice Sheet after local destabilization of the Amundsen Basin. *Proc. Natl Acad. Sci.* **112**, 14191–14196 (2015).

20. Schmidt, B. E. et al. Heterogeneous melting near the Thwaites Glacier grounding line. *Nature* **614**, 471–478 (2023).

21. Nicholls, K. W. et al. A ground-based radar for measuring vertical strain rates and time-varying basal melt rates in ice sheets and shelves. *J. Glaciol.* **61**, 1079–1087 (2015).

22. Wåhlin, A. K. et al. Pathways and modification of warm water flowing beneath Thwaites Ice Shelf, West Antarctica. *Sci. Adv.* **7**, eabd7254 (2021).

23. Stanton, T. P. et al. Channelized ice melting in the ocean boundary layer beneath Pine Island Glacier, Antarctica. *Science* **341**, 1236–1239 (2013).

24. Begeman, C. B. et al. Ocean stratification and low melt rates at the Ross Ice Shelf grounding zone. *J. Geophys. Res.* **123**, 7438–7452 (2018).

25. Stevens, C. et al. Ocean mixing and heat transport processes observed under the Ross Ice Shelf control its basal melting. *Proc. Natl Acad. Sci.* **117**, 16799–16804 (2020).

26. Middleton, L. et al. Double diffusion as a driver of turbulence in the stratified boundary layer beneath George VI Ice Shelf. *Geophys. Res. Lett.* **49**, e2021GL096119 (2022).

27. Jenkins, A. The impact of melting ice on ocean waters. *J. Phys. Oceanogr.* **29**, 2370–2381 (1999).

28. Nakayama, Y. et al. Pathways of ocean heat towards Pine Island and Thwaites grounding lines. *Sci. Rep.* **9**, 16649 (2019).

29. Bett, D. T. et al. The impact of the Amundsen Sea freshwater balance on ocean melting of the West Antarctic Ice Sheet. *J. Geophys. Res.* **125**, e2020JC016305 (2020).

30. Davis, P. E. D. et al. Variability in basal melting beneath Pine Island Ice Shelf on weekly to monthly timescales. *J. Geophys. Res.* **123**, 8655–8669 (2018).

31. Webber, B. G. M. et al. Mechanisms driving variability in the ocean forcing of Pine Island Glacier. *Nat. Commun.* **8**, 14507 (2017).

32. Jenkins, A. et al. Decadal ocean forcing and Antarctic Ice Sheet response: lessons from the Amundsen Sea. *Oceanography* **29**, 106–117 (2016).

33. Zheng, Y. et al. Reversal of ocean gyres near ice shelves in the Amundsen Sea caused by the interaction of sea ice and wind. *Cryosphere Discuss.* **16**, 3005–3019 (2022).

34. Joughin, I. et al. Basal conditions for Pine Island and Thwaites Glaciers, West Antarctica, determined using satellite and airborne data. *J. Glaciol.* **55**, 245–257 (2009).

35. Lepp, A. P. et al. Sedimentary signatures of persistent subglacial meltwater drainage from Thwaites Glacier, Antarctica. *Front. Earth Sci.* **10**, 863200 (2022).

36. Smith, B. E. et al. Connected subglacial lake drainage beneath Thwaites Glacier, West Antarctica. *Cryosphere* **11**, 451–467 (2017).

37. Malczyk, G. et al. Repeat subglacial lake drainage and filling beneath Thwaites Glacier. *Geophys. Res. Lett.* **47**, e2020GL089658 (2020).

38. Hager, A. O. et al. Persistent, extensive channelized drainage modeled beneath Thwaites Glacier, West Antarctica. *Cryosphere* **16**, 3575–3599 (2021).

39. Le Brocq, A. M. et al. Evidence from ice shelves for channelized meltwater flow beneath the Antarctic Ice Sheet. *Nat. Geosci.* **6**, 945–948 (2013).

40. Jenkins, A. et al. Observation and parameterization of ablation at the base of Ronne Ice Shelf, Antarctica. *J. Phys. Oceanogr.* **40**, 2298–2312 (2010).

41. Malyarenko, A. et al. A synthesis of thermodynamic ablation at ice–ocean interfaces from theory, observations and models. *Ocean Model.* **154**, 101692 (2020).

42. Davis, P. E. D. et al. Turbulence observations beneath Larsen C ice shelf, Antarctica. *J. Geophys. Res.* **124**, 5529–5550 (2019).

43. Seroussi, H. et al. Continued retreat of Thwaites Glacier, West Antarctica, controlled by bed topography and ocean circulation. *Geophys. Res. Lett.* **44**, 6191–6199 (2017).

44. Bevan, S. L. et al. Brief communication: Thwaites Glacier cavity evolution. *Cryosphere* **15**, 3317–3328 (2021).

45. Parizek, B. R. et al. Dynamic (in)stability of Thwaites Glacier, West Antarctica. *J. Geophys. Res. Earth Surf.* **118**, 638–655 (2013).

46. Reese, R. et al. The far reach of ice-shelf thinning in Antarctica. *Nat. Clim. Change* **8**, 53–57 (2018).

47. Alley, K. E. et al. Two decades of dynamic change and progressive destabilization on the Thwaites Eastern Ice Shelf. *Cryosphere* **15**, 5187–5203 (2021).

48. Wild, C. T. et al. Weakening of the pinning point buttressing Thwaites Glacier, West Antarctica. *Cryosphere* **16**, 397–417 (2022).

49. Hogan, K. A. et al. Revealing the former bed of Thwaites Glacier using sea-floor bathymetry: implications for warm-water routing and bed controls on ice flow and buttressing. *Cryosphere* **14**, 2883–2908 (2020).

50. Gerrish, L. et al. High resolution vector polylines of the Antarctic coastline - VERSION 7.5. https://data.bas.ac.uk/metadata.php?id=GB/NERC/BAS/PDC/01634 (2022).

51. Mouginot, J. et al. MEaSUREs Antarctic boundaries for IPY 2007–2009 from satellite radar, version 2. https://nsidc.org/data/nsidc-0709/versions/2 (2017).

52. Rignot, E. et al. Ice-shelf melting around Antarctica. *Science* **341**, 266–270 (2013).

53. IOC, SCOR and IAPSO. *The International Thermodynamic Equation of Seawater – 2010: Calculation and Use of Thermodynamics Properties* (UNESCO, 2010).

54. McDougall, T. J. & Barker, P. M. *Getting Started with TEOS-10 and the Gibbs Seawater (GSW) Oceanographic Toolbox* (SCOR/IAPSO WG127, 2011).

55. Brennan, P. V. et al. Phase-sensitive FMCW radar system for high-precision Antarctic ice shelf profile monitoring. *IET Radar Sonar Navig.* **8**, 776–786 (2014).

56. Radko, T. *Double-Diffusive Convection* (Cambridge Univ. Press, 2013).

57. Kimura, S. et al. Estimation of ice shelf melt rate in the presence of a thermohaline staircase. *J. Phys. Oceanogr.* **45**, 133–148 (2015).

58. Timmermans, M.-L. et al. Ice-Tethered Profiler observations of the double-diffusive staircase in the Canada Basin thermocline. *J. Geophys. Res.* **113**, C00A02 (2008).

59. Rosevear, M. G. et al. The role of double-diffusive convection in basal melting of Antarctic ice shelves. *Proc. Natl Acad. Sci.* **118**,

e2007541118 (2021).

60. Middleton, L. et al. Numerical simulations of melt-driven double-diffusive fluxes in a turbulent boundary layer beneath an ice shelf. *J. Phys. Oceanogr.* **51**, 403–418 (2021).

61. Biddle, L. C. et al. Glacial meltwater identification in the Amundsen Sea. *J. Phys. Oceanogr.* **47**, 933–954 (2017).

62. Nakayama, Y. et al. From circumpolar deep water to the glacial meltwater plume on the eastern Amundsen Shelf. *Deep Sea Res. Part I Oceanogr. Res. Pap.* **77**, 50–62 (2013).

63. Zheng, Y. et al. Winter seal-based observations reveal glacial meltwater surfacing in the southeastern Amundsen Sea. *Commun. Earth Environ.* **2**, 40 (2021).

64. Randall-Goodwin, E. et al. Freshwater distributions and water mass structure in the Amundsen Sea Polynya region, Antarctica. *Elem. Sci. Anthr.* **3**, 000065 (2015).

65. Price, J. F. et al. Wind-driven ocean currents and Ekman transport. *Science* **238**, 1534–1538 (1987).

66. Cushman-Roisin, B. & Beckers, J.-M. *Introduction to Geophysical Fluid Dynamics. Physical and Numerical Aspects* (Academic, 2008).

67. Holland, D. M. et al. Modeling thermodynamic ice–ocean interactions at the base of an ice shelf. *J. Phys. Oceanogr.* **29**, 1787–1800 (1999).

68. Paden, J. et al. IceBridge MCoRDS L3 gridded ice thickness, surface, and bottom, version 2 (IRMCR3). https://nsidc.org/data/irmcr3/versions/2 (2013).

Acknowledgements

This work is from the MELT project, a component of the International Thwaites Glacier Collaboration (ITGC). Support from the National Science

Foundation (NSF, grant no. 1739003) and the Natural Environment Research Council (NERC, grant no. NE/S006656/1). Logistics provided by NSF U.S. Antarctic Program and NERC British Antarctic Survey. The ship-based CTD data were supported by the ITGC TARSAN project (NERC grant nos. NE/S006419/1 and NE/S006591/1; NSF grant no. 1929991). ITGC contribution no. ITGC 047.

Author information

Authors and Affiliations

1. British Antarctic Survey, Cambridge, UK

   Peter E. D. Davis, Keith W. Nicholls, Robert J. Arthern, Irena Vaňková, James A. Smith, Paul G. D. Anker & Keith Makinson

2. Courant Institute of Mathematical Sciences, New York University, New York, NY, USA

   David M. Holland & Aurora Basinski-Ferris

3. Center for Global Sea Level Change, New York University Abu Dhabi, Abu Dhabi, UAE

   David M. Holland & Clare Eayrs

4. Department of Astronomy, Cornell University, Ithaca, NY, USA

   Britney E. Schmidt, Peter Washam, Andrew D. Mullen, Daniel Dichek & Matthew M. Meister

5. Department of Environmental Studies, University of Portland, Portland, OR, USA

   Kiya L. Riverman

6. College of Earth, Ocean, and Atmospheric Sciences, Oregon State University, Corvallis, OR, USA

Kiya L. Riverman

7. Georgia Institute of Technology, Atlanta, GA, USA

Justin D. Lawrence

8. Department of Geosciences, Pennsylvania State University, State College, PA, USA

Elisabeth Clyne & Sridhar Anandakrishnan

9. Environmental Studies, Lewis & Clark College, Portland, OR, USA

Elisabeth Clyne

10. Department of Earth System Science, University of California, Irvine, Irvine, CA, USA

Eric Rignot

11. Jet Propulsion Laboratory, California Institute of Technology, Pasadena, CA, USA

Eric Rignot

12. Department of Marine Sciences, University of Gothenburg, Gothenburg, Sweden

Bastien Y. Queste

13. Scottish Oceans Institute, University of St Andrews, St. Andrews, UK

Lars Boehme

14. Centre for Ocean and Atmospheric Sciences, School of Environmental Sciences, University of East Anglia, Norwich, UK

Karen J. Heywood

Contributions

P.E.D.D. wrote the manuscript. P.E.D.D., K.W.N., P.W., I.V. and C.E. analysed the different datasets. P.E.D.D., K.W.N., D.M.H., B.E.S., P.W., K.L.R., J.A.S., P.G.D.A., A.D.M., D.D., E.C., A.B.-F., B.Y.Q. and L.B. contributed to data collection. All authors reviewed and edited the manuscript.

Corresponding author

Correspondence to Peter E. D. Davis.

Ethics declarations

Competing interests

The authors declare no competing interests.

Peer review

Peer review information

Nature thanks Susheel Adusumilli, Craig Lee, Craig McConnochie and the other, anonymous, reviewer(s) for their contribution to the peer review of this work.

Additional information

Publisher's note Springer Nature remains neutral with regard to jurisdictional claims in published maps and institutional affiliations.

Extended data figures and tables

Extended Data Fig. 1 Vertical profiles of buoyancy frequency, density ratio and Turner angle.

a,**b**, Individual vertical profiles of buoyancy frequency (*N*) (**a**) and average vertical profile of the density ratio (blue) and Turner angle (red; see Methods) (**b**) collected over 4 days (9 to 12 January 2020) in the grounding-zone region of Thwaites Glacier (yellow star in Fig. 1). The ice base is indicated by the shaded grey box and the seabed is indicated by the slash-backed line.

Extended Data Fig. 2 Thermal driving and basal melt rate from the three-equation melt-rate model.

a,**b**, Daily averaged time series of thermal driving (red) (**a**) and basal melt rate (blue) (**b**) predicted by the three-equation melt-rate model (see Methods). The grey lines in **a** and **b** show the thermal driving and basal melt rate corrected for effects of ice-base recession using the vertical profiles of Θ and S_A from the CTD data (see Methods).

Extended Data Fig. 3 Subglacial discharge beneath Thwaites Glacier.

Landsat 8 satellite image of Thwaites Glacier and the location of the hot-water-drilled access hole (yellow star; 75.207° S, 104.825° W) in the grounding-zone 'butterfly' region of TEIS. White–blue-coloured contours with hillshade show bed depth in the Amundsen Sea from ship-based survey[49] and BedMachine[5], whereas green-coloured contours show subglacial freshwater pathways and rate of discharge[39]. The purple, green and orange dots show the location of 2019–2020 ship-based CTD profiles from the International Thwaites Glacier Collaboration TARSAN project. The coastline (black) and grounding line (purple) are from the SCAR Antarctic Digital Database[50]. The blue-shaded area shows the location of the 2016–2017 grounding-zone region[18]. Extended Data Figure 3 was created with the QGIS Geographic Information System.

Extended Data Fig. 4 Flow speed, direction and tidal ellipses.

a,**b**, Daily averaged time series of flow speed (**a**) and geographic flow direction (**b**) from the current meter deployed about 1.5 m beneath the ice

base in the grounding-zone region of Thwaites Glacier (yellow star in Fig. 1). For flow direction, 0° indicates flow to the north, 90° indicates flow to the east and 150° indicates flow to the south of southeast. **c**, Amplitude and geographic orientation of the main diurnal (blue) and semidiurnal tidal constituents at the location of the borehole (yellow star). Solid lines indicate ellipses with positive semi-minor axes (anticlockwise rotation in time), whereas dot-dashed lines indicate ellipses with negative semi-minor axes (clockwise rotation in time). The blue polygon shows the location of the 2016–2017 grounding-zone region[18], and the grey area shows where the ice is grounded. The map in panel **c** was created with MATLAB.

Extended Data Fig. 5 Extended ApRES basal melt-rate time series from the borehole location.

Observed ApRES basal melt rate (yellow) at the borehole location (2020; yellow star in Fig. 1) and a secondary location 360 m downstream of the borehole location (2019; yellow diamond in Fig. 1) low-pass-filtered with a 15-day cutoff plotted against the basal melt rate estimated from the three-equation melt-rate model (grey; see Methods).

Extended Data Fig. 6 Bedrock depth along the Thwaites Glacier grounding line.

a, Sentinel-2 image of TEIS and Thwaites Main Trunk from 9 February 2019. Coloured contours show gridded bed depth beneath present-day grounded ice from NASA IceBridge Multichannel Coherent Radar Depth Sounder (MCoRDS) data[68] collected over Thwaites Glacier between 1 January 2006 and 31 December 2012. The green area indicates the location of the 2016–2017 grounding-zone region[18], whereas the yellow star indicates the location of the hot-water-drilled access hole. **b**, Profile of bed depth along the present-day grounding line beneath TEIS and Thwaites Main Trunk from NASA IceBridge MCoRDS data[68]. The dotted line at 106° W marks the boundary between TEIS and the Thwaites Main Trunk. **c**, Profiles of ice base (light grey) and seabed (dark grey) from the Icefin T1 transect. The white triangle marks the location of the 2011

grounding line from satellite interferometry[18]. The map in panel **a** was created with MATLAB.

Extended Data Fig. 7 Temperature–salinity diagram and linear mixing lines between the main sub-ice shelf water masses.

Linear mixing lines between the mCDW (red box), WW (blue box), glacial MW and SD, along with Θ–S_A observations from each individual CTD cast (grey dots) and the sub-ice shelf mooring (dots coloured by time). Note that the endmember properties of MW and SD fall outside the range of the axes (Extended Data Table 2). From the end of September 2020 onwards, individual Θ–S_A observations lie above the mCDW–MW mixing line, indicating the presence of subglacial discharge and the negligible influence of WW.

Extended Data Table 1 Tidal ellipse parameters for the six main tidal constituents
Extended Data Table 2 Temperature and salinity properties of the main sub-ice shelf water masses
Extended Data Table 3 Physical constants used in the three-equation melt-rate model

Rights and permissions

Open Access This article is licensed under a Creative Commons Attribution 4.0 International License, which permits use, sharing, adaptation, distribution and reproduction in any medium or format, as long as you give appropriate credit to the original author(s) and the source, provide a link to the Creative Commons licence, and indicate if changes were made. The images or other third party material in this article are included in the article's Creative Commons licence, unless indicated otherwise in a credit line to the material. If material is not included in the article's Creative Commons licence and your intended use is not permitted by statutory regulation or exceeds the permitted use, you will need to obtain permission directly from the copyright holder. To view a copy of this licence, visit http://creativecommons.org/licenses/by/4.0/.

Reprints and Permissions

About this article

Cite this article

Davis, P.E.D., Nicholls, K.W., Holland, D.M. *et al.* Suppressed basal melting in the eastern Thwaites Glacier grounding zone. *Nature* **614**, 479–485 (2023). https://doi.org/10.1038/s41586-022-05586-0

- Received: 27 April 2022
- Accepted: 22 November 2022
- Published: 15 February 2023
- Issue Date: 16 February 2023
- DOI: https://doi.org/10.1038/s41586-022-05586-0

Share this article

Anyone you share the following link with will be able to read this content:

Get shareable link

Sorry, a shareable link is not currently available for this article.

Copy to clipboard

Provided by the Springer Nature SharedIt content-sharing initiative

Heterogeneous melting near the Thwaites Glacier grounding line

- B. E. Schmidt
- P. Washam
- K. Makinson

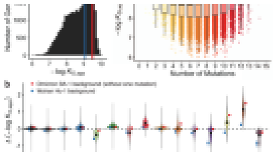
Nature Article Open Access 15 Feb 2023

High variability reveals complexity under Thwaites Glacier

- Craig McConnochie

Nature News & Views 15 Feb 2023

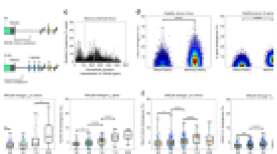
This article was downloaded by **calibre** from https://www.nature.com/articles/s41586-022-05586-0



Compensatory epistasis maintains ACE2 affinity in SARS-CoV-2 Omicron BA.1

16 November 2022

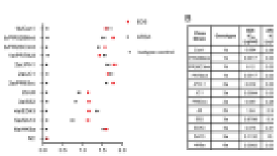
Alief Moulana, Thomas Dupic, … Michael M. Desai



Sequencing HIV-neutralizing antibody exons and introns reveals detailed aspects of lineage maturation

08 October 2018

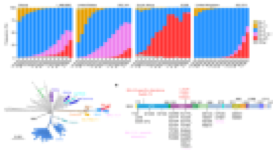
Erik L. Johnson, Nicole A. Doria-Rose, … George Georgiou



Junctional and somatic hypermutation-induced CX4C motif is critical for the recognition of a highly conserved epitope on HCV E2 by a human broadly neutralizing antibody

31 March 2020

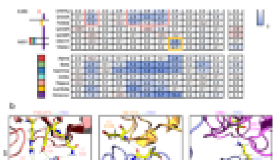
Chunyan Yi, Jing Xia, … Bing Sun



Antibody evasion by SARS-CoV-2 Omicron subvariants BA.2.12.1, BA.4 and BA.5

05 July 2022

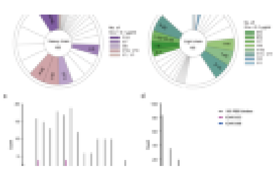
Qian Wang, Yicheng Guo, … David D. Ho



Parallel profiling of antigenicity alteration and immune escape of SARS-CoV-2 Omicron and other variants

08 February 2022

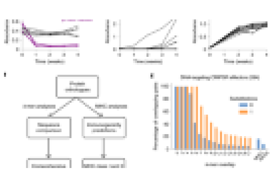
Cong Sun, Yin-Feng Kang, … Mu-Sheng Zeng



Potent and protective IGHV3-53/3-66 public antibodies and their shared escape mutant on the spike of SARS-CoV-2

09 July 2021

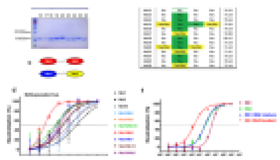
Qi Zhang, Bin Ju, … Zheng Zhang



[Immune-orthogonal orthologues of AAV capsids and of Cas9 circumvent the immune response to the administration of gene therapy]

22 July 2019

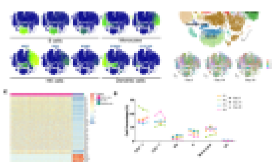
Ana M. Moreno, Nathan Palmer, … Prashant Mali



[An ultrapotent RBD-targeted biparatopic nanobody neutralizes broad SARS-CoV-2 variants]

09 February 2022

Xiaojing Chi, Xinhui Zhang, … Wei Yang



[Integrated single-cell analysis revealed immune dynamics during Ad5-nCoV immunization]

10 August 2021

Qiqi Cao, Shipo Wu, … Wen Wen

- Article
- Open Access
- Published: 19 December 2022

Imprinted SARS-CoV-2 humoral immunity induces convergent Omicron RBD evolution

- Yunlong Cao ,
- Fanchong Jian,
- Jing Wang,
- Yuanling Yu,
- Weiliang Song,
- Ayijiang Yisimayi,
- Jing Wang,
- Ran An,
- Xiaosu Chen,
- Na Zhang,
- Yao Wang,
- Peng Wang,
- Lijuan Zhao,
- Haiyan Sun,
- Lingling Yu,
- Sijie Yang,
- Xiao Niu,
- Tianhe Xiao,
- Qingqing Gu,
- Fei Shao,
- Xiaohua Hao,
- Yanli Xu,
- Ronghua Jin,
- Zhongyang Shen,
- Youchun Wang &
- …
- Xiaoliang Sunney Xie

Show authors

Nature **volume 614**, pages 521–529 (2023)

- 60k Accesses
- 14 Citations
- 712 Altmetric
- Metrics details

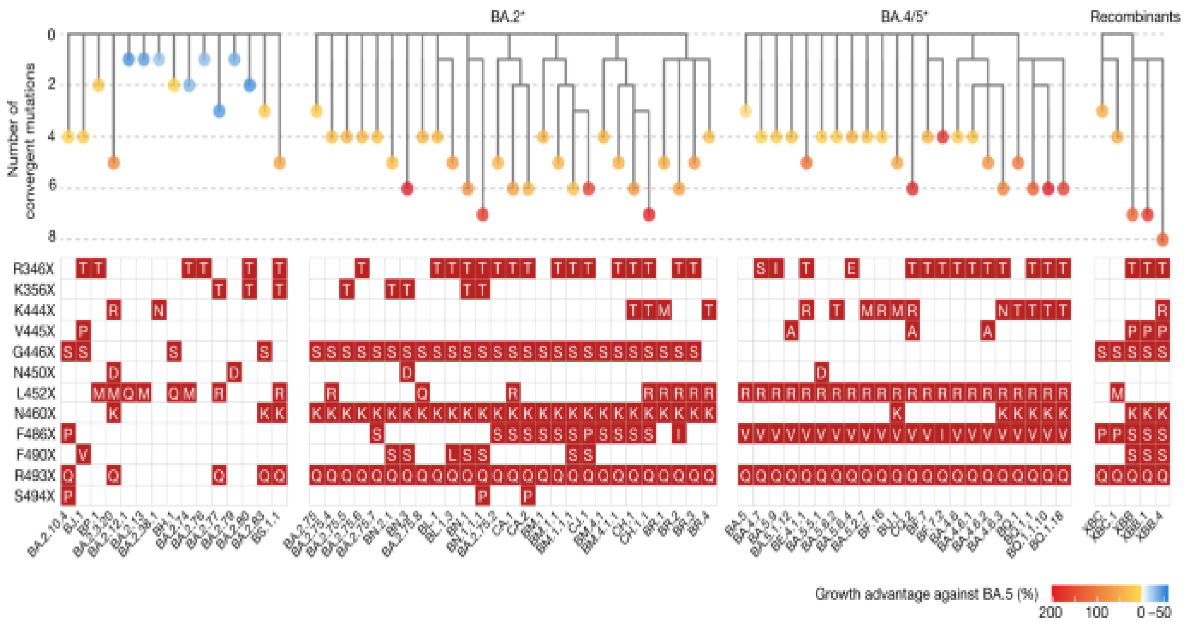
Abstract

Continuous evolution of Omicron has led to a rapid and simultaneous emergence of numerous variants that display growth advantages over BA.5 (ref. [1]). Despite their divergent evolutionary courses, mutations on their receptor-binding domain (RBD) converge on several hotspots. The driving force and destination of such sudden convergent evolution and its effect on humoral immunity remain unclear. Here we demonstrate that these convergent mutations can cause evasion of neutralizing antibody drugs and convalescent plasma, including those from BA.5 breakthrough infection, while maintaining sufficient ACE2-binding capability. BQ.1.1.10 (BQ.1.1 + Y144del), BA.4.6.3, XBB and CH.1.1 are the most antibody-evasive strains tested. To delineate the origin of the convergent evolution, we determined the escape mutation profiles and neutralization activity of monoclonal antibodies isolated from individuals who had BA.2 and BA.5 breakthrough infections[2,3]. Owing to humoral immune imprinting, BA.2 and especially BA.5 breakthrough infection reduced the diversity of the neutralizing antibody binding sites and increased proportions of non-neutralizing antibody clones, which, in turn, focused humoral immune pressure and promoted convergent evolution in the RBD. Moreover, we show that the convergent RBD mutations could be accurately inferred by deep mutational scanning profiles[4,5], and the evolution trends of BA.2.75 and BA.5 subvariants could be well foreseen through constructed convergent pseudovirus mutants. These results suggest that current herd immunity and BA.5 vaccine boosters may not efficiently prevent the infection of Omicron convergent variants.

Main

SARS-CoV-2 Omicron BA.1, BA.2 and BA.5 have demonstrated strong neutralization evasion capability, posing severe challenges to the efficacy of existing humoral immunity established through vaccination and infection[2,3,6,7,8,9,10,11,12,13,14,15]. Nevertheless, Omicron is continuously evolving, leading to various new subvariants, including BA.2.75, BA.4.6 and BF.7 (refs. [16,17,18,19,20,21]). A high proportion of these emerging variants display substantial growth advantages over BA.5, such as BA.2.3.20, BA.2.75.2, BQ.1.1 and especially XBB, a recombinant of BJ.1 and BM.1.1.1 (ref. [1]) (Fig. 1). Such rapid and simultaneous emergence of multiple variants with enormous growth advantages is unprecedented. Of note, although these derivative subvariants appear to diverge along the evolutionary course, the mutations they carry on the RBD converge on the same sites, including R346, K356, K444, V445, G446, N450, L452, N460, F486, F490, R493 and S494 (Fig. 1). These residues were found mutated in at least five independent Omicron sublineages that exhibited a high growth advantage (Extended Data Fig. 1a–c). Most mutations on these residues are known to be antibody-evasive, as revealed by deep mutational scanning (DMS)[2,3,22,23,24]. It is crucial to examine the effect of these convergent mutations on antibody-escaping capability, receptor-binding affinity, and the efficacy of vaccines and antibody therapeutics. It is also important to investigate the driving force behind this suddenly accelerated emergence of convergent RBD mutations, what such mutational convergence would lead to and how we can prepare for such rapid SARS-CoV-2 evolution.

Fig. 1: Convergent evolution of Omicron RBD with growth advantage over BA.5.



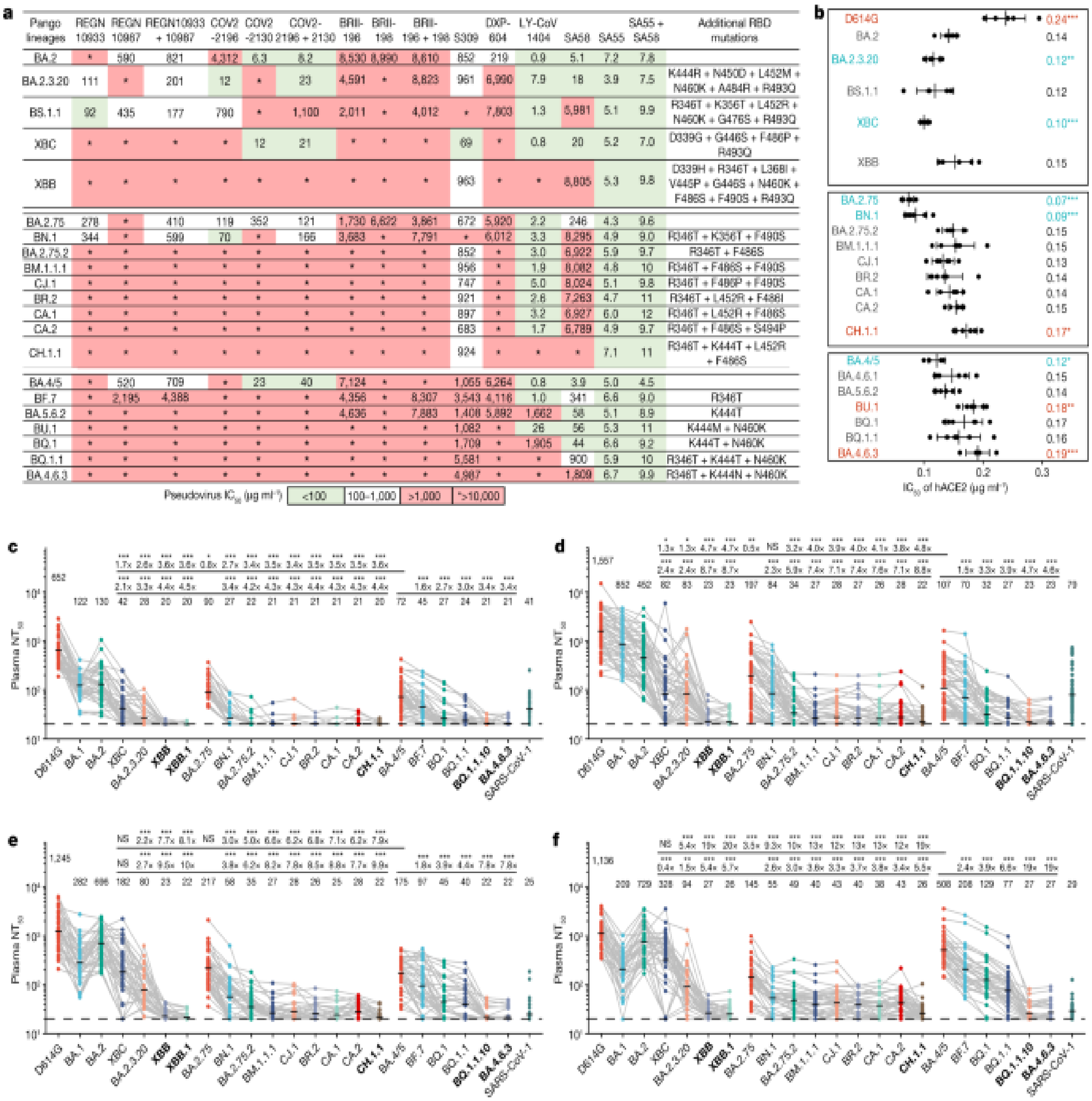
Phylogenetic tree of featured Omicron subvariants carrying convergent mutations. Their relative growth advantage values, calculated using the CoV-Spectrum website, are indicated as a colour scale. Specific convergent mutations carried by each lineage are labelled.

Antibody evasion by convergent variants

First, we tested the antibody evasion capability of these convergent variants. We constructed the vesicular stomatitis virus (VSV)-based spike-pseudotyped virus of Omicron BA.2, BA.2.75 and BA.4/5 sublineages carrying those convergent mutations and examined the neutralizing activities of therapeutic neutralizing antibodies (NAbs) against them (Fig. 2a and Extended Data Fig. 2a). In total, pseudoviruses of 50 convergent variants were constructed and tested. COV2-2196 + COV2-2130 (Evusheld)[25] is vulnerable to F486, R346 and K444–G446 mutations, evaded or highly impaired by BJ.1 (R346T), XBB (R346T + V445P + F486S), BA.2.75.2/CA.1/BM.1.1/BM.1.1.1/CH.1.1 (R346T + F486S), CJ.1/XBF (R346T + F486P), BR.2/BR.2.1 (R346T + F486I), BA.4.6.1 (R346T + F486V), BA.5.6.2/BQ.1 (K444T + F486V), BU.1 (K444M + F486V) and BQ.1.1 (R346T + K444T + F486V). LY-CoV1404 (also known as bebtelovimab) remains potent against BF.16 (K444R) and BA.5.5.1 (N450D) and shows reduced potency against BA.5.1.12 (V445A)[26] (Extended Data Fig. 2a). However, LY-CoV1404 was escaped by BJ.1,

XBB, BR.1, CH.1.1, BA.4.6.3 and BQ.1.1 while exhibiting strongly reduced activity against BA.2.38.1, BA.5.6.2 and BQ.1 due to K444N/T mutations and the combination of K444M–G446S or V445P–G446S[26]. SA55 + SA58 is a pair of broad NAbs isolated from vaccinated individuals who had SARS that target non-competing conserved epitopes[2,27]. SA58 is weak to G339H and R346T mutations and showed reduced neutralization efficacy against BJ.1/XBB and BA.2.75 sublineages. SA55 is the only NAb demonstrating high potency against all tested Omicron subvariants. Among the tested variants, XBB and BQ.1.1 exhibited the strongest resistance to therapeutic monoclonal Abs (mAbs) and cocktails (Fig. 2a). As the SA55 + SA58 cocktail is still in preclinical development, the efficacy of available antibody drugs, including the BA.2.75/BA.5-effective Evusheld (AstraZeneca) and bebtelovimab, is extensively affected by the emerging subvariants with convergent mutations.

Fig. 2: Convergent Omicron subvariants induce NAb evasion.



Pango lineages	REGN 10933	REGN 10987	REGN10933 + 10987	COV2 -2196	COV2 -2130	COV2-2196 + 2130	BRII-196	BRII-198	BRII-196 + 198	S309	DXP-604	LY-CoV 1404	SA58	SA55	SA55 + SA58	Additional RBD mutations
BA.2	*	590	821	4,312	6.3	8.2	8,530	8,990	8,610	852	219	0.9	5.1	7.2	7.8	
BA.2.3.20	111	*	201	12	*	23	4,591	*	8,823	961	6,990	7.9	18	3.9	7.5	K444R + N450D + L452M + N460K + A484R + R493Q
BS.1.1	92	435	177	790	*	1,100	2,011	*	4,012	*	7,803	1.3	5,981	5.1	9.9	R346T + K356T + L452R + N460K + G476S + R493Q
XBC	*	*	*	*	12	21	*	*	*	69	*	0.8	20	5.2	7.0	D339G + G446S + F486P + R493Q
XBB	*	*	*	*	*	*	*	*	*	963	*	*	8,805	5.3	9.8	D339H + R346T + L368I + V445P + G446S + N460K + F486S + F490S + R493Q
BA.2.75	278	*	410	119	352	121	1,730	6,622	3,861	672	5,920	2.2	246	4.3	9.6	
BN.1	344	*	599	70	*	166	3,683	*	7,791	*	6,012	3.3	8,295	4.9	9.0	R346T + K356T + F490S
BA.2.75.2	*	*	*	*	*	*	*	*	*	852	*	3.0	6,922	5.9	9.7	R346T + F486S
BM.1.1.1	*	*	*	*	*	*	*	*	*	956	*	1.9	8,082	4.8	10	R346T + F486S + F490S
CJ.1	*	*	*	*	*	*	*	*	*	747	*	5.0	8,024	5.1	9.8	R346T + F486P + F490S
BR.2	*	*	*	*	*	*	*	*	*	921	*	2.6	7,263	4.7	11	R346T + L452R + F486I
CA.1	*	*	*	*	*	*	*	*	*	897	*	3.2	6,927	6.0	12	R346T + L452R + F486S
CA.2	*	*	*	*	*	*	*	*	*	683	*	1.7	6,789	4.9	9.7	R346T + F486S + S494P
CH.1.1	*	*	*	*	*	*	*	*	*	924	*	*	*	7.1	11	R346T + K444T + L452R + F486S
BA.4/5	*	520	709	*	23	40	7,124	*	*	1,055	6,264	0.8	3.9	5.0	4.5	
BF.7	*	2,195	4,388	*	*	*	4,356	*	8,307	3,543	4,116	1.0	341	6.6	9.0	R346T
BA.5.6.2	*	*	*	*	*	*	4,636	*	7,883	1,408	5,892	1,662	58	5.1	8.9	K444T
BU.1	*	*	*	*	*	*	*	*	*	1,082	*	26	56	5.3	11	K444M + N460K
BQ.1	*	*	*	*	*	*	*	*	*	1,709	*	1,905	44	6.6	9.2	K444T + N460K
BQ.1.1	*	*	*	*	*	*	*	*	*	5,581	*	*	900	5.9	10	R346T + K444T + N460K
BA.4.6.3	*	*	*	*	*	*	*	*	*	4,987	*	*	1,809	6.7	9.9	R346T + K444N + N460K

Pseudovirus IC_{50} (μg ml^{-1}): <100 | 100–1,000 | >1,000 | *>10,000

a, IC_{50} of therapeutic NAbs against VSV-based pseudoviruses with spike glycoproteins of emerging SARS-CoV-2 BA.2, BA.5 or BA.2.75 convergent subvariants. **b**, Relative hACE2-binding capability measured by IC_{50} of hACE2 against pseudoviruses of variants. Error bars indicate mean ± s.d. of $n = 5$ biologically independent replicates. P values were calculated using two-tailed Student's t-test. *$P < 0.05$, **$P < 0.01$ and ***$P < 0.001$. There is no label on variants with $P > 0.05$. Variants with significantly stronger binding are coloured blue, whereas those with weaker binding are coloured red. **c**–**f**, Pseudovirus-neutralizing titres against SARS-CoV-2 D614G and Omicron subvariants of plasma from vaccinated or convalescent individuals

of breakthrough infection. Individuals who had received three doses of CoronaVac ($n = 40$) (**c**), individuals who had been infected with BA.1 after receiving three doses of CoronaVac ($n = 50$) (**d**), individuals who had been infected with BA.2 after receiving three doses of CoronaVac ($n = 39$) (**e**) and individuals who had been infected with BA.5 after receiving three doses of CoronaVac ($n = 36$) (**f**) are shown. The geometric mean titres are labelled. Statistical tests were performed using two-tailed Wilcoxon signed-rank tests of paired samples. $*P < 0.05$, $**P < 0.01$, $***P < 0.001$ and not significant (NS) $P > 0.05$. NT_{50} against BA.2-derived and BA.2.75-derived subvariants were compared with that against BA.4/5 (the upper line) and BA.2.75 (the lower line); BA.4/5-derived subvariants were only compared with BA.4/5. Dashed lines indicate the limit of detection (LOD, $NT_{50} = 20$). Strains showing the strongest evasion are in bold. All neutralization assays were conducted in at least two independent experiments.

Sufficient ACE2-binding affinity is essential for SARS-CoV-2 transmission. Thus, we examined the relative human ACE2 (hACE2)-binding capability of these variants by evaluating hACE2 inhibitory efficiency against the pseudoviruses. Higher inhibitory efficiency of soluble hACE2 against pseudoviruses indicates higher ACE2-binding capability[28]. Overall, these convergent variants all demonstrate sufficient ACE2-binding efficiency, at least higher than that of D614G, including the most antibody-evasive XBB, BQ.1.1 and CH.1.1 (Fig. 2b and Extended Data Fig. 2b). Specifically, R493Q reversion increases the inhibitory efficiency of hACE2, which is consistent with previous reports[6,20,28]. K417T shows a moderate increase in the inhibitory efficiency of hACE2. By contrast, F486S, K444M and K444N have a clear negative effect on inhibitory efficiency, whereas K444T and F486P do not cause significant impairment of ACE2 binding. These observations are also in line with previous DMS results[29].

Most importantly, we investigated how these variants escape the neutralization of plasma samples from individuals with various immune histories. We recruited cohorts of individuals who received three doses of CoronaVac with or without breakthrough infection by BA.1, BA.2 or BA.5. Convalescent plasma samples were collected on average around 4 weeks after hospital discharge (Supplementary Table 1). Plasma from vaccinated individuals who received CoronaVac was obtained 4 weeks after the third

dose. A significant reduction in the 50% neutralization titre (NT_{50}) against most tested BA.2, BA.2.75 or BA.5 subvariants was observed, compared with that against corresponding ancestral BA.2, BA.2.75 or BA.5, respectively (Fig. 2c–f and Extended Data Fig. 3a–d).

Specifically, BA.2.3.20 and BA.2.75.2 are significantly more immune-evasive than BA.5 (Fig. 2c–f), explaining their high growth advantage. Nevertheless, multiple convergent variants showed even stronger antibody evasion capability, including BM.1.1.1 (BM.1.1 + F490S), CJ.1/XBF, CA.1 (BA.2.75.2 + L452R + T604I), CA.2 (BA.2.75.2 + S494P), CH.1 (BA.2.75 + R346T + K444T + F486S) and CH.1.1 (CH.1 + L452R) in the BA.2.75 sublineages, and BQ.1.1, BQ.1.1.10 (BQ.1.1 + Y144del) and BA.4.6.3 (BA.4.6 + K444N + N460K + Y144del) in the BA.4/5 sublineages. BN.1 sublineages also caused heavy immune evasion while retaining high hACE2-binding ability. The BJ.1/BM.1.1.1 recombinant strains XBB and XBB.1 (XBB + G252V) are among the most humoral immune-evasive strains tested, comparable with that of CH.1.1, BQ.1.1.10 and BA.4.6.3. BA.5 breakthrough infection yields higher plasma NT_{50} against BA.5 sublineages, including BQ.1.1; however, plasma from individuals who had BA.5 breakthrough infection neutralize poorly against XBB, CH.1.1, BQ.1.1.10 and BA.4.6.3, suggesting that the N-terminal domain (NTD) mutations these variants carry are extremely effective at evading NAbs elicited by BA.5 breakthrough infection (Fig. 2f). Of note, the strongest immune-evasive convergent variants have displayed even lower NT_{50} than SARS-CoV-1, suggesting immense antigenic drift and potential serotype conversion.

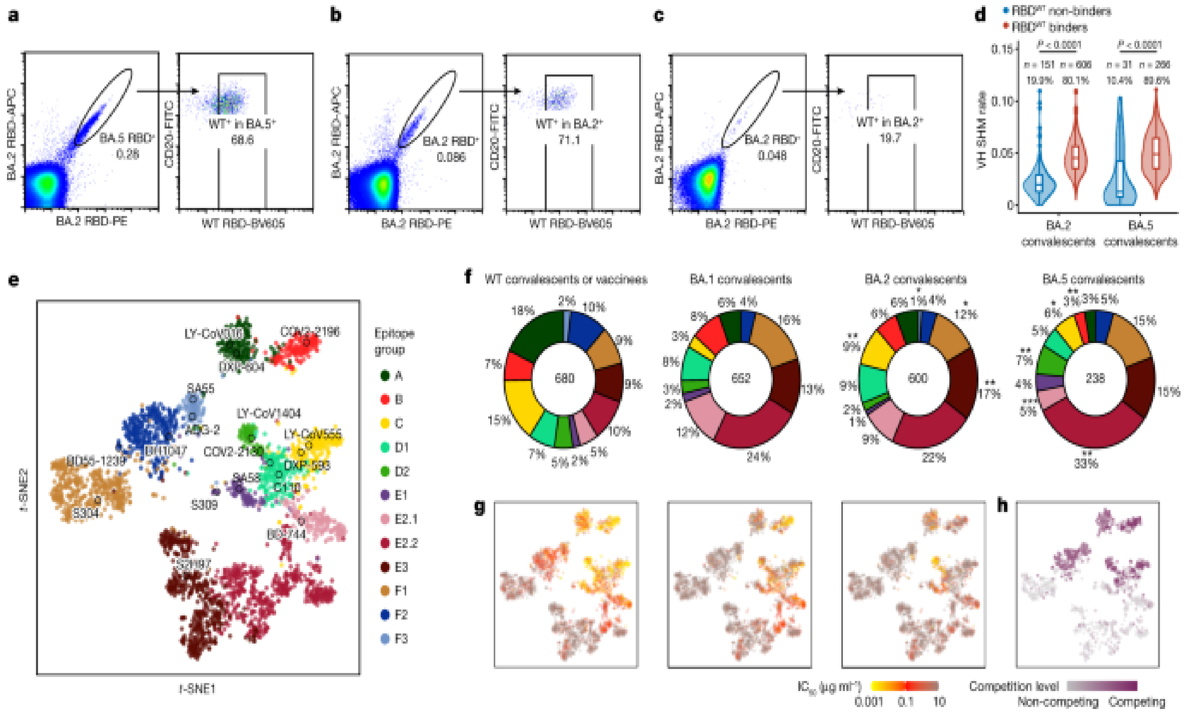
RBD convergence due to immune imprinting

It is crucial to investigate the origin of such accelerated RBD convergent evolution. Therefore, we characterized the antibody repertoires induced by Omicron BA.2 and BA.5 breakthrough infection, which is the dominant immune background of current global herd immunity. Following the strategy described in our previous report using pooled peripheral blood mononuclear cells from individuals with BA.1 breakthrough infection[2], we enriched antigen-specific memory B cells by fluorescence-activated cell sorting

(FACS) for individuals who had recovered from BA.2 and BA.5 breakthrough infection (Supplementary Table 1). RBD-binding $CD27^{+}/IgM^{-}/IgD^{-}$ cells were subjected to single-cell V(D)J sequencing to determine the BCR sequences (Extended Data Fig. 4a,b).

Similar to that reported in BA.1 breakthrough infection, immune imprinting, or 'original antigenic sin', is also observed in BA.2 and BA.5 breakthrough infection[2,30,31,32,33]. Post-vaccination infection with BA.2 and BA.5 mainly recalls cross-reactive memory B cells elicited by wild-type (WT)-based vaccine, but rarely produces BA.2/BA.5-specific B cells, similar to BA.1 breakthrough infection (Fig. 3a,b). This is in marked contrast to Omicron infection without previous vaccination (Fig. 3c and Extended Data Fig. 4c). The RBD-targeting antibody sequences determined by single-cell V(D)J sequencing are then expressed in vitro as human IgG1 mAbs. As expected, only a small proportion of the expressed mAbs specifically bind to the BA.2/BA.5 RBD and are not cross-reactive to the WT RBD, determined by enzyme-linked immunosorbent assay (ELISA) and concordant with the FACS results (Fig. 3d). Cross-reactive mAbs exhibit significantly higher somatic hypermutation (SHM), indicating that these antibodies are more affinity-matured and are indeed most likely recalled from previous vaccination-induced memory (Fig. 3d).

Fig. 3: Epitope characterization of mAbs elicited by Omicron breakthrough infections.



a–**c**, FACS analysis of pooled memory B cells (IgM$^-$, IgD$^-$/CD27$^+$) from Omicron breakthrough-infection convalescent individuals. BA.5 breakthrough infection (**a**), BA.2 breakthrough infection (**b**) and BA.2 convalescent individuals without vaccination (**c**) are shown. APC, allophycocyanine; FITC, fluorescein isothiocyanate; PE, phycoerythrin. **d**, The heavy-chain variable (VH) domain SHM rate of mAbs from individuals with BA.2 ($n = 757$) and BA.5 ($n = 297$) breakthrough infection. Binding specificity was determined by ELISA. Statistical tests were determined using two-tailed Wilcoxon rank-sum tests. Boxes display the 25th percentile, median and 75th percentile, and whiskers indicate median ± 1.5 times the interquartile range. Violin plots show kernel density estimation curves of the distribution. Numbers and ratios of samples in each group are labelled above the violin plots. **e**, *t*-SNE and clustering of SARS-CoV-2 WT RBD-binding antibodies based on DMS profiles of 3,051 antibodies. **f**, Epitope distribution of mAbs from convalescent individuals after WT infection or post-vaccination BA.1, BA.2 or BA.5 infection. Numbers in the centre circles indicate total numbers of mAbs. Colours for epitope groups in **e** also refer to **f**. Two-tailed binomial tests were used to compare the proportion of each epitope group from BA.2 and BA.5 convalescent individuals with that from BA.1. *$P < 0.05$, **$P < 0.01$, ***$P < 0.001$ and no label for $P > 0.05$. **g**, Projection of the neutralizing activity of mAbs against SARS-CoV-2 D614G

(left; $n = 3,046$), BA.2.75 (middle; $n = 3,046$) and BA.4/5 (right; $n = 3,046$). **h**, Projection of the ACE2 competition level of mAbs determined by competition ELISA ($n = 1,317$). All neutralization assays and ELISA were conducted in at least two independent experiments.

Next, we determined the escape mutation profiles of these antibodies by high-throughput DMS and measured their neutralizing activities against SARS-CoV-2 D614G, BA.2, BA.5, BA.2.75, BQ.1.1 and XBB (Fig. 3e,g and Extended Data Fig. 5a,b). Previously, we reported the DMS profiles and the epitope distribution of antibodies isolated from WT vaccinated or infected individuals, SARS-CoV-2-vaccinated individuals who recovered from SARS, and people who had BA.1 infection, which could be classified into 12 epitope groups[2]. Among them, mAbs in groups A, B, C, D1, D2, F2 and F3 compete with ACE2 and exhibit neutralizing activity (Fig. 3h and Extended Data Figs. 6a–d and 7a–d); whereas mAbs in groups E1, E2.1, E2.2, E3 and F1 do not compete with ACE2 (Fig. 3h and Extended Data Fig. 8a–c). Antibodies in groups E2.2, E3, and F1 exhibit low or no neutralizing capability (Extended Data Figs. 5b and 8d). To integrate the previous dataset with DMS profiles of the new mAbs isolated from BA.2 and BA.5 convalescent individuals, we co-embedded all antibodies using multidimensional scaling based on their DMS profiles, followed by *t*-distributed stochastic neighbour embedding (*t*-SNE) for visualization, and used *k*-nearest neighbours-based classification to determine the epitope groups of new mAbs (Fig. 3e). This results in a dataset containing the DMS profiles of 3,051 SARS-CoV-2 WT RBD-targeting mAbs in total (Supplementary Table 2). The epitope distribution of mAbs from BA.2 breakthrough infection is generally similar to those elicited by BA.1, except for the increased proportion of mAbs in group C (Fig. 3f). However, BA.5-elicited mAbs showed a more distinct distribution than BA.1, with a significantly increased proportion of mAbs in groups D2 and E2.2, and decreased ratio of antibodies in groups B and E2.1. The main reason is that the F486 and L452 mutations carried by BA.5 make these cross-reactive memory B cells unable to be activated and recalled (Fig. 3f and Extended Data Figs. 6b, 7a and 8a). Antibody repertoires induced by all Omicron breakthrough infections are distinct from those stimulated by WT infection or vaccination. Compared with WT infection or vaccination, BA.1, BA.2 and BA.5 breakthrough infections mainly elicit mAbs of groups E2.2, E3

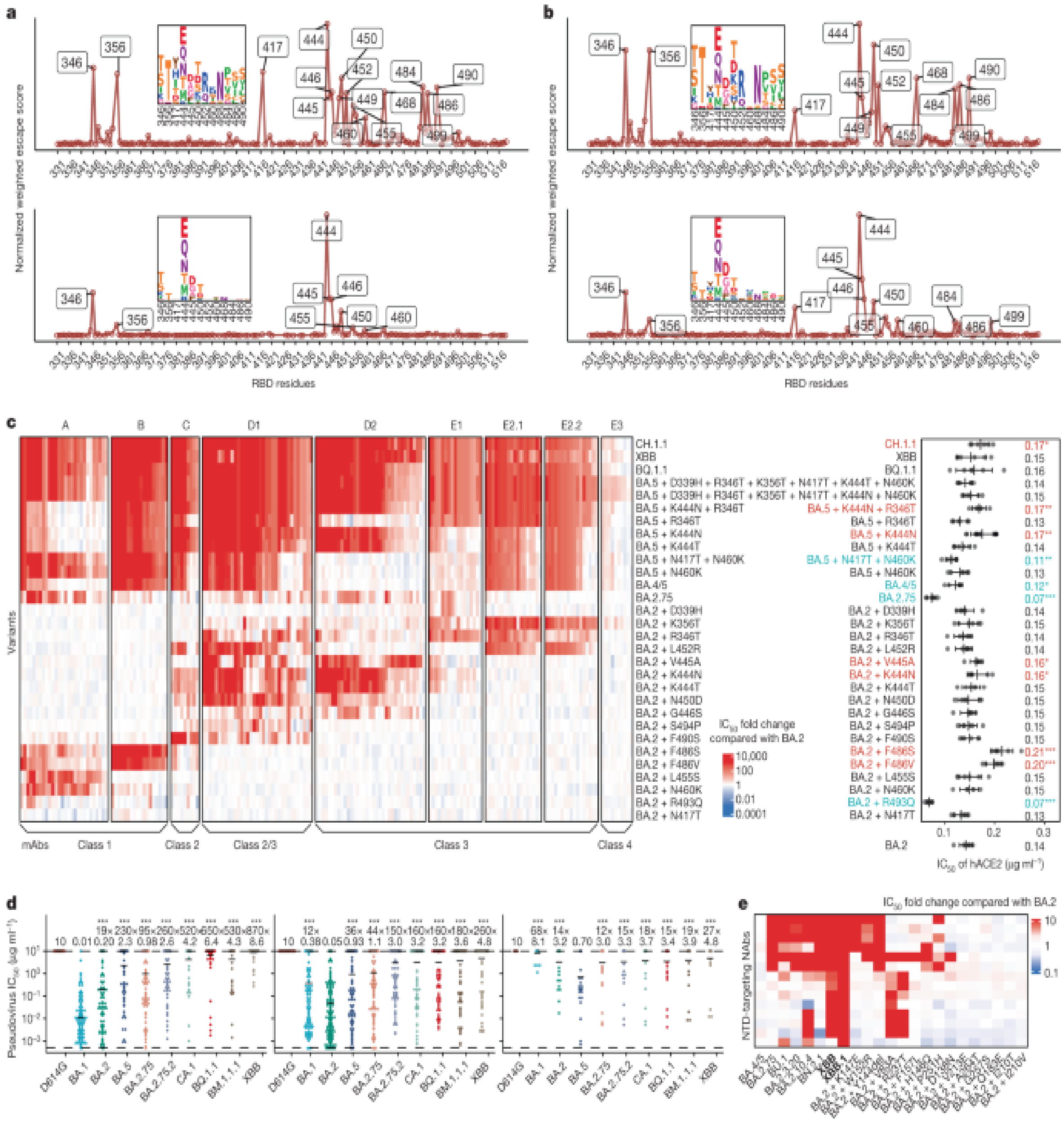
and F1, which do not compete with ACE2 and demonstrate weak neutralizing activity, whereas WT-elicited antibodies enrich mAbs of groups A, B and C, which compete with ACE2 and exhibit strong neutralization potency (Fig. 3f–h). The combined proportion of E2.2, E3 and F1 antibodies rose from 29% in WT convalescent or vaccinated individuals, 53% in BA.1 and 51% in BA.2 convalescent individuals, to 63% in BA.5 convalescent individuals (Fig. 3f). Overall, the proportion and diversity of neutralizing antibody epitopes are reduced in Omicron breakthrough infection, especially in BA.5 breakthrough infection.

To better delineate the effect of immune imprinting and consequent reduction of NAb epitope diversity on the RBD evolutionary pressure, we aggregated the DMS profiles of large collections of mAbs to estimate the effect of mutations on the efficacy of humoral immunity, as inspired by previous works[5] (Supplementary Table 2). It is essential to incorporate the effects of ACE2 binding, RBD expression, neutralizing activity of mAbs and codon usage constraint with the escape profiles to estimate the SARS-CoV-2 evolution trend on the RBD. In brief, each mutation on the RBD would have an effect on each mAb in the set, which is quantified by the escape scores determined by DMS and weighted by its half maximal inhibitory concentration (IC_{50}) against the evolving strain. For each residue, only those amino acids that are accessible by one nucleotide mutation are included. The effects on ACE2-binding capability (as measured by pseudovirus inhibitory efficiency) and RBD expression of each mutation are also considered in the analyses, using data determined by DMS in previous reports[4,29,34]. Finally, the estimated relative preference of each mutation is calculated using the sum of weighted escape scores of all mAbs in the specific set.

The reduced NAb epitope diversity caused by imprinted humoral response could be shown by the estimated mutation preference spectrum (Fig. 4a). Diversified escaping-score peaks, which also represent immune pressure, could be observed when using BA.2-elicited antibodies, whereas only two major peaks could be identified, R346T/S and K444E/Q/N/T/M, when using BA.5-elicited antibodies (Fig. 4a). These two hotspots are the most frequently mutated sites in continuously evolving BA.4/BA.5 subvariants, and convergently occurred in multiple lineages (Fig. 1). Similar analyses for WT and BA.1 also demonstrated diversified peaks; thus, the concentrated

immune pressure reflects the reduced diversity of NAbs elicited by BA.5 breakthrough infection due to immune imprinting, and these concentrated preferred mutations highly overlapped with convergent hotspots observed in the real world (Extended Data Fig. 9a,b). Together, our results indicate that due to immune imprinting, BA.5 breakthrough infection caused significant reductions in NAb epitope diversity and increased proportion of non-neutralizing mAbs, which in turn focused immune pressure and promoted the convergent RBD evolution.

Fig. 4: Immune imprinting promotes convergent evolution of NAb-evasive mutations.



a,**b**, Normalized average escape scores weighted by IC_{50} against BA.2 (top) and BA.5 (bottom) using DMS profiles of NAbs from corresponding convalescent individuals (**a**), and BA.2.75 (top) and BA.5 (bottom) using DMS profiles of all NAbs except those from individuals convalescent from SARS-CoV-1 infection followed by three-dose CoronaVac. (**b**). **c**, IC_{50} of representative potent BA.2-neutralizing antibodies in the epitope group against emerging and constructed Omicron subvariants pseudovirus with escape mutations, in addition to IC_{50} of hACE2 against these variants. The classes of the NAbs as defined in ref. [50] are also annotated below this map.

Error bars indicate mean ± s.d. of $n = 5$ biologically independent replicates. P values were calculated using two-tailed Student's t-test. *$P < 0.05$, **$P < 0.01$, ***$P < 0.001$ and no label on variants with $P > 0.05$. Variants with significantly stronger binding are coloured blue, whereas those with weaker binding are coloured red. **d**, IC_{50} against featured subvariants of RBD-targeting Omicron-specific NAbs from convalescent individuals with BA.1 (left; $n = 100$), BA.2 (middle; $n = 151$) and BA.5 (right; $n = 31$) breakthrough infection. The geometric mean IC_{50}s are labelled, and error bars indicate the geometric standard deviation. Dashed lines indicate the LOD ($IC_{50} = 0.0005$ μg ml^{-1}). P values are calculated using two-tailed Wilcoxon signed-rank tests compared with the corresponding eliciting strain. Antibodies with IC_{50} of more than 10 μg ml^{-1} against the eliciting strain were excluded from the calculation of P values and fold changes. ***$P < 0.001$ and $P > 0.05$ (NS). **e**, IC_{50} of NTD-targeting NAbs against emerging Omicron subvariants and BA.2 mutants with a single NTD substitution. All neutralization assays were conducted in at least two independent experiments.

Inference of RBD evolution hotspots

Moreover, we wondered whether the real-world evolutionary trends of SARS-CoV-2 RBD could be rationalized and even predicted by aggregating this large DMS dataset containing mAbs from various immune histories. Using the mAbs elicited from WT vaccinated or convalescent individuals weighted by IC_{50} against the D614G strain, we identified mutation hotspots including K417N/T, K444–G446, N450, L452R and especially E484K (Extended Data Fig. 9a). Most of these residues were mutated in previous variants of concern, such as K417N/E484K in Beta, K417T/E484K in Gamma, L452R in Delta and G446S/E484A in Omicron BA.1, confirming our estimation and inference. Evidence of the emergence of BA.2.75 and BA.5 could also be found using mAbs elicited by WT, BA.1 and BA.2 with IC_{50} against BA.2, where peaks on 444–446, 452, 460 and 486 could be identified (Extended Data Fig. 9c). To better investigate the evolution trends of BA.2.75 and BA.5, the two major lineages circulating currently, we then included antibodies elicited by various immune background, including WT/BA.1/BA.2/BA.5 convalescents, which we believe is the best way to represent the current heterogeneous global humoral immunity (Fig. 4b and

Extended Data Fig. 9d). For BA.2.75, the most outstanding sites are R346T/S, K356T, N417Y/H/I/T, K444E/Q/N/T/M, V445D/G/A, N450T/D/K/S, L452R, I468N, A484P, F486S/V and F490S/Y. We noticed that these identified residues, even specific mutations, highly overlapped with recent mutation hotspots of BA.2.75 (Fig. 1). Two exceptions are A484 and I468N. E484 is a featured residue of group C antibodies and could be covered by L452 and F490 (Extended Data Fig. 6c). The I468N mutation is also highly associated with K356 mutations, and its function could be covered by K356T (Extended Data Fig. 8a,b). Owing to stronger antibody evasion, the preference spectrum of BA.5 is much more concentrated than BA.2.75, but the remaining sites are highly overlapped and complementary with BA.2.75. The most striking residues are R346, K444–G446 and N450, followed by K356, N417, L455, N460 and A484. As expected, L452R/F486V does not stand out in the BA.5 preference spectrum, whereas N460K harboured by BA.2.75 appears. These sites and mutations are also popular in emerging BA.4/5 subvariants, proving that our RBD evolution inference system works accurately.

Evasion mechanism of convergent mutants

It is important to examine where this convergent evolution would lead. On the basis of the observed and predicted convergent hotpots on RBD of BA.2.75 and BA.5, we wondered whether we could construct the convergent variants in advance and investigate to what extent they will evade the humoral immune response. To do this, we must first evaluate the antibody evasion mechanism and the effect on hACE2-binding capability of the convergent mutations and their combinations. Thus, we selected a panel of 178 NAbs from 8 epitope groups that could potently neutralize BA.2 and determined their neutralizing activity against constructed mutants carrying single or multiple convergent mutations (Fig. 4c and Extended Data Fig. 10a). Most of these sites were selected as we have observed at least five independent emergences in distinct lineages of BA.2 and BA.5 that exhibited a growth advantage. NAbs from F1–F3 epitope groups were not included as they are either completely escaped by BA.2 or too rare in individuals convalescent from Omicron breakthrough infection (Fig. 3f). As expected, R493Q and N417T are not major contributors to antibody evasion, but R493Q significantly benefits ACE2 binding. V445A and K444N caused

slightly, and F486S/V caused significantly, reduced ACE2-binding capability, consistent with the measurement of emerging subvariants (Figs. 2a and 4c and Extended Data Fig. 2a). The neutralization of NAbs in each group is generally in line with DMS profiles. Most group A NAbs are sensitive to N460K and L455S, and BA.5 + N460K escapes the majority of NAbs in group A owing to the combination of F486V and N460K (Extended Data Fig. 6a). All NAbs in group B are escaped by F486S/V, and group C NAbs are heavily escaped by F490S and are strongly affected by L452R and F486S/V (Extended Data Fig. 6b,c). A part of group C NAbs is also slightly affected by K444N/T, S494P and N450D. G446S affects a part of the D1/D2 NAbs, as previously reported[20]. D1/D2 NAbs are more susceptible to K444N/T, V445A and N450D, and some D1 NAbs could also be escaped by L452R, F490S and S494P (Extended Data Fig. 7a,b). E1 is mainly affected by R346T, D339H and K356T (Extended Data Fig. 7c). E2.1 and E2.2 exhibit similar properties, evaded by K356T, R346T and L452R (Extended Data Fig. 8a,b). E3 antibodies seem to be not strongly affected by any of the constructed mutants, as expected (Extended Data Fig. 8c), but they generally exhibit very low neutralization (Extended Data Fig. 8d). BA.5 + R346T escapes most antibodies in D1, E1 and E2.1/E2.2, and an additional K444N further escapes most mAbs in D2, demonstrating the feasibility and effectiveness of combining convergent mutations to achieve further evasion. Adding six mutations to BA.5 could achieve the evasion of the vast majority of RBD NAbs, while exhibiting high hACE2-binding capability, despite the reduction caused by K444N/T and F486V. BQ.1.1, XBB and CH.1.1 could also escape the majority of RBD-targeting NAbs. Together, these findings indicate the feasibility of generating a heavy-antibody-escaping mutant with accumulated convergent escape mutations while maintaining sufficient hACE2-binding capability (Fig. 4c and Extended Data Fig. 10a).

Although the proportion of Omicron-specific mAbs is low due to immune imprinting, it is still necessary to evaluate their neutralization potency and breadth, especially against the convergent mutants. We tested the neutralizing activity of a panel of Omicron-specific RBD-targeting mAbs against D614G, BA.1, BA.2, BA.5, BA.2.75, BA.2.75.2, BR.1, BR.2, CA.1, BQ.1.1 and XBB. These mAbs were isolated from convalescent plasma 1 month after Omicron breakthrough infection (Fig. 4d). They could bind to the RBD of the corresponding exposed Omicron variant but did not cross-

bind WT RBD, as confirmed by ELISA. We found that these mAbs could effectively neutralize against the exposed strain, as expected, but exhibited poor neutralizing breadth, which means their potency would be largely impaired by other Omicron subvariants, consistent with our previous discovery[2]. Of note, BQ.1.1 and XBB could escape most of these Omicron-specific NAbs. Thus, these Omicron-specific antibodies would not effectively expand the breadth of the neutralizing antibody repertoire of Omicron breakthrough infection when facing convergent variants. Further affinity maturation may improve the breadth, but additional experiments are needed.

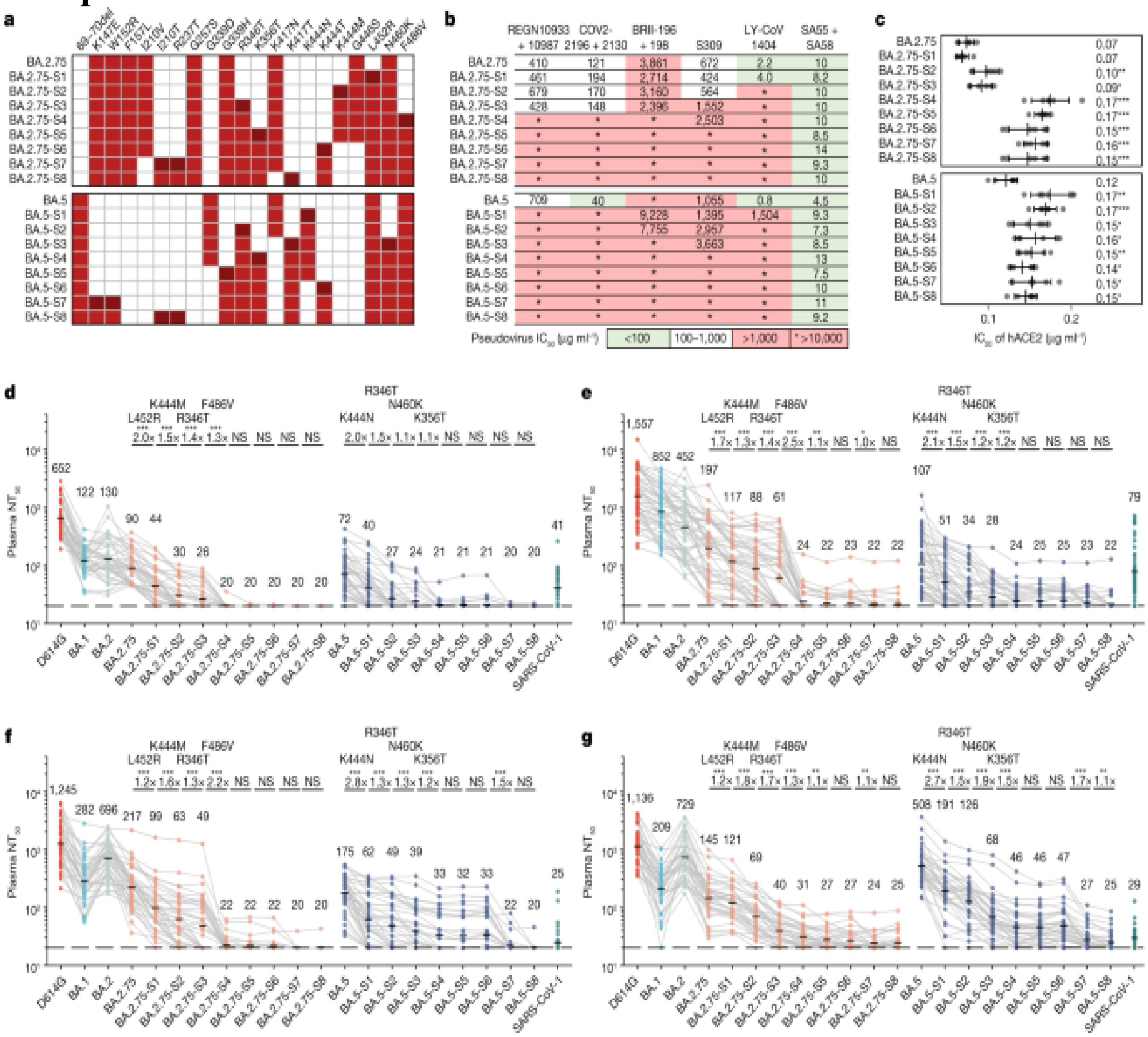
We then evaluated the potency of NTD-targeting NAbs against BA.2, BA.4/5, BA.2.75 and their sublineages and constructed mutants with selected NTD mutations using a panel of 14 NTD-targeting NAbs, as it is reported that NTD-targeting antibodies are abundant in plasma from BA.2 breakthrough infection and contribute to cross-reactivity[35]. Most selected mutations are from recently designated Omicron subvariants, except for R237T, which was near V83A, designed to escape mAbs targeting an epitope recently reported[20]. None of the NTD-targeting NAbs exhibit strong neutralizing potency, and the IC_{50} values are all over 0.2 μg ml^{-1} (refs. [36,37]) (Fig. 4e and Extended Data Fig. 10b). We found that the tested BA.2-effective NTD-targeting NAbs could be separated into two clusters, named group-α and group-δ in our previous report[20] (Extended Data Fig. 10c). NAbs in group-α target the well-known antigenic supersite on NTD[38], which is sensitive to K147E and W152R in BA.2.75* and Y144del in BJ.1/XBB; whereas group-δ is affected by V83A (XBB) and R237T. The other three NTD mutations in BA.2.75, F157L, I210V and G257S did not obviously affect the tested mAbs, consistent with previous sera neutralization data[28]. Two of the NTD mutations in BJ.1 or XBB, Y144del and V83A, each escapes a cluster of them and together would enable XBB to exhibit extremely strong capability of escaping NTD-targeting NAbs. Of note, XBB.1 escaped all NTD-targeting NAbs tested here.

Simulating convergent variant evolution

On the basis of the above results, we designed multiple VSV-based pseudoviruses that gradually gain convergent mutations that could induce RBD-targeting or NTD-targeting NAb resistance (Fig. 5a). The constructed final mutant contains 11 additional mutations on the NTD and RBD compared with BA.5, or 9 mutations compared with BA.2.75. The neutralizing activities of Omicron-effective NAb drugs were first evaluated. As expected, the majority of existing effective NAb drugs, except SA55, are escaped by these mutants (Fig. 5b). Similarly, we also determined the ACE2-binding capability of these mutants by neutralization assays using hACE2 (Fig. 5c). Although some of the designed pseudoviruses, especially those with K444N and F486V, exhibit reduced activity to hACE2 compared with the original BA.2.75 or BA.5 variants, their binding affinities are still higher than that of D614G (Fig. 2b). Our designed pseudoviruses could largely evade the plasma of vaccinated individuals and convalescent individuals after BA.1, BA.2 and even BA.5 breakthrough infection (Fig. 5d–g). Among the derivative mutants of BA.2.75, L452R, K444M, R346T and F486V contribute mainly to the significant reduction in neutralization (Fig. 5d–g). Adding more NTD mutations does not contribute to stronger evasion in BA.2.75-based mutants, but we observed a significant reduction in NT_{50} of BA.2/BA.5 convalescent individuals against BA.5-based mutants with K147E + W152R, suggesting that BA.2/BA.5 convalescent plasma contains a large proportion of NTD-targeting antibodies[35]. As the NTD of BA.1 differs from that of BA.2 and BA.5, we did not observe significant effects of NTD mutations on the efficacy of BA.1 convalescent plasma. Plasma neutralization titres of most vaccinated and convalescent individuals decreased to the lower detection limit against BA.2.75 with five extra RBD mutations: L452R, K444M, R346T, F486V and K356T. The same applies to vaccinated individuals or BA.1 convalescents against BA.5 with four extra RBD mutations: K444N, R346T, N460K and K356T. The plasma from BA.2/BA.5 convalescents can tolerate more mutations based on BA.5, and extra NTD mutations such as K147E and W152R are needed to completely eliminate their neutralization. Together, we demonstrate that as few as five additional mutations on BA.5 or BA.2.75 could completely evade most plasma samples, including those from BA.5 breakthrough infection, while maintaining high hACE2-binding capability. Similar efforts have been made in a recent report despite different construction strategies[39]. The constructed evasive mutants, such as BA.2.75-

S5/6/7/8 and BA.5-S7/8, could serve to examine the effectiveness of broad-spectrum vaccines and NAbs in advance.

Fig. 5: Accumulation of convergent escape mutations leads to complete loss of plasma neutralization.



a, Mutations of multiple designed mutants with key convergent escape mutations based on BA.2.75 and BA.5. Mutations in dark red indicate the additional mutation compared with the former mutant. **b**, IC_{50} of therapeutic mAbs and cocktails against pseudoviruses of designed mutants. **c**, IC_{50} of hACE2 against the designed mutants. Error bars indicate mean ± s.d. of n = 5 biologically independent replicates. P values were calculated using two-tailed Student's t-test, compared with BA.2.75 and BA.5 for BA.2.75-derived and BA.5-derived mutants, respectively. *$P < 0.05$, **$P < 0.01$,

***$P < 0.001$ and no label on variants with $P > 0.05$. **d**–**g**, Pseudovirus neutralizing titres against SARS-CoV-2 D614G, Omicron subvariants and designed mutants of plasma from vaccinated or convalescent individuals with breakthrough infection. Individuals who received three doses of CoronaVac ($n = 40$) (**d**), convalescent individuals infected with BA.1 after receiving three doses of CoronaVac ($n = 50$) (**e**), convalescent individuals infected with BA.2 after receiving three doses of CoronaVac ($n = 39$) (**f**), and convalescent individuals infected with BA.5 after receiving three doses of CoronaVac ($n = 36$) (**g**) are shown. Key additional mutations from each designed mutant are annotated above the points. Dashed lines indicate the limit of detection (LOD, $NT_{50} = 20$). The geometric mean titres are labelled. P values are determined using two-tailed Wilcoxon signed-rank tests of paired samples. *$P < 0.05$, **$P < 0.01$, ***$P < 0.001$ and $P > 0.05$ (NS). All neutralization assays were conducted in at least two independent experiments.

Discussion

Convergent evolution is common in the biological world, given that one mutation can exhibit strong advantage in particular functions and prevail in multiple lineages. This phenomenon has also been observed in other highly mutated RNA viruses, such as HIV and influenza viruses[40,41]. Previously, N501Y was considered as a convergent mutation that appeared in almost all SARS-CoV-2 variants, which was demonstrated to enhance ACE2-binding affinity[42]. K417 and E484, whose mutations were demonstrated to escape a large number of NAbs, have also exhibited some kind of convergence patterns[43]. However, these previous observations were not outstanding and rapid as recent emergence of convergent mutations on RBD during the global BA.4/5 wave, when several convergent mutations appeared in dozens of sublineages independently, exhibiting growth advantages compared with BA.5. In this work, we showed that due to immune imprinting, our humoral immune repertoire is not effectively diversified by infection with new Omicron variants. The immune pressure on the RBD becomes increasingly concentrated and promotes convergent evolution, explaining the observed sudden acceleration of SARS-CoV-2 RBD evolution and the convergence pattern.

Although this study only examines inactivated vaccines, immune imprinting is also observed in those receiving mRNA vaccines[44,45]. In fact, mRNA-vaccinated individuals displayed an even higher proportion of cross-reactive memory B cells, probably because the overall humoral immune response induced by mRNA vaccines is stronger than that induced by inactivated vaccines[45]. In addition, recent studies on mRNA-vaccinated individuals who receive a BA.5 booster or BA.5 breakthrough infection displayed a similar neutralization reduction trend against BA.2.75.2, BQ.1 and BQ.1.1, suggesting high consistency of neutralization data among vaccine types[46,47].

As the antibodies undergo affinity maturation, their SHM rate would increase[45]. This may lead to a higher proportion of variant-specific antibodies, enhanced binding affinity and increased neutralization breadth, which could potentially resist the convergent mutations carried by variants such as XBB and BQ.1.1 (ref. [48]). However, the effect of affinity maturation may be counteracted by waning immunity[45,49]. The affinity-matured memory B cells would require a second booster or reinfection to be effectively deployed.

We also observed that plasma from individuals with BA.5 breakthrough infection exhibited higher neutralization against BA.5-derived variants such as BQ.1 and BQ.1.1, suggesting that BA.5 boosters and infections are beneficial to protection against convergent variants of BA.5 sublineages. However, this may be mainly driven by the enrichment of NTD-targeting antibodies after BA.5 breakthrough infection, which was also reported in BA.2 convalescent individuals[35]. Specific evasive mutations on the NTD, such as Y144del in XBB and BQ.1.1.10, and mutations of many BA.2.75 sublineages, would cause severe reduction in BA.5 breakthrough infection plasma neutralization titres. Therefore, the effectiveness of BA.5-based boosters against the convergent mutants carrying critical NTD mutations should be closely monitored.

Of note, the antibody evasion capability of many variants, such as BQ.1.1, CA.1, BQ.1.18, XBB and CH.1.1, have already reached or even exceeded SARS-CoV-1, indicating extensive antigenic drift (Fig. 5d–g). Indeed, by constructing an antigenic map of the tested SARS-CoV-2/SARS-CoV-1 variants using the plasma NT_{50} data, we found that the antigenicity distances

of SARS-CoV-2 ancestral strain to CA.1, CH.1.1, XBB and BQ.1.1 are already comparable with that of SARS-CoV-1 (Extended Data Fig. 11a,b). Given that there are approximately 50 different amino acids between SARS-CoV-1 and SARS-CoV-2 RBD, but only 21 mutations on the BQ.1.1 RBD compared with the ancestral strain, these results indicate that the global pandemic indeed has greatly promoted the efficiency of the virus to evolve immune escape mutations.

Finally, our prediction demonstrated a remarkable consistency with real-world observations. Some variants close to the predicted and constructed variants have already emerged as we performed the experiments, validating our prediction model. For example, BA.4.6.3 and BQ.1.1 are highly similar to BA.5-S3, and CH.1.1 to BA.2.75-S4/S6 (Fig. 4c). The whole pipeline for constructing pseudoviruses carrying predicted mutations could be safely conducted in biosafety level 2 laboratories, and does not involve any infectious pandemic virus. If we had this prediction model at the beginning of the pandemic, the development of NAb drugs and vaccines might not be so frustrated against the continuously emerging SARS-CoV-2 variants. Broad-spectrum SARS-CoV-2 vaccines and NAb drug development should be of high priority, and the DMS-based prediction of RBD mutations demonstrated in this study could provide effective guidance.

Methods

Sequence analysis of Omicron sublineages

To identify the sites on RBD with convergence patterns, we first gathered a list of designated Pango lineages and only kept the lineages that exhibited growth advantages over their corresponding ancestral Omicron strains (BA.2, BA.2.75 or BA.5). We identified the parent of each strain according to its Pango lineage full name. Only the additional mutations of each strain compared with its parent are counted in the analysis, which means the inherited mutations will not be counted repeatedly. For example, BQ.1 is the parent of BQ.1.1, and BE.1.1.1 is the parent of BQ.1. Therefore, R346T is the only independent mutation carried by BQ.1.1, and N460K is the only independent mutations carried by BQ.1. K444T is only counted in BE.1.1.1 but not repeatedly counted in BQ.1 and BQ.1.1. For recombinants, the

mutations carried by the ancestral recombinant were not counted, but their derivatives were included. Finally, for each site on the RBD, we calculated the number of independent occurrences of mutation on the site, that is, the number of strains that carried mutations on the site and exhibited growth advantage. Sites mutated independently in at least five lineages were considered as convergent mutation sites. The list of strains and the growth advantages over BA.2, BA.2.75 or BA.5 were collected from the #24 collection of CoV-Spectrum (https://cov-spectrum.org)[1]. The full names of designated lineages were collected from the GitHub repository (https://github.com/cov-lineages/pango-designation).

To get the dynamic change of the convergent mutations during the pandemic, spike protein sequences were downloaded from the Global Initiative on Sharing Avian Influenza Data (GISAID; released on 27 October 2022)[16]. The sequences were split according to their date of sampling (from January 2021 to October 2022), and locally aligned to the SARS-CoV-2 WT RBD sequence using biopython (Bio.pairwise2.align.localms, version 1.78) with the scores 2, −1, 8 and 8 for matched, mismatched, gap open and gap extension, respectively. Sequences with an alignment score of less than 200 were excluded from the analysis. ‘X’ in the sequences was also excluded. The frequencies of each of the 20 amino acids on each RBD site were counted.

Isolation of peripheral blood mononuclear cells and plasma

Samples from vaccinated individuals and people who had BA.1, BA.2 or BA.5 infection were obtained under study protocols approved by Beijing Ditan Hospital, Capital Medical University (Ethics committee archiving no. LL-2021-024-02) and the Tianjin Municipal Health Commission, and the Ethics Committee of Tianjin First Central Hospital (Ethics committee archiving no. 2022N045KY). All donors provided written informed consent for the collection of information, the use of blood and blood components, and the publication of data generated from this study. Whole-blood samples were diluted 1:1 with PBS + 2% FBS (Gibco) and subjected to Ficoll (Cytiva) gradient centrifugation. Plasma was collected from the upper layer. Cells were collected at the interface and further prepared by centrifugation, red blood cell lysis (Invitrogen eBioscience) and washing steps. The date of

vaccination, hospitalization and sampling can be found in Supplementary Table 1.

BCR sequencing, analysis and antibody production

$CD19^+$ B cells were isolated from peripheral blood mononuclear cells with EasySep Human CD19 Positive Selection Kit II (17854, STEMCELL). Every 10^6 B cells in 100 μl solution were stained with 3 μl FITC anti-human CD20 antibody (clone 2H7, 302304, BioLegend), 3.5 μl Brilliant Violet 421 anti-human CD27 antibody (clone O323, 302824, BioLegend), 2 μl PE/cyanine-7 anti-human IgM antibody (clone MHM-88, 314532, BioLegend), 2 μl PE/cyanine-7 anti-human IgD antibody (clone IA6-2, 348210, BioLegend), 0.013 μg biotinylated SARS-CoV-2 BA.2 RBD protein (customized from Sino Biological) or 0.013 μg biotinylated SARS-CoV-2 BA.5 RBD protein (customized from Sino Biological) conjugated with PE-streptavidin (405204, BioLegend) and APC-streptavidin (405207, BioLegend), and 0.013 μg SARS-CoV-2 WT biotinylated RBD protein (40592-V27H-B, Sino Biological) conjugated with Brilliant Violet 605 streptavidin (405229, BioLegend). Cells were also labelled with biotinylated RBD conjugated to DNA-oligo-streptavidin. Omicron RBD (BA.2 or BA.5) were labelled with TotalSeq-C0971 streptavidin (405271, BioLegend) and TotalSeq-C0972 streptavidin (405273, BioLegend); WT RBD were labelled with TotalSeq-C0973 streptavidin (405275, BioLegend) and TotalSeq-C0974 streptavidin (405277, BioLegend). Cells were washed twice after 30 min of incubation on ice. 7-AAD (00-6993-50, Invitrogen) was used to label dead cells. 7-$AAD^-CD20^+CD27^+IgM^-IgD^-$ SARS-CoV-2 BA.2 RBD^+ or BA.5 RBD^+ cells were sorted with a MoFlo Astrios EQ Cell Sorter. FACS data were collected by Summit 6.0 (Beckman Coulter). FACS data were analysed using FlowJo v10.8 (BD Biosciences).

Sorted B cells were resuspended in the appropriate volume and then processed with Chromium Next GEM Single Cell V(D)J Reagent Kits v1.1 following the manufacturer's user guide (CG000208, 10X Genomics). Gel beads-in-emulsion (GEMs) were obtained with a 10X Chromium controller. GEMs were subjected to reverse transcription and purification. Reverse transcription products were subject to pre-amplification and purification with the SPRIselect Reagent Kit (B23318, Beckman Coulter). BCR

sequences (paired V(D)J) were enriched with 10X BCR primers. After library preparation, libraries were sequenced with the Illumina sequencing platform.

10X Genomics V(D)J sequencing data were assembled as BCR contigs and aligned using the Cell Ranger (v6.1.1) pipeline according to the GRCh38 BCR reference. Only the productive contigs and the B cells with one heavy chain and one light chain were kept for quality control. The germline V(D)J gene identification and annotation were performed by IgBlast (v1.17.1)[51]. Somatic hypermutation sites in the antibody variable domain were detected using the Change-O toolkit (v1.2.0)[52].

Antibody heavy-chain and light-chain genes were optimized for human cell expression and synthesized by GenScript. VH and VL were inserted separately into plasmids (pCMV3-CH, pCMV3-CL or pCMV3-CK) through infusion (C112, Vazyme). Plasmids encoding the heavy chain and light chain of antibodies were co-transfected by polyethylenimine transfection to Expi293F cells (A14527, Thermo Fisher). Cells were cultured at 36.5 °C in 5% CO_2 at 175 r.p.m. for 6–10 days. Supernatants containing mAbs were collected and the supernatants were further purified with protein A magnetic beads (L00695, Genscript).

High-throughput DMS

The high-throughput DMS platform has been previously described[2,3]. In brief, DMS libraries were constructed by mutagenesis PCR based on the Wuhan-Hu-1 RBD sequence (residues N331–T531; GenBank: MN908947). A unique 26-nucleotide (N26) barcode was appended to each RBD variant in mutant libraries by PCR, and the correspondence between the N26 barcode and mutations in RBD variants was acquired by PacBio sequencing. RBD-mutant libraries were first transformed in the EBY100 strain of *Saccharomyces cerevisiae* and then enriched for properly folded ACE2 binders, which were used for subsequent mutation escape profiling. The above ACE2 binders were grown in SG-CAA medium (2% w/v d-galactose, 0.1% w/v dextrose (d-glucose), 0.67% w/v yeast nitrogen base, 0.5% w/v casamino acids (-ade, -ura and -trp) and 100 mM phosphate buffer, pH 6.0) at room temperature for 16–18 h with agitation. Then, these yeast cells were

washed twice and proceeded to three rounds of magnetic beads-based selection. Obtained yeast cells after sequential sorting were recovered overnight in SD-CAA medium (2% w/v dextrose (d-glucose), 0.67% w/v yeast nitrogen base, 0.5% w/v casamino acids (-ade, -ura and -trp) and 70 mM citrate buffer, pH 4.5). Pre-sorting and post-sorting yeast populations were submitted to plasmid extraction by a 96 Well Plate Yeast Plasmid Preps Kit (PE053, Coolaber). N26 barcode sequences were amplified with the extracted plasmid templates, and PCR products were purified and submitted to Illumina Nextseq 550 sequencing.

Antibody clustering and embedding based on DMS profiles

Data analysis of DMS was performed as described in previous reports[2,3]. In brief, the detected barcode sequences of both the antibody-screened and reference library were aligned to the barcode-variant lookup table generated using dms_variants (v0.8.9). The escape scores of each variant *X* in the library were defined as $F\times(n_{X,\mathrm{ab}} / N_{\mathrm{ab}}) / (n_{X,\mathrm{ref}} / N_{\mathrm{ref}})$, where F is a scale factor to normalize the scores to the 0–1 range, and n and N are the number of detected barcodes for variant X and total barcodes in post-selected (ab) or reference (ref) samples, respectively. The escape scores of each mutation were calculated by fitting an epistasis model as previously described[4,53].

Epitope groups of new antibodies not included in our previous report are determined by the *k*-nearest neighbours-based classification. In brief, site escape scores of each antibody are first normalized and considered as a distribution across RBD residues, and only residues whose standard derivation is among the highest 50% of all residues are retained for further analysis. Then, the dissimilarity or distance of two antibodies is defined by the Jessen–Shannon divergence of the normalized escape scores. Pairwise dissimilarities of all antibodies in the dataset are calculated using the scipy package (scipy.spatial.distance.jensenshannon, v1.7.0). For each antibody, the 15 nearest neighbours whose epitope groups have been determined by unsupervised clustering in our previous paper were identified and simply voted to determine the group of the selected antibody. To project the dataset onto a 2D space for visualization, we performed multidimensional scaling to represent each antibody in a 32-dimensional space, and then *t*-SNE to get the

2D representation, using sklearn.manifold.MDS and sklearn.manifold.TSNE (v0.24.2). Figures were generated by R package ggplot2 (v3.3.3).

Calculation of the estimated preference of RBD mutations

Four different weights are included in the calculation, including the weight for ACE2-binding affinity, RBD expression, codon constraint and neutralizing activity. The effect on ACE2-binding affinity and RBD expression of each mutation based on WT, BA.1 and BA.2 were obtained from public DMS results. For BA.5 (BA.2 + L452R + F486V + R493Q) and BA.2.75 (BA.2 + D339H + G446S + N460K + R493Q), BA.2 results were used except for these mutated residues, whose scores for each mutant were subtracted by the score for the mutation in BA.5 or BA.2.75. As the reported values are log fold changes, the weight is simply defined by the exponential of reported values, that is, $\exp(S_{\mathrm{bind}})$ or $\exp(S_{\mathrm{expr}})$, respectively. For codon constraint, the weight is 1.0 for mutants that could be accessed by one nucleotide mutation, and 0.0 for others. We used the following RBD nucleotide sequences for determination of accessible mutants: WT/D614G (Wuhan-Hu-1 reference genome), BA.1 (EPI_ISL_10000028), BA.2 (EPI_ISL_10000005), BA.4/5 (EPI_ISL_11207535) and BA.2.75 (EPI_ISL_13302209). For neutralizing activity, the weight is $-\log_{10}(\mathrm{IC}_{50})$. The IC_{50} values (μg ml^{-1}), which are smaller than 0.0005 or larger than 1.0 are considered as 0.0005 or 1.0, respectively. The raw escape scores for each antibody were first normalized by the maximum score among all mutants, and the final weighted score for each antibody and each mutation is the product of the normalized scores and four corresponding weights. The final mutation-specific weighted score is the summation of scores of all antibodies in the designated antibody set and then normalized again to make it a value between 0 and 1. Logo plots for visualization of escape maps were generated by the Python package logomaker (v0.8).

Pseudovirus neutralization assay

The gene encoding the spike protein (GenBank: MN908947) was mammalian codon-optimized and inserted into the pcDNA3.1 vector. Site-directed mutagenesis PCR was performed as previously described[54]. The

sequence of mutants is shown in Supplementary Table 3. Pseudotyped viruses were generated by transfection of 293T cells (CRL-3216, American Type Culture Collection) with pcDNA3.1-spike with Lipofectamine 3000 (Invitrogen). The cells were subsequently infected with G*ΔG-VSV (Kerafast) that packages expression cassettes for firefly luciferase instead of VSV-G in the VSV genome. The cell supernatants were discarded after 6–8 h of harvest and replaced with complete culture media. The cell was cultured for 1 day, and then the cell supernatant containing pseudotyped virus was harvested, filtered (0.45-μm pore size; Millipore), aliquoted and stored at −80 °C. Viruses of multiple variants were diluted to the same number of copies before use.

mAbs or plasma were serially diluted and incubated with the pseudotyped virus in 96-well plates for 1 h at 37 °C. Trypsin-treated Huh-7 cells (0403, Japanese Collection of Research Bioresources) were added to the plate. The cells were cultured for 20–28 h in 5% CO_2 and 37 °C incubators. The supernatants were removed and left 100 μl in each well, and 100 μl luciferase substrate (6066769, PerkinElmer) was added and incubated in the dark for 2 min. The cell lysate was removed and the chemiluminescence signals were collected by PerkinElmer Ensight. Each experiment was repeated at least twice.

Inhibitory efficiencies of hACE2 against the pseudoviruses were determined with the same procedure, using the hACE2-Fc dimer (10108-H02H, Sino Biological), and each experiment was conducted in five biologically independent replicates.

DMEM (high glucose; HyClone) with 100 U ml^{-1} penicillin–streptomycin solution (Gibco), 20 mM HEPES (Gibco) and 10% FBS (Gibco) was used in cell culture. Trypsin-EDTA (0.25%; Gibco) was used to detach cells before seeding to the plate.

ELISA

WT/BA.2/BA.1 RBD or spikes in PBS was pre-coated onto ELISA plates at 4 °C overnight and were washed and blocked. Purified antibodies (1 μg ml^{-1}) were added and incubated at room temperature for 20 min.

Peroxidase-conjugated AffiniPure goat anti-human IgG (H+L) (0.25 μg ml^{-1}; 109-035-003, JACKSON) was added to plates and incubated at room temperature for 15 min. Tetramethylbenzidine (54827-17-7, Solarbio) was added and incubated for 10 min, and then the reaction was terminated with 2 M H_2SO_4. Absorbance was measured at 450 nm using a microplate reader (HH3400, PerkinElmer). H7N9 human IgG1 antibody HG1K (1 μg ml^{-1}; HG1K, Sino Biological) was used as negative control.

Reporting summary

Further information on research design is available in the Nature Portfolio Reporting Summary linked to this article.

Data availability

Processed mutation escape scores can be downloaded at https://github.com/jianfcpku/convergent_RBD_evolution. Sequences and neutralization of the antibodies are included in Supplementary Table 2. Raw sequencing data of DMS assays are available on China National GeneBank (db.cngb.org) with project accession CNP0003808. We used vdj_GRCh38_alts_ensembl-5.0.0 as the reference for V(D)J alignment, which can be obtained from https://support.10xgenomics.com/single-cell-vdj/software/downloads/latest. We used Protein Data Bank ID 6M0J for the structural model of the SARS-CoV-2 RBD. A list of strains and the growth advantages was collected from the #24 collection from https://cov-spectrum.org. Designated lineages were from https://github.com/cov-lineages/pango-designation.

Code availability

Custom scripts to analyse the escape mutation profile data are available at https://github.com/jianfcpku/convergent_RBD_evolution.

References

1. Chen, C. et al. CoV-Spectrum: analysis of globally shared SARS-CoV-2 data to identify and characterize new variants. *Bioinformatics* **38**, 1735–1737 (2021).

2. Cao, Y. et al. BA.2.12.1, BA.4 and BA.5 escape antibodies elicited by Omicron infection. *Nature* **608**, 593–602 (2022).

3. Cao, Y. et al. Omicron escapes the majority of existing SARS-CoV-2 neutralizing antibodies. *Nature* **602**, 657–663 (2022).

4. Starr, T. N. et al. Deep mutational scanning of SARS-CoV-2 receptor binding domain reveals constraints on folding and ACE2 binding. *Cell* **182**, 1295–1310.e20 (2020).

5. Greaney, A. J., Starr, T. N. & Bloom, J. D. An antibody-escape estimator for mutations to the SARS-CoV-2 receptor-binding domain. *Virus Evol.* **8**, veac021 (2022).

6. Wang, Q. et al. Antibody evasion by SARS-CoV-2 Omicron subvariants BA.2.12.1, BA.4 and BA.5. *Nature* **608**, 603–608 (2022).

7. Uraki, R. et al. Characterization and antiviral susceptibility of SARS-CoV-2 Omicron/BA.2. *Nature* **607**, 119–127 (2022).

8. Cele, S. et al. Omicron extensively but incompletely escapes Pfizer BNT162b2 neutralization. *Nature* **602**, 654–656 (2022).

9. Cameroni, E. et al. Broadly neutralizing antibodies overcome SARS-CoV-2 Omicron antigenic shift. *Nature* **602**, 664–670 (2022).

10. Yamasoba, D. et al. Virological characteristics of the SARS-CoV-2 Omicron BA.2 spike. *Cell* **185**, 2103–2115.e19 (2022).

11. Tuekprakhon, A. et al. Antibody escape of SARS-CoV-2 Omicron BA.4 and BA.5 from vaccine and BA.1 serum. *Cell* **185**, 2422–2433.e13 (2022).

12. Dejnirattisai, W. et al. SARS-CoV-2 Omicron-B.1.1.529 leads to widespread escape from neutralizing antibody responses. *Cell* **185**,

467–484.e15 (2022).

13. Cui, Z. et al. Structural and functional characterizations of infectivity and immune evasion of SARS-CoV-2 Omicron. *Cell* **185**, 860–871.e13 (2022).

14. Wang, K. et al. Memory B cell repertoire from triple vaccinees against diverse SARS-CoV-2 variants. *Nature* **603**, 919–925 (2022).

15. Kimura, I. et al. Virological characteristics of the SARS-CoV-2 Omicron BA.2 subvariants including BA.4 and BA.5. *Cell* **185**, 3992–4007.e16 (2022).

16. Shu, Y. & McCauley, J. GISAID: global initiative on sharing all influenza data—from vision to reality. *Euro Surveill.* **22**, 30494 (2017).

17. Rambaut, A. et al. A dynamic nomenclature proposal for SARS-CoV-2 lineages to assist genomic epidemiology. *Nat. Microbiol.* **5**, 1403–1407 (2020).

18. Sheward, D. J. et al. Evasion of neutralising antibodies by omicron sublineage BA.2.75. *Lancet Infect. Dis.* **22**, 1421–1422 (2022).

19. Saito, A. et al. Virological characteristics of the SARS-CoV-2 Omicron BA.2.75 variant. *Cell Host Microbe* **30**, 1540-1555.e15 (2022).

20. Cao, Y. et al. Characterization of the enhanced infectivity and antibody evasion of Omicron BA.2.75. *Cell Host Microbe* **30**, 1527–1539.e5 (2022).

21. Jian, F. et al. Further humoral immunity evasion of emerging SARS-CoV-2 BA.4 and BA.5 subvariants. *Lancet Infect. Dis.* **22**, 1535–1537 (2022).

22. Greaney, A. J. et al. Comprehensive mapping of mutations in the SARS-CoV-2 receptor-binding domain that affect recognition by polyclonal human plasma antibodies. *Cell Host Microbe* **29**, 463–476.e6 (2021).

23. Greaney, A. J. et al. Complete mapping of mutations to the SARS-CoV-2 spike receptor-binding domain that escape antibody recognition. *Cell Host Microbe* **29**, 44–57.e9 (2021).

24. Greaney, A. J. et al. Mapping mutations to the SARS-CoV-2 RBD that escape binding by different classes of antibodies. *Nat. Commun.* **12**, 4196 (2021).

25. Zost, S. J. et al. Potently neutralizing and protective human antibodies against SARS-CoV-2. *Nature* **584**, 443–449 (2020).

26. Westendorf, K. et al. LY-CoV1404 (bebtelovimab) potently neutralizes SARS-CoV-2 variants. *Cell Rep.* **39**, 110812 (2022).

27. Cao, Y. et al. Rational identification of potent and broad sarbecovirus-neutralizing antibody cocktails from SARS convalescents. *Cell Rep.* **41**, 111845 (2022).

28. Wang, Q. et al. Antigenic characterization of the SARS-CoV-2 Omicron subvariant BA.2.75. *Cell Host Microbe* **30**, 1512–1517.e4 (2022).

29. Starr, T. N. et al. Deep mutational scans for ACE2 binding, RBD expression, and antibody escape in the SARS-CoV-2 Omicron BA.1 and BA.2 receptor-binding domains. *PLOS Pathogens* https://doi.org/10.1371/journal.ppat.1010951 (2022).

30. Quandt, J. et al. Omicron BA.1 breakthrough infection drives cross-variant neutralization and memory B cell formation against conserved epitopes. *Sci. Immunol.* **7**, eabq2427 (2022).

31. Khan, K. et al. Omicron BA.4/BA.5 escape neutralizing immunity elicited by BA.1 infection. *Nat. Commun.* **13**, 4686 (2022).

32. Park, Y. J. et al. Imprinted antibody responses against SARS-CoV-2 Omicron sublineages. *Science* https://doi.org/10.1126/science.adc9127 (2022).

33. Reynolds, C. J. et al. Immune boosting by B.1.1.529 (Omicron) depends on previous SARS-CoV-2 exposure. *Science* **377**, eabq1841 (2022).

34. Starr, T. N. et al. Shifting mutational constraints in the SARS-CoV-2 receptor-binding domain during viral evolution. *Science* **377**, 420–424 (2022).

35. Muik, A. et al. Omicron BA.2 breakthrough infection enhances cross-neutralization of BA.2.12.1 and BA.4/BA.5. *Sci. Immunol.* **7**, eade2283 (2022).

36. Wang, Z. et al. Analysis of memory B cells identifies conserved neutralizing epitopes on the N-terminal domain of variant SARS-CoV-2 spike proteins. *Immunity* **55**, 998–1012.e8 (2022).

37. Chi, X. et al. A neutralizing human antibody binds to the N-terminal domain of the spike protein of SARS-CoV-2. *Science* **369**, 650–655 (2020).

38. McCallum, M. et al. N-terminal domain antigenic mapping reveals a site of vulnerability for SARS-CoV-2. *Cell* **184**, 2332–2347.e16 (2021).

39. Witte, L. et al. Epistasis lowers the genetic barrier to SARS-CoV-2 neutralizing antibody escape. Preprint at *bioRxiv* https://doi.org/10.1101/2022.08.17.504313 (2022).

40. Scanlan, C. N., Offer, J., Zitzmann, N. & Dwek, R. A. Exploiting the defensive sugars of HIV-1 for drug and vaccine design. *Nature* **446**, 1038–1045 (2007).

41. Xiang, D. et al. Convergent evolution of human-isolated H7N9 avian influenza A viruses. *J. Infect. Dis.* **217**, 1699–1707 (2018).

42. Martin, D. P. et al. The emergence and ongoing convergent evolution of the SARS-CoV-2 N501Y lineages. *Cell* **184**, 5189–5200.e7 (2021).

43. Harvey, W. T. et al. SARS-CoV-2 variants, spike mutations and immune escape. *Nat. Rev. Microbiol.* **19**, 409–424 (2021).

44. Alsoussi, W. B. et al. SARS-CoV-2 Omicron boosting induces de novo B cell response in humans. Preprint at *bioRxiv* https://doi.org/10.1101/2022.09.22.509040 (2022).

45. Kaku, C. I. et al. Evolution of antibody immunity following Omicron BA.1 breakthrough infection. Preprint at *bioRxiv* https://doi.org/10.1101/2022.09.21.508922 (2022).

46. Qu, P. et al. Enhanced neutralization resistance of SARS-CoV-2 Omicron subvariants BQ.1, BQ.1.1, BA.4.6, BF.7, and BA.2.75.2. *Cell Host Microbe* https://doi.org/10.1016/j.chom.2022.11.012 (2022).

47. Wang, Q. et al. Antibody responses to Omicron BA.4/BA.5 bivalent mRNA vaccine booster shot. Preprint at *bioRxiv* https://doi.org/10.1101/2022.10.22.513349 (2022).

48. Marzi, R. et al. Maturation of SARS-CoV-2 spike-specific memory B cells drives resilience to viral escape. Preprint at *bioRxiv* https://doi.org/10.1101/2022.09.30.509852 (2022).

49. Levin, E. G. et al. Waning immune humoral response to BNT162b2 Covid-19 vaccine over 6 months. *N. Engl. J. Med.* **385**, e84 (2021).

50. Barnes, C. O. et al. SARS-CoV-2 neutralizing antibody structures inform therapeutic strategies. *Nature* **588**, 682–687 (2020).

51. Ye, J., Ma, N., Madden, T. L. & Ostell, J. M. IgBLAST: an immunoglobulin variable domain sequence analysis tool. *Nucleic Acids Res.* **41**, W34–W40 (2013).

52. Gupta, N. T. et al. Change-O: a toolkit for analyzing large-scale B cell immunoglobulin repertoire sequencing data. *Bioinformatics* **31**, 3356–3358 (2015).

53. Otwinowski, J., McCandlish, D. M. & Plotkin, J. B. Inferring the shape of global epistasis. *Proc. Natl Acad. Sci. USA* **115**, E7550–E7558 (2018).

54. Nie, J. et al. Quantification of SARS-CoV-2 neutralizing antibody by a pseudotyped virus-based assay. *Nat. Protoc.* **15**, 3699–3715 (2020).

Acknowledgements

We thank J. Bloom for his gift of the yeast SARS-CoV-2 RBD libraries; all volunteers for providing the blood samples; and all the scientists around the globe for performing SARS-CoV-2 sequencing and surveillance analysis. This project is financially supported by the Ministry of Science and Technology of China and Changping Laboratory (2021A0201 and 2021D0102), and the National Natural Science Foundation of China (32222030).

Author information

Author notes

1. These authors contributed equally: Yunlong Cao, Fanchong Jian, Jing Wang, Yuanling Yu, Weiliang Song

Authors and Affiliations

1. Biomedical Pioneering Innovation Center (BIOPIC), Peking University, Beijing, P. R. China

   Yunlong Cao, Fanchong Jian, Jing Wang, Weiliang Song, Ayijiang Yisimayi, Sijie Yang, Xiao Niu, Tianhe Xiao & Xiaoliang Sunney Xie

2. Changping Laboratory, Beijing, P. R. China

   Yunlong Cao, Yuanling Yu, Jing Wang, Ran An, Na Zhang, Yao Wang, Peng Wang, Lijuan Zhao, Haiyan Sun, Lingling Yu, Qingqing Gu, Fei Shao, Youchun Wang & Xiaoliang Sunney Xie

3. College of Chemistry and Molecular Engineering, Peking University, Beijing, P.R. China

Fanchong Jian & Xiao Niu

4. School of Life Sciences, Peking University, Beijing, P. R. China

Jing Wang, Weiliang Song & Ayijiang Yisimayi

5. Institute for Immunology, College of Life Sciences, Nankai University, Tianjin, P. R. China

Xiaosu Chen

6. Peking-Tsinghua Center for Life Sciences, Peking University, Beijing, P. R. China

Sijie Yang

7. Joint Graduate Program of Peking-Tsinghua-NIBS, Academy for Advanced Interdisciplinary Studies, Peking University, Beijing, China

Tianhe Xiao

8. Beijing Ditan Hospital, Capital Medical University, Beijing, P. R. China

Xiaohua Hao, Yanli Xu & Ronghua Jin

9. Organ Transplant Center, NHC Key Laboratory for Critical Care Medicine, Tianjin First Central Hospital, Nankai University, Tianjin, P. R. China

Zhongyang Shen

10. Division of HIV/AIDS and Sex-transmitted Virus Vaccines, Institute for Biological Product Control, National Institutes for Food and Drug Control (NIFDC), Beijing, P. R. China

Youchun Wang

Contributions

Y.C. designed the study. X.S.X. supervised the study. Y.C., F.J., A.Y., Q.G. and X.S.X. wrote the manuscript with input from all authors. A.Y., W.S., R.A., Yao Wang and X.N. performed B cell sorting, single-cell VDJ sequencing and antibody sequence analyses. J.W. (BIOPIC), H.S. and F.J. performed and analysed the DMS data. Y.Y. and Youchun Wang constructed the pseudotyped virus. N.Z., P.W., L.Y., T.X. and F.S. performed the pseudotyped virus neutralization assays. W.S. and Y.C. analysed the neutralization data. X.H., Y.X., X.C., Z.S. and R.J. recruited the SARS-CoV-2 vaccinated and convalescent individuals. J.W. (Changping Laboratory), L.Y. and F.S. performed the antibody expression.

Corresponding authors

Correspondence to Yunlong Cao, Youchun Wang or Xiaoliang Sunney Xie.

Ethics declarations

Competing interests

X.S.X. and Y.C. are founders of Singlomics Biopharmaceuticals. Changping Laboratory is in the process of applying
for provisional patents (PCT/CN2021/090146 and PCT/CN2021/080537) covering BD series SARS-CoV-2 monoclonal antibodies, including BD-604 (DXP-604), BD55-5840 (SA58) and BD55-5514 (SA55), that lists X.S.X. and Y.C. as inventors. All other authors declare no competing interests.

Peer review

Peer review information

Nature thanks Annette Fox and the other, anonymous, reviewer(s) for their contribution to the peer review of this work. Peer reviewer reports are available.

Additional information

Publisher's note Springer Nature remains neutral with regard to jurisdictional claims in published maps and institutional affiliations.

Extended data figures and tables

Extended Data Fig. 1 Emergence of convergent mutations on SARS-CoV-2 RBD.

a, Number of independent Omicron sublineages that gained mutations on the corresponding SARS-CoV-2 RBD residue and exhibited growth advantage compared to its ancestral Omicron strain (BA.2, BA.2.75, or BA.5). Residues that were mutated in at least five independent sublineages are considered convergent (dash threshold). Recombinants were not counted, but their derivatives were included in the analysis (see Methods). **b**, Proportions of each convergent mutation in all detected Spike sequences. Spike sequences were from GISAID (Spike protein sequences released on Oct 27, 2022). The percentage of the wild-type residue is not plotted, except for 493Q, considering the prevalence of R493Q reversion. **c**, List of Pango lineages shown in Extended Data Fig. 1a.

Extended Data Fig. 2 Antibody drug evasion and hACE2 binding capability of convergent Omicron variants.

a, IC50 of therapeutic NAbs against pseudoviruses of additional emerging SARS-CoV-2 Omicron subvariants. **b**, Relative hACE2-binding capability measured by IC50 of hACE2 against pseudoviruses. Error bars indicate mean ± s.d. of $n = 5$ biologically independent replicates. P-values were calculated using a two-tailed Student's *t*-test. *, $p < 0.05$; **, $p < 0.01$; ***, $p < 0.001$. No label on variants with $p > 0.05$. Variants with significantly stronger binding are coloured blue, while those with weaker binding are coloured red. All neutralization assays were conducted in at least two independent experiments.

Extended Data Fig. 3 Plasma neutralization evasion of convergent Omicron variants.

a-**d**, NT50 against SARS-CoV-2 previous variants of concern and additional Omicron subvariants of plasma from vaccinated or convalescent individuals following breakthrough infection. Plasma samples, statistical methods and meaning of labels are the same as in Fig. 2. All neutralization assays were conducted in at least two independent experiments.

Extended Data Fig. 4 FACS gating strategy for isolating mAbs from BA.2 and BA.5 convalescent individuals.

a, FACS gating strategy of antigen-specific B cells from individuals who recovered from BA.5 breakthrough infection. Data from an independent experiment compared to Fig. 3a are shown here. **b**, FACS gating strategy of antigen-specific B cells from individuals who recovered from BA.2 breakthrough infection. Data from an independent experiment compared to Fig. 3b are shown here. **c**, FACS gating strategy of antigen-specific B cells from individuals who recovered from BA.5 infection.

Extended Data Fig. 5 Distribution of antibody sources and neutralizing activities on the DMS landscape.

a, Sources of the 3051 mAbs involved in this study projected on the t-SNE of DMS profiles. **b**, IC50 against SARS-CoV-1 (N = 1870 determined), Omicron BA.1 (N = 3031), BA.2 (N = 3046), BQ.1.1 (N = 3051), and XBB (N = 3033) of these mAbs projected on the embedding. All neutralization assays were conducted in at least two independent experiments.

Extended Data Fig. 6 Escape hotspots and neutralization of mAbs in epitope groups A, B and C.

a-**c**, Average escape scores from DMS of epitope groups A (**a**), B (**b**), C (**c**) and each RBD residue. Scores are projected onto the structure of SARS-CoV-2 RBD (PDB: 6M0J). Average escape maps that indicate the score of each mutation from DMS on escape hotspots of antibodies, grouped by their sources, in epitope groups A (**a**), B (**b**) and C (**c**), and corresponding sequence alignment of SARS-CoV-2 WT and Omicron RBDs are also shown. The height of each amino acid in the escape maps represents its mutation escape score. Mutated sites in Omicron variants are marked in

bold. **d**, Pseudovirus-neutralizing IC50 of antibodies in group A, B, and C, from wild-type vaccinated or convalescent individuals (WT-elicited, n = 133, 50, 106 for A-C, respectively), BA.1 (BA.1-elicited, n = 51, 49, 24), BA.2 (BA.2-elicited, n = 34, 36, 56) and BA.5 convalescent individuals (BA.5-elicited, n = 16, 6, 14). The geometric mean IC50s are labelled, and error bars indicate the geometric standard deviation. P-values are calculated using two-tailed Wilcoxon rank sum tests. *, $p < 0.05$; **, $p < 0.01$; ***, $p < 0.001$; NS, not significant, $p > 0.05$. All neutralization assays were conducted in at least two independent experiments.

Extended Data Fig. 7 Escape hotspots and neutralization of mAbs in epitope group D and E1.

a-**c**, Average escape scores from DMS of epitope groups D1 (**a**), D2 (**b**), E1 (**c**) and each RBD residue. **d**, Pseudovirus-neutralizing IC50 of mAbs in group D1, D2, and E1 from WT vaccinated or convalescent individuals (n = 49, 37, 19 for D1, D2 and E1, respectively), BA.1 (n = 59, 21, 14 for D1, D2 and E1, respectively), BA.2 (n = 56, 15, 9 for D1, D2 and E1, respectively), and BA.5 convalescent individuals (n = 14, 17, 9 for D1, D2 and E1, respectively). The geometric mean IC50s are labelled, and error bars indicate the geometric standard deviation. P-values are calculated using two-tailed Wilcoxon rank sum tests. *, $p < 0.05$; **, $p < 0.01$; ***, $p < 0.001$; NS, not significant, $p > 0.05$. All neutralization assays were conducted in at least two independent experiments.

Extended Data Fig. 8 Escape hotspots and neutralization of mAbs in epitope group E2 and E3.

a-**c**, Average escape scores from DMS of epitope groups E2.1 (**a**), E2.2 (**b**), E3 (**c**) and each RBD residue. **d**, Pseudovirus-neutralizing IC50 of mAbs in group E2.1, E2.2, and E3 from WT vaccinated or convalescent individuals (n = 49, 37, 19 for E2.1, E2.2, and E3, respectively), BA.1 (n = 59, 21, 14 for E2.1, E2.2, and E3, respectively), BA.2 convalescents (n = 56, 15, 9 for E2.1, E2.2, and E3, respectively), and BA.5 convalescent individuals (n = 14, 17, 9 for E2.1, E2.2, and E3, respectively). The geometric mean IC50s are labelled, and error bars indicate the geometric standard deviation. P-values are calculated using two-tailed Wilcoxon rank sum tests. *, $p < 0.05$;

**, $p < 0.01$; ***, $p < 0.001$; NS, not significant, $p > 0.05$. All neutralization assays were conducted in at least two independent experiments.

Extended Data Fig. 9 Predicted escape hotspots of SARS-CoV-2 variants.

a, Normalized average escape scores weighted by IC50 against D614G using DMS profiles of mAbs from ancestral strain infection or vaccination with a logo plot showing specific mutations on important residues. **b**, Normalized average escape scores of mAbs from BA.1 breakthrough infection, weighted by IC50 against BA.1. **c**, Normalized average escape scores of mAbs from ancestral strain infection or vaccination and BA.1 breakthrough infection, weighted by IC50 against BA.2. **d**, WT/BA.1/BA.2-elicited mAbs with IC50 against BA.2.75 and BA.5, similar to Fig. 4b. All neutralization assays were conducted in at least two independent experiments.

Extended Data Fig. 10 IC50 heatmaps of representative mAbs against constructed Omicron variants.

a, Colour shades indicate IC50 of antibodies (columns) against constructed Omicron BA.2 or BA.5 subvariants (rows) carrying mutations on the epitope of each group. The order of mAbs is the same as in Fig. 4c. **b**, IC50 of NTD-targeting antibodies against SARS-CoV-2 variants, which is related to Fig. 4e. **c**, Epitope groups and escape hotspots on BA.2 NTD. All neutralization assays were conducted in at least two independent experiments.

Extended Data Fig. 11 Antigenic map of current SARS-CoV-2 variants.

a, Antigenic map of SARS-CoV-2 variants constructed using plasma neutralization data by principal component analysis (PCA). **b**, Antigenic map of SARS-CoV-2 variants with constructed Omicron subvariants removed.

Supplementary information

Reporting Summary

Peer Review File

Supplementary Table 1

Summarized information of SARS-CoV-2 vaccinated individuals, and convalescents from BA.1, BA.2 and BA.5 breakthrough infections involved in the study.

Supplementary Table 2

Summarized information and experiment results of 3051 SARS-CoV-2 RBD antibodies involved in this study, including their sources, epitope groups, pseudovirus neutralizing IC50 and heavy/light chain sequences.

Supplementary Table 3

Spike mutations carried by the SARS-CoV-2 Omicron variants involved in this study. Spike-pseudotyped viruses (VSV-based) were constructed accordingly.

Rights and permissions

Open Access This article is licensed under a Creative Commons Attribution 4.0 International License, which permits use, sharing, adaptation, distribution and reproduction in any medium or format, as long as you give appropriate credit to the original author(s) and the source, provide a link to the Creative Commons licence, and indicate if changes were made. The images or other third party material in this article are included in the article's Creative Commons licence, unless indicated otherwise in a credit line to the material. If material is not included in the article's Creative Commons licence and your intended use is not permitted by statutory regulation or exceeds the permitted use, you will need to obtain permission directly from the copyright holder. To view a copy of this licence, visit http://creativecommons.org/licenses/by/4.0/.

Reprints and Permissions

About this article

Cite this article

Cao, Y., Jian, F., Wang, J. *et al.* Imprinted SARS-CoV-2 humoral immunity induces convergent Omicron RBD evolution. *Nature* **614**, 521–529 (2023). https://doi.org/10.1038/s41586-022-05644-7

- Received: 23 September 2022
- Accepted: 12 December 2022
- Published: 19 December 2022
- Issue Date: 16 February 2023
- DOI: https://doi.org/10.1038/s41586-022-05644-7

Share this article

Anyone you share the following link with will be able to read this content:

Get shareable link

Sorry, a shareable link is not currently available for this article.

Copy to clipboard

Provided by the Springer Nature SharedIt content-sharing initiative

This article is cited by

- **How your first brush with COVID warps your immunity**
  - Rachel Brazil

Nature (2023)

- **[Repeated vaccination of inactivated SARS-CoV-2 vaccine dampens neutralizing antibodies against Omicron variants in breakthrough infection]**
    - Bo Gao
    - Liheng He
    - Leng-Siew Yeap

  Cell Research (2023)

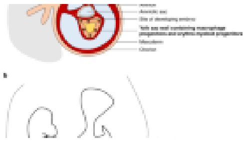
- **[SARS-CoV-2 elicits non-sterilizing immunity and evades vaccine-induced immunity: implications for future vaccination strategies]**
    - Anna L. Beukenhorst
    - Clarissa M. Koch
    - Jaap Goudsmit

  European Journal of Epidemiology (2023)

- **[Resistance of Omicron subvariants BA.2.75.2, BA.4.6, and BQ.1.1 to neutralizing antibodies]**
    - Delphine Planas
    - Timothée Bruel
    - Olivier Schwartz

  Nature Communications (2023)

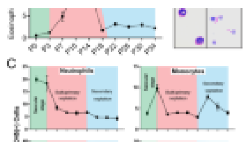
This article was downloaded by **calibre** from https://www.nature.com/articles/s41586-022-05644-7



Role of macrophages in fetal development and perinatal disorders

18 October 2020

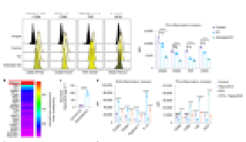
Olachi J. Mezu-Ndubuisi & Akhil Maheshwari



Eosinophil accumulation in postnatal lung is specific to the primary septation phase of development

10 March 2020

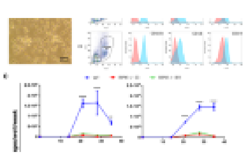
Lucas F. Loffredo, Mackenzie E. Coden, … Sergejs Berdnikovs



The angiocrine Rspondin3 instructs interstitial macrophage transition via metabolic–epigenetic reprogramming and resolves inflammatory injury

24 August 2020

Bisheng Zhou, Lissette Magana, … Asrar B. Malik

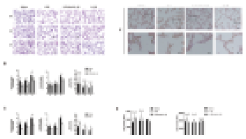


RIPK1 is a critical modulator of both tonic and TLR-responsive inflammatory and cell death pathways in human macrophage

[differentiation](#)

24 September 2018

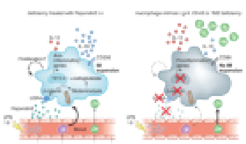
Julian Buchrieser, Maria Jose Oliva-Martin, … Jose Luis Venero



CCR5 signaling promotes lipopolysaccharide-induced macrophage recruitment and alveolar developmental arrest

15 February 2021

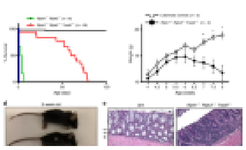
Ze Chen, Xiaohua Xie, … Yongjun Zhang



Endothelial cells instruct macrophages on how to Rspond to lung injury

02 October 2020

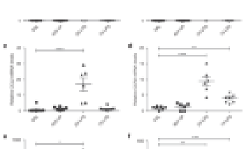
Thomas Marichal



TRADD regulates perinatal development and adulthood survival in mice lacking RIPK1 and RIPK3

11 February 2019

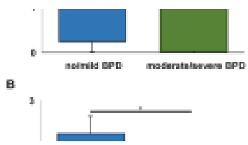
John P. Dowling, Mohamed Alsabbagh, … Jianke Zhang



[Chorioamnionitis induces changes in ovine pulmonary endogenous epithelial stem/progenitor cells in utero]

18 October 2020

Helene Widowski, Daan R. M. G. Ophelders, … Niki L. Reynaert



[TRAIL protects the immature lung from hyperoxic injury]

15 July 2022

Tayyab Shahzad, Cho-Ming Chao, … Harald Ehrhardt

- Article
- Open Access
- Published: 04 January 2023

Neonatal imprinting of alveolar macrophages via neutrophil-derived 12-HETE

- Erwan Pernet ,
- Sarah Sun,
- Nicole Sarden,
- Saideep Gona,
- Angela Nguyen,
- Nargis Khan,
- Martin Mawhinney,
- Kim A. Tran,
- Julia Chronopoulos,
- Dnyandeo Amberkar,
- Mina Sadeghi,
- Alexandre Grant,
- Shradha Wali,

- Renaud Prevel,
- Jun Ding,
- James G. Martin,
- Ajitha Thanabalasuriar,
- Bryan G. Yipp,
- Luis B. Barreiro &
- …
- Maziar Divangahi

Show authors

Nature **volume 614**, pages 530–538 (2023)

- 8498 Accesses
- 68 Altmetric
- Metrics details

Abstract

Resident-tissue macrophages (RTMs) arise from embryonic precursors[1,2], yet the developmental signals that shape their longevity remain largely unknown. Here we demonstrate in mice genetically deficient in 12-lipoxygenase and 15-lipoxygenase (*Alox15*$^{-/-}$ mice) that neonatal neutrophil-derived 12-HETE is required for self-renewal and maintenance of alveolar macrophages (AMs) during lung development. Although the seeding and differentiation of AM progenitors remained intact, the absence of 12-HETE led to a significant reduction in AMs in adult lungs and enhanced senescence owing to increased prostaglandin E_2 production. A compromised AM compartment resulted in increased susceptibility to acute lung injury induced by lipopolysaccharide and to pulmonary infections with influenza A virus or SARS-CoV-2. Our results highlight the complexity of prenatal RTM programming and reveal their dependency on in *trans* eicosanoid production by neutrophils for lifelong self-renewal.

Main

Alveolar macrophages (AMs) are the major embryonically derived population that reside in the airways and play an essential part in the maintenance of pulmonary homeostasis and immunosurveillance[1,2,3]. In contrast to interstitial macrophages derived from bone marrow (BM)[4,5,6,7], AMs originate from fetal liver monocytes that seed the lung during embryogenesis and mature during the first week of life[2,8,9]. At

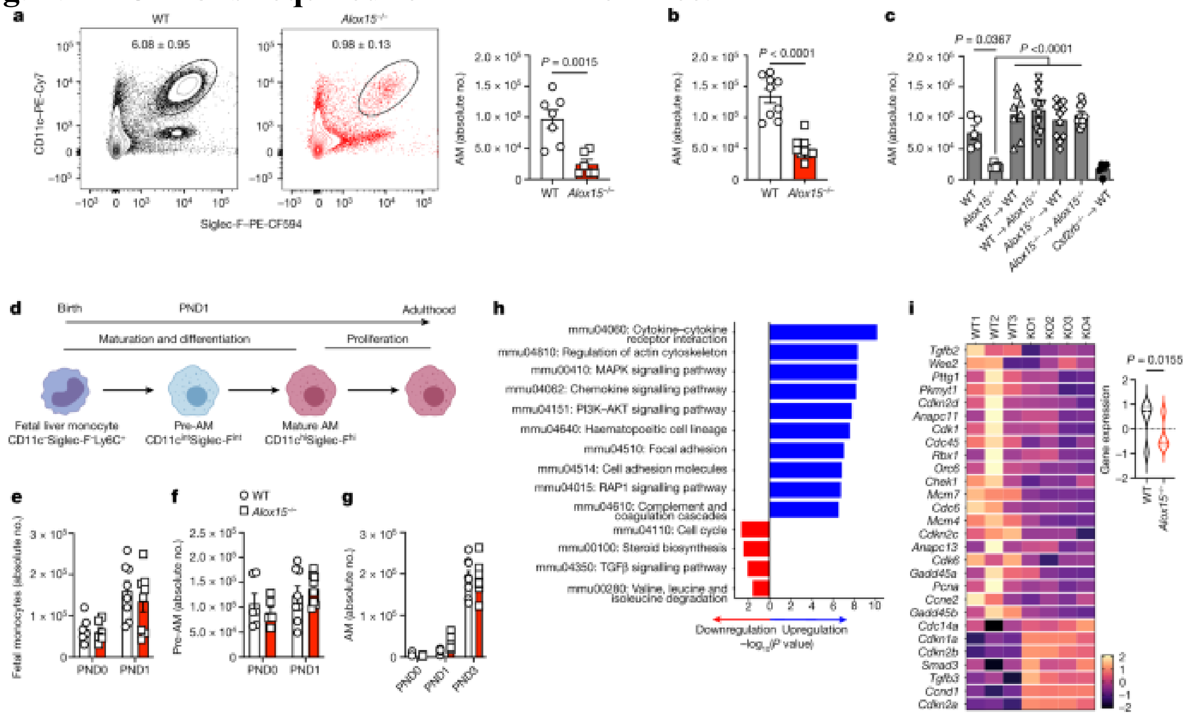
steady state, AMs are maintained by self-renewal, with limited contribution from circulating monocytes[2,10]. The essential role of the lung microenvironment, including granulocyte–macrophage colony-stimulating factor (GM-CSF) and transforming growth factor-β (TGFβ) signalling, in AM development and function has been extensively studied[2,9,11]. However, the potential of other BM-derived immune cells and their specific function in the early AM programming is incompletely understood.

Eicosanoids are evolutionarily conserved bioactive lipids. They are essential mediators of homeostatic and inflammatory processes[12] and potent regulators of macrophage function[13,14,15,16,17]. Eicosanoids are generated through two main pathways: the cyclooxygenase pathway (involving cyclooxygenase 1 (COX1) and COX2) and the lipoxygenase pathway (involving 5-lipoxygenase (ALOX5) and 12-lipoxygenase and 15-lipoxygenase (ALOX12/15)). ALOX15 generates 12-hydroxyeicosatetraenoic acid (12-HETE), 15-HETE and specialized pro-resolving mediators such as lipoxin A_4. Meanwhile, the cyclooxygenase pathway produces prostaglandins, including prostaglandin E_2 (PGE_2)[12]. Although eicosanoid metabolites are produced in the lung at homeostasis[18] and control macrophage-mediated host defence against pathogens[13,19,20], little is known about their contribution to lung alveolarization. In the current study, we demonstrate the crucial role of the ALOX15 pathway in neutrophil-dependent AM programming in the developing lung.

ALOX15 is required for AM maintenance

The frequency and number of AMs in *Alox15*$^{-/-}$ adult mice (6–8 weeks old) were significantly decreased (by about 50%) compared with wild-type (WT) controls at steady state (Fig. 1a,b and Extended Data Fig. 1a–c). This reduction was specific to the ALOX15 pathway, as the AM compartment was intact in ALOX5-deficient (*Alox5*$^{-/-}$) mice (Extended Data Fig. 1d). Notably, the effect of ALOX15 deficiency was specific to AMs, as there was no difference in other populations of lung innate immune cells (Extended Data Fig. 1e and Supplementary Fig. 1) and extrapulmonary RTMs (Extended Data Fig. 1f–h). To validate this observation, we generated BM chimeras in which AMs are replenished by BM-derived monocytes[2,10]. Lethally irradiated WT (CD45.1 or CD45.2) and *Alox15*$^{-/-}$ (CD45.2) mice were reconstituted with BM from *Alox15*$^{-/-}$, *Csf2rb*$^{-/-}$ or WT CD45.1 donor mice (Extended Data Fig. 1i). Following 8 weeks of BM reconstitution, AMs were replenished by donor cells, and there was no difference in AM development between groups. The exception was in mice reconstituted by *Csf2rb*$^{-/-}$ BM, which were used as a control[2,21] (Fig. 1c and Extended Data Fig. 1j–k). Thus, the reduction in AMs in *Alox15*$^{-/-}$ mice is linked to embryonic development.

Fig. 1: ALOX15 is required for AM maintenance.



a, Representative FACS plots (left) and quantification (right) of AM numbers (gated on single live cells, CD45.2$^+$CD11c$^+$Siglec-F$^+$) in the lungs of adult WT ($n = 7$) and *Alox15*$^{-/-}$ ($n = 6$) mice. **b**, AM numbers in BAL ($n = 9$ mice per group). **c**, Quantification of the AM population in the lungs of BM chimeras 8 weeks after reconstitution (left to right, $n = 5$, 5, 8, 11, 11, 9 and 5 mice per group, respectively). **d**, Model of AM development. **e**–**g**, Numbers of fetal monocytes (**e**), pre-AMs (**f**) and AMs (**g**) in WT and *Alox15*$^{-/-}$ lungs at various ages ($n = 6$ (PND0) or 8 (PND1 and PND3) per group). **h**, Top upregulated and downregulated pathways from KEGG Pathway enrichment analysis. **i**, Violin plot (left) and heatmap (right) of mRNA transcripts significantly upregulated and downregulated in the cell cycle pathway ($n =$ 3 (WT) or 4 (*Alox15*$^{-/-}$)). Data are presented as the mean ± s.e.m. and are from one experiment (**h**,**i**) or pooled from two (**a**,**c**,**e**–**g**) or three (**b**) independent experiments. Data were analysed using unpaired two-tailed *t*-test (**a**,**b**), Mann–Whitney two-tailed test (**i**) or one-way analysis of variance (ANOVA) followed by Tukey's multiple comparisons test (**c**). The model in **d** was created using BioRender (https://biorender.com).

Source data

Impaired proliferation in *Alox15*$^{-/-}$ AMs

Because AMs develop from fetal liver monocytes during the first days of life[2] (Fig. 1d), we analysed the progenitors (fetal liver monocytes, pre-AMs) and mature AMs of WT and *Alox15*$^{-/-}$ mice at postnatal day 0 (PND0), PND1 and PND3 (Fig. 1e–g and Extended Data Fig. 2a). There was no difference in the number of progenitors or mature AMs between WT and *Alox15*$^{-/-}$ mice (Fig. 1e–g). There was also no difference in pulmonary levels of the key AM maturation cytokines GM-CSF and TGFβ1 as well as other cytokines (Extended Data Fig. 2b–f) at PND1 and PND3. Moreover, the expression of key AM genes (*Abcg1*, *Pparg*, *Spi1*, *Mmr*, *Ym1* and *Chil3*) (Extended Data Fig. 2g,h) were comparable in PND3 AMs between WT and *Alox15*$^{-/-}$ mice.

As the loss of AMs in adult ALOX15-deficient mice was independent of AM seeding, maturation or differentiation and aberrant cell death (Extended Data Fig. 2i), we next performed bulk RNA sequencing (RNA-seq) to assess the overall effect of ALOX15 deficiency in AMs. We identified 503 differentially expressed genes (false discovery rate (FDR) adjusted P value < 0.05), which included 346 upregulated genes (between WT and *Alox15*$^{-/-}$ mice) and 157 downregulated genes. Pathway enrichment analysis revealed a significant ($P = 0.0021$) downregulation of cell cycle genes in *Alox15*$^{-/-}$ AMs (Fig. 1h,i, Extended Data Fig. 2j–l and Supplementary Table 1). This transcriptomics analysis was further supported by a significant reduction in BrdU incorporation and undetectable Ki-67 in AMs isolated from *Alox15*$^{-/-}$ mice (Fig. 2a–c). This was specific to *Alox15*$^{-/-}$ AMs, as no differences in proliferation were observed in *Alox15*$^{-/-}$ peritoneal macrophages (PMs) or BM-derived macrophages (BMDMs) (Extended Data Fig. 3a–d). Notably, ALOX5 deficiency had no effect on the frequency of Ki-67^{+} AMs (Extended Data Fig. 3e). Finally, we locally depleted AMs using clodronate liposomes (administered intranasally) and followed the dynamics of the AM populations at day 2 (peak of depletion) and day 14 to evaluate their proliferation capacity for repopulating the alveolar space. AMs were depleted at day 2 after clodronate delivery in all groups. By contrast, by day 14, AM numbers from WT and *Ccr2*$^{-/-}$ mice returned to levels that were similar to that of control mice (Extended Data Fig. 3f). This result indicated that AMs are able to proliferate (Extended Data Fig. 3g) and repopulate the airways independent of BM monocytes[10]. However, *Alox15*$^{-/-}$ AMs were not able to proliferate or repopulate the airways (Extended Data Fig. 3f,g). Thus, during homeostasis or local depletion, the self-renewing capacity of AMs is impaired in ALOX15-deficient mice.

Fig. 2: *Alox15*$^{-/-}$ AMs are intrinsically impaired in proliferation.

figure 2

a, Representative FACS plots (left) and quantification (right) of BrdU^{+} AMs in adult WT and *Alox15*$^{-/-}$ lungs after a 7-day BrdU pulse ($n = 5$ mice per group). **b**, Mouse *Ki67* (*mKi67*) expression from the RNA-seq dataset ($n = 3$ (WT) or 4 (*Alox15*$^{-/-}$)). **c**, Representative FACS plots (left) and quantification (right) of Ki-67^{+} AMs in adult WT and *Alox15*$^{-/-}$ lungs ($n = 11$ per group). **d**, Scheme of the adoptive transfer protocol. **e**, Ki-67^{+} AMs before and after transfer (WT CD45.1 (left to right), $n = 4$, 5 or 5; *Alox15*$^{-/-}$ CD45.2, $n = 5$ per group). **f**, Growth of AMs after culture with GM-CSF for 3 days ($n = 4$ biological replicates per group). **g**,**h**, Representative micrographs (left) and quantification (right) of BrdU^{+} (**g**) ($n = 3$ (unstimulated (Uns.) or 5 (GM-CSF) fields of view) and Ki-67^{+} (**h**) ($n = 5$ (Uns.), 12 (WT GM-CSF) or 10 (*Alox15*$^{-/-}$ GM-CSF) fields of view) AMs after 3 days of culture with GM-CSF. Scale bar, 50 µm. **i**, Representative FACS plots (left) and quantification (right) of Ki-67^{+} AMs in PND3 lungs ($n = 12$ mice per group). **j**, Scheme of ATAC-seq of AMs from adult (BAL) or PND3 (sorted) WT and *Alox15*$^{-/-}$ mice ($n = 3$ mice per group). **k**,**l**, Volcano plots for differential accessibility results in adult (**k**; knockout (KO) versus WT) and pups (**l**).

Yellow (**k**) or blue (**l**) highlighted peaks have a *P*-adjusted value of <0.05 and absolute $\log_2$(fold change (FC)) of ≥1. **m**, The $\log_2$(FC) difference in accessibility in adults and pups for all significant peaks within pups. Pink highlighted points are DA in both adults and pups. Green points are significant only in pups. **n**, Top ten enriched pathways in adults and pups from a GSEA of genes matched to the closest DA peaks. Data are presented as the mean ± s.e.m. and are from one (**e**,**k**–**n**) or pooled from three (**c**,**i**) or four (**f**) independent experiments or representative of two (**a**) or three (**g**,**h**) independent experiments. Data were analysed using unpaired two-tailed *t*-test (**a**–**b**,**i**) or two-way ANOVA followed by Sidak's (**e**) or Tukey's (**f–h**) multiple comparisons test. The models in **d** and **j** were created using BioRender (https://biorender.com).

Source data

The impaired proliferative capacity of *Alox15*$^{-/-}$ AMs can be due to either extrinsic signalling (that is, altered eicosanoid composition of the pulmonary microenvironment) or intrinsic signalling. However, the pulmonary microenvironment of *Alox15*$^{-/-}$ mice did not suppress the proliferation of AMs. That is, adoptive transfer of WT CD45.1 AMs into *Alox15*$^{-/-}$ mice (Fig. 2d) repopulated the 'incomplete' *Alox15*$^{-/-}$ AM niche and remained proliferative (Fig. 2e and Extended Data Fig. 3h–j). To examine the intrinsic capacity of AMs to proliferate, we first cultured WT and *Alox15*$^{-/-}$ AMs with GM-CSF or M-CSF and found that *Alox15*$^{-/-}$ AMs remained non-proliferative (Fig. 2f–h and Extended Data Fig. 3k). This phenotype was specific to AMs, as the proliferation of *Alox15*$^{-/-}$ PMs and BMDMs was intact (Extended Data Fig. 3l–m). In vivo, the impaired proliferation in AMs was detected as early as PND3, the development stage at which mature AMs first appear in the airways (Fig. 2i). Next, we generated assay for transposase-accessible chromatin with high-throughput sequencing (ATAC-seq) data from neonatal (PND3) and adult AMs from both WT and *Alox15*$^{-/-}$ mice (Fig. 2j and Extended Data Fig. 3n). ALOX15 deficiency altered the chromatin accessibility landscape of AMs in both neonatal and adult mice. Moreover, the smaller numbers of chromatin changes identified in neonates were amplified in adult AMs. In adult AMs, significant differential chromatin accessibility was detected at 5,369 sites (Fig. 2k and Extended Data Fig. 3o; adjusted $P < 0.05$, absolute($\log_2$(fold change)) > 1). This result demonstrates that *Alox15* plays an overall crucial role in modulating the epigenetic landscape of AMs. Notably, although we detected fewer differentially accessible (DA) sites in neonatal *Alox15*$^{-/-}$ AMs (Fig. 2l and Extended Data Fig. 3o), 42 out of 64 of those sites overlapped DA sites in the adult AMs (Extended Data Fig. 3p). This result represented a more than sevenfold increase over what one would expect by chance ($P < 1 \times 10^{-10}$). Moreover, effect sizes and the directionality of this core set of shared DA peaks were highly correlated when comparing adult with neonate AMs (Fig. 2m). Gene set enrichment analysis (GSEA) performed on the genes closest to DA peaks demonstrated that the top ten most

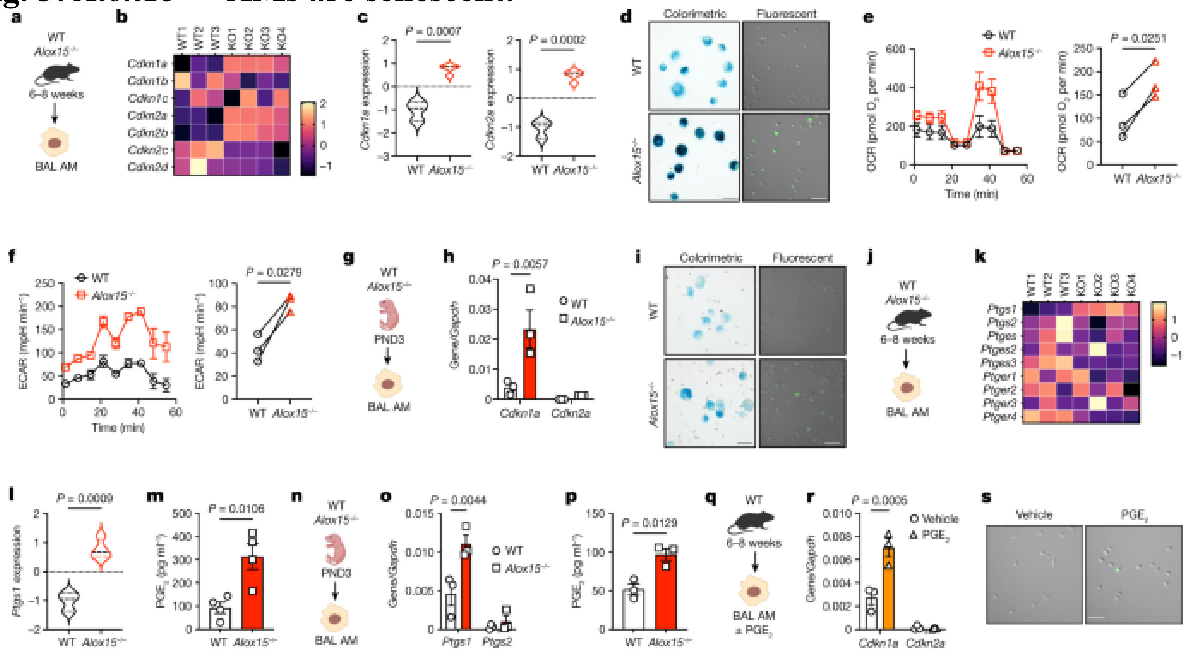
enriched pathways were identical when comparing adult with neonate AMs (Fig. 2n and Extended Data Fig. 3q). The pathway ‘cell cycle mitotic’ was among these top pathways, which was in agreement with our functional data showing that ALOX15 deficiency alters cell proliferation. Moreover, many other pathways directly related to cell division were significantly enriched in both neonate and adult AMs (Extended Data Fig. 3r). Collectively, these data support the notion that ALOX15 signalling imprints epigenetic changes in neonate AMs that are retained and strengthened during development to adult AMs.

Alox15 $^{-/-}$ AMs are senescent

Pathways involved in GM-CSF and TGFβ signalling are key players in the proliferation and differentiation of AMs[9,11]. However, GM-CSF and TGFβ1 production and phosphorylation of AKT1, ERK1, ERK2, SMAD2 and SMAD3 were unchanged between *Alox15*$^{-/-}$ and WT AMs (Extended Data Fig. 4a–e). Furthermore, WT and *Alox15*$^{-/-}$ AMs had similar STAT5 phosphorylation levels at steady state (Extended Data Fig. 4f) and after GM-CSF stimulation (Extended Data Fig. 4g). Thus, impaired proliferation of *Alox15*$^{-/-}$ AMs occurs independent of GM-CSF or TGFβ signalling.

Various biological processes can lead to permanent cell cycle arrest, including cellular senescence[22]. Bulk RNA-seq analysis of adult WT and *Alox15*$^{-/-}$ AMs showed that the expression of two key cell cycle inhibitors, *Cdkn1a* and *Cdkn2a*, was significantly increased in adult *Alox15*$^{-/-}$ AMs (Fig. 3a–c). This was specific to AMs, as there was no difference in *Cdkn1a* expression levels between WT and *Alox15*$^{-/-}$ PMs or BMDMs (Extended Data Fig. 4h). In support of cellular senescence, the expression of senescence-associated β-galactosidase (SA-β-galactosidase) and the frequency of binucleated cells were also significantly increased in *Alox15*$^{-/-}$ AMs (Fig. 3d and Extended Data Fig. 4i–j). Cellular senescence is often associated with metabolic reprogramming and increased cytokine production[23]. Both basal mitochondrial respiration and glycolysis were increased in *Alox15*$^{-/-}$ AMs (Fig. 3e,f), but not *Alox15*$^{-/-}$ PMs or BMDMs (Extended Data Fig. 4k–l). This increased metabolic activity at steady state was associated with increased production of pro-inflammatory cytokines in *Alox15*$^{-/-}$ AMs (Extended Data Fig. 4m). Furthermore, the senescence of *Alox15*$^{-/-}$ AMs initiated during early development, as PND3 *Alox15*$^{-/-}$ AMs showed increased *Cdkn1a* and SA-β-galactosidase expression and cellular metabolism (Fig. 3g–i and Extended Data Fig. 4n) but reduced proliferation (Fig. 2i). Thus, during lung development, ALOX15-deficient AMs become senescent and undergo irreversible cell cycle arrest.

Fig. 3: *Alox15*$^{-/-}$ AMs are senescent.



a, Scheme of BAL-isolated AMs from adult (6–8 weeks) WT and *Alox15*$^{-/-}$ mice. **b**,**c**, Heatmap of selected mRNA transcripts of cell cycle inhibitors (**b**) and expression of *Cdkn1a* and *Cdkn2a* (**c**) in adult WT and *Alox15*$^{-/-}$ AMs ($n = 3$ (WT) or 4 (*Alox15*$^{-/-}$)). **d**, Representative micrographs of SA-β-galactosidase expression assessed by colorimetric or fluorescence assays. Scale bars, 25 μm (left) and 50 μm (right). **e**,**f**, Representative curves (left) and quantification (right) of the oxygen consumption rate (OCR) (**e**) and the extracellular acidification rate (ECAR) (**f**) ($n = 3$ biological replicates/group). **g**–**i**, Scheme of experiment (**g**), *Cdkn1a* and *Cdkn2a* expression (**h**) ($n = 3$ biological replicates per group) and SA-β-galactosidase expression (**i**) in AMs from PND3 WT and *Alox15*$^{-/-}$ mice. Scale bars, 25 μm (left) and 50 μm (right). **j**–**l**, Scheme of experiment (**j**), heatmap of selected mRNA transcripts of the prostanoid pathway (**k**) and expression of *Ptgs1* (**l**) from adult WT and *Alox15*$^{-/-}$ AMs ($n = 3$ (WT) or 4 (*Alox15*$^{-/-}$)) in bulk RNA-seq. **m**, PGE_2 production by resting AMs (24 h) from WT and *Alox15*$^{-/-}$ mice ($n = 4$ biological replicates per group). **n**,**o**, Scheme of experiment (**n**) and *Ptgs1* and *Ptgs2* expression (**o**) by AMs from WT and *Alox15*$^{-/-}$ PND3 mice ($n = 3$ biological replicates per group). **p**, PGE_2 production by resting AMs (24 h) from WT and *Alox15*$^{-/-}$ PND3 mice ($n = 3$ biological replicates per group). **q**, BAL AMs were isolated from adult (6–8 weeks) WT mice, and the AMs were cultured with or without GM-CSF (20 ng ml^{-1}) for 3 days and treated or with or without 10 μM of exogenous PGE_2. **r**,**s**, *Cdkn1a* and *Cdkn2a* expression (**e**) ($n = 3$ biological replicates per group) and SA-β-galactosidase expression (**s**). Scale bar, 50 μm. Data are presented as the mean ± s.e.m. and are from one experiment (**b**,**c**,**k**–**l**) or from three (**e**,**f**,**h**,**o**,**p**,**r**) or four (**m**) independent experiments, or representative of two

(**d**,**l**,**s**) independent experiments. Data were analysed using unpaired (**c**,**l**,**m**,**p**) or paired (**e**,**f**) two-tailed *t*-test or two-way ANOVA followed by Sidak's multiple comparisons test (**h**,**o**,**r**). The models in **a**, **g**, **j** and **n** were created using BioRender (https://biorender.com).

Source data

PGE_2 induces senescence in AMs

Cellular senescence can be triggered by oxidative stress or a DNA damage response, which leads to increased p53 expression. However, there was no difference in the expression or protein levels of p53 in PND3 (Extended Data Fig. 5a) or adult (Extended Data Fig. 5b,c) WT and *Alox15*$^{-/-}$ AMs. This was consistent with similar levels of mitochondrial reactive oxygen species, p38 phosphorylation, the DNA damage marker phospho-γ-H2AX and the oxidative stress response (Extended Data Fig. 5d–g). In addition, there was no difference in the expression of type I interferons (IFN-I) or interferon-stimulated genes (Extended Data Fig. 5h), which has been recently shown to promote senescence[24,25].

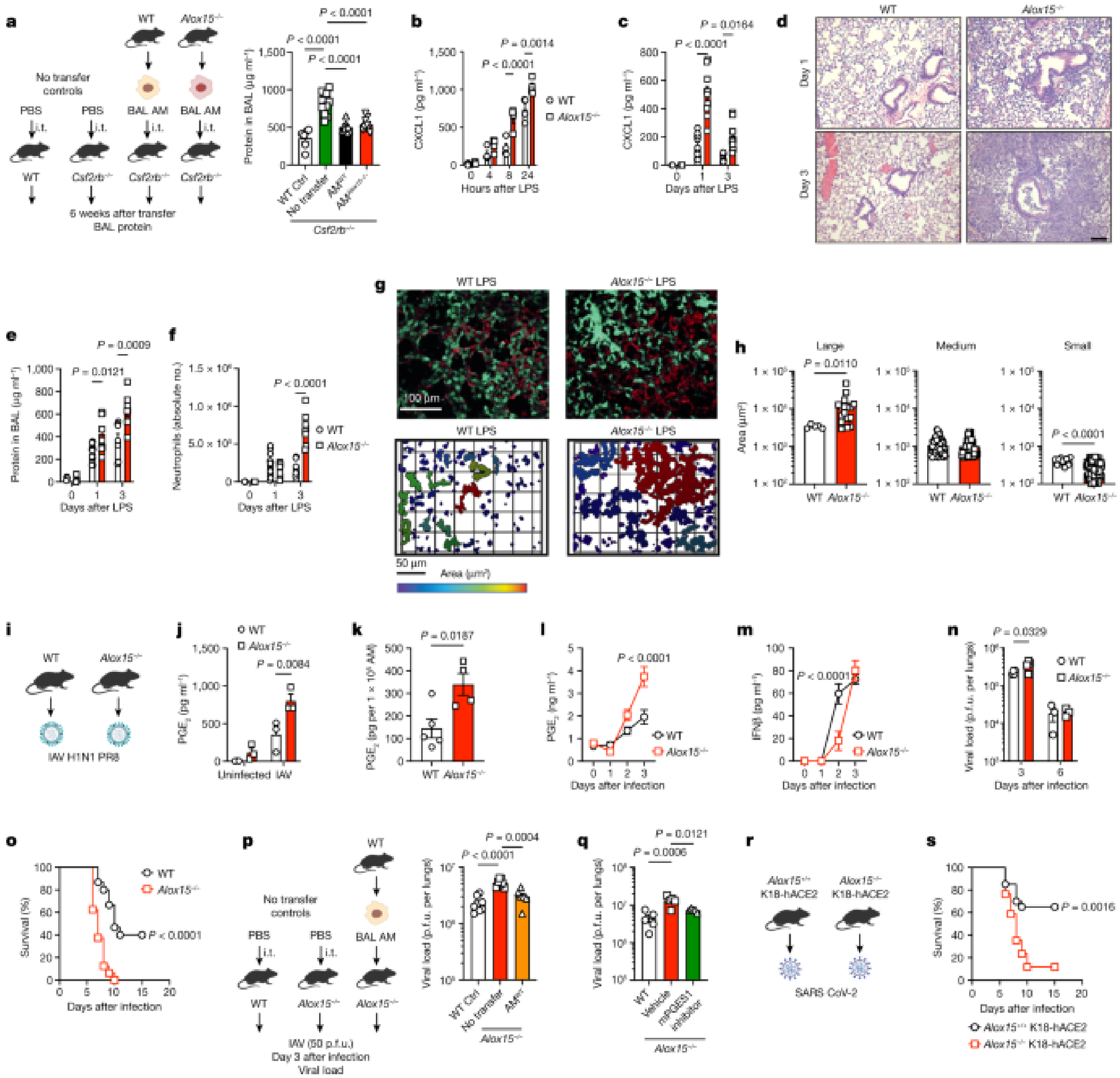
Increased PGE_2 production[26] has been shown to suppress the proliferation of AMs[27] and to maintain the cellular senescence state[28]. Consistently, *Ptgs1* (which encodes COX1) expression and production of PGE_2 were significantly increased in PND3 and adult *Alox15*$^{-/-}$ AMs, but not adult *Alox15*$^{-/-}$ PMs or BMDMs (Fig. 3j–p and Extended Data Fig. 5i–l). PGE_2 production was responsible for inducing the senescence of AMs, as treatment of WT AMs (Fig. 3q) with exogenous PGE_2 substantially decreased GM-CSF-induced Ki-67 expression (Extended Data Fig. 5m), suppressed GM-CSF-mediated proliferation of AMs (Extended Data Fig. 5n) and increased the expression of *Cdkn1a* and SA-β-galactosidase (Fig. 3r,s). Cellular senescence of *Alox15*$^{-/-}$ AMs was specific to PGE_2, as expression of the lipoxygenase pathway and its mediators (leukotriene B_4 (LTB_4) and cysteinyl leukotrienes) remained unchanged (Extended Data Fig. 5o,p). Thus, an increase in the production of PGE_2 induces senescence in *Alox15*$^{-/-}$ AMs.

Alox15$^{-/-}$ AM function is impaired

At steady state, the transcriptomics profile and flow cytometry data showed minimum differences in genes associated with macrophage activation or polarization (Extended Data Fig. 6a–c). Despite a 50% reduction in AMs in adult (6–8 weeks) or elderly (52 weeks) *Alox15*$^{-/-}$ mice (Extended Data Fig. 6d,e), total protein levels in the airways

(Extended Data Fig. 6f), lung structure (Extended Data Fig. 6g) and airway mechanics and responsiveness (Extended Data Fig. 6h–i) were normal in these mice. The phagocytic capacity of *Alox15*$^{-/-}$ AMs (Extended Data Fig. 6j) and surfactant catabolism were also intact (Extended Data Fig. 6k). Consistently, the turbidity of bronchoalveolar lavage (BAL) (Extended Data Fig. 6l), total BAL protein (Extended Data Fig. 6m) and surfactant protein A (SP-A) levels (Extended Data Fig. 6n) in *Alox15*$^{-/-}$ mice were similar to WT mice. The levels of these parameters were also significantly less than in *Csf2rb*$^{-/-}$ mice, which develop pulmonary alveolar proteinosis[11]. Furthermore, adoptive transfer of *Alox15*$^{-/-}$ AMs into the lungs of *Csf2rb*$^{-/-}$ recipient mice restored protein homeostasis in the alveolar space of *Csf2rb*$^{-/-}$ mice (Fig. 4a). Thus, during steady state, *Alox15*$^{-/-}$ AMs are able to maintain alveoli homeostasis.

Fig. 4: *Alox15*$^{-/-}$ AMs have dysregulated responses to sterile inflammation and viral infection.



a, WT or *Alox15*$^{-/-}$ AMs were transferred (intratracheal (i.t.)) into *Csf2rb*$^{-/-}$ mice, and BAL protein levels were determined 6 weeks after transfer (left to right, $n = 6$, 11, 9 or 9 per group). **b**, CXCL1 production by WT or *Alox15*$^{-/-}$ AMs after stimulation with LPS (100 ng ml^{-1}) ($n = 4$ biological replicates per group). **c**–**f**, LPS (20 μg) was delivered intranasally to adult WT and *Alox15*$^{-/-}$ mice. **c**, BAL CXCL1 levels (left to right, $n = 3$, 11 or 7 (WT) or 3, 10 or 8 (*Alox15*$^{-/-}$) mice per time point). **d**, Pulmonary pathology after LPS treatment. Scale bar, 100 μm. **e**, BAL protein levels (left to right, $n = 3$, 11 or 7 (WT) or 3, 9 or 7 (*Alox15*$^{-/-}$) mice per time point). **f**, BAL neutrophil numbers (left to right, $n = 3$, 11 or 7 (WT) or 3, 10 or 8 (*Alox15*$^{-/-}$) mice per time point). **g**,**h**, Intravital microscopy following 2 h of intravenous LPS (20 μg) treatment. **g**, Intravascular neutrophil (cyan) aggregation (top) and cluster formation quantified (bottom) by defining contiguous objects and measuring the areas (blue, low; red, high area clusters). Vascular endothelium is red. **h**, Clusters were classified as large

(≥3,000 μm^2) ($n = 5$ (WT) or 17 (*Alox15*$^{-/-}$) cells), medium (500–2,999 μm^2) ($n = 105$ (WT) or 66 (*Alox15*$^{-/-}$) cells) or small or individual neutrophils (500 μm^2) ($n = 16$ (WT) or 161 (*Alox15*$^{-/-}$) cells). $n = 3$ per group with 3 fields of view per mouse. **i**,**j**, Scheme (**i**) and quantification (**j**) of PGE_2 production by WT and *Alox15*$^{-/-}$ AMs 4 h after IAV infection (multiplicity of infection of 1) ($n = 3$ biological replicates per group). **k**, PGE_2 production by BAL AMs from IAV-infected mice (day 1, 50 p.f.u.) after 4 h of culture ($n = 5$ (WT) or 4 (*Alox15*$^{-/-}$)). **l**–**n**, WT and *Alox15*$^{-/-}$ mice were infected with IAV (50 p.f.u.). **l**, BAL levels of PGE_2 (left to right, $n = 6$, 9, 9 or 8 (WT) or 5, 7, 9 or 7 (*Alox15*$^{-/-}$) per time point). **m**, IFNβ (left to right, $n = 3$, 7, 9 or 8 (WT) or 3, 6, 10 or 7 (*Alox15*$^{-/-}$) per time point). **n**, Pulmonary viral loads ($n = 4$ (day 3) or 3 (day 6) mice per group). **o**, Survival of WT ($n = 15$) and *Alox15*$^{-/-}$ ($n = 16$) animals infected with IAV (90 p.f.u.). **p**, WT AMs were transferred into *Alox15*$^{-/-}$ mice. Animals were infected 2 h after transfer with IAV (50 p.f.u.). Pulmonary viral loads were determined 3 days after infection (left to right, $n = 8$, 7 or 6 per group). **q**, Pulmonary viral loads in IAV-infected (50 p.f.u.) WT and *Alox15*$^{-/-}$ mice (treated or with or without mPGES1 inhibitor) ($n = 5$ per group). **r**,**s**, Scheme (**r**) and survival of *Alox15*$^{+/+}$ ($n = 20$) and *Alox15*$^{-/-}$ ($n = 17$) K18-hACE2 mice infected with SARS-CoV-2. Data are presented as the mean ± s.e.m. and are from one experiment (**k**,**q**), pooled from two (**a**,**c**,**e**,**f**,**m**,**p**,**s**), three (**g**,**h**,**j**,**l**,**o**) or four (**b**) independent experiments, or representative of two (n) independent experiments or six biological replicates (**d**). Data were analysed using two-tailed unpaired *t*-test (**k**), two-tailed Mann–Whitney test (**h**), one-way ANOVA followed by Tukey's multiple comparisons test (**a**,**p**,**q**), two-way ANOVA followed by Sidak's multiple comparisons test (**b**,**c**,**e**,**f**,**j**,**l**–**n**) or log-rank test (**o**,**s**). The models in **a**, **I**, **p** and **r** were created using BioRender (https://biorender.com).

Source data

By contrast, *Alox15*$^{-/-}$ AMs, but not BMDMs or PMs, produced significantly more tumour necrosis factor (TNF)-α, C-X-C motif chemokine 1 (CXCL1; also known as KC) and interleukin-6 (IL-6) in response to lipopolysaccharide (LPS) in vitro (Fig. 4b and Extended Data Fig. 7a–c) and in vivo (Fig. 4c and Extended Data Fig. 7d). This increase in cytokine production was associated with increased lung inflammation (Fig. 4d), tissue damage (Fig. 4e) and a significant increase in neutrophil recruitment (Fig. 4f and Extended Data Fig. 7e). Imaging of the lung microvasculature by intravital microscopy showed that in LPS-treated *Alox15*$^{-/-}$ mice, LPS induced neutrophil recruitment, with significant neutrophil–neutrophil interactions leading to the formation of large, complex cellular aggregates termed clusters. This highly activated neutrophil behaviour (Fig. 4g,h and Supplementary Video 1) contributes significantly to pulmonary tissue damage[29]. Similar to LPS, *Alox15*$^{-/-}$ AMs stimulated with

polyinosinic:polycytidylic acid (poly(I:C)) also showed increased levels of CXCL1, C-C chemokine 2 (CCL2) and TNF-α (Extended Data Fig. 7f).

Considering that senescent *Alox15*$^{-/-}$ AMs produced more PGE_2, and we have previously shown that PGE_2 is detrimental during influenza A virus (IAV) infection[14], we infected *Alox15*$^{-/-}$ mice with IAV (Fig. 4i). The production of PGE_2 in *Alox15*$^{-/-}$ AMs infected with IAV in vitro, ex vivo and in vivo was significantly increased (Fig. 4j–l). In line with the PGE_2-mediated suppression of early IFN-I production during IAV infection[14], the production of IFN-I, IFNβ (Fig. 4m) and IFNα (Extended Data Fig. 7g), but not IFN-III or IFNλ (Extended Data Fig. 7h), was significantly reduced in the BAL at day 2 after infection. A delay in the early IFN-I response resulted in increased pulmonary viral loads at day 3 after infection (Fig. 4n). This was associated with a significant increase in the production of CCL2 (Extended Data Fig. 7i), an accumulation of pulmonary inflammatory monocytes (Extended Data Fig. 7j,k), lung damage (Extended Data Fig. 7l–q) and an increase in mortality (Fig. 4o and Extended Data Fig. 7r). The expression of ALOX15 was not detectable in the lung at steady state (Extended Data Fig. 8a). However, following IAV infection, different cell types showed detectable levels of ALOX15 expression at day 1 and day 2, including AMs, neutrophils and eosinophils. Levels were undetectable by day 3 after IAV infection (Extended Data Fig. 8a). Concomitantly, the production of 12-HETE and 15-HETE in the BAL of IAV-infected mice was significantly increased at day 3 after infection (Extended Data Fig. 8b). Similar to the results obtained with 50 plaque-forming units (p.f.u.) of IAV, *Alox15*$^{-/-}$ animals infected with a low dose of IAV (20 p.f.u.), which causes no mortality, displayed an increase in pulmonary viral load, PGE_2, CXCL1, CCL2, neutrophils and inflammatory monocytes and a decrease in IFNβ (Extended Data Fig. 8c–g). This led to increased alveolar damage (Extended Data Fig. 8h) and pulmonary inflammation (Extended Data Fig. 8i). Thus, the lack of ALOX15 pathway has a significant impact on the initial antiviral response, which in turn dictates the magnitude of the inflammatory responses.

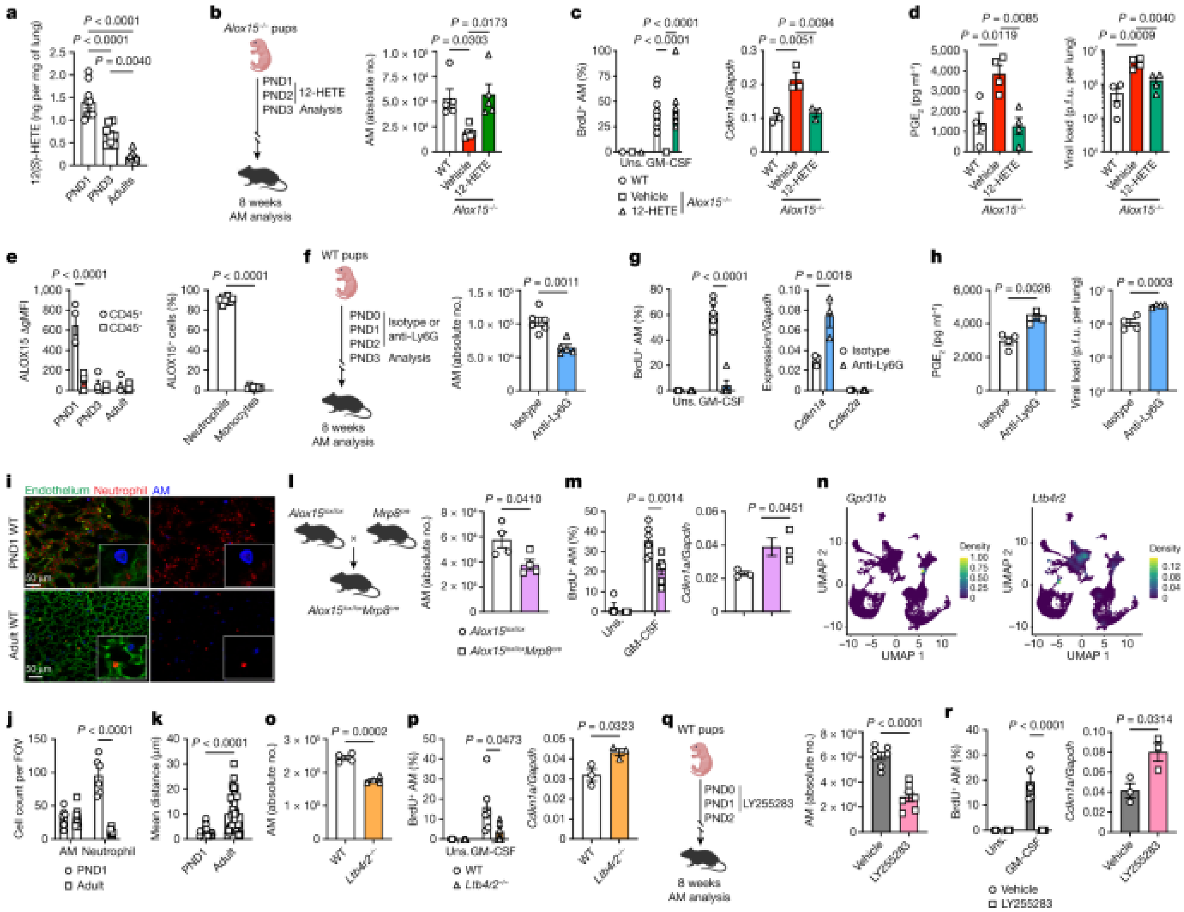
Notably, treatment of *Alox15*$^{-/-}$ with 12-HETE or 15-HETE had no effect on the pulmonary viral load or the outcome of IAV infection (Extended Data Fig. 8j,k). However, adoptive transfer of WT AMs into the airways of *Alox15*$^{-/-}$ mice (Fig. 4p) or inhibition of PGE_2 production in *Alox15*$^{-/-}$ mice (Fig. 4q) significantly reduced the pulmonary viral load. These data suggest that impaired function of *Alox15*$^{-/-}$ AMs is responsible for the susceptibility of the host to IAV infection, which cannot be reversed by exogenous 12-HETE or 15-HETE. Finally, we generated *Alox15*$^{-/-}$ K18-hACE2 mice and infected them with a sublethal dose of SARS-CoV-2 (Fig. 4r). *Alox15*$^{-/-}$ K18-hACE2 mice were highly susceptible to infection, with almost 100% mortality (Fig. 4r,s and Extended Data Fig. 8l). Thus, impaired proliferation and

increased senescence in *Alox15*$^{-/-}$ AMs leads to increased susceptibility to acute pulmonary viral infections.

AM programming by neutrophils

ALOX15-deficient AMs exhibit impaired proliferation, even though *Alox15* is not expressed in mouse adult lungs[30] or by AMs themselves at steady state (Extended Data Fig. 9a). Therefore we asked whether a burst of ALOX15 occurs during postnatal lung development. ALOX15-derived 12(*S*)-HETE and 15(*S*)-HETE were significantly increased in the lungs of WT mice at PND1 compared with PND3 and gradually decreased with age (Fig. 5a and Extended Data Fig. 9b). Moreover, delivery of exogenous 12-HETE, but not 15-HETE, at PND1 and PND2 significantly increased the proliferation of AMs, but had no effect on their differentiation (Extended Data Fig. 9c–e). The effects of perinatal 12-HETE treatment in *Alox15*$^{-/-}$ mice was long term, as the number of AMs in the BAL was maintained and comparable to WT in adult mice (Fig. 5b). Notably, AMs from prenatal 12-HETE-treated *Alox15*$^{-/-}$ mice restored their proliferative capacity with decreased expression of the senescence marker *Cdkn1a* (Fig. 5c and Extended Data Fig. 9f). Functionally, IAV-infected 12-HETE-treated *Alox15*$^{-/-}$ mice showed significantly lower levels of PGE_2 in the BAL, which was associated with a reduced viral load (Fig. 5d). Thus, 12-HETE is required for imprinting the self-renewal capacity of AMs during the differentiation of fetal liver monocytes into AMs to prevent senescence and restore the antimicrobial capacity of AMs.

Fig. 5: Neonatal neutrophil-derived 12-HETE programmes AM proliferation.



a, Pulmonary levels of 12(*S*)-HETE in PND1, PND3 and adult WT mice (left to right, $n = 10$, 8 or 8 per group). **b**, Scheme (left) and BAL AM numbers (right) in 12-HETE-treated *Alox15*$^{-/-}$ pups that were left to age until adulthood ($n = 5$ per group). **c**, Left, BrdU^{+} AMs after GM-CSF culture ($n = 5$ (Uns.) or 11, 10 or 12 (GM-CSF) fields of view (FOVs) per group). Right, basal *Cdkn1a* expression in AMs ($n = 3$ biological replicates per group). **d**, BAL PGE_2 levels (left) and pulmonary viral loads (right) at day 3 after IAV infection (50 p.f.u.) ($n = 4$ per group). **e**, Left, quantification of ALOX15 expression in CD45^{+} or CD45^{-} lung cells at various ages ($n = 4$ mice per group). MFI, mean fluorescence intensity. Right, ALOX15^{+} CD45^{+} cells were further gated using CD11b, Ly6C and Ly6G in PND1 lungs ($n = 8$ mice per group). **f**, Postnatal neutrophil depletion in WT mice using anti-Ly6G (left) and quantification (right) of BAL AMs in animals that were left to age until adulthood ($n = 6$ (isotype) or 5 (anti-Ly6G) mice per group). **g**, Left, BrdU^{+} AMs after GM-CSF culture ($n = 3$ (Uns.) or 5 (GM-CSF) fields of view per group). Right, basal *Cdkn1a* and *Cdkn2a* expression in AMs ($n = 3$ biological replicates per group). **h**, BAL PGE_2 levels (left) and pulmonary viral loads (right) at day 3 after IAV infection (50 p.f.u.) ($n = 4$ mice per group). **i**, Lungs were isolated from PND1 or adult (6–8 weeks) WT mice and stained for Ly6G (neutrophils, red), CD11c (AMs, blue) and CD31 (endothelial cells,

green). **j**, Quantification of macrophages and neutrophils (PND1: n = 6, Adults: n = 11). **k**, Mean distance between neutrophils and macrophages (PND1: n = 45, Adult: n = 43). **l**, Left, generation of neutrophil-specific $Alox15^{lox/lox}Mrp8^{cre}$ mouse model. Right, BAL AM numbers in adult mice (*n* = 4 per group). **m**, Left, BrdU^{+} AMs after GM-CSF culture (*n* = 4 (Uns.) or 6 (GM-CSF) fields of view). Right, basal *Cdkn1a* expression (*n* = 3 biological replicates per group). **n**, Representative uniform manifold approximation and projection (UMAP) plots of *Gpr31b* and *Ltb4r2* expression by single-cell RNA-seq in PND1 lungs. **o**, BAL AM numbers in adult WT and $Ltb4r2^{-/-}$ mice (*n* = 4 per group). **p**, BrdU^{+} AMs after GM-CSF culture (left; *n* = 3 (Uns.) or 6 (GM-CSF) fields of view per group) and basal *Cdkn1a* expression (right; *n* = 3 biological replicates per group) in adult WT and $Ltb4r2^{-/-}$ AMs. **q**, Postnatal inhibition of LTB4R2 signalling using LY255283 in WT mice (left) and BAL AM numbers in adult mice (right) (*n* = 7 per group). **r**, BrdU^{+} AMs after GM-CSF culture (left; *n* = 3 (Uns.) or 5 (GM-CSF) fields of view per group) and basal expression of *Cdkn1a* (right; *n* = 3 biological replicates per group) in adult AMs. Data are presented as the mean ± s.e.m. and are pooled from one (**d**,**h**,**n**), two (**a**,**b**,**e**,**f**,**l**,**o**,**q**) or three (**c**,**g**,**i**–**k**,**m**,**p**,**r**) independent experiments or representative of two (**c**,**g**,**m**,**p**,**r** (left)) independent experiments and were analysed using two-tailed unpaired *t*-test (**e**–**h**,**k**–**m**,**o**–**r**), one-way ANOVA followed by Tukey's multiple comparisons test (**a**–**d**) or two-way ANOVA followed by Tukey's (**c**) or Sidak's (**e**,**g**,**j**,**m**,**p**,**r**) multiple comparisons test. The models in **b**, **f**, **l** and **q** were created using BioRender (https://biorender.com).

Source data

To identify the source of 12-HETE in the neonatal lung, we first depleted basophils, which have been shown to express ALOX15 in the neonatal lung and play an important part in the differentiation of AMs[31]. However, basophil depletion in WT mice affected neither the seeding of AMs nor their proliferation (Extended Data Fig. 9g–i). We next analysed the expression of ALOX15 in leukocytes (CD45^{+}) or structural cells (CD45^{-}) in the lungs of PND1, PND3 and adult mice by flow cytometry (Fig. 5e and Extended Data Fig. 9j,k). The number of ALOX15-expressing leukocytes, in particular neutrophils (CD11b^{+}Ly6G^{+}), was significantly increased in the lungs of PND1 mice, but not adult lungs (Fig. 5e and Extended Data Fig. 9l,m). We next performed single-cell RNA-seq on isolated CD45^{+} cells from the lungs of WT and $Alox15^{-/-}$ mice at PND1. This analysis revealed marked compositional differences in neutrophil populations between $Alox15^{-/-}$ mice and WT mice (Extended Data Fig. 10a–d). $Alox15^{-/-}$ mice showed an almost complete absence of an entire subpopulation of neutrophils that represented 63% of all mature neutrophils found in WT mice (Extended Data Fig. 10b,c). By comparison, the compositional differences detected among other cell types were negligible, which further implicates

neutrophils in the programming of AMs. Indeed, neutrophil depletion from PND0 to PND2 significantly reduced the proliferative capacity of AMs, but not seeding, at PND3 (Extended Data Fig. 10e–g). This in turn led to reduced numbers of AMs in adult mice (Fig. 5f), which was due to decreased proliferation of AMs and increased expression of the senescence marker *Cdkn1a* (Fig. 5g and Extended Data Fig. 10h). Of note, this was associated with increased PGE_2 production and pulmonary viral load following IAV infection (Fig. 5h). Whole-lung imaging and intravascular staining showed that neutrophils specifically accumulated in the lung parenchyma of PND1 mice (Fig. 5i,j and Extended Data Fig. 10i,j). Moreover, the distance between AMs and neutrophils in the neonatal lungs was significantly reduced compared with adult lungs of WT mice (Fig. 5k). This result suggests a potential interaction between neutrophils and AMs in the early days of life. Finally, we generated a conditional knockout strain in which *Alox15* is selectively deleted in neutrophils by crossing $Alox15^{lox/lox}$ mice with $Mrp8^{cre}$ mice (Fig. 5l). Similar to $Alox15^{-/-}$ mice, $Alox15^{lox/lox}Mrp8^{cre}$ mice had significantly fewer numbers of AMs in the BAL, which was associated with impaired proliferation, increased expression of *Cdkn1a* and β-galactosidase (Fig. 5l,m and Extended Data Fig. 10k,l).

Two receptors have been identified for 12-HETE: GPR31 (encoded by *Gpr31b*)[32] and LTB4R2 (encoded by *Ltb4r2*)[33]. Our single-cell RNA-seq datasets showed no detectable *Gpr31b* expression, whereas there was a strong expression of *Ltb4r2* in PND1 macrophages (Fig. 5n). Similar to $Alox15^{-/-}$ mice, $Ltb4r2^{-/-}$ mice had significantly fewer numbers of AMs in the BAL at steady state (Fig. 5o). The reduced numbers of AMs were associated with a decrease in their proliferation and an increase in the expression of *Cdkn1a* in $Ltb4r2^{-/-}$ mice (Fig. 5p). We next treated WT mice at PND0, PND1 and PND2 with a pharmacological antagonist of LTB4R2 (LY255283) and mice were left to age until adulthood (Fig. 5q). AMs from mice that were treated with LY255283 perinatally had significantly fewer AMs in the BAL (Fig. 5q). This was associated with a significant decrease in proliferation of AMs and an increase in the expression of the cell cycle inhibitor *Cdkn1a* (Fig. 5r). An analysis of the AM populations and proliferation after blocking PGE_2 signalling with an EP_2 antagonist (TG6-10-1) in $Alox15^{-/-}$ mice showed that the number of AMs in the BAL was significantly increased, reaching a level similar to that of WT mice (Extended Data Fig. 10m). This was associated with an increase in proliferation and a decrease in *Cdkn1a* expression in AMs (Extended Data Fig. 10n). These processes were specific to the perinatal window, as no effect was observed in adult mice (Extended Data Fig. 10o,p). Collectively, these data indicate that perinatal ALOX15-derived 12-HETE from neutrophils is required to imprint the long-term self-renewing programme of AMs through the LTB4R2 receptor.

Since the advent of fate-mapping approaches demonstrating the prenatal origins of some RTMs, the cellular and molecular mechanisms of self-renewing, embryo-derived

macrophages have remained elusive. Although GM-CSF and TGFβ are required for the differentiation of fetal liver monocytes to mature AMs during the first days of lung development[2,9], our results demonstrated that these cytokines are not sufficient for RTM self-renewal and maintenance. Specifically, we showed that neutrophil-derived 12-HETE during early life is essential for the programming of AM self-proliferation, revealing a new role for innate immunity and eicosanoids during the perinatal period (Extended Data Fig. 10q). It is unclear whether similar mechanisms of reprogramming are engaged to replace AMs by BMDMs. Furthermore, the location of this imprinting (for example, BM or lung) remains unknown. Although ageing is associated with alterations in haematopoiesis and increased numbers of circulating monocytes and neutrophils, the number of AMs declines with age[34,35]. The AM reduction in ageing individuals and their increased susceptibility to pulmonary infection or inflammation may be related to the attenuation of neutrophil function with age[36], including their reduced capacity to produce 12-HETE. Although we did not investigate the origin of neutrophils (BM compared to fetal liver haemopoietic stem cells) during prenatal lung development, the increased number of neutrophils in the lung parenchymal tissue raises questions on the specific age-dependent origin of neutrophils that might still derive from fetal haematopoiesis. Further studies are required to examine the ontogeny and functions of neutrophils with age and the therapeutic potential of eicosanoid pathways in modulating the quantity or quality of AMs during pulmonary infection, resolution of inflammation and mucosal healing.

Methods

Mice

C57BL/6 mice, *Alox15*$^{-/-}$ mice (B6.129S2-*Alox15*^{tm1Fun}/J), *Alox5*$^{-/-}$ mice (B6.129S2-*Alox5*^{tm1Fun}/J), CD45.1 mice (B6.SJL-*Ptprc*^{a} *Pepc*^{b}/BoyJ), *Mrp8*^{cre} mice (B6.Cg-Tg(S100A8-cre,-EGFP)1Ilw/J), *Csf2rb*$^{-/-}$ mice (B6.129S1-*Csf2rb*^{tm1Cgb}/J) and K18-hACE2 (B6.Cg-Tg(K18-ACE2)2Prlmn/J) mice were purchased from Jackson Laboratories. *Alox15*$^{-/-}$ K18-hACE2 mice were generated by crossing K18-hACE2 mice with *Alox15*$^{-/-}$ animals. *Alox15*$^{lox/lox}$ mice on a C57BL/6 background were a gift from S. Tersey (University of Chicago, USA) and were crossed with *Mrp8*^{cre} mice to generate specific deletion of the ALOX15 pathway in neutrophils. *Ltb4r2*$^{-/-}$ mice on a C3HeJ background were a gift from C. Brown (University of Missouri, USA). All animals were housed and inbred at the animal facility of the Research Institute of McGill University under specific pathogen-free conditions with ad libitum access to food and water, a temperature of 21 °C (±1 °C), relative humidity of 40–60% (±5%) and light cycle of 12 h on, 12 h off (daily cycle). Mice were randomly allocated to experimental groups, and experiments were performed using both female and male age- and sex-matched mice.

Isolation and culture of primary macrophages and cell lines

AMs were collected by BAL of naive mice using cold, sterile PBS (5 × 1 ml for adult mice; 5 × 50–100 µl for PND3). AMs were cultured in RPMI-1640 medium supplemented with 10% (v/v) FBS, 2 mM l-glutamine, 10 mM HEPES and 100 U ml^{-1} penicillin–streptomycin. After 1 h of adhesion, AMs were washed with PBS and placed in fresh medium. Mouse BMDMs were isolated following aseptic flushing of tibiae and femurs of 6–8-week-old mice. Macrophages were differentiated from BM precursors for 6 days in RPMI-1640 supplemented with 30% (v/v) L929 cell-conditioned (American Type Culture Collection (ATCC)) medium, 10% (v/v) FBS, 2 mM l-glutamine, 1 mM sodium pyruvate, 1% essential and nonessential amino acids, 10 mM HEPES and 100 U ml penicillin–streptomycin. PMs were collected by peritoneal lavage of naive mice using cold, sterile PBS. PMs were cultured in RPMI-1640 supplemented with 10% (v/v) FBS, 2 mM l-glutamine, 10 mM HEPES and 100 U ml^{-1} penicillin–streptomycin. After 1 h of adhesion, PMs were washed with PBS and placed in fresh medium. All reagents and supplements pertaining to cell culture were purchased from Gibco.

Viruses, infections and stimulation

All influenza in vitro and in vivo infections were performed using influenza A/Puerto Rico/8/34 (H1N1) virus, which was provided by J. A. McCullers (St Jude Children Research Hospital). Virus was propagated and titrated in MDCK (ATCC) cells using standard plaque assay[37]. Mice were intranasally challenged (in 25 µl PBS) with IAV at a sublethal dose of 20 or 50 p.f.u. (immunophenotyping, ELISA) or a median lethal dose (LD_{50}) of 90 p.f.u. In some experiments, *Alox15*$^{-/-}$ mice were treated intraperitoneally with a chemical inhibitor of mPGES1 (CAY10526, 5 mg kg^{-1}, in 100 µl of PBS, daily) or exogenous 12-HETE or 15-HETE (1 µg per mouse in 100 µl of PBS) starting from the day of infection. Virus titres were determined in lung homogenates homogenized in PBS using standard MDCK plaque assay.

For SARS-CoV-2 infection in vivo, SARS-CoV-2/RIM-1 was isolated from a patient at The McGill University Health Center, Montreal, Quebec. SARS-CoV-2 was propagated in VeroE6 cells (ATCC). Mice were intratracheally infected as previously described[38] with 4,000 median tissue culture infectious dose ($TCID_{50}$) of SARS-CoV-2/SB2.

In specific experiments, AMs, PMs or BMDMs were stimulated with 100 ng ml^{-1} of LPS (Sigma) or AMs were stimulated with 50 µg ml^{-1} of poly(I:C) (Invivogen).

Protein in BAL

BAL samples collected by cannulating the trachea with a 22-gauge cannula, then washing the lungs with 3× 1 ml of cold, sterile PBS. The total volume of the recovered fluid after lavage was around 0.7 ml. Samples were centrifuged (1,500 r.p.m., 10 min), and total protein content was assessed using a Pierce BCA Protein assay (ThermoFisher).

Wet-to-dry ratio

Lungs were collected from naive or IAV-infected mice (50 p.f.u., day 6 after infection) and blood clots were carefully removed. Then the lungs were weighed (wet weight), dried in an oven (56 °C, 2 days) and the dry weight was measured. Data are presented as the ratio wet/dry (w/w).

Flow cytometry

Lung tissues were perfused with 10 ml of PBS, collected and minced before collagenase IV digestion (150 U ml^{-1}, Sigma) for 1 h at 37 °C. Lungs were filtered through a 70 μm nylon mesh, and red blood cells were lysed. Peritoneal cells were obtained following lavage with 5 ml of cold PBS intraperitoneally injected. Cells were then spun down, and red blood cells were lysed. Spleen cells were obtained by crushing the spleen through a 70 μm nylon mesh followed by red blood cells lysis. Liver cells (median lobe) were obtained after mincing and digestion with collagenase VIII (1 mg ml^{-1}, Sigma) for 30 min at 37 °C. The cells were passed sequentially through 100 and 70 μm cell strainers before red blood cell lysis. Brain cells were obtained after passing through 100 and 70 μm cell strainers followed by Percoll gradient (30% and 70% solutions). Total lung, peritoneal, liver, brain and spleen cell counts were determined with a haemocytometer, and 1–2 million cells were used for staining.

Cells were initially stained with viability dye e450 or e506 (Invitrogen, 20 min, 4 °C) and surface stained with anti-CD16/32 (BD Bioscience) in 0.5% BSA/PBS solution to block nonspecific AB interaction with Fc receptors (10 min, 4 °C). Cells were then surface-stained with different combinations of PE-Cy7-conjugated anti-CD11c, PE-CF594-conjugated anti-Siglec-F, PE-Cy7-conjugated or BUV395-conjugated anti-CD11b, PerCP-eFluor710-conjugated anti-Ly6G, FITC-conjugated or APC-conjugated anti-Ly6C, APC-eFluor780-conjugated anti-F4/80, PE-conjugated anti-CD103, PerCP-conjugated anti-CD64, BUV395-conjugated anti-CD45.2 and APC-conjugated anti-CD45.1 (all from BD Biosciences). For Ki-67, p53, pSTAT5, pSMAD2/3, p-p38, pAKT and pERK1/2, cells were fixed and permeabilized using BD CytoFix/CytoPerm (BD Bioscience) before intracellular staining with APC-conjugated or PE-conjugated anti-Ki-67, PE-conjugated anti-p53, AlexaFluor647-conjugated anti-p-p38, PE-conjugated anti-pSMAD2/3, APC-conjugated anti-pAKT1, PerCP-eFluor710-

cojugated anti-pERK1/2, PE-Cy7-conjugated anti-p-γH2AX, AlexaFluor 647-conjugated anti-15-lipoxygenase and APC-conjugated anti-pSTAT5 (from BD Bioscience, Life Technologies, Bioss or Cell Signaling Technologies). In some experiments, AMs were stained with MitoSox (Invitrogen) for analysis of mitochondrial reactive oxygen species production or DAPI (1:2,000 in PBS) to evaluate the total DNA content. Flow cytometry was performed using a BD LSR Fortessa X-20 instrument (BD Biosciences) with FACSDiva software v.8.0.1 (BD Biosciences). Analysis was performed using FlowJo software v.10.7.1 (Tree Star).

Cell death analysis

Necrosis and apoptosis levels of BAL AMs were assessed using a PE-AnnexinV and 7-amino-actinomycin D (7-AAD) Apoptosis Detection Kit I (BD Biosciences) according to the manufacturer's instructions and analysed by flow cytometry.

BrdU incorporation studies

For in vivo analysis, BrdU was intraperitoneally administered (1 mg per 100 µl per mouse) daily for 7 days before euthanasia. BrdU incorporation in AMs and PMs was assessed using a BrdU APC kit (BD) following the manufacturer's instructions before analysis by flow cytometry.

For in vitro analysis, BrdU (10 µM) was added to AMs on day 2 after GM-CSF (20 ng ml^{-1}) stimulation. On day 3, AMs were fixed with 4% paraformaldehyde (PFA) and then DNA was denatured using 1.5 M HCl for 30 min at room temperature. Cells were washed with PBS then stained with anti-BrdU antibody (BioLegend). BrdU (10 µM) was added to cells at day 3 and day 5 of BMDM differentiation. BrdU incorporation was assessed by flow cytometry at day 6 using a BrdU APC kit (BD) following the manufacturer's instructions.

Histopathological analysis

Lungs were inflated and fixed for 48 h with 10% formalin, and then embedded in paraffin. Sections (5 µm) were cut and stained with haematoxylin and eosin. Slides were scanned at a resolution of ×40 magnification, and pictures were taken using a Leica Aperio slide scanner (Leica).

For frozen sectioning and ALOX15 and Ly6G staining, lungs were inflated with 10% OCT in PBS and embedded in OCT before being frozen at −80 °C. Sections (5 µm) were dried on slides and fixed for 5 min in ice-cold acetone:methanol solution (1:3, v/v) and then washed in PBS. Lung sections were incubated for 1 h with cold block buffer (2% BSA diluted in PBS with 1:100 Fc-block). Sections were then incubated

with AlexaFluor 594-conjugated anti-Ly6G (BioLegend) or a rabbit anti-ALOX15 antibody (Abcam) for 24 h in 2% BSA in PBS. Slides were then incubated with a goat anti-rabbit AlexaFluor 647-conjugated antibody (Life Technologies) for 1 h at room temperature. Slides were washed with PBS and mounted in Prolong Diamond antifade with DAPI (Invitrogen). Images were acquired using a Zeiss LSM 700 laser-scanning confocal microscope.

For whole-lung imaging of adult or PND1 mice, animals were euthanized, and 1.5% agarose was used to fill the lungs. The trachea was opened, and agarose was added to the lungs using a 25-gauge needle syringe. Lungs were removed and fixed using 4% PFA overnight and sliced into 300 μm sections using a vibratome. Lungs were stained using AlexaFluor 647-conjugated anti-mouse CD11c, AlexaFluor 594-conjugated anti-mouse Ly6G and AlexaFluor 488-conjugated anti-mouse CD31 fluorescent antibodies (all from BioLegend). Samples were mounted on slides and imaged using a Leica SP8 confocal microscope.

Confocal microscopy

AMs were seeded in a media chamber of a glass microscopy slide (Millipore). Cells were fixed in 4% PFA for 15 min and then permeabilized by incubating with 0.1% Triton X-100 in PBS or ice-cold methanol for 15 min. Samples were blocked with 1% milk in PBS Triton X-100 0.1% for 1 h and then incubated with a specific rabbit polyclonal anti-pSTAT5, rat anti-Ki-67 or mouse anti-BrdU overnight at 4 °C (Cell Signaling Technology, Life Technologies or BioLegend). Cells were incubated for 1 h with secondary antibody Alexa Fluor 555-conjugated or 647-conjugated goat anti-rabbit or anti-mouse (1:1,000, Invitrogen) and nuclei were stained with DAPI (1:2,000, Molecular Probes). Coverslips were mounted (ProLong Diamond Anti Fade, Invitrogen) onto microscope slides. Images were acquired using a Zeiss LSM 700 laser-scanning confocal microscope and analysed using ImageJ software.

In some experiments, lung and blood neutrophils from PND1 and adult WT or *Alox15*$^{-/-}$ mice were isolated using a neutrophil enrichment kit (StemCell Technologies). Pooled neutrophils were seeded onto poly-l-lysine-treated microscopy chambers and fixed with 4% PFA at room temperature for 15 min. Cells were then permeabilized using Triton X-100 0.1% and then incubated with a rabbit anti-ALOX15 antibody (Abcam) for 24 h in 2% BSA in PBS. Slides were then incubated with AlexaFluor 594-conjugated anti-Ly6G (BioLegend) and a goat anti-rabbit AlexaFluor 647-conjugated antibody (Life Technologies) for 1 h at room temperature. Slides were washed with PBS and mounted in Prolong Diamond antifade with DAPI (Invitrogen). Images were acquired using a Zeiss LSM 700 laser-scanning confocal microscope.

ELISA and cytokine array

IFNβ and IFNα levels in BAL were measured using a Verikine Mouse IFNβ ELISA kit (PBL Assay Science) or a Mouse IFNβ ELISA kit (Abcam) and Verikine Mouse IFNα ELISA kit (PBL Assay) or an IFNα Mouse ELISA kit (Invitrogen), respectively. TNF, CXCL1C, GM-CSF, TGFβ1, IL-6, IFNλ and CCL2 levels were assessed by ELISA (R&D Systems). PGE_2, 12(*S*)-HETE, 15(*S*)-HETE, cysteinyl leukotrienes and LTB_4 levels were determined by ELISA (Cayman Chemical or Abcam). Surfactant protein-A ELISA was from Cusabio. Cytokines were measured in resting AM supernatant (24 h) using a Proteome Profiler Mouse Cytokine Array Kit, Panel A (R&D Systems) following the manufacturer's instructions. The pixel intensity was analysed using ImageJ.

RNA isolation and quantitative PCR with reverse transcription

RNA from AMs, PMs and BMDMs was extracted using a RNeasy kit (Qiagen) according to the manufacturer's instructions. RNA was reverse transcribed using ABM 5X RT MasterMix (ABM) or LunaScript RT SuperMix (New England Biolabs) as directed by the manufacturer. cDNA was generated by quantitative PCR using BrightGreen Sybr Green (ABM) or PowerUp Sybr Green (Life Technologies). Primers are listed in Supplementary Table 2. C_q values obtained using a CFX96 PCR system (Bio-Rad) were analysed using the formula \({2}^{-\Delta {{\rm{C}}}_{{\rm{q}}}}\), normalizing target gene expression to *Gapdh*.

Adoptive transfer models

AMs from WT or *Alox15*$^{-/-}$ mice were collected as described above and resuspended at a density of 5×10^4 cells per 50 µl. AMs were then transferred by the intratracheal route into *Alox15*$^{-/-}$ mice (AM populations, IAV infection model) or *Csf2rb*$^{-/-}$ mice (BAL protein analysis). For the IAV infection model, mice were infected with IAV PR8 (50 p.f.u., intranasally) 2 h after transfer. BAL and lung tissue were collected and processed as described above for flow cytometry, viral load or total BAL protein content evaluation.

Administration of 12-HETE or 15-HETE, TG6-10-1, LY255283 or anti-FcεRI and anti-Ly6G antibodies

Exogenous 12-HETE and 15-HETE were purchased from Cayman Chemicals. PND1 and PND2 *Alox15*$^{-/-}$ pups or adult mice were intranasally administered with vehicle, 12-HETE or 15-HETE (200 ng in 6 µl or 25 µl of PBS).

TG6-10-1 (5 mg kg^{-1} in 25 µl or 100 µl of PBS) and LY255283 (5 mg kg^{-1} in 25 µl or 100 µl of PBS) were purchased from Cayman Chemicals and intraperitoneally administered to pups (PND0, PND1 or PND2) or adult mice.

Isotype control (rat IgG2a) or anti-Ly6G (50 µg per mouse in 25 µl, both from BioLegend) were given intraperitoneally to PND0, PND1 and PND2 WT pups.

Isotype control (Armenian hamster IgG) or anti-FcεR1 (7 µl of a 100 µg solution per mouse, both from Life Technologies) were given intranasally to WT pups at PND1 and PND2.

Macrophage proliferation and growth assays

For the macrophage growth assay, 20×10^4 cells were seeded in a 24-well plate and cultured with 20 ng ml^{-1} recombinant murine GM-CSF, 50 ng ml^{-1} M-CSF alone or in combination with IL-4 (20 ng ml^{-1}) for 3 days. Cells were then stained with crystal violet, resuspended in ethanol and the optical density read at 595 nm. In some experiments, macrophages were treated with various concentrations of PGE_2 (1–10 µM, Cayman Chemical).

Endothelial permeability

Infected or uninfected mice were intraperitoneally injected with 400 µl of Evan's blue dye (2% in PBS). After 1 h, mice were euthanized, BAL collected and lungs were perfused with 10 ml of PBS. Evan's blue was then extracted by overnight incubation in formamide at 56 °C (lungs) or overnight incubation with 50% trichloroacetic acid at 4 °C (BAL) and quantified by spectrophotometry analysis using a standard curve of Evan's blue in formamide or 50% trichloroacetic acid.

BM chimeras

$CD45.1^+$ WT mice or $CD45.2^+$ WT or *Alox15*$^{-/-}$ mice were lethally irradiated with 9 Gy following 3 days of antibiotic treatment (0.5 g Enrofloxacin (Bayer) per litre of drinking water). After 16 h, the BM compartment was reconstituted with 4×10^6 nucleated cells from either $CD45.1^+$ mice (*Alox15*$^{-/-}$ or WT $CD45.2^+$ recipient) or *Csf2rb*$^{-/-}$ or *Alox15*$^{-/-}$ mice (*Alox15*$^{-/-}$ or $CD45.1^+$ recipient) and antibiotic treatment was maintained for 2 additional weeks. Eight weeks after injection, mice were then used for downstream assays.

AM depletion

WT, *Alox15*$^{-/-}$ or *Ccr2*$^{-/-}$ mice were treated with control or clodronate liposomes (70 μl, intranasally; Liposoma BV). The AM populations were evaluated at day 2 and day 14 after delivery in the BAL by flow cytometry.

Extracellular flux analysis

Real-time OCRs of AMs, PMs and BMDMs were measured in XF medium (non-buffered RPMI containing 2 mM l-glutamine, 25 mM glucose and 1 mM sodium pyruvate) using a Seahorse Xfe 96 Analyzer (Agilent Technologies). For the mitochondrial stress test, mitochondrial inhibitors oligomycin (1.5 μM), fluorocarbonyl cyanide phenylhydrazone (FCCP) (1 μM), antimycin A and rotenone (0.5 μM) were used as per the manufacturer's recommendations. In brief, cells were seeded at a density of 100,000 cells per well and 3 basal measurements were taken. Following this, two consecutive measurements were taken following each injection of oligomycin, FCCP and antimycin A with rotenone. All measurements were normalized to cell number using crystal violet dye extraction assay. Oxygen consumption curves, OCRs and ECARs were generated using Wave Desktop 2.3 (Agilent Technologies).

Library preparation and RNA-seq

Bulk RNA was collected from BAL AMs from four WT and four *Alox15*$^{-/-}$ mice. Sequencing libraries were constructed using the Illumina TruSeq protocol. Libraries were sequenced on an Illumina NovaSeq (paired-end 100 base pair) to an average depth of 42.6 million reads per sample.

Quantification of gene expression and identification of differential genes

All the reads were mapped to the mouse genome (UCSC mm10) (http://www.ccb.jhu.edu/software/hisat/index.shtml) using HISAT2 (v.2.1.0)[39] with the default settings. We then used HTSeq-count[40] to quantify the raw counts for all genes based on the mapped reads using the mm10 gene annotation GTF file downloaded from the UCSC genome browser. With the quantified raw count for all samples, DESeq2 (ref. [41]) was used to identify differentially expressed genes between samples of the WT and *Alox15* knockout (KO) macrophages in our study. DESeq2 also normalizes gene expression of all samples. The normalized gene expression was further converted into the $\log_2$ space. We obtained four replicates each from WT (WT0–WT4) and KO (KO1–KO4) macrophage cells. The gene expression pattern of WT4 was different (Mann–Whitney U-test $P = 0$) to all other WT samples (WT0–WT3). Therefore we removed WT4 from all subsequent analyses; this decision was supported by the principal component analysis plot (WT4 is far from the other three WT samples in the plot).

We also wrote a JavaScript-based web service to interactively plot the gene expression pattern in different samples and to perform statistical comparison analysis (that is, Mann–Whitney *U*-test) between macrophages in different conditions (for example, WT compared with KO). For any input gene (or gene list), the web service can automatically plot the heatmap (to show gene expression across samples) and violin plot (to show the expression difference between macrophages in different samples and conditions). The normalized gene expression for the queried gene (gene list) can also be directly downloaded from the web service. The web service is freely available at http://junding.lab.mcgill.ca/reseach/maziar/GeneSetEnrichment for easier and interactive use of the RNA-seq datasets generated in this study.

KEGG Pathway enrichment analyses

We performed pathway enrichment analyses on the identified differential gene list. We first downloaded the mouse pathway annotation from the KEGG database[42]. For a given gene list of interest, we used the hypergeometric test to check whether it was significantly enriched with specific pathways (that is, whether the gene list was significantly enriched with genes from a specific KEGG Pathway). All the obtained *P* values were corrected for multiple comparison.

Single-cell RNA-seq data generation

Lungs were collected from WT and *Alox15*$^{-/-}$ PND1 pups and then the total CD45^{+} cells were isolated using magnetic sorting (StemCell Technologies). Single-cell gel beads in emulsion (GEMs) were generated using a Chromium Controller instrument (10x Genomics). Sequencing libraries were prepared using Chromium Single Cell 3′ Reagent kits (10x Genomics) according to the manufacturer's instructions. In brief, GEM-RT was performed in a thermal cycler with the following parameters: 53 °C for 45 min; and 85 °C for 5 min. cDNA was cleaned up with DynaBeads MyOne Silane Beads (ThermoFisher Scientific) and amplified with a thermal cycler with the following parameters: 98 °C for 3 min; cycled 12× 98 °C for 15 s; 67 °C for 20 s; 72 °C for 1 min; and 72 °C 1 min. After a clean-up using a SPRIselect Reagent kit, the libraries were constructed by performing the following steps: fragmentation, end repair, A-tailing, SPRIselect cleanup, adaptor ligation, SPRIselect cleanup, sample index PCR and SPRIselect size selection. Libraries were sequenced on a NovaSeq S2 flowcell.

Single-cell RNA-seq data analyses

Raw fastq files were processed using Cellranger (v.3.1.0)[43]. After filtering for low counts cells using Cellranger's default parameters, 7,755 and 10,098 cells were retained for WT and *Alox15*$^{-/-}$ samples, respectively. The two datasets were

integrated using SCTransform[44]. To account for potential variation in cell death and the proliferative status of the cells, we included as covariables the percentage of mitochondrial reads and the expression level of cell cycles genes, respectively. Integration was performed using 3,000 hypervariable genes followed by dimensionality reductions runPCA (retaining 20 principal components for all dependent analysis) and runUMAP. After dimensionality reduction, unsupervised clustering was performed using FindNeighbors and FindClusters (resolution of 1).

Owing to the unprofiled nature of developing mouse lung cells, a combination approach was taken to annotate the different cell type clusters identified. First, we used canonical markers of the different cell types expected to be found in mature lung cells. This was followed by a more systematic cell-type annotation using signature gene sets. Gene sets were derived from the full Panglao cell-type marker database[45], which were converted to mouse gene nomenclature before use. Annotation was performed using the procedure as described in the R package Cell-ID[46]. In brief, the SCTransform normalized count matrix is evaluated against reference gene lists using a multiclass hypergeometric test. For each cell, the predicted class with the lowest FDR (Benjamini–Hochberg) *P* value was considered the likely true class. *P* values greater than 0.01 were considered ambiguous for this analysis.

To provide more detailed insight, we sought to further characterize neutrophil heterogeneity. To do so, we leveraged a previous a single-cell study[46] that characterized distinct mouse peripheral blood neutrophil subpopulations through their development. Raw count and per-barcode labels were downloaded from the Gene Expression Omnibus (identifier GSE137539). Counts were $\log_{10}$-normalized and then genes were scaled using default parameters of Seurat's NormalizeData and ScaleData functions. Next, multiple correspondence analysis (MCA and RunMCA function) dimensionality reduction from the Cell-ID package was performed followed by the GetCellGeneSet Cell-ID function. This procedure resulted in a series of custom gene lists ($n = 200$ per list) that defined each neutrophil class. Cell annotation was again performed using these lists to obtain neutrophil subtype predictions. Final labelling was done by assigning unsupervised clusters by their consensus label and manually curating when necessary.

Characterization of differences between WT and *Alox15*$^{-/-}$ samples was performed by observing variation in abundance among annotated cell types. We did so using neighbourhood-based differential-abundance testing and visualization with Milo[47]. Because Milo requires at least two samples per condition, each sample was randomly split into two equal 'pseudosamples' for use with Milo differential-abundance testing using the following R function: ≈condition + pseudosample. Differential-abundance neighbourhood graph construction was completed with the plotNhoodGraphDA.

ATAC-seq

ATAC-seq was performed on FACS-sorted neonatal (PND3) and BAL-isolated adult alveolar macrophages. Fifty thousand cells were washed once in ice-cold PBS by centrifugation at 500*g* for 5 min at 4 °C. Cells were resuspended in 50 µl lysis buffer (10 mM Tris-HCl, pH 7.4, 10 mM NaCl, 3 mM $MgCl_2$ and 0.1% IGEPAL CA-630) and spun down immediately at 500*g* for 10 min at 4 °C. Pellets were resuspended in transposition reaction mix (25 µl 2× TD Buffer (Illumina, FC-121-1030), 2.5 µl Tn5 Transposes (Illumina, FC-121-1030) and 22.5 µl nuclease-free H_2O) and incubated at 37 °C for 30 min. DNA was purified with a Qiagen MiniElute kit and amplified with Nextera PCR primers (Illumina Nextera Index kit) and NEBNext PCR master mix (M0541, New England BioLabs). Amplified DNA was purified with a Qiagen Mini Elute kit. Libraries were sequenced paired-end on a Novaseq sequencer at the University of Chicago Genomics Facility.

Initial processing of ATAC-seq data

ATAC-seq reads were mapped to the mouse reference genome (GRCm38/mm10) using Bowtie2. Mapped reads were filtered and sorted using the samtools 'view' and 'sort', respectively. PCR duplicates were removed using the Picard MarkDuplicates program with parameter REMOVE_DUPLICATES=True. Peaks were subsequently called using the MACS2 software suite[48] with parameters -q 0.05 and –keep-dup all.

Differential chromatin accessibility analysis

Differentially accessible peaks were determined first by counting the number of reads overlapping each called peak region (using a merged peak file from all samples and replicates across the time course) using featureCounts software (from the subread package). The resulting count matrix was then further analysed using the limma package for R (v.4.1.1). Features were first filtered by removing those with median log(counts per million) of ≤1 across all samples and replicates. Then we normalized raw counts across all samples using the calcNormFactors function implemented in the R package edgeR (v.3.34.0), which utilizes the TMM algorithm (weighted trimmed mean of *M*-values) to compute normalization factors and we log-transformed the data using the voom function from the limma package (v.3.48.3). After filtering and normalization, we performed a weighted fit with the voom-calculated weights using the lmFit function from limma. The normalized, log-transformed counts were fit to a linear model with the following design: chromatin accessibility ≈1 + age + genotype:age. This enabled us to capture the effect of *Alox15* KO (genotype) on peak accessibility levels independently for adults and pups. Features with adjusted *P* values smaller than 0.05 were considered significant.

GSEAs

GSEAs were performed using the R package fgsea (v.1.18.0) with the following parameters: minSize = 15, maxSize = 500, nperm = 100000. To investigate biological pathway enrichments among genes close to differentially accessible peaks, we first assigned all peaks to their nearest gene using the Homer function annotatePeaks with default parameters. Then we ordered genes by their peak associated *t*-statistic derived from limma (see above) and compared the rank-ordered gene list to the reactome gene sets from the MsigDB collections (category = C2, subcategory = CP:REACTOME).

LPS lung injury

Mice were administered with 20 μg of LPS in PBS (25 μl per mouse, intranasally). BAL and lungs were collected 1 or 3 days after delivery for downstream analyses.

Intravascular staining

PND1, PND3 or adult WT mice were given 2 μg of FITC-conjugated anti-CD45.2 intravenously to label all circulating cells. Three minutes later, mice were euthanized and lungs collected, stained ex vivo with BUV395-conjugated anti-CD45.2 antibody to determine the parenchymal (cells only labelled with the ex vivo antibody) or vascular localization of the cells (cells labelled with both antibodies).

SA-β-galactosidase staining

AMs from WT, $Alox15^{-/-}$, $Alox15^{lox/lox}$ and $Alox15^{lox/lox}Mrp8^{cre}$ mice were collected as described above and stained using a colorimetric SA-β-galactosidase staining kit (Cell Signaling Technology) or a CellEvent Senescence kit (Life Technologies) according to manufacturer's instructions.

Intravital microscopy

For imaging experiments, male mice were used between 6 and 12 weeks of age. Mice were anaesthetized by an intraperitoneal injection of ketamine (100 mg kg^{-1}) and xylazine (10 mg kg^{-1}). Anaesthetized mice were cannulated at the internal jugular veins to allow for intravenous injection of antibodies, reagents and additional anaesthetics before and during imaging. Mice were placed on mechanical ventilation through a tracheal catheter. The left lung was exposed by removing two or three ribs. A vacuum chamber with a glass slide fitted on top was used to gently stabilize a portion of the lung for imaging. Anti-Ly6G (clone 1A8, BioLegend) and anti-CD31 (clone MEC13.3, BioLegend) antibodies conjugated with either AlexaFluor 647 or

594 fluorochromes were intravenously injected (7 µl per mouse) to visualize neutrophils and the vasculature, respectively. A resonant-scanner confocal microscope (Leica SP8) was used for all pulmonary imaging. A ×25/0.95 water-objective lens was used for imaging for all videos. A tuneable multiline white light laser was used to simultaneously excite the required fluorochromes. Videos (each 10 min in length) from 3 different field of views were recorded at identical time points and repeated over 2 h of the imaging experiment. Videos were processed using Imaris 9.3. Analysis of cell behaviour and cluster quantification was performed with Imaris 9.3.

Oil Red O staining

BAL AMs were stained using an Oil Red O staining kit (Abcam) following the manufacturer's instructions.

Analysis of pulmonary function

Airway responses to methacholine were evaluated using a small animal ventilator (flexiVent apparatus and flexiVent 5.1 software) as previously described[49].

AM phagocytosis assay

BAL phagocytosis was evaluated using pHrodo Green *Escherichia coli* BioParticles Conjugate for Phagocytosis (Invitrogen) following the manufacturer's instructions. Fluorescence was measured using a Tecan plate reader.

BAL turbidity

BAL from naive mice were collected as described above, and 200 µl was used to determine the optical density at 600 nm.

Ethics statement

All experiments involving animals were approved by the McGill University Animal Care Committee (permit number 2010–5860) in accordance with the guidelines set out by the Canadian Council on Animal Care. All animal protocols for intravital lung imaging were approved by the University of Calgary Animal Care Committee (protocol number AC18-0038).

Statistical analysis

Data are presented as the mean ± s.e.m. Statistical analyses were performed using GraphPad Prism v.9.1.2 software (GraphPad). Statistical differences were determined using two-sided log-rank test (survival studies), one-way analysis of variance (ANOVA) followed by Tukey's multiple comparisons test, two-way ANOVA followed by Sidak's or Tukey's multiple comparisons test, paired or unpaired two-tailed *t*-test or two-tailed Mann–Whitney test.

Reporting Summary

Further information on research design is available in the Nature Portfolio Reporting Summary linked to this article.

Data availability

All data supporting the findings of this study are included in the published article and supplementary materials. Bulk RNA-seq, ATAC-seq and single-cell RNA-seq data have been deposited into the Gene Expression Omnibus and are publicly available under accession numbers GSE216531 and GSE219042. Source data are provided with this paper.

References

1. Schneider, C. et al. Induction of the nuclear receptor PPAR-γ by the cytokine GM-CSF is critical for the differentiation of fetal monocytes into alveolar macrophages. *Nat. Immunol.* **15**, 1026–1037 (2014).

2. Guilliams, M. et al. Alveolar macrophages develop from fetal monocytes that differentiate into long-lived cells in the first week of life via GM-CSF. *J. Exp. Med.* **210**, 1977–1992 (2013).

3. Hussell, T. & Bell, T. J. Alveolar macrophages: plasticity in a tissue-specific context. *Nat. Rev. Immunol.* **14**, 81–93 (2014).

4. Sabatel, C. et al. Exposure to bacterial CpG DNA protects from airway allergic inflammation by expanding regulatory lung interstitial macrophages. *Immunity* **46**, 457–473 (2017).

5. Gibbings, S. L. et al. Three unique interstitial macrophages in the murine lung at steady state. *Am. J. Respir. Cell Mol. Biol.* **57**, 66–76 (2017).

6. Schyns, J. et al. Non-classical tissue monocytes and two functionally distinct populations of interstitial macrophages populate the mouse lung. *Nat. Commun.* **10**, 3964 (2019).

7. Chakarov, S. et al. Two distinct interstitial macrophage populations coexist across tissues in specific subtissular niches. *Science* **363**, eaau0964 (2019).

8. Kawasaki, T., Ito, K., Miyata, H., Akira, S. & Kawai, T. Deletion of PIKfyve alters alveolar macrophage populations and exacerbates allergic inflammation in mice. *EMBO J.* **36**, 1707–1718 (2017).

9. Yu, X. et al. The cytokine TGF-β promotes the development and homeostasis of alveolar macrophages. *Immunity* **47**, 903–912.e4 (2017).

10. Hashimoto, D. et al. Tissue-resident macrophages self-maintain locally throughout adult life with minimal contribution from circulating monocytes. *Immunity* **38**, 792–804 (2013).

11. Suzuki, T. et al. Pulmonary macrophage transplantation therapy. *Nature* **514**, 450–454 (2014).

12. Dennis, E. A. & Norris, P. C. Eicosanoid storm in infection and inflammation. *Nat. Rev. Immunol.* **15**, 511–523 (2015).

13. Pernet, E., Downey, J., Vinh, D. C., Powell, W. S. & Divangahi, M. Leukotriene B4-type I interferon axis regulates macrophage-mediated disease tolerance to influenza infection. *Nat. Microbiol.* **4**, 1389–1400 (2019).

14. Coulombe, F. et al. Targeted prostaglandin E2 inhibition enhances antiviral immunity through induction of type I interferon and apoptosis in macrophages. *Immunity* **40**, 554–568 (2014).

15. Divangahi, M. et al. *Mycobacterium tuberculosis* evades macrophage defenses by inhibiting plasma membrane repair. *Nat. Immunol.* **10**, 899–906 (2009).

16. Serezani, C. H., Lewis, C., Jancar, S. & Peters-Golden, M. Leukotriene B4 amplifies NF-κB activation in mouse macrophages by reducing SOCS1 inhibition of MyD88 expression. *J. Clin. Invest.* **121**, 671–682 (2011).

17. Lee, S. P., Serezani, C. H., Medeiros, A. I., Ballinger, M. N. & Peters-Golden, M. Crosstalk between prostaglandin E2 and leukotriene B4

regulates phagocytosis in alveolar macrophages via combinatorial effects on cyclic AMP. *J. Immunol.* **182**, 530–537 (2009).

18. Morita, M. et al. The lipid mediator protectin D1 inhibits influenza virus replication and improves severe influenza. *Cell* **153**, 112–125 (2013).

19. Coulombe, F. & Divangahi, M. Targeting eicosanoid pathways in the development of novel anti-influenza drugs. *Exp. Rev. Anti Infect. Ther.* **12**, 1337–1343 (2014).

20. Divangahi, M., Desjardins, D., Nunes-Alves, C., Remold, H. G. & Behar, S. M. Eicosanoid pathways regulate adaptive immunity to *Mycobacterium tuberculosis*. *Nat. Immunol.* **11**, 751–758 (2010).

21. Schneider, C. et al. Alveolar macrophages are essential for protection from respiratory failure and associated morbidity following influenza virus infection. *PLoS Pathog.* **10**, e1004053 (2014).

22. Hernandez-Segura, A., Nehme, J. & Demaria, M. Hallmarks of cellular senescence. *Trends Cell Biol.* **28**, 436–453 (2018).

23. Coppe, J. P., Desprez, P. Y., Krtolica, A. & Campisi, J. The senescence-associated secretory phenotype: the dark side of tumor suppression. *Annu. Rev. Pathol.* **5**, 99–118 (2010).

24. Yu, Q. et al. DNA-damage-induced type I interferon promotes senescence and inhibits stem cell function. *Cell Rep.* **11**, 785–797 (2015).

25. Gluck, S. et al. Innate immune sensing of cytosolic chromatin fragments through cGAS promotes senescence. *Nat. Cell Biol.* **19**, 1061–1070 (2017).

26. Huang, N. N., Wang, D. J. & Heppel, L. A. Stimulation of aged human lung fibroblasts by extracellular ATP via suppression of arachidonate metabolism. *J. Biol. Chem.* **268**, 10789–10795 (1993).

27. Penke, L. R. et al. PGE_2 accounts for bidirectional changes in alveolar macrophage self-renewal with aging and smoking. *Life Sci. Alliance* **3**, e202000800 (2020).

28. Dagouassat, M. et al. The cyclooxygenase-2-prostaglandin E2 pathway maintains senescence of chronic obstructive pulmonary disease fibroblasts. *Am. J. Respir. Crit. Care Med.* **187**, 703–714 (2013).

29. Lee, E. K. S. et al. Leukotriene B4-mediated neutrophil recruitment causes pulmonary capillaritis during lethal fungal sepsis. *Cell Host Microbe* **23**, 121–133.e4 (2018).

30. Zarbock, A. et al. Improved survival and reduced vascular permeability by eliminating or blocking 12/15-lipoxygenase in mouse models of acute lung injury (ALI). *J. Immunol.* **183**, 4715–4722 (2009).

31. Cohen, M. et al. Lung single-cell signaling interaction map reveals basophil role in macrophage imprinting. *Cell* **175**, 1031–1044.e18 (2018).

32. Guo, Y. et al. Identification of the orphan G protein-coupled receptor GPR31 as a receptor for 12-(*S*)-hydroxyeicosatetraenoic acid. *J. Biol. Chem.* **286**, 33832–33840 (2011).

33. Yokomizo, T., Kato, K., Hagiya, H., Izumi, T. & Shimizu, T. Hydroxyeicosanoids bind to and activate the low affinity leukotriene B4 receptor, BLT2. *J. Biol. Chem.* **276**, 12454–12459 (2001).

34. McQuattie-Pimentel, A. C. et al. The lung microenvironment shapes a dysfunctional response of alveolar macrophages in aging. *J. Clin. Invest.* **131**, e140299 (2021).

35. Wong, C. K. et al. Aging impairs alveolar macrophage phagocytosis and increases influenza-induced mortality in mice. *J. Immunol.* **199**, 1060–1068 (2017).

36. Zhang, D. et al. Neutrophil ageing is regulated by the microbiome. *Nature* **525**, 528–532 (2015).

37. Gaush, C. R. & Smith, T. F. Replication and plaque assay of influenza virus in an established line of canine kidney cells. *Appl. Microbiol.* **16**, 588–594 (1968).

38. Kaufmann, E. et al. BCG educates hematopoietic stem cells to generate protective innate immunity against tuberculosis. *Cell* **172**, 176–190.e19 (2018).

39. Kim, D., Paggi, J. M., Park, C., Bennett, C. & Salzberg, S. L. Graph-based genome alignment and genotyping with HISAT2 and HISAT-genotype. *Nat. Biotechnol.* **37**, 907–915 (2019).

40. Anders, S., Pyl, P. T. & Huber, W. HTSeq-a Python framework to work with high-throughput sequencing data. *Bioinformatics* **31**, 166–169 (2015).

41. Love, M. I., Huber, W. & Anders, S. Moderated estimation of fold change and dispersion for RNA-seq data with DESeq2. *Genome Biol.* **15**, 550 (2014).

42. Kanehisa, M., Furumichi, M., Sato, Y., Ishiguro-Watanabe, M. & Tanabe, M. KEGG: integrating viruses and cellular organisms. *Nucleic Acids Res.* **49**, D545–D551 (2021).

43. Zheng, G. X. et al. Massively parallel digital transcriptional profiling of single cells. *Nat. Commun.* **8**, 14049 (2017).

44. Hafemeister, C. & Satija, R. Normalization and variance stabilization of single-cell RNA-seq data using regularized negative binomial regression. *Genome Biol.* **20**, 296 (2019).

45. Franzen, O., Gan, L. M. & Bjorkegren, J. L. M. PanglaoDB: a web server for exploration of mouse and human single-cell RNA sequencing data. *Database (Oxford)* **2019**, baz046 (2019).

46. Xie, X. et al. Single-cell transcriptome profiling reveals neutrophil heterogeneity in homeostasis and infection. *Nat. Immunol.* **21**, 1119–1133 (2020).

47. Dann, E., Henderson, N. C., Teichmann, S. A., Morgan, M. D. & Marioni, J. C. Differential abundance testing on single-cell data using *k*-nearest neighbor graphs. *Nat. Biotechnol.* **40**, 245–253 (2022).

48. Zhang, Y. et al. Model-based analysis of ChIP-Seq (MACS). *Genome Biol.* **9**, R137 (2008).

49. Downey, J. et al. RIPK3 interacts with MAVS to regulate type I IFN-mediated immunity to influenza A virus infection. *PLoS Pathog.* **13**, e1006326 (2017).

50. Cortal, A., Martignetti, L., Six, E. & Rausell, A. Gene signature extraction and cell identity recognition at the single-cell level with Cell-ID. *Nat. Biotechnol.* **39**, 1095–1102 (2021).

Acknowledgements

The authors acknowledge technical help from staff at the RI-MUHC histopathology platform; M. Orlova and P. Cassart; I. King for critical reading of the manuscript; S. Tersey (University of Chicago) and C. Brown (University of Missouri) for providing *Alox15*$^{lox/lox}$ and *Ltb4r2*$^{-/-}$ mice, respectively. M.D. is funded by Canadian Institute of Health Research (CIHR) Project Grant-168885 and MM1174910, a Fonds de recherche du Québec–Santé (FRQS) Award, holds the Strauss Chair in Respiratory Diseases and is a fellow member of the Royal Society of Canada. E.P. is a fellow supported by a Postdoctoral Fellowship from the Fonds de Recherche du Québec Santé. The models in Figs. 1d, 2d,j, 3a,g,j,n, 4a,l,p,r and 5b,f,lq and Extended Data Figs. 1i and 10a,m,q were created using BioRender (https://biorender.com).

Author information

Authors and Affiliations

1. McGill University Health Centre, Meakins-Christie Laboratories, McGill University, Montreal, Quebec, Canada

   Erwan Pernet, Nargis Khan, Kim A. Tran, Julia Chronopoulos, Dnyandeo Amberkar, Shradha Wali, Renaud Prevel, Jun Ding, James G. Martin & Maziar Divangahi

2. Department of Medicine, Section of Genetic Medicine, University of Chicago, Chicago, IL, USA

   Sarah Sun, Saideep Gona & Luis B. Barreiro

3. Calvin, Phoebe and Joan Snyder Institute for Chronic Diseases and Department of Critical Care, Cumming School of Medicine, University of Calgary, Calgary, Alberta, Canada

   Nicole Sarden, Angela Nguyen & Bryan G. Yipp

4. Department of Pharmacology and Therapeutics, McGill University, Montreal, Quebec, Canada

   Martin Mawhinney & Ajitha Thanabalasuriar

5. Department of Microbiology and Immunology, McGill University, Montreal, Quebec, Canada

   Mina Sadeghi, Alexandre Grant & Maziar Divangahi

6. Department of Genetics, CHU Sainte-Justine Research Center, Montreal, Quebec, Canada

   Luis B. Barreiro

7. Department of Pathology, McGill University, Montreal, Quebec, Canada

   Maziar Divangahi

8. McGill International TB Centre, McGill University, Montreal, Quebec, Canada

Maziar Divangahi

Contributions

Conceptualization: E.P. and M.D. Methodology: E.P., S.S., S.G., N.S., A.N., N.K., K.A.T., J.C., D.A., M.S., A.G., M.M., S.W., R.P., J.D., J.G.M., A.T., B.G.Y., L.B.B. and M.D. Investigation: E.P., B.G.Y., J.D., L.B.B. and M.D. Funding acquisition: M.D. Project administration: E.P. and M.D. Supervision: J.G.M., A.T., B.G.Y., L.B.B. and M.D. Writing original draft: E.P. and M.D. Writing, review and editing: J.D., J.M., A.T., B.G.Y., L.B.B., E.P. and M.D.

Corresponding authors

Correspondence to Erwan Pernet or Maziar Divangahi.

Ethics declarations

Competing interests

The authors declare no competing interests.

Peer review

Peer review information

Nature thanks Frederic Geissmann, Klaus Ley and the other, anonymous, reviewer(s) for their contribution to the peer review of this work.

Additional information

Publisher's note Springer Nature remains neutral with regard to jurisdictional claims in published maps and institutional affiliations.

Extended data figures and tables

Extended Data Fig. 1 ALOX15, but not ALOX5, is required for AM homeostasis.

(a) AM frequencies in the lungs of adult WT (n = 7) and *Alox15*$^{-/-}$ (n = 6) mice. (b) Representative FACS plot and quantification of AM frequencies in the BAL of adult WT and *Alox15*$^{-/-}$ mice (n = 9 mice/group). (c) Representative FACS plot and quantification of AM frequencies and numbers in the lungs of adult *Alox15*$^{-/-}$ (n = 9) and *Alox15*$^{+/+}$ (n = 7) littermate control mice. (d) Representative FACS plot and quantification of AM frequencies and numbers in the lungs of adult WT (n = 10) and *Alox5*$^{-/-}$ (n = 9) mice. (e) Quantification of lung innate cells in adult WT and *Alox15*$^{-/-}$ mice (n = 8/8/8/8/6/6/6/group). See also Supplementary Fig. 1 for gating strategy. (f) Weight of spleen, lungs, brain and top liver lobe from WT and *Alox15*$^{-/-}$ adult mice (n = 8 mice/group). (g-h) Representative FACS plot (g) and quantification (h) of resident tissue macrophages in adult WT (n = 3/6/7/7/group) and *Alox15*$^{-/-}$ mice (n = 3/5/6/6/group). (i) Bone marrow chimera model. (j-k) Representative FACS plots (j) and AM chimerism 8 weeks post-BM reconstitution (right) (n = 8/11/11/9/group). Data are presented as mean ± s.e.m and are pooled from two (a, c-e, f-k) or three (b-e) independent experiments and were analyzed using unpaired two-tailed t-test (a, c) or two-way ANOVA followed by Sidak's multiple comparisons test (k). The model in (i) was created using BioRender (https://biorender.com).

Source data

Extended Data Fig. 2 *Alox15*$^{-/-}$ AM seeding and maturation.

(a) Representative FACS plot for the determination of AM progenitors (pre-AM and fetal liver monocytes) and AM in the lungs of PND0, PND1 and

PND3 WT and *Alox15*$^{-/-}$ mice. (b) Weight of lungs from PND1 and PND3 WT (n = 7/group) and *Alox15*$^{-/-}$ mice (n = 6/group). (c-f) Lungs from PND1 or PND3 WT and *Alox15*$^{-/-}$ mice were harvested and the levels of TGF-β1 (c) (PND1, WT: n = 6, *Alox15*$^{-/-}$: n = 7; PND3, WT: n = 8, *Alox15*$^{-/-}$: n = 7), GM-CSF (d) (PND1, WT: n = 6, *Alox15*$^{-/-}$: n = 7; PND3, WT: n = 8, *Alox15*$^{-/-}$: n = 8), type 1 and type 2 cytokines (e- PND1: WT: n = 6, *Alox15*$^{-/-}$: n = 7, f- PND3: n = 8/group) were determined by ELISA. (g-h) BAL-AM were isolated from PND3 WT and *Alox15*$^{-/-}$ mice for gene expression analysis (n = 3 biological replicates/group). (i) BAL-AM were isolated from adult naïve animals and cell death was assessed by flow cytometry using AnnexinV/7AAD staining (n = 7/group). (j-l) Batch effect examinations. (j) PCA and (k) heatmap plots that suggest WT4 is an outlier. (l) A heatmap that indicates the similarity between different samples. Data are presented as mean ± s.e.m and are pooled from two (b-f, i) or three (g-h) independent experiments.

Source data

Extended Data Fig. 3 Intact PM and BMDM proliferation.

(a-b) Peritoneal macrophages (PM) were harvested from adult naïve WT and *Alox15*$^{-/-}$ mice and BrdU incorporation after 7 days pulse (a) or Ki67 expression (b) were determined by flow cytometry (n = 5/group). (c-d) Bone marrow-derived macrophages were generated from adult WT and *Alox15*$^{-/-}$ mice and were treated with BrdU (day 3 and 5 of differentiation). At day 6 BrdU incorporation (c) (n = 6/group) and Ki67 expression (d) (n = 9/group) were evaluated by flow cytometry. (e) Representative FACS plot and quantification of Ki67^{+} AM frequencies in the lungs of adult WT and *Alox5*$^{-/-}$ mice (n = 4/group). (f-g) AM kinetics following local depletion by clodronate liposomes. Adult WT (control: n = 3/6/9/timepoint, clodronate: n = 3/6/10/timepoint), *Alox15*$^{-/-}$ (control: n = 3/6/10 mice/timepoint, clodronate: n = 3/6/9/timepoint) or *Ccr2*$^{-/-}$ (n = 3/3/5/group/timepoint) mice were given control or clodronate liposomes intranasally (70 µl). AM populations were assessed in the airways at day 2 and 14 post-delivery. (f) Numbers of AM in the BAL at various days post-infection. (g) Frequency of Ki67^{+} AM in the BAL at day 14 (n = 5/group). (h) Representative FACS

plot of Ki67^{+} CD45.1 BAL AM before adoptive transfer. (i) Representative FACS plots of AM in the lungs of *Alox15*$^{-/-}$ mice 2 and 8 weeks after WT CD45.1 AM transfer. (j) Quantification of WT CD45.1^{+} or *Alox15*$^{-/-}$ CD45.2^{+} AM post-adoptive transfer in ALOX15-deficient mice (n = 5/group). (k) BAL AM from adult WT and *Alox15*$^{-/-}$ mice were cultured with M-CSF for 3 days before cell growth was evaluated (n = 3 biological replicates/group). (l) PM isolated from adult WT and *Alox15*$^{-/-}$ mice were cultured with M-CSF+IL-4 for 3 days before cell growth was evaluated (n = 3 biological replicates/group). (m) BMDM generated from adult WT (n = 4 biological replicates) and *Alox15*$^{-/-}$ (n = 3 biological replicates) mice were cultured with M-CSF for 3 days before cell growth was evaluated. (n-r) WT and *Alox15*$^{-/-}$ AM from adult and PND3 mice were subjected to ATAC-Seq (n = 3/group). (n) Principal component analysis of WT versus KO adult and pup cells. (o) The number of differentially accessible peaks comparing ALOX15-deficient and WT cells using the cutoffs: p.adj < 0.05 and abs(log2FC) > 1. Upward bars indicate increased accessibility in the KO condition and downward bars indicate decreased accessibility. (p) Venn diagram showing the relative numbers of DA peaks in adults and pups. Circle size is proportional to the number of DA peaks. Out of 64 total peaks with p.adj < 0.05 and abs(log2FC) > 1 in pups, ~65% (42/64) overlapped with the DA peaks set in adults. (q) Correlation (pearson cor = 0.702, p < 2.2e-16) of normalized enrichment scores (NES) for all enriched pathways in adults and pups. Pink highlighted points are the top 10 pathways in both adults and pups. (r) Heatmap showing the gene set enrichment results specifically for reactome pathways related to proliferation. Shading is indicative of significance with darker red colors indicating lower p.adjusted values. Data are presented as mean ± s.e.m and are from one (e, g-j, n-r), or pooled from two (c, f) or three (d, k-m) or representative of two (a-b) independent experiments. Data were analyzed using two-way ANOVA followed by Tukey's (f) or Sidak's (g, j-k) multiple comparisons test.

Source data

Extended Data Fig. 4 Intact GM-CSF and TGF-β1 signalling in *Alox15*$^{-/-}$ AM.

BAL (a) (WT: n = 11/10/group, *Alox15*$^{−/−}$: n = 12/11/group) and lung tissue (b) (WT: n = 9/group, *Alox15*$^{−/−}$: n = 9/8/group) levels of GM-CSF and TGF-β1 in adult WT and *Alox15*$^{−/−}$ mice. (c-f) BAL-AM were isolated from adult naïve animals and phosphorylation of pAKT1 (c) (n = 6/group), pERK1/2 (d) (n = 6/group), pSMAD2/3 (e) (n = 3/group), pSTAT5 (f) (WT: n = 17, *Alox15*$^{−/−}$: n = 16) were assessed by flow cytometry. (g) BAL-AM were isolated from adult naïve animals and cultured with GM-CSF (10 ng/ml) for various time points before phosphorylation of STAT5 was evaluated. Bar = 50 µm. (h) Expression of *Cdkn1a* in AM, PM and BMDM from adult WT and *Alox15*$^{−/−}$ mice by qPCR (n = 6/group). (i) Left, representative micrographs of H&E-stained adult WT and *Alox15*$^{−/−}$ AM harvested by BAL. Bar = 10 µm. Right, percentage of bi-nucleated cells in BAL AM (n = 5 fields of view/group). (j) Representative histograms (left) and quantification (right) of DNA content in BAL AM from adult WT and *Alox15*$^{−/−}$ mice (n = 6/group). (k) Representative curve (left, n = 3/group) and quantification (right, n = 3 biological replicates/group) of OCR in PM isolated from adult WT and *Alox15*$^{−/−}$ mice. (l) Representative curve (left, n = 5/group) and quantification (right, n = 5 biological replicates/group) of OCR in BMDM generated from adult WT and *Alox15*$^{−/−}$ mice. (m) Representative immunoblot (left) and quantification (right) of cytokine production in the supernatant of resting (24 h) pooled from adult WT or *Alox15*$^{−/−}$ BAL AM. (n) Representative curve (left, WT: n = 5, *Alox15*$^{−/−}$: n = 3) and quantification (right, n = 3 biological replicates/group) of OCR in AM from PND3 WT and *Alox15*$^{−/−}$ mice. Data are presented as mean ± s.e.m and are from one (e, m) or pooled from two (c-d, h, j), three (a-b, k-l, n), or five (f, i) independent experiments or representative of two (g) independent experiments. Data were analyzed using unpaired two-tailed t-test (i) or two-way ANOVA followed by Sidak's multiple comparisons test (h, j).

Source data

Extended Data Fig. 5 No difference in canonical senescence pathways.

(a) Representative histograms and quantification of p53 MFI in PND3 AM from WT (n = 5) and *Alox15*$^{-/-}$ (n = 6) animals. (b) Expression of *Trp53* in adult AM from WT and *Alox15*$^{-/-}$ mice (n = 6/group). (c-f) Representative histograms and quantification of p53 (c) (n = 5/group), MitoSox (d) (n = 3/group), p-p38 (e) (n = 3/group) and p-γH2AX (f) (n = 5/group) in BAL AM isolated from adult WT and *Alox15*$^{-/-}$ mice. (g-h) Heatmap and quantification of genes involved in antioxidant response (g) or interferon response (h) in BAL AM isolated from adult WT (n = 3) and *Alox15*$^{-/-}$ (n = 4) mice in bulk RNA-Seq dataset. (i) Expression of *Ptgs*/*Ptges* (WT n = 5/group, *Alox15*$^{-/-}$ n = 6/5/6/6/6/group) and *Ptger* genes by BAL AM from adult WT and *Alox15*$^{-/-}$ mice (n = 6/group). (j) Expression of *Ptgs1* by AM, PM and BMDM from adult WT and *Alox15*$^{-/-}$ mice (n = 6/group). (k-l) PGE_2 production by naïve resting (24 h) peritoneal macrophages (k) or bone marrow derived macrophages (l) from adult WT and *Alox15*$^{-/-}$ mice (n = 6/group). (m-n) BAL AM were isolated from adult (6–8 weeks) WT mice, and they were cultured or not with GM-CSF (20 ng/ml) for 3 days and treated or not with various concentrations of exogenous PGE_2. (m) Representative micrographs of Ki67$^+$ AM after 3 days of culture with GM-CSF and treated or not with PGE_2 (1–10 µM). Bar = 50 µm. (n) AM growth was assessed after culture with GM-CSF and treatment with PGE_2 (10 µM) (n = 3 biological replicates/group). (o) Heatmap and quantification of lipoxygenase pathway related genes in BAL AM from adult WT (n = 3) and *Alox15*$^{-/-}$ (n = 4). (p) Production of LTB_4 and cysteinyl leukotrienes by resting adult WT and *Alox15*$^{-/-}$ BAL AM (24 h) (n = 3 biological replicates/group). Data are presented as mean ± s.e.m and are from one (e, g-h, o) or pooled from two (b, i-l) or three (n, p) independent experiments or representative of two experiments (a, c-f, m) independent experiments. Data were analysed using two-way ANOVA followed by Sidak’s multiple comparisons test (i-j, n).

Source data

Extended Data Fig. 6 Homeostatic *Alox15*$^{-/-}$ AM are similar to WT AM.

(a) Heatmap and quantification of genes previously associated with alveolar macrophages or monocytes lineages (WT: n = 3, *Alox15*$^{-/-}$: n = 4). (b) Representative FACS plots and quantification of surface markers expression determined by flow cytometry. (c) Heatmap and quantification of genes previously associated with alveolar macrophages phenotype (WT: n = 3, *Alox15*$^{-/-}$: n = 4). (d) Representative FACS plots of AM population in 6–8 weeks and 52 weeks old WT and *Alox15*$^{-/-}$ mice. (e) AM numbers in the lungs of 6–8 (WT: n = 3, *Alox15*$^{-/-}$: n = 5) or 52-weeks old (n = 5/group) WT and *Alox15*$^{-/-}$ mice. (f) BAL total protein levels in 6–8 (n = 3/group) or 52-weeks old (n = 5/group) WT and *Alox15*$^{-/-}$ mice. (g) Representative micrographs of lung sections from naïve 6–8 weeks and 52 weeks old WT and *Alox15*$^{-/-}$ mice. Bar = 100 µm. (h-i) Adult WT (n = 5) and *Alox15*$^{-/-}$ (n = 6) mice were used to measure resistance (h) and elastance (i). (j) Phagocytic capacity of naïve BAL AM from adult WT and *Alox15*$^{-/-}$ mice (WT: n = 7, *Alox15*$^{-/-}$: n = 6 biological replicates). (k) Representative micrographs of BAL AM, cytospun, and stained with H&E (top) or Oil red O (bottom). Bar = 20 µm. (l-n) BAL was collected from adult WT, *Alox15*$^{-/-}$ and *Csf2rb*$^{-/-}$ mice, and BAL turbidity (l) (n = 10/14/11/group), total protein content (p) (n = 13/15/15/group) and SP-A levels (q) (n = 5/6/5/group) were measured. Data are presented as mean ± s.e.m and are from one (a, c, d-f) or pooled from two (h-j) or three (l-m) independent experiments or representative of two (b, k) independent experiments or 5 biological replicates (g). Data were analyzed using two-way ANOVA followed by Tukey's multiple comparison test (f), two-tailed unpaired t-test (e), or one-way ANOVA followed by Tukey's multiple comparisons test (l-n).

Source data

Extended Data Fig. 7 *Alox15*$^{-/-}$ mice are more susceptible to acute viral infections.

(a) BAL AM from adult WT and *Alox15*$^{-/-}$ mice were stimulated *in vitro* using LPS (100 ng/ml) and TNFa (left) or IL6 (right) production was assessed by ELISA (n = 3 biological replicates/group). (b-c) Peritoneal

macrophages (b) or BMDM (c) from adult WT and *Alox15*$^{-/-}$ were stimulated with LPS (100 ng/ml) and production of TNFα and CXCL1/KC was evaluated by ELISA (n = 3 biological replicates/group). (d) TNFα and IL6 levels in BAL from adult WT and *Alox15*$^{-/-}$ mice treated or not with 20 µg LPS intranasally (WT: n = 3/11/7/timepoint, *Alox15*$^{-/-}$: TNFα n = 3/10/8 and IL6 3/10/9/timepoint). (e) BAL cellularity in LPS-treated (20 µg/mouse) WT and *Alox15*$^{-/-}$ mice at various days post-delivery (WT: n = 3/11/7/timepoint, *Alox15*$^{-/-}$: n = 3/10/8/timepoint). (f) BAL AM from adult WT and *Alox15*$^{-/-}$ mice were stimulated *in vitro* using poly(I:C) (50 µg/ml) and CXCL1/KC, CCL2 and TNFα production were assessed by ELISA (n = 3 biological replicates/group). (g-o) Adult WT and *Alox15*$^{-/-}$ mice were infected with IAV (50 pfu). (g-i) BAL levels of IFNα (g) (WT: n = 3/5/8/7/timepoint, *Alox15*$^{-/-}$: n = 3/5/9/7/timepoint), IFNλ (h) (WT: n = 3/5/7/8 /timepoint, *Alox15*$^{-/-}$: n = 3/4/7/7/timepoint) and CCL2 (i) (WT: n = 3/6/6/11/7/timepoint, *Alox15*$^{-/-}$: n = 3/6/6/10/5/timepoint) at various days post-infection. (j-k) Numbers of monocytes in the BAL (j) (WT: n = 3/8/9/timepoint, *Alox15*$^{-/-}$: n = 3/7/8/timepoint) and lungs (k) (WT: n = 5/4/5/timepoint, *Alox15*$^{-/-}$: n = 5/3/5/timepoint) at various days post-infection. (l) Protein levels in BAL (WT: n = 4/5/6/timepoint, *Alox15*$^{-/-}$: n = 4/4/5/timepoint). (m) Representative micrographs of lung sections at day 6 post-IAV infection. Bar = 100 µm. (n) Oxygen saturation at various days post-infection (WT: n = 3/5/9/timepoint, *Alox15*$^{-/-}$: n = 3/5/8/timepoint). (o) Wet/dry ratio (Uninf.: n = 3/group, IAV: n = 4/group). (p-q) Representative micrographs and quantification of Evans blue extravasation in the lungs (p) and BAL (q) of IAV-infected mice at day 6 post-infection (Uninf.: n = 3/group, IAV: 5/group). (r) Representatives weight loss curves after infection with LD50 dose (90 pfu) of IAV (n = 11/group). Data are presented as mean ± s.e.m and are pooled from two (d-e, g-j, n, r) or three (a-c, f) or representative of two (k, o-q) independent experiments or 6 biological replicates (m). Data were analyzed using two-way ANOVA followed by Sidak’s multiple comparisons test (a, d-g, i-l, n-r).

Source data

Extended Data Fig. 8 ALOX15-deficient mice are more susceptible to a low dose of IAV.

(a-c) WT and *Alox15*$^{-/-}$ animals were infected with IAV (50 pfu, in). (a) At various days post-infection, expression of ALOX15 was evaluated by flow cytometry (ICS) in CD45^{-} cells as well as various leukocyte populations. The expression was normalized to *Alox15*$^{-/-}$ mice used as controls for gating (n = 4/5/3/5/group). (b) Levels of 12-HETE (left, n = 5/10/8/13/group) and 15-HETE (right, n = 6/12/8/13/group) in the BAL at various days post-infection. (c-i) WT and *Alox15*$^{-/-}$ animals were infected with IAV (20 pfu, in). (c) Pulmonary viral loads at day 3 post-infection (n = 4/group). (d-h) BAL levels of IFNβ (d) (0: n = 3/group, 3: n = 5/group) and PGE_2 (e) (n = 5/group) at day 3 post-infection. (f) BAL levels of CCL2 (left) and CXCL1/KC (right) at various days post-infection (WT: n = 3/5/9/5/6/3/group, *Alox15*$^{-/-}$: n = 3/5/8/6/5/3 mice/group). (g) BAL numbers of AM (left), monocytes (middle) and neutrophils (right) at various days post-infection (WT: n = 3/5/5/5/6/3/timepoint, *Alox15*$^{-/-}$: n = 3/5/5/6/5/3/timepoint). (h) Total BAL protein levels at various days post-infection (WT: n = 3/5/9/5/6/3/group, *Alox15*$^{-/-}$: n = 3/5/7/6/5/3/group). (i) Representative micrographs of H&E lung sections at various days post-infection. (j) *Alox15*$^{-/-}$ mice were treated daily with exogenous 12-HETE or 15-HETE or vehicle. Lungs were harvested at day 3 post-infection for assessment of pulmonary viral loads (n = 8/8/7/8/group). (k) *Alox15*$^{-/-}$ mice were treated daily with exogenous 12-HETE or 15-HETE or vehicle starting on the day of infection (IAV, 90 pfu, in) for 3 days. The survival was monitored overtime (n = 8/10/9/9/group). (l) Weight loss curves after SARS-CoV-2 infection (k18-hACE2 *Alox15*$^{+/+}$: n = 19, k18-hACE2 *Alox15*$^{-/-}$: n = 17). Data are presented as mean ± s.e.m and are from one (a, c-e, k) or pooled from two (b, f-h, j, l) independent experiments or representative of 5 (i) biological replicates. Data were analyzed using two-tailed unpaired t-test (c, e), one-way ANOVA followed by Tukey's multiple comparisons test (b, j), two-way ANOVA followed by Sidak's multiple comparisons test (d, f-h) or log-rank test (k).

Source data

Extended Data Fig. 9 12-HETE-treated pups have restored proliferation.

(a) *Alox15* expression was measured in BAL AM (PND3 and adult mice) or peritoneal macrophages using qPCR (n = 5/3/3 biological replicates/group). (b) Pulmonary levels of 15(S)-HETE in PND1, PND3 and adult WT mice (n = 10/8/8/group). (c) Representative FACS plots and quantification of Ki67$^+$ AM after 12-HETE treatment (Veh.: n = 7, 12-HETE: n = 5). (d) AM populations after 12-HETE treatment (Veh.: n = 7, 12-HETE: n = 6). (e) Representative FACS plots and quantification of Ki67$^+$ AM after 15-HETE treatment (Veh.: n = 3, 15-HETE: n = 4). (f) Representative micrographs of BrdU staining *in vitro* after AM culture with GM-CSF. Bar=50 µm. (g-i) PND1 WT pups were delivered intranasally anti-FcεR1 antibodies or isotype controls for two consecutive days. (g) Basophil depletion, (h) AM populations and (i) Ki67$^+$ AM were determined at PND3 (Iso.: n = 4, α-FcεRI: n = 6). (j) Representative histograms of ALOX15 expression in CD45$^+$ or CD45$^−$ lung cells at various ages of WT and *Alox15*$^{−/−}$ mice. (k) PND1 ALOX15$^+$ CD45$^+$ cells were further gated using CD11b, Ly6C and Ly6G. (l) Lung and blood neutrophils were isolated from PND1 or adults (6–8 weeks) WT or *Alox15*$^{−/−}$ mice. Expression of ALOX15 and Ly6G were assessed by immunofluorescence. Blue: DAPI. Bar = 20 µm. (m) Representative micrographs of ALOX15 and Ly6G expression in frozen lung sections of PND1 WT pups. Data are presented as mean ± s.e.m and are from one (g-i) or pooled from two (c-e) or three (a-b) independent experiments or representative from two (f, j, k, l, m) independent experiments. Data were analyzed using two-tailed unpaired t-test (c, g) or one-way ANOVA followed by Tukey's multiple comparisons test (b).

Source data

Extended Data Fig. 10 Neonatal neutrophils program AM proliferative capacity.

(a) CD45$^+$ cells were isolated from the lungs of PND1 WT and *Alox15*$^{−/−}$ pups and subjected to scRNA-Sequencing. (b) Uniform Manifold Approximation and Projection (UMAP) embedding of integrated CD45$^+$ cells from the lungs of WT and *Alox15*$^{−/−}$ mice. Unsupervised clusters were labelled using CelliD[50] and the expression levels of canonical cell type markers. Neutrophils were further partitioned through label transfer from

adult mouse neutrophil cell atlas to create a final assignment (left). A graph representation of the results from Milo differential abundance testing (right). Nodes are neighbourhoods, coloured by their log fold change between WT and *Alox15*$^{-/-}$ cells. Non-DA neighbourhoods (FDR > 10%) are coloured white, and sizes correspond to the number of cells in a neighbourhood. There is a marked increase in the relative abundance of WT cells in the "Neutrophil-G5b" cluster compared to *Alox15*$^{-/-}$ cells. (c) Beeswarm plot showing the distribution of log-fold change between WT and *Alox15*$^{-/-}$ cells in neighborhoods containing cells from different cell type clusters. Blue refers to neighborhoods within particular cell types that are significantly enriched (FDR<5%) in WT compared to *Alox15*$^{-/-}$ animals and brown neighborhoods enriched in *Alox15*$^{-/-}$ animals relative to WT. (d) Cell type label frequencies from PanglaoDB predictions within finalized manual labeling clusters (vertical facets) and split by condition. Confirms finalized labels as consistent with automated predictions. (e-g) quantification of neutrophils (e), total (f) and Ki67^{+} (g) alveolar macrophages in the lungs of PND3 WT mice following isotype or anti-Ly6G treatment (Iso.: n = 8, α-Ly6G: n = 10). (h) Representative micrographs of BrdU staining *in vitro* after AM culture with GM-CSF. Bar = 50 µm. (i-j) Parenchymal neutrophils were determined in WT mice at various ages by intravascular and *ex vivo* CD45.2 staining. Representative FACS plots (i) and quantification (j) (n = 11/4/5/group). (k) Expression of various genes involved in proliferation in BAL AM from adult *Alox15*$^{lox/lox}$ and *Alox15*$^{lox/lox}$ MRP8^{Cre} (n = 3 biological replicates/group). The genes were previously identified in our bulk RNA-Seq dataset on whole body *Alox15*$^{-/-}$ mice. (l) Representative micrographs of SA-β-galactosidase in BAL AM from *Alox15*$^{lox/lox}$ and *Alox15*$^{lox/lox}$ MRP8^{Cre} mice. Bar=10 µm. (m) Model of EP2 signaling inhibition with TG6-10-1 in pups (left) and BAL AM numbers in adult mice (right) (n = 5/6/8/group). (n) BrdU^{+} AM following GM-CSF culture *in vitro* (left) (Uns.: n = 3, GM-CSF: n = 5 fields of view/group) and basal *Cdkn1a* expression (right) (n = 3 biological replicates/group) in BAL AM from adult mice. (o-p) Adult WT mice were treated with LY255283 and adult *Alox15*$^{-/-}$ mice were treated with TG6-10-1 or 12-HETE for three consecutive days. AM populations in the BAL were evaluated after 7 days resting period (o) (left, n = 5/group; right, WT: n = 5, Untreated: n = 5, 12-HETE: n = 5, TG6-10-1: n = 6) and BrdU^{+} AM

after 3 days of culture with GM-CSF *in vitro* (p) (Uns.: n = 3, GM-CSF: n = 4 fields of view/group). Data are presented as mean ± s.e.m and are from one (a-d, o-p) or pooled from two (e-g, i-j, m) or three (k, n) independent experiments or representative of two (h, l, n, p) independent experiments. Data were analyzed using two-tailed unpaired t-test (e, g, k), one-way ANOVA followed by Tukey's multiple comparison test (j, m-o) or two-way ANOVA followed by Sidak's multiple comparisons test (n, p). The models in (a, m, q) were created using BioRender (https://biorender.com).

Source data

Supplementary information

Supplementary Figure 1

Flow cytometry gating strategies for the evaluation of immune cells in the lungs of naive adult (6–8 weeks) WT or *Alox15*$^{-/-}$ mice. **a**, Cells were gated on single live CD45.2^{+} cells then further gated on CD11c^{+} and Siglec-F^{+} (AMs), CD11c^{-}Siglec-F^{-}Ly6G^{+}CD11b^{+} (neutrophils), Ly6G^{-}CD11b^{+}F4/80^{+}Ly6C$^{+/-}$ for monocytes/macrophages. **b**, Natural killer cells were gated on single live cells, CD64^{-}Ly6G^{-}NK1.1^{+}. **c**, Conventional dendritic cells were gated on single live cells, CD64^{-}Ly6C^{-}CD11c^{+}, CD11b^{-}CD103^{+} (cDC1) or CD11b^{+}CD103^{-} (cDC2).

Reporting Summary

Supplementary Table 1

List of differentially expressed genes in adult WT and *Alox15*$^{-/-}$ AM bulk RNA-seq dataset.

Supplementary Table 2

List of primers used in this study.

Supplementary Video 1

Pulmonary intravital microscopy was used to compare the effects of intravenous LPS (20 µg intravenously) in WT or *Alox15*$^{-/-}$ mice. Neutrophils (cyan) are labelled with AlexaFluor-647 anti-Ly6G antibody and the vascular endothelium (red) is labelled with AlexaFluor-594 conjugated anti-CD31 antibody. A large neutrophil cluster is demonstrated in the second part of the movie with an arrow.

Source data

Source Data Fig. 1

Source Data Fig. 2

Source Data Fig. 3

Source Data Fig. 4

Source Data Fig. 5

Source Data Extended Data Fig. 1

Source Data Extended Data Fig. 2

Source Data Extended Data Fig. 3

Source Data Extended Data Fig. 4

Source Data Extended Data Fig. 5

Source Data Extended Data Fig. 6

Source Data Extended Data Fig. 7

Source Data Extended Data Fig. 8

Source Data Extended Data Fig. 9

Source Data Extended Data Fig. 10

Rights and permissions

Open Access This article is licensed under a Creative Commons Attribution 4.0 International License, which permits use, sharing, adaptation, distribution and reproduction in any medium or format, as long as you give appropriate credit to the original author(s) and the source, provide a link to the Creative Commons licence, and indicate if changes were made. The images or other third party material in this article are included in the article's Creative Commons licence, unless indicated otherwise in a credit line to the material. If material is not included in the article's Creative Commons licence and your intended use is not permitted by statutory regulation or exceeds the permitted use, you will need to obtain permission directly from the copyright holder. To view a copy of this licence, visit http://creativecommons.org/licenses/by/4.0/.

Reprints and Permissions

About this article

Cite this article

Pernet, E., Sun, S., Sarden, N. *et al.* Neonatal imprinting of alveolar macrophages via neutrophil-derived 12-HETE. *Nature* **614**, 530–538 (2023). https://doi.org/10.1038/s41586-022-05660-7

- Received: 15 July 2021
- Accepted: 14 December 2022
- Published: 04 January 2023

- Issue Date: 16 February 2023
- DOI: https://doi.org/10.1038/s41586-022-05660-7

Share this article

Anyone you share the following link with will be able to read this content:

Get shareable link

Sorry, a shareable link is not currently available for this article.

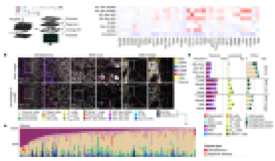
Copy to clipboard

Provided by the Springer Nature SharedIt content-sharing initiative

---

This article was downloaded by **calibre** from https://www.nature.com/articles/s41586-022-05660-7

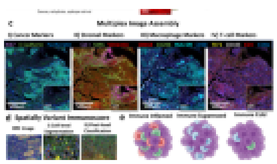
| Section menu | Main menu |



Single-cell spatial immune landscapes of primary and metastatic brain tumours

01 February 2023

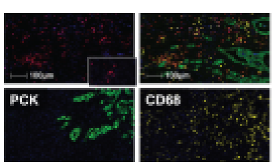
Elham Karimi, Miranda W. Yu, … Logan A. Walsh



Spatially variant immune infiltration scoring in human cancer tissues

01 September 2022

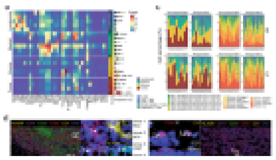
Mayar Allam, Thomas Hu, … Ahmet F. Coskun



Spatial immune profiling of the colorectal tumor microenvironment predicts good outcome in stage II patients

15 May 2020

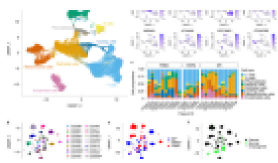
Ines P. Nearchou, Bethany M. Gwyther, … Peter D. Caie



[Multiplexed imaging mass cytometry reveals distinct tumor-immune microenvironments linked to immunotherapy responses in melanoma]

21 October 2022

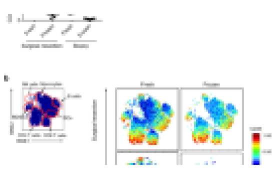
Xu Xiao, Qian Guo, … Rongshan Yu



[A single-cell and spatially resolved atlas of human breast cancers]

06 September 2021

Sunny Z. Wu, Ghamdan Al-Eryani, … Alexander Swarbrick



[Potentiality of multiple modalities for single-cell analyses to evaluate the tumor microenvironment in clinical specimens]

11 January 2021

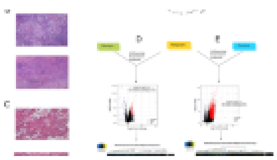
Yukie Kashima, Yosuke Togashi, … Toshihiko Doi



[VoPo leverages cellular heterogeneity for predictive modeling of single-cell data]

27 July 2020

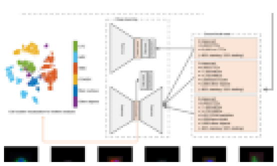
Natalie Stanley, Ina A. Stelzer, … Nima Aghaeepour



[Differential early diagnosis of benign versus malignant lung cancer using systematic pathway flux analysis of peripheral blood leukocytes]

24 March 2022

Jian Li, Xiaoyu Li, … Qi Mei



[Deep learning of circulating tumour cells]

10 February 2020

Leonie L. Zeune, Yoeri E. Boink, … Christoph Brune

- Article
- Open Access
- [Published: 01 February 2023]

Single-cell spatial landscapes of the lung tumour immune microenvironment

- Mark Sorin,
- Morteza Rezanejad,
- Elham Karimi,
- Benoit Fiset,
- Lysanne Desharnais,
- Lucas J. M. Perus,
- Simon Milette,
- Miranda W. Yu,
- Sarah M. Maritan,
- Samuel Doré,
- Émilie Pichette,
- William Enlow,
- Andréanne Gagné,
- Yuhong Wei,
- Michele Orain,
- Venkata S. K. Manem,
- Roni Rayes,
- Peter M. Siegel,
- Sophie Camilleri-Broët,
- Pierre Olivier Fiset,
- Patrice Desmeules,
- Jonathan D. Spicer,
- Daniela F. Quail ,
- Philippe Joubert &
- …
- Logan A. Walsh

Show authors

Nature **volume 614**, pages 548–554 (2023)

- 23k Accesses
- 145 Altmetric
- Metrics details

Abstract

Single-cell technologies have revealed the complexity of the tumour immune microenvironment with unparalleled resolution[1,2,3,4,5,6,7,8,9]. Most clinical strategies rely on histopathological stratification of tumour subtypes, yet the spatial context of single-cell phenotypes within these stratified subgroups is poorly understood. Here we apply imaging mass cytometry to characterize the tumour and immunological landscape of samples from 416 patients with lung adenocarcinoma across five histological patterns. We resolve more than 1.6 million cells, enabling spatial analysis of immune lineages and activation states with distinct clinical correlates, including survival. Using deep learning, we can predict with high accuracy those patients who will progress after surgery using a single 1-mm^2 tumour core, which could be informative for clinical management following surgical resection. Our dataset represents a valuable resource for the non-small cell lung cancer research community and exemplifies the utility of spatial resolution within single-cell analyses. This study also highlights how artificial intelligence can improve our understanding of microenvironmental features that underlie cancer progression and may influence future clinical practice.

Main

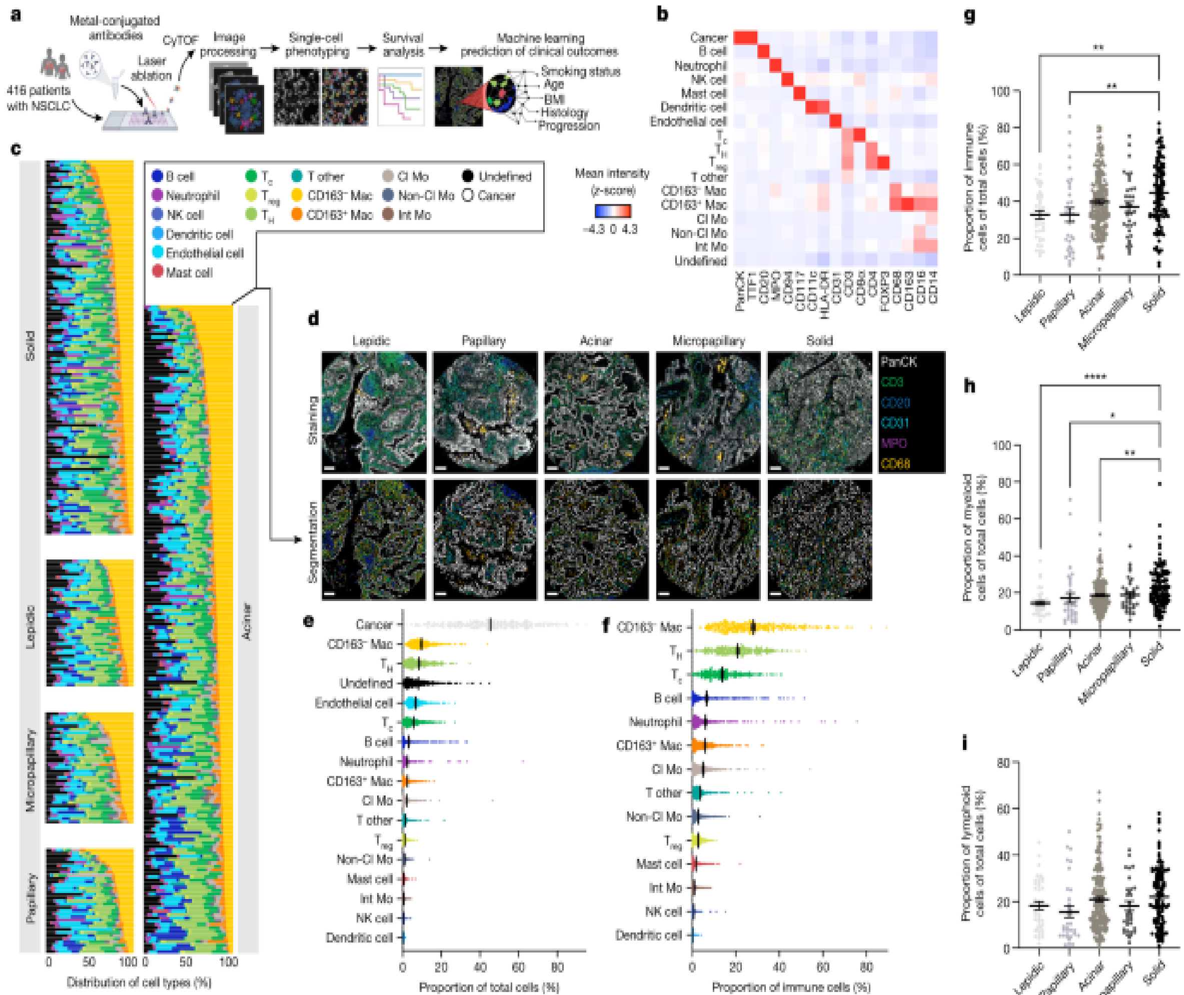
Lung cancer remains the leading cause of cancer-related death, accounting for greater than 20% of all cancer mortalities[10]. Lung adenocarcinoma (LUAD), a type of non-small cell lung cancer (NSCLC), is the most common subtype and is characterized by distinct cellular and molecular features[11]. The tumour immune microenvironment (TIME) is a major source of LUAD heterogeneity and influences both disease progression and response to therapy[1,3,5]. The positioning of immune cells within tumours is

known to dictate their function[12,13,14]; therefore, understanding the spatial landscape of the lung TIME would provide mechanistic insights into disease progression, reveal novel therapeutic vulnerabilities and unveil biomarkers of response to existing treatments. Here, using highly multiplexed imaging mass cytometry (IMC), we interrogated spatially resolved features of the TIME that are associated with clinical outcomes in patients with LUAD. Using a deep neural network model, we demonstrated that various clinical outcomes, such as progression, can be predicted using features that an artificial intelligence-based system can extract from raw IMC images. The ability to identify patients who will progress with a high degree of certainty could guide future post-surgical management.

LUAD tumour immune microenvironment

To spatially characterize the cellular landscape of the lung TIME, we applied IMC to samples from 416 patients with LUAD (Fig. 1a, Extended Data Fig. 1a and Supplementary Table 1). We optimized a 35-plex antibody panel to identify cancer cells, stromal cells, and innate and adaptive immune lineages with diverse functional substates (Extended Data Figs. 1b–d and 2–4 and Supplementary Table 2). In total, we detected 1,644,178 cells and used a supervised lineage assignment approach to classify 14 distinct immune cell populations, along with tumour cells and endothelial cells using canonical lineage markers (Fig. 1b–f and Extended Data Figs. 1c and 5a).

Fig. 1: IMC defines the spatial landscape of LUAD.



a, Schematic depicting IMC acquisition of multiplexed images from 416 patients with LUAD, single-cell phenotyping, survival and machine learning prediction of clinical outcomes. CyTOF, cytometry by time of flight. Images were created with BioRender. **b**, Average expression of lineage markers across cell types in the LUAD tissue using the panel of isotope-conjugated antibodies. Cl Mo, classical monocyte; Int Mo, intermediate monocyte; Mac, macrophage; NK, natural killer; non-Cl Mo, non-classical monocyte; T_c, cytotoxic T cell; T_H, helper T cell. **c**, Waterfall plot depicting the distribution of 16 stromal and immune cell types across histological subgroups. **d**, Representative images of antibody staining and corresponding single-cell segmented images across histological subgroups. Scale bars, 100 µm. **e**,**f**, Prevalence of 17 cell types, including 14 immune cell types, across 416 patients with LUAD as a proportion of total cells (**e**) and immune cells (**f**). **g**–**i**, Prevalence of all immune (**g**), myeloid (**h**) and lymphoid (**i**) cells across

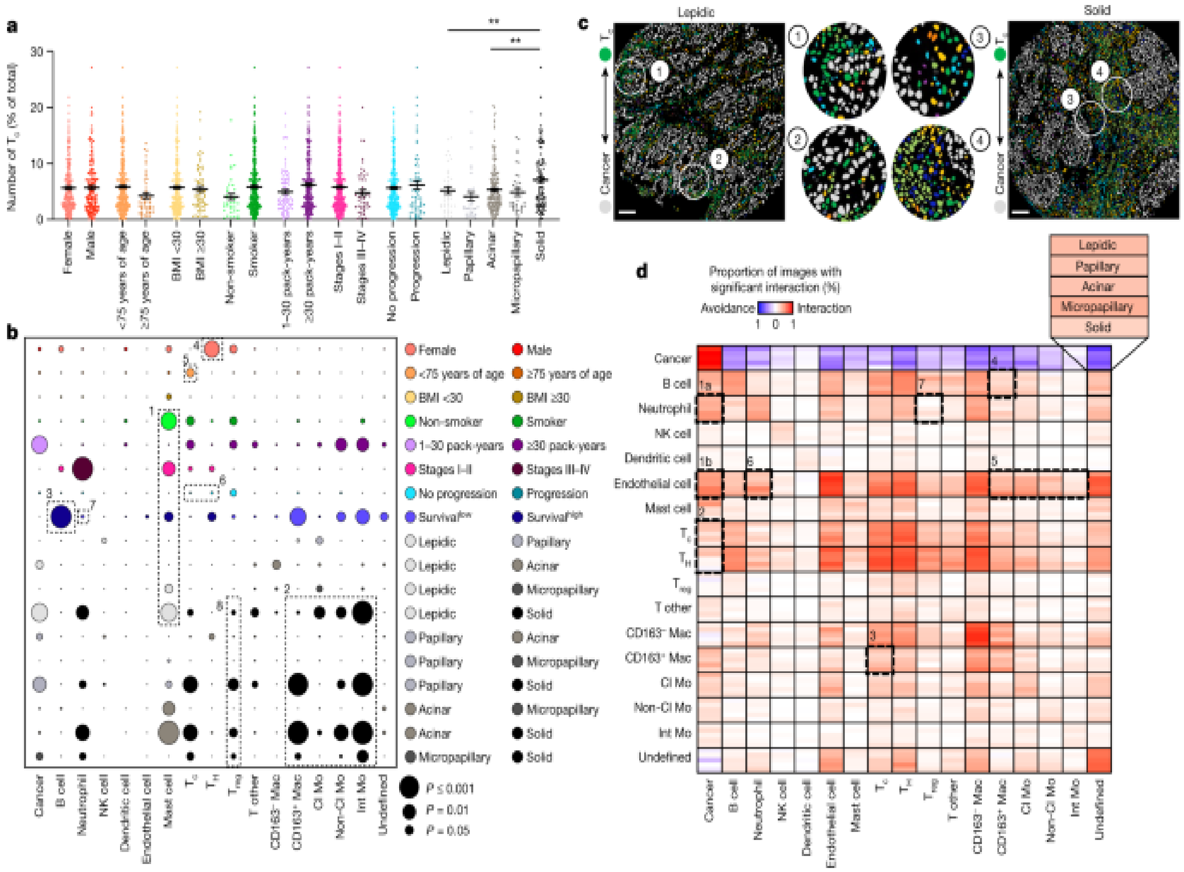
lepidic ($n = 40$), papillary ($n = 33$), acinar ($n = 190$), micropapillary ($n = 35$) and solid ($n = 118$) architectural patterns as a proportion of total cells. Comparison between lepidic and solid (immune cells): $^{**}P = 0.0013$. Comparison between papillary and solid (immune cells): $^{**}P = 0.0039$. Comparison between lepidic and solid (myeloid cells): $^{****}P \leq 0.0001$. Comparison between papillary and solid (myeloid cells): $^{*}P = 0.0474$. Comparison between acinar and solid (myeloid cells): $^{**}P = 0.0072$. Data shown as mean ± s.e.m. (**e**–**i**). One-way ANOVA with Tukey multiple comparison test was used for statistical analysis (**g**–**i**).

Consistent with previous work[15], high-grade solid tumours had the greatest immune infiltrate (44.6%) compared with micropapillary, acinar, papillary and lepidic architectures (37.0%, 39.7%, 32.8% and 32.7% respectively; Fig. 1g). This was driven by shifts within the myeloid compartment, as there were no significant differences in the average frequency of total lymphoid cells across histological patterns (Fig. 1h,i). In particular, macrophages were the most frequent cell population within the lung TIME, representing 12.3% of total cells (Fig. 1e) and 34.1% of immune cells (Fig. 1f), consistent with their critical role in the NSCLC niche[16]. We found the highest enrichment of $CD163^{+}$ macrophages (putative 'M2-like' or protumorigenic) in solid tumours, which are one of the most aggressive architectures (Extended Data Fig. 5b, Supplementary Table 3, Supplementary Fig. 1, xii). The prevalence of $CD163^{+}$ macrophages was strongly correlated with $FOXP3^{+}$ immunoregulatory T cells (T_{reg} cells) in the solid pattern (Extended Data Fig. 5c, box 1). This relationship was much less pronounced in low-grade lepidic and papillary architectures, which had a strong correlation between $CD163^{+}$ macrophages and cytotoxic $CD8^{+}$ T cells (Extended Data Fig. 5c, box 2). These associations suggest a potential interplay between macrophage and T cell populations in the TIME across LUAD patterns. Of note, solid tumours were also enriched for additional myeloid components, including neutrophils, non-classical monocytes and intermediate monocytes (Supplementary Fig. 1, ii, xiv and xv). Similarly to macrophages, these myeloid populations all exhibit diverse functional states in NSCLC biology[4] and exemplify the complex heterogeneity that exists in the lung TIME.

LUAD multicellular spatial interactions

We next assessed the relationship between immune populations and clinical or pathological variables by interrogating the frequency of individual cell types as a percentage of total cells within each image (Fig. 2a,b, Supplementary Tables 1 and 4 and Supplementary Fig. 1). Each image was cross-referenced with clinical data from patients, including sex, age, body mass index (BMI), smoking status, stage, progression, survival and histological subtype. Although we discovered established survival associations for several cell types[17,18], most were driven by an enrichment in specific clinical or pathological groups. For example, although mast cells were associated with prolonged survival, they were overrepresented in non-smokers, early-stage patients and those with lepidic tumours (Fig. 2b, box 1)—all clinical variables associated with good outcomes. Similarly, CD163^{+} macrophages, non-classical monocytes and intermediate monocytes were enriched in solid tumours, which have poor outcomes (Fig. 2b, box 2). By contrast, B cell frequency was most significantly associated with better overall survival, independent of any confounding clinical or pathological variables (Fig. 2b, box 3).

Fig. 2: Variability in single-cell distributions across clinical variables and in cell–cell interaction profiles across histological patterns in LUAD.



a, Prevalence of T_c cells (CD8$^+$ T cells) across sex (female $n = 233$, male $n = 183$), age (younger than 75 years of age $n = 369$, 75 years of age or older $n = 47$), BMI (less than 30 $n = 346$, 30 or higher $n = 70$), smoking status (smoker $n = 376$, non-smoker $n = 38$), pack-years (1–30 $n = 89$, 30 or more $n = 256$), stage (I-II $n = 365$, III–IV $n = 50$), progression status (progression $n = 64$, no progression $n = 340$) and histological subgroup (lepidic $n = 40$, papillary $n = 33$, acinar $n = 190$, micropapillary $n = 35$, solid $n = 118$). Comparison between papillary and solid: $^{**}P = 0.0070$, and acinar and solid: $^{**}P = 0.0076$. Data shown as mean ± s.e.m. **b**, Bubble plot in which the circle size represents the level of significance and the circle colour indicates which of the two comparisons on the *y* axis has higher levels of the cell type on the *x* axis. Survival^{low}, survival in the context of low (*z*-score < 0) cell prevalence. For *P* values, see Supplementary Table 4. **c**, Segmented images showing increased interaction of cancer and T_c cells in lepidic versus solid predominant LUAD. Scale bars, 100 μm. **d**, Heat map depicting significant pairwise cell–cell interaction (red) or avoidance (blue) across the five histological subgroups (lepidic $n = 40$ images, papillary $n = 33$ images,

acinar $n = 190$ images, micropapillary $n = 35$ images, solid $n = 118$ images; 1,000 permutations each). The black boxes depict associations referenced in the text. FDR-corrected two-tailed Student's t-test for sex, age, BMI, smoking status, pack-years, stage and progression status; one-way ANOVA with Tukey multiple comparison test for histological subgroup; and log-rank test for survival were used for statistical analysis (**a**,**b**).

Beyond survival associations, we found additional relationships between cell frequencies and specific clinical subgroups. For example, T cell subsets exhibited specific enrichment based on sex and age. Consistent with previous reports[19], $CD4^+$ helper T cells were significantly enriched in female patients (Fig. 2b, box 4), who have better overall survival than male patients[20,21]—an association also observed in our dataset (Extended Data Fig. 5d). Moreover, older patients (more than 75 years of age) had fewer intratumoural $CD8^+$ T cells (Fig. 2b, box 5), reminiscent of immune ageing that is linked to reduced expression of co-stimulatory molecules, antigen receptor diversity and immunotherapy response[22,23,24,25]. Overall, these data reveal new relationships and add biological insight into established associations between cell frequencies and clinical outcomes within the TIME.

To gain insight into the cellular architecture and spatial organization of the LUAD TIME, we characterized direct interactions and communication patterns between single cells by quantifying cell–cell spatial relationships. Using permutation testing, we assigned the likelihood of interaction or avoidance behaviours between cell pairs across LUAD architectures ranging from least to most aggressive (Fig. 2c,d). Tumour cells had a universal tendency towards homotypic interactions and a relative avoidance with other cell types (Fig. 2d), consistent with spatial analyses in breast cancer[12]. Homotypic interactions were high across several immune cell populations, suggestive of a spatially coordinated TIME. Many of these interactions were discordant with the pattern of cell frequencies, revealing that the spatial relationship of cell–cell interactions may hold greater prognostic value than frequency alone. In higher-grade histological patterns (solid and micropapillary), both neutrophils and endothelial cells had an increased tendency for interactions with cancer cells compared with lower-grade subtypes (Fig. 2d, box 1a,b). These relationships are consistent with the

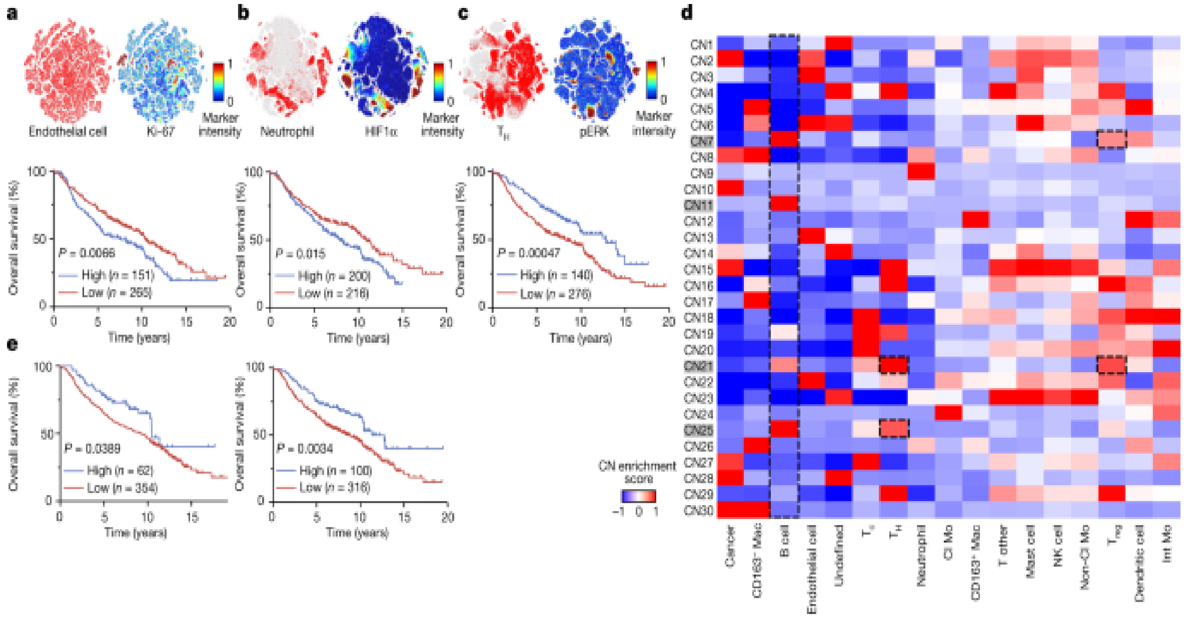
ability of neutrophils to facilitate tumour cell extravasation into blood vessels, thereby promoting haematogenic metastasis[26,27], and solid-predominant LUAD has the highest rate of metastasis compared with other histologies[28].

In low-grade lepidic and papillary tumours, $CD8^+$ and $CD4^+$ T cells had a stronger tendency for interaction with cancer cells than high-grade solid LUAD (Fig. 2c,d, box 2), despite the fact that overall $CD8^+$ and $CD4^+$ T cell frequencies were not associated with progression (Fig. 2b, box 6). This relationship echoes previous findings that the spatial interaction of T cells and tumour cells is a stronger indicator of non-recurrence than T cell density alone[29]. Moreover, despite the co-occurrence of $CD163^+$ macrophages and $CD8^+$ T cells in low-grade tumours (Extended Data Fig. 5c, box 2), their tendency to directly interact was strongest in high-grade tumours and decreased as tumors became lower grade (Fig. 2d, box 3). This is consistent with the role for $CD163^+$ macrophages in suppressing $CD8^+$ T cell function within the TIME[30]. Similarly, B cells exhibited a greater tendency to interact with $CD163^+$ macrophages in high-grade tumours (Fig. 2d, box 4), despite the observation that high B cell frequency was indicative of prolonged survival (Fig. 2b, box 3). In patient tumours specifically enriched in mature antigen-presenting $CD40^+$ B cells[31], these cells became generally more interactive across TIME populations (Extended Data Fig. 5e). Finally, endothelial cells tended to interact with many immune populations in high-grade tumours compared with low-grade tumours, including $CD163^+$ macrophages and monocytes (Fig. 2d, box 5); these interactions may be reminiscent of innate regulation of vascular inflammation, consistent with our observation that immune infiltration was highest in the solid pattern (Fig. 1g), driven largely by differences within the myeloid compartment (Fig. 1h). Together, these analyses paint an overall picture of how stromal interactions shift among histological patterns and exemplify how spatial relationships, rather than cell frequency alone, are important to understand TIME biology.

LUAD architecture and survival outcomes

To complement our analyses of cell frequencies and interactions, we next explored how cellular phenotypes within the microenvironment relate to survival. We extracted all microenvironmental populations represented in our dataset (including endothelial, myeloid or lymphoid compartments) and performed *t*-distributed stochastic neighbour embedding (*t*-SNE) based on functional markers in our antibody panel (Extended Data Fig. 6a–c). First, outside the immune compartment, we observed a distinct population of proliferative Ki-67^+ endothelial cells, whose frequency was associated with poor overall survival (Fig. 3a and Supplementary Table 5) and high-grade solid tumours (Extended Data Fig. 6d). Proliferation of the endothelium underlies angiogenesis in response to hypoxia, a common feature of aggressive tumours[32]. We therefore explored vascular interactions in high-grade patterns and found an enrichment in endothelial cell interactions with neutrophils (Fig. 2d, box 6), leading us to question how specific neutrophil subsets may respond to hypoxic conditions. We observed several neutrophil states based on the expression pattern of three markers: HIF1α^+, ARG1^+ and MMP9^+ (Fig. 3b and Extended Data Fig. 6b). Despite a high frequency of total neutrophils not being correlated with survival in our cohort (Fig. 2b, box 7), an increase in the proportion of the HIF1α^+ subset was significantly associated with worse overall survival (Fig. 3b and Supplementary Table 5), which may reflect cases in which angiogenesis is insufficient to alleviate hypoxia. Neutrophils and other granulocytes are sensitive to low-oxygen conditions, and can adopt immunosuppressive behaviours against T cells in this setting[33]. Indeed, we observed that neutrophils exhibit a higher tendency to interact with immunosuppressive T_{reg} cells in high-grade tumours (Fig. 2d, box 7). Phenotypic analysis within the lymphoid compartment revealed active ERK signalling within a subset of $CD4^+$ T cells associated with prolonged survival (Fig. 3c and Supplementary Table 5), which is known to suppress differentiation into T_{reg} cells[34]. Consistently, $pERK^+CD4^+$ T cells were enriched in low-grade lepidic tumours (Extended Data Fig. 6e) where neutrophil–T_{reg} cell interactions were the lowest (Fig. 2d, box 7), and reduced in high-grade solid tumours (Extended Data Fig. 6e) where T_{reg} cells were most abundant (Fig. 2b, box 8). Together, these findings provide a snapshot of spatially resolved phenotypic programs associated with more aggressive tumours, as they relate to tumour hypoxia and an immunosuppressive niche.

Fig. 3: Single-cell populations and neighbourhoods are associated with distinct outcomes in LUAD.



a–**c**, *t*-SNE of endothelial, myeloid and lymphoid cell populations highlighting the distribution of 108,387 endothelial cells (**a**), 42,427 neutrophils (**b**) and 147,980 CD4$^+$ T_H cells (**c**), and the positivity of the Ki-67 (endothelial cells), HIF1α (neutrophils) and pERK (T_H cells) markers. Kaplan–Meier curves of overall survival for 416 patients with LUAD based on low (*z*-score < 0) and high (*z*-score ≥ 0) prevalence of the indicated cell types are also shown. **d**, Heatmap of 30 CNs discovered in 416 patients with LUAD. The CNs highlighted in grey refer to B-cell-enriched neighbourhoods. **e**, Kaplan–Meier curves of overall survival for 416 patients with LUAD based on low (*z*-score < 0) and high (*z*-score ≥ 0) prevalence of B cell CN11 (left) and CN25 (right). log-rank test was used for statistical analysis (**a**–**c**,**e**).

Beyond pairwise interactions, our data hint at the existence of larger cellular communities that are distinctively organized within the TIME across LUAD subtypes. To assess this, we followed a canonical approach to establish cellular neighbourhoods by first identifying the ten nearest spatial neighbours for each individual cell[12,14]. We then reclassified cells on the basis of their spatially defined cellular neighbourhood (CN). Using this approach, we discovered ten CNs that recapitulated both new and known tissue architectures, which we named: tumour boundary (CN1), undefined

(CN2), pan-immune hotspot 1 (CN3), lymphoid enriched (CN4), tumour core (CN5), macrophage enriched (CN6), neutrophil enriched (CN7), pan-immune hotspot 2 (CN8), B cell enriched (CN9) and vascular niche (CN10) (Extended Data Fig. 7a,b). To identify CNs associated with survival, we performed Kaplan–Meier analysis by designating the frequency of CNs for each patient as high (CN^{high}; z-score ≥ 0) or low (CN^{low}; z-score < 0). Consistent with our findings related to B cell frequency (Fig. 2b, box 3, and Supplementary Table 4), $CN9^{high}$ (B cell-enriched) was significantly associated with increased overall survival (Extended Data Fig. 7a and Supplementary Table 6), despite minimal differences in CN9 representation across histological patterns (Extended Data Fig. 7c, box 1). $CN3^{high}$ (pan-immune hotspot 1) and $CN4^{high}$ (lymphoid enriched) were also significantly correlated with increased overall survival across LUAD histologies (Extended Data Fig. 7a,c, box 2). When survival was analysed within histological patterns, associations with increased survival were noted for $CN4^{low}$ (lymphoid enriched) within the lepidic pattern, $CN9^{high}$ (B cell enriched) in the acinar pattern and $CN2^{low}$ (undefined) and $CN4^{high}$ (lymphoid enriched) in the solid pattern (Supplementary Fig. 2).

We were particularly interested in dissecting B cell neighbourhoods in greater detail, given the prognostic value of B cells in our dataset (Fig. 2b, box 3). Two variables that affect CN analysis include the number of interacting cells within a neighbourhood (denoted as n) and the number of total neighbourhoods (denoted as tCN). To further explore the spatial relationship between CNs and survival, we first altered the number of nearest spatial neighbours for each individual cell (n) while maintaining a constant number of neighbourhoods (tCN = 10). Across a wide range of n values ($n = 3$–30), CNs enriched in B cells were significantly associated with survival (Extended Data Fig. 8a), with the most significant association resulting from $n = 10$ and tCN = 10 (Extended Data Fig. 7a). To resolve B cell interactions that drive this survival advantage, we increased the tCN to 30. Using this approach, we were able to resolve four B cell-enriched neighbourhoods (CN7, CN11, CN21 and CN25) (Fig. 3d). Across these neighbourhoods, the survival advantage associated with B cells was negated when CNs concurrently displayed an enrichment in T_{reg} cells (CN7 and CN21), whereas the survival advantage was maintained for CN11 ($P = 0.0389$) and CN25 ($P = 0.0034$) where T_{reg} cells were lower (Fig. 3e and

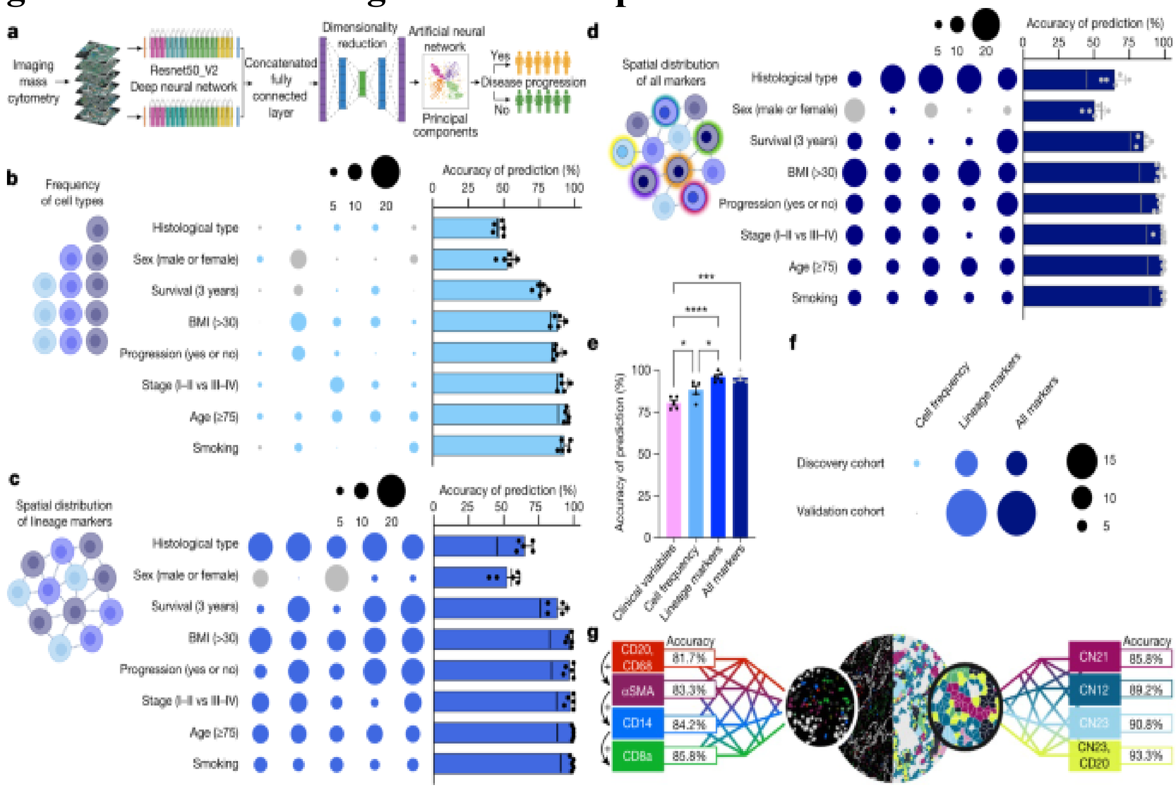
Supplementary Table 7). When comparing these two neighbourhoods, we noted a greater survival advantage for CN25, which was also enriched for $CD4^+$ helper T cells (by contrast, CN11 was enriched for B cells alone). To determine whether the improved survival benefit associated with CN25 was related to the interaction of B cells and $CD4^+$ helper T cells or to the prevalence of both cell types independent of their interaction, we plotted the survival association of patients who were B cell-high and $CD4^+$ helper T cell-high versus patients who were B cell-high and $CD4^+$ helper T cell-low and observed no significant difference ($P = 0.644$; Extended Data Fig. 8b). Moreover, the correlation between T cells and B cells in our cohort was low with an R^2 of 0.210, thus making it less likely that $CD4^+$ helper T cells and B cells are interacting as a result of a strong correlation in the prevalence of both cell types (Extended Data Fig. 8c,d). These data suggest that the improved survival association for CN25 is related to the interaction of B cells and $CD4^+$ helper T cells beyond the prevalence of both cell types alone. However, an enrichment in T_{reg} cells was still sufficient to negate this survival benefit (CN21), emphasizing the importance of multicellular B cell interactions within the TIME. Finally, there was no significant association between these B cell-enriched CNs and any other clinical variable, including histological subtype (Extended Data Fig. 9a,b and Supplementary Table 7). Together, these findings suggest that the spatial organization of TIME interactions may provide additional insight into individual patient survival beyond histological subtype classifications and cell prevalence.

Predicting outcomes using deep learning

Given our finding that spatial neighbourhoods are predictive of survival regardless of LUAD architectures, we wondered whether we could leverage spatial data to predict clinical outcomes by using a deep-learning approach (Fig. 4a). We took advantage of transfer learning by using a pretrained convolutional neural network model. We chose the deep residual networks[35] architecture pretrained on the ImageNet dataset[36]. Using the *k*-fold cross-validation method, we split the data into five folds, with 20% of the data for each fold. In our experiments, we considered four of the folds (80% of the patients) as the training data and the remaining fold (20%) for testing to evaluate the prediction accuracy. We repeated this for all possible

combinations. For proof of principle, we first assessed whether the frequency of cells alone within each image would be sufficient to predict clinical variables. We tested routine clinical variables that demonstrated some variation in cell-type frequencies including histological subtype, sex, survival, BMI, cancer progression, cancer stage, age and smoking. Our goal was to increase the ability to predict clinical outcomes above the baseline prediction score, which reflects the chance of predicting the major class over the total number of examples involved for that specific variable. However, we saw negligible increases in prediction score above baseline for most of the clinical variables, suggesting that cell frequency alone does not capture the tumour architecture with enough resolution to predict clinical variables with high confidence (Fig. 4b and Supplementary Table 8).

Fig. 4: Machine learning of IMC data predicts clinical outcomes.



a, Schematic of the deep-learning-based strategy involving deep residual networks (Resnet50) architecture on the ImageNet dataset for feature extraction from IMC image channels. **b**–**d**, Fivefold cross-validation across clinical outcomes: histological patterns, sex (male or female), BMI (less than 30 or 30 or higher) and age (younger than 75 years of age or 75 years of age or older) $n = 416$; survival (less than 3 years, 3 years or longer) $n = 407$;

progression status (progression or no progression) *n* = 404; stage (I–II or III–IV) *n* = 415; smoking status (smoker or non-smoker) *n* = 414 using frequency of cell types (**b**); spatial distribution of lineage markers (**c**) and spatial distribution of all markers (**d**). The size of the bubble represents deviation from baseline, with blue and grey indicating an improvement or worsening in predictive performance, respectively. The line in the bar plot represents the baseline. Schematics in **a**–**d** were created with BioRender. **e**, Accuracy of clinical progression prediction in patients with stage I LUAD (*n* = 286) using clinical variables, cell frequency, lineage marker and 'all markers' models. Comparison between the clinical variables and the cell frequency model: *$P = 0.0319$. Comparison between the clinical variables and lineage marker model: ****$P < 0.0001$. Comparison between the clinical variables and all markers model: ***$P = 0.0001$. Comparison between the cell frequency and lineage marker model: *$P = 0.0321$. **f**, Accuracy of clinical progression prediction in patients with stage I LUAD; discovery cohort (*n* = 286) and validation cohort (*n* = 60; 120 cores) in the cell frequency, lineage and all markers models compared with baseline. The size of the bubble represents deviation from baseline, with blue and grey indicating an improvement or worsening in predictive performance, respectively. **g**, Accuracy of clinical progression prediction in patients with stage I LUAD (validation cohort *n* = 60; 120 cores) using combinations of top-ranked (left) and neighbourhood-derived (right) lineage markers. For all combinations, see Supplementary Table 15. Data shown as mean ± s.e.m. (**b**–**e**). One-way ANOVA with Tukey multiple comparison test was used for statistical analysis (**e**).

We next investigated whether the integration of spatial information, obtained by inputting all the raw lineage marker images into our model, would help recognition performance. Using this approach, we observed a significant boost in performance for all clinical variables tested compared with cell frequency alone, suggesting that single-cell positional information that is encoded in each of the multiplex image scans is critical to interpreting the complex TIME that underlies clinical correlates (Fig. 4c and Supplementary Table 9). Spatial information did not confer an increase above baseline for sex, indicating that the TIME that underlies tumours from male individuals versus female individuals is indistinguishable using our model. Finally, to compare whether additional channels from our IMC images would lead to better recognition performance (that is, integration of spatially resolved

immune functional substates), we used all the markers in our panel and repeated the predictions. The additional channels did not boost performance, suggesting that there is a certain threshold beyond which additional markers do not add value to clinical predictions based on our model (Fig. 4d and Supplementary Table 10).

We next sought to leverage our deep-learning approach to address a clinically meaningful problem. Although adjuvant chemotherapy has long been demonstrated to improve overall survival in patients with NSCLC who have stage IIA to IIIA disease, patients with stage I tumours smaller than 4 cm currently do not receive adjuvant chemotherapy[37,38], despite that many of these patients are at increased risk for progression[39]. In fact, these patients currently have minimal approved peri-adjuvant therapeutic options[37]. Even with complete lung tumour resection, a significant proportion of these patients will relapse[39]. Therefore, we next assessed whether we could predict progression in patients with stage IA–IB lung cancer. The use of standard clinical information in our model (sex, age, BMI, smoking status, pack-years, surgery type, maximum tumour size, tumour grade, predominant histological pattern and stage) was insufficient to predict progression over baseline (Fig. 4e, Extended Data Fig. 10a and Supplementary Table 11). Consistent with our previous results, the frequency of cells alone was also insufficient to significantly predict progression (Fig. 4e, Extended Data Fig. 10b and Supplementary Table 11). When we included spatial information, however, our model predicted progression with 95.9% accuracy from a single 1-mm^2 tumour core, smaller than most standard needle biopsies used to establish a diagnosis of lung cancer (Fig. 4e, Extended Data Fig. 10c and Supplementary Table 11). Additional markers, again, did not boost the prediction accuracy (Fig. 4e, Extended Data Fig. 10d and Supplementary Table 11), indicating that there is a minimum threshold of markers required to ascertain accurate predictions, a promising finding for translational practicality.

To validate our findings and to assess how heterogeneity within the lung TIME may affect our predictions, we performed IMC on an independent validation cohort consisting of 60 patients with primary LUAD that included two spatially distinct cores per tumour (Supplementary Table 12). In this new dataset, after training on our discovery cohort, the use of raw images

from our lineage markers was able to predict progression with high accuracy (94.2% accuracy; Fig. 4f and Supplementary Table 13), with no added benefit from integrating the entire panel (93.3% accuracy). Of note, our validation cohort was more balanced, with a lower baseline prediction score (75.0%), confirming that there are spatially defined features within these images that probably reflect clinical outcomes. When assessing intratumour heterogeneity, we found substantial agreement in the predictions between two distinct cores from the same tumour (91.7%, lineage markers model). Despite these promising results, we acknowledge that tumour heterogeneity remains a challenge for accurate clinical and pathological diagnosis, an area of research that may benefit greatly from the application of artificial intelligence approaches.

One limitation of highly multiplexed imaging is the impracticality of translating discoveries into a clinically actionable assay that is broadly accessible. We thus sought to determine the minimum threshold of markers that could be used to predict progression without compromising prediction accuracy, with the goal of reducing our panel to approximately five markers (which is more likely to be amenable to clinical pathology practice). We first assessed the predictive performance of the spatial information derived from each individual marker in our antibody panel. Not surprisingly, we found that CD20 (a B cell marker) was most associated with an improved prediction of progression in our discovery cohort (Supplementary Table 14). Next, on the basis of the ranking of individual prediction scores, we combined the top two, three, four or five markers and tested whether combinations could predict progression in our validation dataset with high accuracy. Using this approach, we did not reach the level of accuracy that was achieved when all lineage markers were used (Fig. 4g and Supplementary Table 15). As an alternative approach, we took advantage of the spatial information embedded within our dataset, by using our CN analysis as a guide to identify rational combinations of markers whose spatial distribution are strongly correlated with survival (Fig. 3d and Supplementary Table 7). We reasoned that specific interactions may have prognostic value and would therefore be informative in predicting progression. Using this approach, we discovered that the combination of five markers—CD14, CD16, CD94, αSMA and CD117 (enriched in CN23, the neighbourhood most significantly associated with overall survival)—resulted in 90.8% accuracy (Fig. 4g and Supplementary Table 15). When we

added CD20 (the individual marker demonstrating the highest predictive potential for progression), we increased accuracy to 93.3%, with 95.6% precision and recall. Overall, these data suggest that spatially resolved single-cell datasets may be highly valuable in the future to help to inform personalized peri-operative care plans to minimize toxicity for those destined to be cured, or to increase cure rates for those destined to recur.

Discussion

Here we applied highly multiplexed IMC to characterize the cellular landscape of the LUAD TIME. We identified cellular dynamics and spatial features that correlate with distinct clinical outcomes including patient survival. Our data represent a valuable resource that adds to a quickly evolving body of literature supporting the importance of spatially resolved single-cell datasets in understanding how the TIME architecture relates to tumour biology. As lung cancer remains by far the largest cause of cancer-related death, there is untapped value in combining single-cell technology with deep-learning approaches to develop intelligent predictive algorithms to help to triage patients onto the therapeutic regimens that are best suited for their individual cancer. Our findings utilize a 5-μm section of a single 1-mm^2 core of formalin-fixed paraffin-embedded tumour tissue to predict recurrence with high accuracy, which can be obtained from surgical resection or a biopsy. Nevertheless, clinical sampling bias remains a challenge in studies in which small regions of tumours are captured within a small amount of material. Future work will focus on using lower-plex technologies while attempting to maintain predictive accuracy to achieve translational feasibility. Our findings represent an important advance over existing prediction tools that use clinical and pathological variables and may enable more effective utilization of a growing armamentarium of peri-adjuvant systemic therapies to improve cancer outcomes[40,41].

Methods

Clinical cohort

A cohort of 416 patients with LUAD were included in this study with follow-up time ranging from February 1996 to July 2020. For the validation cohort, 60 patients with LUAD with follow-up time ranging from February 2012 to May 2022 were included with two distinct cores per patient. All samples obtained were primary treatment-naive LUADs diagnosed by a board-certified pathologist following surgical resection or biopsy. Clinical information on all patients included can be found in Supplementary Tables 1 and 12. Tissue microarrays were constructed by selecting one 1-mm^2 core from the surgical tumour specimen. Patient samples and clinical information were obtained following written informed patient consent. The protocols for human sample biobanking were approved (ethics, scientific and final) through the IUCPQ Biobank, protocol number IRB #2022-3474, 22090, and the MUHC protocol numbers IRB #2014-1119 and 2019-5253.

Sample staining and IMC

Formalin-fixed paraffin-embedded (FFPE) slides were deparaffinized at 70 °C by incubation in EZ Prep solution (Roche Diagnostics) followed by antigen retrieval at 95 °C in standard cell conditioning 1 solution (Roche Diagnostics). The Ventana Discovery Ultra auto-stainer platform (Roche Diagnostics) was used for antigen retrieval. Slides were rinsed with 1× PBS and incubated for 45 min in Dako serum-free protein block solution (Agilent). Slides were stained with a cocktail containing metal-tagged antibodies at optimized dilutions overnight at 4 °C. All conjugations were performed by the Single Cell and Imaging Mass Cytometry Platform at the Goodman Cancer Institute (McGill University), using Maxpar Conjugation Kits (Fluidigm). Information on the antibodies used can be found in Supplementary Table 2. Slides were then washed with 0.2% Triton X and 1× PBS. An optimized dilution of the secondary antibody cocktail containing metal-conjugated anti-biotin was prepared in Dako antibody diluent. After a 1-h incubation, slides were washed with 0.2% Triton X and 1× PBS. Before IMC acquisition, Cell-ID Intercalator-Ir (Fluidigm) at a dilution of 1:400 was used to counterstain slides in 1× PBS for 30 min at room temperature. Slides were then rinsed for 5 min with distilled water and air-dried. IMC images were acquired at a resolution of roughly 1 μm. Cores were laser-ablated at a frequency of 200 Hz using the Hyperion Imaging System (Fluidigm) and raw data were compiled using the Fluidigm commercial

acquisition software. Of note, in our validation cohort, we stained with alpha cleaved H3 (176Yb) instead of histone H3 (176Yb). Accordingly, this marker was excluded from validating our deep-learning predictions of progression.

Antibody optimization

Antibodies were optimized on control tissues including the spleen, tonsil, appendix, placenta, thymus, normal lung and LUAD. Multiplex quality-control staining of positive and negative control tissue can be seen in Extended Data Figs. 2–4, with four representative images staining for each of the 35 markers in our panel.

Data transformation and normalization

Data presented were not transformed. All analyses were based on raw IMC measurements. For heatmap visualization, expression data were normalized to the 95th percentile and *z*-scored cluster means were plotted. Single-cell marker expressions were summarized by mean pixel values for each channel.

Cell segmentation and lineage assignment

All markers underwent a staining quality check before cell segmentation (Extended Data Figs. 2–4). A small number of markers did not consistently stain every sample in our cohort, so we chose not to make any conclusions based on those markers (GM-CSFR, PD-1, PD-L1 and B7-H3). Note that CD163 (a putative 'M2-like' marker) was chosen to subdivide macrophage populations on the basis that this marker is often upregulated in tumour-associated macrophages and has been used to categorize macrophages in multiplex imaging studies[14,42,43]. Although the terms 'M1/pro-inflammatory' and 'M2/anti-inflammatory' have traditionally been used to classify macrophage activation states, these terms are outdated and were therefore avoided[44,45]. Using a novel cell segmentation pipeline that combines classical and modern machine-learning-based computer vision algorithms, we segmented all cells contained within the IMC images. The model used is a fully automated hybrid cell detection model that eliminates

subjective bias and enables high-throughput image segmentation. It allows us to accurately distinguish cells across diverse tissue microenvironments and resolve low-resolution structures. The details of our image segmentation approach can be found here: https://biorxiv.org/cgi/content/short/2022.02.27.482183v1. Owing to existing phenotyping challenges for highly multiplexed imaging, we created a cell phenotyping pipeline to assign cell phenotypes. Our strategy relies on canonical lineage markers and uses a supervised hierarchal approach that integrates the staining quality, the expected population abundance and cell lineage maturation to assign cells. We used *k*-means clustering[46] and a mixture of generalized Gaussian models[47] to generate a mask or level for each marker within a multi-level image stack created based on staining intensity. This allowed us to evaluate the existence of a marker at a particular location. Each marker in our panel was assessed using six levels and the appropriate mask was subsequently manually curated for each marker. Each mask is produced using the following procedure:

1. (1)

   The greyscale image channel is convolved with a median filter with a particular window size (3×3).

2. (2)

   Each pixel in the image is clustered into six groups of intensity levels using the *k*-means algorithm.

3. (3)

   For each channel, we then selected all groups up to a particular level as foreground (1) and the rest as background (0).

4. (4)

   To obtain smoother binary masks, we also applied a morphological blob removal process in which binary blobs of a particular area are removed from masks to avoid noisy regions.

5. (5)

   To further refine the accuracy of select markers, additional channel-specific morphological operations were applied by computing an additional binary mask obtained using the adaptive binarization method with a sensitivity of 0.4. This mask is then amalgamated with the mask obtained in step 4.

As a formula, for each cell ${c}_{i}$, we consider the curated mask for each lineage marker ${M}_{k}$, where $k=1,\ldots ,n$ and *n* is the number of lineage markers. Let us assume ${p}_{{c}_{i}}^{j}$ be the *j*th pixel that lies in the surrounding of ${c}_{i}$ and each pixel has the following presence vector based on the lineage markers:

$$E({p}_{{c}_{i}}^{j})=\{{p}_{{M}_{1}}^{j},{p}_{{M}_{2}}^{j},\ldots ,{p}_{{M}_{n}}^{j}\}$$

where ${p}_{{M}_{i}}=\{0\,\text{or}\,1\}$, which determines whether the pixel ${p}_{{c}_{i}}^{j}$ is positive for a particular marker. Next, to determine whether each pixel within a cell is positive or negative for a given marker, we determined the majority vector by summing the presence of all vectors as:

$${M}_{{c}_{i}}=\left\{\mathop{\sum }\limits_{j=1}^{{N}_{{c}_{i}}}{p}_{{M}_{1}}^{j},\mathop{\sum }\limits_{j=1}^{{N}_{{c}_{i}}}{p}_{{M}_{2}}^{j},\ldots ,\mathop{\sum }\limits_{j=1}^{{N}_{{c}_{i}}}{p}_{{M}_{n}}^{j}\right\}$$

where ${N}_{{c}_{i}}$ is the number of pixels in the cell ${c}_{i}$. The maximum value in vector ${M}_{{c}_{i}}$ determines the cell-type assignment. Cell lineages were assigned in rank priority order (Extended Data Fig. 1c). See the ‘Code availability’ section for additional details.

Cell–cell pairwise interaction

We performed a permutation-test-based analysis of spatial single-cell interactions to identify significant pairwise interaction–avoidance between

cells[12]. Interacting cells were defined as those within six pixels. *P* values less than 0.01 were deemed significant.

Neighbourhood identification

To generate CNs, we used a 'window' capture strategy consisting of the number of cells (*n*) in closest proximity to a given cell as previously described[14]. Each window is a frequency vector consisting of the types of X (as indicated) closest cells to a given cell. Obtaining all the window vectors for each cell, initial cells (Extended Data Fig. 7a) were clustered using Scikit-learn, a software machine-learning library for Python, and MiniBatchKMeans clustering algorithm version 0.24.2 with default batch size = 100 and random_state = 0. Subsequent CN analysis was performed using the MiniBatchKMeans clustering algorithm version 1.1.2 with default batch size = 1,024 and random_state = 0. Every cell was subsequently allocated to a CN based on their defining window. The prevalence of each neighbourhood in each core was normalized so that the sum of neighbourhood prevalence for that core was 100%. Values were then *z*-scored and cores with a *z*-score above or equal to 0 and below 0 were compared for survival outcomes.

t-SNE

All *t*-SNE plots were generated in MATLAB (version 2019b) using default parameters. For visualization, expression data were normalized to the 95th percentile.

Deep learning

All deep-learning analysis steps were performed in Python (version 3.7.12). We used the TensorFlow (version 2.8.0) framework alongside Keras, which now acts as an interface for the TensorFlow library. We have two modes of data for our experiments: (1) raw IMC images, and (2) cell frequencies obtained from cell phenotyping. For raw IMC images, the pretrained ResNet-50 model with weights pretrained on ImageNet is first utilized to extract embeddings from each channel within the multiplex IMC channels. Each channel is fed to the three-channels of ResNet-50 and the embeddings

are computed before the classificationlayers are obtained. Each channel produces an embedding vector size of 2,048 and then these are all concatenated into a single vector of features representing that specific core. We then reduced the dimensionality of the extracted feature vectors using mini-batch sparse principal components analysis to a specific number of principal components (for most applications we tried nine principal components). Principal components were later used to train a support vector machine with a radial basis function kernel with the parameters specified in our codebase. For the imbalanced datasets, we used a random oversampling to achieve an equal number of samples for each class during the training. The function used is RandomOverSampler (version 0.9.1) and it is available at: https://imbalanced-learn.org/stable/references/generated/imblearn.over_sampling.RandomOverSampler.html. To compare with cell frequencies, we imagined that cell-frequency vectors also represent a core (in which each vector is simply a vector of cell prevalence of each type). Similar to images, we reduced the dimensionality of the extracted feature vectors to nine principal components and then trained a support vector machine with a radial basis function kernel with the same parameters. Various classes of Scikit-learn (version 1.0.2) machine-learning libraries have been utilized for the tasks of splitting the dataset, dimensionality reduction and training support vector machines for the prediction tasks. All feature extraction and training steps were performed on Google Cloud GPU/TPU servers. See the ‘Code availability’ section for additional details.

Statistical analysis and workflow

All image analysis steps were performed in MATLAB (version 2019b) and Python (version 3.7.12). Statistical analyses were performed using RStudio version 4.2.2 and GraphPad Prism 9 statistical software. Data are expressed as mean ± s.e.m. or mean ± s.d.; $P < 0.05$ was considered significant unless otherwise indicated. All statistical tests are indicated in the figure legends. Survival data were analysed by log-rank (Mantel–Cox) test.

Reporting summary

Further information on research design is available in the Nature Portfolio Reporting Summary linked to this article.

Data availability

Data supporting the findings in this study, including high-dimensional TIFF images, are available at https://doi.org/10.5281/zenodo.7383627. Raw primary imaging data can be obtained from the authors directly on reasonable request.

Code availability

The original code used to produce the results of this study is available at https://github.com/walsh-quail-labs/IMC-Lung.

References

1. Leader, A. M. et al. Single-cell analysis of human non-small cell lung cancer lesions refines tumor classification and patient stratification. *Cancer Cell* **39**, 1594–1609.e12 (2021).

2. Melms, J. C. et al. A molecular single-cell lung atlas of lethal COVID-19. *Nature* **595**, 114–119 (2021).

3. Marjanovic, N. D. et al. Emergence of a high-plasticity cell state during lung cancer evolution. *Cancer Cell* **38**, 229–246.e13 (2020).

4. Zilionis, R. et al. Single-cell transcriptomics of human and mouse lung cancers reveals conserved myeloid populations across individuals and species. *Immunity* **50**, 1317–1334.e10 (2019).

5. Liu, B. et al. Temporal single-cell tracing reveals clonal revival and expansion of precursor exhausted T cells during anti-PD-1 therapy in lung cancer. *Nat. Cancer* **3**, 108–121 (2022).

6. Zheng, L. et al. Pan-cancer single-cell landscape of tumor-infiltrating T cells. *Science* **374**, abe6474 (2021).

7. Cheng, S. et al. A pan-cancer single-cell transcriptional atlas of tumor infiltrating myeloid cells. *Cell* **184**, 792–809.e23 (2021).

8. Kumar, V. et al. Single-cell atlas of lineage states, tumor microenvironment, and subtype-specific expression programs in gastric cancer. *Cancer Discov.* **12**, 670–691 (2022).

9. Zhang, Y. et al. Single-cell analyses of renal cell cancers reveal insights into tumor microenvironment, cell of origin, and therapy response. *Proc. Natl Acad. Sci. USA* **118**, e2103240118 (2021).

10. Siegel, R. L., Miller, K. D., Fuchs, H. E. & Jemal, A. Cancer statistics, 2021. *CA Cancer J. Clin.* **71**, 7–33 (2021).

11. Gridelli, C. et al. Non-small-cell lung cancer. *Nat. Rev. Dis. Primers* **1**, 15009 (2015).

12. Jackson, H. W. et al. The single-cell pathology landscape of breast cancer. *Nature* **578**, 615–620 (2020).

13. Ali, H. R. et al. Imaging mass cytometry and multiplatform genomics define the phenogenomic landscape of breast cancer. *Nat. Cancer* **1**, 163–175 (2020).

14. Schurch, C. M. et al. Coordinated cellular neighborhoods orchestrate antitumoral immunity at the colorectal cancer invasive front. *Cell* **182**, 1341–1359.e19 (2020).

15. Tavernari, D. et al. Nongenetic evolution drives lung adenocarcinoma spatial heterogeneity and progression. *Cancer Discov.* **11**, 1490–1507 (2021).

16. Casanova-Acebes, M. et al. Tissue-resident macrophages provide a pro-tumorigenic niche to early NSCLC cells. *Nature* **595**, 578–584 (2021).

17. Welsh, T. J. et al. Macrophage and mast-cell invasion of tumor cell islets confers a marked survival advantage in non-small-cell lung cancer. *J. Clin. Oncol.* **23**, 8959–8967 (2005).

18. Wu, P. et al. Inverse role of distinct subsets and distribution of macrophage in lung cancer prognosis: a meta-analysis. *Oncotarget* **7**, 40451–40460 (2016).

19. Conforti, F. et al. Sex-based dimorphism of anticancer immune response and molecular mechanisms of immune evasion. *Clin. Cancer Res.* **27**, 4311–4324 (2021).

20. Tong, B. C. et al. Sex differences in early outcomes after lung cancer resection: analysis of the Society of Thoracic Surgeons General Thoracic Database. *J. Thorac. Cardiovasc. Surg.* **148**, 13–18 (2014).

21. International Early Lung Cancer Action Program Investigators. Women's susceptibility to tobacco carcinogens and survival after diagnosis of lung cancer. *JAMA* **296**, 180–184 (2006).

22. Weng, N. P. Aging of the immune system: how much can the adaptive immune system adapt? *Immunity* **24**, 495–499 (2006).

23. Kugel, C. H. 3rd et al. Age correlates with response to anti-PD1, reflecting age-related differences in intratumoral effector and regulatory T-cell populations. *Clin. Cancer Res.* **24**, 5347–5356 (2018).

24. Fane, M. & Weeraratna, A. T. How the ageing microenvironment influences tumour progression. *Nat. Rev. Cancer* **20**, 89–106 (2020).

25. Yager, E. J. et al. Age-associated decline in T cell repertoire diversity leads to holes in the repertoire and impaired immunity to influenza virus. *J. Exp. Med.* **205**, 711–723 (2008).

26. Szczerba, B. M. et al. Neutrophils escort circulating tumour cells to enable cell cycle progression. *Nature* **566**, 553–557 (2019).

27. Saini, M., Szczerba, B. M. & Aceto, N. Circulating tumor cell–neutrophil tango along the metastatic process. *Cancer Res.* **79**, 6067–6073 (2019).

28. Xu, L., Tavora, F. & Burke, A. Histologic features associated with metastatic potential in invasive adenocarcinomas of the lung. *Am. J.*

Surg. Pathol. **37**, 1100–1108 (2013).

29. Enfield, K. S. S. et al. Hyperspectral cell sociology reveals spatial tumor-immune cell interactions associated with lung cancer recurrence. *J. Immunother. Cancer* **7**, 13 (2019).

30. Peranzoni, E. et al. Macrophages impede CD8 T cells from reaching tumor cells and limit the efficacy of anti-PD-1 treatment. *Proc. Natl Acad. Sci. USA* **115**, E4041–E4050 (2018).

31. Schultze, J. L. et al. CD40-activated human B cells: an alternative source of highly efficient antigen presenting cells to generate autologous antigen-specific T cells for adoptive immunotherapy. *J. Clin. Invest.* **100**, 2757–2765 (1997).

32. Folkman, J. Tumor angiogenesis: therapeutic implications. *N. Engl. J. Med.* **285**, 1182–1186 (1971).

33. Noman, M. Z. et al. PD-L1 is a novel direct target of HIF-1α, and its blockade under hypoxia enhanced MDSC-mediated T cell activation. *J. Exp. Med.* **211**, 781–790 (2014).

34. Chang, C. F. et al. Polar opposites: Erk direction of CD4 T cell subsets. *J. Immunol.* **189**, 721–731 (2012).

35. He, K., Zhang, X., Ren, S. & Sun, J. Deep residual learning for image recognition. In *2016 IEEE Conference on Computer Vision and Pattern Recognition (CVPR)* 770–778 (IEEE, 2016).

36. Deng, J. et al. ImageNet: a large-scale hierarchical image database. In *2009 IEEE Conference on Computer Vision and Pattern Recognition* 248–255 (IEEE, 2009).

37. Ettinger, D. S. et al. Non-small cell lung cancer, version 3.2022, NCCN Clinical Practice Guidelines in Oncology. *J. Natl Compr. Canc. Netw.* **20**, 497–530 (2022).

38. Pisters, K. et al. Cancer Care Ontario and American Society of Clinical Oncology adjuvant chemotherapy and adjuvant radiation therapy for

stages I–IIIA resectable non small-cell lung cancer guideline. *J. Clin. Oncol.* **25**, 5506–5518 (2007).

39. Martini, N. et al. Incidence of local recurrence and second primary tumors in resected stage I lung cancer. *J. Thorac. Cardiovasc. Surg.* **109**, 120–129 (1995).

40. Felip, E. et al. Adjuvant atezolizumab after adjuvant chemotherapy in resected stage IB–IIIA non-small-cell lung cancer (IMpower010): a randomised, multicentre, open-label, phase 3 trial. *Lancet* **398**, 1344–1357 (2021).

41. Wu, Y. L. et al. Osimertinib in resected EGFR-mutated non-small-cell lung cancer. *N. Engl. J. Med.* **383**, 1711–1723 (2020).

42. Liudahl, S. M. et al. Leukocyte heterogeneity in pancreatic ductal adenocarcinoma: phenotypic and spatial features associated with clinical outcome. *Cancer Discov.* **11**, 2014–2031 (2021).

43. Peng, H. et al. Profiling tumor immune microenvironment of non-small cell lung cancer using multiplex immunofluorescence. *Front. Immunol.* **12**, 750046 (2021).

44. Ginhoux, F., Schultze, J. L., Murray, P. J., Ochando, J. & Biswas, S. K. New insights into the multidimensional concept of macrophage ontogeny, activation and function. *Nat. Immunol.* **17**, 34–40 (2016).

45. Murray, P. J. et al. Macrophage activation and polarization: nomenclature and experimental guidelines. *Immunity* **41**, 14–20 (2014).

46. Vassilvitskii, S. & Arthur, D. in *SODA '07: Proc. 18th Annual ACM–SIAM Symposium on Discrete Algorithms*, 1027–1035 (Society for Industrial and Applied Mathematics, 2007).

47. MacLahlan, G. & Peel, D. *Finite Mixture Models* (John Wiley & Sons, 2000).

Acknowledgements

We thank the IUCPQ Biobank of the Quebec Respiratory Health Research Network and TOCDB at the MUHC for providing access to tissue and clinical data; the Single Cell and Imaging Mass Cytometry Platform (SCIMAP; Y. Wei) and Histology Core Facility (N. Robinson and P. Cruz) at the Rosalind and Morris Goodman Cancer Institute and the Quebec Cancer Consortium; and the Ministère de l'Économie et de l'Innovation du Québec through the Fonds d'accélération des collaborations en santé for financial support. We acknowledge support from the McGill Interdisciplinary Initiative in Infection and Immunity (Mi4). L.A.W. and D.F.Q. acknowledge funding from the Brain Tumour Funders' Collaborative. L.A.W. acknowledges funding from the Canadian Institutes of Health Research (CIHR; PJT-162137) and the Canadian Foundation for Innovation, and holds a Rosalind and Morris Goodman Chair in Lung Cancer Research. D.F.Q. acknowledges funding from the CIHR (PJT-159742 and PJT-178306), the Canadian Foundation for Innovation, and the Canada Research Chairs Program. P.J. acknowledges support from the Fonds de recherche du Québec-Health-Junior 2-Clinical Research Scholars program. M.S. is supported by a Fonds de recherche du Québec-Santé Doctoral award and a Vanier Canada Graduate Scholarship. M.R. is funded by an Arts & Science PDF, University of Toronto.

Author information

Author notes

1. These authors contributed equally: Mark Sorin, Morteza Rezanejad, Elham Karimi

Authors and Affiliations

1. Rosalind and Morris Goodman Cancer Institute, McGill University, Montreal, Quebec, Canada

   Mark Sorin, Elham Karimi, Benoit Fiset, Lysanne Desharnais, Lucas J. M. Perus, Simon Milette, Miranda W. Yu, Sarah M. Maritan, Samuel Doré, Yuhong Wei, Roni Rayes, Peter M. Siegel, Jonathan D. Spicer, Daniela F. Quail & Logan A. Walsh

2. Department of Human Genetics, McGill University, Montreal, Quebec, Canada

Mark Sorin, Lysanne Desharnais, Samuel Doré & Logan A. Walsh

3. Department of Psychology, University of Toronto, Toronto, Ontario, Canada

Morteza Rezanejad

4. Department of Computer Science, University of Toronto, Toronto, Ontario, Canada

Morteza Rezanejad

5. Department of Physiology, Faculty of Medicine, McGill University, Montreal, Quebec, Canada

Lucas J. M. Perus, Simon Milette, Miranda W. Yu & Daniela F. Quail

6. Department of Medicine, Division of Experimental Medicine, McGill University, Montreal, Quebec, Canada

Sarah M. Maritan, Peter M. Siegel, Jonathan D. Spicer & Daniela F. Quail

7. Faculty of Medicine and Health Sciences, McGill University, Montreal, Quebec, Canada

Émilie Pichette

8. Institut Universitaire de Cardiologie et de Pneumologie de Québec, Laval University, Québec City, Quebec, Canada

William Enlow, Andréanne Gagné, Michele Orain, Venkata S. K. Manem, Patrice Desmeules & Philippe Joubert

9. Department of Mathematics and Computer Science, University of Quebec at Trois-Rivières, Trois-Rivières, Quebec, Canada

Venkata S. K. Manem

10. Department of Biochemistry, Faculty of Medicine, McGill University, Montreal, Quebec, Canada

Peter M. Siegel

11. Department of Pathology, McGill University, Montreal, Quebec, Canada

Sophie Camilleri-Broët & Pierre Olivier Fiset

12. Department of Surgery, McGill University Health Center, Montreal, Quebec, Canada

Jonathan D. Spicer

Contributions

M.S., M.R., E.K., P.M.S., J.D.S., D.F.Q., P.J. and L.A.W. designed the study, reviewed the data and wrote the manuscript. M.S., E.K., M.R. and L.A.W. oversaw and performed all experiments and data analysis. E.K., M.R. and B.F. wrote all the code. L.J.M.P., Y.W., D.F.Q. and L.A.W. designed, optimized and performed IMC protocols. L.D., L.J.M.P., S.M., M.W.Y., S.M.M., S.D., Y.W. and R.R. provided experimental support, which included antibody and protocol optimization, image acquisition, data analysis and generating schematics. É.P., W.E., A.G., M.O., V.S.K.M., S.C.-B., P.D. and P.J. provided human tissue samples, built the patient tissue microarrays (TMAs), and collected and curated all clinical data including the assessment of pathological patterns. Clinical pathologists P.O.F., S.C.-B., P.D. and P.J. reviewed all samples. All authors reviewed and approved the manuscript.

Corresponding authors

Correspondence to Daniela F. Quail, Philippe Joubert or Logan A. Walsh.

Ethics declarations

Competing interests

The authors declare no competing interest.

Peer review

Peer review information

Nature thanks Benjamin Izar and the other, anonymous, reviewer(s) for their contribution to the peer review of this work.

Additional information

Publisher's note Springer Nature remains neutral with regard to jurisdictional claims in published maps and institutional affiliations.

Extended data figures and tables

Extended Data Fig. 1 Imaging mass cytometry segmentation pipeline and antibody panel.

a, Flowchart for inclusion and exclusion criteria of 576 lung adenocarcinoma cores. **b**, Schematic of IMC segmentation pipeline representing antibody conjugation of metal isotopes, labeling, laser ablation, CyTOF acquisition, image tiling, structure tensor response, scale selection and final output. **c**, Schematic depiction of the workflow and specific markers used for lineage assignment. Panels **a**–**c** were created with BioRender. **d**, Average expression of non-lineage markers across cell types in lung adenocarcinoma tissue stained with the panel of isotope-conjugated antibodies; $CD163^{-}$Mac, $CD163^{-}$ macrophage; $CD163^{+}$ Mac, $CD163^{+}$ macrophage; T_c, $CD8^{+}$ T cell; T_{reg}, regulatory T cell, T_H, $CD4^{+}$ T cell; Cl Mo, classical monocyte; Int Mo, intermediate monocyte; Non-Cl Mo, non-classical monocyte; NK Cell, natural killer cell.

Extended Data Fig. 2 Antibody panel validation 1.

Validation of 18 antibodies used for multiplex IMC across positive and negative controls. Scale bars represent 50 µm.

Extended Data Fig. 3 Antibody panel validation 2.

Validation of 17 antibodies used for multiplex IMC across positive and negative controls. Scale bars represent 50 µm.

Extended Data Fig. 4 Antibody panel validation 3.

Lineage marker staining and corresponding cell segmentation in control tissue. Colour code for cell segmentation is provided. Scale bars represent 100 µm.

Extended Data Fig. 5 Survival analysis of distinct clinical variables.

a, Pie chart depicting the proportion of undefined cells that are $CD45^{+}$ across 416 lung adenocarcinoma patients. **b**, Kaplan–Meier curves of overall survival for 416 lung adenocarcinoma patients based on histological subgroup (Lepidic n = 40, Papillary n = 33, Acinar n = 190, Micropapillary n = 35, Solid n = 118. For P values, see Supplementary Table 3. **c**, Heatmap depicting the Spearman's rank correlation coefficient with high coefficients in red and low coefficients in blue between indicated cell types across the five histological subgroups (Lepidic n = 40 images, Papillary n = 33 images, Acinar n = 190 images, Micropapillary n = 35 images, Solid n = 118 images). **d**, Kaplan–Meier curves of overall survival for 416 lung adenocarcinoma patients based on sex (Female n = 233, Male n = 183). **e**, Heatmap depicting cell-cell interaction/avoidance among B cells in the $CD40^{+}$ B cell high (z score ≥0; %total B cells) and $CD40^{+}$ B cell low (z score <0; %total B cells) groups. Each rectangle depicts significant pairwise cell-type interaction (red) or avoidance (blue) between indicated cell types (n = 186 images for the $CD40^{+}$ B cell high group; n = 230 images for the $CD40^{+}$ B cell low group; 1,000 permutations each). Statistical analysis (**b, d:** log-rank test).

Extended Data Fig. 6 Activation markers and single-cell phenotypes in lung adenocarcinoma.

a, T-distributed stochastic neighbour embedding (t-SNE) of 108,387 endothelial cells. pSTAT3, Ki-67, CD39 and pERK expression within the endothelial cluster is shown. **b**, t-SNE plots of 9,480 mast cells, 42,427 neutrophils, 1,407 dendritic cells, 10,000 subsampled CD163- macrophages, 39,502 $CD163^+$ macrophages, 37,653 classical monocytes, 8,330 intermediate monocytes and 17,029 non-classical monocytes. Ki-67, HIF1α, MMP9, ARG1, pERK, MCSFR, PD-1, B7-H3, BCL2, B7-H4, CD40, CC3, CD39, PD-L1 and pSTAT3 expression in the myeloid compartment is shown. **c**, t-SNE plots of 62,941 B cells, 98,396 T_c, 147,980 T_H, 19,839 T_{reg} and 23,995 T other cells. Ki-67, FOXP3, pERK, CD40, CD39, BCL2, PD-1 and pSTAT3 expression in the lymphoid compartment is shown. **d-e**, Prevalence of Ki-67^+ endothelial cells (Comparison between Lepidic and Solid: * $P = 0.0362$. Comparison between Acinar and Solid: * $P = 0.0185$) and pERK+ T_H cells (Comparison between Lepidic and Solid: **** $P = <0.0001$. Comparison between Lepidic and Micropapillary: *** $P = 0.0004$. Comparison between Lepidic and Acinar: *** $P = 0.0003$. Comparison between Lepidic and Papillary: * $P = 0.0102$. Comparison between Acinar and Solid: * $P = 0.0288$) as a proportion of endothelial and T_H cells respectively, across histological subgroups in 416 lung adenocarcinoma patients (Lepidic n = 40, Papillary n = 33, Acinar n = 190, Micropapillary n = 35, Solid n = 118). Mean ± SEM. Statistical analysis (**d-e:** one-way ANOVA with Tukey multiple comparison test).

Extended Data Fig. 7 Variability in 10 cellular neighbourhoods across clinical variables in lung adenocarcinoma.

a, Heatmap of 10 cellular neighbourhoods discovered in 416 lung adenocarcinoma patients. **b**, Representative images of 10 cellular neighbourhoods using Voronoi diagrams. **c**, Bubble plot where circle colour indicates which of the two comparisons on the y-axis has higher levels of the cell type on the x-axis (Female n = 233, Male n = 183), age (<75 yo n = 369, ≥75 yo n = 47), BMI (<30 n = 346, ≥30 n = 70), smoking status (Smoker n = 376, Non-smoker n = 38), pack-years (1—30 n = 89, ≥30 n = 256), stage (I-II

n = 365, III-IV n = 50), progression status (Progression n = 64, No progression n = 340) and histological subgroup (Lepidic n = 40, Papillary n = 33, Acinar n = 190, Micropapillary n = 35, Solid n = 118). The size of the circle represents the level of significance. Survival^{low} refers to survival in the context of low (z score <0) prevalence of depicted 10 cellular neighbourhoods. The black boxes depict associations referenced in the text. For exact P values, see Supplementary Table 6. Statistical analysis (**a:** log-rank test, **c:** FDR-corrected two-tailed Student t-test for sex, age, BMI, smoking status, pack-years, stage, progression status; one-way ANOVA with Tukey multiple comparison test for histological subgroup; log-rank test for survival).

Extended Data Fig. 8 Heatmaps of 10 cellular neighbourhoods with 3, 5, 20 and 30 closest cells (n) discovered in 416 lung adenocarcinoma patients.

a, Tables depict result of log-rank test of the overall survival for 416 lung adenocarcinoma patients based on low (z score <0) and high (z score ≥0) prevalence. Black p values indicate no significant difference ($p \geq 0.05$) in survival between the two groups. Blue p values indicate better survival ($p < 0.05$) with high prevalence and red p values indicate better survival ($p < 0.05$) with low prevalence of the depicted groups. **b**, Kaplan–Meier curves of overall survival for lung adenocarcinoma patients based on low (z score <0) and high (z score ≥0) prevalence of T_H cells and high (z score ≥0) prevalence of B cells. **c**, Correlation of T cell and B cell prevalence. **d**, Correlation of immune infiltrate and B cell prevalence. Statistical analysis (**b:** Log-rank test).

Extended Data Fig. 9 Variability in 30 cellular neighbourhoods across clinical variables in lung adenocarcinoma.

a, Bubble plot where circle colour indicates which of the two comparisons on the y-axis has higher levels of the cell type on the x-axis (Female n = 233, Male n = 183), age (<75 yo n = 369, ≥75 yo n = 47), BMI (<30 n = 346, ≥30 n = 70), smoking status (Smoker n = 376, Non-smoker n = 38), pack-years (1-30 n = 89, ≥30 n = 256), stage (I-II n = 365, III-IV n = 50), progression

status (Progression n = 64, No progression n = 340) and histological subgroup (Lepidic n = 40, Papillary n = 33, Acinar n = 190, Micropapillary n = 35, Solid n = 118). The size of the circle represents the level of significance. $Survival^{low}$ refers to survival in the context of low (z score <0) prevalence of depicted 30 cellular neighbourhoods. For exact P values, see Supplementary Table 7. The black boxes depict associations referenced in the text. **b**, Prevalence of 30 cellular neighbourhoods across 5 histological subtypes (Lepidic n = 40, Papillary n = 33, Acinar n = 190, Micropapillary n = 35, Solid n = 118). Mean ± SEM. Statistical analysis (**a:** FDR-corrected two-tailed Student t-test for sex, age, BMI, smoking status, pack-years, stage, progression status; one-way ANOVA with Tukey multiple comparison test for histological subgroup; log-rank test for survival).

Extended Data Fig. 10 Machine learning of imaging mass cytometry data improves prediction of progression.

Accuracy of clinical progression prediction in stage I lung adenocarcinoma patients (n = 286) in the **a**, clinical variables; **b**, cell frequency; **c**, lineage markers and **d**, "all markers" models. Comparison between baseline and the lineage marker model: * P = 0.0343. Comparison between baseline and the "all marker" model : * P = 0.0355. Mean ± SEM. Statistical analysis (**a—d:** two-tailed Student t-test).

Supplementary information

Supplementary Information

This file contains Supplementary Data 1–2 and Supplementary Tables 1–15. The Supplementary Data describes single cell prevalence across clinical variables and the association of cellular neighborhood prevalence with survival across the five predominant histological patterns of lung adenocarcinoma. The Supplementary Tables describe the clinical information and summarize statistical analyses.

Reporting Summary

Rights and permissions

Open Access This article is licensed under a Creative Commons Attribution 4.0 International License, which permits use, sharing, adaptation, distribution and reproduction in any medium or format, as long as you give appropriate credit to the original author(s) and the source, provide a link to the Creative Commons licence, and indicate if changes were made. The images or other third party material in this article are included in the article's Creative Commons licence, unless indicated otherwise in a credit line to the material. If material is not included in the article's Creative Commons licence and your intended use is not permitted by statutory regulation or exceeds the permitted use, you will need to obtain permission directly from the copyright holder. To view a copy of this licence, visit http://creativecommons.org/licenses/by/4.0/.

Reprints and Permissions

About this article

Cite this article

Sorin, M., Rezanejad, M., Karimi, E. *et al.* Single-cell spatial landscapes of the lung tumour immune microenvironment. *Nature* **614**, 548–554 (2023). https://doi.org/10.1038/s41586-022-05672-3

- Received: 24 March 2022
- Accepted: 20 December 2022
- Published: 01 February 2023
- Issue Date: 16 February 2023
- DOI: https://doi.org/10.1038/s41586-022-05672-3

Share this article

Anyone you share the following link with will be able to read this content:

Get shareable link

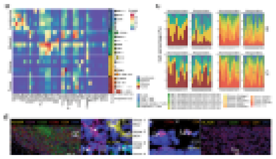
Sorry, a shareable link is not currently available for this article.

Copy to clipboard

Provided by the Springer Nature SharedIt content-sharing initiative

---

This article was downloaded by **calibre** from https://www.nature.com/articles/s41586-022-05672-3



Multiplexed imaging mass cytometry reveals distinct tumor-immune microenvironments linked to immunotherapy responses in melanoma

21 October 2022

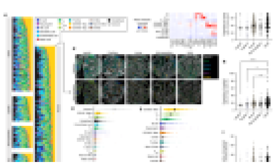
Xu Xiao, Qian Guo, … Rongshan Yu



An integrated pipeline for comprehensive analysis of immune cells in human brain tumor clinical samples

30 August 2021

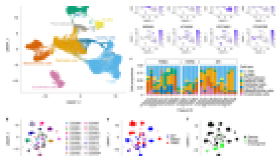
Roeltje R. Maas, Klara Soukup, … Johanna A. Joyce



Single-cell spatial landscapes of the lung tumour immune microenvironment

01 February 2023

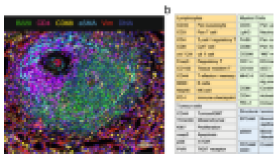
Mark Sorin, Morteza Rezanejad, … Logan A. Walsh



[A single-cell and spatially resolved atlas of human breast cancers]

06 September 2021

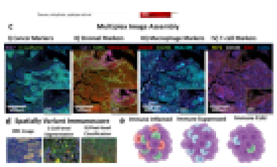
Sunny Z. Wu, Ghamdan Al-Eryani, … Alexander Swarbrick



[Characterisation of tumour microenvironment remodelling following oncogene inhibition in preclinical studies with imaging mass cytometry]

08 October 2021

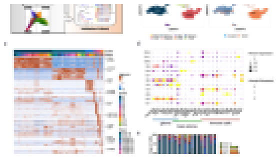
Febe van Maldegem, Karishma Valand, … Julian Downward



[Spatially variant immune infiltration scoring in human cancer tissues]

01 September 2022

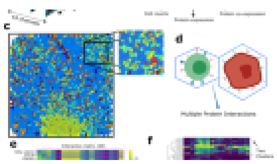
Mayar Allam, Thomas Hu, … Ahmet F. Coskun



[**Single-cell analysis of human glioma and immune cells identifies S100A4 as an immunotherapy target**]

09 February 2022

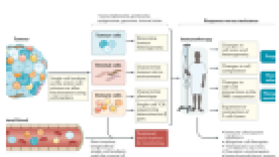
Nourhan Abdelfattah, Parveen Kumar, … Kyuson Yun



[**Multiplexed imaging analysis of the tumor-immune microenvironment reveals predictors of outcome in triple-negative breast cancer**]

09 July 2021

Aalok Patwa, Rikiya Yamashita, … Daniel L. Rubin



[**Applying high-dimensional single-cell technologies to the analysis of cancer immunotherapy**]

04 December 2020

Satyen H. Gohil, J. Bryan Iorgulescu, … Kenneth J. Livak

- Article
- Open Access

- Published: 01 February 2023

Single-cell spatial immune landscapes of primary and metastatic brain tumours

- Elham Karimi,
- Miranda W. Yu,
- Sarah M. Maritan,
- Lucas J. M. Perus,
- Morteza Rezanejad,
- Mark Sorin,
- Matthew Dankner,
- Parvaneh Fallah,
- Samuel Doré,
- Dongmei Zuo,
- Benoit Fiset,
- Daan J. Kloosterman,
- LeeAnn Ramsay,
- Yuhong Wei,
- Stephanie Lam,
- Roa Alsajjan,
- Ian R. Watson,
- Gloria Roldan Urgoiti,
- Morag Park,
- Dieta Brandsma,
- Donna L. Senger,
- Jennifer A. Chan,
- Leila Akkari,
- Kevin Petrecca,
- Marie-Christine Guiot,
- Peter M. Siegel ,
- Daniela F. Quail &
- …

- Logan A. Walsh

Show authors

Nature **volume 614**, pages 555–563 (2023)

- 29k Accesses
- 149 Altmetric
- Metrics details

Abstract

Single-cell technologies have enabled the characterization of the tumour microenvironment at unprecedented depth and have revealed vast cellular diversity among tumour cells and their niche. Anti-tumour immunity relies on cell–cell relationships within the tumour microenvironment[1,2], yet many single-cell studies lack spatial context and rely on dissociated tissues[3]. Here we applied imaging mass cytometry to characterize the immunological landscape of 139 high-grade glioma and 46 brain metastasis tumours from patients. Single-cell analysis of more than 1.1 million cells across 389 high-dimensional histopathology images enabled the spatial resolution of immune lineages and activation states, revealing differences in immune landscapes between primary tumours and brain metastases from diverse solid cancers. These analyses revealed cellular neighbourhoods associated with survival in patients with glioblastoma, which we leveraged to identify a unique population of myeloperoxidase (MPO)-positive macrophages associated with long-term survival. Our findings provide insight into the biology of primary and metastatic brain tumours, reinforcing the value of integrating spatial resolution to single-cell datasets to dissect the microenvironmental contexture of cancer.

Main

Brain tumours comprise a diverse repertoire of malignancies that arise either from within the brain or from cancer cells that have spread from other

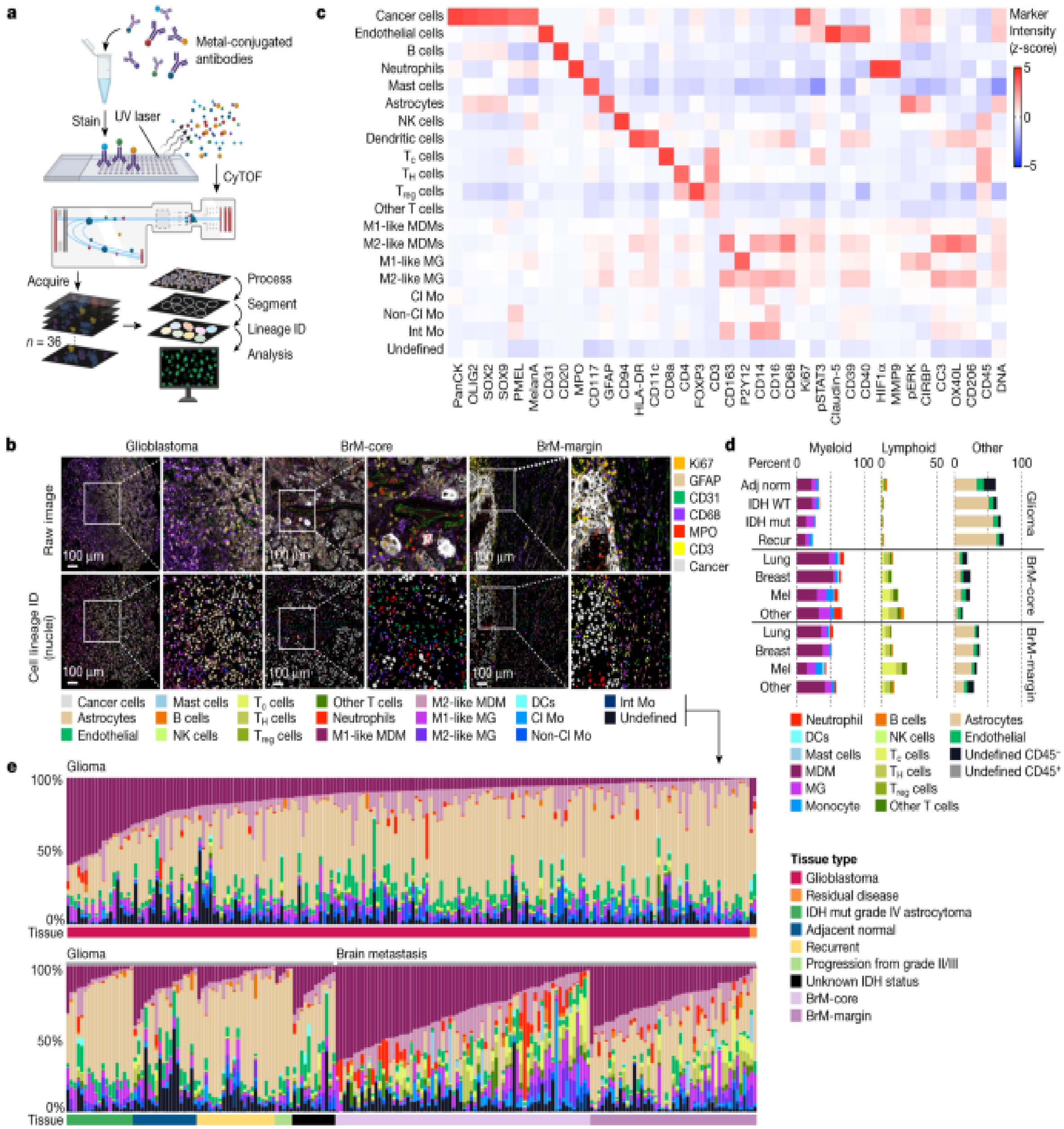
primary sites. The most common types of cancer representing these two classes include glioblastoma (around 50% of all primary brain malignancies in adults[4]) and brain metastasis (BrM) (about 90% of all brain malignancies), with BrM most frequently arising from melanoma, lung or breast tumours[5]. Besides surgery, cytotoxic therapies that target tumour cells—such as stereotactic radiotherapy—are often the first line of treatment, but they yield minimal benefit, with survival beyond 2 years being rare[6,7]. The tumour microenvironment (TME) is a major regulator of cancer progression, whose therapeutic value has grown with the advent of immune checkpoint blockade[1,2]. Compared with other tissues, the brain TME has a distinct composition, dominated by functionally diverse astrocytes and pro-tumorigenic macrophages that are ontogenically distinct, with the exclusion of infiltrating lymphocytes[8]. Many promising therapeutic targets within the TME of other cancers have been revealed by single-cell profiling technologies; for example, multiplex imaging has enabled the discovery of several new biomarkers that are predictive of outcomes and therapeutic efficacy in breast[9,10,11,12], colorectal[13] and pancreatic cancer[14]. However, comprehensive profiling of the brain TME has seen fewer (albeit important[15,16,17,18,19]) advances compared with other malignancies, and so far none have included the spatial characterization of individual cells within their niche using highly multiplexed histology. Here we use imaging mass cytometry (IMC) on patient samples to characterize the brain TME of glioblastoma and BrM, and explore how spatially resolved features relate to clinical outcomes.

Mapping the brain TME with IMC

To comprehensively profile the cellular composition and spatial organization of the brain TME, we optimized a highly multiplexed antibody panel and IMC pipeline (Extended Data Figs. 1–3, Supplementary Figs. 1–3 and Supplementary Table 1). Antibodies were validated in normal and malignant tissues on the basis of their expected staining pattern (Extended Data Fig. 3a and Supplementary Figs. 1 and 2). We acquired 389 high-dimensional histopathology images representing 139 high-grade glioma and 46 BrM patient tumours (Fig. 1a,b and Extended Data Fig. 1a). Gliomas comprised resected tissues obtained during surgery (270 images in total, 192 from

primary glioblastoma), including a subset from long-term survivors (78 images). BrM images were derived from multiple primary malignancies, including lung (51 images), breast (29 images), melanoma (19 images) and other primary sources (20 images), with patient-matched samples from the centre of the metastatic lesion (BrM-core) and tissue interface (BrM-margin). Images were segmented into 1,163,362 total cells and a supervised lineage assignment approach was used to classify tumour cells, astrocytes, blood vessels and more than 16 immune cell populations using canonical identity markers (Fig. 1c and Extended Data Figs. 1b and 2). As expected, within the stromal compartment across all tissues, major cell populations included $GFAP^+$ astrocytes and $CD68^+$ macrophages, whereas lymphocytes were relatively infrequent (Fig. 1d,e).

Fig. 1: IMC reveals cell dynamics within the brain TME.



a, Schematic of the IMC pipeline applied to glioma and BrM tissue microarrays. Samples were subject to multiplex staining and data were acquired using cytometry by time-of-flight (CyTOF). Cell segmentation and lineage assignment was performed prior to spatial analysis. Created with BioRender.com. **b**, IMC images from glioblastoma, BrM-core and BrM-margin samples (top) and corresponding lineage assignment (bottom), with magnified regions to the right of each image. The colour codes for IMC markers (top right) and lineage assignment (bottom) are provided (representative of $n = 389$ images). Scale bars, 100 μm. **c**, Heat map showing

relative average expression of all markers across cell populations identified using IMC ($n = 389$ images). A subset of markers was specific to the glioma IMC antibody panel (SOX2, SOX9, OLIG2, CD40, CD206; $n = 270$ images) and a second subset to the BrM IMC antibody panel (pan-cytokeratin, PMEL, MelanA, pERK, CIRBP; $n = 119$ images). **d**, Stacked bar graph of the indicated cell types as a percentage of all cells within the TME according to clinical subgroups. Glioma: adjacent normal (adj norm), $n = 18$; primary isocitrate dehydrogenase (IDH) wild type (WT), $n = 192$; primary IDH mutant (mut), $n = 19$; recurrent (recur), $n = 22$. BrM-core: lung, $n = 29$; breast, $n = 17$; melanoma (mel), $n = 13$; other, $n = 13$. BrM-margin: lung, $n = 22$; breast, $n = 12$; melanoma, $n = 6$; other, $n = 7$. Data are mean values; n refers to number of images. **e**, The distribution of cell populations as a percentage of all cells in the TME, sorted by tissue type. Cell frequencies for each image ($n = 389$ images) are displayed as vertical bars (colours correspond to cell lineages in **b**) and the associated tissue type is indicated in the horizontal panels below (colours indicated in the legend, right). Cl Mo, classical monocyte; DC, dendritic cells; Int Mo, intermediate monocyte; MG, microglia; Non-Cl Mo, non-classical monocyte; NK cells, natural killer cells; panCK, pan-cytokeratin; T_c, cytotoxic T cell; T_H, T helper; T_{reg}, T regulatory cell; other T cells, $CD8^{-}CD4^{-}$ double-negative T cells.

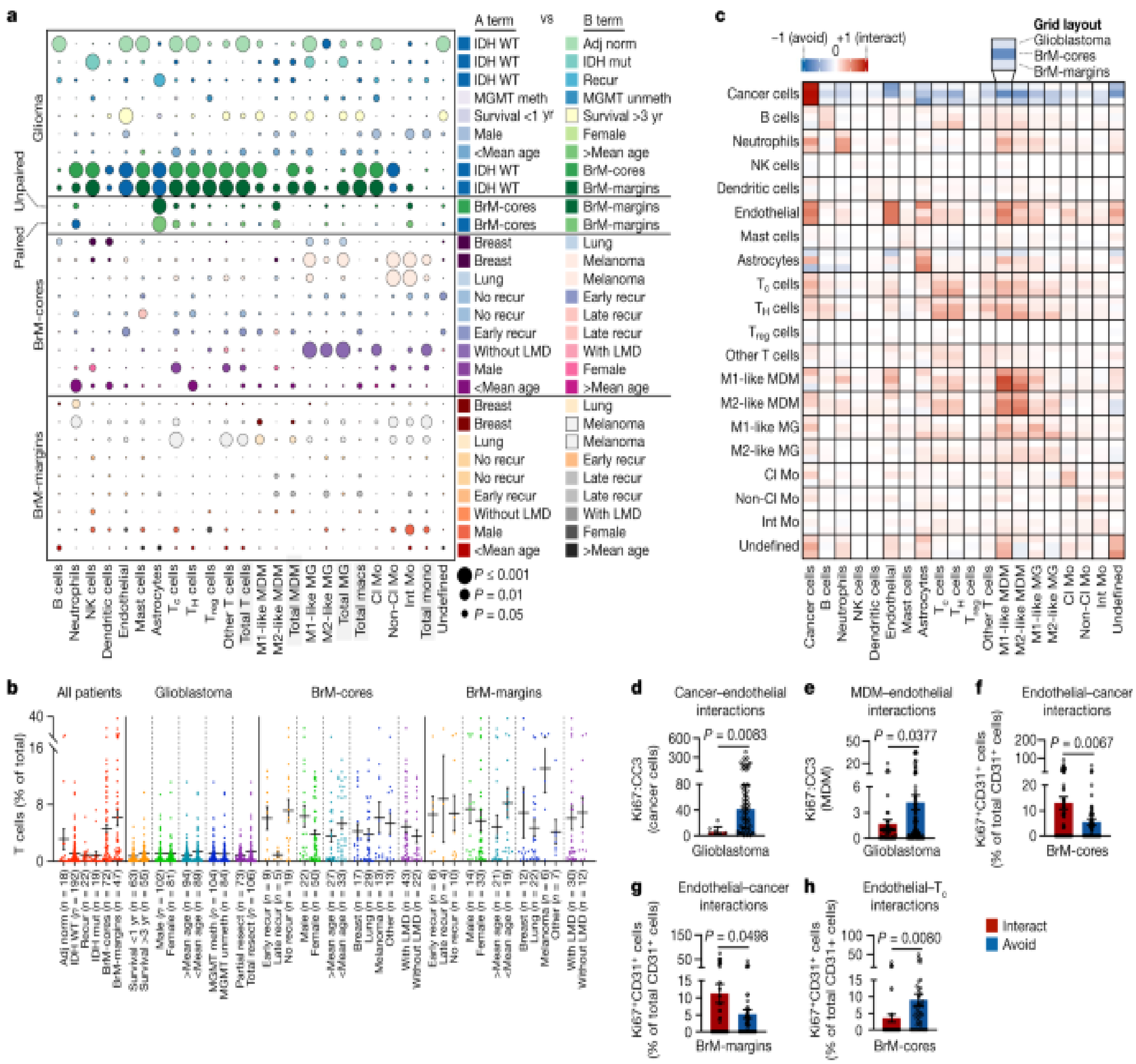
Macrophages stimulated in vitro can be defined along a continuum of activation states; although usually considered M2-like, tumour-associated macrophage activation is much more complex in situ and does not necessarily conform to the M1/M2 paradigm[19,20]. With this limitation in mind, we subdivided macrophages by ontogeny and activation state; expression of the purinergic receptor P2Y12 distinguished tissue-resident microglia from monocyte-derived macrophages[19] (MDMs), and CD163 expression distinguished putative ‘M2-like’ from ‘M1-like’ cells[21,22] (Fig. 1c and Supplementary Figs. 3, 4 and 5a). Additional pro-tumorigenic markers, including CD206 and CD39, were also enriched in the $CD163^{+}$ M2-like macrophage fraction (Supplementary Fig. 5b,c). Consistent with previous reports[15,16], MDMs and microglia were the dominant immune populations across all samples, comprising approximately 30.5% and 9.2% of the TME, respectively (Fig. 1d).

Single-cell interaction networks

We quantified the frequency of each cell type as a percentage of the total number of cells within each image, and compared clinically relevant subgroups of patients (Fig. 2a,b and Supplementary Figs. 6 and 7). Cell density within each image area was similarly assessed (Extended Data Fig. 4a and Supplementary Fig. 8). As expected, there was an increase in the frequency of most cell types in adjacent normal tissue compared with glioblastoma (Fig. 2a), whereas this trend was reversed when examining cell density (Extended Data Fig. 4a), reflecting the sparse cellular landscape of the normal brain niche. In IDH wild-type (glioblastoma) versus IDH mutant (grade IV astrocytoma) tumours[23], NK cells were reduced in frequency (Fig. 2a). Moreover, there was a lower proportion of $CD16^+$ (cytotoxic) than $CD16^−$ (immature) NK cell subsets in glioblastoma tumours (Supplementary Fig. 7b,c), consistent with previous findings[15]. We also found a higher frequency and density of recruited MDMs (but not microglia) in IDH wild-type versus mutant tumours (Fig. 2a and Extended Data Fig. 4a), suggestive of enhanced peripheral recruitment of macrophages with greater disease severity[24]. Parsing glioblastoma samples by MGMT methylation status (a prognostic indicator) unveiled minimal immunological differences; however, subdivision by survival time revealed a higher endothelial frequency in tumours from long-term survivors (LTSs) (overall survival more than three years) compared with those from short-term survivors (STSs) (overall survival less than one year) (Fig. 2a). This was unexpected, and may be related to efficiencies in chemotherapy delivery. Alternatively, features of the vascular niche may confer a survival benefit in some patients. Compared with STS tumours, LTS tumours also had a higher frequency of $CD8^−CD4^−$ T cells (potentially including γδ T cells, which are associated with increased survival[25]) and M1-like macrophage accumulation, with no difference in M2-like macrophages (Fig. 2a). Across glioblastoma clinical subgroups, very few lymphocytes were observed based on frequency (Fig. 2b) as well as density (Supplementary Fig. 8), supporting observations that glioblastomas are T cell deserts that exhibit poor responses to immune checkpoint blockade[26]. However, a subset of glioblastoma images exhibited unusually high T cell frequencies (more than 5% of cells in the TME). These samples were enriched for $CD8^+$, $CD4^+$ and $CD8^−CD4^−$ T cell subsets, but

not immunosuppressive T_{reg} cells, and exhibited a 62% increase in mean survival time compared with samples with low numbers of T cells (less than 5% of cells in the TME) (Extended Data Fig. 4b,c). Finally, we observed higher frequencies of peripherally derived monocytes in tumours from male patients than in those from female patients, coinciding with higher frequencies of endothelial cells (Fig. 2a), highlighting putative sexual dimorphism in immune responses to cancer.

Fig. 2: Single-cell interaction networks in high-dimensional histopathology images represent clinical subgroups of patients with brain tumours.



a, Cell frequency comparisons between clinical subgroups of patients, corresponding to data in **b** and Supplementary Fig. 6. Within each row, the bubble colour indicates the clinical subgroup with the higher cell type representation (A term versus B term, right), and the bubble size indicates the *P*-value. Two-sided Student's *t*-test, unpaired unless indicated otherwise; paired analyses are from patient-matched samples. LMD, leptomeningeal disease; Meth, methylated; unmeth, unmethylated; recur, recurrence. **b**, T cell frequencies as a percentage of total cells across clinical subgroups. Data are mean ± s.e.m.; all data points overlaid; *n* refers to the number of images. Resect, resection. **c**, Heat map of pairwise interaction–avoidance scores for glioblastoma (top rows, $n = 192$ images), BrM-cores (middle rows, $n = 59$ images) and BrM-margins (bottom rows, $n = 40$ images). Associations should be read row-to-column. **d**, Ki67:CC3 ratio in cancer cells interacting with (red; $n = 107$ cells across 6 images) or avoiding (blue; $n = 11{,}163$ cells across 67 images) endothelial cells in glioblastoma. Data are median ± interquartile range; two-sided Mann–Whitney test. **e**, Ki67:CC3 ratio in MDMs interacting with (red; $n = 270$ cells across 51 images) or avoiding (blue; $n = 2{,}808$ cells across 94 images) endothelial cells in glioblastoma. Data are mean ± s.e.m.; two-sided Student's *t*-test. **f**, Ki67 expression in endothelial cells interacting with (red) or avoiding (blue) cancer cells in BrM-cores. Data are mean ± s.e.m.; $n = 347$ cells across 61 images per group; two-sided Student's *t*-test. **g**, Ki67 expression in endothelial cells interacting with (red) or avoiding (blue) cancer cells in BrM-margins. Data are mean ± s.e.m.; $n = 156$ cells across 45 images per group; two-sided Student's *t*-test. **h**, Ki67 expression in endothelial cells interacting with (red) or avoiding (blue) T_c cells in BrM-cores. Data are mean ± s.e.m.; $n = 235$ cells across 41 images per group; two-sided Student's *t*-test. In **d**–**h**, images with zero cells of interest or lacking pairwise interactions of interest were excluded from analysis.

We next examined immune cell dynamics across BrM samples. We found an increase in the frequency and density of NK cells (notably, those that were $CD16^+$[15]), neutrophils, macrophages, classical monocytes and T cells (including T_{reg} cells[15]) compared with glioblastoma, and a decrease in dendritic cells and non-classical monocytes (Fig. 2a, Extended Data Fig. 4a and Supplementary Fig. 7b,c). When examining immunological changes associated with BrM progression in BrM-cores, we found increases in

monocytes and microglia in patients without leptomeningeal disease (Fig. 2a) or local recurrence (after more than 724 days) (Supplementary Fig. 9a), suggesting a putative protective role for these cells in this context. In comparing BrMs arising from distinct primary tumour sites, the degree of BrM-associated inflammation (that is, the frequency of immune cell types analysed) was generally lowest in tumours originating from breast tumours, highest in those from melanoma, with an intermediate level in tumours originating from lung. Melanoma BrM were enriched for monocytes and microglia compared with lung and breast BrM, and exhibited a pronounced accumulation of $CD8^+$ T cells in the tumour margin as a percentage of total cells (Fig. 2a and Supplementary Fig. 9b). This is consistent with observations that, unlike glioblastoma, BrM displays some vulnerability to immune checkpoint blockade—particularly melanoma BrM[27,28]. Similar to glioblastoma, we observed sexual dimorphism in BrM-cores, with more $CD8^+$ T cells in those from male patients compared with those from female patients. We additionally found more neutrophils, dendritic cells and $CD4^+$ T cells in BrM-cores from younger patients compared with those from older patients (Fig. 2a).

To characterize the patterns of communication between individual cells, we interrogated the positional architecture of brain tumours using permutation tests to quantify cell–cell co-localization and identify interaction or avoidance behaviours between cell pairs[11] (Fig. 2c). This approach revealed that cancer cells in BrM were more likely to avoid most non-cancer lineages within the TME compared with glioblastoma (Fig. 2c and Extended Data Fig. 5a), indicating that the topography of cancer cells in BrM is more compact relative to the dispersed nature of glioblastoma, consistent with the observed pattern of homotypic cellular interactions (Fig. 2c). Global heterotypic cellular interactions were increased in BrM compared with glioblastoma (Fig. 2c and Extended Data Fig. 5b), suggesting that the ways in which glioblastoma and BrM interface with the surrounding brain parenchyma are fundamentally different, despite sharing a common tissue niche.

The vasculature is a key component of the brain TME in both glioblastoma and BrM; for example, the perivascular niche maintains the glioma-initiating cell pool[29], and the blood-brain barrier (BBB) regulates BrM dissemination.

Given our observation of endothelial enrichment in LTS tumours (Fig. 2a), we examined cellular dynamics within the vascular niche of glioblastoma. As expected, endothelial cells exhibited a strong likelihood of interacting with astrocytes in glioblastoma, essential for BBB function (Fig. 2c). Endothelial cells also showed strong interactions with cancer cells (Fig. 2c); in particular, perivascular cancer cells exhibited reduced Ki67:CC3 ratios compared with those that avoided blood vessels (Fig. 2d and Extended Data Fig. 6a), suggesting that direct contact with the vasculature may impede cancer cell expansion[30]—a finding that may provide insight into LTS tumour biology. Consistent with previous reports, we observed that MDMs, but not monocytes or microglia, also displayed a strong tendency to interact with endothelial cells in glioblastoma[15,16] (Fig. 2c), despite a weak correlation between the frequencies of MDMs and endothelial cells (Extended Data Fig. 6b). This highlights that these interactions are spatially coordinated rather than simply resulting from associations in abundance. Mirroring tumour cells, MDMs displayed lower Ki67:CC3 ratios when engaged with the endothelium compared with those that avoided direct endothelial interactions (Fig. 2e and Extended Data Fig. 6a), recapitulating the relationship between proliferating brain macrophages and glioma progression[31]. Finally, despite their low prevalence, there was a modest tendency for T cells to interact with endothelial cells or MDMs (Fig. 2c), prompting us to further dissect these relationships. Specifically, we found more $CD40^{+}$ MDMs interacting with T_H cells than $CD40^{-}$ MDMs (Extended Data Fig. 6c), CD40 being a co-stimulatory protein implicated in T cell recruitment in glioma[32]. When examining vessel proximity, perivascular M1-like MDMs exhibited higher CD40 expression than those further away from blood vessels (Extended Data Fig. 6d) and similarly, perivascular M2-like MDMs expressed high levels of OX40L (another co-stimulatory molecule) (Extended Data Fig. 6e). Together, these data allude to the existence of vascular microniches—where macrophages may provide beneficial signalling cues to T cells and cancer cell expansion is kept in check—and support a role for blood vessels in shaping the brain TME contexture.

We next explored vascular interactions in BrM. Similar to glioblastoma, endothelial cells had a high tendency to interact with cancer cells in BrM (Fig. 2c), which is essential for metastatic colonization following

extravasation[33,34]. Within both BrM-cores and BrM-margins, endothelial cells that were associated with cancer cells displayed increased Ki67 expression, reminiscent of microvascular proliferation (Fig. 2f,g and Extended Data Fig. 6a). This was of interest given the relationship between microvascular proliferation and high-grade glioma[35], potentially suggesting localized cellular niches of more aggressive tumour features within metastases. Endothelial cell proliferation appeared to be suppressed via interactions with $CD8^+$ T cells—an effect that was specific to BrM-cores (Fig. 2h and Extended Data Fig. 6f). Notably, the expression of claudin-5—a tight junction protein in the BBB implicated in vascular permeability in BrM[36,37]—was spatially regulated. Within BrM-cores (but not BrM-margins), cancer-adjacent endothelial cells exhibited lower claudin-5 expression compared with cancer-avoiding endothelial cells (Extended Data Fig. 6g). Moreover, the frequency of claudin-5^+ cancer-adjacent endothelial cells was lower in BrM-cores compared with BrM-margins (Extended Data Fig. 6g), supporting a model of vascular co-option during BrM colonization that is initiated in regions of weakened endothelial junctions[34,38,39]. As downregulation of claudin-5 is associated with peritumoural brain oedema[40], we subdivided BrM-cores by the degree of oedema as assessed by pre-operative MRI. Endothelial cells that were associated with cancer cells displayed reduced claudin-5 in BrMs with a moderate-high degree of peritumoural oedema (oedema score 2–3); this relationship was absent in BrMs with absent or low peritumoural oedema (oedema score 0–1.5) (Extended Data Fig. 6h). These data highlight a spatially resolved link between BBB integrity and metastasis, and how it relates to vascular proliferation and oedema.

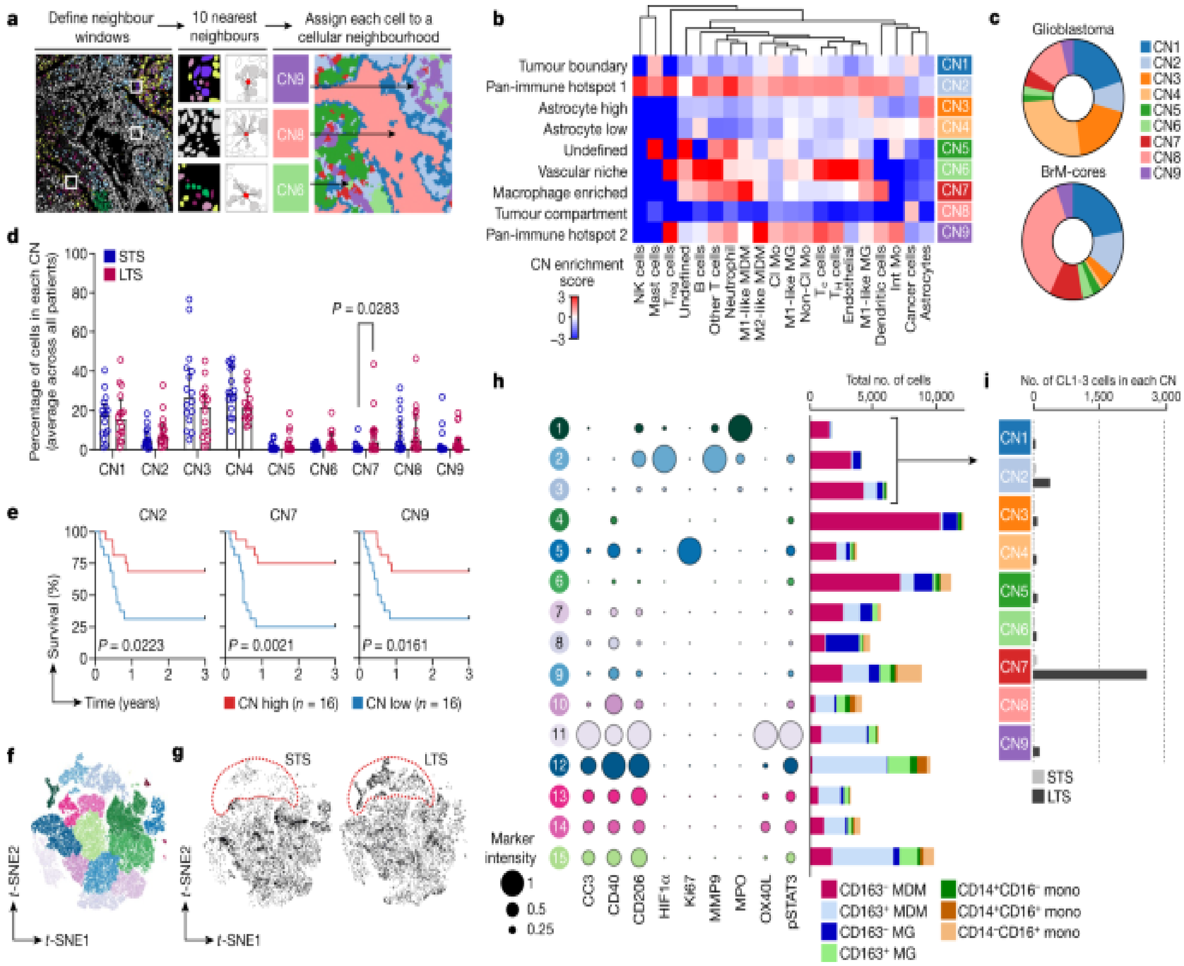
Spatial cellular neighbourhoods

We next explored whether multicellular structures within tumours, rather than pairwise interactions, would provide meaningful insights into the organization and prognostic value of brain TME dynamics. Two variables affect cellular neighbourhood assessment: the number of interacting cells within a neighbourhood (N) and the number of total cellular neighbourhoods (CNs). To gain insight into how the size and complexity of neighbourhoods relate to survival, we first used our glioblastoma dataset as a

model, and altered the number of nearest spatial neighbours for each individual cell ($N = 3,5,10,20,30$) while maintaining a constant number of neighbourhoods (CN = 9, as in previous work[13]). In most cases, CNs enriched in M1-like MDMs were associated with increased survival, regardless of the number of nearest spatial neighbours (Extended Data Fig. 7). Notably, the frequency of M1-like MDMs was not associated with overall survival (Supplementary Fig. 7a), highlighting the value of spatial relationships rather than abundance alone. To resolve specific cellular interactions that underlie this survival advantage, we forced the number of CNs to 30 (rather than 9) while maintaining $N = 10$ nearest neighbours. Using this approach, we resolved six CNs that were enriched for M1-like MDMs (Extended Data Fig. 8a). Of these, only two maintained their relationship with prolonged survival; these CNs were both primarily composed of M1-like MDMs, neutrophils and M1-like microglia. In the remaining M1-like MDM-enriched CNs, the survival relationship was lost if either neutrophils or M1-like microglia were reduced (Extended Data Fig. 8a). Importantly, we saw no correlation in the prevalence of M1-like MDMs, neutrophils and M1-like microglia (Extended Data Fig. 8b), suggesting that spatial interactions between these cells are purposeful and not a product of their coordinated abundance.

We next compared multicellular interactions between glioblastoma and BrM. Using $N = 10$ nearest neighbours (the mid-point of our model and similar to other studies[13]), we identified 9 CNs across glioblastoma and BrM images (Fig. 3a,b and Extended Data Fig. 9a,b). The cellular composition of CNs recapitulated known tissue features, including the tumour boundary (CN1) or tumour compartment (CN8), two pan-immune hotspots with either high levels of all immune populations (CN2) or deficiencies in select subsets (CN9), high (CN3) or low (CN4) astrocytes, vascular niche (CN6), macrophage-enriched (CN7), and a neighbourhood largely represented by cells undefined by our panel (CN5) (Fig. 3b). As expected, glioblastoma was dominated by CN3 and CN4 (astrocyte-enriched) whereas BrM-cores were enriched for CN8 (tumour compartment), reflecting the infiltrative nature of gliomas compared with metastatic tumours (Fig. 3c).

Fig. 3: Spatial cellular neighbourhoods relate to survival in glioblastoma.



a, Schematic of cellular neighbourhood (CN) assignments. CNs are projected as a Voronoi diagram (right). **b**, Heat map of cell types represented across 9 CNs discovered in glioblastoma and BrM-cores ($n = 251$ images; $N = 10$ nearest neighbours, CN = 9 neighbourhoods). **c**, The distribution of CNs across glioblastoma ($n = 192$ images) and BrM-cores ($n = 59$ images). For each image, the percentage of cells from each CN was determined and then averaged for each disease type. **d**–**i**, Analysis of a controlled glioblastoma cohort of LTS (overall survival >3 years) and STS (overall survival <1 year) (see Extended Data Fig. 9f). **d**, The distribution of CNs in the LTS and STS glioblastoma cohort. CN frequencies were averaged where there were multiple samples from the same patient. Data are median ± interquartile range; $n = 16$ patients per group; two-sided Mann–Whitney test. **e**, Kaplan–Meier analysis of the LTS and STS glioblastoma cohort based on the median CN frequency. CN frequencies were averaged where there were multiple samples from the same patient. Log-rank (Mantel–Cox) test; $n = 16$ patients per group. **f**, t-SNE unsupervised clustering of macrophages and

monocytes from all glioblastoma images ($n = 93,513$ cells across 192 images). **g**, *t*-SNE projection of monocytes and macrophages from patients with glioblastoma, with cells in clusters CL1–3 outlined in red. LTS, $n = 17,752$ cells across 32 images; STS, $n = 10,456$ cells across 28 images. **h**, Relative expression of functional markers (left) and the distribution of cell types (right) across 15 monocyte and macrophage clusters (CL1–15). **i**, The number of cells from CL1–3 found within each cellular neighbourhood in the LTS and STS glioblastoma cohort.

Many patients with BrM exhibit metastatic involvement outside the brain, confounding survival analysis; we therefore correlated CN enrichment with local recurrence. The strongest trend was an association between high CN5 (undefined) and reduced time to local recurrence (Extended Data Fig. 9c). We confirmed that 96% of undefined cells in our dataset were $CD45^{-}$ (non-immune) (Extended Data Fig. 9d). We next investigated the distributions of CNs between BrM-margins and BrM-cores from distinct primary sites. Neighbourhood similarities among BrMs was dictated regionally, rather than by primary tumour type, with BrM-margins being more similar to glioblastoma than BrM-cores (Fig. 3c and Extended Data Fig. 9e). For example, lung BrM-cores were more similar to melanoma or breast BrM-cores than they were to lung BrM-margins (Extended Data Fig. 9e). Despite a high degree of variability in the cell frequencies between BrM from distinct primary tumours (Supplementary Fig. 6), CN distribution was relatively constant, highlighting an ability to identify unifying features in brain tumours that may be therapeutically informative.

We next examined a balanced glioblastoma cohort of STS and LTS by excluding patients with the greatest confounding clinical variable (partial resection) and controlled for other variables that affect survival, such as MGMT methylation status (Extended Data Fig. 9f and Supplementary Table 2). We compared the proportion of cells representing each CN within a given tumour sample, and found that LTS tumours had significantly higher representation of macrophage-enriched CN7 than STS tumours (Fig. 3d). Moreover, using this refined cohort, we confirmed the association between CN7 and improved survival (Fig. 3e and Extended Data Fig. 9g). This aligned with our neighbourhood analysis using variable numbers of interacting cells, where CNs enriched in M1-like MDMs were associated with prolonged survival (Extended Data Fig. 7). Notably, CN2 and CN9

(pan-immune hotspots) were also associated with improved survival (Fig. 3e); analysis of cell dynamics revealed elevated numbers of $CD4^+$ T cells in LTS tumours compared with STS tumours (Supplementary Fig. 10), which were enriched in both CN2 and CN9 (Fig. 3b). These data suggest a potential beneficial role for T cell neighbourhoods in glioblastoma, despite their low frequency.

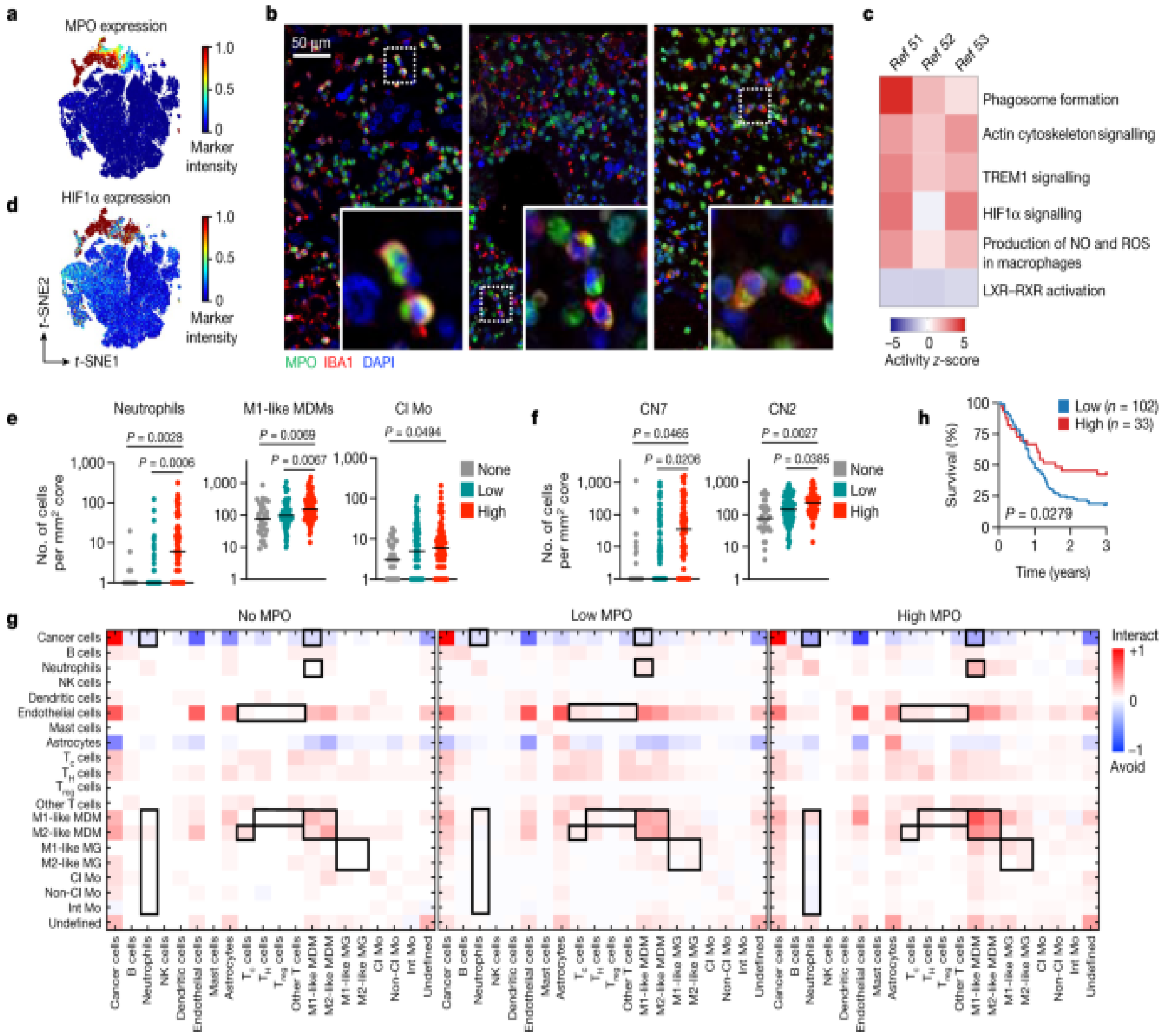
We focused on the prognostic relevance of CN7 in glioblastoma, since it was most consistently associated with survival compared with other CNs. Moreover, targeting macrophages in brain tumours in the clinical setting is receiving increasing interest in light of promising preclinical studies[41,42,43]. To define macrophage identities across neighbourhoods, we extracted all macrophage and monocyte subsets from glioblastoma samples and performed *t*-stochastic neighbour embedding (*t*-SNE) dimensionality reduction and spectral clustering based on phenotypic markers in our panel (Fig. 3f). Cellular clusters (CL)1–3 were significantly enriched in LTS tumours compared with STS tumours (Fig. 3g and Supplementary Fig. 11), the majority of which were $CD163^-P2Y12^-$, suggestive of an M1-like MDM phenotype (Fig. 3h). However, they co-expressed CD206, indicating these cells do not follow the M1/M2 paradigm, unlike other clusters with high CD206 that were enriched for $CD163^+$ cells (for example CL11–15; Fig. 3h). In comparing the relative representation of CL1–3 across each CN (Fig. 3b), we observed an enrichment in CN7 specifically in patients with LTS tumours (Fig. 3i). Together, these data indicate that macrophage spatial relationships may contain critical prognostic information, as we have identified a unique macrophage-enriched neighbourhood associated with long-term survival—a rarity in this disease.

MPO^+ macrophages are associated with survival

Given the relationship between CL1–3 macrophages and LTS tumours, we explored their putative function. CL1–3 macrophages expressed high levels of MPO (Fig. 4a), and more than 80% of MPO^+ macrophages were $CD163^-P2Y12^-$ (Extended Data Fig. 10a,b), suggesting a pro-inflammatory phenotype dominated by peripherally derived MDMs. MPO is often used as a marker for neutrophils, where it mediates production of reactive oxygen

species and oxidative burst. Although it is likely that MPO staining within macrophages partially reflects enhanced phagocytosis of neutrophils, *MPO* transcript is also detectable in brain tumour MDMs (Extended Data Fig. 10c) and peripheral monocytes (Extended Data Fig. 10d) at comparable levels to neutrophils. Indeed, neutrophil-like monocytes and macrophages have been identified in several immunopathologic contexts, including atherosclerosis[44], neuroinflammation[45,46] and lung cancer[47]. It is possible they arise either from a shift in monocyte developmental trajectories to favour granulocyte-monocyte progenitor (GMP)-derived lineages[48] or through MPO induction within the tissue niche. We confirmed the presence of $MPO^{+}IBA1^{+}$ macrophages in glioblastoma tumours using immunofluorescence (Fig. 4b; IBA1 was used as an alternative macrophage marker to CD68 for validation purposes). Using single-cell RNA-sequencing datasets from patients with glioblastoma, we identified genes enriched in MPO^{+} macrophages versus MPO^{-} macrophages (Extended Data Fig. 10e). Among the top differentially expressed genes were *S100A8* and *S100A9*, markers of GMP-derived lineages[48,49]. We observed signatures associated with reactive oxygen species biosynthesis and phagosome formation (indicative of cytotoxicity), and HIF1α signalling (suggesting distance from blood vessels) (Fig. 4c). Consistently, MPO^{+} macrophages were less likely to interact with endothelial cells compared with MPO^{-} macrophages (Extended Data Fig. 10f), coinciding with enriched HIF1α in CL1–3 (Fig. 4d). We also saw reduced LXR–RXR signalling (Fig. 4c), suggesting altered fatty acid metabolism within these cells that is consistent with their avoidance of fatty streaks in atherosclerosis[44]. These data suggest that, although rare in the TME, MPO^{+} macrophages may have anti-tumorigenic properties.

Fig. 4: MPO^{+} macrophages are enriched in LTS tumours and are associated with enhanced cytotoxic functions.



a, Heat map of MPO expression projected onto a *t*-SNE map (Fig. 3f) of monocytes and macrophages from patients with glioblastoma ($n = 93,513$ cells across 192 images). **b**, Representative immunohistofluorescence (IHF) images showing MPO and IBA1 (a macrophage marker) co-localization in glioblastoma tumours. Expanded regions show examples of MPO^+ macrophages ($n = 5$ images). **c**, Ingenuity pathway analysis of enriched pathways in MPO^+ versus MPO^- macrophages from three publicly available datasets[51,52,53]. **d**, HIF1α expression projected onto a *t*-SNE map of monocytes and macrophages from patients with glioblastoma ($n = 93,513$ cells across 192 images). **e**, The number of cells per 1 mm^2 core in glioblastoma samples with zero ($n = 32$ images), low ($n = 79$ images) or high ($n = 81$ images) MPO^+ M1-like MDMs. The graph shows mean values (black horizontal line) and all data points; one-way ANOVA; data are

presented in log scale, so images with 0 cells were assigned a value of 1. **f**, The raw number of cells in each cellular neighbourhood per 1 mm^2 core from patients with glioblastoma with zero (*n* = 32 images), low (*n* = 79 images) or high (*n* = 81 images) numbers of MPO^+ M1-like MDMs. The graph shows mean values (black horizontal line) and all data points; one-way ANOVA; images with 0 cells were assigned a value of 1. **g**, Pairwise interactions across two-sided permutation tests on individual images (1,000 permutations each) for patients with zero, low or high numbers of MPO^+ M1-like MDMs. Red, interactions (interact); blue, avoidances (avoid). **h**, Kaplan–Meier analysis based on MPO^+IBA1^+ cell frequency as determined by IHF staining in 135 tumours from patients with glioblastoma (*z*-score). Cell frequencies were averaged when multiple samples corresponded to the same individual. Log-rank (Mantel–Cox) test.

We next categorized tissues on the basis of the median density of MPO^+ M1-like MDM: none, low (1–5 cells per mm^2) and high (6 or more cells per mm^2). Higher numbers of MPO^+ macrophages corresponded with an increase in total neutrophils, M1-like MDMs and classical monocytes (Fig. 4e), supporting the notion that these tumours may be primed for strong innate effector responses. We also compared CN prevalence and found an enrichment in cells associated with CN7 (macrophage-enriched, as expected) and CN2 (pan-immune hotspot) (Fig. 4f), both of which provided a significant survival benefit in patients (Fig. 3e). To gain insight into the tumour architecture, we compared spatial interactions between major immune lineages across MPO categories. Cancer cells displayed a greater tendency to avoid neutrophils and M1-like MDMs as the density of MPO^+ macrophages increased (Fig. 4g). Indeed, most myeloid cell populations avoided neutrophils as MPO^+ macrophage density increased, with the exception of M1-like MDMs (Fig. 4g). The relationship between neutrophils and MPO^+ macrophages was confirmed by immunohistofluorescence, as samples with high MPO^+IBA1^- neutrophils also had high MPO^+IBA1^+ macrophages (Extended Data Fig. 10g). Similarly, interaction analysis of MPO^+ M1-like MDMs revealed interactions with both neutrophils and M1-like microglia (Extended Data Fig. 10h), echoing our CN findings (Extended Data Fig. 8a). Higher densities of MPO^+ macrophages were also associated with increased interactions between endothelial cells and M1-like MDMs

with T cells, concomitant with reduced interactions between M2-like MDMs and $CD8^+$ T cells (Fig. 4g), which can be immunoregulatory in cancer. Within the macrophage compartment, associations between MDMs increased, whereas they were relatively less pronounced for microglia (Fig. 4g)—suggesting that the dynamics of tissue-resident versus monocyte-derived macrophages may have distinct effects on tumour biology, as has been suggested in preclinical models[41]. These data illuminate gradual shifts in TME composition with changes in the density of MPO^+ macrophages.

Finally, to further probe clinical relevance, we confirmed that increased levels of $MPO^+CD163^-P2Y12^-CD68^+$ macrophages were associated with prolonged survival using our balanced glioblastoma cohort (Extended Data Fig. 10i). Consistently, recurrent glioblastomas contained fewer $MPO^+CD163^-P2Y12^-CD68^+$ macrophages compared with either STS or LTS tumours (Extended Data Fig. 10j). To test the practicality of our findings using a lower-plex technology, we performed immunohistofluorescence co-staining for MPO and IBA1 to evaluate survival outcomes in a cohort of 135 patients with glioblastoma. As the vast majority (83.96%) of MPO^+ macrophages are $CD163^-$ and $P2Y12^-$ (Extended Data Fig. 10a), the combination of MPO with IBA1 was sufficient to confirm significantly prolonged survival in patients with high frequencies of double-positive cells (Fig. 4h). Building on previous work showing that macrophage accumulation in brain tumours is associated with advanced disease[24], our findings highlight an MPO^+ subpopulation associated with an unexpected survival benefit. This suggests that therapies that broadly target macrophages in glioblastoma may deplete a beneficial macrophage subset, adding insight to clinical trials with CSF-1R inhibitors that have been largely unsuccessful[50], and deepening our understanding of macrophage complexity in this disease.

Discussion

We have provided a high-dimensional spatial map of the brain TME using IMC. We performed a comprehensive analysis of cellular dynamics, interactions and neighbourhoods in glioblastoma and BrM, and correlated spatial features of glioblastoma with patient survival. We defined

multicellular structures that are common across disease states and regions, which are superior for predicting patient survival compared with cell frequencies alone. We identified a unique subset of neutrophil-like macrophages that stain positively for MPO, which appear to be beneficial for the survival of patients with glioblastoma. We speculate that host immunity favouring GMP-derived neutrophil-like states may be advantageous for patient outcomes[48]. Alternatively, programming macrophages to adopt neutrophil-like characteristics or enhanced phagocytosis may occur within specific tumour niches. Our dataset adds to the growing evidence that the spatial organization of tumours at the cellular level is critical for understanding immunological mechanisms governing cancer. Given the limited therapeutic options for patients with brain tumours and dismal prognosis, there is untapped translational value in understanding how the spatial architecture of the brain TME relates to tumour biology, and whether specific immune cell subsets can be harnessed to improve outcomes.

Methods

Clinical samples for IMC

A cohort of 185 patients underwent surgical resection for primary brain tumours or BrM between 2006–2019. A breakdown of the patients whose tumour samples were used in this study can be found in Extended Data Fig. 1a. The clinical data for all patients was obtained from surgical and pathological reports. All tumour samples obtained from patients with glioblastoma were previously untreated and classified by a certified neuropathologist (M.C.G.) following primary surgical debulking. A subset of tumours was removed during a second follow-up surgery (residual tumour) or following tumour recurrence (recurrent tumour). In accordance with World Health Organization 2021 guidelines[23], tumours formerly classified as IDH mutant glioblastoma are now considered grade IV IDH mutant astrocytoma; therefore, in this study, only grade IV IDH wild-type tumours were designated as glioblastoma. We further distinguished glioblastomas that resulted from progression from grade II/III tumours (Extended Data Fig. 1a). LTSs were defined as patients with an overall survival greater than three years (much longer than expected survival time),

and STSs were defined as patients with an overall survival less than one year (shorter than expected survival time). Brain metastases samples[54] were surgically removed from patients bearing lung (n = 51 images), breast (n = 29 images), and melanoma (n = 19 images) primary tumours as well as a small number of bladder, colorectal, gastric, gastrointestinal and ovarian tumours, collectively called 'other' (n = 20 images) in this study. Pre-operative MRI images were used to determine the extent of peritumoural oedema (scored 0–3) by a neuroradiologist (S.L.). Leptomeningeal disease[55] was determined by contrast-enhancing lesions in the subarachnoid or ventricles as determined on MRI by a neuroradiologist (S.L.). All patients underwent standard of care (SOC) following surgery, unless otherwise specified. Cores (1–1.5 mm in diameter) were removed from formalin-fixed, paraffin embedded (FFPE) tissue blocks and assembled into tissue microarrays (TMAs). Within the glioma cohort, we included tumour-adjacent 'normal' tissues as well as primary brain tumour samples extracted from the tumour bulk, which were confirmed using corresponding haematoxylin and eosin (H&E) staining by a neuropathologist (M.C.G.). BrM samples were extracted from the tumour bulk and/or tumour–brain interface (termed BrM-cores and BrM- margins, respectively). A total of 242 tissue regions were sampled across the 185 patients including 139 high-grade glioma, 18 glioma-adjacent normal, 41 BrM-cores and 44 BrM-margins. Of these 242 regions, 142 were sampled in duplicate and 2 were sampled in triplicate for a total of 389 cores. Additionally, 39 patients with BrM had matched core-margin pairs. All surgical specimens and clinical information were obtained following written informed patient consent. Clinical information was de-identified and used in accordance with the institutional review boards of McGill University and Montreal Neurological Institute-Hospital (REB: NEU-10-066, 2018-4150).

Antibody optimization

Antibodies were optimized on control tissues including spleen, tonsil, lymph node, liver, kidney, normal lung, normal brain, lung cancer, glioblastoma and/or BrM. In Extended Data Fig. 3a and Supplementary Figs. 1 and 2, we show representative optimization images of both immunohistofluorescence (IHF) and IMC staining for all markers in our panel, with some exceptions: IHF was not performed for antibodies that

were commercially available with conjugated metal isotopes (except CD20 and CD45; unconjugated forms were used for IHF), and IHF was not performed for Ki67 as the B56 clone is routinely used. A list of all antibodies can be found in Supplementary Table 1. For IHF staining, FFPE sections underwent deparaffinization and heat-mediated antigen retrieval using the Ventana Discovery Ultra auto-stainer platform (Roche Diagnostics) according to manufacturer instructions. FFPE slides were incubated at 70 °C in pre-formulated EZ Prep solution (Roche Diagnostics), followed by incubation at 95 °C in pre-formulated Cell Conditioning 1 solution (Roche Diagnostics) for a total run time of ~2.5 h. Slides were rinsed in 1× PBS and incubated for 1 h at room temperature in Dako Serum-free Protein Block solution (Agilent). An antibody cocktail was prepared in Dako Antibody Diluent and slides were incubated with primary antibodies overnight at 4 °C. Slides were rinsed with 1× PBS and incubated with secondary antibody cocktail prepared in Dako Antibody Diluent for 1 h at room temperature. Slides were counterstained with DAPI for 5 min at room temperature and mounted using Dako Mounting Medium. An AxioScan Z1 scanner was used to capture tissue images.

Immunostaining and IMC

FFPE TMA slides underwent deparaffinization and heat-mediated antigen retrieval using the Ventana Discovery Ultra auto-stainer platform (Roche Diagnostics) according to the manufacturer's instructions. FFPE slides were incubated at 70 °C in pre-formulated EZ Prep solution (Roche Diagnostics), followed by incubation at 95 °C in pre-formulated Cell Conditioning 1 solution (Roche Diagnostics) for a total run time of ~2.5 h. Slides were rinsed in 1× PBS and incubated for 45 min at room temperature in Dako Serum-free Protein Block solution (Agilent). An antibody cocktail containing metal-conjugated antibodies was prepared in Dako Antibody Diluent at optimized dilutions. Slides were stained with primary antibodies at 4 °C overnight and subsequently washed with 0.2% Triton X-100 and 1× PBS. A secondary antibody cocktail containing metal-conjugated anti-biotin was prepared in Dako Antibody Diluent at the optimized dilution. Slides were incubated with anti-biotin for 1 h at room temperature and subsequently washed with 0.2% Triton X-100 and 1× PBS. Slides were counterstained with Cell-ID Intercalator-Ir (Fluidigm) diluted at 1:400 in 1×

PBS for 30 min at room temperature, rinsed for 5 min with distilled water, and air-dried prior to IMC acquisition. IMC acquisition was performed using the Hyperion Imaging System (Fluidigm).

Data transformation and normalization

All IMC data presented were not transformed and analyses were based on raw measurements. Single-cell marker expressions are summarized by mean pixel values for each channel. For heat map visualization, expression data were normalized to the 95th percentile and *z*-scored cluster means were plotted.

Cell segmentation and lineage assignment

All lineage and functional markers underwent a staining quality check prior to cell segmentation. A subset of functional markers passed initial quality control, but did not stain consistently with IMC, and were subsequently removed from analysis (GM-CSF-R, M-CSF-R, PD-1, PD-L1 and CTLA-4; see Supplementary Fig. 1). Cell segmentation was done using a combination of classical and modern machine learning-based computer vision algorithms. This pipeline enables high-throughput segmentation and accurately resolves individual cells across diverse tissues and structures. Importantly, this algorithm fully automates the detection of cells, thus eliminating subjective bias. The DNA channel is pre-processed for nuclei segmentation to obtain foreground regions of interest using mixtures of generalized Gaussian distributions (MoGG). The channels are also tiled for segmentation so we can pass them as inputs for inference to the MaskRCNN model. A detailed description of our segmentation and image analysis pipeline is available[56]. To assign cell phenotypes, we established a supervised approach based on canonical lineage markers, expected population abundance, staining quality, and maturity of cell lineage (Extended Data Fig. 1b). We first used *k*-means clustering[57] and a mixture of generalized Gaussian models[58] to create multi-level image stacks based on the staining intensity of each marker. Masks were curated for each lineage marker in the panel based on consideration of 6 levels using the following procedure. (1) Greyscale image channel is convolved with a median filter with a 3 × 3 window size. (2) Each pixel is clustered into 6 groups of intensity levels using the *k*-means algorithm. (3)

For each channel we select all groups up to a particular level as foreground (1) and the rest are designated as background (0). (4) We apply morphological blob removal to obtain smoother binary masks, where binary blobs of a particular area are removed from masks to avoid noisy regions. (5) To further refine the accuracy of select markers, additional channel-specific morphological operations are applied by computing an additional binary mask obtained using the adaptive binarization method with a sensitivity of 0.4. This mask is then amalgamated with the mask obtained in step 4. (6) To enhance the image intensity of select channels, we apply a simple contrast enhancement filter by saturating the bottom and top intensity levels of pixels in particular channels. This process enables us to capture more accurate masks from channels when phenotyping cells within our cores.

The method of lineage assignment is represented in the following formula: for each cell c_i we consider the curated mask for each lineage marker M_k, where $k = 1,\ldots,n$ and n is the number of lineage markers. Let us assume $p_{c_i}^{j}$ be the j^{th} pixel that lies in the surrounding of c_i and each pixel has the following presence vector based on the lineage markers:

$$E\left(p_{c_i}^{j}\right)=\{p_{M_1}^{j}, p_{M_2}^{j},\ldots ,p_{M_n}^{j}\}$$

where $p_{M_i}=\{0\,\text{or}\,1\}$, which determines whether the pixel $p_{c_i}^{j}$ is positive for a particular marker. Next, to determine whether each pixel within a cell is positive or negative for a given marker, we determine the majority vector by summing over the presence of all vectors as:

$$M_{c_i}=\left\{\mathop{\sum }\limits_{j=1}^{N_{c_i}} p_{M_1}^{j},\mathop{\sum }\limits_{j=1}^{N_{c_i}} p_{M_2}^{j},\ldots ,\mathop{\sum }\limits_{j=1}^{N_{c_i}} p_{M_n}^{j}\right\}$$

where N_{c_i} is the number of pixels in the cell c_i. The maximum value in vector M_{c_i} determines the cell type

assignment. Cell lineages are assigned in rank priority order (Extended Data Fig. 1b).

All code used to perform these analyses is available at https://github.com/walsh-quail-labs/IMC-Brain.

Cell–cell pairwise interaction analysis

To identify significant pairwise interaction and avoidance behaviours between cell types, we performed permutation tests of single-cell interactions as previously described[11,59]. Cells within a 6 pixel radius (6 μm) were considered interacting. Significant interaction or avoidance behaviours were defined as having a *P*-value of less than 0.01.

Cellular neighbourhood identification

To identify spatial cellular neighbourhoods, we first computed neighbour windows, which we defined as being the number (*N*) of nearest cells to each cell (as indicated), as previously described[60]. Each window is a frequency vector consisting of the types of *N* closest cells to a given cell. Neighbour windows were clustered. Cellular neighbourhood discovery on glioblastoma and BrM-cores combined (performed in 2021) was performed using Scikit-learn, a software machine learning library for Python. Clustering was performed using MiniBatchKMeans clustering algorithm version 0.24.2 with default batch size = 100 and random_state = 0. BrM-margins were excluded from cellular neighbourhood discovery due to their variable mix of tumour versus stromal content. Cellular neighbourhood analysis on glioblastoma cores alone (performed in 2022) used MiniBatchKMeans clustering algorithm version 1.1.2 with default batch size = 1,024 and random_state = 0. Every cell was then assigned to a particular cellular neighbourhood based on their neighbour window. Cellular neighbourhood prevalence in each core was normalized so the sum of cellular neighbourhood prevalence for that core was 100%. Values were then *z*-scored and cores with *z*-score above or equal to 0 and below 0 were compared for survival outcome.

IMC survival analysis

Glioblastoma survival analysis was conducted using a clinically controlled cohort of patients that received gross total resection of the tumour prior to treatment, as confirmed by post-surgical MRI, and were treated with SOC (Extended Data Fig. 9f and Supplementary Table 2). Overall survival was calculated from the date of surgery to date of death. For patients with glioblastoma whose date of death was not specified, overall survival was estimated using the date of their last known follow-up. For BrM survival analyses, local recurrence-free survival was assessed in previously untreated lesions with complete macroscopic gross total resections as confirmed by post-surgical MRI. For all Kaplan–Meier analyses, images were averaged when multiple cores were collected from the same patient's tumour (that is, each patient had only one survival value represented in the analysis).

t-SNE

Using default parameters, *t*-SNE dimensionality reduction plots were generated in MATLAB (version 2019b). Clustering was performed using a customized high-dimensional spectral-based clustering algorithm, due to the curse dimensionality of our cells (order of million number of cells). In our customized algorithm, we first use the DBSCAN to isolate clusters that have a similar density (with fixed parameters of a maximum distance of 3 pixels minimum number of 30 points per cluster). This approach produces some small and some big clusters with densities that are similar to each other. The big cluster group is then re-clustered using a spectral clustering algorithm. To be able to achieve a spectral clustering result on our massive dimensional data, we do a subsampling of the data (with a subsampling rate of 10), which gives us the overall shape of the data. Next, we assign each cluster with its cluster labels obtained from spectral clustering. Finally, we fit a *k*-nearest neighbour classifier (with $k = 5$) to our labelled subsampled data, to identify the cluster labels of all samples. Markers used for *t*-SNE analysis include CD14, CD16, CD68, CD163, P2Y12, CC3, Ki67, CD40, CD206, HIF1α, MMP9, MPO, OX40L and pSTAT3. For visualization, expression data were normalized to the 95th percentile.

Immunohistofluorescence co-staining

FFPE tissue sections were deparaffinized and underwent heat-mediated antigen retrieval in citrate buffer pH 6.0 or EDTA buffer pH 9.0. Slides were blocked with Power Block for 5 min at room temperature and incubated with the primary antibody for 30 min at room temperature. Slides were rinsed with TBS-T and subsequently incubated with secondary antibody–horseradish peroxidase (HRP) for 30 min at room temperature. Slides were rinsed with TBS-T and stained with Opal fluorophore working solution for 10 min (AKOYA Biosciences; Opal 520: FP1487001KT, lot 202212718; Opal 570: FP1488001KT, lot 20212821). This was followed by heat-mediated antibody stripping to remove primary and secondary antibodies. These steps were repeated for each primary antibody for a total of two rounds of labelling: MPO, Abcam, EPR20257, ab208670, lot GR3390666-13, 1:500; IBA1, Fujifilm Wako Pure Chemicals, polyclonal, 019-19741, lot 41375175, 1:400; and Horse Anti-Rabbit IgG HRP Polymer Kit, Vector Laboratories, MP-7801, lot ZH0611, 1:1.

Antibody specificities and dilutions were optimized individually before multiplexing was performed. Tissue images were captured using the AxioScan Z1 scanner and processed using HALO software (version 3.5).

Clinical samples for IHF

Tissue microarrays containing glioblastoma primary tumour samples from n = 135 patients were consolidated from McGill University (Quebec, Canada), University of Calgary (Alberta, Canada) and the Netherlands Cancer Institute (NKI, Amsterdam, The Netherlands). All patients were previously untreated and classified as IDH wild-type glioblastoma by a certified neuropathologist following primary surgical debulking, and later treated with SOC. All patient information and tissues were obtained after written informed consent and used in accordance with the following ethics oversight.

McGill University cohort

$n = 70$ patients underwent surgical resection between 2006–2019; McGill University Health Centre and the Montreal Neurological Institute and Hospital institutional review boards (NEU-10-066, 2018-4150); a

neuropathologist reviewed all cases and provided the TMA (M.C.G.). These samples represent a subset of our original IMC cohort based on tissue availability on the TMA (an independent section was used). Survival <1 year, *n* = 25 patients; survival 1–3 years, *n* = 18 patients; survival >3 years, *n* = 27 patients.

University of Calgary cohort

n = 58 patients underwent surgical resection between 2002 and 2020; Health Research Ethics Board of Alberta, Cancer Committee (HREBA.CC-16-0762), Clark Smith Tumour Biobank; a neuropathologist reviewed all cases and provided the TMA (J.A.C.). Survival <1 year, *n* = 31 patients; survival 1–3 years, *n* = 23 patients; survival >3 years, *n* = 4 patients.

NKI cohort

n = 7 patients; Institutional Review Board of the NKI-AvL and NKI-biobank (CFMPB541); TMA provided by D.B. Survival <1 year, *n* = 5 patients; survival 1–3 years, *n* = 1 patient; >3 years, *n* = 1 patient.

Publicly available RNA-sequencing data

Single-cell RNA-sequencing datasets were downloaded from the following.

1. (1)

   GSE154795 (ref. [51]) (GSE154795_GBM.AllCell.Integrated.Scaled.ClusterRes.0.1.rds.gz). Using the Seurat object file GSE154795_GBM.AllCell.Integrated.Scaled.ClusterRes.0.1.rds, a new Seurat object was created (Seurat 4.1.1), with the RNA assay counts from the subset of the 14 new patients with glioblastoma and was normalized with the default parameters of the Seurat function NormalizeData.

2. (2)

GSE162631 (ref. [53]) (GSE162631_raw_counts_matrix.zip.gz). A Seurat object was created using Seurat 4.1.1 from the expression matrix count files with the parameters min.cells = 0 and min.features = 200. The counts were normalized with the default parameters of the Seurat function NormalizeData.

3. (3)

https://doi.org/10.17605/OSF.IO/4Q32E[52]. Using the Seurat object file seurat.obj_MNN_ref.RDS, a new Seurat object was created using Seurat 4.1.1 with the RNA assay counts of the source Seurat object and were normalized with the default parameters of the Seurat function NormalizeData.

MDMs from each dataset were characterized as *CD68*^{high} (normalized expression >0) and *P2RY12*^{low} (normalized expression <0.1) and were isolated for further downstream analysis. MDMs were subdivided by *MPO*^{high} (normalized expression >0.05) or *MPO*^{low} (normalized expression <0.05). For each individual patient, an average expression matrix was generated from the *MPO*^{high} and *MPO*^{low} MDMs. The FindMarkers function in Seurat was used to generate a list of differentially expressed genes between the *MPO*^{high} and *MPO*^{low} MDMs. Pathway enrichment was assessed using Ingenuity Pathway Analysis software v.01–13 (Qiagen). Differentially expressed genes (adjusted $P < 0.05$) were selected for each dataset and 'Core Analysis' was used with all default parameters.

The following data were also used. Transcriptomic data from human immune cells in blood[61], accessed via Human Protein Atlas (https://www.proteinatlas.org/ENSG00000005381-MPO/immune+cell); glioblastoma RNA-sequencing data from The Cancer Genome Atlas (TCGA Firehose Legacy), accessed via the cBioPortal for cancer genomics (https://www.cbioportal.org); and bulk RNA-sequencing data from sorted immune cells from brain tumours[16], accessed via https://joycelab.shinyapps.io/braintime/.

Statistics and reproducibility

All image analysis steps were performed in MATLAB (version 2019b) and Python (version 3.7.12). Statistical analyses were performed using GraphPad Prism 9 statistical software. *P*-values of <0.05 were considered significant and data were expressed as mean ± s.e.m. unless indicated otherwise in the figure legends. Normal distribution was examined via the Shapiro–Wilk test. Parametric data were analysed by Student's *t*-test, one-way or two-way ANOVA. Non-parametric data were analysed by Mann–Whitney test; for large sample size comparisons, Student's *t*-test was used[62]. Survival data were analysed by log-rank (Mantel–Cox) tests, as indicated in the relevant figure legends. Contingency tables were analysed by Fisher's exact test. Tukey's test was used for multiple comparisons. For all analyses related to survival, including Kaplan–Meier analysis and the LTS and STS cohort, images were averaged when multiple cores were collected from the same patient's tumour to prevent biasing results toward individuals with more images. All other analyses unrelated to survival (for example, population dynamics) were performed using individual images to appropriately capture heterogeneity within the TME. Area analysis of IMC images was performed using ImageJ (version 1.53k). All antibody optimization was repeated at least two times by IHF and an additional two times by IMC, using a broad variety of tissues as shown in Extended Data Fig. 3 and Supplementary Fig. 1. Additional representative IMC images (including Fig. 1b, Extended Data Figs. 6a and 10b and Supplementary Fig. 3) were selected from 389 total images and depict the statistical changes and/or staining quality as described; similar results in staining quality were obtained for all samples included in analysis. All other representative immunostaining (Fig. 4b, Extended Data Fig. 10g and Supplementary Fig. 2) was performed on at least five full tissue samples with similar results.

Reporting summary

Further information on research design is available in the Nature Portfolio Reporting Summary linked to this article.

Data availability

The source data supporting findings in this study, including high-dimensional TIFF images and clinical information corresponding to IMC,

have been deposited at https://doi.org/10.5281/zenodo.7383719. Raw primary imaging data can be obtained from the authors directly upon reasonable request.

Code availability

All original code has been deposited at GitHub and can be accessed at: https://github.com/walsh-quail-labs/IMC-Brain.

References

1. Quail, D. F. & Joyce, J. A. Microenvironmental regulation of tumor progression and metastasis. *Nat. Med.* **19**, 1423–1437 (2013).

2. Binnewies, M. et al. Understanding the tumor immune microenvironment (TIME) for effective therapy. *Nat. Med.* **24**, 541–550 (2018).

3. Baslan, T. & Hicks, J. Unravelling biology and shifting paradigms in cancer with single-cell sequencing. *Nat. Rev. Cancer* **17**, 557–569 (2017).

4. Ostrom, Q. T. et al. CBTRUS statistical report: primary brain and other central nervous system tumors diagnosed in the United States in 2010–2014. *Neuro Oncol.* **19**, v1–v88 (2017).

5. Barnholtz-Sloan, J. S. et al. Incidence proportions of brain metastases in patients diagnosed (1973 to 2001) in the Metropolitan Detroit Cancer Surveillance System. *J. Clin. Oncol.* **22**, 2865–2872 (2004).

6. Stupp, R. et al. Radiotherapy plus concomitant and adjuvant temozolomide for glioblastoma. *N. Engl. J. Med.* **352**, 987–996 (2005).

7. Cagney, D. N. et al. Incidence and prognosis of patients with brain metastases at diagnosis of systemic malignancy: a population-based study. *Neuro Oncol.* **19**, 1511–1521 (2017).

8. Quail, D. F. & Joyce, J. A. The microenvironmental landscape of brain tumors. *Cancer Cell* **31**, 326–341 (2017).

9. Carvajal-Hausdorf, D. E. et al. Multiplexed (18-Plex) measurement of signaling targets and cytotoxic T cells in trastuzumab-treated patients using imaging mass cytometry. *Clin. Cancer Res.* **25**, 3054–3062 (2019).

10. Ali, H. R. et al. Imaging mass cytometry and multiplatform genomics define the phenogenomic landscape of breast cancer. *Nat. Cancer* **1**, 163–175 (2020).

11. Jackson, H. W. et al. The single-cell pathology landscape of breast cancer. *Nature* **578**, 615–620 (2020).

12. Keren, L. et al. A structured tumor–immune microenvironment in triple negative breast cancer revealed by multiplexed ion beam imaging. *Cell* **174**, 1373–1387.e1319 (2018).

13. Schürch, C. M. et al. Coordinated cellular neighborhoods orchestrate antitumoral immunity at the colorectal cancer invasive front. *Cell* **182**, 1341–1359 (2020).

14. Liudahl, S. M. et al. Leukocyte heterogeneity in pancreatic ductal adenocarcinoma: phenotypic and spatial features associated with clinical outcome. *Cancer Discov.* **11**, 2014–2031 (2021).

15. Friebel, E. et al. Single-cell mapping of human brain cancer reveals tumor-specific instruction of tissue-invading leukocytes. *Cell* **181**, 1626–1642.e1620 (2020).

16. Klemm, F. et al. Interrogation of the microenvironmental landscape in brain tumors reveals disease-specific alterations of immune cells. *Cell* **181**, 1643–1660.e1617 (2020).

17. Schaettler, M. O. et al. Characterization of the genomic and immunologic diversity of malignant brain tumors through multisector analysis. *Cancer Discov.* **12**, 154–171 (2022).

18. Puchalski, R. B. et al. An anatomic transcriptional atlas of human glioblastoma. *Science* **360**, 660–663 (2018).

19. Muller, S. et al. Single-cell profiling of human gliomas reveals macrophage ontogeny as a basis for regional differences in macrophage activation in the tumor microenvironment. *Genome Biol.* **18**, 234 (2017).

20. Ginhoux, F., Schultze, J. L., Murray, P. J., Ochando, J. & Biswas, S. K. New insights into the multidimensional concept of macrophage ontogeny, activation and function. *Nat. Immunol.* **17**, 34–40 (2016).

21. Komohara, Y., Ohnishi, K., Kuratsu, J. & Takeya, M. Possible involvement of the M2 anti-inflammatory macrophage phenotype in growth of human gliomas. *J. Pathol.* **216**, 15–24 (2008).

22. Lu-Emerson, C. et al. Increase in tumor-associated macrophages after antiangiogenic therapy is associated with poor survival among patients with recurrent glioblastoma. *Neuro Oncol.* **15**, 1079–1087 (2013).

23. Louis, D. N. et al. The 2021 WHO Classification of Tumors of the Central Nervous System: a summary. *Neuro Oncol.* **23**, 1231–1251 (2021).

24. Prosniak, M. et al. Glioma grade is associated with the accumulation and activity of cells bearing M2 monocyte markers. *Clin. Cancer Res.* **19**, 3776–3786 (2013).

25. Park, J. H. et al. Tumor hypoxia represses γδ T cell-mediated antitumor immunity against brain tumors. *Nat. Immunol.* **22**, 336–346 (2021).

26. Reardon, D. A. et al. Effect of nivolumab vs bevacizumab in patients with recurrent glioblastoma: the CheckMate 143 Phase 3 Randomized Clinical Trial. *JAMA Oncol.* **6**, 1003–1010 (2020).

27. Tawbi, H. A. et al. Combined nivolumab and ipilimumab in melanoma metastatic to the brain. *N. Engl. J. Med.* **379**, 722–730 (2018).

28. Long, G. V. et al. Combination nivolumab and ipilimumab or nivolumab alone in melanoma brain metastases: a multicentre randomised phase 2 study. *Lancet Oncol.* **19**, 672–681 (2018).

29. Calabrese, C. et al. A perivascular niche for brain tumor stem cells. *Cancer Cell* **11**, 69–82 (2007).

30. Ghajar, C. M. et al. The perivascular niche regulates breast tumour dormancy. *Nat. Cell Biol.* **15**, 807–817 (2013).

31. Liu, H. et al. Pro-inflammatory and proliferative microglia drive progression of glioblastoma. *Cell Rep.* **36**, 109718 (2021).

32. van Hooren, L. et al. Agonistic CD40 therapy induces tertiary lymphoid structures but impairs responses to checkpoint blockade in glioma. *Nat. Commun.* **12**, 4127 (2021).

33. Kienast, Y. et al. Real-time imaging reveals the single steps of brain metastasis formation. *Nat. Med.* **16**, 116–122 (2010).

34. Valiente, M. et al. Serpins promote cancer cell survival and vascular co-option in brain metastasis. *Cell* **156**, 1002–1016 (2014).

35. Gi, T. et al. Microvascular proliferation of brain metastases mimics glioblastomas in squash cytology. *Cytopathology* **28**, 228–234 (2017).

36. Vanlandewijck, M. et al. A molecular atlas of cell types and zonation in the brain vasculature. *Nature* **554**, 475–480 (2018).

37. Arvanitis, C. D., Ferraro, G. B. & Jain, R. K. The blood–brain barrier and blood–tumour barrier in brain tumours and metastases. *Nat. Rev. Cancer* **20**, 26–41 (2020).

38. Avraham, H. K. et al. Angiopoietin-2 mediates blood-brain barrier impairment and colonization of triple-negative breast cancer cells in brain. *J. Pathol.* **232**, 369–381 (2014).

39. Carbonell, W. S., Ansorge, O., Sibson, N. & Muschel, R. The vascular basement membrane as “soil” in brain metastasis. *PLoS ONE* **4**, e5857

(2009).

40. Liebner, S. et al. Claudin-1 and claudin-5 expression and tight junction morphology are altered in blood vessels of human glioblastoma multiforme. *Acta Neuropathol.* **100**, 323–331 (2000).

41. Akkari, L. et al. Dynamic changes in glioma macrophage populations after radiotherapy reveal CSF-1R inhibition as a strategy to overcome resistance. *Sci. Transl. Med.* **12**, eaaw7843 (2020).

42. Pyonteck, S. M. et al. CSF-1R inhibition alters macrophage polarization and blocks glioma progression. *Nat. Med.* **19**, 1264–1272 (2013).

43. Quail, D. F. et al. The tumor microenvironment underlies acquired resistance to CSF-1R inhibition in gliomas. *Science* **352**, aad3018 (2016).

44. Sugiyama, S. et al. Macrophage myeloperoxidase regulation by granulocyte macrophage colony-stimulating factor in human atherosclerosis and implications in acute coronary syndromes. *Am. J. Pathol.* **158**, 879–891 (2001).

45. Amorim, A. et al. IFNγ and GM-CSF control complementary differentiation programs in the monocyte-to-phagocyte transition during neuroinflammation. *Nat. Immunol.* **23**, 217–228 (2022).

46. Reynolds, W. F. et al. Myeloperoxidase polymorphism is associated with gender specific risk for Alzheimer's disease. *Exp. Neurol.* **155**, 31–41 (1999).

47. Zilionis, R. et al. Single-cell transcriptomics of human and mouse lung cancers reveals conserved myeloid populations across individuals and species. *Immunity* **50**, 1317–1334.e1310 (2019).

48. Yanez, A. et al. Granulocyte–monocyte progenitors and monocyte–dendritic cell progenitors independently produce functionally distinct monocytes. *Immunity* **47**, 890–902.e894 (2017).

49. Lagasse, E. & Weissman, I. L. Mouse MRP8 and MRP14, two intracellular calcium-binding proteins associated with the development of the myeloid lineage. *Blood* **79**, 1907–1915 (1992).

50. Butowski, N. et al. Orally administered colony stimulating factor 1 receptor inhibitor PLX3397 in recurrent glioblastoma: an Ivy Foundation Early Phase Clinical Trials Consortium phase II study. *Neuro Oncol.* **18**, 557–564 (2016).

51. Lee, A. H. et al. Neoadjuvant PD-1 blockade induces T cell and cDC1 activation but fails to overcome the immunosuppressive tumor associated macrophages in recurrent glioblastoma. *Nat. Commun.* **12**, 6938 (2021).

52. Ravi, V. M. et al. T-cell dysfunction in the glioblastoma microenvironment is mediated by myeloid cells releasing interleukin-10. *Nat. Commun.* **13**, 925 (2022).

53. Xie, Y. et al. Key molecular alterations in endothelial cells in human glioblastoma uncovered through single-cell RNA sequencing. *JCI Insight* **6**, e150861 (2021).

54. Dankner, M. et al. Invasive growth associated with cold-inducible RNA-binding protein expression drives recurrence of surgically resected brain metastases. *Neuro Oncol.* **23**, 1470–1480 (2021).

55. Dankner, M. et al. The underlying biology and therapeutic vulnerabilities of leptomeningeal metastases in adult solid cancers. *Cancers* **13**, 732 (2021).

56. Karimi, E. et al. Machine learning meets classical computer vision for accurate cell identification. Preprint at *BioRxiv*, https://doi.org/10.1101/2022.02.27.482183 (2022).

57. Arthur, D. & Vassilvitskii, S. *k*-means++: The advantages of careful seeding. In *Proc. 18th annual ACM-SIAM Symposium on Discrete Algorithms* 1027–1035 (Society for Industrial and Applied Mathematics, 2006).

58. Peel, D. M. G. *Finite Mixture Models* (John & Sons, 2000).

59. Schapiro, D. et al. histoCAT: analysis of cell phenotypes and interactions in multiplex image cytometry data. *Nat. Methods* **14**, 873–876 (2017).

60. Schurch, C. M. et al. Coordinated cellular neighborhoods orchestrate antitumoral immunity at the colorectal cancer invasive front. *Cell* **182**, 1341–1359.e1319 (2020).

61. Uhlen, M. et al. A genome-wide transcriptomic analysis of protein-coding genes in human blood cells. *Science* **366**, eaax9198 (2019).

62. Fagerland, M. W. *t*-tests, non-parametric tests, and large studies-a paradox of statistical practice? *BMC Med. Res. Methodol.* **12**, 78 (2012).

Acknowledgements

The authors are grateful for technical support from core facilities from the Rosalind and Morris Goodman Cancer Institute (GCI) and Life Sciences Complex at McGill University, including the Single Cell and Imaging Mass Cytometry Platform (SCIMAP) and Histology core facility (N. Robinson and P. Cruz). The authors acknowledge financial support from the McGill Interdisciplinary Initiative in Infection and Immunity, the Quebec Cancer Consortium and the Ministère de l'Économie et de l'Innovation du Québec through the Fonds d'accélération des collaborations en santé. L.A.W., D.F.Q., L.A., K.P. and M.C.G. acknowledge funding from the Brain Tumour Funders' Collaborative. L.A.W acknowledges funding from the Canadian Institutes of Health Research (CIHR; PJT-162137) and the Canadian Foundation for Innovation, and holds a Rosalind and Morris Goodman Chair in Lung Cancer Research. D.F.Q. acknowledges funding from the CIHR (PJT-159742, PJT-178306), Canadian Foundation for Innovation, and the Canada Research Chairs Program. P.M.S. acknowledges funding from the CIHR (PJT-175066) and is a McGill University William Dawson Scholar. I.R.W. acknowledges funding from the Terry Fox Research Institute (1084), CIHR (PJT-152975) and Canada Research Chairs Program. M.P.

acknowledges funding from the Réseau de Recherche en Cancer of the Fonds de Recherche du Québec-Santé and the Québec Breast Cancer Foundation, and holds the Diane and Sal Guererra Chair in Cancer Genetics. Fellowship support was provided by the McGill University MD/PhD Program (S.M.M.), the GCI Charlotte and Leo Karassik Foundation Oncology PhD fellowship (M.W.Y. and L.J.M.P.), Fonds de Recherche du Québec (M.W.Y. and L.J.M.P.) and the GCI Canderel Graduate Studentship Program.

Author information

Author notes

1. These authors contributed equally: Elham Karimi, Miranda W. Yu, Sarah M. Maritan, Lucas J. M. Perus

Authors and Affiliations

1. Rosalind and Morris Goodman Cancer Institute, McGill University, Montreal, Quebec, Canada

   Elham Karimi, Miranda W. Yu, Sarah M. Maritan, Lucas J. M. Perus, Mark Sorin, Matthew Dankner, Samuel Doré, Dongmei Zuo, Benoit Fiset, LeeAnn Ramsay, Yuhong Wei, Ian R. Watson, Morag Park, Marie-Christine Guiot, Peter M. Siegel, Daniela F. Quail & Logan A. Walsh

2. Department of Physiology, Faculty of Medicine, McGill University, Montreal, Quebec, Canada

   Miranda W. Yu, Lucas J. M. Perus & Daniela F. Quail

3. Department of Medicine, Division of Experimental Medicine, McGill University, Montreal, Quebec, Canada

   Sarah M. Maritan, Matthew Dankner, Peter M. Siegel & Daniela F. Quail

4. Departments of Psychology and Computer Science, University of Toronto, Toronto, Ontario, Canada

Morteza Rezanejad

5. Department of Human Genetics, Faculty of Medicine, McGill University, Montreal, Quebec, Canada

Mark Sorin, Samuel Doré & Logan A. Walsh

6. Gerald Bronfman Department of Oncology, McGill University, Montreal, Quebec, Canada

Parvaneh Fallah, Morag Park & Donna L. Senger

7. Division of Tumor Biology and Immunology, Oncode Institute, Netherlands Cancer Institute, Amsterdam, Netherlands

Daan J. Kloosterman & Leila Akkari

8. Department of Diagnostic Radiology, Faculty of Medicine, McGill University, Montreal, Quebec, Canada

Stephanie Lam

9. Department of Medicine, Division of Neurology, King Saud University College of Medicine, Riyadh, Saudi Arabia

Roa Alsajjan

10. Department of Neurology and Neurosurgery, Faculty of Medicine, McGill University, Montreal, Quebec, Canada

Roa Alsajjan, Kevin Petrecca & Marie-Christine Guiot

11. Department of Biochemistry, Faculty of Medicine, McGill University, Montreal, Quebec, Canada

Ian R. Watson, Morag Park & Peter M. Siegel

12. Department of Oncology, University of Calgary, Calgary, Alberta, Canada

Gloria Roldan Urgoiti

13. Arnie Charbonneau Cancer Institute, University of Calgary, Calgary, Alberta, Canada

Gloria Roldan Urgoiti & Jennifer A. Chan

14. Department of Neuro-Oncology, Netherlands Cancer Institute, Antoni van Leeuwenhoek Hospital, Amsterdam, Netherlands

Dieta Brandsma

15. Lady Davis Institute for Medical Research, Jewish General Hospital, Montreal, Quebec, Canada

Donna L. Senger

16. Department of Pathology and Laboratory Medicine, University of Calgary, Calgary, Alberta, Canada

Jennifer A. Chan

17. Montreal Neurological Institute-Hospital, McGill University Health Centre, Montreal, Quebec, Canada

Kevin Petrecca & Marie-Christine Guiot

18. Department of Pathology, Faculty of Medicine, McGill University, Montreal, Quebec, Canada

Marie-Christine Guiot

19. Department of Anatomy and Cell Biology, Faculty of Medicine, McGill University, Montreal, Quebec, Canada

Peter M. Siegel

Contributions

P.M.S., D.F.Q. and L.A.W. designed the study. D.F.Q., L.A.W., P.M.S., M.W.Y. and S.M.M. wrote the manuscript and coordinated experiments. E.K., M.R., M.W.Y., S.M.M., P.M.S., D.F.Q. and L.A.W. performed all IMC analysis and interpreted data. E.K., M.R. and B.F. wrote all original code used in the study. L.J.M.P., Y.W., I.R.W. and D.F.Q. designed, optimized and/or performed IMC. M.S., S.D. and B.F. performed analysis of publicly available datasets. L.R., I.R.W., D.J.K. and L.A. provided analysis critical to data interpretation. M.P. and D.Z. provided materials and optimized and performed IHF for validation of IMC. K.P. and M.C.-G. provided human tissue samples used for IMC. M.D., P.F., S.L., R.A. and M.C.G. assisted with collection and/or curation of clinical data for the IMC TMAs. For glioblastoma IHF, the following authors provided TMAs, pathology expertise and/or clinical data for patient samples from McGill University (K.P., M.C.G. and R.A.), the University of Calgary (J.A.C., D.L.S. and G.R.U.) and the Netherlands Cancer Institute (D.B. and L.A.). All authors reviewed and approved the manuscript.

Corresponding authors

Correspondence to Peter M. Siegel, Daniela F. Quail or Logan A. Walsh.

Ethics declarations

Competing interests

The authors declare no competing interests.

Peer review

Peer review information

Nature thanks Robert Prins and the other, anonymous, reviewer(s) for their contribution to the peer review of this work.

Additional information

Publisher's note Springer Nature remains neutral with regard to jurisdictional claims in published maps and institutional affiliations.

Extended data figures and tables

Extended Data Fig. 1 Study cohort and cell lineage assignment.

a, Summary of patient samples. Patients underwent surgical resection and tumours were classified by a neuropathologist (M.C.G.). Gliomas were classified as: primary (first surgical resection), residual (second surgery to remove any remaining tumour), recurrent (surgical resection after tumour recurrence), or progression from grade II/III (resection of grade IV tumour that progressed from low grade glioma). Glioma samples were extracted from the tumour bulk or the tumour-adjacent normal. Brain metastasis samples were extracted from the tumour bulk (core) or the tumour/brain interface (margin). All clinical information was obtained from surgical and pathological reports. Number of cells acquired corresponds to the total number of cells segmented across all images. **b**, Schematic for cell lineage assignment strategy. Created with BioRender.com.

Extended Data Fig. 2 Cellular dynamics in primary & metastatic brain tumours.

a, Cell frequencies as a percentage of all TME cells in glioblastoma ($n = 192$ images), BrM-cores ($n = 72$ images) and BrM-margins ($n = 47$ images). Data are mean ± s.e.m.; two-way ANOVA; significant adjusted P-values are highlighted. **b**, Left: number of cells/image for each cell type in glioblastoma ($n = 192$ images), BrM-cores ($n = 72$ images) and BrM-margins ($n = 47$ images); data are mean ± s.e.m. Right: absolute number of cells (total across all images) in glioblastoma ($n = 192$ images), BrM-core ($n = 72$ images) and BrM-margin ($n = 47$ images).

Extended Data Fig. 3 Representative staining of control tissues and brain tumours.

a, Representative IMC images of expected co-staining patterns in tonsil, spleen or tumour margins. Blue, DNA (191Ir and 193Ir). **b**, Representative IMC images of major lineage markers (left, centre) and corresponding cell segmentation and lineage assignment (right). The colour code for the cell segmentation image is provided (right).

Extended Data Fig. 4 Single-cell frequencies correlate with clinical subgroups in patients with brain tumours.

a, Cell density comparisons between clinical subgroups of patients, corresponding to Supplementary Fig. 8. Within each row, bubble colour indicates the clinical subgroup (A term versus B term, right) with higher cell type representation; bubble size indicates *P*-value. Two-sided student's t test, unpaired unless indicated otherwise; paired analyses are from patient-matched samples. **b**, Cell frequencies as a percentage of total cells per image in glioblastoma tumours with low T cells (<5% of TME, $n = 144$ images) versus high T cells (>5% of TME, $n = 13$ images). Data are mean ± s.e.m.; two-sided student's t test. **c**, Mean overall survival time of glioblastoma patients (for whom this information was available) with low T cells (<5% of TME, $n = 142$ images) versus high T cells (>5% of TME, $n = 13$ images). Data are mean ± s.e.m.; two-sided student's t test.

Extended Data Fig. 5 Cellular interactions in primary versus metastatic brain tumours.

a, Avoidance scores corresponding to Fig. 2c for cancer cell interactions with non-cancer lineages in glioblastoma ($n = 192$ images) and BrM-cores ($n = 59$ images). Data are mean ± s.e.m.; two-sided student's t test. **b**, Statistical significance of cellular interaction/avoidance scores in glioblastoma ($n = 192$ images) and BrM-cores ($n = 59$ images) corresponding to Fig. 2c. *P*-values calculated by two-sided student's t test. Colours indicate significantly greater interaction (red) or avoidance (blue) in BrM versus glioblastoma (upper table) or glioblastoma versus BrM (lower table).

Extended Data Fig. 6 Single-cell spatial interactions in patients with brain tumours.

a, IMC images of interacting cells in the perivascular niche of glioblastoma and BrM samples, representative of analysis in Fig. 2d–g. First row, perivascular cancer cell proliferation in glioblastoma; second row, perivascular macrophage proliferation in glioblastoma; third row, peritumoural endothelial proliferation in BrM-cores; fourth row, peritumoural endothelial proliferation in BrM-margins. High-magnification insets are provided to the right of each image. **b**, Heatmap of Spearman's correlation between cell types in glioblastoma (top rows, $n = 192$ images), BrM-cores (middle rows, $n = 59$ images) and BrM-margins (bottom rows, $n = 40$ images). Red, positive correlation; blue, negative correlation. **c**, Frequency of CD40+ MDMs and CD40- MDMs interacting with Th. Data are mean ± s.e.m.; $n = 1{,}048$ cells across 74 images; two-sided student's t test. **d**, CD40 in M1-like MDMs interacting with (red) or avoiding (blue) endothelial cells in glioblastoma. Data are mean ± s.e.m.; $n = 415$ cells across 188 images/group; two-sided student's t test. **e**, Ox40L in M2-like MDMs interacting with (red) or avoiding (blue) endothelial cells in glioblastoma. Data are mean ± s.e.m.; $n = 4{,}248$ cells across 183 images/group; Two-sided student's t test. **f**, Ki67 in endothelial cells interacting with (red) or avoiding (blue) Tc cells in BrM-margins. Data are mean ± s.e.m.; $n = 98$ cells across 28 images; two-sided student's t test. **g**, Claudin-5 in endothelial cells interacting with (red) or avoiding (blue) cancer cells in BrM-cores and -margins. Data are mean ± s.e.m.; BrM-cores, $n = 1{,}503$ cells across 61 images; BrM-margins, $n = 1507$ cells across 45 images; two-sided student's t test. **h**, Claudin-5 expression in endothelial cells interacting with (red) or avoiding (blue) cancer cells in BrM-cores subdivided by extent of peritumoural edema. Data are mean ± s.e.m.; none/low edema, $n = 369$ cells across 13 images; moderate/high edema, $n = 1{,}046$ cells across 42 images; two-sided student's t test. All images lacking pairwise interactions of interest were excluded from analysis.

Extended Data Fig. 7 Survival associations of spatial cellular neighbourhoods in glioblastoma.

Heatmaps depicting the cellular composition of glioblastoma cellular neighbourhoods (CN), with $N = 3$, 5, 10, 20 or 30 nearest neighbours and CN = 9 neighbourhoods. Tables show *P*-values of survival analyses (Log-rank (Mantel-Cox) test) for samples based on median CN frequency. CNs enriched in M1-like MDM that are significantly associated with survival are highlighted in grey. CN frequencies were averaged when multiple samples corresponded to the same patient.

Extended Data Fig. 8 M1-like MDM enriched cellular neighbourhoods are associated with survival in glioblastoma.

a, Heatmap depicting the cellular composition of glioblastoma cellular neighbourhoods (CN), with $N = 10$ nearest neighbours and CN = 30 neighbourhoods ($n = 192$ images). 6 CNs are enriched with >3000 M1-like MDM (grey highlight; number of M1-like MDM in each CN is indicated). Of these, 2 (red text) are associated with prolonged survival. Table shows *P*-values of survival analyses (Log-rank (Mantel-Cox) test) for samples based on median CN frequency. CN frequencies were averaged when multiple samples corresponded to the same patient. **b**, Cell frequency correlation graphs of neutrophils, M1-like MDM and M1-like MG. Linear regression with 95% confidence interval is shown.

Extended Data Fig. 9 The spatial cellular neighbourhoods of glioblastoma and brain metastases.

a, Representative Voronoi diagrams of CNs mapped onto glioblastoma IMC images. **b**, Representative Voronoi diagrams of CNs mapped onto BrM-core IMC images. **c**, Kaplan-Meier analysis of BrM patients (lung, melanoma and breast primaries) based on median CN5 frequency in BrM-cores. CN frequencies were averaged when multiple samples corresponded to the same patient. Log-rank (Mantel-Cox) test, $n = 13$ patients/group. **d**, CD45 expression in undefined cells across glioblastoma and BrM samples ($n = 389$ images). **e**, Distribution of CNs across BrM samples. BrM-margins: melanoma $n = 6$ images, lung $n = 22$ images, breast $n = 12$ images; BrM-cores: melanoma $n = 13$ images, lung $n = 29$ images, breast $n = 17$ images. For each image, the percentage of cells from each CN was determined, then averaged for each group. **f**, Schematic of the glioblastoma LTS/STS cohort

and inclusion/exclusion criteria, pertaining to Supplementary Table 2. Created with BioRender.com. **g**, Kaplan-Meier analysis of glioblastoma LTS/STS cohort based on median CN frequency. CN frequencies were averaged when multiple samples corresponded to the same patient. Log-rank (Mantel-Cox) test, $n = 16$ patients/group.

Extended Data Fig. 10 MPO+ macrophages are associated with enhanced cytotoxic functions.

a, Pie chart depicting the distribution of macrophage subsets within the total pool of MPO+ CD68+ macrophages in glioblastoma ($n = 192$ images). Percentages reflect the proportion of total MPO+ CD68+ cells. **b**, Representative IMC images of MPO+ MDMs in two glioblastoma samples. **c**, Normalized expression of *MPO* in glioblastoma and BrM immune cell subsets via RNA-seq (data from ref. [16]). Data are mean ± s.e.m.; *n*-values depicted indicate number of patients. **d**, Normalized expression of *MPO* in human blood immune cell subsets via RNA-seq (data from ref. [61]). **e**, Heatmap displaying the top 50 differentially expressed genes in MPO+ versus MPO- macrophages that were common to three independent publicly available glioblastoma scRNA-seq datasets (data from refs. [51,52,53]). **f**, Pairwise interaction/avoidance scores using two-sided permutation tests on individual images (1,000 permutations each) between endothelial cells and MPO+ versus MPO- M1-like MDMs ($n = 192$ images). Colour indicates interaction (red) or avoidance (blue) and circle size reflects the magnitude of the interaction score. **g**, Representative immunohistofluorescence images of MPO (green) and IBA1 (red; macrophage marker) co-localization in glioblastoma tumours. Examples of MPO+ IBA1+ macrophages are shown in insets, along with MPO+ IBA1- neutrophils or MPO- IBA1+ macrophages ($n = 5$ images). **h**, Pairwise interaction/avoidance scores using two-sided permutation tests on individual images (1,000 permutations each) for MPO+ M1-like MDM with other cell types ($n = 192$ images); interaction (red), avoidance (blue). **i**, Kaplan-Meier analysis of glioblastoma LTS/STS cohort based on median MPO+CD163-P2Y12-CD68+ macrophage enrichment. Cell frequencies were averaged when multiple samples corresponded to the same patient. Log-rank (Mantel-Cox) test, $n = 16$ patients/group. **j**, Frequency of MPO+ M1-like MDM as a percentage of total cells in the glioblastoma LTS/STS cohort ($n = 16$ patients/group) and

recurrent glioblastoma (n = 10 patients). Frequencies were averaged when multiple samples corresponded to the same patient. Data are median ± interquartile range; two-sided Mann-Whitney test.

Supplementary information

Supplementary Information

This file contains representative images and other panel validation data (Supplementary Figs. 1–5), analysis of cell frequencies and densities across clinical groups (Supplementary Figs. 6–11), and antibody and patient cohort information (Supplementary Tables 1 and 2).

Reporting Summary

Rights and permissions

Open Access This article is licensed under a Creative Commons Attribution 4.0 International License, which permits use, sharing, adaptation, distribution and reproduction in any medium or format, as long as you give appropriate credit to the original author(s) and the source, provide a link to the Creative Commons licence, and indicate if changes were made. The images or other third party material in this article are included in the article's Creative Commons licence, unless indicated otherwise in a credit line to the material. If material is not included in the article's Creative Commons licence and your intended use is not permitted by statutory regulation or exceeds the permitted use, you will need to obtain permission directly from the copyright holder. To view a copy of this licence, visit http://creativecommons.org/licenses/by/4.0/.

Reprints and Permissions

About this article

Cite this article

Karimi, E., Yu, M.W., Maritan, S.M. *et al.* Single-cell spatial immune landscapes of primary and metastatic brain tumours. *Nature* **614**, 555–563 (2023). https://doi.org/10.1038/s41586-022-05680-3

- Received: 24 March 2022
- Accepted: 22 December 2022
- Published: 01 February 2023
- Issue Date: 16 February 2023
- DOI: https://doi.org/10.1038/s41586-022-05680-3

Share this article

Anyone you share the following link with will be able to read this content:

Get shareable link

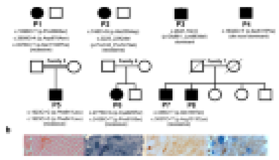
Sorry, a shareable link is not currently available for this article.

Copy to clipboard

Provided by the Springer Nature SharedIt content-sharing initiative

---

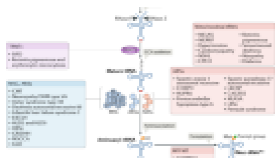
This article was downloaded by **calibre** from https://www.nature.com/articles/s41586-022-05680-3



POLRMT mutations impair mitochondrial transcription causing neurological disease

18 February 2021

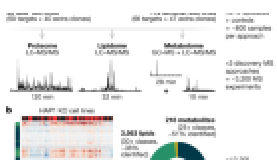
Monika Oláhová, Bradley Peter, … Robert W. Taylor



Translation deregulation in human disease

23 July 2018

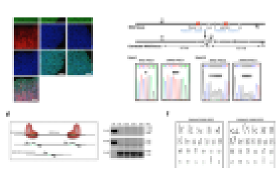
Soroush Tahmasebi, Arkady Khoutorsky, … Nahum Sonenberg



Defining mitochondrial protein functions through deep multiomic profiling

25 May 2022

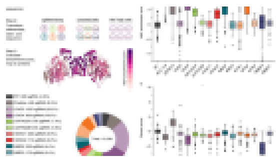
Jarred W. Rensvold, Evgenia Shishkova, … David J. Pagliarini



[Wiskott-Aldrich syndrome protein forms nuclear condensates and regulates alternative splicing]

25 June 2022

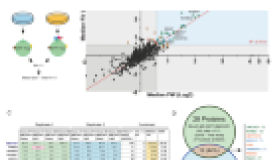
Baolei Yuan, Xuan Zhou, … Mo Li



[Rational targeting of a NuRD subcomplex guided by comprehensive in situ mutagenesis]

28 June 2019

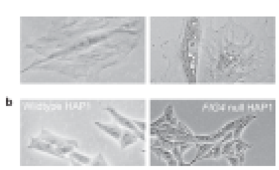
Falak Sher, Mir Hossain, … Daniel E. Bauer



[A proteomics study identifying interactors of the FSHD2 gene product SMCHD1 reveals RUVBL1-dependent DUX4 repression]

08 December 2021

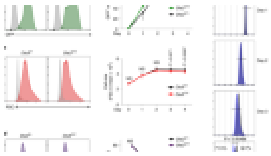
Remko Goossens, Mara S. Tihaya, … Silvère M. van der Maarel



[CRISPR knockout screen implicates three genes in lysosome function]

03 July 2019

Guy M. Lenk, Young N. Park, … Jacob O. Kitzman



[Noncoding RNA processing by DIS3 regulates chromosomal architecture and somatic hypermutation in B cells]

01 February 2021

Brice Laffleur, Junghyun Lim, … Uttiya Basu



[Reversible mislocalization of a disease-associated MRE11 splice variant product]

04 July 2018

Andrea J. Hartlerode, Joshua A. Regal & David O. Ferguson

- Article
- Open Access
- Published: 08 February 2023

Aberrant phase separation and nucleolar dysfunction in rare genetic diseases

- Martin A. Mensah,
- Henri Niskanen,
- Alexandre P. Magalhaes,
- Shaon Basu,
- Martin Kircher,
- Henrike L. Sczakiel,
- Alisa M. V. Reiter,
- Jonas Elsner,
- Peter Meinecke,
- Saskia Biskup,
- Brian H. Y. Chung,
- Gregor Dombrowsky,
- Christel Eckmann-Scholz,
- Marc Phillip Hitz,
- Alexander Hoischen,
- Paul-Martin Holterhus,
- Wiebke Hülsemann,
- Kimia Kahrizi,
- Vera M. Kalscheuer,
- Anita Kan,
- Mandy Krumbiegel,
- Ingo Kurth,
- Jonas Leubner,
- Ann Carolin Longardt,
- Jörg D. Moritz,
- Hossein Najmabadi,
- Karolina Skipalova,
- Lot Snijders Blok,
- Andreas Tzschach,
- Eberhard Wiedersberg,
- Martin Zenker,
- Carla Garcia-Cabau,
- René Buschow,
- Xavier Salvatella,
- Matthew L. Kraushar,
- Stefan Mundlos,
- Almuth Caliebe,

- Malte Spielmann ,
- Denise Horn &
- …
- Denes Hnisz

Show authors

Nature **volume 614**, pages 564–571 (2023)

- 21k Accesses
- 367 Altmetric
- Metrics details

Abstract

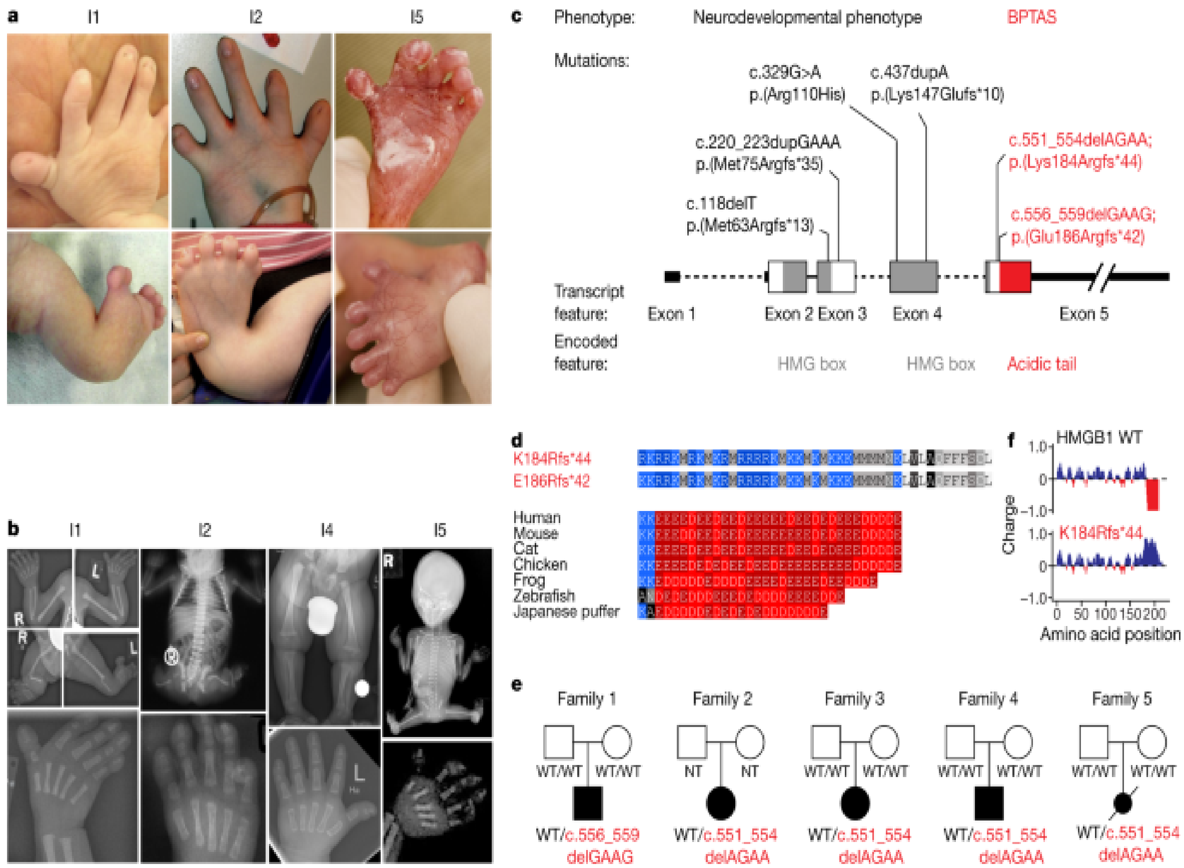
Thousands of genetic variants in protein-coding genes have been linked to disease. However, the functional impact of most variants is unknown as they occur within intrinsically disordered protein regions that have poorly defined functions[1,2,3]. Intrinsically disordered regions can mediate phase separation and the formation of biomolecular condensates, such as the nucleolus[4,5]. This suggests that mutations in disordered proteins may alter condensate properties and function[6,7,8]. Here we show that a subset of disease-associated variants in disordered regions alter phase separation, cause mispartitioning into the nucleolus and disrupt nucleolar function. We discover de novo frameshift variants in *HMGB1* that cause brachyphalangy, polydactyly and tibial aplasia syndrome, a rare complex malformation syndrome. The frameshifts replace the intrinsically disordered acidic tail of HMGB1 with an arginine-rich basic tail. The mutant tail alters HMGB1 phase separation, enhances its partitioning into the nucleolus and causes nucleolar dysfunction. We built a catalogue of more than 200,000 variants in disordered carboxy-terminal tails and identified more than 600 frameshifts that create arginine-rich basic tails in transcription factors and other proteins. For 12 out of the 13 disease-associated variants tested, the mutation enhanced partitioning into the nucleolus, and several variants altered rRNA biogenesis. These data identify the cause of a rare complex syndrome and

suggest that a large number of genetic variants may dysregulate nucleoli and other biomolecular condensates in humans.

Main

Monogenic and common diseases are frequently associated with mutations in transcriptional regulatory proteins, including DNA-binding transcription factors. However, the functional impact of the majority of such mutations is unknown, and many complex diseases still lack a clear underlying genetic component[1,9,10,11,12]. We initially set out to identify the molecular basis of brachyphalangy, polydactyly and tibial aplasia/hypoplasia syndrome (BPTAS; Online Mendelian Inheritance in Man database identifier: 609945), an extremely rare complex malformation syndrome with an as yet unknown molecular aetiology[13,14,15,16,17,18,19]. During the study, five individuals (I1–I5) were diagnosed with BPTAS. All five exhibited a distinct skeletal phenotype, including short and malformed lower limbs characterized by tibia aplasia or hypoplasia, preaxial polysyndactyly and contractures of large joints (Fig. 1a,b). In all five individuals, anomalies of the upper limbs were less severe compared with those of the lower limbs, and included brachydactyly or brachyphalangy of fingers with an irregular finger length (Fig. 1a,b). Short radius and ulna and contractures or pterygia of the elbow joints were present in four out of five individuals. All individuals with BPTAS diagnosed during our study or described in previous reports also presented with distinct craniofacial, neurological and genitourinary features. Phenotypic findings are summarized in Supplementary Table 1. Detailed clinical and family histories are provided in Supplementary Note and Extended Data Fig. 1.

Fig. 1: De novo frameshifts in *HMGB1* cause BPTAS.



a, Photographs of individuals diagnosed with BPTAS. Top row, hands of I1, I2 and I5. Note brachydactyly, irregular finger length and hypoplasia of the nails. Bottom row, lower extremities of I1, I2 and I5, presenting with malformed legs, joint contractures, preaxial polysyndactyly and hypoplasia of the nails. **b**, Radiograms of I1, I2, I4 and I5. Top far left, limb radiograms (at newborn age) of I1 showing brachydactyly and brachyphalangy, tibial aplasia, hypoplastic fibulae and preaxial polysyndactyly. Top middle left, babygram of I2. Note tibial aplasia, hypoplastic and absent fibulae, hypoplastic pelvic bones and hypoplastic right femur. Top middle right, lower extremities of I4 (at 6 months) showing asymmetric shortness of tibiae and fibulae. Top far right, fetogram of I5 showing tibial aplasia, hypoplastic and absent fibulae, hypoplastic pelvic bones and contractures of joints. Bottom row, hand radiograms of I1, I2 (both at newborn age), I4 (at 6 months) and of I5 (at 21 weeks of gestation). Note the short middle phalanges and short proximal phalanges of the thumbs. **c**, Pathogenic frameshift variants in the acidic tail of HMGB1 in the individuals with BPTAS reported in this article are highlighted in red. Previously reported variants associated with developmental delay are in black. Note the

genotype–phenotype correlation: C-terminal frameshifts result in BPTAS, whereas other variants lead to a neurodevelopmental phenotype. **d**, Amino acid sequence of the C terminus of HMGB1 in individuals with BPTAS and in selected vertebrates. Acidic residues glutamate and aspartate are shaded in red, basic residues arginine and lysine are shaded in blue. Note the replacement of the conserved acidic tail in individuals with BPTAS. **e**, Family pedigrees. Individuals with BPTAS are highlighted with black boxes, and the genotypes are below the boxes. **f**, Charge plots of WT and mutant HMGB1. I, individual; L, left; NT, not tested; R, right; WT, wild type.

De novo *HMGB1* frameshifts in BPTAS

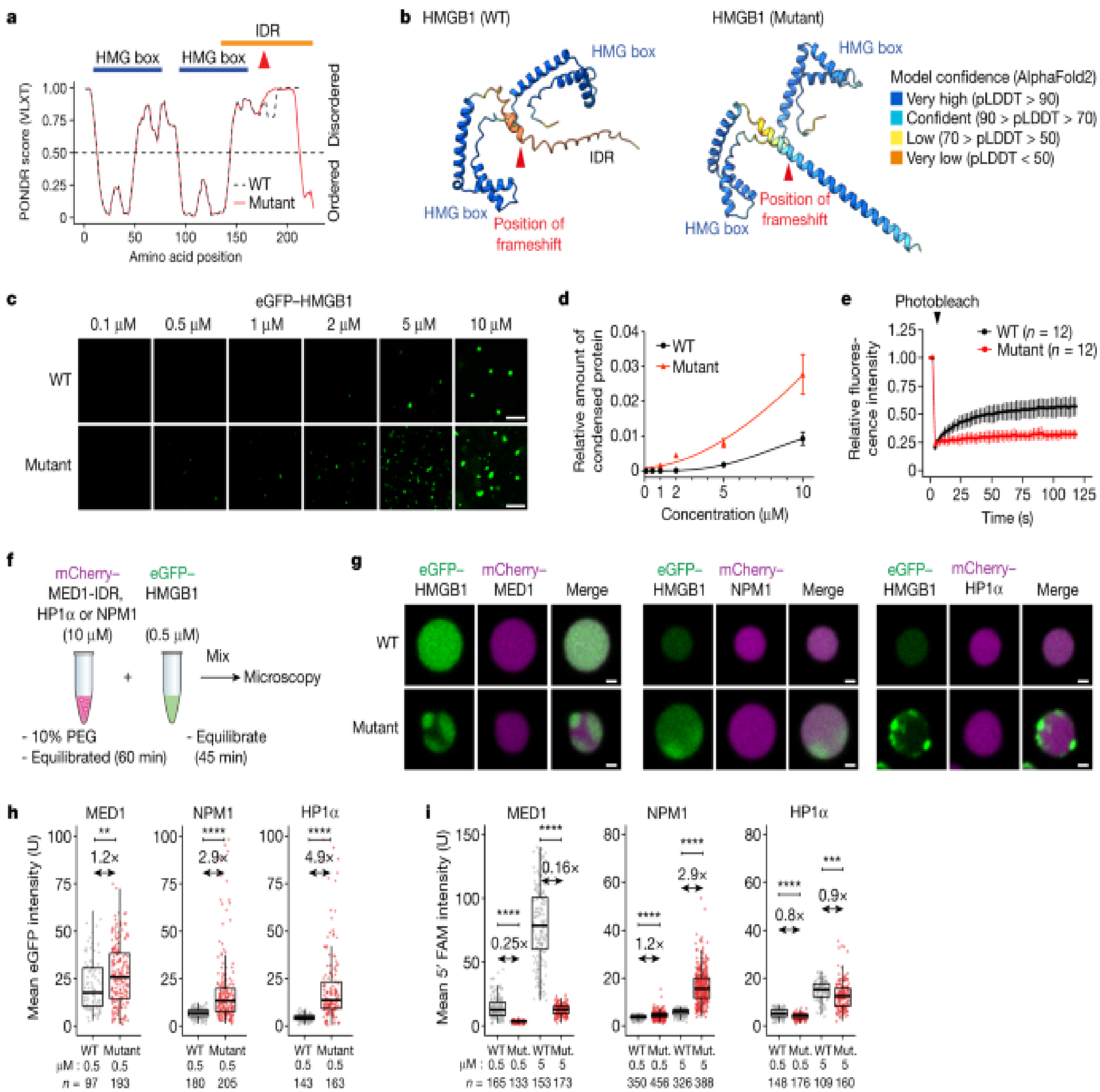
We performed genome sequencing of I1 and detected a potentially pathogenic variant: the heterozygous frameshift NM_002128.7(*HMGB1*):c.556_559delGAAG;p.(Glu186Argfs*42) in the final exon of *HMGB1* (Extended Data. Fig. 2a). *HMGB1* encodes a highly conserved, low-specificity DNA binding factor associated with cell signalling[20], cell motility[21,22], base excision repair[23,24] and chromatin looping[25]. Sanger sequencing of I1 and his parents confirmed the presence of the frameshift variant and revealed de novo occurrence (Fig. 1c–e and Extended Data Fig. 2b). Sanger sequencing of *HMGB1* in I2 and I3, and trio exome sequencing of I4 identified a similar de novo heterozygous frameshift: NM_002128.7(*HMGB1*):c.551_554delAGAA;p.(Lys184Argfs*44), a variant also detected in a previously described female fetus[26] (I5) (Fig. 1c–e and Extended Data Fig. 2c,d). Sequencing of cDNA from a lymphoblastoid cell line derived from peripheral blood cells from I3 confirmed the presence of both wild-type and mutant *HMGB1* transcripts (Extended Data Fig. 2e). The two frameshift mutations result in almost identical, positively charged sequences (Fig. 1d,f).

Altered HMGB1 phase separation in vitro

To investigate the potential pathogenic role of the frameshift variant in HMGB1, we first explored structural and sequence features of the wild-type and mutant proteins. HMGB1 is a low-specificity DNA-binding protein that contains two HMG boxes that are responsible for DNA binding[27] and a C-

terminal acidic tail (Fig. 2a,b). The acidic tail is predicted to be intrinsically disordered and resides within an approximately 60-amino-acid long conserved intrinsically disordered region (IDR), as revealed by AlphaFold2 and PONDR analyses (Fig. 2a,b and Extended Data Fig. 3a). Both algorithms predicted a slight propensity of the C-terminal portion of the IDR to assume a helical conformation in the frameshift mutant HMGB1 (Fig. 2a,b and Extended Data Fig. 3b). This prediction was confirmed by circular dichroism experiments on synthetic peptides that corresponded to the C-terminal 80–90 amino acid region (Extended Data Fig. 3c–e). IDRs of numerous proteins, including transcription factors, co-activators (for example, Mediator) and RNA polymerase II (RNAPII), contribute to phase separation by mediating multivalent low-affinity interactions[6,28,29,30,31]. Therefore, we hypothesized that the potentially BPTAS-causing frameshift may alter the phase-separation capacity of HMGB1.

Fig. 2: A BPTAS-causing frameshift alters HMGB1 phase separation in vitro.



a, Graph plotting the intrinsic disorder of HMGB1. Red arrowhead shows the position of the BPTAS frameshift. The position of the IDR is highlighted with an orange bar and the position of HMG boxes with blue bars. **b**, Structures of WT and mutant HMGB1 predicted with AlphaFold2. Colours ranging from blue to orange depict the per-residue measure of local confidence (pLDDT) for the model. **c**, Representative images from droplet formation assays of eGFP–HMGB1 variants at the indicated concentrations. The experiment was repeated three times, with similar results obtained. **d**, Quantification of the relative amount of condensed protein at the indicated concentrations. Data displayed as the mean ± s.d. **e**, Relative fluorescence intensity of the bleached area from eGFP–HMGB1 condensates before and

after photobleaching. Data displayed as the mean ± s.d. **f**, Scheme of co-droplet assays. **g**, Representative images of eGFP–HMGB1 proteins mixed with preassembled mCherry-labelled MED1-IDR, HP1α or NPM1 droplets. **h**,**i**, Quantification of eGFP (**h**) and 5′ FAM (**i**) fluorescence intensity in mCherry-labelled MED1-IDR, HP1α and NPM1 droplets mixed with full-length mEGFP–HMGB1 proteins (**h**) or 5′ FAM–HMGB1-IDR peptides (**i**). Fold change values between the mean intensities of WT and mutants (Mut.) are indicated above the plot. Median is shown as a line within the boxplot, which spans from the 25th to 75th percentiles. Whiskers depict a 1.5× interquartile range. *P* values are from two-tailed Welch's *t*-test. $^{**}P < 1 \times 10^{-2}$, $^{***}P < 1 \times 10^{-3}$, $^{****}P < 1 \times 10^{-4}$. Scale bars, 5 μm (**c**) and 10 μm (**g**).

To test the phase-separation capacity of HMGB1, we purified recombinant HMGB1 proteins tagged with enhanced green fluorescent protein (eGFP) and examined their behaviour in vitro. Wild-type full-length HMGB1 formed droplets in the presence of a crowding agent (10% polyethylene glycol (PEG)), and the number and size of droplets scaled with the concentration of the protein (Fig. 2c,d and Extended Data Fig. 4a–c). The droplets were spherical, settled on the surface and occasionally underwent fusion (Supplementary Video 1), which are hallmarks of phase separation[32]. By contrast, the frameshift mutant HMGB1 formed amorphous condensates that appeared at a lower saturation concentration (Fig. 2c,d) and, after photobleaching, recovered fluorescence slower than wild-type HMGB1 droplets (Fig. 2e). Similar results were observed using synthetic peptides that corresponded to the C-terminal 80–90 amino acid region of wild-type and frameshift mutant HMGB1 (Extended Data Fig. 4d–g). These results indicate that the frameshift in HMGB1 enhances condensate formation and alters condensate properties in vitro.

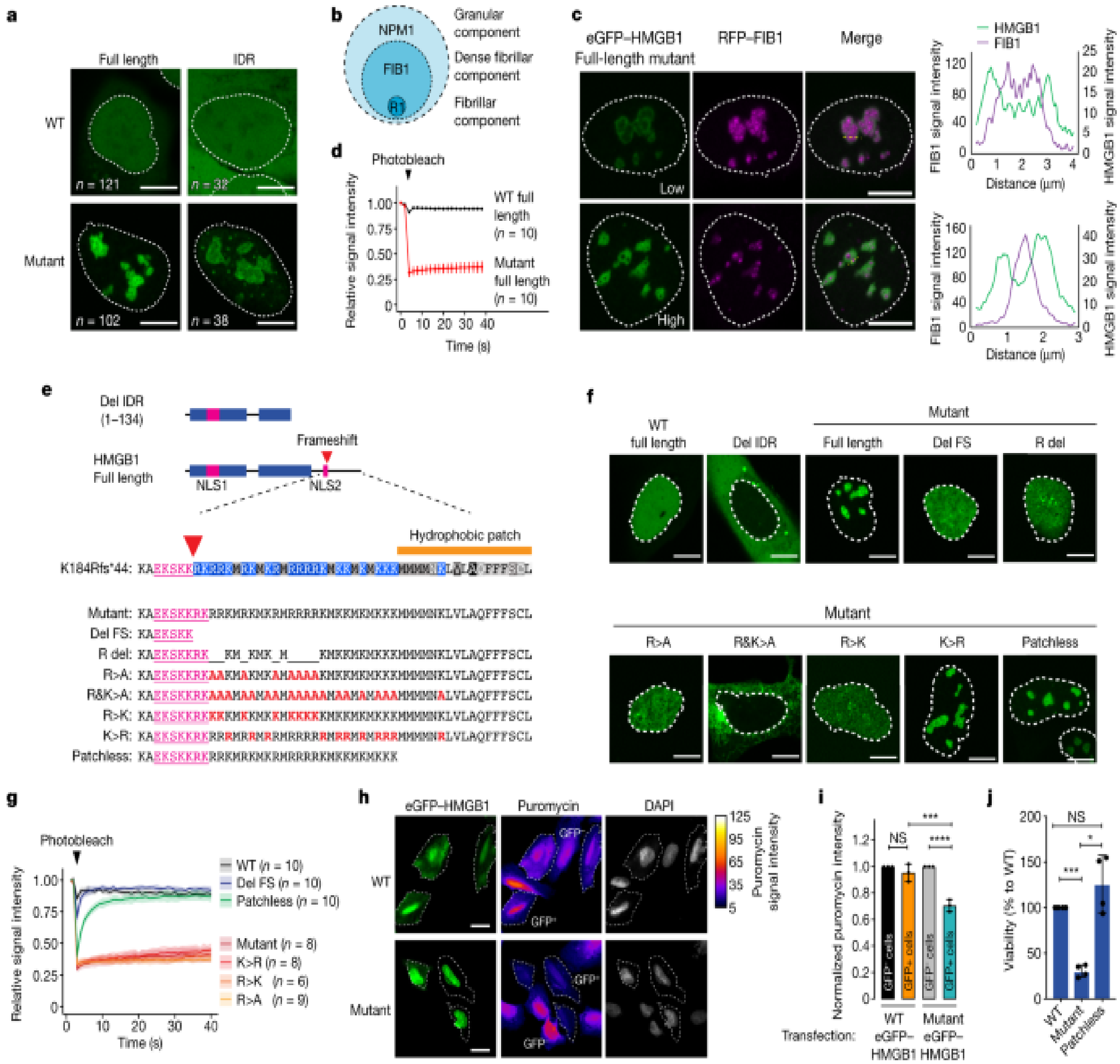
Mammalian nuclei contain numerous biomolecular condensates, for example, the nucleolus, heterochromatin, co-activator and RNAPII condensates[4,5]. IDRs play important roles in the partitioning of proteins into nuclear condensates[4,5]. We therefore tested whether the frameshift mutation alters the partitioning of HMGB1 into nuclear condensates. Using purified marker proteins, we assembled the following model condensates: recombinant mCherry-tagged MED1 IDR droplets as an in vitro model for

Mediator co-activator condensates[29,31,33]; mCherry-tagged HP1α droplets as an in vitro model for heterochromatin[34]; and mCherry-tagged NPM1 droplets as an in vitro model for the granular component of the nucleolus[35]. Wild-type and mutant HMGB1 proteins were then added to the droplets (Fig. 2f). Wild-type eGFP-tagged HMGB1 partitioned into all three model condensates, with the highest partitioning observed in MED1-IDR droplets (Fig. 2g,h). The mutant HMGB1 protein displayed enhanced partitioning into NPM1 droplets (threefold compared with wild type, $P < 1 \times 10^{-5}$, Welch's *t*-test) and to some extent in HP1α droplets (Fig. 2g,h). Mutant HMGB1 also tended to form dense foci within the MED1-IDR, HP1α and NPM1 droplets over time that appeared sequestered to the surface of the droplets (Fig. 2g). Enhanced partitioning into NPM1 condensates and foci formation were also observed using a 5′-carboxyfluorescein (5′ FAM)-labelled synthetic HMGB1 IDR mutant peptide, tested at multiple concentrations (Fig. 2i and Extended Data Fig. 4h–j). These results reveal that mutant HMGB1 exhibits enhanced partitioning into NPM1 condensates in vitro.

Nucleolar HMGB1 mispartitioning in vivo

We next sought to investigate the condensate behaviour of mutant HMGB1 in human cells. As primary culturable cells from individuals with BPTAS were not available, we ectopically expressed eGFP-tagged HMGB1 in U2OS cells. Wild-type HMGB1 displayed diffuse nuclear localization in live cells (Fig. 3a and Extended Data Fig. 5a,b). By contrast, mutant HMGB1 localized to discrete nuclear inclusions (Fig. 3a, Extended Data Fig. 5a,b and Supplementary Video 2). Ectopic expression of the mutant HMGB1 IDR also led to the formation of nuclear inclusions in live U2OS cells (Fig. 3a and Extended Data Fig. 5a–c), which indicated that the replaced IDR of the mutant HMGB1 is responsible for its altered subnuclear localization. Nuclear inclusions were observed in several other human cell types expressing mutant HMGB1 (Extended Data Fig. 5d).

Fig. 3: Mutant HMGB1 replaces the granular component of the nucleolus in vivo.



a, Representative images of live U2OS cells expressing eGFP–HMGB1 proteins. Nuclear area revealed by Hoechst staining is shown as dashed white lines in **a**, **c** and **f**. **b**, Model of the nucleolus. R1, RNA polymerase I. **c**, Left, representative images of U2OS cells expressing RFP–FIB1 and mutant eGFP–HMGB1. Right, fluorescence intensity profiles from the region highlighted by the dashed yellow line. Low and high indicate nuclei with a relatively low or high amount, respectively, of the mutant protein. **d**, Relative fluorescence intensity of eGFP–HMGB1 before and after photobleaching. Data displayed as the mean ± s.d. **e**, Schematic and sequence representation of HMGB1 variants. Blue bars, HMG boxes. NLS, nuclear localization signal. Red arrow marks the position of the frameshift mutation (K184Rfs*44) and red letters highlight mutagenized amino acids.

f, Representative images of live U2OS cells expressing the indicated eGFP–HMGB1 variants. **g**, Relative fluorescence intensity of eGFP–HMGB1 variants before and after photobleaching. Data are displayed as a line for the mean signal, with the shaded region representing ± s.d., n = number of cells examined. **h**, Representative images from puromycin-staining experiments with U2OS cells ectopically expressing eGFP–HMGB1 proteins. The puromycin signal was used to trace the cell area to highlight GFP^+ cells with a dashed line. **i**, Normalized puromycin intensities displayed as the mean ± s.d. from three independent biological replicate experiments. ***$P < 0.0002$, ****$P < 0.0001$ by one-way ANOVA. **j**, Quantification of the viability of cells expressing the indicated HMGB1 proteins. Data displayed as individual points from independent biological replicates ($n = 4$). Bar charts show mean ± s.d. *** $P = 0.0005$, * $P = 0.0177$ by one-way ANOVA. Scale bars, 10 µm (**a**,**c**,**f**) or 20 µm (**h**).

Mutant HMGB1 nuclear inclusions frequently contained cavities and resembled nucleoli. Nucleoli are phase-separated multiphasic condensates that contain an outer granular component enriched in NPM1 and an inner dense fibrillar component enriched in FIB1 (ref. [35]) (Fig. 3b). To gain initial insights into the nature of the mutant HMGB1 nuclear inclusions, we expressed FIB1 tagged with red fluorescent protein (RFP–FIB1) and eGFP–HMGB1 in live U2OS cells. The cavities in the mutant HMGB1 inclusions tended to encapsulate FIB1 (Fig. 3c). Fluorescence recovery after photobleaching (FRAP) experiments revealed that the HMGB1 shell displayed arrested dynamics around the FIB1 cores (Fig. 3d and Extended Data Fig. 5e). These results suggest that the mutant HMGB1 inclusions may be abnormal, arrested nucleoli.

To further probe the identity of mutant HMGB1 nuclear inclusions, we performed immunofluorescence against various nuclear proteins known to form condensates. The immunofluorescence analyses revealed that mutant HMGB1 inclusions were distinct from RNAPII and MED1 puncta, nuclear speckles and heterochromatin (Extended Data Fig. 5f–h). However, they overlapped with NPM1 and FIB1 (Extended Data Fig. 5h). The NPM1 signal within the HMGB1 inclusions inversely correlated with the HMGB1 signal (Pearson's $r = -0.70$) (Extended Data Fig. 5i). Moreover, the amount of diffuse NPM1 outside nucleoli correlated with the amount of HMGB1 in the inclusions (Pearson's $r = 0.50$) (Extended Data Fig. 5j). These results

indicate that the mutant HMGB1 inclusions replace the NPM1-enriched granular component of nucleoli.

Targeted mutagenesis experiments revealed that arginine residues in the mutant HMGB1 tail drive nucleolar mispartitioning, and a hydrophobic patch drives nucleolar arrest. Various mutant HMGB1 sequences were expressed in live U2OS cells. A HMGB1 protein lacking the entire IDR (Del IDR) or the sequence after the frameshift position (Del FS) was not enriched in the nucleolus (Fig. 3e,f). Deletion of arginine residues (R del), substitution of arginine residues with alanine residues (R>A), substitution of arginine and lysine residues with alanine residues (R&K>A), and substitution of arginine residues with lysine residues (R>K) within the sequence created by the frameshift led to failure of the mutant protein to partition into the nucleolus (Fig. 3e,f). Furthermore, deletion of the short hydrophobic patch at the C terminus of the frameshifted sequence (Patchless) did not alter nucleolar mispartitioning (Fig. 3e,f and Extended Data Fig. 5k), but it did rescue the arrested dynamics of the mutant HMGB1 nucleoli assessed by FRAP (Fig. 3e,g). These results demonstrate that nucleolar mispartitioning of the frameshift mutant HMGB1 depends on arginine residues within the sequence created by the frameshift and that the hydrophobic patch contributes to nucleolar arrest.

Mutant HMGB1 and nucleolar dysfunction

To test whether the nucleolar mispartitioning of HMGB1 affects nucleolar function, we investigated ribosomal RNA (rRNA) production using quantitative PCR with reverse transcription (RT–qPCR)[36]. The level of 28S rRNA in U2OS cells expressing the frameshift mutant HMGB1 was significantly reduced by about 1.5-fold ($P < 0.05$, Student's t-test) (Extended Data Fig. 6a). Ribosomal dysfunction was subsequently probed using an assay of nascent translation that measures puromycin incorporation[37]. U2OS cells expressing mutant eGFP–HMGB1 consistently displayed lower levels of puromycin intensity than non-transfected (that is, GFP^-) cells and cells transfected with wild-type eGFP–HMGB1 (Fig. 3h,i and Extended Data Fig. 6b,c). Furthermore, U2OS cells expressing the mutant HMGB1 exhibited substantially reduced viability after several days of culture compared with cells expressing wild-type HMGB1 ($P < 5 \times 10^{-4}$, one-way analysis of

variance (ANOVA)) (Fig. 3j and Extended Data Fig. 6d). The reduced viability was associated with nucleolar arrest, as transfection of cells with the Patchless mutant did not compromise viability (Fig. 3j and Extended Data Fig. 6d). The findings of nucleolar mispartitioning, nucleolar arrest and viability were corroborated using cell lines expressing stably integrated eGFP–HMGB1 transgenes from a PiggyBac transposon (Extended Data Fig. 6e–j). These results indicate that the presence of the HMGB1 frameshift mutant in cells disrupts nucleolar function and is cytotoxic.

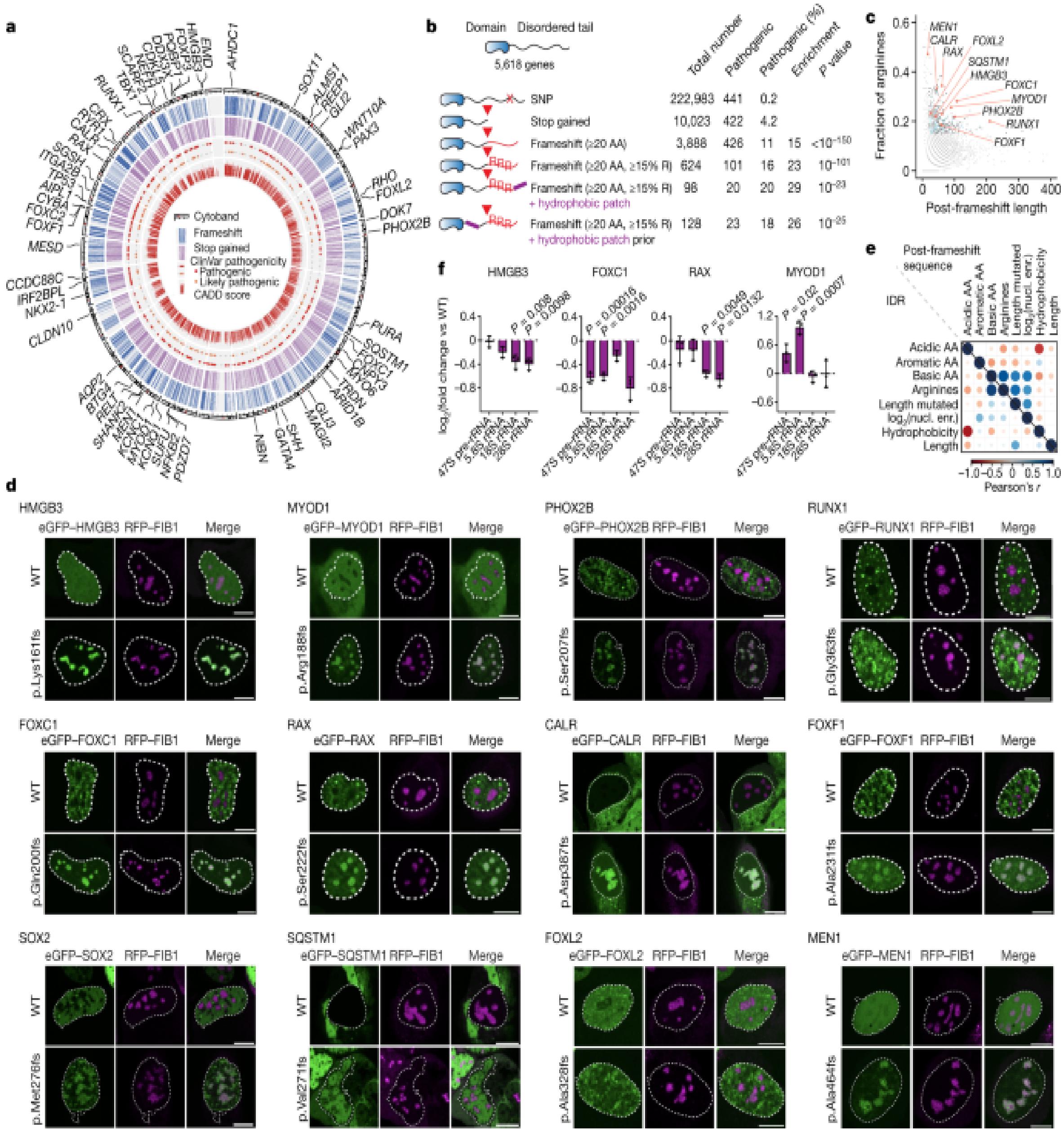
ACMG classification of HMGB1 variants

The clinical and genetic information of the five individuals with BPTAS and the functional data were used to classify the *HMGB1* frameshift variants as pathogenic. This classification was made in accordance with the criteria of the American College of Medical Genetics and Genomics (ACMG)[38]. Both frameshifts observed in individuals with BPTAS result in the replacement of the highly conserved acidic tail of the protein (ACMG criterion PM1), and were classified as pathogenic by MutationTaster (ACMG criterion PP3). Notably, of the 43 nonsynonymous variants in the HMGB1 tail (1,123 alleles) listed in the gnomAD database (v.2.1.1)[39], only 4 variants (5 alleles) introduce amino acids other than aspartate and glutamate (ACMG criterion PM2) (Extended Data Fig. 2f,g). All previously described pathogenic *HMGB1* variants are associated with neurodevelopmental phenotypes without severe skeletal anomalies, which are therefore distinct from BPTAS (Fig. 1c and Supplementary Table 2), including a chromosomal microdeletion encompassing the *HMGB1* locus in an individual (I6) diagnosed in our study (Extended Data Fig. 2h–j, Supplementary Note and Supplementary Table 2). The functional data presented in this study suggest a deleterious effect (ACMG criterion PS3). In summary, the identification of almost the same (ACMG criterion PS4) *HMGB1* frameshift variants in five (shown to be de novo in four; ACMG criteria PS2 and PM6) unrelated individuals with the same ultrarare diagnosis of BPTAS (ACMG criterion PP4) argues for the classification of these variants as pathogenic (ACMG evidence level: 3S+2M+2P; Supplementary Note).

Catalogue of variants in C-terminal IDRs

We then sought to investigate whether replacement of a disordered C-terminal tail with an arginine-rich basic tail and the consequent nucleolar mispartitioning and dysfunction could occur in other diseases. To this end, we generated a catalogue of genetic variants in intrinsically disordered tails of cellular proteins. First, we annotated 9,303 isoforms of 5,618 genes that have a C-terminal IDR consisting of at least 20 amino acids (Supplementary Table 3). We then identified genetic variants that occur in the disordered tails of the 5,618 genes annotated in the 1000 Genomes Project, ClinVar, COSMIC and dbSNP databases. These analyses revealed 249,464 genetic variants in C-terminal IDRs, including 10,023 truncating variants and 3,888 frameshifts that replace the C-terminal sequence with ≥20 amino acids (Fig. 4a, Extended Data Fig. 7a–c and Supplementary Tables 4 and 5). Of the 3,888 frameshifts, 426 were annotated as pathogenic in ClinVar, 763 were common variants curated in the 1000 Genomes Project and 189 in the dbSNP databases (Fig. 4b, Extended Data Fig. 7b,c and Supplementary Table 5). The frameshifts were associated with higher-than-average pathogenicity (Fig. 4a), and frameshifts were enriched for pathogenic variants (Fig. 4b and Extended Data Fig. 7c). Genes encoding transcription factors were highly enriched among those that contained C-terminal IDR mutations (Extended Data Fig. 7d). Among the 3,888 frameshift variants, 624 were predicted to result in a sequence consisting of at least 15% arginine residues, of which 101 were classified as pathogenic in ClinVar (Fig. 4b,c and Supplementary Fig. 2a–g). Overall, 29 out of 66 genes containing arginine-rich frameshift variants had a probability of loss-of-function intolerance (pLI) score of <0.05, which is consistent with a potential gain-of-function effect of the variants (Extended Data Fig. 7e). The variants were associated with various pathogenic conditions, including neurodevelopmental diseases and cancer predisposition (Extended Data Fig. 7f–h). Moreover, 98 of the frameshifts also created a sequence resembling the short hydrophobic patch encoded by the HMGB1 frameshift (Fig. 4b), and 128 of the frameshifts occurred in genes that contained at least one hydrophobic patch in their IDR (Fig. 4b). Overall, the catalogue revealed >200,000 variants in C-terminal IDRs, including 624 frameshifts that replace a C-terminal tail with an arginine-rich basic tail, of which 101 frameshifts were classified as pathogenic.

Fig. 4: A catalogue of variants in C-terminal IDRs reveals frameshifts associated with nucleolar mispartitioning and dysfunction.



a, Circos plot of the IDR variant catalogue. The circles indicate the location of genes that contain a truncation (stop gained) or frameshift variant in the dbSNP, 1000 Genomes Project, COSMIC and ClinVar databases. The highlighted genes contain a pathogenic frameshift that creates a sequence of ≥20 amino acids comprising ≥15% arginine residues. **b**, Summary statistics and features of variant types in C-terminal IDRs. *P* values are from hypergeometric tests. **c**, Identification of frameshifts creating a sequence of ≥20 amino acids that consist of ≥15% arginine residues. Plotted is the fraction of arginine residues against the length of the sequence created by

the frameshift. The genes containing the variants selected for further validation are highlighted orange. Pathogenic gene variants are in blue. **d**, Representative images of U2OS cells co-expressing RFP–FIB1 and the indicated eGFP-tagged proteins. Nuclear area revealed by Hoechst staining is shown as dashed white lines. Mutations in the following genes are associated with the indicated conditions: microphthalmia (*HMGB3* and *RAX*); myopathy (*MYOD1*); congenital central hypoventilation (*PHOX2B*); myelodysplasia (*RUNX1*); Axenfeld–Rieger syndrome type 3 (*FOXC1*); myelofibrosis (*CALR*); alveolar capillary dysplasia (*FOXF1*); anophthalmia/microphthalmia-oesophaegalatresia syndrome (*SOX2*); Paget disease of bone 2, early-onset frontotemporal dementia and amyotrophic lateral sclerosis (*SQSTM1*); blepharophimosis, ptosis and epicanthus inversus (*FOXL2*); and hereditary cancer predisposing syndrome (*MEN1*). Scale bar, 10 μm. **e**, Nucleolar mispartitioning strongly correlates with the fraction of arginine residues in the frameshift sequence. Plotted are Pearson's correlation coefficients of the extent of nucleolar mispartitioning of mutant proteins with protein features of their IDRs (left triangle) and features of the sequences created by the frameshifts (right triangle). The colour corresponds to the value of Pearson's correlation coefficients, and the size of the circles is proportional to the *P* value of the Pearson's *r*. **f**, RT–qPCR analysis of rRNA species in U2OS cells expressing the indicated WT and mutant proteins. rRNA levels are normalized against an RNAPII transcript (*GAPDH*), and fold changes are calculated against the rRNA/*GAPDH* level measured in the cells expressing WT protein. Data are shown as mean ± s.d., *P* values are from two-tailed Welch's *t*-test. AA, amino acid; SNP, single nucleotide polymorphism; nucl. enr., nucleolar enrichment.

Genes containing pathogenic frameshift variants that create an arginine-rich basic tail were expressed in U2OS cells. As such frameshifts are highly enriched in genes that encode transcription factors, we selected nine transcription factors (HMGB3, FOXC1, FOXF1, MYOD1, RAX, RUNX1, SOX2, PHOX2B and FOXL2) and four additional proteins (MEN1, SQSTM1, CALR and DVL1) for functional testing (Fig. 4d, Extended Data Figs. 8 and 9a–d and Supplementary Fig. 3a–d). The frameshift mutants of 12 out of the 13 proteins formed nuclear inclusions that overlapped the FIB1–RFP-labelled dense fibrillar component of the nucleolus in live cells (Fig. 4d and Extended Data Fig. 9e–i). The extent of mispartitioning into the

nucleolus strongly correlated with the length of the IDR sequence replaced by the frameshift and the fraction of arginine residues in the sequence created by the frameshifts (Fig. 4e and Supplementary Fig. 4a,b). For six variant proteins, cavities enriched in FIB1–RFP were apparent (Fig. 4d and Extended Data Fig. 10a). FRAP experiments showed that condensate properties for 7 out of the 13 variants were affected (Extended Data Figs. 9g and 10b). Six of the mutant proteins that showed significant nucleolar enrichment were further analysed. For four out of six, changes in the level of rRNA species in cells expressing the frameshift mutants were detectable (Fig. 4f and Extended Data Fig. 10c,d). These results indicate that disease-associated frameshifts that generate an arginine-rich basic tail in C-terminal IDRs can cause nucleolar mispartitioning and dysfunction.

Discussion

We propose that disease-associated and common variants in disordered regions may alter phase separation and partitioning of proteins into biomolecular condensates. In particular, the results presented here indicate that frameshift variants that substantially increase the arginine content of various proteins lead to mispartitioning into the nucleolus and disruption of nucleolar function. Our data identified the replacement of the disordered tail with an arginine-rich basic tail in HMGB1 as the pathomechanism underlying BPTAS, a rare complex malformation syndrome[13]. The HMGB1 variant appears to encode a sequence that combines high arginine content, reminiscent of the phase-separation grammar of native nucleolar proteins[40], and a hydrophobic patch that predominantly contributes to nucleolar arrest and dysfunction (Fig. 3e–j). The frameshift therefore interferes with the 'molecular grammar' of phase separation encoded in *HMGB1*, and the resulting mutant protein disrupts condensate features and function of the nucleolus where it accumulates. The extent to which the minimal propensity of the HMGB1 mutant sequence to form a helix contributes to these effects remains to be tested.

We provided evidence that arginine-rich frameshifts occur in hundreds of proteins, which implies that there is a common mechanism for hundreds of disease-associated and common genetic variants with previously unknown functions. The organismal effects of such frameshifts are probably

influenced by tissue-specific expression and haplosufficiency (or haploinsufficiency) of the genes in which they occur. For example, BPTAS is associated with a frameshift in *HMGB1* that is broadly expressed and haploinsufficient (pLI score of 0.83), which is consistent with phenotypic features presenting in multiple organ systems and partially overlapping with those seen when the locus is deleted (Supplementary Note). Of note, mispartitioning into the nucleolus and nucleolar dysfunction have been reported for poly-(proline:arginine)-dipeptides produced by repeat-expanded variants of *C9orf72* linked to amyotrophic lateral sclerosis[36,41,42]. Aberrant phase separation and nucleolar dysfunction may therefore occur in a wide range of genetic conditions as a shared underlying molecular pathomechanism.

Finally, the IDR variant catalogue provides a resource for exploring further models of how disease-associated variants may alter biomolecular condensates. For example, the >10,000 variants that truncate a C-terminal IDR may inhibit biogenesis of condensates, and several such variants have been associated with condensate dissolution in cultured cells[43]. Disease-associated alanine repeat expansions in a few transcription factors have been shown to alter the composition of their condensates[6], and our catalogue contains >200 frameshift sequences consisting of at least 25% alanine residues. In summary, we propose that disruption of phase separation may frequently occur in genetic diseases. Further investigation of the underlying molecular basis may lead to future strategies that alter phase separation with therapeutic intent.

Methods

DNA sequencing, array comparative genomic hybridization and qPCR

Genome sequencing and exome sequencing were performed using Illumina technology with a paired-end sequencing approach[26]. Genome sequencing data were filtered using VarFish. Information on excluded variants and filtering strategy are displayed in Extended Data Fig. 2a. Sanger sequencing and real-time qPCR were performed on a 3730 DNA analyzer (Thermo

Fisher Scientific). Sanger sequencing of *HMGB1* from gDNA from individuals included in this study was performed using primers listed in Supplementary Table 6. For cDNA Sanger sequencing and RT–qPCR of I3, RNA was extracted from a patient and a control lymphoblastoid cell line using a Direct-zol RNA Miniprep kit (Zymo Research Europe). RNA was measured on a Nanodrop instrument (Thermo Fisher Scientific), and 1 µg of RNA was transcribed to cDNA using a RevertAid H Minus First Strand cDNA Synthesis kit (Thermo Fisher Scientific). Raw data of RT–qPCRs were analysed using the $2^{(-\Delta\Delta CT)}$ method normalized to *GAPDH*. For cDNA Sanger sequencing, the primers used for amplification and sequencing are listed in Supplementary Table 6. For RT–qPCR of cDNA from individuals included in this study, *HMGB1* and *GAPDH* primers are listed in Supplementary Table 6. Chromosomal microarray analysis was performed using a 4 × 180 k oligonucleotide slide from Agilent on a DNA microarray scanner (Agilent). Chromosomal microarray analysis results were confirmed by RT–qPCR. All procedures were performed using the manufacturers' protocols. All variants were annotated according to genome build hg19 and the *HMGB1* transcript NM_002128.7.

Patient consent

Parental consent was obtained for all clinical and molecular studies of this article and for the publication of the relevant causative variants and of clinical photographs. Patient consent did not cover the release of personal sequence information other than the causative pathogenic variants. Therefore, whole-genome sequencing and exome sequencing data cannot be made publicly available. All studies and investigations were performed according to the declaration of Helsinki principles of medical research involving human participants, and the study was approved by the ethics committee of the Charité–Universitätsmedizin Berlin (EA2/087/15).

Patient recruitment and clinical protocol

Individuals were recruited during routine patient care at five departments of genetics (Berlin, Kiel, Nuremberg, Schwerin, Hong Kong). Fetuses from spontaneous abortions were not systematically screened for BPTAS. No

statistical methods were used to predetermine sample sizes. Investigators were not blinded and no randomization was used.

Computer-aided facial phenotyping

Facial frontal images were analysed using the Face2Gene suite (v.20.1.4, https://www.face2gene.com). Face2Gene Clinic was used for computer-aided facial phenotyping[44]. We created a composite mask using Face2Gene Research. If several images of the same patient were available, the image depicting the individual at the oldest age was used for facial analysis by Face2Gene Clinic. Seven images of unrelated individuals diagnosed with BPTAS were taken from the literature (of those reported in ref. [15], only the father was included)[13,14,15,16,17,18,19]. In addition, I1 and I2 of the current study were included in the analysis. Each selected BPTAS image was used twice for Face2Gene Research analysis to reach more than the ten images necessary for composite mask creation (Extended Data Fig. 1s).

AlphaFold predictions for protein structures

AlphaFold predictions were computed using an in-house implementation of AlphaFold[45] using v.2.0.0 from 16 July 2021. The preset parameter was set to --preset=casp14 to use all genetic databases and eight ensembles, matching the CASP14 prediction pipeline. Templates were restricted to those available before the CASP14 predictions using the parameter --max_template_date=2020-05-14. Models were rendered using UCSF ChimeraX (v.1.5)[46,47], colouring the structure with the pLDDT score. Multiple sequence analysis depth plots and per-model pLDDT sequence plots were made using custom scripts based on ColabFold notebook AlphaFold2 with MMseqs2 (ref. [48]). Predictions of *Mus musculus*, *Rattus norvegicus* and *Danio rerio* HMGB1(A) protein structures, shown in Extended Data Fig. 4a, are from the AlphaFold Protein Structure Database[45].

Generation of DNA constructs for protein purification and expression in human cells

To generate plasmids for recombinant protein expression, *HMGB1* cDNA sequences containing the wild-type or NM_002128.7(*HMGB1*):c.551_554delAGAA;p.(Lys184Argfs*44) variant were ordered from Twist Bioscience. Full-length cDNAs and the regions encoding IDR sequences were cloned into a monomeric eGFP (meGFP)-pET45 backbone by Gibson assembly using NEBuilder HiFi DNA Assembly MasterMix (NEB); primers are listed in Supplementary Table 6. For the generation of pET45-mCherry–NPM1 and pET45-mCherry–HP1a, *NPM1* and *HP1A* open-reading frames were amplified from mouse cDNA using primers flanked with Gibson overhangs (sequences listed in Supplementary Table 6). The resulting amplicons were gel purified and cloned into pET45-mCherry (Addgene, 145279) linearized with AscI and HindIII restriction enzymes. For the generation of pET28-mCherry–MED1-IDR, mCherry was subcloned into the pET28-meGFP–MED1-IDR vector as previously described[6,31] using NcoI and BsrGI restriction sites.

To express monomeric eGFP–HMGB1 variants in mammalian cells, eGFP–HMGB1 sequences were subcloned from pET45-meGFP vectors into a pRK5-meGFP vector digested with AgeI and XbaI (Addgene, 18696); primers used are listed below. To express wild-type and frameshift variants of FOXC1, FOXF1, HMGB3, MYOD1, RAX, RUNX1, PHOX2B, CALR, SOX2, SQSTM1, FOXL2, MEN1 and DVL1, the following cDNA sequences were ordered from Twist Bioscience: NM_001453.3(*FOXC1*):c.599_617del;p.(Gln200Argfs*109), variant rs1057519478; NM_001451.3(*FOXF1*):c.691_698del;p.(Ala231Argfs*61), variant 692054; NM_005342.4(*HMGB3*):c.480_481dup;p.(Lys161Ilefs*55), variant rs431825172; NM_002478.5(*MYOD1*):c.557dup;p.(Arg188Profs*90), variant rs1179926739; NM_013435.3(*RAX*):c.664del;p(Ser222Argfs*63), variant rs1603388837; NM_001754.5(*RUNX1*):c.1088_1094del;p.(Gly363Alafs*229), variant 1013621; NM_004343.4(*CALR*):c.1157_1158dup;p.(Asp387Argfs*44), variant COSV104394382; NM_003924.4(*PHOX2B*):c.618del;p.(Ser207Alafs*102), variant 658418; NM_023067.4(*FOXL2*):c.982del;p.(Ala328Profs*28), variant 369937; NM_003106.4(*SOX2*):c.828del;p(Met276Ilefs*95) variant 986766; NM_003900.5(*SQSTM1*):c.810del;p.(Val271Serfs*41) variant 967349; NM_001370259.2(*MEN1*):c.1382_1389dup;p.(Ala464Argfs*98) variant

428075; NM_004421.2(*DVL1*):c.1505_1517del;p.(His502Profs*143). For genotype–phenotype correlations see Supplementary Note.

cDNAs were amplified with primers listed in Supplementary Table 6 and cloned into a pRK5-meGFP–HMGB1 vector using Gibson assembly after removing the *HMGB1* sequence with BsrGI and XbaI restriction enzymes. To test the contribution of arginine and lysine residues of the mutant HMGB1 sequence, cDNA sequences were ordered from Twist Bioscience, in which all arginine and lysine residues after Lys185 were replaced with alanine (R&K>A variant), all arginine residues after Lys185 were deleted (R del variant) or replaced with alanine or lysine (R>A and R>K, respectively, variants). cDNAs were amplified using the primers listed below and cloned into a pRK5-meGFP–HMGB1 vector as described above. To create truncated versions of HMGB1, in which the IDR (amino acids after Asn134), or the sequence after the frameshift position (del FS) or the hydrophobic patch of the mutant sequence (amino acids after Lys209) is deleted, cDNA was amplified from pRK5-meGFP-HMGB1 using the primers listed in Supplementary Table 6 and cloned back to a vector digested with BsrGI and XbaI as described above. All constructs were sequence-verified. Plasmids are available from Addgene (https://www.addgene.org/Denes_Hnisz/).

Protein purification and peptide synthesis

Protein expression of mCherry constructs was performed as previously described[6,33], but with modifications to mCherry–MED1-IDR expression, which was performed in the presence of 400 μg ml^{-1} kanamycin. Protein expression of meGFP–HMGB1 constructs was performed in Rosetta (DE3)pLysS cells (Sigma-Aldrich) in the presence of 25 μg ml^{-1} chloramphenicol and 100 μg ml^{-1} ampicillin. All bacterial pellets were stored at −80 °C. Pellets were resuspended in 20 ml of ice-cold buffer A (50 mM Tris pH 7.5, 500 mM NaCl, 20 mM imidazole and complete protease inhibitors (Sigma-Aldrich, 11697498001)), and cells were lysed using a Qsonica Q700 sonicator. Lysate was cleared by centrifugation at 15,500*g* for 30 min at 4 °C, and proteins were purified using an Äkta avant 25 chromatography system and a complete His-Tag purification column (Merck, 6781543001). Columns were pre-equilibrated in buffer A, loaded

with cleared lysate and washed with 15 column volumes of buffer A. Fusion proteins were eluted in 10 column volumes of elution buffer (50 mM Tris pH 7.5, 500 mM NaCl and 250 mM imidazole). Protein preparations were diluted in storage buffer (50 mM Tris pH 7.5, 125 mM NaCl, 1 mM DTT and 10% glycerol) and concentrated using 3000 MWCO Amicon Ultra centrifugal filters (Merck, UFC803024) and stored at −80 °C. After His-Tag column purification, meGFP–HMGB1 protein preparations were further purified using Superdex 200 10/300 GL columns (GE28-9909-44) and concentrated and stored as noted above. Elution profiles are shown in Extended Data Fig. 4a. We note that the mutant protein elutes at lower elution volumes, which indicates that it may form soluble oligomers and that the potential to form soluble oligomers may be associated with the slight propensity of the mutant IDR to form a helix (Extended Data Fig. 3c,d). Immunoreactivity of purified meGFP–HMGB1 proteins were evaluated by western blotting. Equal amounts of protein were diluted in NuPAGE LDS buffer (Thermo Fisher Scientific, NP0007) with NuPAGE sample-reducing agent and heated at 70 °C for 10 min. Samples were run using NuPAGE 4–12% Bis-Tris protein gels (Invitrogen, NP0321PK2) and transferred to a nitrocellulose membrane with an iBlot2 device. The membrane was blocked with 5% non-fat milk TBST for 1 h and incubated 1 h with anti-HMGB1 (Sigma-Aldrich, H9664) or anti-eGFP (Invitrogen, A-11122) antibodies diluted 1:1,000 in 5% non-fat milk TBST. Membranes were washed five times with TBST, incubated with HRP-conjugated donkey anti-rabbit antibody (1:2,000, Jackson Immuno Research, 711-035-152) for 1 h, washed five times in TBST and visualized using SuperSignal West Dura Extended Duration substrate (Thermo Scientific, 34075). The identity of the fusion protein products was confirmed by mass spectrometry.

Synthetic peptides with amino-terminal 5′ FAM-labelling for in vitro droplet formation assays (Fig. 2i and Extended Data Fig. 4d–i) and circular dichroism (CD) spectroscopy experiments (Extended Data Fig. 3c,d) were ordered for wild-type and mutant HMGB1 C-terminal sequences (Asp135 onwards) from ProteoGenix. The synthetic peptides had >90% purity.

CD experiments

The synthetic peptides were dissolved in 20 mM sodium phosphate buffer, pH 7.4. The samples were centrifuged for 10 min at 15,000 r.p.m. to remove undissolved solid. The supernatant was extensively dialysed against 20 mM sodium phosphate buffer, pH 7.4, to remove traces of impurities from peptide synthesis. The protein concentration was determined by amino acid analysis. CD spectra were acquired on 10.6 μM samples in a Jasco 815 UV spectrophotopolarimeter at 278 K with a 1 mm optical path cuvette. Each spectrum is the result of 20 cumulative scans acquired at a scanning speed of 50 nm min^{-1} with a data pitch of 0.2 nm (Extended Data Fig. 4c,d).

Reference CD spectra in Extended Data Fig. 4e are included from the Protein Circular Dichroism Data Bank[49]. The following reference proteins were used: myoglobin (blue)[50], with a DSSP α-helix of 73.9%; outer membrane protein g (OmpG, purple)[51], with a DSSP β-strand of 67.6%; and translocated actin recruiting phosphoprotein (Tarp, green)[52], with a DSSP loop of 71.0%.

In vitro droplet formation experiments

For droplet formation experiments in Fig. 2c–e, proteins were diluted to desired concentrations in storage buffer, further diluted 1:1 in 20% PEG-8000 and mixed well with pipetting. Next, 10 μl of solution was immediately transferred on a chambered coverslip (Ibidi, 80826-96). Droplets were imaged using a LSM880 confocal microscope (Zeiss) with a ×63, 1.40 oil DIC objective. Images were acquired slightly above the solution interface; for FRAP experiments, images were acquired directly on the solution interface. Time series for FRAP experiments were acquired using 60 cycles of 2 s intervals, during which the eGFP signal was bleached using a 488 nm laser with 95% intensity after the second interval. FRAP was performed for at least ten droplets for both wild-type and mutant HMGB1 using 10 μM concentration. Recovery curves were fitted to a power-law model. For droplet assays using preassembled mCherry–HP1α, mCherry–MED1-IDR and mCherry–NPM1 condensates (Fig. 2g–i), mCherry-labelled proteins were diluted to 20 μM concentration in storage buffer, diluted 1:1 in 20% PEG-8000 and droplets were allowed to form for 1 h at room temperature, shielded from light. Next, eGFP–HMGB1 proteins or 5′ FAM-labelled synthetic IDR peptides were added to the desired concentration,

thoroughly mixed and solutions were left to equilibrate for 45 min at room temperature, shielded from light. Droplets were imaged as described above. To test the contribution of RNA for the condensation propensity of HMGB1 IDR peptides, total RNA from V6.5 mouse embryonic stem cells was isolated using a Direct-zol RNA Miniprep kit and added in indicated concentrations into peptide dilutions. RNA–peptide dilutions were thoroughly mixed with pipetting, crowding agent was added and imaging was performed as described above.

Cell culture

U2OS, HCT116 and HEK293T cells were cultured in DMEM with GlutaMAX (Thermo Fisher Scientific, 31966-021) supplemented with 10% FBS and 100 U ml^{-1} penicillin–streptomycin (Gibco). MCF7 cells were cultured in RPMI-1640 supplemented with 20% FBS and 100 U ml^{-1} penicillin–streptomycin (Gibco). Human induced pluripotent stem (iPS) cells ZIP13K2 (ref. [53]), were grown in mTeSR Plus (Stem Cell Technologies, 100-0276) on plates coated with 1:100 diluted Matrigel (Corning, 354234) in KnockOut DMEM (Thermo Fisher Scientific, 10829-018) and supplemented with 10 µM of the Rho kinase inhibitor Y-27632 (Abcam, ab120129) once detached during passaging. Cells were cultured at 37 °C with 5% CO_2 in a humidified incubator. All cell lines were tested negative for mycoplasma contamination. For live-cell imaging and immunofluorescence, cells were seeded on chambered coverslips (Ibidi, 80826-96). On the next day, cells were transfected using FuGENE HD (Promega) according to the manufacturer's instructions. Human iPS cells were transfected using Lipofectamine 3000 according to the manufacturer's instructions. For viability experiments, cells were cultured on 6-well plates. Transfection series were repeated at least twice for each experiment.

RT–qPCR after expression of frameshift variants in U2OS cells

Cells were grown on 6-well plates, transfected with FuGENE HD according to manufacturer's instructions, and $eGFP^+$ cells were sorted by FACS 48 h after transfections and lysed in TRIzol reagent (Thermo Fisher Scientific). Experiments were performed in at least three biological replicates. RNA was

extracted and cDNA synthesis was performed as described above, except that 125 ng of RNA was used. Primers are listed in Supplementary Table 6.

Live-cell imaging

Cells were imaged 24 h after transfections using a LSM880 confocal microscope (Zeiss) equipped with an incubation chamber with 5% CO_2 and a heated stage at 37 °C. Images were acquired using a ×63, 1.40 oil DIC objective. To visualize cell nuclei, cells were incubated with 0.2 µg ml^{-1} Hoechst (Thermo Scientific, 33342) at least 10 min before imaging. To visualize nucleoli in living cells, we expressed RFP–fibrillarin fusion proteins by transfecting cells with pTagRFP-C1-fibrillarin plasmid (Addgene, 70649) together with plasmids for eGFP–HMGB1 and other transcription factor variants.

FRAP experiments were performed for nucleolar regions in cells expressing wild-type or mutant eGFP–HMGB1, guided by the RFP–fibrillarin fluorescence channel. Time series for FRAP experiments were acquired using 20 cycles of 2 s intervals, during which the eGFP signal was bleached using a 488 nm laser with 85% intensity after the second interval. FRAP experiments with designed variants of HMGB1 and other frameshift variants were performed as described above, but using 85–100% laser intensities for bleaching with identical settings for each wild type–mutant comparison. Fluorescence intensities were acquired from around ten regions of interest from separate nuclei, quantified using ZEN Black 2.3 software and reported as relative values to the pre-bleaching time point.

Time-lapse imaging of mutant HMGB1 expressing U2OS cells was performed on a Screenstar microplate (Greiner bio-one, 655866) with Zeiss Celldiscoverer 7. Images were acquired fully automated with a Plan-ApoChromat ×20 objective, NA = 0.7 and 1× tubelense (Optovar) using 15 min intervals and a camera binning of 1 × 1 pixel in 8-bit mode (Supplementary Video 2).

Immunofluorescence

For fixed-cell immunofluorescence, cells were fixed 24 h after transfections with 4% PFA in PBS for 10 min. After two washes with PBS, cells were permeabilized by incubating 30 min with 0.5% Triton X-100 at room temperature, washed three times with PBS and blocked for 1 h with blocking buffer (1% BSA, 0.1% Triton X-100 in PBS) at room temperature. Samples were incubated with primary antibodies diluted in blocking buffer (1:500 rabbit anti-HP1α, Cell Signaling, 2616S; 1:500 rabbit anti-MED1, Abcam, ab64965; 1:500 rabbit anti-RNAPII, ab26721; 1:250 mouse anti-NPM1, Thermo Fisher Scientific, 32–5200; 1:100 mouse anti-FIB1, Santa Cruz, sc-374022; 1:200 mouse anti-SC35, Sigma-Aldrich, S4045) overnight in 4 °C with gentle agitation. After four washes with blocking buffer, samples were incubated with secondary antibodies (1:1,000 dilutions of Alexa Fluor 647 donkey anti-mouse or anti-rabbit antibodies, Jackson Immuno Research, 715-605-150 and 711-605-152) for 1 h at room temperature. Samples were washed two times with blocking buffer, incubated for 3 min with 0.25 μg ml^{-1} DAPI (Invitrogen, D1306) in PBS and washed five times with PBS.

Protein synthesis labelling by puromycylation

U2OS cells were seeded on 24-well plates (15,000 cells per well) on sterilized 13 mm glass coverslips pretreated with 0.2% gelatin. The next day, cells were transfected with meGFP–HMGB1 full-length wild-type or mutant constructs using FuGENE HD according to the manufacturer's instructions. After 24 h, pulse labelling of nascent peptide chains actively translated by the ribosome was performed by replacing the medium supplemented with 20 μM puromycin (Sigma Aldrich, P8833) for 15 min at 37 °C, 5% CO_2. Cells were then washed three times with cold PBS, followed by fixation with 4% formaldehyde (Roth, P087.5) at room temperature, with shaking, for 20 min. Fixative was removed, and cells were washed two times with PBS, followed by incubation in blocking solution (1× PBS, 5% v/v normal donkey serum, 1% w/v BSA, 0.1% w/v glycine and lysine) with shaking for 45 min at room temperature. Anti-puromycin (1:1,000, mouse, Sigma Aldrich, MABE343, RRID:AB_2566826) and anti-GFP (1:2,000, chicken, Abcam, ab13970, RRID:AB_300798) primary antibodies were applied in blocking solution supplemented with 0.4% Triton-X-100 and incubated overnight with shaking at 4 °C. Cells were then washed three times with PBS for 5 min at room temperature, followed by secondary antibodies

(1:250, Jackson ImmunoResearch, 488-anti-chicken, 703-545-155, RRID:AB_2340375; 647-anti-mouse, 715-605-151, RRID:AB_2340863) incubated in blocking solution with 0.4% Triton-X-100 shaking for 2 h at room temperature. After three PBS washes, cells were incubated in DAPI (1:2,500) in PBS for 30 min with shaking at room temperature, and washed with PBS an additional two times. Coverslips were removed from wells and sealed on poly-l-lysine slides (Thermo, J2800AMNZ) with ProLong Gold Antifade Mountant (Invitrogen, P36930). The experiment was performed in independent biological triplicates, with two to four technical replicate coverslips per conditions per experiment.

Coverslips were imaged using a Zeiss Celldiscoverer 7 running Zen Blue v.3.2 (Zeiss). All images were acquired in a fully automated fashion with a Plan-ApoChromat ×20 objective, NA = 0.95 and a ×2 tube lens (Optovar), and camera binning 2 × 2 pixels in 8-bit mode. The resulting lateral resolution (*xy*) is 0.227 µm pixel^{-1}. All images were acquired in tile regions of typically 20 × 20 individual tiles, resulting in 400 individual images per coverslip. Focus stabilization was achieved with an automated combined hardware and software focusing strategy at each second position (Fig. 3h,i and Extended Data Fig. 6b,c).

Viability experiments

For viability experiments, cells were collected 24 h after transfections or doxycycline inductions and sorted for eGFP$^+$ cells using a FACS Aria II flow cytometer (BD Biosciences) with BD FACS Diva v.6.1.3. software. The FACS gating strategy is shown in Supplementary Fig. 6. One thousand cells per well were seeded on white microwell plates and were cultured for an additional 48 h. Viability was measured using a CellTiter-Glo 2.0 Cell Viability assay (Promega, G9242) according to the manufacturer's instructions. Measurements were done in three to five technical replicate wells and performed in four to five independent biological replicates. For imaging cells at the end of viability assay, 40,000 sorted cells were seeded per well on 24-well plates and imaged 48 h later with a Nikon Eclipse Ti2 microscope with a ×10 objective.

Generation of doxycycline-inducible meGFP–HMGB1 transgenic cell lines

A PiggyBAC transposon system was used to integrate meGFP–HMGB1 wild-type and mutant sequences into U2OS cells. To generate the doxycycline-inducible expression cassette, *meGFP–HMGB1* cDNA was amplified from pRK5-meGFP–HMGB1 plasmids (primers listed in Supplementary Table 6), and Gibson assembly cloned into the backbone of a Caspex expression vector (Addgene, 97421) digested with NcoI and BsrGI restriction enzymes. Generated plasmids were transfected with a PiggyBAC transposase expression vector (SBI, PB210PA-1) into U2OS cells with FuGENE HD reagent according to the manufacturer's instructions using a molar ratio of 6:1 with meGFP–HMGB1 and transposase expression plasmids. Transfected cells were kept under puromycin (2 $\mu g\ ml^{-1}$) selection for 4 days, after which all untransfected control cells had died. Bulk populations of surviving cells were induced by adding 2 $\mu g\ ml^{-1}$ doxycycline (Sigma) and imaged 24 h after doxycycline treatments (Extended Data Fig. 6e–j). GFP^{+} cells were sorted by FACS for viability experiments, which were performed as described above. Single-cell clones of meGFP–HMGB1 mutant-expressing U2OS cells was used for time-lapse imaging (Supplementary Video 2).

Image analysis

For the detection of droplet regions for phase diagrams, we used the ZEN blue 3.2 Image Analysis and Intellesis software packages to analyse at least five images for each experimental condition. Image segmentation was performed using the Intellesis Trainable segmentation algorithm, which was trained on five representative images from the image series to classify each pixel into the droplet area and image background. Regions of interest were automatically detected for the entire image series, and mean signal intensities for the eGFP or 5′ FAM channel and object areas for droplets and background are reported. In Fig. 2d, the phase-shifted fraction was calculated as the total area of detected droplets divided by the total area.

Data for dual-colour in vitro condensation experiments were acquired from 15–20 image fields for each condition (corresponding to Fig. 2g–i and

Extended Data Fig. 4i,j) using ZEN Blue 3.2. For Extended Data Fig. 4j,k, droplets were first detected using triangle thresholding for light regions in the meGFP or 5′ FAM channel. For data analyses in Fig. 2h,i, droplets were detected using Otsu thresholding for light regions in the mCherry channel. Mean fluorescence intensity within droplet regions, area and diameter were then measured on both channels and plotted as described.

To quantify nuclear enrichment of eGFP–HMGB1, Hoechst stain was used to identify nuclei as the regions of interest using the ZEN Blue 3.2 zones of influence method. Images were automatically segmented with Otsu thresholding, parameters of which were adjusted on the basis of five representative images from the image series. The cytoplasmic region was defined as a ring surrounding the nucleus with a distance of 9 and a width of 29 pixels. Mean and standard deviation values for eGFP fluorescence intensity were recorded for nuclear and cytoplasmic regions, and nuclear enrichment, calculated as a ratio between the two, was plotted in Extended Data Fig. 5a. Cells with no expression (eGFP fluorescence intensity below 5) were excluded from the analysis.

To quantify the correlation between eGFP–HMGB1 fluorescence and NPM1 staining intensities inside and outside nucleoli, images from around 120 cells per condition were analysed using ZEN Blue 3.2 software. Images were first segmented to nuclear regions of interest with Otsu thresholding on the basis of DAPI channel intensity. Nuclei were further segmented to nucleolar regions of interest and regions outside the nucleoli, based on NPM1 staining intensity, using fixed thresholds that detected nucleoli in cells with high and low NPM1 intensities. Parameters were empirically set with ten representative images for each experimental set. Mean signal intensities for eGFP and NPM1 staining were recorded for each region of interest and reported as an average for each detected nucleus.

To quantify nucleolar enrichment of wild-type and frameshift variant proteins (Extended Data Fig. 9e), nuclear regions of interest were defined with Hoechst staining as outlined above and nucleolar regions with RFP–FIB1 intensity using two fixed thresholds that detect nucleoli in cells with high and low RFP–FIB1 expression. Mean signal intensities for eGFP were recorded, and nucleolar enrichment was plotted as $\log_2$(mean signal intensity for regions within nucleoli/mean intensity outside nucleoli). When imaging

human iPS cells, nuclear regions of interest were eroded by 8 pixels to avoid signals at the nuclear periphery.

Data wrangling was performed in base R, and plots were generated using the ggplot2 package.

Image analysis for puromycylation experiments was performed using Zen Blue software v.3.4. DAPI was used to localize each cell. In brief, DAPI images were smoothed, an Otsu threshold was applied to binarize images and watershedding was used to separate neighbouring objects. The resulting nuclei masks were filtered to fit an area of 75–900 μm^2 and a circularity (sqrt(4 × area/π × FeretMax^2)) of 0.6–1. The resulting primary objects were dilated with a total of 17 pixels, 3.9 μm. Puromycin and GFP signal intensities were quantified per cell. Puromycin intensity in each GFP$^+$ cell was normalized by the mean puromycin intensity in GFP$^-$ cells in the same image, for wild-type and mutant conditions, and plotted using R and GraphPad Prism, followed by comparisons for significant differences (one-way ANOVA) between condition means from biological replicates. A total of 37,979 single cells for mutant and 39,528 for wild-type conditions were identified and analysed (Fig. 3h,i and Extended Data Fig. 6b,c).

C-terminal IDR identification

Prediction of IDRs was performed using metapredict (v.1.51)[54], a deep-learning-based predictor for consensus disordered sequences. The threshold score was set to 0.5, the minimum IDR length was set to 20 amino acids and the analysis was restricted to only GENCODE canonical or GENCODE basic isoforms. To complete the IDR catalogue, sequences from MobiDB[55] were added to the database. Protein coordinates for each IDR and Interpro domain were used to define the C-terminal IDR. Using a combination of custom scripts, the C-terminal IDR of each isoform was defined as any IDR that started 20 amino acids downstream of the start of the protein, to filter all disordered proteins. The region where the start of the IDR was downstream of the start of the most C-terminal domain was mapped.

Variant identification and characterization

The resulting C-terminal IDR coordinates were then converted to genomic coordinates using the R package ensembldb[56] and the ensembl v.104 human annotation (v.2.22.0). The annotation version can affect the canonical isoforms that are selected for analysis, so the downstream analysis was locked to this version on Ensembl annotation. The resulting BED file was then used to filter ClinVar[57], COSMIC[58], dbSNP[59] and 1000 Genomes[60] to the designated genomic coordinates of the C-terminal IDR regions using BEDtools (v.2.30.0.)[61]. The resulting VCF file was filtered for protein-coding variant consequences using Ensembl Variant Effect Predictor (VEP, v.104)). The filtered VCF was then used to conduct downstream analysis using OpenCRAVAT[62] to annotate the variants for ClinVar annotation using the ClinVar and ClinGen[63] plugins, genomic frequencies using the 1000 Genome plugin, and CADD score[64,65] using the CADD plugin (v.1.6). The CADD score is a metric for the predicted effect of the variant on protein function (Fig. 4a). The same VCF file was also used to retrieve frameshift variant sequences using the Frameshift VEP plugin from pVACtools (v.3.1.0.)[66] and Downstream plugin for the stop gained sequences.

Sequences were then characterized using a combination of custom scripts to obtain protein sequence feature parameters based on localCIDER (v.0.1.18.)[67] and biopython (v.1.79.)[68] packages. All scatter and violin plots were made using the R package ggplot2. The fraction of amino acids was defined as the sum of the count of amino acids over the sequence length. The acidic fraction was defined as the sum of aspartic acid and glutamic acid. The basic fraction was defined as the sum of arginine, lysine and histidine. The RK fraction was defined as the sum of arginine, lysine, and the aromatic fraction as phenylalanine, tyrosine and tryptophan. Hydrophobic patches were identified using custom regex expression (r'([CAVILMFYW]..?)<6,>') using hydrophobic amino acids as the dictionary, allowing 1 or 2 amino acid gap and 6 residue minimum match. Nucleolar signal prediction was caried using NoD program (v.1.0.0.) with the command line with default settings[69]. Characterization of nonsense-mediated mRNA decay of variants was done using a custom script. In brief, wild-type exon boundaries were retrieved from GENECODE and mapped to the wild-type coding sequence. An NMD sensitive zone was established for each wild-type sequence with the following rules: >100 bp downstream of starting codon and <51 bp of the second to last exon boundary. Variants with

only one exon were marked 'NMD_escaping', then the stop codon coordinate of the variant was compared with the NMD sensitive zone coordinates and variants of which the stop codon did not overlap with the NMD sensitive zone were also marked as 'NMD_escaping'. All other variants were left empty.

Combined disordered and pLDDT score plots were plotted with the metapredict meta.graph_disorder function and pLDDT_scores parameter set to 'true', using v.2 of the metapredict network and v.7 of the pLDDT score prediction network.

Circos visualization of the variant catalogue was done using Circos implementation in R, and Granges package in R (Fig. 4a).

Enrichment analysis of pathogenic variants was done using hypergeometric nonaccumulative test with N set as the full number of variants in the catalogue and M set as the full set of pathogenic variants ($N = 249,468$ and $M = 1,805$). Reported P values correspond to the calculated hypergeometric P value and fold change as the number of pathogenic variants/expected number of pathogenic variants (Fig. 4b).

Sequence feature correlation matrices in Fig. 4e and Supplementary Fig. 4 were calculated using the cor package in R using Pearson parametric correlation test and plotted using the corrplot package in R. The P value cut-off was set to 0.01. The fraction of mutated IDRs was defined as 1 – (frameshift position – IDR start)/IDR length. The *SQSTM1* wild-type sequence was excluded from correlation analysis because the wild-type isoform ENST00000510187.5 in our catalogue was replaced with isoform ENST00000389805.9 (NM_003900.5) in the imaging experiments owing to low transcript support level (TSL:5) for ENST00000510187.

Gene Ontology enrichment analysis (Extended Data Fig. 7d) for the variant type 'stop gained', 'frameshift' and 'ARG-rich FS' was done using gProfiler[70]. Multiple testing correction for P values was done using the g:SCS method from g:Profiler.

Scores for the predicted disorder plotted in Fig. 2a and Extended Data Fig. 9a,c were obtained using PONDR (http://www.pondr.com). Charge plots in

Fig. 1f and Extended Data Fig. 9b,d were prepared using EMBOSS Charge tool (https://www.bioinformatics.nl/cgi-bin/emboss/charge) with a window size of 8. Isoelectric points (pI) for post-frameshift sequences were calculated using Expasy compute pI tool (https://web.expasy.org/compute_pi/).

The DVL1 variant NM_004421.2(*DVL1*):c.1505_1517del was not part of the catalogue because the frameshift sequence from the canonical isoform used in ensembl v.104 did not fulfil all selection criteria. Instead, this variant was identified through a literature search that revealed Robinow syndrome-associated frameshift variants in the *DVL*1 gene that occur in a C-terminal IDR that generates arginine-rich sequences[71,72].

Reporting summary

Further information on research design is available in the Nature Portfolio Reporting Summary linked to this article.

Data availability

CD spectra have been deposited at the Protein Circular Dichroism Data Bank under the accession identifiers CD0006401000, CD0006401001, CD0006404000, CD0006404001. Genome and exome-wide summary statistics of I1, I4 and I5, and direct sequencing results of HMGB1 of I1–I4 and array comparative genomic hybridization and qPCR results of the *HMGB1* locus of I6 are made available in this manuscript (Extended Data Fig. 2). Patient consent did not cover the public release of personal sequence information other than the causative pathogenic variants. Therefore, the pathogenic variants are disclosed in this article, but individual-level whole-genome sequencing (WGS) and exome sequencing data cannot be made publicly available for reasons of data protection and patient privacy and are available only upon reasonable request from the corresponding authors. Access to individual-level sequencing data is subject to the policies and approval of the data protection officer of the institution that stores the patient data. WGS and Sanger sequencing data of I1 are stored at the Institute of Human Genetics, University Hospitals Schleswig-Holstein. WGS data of I4 is stored at the Center for Genomics and Transcriptomics (CeGaT)

Tübingen. WGS data of I5, and Sanger Sequencing data of I2–I5, and qPCR and array comparative genomic hybridization data of I6 are stored at the Institute of Medical Genetics and Human Genetics, Charité–Universitätsmedizin Berlin. The respective servers are physically located in Germany.

Code availability

Custom code is available at GitHub: https://github.com/hniszlab/HMGB1_2022; https://github.com/alexpmagalhaes/IDR-variant-catalog. Custom code and raw data for this study have been deposited at Zenodo (https://doi.org/10.5281/zenodo.7311150).

References

1. Claussnitzer, M. et al. A brief history of human disease genetics. *Nature* **577**, 179–189 (2020).

2. Tsang, B., Pritisanac, I., Scherer, S. W., Moses, A. M. & Forman-Kay, J. D. Phase separation as a missing mechanism for interpretation of disease mutations. *Cell* **183**, 1742–1756 (2020).

3. Dyson, H. J. & Wright, P. E. Intrinsically unstructured proteins and their functions. *Nat. Rev. Mol. Cell Biol.* **6**, 197–208 (2005).

4. Banani, S. F., Lee, H. O., Hyman, A. A. & Rosen, M. K. Biomolecular condensates: organizers of cellular biochemistry. *Nat. Rev. Mol. Cell Biol.* **18**, 285–298 (2017).

5. Shin, Y. & Brangwynne, C. P. Liquid phase condensation in cell physiology and disease. *Science* **357**, eaaf4382 (2017).

6. Basu, S. et al. Unblending of transcriptional condensates in human repeat expansion disease. *Cell* **181**, 1062–1079.e30 (2020).

7. Molliex, A. et al. Phase separation by low complexity domains promotes stress granule assembly and drives pathological fibrillization. *Cell* **163**, 123–133 (2015).

8. Patel, A. et al. A liquid-to-solid phase transition of the ALS protein FUS accelerated by disease mutation. *Cell* **162**, 1066–1077 (2015).

9. Deciphering Developmental Disorders Study. Large-scale discovery of novel genetic causes of developmental disorders. *Nature* **519**, 223–228 (2015).

10. Amberger, J. S., Bocchini, C. A., Schiettecatte, F., Scott, A. F. & Hamosh, A. OMIM.org: Online Mendelian Inheritance in Man (OMIM®), an online catalog of human genes and genetic disorders. *Nucleic Acids Res.* **43**, D789–D798 (2015).

11. Manolio, T. A. et al. Finding the missing heritability of complex diseases. *Nature* **461**, 747–753 (2009).

12. Kandoth, C. et al. Mutational landscape and significance across 12 major cancer types. *Nature* **502**, 333–339 (2013).

13. Baraitser, M. et al. A syndrome of brachyphalangy, polydactyly and absent tibiae. *Clin. Dysmorphol.* **6**, 111–121 (1997).

14. Faravelli, F., Di Rocco, M., Stella, G., Selicorni, A. & Camera, G. Brachyphalangy, feet polydactyly, absent/hypoplastic tibiae: a further case and review of main diagnostic findings. *Clin. Dysmorphol.* **10**, 101–103 (2001).

15. Pierson, D. M. et al. Total anomalous pulmonary venous connection and a constellation of craniofacial, skeletal, and urogenital anomalies in a newborn and similar features in his 36-year-old father. *Clin. Dysmorphol.* **10**, 95–99 (2001).

16. Olney, R. S. et al. Limb/pelvis hypoplasia/aplasia with skull defect (Schinzel phocomelia): distinctive features and prenatal detection. *Am. J. Med. Genet.* **103**, 295–301 (2001).

17. Wechsler, S. B., Lehoczky, J. A., Hall, J. G. & Innis, J. W. Tibial aplasia, lower extremity mirror image polydactyly, brachyphalangy, craniofacial dysmorphism and genital hypoplasia: further delineation and mutational analysis. *Clin. Dysmorphol.* **13**, 63–69 (2004).

18. Bernardi, P. et al. Additional features in a new case of a girl presenting brachyphalangy, polydactyly and tibial aplasia/hypoplasia. *Am. J. Med. Genet. A* **149A**, 1532–1538 (2009).

19. Shafeghati, Y. et al. Brachyphalangy, polydactyly and tibial aplasia/hypoplasia syndrome (OMIM 609945): case report and review of the literature. *Eur. J. Pediatr.* **169**, 1535–1539 (2010).

20. Itou, J. et al. HMGB factors are required for posterior digit development through integrating signaling pathway activities. *Dev. Dyn.* **240**, 1151–1162 (2011).

21. Yanai, H. et al. HMGB proteins function as universal sentinels for nucleic-acid-mediated innate immune responses. *Nature* **462**, 99–103 (2009).

22. Scaffidi, P., Misteli, T. & Bianchi, M. E. Release of chromatin protein HMGB1 by necrotic cells triggers inflammation. *Nature* **418**, 191–195 (2002).

23. Bianchi, M. E., Beltrame, M. & Paonessa, G. Specific recognition of cruciform DNA by nuclear protein HMG1. *Science* **243**, 1056–1059 (1989).

24. Prasad, R. et al. HMGB1 is a cofactor in mammalian base excision repair. *Mol. Cell* **27**, 829–841 (2007).

25. Sofiadis, K. et al. HMGB1 coordinates SASP-related chromatin folding and RNA homeostasis on the path to senescence. *Mol. Syst. Biol.* **17**, e9760 (2021).

26. Elsner, J. et al. Genome sequencing in families with congenital limb malformations. *Hum. Genet.* **140**, 1229–1239 (2021).

27. Lambert, S. A. et al. The human transcription factors. *Cell* **175**, 598–599 (2018).

28. Boehning, M. et al. RNA polymerase II clustering through carboxy-terminal domain phase separation. *Nat. Struct. Mol. Biol.* **25**, 833–840 (2018).

29. Boija, A. et al. Transcription factors activate genes through the phase-separation capacity of their activation domains. *Cell* **175**, 1842–1855.e16 (2018).

30. Cho, W. K. et al. Mediator and RNA polymerase II clusters associate in transcription-dependent condensates. *Science* **361**, 412–415 (2018).

31. Sabari, B. R. et al. Coactivator condensation at super-enhancers links phase separation and gene control. *Science* **361**, eaar3958 (2018).

32. Alberti, S., Gladfelter, A. & Mittag, T. Considerations and challenges in studying liquid–liquid phase separation and biomolecular condensates. *Cell* **176**, 419–434 (2019).

33. Asimi, V. et al. Hijacking of transcriptional condensates by endogenous retroviruses. *Nat. Genet.* **54**, 1238–1247 (2022).

34. Larson, A. G. et al. Liquid droplet formation by HP1α suggests a role for phase separation in heterochromatin. *Nature* **547**, 236–240 (2017).

35. Feric, M. et al. Coexisting liquid phases underlie nucleolar subcompartments. *Cell* **165**, 1686–1697 (2016).

36. Kwon, I. et al. Poly-dipeptides encoded by the *C9orf72* repeats bind nucleoli, impede RNA biogenesis, and kill cells. *Science* **345**, 1139–1145 (2014).

37. Aviner, R. The science of puromycin: from studies of ribosome function to applications in biotechnology. *Comput. Struct. Biotechnol. J.* **18**, 1074–1083 (2020).

38. Richards, S. et al. Standards and guidelines for the interpretation of sequence variants: a joint consensus recommendation of the American College of Medical Genetics and Genomics and the Association for Molecular Pathology. *Genet. Med.* **17**, 405–424 (2015).

39. Lek, M. et al. Analysis of protein-coding genetic variation in 60,706 humans. *Nature* **536**, 285–291 (2016).

40. Mitrea, D. M. et al. Nucleophosmin integrates within the nucleolus via multi-modal interactions with proteins displaying R-rich linear motifs and rRNA. *eLife* **5**, e13571 (2016).

41. White, M. R. et al. *C9orf72* poly(PR) dipeptide repeats disturb biomolecular phase separation and disrupt nucleolar function. *Mol. Cell* **74**, 713–728.e6 (2019).

42. Lee, K. H. et al. C9orf72 dipeptide repeats impair the assembly, dynamics, and function of membrane-less organelles. *Cell* **167**, 774–788.e17 (2016).

43. Banani, S. F. et al. Genetic variation associated with condensate dysregulation in disease. *Dev. Cell* **57**, 1776–1788.e8 (2022).

44. Gurovich, Y. et al. Identifying facial phenotypes of genetic disorders using deep learning. *Nat. Med.* **25**, 60–64 (2019).

45. Jumper, J. et al. Highly accurate protein structure prediction with AlphaFold. *Nature* **596**, 583–589 (2021).

46. Pettersen, E. F. et al. UCSF ChimeraX: structure visualization for researchers, educators, and developers. *Protein Sci.* **30**, 70–82 (2021).

47. Goddard, T. D. et al. UCSF ChimeraX: meeting modern challenges in visualization and analysis. *Protein Sci.* **27**, 14–25 (2018).

48. Mirdita, M. et al. ColabFold—making protein folding accessible to all. *Nat Methods* **19**, 679–682 (2022).

49. Whitmore, L., Miles, A. J., Mavridis, L., Janes, R. W. & Wallace, B. A. PCDDB: new developments at the Protein Circular Dichroism Data Bank. *Nucleic Acids Res.* **45**, D303–D307 (2017).

50. Lees, J. G., Miles, A. J., Wien, F. & Wallace, B. A. A reference database for circular dichroism spectroscopy covering fold and secondary structure space. *Bioinformatics* **22**, 1955–1962 (2006).

51. Abdul-Gader, A., Miles, A. J. & Wallace, B. A. A reference dataset for the analyses of membrane protein secondary structures and transmembrane residues using circular dichroism spectroscopy. *Bioinformatics* **27**, 1630–1636 (2011).

52. Tolchard, J. et al. The intrinsically disordered Tarp protein from chlamydia binds actin with a partially preformed helix. *Sci. Rep.* **8**, 1960 (2018).

53. Tandon, R. et al. Generation of two human isogenic iPSC lines from fetal dermal fibroblasts. *Stem Cell Res.* **33**, 120–124 (2018).

54. Emenecker, R. J., Griffith, D. & Holehouse, A. S. Metapredict: a fast, accurate, and easy-to-use predictor of consensus disorder and structure. *Biophys. J.* **120**, 4312–4319 (2021).

55. Piovesan, D. et al. MobiDB: intrinsically disordered proteins in 2021. *Nucleic Acids Res.* **49**, D361–d367 (2021).

56. Rainer, J., Gatto, L. & Weichenberger, C. X. ensembldb: an R package to create and use Ensembl-based annotation resources. *Bioinformatics* **35**, 3151–3153 (2019).

57. Landrum, M. J. et al. ClinVar: improving access to variant interpretations and supporting evidence. *Nucleic Acids Res.* **46**, D1062–D1067 (2018).

58. Tate, J. G. et al. COSMIC: the Catalogue Of Somatic Mutations In Cancer. *Nucleic Acids Res.* **47**, D941–D947 (2018).

59. Sherry, S. T. et al. dbSNP: the NCBI database of genetic variation. *Nucleic Acids Res.* **29**, 308–311 (2001).

60. Auton, A. et al. A global reference for human genetic variation. *Nature* **526**, 68–74 (2015).

61. Quinlan, A. R. & Hall, I. M. BEDTools: a flexible suite of utilities for comparing genomic features. *Bioinformatics* **26**, 841–842 (2010).

62. Pagel, K. A. et al. Integrated informatics analysis of cancer-related variants. *JCO Clin. Cancer Inform.* **4**, 310–317 (2020).

63. Rehm, H. L. et al. ClinGen—the clinical genome resource. *N. Engl. J. Med.* **372**, 2235–2242 (2015).

64. Kircher, M. et al. A general framework for estimating the relative pathogenicity of human genetic variants. *Nat. Genet.* **46**, 310–315 (2014).

65. Rentzsch, P., Schubach, M., Shendure, J. & Kircher, M. CADD-Splice—improving genome-wide variant effect prediction using deep learning-derived splice scores. *Genome Med.* **13**, 31 (2021).

66. Hundal, J. et al. pVACtools: a computational toolkit to identify and visualize cancer neoantigens. *Cancer Immunol. Res.* **8**, 409–420 (2020).

67. Holehouse, A. S., Das, R. K., Ahad, J. N., Richardson, M. O. & Pappu, R. V. CIDER: resources to analyze sequence-ensemble relationships of intrinsically disordered proteins. *Biophys. J.* **112**, 16–21 (2017).

68. Cock, P. J. et al. Biopython: freely available Python tools for computational molecular biology and bioinformatics. *Bioinformatics* **25**, 1422–1423 (2009).

69. Scott, M. S., Troshin, P. V. & Barton, G. J. NoD: a nucleolar localization sequence detector for eukaryotic and viral proteins. *BMC Bioinformatics* **12**, 317 (2011).

70. Raudvere, U. et al. g:Profiler: a web server for functional enrichment analysis and conversions of gene lists (2019 update). *Nucleic Acids Res.* **47**, W191–W198 (2019).

71. Bunn, K. J. et al. Mutations in *DVL1* cause an osteosclerotic form of Robinow syndrome. *Am. J. Hum. Genet.* **96**, 623–630 (2015).

72. White, J. et al. *DVL1* frameshift mutations clustering in the penultimate exon cause autosomal-dominant Robinow syndrome. *Am. J. Hum. Genet.* **96**, 612–622 (2015).

Acknowledgements

We thank the patients and their families for participating in this study; V. Suckow, G. Hildebrand, V. Johnston and Y. Zhang for technical assistance; T. Aktas (MPI-MG) for comments on the manuscript; A. Papantonis (GAU, Göttingen) for advice on HMGB1 immunofluorescence; and U. Marchfelder and E. Weiß from the Flow Cytometry Facility of the MPI-MG for their assistance with cell sorting; D. Meierhofer and B. Lukaszewska-McGreal for performing mass spectrometry; and J. Naderi for mCherry constructs and human iPS cells. M.A.M. is a participant in the Digital Clinician Scientist Program and H.L.S. in the Junior Clinician Scientist Program founded by the late D. Dragun and funded by the Berlin Institute of Health and the Charité–Universitätsmedizin Berlin. This work was partially funded by the Max Planck Society. Work in the Hnisz Lab is supported by the Deutsche Forschungsgemeinschaft (DFG) Priority Program Grants HN 4/1-1 and HN 4/3-1 and a Worldwide Cancer Research grant (20-0232). M.S. is supported by grants from the DFG (SP1532/3-2, SP1532/4-1 and SP1532/5-1) and the Deutsches Zentrum für Luft- und Raumfahrt (DLR 01GM1925). S.M. was funded by grant MU 880/16-1 from the DFG. H. Niskanen is supported by fellowships from the Orion Research Foundation and the Instrumentarium Science Foundation. C.G.-C. acknowledges a graduate fellowship from MINECO (PRE2018-084684) and X.S. acknowledges funding from AGAUR (2017 SGR 324), MINECO (PID2019-110198RB-I00) and the European Research Council (CONCERT, contract number 648201). IRB Barcelona is the recipient of a Severo Ochoa Award of Excellence from MINECO (Government of Spain).

Funding

Open access funding provided by Max Planck Society.

Author information

Author notes

1. These authors contributed equally: Martin A. Mensah, Henri Niskanen
2. These authors jointly supervised this work: Malte Spielmann, Denise Horn, Denes Hnisz

Authors and Affiliations

1. Institute of Medical Genetics and Human Genetics, Charité–Universitätsmedizin Berlin, corporate member of Freie Universität Berlin and Humboldt-Universität zu Berlin, Berlin, Germany

   Martin A. Mensah, Henrike L. Sczakiel, Alisa M. V. Reiter, Jonas Elsner, Karolina Skipalova, Stefan Mundlos & Denise Horn

2. BIH Biomedical Innovation Academy, Berlin Institute of Health at Charité–Universitätsmedizin Berlin, Berlin, Germany

   Martin A. Mensah, Henrike L. Sczakiel & Stefan Mundlos

3. RG Development and Disease, Max Planck Institute for Molecular Genetics, Berlin, Germany

   Martin A. Mensah, Henrike L. Sczakiel, Vera M. Kalscheuer, Stefan Mundlos & Malte Spielmann

4. Department of Genome Regulation, Max Planck Institute for Molecular Genetics, Berlin, Germany

   Henri Niskanen, Alexandre P. Magalhaes, Shaon Basu, Matthew L. Kraushar & Denes Hnisz

5. Exploratory Diagnostic Sciences, Berlin Institute of Health at Charité–Universitätsmedizin Berlin, Berlin, Germany

Martin Kircher

6. Institute of Human Genetics, University Hospitals Schleswig-Holstein, University of Lübeck and Kiel University, Lübeck, Kiel, Germany

Martin Kircher, Almuth Caliebe & Malte Spielmann

7. Institute of Human Genetics, University Medical Center Hamburg-Eppendorf, Hamburg, Germany

Peter Meinecke

8. Center for Genomics and Transcriptomics (CeGaT), Tübingen, Germany

Saskia Biskup

9. Department of Pediatrics and Adolescent Medicine, School of Clinical Medicine, LKS Faculty of Medicine, The University of Hong Kong, Pok Fu Lam, Hong Kong

Brian H. Y. Chung

10. Department of Congenital Heart Disease and Pediatric Cardiology, University Hospital Schleswig-Holstein, Kiel, Germany

Gregor Dombrowsky & Marc Phillip Hitz

11. Department of Medical Genetics, Carl von Ossietzky University, Oldenburg, Germany

Gregor Dombrowsky & Marc Phillip Hitz

12. Department of Obstetrics and Gynecology, University Hospital Schleswig-Holstein, Kiel, Germany

Christel Eckmann-Scholz

13. Department of Internal Medicine, Radboud Institute for Molecular Life Sciences, Radboud Expertise Center for Immunodeficiency and Autoinflammation and Radboud Center for Infectious Disease (RCI), Radboud University Medical Center, Nijmegen, The Netherlands

Alexander Hoischen

14. Department of Human Genetics, Radboud University Medical Center, Nijmegen, The Netherlands

Alexander Hoischen & Lot Snijders Blok

15. Department of Pediatrics, Pediatric Endocrinology and Diabetes, University Hospital Schleswig-Holstein, Schleswig-Holstein, Germany

Paul-Martin Holterhus

16. Handchirurgie, Katholisches Kinderkrankenhaus Wilhelmstift, Hamburg, Germany

Wiebke Hülsemann

17. Genetics Research Center, University of Social Welfare and Rehabilitation Sciences, Tehran, Iran

Kimia Kahrizi & Hossein Najmabadi

18. Department of Obstetrics and Gynaecology, Queen Mary Hospital, Pok Fu Lam, Hong Kong

Anita Kan

19. Institute of Human Genetics, Universitätsklinikum Erlangen, Friedrich-Alexander-Universität Erlangen-Nürnberg (FAU), Erlangen, Germany

Mandy Krumbiegel

20. Institute for Human Genetics and Genomic Medicine, Medical Faculty, RWTH Aachen University Hospital, Aachen, Germany

Ingo Kurth

21. Department of Pediatric Neurology, Charité–Universitätsmedizin Berlin, corporate member of Freie Universität Berlin and Humboldt-Universität zu Berlin, Berlin, Germany

Jonas Leubner

22. Department of Pediatrics, University Hospital Center Schleswig-Holstein, Kiel, Germany

Ann Carolin Longardt

23. Department of Radiology and Neuroradiology, Pediatric Radiology, University Hospital Schleswig-Holstein, Kiel, Germany

Jörg D. Moritz

24. Institute of Human Genetics, Medical Center, University of Freiburg, Faculty of Medicine, University of Freiburg, Freiburg, Germany

Andreas Tzschach

25. Zentrum für Kinder-und Jugendmedizin, Helios Kliniken Schwerin, Schwerin, Germany

Eberhard Wiedersberg

26. Institute of Human Genetics, University Hospital, Otto-von-Guericke University, Magdeburg, Germany

Martin Zenker

27. Institute for Research in Biomedicine (IRB Barcelona), The Barcelona Institute of Science and Technology, Barcelona, Spain

Carla Garcia-Cabau & Xavier Salvatella

28. Microscopy Core Facility, Max Planck Institute for Molecular Genetics, Berlin, Germany

René Buschow

29. ICREA, Passeig Lluís Companys 23, Barcelona, Spain

Xavier Salvatella

30. BCRT-Berlin Institute of Health Center for Regenerative Therapies, Berlin, Germany

Stefan Mundlos

31. DZHK (German Centre for Cardiovascular Research), partner site Hamburg, Lübeck, Kiel, Lübeck, Germany

Malte Spielmann

Contributions

M.A.M., H. Niskanen and A.P.M. conceived and planned the study with input from S. Basu, S.M., M.S., D. Hnisz and D. Horn. M.A.M. managed the collection, analysis and interpretation of patient clinical and molecular data with M.S. and D. Horn. H. Niskanen designed and performed the cell biology experiments. M.L.K. performed the puromycin experiments. H. Niskanen designed and performed the biochemistry experiments with S. Basu. H. Niskanen, S. Basu and R.B. performed image analyses. A.P.M. performed AlphaFold2 modelling and built the variant catalogue with input from M.A.M., H. Niskanen and D. Hnisz. C.G.-C. performed the CD experiments. M.A.M., H. Niskanen, M.S., D. Hnisz and D. Horn wrote the manuscript with contributions from A.P.M. and S. Basu. M.S., D. Hnisz and D. Horn supervised the study. All other authors contributed clinical or molecular data. All authors approved the final manuscript.

Corresponding authors

Correspondence to Malte Spielmann, Denise Horn or Denes Hnisz.

Ethics declarations

Competing interests

D. Hnisz and X.S. are founders and scientific advisors of Nuage Therapeutics. The other authors declare no competing interests.

Peer review

Peer review information

Nature thanks Marco Bianchi, Diana Mitrea and Stephen Robertson for their contribution to the peer review of this work. Peer reviewer reports are available.

Additional information

Publisher's note Springer Nature remains neutral with regard to jurisdictional claims in published maps and institutional affiliations.

Extended data figures and tables

Extended Data Fig. 1 Clinical findings in BPTAS individuals.

(**a**-**c**) I1 at age of 9 months. (**a**) Palmar view, left hand: brachydactyly and reduced creases of fingers. (**b**) Right foot: preaxial polysyndactyly, syndactyly between the second and third toes, increased soft tissue of distal toes in the dorso-ventral axis, hypoplastic/missing nails. (**c**) Malformed upper and lower limbs, contractures of large joints. (**d**-**i**) I2. (**d**) Lateral babygram (after birth): normal lateral spine apart from limb anomalies. (**e**-**f**) X-rays of upper extremities: contractures of the elbows, dislocation of the radius head, short radius and ulna, short middle phalanges. (**g**-**i**) I2, photos at age of 11 years. Plantar and dorsal views of the feet: preaxial

polysyndactyly, hypoplastic nails. (**j**-**l**) I4. (**j**) Left foot, (**k**) Right foot, (**l**) Right hand. Radiograms of the feet at the age of 6 months showing symmetrical preaxial polysyndactyly. Radiogram of the right hand at age of 6 months: Note retarded bone age and short tubular bones, the middle phalanges are slightly more affected than the other ones. (**m**-**r**) I5 at 21 weeks of gestation. (**m**) Note webbed elbows. (**n**) Contractures of large joints. (**o**) Dorsal view of hands showing brachydactyly with hypoplastic nails. (**p**) Abnormal female genitalia. (**q**-**r**) Radiograms of the lower extremities and pelvis: hypoplastic iliac wings, lack of tibiae, hypoplastic fibulae, and preaxial polydactyly of feet. (**s**) Histogram of the syndromes suggested among the top-10 Face2Gene-suggestions of the images of individuals affected with BPTAS and the composite mask of this syndrome showing telecanthus and blepharophimosis.

Extended Data Fig. 2 Patient genotyping and population-genetic data.

(**a**) Variant detection and filtering scheme of the whole genome (I1 and I5) and exome sequencing data (I4). (**b**) gDNA Sanger sequencing data of *HMGB1* in I1. (**c**) gDNA Sanger sequencing data of *HMGB1* in I2, and I3, note identical de novo frameshift also found in I2 c.551_554delAGAA, de novo occurrence in I3. (**d**) Exome sequencing data of *HMGB1* in I4. Note identical frameshift as in I2 in I3, and de novo occurrence. (**e**) Sequencing of *HMGB1* cDNA in I3 and an unaffected control. Note the detection of both the wildtype and mutant cDNA in I3. (**f**) Allele counts of non-synonymous variants in HMGB1's acidic tail in the gnomAD database (v.2.1.1). Note that especially non-acidic substitutions are rare, and no frameshifts of *HMGB1* are listed in gnomAD. (**g**) Position of nonsynonymous variants in HMGB1's acidic tail. Note that most variants do not significantly shorten the uninterrupted succession of aspartic acid (D) and glutamic acid (E). The 4 non-acidic substitutions comprise merely 5 of 1123 non-synonymous alleles of the acidic tail listed in gnomAD. (**h**) Pedigree of family 6. Squares denote male, circles denote female individuals. Individuals diagnosed with BPTAS are highlighted with solid black boxes, and the genotypes are displayed below the boxes. WT = wildtype. (**i**) Microdeletion in 13q12.3 in I5. CMA data showing loss of *HMGB1* in I6. (**j**) qPCR showing de novo occurrence and revealing deletion of all exons, colored primers are positioned between

the last non-deleted and first deleted oligo of the CMA, black primer X chromosomal control. Data are from one biological replicate.

Extended Data Fig. 3 Computational and biochemical characterization of HMGB1.

(**a**) Predicted structures of Hmgb1 proteins from AlphaFold2 Protein Structure Database. Colors ranging from blue to orange depict the per-residue measure of local confidence for the model. (**b**) Left: MSA depth assessment for the sequences for quality assessment of the predicted HMGB1 models. Aligned sequences are colored by sequence identity. Sequence coverage frequency is depicted by a black line. The dotted red line marks the frameshift in the mutant. Right: Disorder analysis of wild type and mutant HMGB1 sequences using AlphaFold2 pLDDT scores (yellow) and Metapredict scores (blue). (**c**) Circular dichroism (CD) data of the WT HMGB1 IDR peptide in the absence (black) and in the presence (gray) of 2.5 % trifluoroethanol (TFE). On the upper panel, the CD spectra are shown as the mean residue ellipticity (MRE) as a function of wavelength. On the lower panel, the high-tension voltage (HT) values are shown as a function of wavelength. Vertical dotted lines indicate the wavelength value corresponding to HT = 600 V. (**d**) Circular dichroism (CD) data of the Mutant HMGB1 IDR peptide in the absence (red) and in the presence (orange) of 2.5 % trifluoroethanol TFE. On the upper panel, the CD spectra are shown as the mean residue ellipticity (MRE) as a function of wavelength. On the lower panel, the high-tension voltage (HT) values are shown as a function of wavelength. Vertical dotted lines indicate the wavelength value corresponding to HT = 600 V. (**e**) Representative CD spectra of α-helix, β-strand and disordered proteins, shown as the mean residue ellipticity (MRE) as a function of wavelength. The data was obtained from the Protein Circular Dichroism Data Bank (PCDDB) (see Methods).

Extended Data Fig. 4 Mutant HMGB1 protein and synthetic IDR peptide.

(**a**) Chromatograms from size-exclusion chromatography (SEC) of wild type and mutant mEGFP-HMGB1 fusion proteins. Selected fractions highlighted with red. (**b**) SDS-PAGE analysis of purified proteins after His-Tag column

purification before SEC and after SEC purification steps. Analysis was performed once for each protein prep. (**c**) SDS-PAGE of SEC purified HMGB1 proteins followed by immunoblotting with anti-EGFP and anti-HMGB1 antibodies. Analysis was performed once for each protein prep. (**d**) Representative images from droplet formation assays performed with 5'FAM-labeled HMGB1-IDR variant peptides at indicated concentrations in the presence of 20 ng/µl RNA or without RNA. Experiment was replicated 2 times with similar results. (**e**) Quantification of the relative amount of condensed protein of 5'FAM-HMGB1-IDR peptides at the indicated concentrations. Data displayed as mean ± SD from 5 image fields examined per condition. (**f**) Representative images from droplet formation assays performed with 2.5 µM 5'FAM-labeled HMGB1-IDR synthetic peptides at indicated RNA concentrations. Experiment was replicated 2 times with similar results. (**g**) Quantification of the relative amount of condensed protein of 2.5 µM 5'FAM-HMGB1-IDR peptides at the indicated RNA concentrations. Data displayed as mean ± SD from 5 image fields examined per condition. (**h**) Scheme of co-droplet assays. (**i**) (top) Representative images of droplets formed by 5'FAM-HMGB1-IDR peptide mixed with pre-assembled mCherry-labeled MED1-IDR, HP1α or NPM1 droplets. (bottom) Example images from 5 µM 5'FAM-HMGB1 mutant peptide mixed with mCherry labeled NPM1 droplets with uneven distribution of the peptide within droplet. (**j**) Dual fluorescence plot quantification of 5'FAM and mCherry fluorescence intensities in mCherry-labeled NPM1, MED1-IDR or HP1α droplets mixed with synthetic HMGB1 IDR peptides. Each dot represents one droplet, and the size of the dot is proportional to the size of the droplet. Scale bars, 5 µm (**d,f**) or 1 µm (**g,i**).

Extended Data Fig. 5 Mutant HMGB1 forms nuclear inclusions in human cells.

(**a**) Quantification of the nuclear enrichment of EGFP as the ratio of mean signal intensities inside and outside the nucleus. Red dashed line depicts a value of 1 (no enrichment). For all boxplots in this figure, the median is shown as a line within the boxplot, which spans from 25th to 75th percentiles. Whiskers depict a 1.5x interquartile range. **** $P < 2.2 \times 10^{-16}$, two-tailed Welch's t-test. (**b**) Quantification of nuclear inclusions as the standard deviation of nuclear EGFP fluorescence intensity normalized by

mean intensity. **** $P < 2.2 \times 10^{-16}$, two-tailed Welch's t-test. (**c**) (left) Graph plotting the intrinsic disorder of HMGB1 predicted by PONDR VLXT algorithm. The positions two different IDR definitions are highlighted with orange bars and the position of HMG boxes with blue bars. IDR1 begins from Asn135 as defined by PONDR analysis and IDR2 begins from Ala164, excluding any sequence belonging to HMG box. (middle) Representative image from U2OS cells expressing EGFP-HMGB1-mutant-IDR2. Scale bar = 10 µm. (right) Relative fluorescence intensity of bleached EGFP-HMGB1 WT full-length, mutant full length and mutant IDRs 1 and 2 before and after photobleaching. Data is displayed with a line showing the mean and lighter shade represents ± SD. (**d**) Representative images of live MCF7, HCT116 and HEK293T cells expressing mEGFP-HMGB1 variants. The nuclear area is shown as dashed white lines. Scale bar = 10 µm. (**e**) Representative images of EGFP-HMGB1 within live U2OS cell nuclei before and after photobleaching. FRAP recovery quantified in (Fig. 3d). Scale bar = 1 µm. (**f**) Representative images of formaldehyde-fixed U2OS cells ectopically expressing EGFP-HMGB1 WT or mutant proteins. Scale bar = 5 µm. (**g**) Quantification of presence of nuclear inclusions in fixed cells in panel (f) represented as the standard deviation of nuclear EGFP fluorescence intensity normalized by mean intensity. (**h**) Immunofluorescence for RNAPII, MED1, SC35, HP1α, NPM1 and FIB1 in U2OS cells expressing full length mutant EGFP-HMGB1. (low) indicates a nucleus with a relatively low amount of the mutant protein, (high) indicates a nucleus with a relatively high amount of the mutant protein. Scale bar = 10 µm. (**i**) Quantification of the ratio between intra- /extranucleolar NPM1 intensity and EGFP-HMGB1 intensity inside nucleoli. *r* = Pearson's correlation coefficient, *P*-value from a two-tailed t-test. (**j**) Quantification of the average NPM1 fluorescence outside the nucleoli and EGFP-HMGB1 intensity inside the nucleoli for the IF experiments shown in panel (h). *r* = Pearson's correlation coefficient, p-value from a two-tailed t-test. (**k**) Quantification of nuclear inclusions in the panel of EGFP-HMGB1 mutants (Fig. 3e–g) as the standard deviation (SD) of nuclear EGFP signal normalized to the mean nuclear EGFP signal intensity. FL = full length.

Extended Data Fig. 6 Additional characterization of HMGB1 mutant nuclear inclusions in U2OS cells.

(**a**) qRT-PCR analysis of rRNA species in U2OS cells expressing wild type and mutant HMGB1 variants. rRNA levels are normalized against an RNAPII transcript (*actin*), and the values are normalized against the rRNA/*actin* level measured in the cells expressing wild type HMGB1. Data is shown as mean +/− SD, * $p < 0.05$, two-tailed Student's t-test. (**b**) Representative images from Puromycylation experiments with U2OS cells ectopically expressing EGFP-tagged WT or mutant HMGB1 proteins with (Puro +) and without (Puro -) Puromycin pulse labeling. Scale bar = 20 µm. (**c**) Histograms depicting % of cells and their normalized puromycin intensities from EGFP+ and EGFP- cells ectopically expressing WT or Mutant full length HMGB1 combined from three independent puromycylation experiments. (**d**) (top) Scheme of the viability experiment. (bottom) Representative mages of U2OS cells at the end of viability experiments (Fig. 3j). Scale bar = 50 µm. (**e**) Representative live cell imaging of U2OS cells with doxycycline inducible overexpression of EGFP-HMGB1 variants. Dashed lines show nuclear area defined by Hoechst staining. Scale bar = 10 µm. (**f**) Quantification of nuclear inclusions as the standard deviation (SD) of nuclear EGFP signal normalized to the mean nuclear EGFP signal intensity. **** $P < 2.2 \times 10^{-16}$, two-tailed Welch's t-test, n = number of nuclei examined for each condition. (**g**) Relative fluorescence intensity of EGFP-HMGB1 before and after photobleaching with identical laser settings in cells described in (panels e-f). Data displayed as mean ± SD. (**h**) Representative images of EGFP-HMGB1 within live U2OS cell nuclei before and after photobleaching with identical laser settings, FRAP recovery quantified in (panel g). Scale bar = 2 µm. (**i**) (top) Scheme for experiments testing the viability of U2OS cells with Doxycycline-inducible expression of HMGB1 variants. (bottom) representative images from viability experiments 48h after sorting for GFP+ cells. Scale bar = 100 µm. (**j**) Quantification of viability of cells expressing the indicated HMGB1 proteins. Mean relative light units (RLU) displayed as individual points from independent biological replicate experiments (n = 5 for WT and Mutant, 4 for "Patchless"). Bar charts show the mean ± SD. p-values are from one-way ANOVA.

Extended Data Fig. 7 Characterization of genetic variants in C-terminal IDRs.

(**a**) Scheme of the IDR catalog identification algorithm. (**b**) Summary of all variants identified in C-terminal IDRs. (**c**) Frameshift variants are enriched for pathogenic variants. (**d**) Gene Ontology (GO) term enrichment analysis of (left) genes that contain at least one 'stop gained' (i.e. truncating) mutation in the catalog; (middle) genes that contain at least one frameshift (≥20 amino acids) in the catalog; (right) genes that contain at least one frameshift (≥20 amino acids) that creates a sequence consisting of at least 15% arginines. (**e**) pLI score distributions for indicated gene sets. Disease genes: genes that have at least one "pathogenic", "likely pathogenic", or "conflicting interpretations" entry in ClinVar. (**f**) Word cloud plot of diseases associated with 'stop gained' (i.e. truncating) variants. Font size of words correlates with frequency of occurrence. (**g**) Word cloud plot of diseases associated with frameshift variants that create an at least 20 amino acid long sequence. Font size of words correlates with frequency of occurrence. (**h**) Word cloud plot of diseases associated with frameshift variants that create an at least 20 amino acid long sequence that consists of at least 15% arginines. Font size of words correlates with frequency of occurrence.

Extended Data Fig. 8 Sequences of candidate proteins.

Sequences of the thirteen wild type and mutant HMGB3, FOXC1, FOXF1, MYOD1, RAX, RUNX1, PHOX2B, CALR, FOXL2, SOX2, SQSTM1, MEN1 and DVL1 proteins. In the wild type variants, only the sequences replaced by the frameshift variants are shown underlined. The sequences created by the frameshift variants are colored red and are underlined.

Extended Data Fig. 9 Disorder and charge analyses of proteins created by frameshifts in candidate proteins.

(**a**, **c**) Disorder analysis of HMGB1, HMGB3, FOXC1, FOXF1, MYOD1, RAX, RUNX1, CALR, FOXL2, PHOX2B, SOX2 and SQSTM1 wild type and frameshift mutant sequences using the PONDR algorithm. The PONDR scores for the wild type sequences are plotted with grey dashed line, the PONDR scores for the mutant sequences are plotted in red. The positions of the DNA binding domains (DBD) are highlighted with black bars and frameshift position is highlighted with red arrow. (**b**, **d**) Charge plots of wild type and mutant sequences. Note the increased positive charge in C-terminus

of frameshift variants. Isoelectric points (pI) for the protein sequence following the frameshift position in wild type and mutant sequences are shown beside the charge plots. (**e**) Quantification of nucleolar enrichment of the indicated proteins in the FIB1-RFP co-expression experiments. Median is shown as a line within the boxplot, which spans from 25th to 75th percentiles. Whiskers depict a 1.5x interquartile range. *** $P < 10^{-3}$, **** $P < 10^{-4}$ from two-tailed Welch's t-test, n = number of nuclei examined per condition. (**f**) Representative images of U2OS cells co-expressing RFP-Fibrillarin and EGFP-tagged DVL1 proteins. Scale bar = 10 µm. (**g**) Relative fluorescence intensity of bleached EGFP-tagged DVL1 in U2OS cells before and after photobleaching with identical laser settings. Line: mean, lighter shade: ± SD. (**h**) Representative images of hiPSCs co-expressing RFP-Fibrillarin and EGFP-tagged DVL1 proteins. Note the nucleolar signal in the cells expressing Mutant EGFP-DVL1. Scale bar = 10 µm. (**i**) Quantification of nucleolar enrichment of DVL1 in the FIB1-RFP co-expression experiments in hiPSCs. Median is shown as a line within the boxplot, which spans from 25th to 75th percentiles. Whiskers depict a 1.5x interquartile range, **** $P < 10^{-4}$, two-tailed Welch's t-test, n = number of nuclei examined per condition.

Extended Data Fig. 10 Nucleolar mispartitioning and dysfunction in cells expressing mutant proteins with disease-associated frameshifts.

(**a**) Cavitation of the nuclear inclusion formed by frameshift mutant FOXC1, FOXF1, RAX, HMGB3, PHOX2B and SOX2. Representative images of U2OS cells co-expressing RFP-Fibrillarin and EGFP-tagged mutant proteins are shown. Scale bar = 5 µm. Right: fluorescence intensity profiles of EGFP (green) and RFP (purple) quantified from the region highlighted with yellow a dashed line on images on the left. (**b**) Relative fluorescence intensity of bleached EGFP-tagged proteins before and after photobleaching with identical laser settings. Data displayed as mean ± SD. (**c**) qRT-PCR analysis of rRNA species in U2OS cells expressing the indicated wild type and mutant proteins. rRNA levels are normalized against a control RNAPII transcript (*GAPDH*, *actin, or Cyclophilin*), and the values are normalized against the rRNA/*control transcript* level measured in the cells expressing wild type proteins. Data displayed as mean +/− SD. *P*-values are from two-

tailed Student's t-tests, n = 3 biologically independent experiments. (**d**) Actinomycin D control experiments for measuring rRNA levels. U2OS cells were treated with Actinomycin D (30 nM for 2 h), and rRNA levels were quantified using qRT-PCR. rRNA levels are normalized against a control RNAPII transcript (*actin*, *GAPDH* or *Cyclophilin*), and the values are normalized against the rRNA/*control transcript* level measured in the control (i.e. untreated) cells. Data displayed as mean +/− SD. *P*-values are from two-tailed Welch's t-test, n = 3 biologically independent experiments. On the right, light microscopy images of control and Actinomycin D-treated cells are shown. Note the dimming of the dark spots in the nucleus (corresponding to nucleoli).

Supplementary information

Supplementary Information

This file contains Supplementary Note, Supplementary Figs. 1–6, Supplementary Table legends, Supplementary Video legends and supplementary references.

Reporting Summary

Peer Review File

Supplementary Table 1

Clinical characteristics of affected individuals with BPTAS.

Supplementary Table 2

Clinical features of individuals with 13q12.3 deletion syndrome from this study and previous studies.

Supplementary Table 3

Genes and isoforms for which protein products contain a C-terminal IDR.

Supplementary Table 4

List of variants in C-terminal IDRs.

Supplementary Table 5

Features of proteins affected by frameshift variants, including sequence, length, pathogenicity and disease association.

Supplementary Table 6

Primer sequences.

Supplementary Video 1

Fusion event between eGFP–HMG1 protein droplets in vitro. Time (mm:ss) is displayed on the bottom left. Scale bar, 1 µm.

Supplementary Video 2

Live U2OS cells expressing mutant eGFP–HMGB1 protein undergoing mitosis. Time after doxycycline induction (hh:mm) is shown on bottom left of the image. Scale bar, 10 µm.

Rights and permissions

Open Access This article is licensed under a Creative Commons Attribution 4.0 International License, which permits use, sharing, adaptation, distribution and reproduction in any medium or format, as long as you give appropriate credit to the original author(s) and the source, provide a link to the Creative Commons licence, and indicate if changes were made. The images or other third party material in this article are included in the article's Creative Commons licence, unless indicated otherwise in a credit line to the material. If material is not included in the article's Creative Commons licence and your intended use is not permitted by statutory regulation or exceeds the permitted use, you will need to obtain permission directly from

the copyright holder. To view a copy of this licence, visit http://creativecommons.org/licenses/by/4.0/.

Reprints and Permissions

About this article

Cite this article

Mensah, M.A., Niskanen, H., Magalhaes, A.P. *et al.* Aberrant phase separation and nucleolar dysfunction in rare genetic diseases. *Nature* **614**, 564–571 (2023). https://doi.org/10.1038/s41586-022-05682-1

- Received: 09 November 2021
- Accepted: 22 December 2022
- Published: 08 February 2023
- Issue Date: 16 February 2023
- DOI: https://doi.org/10.1038/s41586-022-05682-1

Share this article

Anyone you share the following link with will be able to read this content:

Get shareable link

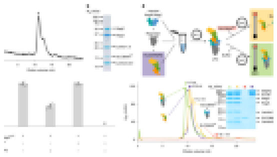
Sorry, a shareable link is not currently available for this article.

Copy to clipboard

Provided by the Springer Nature SharedIt content-sharing initiative

---

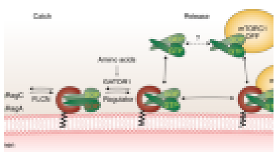
This article was downloaded by **calibre** from https://www.nature.com/articles/s41586-022-05682-1



Structural mechanism for amino acid-dependent Rag GTPase nucleotide state switching by SLC38A9

31 August 2020

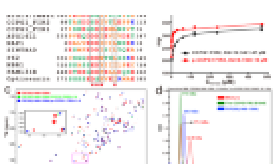
Simon A. Fromm, Rosalie E. Lawrence & James H. Hurley



Lysosomal catch-and-release controls mTORC1

28 August 2018

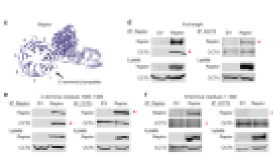
Aaron M. Hosios & Brendan D. Manning



Phosphorylation regulates the binding of autophagy receptors to FIP200 Claw domain for selective autophagy initiation

10 March 2021

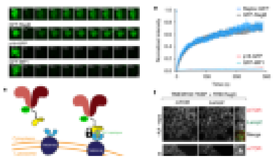
Zixuan Zhou, Jianping Liu, … Lifeng Pan



[Structural and functional analysis of the role of the chaperonin CCT in mTOR complex assembly]

28 June 2019

Jorge Cuéllar, W. Grant Ludlam, … José M. Valpuesta



[A nutrient-induced affinity switch controls mTORC1 activation by its Rag GTPase–Ragulator lysosomal scaffold]

30 July 2018

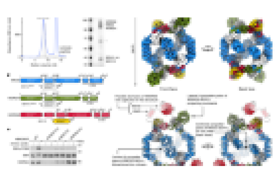
Rosalie E. Lawrence, Kelvin F. Cho, … Roberto Zoncu



[Crystal structure of the Rab33B/Atg16L1 effector complex]

31 July 2020

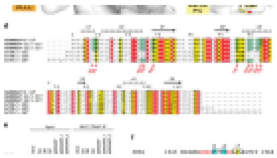
Janina Metje-Sprink, Johannes Groffmann, … Beyenech Binotti



[Structure of the nutrient-sensing hub GATOR2]

13 July 2022

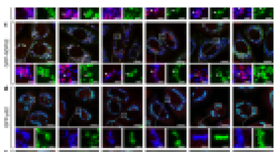
Max L. Valenstein, Kacper B. Rogala, … David M. Sabatini



[Molecular determinants regulating selective binding of autophagy adapters and receptors to ATG8 proteins]

03 May 2019

Martina Wirth, Wenxin Zhang, … Stéphane Mouilleron



[LC3/GABARAPs drive ubiquitin-independent recruitment of Optineurin and NDP52 to amplify mitophagy]

24 January 2019

Benjamin Scott Padman, Thanh Ngoc Nguyen, … Michael Lazarou

- Article
- Open Access
- Published: 25 January 2023

Structure of the lysosomal mTORC1–TFEB–Rag–Ragulator megacomplex

- Zhicheng Cui,
- Gennaro Napolitano,
- Mariana E. G. de Araujo,

- Alessandra Esposito,
- Jlenia Monfregola,
- Lukas A. Huber,
- Andrea Ballabio &
- …
- James H. Hurley

Show authors

Nature **volume 614**, pages 572–579 (2023)

- 14k Accesses
- 54 Altmetric
- Metrics details

Abstract

The transcription factor TFEB is a master regulator of lysosomal biogenesis and autophagy[1]. The phosphorylation of TFEB by the mechanistic target of rapamycin complex 1 (mTORC1)[2,3,4,5] is unique in its mTORC1 substrate recruitment mechanism, which is strictly dependent on the amino acid-mediated activation of the RagC GTPase activating protein FLCN[6,7]. TFEB lacks the TOR signalling motif responsible for the recruitment of other mTORC1 substrates. We used cryogenic-electron microscopy to determine the structure of TFEB as presented to mTORC1 for phosphorylation, which we refer to as the 'megacomplex'. Two full Rag–Ragulator complexes present each molecule of TFEB to the mTOR active site. One Rag–Ragulator complex is bound to Raptor in the canonical mode seen previously in the absence of TFEB. A second Rag–Ragulator complex (non-canonical) docks onto the first through a RagC GDP-dependent contact with the second Ragulator complex. The non-canonical Rag dimer binds the first helix of TFEB with a $RagC^{GDP}$-dependent aspartate clamp in the cleft between the Rag G domains. In cellulo mutation of the clamp drives TFEB constitutively into the nucleus while having no effect on mTORC1 localization. The remainder of the 108-amino acid TFEB docking domain

winds around Raptor and then back to RagA. The double use of RagC GDP contacts in both Rag dimers explains the strong dependence of TFEB phosphorylation on FLCN and the RagC GDP state.

Main

TFEB is one of four members of the microphthalmia family of basic helix-loop-helix leucine zipper (bHLH-Zip) transcription factors[8]. Overexpression of TFEB promotes degradation of long-lived proteins[9], lipid droplets[10] and damaged mitochondria[11], and can induce lysosomal exocytosis[12]. Indeed, data from cellular and mouse models show that TFEB activation increases autophagic and lysosomal clearance capacity, and is therefore a potential therapeutic target for the treatment of lysosomal storage disorders[13,14] and neurodegenerative diseases involving damaged organelles and accumulation of protein aggregates[15,16,17,18]. The last include Parkinson's Disease and Alzheimer's Disease. TFEB is regulated by cellular nutrient status through the phosphorylation at several serine residues, including Ser122, Ser142 and Ser211, by the mechanistic target of rapamycin complex 1 (mTORC1) under nutrient-replete conditions[2,3,4,5]. Phosphorylation of these sites allows TFEB cytosolic retention and inactivation[3,4,19]. mTORC1 is recruited to the lysosomal membrane for activation by the Rag GTPases, which are heterodimers composed of Rag A or B bound to Rag C or D[20,21,22]. The pentameric Ragulator–Lamtor complex, composed of Lamtor1–5 proteins, is a scaffold that anchors the Rag GTPases to the lysosomal membrane through myristoyl and palmitoyl posttranslational modifications of its Lamtor1 subunit[23].

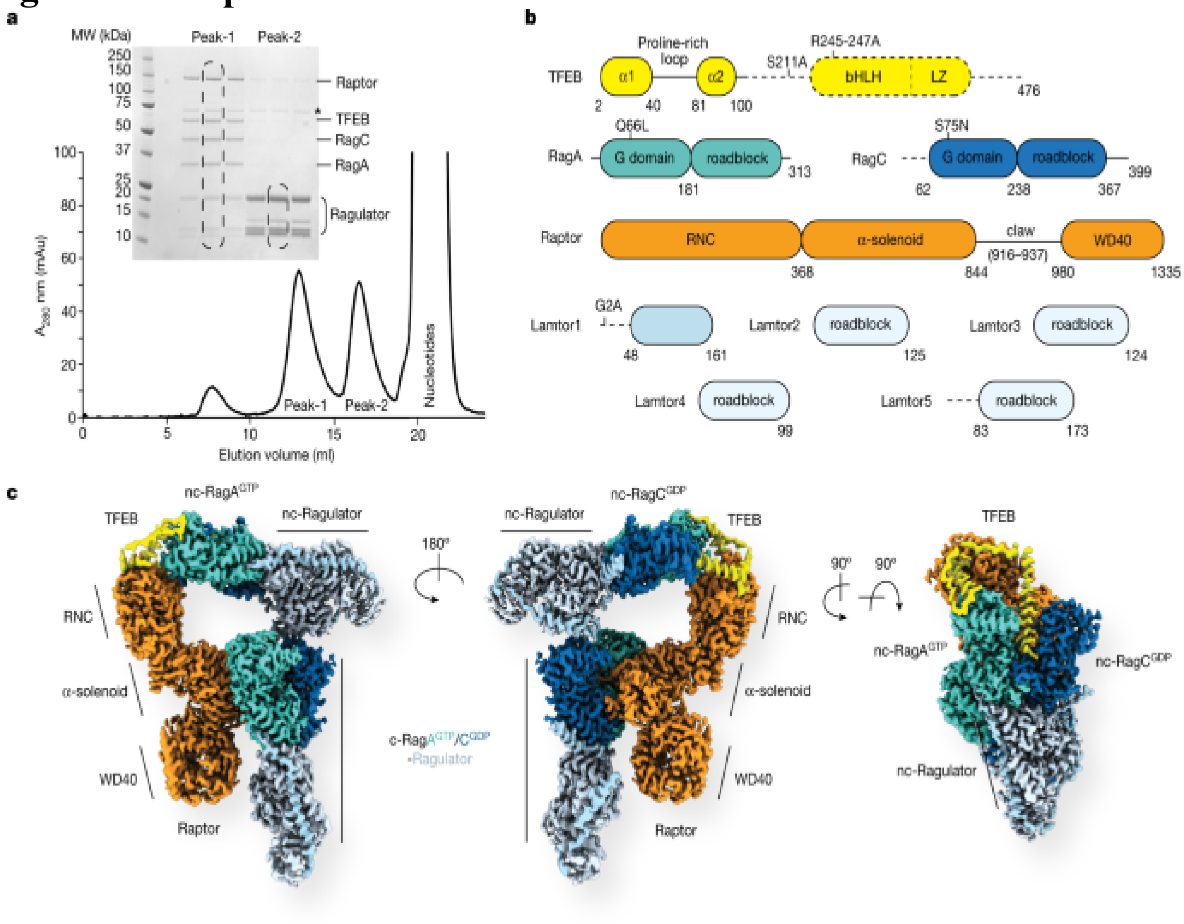
The cryogenic-electron microscopy (cryo-EM) structures of Rag dimers bound to mTORC1 (ref. [24]) or its Raptor subunit[25] showed that $RagA^{GTP}$ extensively contacts Raptor. Despite the importance of $RagC^{GDP}$ in mTORC1 physiology, these structures also showed $RagC^{GDP}$ interacts with Raptor to a lesser degree and without stringent dependence on the RagC nucleotide state. The tumour suppressor FLCN is the GTPase activating protein (GAP) for RagC[26]. FLCN activity is required for the phosphorylation of TFEB, but not for other mTORC1 substrates[7]. FLCN is maintained in the inactive lysosomal FLCN complex (LFC) during amino

acid starvation[6]. FLCN is reactivated under amino acid replete condition when the LFC is destabilized by the amino acid transporter SLC38A9 (ref. [27]). TFEB phosphoregulation accounts for the tumour suppressor function of FLCN in Birt–Hogg–Dubé (BHD) syndrome[7]. TFEB lacks the TOR signalling (TOS) motif found in other mTORC1 substrates[28], which enables presentation of substrates to the catalytic subunit by Raptor[29]. Instead, TFEB was shown to interact with the Rag GTPases[30], which serve as a substrate recruitment mechanism that allows TFEB phosphorylation by mTORC1 (ref. [7]). We therefore proposed that a unique structural platform directly involving RagC^{GDP} might be responsible for selectively presenting TFEB as a substrate of mTORC1. We set out to test the hypothesis by reconstituting and determining the structure of the complex.

Cryo-EM of Raptor–TFEB–Rag–Ragulator

A complex of TFEB–RagA–RagC was obtained by co-expression of full-length TFEB (R245-247A, S211A) and Rag GTPases (RagA^{Q66L}, RagC^{S75N}) in human embryonic kidney (HEK)-293F GnTI^{-} cells, and found to be stable under size-exclusion chromatography (Extended Data Fig. 1a,b). Mutations in the nuclear localization signal of TFEB (R245A, R246A, R247A) were introduced to prevent nuclear translocation[30] during expression in HEK cells. We also introduced the S211A mutation in TFEB because it had been reported to stabilize TFEB association with the Rag GTPases in cells[30]. The mutations RagA (Q66L) and RagC (S75N) were incorporated to promote the active configuration of Rag GTPases (RagA^{GTP}–RagC^{GDP}). We reconstituted the TFEB–Rag complex with purified Ragulator complex and solved the cryo-EM structure (Extended Data Fig. 1a,c–e). However, no TFEB density was observed (Extended Data Fig. 1f,g), indicating that further interactions were required to stabilize TFEB for structural studies. Previous structures[24,25] suggested that Raptor would be structurally proximal to the TFEB binding site. We then repeated the reconstitution in the presence of purified Raptor, assembled a Raptor–TFEB–Rag–Ragulator complex (Fig. 1a), and determined its cryo-EM structure to an overall 3.1-Å resolution (Extended Data Fig. 2d and Extended Data Table 1).

Fig. 1: Reconstitution and structure of the Raptor–TFEB–Rag–Ragulator complex.



a, Size-exclusion chromatography and SDS–PAGE of assembled Raptor–TFEB–Rag–Ragulator complex. Peak-1 corresponds to the fully assembled complex, and peak-2 represents Ragulator alone. All the corresponding bands are labelled, the asterisk indicates HSP70 contamination. MW, molecular weight; A_{280}, absorbance at 280 nm. **b**, Domain arrangement of all the subunits in the complex. Unresolved domains are indicated by dashed lines. **c**, A composite cryo-EM density map of the complex, assembled from three focused-refinement maps (Raptor, c-RagA^{GTP}/RagC^{GDP}–Ragulator and TFEB-nc–RagA^{GTP}/RagC^{GDP}–Ragulator). Different contour levels were used for optimal visualization using UCSF ChimeraX[46]. c, canonical; nc, non-canonical.

The structure of Raptor–TFEB–Rag–Ragulator showed a 2:1 stoichiometry for Rag–Ragulator with respect to Raptor, as compared to 1:1 observed in

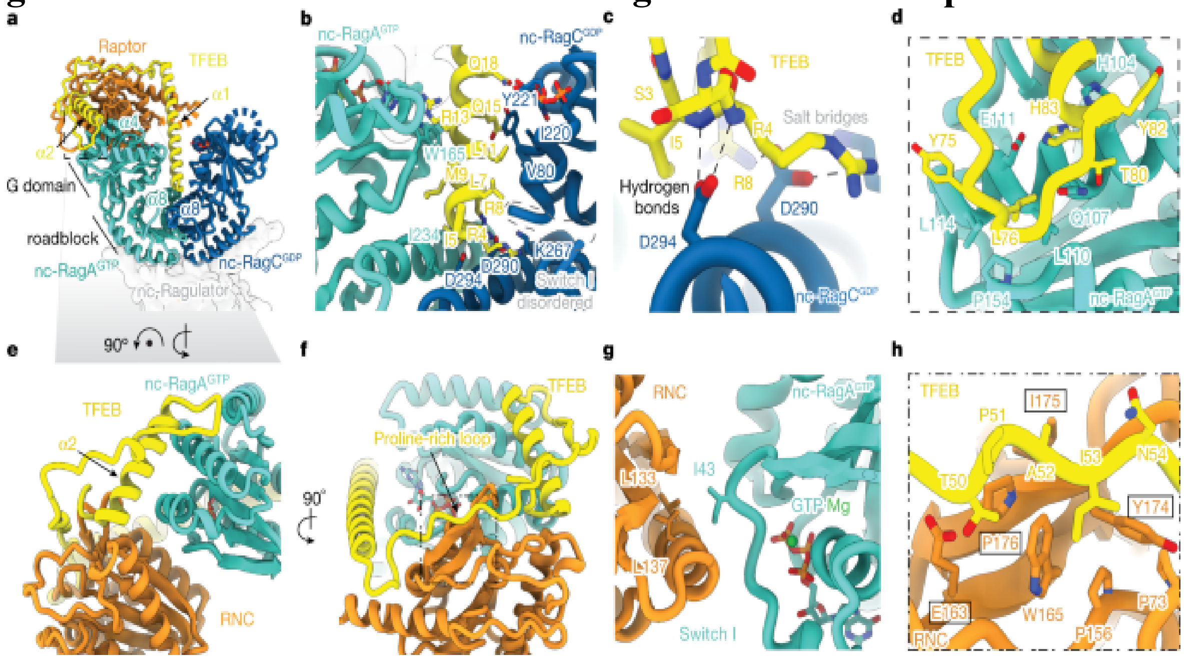
the structures of mTORC1/Raptor–Rag–Ragulator[24,25] (Fig. 1c). We refer to the Rag–Ragulator module that binds to Raptor as previously reported as the 'canonical' (c) Rag–Ragulator, and the second module as the 'non-canonical' (nc) Rag–Ragulator. Further local refinement of Raptor, canonical Rag–Ragulator and TFEB-nc–Rag–Ragulator yielded 2.8, 2.9 and 2.9 Å cryo-EM maps, respectively, which allowed us to build accurate atomic models (Extended Data Fig. 2a,d). The cryo-EM density of TFEB was clearly visible and corresponds to residues 2–105 (Extended Data Fig. 3a). The N and C termini of this segment are helical and referred to as α1 and α2, and they are connected to a Pro-rich loop. The TFEB-nc–Rag–Ragulator spans the Raptor and the canonical Rag dimer, forming a closed triangle with extensive contacts at both ends (Extended Data Fig. 4a,b). Both Rag heterodimers are in active states, on the basis of the high-resolution cryo-EM density of the corresponding nucleotide (Extended Data Fig. 3b). The conformations of the c-Rag–Ragulator and nc-Rag–Ragulator complexes are virtually identical (Extended Data Fig. 4c).

Interactions between TFEB and Rags

The structure showed that TFEB residues 2–105 were ordered, suggesting that these residues were both necessary and sufficient to form a stable complex with active Rag GTPases, and we confirmed that a slightly longer TFEB 1–109 construct was competent to form such a complex in vitro (Extended Data Fig. 5). The first 40 residues of TFEB form a long helix (α1) and occupy the cleft between the two G domains of the non-canonical dimer of $RagA^{GTP}$ and $RagC^{GDP}$ (Fig. 2a). Residues 2–18 of TFEB α1 are embedded in the inter-Rag G domain cleft and form a roughly 570 Å interaction interface with the $RagC^{GDP}$ G domain (Fig. 2b and Extended Data Fig. 4b). The N terminus of TFEB α1 sits directly on top of the α8 of $RagC^{GDP}$ roadblock domain, which is, in turn, at the dimerization interface of Rag heterodimer. TFEB helix α1 is thus clamped within the G domain cleft by hydrogen bonds between Asp^{294} of $RagC^{GDP}$ and the backbone of Arg^{4} and Ile^{5} of TFEB, and salt bridges between Asp^{290} of $RagC^{GDP}$ and Arg^{4}, Arg^{8} of TFEB (Fig. 2c). The α1 of TFEB also contacts $RagC^{GDP}$ through hydrophobic interactions between Leu^{7}, Leu^{11} of TFEB and Val^{80}, Ile^{220} of $RagC^{GDP}$ and between the side chain of Gln^{15} of TFEB and Tyr^{221}

of RagC^{GDP} (Fig. 2b). A stacking interaction is also present between the carbon chain of Arg^{13} of TFEB and Trp^{165} of RagA^{GTP}. There are fewer contacts between TFEB α1 and RagA^{GTP}, primarily through hydrophobic interactions between Ile^{5}, Met^{9} of TFEB and Ile^{234} of RagA^{GTP} (Fig. 2b). These data show how the TFEB N terminus is clamped between the Rag G domains in a strictly RagC^{GDP}-dependent manner.

Fig. 2: TFEB interacts with both nc-Rag GTPases and Raptor.

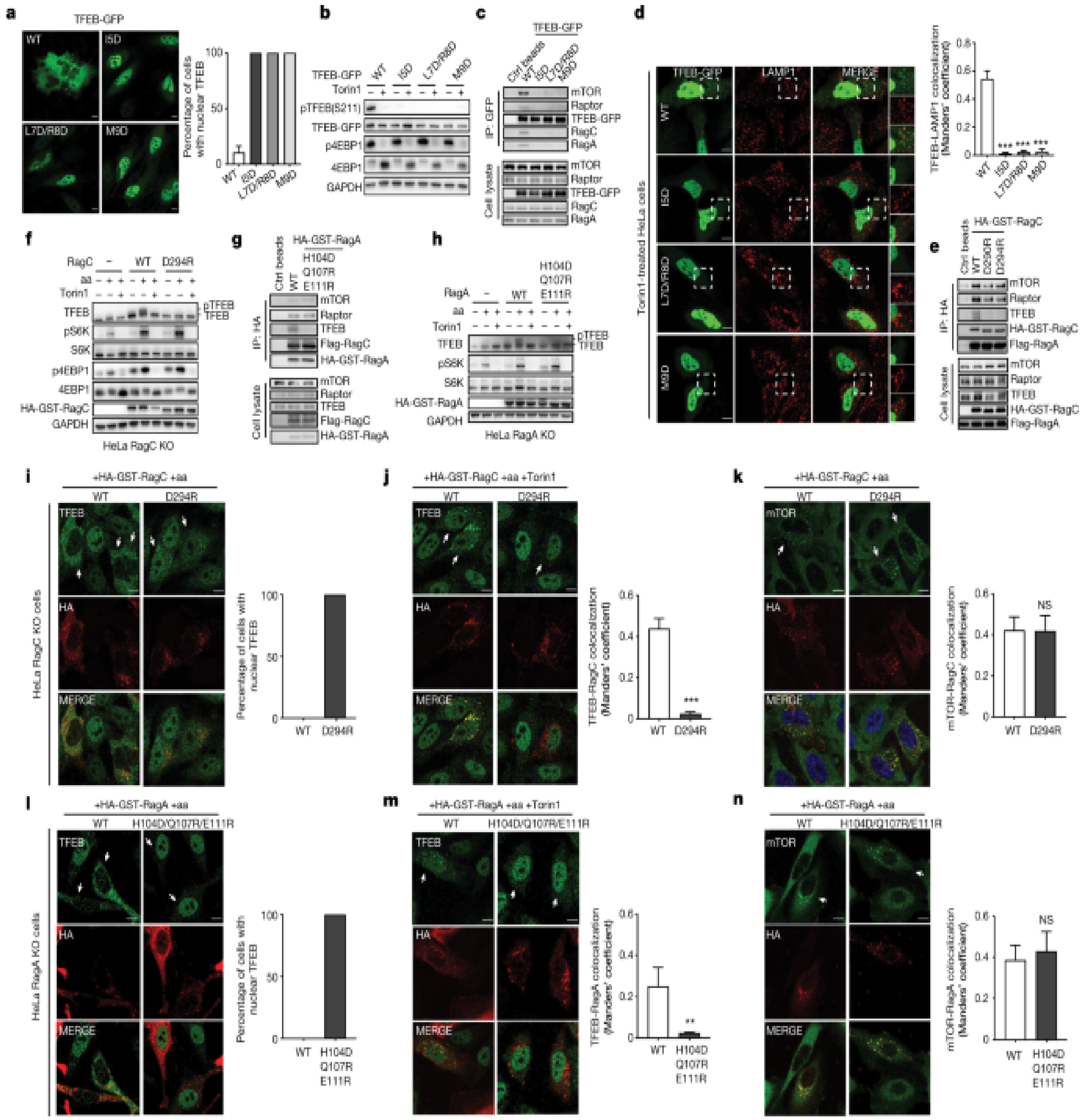


a, Overall interaction between TFEB and nc-Rag GTPases is shown as ribbon models from the front view. nc-Ragulator is shown as transparent surfaces. Disordered switches I and II of nc-RagC^{GDP} are shown with dashed lines. **b**, Interactions between TFEB and inter-Rag G domains at the dimer interface. **c**, Close-up view of the interaction between TFEB N terminus and α8 of RagC^{GDP}. Hydrogen bonds and salt bridges are labelled and indicated with black and grey dashed lines, respectively. **d**, Close-up view of the interaction between TFEB and outer-G domain of RagA^{GTP} as outlined in **a**. **e**, Ribbon model showing the interactions among TFEB, Raptor and nc-RagA^{GTP}. TFEB bridges the interaction between Raptor and nc-RagA^{GTP} through its Pro-rich loop and α2 region. **f**, 90°-rotated view of **e** shows the interaction between the Pro-rich loop of TFEB and RNC domain. **g**, Close-up view of the interaction between RNC domain and nc-RagA^{GTP}.

Ordered switch I of nc-RagA^{GTP} facilitates its interaction with the RNC domain. **h**, Close-up view as outlined in **f** shows the residues responsible for the interaction between ^{50}TPAI^{53} of TFEB and RNC domain. Raptor residues that interact with the RAIP motif of 4E-BP1 are highlighted with boxes[33].

To validate the functional role of the TFEB N terminus, TFEB mutants I5D, L7D/R8D and M9D were expressed in HeLa cells as green fluorescent protein (GFP) fusions. Cytosolic localization and Ser211 phosphorylation of wild-type TFEB was observed robustly in the absence of Torin1, as expected (Fig. 3a,b). Instead, all three of the mutants showed constitutively nuclear localization and defective Ser211 phosphorylation, even in the absence of Torin1 (Fig. 3a,b). TFEB lysosomal localization and mTORC1 interaction, which are observed for wild-type TFEB in Torin1-treated cells, were essentially abolished for all the mutants (Fig. 3c,d), confirming the functional requirement for these extreme N-terminal residues of TFEB in the G domain clamp. Next, we used a HeLa RagC knockout (KO) cell line to validate the role of the RagC clamp. The interaction between TFEB and the transiently transfected Rag GTPases was significantly impaired in both RagC^{D290R} and RagC^{D294R} in comparison to wild-type RagC (Fig. 3e). Moreover, expression of RagC^{D294R} in the RagC KO cells prevented TFEB phosphorylation in amino acid replete cells, even in the absence of Torin1 (Fig. 3f). However, the phosphorylation of S6K and 4E-BP1 was normal, indicating that these TOS motif substrates do not require the RagC clamp. RagC^{D294R} expression supported mTOR–RagC colocalization in amino acid replete conditions (Fig. 3k), but not cytosolic localization and RagC colocalization of TFEB in the absence and presence of Torin1, respectively (Fig. 3i,j). These data support that the RagC G domain clamp uniquely regulates TFEB phosphorylation.

Fig. 3: Function of the TFEB-nc-Rag GTPases interface.



a, Cells expressing wild-type (WT) or mutant TFEB-GFP were analysed using immunofluorescence to determine the percentage of cells showing nuclear TFEB, shown as mean ± s.e. throughout; $n = 12$ independent fields per condition. **b**, Immunoblot of HeLa cells expressing wild-type or mutant TFEB-GFP. **c**, Representative co-immunoprecipitation of Flp-In 293 T-REx cells transfected with wild-type or mutant TFEB-GFP. **d**, Microscopy analysis of Torin1-treated HeLa cells, $n \geq 5$ independent fields per condition. ***$P \leq 0.0001$ throughout. One-way analysis of variance (ANOVA), Dunnett's multiple comparisons test. **e**, Representative co-immunoprecipitation of HeLa RagC KO cells transfected with the indicated

constructs. **f**, Immunoblot of RagC KO HeLa cells transfected with empty vector or wild-type RagC or RagC(D294R). Cells were amino acid starved and refed in the presence or absence of 250 nM Torin1. **g**, Representative co-immunoprecipitation of HeLa RagA KO cells transfected with the indicated constructs. **h**, Immunoblot of RagA KO HeLa cells transfected with empty vector or wild-type RagA or RagA(H104D/Q107R/E111R). **i**–**k**, Cells as in **f** were analysed using immunofluorescence and the percentage of the cells were determined to show nuclear TFEB (**i**) ($n = 5$ fields per condition); TFEB–RagC colocalization (**j**) ($n \geq 5$ fields per condition, $***P \leq 0.0001$, unpaired *t*-test) and mTOR–RagC colocalization (**k**) ($n \geq 12$ fields per condition, unpaired *t*-test). **l**–**n**, Cells as in **h** were analysed using immunofluorescence and quantified to calculate the percentage of the cells showing nuclear TFEB (**l**) ($n \geq 4$ independent fields per condition), TFEB–RagA colocalization (**m**) ($n \geq 4$ fields per condition, $**P \leq 0.002$, unpaired *t*-test) and mTOR–RagA colocalization (**n**) ($n = 5$ independent fields per condition, unpaired *t*-test). Scale bar, 10 μm. NS, not significant; aa, amino acid; Ctrl, control; HA, haemagglutinin; IP, immunoprecipitation; GST, glutathione *S*-transferase.

Notably, a previously unknown interaction interface between residues 76–83 of TFEB and α4 of $RagA^{GTP}$ is also shown in our structure (Fig. 2d). Leu^{76} of TFEB inserts into a hydrophobic pocket formed by Leu^{110}, Leu^{114}, Pro^{154} and Leu^{155} of $RagA^{GTP}$. A salt bridge between His^{84} of TFEB and Glu^{111} of $RagA^{GTP}$ is also observed. We then used a RagA KO cell line to validate whether the structural analysis faithfully reflects cell physiology. The interaction between TFEB and the transiently transfected Rag GTPases was significantly impaired in the RagA triple mutant (H104D/Q107R/E111R) in comparison to wild-type RagA (Fig. 3g). The expression of $RagA^{H104D/Q107R/E111R}$ prevented TFEB phosphorylation in amino acid replete cells (Fig. 3h), but did not affect the phosphorylation of S6K and 4E-BP1. In addition, $RagA^{H104D/Q107R/E111R}$ expression supported mTOR–RagA colocalization in amino acid replete conditions (Fig. 3n), but not cytosolic localization and RagA colocalization of TFEB in the absence and presence of Torin1, respectively (Fig. 3l,m). Therefore, the unique RagA–TFEB interaction is necessary for TFEB phosphorylation.

TFEB interacts only with the active $RagC^{GDP}$-containing Rag dimer. Alignment of the TFEB bound active Rag GTPases and inactive Rag GTPases ($RagA^{GDP}$–$RagC^{GTP}$)[6,27,31,32] based on the α8 of RagC roadblock domains indicated that the switch I of $RagC^{GTP}$ sterically clashes with the α1 of TFEB, therefore precluding TFEB binding (Extended Data Fig. 6a). In addition, the wide opening conformation of G domains in the inactive Rag GTPases ($RagA^{GDP}$–$RagC^{GTP}$) effectively prevent the interaction between TFEB and the Rag heterodimer in the inactive state. Alignment of the TFEB bound active $RagA^{GTP}$ and inactive $RagA^{GDP}$ based on the α4 of RagA G domain showed apparently trivial structural differences in the TFEB binding region (Extended Data Fig. 6b), suggesting the nucleotide loading state of RagA does not impose selectivity towards TFEB binding at the unique RagA–TFEB interface. However, $RagA^{GTP}$ is required for mTORC1 recruitment to the lysosome and subsequent phosphorylation of both TFEB and TOS motif-containing substrates. In summary, $RagC^{GDP}$ and the unique RagA–TFEB interaction are specifically important for TFEB phosphorylation.

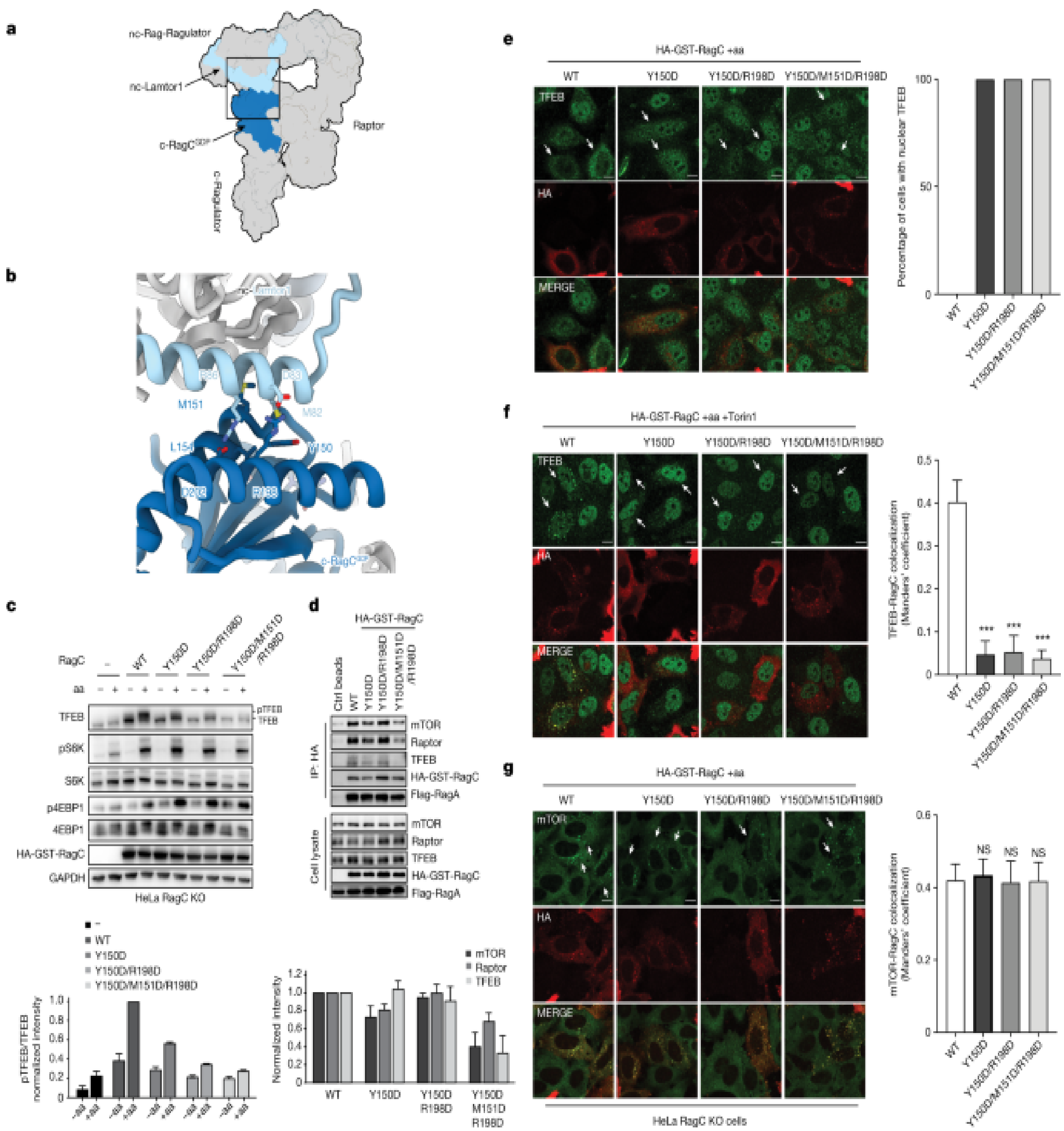
Bridging Rag–Ragulator complexes

The TFEB-nc–Rag–Ragulator complex is stabilized by interactions at both ends. On one end, the Pro-loop and α2 of TFEB bridge the Raptor N-terminal conserved (RNC) domain and the ordered switch I of nc-$RagA^{GTP}$ (Fig. 2e,f). As the switch I of RagA is disordered in the GDP-bound state[6,27], it emphasizes the importance of nc-Rag GTPases being in the active state ($RagA^{GTP}$–$RagC^{GDP}$). The contact between Raptor and nc-$RagA^{GTP}$ is maintained by hydrophobic interaction between Leu^{133}, Leu^{137} of Raptor and Ile^{43} of nc-$RagA^{GTP}$ (Fig. 2g). The residues Thr^{50}, Pro^{51}, Ala^{52} and Ile^{53} of TFEB (TPAI) cover a patch on the RNC domain, formed by residues Pro^{73}, Pro^{156}, Glu^{163}, Trp^{165}, Tyr^{174}, Ile^{175} and Pro^{176} (Fig. 2h). The mTORC1 substrate 4E-BP1 contains an N-terminal RAIP sequence that binds to the same site on the RNC domain[33]. TFEB Ala^{52} and Ile^{53} also interact with Raptor residues Tyr^{174} and Ile^{175} by β strand augmentation, as had been proposed for the 4E-BP1 RAIP–RNC interaction[33]. However,

mutational disruption of the ^{50}TPAI^{53} sequence had no effect on TFEB phosphorylation or subcellular localization (Extended Data Fig. 7d,e).

On the other side of the interface, the Lamtor1 subunit of the non-canonical Ragulator makes close contacts with the G domain of canonical RagC^{GDP} (Fig. 4a). The α2 of Lamtor1 resides on top of the α4 and α5 helices of RagC, stabilized by Met^{82} of Lamtor1 inserting into the hydrophobic pocket formed by Tyr^{150}, Met^{151}, Leu^{154} of RagC^{GDP} (Fig. 4b). Salt bridges are formed between Asp^{83}, Arg^{86} of Lamtor1 and Arg^{198}, Asp^{202} of RagC^{GDP}, respectively. These data indicate that the RagC^{GDP} state in the canonical Rag dimer is important for nc-Lamtor1 interaction and stabilization of the nc-Rag–Ragulator binding, thus heightening the sensitivity of the entire assembly to the RagC nucleotide state and thus the dependency of TFEB phosphorylation on FLCN.

Fig. 4: Function of the nc-Ragulator and c-RagC^{GDP} interface.



a, Cartoon representation that highlights the interacting subunits at the end with nc-Ragulator. **b**, Close-up view as outlined in **a** shows the residues responsible for the interaction between nc-Lamtor1 and c-RagC^{GDP}. **c**, Representative immunoblot of RagC KO HeLa cells transfected with empty vector or wild-type RagC or RagC mutants (Y150, Y150/R198D or Y150/M151/R198D). Cells were amino acid starved and refed in the presence or absence of 250 nM Torin1. Quantifications are shown with mean ± s.e. throughout; *n* = 2 experiments. **d**, Representative co-immunoprecipitation of HeLa RagC KO cells transfected with the indicated

constructs; $n = 3$ experiments. **e**–**g**, Cells as in **c** were analysed using immunofluorescence and quantified to calculate the percentage of the cells showing nuclear TFEB (**e**) ($n = 5$ independent fields per condition); TFEB–RagC colocalization (**f**) ($n \geq 5$ independent fields per condition, $^{***}P \leq 0.0001$, one-way ANOVA, Dunnett's multiple comparisons test) and mTOR–RagC colocalization (**g**) ($n \geq 8$ independent fields per condition; NS, not significant; one-way ANOVA, Dunnett's multiple comparisons test). Scale bar, 10 μm.

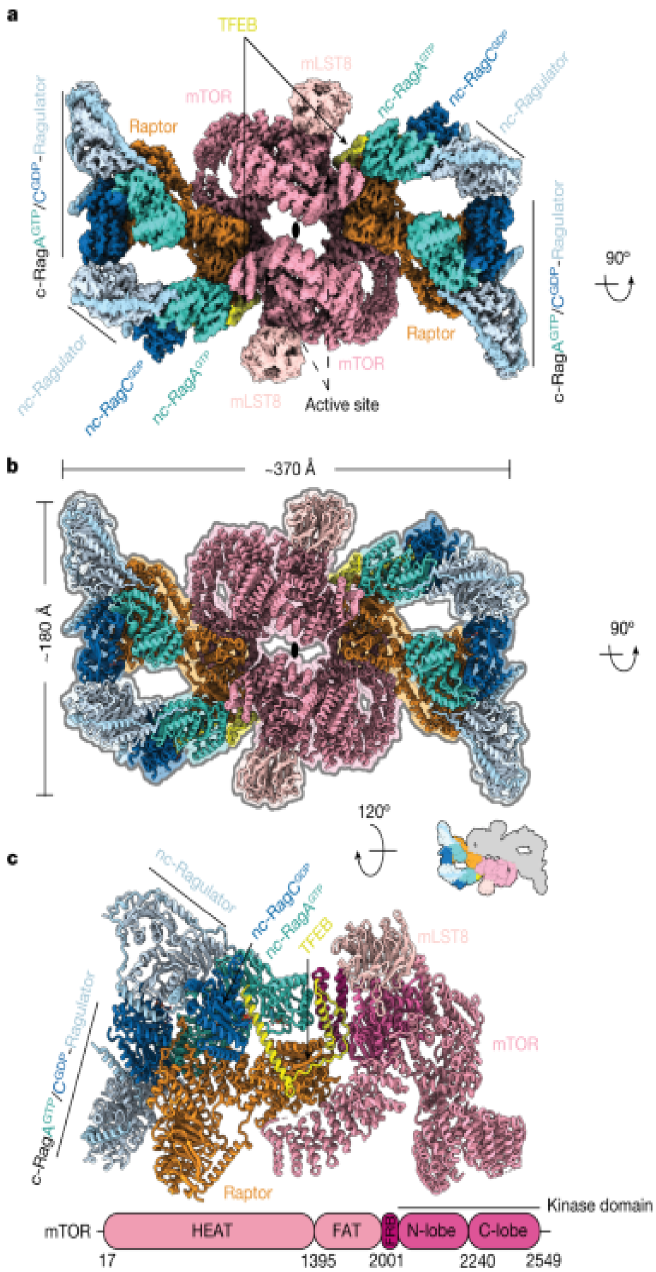
To validate the role of the c-RagC and nc-Ragulator bridging interaction, RagC residues Tyr^{150}, Met^{151} and Arg^{198} were mutated and expressed in RagC KO HeLa cells. The constructs $RagC^{Y150D}$, $RagC^{Y150D/R198D}$ and $RagC^{Y150D/M151D/R198D}$ all showed normal S6K and 4E-BP1 phosphorylation in amino acid replete conditions, but reduced or no TFEB phosphorylation under these same conditions (Fig. 4c). Consistently, only wild-type RagC restored TFEB cytosolic localization in RagC KO cells (Fig. 4e). Furthermore, in contrast to wild-type RagC, none of the RagC mutants were able to restore TFEB–RagC colocalization in Torin1-treated RagC KO cells (Fig. 4f). Wild-type and all three RagC mutants were all, however, able to restore mTOR lysosomal localization in RagC KO cells (Fig. 4g), consistent with a selective role for this interaction in regulating the phosphorylation of TFEB, but not other mTORC1 substrates. Transfected $RagC^{Y150D}$ and $RagC^{Y150D/R198D}$ had no defect in their interactions with TFEB, Raptor or mTOR, but a modest defect was noted for $RagC^{Y150D/M151D/R198D}$ (Fig. 4d). The co-immunoprecipitation results confirm that the megacomplex can still be formed in bulk, whereas the microscopy results indicate that significant recruitment of TFEB at any given time point is low because of decreased affinity for Ragulator, which in turn effectively prevents TFEB phosphorylation.

Cryo-EM structure of the megacomplex

To understand how TFEB is phosphorylated by mTORC1 as presented by the Raptor–Rag–Ragulator complex, we reconstituted mTORC1–TFEB–Rag–Ragulator megacomplex and determined its structure by cryo-EM. Two main populations of the megacomplex were resolved, showing that either one or two copies of TFEB are present on mTORC1 (Extended Data Fig.

8a). The reconstruction in C2 symmetry for the mTORC1 with two copies of TFEB resulted in a 3.7-Å resolution cryo-EM map. Further symmetry expansion and local refinement of the asymmetric unit improved the resolution to 3.2 Å (Extended Data Fig. 8e). A composite map was generated by superimposing the local reconstructions to the C2 symmetric reconstruction (Fig. 5a). We then built the atomic model for the entire complex, which contains mTOR, Raptor, mLST8, TFEB, active Rag GTPases, Ragulator with a stoichiometry of 2:2:2:2:4:4, containing a total of 36 polypeptide chains (Fig. 5b, Extended Data Table 1 and Supplementary Video 1).

Fig. 5: Structure of the mTORC1–TFEB–Rag–Ragulator megacomplex.



a, Composite cryo-EM density map of the dimeric mTORC1–TFEB–Rag–Ragulator megacomplex shown from top and side views. The active sites of mTOR are labelled with dashed arrows. The twofold axis is labelled as an oval symbol in the top view and a dash line in the side view. Different contour levels were used for optimal visualization using UCSF ChimeraX[46]. **b**, Atomic model of the dimeric megacomplex shown in the same orientation as in **a**. **c**, The ribbon model of an asymmetric unit. The domain organization of mTOR is shown. **d**, Focused view of the active site of mTOR, the HEAT and FAT domains are omitted for clarity. The ATP binding site is outlined

with a dashed line. The distance between Pro^{66} of TFEB and Lys^{2166} of mTOR is drawn with a double-headed arrow. The distance between Ile^{108} of TFEB and the active site of mTOR is calculated on the basis of the distance between Ile^{108} of TFEB and Asp^{2338} of mTOR. The inset highlights the distance between TFEB and the hinge loop (residues 2115–2118) at the end of mTOR FRB domain. Distances are calculated on the basis of the Cα atoms.

The long axis of the megacomplex is about 370 Å, and shows a curved geometry, with the HEAT domain and FAT domain of mTOR facing the convex and concave side, respectively. The binding mode of TFEB to the Rag GTPases and Raptor is essentially unchanged in the presence of the entire mTORC1 complex. Residues 2–108 of TFEB were resolved in the cryo-EM structure, essentially as before, but with the rest of TFEB not visualized and an empty active site despite the presence of a non-hydrolysable ATP analogue and the presence of sequences containing phosphorylation sites (Extended Data Fig. 9a,b). The inability to visualize these regions is probably due to inherent flexibility in the sequences containing phosphorylation sites. The Pro-loop and α2 of TFEB are positioned near the active site of mTOR, surrounded by the FKBP12-rapamycin-binding (FRB) domain, the kinase domain (KD) N lobe and C lobe (Fig. 5c). TFEB shows limited overlap with the PRAS40 (ref. [29]), but no overlap with the S6K, at the FRB binding site (Extended Data Fig. 9c,d). In addition, Tyr^{95} and Thr^{99} of TFEB are close to, but do not directly contact, a hinge loop (residues 2115–2118) at the end of mTOR FRB domain (Fig. 5d)

Whereas the last ordered residue of TFEB is roughly 34 Å from the catalytic residue Asp^{2338} of mTOR (Fig. 5d), this still places Ser122 and Ser142 of TFEB close enough for delivery to the active site. In principle, the predicted flexible sequence from 109–210 could be long enough to deliver Ser211 to the second (distal) active site in the mTOR dimer, which is roughly 116 Å (linear distance) from TFEB residue 108. TFEB phosphorylation by mTORC1 is independent of Rheb[7]. In the case of Rheb-dependent mTORC1 activation, a large-scale conformational change of mTORC1 was observed in the Rheb-bound state, which is thought to be essential for phosphorylation of TOS-containing substrates[29]. Our results shed light on the alternative

structural mechanism of Rheb-independent TFEB phosphorylation by mTORC1, with compatible anchoring geometry on the lysosomal membrane (Extended Data Fig. 10).

Discussion

The work described above provides structural evidence in support of the findings that TFEB phosphorylation by mTORC1 is uniquely regulated through an elaborate $RagC^{GDP}$-dependent mechanism[7]. The $RagC^{GDP}$ state is required, in the first instance, to maintain favourable contacts with the TFEB N-terminal helix in the non-canonical Rag dimer. In the canonical Rag dimer, the $RagC^{GDP}$ state is also important, in this case, for recruitment of the non-canonical Ragulator to the rest of the complex. The elaborate complex involved in presenting TFEB for phosphorylation by mTORC1 thus depends on two molecules of $RagC^{GDP}$. This mechanism serves to increase the stringency of TFEB regulation by the RagC GAP, FLCN. In the past few years, it has emerged that FLCN controls the phosphorylation of TFEB and other microphthalmia-associated transcription factors, but not that of many other well-known mTORC1 substrates such as S6 kinase, ULK1 and 4E-BP1 (refs. [6,7,34,35]). As the tumour suppressor whose mutation is responsible for BHD syndrome[36], FLCN is under exceptionally tight regulation. An elaborate set of structural gymnastics keep FLCN inactive by retaining it in the lysosomal LFC under starvation conditions[6], and reactivating it through intercleft competition with nutrient-activated SLC38A9 on refeeding[27]. The intercleft binding site for TFEB in the nc-Rag dimer overlaps with the site occupied by FLCN-FNIP2 in the LFC[6,31] and with SLC38A9 (ref. [27]), highlighting the complex time-sharing of different regulatory factors in the cleft. To this picture of stringent regulation of FLCN, we have now added an even more elaborate mode of regulation of TFEB phosphorylation downstream of FLCN.

The structures described here confirm several predictions in the literature while also showing many unexpected features. The interaction of Raptor with the canonical Rag–Ragulator complex was just as expected[24,25]. The N-terminal 30 amino acids of TFEB were correctly predicted to be essential for its Rag binding, lysosomal localization and mTORC1 phosphorylation[30].

The role of the subsequent 80 TFEB residues, however, was unanticipated. The presence of direct TFEB–Raptor interactions was completely unexpected. An Ile- and Pro-containing TPAI motif of TFEB binds directly to a surface patch on the RNC domain of Raptor that was previously shown to bind the RAIP sequence of 4E-BP1 (ref. [33]). The TOS-containing mTORC1 inhibitor PRAS40 also contains an RAIP-like motif that interacts with the same patch on the RNC domain[24], although its functional role has not been assessed. We found that a quadruple TPAI mutant of TFEB has no effect on TFEB phosphorylation by mTORC1 and subcellular localization. This is consistent with the finding that TFEB is not stably bound to Raptor in RagA/B deficient cells[7], in the presence of inactive Rag GTPases[2,5], or when the Rag-binding N-terminal residues of TFEB are absent[3,7,37]. The 4E-BP1 RAIP motif is separated from the TOS motif by 100 residues, and the RAIP–Raptor interaction makes a secondary contribution to mTORC1 binding relative to the TOS motif. Despite the fact structures show that the Raptor–TFEB binding interface is a prominent feature, the TPAI mutational data and previously published evidence indicate that TFEB–Raptor interaction is secondary to the contacts with the Rags and may have an auxiliary role in complex stabilization. Our structure illuminates a direct interaction between a Rag G domain and Ragulator (canonical RagC with non-canonical Ragulator), which we found to be important for TFEB phosphorylation. The question of how the megacomplex dissociates in cells following Ser211 phosphorylation remains open. Dissociation might be mediated by phosphorylation-triggered structural rearrangements within TFEB or other megacomplex components, or binding to 14-3-3 proteins[2,3,4,5] or other factors.

All of the TFEB-contacting residues of RagC are conserved in RagD, consistent with the finding that expression of either RagC or RagD can rescue TFEB recruitment to lysosomes in RagC/D double KO cells[7]. However, a recent publication[38] suggested that RagC plays only a minor role in the recruitment and phosphorylation of TFEB. By contrast with this conclusion, here we showed that TFEB forms a stable complex with a RagA–RagC dimer, and that TFEB phosphorylation and subcellular localization are drastically affected in RagC KO cells, despite the presence of endogenous RagD. These results are in line with previous publications showing that RagC depletion promotes TFEB/TFE3 dephosphorylation and

nuclear translocation[39,40] and that the expression of a constitutively active RagC mutant is sufficient to rescue TFEB/TFE3 phosphorylation and subcellular localization in FLCN KO cells[7,40]. Together, these data clearly demonstrate that RagC plays a major role in TFEB phosphorylation.

Overall, this work provides structural evidence of a non-canonical mTORC1 signalling that allows selective control of TFEB activity under specific conditions[7,39,41,42,43,44]. The hypophosphorylation and consequent hyperactivation of TFEB in the absence of FLCN drives increased mTORC1 activity and tumorigenesis in BHD syndrome[7]. Thus, in BHD, there might be therapeutic benefits to enhancing TFEB phosphorylation by bypassing $RagC^{GDP}$. The complexity and stringency of the structural mechanism for $RagC^{GDP}$-dependent phosphorylation suggests this will be challenging. On the other hand, enhanced activation of TFEB may be desirable in treating lysosomal storage disorders[13,14], promoting clearance of toxic aggregates and debris in neurons[15,16,17,18] and preventing non-alcoholic fatty liver disease through lipid clearance[45]. The structure presented here identifies several new interfaces that could be targeted to such an end.

Methods

Protein expression and purification

The full-length codon-optimized human TFEB with S211A and R245-247A mutations, human RagC with S75N mutation and human RagA with Q66L mutation were synthesized (Twist Bioscience) and cloned into a pCAG vector individually. The TFEB (S211A, R245-247A) construct included a TEV-cleavable GFP-His_{10} tag at the C terminus. The RagC (S75N) construct included a tobacco etch virus (TEV)-cleavable GST tag at the N terminus, whereas the RagA (Q66L) was tagless. For the expression and purification of the TFEB–Rag GTPases complex, the HEK293F $GnTI^{-}$ cells were transfected with a total of 1 mg of plasmid DNA (333 µg TFEB, 400 µg RagA and 267 µg RagC) and 4 mg polyethylenimine (Sigma-Aldrich) per litre at a density of $1.5–1.8 \times 10^6$ cells per ml. Cells were collected after 48 h, and lysed by gentle nutating in wash buffer (50 mM HEPES, 150 mM NaCl, 2.5 mM $MgCl_2$, 1 mM TCEP, pH 7.4) supplemented with 0.4%

CHAPS and Protease Inhibitor (Roche) for 1 h. Lysate was cleared by centrifugation at 35,000*g* for 35 min. Supernatant was incubated with glutathione Sepharose 4B (GE Healthcare) resin for 2 h. The resin was then first washed in the modified wash buffer with 200 mM NaCl and 0.3% CHAPS, and then in the wash buffer. The complex was eluted from the resin by a wash buffer with 10 mM reduced glutathione, and then incubated with TEV protease overnight. Eluted complexes were concentrated and further purified by size-exclusion chromatography using a Superose 6 10/300 GL (GE Healthcare) column equilibrated in the wash buffer. All purification steps were performed at 4 °C. Proteins were flash frozen in liquid nitrogen and stored in −80 °C. Attempted co-expression and purification of wild-type TFEB-GFP with active Rag GTPases was carried out as described above, however, wild-type TFEB-GFP did not co-elute with the Rags (Supplementary Fig. 2).

The human Ragulator complex (GST-TEV–Lamtor1, His_6-TEV–Lamtor2) was expressed in *Spodoptera frugiperda* (Sf9) cells through baculovirus infection and purified as previously described[47]. In brief, Sf9 cells were pelleted after 72 h of baculovirus infection and lysed in the wash buffer with 1% Triton X-100 and protease inhibitor. The cleared supernatant after centrifugation was applied to Ni-nitrilotriacetic acid gravity column (Thermo Scientific), washed with the wash buffer containing 200 mM NaCl, and eluted with the wash buffer with 250 mM imidazole. The elution was then applied to glutathione Sepharose 4B (GE Healthcare) gravity column, washed with the wash buffer. The complex was then eluted by on-column TEV cleavage overnight without nutation. Further purification was done by size-exclusion chromatography with a Superdex 200 10/300 GL column (GE Healthcare) column.

Three subunits of the human mTORC1 complex (mTOR, Raptor, mLST8) were codon-optimized and synthesized (GenScript). The mTOR gene was cloned into a pCAG vector without a tag, the Raptor gene was cloned into a pCAG vector with an uncleavable tandem 2× Strep II-1× FLAG-tag at the N terminus, and the mLST8 gene was also cloned into a pCAG vector with an uncleavable tandem 2× Strep II-1× FLAG-tag at the N terminus. The mTORC1 complex was produced in a similar manner to the TFEB–Rag GTPases complex, except that the total amount of DNA was increased to

1.35 mg (900 μg of mTOR, 250 μg of Raptor and 200 μg of mLST8) per litre of cells. The purification procedure of the mTORC1 complex is similar to that previously described[24]. On the other hand, Strep-Tactin resin (IBA Lifesciences) was used for the affinity purification and the complex was eluted with the wash buffer (50 mM HEPES, 150 mM NaCl, 1 mM TCEP, pH 7.4) containing 10 mM d-desthiobiotin. The elution was diluted into equal volume of salt-free buffer (50 mM HEPES, 1 mM TCEP, pH 7.4) and applied to a 5 ml HiTrap Q column (GE Healthcare). The mTORC1 complex and free RAPTOR were separated by a 100 ml salt gradient with salt-free buffer and high salt buffer (50 mM HEPES, 1 M NaCl, 1 mM TCEP, pH 7.4). The fractions containing mTORC1 complex and free Raptor were concentrated to 1.3 and 0.5 mg ml^{-1}, respectively. Purified proteins were flash frozen in liquid nitrogen and stored at −80 °C.

Cryo-EM sample preparation and imaging

The Raptor–TFEB–Rag–Ragulator complex was prepared by incubating 0.48 μM Raptor, 0.59 μM TFEB–Rag GTPases, 1.42 μM Ragulator, 9.5 μM GTP and 9.5 μM GDP in the wash buffer on ice for 5 h. Further purification of the complex was achieved by running a Superose 6 10/300 GL column. Fractions containing the fully assembled Raptor–TFEB–Rag–Ragulator complex were concentrated to 0.8 mg ml^{-1} for cryo-EM sample preparation.

The mTORC1–TFEB–Rag–Ragulator megacomplex was reconstituted in two steps. First, the TFEB–Rag–Ragulator complex was formed by incubating 2.5 μM TFEB–Rag GTPases, 7.4 μM Ragulator, 25 μM GTP and 25 μM GDP in the wash buffer on ice for 1 h. It is further purified through a Superose 6 10/300 GL column and concentrated to 1.2 mg ml^{-1}. And then, 0.36 μM mTORC1 complex, 1.8 μM TFEB–Rag–Ragulator complex, 18 μM GTP, 18 μM GDP and 36 μM AMPPNP were incubated in 100 μl of wash buffer containing 5 mM TCEP on ice for 5 h. Assembled mTORC1–TFEB–Rag–Ragulator megacomplex was further concentrated to roughly 1 mg ml^{-1} for cryo-EM sample preparation.

Cryo-EM specimens were prepared by applying 3 μl of freshly reconstituted complex to a glow-discharged (PELCO easiGlow, 45 s in air at 15 mA and 0.37 mbar) holey carbon grid (C-flat, 2/1-3C-T) and vitrified using a FEI

Vitrobot Mark IV (Thermo Fisher Scientific) after blotting for 3 s with blot force 18, two Whatman 595 papers on the sample side and one Whatman 595 paper on the back side at 6 °C with 100% relative humidity.

Cryo-EM images of the Raptor–TFEB–Rag–Ragulator complex and mTORC1–TFEB–Rag–Ragulator megacomplex were recorded under a Titan Krios G3 microscope (Thermo Fisher Scientific) equipped with a Gatan Quantum energy filter (slit width 20 eV) and operated at 300 kV. Automated data acquisition was achieved using SerialEM[48] on a K3 Summit direct detection camera (Gatan) in the super-resolution correlated-double sampling mode with a pixel size of 0.525 Å and a defocused range of −0.8 to −2.2 µm. Beam shift was enabled to encompass four exposures per hole and nine holes per stage shift. The beam intensity was adjusted to a dose rate of roughly 1 e^- per $Å^2$ per frame for a 50-frame video stack with a total exposure time of 7.6 s. A total of 10,080 and 17,028 video stacks were recorded for the Raptor–TFEB–Rag–Ragulator complex and the mTORC1–TFEB–Rag–Ragulator megacomplex, respectively.

Cryo-EM images of the TFEB–Rag–Ragulator complex were recorded under a Talos Arctica microscope (Thermo Fisher Scientific) operated at 200 kV. Automated data acquisition was achieved using SerialEM[48] on a K3 Summit direct detection camera (Gatan) in the super-resolution correlated-double sampling mode with a pixel size of 0.5575 Å and a defocused range of −0.8 to −2.2 µm. Beam shift was enabled to encompass nine exposures per stage shift. The beam intensity was adjusted to a dose rate of roughly 1 e^- per $Å^2$ per frame for a 50-frames video stack with a total exposure time of 8.6 s. A total of 3,438 video stacks were recorded for the TFEB–Rag–Ragulator complex.

Cryo-EM data processing

Super-resolution video stacks were motion-corrected and binned 2× by Fourier cropping using MotionCor2 (ref. [49]). Motion-corrected micrographs were primarily processed following the workflow in cryoSPARC v.3 (ref. [50]).

The data processing scheme for the Raptor–TFEB–Rag–Ragulator complex and mTORC1–TFEB–Rag–Ragulator megacomplex is shown in Extended Data Figs. 2 and 8, respectively. Owing to the size of the datasets, micrographs were split and processed following the same protocol and then combined for homogeneous refinement. Contrast transfer function determination was done using patch CTF in cryoSPARC v.3. Blob picker and template picker were both used to maximize the number of initially picked particles. Two-dimensional (2D) classification was only used to remove obvious 'junk' particles (for example, ice and chaperonin contaminants). Heterogeneous refinement following the ab initio reconstruction was used to select good particles, preserving potential particles with rare views that could not be identified in 2D classification. After extensive cleaning using 2D classification and heterogeneous refinement, particles were merged and the duplicates were removed with a 100-Å cut-off distance. Homogeneous refinement was then performed for the full dataset. Further cleaning of the full dataset was accomplished either by three-dimensional (3D) classification with the 'skip_align' option using RELION3 (ref. [51]) or 3D classification function in cryoSPARC v.3. The conversion of data files between cryoSPARC v.3 and RELION3 was done using University of California San Francisco (UCSF) pyem[52]. Local refinement was used to produce final cryo-EM maps for model building. For the mTORC1–TFEB–Rag–Ragulator megacomplex, symmetry expansion followed by local refinement was used to generate the cryo-EM map of an asymmetric unit.

In summary, a 3.6 Å resolution map was obtained from 169,720 particles for the TFEB–Rag–Ragulator complex. Three local refinement maps were resolved for the Raptor–TFEB–Rag–Ragulator complex, including Raptor (377,569 particles), canonical Rag–Ragulator (377,569 particles) and non-canonical Rag–Ragulator (273,453 particles) to the resolutions of 2.8, 2.9 and 2.9 Å, respectively. For the mTORC1–TFEB–Rag–Ragulator megacomplex, two main populations containing either one (103,274 particles) or two copies (96,166 particles) of the TFEB and non-canonical Rag–Ragulator were both resolved with C1 symmetry to the resolution of 3.8 Å. Symmetry expansion and local refinement of the population with two copies of the TFEB and non-canonical Rag–Ragulator yielded a 3.2 Å resolution map.

The overall resolution of all these reconstructed maps was assessed using the gold-standard criterion of Fourier shell correlation[53] at 0.143 cut-off[54]. Local resolution estimation[55] and local filtering were done in cryoSPARC v.3.

Atomic model building and refinement

To build the atomic model for Raptor–TFEB–Rag–Ragulator complex, we first fit the previous Raptor–Rag–Ragulator (Protein Data Bank (PDB) 6U62) structure in our cryo-EM map as rigid body using UCSF ChimeraX[46]. The fragments of the TFEB model were initially obtained from AlfaFold2 prediction[56], and manually docked into our cryo-EM map. A composite map combining the three focused-refinement maps was assembled using PHENIX[57]. Model refinement against the composite map was performed by real-space refinement in PHENIX[58]. Manual model building was done with COOT[59] and ISOLDE[60] to inspect and improve local fitting. The iterative process of refinement and the manual building was conducted to achieve the best model. For the mTORC1–TFEB–Rag–Ragulator megacomplex, the refined Raptor–TFEB–Rag–Ragulator and previous mTORC1 (PDB 6BCX) structures were docked in our cryo-EM map. A composite map of the symmetric complex using the focused-refinement asymmetric unit was generated. The same model building procedure was performed as described above. All the figures and videos were made using UCSF ChimeraX.

Materials and plasmids for cellular assays

Reagents used in this study were obtained from the following sources: antibodies to mTOR (catalogue no. 2983, 1:100 immunofluorescence), Phospho-p70 S6 Kinase (Thr389) (1A5) (catalogue no. 9206, 1:1,000 western blot), p70 S6 Kinase (catalogue no. 9202, 1:1,000 western blot), 4E-BP1 (catalogue no. 9644, 1:1,000 western blot), Phospho-4E-BP1 (Ser65) (catalogue no. 9456, 1:1,000 western blot), TFEB (catalogue no. 4240, 1:1,000 western blot) and Phospho-TFEB S211 (catalogue no. 37681, 1:1,000 western blot) were from Cell Signalling Technology; antibodies to GAPDH (6C5) (catalogue no. sc-32233, 1:15,000 western blot) and LAMP-1 (H4A3) (catalogue no. sc-20011, 1:500 immunofluorescence) were from Santa Cruz; antibody to HA.11 Epitope Tag (catalogue no. 901513) was from Biolegend and HRP-conjugated secondary antibodies to mouse

(catalogue no. 401215, 1:5,000 dilution) and rabbit (catalogue no. 401315, 1:5,000 dilution) IgGs were from Calbiochem.

Chemicals used were Torin1 (catalogue no. 4247) that came from Tocris, Protease Inhibitor Cocktail (catalogue no. P8340) and puromycin (catalogue no. P9620) were from Sigma-Aldrich and PhosSTOP phosphatase inhibitor cocktail tablets (catalogue no. 04906837001) were from Roche.

Plasmids used were the plasmid encoding full-length TFEB-GFP, previously described in ref. [9]. pRK5-HA-GST RagC wild-type (no. 19304) and pRK5-HA-GST-RagA wild-type (no. 19298) plasmids, which were a kind gift from D. Sabatini (Addgene plasmids). All the mutants used in these cellular assays were generated by using QuikChange II-E Site-Directed Mutagenesis Kit (no. 200555, Agilent Technologies).

Cell culture

HeLa cells were cultured in MEM (catalogue no. ECB2071L, Euroclone) supplemented with 10% inactivated fetal bovine serum (FBS) (catalogue no. ECS0180L, Euroclone), 2 mM glutamine (catalogue no. ECB3000D, Euroclone), penicillin (100 IU ml^{-1}) and streptomycin (100 μg ml^{-1}) (catalogue no. ECB3001D, Euroclone) and maintained at 37 °C and 5% CO_2. RagC KO HeLa cells and RagA KO HeLa cells were previously generated and described in ref. [7]. Flp-In 293 T-REx cells (catalogue no. R78007 Thermo Fisher) were grown in DMEM (catalogue no. D6429 Sigma-Aldrich), supplemented with 10% (vol/vol) FBS (catalogue no. 10270 Thermo Fisher), 100 U ml^{-1} penicillin and 100 μg ml^{-1} streptomycin (catalogue no. P0781 Sigma-Aldrich), 100 μg ml^{-1} Zeocin (catalogue no. ant-zn-5b InvivoGen, Toulouse, France) and 15 μg ml^{-1} Blasticidin (ant-bl-5b InvivoGen). Cell lines were validated by morphological analysis and routinely tested for absence of mycoplasma.

Cell treatment

For experiments involving amino acid starvation, cells were rinsed twice with PBS and incubated for 60 min (unless stated otherwise) in amino acid-free Roswell Park Memorial Institute medium (catalogue no. R9010-01,

USBiological) supplemented with 10% dialysed FBS. Serum was dialysed against 1× PBS through 3,500 molecular weight cut-off dialysis tubing to ensure absence of contaminating amino acids. For amino acid refeeding, cells were restimulated for 30 min with 1× water-solubilized mix of essential (catalogue no. 11130036, Thermo Fisher Scientific) and non-essential (catalogue no. 11140035, Thermo Fisher Scientific) amino acids resuspended in amino acid-free Roswell Park Memorial Institute medium supplemented with 10% dialysed FBS, plus glutamine. Where reported, cells were incubated with 250 nM Torin1 during amino acid restimulation.

Cell lysis and western blotting

Cells were rinsed once with PBS and lysed in ice-cold lysis buffer (250 mM NaCl, 1% Triton, 25mM HEPES pH 7.4) supplemented with protease and phosphatase inhibitors. Total lysates were passed ten times through a 25-gauge needle with syringe, kept at 4 °C for 10 min and then cleared by centrifugation in a microcentrifuge (14,000 rpm at 4 °C for 10 min). Protein concentration was measured by Bradford assay. Cell lysates were resolved by SDS–PAGE on 4–12% Bis-Tris gradient gels (catalogue no. NP0323PK2 NuPage, Thermo Fisher Scientific) and analysed by immunoblotting with the indicated primary antibodies.

Confocal microscopy

Cells were grown on eight-well Lab-Tek II Chamber Slides, treated as indicated and fixed with 4% paraformaldehyde for 10 min at room temperature. Blocking was performed with 3% bovine serum albumin in PBS + 0.02% saponin for 1 h at room temperature. Immunostainings were performed on dilution of primary antibodies in blocking solution and overnight incubation at 4 °C, followed by three washes and secondary antibody incubation in blocking solution for 1 h at room temperature. After three more washes, coverslips were finally mounted in VECTASHIELD mounting medium with 4,6-diamidino-2-phenylindole and analysed using LSM 800 or LSM 880+ Airyscan systems (Carl Zeiss), with a Plan-Apochromat ×63/1.4 NA M27 oil immersion objective using immersion oil (catalogue no. 518F, Carl Zeiss) at room temperature. The microscopes were operated on the ZEN 2013 software platform (Carl Zeiss). After calculation

of processing for the airyscan, images were processed in the ImageJ v.1.47. Mander's colocalization coefficient was calculated using JACoP ImageJ Plugin[61].

Immunoprecipitation

Flp-In 293 T-REx cells were transfected with wild-type or mutant TFEB-GFP. HeLa RagC KO cells or RagA KO cells grown on 10 cm culture dishes were transiently transfected with the different HA-GST-RagC mutants and wild-type Flag-RagA or HA-GST-RagA$^{H104D/D107R/E111R}$ and Flag-RagC, respectively, using Fugene HD (catalogue no. E2311, Promega). As a control, cell lines were transfected with STREP-HA-GFP (control beads lane on immunoprecipitation blots). The following day, cells were treated with 330 nM Torin1 (catalogue no. 4247, Tocris) for 1 h. Subsequently, cells were washed twice with ice-cold PBS and incubated with 1 mg ml^{-1} dithiobis(succinimidyl propionate) crosslinker (catalogue no. 22586, Thermo Fisher Scientific) for 10 min at room temperature. The crosslinking reaction was quenched by adding Tris-HCl pH 8.5 to a final concentration of 100 mM, the cells rinsed again with ice-cold PBS and lysed in 25 mM HEPES pH 7.4, 250 mM NaCl, 1% Triton supplemented with protease and phosphatase inhibitors. For immunoprecipitations performed with TFEB as a bait, the lysis buffer also included 0.1% SDS and 2 mM EDTA. Lysates were passed five times through a 25-gauge needle with syringe and then cleared by centrifugation (14,000 rpm at 4 °C for 10 min). Lysates were then incubated with GFP trap magnetic agarose beads (no, gtma-20, ProteinTech Group, Inc) or with haemagglutinin beads (catalogue no. A2095, Sigma) at 4 °C for 2 h, washed with 40× the beads volume of lysis buffer, and eluted from the beads. Aliquots of the lysates and eluates were resolved by SDS–PAGE on 8, 10 or 15% SDS–PAGE gels and analysed by immunoblotting with the indicated primary antibodies. The emitter-coupled logic signal was detected and recorded with Fusion FX EDGE. Quantification of western blots was performed by calculating the intensity of the protein bands using the densitometry analysis function of ImageJ. Values were normalized to the respective control in each experiment.

Reporting summary

Further information on research design is available in the Nature Portfolio Reporting Summary linked to this article.

Data availability

Structural coordinates were deposited in the PDB with accession codes 7UX2 (Raptor–TFEB–Rag–Ragulator), 7UXC (asymmetric unit of mTORC1–TFEB–Rag–Ragulator) and 7UXH (mTORC1–TFEB–Rag–Ragulator). The cryo-EM density maps were deposited in the Electron Microscopy Data Bank with accession numbers EMD-26840 (Raptor–TFEB–Rag–Ragulator complex with Raptor mask), EMD-26842 (Raptor–TFEB–Rag–Ragulator complex with c-Rag–Ragulator mask), EMD-26843 (Raptor–TFEB–Rag–Ragulator complex with TFEB-nc-Rag–Ragulator mask), EMD-26844 (consensus refinement of the Raptor–TFEB–Rag–Ragulator complex), EMD-26846 (composite map of the Raptor–TFEB–Rag–Ragulator complex), EMD-26852 (consensus refinement of mTORC1–TFEB–Rag–Ragulator complex with C2 symmetry), EMD-26857 (symmetry expansion of the mTORC1–TFEB–Rag–Ragulator complex) and EMD-26861 (composite map of the mTORC1–TFEB–Rag–Ragulator complex).

References

1. Sardiello, M. et al. A gene network regulating lysosomal biogenesis and function. *Science* **325**, 473–477 (2009).

2. Settembre, C. et al. A lysosome-to-nucleus signalling mechanism senses and regulates the lysosome via mTOR and TFEB. *EMBO J.* **31**, 1095–1108 (2012).

3. Roczniak-Ferguson, A. et al. The transcription factor TFEB links mTORC1 signaling to transcriptional control of lysosome homeostasis. *Sci. Signal* **5**, ra42 (2012).

4. Martina, J. A., Chen, Y., Gucek, M. & Puertollano, R. MTORC1 functions as a transcriptional regulator of autophagy by preventing nuclear transport of TFEB. *Autophagy* **8**, 903–914 (2012).

5. Vega-Rubin-de-Celis, S., Pena-Llopis, S., Konda, M. & Brugarolas, J. Multistep regulation of TFEB by MTORC1. *Autophagy* **13**, 464–472 (2017).

6. Lawrence, R. E. et al. Structural mechanism of a Rag GTPase activation checkpoint by the lysosomal folliculin complex. *Science* **366**, 971–977 (2019).

7. Napolitano, G. et al. A substrate-specific mTORC1 pathway underlies Birt-Hogg-Dubé syndrome. *Nature* **585**, 597–602 (2020).

8. Napolitano, G. & Ballabio, A. TFEB at a glance. *J. Cell Sci.* **129**, 2475–2481 (2016).

9. Settembre, C. et al. TFEB links autophagy to lysosomal biogenesis. *Science* **332**, 1429–1433 (2011).

10. Settembre, C. et al. TFEB controls cellular lipid metabolism through a starvation-induced autoregulatory loop. *Nat. Cell Biol.* **15**, 647–658 (2013).

11. Nezich, C. L., Wang, C., Fogel, A. I. & Youle, R. J. MiT/TFE transcription factors are activated during mitophagy downstream of Parkin and Atg5. *J. Cell Biol.* **210**, 435–450 (2015).

12. Medina, D. L. et al. Transcriptional activation of lysosomal exocytosis promotes cellular clearance. *Dev. Cell* **21**, 421–430 (2011).

13. Rega, L. R. et al. Activation of the transcription factor EB rescues lysosomal abnormalities in cystinotic kidney cells. *Kidney Int.* **89**, 862–873 (2016).

14. Spampanato, C. et al. Transcription factor EB (TFEB) is a new therapeutic target for Pompe disease. *EMBO Mol. Med.* **5**, 691–706 (2013).

15. Decressac, M. et al. TFEB-mediated autophagy rescues midbrain dopamine neurons from α-synuclein toxicity. *Proc. Natl Acad. Sci. USA* **110**, E1817–E1826 (2013).

16. Dehay, B. et al. Pathogenic lysosomal depletion in Parkinson's disease. *J. Neurosci.* **30**, 12535–12544 (2010).

17. Polito, V. A. et al. Selective clearance of aberrant tau proteins and rescue of neurotoxicity by transcription factor EB. *EMBO Mol. Med.* **6**, 1142–1160 (2014).

18. Xiao, Q. et al. Neuronal-targeted TFEB accelerates lysosomal degradation of APP, reducing Aβ generation and amyloid plaque pathogenesis. *J. Neurosci.* **35**, 12137–12151 (2015).

19. Napolitano, G. et al. mTOR-dependent phosphorylation controls TFEB nuclear export. *Nat. Commun.* **9**, 3312 (2018).

20. Kim, E., Goraksha-Hicks, P., Li, L., Neufeld, T. P. & Guan, K. L. Regulation of TORC1 by Rag GTPases in nutrient response. *Nat. Cell Biol.* **10**, 935–945 (2008).

21. Sancak, Y. et al. Ragulator-Rag complex targets mTORC1 to the lysosomal surface and is necessary for its activation by amino acids. *Cell* **141**, 290–303 (2010).

22. Sancak, Y. et al. The Rag GTPases bind raptor and mediate amino acid signaling to mTORC1. *Science* **320**, 1496–1501 (2008).

23. Nada, S. et al. The novel lipid raft adaptor p18 controls endosome dynamics by anchoring the MEK-ERK pathway to late endosomes. *EMBO J.* **28**, 477–489 (2009).

24. Anandapadamanaban, M. et al. Architecture of human Rag GTPase heterodimers and their complex with mTORC1. *Science* **366**, 203–210 (2019).

25. Rogala, K. B. et al. Structural basis for the docking of mTORC1 on the lysosomal surface. *Science* **366**, 468–475 (2019).

26. Tsun, Z. Y. et al. The Folliculin tumor suppressor is a GAP for the RagC/D GTPases that signal amino acid levels to mTORC1. *Mol. Cell* **52**, 495–505 (2013).

27. Fromm, S. A., Lawrence, R. E. & Hurley, J. H. Structural mechanism for amino acid-dependent Rag GTPase nucleotide state switching by SLC38A9. *Nat. Struct. Mol. Biol.* **27**, 1017–1023 (2020).

28. Schalm, S. S. & Blenis, J. Identification of a conserved motif required for mTOR signaling. *Curr. Biol.* **12**, 632–639 (2002).

29. Yang, H. et al. Mechanisms of mTORC1 activation by RHEB and inhibition by PRAS40. *Nature* **552**, 368–373 (2017).

30. Martina, J. A. & Puertollano, R. Rag GTPases mediate amino acid-dependent recruitment of TFEB and MITF to lysosomes. *J. Cell Biol.* **200**, 475–491 (2013).

31. Shen, K. et al. Cryo-EM structure of the human FLCN-FNIP2-Rag-Ragulator complex. *Cell* **179**, 1319–1329.e8 (2019).

32. Gong, R. et al. Crystal structure of the Gtr1p-Gtr2p complex reveals new insights into the amino acid-induced TORC1 activation. *Genes Dev.* **25**, 1668–1673 (2011).

33. Bohm, R. et al. The dynamic mechanism of 4E-BP1 recognition and phosphorylation by mTORC1. *Mol. Cell* **81**, 2403–2416 e5 (2021).

34. Wada, S. et al. The tumor suppressor FLCN mediates an alternate mTOR pathway to regulate browning of adipose tissue. *Genes Dev.* **30**, 2551–2564 (2016).

35. Li, J. et al. Myeloid Folliculin balances mTOR activation to maintain innate immunity homeostasis. *JCI Insight* **5**, e126939 (2019).

36. Schmidt, L. S. & Linehan, W. M. FLCN: the causative gene for Birt-Hogg-Dube syndrome. *Gene* **640**, 28–42 (2018).

37. Hsu, C. L. et al. MAP4K3 mediates amino acid-dependent regulation of autophagy via phosphorylation of TFEB. *Nat. Commun.* **9**, 942 (2018).

38. Gollwitzer, P., Grutzmacher, N., Wilhelm, S., Kummel, D. & Demetriades, C. A Rag GTPase dimer code defines the regulation of

mTORC1 by amino acids. *Nat. Cell Biol.* **24**, 1394–1406 (2022).

39. Alesi, N. et al. TSC2 regulates lysosome biogenesis via a non-canonical RAGC and TFEB-dependent mechanism. *Nat. Commun.* **12**, 4245 (2021).

40. Li, K. et al. Folliculin promotes substrate-selective mTORC1 activity by activating RagC to recruit TFE3. *PLoS Biol.* **20**, e3001594 (2022).

41. Napolitano, G., Di Malta, C. & Ballabio, A. Non-canonical mTORC1 signaling at the lysosome. *Trends Cell Biol.* **32**, 920–931 (2022).

42. Goodwin, J. M. et al. GABARAP sequesters the FLCN-FNIP tumor suppressor complex to couple autophagy with lysosomal biogenesis. *Sci. Adv.* **7**, eabj2485 (2021).

43. Nakamura, S. et al. LC3 lipidation is essential for TFEB activation during the lysosomal damage response to kidney injury. *Nat. Cell Biol.* **22**, 1252–1263 (2020).

44. Kimura, T., Hayama, Y., Okuzaki, D., Nada, S. & Okada, M. The Ragulator complex serves as a substrate-specific mTORC1 scaffold in regulating the nuclear translocation of transcription factor EB. *J. Biol. Chem.* **298**, 101744 (2022).

45. Gosis, B. S. et al. Inhibition of nonalcoholic fatty liver disease in mice by selective inhibition of mTORC1. *Science* **376**, eabf8271 (2022).

46. Goddard, T. D. et al. UCSF ChimeraX: meeting modern challenges in visualization and analysis. *Protein Sci.* **27**, 14–25 (2018).

47. Su, M. Y. et al. Hybrid structure of the RagA/C-Ragulator mTORC1 activation complex. *Mol. Cell* **68**, 835–846.e3 (2017).

48. Mastronarde, D. N. Automated electron microscope tomography using robust prediction of specimen movements. *J. Struct. Biol.* **152**, 36–51 (2005).

49. Zheng, S. Q. et al. MotionCor2: anisotropic correction of beam-induced motion for improved cryo-electron microscopy. *Nat. Methods* **14**, 331–332 (2017).

50. Punjani, A., Rubinstein, J. L., Fleet, D. J. & Brubaker, M. A. cryoSPARC: algorithms for rapid unsupervised cryo-EM structure determination. *Nat. Methods* **14**, 290–296 (2017).

51. Zivanov, J. et al. New tools for automated high-resolution cryo-EM structure determination in RELION-3. *eLife* **7**, e42166 (2018).

52. Asarnow, D., Palovcak, E. & Cheng, Y. UCSF pyem v.0.5. *Zenodo* https://doi.org/10.5281/zenodo.3576630 (2019).

53. Scheres, S. H. & Chen, S. Prevention of overfitting in cryo-EM structure determination. *Nat. Methods* **9**, 853–854 (2012).

54. Rosenthal, P. B. & Henderson, R. Optimal determination of particle orientation, absolute hand, and contrast loss in single-particle electron cryomicroscopy. *J. Mol. Biol.* **333**, 721–745 (2003).

55. Cardone, G., Heymann, J. B. & Steven, A. C. One number does not fit all: mapping local variations in resolution in cryo-EM reconstructions. *J. Struct. Biol.* **184**, 226–236 (2013).

56. Jumper, J. et al. Highly accurate protein structure prediction with AlphaFold. *Nature* **596**, 583–589 (2021).

57. Liebschner, D. et al. Macromolecular structure determination using X-rays, neutrons and electrons: recent developments in Phenix. *Acta Crystallogr. D Struct. Biol.* **75**, 861–877 (2019).

58. Afonine, P. V. et al. Real-space refinement in PHENIX for cryo-EM and crystallography. *Acta Crystallogr. D Struct. Biol.* **74**, 531–544 (2018).

59. Emsley, P. & Cowtan, K. Coot: model-building tools for molecular graphics. *Acta Crystallogr. D Biol. Crystallogr.* **60**, 2126–2132 (2004).

60. Croll, T. I. ISOLDE: a physically realistic environment for model building into low-resolution electron-density maps. *Acta Crystallogr. D Struct. Biol.* **74**, 519–530 (2018).

61. Dunn, K. W., Kamocka, M. M. & McDonald, J. H. A practical guide to evaluating colocalization in biological microscopy. *Am. J. Physiol. Cell Physiol.* **300**, C723–C742 (2011).

62. Krissinel, E. & Henrick, K. in *Computational Life Sciences. CompLife 2005. Lecture Notes in Computer Science* (eds Berthold, R. et al.) Vol. 3695, 163–174 (Springer, 2005).

Acknowledgements

We thank S. Fromm and T. Stasyk for contributions to early stages of the project, J. Remis and D. Toso for cryo-EM facility support, A. Joiner for comments on the manuscript, and H. R. Shin, R. Zoncu and many members of the Zoncu and Hurley laboratories for discussions. This work was supported by Genentech as part of the Alliance for Therapies in Neuroscience and the National Institute of General Medical Sciences, National Institutes of Health, grant no. R01 GM111730 (J.H.H.), the Italian Telethon Foundation (to G.N. and A.B.), Associazione Italiana per la Ricerca sul Cancro A.I.R.C. (grant nos. MFAG-23538 to G.N. and IG-22103 and 5x1000-21051 to A.B.), MIUR (grant nos. PRIN 2017YF9FBS to G.N. and PRIN 2017E5L5P3 to A.B.) and the European Research Council H2020 AdG (grant no. LYSOSOMICS 694282 to A.B.).

Author information

Authors and Affiliations

1. Department of Molecular and Cell Biology, University of California Berkeley, Berkeley, CA, USA

   Zhicheng Cui & James H. Hurley

2. California Institute for Quantitative Biosciences, University of California, Berkeley, CA, USA

Zhicheng Cui & James H. Hurley

3. Telethon Institute of Genetics and Medicine (TIGEM), Naples, Italy

Gennaro Napolitano, Alessandra Esposito, Jlenia Monfregola & Andrea Ballabio

4. Medical Genetics Unit, Department of Medical and Translational Science, Federico II University, Naples, Italy

Gennaro Napolitano, Alessandra Esposito, Jlenia Monfregola & Andrea Ballabio

5. Institute of Cell Biology, Biocenter, Medical University of Innsbruck, Innsbruck, Austria

Mariana E. G. de Araujo & Lukas A. Huber

6. Department of Molecular and Human Genetics, Baylor College of Medicine, Houston, TX, USA

Andrea Ballabio

7. Jan and Dan Duncan Neurological Research Institute, Texas Children's Hospital, Houston, TX, USA

Andrea Ballabio

8. SSM School for Advanced Studies, Federico II University, Naples, Italy

Andrea Ballabio

9. Helen Wills Neuroscience Institute, University of California, Berkeley, Berkeley, CA, USA

James H. Hurley

Contributions

Z.C. expressed and purified proteins, reconstituted the protein complexes and carried out cryo-EM imaging and structural analysis. G.N., A.E. and J.M. carried out mutational analysis, cell culture and cell imaging and protein phosphorylation analysis. M.E.G.A. carried out immunoblotting. L.A.H., A.B. and J.H.H. supervised research. Z.C., G.N., A.B. and J.H.H. wrote the first draft of the manuscript. All authors contributed to editing and revising.

Corresponding authors

Correspondence to Andrea Ballabio or James H. Hurley.

Ethics declarations

Competing interests

J.H.H. is a cofounder and shareholder of Casma Therapeutics and receives research funding from Casma Therapeutics, Genentech and Hoffmann-La Roche. A.B. is a cofounder and shareholder of Casma Therapeutics and advisory board member of Next Generation Diagnostics, Avilar Therapeutics and Coave. The other authors declare no competing interests.

Peer review

Peer review information

Nature thanks the anonymous reviewers for their contribution to the peer review of this work. Peer reviewer reports are available.

Additional information

Publisher’s note Springer Nature remains neutral with regard to jurisdictional claims in published maps and institutional affiliations.

Extended data figures and tables

Extended Data Fig. 1 Purification, reconstitution, and cryo-EM structure determination of the TFEB-Rag-Ragulator complex.

a, Gel filtration chromatography of the TFEB-Rag and TFEB-Rag-Ragulator complexes, using a Superose 6 10/300 GL (GE Healthcare) column. Corresponding peaks are labelled and analyzed by Coomassie blue staining SDS-PAGE in **b** and **c** for TFEB-Rag and TFEB-Rag-Ragulator complexes, respectively. **d**-**f**, cryo-EM structure determination of TFEB-Rag-Ragulator complex. **d**, Resolution estimation based on the gold standard FSC. **e**, Orientation distribution of the reconstructed cryo-EM map. **f**, Side-by-side view of the cryo-EM density map and atomic model of the TFEB-Rag-Ragulator complex. Cryo-EM density for TFEB is not resolved. Asterisks in (**b)** and (**c)** indicate HSP70 contamination. **g**, Masked 3D classification of TFEB-Rag-Ragulator without alignment using the reconstruction in **f**. The TFEB mask is shown in grey density. The classification results are shown in blue. Rag-Ragulator is shown in light gray and shown as reference to identify TFEB. Only the least populated class (0.15%) shows density in the TFEB binding site.

Extended Data Fig. 2 Cryo-EM workflow of the Raptor–TFEB-Rag-Ragulator complex.

a, Cryo-EM data processing diagram of the Raptor–TFEB-Rag-Ragulator complex. **b**, A representative micrograph of the dataset after motion correction. **c**, Selected 2D class average images showing different orientations of the complex. **d**, Resolution plots of the cryo-EM reconstructions with different masks. Orientation distribution of reconstructed cryo-EM maps with Raptor, c-Rag-Ragulator, and nc-Rag-Ragulator masks are shown in **e**, **f**, and **g**, respectively. Scale bars in **b** and **c** represent 20 nm.

Extended Data Fig. 3 Representative cryo-EM density of the Raptor-TFEB-Rag-Ragulator complex.

a, Cryo-EM density of TFEB (2–105) at contour level 6 (left) and level 4 (right). **b**, Cryo-EM density of the nucleotides at contour level 8.9.

Extended Data Fig. 4 Interaction surface aera estimation of the Raptor-TFEB-Rag-Ragulator complex and structural comparison between nc-Rag-Ragulator and c-Rag-Ragulator.

a, A cartoon representation of the complex, labelled with red circles indicating different interaction surface. **b**, A table showing the interaction surface aera labelled in **a**, estimated by PISA[62]. **c**, Structures are superimposed based on RagC. The TFEB-nc-Rag-Ragulator are colored as in Fig. 1. The c-Rag-Ragulator is colored in gray.

Extended Data Fig. 5 Assembly of Raptor-TFEB$^{1–109}$-Rag-Ragulator complex.

a, SDS-PAGE analysis of the purified TFEB$^{1–109}$-Rag complex before TEV cleavage and gel filtration. **b**, Gel filtration chromatography of the Raptor-Rag-Ragulator and Raptor-TFEB$^{1–109}$-Rag-Ragulator complexes, using a Superose 6 10/300 GL (GE Healthcare) column. The peaks corresponding to the largest complex are analyzed by SDS-PAGE and stained by Coomassie blue.

Extended Data Fig. 6 Structural comparison between the active nc-Rag GTPases (RagA^{GTP}-RagC^{GDP}) and RagC in GTP-bound states, and between the nc-RagA^{GTP} and RagA in GDP-bound states at the unique TFEB contact site.

a, Structures are superimposed based on the α8 of RagC. Structures of RagC in GTP-bound states are colored as gray, while the switch I regions are colored as pink. Residues 41–105 of TFEB are omitted. **b**, Structures are

superimposed based on the α4 of RagA. Structures of RagA at GDP-bound states are colored in gray. The TFEB and nc-Rag GTPases are colored as in Fig. 1.

Extended Data Fig. 7 Quantification of the co-immunoprecipitation of mutants in the TFEB-nc-Rag GTPases interface and in cellulo assessment of the TFEB ^{50}TPAI^{53} mutation.

a-**c**, Quantifications of TFEB mutants in Fig. 3c, RagC mutants in Fig. 3e, and RagA mutants in Fig. 3g are calculated with mean ± s.e.m.; n = 3 experiments. **d**, Representative immunofluorescence analysis of cells expressing GFP tagged wild type or ^{50}TPAI^{53} mutant TFEB, in the presence and absence of amino acids. Quantification on the right shows the percentage of cells with TFEB nuclear localization. Results are mean ± s.e.; n = 5 independent fields per condition. Scale bar, 10 µm. **e**, TFEB phosphorylation was analyzed by immunoblotting for wild type and ^{50}TPAI^{53} mutant, in the presence and absence of Torin1.

Extended Data Fig. 8 Cryo-EM workflow of the mTORC1-TFEB-Rag-Ragulator megacomplex.

a, Cryo-EM data processing diagram of the mTORC1-TFEB-Rag-Ragulator megacomplex. **b**, A representative micrograph of the dataset after motion correction. **c**, SDS-PAGE of the reconstituted megacomplex stained by Coomassie blue. Asterisk indicates HSP70 contamination. **d**, Selected 2D class average images showing different orientations of the complex. **e**, Resolution plots of the asymmetric unit of mTORC1-TFEB-Rag-Ragulator megacomplex after symmetry expansion. **f**, Orientation distribution of local refinement after symmetry expansion of the mTORC1-TFEB-Rag-Ragulator complex. Scale bars in **b** and **d** represent 20 nm.

Extended Data Fig. 9 Cryo-EM map of the active site of mTOR and overlapping between TFEB, S6K and PRAS40.

a, Cryo-EM map in the active site of mTOR is shown as transparent surface. The density is zoned within 3Å of the model. **b**, The cryo-EM density outside the zone range is shown as solid surface colored in gray. **c**-**d**, Superimposed structure of S6K (PDB: 5WBH) and PRAS40 (PDB: 5WBU) with mTORC1-TFEB-Rag-Ragulator based on the FRB domain of mTOR.

Extended Data Fig. 10 Proposed membrane tethering of the mTORC1-TFEB-Rag-Ragulator megacomplex.

The Red dots represent the position of residue 47 of Lamtor 1 subunit. The dashed curved lines indicate the disordered 46 residues of Lamtor1. The long linker of Lamtor 1 at N-terminus could also permit the complex facing toward the lysosomal membrane in an opposite orientation as shown above.

Extended Data Table 1 Cryo-EM data collection, refinement, and validation statistics

Supplementary information

Supplementary Figures

This file contains Supplementary Fig. 1: Original images of SDS–PAGE and immunoblots and Supplementary Fig. 2: Wild-type TFEB does not copurify with Rags.

Reporting Summary

Peer Review File

Supplementary Video 1

Atomic model of mTORC1–TFEB–Rag–Ragulator megacomplex. Overview of the model built on the cryo-EM density, highlighting new interaction interfaces discussed in the article.

Rights and permissions

Open Access This article is licensed under a Creative Commons Attribution 4.0 International License, which permits use, sharing, adaptation, distribution and reproduction in any medium or format, as long as you give appropriate credit to the original author(s) and the source, provide a link to the Creative Commons licence, and indicate if changes were made. The images or other third party material in this article are included in the article's Creative Commons licence, unless indicated otherwise in a credit line to the material. If material is not included in the article's Creative Commons licence and your intended use is not permitted by statutory regulation or exceeds the permitted use, you will need to obtain permission directly from the copyright holder. To view a copy of this licence, visit http://creativecommons.org/licenses/by/4.0/.

Reprints and Permissions

About this article

Cite this article

Cui, Z., Napolitano, G., de Araujo, M.E.G. *et al.* Structure of the lysosomal mTORC1–TFEB–Rag–Ragulator megacomplex. *Nature* **614**, 572–579 (2023). https://doi.org/10.1038/s41586-022-05652-7

- Received: 03 May 2022
- Accepted: 13 December 2022
- Published: 25 January 2023
- Issue Date: 16 February 2023
- DOI: https://doi.org/10.1038/s41586-022-05652-7

Share this article

Anyone you share the following link with will be able to read this content:

Get shareable link

Sorry, a shareable link is not currently available for this article.

Copy to clipboard

Provided by the Springer Nature SharedIt content-sharing initiative

A transient protein megacomplex that controls degradation of cell components

Nature Research Briefing 25 Jan 2023

This article was downloaded by **calibre** from https://www.nature.com/articles/s41586-022-05652-7

- Matters Arising
- Open Access
- Published: 15 February 2023

The case for standardizing gene nomenclature in vertebrates

- Fiona M. McCarthy,
- Tamsin E. M. Jones,
- Anne E. Kwitek,
- Cynthia L. Smith,
- Peter D. Vize,
- Monte Westerfield &
- …
- Elspeth A. Bruford

Show authors

Nature **volume 614**, pages E31–E32 (2023)

- 1709 Accesses

- 22 Altmetric

- Metrics details

Matters Arising to this article was published on 15 February 2023

The Original Article was published on 28 April 2021

arising from C. Theofanopoulou et al. *Nature* https://doi.org/10.1038/s41586-020-03040-7 (2021)

Standardized gene nomenclature supports unambiguous communication and identification of the scientific literature associated with genes; to support the increasing number of annotated genomes that are now available for comparative studies, gene nomenclature authorities coordinate the assignment of approved gene names that can be readily applied across species. Theofanopoulou et al.[1] propose a new nomenclature for the genes that encode oxytocin and arginine vasopressin and their receptors. Rather than changing to a different nomenclature, we suggest minor updates to the current approved nomenclature of these vertebrate genes to better reflect their evolutionary history. We call on authors, journal editors and reviewers to help support communication and indexing of gene-related publications by working with existing gene nomenclature committees and ensuring that standardized gene nomenclature is routinely used.

Standardized gene nomenclature provides a common language for the biomedical community and beyond. Gene nomenclature refers to both the full gene name and the unique gene symbol; aliases (or synonyms) used in published literature are also often recorded to facilitate disambiguation, indexing and text mining. In vertebrates, gene nomenclature committees focus on species that represent key groups, including mammals[2,3,4], birds[5], fish[6] and amphibians[7], and coordinate their efforts to ensure that approved gene names are assigned consistently across species. Historically, mammalian and avian gene symbols are in upper case, with the exception of rodents, which have gene symbols in title case; by contrast, *Xenopus* and zebrafish gene symbols are in lower case. These case conventions were originally established to help researchers distinguish references to genes in different model organisms[8], and the standardized nomenclature is widely disseminated through all of the major genomic resources and model organism databases. Notably, this approach takes into account genetic and evolutionary similarities in addition to function, exactly as proposed by Theofanopoulou et al.[1], and many genes are named on the basis of their homologues in yeast, flies and other non-vertebrates. Gene nomenclature groups work closely with community experts[9], researchers, clinicians, bioinformaticians and biocurators to ensure that the approved gene names

and symbols are informative, non-redundant and broadly applicable across diverse biological fields of study. One rationale cited for the newly proposed nomenclature of Theofanopoulou et al. is to create a universal nomenclature system that can be consistently used across vertebrates. However, such a system is already established by the existing vertebrate nomenclature authorities.

Theofanopoulou et al. propose a new nomenclature for the genes that encode oxytocin, arginine vasopressin and their receptors on the basis of their evolutionary analysis of these genes in the context of newly sequenced, high-quality genomes generated by the Vertebrate Genomes Project (VGP)[10]. Although we share their desire to ensure that gene nomenclature reflects evolutionary relationships, we believe that the existing approved nomenclature, first established in vertebrates 30 years ago, already largely represents these relationships (Table 1). Instead, only minor updates are needed in some species to better reflect the orthology and paralogy between these genes (Supplementary Information). We consider many factors when making nomenclature decisions: structure and function of genes and gene products; evolutionary history (including consideration of gene synteny); current and historical nomenclature usage; utility of nomenclature as search terms (including avoiding symbol clashes with other genes across the tree of life); levels of support for nomenclature updates in the research community; and concordance with nomenclature guidelines in several model systems (see Supplementary Information). In addition, the current remit of the HUGO Gene Nomenclature Committee (HGNC) includes a commitment to move towards gene-symbol stability in humans[2]—especially for genes that are clinically relevant, which include the genes encoding oxytocin and arginine vasopressin and their receptors. Confusion about gene nomenclature in the medical literature could have serious negative consequences for patient safety[11].

Table 1 Comparison of approved and proposed symbols for the oxytocin and arginine vasopressin ligand and receptor genes

Major revisions to approved nomenclature are considered when the benefits clearly outweigh the downsides. Benefits can include the correction of incorrect or misleading gene nomenclature, better representation of

evolutionary relationships, standardizing nomenclature throughout a gene family and providing nomenclature that can be used across all vertebrate species. Theofanopoulou et al. argue that the nomenclature of the oxytocin and arginine vasopressin genes and their receptors merits an update for all of these benefits. We believe that the existing approved nomenclature does not merit major revision as it is widely used, is not incorrect or misleading in the vast majority of vertebrate species, largely represents evolutionary relationships (with only minor additions needed to represent subclades in the AVPR2 subfamily) and has long been standardized across species (see Supplementary Information). The drawback is the introduction of additional identifiers in databases and the literature, which increases the risk of confusion to researchers and readers. Unfortunately, the potential for confusion has already been exemplified in a recent paper by Ocampo Daza et al.[12], who disagreed with Theofanopoulou et al.'s assignment of ABC suffixes in the AVPR2/VTR2 subfamily and therefore used the same symbols to refer to different genes.

Theofanopoulou et al. argue that their study acts as a model for the revision of gene nomenclature in the context of large-scale vertebrate-sequencing projects, including the VGP. Their stated intent is to completely revise vertebrate gene nomenclature, including that of human genes, to fully reflect evolutionary histories that are revealed by large-scale sequencing projects. We are concerned that the authors may not fully appreciate the level of disruption that would be caused by major revisions to gene nomenclature on this scale. It is worth noting that the gene family analysed in their study is relatively simple with regard to its evolutionary history, and to perform such an analysis for every vertebrate gene family is an inconceivably large task. Given that over 40 years and millions of dollars of public funding have been invested in the current standardized nomenclature projects, we propose that an overhaul of the entire system would not be a prudent use of the limited resources we have in genomics.

Requiring scientists to consistently use approved nomenclature avoids confusion and supports search indexing. Although an increasing number of scientific journals mandate the use of standardized gene nomenclature, this requirement is not always clearly stated or strictly enforced for authors, and citing the approved gene symbol and its associated gene ID should be

compulsory in all journals. The instructions provided by *Nature* to authors state that authors can “use their preferred terminology” for genes and proteins, which enables authors to publish novel nomenclature without first checking with the relevant authority. If all journals—and especially influential ones such as *Nature*—were to insist that authors consult with nomenclature committees when suggesting updates, much confusion could potentially be avoided. Unequivocally communicating about genes will facilitate research and development in all biological and clinical fields.

We assert that the changes suggested by Theofanopoulou et al. to the official vertebrate gene nomenclature would cause considerable confusion with little perceivable benefit.

Our analysis of their study (Supplementary Information) demonstrates how the integration of genomic data from a broader range of species can help us to update and improve an already-established nomenclature with only minor modifications. Theofanopoulou et al. call for collaboration between the gene nomenclature committees and genomic initiatives, which we have always wholeheartedly supported. We continue to encourage researchers and communities to collaborate with the gene nomenclature committees when proposing nomenclature updates.

Reporting summary

Further information on experimental design is available in the Nature Portfolio Reporting Summary linked to this article.

References

1. Theofanopoulou, C., Gedman, G., Cahill, J. A., Boeckx, C. & Jarvis, E. D. Universal nomenclature for oxytocin–vasotocin ligand and receptor families. *Nature* **592**, 747–755 (2021).

2. Bruford, E. A. et al. Guidelines for human gene nomenclature. *Nat. Genet.* **52**, 754–758 (2020).

3. Smith, J. R. et al. The year of the rat: the rat genome database at 20: a multi-species knowledgebase and analysis platform. *Nucleic Acids Res.* **48**, D731–D742 (2020).

4. Blake, J. A. et al. Mouse Genome Database (MGD): knowledgebase for mouse–human comparative biology. *Nucleic Acids Res.* **49**, D981–D987 (2021).

5. Burt, D. W. et al. The chicken gene nomenclature committee report. *BMC Genomics* **10**, S5 (2009).

6. Howe, D. G. et al. The Zebrafish Information Network: major gene page and home page updates. *Nucleic Acids Res.* **49**, D1058–D1064 (2021).

7. James-Zorn, C. et al. Xenbase: core features, data acquisition, and data processing. *Genesis* **53**, 486–497 (2015).

8. Bruford, E. A. Highlights of the 'Gene Nomenclature Across Species' meeting. *Hum. Genomics* **4**, 213–217 (2010).

9. Olender, T., Jones, T. E. M., Bruford, E. A. & Lancet, D. A unified nomenclature for vertebrate olfactory receptors. *BMC Evol. Biol.* **20**, 42 (2020).

10. Rhie, A. et al. Towards complete and error-free genome assemblies of all vertebrate species. *Nature* **592**, 737–746 (2021).

11. Braschi, B., Seal, R. L., Tweedie, S., Jones, T. E. M. & Bruford, E. A. The risks of using unapproved gene symbols. *Am. J. Hum. Genet.* **108**, 1813–1816 (2021).

12. Ocampo Daza, D., Bergqvist, C. A. & Larhammar, D. The evolution of oxytocin and vasotocin receptor genes in jawed vertebrates: a clear case for gene duplications through ancestral whole-genome duplications. *Front. Endocrinol.* **12**, 792644 (2021).

Acknowledgements

T.E.M.J. and E.A.B. are currently funded by the National Human Genome Research Institute (NHGRI) grant U24HG003345 and Wellcome Trust grant 208349/Z/17/Z. F.M.M. is supported by the US Department of Agriculture National Institute of Food and Agriculture projects ARZT-1370570-R50-131 and ARZT-1370520-R50-130. A.E.K. is supported by National Institutes of Health (NIH) grants from the NHGRI (U24HG010859) and the National Heart Lung and Blood Institute (NHLBI; R01HL064541). C.L.S. is supported by NHGRI grant U24HG000330. P.D.V. is supported by NIH grants P41 HD095831 and P41 HD064556. M.W. is supported by NHGRI grants U24HG002659 and U24HG010859. The content is solely the responsibility of the authors and does not necessarily represent the official views of the NIH or any of the funders.

Author information

Author notes

1. These authors contributed equally: Fiona M. McCarthy, Tamsin E.M. Jones

Authors and Affiliations

1. The Chicken Gene Nomenclature Committee (CGNC), School of Animal and Comparative Biomedical Sciences, University of Arizona, Tucson, AZ, USA

   Fiona M. McCarthy

2. HUGO Gene Nomenclature Committee (HGNC), European Molecular Biology Laboratory, European Bioinformatics Institute, Wellcome Genome Campus, Hinxton, UK

   Tamsin E. M. Jones & Elspeth A. Bruford

3. Rat Genome Database, Medical College of Wisconsin, Milwaukee, WI, USA

Anne E. Kwitek

4. Mouse Genome Database, The Jackson Laboratory, Bar Harbor, ME, USA

   Cynthia L. Smith

5. Xenbase, Departments of Biological Sciences and Computer Science, University of Calgary, Calgary, Alberta, Canada

   Peter D. Vize

6. ZFIN, Institute of Neuroscience, University of Oregon, Eugene, OR, USA

   Monte Westerfield

7. Department of Haematology, University of Cambridge School of Clinical Medicine, Cambridge, UK

   Elspeth A. Bruford

Contributions

Study conceptualization: E.A.B. Analysis of gene nomenclature and evolutionary relationships: T.E.M.J. and E.A.B. Manuscript writing and reviewing: initial writing by F.M.M., T.E.M.J. and E.A.B., with input from all authors.

Corresponding author

Correspondence to Elspeth A. Bruford.

Ethics declarations

Competing interests

The authors declare no competing interests.

Additional information

Publisher's note Springer Nature remains neutral with regard to jurisdictional claims in published maps and institutional affiliations.

Supplementary information

Supplementary Information

This file contains additional discussion of the guidelines and procedures used by the gene nomenclature committees, followed by detailed discussion of the nomenclature of each gene in the oxytocin/arginine vasopressin ligand and receptor gene families. Supplementary Tables 1–5 outline the key factors considered by the gene nomenclature committees when deciding whether to update approved gene nomenclature. Supplementary Tables 6–13 specify the approved gene nomenclature and unique database IDs for all genes as well as indicating where the approved nomenclature was updated concurrently with this publication. Supplementary Fig. 1 shows a maximum likelihood phylogeny of the vertebrate AVPR2* amino acid sequences.

Reporting Summary

Rights and permissions

Open Access This article is licensed under a Creative Commons Attribution 4.0 International License, which permits use, sharing, adaptation, distribution and reproduction in any medium or format, as long as you give appropriate credit to the original author(s) and the source, provide a link to the Creative Commons license, and indicate if changes were made. The images or other third party material in this article are included in the article's Creative Commons license, unless indicated otherwise in a credit line to the material. If material is not included in the article's Creative Commons license and your intended use is not permitted

by statutory regulation or exceeds the permitted use, you will need to obtain permission directly from the copyright holder. To view a copy of this license, visit http://creativecommons.org/licenses/by/4.0/.

Reprints and Permissions

About this article

Cite this article

McCarthy, F.M., Jones, T.E.M., Kwitek, A.E. *et al.* The case for standardizing gene nomenclature in vertebrates. *Nature* **614**, E31–E32 (2023). https://doi.org/10.1038/s41586-022-05633-w

- Received: 14 September 2021
- Accepted: 06 December 2022
- Published: 15 February 2023
- Issue Date: 16 February 2023
- DOI: https://doi.org/10.1038/s41586-022-05633-w

Share this article

Anyone you share the following link with will be able to read this content:

Get shareable link

Sorry, a shareable link is not currently available for this article.

Copy to clipboard

Provided by the Springer Nature SharedIt content-sharing initiative

This article was downloaded by **calibre** from https://www.nature.com/articles/s41586-022-05633-w

- Matters Arising
- Open Access
- Published: 15 February 2023

Reply to: The case for standardizing gene nomenclature in vertebrates

- Constantina Theofanopoulou &
- Erich D. Jarvis

Nature **volume 614**, pages E33–E36 (2023)

- 1543 Accesses
- 6 Altmetric
- Metrics details

The Original Article was published on 15 February 2023

replying to F. M. McCarthy et al. *Nature* https://doi.org/10.1038/s41586-022-05633-w (2023)

Here we reply to points raised by McCarthy et al. in the accompanying Comment[1] concerning our proposal[2] for an evolution-based and universal vertebrate nomenclature for the oxytocin and vasotocin ligand and receptor families, and the principles considered for homology-based gene nomenclatures. We strengthen our claims with additional evidence and propose evidence-based criteria for homologous gene nomenclature, in the following order of reliability: synteny, phylogenetic inference, sequence

identity and gene function. We believe that the time is ripe for gene nomenclature committees and initiatives generating high-quality assemblies to join forces in a universal gene nomenclature committee.

Our proposed universal gene nomenclature (that is, naming) for the oxytocin and vasotocin ligands and receptors[2] was based on several criteria, including gene synteny, phylogeny, identity and function, and provides a case study that is applicable across gene families. McCarthy et al.[1] argue that a standardized system of nomenclature already exists, "first established in vertebrates 30 years ago", and that only minor changes are needed in this gene family, with a focus on tradition, name stability, phylogeny, identity and gene function, and with the order of priority of evidence determined on a case-by-case basis. We disagree with both of these claims, especially because determining gene orthology was not fully possible until the recent availability of high-quality genomes. Below, we discuss the principles that we suggest should be applied across gene families and future initiatives. In the Supplementary Information, we respond to the gene-specific claims made by McCarthy et al.[1].

In our study[2], for each of the oxytocin and vasotocin ligands and receptors, we listed two to six commonly used aliases (Table 1 in Theofanopoulou et al.[2]). Many of these reflect incorrect orthologies or paralogies, indicating that there was not a universally used standard before our study, nor one that sufficiently portrayed gene orthology. We view the vertebrate-wide gene nomenclature that McCarthy et al.[1] present as "approved" in their Table 1 as newly proposed. They adopted the most common gene names for mammals, revised some on the basis of our study and others, and applied them to all other vertebrates where possible (Supplementary Note 1). None of the other aliases were listed, which makes the translation of findings across species and the literature difficult. Furthermore, in their newly proposed nomenclature, tradition overrides orthology and paralogy. For example, they maintain very different names for the genes oxytocin and vasotocin that do not echo their paralogy (that is, oxytocin and arginine vasopressin); and for species that do not have the arginine amino acid, they change the name to another alias (vasopressin), but still abbreviate it *to AVP*. We think that allowing tradition and stability to override naming rules of orthology and paralogy could lead to confusion.

However, we believe it is possible to consider both tradition and orthology/paralogy. For example, because vasotocin is the evolutionarily older gene, with oxytocin resulting from a local duplication of it[2], if we were strict with evolutionary naming, we would have renamed vasotocin to 'vasotocin 1' and oxytocin to 'vasotocin 2'. But to conserve some continuity with traditional use, we proposed the already used 'vasotocin' for vasopressin, to mirror the ending of 'oxytocin'. In forming this proposal, we consulted with experts, whom we acknowledged[2], and with the leaders of the Ensembl annotation team.

Valuing accuracy over tradition comes with some downsides. Perhaps the greatest would be the effort required to ensure continuity between previous publications and annotated genomes with the new nomenclature. To mitigate this, we suggest a translation table from old to revised gene names (for example, Table 1 in Theofanopoulou et al.[2]), which would be available in platforms like the National Center for Biotechnology Information. Current committees already use such tables, but their practices of establishing nomenclature changes are either different than the ones we propose or not consistent with each other (Supplementary Notes 2–4).

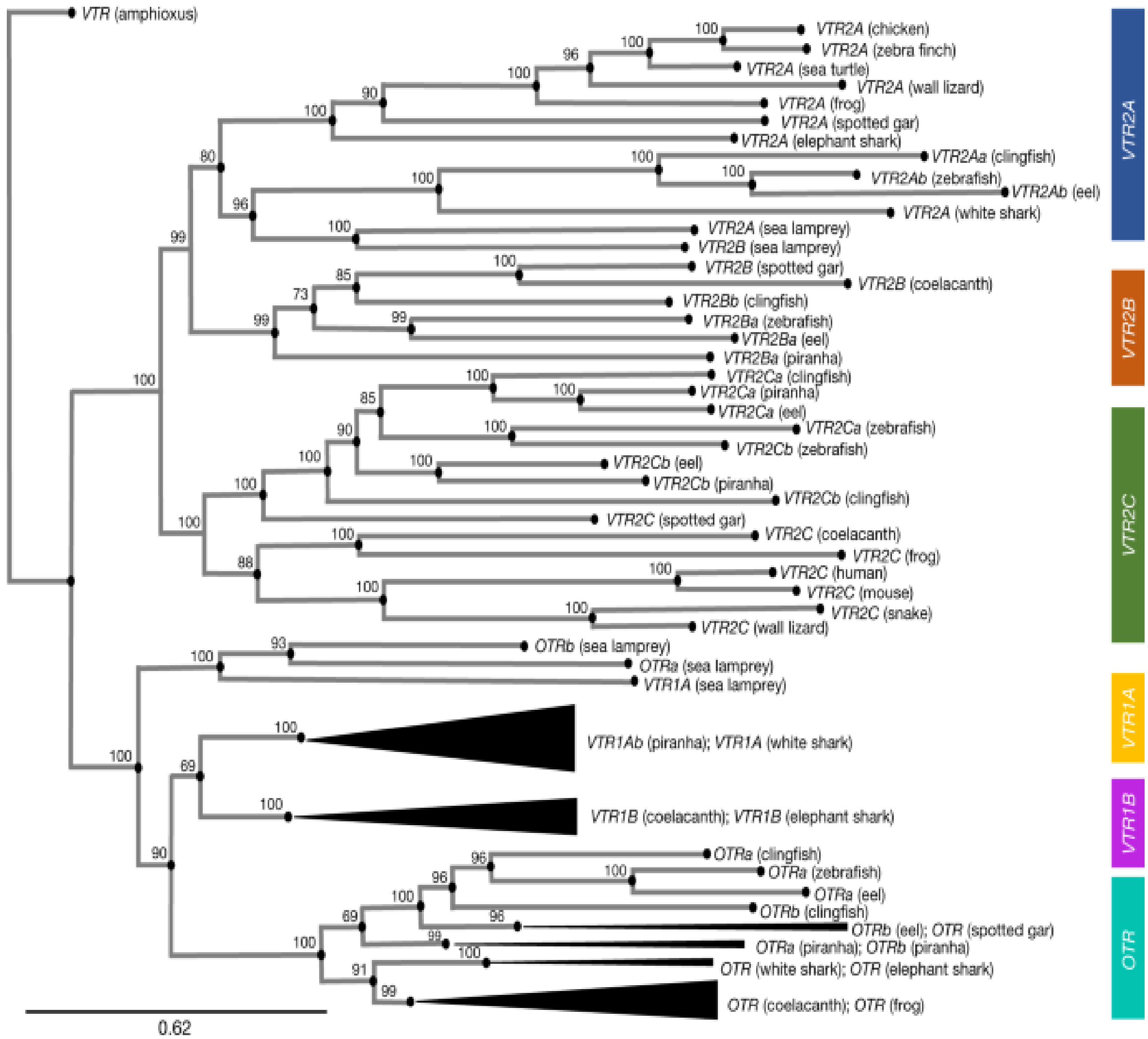
McCarthy et al.[1] also criticize our proposed two-letter symbols for oxytocin and vasotocin (*OT* and *VT*), in that they give broader results in a literature search compared to three-letter symbols (such as *OXT* and *AVP*). We agree and further argue that three-letter symbols could still reflect an evolution-based nomenclature; for example, *OTC* (oxytocin) and *VTC* (vasotocin). We also suggest that gene-symbol consistency across species should be adopted in their letter capitalization. The landscape at present, in which only some mammalian and avian gene symbols are upper case, mouse and rat symbols are lower case except for an initial upper-case letter and amphibian and fish species are all lower case, does not depict the real orthology of these genes, and perpetuates anthropocentric practices. In our universal nomenclature proposal[2], we suggest that gene symbols should be upper case across species.

We agree with McCarthy et al.[1] that for name revisions, the benefits should outweigh the risks. We are guided by the belief that "names have a powerful influence on the experiments we do and the way in which we think"[3], and

hence it is important that names do not give rise to false expectations. For example, the binding of oxytocin to the 'vasopressin' receptors has been often identified as surprising—something that could be avoided with names that reflect their common origin (-tocin). This knowledge will also be useful for medicine, so that physicians are more aware of drug interactions between the two receptor families. Similarly, in other gene families, McCarthy et al.[1] endorse a nomenclature that differs in orthologous genes with a different function across species. For example, the *CSAD* gene is named 'cysteine sulfinic acid decarboxylase' in all species except chickens, in which it is called 'cysteine acid decarboxylase'. If sequence and/or function changes were routinely used to change gene names, then nearly all orthologous genes would have different names across species.

McCarthy et al.[1] decided not to suggest blanket 'rules' about which factors should be weighed more heavily than others, as each case will differ depending on the context. In our experience, not all evidence has equal weight. For example, McCarthy et al.[1] did not accept our nomenclature in part due to the lack of sequence-identity resolution (Basic Local Alignment Search Tool (BLAST) analyses). However, sequence-identity percentages do not always provide a solid basis for gene nomenclature, because orthologous syntenic genes can misleadingly have higher sequence identity with a paralogous gene (Supplementary Table 12 in Theofanopoulou et al.[2]). In addition, McCarthy et al.[1] presented an amino acid phylogeny as not being conclusive enough for some of our interpretations. However, we showed[2] that amino acid phylogenies have low bootstrap support on some branches, whereas exonic nucleotide phylogenies yielded a higher resolution that supports our conclusions (Fig. 4 in Theofanopoulou et al.[2]). With more high-quality genome assemblies generated by the Vertebrate Genomes Project (VGP) since our original publication, we ran a new exonic phylogeny that even more strongly supports our conclusions (Fig. 1 and Supplementary Notes 3 and 4).

Fig. 1: Family tree for genes that encode the oxytocin and vasopressin receptors.



Tree topology inferred with the phylogenetic maximum likelihood method on an exon nucleotide alignment (MAFFT), with 1,000 non-parametric bootstrap replicates (IQ-TREE). Bootstrap values are shown as percentages at the branch points. The tree is rooted with the *VTR* gene in amphioxus. The gene names of the current accessions (see Table 1 in Theofanopoulou et al.[2] and Supplementary Tables 4a–e in Theofanopoulou et al.[2] for a full list of synonyms) were written over according to our revised synteny- and phylogeny-based orthology. All sequences used, FASTA alignment and Newick tree files can be accessed here at https://github.com/constantinatheo/universalnomenclature/. Scale bar, 0.62 substitutions. For a discussion on interchanging *VTR2A* and *VTR2C* naming, see Supplementary Note 3.

We find[2,4] that synteny-based approaches in most cases give the best resolution for gene orthologies and paralogies, and hence for gene nomenclature. Wherever available, we propose using chromosome-scale genomes that are highly contiguous and have a high base-call accuracy[2]. When synteny is not clear, we suggest that priority is given to nucleotide phylogenetic inference with the same prerequisites for genome quality. In Extended Data Fig. 1 and Supplementary Note 5, we provide specific suggestions and caveats with regard to our recommended practices for synteny and phylogenetic analyses. We propose that a combination of synteny and highly supported phylogeny is the backbone of a universal gene nomenclature.

According to the guidelines for human gene nomenclature[5], initiatives that aim to revise a nomenclature when the old one is "misleading…are welcomed". We agree with this practice. However, we believe that the process that is used to approve those revisions should take a different approach to the ones proposed by McCarthy et al.[1] We do not think that journal editors should require "scientists to consistently use approved nomenclature"[1] by a limited committee. Rather, we believe that they should allow new uses in the light of new evidence (see checklist in Extended Data Fig. 1).

Moreover, the current nomenclature committees represent nomenclature focused on only 0.01% of the 70,000 extant vertebrates, with genome assemblies that were much more fragmented, and with traditions that we think need reconsideration. Although several authors of the accompanying Comment by McCarthy et al.[1] are part of a recently formed Vertebrate Gene Nomenclature Committee (VGNC), in their database (https://vertebrate.genenames.org/) at the time of writing (19 November 2022) there is no inclusion of gene aliases used in the literature (versus Table 1 in Theofanopoulou et al.[2]).

The high-quality genomes generated by the VGP (https://vertebrategenomesproject.org/) and related initiatives such as the Earth BioGenome Project (https://www.earthbiogenome.org/)[6,7] are greatly improving the identification of gene orthology and thereby gene annotation, bringing about an opportunity to establish a universal nomenclature for most

genes. Our experience in these initiatives is that existing gene annotation and nomenclature bodies are not yet coordinated or consistent in their approaches. We envisage a universal gene nomenclature committee that involves scientists working on sequencing, assembly, annotation, phylogeny and genome evolution, as well as on the respective lineages and genes for all life.

One possible organizing principle would be to create one committee per major lineage (for example, cyclostomes), group these as subcommittees under one larger committee (for example, all vertebrate species), group all of them under a committee for all species of one of the animal kingdoms (for example, eukaryotic species) and then group all of them under all life. We believe that such an effort would be likely to require changes both to infrastructure (for example, committees and publication policies) and to the way systems operate (for example, high-quality genomes, synteny and phylogenetics).

Reporting summary

Further information on research design is available in the Nature Portfolio Reporting Summary linked to this article.

Data availability

All of the data used can be found in the Supplementary Notes and in the following repository: https://github.com/constantinatheo/universalnomenclature.

Code availability

All the code used in this study can be found in the following repository: https://github.com/constantinatheo/universalnomenclature.

References

1. McCarthy, F. M. et al. The case for standardizing gene nomenclature in vertebrates. *Nature* https://doi.org/10.1038/s41586-022-05633-w (2022).

2. Theofanopoulou, C., Gedman, G., Cahill, J. A., Boeckx, C. & Jarvis, E. D. Universal nomenclature for oxytocin–vasotocin ligand and receptor families. *Nature* **592**, 747–755 (2021).

3. Jarvis, E. D. et al. Avian brains and a new understanding of vertebrate brain evolution. *Nat. Rev. Neurosci.* **6**, 151–159 (2005).

4. Theofanopoulou, C. Reconstructing the evolutionary history of the oxytocin and vasotocin receptor gene family: Insights on whole genome duplication scenarios. *Dev. Biol.* **479**, 99–106 (2021).

5. Wain, H. M. et al. Guidelines for human gene nomenclature. *Genomics* **79**, 464–470 (2002).

6. Rhie, A. et al. Towards complete and error-free genome assemblies of all vertebrate species. *Nature* **592**, 737–746 (2021).

7. Lewin, H. A. et al. Earth BioGenome Project: sequencing life for the future of life. *Proc. Natl Acad. Sci. USA* **115**, 4325–4333 (2018).

Acknowledgements

We thank all the members, and especially the genome annotation committees, of the Vertebrate Genomes Project, the Earth BioGenome Project and the European Reference Genome Atlas for helping us to appreciate, over the past years, the complexity of the issues we have touched on here. C.T. was supported by funds from the Rockefeller University and E.D.J. by funds from the Howard Hughes Medical Institute and the Rockefeller University.

Author information

Authors and Affiliations

1. Laboratory of Neurogenetics of Language, Rockefeller University, New York, NY, USA

   Constantina Theofanopoulou & Erich D. Jarvis

2. Hunter College, City University of New York, New York, NY, USA

   Constantina Theofanopoulou & Erich D. Jarvis

3. Howard Hughes Medical Institute, Chevy Chase, MD, USA

   Erich D. Jarvis

Contributions

For this Matters Arising Reply, the corresponding authors of the original study[2], C.T. and E.D.J., conceived the ideas for the response. C.T. performed the additional BLAST/BLAT, synteny and phylogenetic analyses and wrote the first draft; E.D.J. supervised the study and helped write the manuscript. The three other co-authors of the original study[2] (G. Gedman, J. A. Cahill and C. Boeckx) did not participate in this Reply, owing to the challenge being on the specific concepts and work that the corresponding authors had developed, but all continue to support the original study.

Corresponding authors

Correspondence to Constantina Theofanopoulou or Erich D. Jarvis.

Ethics declarations

Competing interests

The authors declare no competing interests.

Additional information

Publisher's note Springer Nature remains neutral with regard to jurisdictional claims in published maps and institutional affiliations.

Extended data figures and tables

Extended Data Fig. 1 Checklist and caveats.

Suggested checklist and caveats to be considered for synteny (top) and phylogeny (bottom) evidence used to propose gene nomenclature.

Supplementary information

Supplementary Notes

This document contains detailed observations on the following topics: Supplementary Note 1: standardization biases; Supplementary Note 2: factors in favour of or against nomenclature change; Supplementary Note 3: *VTR2A* and *VTR2C*: which is most likely the oldest and why; Supplementary Note 4: is *VTR2Ab* in teleost fish a *VTR2A* duplicate?; and Supplementary Note 5: suggested checklist for evolution-based gene nomenclatures.

Reporting Summary

Supplementary Tables

This file contains information on the species' genomes (Supplementary Table 1) and specific genes analysed (Supplementary Table 2) for the exonic phylogeny in Fig. 1.

Rights and permissions

Open Access This article is licensed under a Creative Commons Attribution 4.0 International License, which permits use, sharing, adaptation, distribution and reproduction in any medium or format, as long as you give appropriate credit to the original author(s) and the source, provide a link to

the Creative Commons license, and indicate if changes were made. The images or other third party material in this article are included in the article's Creative Commons license, unless indicated otherwise in a credit line to the material. If material is not included in the article's Creative Commons license and your intended use is not permitted by statutory regulation or exceeds the permitted use, you will need to obtain permission directly from the copyright holder. To view a copy of this license, visit http://creativecommons.org/licenses/by/4.0/.

Reprints and Permissions

About this article

Cite this article

Theofanopoulou, C., Jarvis, E.D. Reply to: The case for standardizing gene nomenclature in vertebrates. *Nature* **614**, E33–E36 (2023). https://doi.org/10.1038/s41586-022-05634-9

- Published: 15 February 2023
- Issue Date: 16 February 2023
- DOI: https://doi.org/10.1038/s41586-022-05634-9

Share this article

Anyone you share the following link with will be able to read this content:

Get shareable link

Sorry, a shareable link is not currently available for this article.

Copy to clipboard

Provided by the Springer Nature SharedIt content-sharing initiative

Universal nomenclature for oxytocin–vasotocin ligand and receptor families

- Constantina Theofanopoulou
- Gregory Gedman
- Erich D. Jarvis

Nature Article Open Access 28 Apr 2021

This article was downloaded by **calibre** from https://www.nature.com/articles/s41586-022-05634-9

| Section menu | Main menu |

Amendments & Corrections

- **Author Correction: Genomic basis for RNA alterations in cancer** [25 Jan 2023]
- **Author Correction: Patterns of somatic structural variation in human cancer genomes** [25 Jan 2023]
- **Author Correction: Pan-cancer analysis of whole genomes** [25 Jan 2023]
- **Author Correction: Analyses of non-coding somatic drivers in 2,658 cancer whole genomes** [25 Jan 2023]
- **Author Correction: The repertoire of mutational signatures in human cancer** [25 Jan 2023]
- **Author Correction: The evolutionary history of 2,658 cancers** [25 Jan 2023]

- Author Correction
- Open Access
- Published: 25 January 2023

Author Correction: Genomic basis for RNA alterations in cancer

- PCAWG Transcriptome Core Group,
- Claudia Calabrese,
- Natalie R. Davidson,
- Deniz Demircioğlu,
- Nuno A. Fonseca,
- Yao He,
- André Kahles,
- Kjong-Van Lehmann,
- Fenglin Liu,
- Yuichi Shiraishi,
- Cameron M. Soulette,
- Lara Urban,
- Liliana Greger,
- Siliang Li,
- Dongbing Liu,
- Marc D. Perry,
- Qian Xiang,
- Fan Zhang,
- Junjun Zhang,
- Peter Bailey,
- Serap Erkek,
- Katherine A. Hoadley,
- Yong Hou,
- Matthew R. Huska,
- Helena Kilpinen,
- Jan O. Korbel,

- Maximillian G. Marin,
- Julia Markowski,
- Tannistha Nandi,
- Qiang Pan-Hammarström,
- Chandra Sekhar Pedamallu,
- Reiner Siebert,
- Stefan G. Stark,
- Hong Su,
- Patrick Tan,
- Sebastian M. Waszak,
- Christina Yung,
- Shida Zhu,
- Philip Awadalla,
- Chad J. Creighton,
- Matthew Meyerson,
- B. F. Francis Ouellette,
- Kui Wu,
- Huanming Yang,
- PCAWG Transcriptome Working Group,
- Alvis Brazma ,
- Angela N. Brooks ,
- Jonathan Göke,
- Gunnar Rätsch ,
- Roland F. Schwarz,
- Oliver Stegle,
- Zemin Zhang &
- PCAWG Consortium

Show authors

Nature **volume 614**, page E37 (2023)

- 2299 Accesses
- 1 Altmetric
- Metrics details

The Original Article was published on 05 February 2020

Correction to: *Nature* https://doi.org/10.1038/s41586-020-1970-0 Published online 5 February 2020

In the published version of this paper, the members of the Pan-Cancer Analysis of Whole Genomes (PCAWG) Consortium were listed in the Supplementary Information; however, these members should have been included in the main paper. The original Article has been corrected to include the members and affiliations of the PCAWG Consortium in the main paper; the corrections have been made to the HTML version of the Article but not the PDF version. Additional minor corrections to affiliations have been made to the PDF and HTML versions of the original Article for consistency of information between the PCAWG list and the main paper. An additional affiliation has been added for Aurélien Chateigner (BioForA, French National Institute for Agriculture, Food, and Environment (INRAE), ONF, Orléans, France).

Author information

Author notes

1. A list of members and their affiliations appears online
2. These authors contributed equally: PCAWG Transcriptome Core Group, Claudia Calabrese, Natalie R. Davidson, Deniz Demircioğlu, Nuno A. Fonseca, Yao He, André Kahles, Kjong-Van Lehmann, Fenglin Liu, Yuichi Shiraishi, Cameron M. Soulette, Lara Urban
3. These authors jointly supervised this work: Alvis Brazma, Angela N. Brooks, Jonathan Göke, Gunnar Rätsch, Roland F. Schwarz, Oliver Stegle, Zemin Zhang
4. A list of members and their affiliations appears at the end of the paper

Authors and Affiliations

1. European Molecular Biology Laboratory, European Bioinformatics Institute, Hinxton, UK

Claudia Calabrese, Nuno A. Fonseca, Lara Urban, Claudia Calabrese, Nuno A. Fonseca, Lara Urban, Liliana Greger, Nuno A. Fonseca, Lara Urban, Claudia Calabrese, Liliana Greger, Roland F. Schwarz, Oliver Stegle, Alvis Brazma, Alvis Brazma, Roland F. Schwarz & Oliver Stegle

2. ETH Zurich, Zurich, Switzerland

Natalie R. Davidson, André Kahles, Kjong-Van Lehmann, Natalie R. Davidson, André Kahles, Kjong-Van Lehmann, Stefan G. Stark, André Kahles, Kjong-Van Lehmann, Natalie R. Davidson, Stefan G. Stark, Gunnar Rätsch & Gunnar Rätsch

3. Memorial Sloan Kettering Cancer Center, New York, NY, USA

Natalie R. Davidson, André Kahles, Kjong-Van Lehmann, Natalie R. Davidson, André Kahles, Kjong-Van Lehmann, Stefan G. Stark, André Kahles, Kjong-Van Lehmann, Natalie R. Davidson, Stefan G. Stark, Gunnar Rätsch & Gunnar Rätsch

4. Weill Cornell Medical College, New York, NY, USA

Natalie R. Davidson, Natalie R. Davidson, Natalie R. Davidson, Ekta Khurana, Gunnar Rätsch & Gunnar Rätsch

5. SIB Swiss Institute of Bioinformatics, Lausanne, Switzerland

Natalie R. Davidson, André Kahles, Kjong-Van Lehmann, Natalie R. Davidson, André Kahles, Kjong-Van Lehmann, Stefan G. Stark, André Kahles, Kjong-Van Lehmann, Natalie R. Davidson, Stefan G. Stark, Gunnar Rätsch & Gunnar Rätsch

6. University Hospital Zurich, Zurich, Switzerland

Natalie R. Davidson, André Kahles, Kjong-Van Lehmann, Natalie R. Davidson, André Kahles, Kjong-Van Lehmann, Stefan G. Stark, André

Kahles, Kjong-Van Lehmann, Natalie R. Davidson, Stefan G. Stark, Gunnar Rätsch & Gunnar Rätsch

7. National University of Singapore, Singapore, Singapore

Deniz Demircioğlu, Deniz Demircioğlu & Deniz Demircioğlu

8. Genome Institute of Singapore, Singapore, Singapore

Deniz Demircioğlu, Deniz Demircioğlu, Tannistha Nandi, Patrick Tan, Deniz Demircioğlu, Tannistha Nandi, Patrick Tan, Jonathan Göke & Jonathan Göke

9. Peking University, Beijing, China

Yao He, Fenglin Liu, Yao He, Fenglin Liu, Fan Zhang, Fenglin Liu, Yao He, Fan Zhang, Liangtao Zheng, Zemin Zhang & Zemin Zhang

10. The University of Tokyo, Minato-ku, Japan

Yuichi Shiraishi, Yuichi Shiraishi & Yuichi Shiraishi

11. University of California, Santa Cruz, Santa Cruz, CA, USA

Cameron M. Soulette, Cameron M. Soulette, Maximillian G. Marin, Cameron M. Soulette, Brian Craft, Mary Goldman, Maximillian G. Marin, Jingchun Zhu, Angela N. Brooks & Angela N. Brooks

12. BGI-Shenzhen, Shenzhen, China

Siliang Li, Dongbing Liu, Yong Hou, Qiang Pan-Hammarström, Hong Su, Shida Zhu, Kui Wu, Huanming Yang, Siliang Li, Dongbing Liu, Yong Hou, Chang Li, Xiaobo Li, Xinyue Li, Xingmin Liu, Qiang Pan-Hammarström, Hong Su, Jian Wang, Heng Xiong, Chen Ye, Xiuqing Zhang, Shida Zhu, Kui Wu & Huanming Yang

13. China National GeneBank-Shenzhen, Shenzhen, China

Siliang Li, Dongbing Liu, Yong Hou, Hong Su, Shida Zhu, Kui Wu, Siliang Li, Dongbing Liu, Yong Hou, Chang Li, Xiaobo Li, Xingmin Liu, Hong Su, Heng Xiong, Chen Ye, Shida Zhu & Kui Wu

14. Ontario Institute for Cancer Research, Toronto, Ontario, Canada

Marc D. Perry, Qian Xiang, Junjun Zhang, Christina Yung, Philip Awadalla, Junjun Zhang, Marc D. Perry, Qian Xiang, Aurélien Chateigner, Fabien C. Lamaze, Christina Yung & Philip Awadalla

15. University of California, San Francisco, San Francisco, CA, USA

Marc D. Perry & Marc D. Perry

16. University of Glasgow, Glasgow, UK

Peter Bailey & Peter Bailey

17. European Molecular Biology Laboratory, Genome Biology Unit, Heidelberg, Germany

Serap Erkek, Jan O. Korbel, Sebastian M. Waszak, Serap Erkek, Jan O. Korbel, Sebastian M. Waszak, Sergei Yakneen, Oliver Stegle & Oliver Stegle

18. The University of North Carolina at Chapel Hill, Chapel Hill, NC, USA

Katherine A. Hoadley & Katherine A. Hoadley

19. Berlin Institute for Medical Systems Biology, Max Delbruck Center for Molecular Medicine, Berlin, Germany

Matthew R. Huska, Julia Markowski, Matthew R. Huska, Julia Markowski, Roland F. Schwarz & Roland F. Schwarz

20. University College London, London, UK

Helena Kilpinen & Helena Kilpinen

21. Karolinska Institutet, Stockholm, Sweden

Qiang Pan-Hammarström & Qiang Pan-Hammarström

22. Broad Institute, Cambridge, MA, USA

Chandra Sekhar Pedamallu, Matthew Meyerson, Akinyemi I. Ojesina, Chandra Sekhar Pedamallu, Matthew Meyerson, Angela N. Brooks & Angela N. Brooks

23. Ulm University and Ulm University Medical Center, Ulm, Germany

Reiner Siebert & Reiner Siebert

24. Duke-NUS Medical School, Singapore, Singapore

Patrick Tan & Patrick Tan

25. University of Toronto, Toronto, Ontario, Canada

Philip Awadalla & Philip Awadalla

26. Baylor College of Medicine, Houston, TX, USA

Chad J. Creighton & Chad J. Creighton

27. Dana-Farber Cancer Institute, Boston, MA, USA

Chandra Sekhar Pedamallu, Matthew Meyerson, Akinyemi I. Ojesina, Chandra Sekhar Pedamallu, Matthew Meyerson, Angela N. Brooks & Angela N. Brooks

28. Harvard Medical School, Boston, MA, USA

Chandra Sekhar Pedamallu, Matthew Meyerson, Isidro Cortés-Ciriano, Peter J. Park, Chandra Sekhar Pedamallu & Matthew Meyerson

29. University of Toronto, Toronto, Ontario, Canada

B. F. Francis Ouellette & B. F. Francis Ouellette

30. National Cancer Centre Singapore, Singapore, Singapore

Bin Tean Teh, Jonathan Göke & Jonathan Göke

31. German Cancer Consortium (DKTK), partner site Berlin, Germany

Roland F. Schwarz & Roland F. Schwarz

32. German Cancer Research Center (DKFZ), Heidelberg, Germany

Roland F. Schwarz, Oliver Stegle, Roland F. Schwarz & Oliver Stegle

33. The UT MD Anderson Cancer Center, Houston, TX, USA

Samirkumar B. Amin

34. BioForA, French National Insitute for Agriculture, Food, and Environment (INRAE), ONF, Orléans, France

Aurélien Chateigner

35. Ludwig Center at Harvard, Boston, MA, USA

Isidro Cortés-Ciriano & Peter J. Park

36. University of Cambridge, Cambridge, UK

Isidro Cortés-Ciriano

37. The Azrieli Faculty of Medicine, Bar-Ilan University, Safed, Israel

Milana Frenkel-Morgenstern

38. Aarhus University, Aarhus, Denmark

Morten M. Nielsen & Jakob S. Pedersen

39. HudsonAlpha Institute for Biotechnology, Huntsville, AL, USA

Akinyemi I. Ojesina

40. University of Alabama at Birmingham, Birmingham, AL, USA

Akinyemi I. Ojesina

41. Applied Tumor Genomics Research Program, Research Programs Unit, University of Helsinki, Helsinki, Finland

Lauri A. Aaltonen

42. Wellcome Sanger Institute, Wellcome Genome Campus, Hinxton, UK

Federico Abascal, David J. Adams, Ludmil B. Alexandrov, Sam Behjati, Shriram G. Bhosle, David T. Bowen, Adam P. Butler, Peter J. Campbell, Peter Clapham, Helen Davies, Kevin J. Dawson, Stefan C. Dentro, Serge Serge, Erik Garrison, Mohammed Ghori, Dominik Glodzik, Jonathan Hinton, David R. Jones, Young Seok Ju, Stian Knappskog, Barbara Kremeyer, Henry Lee-Six, Daniel A. Leongamornlert, Yilong Li, Sancha Martin, Iñigo Martincorena, Ultan McDermott, Andrew Menzies, Thomas J. Mitchell, Sandro Morganella, Jyoti Nangalia, Jonathan Nicholson, Serena Nik-Zainal, Sarah O'Meara, Elli Papaemmanuil, Keiran M. Raine, Manasa Ramakrishna, Kamna Ramakrishnan, Nicola D. Roberts, Rebecca Shepherd, Lucy Stebbings, Michael R. Stratton, Maxime Tarabichi, Jon W. Teague, Ignacio Vázquez-García, David C. Wedge, Lucy Yates, Jorge Zamora & Xueqing Zou

43. Memorial Sloan Kettering Cancer Center, New York, NY, USA

Adam Abeshouse, Hikmat Al-Ahmadie, Gunes Gundem, Zachary Heins, Jason Huse, Douglas A. Levine, Eric Minwei Liu & Angelica Ochoa

44. Genome Science Division, Research Center for Advanced Science and Technology, University of Tokyo, Tokyo, Japan

Hiroyuki Aburatani, Genta Nagae, Akihiro Suzuki, Kenji Tatsuno & Shogo Yamamoto

45. Department of Surgery, University of Chicago, Chicago, IL, USA

Nishant Agrawal

46. Department of Surgery, Division of Hepatobiliary and Pancreatic Surgery, School of Medicine, Keimyung University Dongsan Medical Center, Daegu, South Korea

Keun Soo Ahn & Koo Jeong Kang

47. Department of Oncology, Gil Medical Center, Gachon University, Incheon, South Korea

Sung-Min Ahn

48. Hiroshima University, Hiroshima, Japan

Hiroshi Aikata, Koji Arihiro, Kazuaki Chayama, Yoshiiku Kawakami & Hideki Ohdan

49. Department of Bioinformatics and Computational Biology, The University of Texas MD Anderson Cancer Center, Houston, TX, USA

Rehan Akbani, Shaolong Cao, Yiwen Chen, Zechen Chong, Yu Fan, Jun Li, Han Liang, Wenyi Wang, Yumeng Wang & Yuan Yuan

50. University of Texas MD Anderson Cancer Center, Houston, TX, USA

Kadir C. Akdemir & Ken Chen

51. King Faisal Specialist Hospital and Research Centre, Al Maather, Riyadh, Saudi Arabia

Sultan T. Al-Sedairy

52. Bioinformatics Unit, Spanish National Cancer Research Centre (CNIO), Madrid, Spain

Fatima Al-Shahrour & Elena Piñeiro-Yáñez

53. Bioinformatics Core Facility, University Medical Center Hamburg, Hamburg, Germany

Malik Alawi

54. Heinrich Pette Institute, Leibniz Institute for Experimental Virology, Hamburg, Germany

Malik Alawi & Adam Grundhoff

55. Ontario Tumour Bank, Ontario Institute for Cancer Research, Toronto, ON, Canada

Monique Albert & John Bartlett

56. Department of Pathology, The University of Texas MD Anderson Cancer Center, Houston, TX, USA

Kenneth Aldape, Russell R. Broaddus, Bogdan Czerniak, Adel El-Naggar, Savitri Krishnamurthy, Alexander J. Lazar & Xiaoping Su

57. Laboratory of Pathology, Center for Cancer Research, National Cancer Institute, Bethesda, MD, USA

Kenneth Aldape

58. Department of Cellular and Molecular Medicine and Department of Bioengineering, University of California San Diego, La Jolla, CA, USA

Ludmil B. Alexandrov & Erik N. Bergstrom

59. UC San Diego Moores Cancer Center, San Diego, CA, USA

Ludmil B. Alexandrov, Erik N. Bergstrom & Olivier Harismendy

60. Canada’s Michael Smith Genome Sciences Centre, BC Cancer, Vancouver, BC, Canada

Adrian Ally, Miruna Balasundaram, Reanne Bowlby, Denise Brooks, Rebecca Carlsen, Eric Chuah, Noreen Dhalla, Robert A. Holt, Steven J. M. Jones, Katayoon Kasaian, Darlene Lee, Haiyan Irene Li, Yussanne Ma, Marco A. Marra, Michael Mayo, Richard A. Moore, Andrew J. Mungall, Karen Mungall, A. Gordon Robertson, Sara Sadeghi, Jacqueline E. Schein, Payal Sipahimalani, Angela Tam, Nina Thiessen & Tina Wong

61. Sir Peter MacCallum Department of Oncology, Peter MacCallum Cancer Centre, University of Melbourne, Melbourne, VIC, Australia

Kathryn Alsop, David D. L. Bowtell, Elizabeth L. Christie, Dariush Etemadmoghadam, Sian Fereday, Dale W. Garsed, Linda Mileshkin, Chris Mitchell, Mark Shackleton, Heather Thorne & Nadia Traficante

62. Centre for Research in Molecular Medicine and Chronic Diseases (CiMUS), Universidade de Santiago de Compostela, Santiago de Compostela, Spain

Eva G. Alvarez, Alicia L. Bruzos, Bernardo Rodriguez-Martin, Javier Temes, Jose M. C. Tubio & Jorge Zamora

63. Department of Zoology, Genetics and Physical Anthropology, (CiMUS), Universidade de Santiago de Compostela, Santiago de Compostela, Spain
Eva G. Alvarez, Alicia L. Bruzos, Bernardo Rodriguez-Martin, Javier Temes, Jose M. C. Tubio & Jorge Zamora
64. The Biomedical Research Centre (CINBIO), Universidade de Vigo, Vigo, Spain

Eva G. Alvarez, Alicia L. Bruzos, Bernardo Rodriguez-Martin, Marta Tojo, Jose M. C. Tubio & Jorge Zamora

65. Royal National Orthopaedic Hospital - Bolsover, London, UK

Fernanda Amary

66. Department of Genomic Medicine, The University of Texas MD Anderson Cancer Center, Houston, TX, USA

Samirkumar B. Amin, P. Andrew Futreal & Alexander J. Lazar

67. Quantitative and Computational Biosciences Graduate Program, Baylor College of Medicine, Houston, TX, USA

Samirkumar B. Amin, Han Liang & Yumeng Wang

68. The Jackson Laboratory for Genomic Medicine, Farmington, CT, USA

Samirkumar B. Amin, Joshy George & Lucas Lochovsky

69. Genome Informatics Program, Ontario Institute for Cancer Research, Toronto, ON, Canada

Brice Aminou, Niall J. Byrne, Aurélien Chateigner, Nodirjon Fayzullaev, Vincent Ferretti, George L. Mihaiescu, Hardeep K. Nahal-Bose, Brian D. O’Connor, B. F. Francis Ouellette, Marc D. Perry, Kevin Thai, Qian Xiang, Christina K. Yung & Junjun Zhang

70. Institute of Human Genetics, Christian-Albrechts-University, Kiel, Germany

Ole Ammerpohl, Andrea Haake, Cristina López, Julia Richter & Rabea Wagener

71. Institute of Human Genetics, Ulm University and Ulm University Medical Center, Ulm, Germany

Ole Ammerpohl, Sietse Aukema, Cristina López, Reiner Siebert & Rabea Wagener

72. Queensland Centre for Medical Genomics, Institute for Molecular Bioscience, University of Queensland, St. Lucia, Brisbane, QLD, Australia

Matthew J. Anderson, Timothy J. C. Bruxner, Angelika N. Christ, J. Lynn Fink, Ivon Harliwong, Karin S. Kassahn, David K. Miller, Alan J. Robertson & Darrin F. Taylor

73. Salford Royal NHS Foundation Trust, Salford, UK

Yeng Ang, Hsiao-Wei Chen, Ritika Kundra & Francisco Sanchez-Vega

74. Department of Surgery, Pancreas Institute, University and Hospital Trust of Verona, Verona, Italy

Davide Antonello, Claudio Bassi, Narong Khuntikeo, Luca Landoni, Giuseppe Malleo, Giovanni Marchegiani, Neil D. Merrett, Marco Miotto, Salvatore Paiella, Antonio Pea, Paolo Pederzoli, Roberto Salvia, Jaswinder S. Samra, Elisabetta Sereni & Samuel Singer

75. Molecular and Medical Genetics, OHSU Knight Cancer Institute, Oregon Health and Science University, Portland, OR, USA

Pavana Anur, Myron Peto & Paul T. Spellman

76. Department of Molecular Oncology, BC Cancer Research Centre, Vancouver, BC, Canada

Samuel Aparicio

77. The McDonnell Genome Institute at Washington University, St. Louis, MO, USA

Elizabeth L. Appelbaum, Matthew H. Bailey, Matthew G. Cordes, Li Ding, Catrina C. Fronick, Lucinda A. Fulton, Robert S. Fulton, Kuan-

lin Huang, Reyka Jayasinghe, Elaine R. Mardis, R. Jay Mashl, Michael D. McLellan, Christopher A. Miller, Heather K. Schmidt, Jiayin Wang, Michael C. Wendl, Richard K. Wilson & Tina Wong

78. University College London, London, UK

Elizabeth L. Appelbaum, Jonathan D. Kay, Helena Kilpinen, Laurence B. Lovat, Hayley J. Luxton & Hayley C. Whitaker

79. Division of Cancer Genomics, National Cancer Center Research Institute, National Cancer Center, Tokyo, Japan

Yasuhito Arai, Natsuko Hama, Fumie Hosoda, Hiromi Nakamura, Tatsuhiro Shibata, Yasushi Totoki & Shinichi Yachida

80. DLR Project Management Agency, Bonn, Germany

Axel Aretz

81. Tokyo Women's Medical University, Tokyo, Japan

Shun-ichi Ariizumi & Masakazu Yamamoto

82. Center for Molecular Oncology, Memorial Sloan Kettering Cancer Center, New York, NY, USA

Joshua Armenia, Hsiao-Wei Chen, Jianjiong Gao, Ritika Kundra, Francisco Sanchez-Vega, Nikolaus Schultz & Hongxin Zhang

83. Los Alamos National Laboratory, Los Alamos, NM, USA

Laurent Arnould

84. Department of Pathology, University Health Network, Toronto General Hospital, Toronto, ON, Canada

Sylvia Asa, Michael H. A. Roehrl & Theodorus Van der Kwast

85. Nottingham University Hospitals NHS Trust, Nottingham, UK

Sylvia Asa, Simon L. Parsons & Ming Tsao

86. Epigenomics and Cancer Risk Factors, German Cancer Research Center (DKFZ), Heidelberg, Germany

Yassen Assenov

87. Computational Biology Program, Ontario Institute for Cancer Research, Toronto, ON, Canada

Gurnit Atwal, Philip Awadalla, Jonathan Barenboim, Vinayak Bhandari, Ivan Borozan, Paul C. Boutros, Lewis Jonathan Dursi, Shadrielle M. G. Espiritu, Natalie S. Fox, Michael Fraser, Syed Haider, Vincent Huang, Keren Isaev, Wei Jiao, Christopher M. Lalansingh, Emilie Lalonde, Fabien C. Lamaze, Constance H. Li, Julie Livingstone, Christine P'ng, Marta Paczkowska, Stephenie D. Prokopec, Jüri Reimand, Veronica Y. Sabelnykova, Adriana Salcedo, Yu-Jia Shiah, Solomon I. Shorser, Shimin Shuai, Jared T. Simpson, Lincoln D. Stein, Ren X. Sun, Lina Wadi, Gavin W. Wilson, Adam J. Wright, Takafumi N. Yamaguchi, Fouad Yousif & Denis Yuen

88. Department of Molecular Genetics, University of Toronto, Toronto, ON, Canada

Gurnit Atwal, Philip Awadalla, Gary D. Bader, Shimin Shuai & Lincoln D. Stein

89. Vector Institute, Toronto, ON, Canada

Gurnit Atwal, Quaid D. Morris, Yulia Rubanova & Jeffrey A. Wintersinger

90. Hematopathology Section, Institute of Pathology, Christian-Albrechts-University, Kiel, Germany

Sietse Aukema, Wolfram Klapper, Julia Richter & Monika Szczepanowski

91. Department of Pathology and Laboratory Medicine, School of Medicine, University of North Carolina at Chapel Hill, Chapel Hill, NC, USA

J. Todd Auman & Charles M. Perou

92. Department of Cancer Genetics, Institute for Cancer Research, Oslo University Hospital, The Norwegian Radium Hospital, Oslo, Norway

Miriam R. R. Aure, Anne-Lise Børresen-Dale & Anita Langerød

93. Pathology, Hospital Clinic, Institut d'Investigacions Biomèdiques August Pi i Sunyer (IDIBAPS), University of Barcelona, Barcelona, Spain

Marta Aymerich

94. Department of Veterinary Medicine, Transmissible Cancer Group, University of Cambridge, Cambridge, UK

Adrian Baez-Ortega

95. Alvin J. Siteman Cancer Center, Washington University School of Medicine, St. Louis, MO, USA

Matthew H. Bailey, Li Ding, Robert S. Fulton, Ramaswamy Govindan & Michael D. McLellan

96. Wolfson Wohl Cancer Research Centre, Institute of Cancer Sciences, University of Glasgow, Glasgow, UK

Peter J. Bailey, Andrew V. Biankin, David K. Chang, Susanna L. Cooke, Fraser R. Duthie, Janet S. Graham, Nigel B. Jamieson, Elizabeth A. Musgrove & Derek W. Wright

97. Lineberger Comprehensive Cancer Center, University of North Carolina at Chapel Hill, Chapel Hill, NC, USA

Saianand Balu, Tom Bodenheimer, D. Neil Hayes, Austin J. Hepperla, Katherine A. Hoadley, Alan P. Hoyle, Stuart R. Jefferys, Shaowu Meng, Lisle E. Mose, Grant Sanders, Yan Shi, Janae V. Simons & Matthew G. Soloway

98. Broad Institute of MIT and Harvard, Cambridge, MA, USA

Pratiti Bandopadhayay, Rameen Beroukhim, Angela N. Brooks, Susan Bullman, John Busanovich, Andrew D. Cherniack, Juok Cho, Carrie Cibulskis, Kristian Cibulskis, David Craft, Timothy Defreitas, Andrew J. Dunford, Scott Frazer, Stacey B. Gabriel, Nils Gehlenborg, Gad Getz, Manaswi Gupta, Gavin Ha, Nicholas J. Haradhvala, David I. Heiman, Julian M. Hess, Manolis Kellis, Jaegil Kim, Kiran Kumar, Kirsten Kübler, Eric Lander, Michael S. Lawrence, Ignaty Leshchiner, Pei Lin, Ziao Lin, Dimitri Livitz, Yosef E. Maruvka, Samuel R. Meier, Matthew Meyerson, Michael S. Noble, Chandra Sekhar Pedamallu, Paz Polak, Esther Rheinbay, Daniel Rosebrock, Mara Rosenberg, Gordon Saksena, Richard Sallari, Steven E. Schumacher, Ayellet V. Segre, Ofer Shapira, Juliann Shih, Nasa Sinnott-Armstrong, Oliver Spiro, Chip Stewart, Amaro Taylor-Weiner, Grace Tiao, Douglas Voet, Jeremiah A. Wala, Cheng-Zhong Zhang & Hailei Zhang

99. Dana-Farber/Boston Children’s Cancer and Blood Disorders Center, Boston, MA, USA

Pratiti Bandopadhayay

100. Department of Pediatrics, Harvard Medical School, Boston, MA, USA

Pratiti Bandopadhayay

101. Leeds Institute of Medical Research @ St. James’s, University of Leeds, St. James’s University Hospital, Leeds, UK

Rosamonde E. Banks & Naveen Vasudev

102. Department of Pathology and Diagnostics, University and Hospital Trust of Verona, Verona, Italy

Stefano Barbi, Vincenzo Corbo & Michele Simbolo

103. Department of Surgery, Princess Alexandra Hospital, Brisbane, QLD, Australia

Andrew P. Barbour

104. Surgical Oncology Group, Diamantina Institute, University of Queensland, Brisbane, QLD, Australia

Andrew P. Barbour

105. Department of Population and Quantitative Health Sciences, Case Western Reserve University School of Medicine, Cleveland, OH, USA

Jill Barnholtz-Sloan

106. Research Health Analytics and Informatics, University Hospitals Cleveland Medical Center, Cleveland, OH, USA

Jill Barnholtz-Sloan

107. Gloucester Royal Hospital, Gloucester, UK

Hugh Barr

108. European Molecular Biology Laboratory, European Bioinformatics Institute (EMBL-EBI), Cambridge, UK

Elisabet Barrera, Wojciech Bazant, Ewan Birney, Rich Boyce, Alvis Brazma, Andy Cafferkey, Claudia Calabrese, Paul Flicek, Nuno A. Fonseca, Anja Füllgrabe, Moritz Gerstung, Santiago Gonzalez, Liliana Greger, Maria Keays, Jan O. Korbel, Alfonso Muñoz, Steven J. Newhouse, David Ocana, Irene Papatheodorou, Robert Petryszak, Roland F. Schwarz, Charles Short, Oliver Stegle & Lara Urban

109. Diagnostic Development, Ontario Institute for Cancer Research, Toronto, ON, Canada

John Bartlett & Ilinca Lungu

110. Barcelona Supercomputing Center (BSC), Barcelona, Spain

Javier Bartolome, Mattia Bosio, Ana Dueso-Barroso, J. Lynn Fink, Josep L. L. Gelpi, Ana Milovanovic, Montserrat Puiggròs, Javier Bartolomé Rodriguez, Romina Royo, David Torrents, Alfonso Valencia, Miguel Vazquez, David Vicente & Izar Villasante

111. Arnie Charbonneau Cancer Institute, University of Calgary, Calgary, AB, Canada

Oliver F. Bathe

112. Departments of Surgery and Oncology, University of Calgary, Calgary, AB, Canada

Oliver F. Bathe

113. Department of Pathology, Oslo University Hospital, The Norwegian Radium Hospital, Oslo, Norway

Daniel Baumhoer & Bodil Bjerkehagen

114. PanCuRx Translational Research Initiative, Ontario Institute for Cancer Research, Toronto, ON, Canada

Prashant Bavi, Michelle Chan-Seng-Yue, Sean Cleary, Robert E. Denroche, Steven Gallinger, Robert C. Grant, Gun Ho Jang, Sangeetha Kalimuthu, Ilinca Lungu, John D. McPherson, Faiyaz Notta, Michael H. A. Roehrl, Gavin W. Wilson & Julie M. Wilson

115. Department of Oncology, Sidney Kimmel Comprehensive Cancer Center at Johns Hopkins University School of Medicine, Baltimore, MD, USA

Stephen B. Baylin, Nilanjan Chatterjee, Leslie Cope, Ludmila Danilova & Ralph H. Hruban

116. University Hospital Southampton NHS Foundation Trust, Southampton, UK

Stephen B. Baylin & Tim Dudderidge

117. Royal Stoke University Hospital, Stoke-on-Trent, UK

Duncan Beardsmore & Christopher Umbricht

118. Genome Sequence Informatics, Ontario Institute for Cancer Research, Toronto, ON, Canada

Timothy A. Beck, Bob Gibson, Lawrence E. Heisler, Xuemei Luo & Morgan L. Taschuk

119. Human Longevity Inc, San Diego, CA, USA

Timothy A. Beck

120. Olivia Newton-John Cancer Research Institute, La Trobe University, Heidelberg, VIC, Australia

Andreas Behren & Jonathan Cebon

121. Computer Network Information Center, Chinese Academy of Sciences, Beijing, China

Beifang Niu

122. Genome Canada, Ottawa, ON, Canada

Cindy Bell

123. CNAG-CRG, Centre for Genomic Regulation (CRG), Barcelona Institute of Science and Technology (BIST), Barcelona, Spain

Sergi Beltran, Ivo G. Gut, Marta Gut, Simon C. Heath, Tomas Marques-Bonet, Arcadi Navarro, Miranda D. Stobbe, Jean-Rémi Trotta & Justin P. Whalley

124. Universitat Pompeu Fabra (UPF), Barcelona, Spain

Sergi Beltran, Mattia Bosio, German M. Demidov, Oliver Drechsel, Ivo G. Gut, Marta Gut, Simon C. Heath, Francesc Muyas, Stephan Ossowski, Aparna Prasad, Raquel Rabionet, Miranda D. Stobbe & Hana Susak

125. Buck Institute for Research on Aging, Novato, CA, USA

Christopher Benz & Christina Yau

126. Duke University Medical Center, Durham, NC, USA

Andrew Berchuck

127. Department of Human Genetics, Hannover Medical School, Hannover, Germany

Anke K. Bergmann

128. Center for Bioinformatics and Functional Genomics, Cedars-Sinai Medical Center, Los Angeles, CA, USA

Benjamin P. Berman & Huy Q. Dinh

129. Department of Biomedical Sciences, Cedars-Sinai Medical Center, Los Angeles, CA, USA

Benjamin P. Berman

130. The Hebrew University Faculty of Medicine, Jerusalem, Israel

Benjamin P. Berman

131. Barts Cancer Institute, Barts and the London School of Medicine and Dentistry, Queen Mary University of London, London, UK

Daniel M. Berney & Yong-Jie Lu

132. Department of Computer Science, Bioinformatics Group, University of Leipzig, Leipzig, Germany

Stephan H. Bernhart, Hans Binder, Steve Hoffmann & Peter F. Stadler

133. Interdisciplinary Center for Bioinformatics, University of Leipzig, Leipzig, Germany

Stephan H. Bernhart, Hans Binder, Steve Hoffmann, Helene Kretzmer & Peter F. Stadler

134. Transcriptome Bioinformatics, LIFE Research Center for Civilization Diseases, University of Leipzig, Leipzig, Germany

Stephan H. Bernhart, Steve Hoffmann, Helene Kretzmer & Peter F. Stadler

135. Department of Medical Oncology, Dana-Farber Cancer Institute, Boston, MA, USA

Rameen Beroukhim, Angela N. Brooks, Susan Bullman, Andrew D. Cherniack, Levi Garraway, Matthew Meyerson, Chandra Sekhar Pedamallu, Steven E. Schumacher, Juliann Shih & Jeremiah A. Wala

136. Department of Cancer Biology, Dana-Farber Cancer Institute, Boston, MA, USA

Rameen Beroukhim, Aquila Fatima, Andrea L. Richardson, Steven E. Schumacher, Ofer Shapira, Andrew Tutt & Jeremiah A. Wala

137. Harvard Medical School, Boston, MA, USA

Rameen Beroukhim, Gad Getz, Kirsten Kübler, Matthew Meyerson, Chandra Sekhar Pedamallu, Paz Polak, Esther

Rheinbay & Jeremiah A. Wala

138. USC Norris Comprehensive Cancer Center, University of Southern California, Los Angeles, CA, USA

Mario Berrios, Moiz S. Bootwalla, Andrea Holbrook, Phillip H. Lai, Dennis T. Maglinte, David J. Van Den Berg & Daniel J. Weisenberger

139. Department of Diagnostics and Public Health, University and Hospital Trust of Verona, Verona, Italy

Samantha Bersani, Ivana Cataldo, Claudio Luchini & Maria Scardoni

140. Department of Mathematics, Aarhus University, Aarhus, Denmark

Johanna Bertl & Asger Hobolth

141. Department of Molecular Medicine (MOMA), Aarhus University Hospital, Aarhus N, Denmark

Johanna Bertl, Henrik Hornshøj, Malene Juul, Randi Istrup Juul, Tobias Madsen, Morten Muhlig Nielsen & Jakob Skou Pedersen

142. Instituto Carlos Slim de la Salud, Mexico City, Mexico

Miguel Betancourt

143. Department of Medical Biophysics, University of Toronto, Toronto, ON, Canada

Vinayak Bhandari, Paul C. Boutros, Robert G. Bristow, Keren Isaev, Constance H. Li, Jüri Reimand, Michael H. A. Roehrl & Bradly G. Wouters

144. Cancer Division, Garvan Institute of Medical Research, Kinghorn Cancer Centre, University of New South Wales (UNSW Sydney), Sydney, NSW, Australia

Andrew V. Biankin, David K. Chang, Lorraine A. Chantrill, Angela Chou, Anthony J. Gill, Amber L. Johns, James G. Kench, David K. Miller, Adnan M. Nagrial, Marina Pajic, Mark Pinese, Ilse Rooman, Christopher J. Scarlett, Christopher W. Toon & Jianmin Wu

145. South Western Sydney Clinical School, Faculty of Medicine, University of New South Wales (UNSW Sydney), Liverpool, NSW, Australia

Andrew V. Biankin

146. West of Scotland Pancreatic Unit, Glasgow Royal Infirmary, Glasgow, UK

Andrew V. Biankin & Nigel B. Jamieson

147. Center for Digital Health, Berlin Institute of Health and Charitè - Universitätsmedizin Berlin, Berlin, Germany

Matthias Bieg

148. Heidelberg Center for Personalized Oncology (DKFZ-HIPO), German Cancer Research Center (DKFZ), Heidelberg, Germany

Matthias Bieg, Ivo Buchhalter, Barbara Hutter & Nagarajan Paramasivam

149. The Preston Robert Tisch Brain Tumor Center, Duke University Medical Center, Durham, NC, USA

Darell Bigner

150. Massachusetts General Hospital, Boston, MA, USA

Michael Birrer, Vikram Deshpande, William C. Faquin, Nicholas J. Haradhvala, Kirsten Kübler, Michael S. Lawrence, David N. Louis, Yosef E. Maruvka, G. Petur Nielsen, Esther Rheinbay, Mara Rosenberg, Dennis C. Sgroi & Chin-Lee Wu

151. National Institute of Biomedical Genomics, Kalyani, West Bengal, India

Nidhan K. Biswas, Arindam Maitra & Partha P. Majumder

152. Institute of Clinical Medicine and Institute of Oral Biology, University of Oslo, Oslo, Norway

Bodil Bjerkehagen

153. University of North Carolina at Chapel Hill, Chapel Hill, NC, USA

Lori Boice, Mei Huang, Sonia Puig & Leigh B. Thorne

154. ARC-Net Centre for Applied Research on Cancer, University and Hospital Trust of Verona, Verona, Italy

Giada Bonizzato, Cinzia Cantù, Ivana Cataldo, Vincenzo Corbo, Sonia Grimaldi, Rita T. Lawlor, Andrea Mafficini, Borislav C. Rusev, Aldo Scarpa, Katarzyna O. Sikora, Nicola Sperandio, Alain Viari & Caterina Vicentini

155. The Institute of Cancer Research, London, UK

Johann S. De Bono, Niedzica Camacho, Colin S. Cooper, Sandra E. Edwards, Rosalind A. Eeles, Zsofia Kote-Jarai, Daniel A. Leongamornlert, Lucy Matthews & Sue Merson

156. Centre for Computational Biology, Duke-NUS Medical School, Singapore, Singapore

Arnoud Boot, Ioana Cutcutache, Mi Ni Huang, John R. McPherson, Steven G. Rozen & Yang Wu

157. Programme in Cancer and Stem Cell Biology, Duke-NUS Medical School, Singapore, Singapore

Arnoud Boot, Ioana Cutcutache, Mi Ni Huang, John R. McPherson, Steven G. Rozen, Patrick Tan, Bin Tean Teh & Yang Wu

158. Division of Oncology and Pathology, Department of Clinical Sciences Lund, Lund University, Lund, Sweden

Ake Borg, Markus Ringnér & Johan Staaf

159. Department of Pediatric Oncology, Hematology and Clinical Immunology, Heinrich-Heine-University, Düsseldorf, Germany

Arndt Borkhardt & Jessica I. Hoell

160. Laboratory for Medical Science Mathematics, RIKEN Center for Integrative Medical Sciences, Yokohama, Japan

Keith A. Boroevich, Todd A. Johnson, Michael S. Lawrence & Tatsuhiko Tsunoda

161. RIKEN Center for Integrative Medical Sciences, Yokohama, Japan

Keith A. Boroevich, Akihiro Fujimoto, Masashi Fujita, Mayuko Furuta, Kazuhiro Maejima, Hidewaki Nakagawa, Kaoru Nakano & Aya Sasaki-Oku

162. Department of Internal Medicine/Hematology, Friedrich-Ebert-Hospital, Neumünster, Germany

Christoph Borst & Siegfried Haas

163. Departments of Dermatology and Pathology, Yale University, New Haven, CT, USA

Marcus Bosenberg

164. Centre for Genomic Regulation (CRG), The Barcelona Institute of Science and Technology, Barcelona, Spain

Mattia Bosio, German M. Demidov, Oliver Drechsel, Georgia Escaramis, Xavier Estivill, Aliaksei Z. Holik, Francesc Muyas, Stephan Ossowski, Raquel Rabionet & Hana Susak

165. Radcliffe Department of Medicine, University of Oxford, Oxford, UK

Jacqueline Boultwood

166. Canadian Center for Computational Genomics, McGill University, Montreal, QC, Canada

Guillaume Bourque

167. Department of Human Genetics, McGill University, Montreal, QC, Canada

Guillaume Bourque, Mark Lathrop & Yasser Riazalhosseini

168. Department of Human Genetics, University of California Los Angeles, Los Angeles, CA, USA

Paul C. Boutros

169. Department of Pharmacology, University of Toronto, Toronto, ON, Canada

Paul C. Boutros

170. Faculty of Medicine and Health Technology, Tampere University and Tays Cancer Center, Tampere University Hospital, Tampere, Finland

G. Steven Bova & Tapio Visakorpi

171. Haematology, Leeds Teaching Hospitals NHS Trust, Leeds, UK

David T. Bowen

172. Translational Research and Innovation, Centre Léon Bérard, Lyon, France

Sandrine Boyault

173. Fox Chase Cancer Center, Philadelphia, PA, USA

Jeffrey Boyd & Elaine R. Mardis

174. International Agency for Research on Cancer, World Health Organization, Lyon, France

Paul Brennan & Ghislaine Scelo

175. Earlham Institute, Norwich, UK

Daniel S. Brewer & Colin S. Cooper

176. Norwich Medical School, University of East Anglia, Norwich, UK

Daniel S. Brewer & Colin S. Cooper

177. Department of Molecular Biology, Faculty of Science, Radboud Institute for Molecular Life Sciences, Radboud University, Nijmegen, HB, The Netherlands

Arie B. Brinkman

178. CRUK Manchester Institute and Centre, Manchester, UK

Robert G. Bristow

179. Department of Radiation Oncology, University of Toronto, Toronto, ON, Canada

Robert G. Bristow

180. Division of Cancer Sciences, Manchester Cancer Research Centre, University of Manchester, Manchester, UK

Robert G. Bristow

181. Radiation Medicine Program, Princess Margaret Cancer Centre, Toronto, ON, Canada

Robert G. Bristow & Fei-Fei Fei Liu

182. Department of Pathology, Brigham and Women's Hospital, Harvard Medical School, Boston, MA, USA

Jane E. Brock & Sabina Signoretti

183. Department of Surgery, Division of Thoracic Surgery, The Johns Hopkins University School of Medicine, Baltimore, MD, USA

Malcolm Brock

184. Division of Molecular Pathology, The Netherlands Cancer Institute, Oncode Institute, Amsterdam, CX, The Netherlands

Annegien Broeks & Jos Jonkers

185. Department of Biomolecular Engineering, University of California Santa Cruz, Santa Cruz, CA, USA

Angela N. Brooks, David Haan, Maximillian G. Marin, Thomas J. Matthew, Yulia Newton, Cameron M. Soulette & Joshua M. Stuart

186. UC Santa Cruz Genomics Institute, University of California Santa Cruz, Santa Cruz, CA, USA

Angela N. Brooks, Brian Craft, Mary J. Goldman, David Haussler, Joshua M. Stuart & Jingchun Zhu

187. Division of Applied Bioinformatics, German Cancer Research Center (DKFZ), Heidelberg, Germany

Benedikt Brors, Lars Feuerbach, Chen Hong, Charles David Imbusch & Lina Sieverling

188. German Cancer Consortium (DKTK), German Cancer Research Center (DKFZ), Heidelberg, Germany

Benedikt Brors, Barbara Hutter, Peter Lichter, Dirk Schadendorf & Holger Sültmann

189. National Center for Tumor Diseases (NCT) Heidelberg, Heidelberg, Germany

Benedikt Brors, Barbara Hutter, Holger Sültmann & Thorsten Zenz

190. Center for Biological Sequence Analysis, Department of Bio and Health Informatics, Technical University of Denmark, Lyngby, Denmark

Søren Brunak

191. Novo Nordisk Foundation Center for Protein Research, University of Copenhagen, Copenhagen, Denmark

Søren Brunak

192. Institute for Molecular Bioscience, University of Queensland, St. Lucia, Brisbane, QLD, Australia

Timothy J. C. Bruxner, Oliver Holmes, Stephen H. Kazakoff, Conrad R. Leonard, Felicity Newell, Katia Nones, Ann-Marie Patch, John V. Pearson, Michael C. Quinn, Nick M. Waddell, Nicola Waddell, Scott Wood & Qinying Xu

193. Biomedical Engineering, Oregon Health and Science University, Portland, OR, USA

Alex Buchanan & Kyle Ellrott

194. Division of Theoretical Bioinformatics, German Cancer Research Center (DKFZ), Heidelberg, Germany

Ivo Buchhalter, Calvin Wing Yiu Chan, Roland Eils, Michael C. Heinold, Carl Herrmann, Natalie Jäger, Rolf Kabbe, Jules N. A. Kerssemakers, Kortine Kleinheinz, Nagarajan Paramasivam, Manuel Prinz, Matthias Schlesner & Johannes Werner

195. Institute of Pharmacy and Molecular Biotechnology and BioQuant, Heidelberg University, Heidelberg, Germany

Ivo Buchhalter, Roland Eils, Michael C. Heinold, Carl Herrmann, Daniel Hübschmann, Kortine Kleinheinz & Umut H. Toprak

196. Federal Ministry of Education and Research, Berlin, Germany

Christiane Buchholz

197. Melanoma Institute Australia, University of Sydney, Sydney, NSW, Australia

Hazel Burke, Ricardo De Paoli-Iseppi, Nicholas K. Hayward, Peter Hersey, Valerie Jakrot, Hojabr Kakavand, Georgina V. Long, Graham J. Mann, Robyn P. M. Saw, Richard A. Scolyer, Ping Shang, Andrew J. Spillane, Jonathan R. Stretch, John F. F. Thompson & James S. Wilmott

198. Pediatric Hematology and Oncology, University Hospital Muenster, Muenster, Germany

Birgit Burkhardt

199. Department of Pathology, Johns Hopkins University School of Medicine, Baltimore, MD, USA

Kathleen H. Burns & Christopher Umbricht

200. McKusick-Nathans Institute of Genetic Medicine, Sidney Kimmel Comprehensive Cancer Center at Johns Hopkins University School of Medicine, Baltimore, MD, USA

Kathleen H. Burns

201. Foundation Medicine, Inc, Cambridge, MA, USA

John Busanovich

202. Department of Biomedical Data Science, Stanford University School of Medicine, Stanford, CA, USA

Carlos D. Bustamante & Francisco M. De La Vega

203. Department of Genetics, Stanford University School of Medicine, Stanford, CA, USA

Carlos D. Bustamante, Francisco M. De La Vega, Suyash S. Shringarpure, Nasa Sinnott-Armstrong & Mark H. Wright

204. Bakar Computational Health Sciences Institute and Department of Pediatrics, University of California, San Francisco, CA, USA

Atul J. Butte & Jieming Chen

205. Institute of Clinical Medicine, Faculty of Medicine, University of Oslo, Oslo, Norway

Anne-Lise Børresen-Dale

206. National Cancer Institute, National Institutes of Health, Bethesda, MD, USA

Samantha J. Caesar-Johnson, John A. Demchok, Ina Felau, Roy Tarnuzzer, Zhining Wang, Liming Yang, Jean C. Zenklusen & Jiashan Zhang

207. Royal Marsden NHS Foundation Trust, London and Sutton, UK

Declan Cahill, Nening M. Dennis, Tim Dudderidge, Rosalind A. Eeles, Cyril Fisher, Steven Hazell, Vincent Khoo, Pardeep Kumar, Naomi Livni, Erik Mayer, David Nicol, Christopher Ogden, Edward W. Rowe, Sarah Thomas, Alan Thompson & Nicholas van As

208. Genome Biology Unit, European Molecular Biology Laboratory (EMBL), Heidelberg, Germany

Claudia Calabrese, Serap Erkek, Moritz Gerstung, Santiago Gonzalez, Nina Habermann, Wolfgang Huber, Lara Jerman, Jan O. Korbel, Esa Pitkänen, Benjamin Raeder, Tobias Rausch, Vasilisa A.

Rudneva, Oliver Stegle, Stephanie Sungalee, Lara Urban, Sebastian M. Waszak, Joachim Weischenfeldt & Sergei Yakneen

209. Department of Oncology, University of Cambridge, Cambridge, UK

Carlos Caldas & Suet-Feung Chin

210. Li Ka Shing Centre, Cancer Research UK Cambridge Institute, University of Cambridge, Cambridge, UK

Carlos Caldas, Suet-Feung Chin, Ruben M. Drews, Paul A. Edwards, Matthew Eldridge, Steve Hawkins, Andy G. Lynch, Geoff Macintyre, Florian Markowetz, Charlie E. Massie, David E. Neal, Simon Tavaré & Ke Yuan

211. Institut Gustave Roussy, Villejuif, France

Fabien Calvo

212. Cambridge University Hospitals NHS Foundation Trust, Cambridge, UK

Peter J. Campbell, Vincent J. Gnanapragasam, William Howat, Thomas J. Mitchell, David E. Neal, Nimish C. Shah & Anne Y. Warren

213. Department of Haematology, University of Cambridge, Cambridge, UK

Peter J. Campbell

214. Anatomia Patológica, Hospital Clinic, Institut d'Investigacions Biomèdiques August Pi i Sunyer (IDIBAPS), University of Barcelona, Barcelona, Spain

Elias Campo

215. Spanish Ministry of Science and Innovation, Madrid, Spain

Elias Campo

216. University of Michigan Comprehensive Cancer Center, Ann Arbor, MI, USA

Thomas E. Carey

217. Department for BioMedical Research, University of Bern, Bern, Switzerland

Joana Carlevaro-Fita

218. Department of Medical Oncology, Inselspital, University Hospital and University of Bern, Bern, Switzerland

Joana Carlevaro-Fita, Rory Johnson & Andrés Lanzós

219. Graduate School for Cellular and Biomedical Sciences, University of Bern, Bern, Switzerland

Joana Carlevaro-Fita & Andrés Lanzós

220. University of Pavia, Pavia, Italy

Mario Cazzola & Luca Malcovati

221. University of Alabama at Birmingham, Birmingham, AL, USA

Robert Cerfolio

222. UHN Program in BioSpecimen Sciences, Toronto General Hospital, Toronto, ON, Canada

Dianne E. Chadwick, Sheng-Ben Liang, Michael H. A. Roehrl & Sagedeh Shahabi

223. Department of Urology, Icahn School of Medicine at Mount Sinai, New York, NY, USA

Dimple Chakravarty

224. Centre for Law and Genetics, University of Tasmania, Sandy Bay Campus, Hobart, TAS, Australia

Don Chalmers

225. Faculty of Biosciences, Heidelberg University, Heidelberg, Germany

Calvin Wing Yiu Chan, Chen Hong & Lina Sieverling

226. Department of Biochemistry, Microbiology and Immunology, Faculty of Medicine, University of Ottawa, Ottawa, ON, Canada

Kin Chan

227. Division of Anatomic Pathology, Mayo Clinic, Rochester, MN, USA

Vishal S. Chandan

228. Division of Cancer Epidemiology and Genetics, National Cancer Institute, National Institutes of Health, Bethesda, MD, USA

Stephen J. Chanock, Xing Hua, Lisa Mirabello, Lei Song & Bin Zhu

229. Illawarra Shoalhaven Local Health District L3 Illawarra Cancer Care Centre, Wollongong Hospital, Wollongong, NSW, Australia

Lorraine A. Chantrill

230. BioForA, French National Institute for Agriculture, Food, and Environment (INRAE), ONF, Orléans, France

Aurélien Chateigner

231. Department of Biostatistics, Bloomberg School of Public Health, Johns Hopkins University, Baltimore, MD, USA

Nilanjan Chatterjee

232. University of California San Diego, San Diego, CA, USA

Zhaohong Chen, Michelle T. Dow, Claudiu Farcas, S. M. Ashiqul Islam, Antonios Koures, Lucila Ohno-Machado, Christos Sotiriou & Ashley Williams

233. Division of Experimental Pathology, Mayo Clinic, Rochester, MN, USA

Jeremy Chien

234. Centre for Cancer Research, The Westmead Institute for Medical Research, University of Sydney, Sydney, NSW, Australia

Yoke-Eng Chiew, Angela Chou, Jillian A. Hung, Catherine J. Kennedy, Graham J. Mann, Gulietta M. Pupo, Sarah-Jane Schramm, Varsha Tembe & Anna deFazio

235. Department of Gynaecological Oncology, Westmead Hospital, Sydney, NSW, Australia

Yoke-Eng Chiew, Jillian A. Hung, Catherine J. Kennedy & Anna deFazio

236. PDXen Biosystems Inc, Seoul, South Korea

Sunghoon Cho

237. Korea Advanced Institute of Science and Technology, Daejeon, South Korea

Jung Kyoon Choi, Young Seok Ju & Christopher J. Yoon

238. Electronics and Telecommunications Research Institute, Daejeon, South Korea

Wan Choi, Seung-Hyup Jeon, Hyunghwan Kim & Youngchoon Woo

239. Institut National du Cancer (INCA), Boulogne-Billancourt, France

Christine Chomienne & Iris Pauporté

240. Department of Genetics, Informatics Institute, University of Alabama at Birmingham, Birmingham, AL, USA

Zechen Chong

241. Division of Medical Oncology, National Cancer Centre, Singapore, Singapore

Su Pin Choo

242. Medical Oncology, University and Hospital Trust of Verona, Verona, Italy

Sara Cingarlini & Michele Milella

243. Department of Pediatrics, University Hospital Schleswig-Holstein, Kiel, Germany

Alexander Claviez

244. Hepatobiliary/Pancreatic Surgical Oncology Program, University Health Network, Toronto, ON, Canada

Sean Cleary, Ashton A. Connor & Steven Gallinger

245. School of Biological Sciences, University of Auckland, Auckland, New Zealand

Nicole Cloonan

246. Department of Surgery, University of Melbourne, Parkville, VIC, Australia

Marek Cmero

247. The Murdoch Children’s Research Institute, Royal Children’s Hospital, Parkville, VIC, Australia

Marek Cmero

248. Walter and Eliza Hall Institute, Parkville, VIC, Australia

Marek Cmero

249. Vancouver Prostate Centre, Vancouver, Canada

Colin C. Collins, Nilgun Donmez, Faraz Hach, Salem Malikic, S. Cenk Sahinalp, Iman Sarrafi & Raunak Shrestha

250. Lunenfeld-Tanenbaum Research Institute, Mount Sinai Hospital, Toronto, ON, Canada

Ashton A. Connor, Steven Gallinger, Robert C. Grant, Treasa A. McPherson & Iris Selander

251. University of East Anglia, Norwich, UK

Colin S. Cooper

252. Norfolk and Norwich University Hospital NHS Trust, Norwich, UK

Matthew G. Cordes, Catrina C. Fronick & Tom Roques

253. Victorian Institute of Forensic Medicine, Southbank, VIC, Australia

Stephen M. Cordner

254. Department of Biomedical Informatics, Harvard Medical School, Boston, MA, USA

Isidro Cortés-Ciriano, Jake June-Koo Lee & Peter J. Park

255. Department of Chemistry, Centre for Molecular Science Informatics, University of Cambridge, Cambridge, UK

Isidro Cortés-Ciriano

256. Ludwig Center at Harvard Medical School, Boston, MA, USA

Isidro Cortés-Ciriano, Jake June-Koo Lee & Peter J. Park

257. Human Genome Sequencing Center, Baylor College of Medicine, Houston, TX, USA

Kyle Covington, HarshaVardhan Doddapaneni, Richard A. Gibbs, Jianhong Hu, Joy C. Jayaseelan, Viktoriya Korchina, Lora Lewis, Donna M. Muzny, Linghua Wang, David A. Wheeler & Liu Xi

258. Peter MacCallum Cancer Centre, University of Melbourne, Melbourne, VIC, Australia

Prue A. Cowin, Anne Hamilton, Gisela Mir Arnau & Ravikiran Vedururu

259. Physics Division, Optimization and Systems Biology Lab, Massachusetts General Hospital, Boston, MA, USA

David Craft

260. Department of Medicine, Baylor College of Medicine, Houston, TX, USA

Chad J. Creighton

261. University of Cologne, Cologne, Germany

Yupeng Cun, Martin Peifer & Tsun-Po Yang

262. International Genomics Consortium, Phoenix, AZ, USA

Erin Curley & Troy Shelton

263. Genomics Research Program, Ontario Institute for Cancer Research, Toronto, ON, Canada

Karolina Czajka, Jenna Eagles, Thomas J. Hudson, Jeremy Johns, Faridah Mbabaali, John D. McPherson, Jessica K. Miller, Danielle Pasternack, Michelle Sam & Lee E. Timms

264. Barking Havering and Redbridge University Hospitals NHS Trust, Romford, UK

Bogdan Czerniak, Adel El-Naggar & David Khoo

265. Children's Hospital at Westmead, University of Sydney, Sydney, NSW, Australia

Rebecca A. Dagg

266. Department of Medicine, Section of Endocrinology, University and Hospital Trust of Verona, Verona, Italy

Maria Vittoria Davi

267. Computational Biology Center, Memorial Sloan Kettering Cancer Center, New York, NY, USA

Natalie R. Davidson, Andre Kahles, Kjong-Van Lehmann, Alessandro Pastore, Gunnar Rätsch, Chris Sander, Yasin Senbabaoglu & Nicholas D. Socci

268. Department of Biology, ETH Zurich, Zürich, Switzerland

Natalie R. Davidson, Andre Kahles, Kjong-Van Lehmann, Gunnar Rätsch & Stefan G. Stark

269. Department of Computer Science, ETH Zurich, Zurich, Switzerland

Natalie R. Davidson, Andre Kahles, Kjong-Van Lehmann & Gunnar Rätsch

270. SIB Swiss Institute of Bioinformatics, Lausanne, Switzerland

Natalie R. Davidson, Andre Kahles, Kjong-Van Lehmann, Gunnar Rätsch & Stefan G. Stark

271. Weill Cornell Medical College, New York, NY, USA

Natalie R. Davidson, Bishoy M. Faltas & Gunnar Rätsch

272. Academic Department of Medical Genetics, University of Cambridge, Addenbrooke's Hospital, Cambridge, UK

Helen Davies & Serena Nik-Zainal

273. MRC Cancer Unit, University of Cambridge, Cambridge, UK

Helen Davies, Rebecca C. Fitzgerald, Nicola Grehan, Serena Nik-Zainal & Maria O'Donovan

274. Departments of Pediatrics and Genetics, University of North Carolina at Chapel Hill, Chapel Hill, NC, USA

Ian J. Davis

275. Seven Bridges Genomics, Charlestown, MA, USA

Brandi N. Davis-Dusenbery, Sinisa Ivkovic, Milena Kovacevic, Ana Mijalkovic Lazic, Sanja Mijalkovic, Mia Nastic, Petar Radovic & Nebojsa Tijanic

276. Annai Systems, Inc, Carlsbad, CA, USA

Francisco M. De La Vega, Tal Shmaya & Dai-Ying Wu

277. Department of Pathology, General Hospital of Treviso, Department of Medicine, University of Padua, Treviso, Italy

Angelo P. Dei Tos

278. Department of Computational Biology, University of Lausanne, Lausanne, Switzerland

Olivier Delaneau

279. Department of Genetic Medicine and Development, University of Geneva Medical School, Geneva, CH, Switzerland

Olivier Delaneau

280. Swiss Institute of Bioinformatics, University of Geneva, Geneva, CH, Switzerland

Olivier Delaneau

281. The Francis Crick Institute, London, UK

Jonas Demeulemeester, Stefan C. Dentro, Matthew W. Fittall, Kerstin Haase, Clemency Jolly, Maxime Tarabichi & Peter Van Loo

282. University of Leuven, Leuven, Belgium

Jonas Demeulemeester & Peter Van Loo

283. Institute of Medical Genetics and Applied Genomics, University of Tübingen, Tübingen, Germany

German M. Demidov, Francesc Muyas & Stephan Ossowski

284. Computational and Systems Biology, Genome Institute of Singapore, Singapore, Singapore

Deniz Demircioğlu & Jonathan Göke

285. School of Computing, National University of Singapore, Singapore, Singapore

Deniz Demircioğlu

286. Big Data Institute, Li Ka Shing Centre, University of Oxford, Oxford, UK

Stefan C. Dentro & David C. Wedge

287. Biomedical Data Science Laboratory, Francis Crick Institute, London, UK

Nikita Desai

288. Bioinformatics Group, Department of Computer Science, University College London, London, UK

Nikita Desai

289. The Edward S. Rogers Sr. Department of Electrical and Computer Engineering, University of Toronto, Toronto, ON, Canada

Amit G. Deshwar

290. Breast Cancer Translational Research Laboratory JC Heuson, Institut Jules Bordet, Brussels, Belgium

Christine Desmedt

291. Department of Oncology, Laboratory for Translational Breast Cancer Research, KU Leuven, Leuven, Belgium

Christine Desmedt

292. Institute for Research in Biomedicine (IRB Barcelona), The Barcelona Institute of Science and Technology, Barcelona, Spain

Jordi Deu-Pons, Joan Frigola, Abel Gonzalez-Perez, Ferran Muiños, Loris Mularoni, Oriol Pich, Iker Reyes-Salazar, Carlota Rubio-Perez, Radhakrishnan Sabarinathan & David Tamborero

293. Research Program on Biomedical Informatics, Universitat Pompeu Fabra, Barcelona, Spain

Jordi Deu-Pons, Abel Gonzalez-Perez, Ferran Muiños, Loris Mularoni, Oriol Pich, Carlota Rubio-Perez, Radhakrishnan

Sabarinathan & David Tamborero

294. Division of Medical Oncology, Princess Margaret Cancer Centre, Toronto, ON, Canada

Neesha C. Dhani, David Hedley & Malcolm J. Moore

295. Department of Physiology and Biophysics, Weill Cornell Medicine, New York, NY, USA

Priyanka Dhingra, Ekta Khurana, Eric Minwei Liu & Alexander Martinez-Fundichely

296. Institute for Computational Biomedicine, Weill Cornell Medicine, New York, NY, USA

Priyanka Dhingra, Ekta Khurana, Eric Minwei Liu & Alexander Martinez-Fundichely

297. Department of Pathology, UPMC Shadyside, Pittsburgh, PA, USA

Rajiv Dhir

298. Independent Consultant, Wellesley, USA

Anthony DiBiase

299. Department of Cell and Molecular Biology, Science for Life Laboratory, Uppsala University, Uppsala, Sweden

Klev Diamanti, Jan Komorowski & Husen M. Umer

300. Department of Medicine and Department of Genetics, Washington University School of Medicine, St. Louis, St. Louis, MO, USA

Li Ding, Robert S. Fulton, Michael D. McLellan, Michael C. Wendl & Venkata D. Yellapantula

301. Hefei University of Technology, Anhui, China

Shuai Ding & Shanlin Yang

302. Translational Cancer Research Unit, GZA Hospitals St.-Augustinus, Center for Oncological Research, Faculty of Medicine and Health Sciences, University of Antwerp, Antwerp, Belgium

Luc Dirix, Steven Van Laere, Gert G. Van den Eynden & Peter Vermeulen

303. Simon Fraser University, Burnaby, BC, Canada

Nilgun Donmez, Ermin Hodzic, Salem Malikic, S. Cenk Sahinalp & Iman Sarrafi

304. University of Pennsylvania, Philadelphia, PA, USA

Ronny Drapkin

305. Faculty of Science and Technology, University of Vic—Central University of Catalonia (UVic-UCC), Vic, Spain

Ana Dueso-Barroso

306. The Wellcome Trust, London, UK

Michael Dunn

307. The Hospital for Sick Children, Toronto, ON, Canada

Lewis Jonathan Dursi

308. Department of Pathology, Queen Elizabeth University Hospital, Glasgow, UK

Fraser R. Duthie

309. Department of Genetics and Computational Biology, QIMR Berghofer Medical Research Institute, Brisbane, QLD, Australia

Ken Dutton-Regester, Nicholas K. Hayward, Oliver Holmes, Peter A. Johansson, Stephen H. Kazakoff, Conrad R. Leonard, Felicity Newell, Katia Nones, Ann-Marie Patch, John V. Pearson, Antonia L. Pritchard, Michael C. Quinn, Paresh Vyas, Nicola Waddell, Scott Wood & Qinying Xu

310. Department of Oncology, Centre for Cancer Genetic Epidemiology, University of Cambridge, Cambridge, UK

Douglas F. Easton

311. Department of Public Health and Primary Care, Centre for Cancer Genetic Epidemiology, University of Cambridge, Cambridge, UK

Douglas F. Easton

312. Prostate Cancer Canada, Toronto, ON, Canada

Stuart Edmonds

313. University of Cambridge, Cambridge, UK

Paul A. Edwards, Anthony R. Green, Andy G. Lynch, Florian Markowetz & Thomas J. Mitchell

314. Department of Laboratory Medicine, Translational Cancer Research, Lund University Cancer Center at Medicon Village, Lund University, Lund, Sweden

Anna Ehinger

315. Heidelberg University, Heidelberg, Germany

Juergen Eils, Roland Eils & Daniel Hübschmann

316. New BIH Digital Health Center, Berlin Institute of Health (BIH) and Charité - Universitätsmedizin Berlin, Berlin, Germany

Juergen Eils, Roland Eils & Chris Lawerenz

317. CIBER Epidemiología y Salud Pública (CIBERESP), Madrid, Spain

Georgia Escaramis

318. Research Group on Statistics, Econometrics and Health (GRECS), UdG, Barcelona, Spain

Georgia Escaramis

319. Quantitative Genomics Laboratories (qGenomics), Barcelona, Spain

Xavier Estivill

320. Icelandic Cancer Registry, Icelandic Cancer Society, Reykjavik, Iceland

Jorunn E. Eyfjord, Holmfridur Hilmarsdottir & Jon G. Jonasson

321. State Key Laboratory of Cancer Biology, and Xijing Hospital of Digestive Diseases, Fourth Military Medical University, Shaanxi, China

Daiming Fan & Yongzhan Nie

322. Department of Medicine (DIMED), Surgical Pathology Unit, University of Padua, Padua, Italy

Matteo Fassan

323. Rigshospitalet, Copenhagen, Denmark

Francesco Favero

324. Center for Cancer Genomics, National Cancer Institute, National Institutes of Health, Bethesda, MD, USA

Martin L. Ferguson

325. Department of Biochemistry and Molecular Medicine, University of Montreal, Montreal, QC, Canada

Vincent Ferretti

326. Australian Institute of Tropical Health and Medicine, James Cook University, Douglas, QLD, Australia

Matthew A. Field

327. Department of Neuro-Oncology, Istituto Neurologico Besta, Milano, Italy

Gaetano Finocchiaro

328. Bioplatforms Australia, North Ryde, NSW, Australia

Anna Fitzgerald & Catherine A. Shang

329. Department of Pathology (Research), University College London Cancer Institute, London, UK

Adrienne M. Flanagan

330. Department of Surgical Oncology, Princess Margaret Cancer Centre, Toronto, ON, Canada

Neil E. Fleshner

331. Department of Medical Oncology, Josephine Nefkens Institute and Cancer Genomics Centre, Erasmus Medical Center, Rotterdam, CN, The Netherlands

John A. Foekens, John W. M. Martens, F. Germán Rodríguez-González, Anieta M. Sieuwerts & Marcel Smid

332. The University of Queensland Thoracic Research Centre, The Prince Charles Hospital, Brisbane, QLD, Australia

Kwun M. Fong

333. CIBIO/InBIO - Research Center in Biodiversity and Genetic Resources, Universidade do Porto, Vairão, Portugal

Nuno A. Fonseca

334. HCA Laboratories, London, UK

Christopher S. Foster

335. University of Liverpool, Liverpool, UK

Christopher S. Foster

336. The Azrieli Faculty of Medicine, Bar-Ilan University, Safed, Israel

Milana Frenkel-Morgenstern

337. Department of Neurosurgery, University of Florida, Gainesville, FL, USA

William Friedman

338. Department of Pathology, Graduate School of Medicine, University of Tokyo, Tokyo, Japan

Masashi Fukayama & Tetsuo Ushiku

339. University of Milano Bicocca, Monza, Italy

Carlo Gambacorti-Passerini

340. BGI-Shenzhen, Shenzhen, China

Shengjie Gao, Yong Hou, Chang Li, Lin Li, Siliang Li, Xiaobo Li, Xinyue Li, Dongbing Liu, Xingmin Liu, Qiang Pan-Hammarström, Hong Su, Jian Wang, Kui Wu, Heng Xiong, Huanming Yang, Chen Ye, Xiuqing Zhang, Yong Zhou & Shida Zhu

341. Department of Pathology, Oslo University Hospital Ulleval, Oslo, Norway

Øystein Garred

342. Center for Biomedical Informatics, Harvard Medical School, Boston, MA, USA

Nils Gehlenborg

343. Department Biochemistry and Molecular Biomedicine, University of Barcelona, Barcelona, Spain

Josep L. L. Gelpi

344. Office of Cancer Genomics, National Cancer Institute, National Institutes of Health, Bethesda, MD, USA

Daniela S. Gerhard

345. Cancer Epigenomics, German Cancer Research Center (DKFZ), Heidelberg, Germany

Clarissa Gerhauser, Christoph Plass & Dieter Weichenhan

346. Department of Cancer Biology, The University of Texas MD Anderson Cancer Center, Houston, TX, USA

Jeffrey E. Gershenwald

347. Department of Surgical Oncology, The University of Texas MD Anderson Cancer Center, Houston, TX, USA

Jeffrey E. Gershenwald

348. Department of Computer Science, Yale University, New Haven, CT, USA

Mark Gerstein & Fabio C. P. Navarro

349. Department of Molecular Biophysics and Biochemistry, Yale University, New Haven, CT, USA

Mark Gerstein, Sushant Kumar, Lucas Lochovsky, Shaoke Lou, Patrick D. McGillivray, Fabio C. P. Navarro, Leonidas Salichos & Jonathan Warrell

350. Program in Computational Biology and Bioinformatics, Yale University, New Haven, CT, USA

Mark Gerstein, Arif O. Harmanci, Sushant Kumar, Donghoon Lee, Shantao Li, Xiaotong Li, Lucas Lochovsky, Shaoke Lou, William Meyerson, Leonidas Salichos, Jonathan Warrell, Jing Zhang & Yan Zhang

351. Center for Cancer Research, Massachusetts General Hospital, Boston, MA, USA

Gad Getz & Paz Polak

352. Department of Pathology, Massachusetts General Hospital, Boston, MA, USA

Gad Getz

353. Department of Pathology, Memorial Sloan Kettering Cancer Center, New York, NY, USA

Ronald Ghossein, Dilip D. Giri, Christine A. Iacobuzio-Donahue, Jorge Reis-Filho & Victor Reuter

354. Division of Gastroenterology and Hepatology, Mayo Clinic, Rochester, MN, USA

Nasra H. Giama, Catherine D. Moser & Lewis R. Roberts

355. University of Sydney, Sydney, NSW, Australia

Anthony J. Gill & James G. Kench

356. University of Oxford, Oxford, UK

Pelvender Gill, Freddie C. Hamdy, Katalin Karaszi, Adam Lambert, Luke Marsden, Clare Verrill & Paresh Vyas

357. Department of Surgery, Academic Urology Group, University of Cambridge, Cambridge, UK

Vincent J. Gnanapragasam

358. Department of Medicine II, University of Würzburg, Wuerzburg, Germany

Maria Elisabeth Goebler

359. Sylvester Comprehensive Cancer Center, University of Miami, Miami, FL, USA

Carmen Gomez

360. Institut Hospital del Mar d’Investigacions Mèdiques (IMIM), Barcelona, Spain

Abel Gonzalez-Perez

361. Genome Integrity and Structural Biology Laboratory, National Institute of Environmental Health Sciences (NIEHS), Durham, NC, USA

Dmitry A. Gordenin & Natalie Saini

362. St. Thomas’s Hospital, London, UK

James Gossage

363. Osaka International Cancer Center, Osaka, Japan

Kunihito Gotoh

364. Department of Pathology, Skåne University Hospital, Lund University, Lund, Sweden

Dorthe Grabau

365. Department of Medical Oncology, Beatson West of Scotland Cancer Centre, Glasgow, UK

Janet S. Graham

366. National Human Genome Research Institute, National Institutes of Health, Bethesda, MD, USA

Eric Green, Carolyn M. Hutter & Heidi J. Sofia

367. Centre for Cancer Research, Victorian Comprehensive Cancer Centre, University of Melbourne, Melbourne, VIC, Australia

Sean M. Grimmond

368. Department of Medicine, Section of Hematology/Oncology, University of Chicago, Chicago, IL, USA

Robert L. Grossman

369. German Center for Infection Research (DZIF), Partner Site Hamburg-Borstel-Lübeck-Riems, Hamburg, Germany

Adam Grundhoff

370. Bioinformatics Research Centre (BiRC), Aarhus University, Aarhus, Denmark

Qianyun Guo, Asger Hobolth & Jakob Skou Pedersen

371. Department of Biotechnology, Ministry of Science and Technology, Government of India, New Delhi, Delhi, India

Shailja Gupta & K. VijayRaghavan

372. National Cancer Centre Singapore, Singapore, Singapore

Jonathan Göke

373. Brandeis University, Waltham, MA, USA

James E. Haber

374. Department of Urologic Sciences, University of British Columbia, Vancouver, BC, Canada

Faraz Hach

375. Department of Internal Medicine, Stanford University, Stanford, CA, USA

Mark P. Hamilton

376. The University of Texas Health Science Center at Houston, Houston, TX, USA

Leng Han, Yang Yang & Xuanping Zhang

377. Imperial College NHS Trust, Imperial College, London, INY, UK

George B. Hanna

378. Senckenberg Institute of Pathology, University of Frankfurt Medical School, Frankfurt, Germany

Martin Hansmann

379. Department of Medicine, Division of Biomedical Informatics, UC San Diego School of Medicine, San Diego, CA, USA

Olivier Harismendy

380. Center for Precision Health, School of Biomedical Informatics, The University of Texas Health Science Center, Houston, TX, USA

Arif O. Harmanci

381. Oxford Nanopore Technologies, New York, NY, USA

Eoghan Harrington & Sissel Juul

382. Institute of Medical Science, University of Tokyo, Tokyo, Japan

Takanori Hasegawa, Shuto Hayashi, Seiya Imoto, Mitsuhiro Komura, Satoru Miyano, Naoki Miyoshi, Kazuhiro Ohi, Eigo Shimizu, Yuichi Shiraishi, Hiroko Tanaka & Rui Yamaguchi

383. Howard Hughes Medical Institute, University of California Santa Cruz, Santa Cruz, CA, USA

David Haussler

384. Wakayama Medical University, Wakayama, Japan

Shinya Hayami, Masaki Ueno & Hiroki Yamaue

385. Department of Internal Medicine, Division of Medical Oncology, Lineberger Comprehensive Cancer Center, University of North Carolina at Chapel Hill, Chapel Hill, NC, USA

D. Neil Hayes

386. University of Tennessee Health Science Center for Cancer Research, Memphis, TN, USA

D. Neil Hayes

387. Department of Histopathology, Salford Royal NHS Foundation Trust, Salford, UK

Stephen J. Hayes

388. Faculty of Biology, Medicine and Health, University of Manchester, Manchester, UK

Stephen J. Hayes

389. BIOPIC, ICG and College of Life Sciences, Peking University, Beijing, China

Yao He & Zemin Zhang

390. Peking-Tsinghua Center for Life Sciences, Peking University, Beijing, China

Yao He & Zemin Zhang

391. Children’s Hospital of Philadelphia, Philadelphia, PA, USA

Allison P. Heath

392. Department of Bioinformatics and Computational Biology and Department of Systems Biology, The University of Texas MD Anderson Cancer Center, Houston, TX, USA

Apurva M. Hegde, Yiling Lu & John N. Weinstein

393. Karolinska Institute, Stockholm, Sweden

Eva Hellstrom-Lindberg & Jesper Lagergren

394. The Donnelly Centre, University of Toronto, Toronto, ON, Canada

Mohamed Helmy & Jeffrey A. Wintersinger

395. Department of Medical Genetics, College of Medicine, Hallym University, Chuncheon, South Korea

Seong Gu Heo, Eun Pyo Hong & Ji Wan Park

396. Department of Experimental and Health Sciences, Institute of Evolutionary Biology (UPF-CSIC), Universitat Pompeu Fabra, Barcelona, Spain

José María Heredia-Genestar, Tomas Marques-Bonet & Arcadi Navarro

397. Health Data Science Unit, University Clinics, Heidelberg, Germany

Carl Herrmann

398. Massachusetts General Hospital Center for Cancer Research, Charlestown, MA, USA

Julian M. Hess & Yosef E. Maruvka

399. Hokkaido University, Sapporo, Japan

Satoshi Hirano & Toru Nakamura

400. Department of Pathology and Clinical Laboratory, National Cancer Center Hospital, Tokyo, Japan

Nobuyoshi Hiraoka

401. Department of Genetics, University of North Carolina at Chapel Hill, Chapel Hill, NC, USA

Katherine A. Hoadley & Tara J. Skelly

402. Computational Biology, Leibniz Institute on Aging - Fritz Lipmann Institute (FLI), Jena, Germany

Steve Hoffmann

403. University of Melbourne Centre for Cancer Research, Melbourne, VIC, Australia

Oliver Hofmann

404. University of Nebraska Medical Center, Omaha, NE, USA

Michael A. Hollingsworth & Sarah P. Thayer

405. Syntekabio Inc, Daejeon, South Korea

Jongwhi H. Hong

406. Department of Pathology, Academic Medical Center, Amsterdam, AZ, The Netherlands

Gerrit K. Hooijer

407. China National GeneBank-Shenzhen, Shenzhen, China

Yong Hou, Chang Li, Siliang Li, Xiaobo Li, Dongbing Liu, Xingmin Liu, Henk G. Stunnenberg, Hong Su, Kui Wu, Heng Xiong, Chen Ye & Shida Zhu

408. Division of Molecular Genetics, German Cancer Research Center (DKFZ), Heidelberg, Germany

Volker Hovestadt, Murat Iskar, Peter Lichter, Bernhard Radlwimmer & Marc Zapatka

409. Division of Life Science and Applied Genomics Center, Hong Kong University of Science and Technology, Clear Water Bay, Hong Kong, China

Taobo Hu, Yogesh Kumar, Eric Z. Ma, Zhenggang Wu & Hong Xue

410. Icahn School of Medicine at Mount Sinai, New York, NY, USA

Kuan-lin Huang

411. Geneplus-Shenzhen, Shenzhen, China

Yi Huang

412. School of Computer Science and Technology, Xi’an Jiaotong University, Xi’an, China

Yi Huang, Jiayin Wang, Xiao Xiao & Xuanping Zhang

413. AbbVie, North Chicago, IL, USA

Thomas J. Hudson

414. Institute of Pathology, Charité – University Medicine Berlin, Berlin, Germany

Michael Hummel & Dido Lenze

415. Centre for Translational and Applied Genomics, British Columbia Cancer Agency, Vancouver, BC, Canada

David Huntsman

416. Edinburgh Royal Infirmary, Edinburgh, UK

Ted R. Hupp

417. Berlin Institute for Medical Systems Biology, Max Delbrück Center for Molecular Medicine, Berlin, Germany

Matthew R. Huska, Julia Markowski & Roland F. Schwarz

418. Department of Pediatric Immunology, Hematology and Oncology, University Hospital, Heidelberg, Germany

Daniel Hübschmann

419. German Cancer Research Center (DKFZ), Heidelberg, Germany

Daniel Hübschmann, Christof von Kalle & Roland F. Schwarz

420. Heidelberg Institute for Stem Cell Technology and Experimental Medicine (HI-STEM), Heidelberg, Germany

Daniel Hübschmann

421. Institute for Computational Biomedicine, Weill Cornell Medical College, New York, NY, USA

Marcin Imielinski

422. New York Genome Center, New York, NY, USA

Marcin Imielinski & Xiaotong Yao

423. Department of Urology, James Buchanan Brady Urological Institute, Johns Hopkins University School of Medicine, Baltimore, MD, USA

William B. Isaacs

424. Department of Preventive Medicine, Graduate School of Medicine, The University of Tokyo, Tokyo, Japan

Shumpei Ishikawa, Hiroto Katoh & Daisuke Komura

425. Department of Molecular and Cellular Biology, Baylor College of Medicine, Houston, TX, USA

Michael Ittmann

426. Department of Pathology and Immunology, Baylor College of Medicine, Houston, TX, USA

Michael Ittmann

427. Michael E. DeBakey Veterans Affairs Medical Center, Houston, TX, USA

Michael Ittmann

428. Technical University of Denmark, Lyngby, Denmark

Jose M. G. Izarzugaza

429. Department of Pathology, College of Medicine, Hanyang University, Seoul, South Korea

Jocelyne Jacquemier, Hyung-Yong Kim & Gu Kong

430. Academic Unit of Surgery, School of Medicine, College of Medical, Veterinary and Life Sciences, University of Glasgow, Glasgow Royal Infirmary, Glasgow, UK

Nigel B. Jamieson

431. Department of Pathology, Asan Medical Center, College of Medicine, Ulsan University, Songpa-gu, Seoul, South Korea

Se Jin Jang & Hee Jin Lee

432. Science Writer, Garrett Park, MD, USA

Karine Jegalian

433. International Cancer Genome Consortium (ICGC)/ICGC Accelerating Research in Genomic Oncology (ARGO) Secretariat, Ontario Institute for Cancer Research, Toronto, ON, Canada

Jennifer L. Jennings

434. University of Ljubljana, Ljubljana, Slovenia

Lara Jerman

435. Department of Public Health Sciences, University of Chicago, Chicago, IL, USA

Yuan Ji

436. Research Institute, NorthShore University HealthSystem, Evanston, IL, USA

Yuan Ji

437. Department for Biomedical Research, University of Bern, Bern, Switzerland

Rory Johnson, Andrés Lanzós & Mark A. Rubin

438. Centre of Genomics and Policy, McGill University and Génome Québec Innovation Centre, Montreal, QC, Canada

Yann Joly, Bartha M. Knoppers, Mark Phillips & Adrian Thorogood

439. Carolina Center for Genome Sciences, University of North Carolina at Chapel Hill, Chapel Hill, NC, USA

Corbin D. Jones

440. Hopp Children's Cancer Center (KiTZ), Heidelberg, Germany

David T. W. Jones, Marcel Kool & Stefan M. Pfister

441. Pediatric Glioma Research Group, German Cancer Research Center (DKFZ), Heidelberg, Germany

David T. W. Jones

442. Cancer Research UK, London, UK

Nic Jones & David Scott

443. Indivumed GmbH, Hamburg, Germany

Hartmut Juhl

444. Genome Integration Data Center, Syntekabio, Inc, Daejeon, South Korea

Jongsun Jung

445. University Hospital Zurich, Zurich, Switzerland

Andre Kahles, Kjong-Van Lehmann & Gunnar Rätsch

446. Clinical Bioinformatics, Swiss Institute of Bioinformatics, Geneva, Switzerland

Abdullah Kahraman

447. Institute for Pathology and Molecular Pathology, University Hospital Zurich, Zurich, Switzerland

Abdullah Kahraman

448. Institute of Molecular Life Sciences, University of Zurich, Zurich, Switzerland

Abdullah Kahraman & Christian von Mering

449. MRC Human Genetics Unit, MRC IGMM, University of Edinburgh, Edinburgh, UK

Vera B. Kaiser & Colin A. Semple

450. Women's Cancer Program at the Samuel Oschin Comprehensive Cancer Institute, Cedars-Sinai Medical Center, Los Angeles, CA, USA

Beth Karlan

451. Department of Biology, Bioinformatics Group, Division of Molecular Biology, Faculty of Science, University of Zagreb, Zagreb, Croatia

Rosa Karlić

452. Department for Internal Medicine II, University Hospital Schleswig-Holstein, Kiel, Germany

Dennis Karsch & Michael Kneba

453. Genetics and Molecular Pathology, SA Pathology, Adelaide, SA, Australia

Karin S. Kassahn

454. Department of Gastric Surgery, National Cancer Center Hospital, Tokyo, Japan

Hitoshi Katai

455. Department of Bioinformatics, Division of Cancer Genomics, National Cancer Center Research Institute, Tokyo, Japan

Mamoru Kato, Hirofumi Rokutan & Mihoko Saito-Adachi

456. A.A. Kharkevich Institute of Information Transmission Problems, Moscow, Russia

Marat D. Kazanov

457. Oncology and Immunology, Dmitry Rogachev National Research Center of Pediatric Hematology, Moscow, Russia

Marat D. Kazanov

458. Skolkovo Institute of Science and Technology, Moscow, Russia

Marat D. Kazanov

459. Department of Surgery, The George Washington University, School of Medicine and Health Science, Washington, DC, USA

Electron Kebebew

460. Endocrine Oncology Branch, Center for Cancer Research, National Cancer Institute, National Institutes of Health, Bethesda, MD, USA

Electron Kebebew

461. Melanoma Institute Australia, Macquarie University, Sydney, NSW, Australia

Richard F. Kefford

462. MIT Computer Science and Artificial Intelligence Laboratory, Massachusetts Institute of Technology, Cambridge, MA, USA

Manolis Kellis

463. Tissue Pathology and Diagnostic Oncology, Royal Prince Alfred Hospital, Sydney, NSW, Australia

James G. Kench & Richard A. Scolyer

464. Cholangiocarcinoma Screening and Care Program and Liver Fluke and Cholangiocarcinoma Research Centre, Faculty of Medicine, Khon Kaen University, Khon Kaen, Thailand

Narong Khuntikeo

465. Controlled Department and Institution, New York, NY, USA

Ekta Khurana

466. Englander Institute for Precision Medicine, Weill Cornell Medicine, New York, NY, USA

Ekta Khurana & Alexander Martinez-Fundichely

467. National Cancer Center, Gyeonggi, South Korea

Hark Kyun Kim

468. Department of Biochemistry, College of Medicine, Ewha Womans University, Seoul, South Korea

Hyung-Lae Kim

469. Health Sciences Department of Biomedical Informatics, University of California San Diego, La Jolla, CA, USA

Jihoon Kim

470. Research Core Center, National Cancer Centre Korea, Goyang-si, South Korea

Jong K. Kim

471. Department of Health Sciences and Technology, Sungkyunkwan University School of Medicine, Seoul, South Korea

Youngwook Kim

472. Samsung Genome Institute, Seoul, South Korea

Youngwook Kim

473. Breast Oncology Program, Dana-Farber/Brigham and Women's Cancer Center, Boston, MA, USA

Tari A. King

474. Department of Surgery, Memorial Sloan Kettering Cancer Center, New York, NY, USA

Tari A. King & Samuel Singer

475. Division of Breast Surgery, Brigham and Women's Hospital, Boston, MA, USA

Tari A. King

476. Integrative Bioinformatics Support Group, National Institute of Environmental Health Sciences (NIEHS), Durham, NC, USA

Leszek J. Klimczak

477. Department of Clinical Science, University of Bergen, Bergen, Norway

Stian Knappskog & Ola Myklebost

478. Center For Medical Innovation, Seoul National University Hospital, Seoul, South Korea

Youngil Koh

479. Department of Internal Medicine, Seoul National University Hospital, Seoul, South Korea

Youngil Koh & Sung-Soo Yoon

480. Institute of Computer Science, Polish Academy of Sciences, Warsawa, Poland

Jan Komorowski

481. Functional and Structural Genomics, German Cancer Research Center (DKFZ), Heidelberg, Germany

Marcel Kool, Andrey Korshunov, Michael Koscher, Stefan M. Pfister & Qi Wang

482. Laboratory of Translational Genomics, Division of Cancer Epidemiology and Genetics, National Cancer Institute, , National Institutes of Health, Bethesda, MD, USA

Roelof Koster

483. Institute for Medical Informatics Statistics and Epidemiology, University of Leipzig, Leipzig, Germany

Markus Kreuz & Markus Loeffler

484. Morgan Welch Inflammatory Breast Cancer Research Program and Clinic, The University of Texas MD Anderson Cancer Center, Houston, TX, USA

Savitri Krishnamurthy

485. Department of Hematology and Oncology, Georg-Augusts-University of Göttingen, Göttingen, Germany

Dieter Kube & Lorenz H. P. Trümper

486. Institute of Cell Biology (Cancer Research), University of Duisburg-Essen, Essen, Germany

Ralf Küppers

487. King's College London and Guy's and St. Thomas' NHS Foundation Trust, London, UK

Jesper Lagergren

488. Center for Epigenetics, Van Andel Research Institute, Grand Rapids, MI, USA

Peter W. Laird

489. The University of Queensland Centre for Clinical Research, Royal Brisbane and Women's Hospital, Herston, QLD, Australia

Sunil R. Lakhani & Peter T. Simpson

490. Department of Pediatric Oncology and Hematology, University of Cologne, Cologne, Germany

Pablo Landgraf

491. University of Düsseldorf, Düsseldorf, Germany

Pablo Landgraf & Guido Reifenberger

492. Department of Pathology, Institut Jules Bordet, Brussels, Belgium

Denis Larsimont

493. Institute of Biomedicine, Sahlgrenska Academy at University of Gothenburg, Gothenburg, Sweden

Erik Larsson

494. Children's Medical Research Institute, Sydney, NSW, Australia

Loretta M. S. Lau & Hilda A. Pickett

495. ILSbio, LLC Biobank, Chestertown, MD, USA

Xuan Le

496. Division of Genetics and Genomics, Boston Children's Hospital, Harvard Medical School, Boston, MA, USA

Eunjung Alice Lee

497. Institute for Bioengineering and Biopharmaceutical Research (IBBR), Hanyang University, Seoul, South Korea

Jeong-Yeon Lee

498. Department of Statistics, University of California Santa Cruz, Santa Cruz, CA, USA

Juhee Lee

499. National Genotyping Center, Institute of Biomedical Sciences, Academia Sinica, Taipei, Taiwan

Ming Ta Michael Lee

500. Department of Vertebrate Genomics/Otto Warburg Laboratory Gene Regulation and Systems Biology of Cancer, Max Planck Institute for Molecular Genetics, Berlin, Germany

Hans Lehrach, Hans-Jörg Warnatz & Marie-Laure Yaspo

501. McGill University and Genome Quebec Innovation Centre, Montreal, QC, Canada

Louis Letourneau

502. biobyte solutions GmbH, Heidelberg, Germany

Ivica Letunic

503. Gynecologic Oncology, NYU Laura and Isaac Perlmutter Cancer Center, New York University, New York, NY, USA

Douglas A. Levine

504. Division of Oncology, Stem Cell Biology Section, Washington University School of Medicine, St. Louis, MO, USA

Tim Ley

505. Department of Systems Biology, The University of Texas MD Anderson Cancer Center, Houston, TX, USA

Han Liang

506. Harvard University, Cambridge, MA, USA

Ziao Lin

507. Urologic Oncology Branch, Center for Cancer Research, National Cancer Institute, National Institutes of Health, Bethesda, MD, USA

W. M. Linehan

508. University of Oslo, Oslo, Norway

Ole Christian Lingjærde & Torill Sauer

509. University of Toronto, Toronto, ON, Canada

Fei-Fei Fei Liu, Quaid D. Morris, Ruian Shi, Shankar Vembu & Fan Yang

510. Peking University, Beijing, China

Fenglin Liu, Fan Zhang, Liangtao Zheng & Xiuqing Zheng

511. School of Life Sciences, Peking University, Beijing, China

Fenglin Liu

512. Leidos Biomedical Research, Inc, McLean, VA, USA

Jia Liu

513. Hematology, Hospital Clinic, Institut d'Investigacions Biomèdiques August Pi i Sunyer (IDIBAPS), University of Barcelona, Barcelona, Spain

Armando Lopez-Guillermo

514. Second Military Medical University, Shanghai, China

Yong-Jie Lu & Hongwei Zhang

515. Chinese Cancer Genome Consortium, Shenzhen, China

Youyong Lu

516. Department of Medical Oncology, Beijing Hospital, Beijing, China

Youyong Lu

517. Laboratory of Molecular Oncology, Key Laboratory of Carcinogenesis and Translational Research (Ministry of Education), Peking University Cancer Hospital and Institute, Beijing, China

Youyong Lu & Rui Xing

518. School of Medicine/School of Mathematics and Statistics, University of St. Andrews, St, Andrews, Fife, UK

Andy G. Lynch

519. Institute for Systems Biology, Seattle, WA, USA

Lisa Lype, Sheila M. Reynolds & Ilya Shmulevich

520. Department of Biochemistry and Molecular Biology, Faculty of Medicine, University Institute of Oncology-IUOPA, Oviedo, Spain

Carlos López-Otín & Xose S. Puente

521. Institut Bergonié, Bordeaux, France

Gaetan MacGrogan

522. Cancer Unit, MRC University of Cambridge, Cambridge, UK

Shona MacRae

523. Department of Pathology and Laboratory Medicine, Center for Personalized Medicine, Children's Hospital Los Angeles, Los Angeles, CA, USA

Dennis T. Maglinte

524. John Curtin School of Medical Research, Canberra, ACT, Australia

Graham J. Mann

525. MVZ Department of Oncology, PraxisClinic am Johannisplatz, Leipzig, Germany

Luisa Mantovani-Löffler

526. Department of Information Technology, Ghent University, Ghent, Belgium

Kathleen Marchal & Sergio Pulido-Tamayo

527. Department of Plant Biotechnology and Bioinformatics, Ghent University, Ghent, Belgium

Kathleen Marchal, Sergio Pulido-Tamayo & Lieven P. C. Verbeke

528. Institute for Genomic Medicine, Nationwide Children’s Hospital, Columbus, OH, USA

Elaine R. Mardis

529. Computational Biology Program, School of Medicine, Oregon Health and Science University, Portland, OR, USA

Adam A. Margolin & Adam J. Struck

530. Department of Surgery, Duke University, Durham, NC, USA

Jeffrey Marks

531. Institució Catalana de Recerca i Estudis Avançats (ICREA), Barcelona, Spain

Tomas Marques-Bonet, Jose I. Martin-Subero, Arcadi Navarro, David Torrents & Alfonso Valencia

532. Institut Català de Paleontologia Miquel Crusafont, Universitat Autònoma de Barcelona, Barcelona, Spain

Tomas Marques-Bonet

533. University of Glasgow, Glasgow, UK

Sancha Martin & Ke Yuan

534. Institut d’Investigacions Biomèdiques August Pi i Sunyer (IDIBAPS), Barcelona, Spain

Jose I. Martin-Subero

535. Division of Oncology, Washington University School of Medicine, St. Louis, MO, USA

R. Jay Mashl

536. Department of Surgery and Cancer, Imperial College, London, INY, UK

Erik Mayer

537. Applications Department, Oxford Nanopore Technologies, Oxford, UK

Simon Mayes & Daniel J. Turner

538. Department of Obstetrics, Gynecology and Reproductive Services, University of California San Francisco, San Francisco, CA, USA

Karen McCune & Karen Smith-McCune

539. Department of Biochemistry and Molecular Medicine, University California at Davis, Sacramento, CA, USA

John D. McPherson

540. STTARR Innovation Facility, Princess Margaret Cancer Centre, Toronto, ON, Canada

Alice Meng

541. Discipline of Surgery, Western Sydney University, Penrith, NSW, Australia

Neil D. Merrett

542. Yale School of Medicine, Yale University, New Haven, CT, USA

William Meyerson

543. Department of Genetics, Lineberger Comprehensive Cancer Center, University of North Carolina at Chapel Hill, Chapel Hill, NC, USA

Piotr A. Mieczkowski, Joel S. Parker, Charles M. Perou, Donghui Tan, Umadevi Veluvolu & Matthew D. Wilkerson

544. Departments of Neurology and Neurosurgery, Henry Ford Hospital, Detroit, MI, USA

Tom Mikkelsen

545. Precision Oncology, OHSU Knight Cancer Institute, Oregon Health and Science University, Portland, OR, USA

Gordon B. Mills

546. Institute of Pathology, University Medical Center Hamburg-Eppendorf, Hamburg, Germany

Sarah Minner, Guido Sauter & Ronald Simon

547. Department of Health Sciences, Faculty of Medical Sciences, Kyushu University, Fukuoka, Japan

Shinichi Mizuno

548. Heidelberg Academy of Sciences and Humanities, Heidelberg, Germany

Fruzsina Molnár-Gábor

549. Department of Clinical Pathology, University of Melbourne, Melbourne, VIC, Australia

Carl Morrison, Karin A. Oien, Chawalit Pairojkul, Paul M. Waring & Marc J. van de Vijver

550. Department of Pathology, Roswell Park Cancer Institute, Buffalo, NY, USA

Carl Morrison

551. Department of Computer Science, University of Helsinki, Helsinki, Finland

Ville Mustonen

552. Institute of Biotechnology, University of Helsinki, Helsinki, Finland

Ville Mustonen

553. Organismal and Evolutionary Biology Research Programme, University of Helsinki, Helsinki, Finland

Ville Mustonen

554. Department of Obstetrics and Gynecology, Division of Gynecologic Oncology, Washington University School of Medicine, St. Louis, MO, USA

David Mutch

555. Penrose St. Francis Health Services, Colorado Springs, CO, USA

Jerome Myers

556. Institute of Pathology, Ulm University and University Hospital of Ulm, Ulm, Germany

Peter Möller

557. National Cancer Center, Tokyo, Japan

Hitoshi Nakagama

558. Genome Institute of Singapore, Singapore, Singapore

Tannistha Nandi & Patrick Tan

559. 32Program in Computational Biology and Bioinformatics, Yale University, New Haven, CT, USA

Fabio C. P. Navarro

560. German Cancer Aid, Bonn, Germany

Gerd Nettekoven & Laura Planko

561. Programme in Cancer and Stem Cell Biology, Centre for Computational Biology, Duke-NUS Medical School, Singapore, Singapore

Alvin Wei Tian Ng

562. The Chinese University of Hong Kong, Shatin, NT, Hong Kong, China

Anthony Ng

563. Fourth Military Medical University, Shaanxi, China

Yongzhan Nie

564. The University of Cambridge School of Clinical Medicine, Cambridge, UK

Serena Nik-Zainal

565. St. Jude Children's Research Hospital, Memphis, TN, USA

Paul A. Northcott

566. University Health Network, Princess Margaret Cancer Centre, Toronto, ON, Canada

Faiyaz Notta & Ming Tsao

567. Center for Biomolecular Science and Engineering, University of California Santa Cruz, Santa Cruz, CA, USA

Brian D. O'Connor

568. Department of Medicine, University of Chicago, Chicago, IL, USA

Peter O'Donnell

569. Department of Neurology, Mayo Clinic, Rochester, MN, USA

Brian Patrick O'Neill

570. Cambridge Oesophagogastric Centre, Cambridge University Hospitals NHS Foundation Trust, Cambridge, UK

J. Robert O'Neill

571. Department of Computer Science, Carleton College, Northfield, MN, USA

Layla Oesper

572. Institute of Cancer Sciences, College of Medical Veterinary and Life Sciences, University of Glasgow, Glasgow, UK

Karin A. Oien

573. Department of Epidemiology, University of Alabama at Birmingham, Birmingham, AL, USA

Akinyemi I. Ojesina

574. HudsonAlpha Institute for Biotechnology, Huntsville, AL, USA

Akinyemi I. Ojesina

575. O'Neal Comprehensive Cancer Center, University of Alabama at Birmingham, Birmingham, AL, USA

Akinyemi I. Ojesina

576. Department of Pathology, Keio University School of Medicine, Tokyo, Japan

Hidenori Ojima

577. Department of Hepatobiliary and Pancreatic Oncology, National Cancer Center Hospital, Tokyo, Japan

Takuji Okusaka

578. Sage Bionetworks, Seattle, WA, USA

Larsson Omberg

579. Lymphoma Genomic Translational Research Laboratory, National Cancer Centre, Singapore, Singapore

Choon Kiat Ong

580. Department of Clinical Pathology, Robert-Bosch-Hospital, Stuttgart, Germany

German Ott

581. Department of Cell and Systems Biology, University of Toronto, Toronto, ON, Canada

B. F. Francis Ouellette

582. Department of Biosciences and Nutrition, Karolinska Institutet, Stockholm, Sweden

Qiang Pan-Hammarström

583. Center for Liver Cancer, Research Institute and Hospital, National Cancer Center, Gyeonggi, South Korea

Joong-Won Park

584. Division of Hematology-Oncology, Samsung Medical Center, Sungkyunkwan University School of Medicine, Seoul, South Korea

Keunchil Park

585. Samsung Advanced Institute for Health Sciences and Technology, Sungkyunkwan University School of Medicine, Seoul, South Korea

Keunchil Park

586. Cheonan Industry-Academic Collaboration Foundation, Sangmyung University, Cheonan, South Korea

Kiejung Park

587. NYU Langone Medical Center, New York, NY, USA

Harvey Pass

588. Department of Hematology and Medical Oncology, Cleveland Clinic, Cleveland, OH, USA

Nathan A. Pennell

589. Department of Radiation Oncology, University of California San Francisco, San Francisco, CA, USA

Marc D. Perry

590. Department of Health Sciences Research, Mayo Clinic, Rochester, MN, USA

Gloria M. Petersen

591. Helen F. Graham Cancer Center at Christiana Care Health Systems, Newark, DE, USA

Nicholas Petrelli

592. Heidelberg University Hospital, Heidelberg, Germany

Stefan M. Pfister

593. CSRA Incorporated, Fairfax, VA, USA

Todd D. Pihl

594. Research Department of Pathology, University College London Cancer Institute, London, UK

Nischalan Pillay

595. Department of Research Oncology, Guy's Hospital, King's Health Partners AHSC, King's College London School of Medicine, London, UK

Sarah Pinder

596. Faculty of Medicine and Health Sciences, Macquarie University, Sydney, NSW, Australia

Andreia V. Pinho

597. University Hospital of Minjoz, INSERM UMR 1098, Besançon, France

Xavier Pivot

598. Spanish National Cancer Research Centre, Madrid, Spain

Tirso Pons

599. Center of Digestive Diseases and Liver Transplantation, Fundeni Clinical Institute, Bucharest, Romania

Irinel Popescu

600. Cureline, Inc, South San Francisco, CA, USA

Olga Potapova

601. St. Luke's Cancer Centre, Royal Surrey County Hospital NHS Foundation Trust, Guildford, UK

Shaun R. Preston

602. Cambridge Breast Unit, Addenbrooke's Hospital, Cambridge University Hospital NHS Foundation Trust and NIHR Cambridge Biomedical Research Centre, Cambridge, UK

Elena Provenzano

603. East of Scotland Breast Service, Ninewells Hospital, Aberdeen, UK

Colin A. Purdie

604. Department of Genetics, Microbiology and Statistics, University of Barcelona, IRSJD, IBUB, Barcelona, Spain

Raquel Rabionet

605. Department of Obstetrics and Gynecology, Medical College of Wisconsin, Milwaukee, WI, USA

Janet S. Rader

606. Hematology and Medical Oncology, Winship Cancer Institute of Emory University, Atlanta, GA, USA

Suresh Ramalingam

607. Department of Computer Science, Princeton University, Princeton, NJ, USA

Benjamin J. Raphael & Matthew A. Reyna

608. Vanderbilt Ingram Cancer Center, Vanderbilt University, Nashville, TN, USA

W. Kimryn Rathmell

609. Ohio State University College of Medicine and Arthur G. James Comprehensive Cancer Center, Columbus, OH, USA

Matthew Ringel

610. Department of Surgery, Yokohama City University Graduate School of Medicine, Kanagawa, Japan

Yasushi Rino

611. Division of Chromatin Networks, German Cancer Research Center (DKFZ) and BioQuant, Heidelberg, Germany

Karsten Rippe

612. Research Computing Center, University of North Carolina at Chapel Hill, Chapel Hill, NC, USA

Jeffrey Roach

613. School of Molecular Biosciences and Center for Reproductive Biology, Washington State University, Pullman, WA, USA

Steven A. Roberts

614. Finsen Laboratory and Biotech Research and Innovation Centre (BRIC), University of Copenhagen, Copenhagen, Denmark

F. Germán Rodríguez-González, Nikos Sidiropoulos & Joachim Weischenfeldt

615. Department of Laboratory Medicine and Pathobiology, University of Toronto, Toronto, ON, Canada

Michael H. A. Roehrl & Stefano Serra

616. Department of Pathology, Human Oncology and Pathogenesis Program, Memorial Sloan Kettering Cancer Center, New York, NY, USA

Michael H. A. Roehrl

617. University Hospital Giessen, Pediatric Hematology and Oncology, Giessen, Germany

Marius Rohde

618. Oncologie Sénologie, ICM Institut Régional du Cancer, Montpellier, France

Gilles Romieu

619. Institute of Clinical Molecular Biology, Christian-Albrechts-University, Kiel, Germany

Philip C. Rosenstiel & Markus B. Schilhabel

620. Institute of Pathology, University of Wuerzburg, Wuerzburg, Germany

Andreas Rosenwald

621. Department of Urology, North Bristol NHS Trust, Bristol, UK

Edward W. Rowe

622. SingHealth, Duke-NUS Institute of Precision Medicine, National Heart Centre Singapore, Singapore, Singapore

Steven G. Rozen, Patrick Tan & Bin Tean Teh

623. Department of Computer Science, University of Toronto, Toronto, ON, Canada

Yulia Rubanova, Jared T. Simpson & Jeffrey A. Wintersinger

624. Bern Center for Precision Medicine, University Hospital of Bern, University of Bern, Bern, Switzerland

Mark A. Rubin

625. Englander Institute for Precision Medicine, Weill Cornell Medicine and New York Presbyterian Hospital, New York, NY, USA

Mark A. Rubin

626. Meyer Cancer Center, Weill Cornell Medicine, New York, NY, USA

Mark A. Rubin

627. Pathology and Laboratory, Weill Cornell Medical College, New York, NY, USA

Mark A. Rubin

628. Vall d'Hebron Institute of Oncology: VHIO, Barcelona, Spain

Carlota Rubio-Perez

629. General and Hepatobiliary-Biliary Surgery, Pancreas Institute, University and Hospital Trust of Verona, Verona, Italy

Andrea Ruzzenente

630. National Centre for Biological Sciences, Tata Institute of Fundamental Research, Bangalore, India

Radhakrishnan Sabarinathan

631. Indiana University, Bloomington, IN, USA

S. Cenk Sahinalp

632. Department of Pathology, GZA-ZNA Hospitals, Antwerp, Belgium

Roberto Salgado

633. Analytical Biological Services, Inc, Wilmington, DE, USA

Charles Saller

634. Sydney Medical School, University of Sydney, Sydney, NSW, Australia

Jaswinder S. Samra & Richard A. Scolyer

635. cBio Center, Dana-Farber Cancer Institute, Harvard Medical School, Boston, MA, USA

Chris Sander & Ciyue Shen

636. Department of Cell Biology, Harvard Medical School, Boston, MA, USA

Chris Sander & Ciyue Shen

637. Advanced Centre for Treatment Research and Education in Cancer, Tata Memorial Centre, Navi Mumbai, Maharashtra, India

Rajiv Sarin

638. School of Environmental and Life Sciences, Faculty of Science, The University of Newcastle, Ourimbah, NSW, Australia

Christopher J. Scarlett

639. Department of Dermatology, University Hospital of Essen, Essen, Germany

Dirk Schadendorf

640. Bioinformatics and Omics Data Analytics, German Cancer Research Center (DKFZ), Heidelberg, Germany

Matthias Schlesner

641. Department of Urology, Charité Universitätsmedizin Berlin, Berlin, Germany

Thorsten Schlomm & Joachim Weischenfeldt

642. Martini-Clinic, Prostate Cancer Center, University Medical Center Hamburg-Eppendorf, Hamburg, Germany

Thorsten Schlomm

643. Department of General Internal Medicine, University of Kiel, Kiel, Germany

Stefan Schreiber

644. German Cancer Consortium (DKTK), Partner site Berlin, Berlin, Germany

Roland F. Schwarz

645. Cancer Research Institute, Beth Israel Deaconess Medical Center, Boston, MA, USA

Ralph Scully

646. University of Pittsburgh, Pittsburgh, PA, USA

Raja Seethala

647. Department of Ophthalmology and Ocular Genomics Institute, Massachusetts Eye and Ear, Harvard Medical School, Boston, MA, USA

Ayellet V. Segre

648. Center for Psychiatric Genetics, NorthShore University HealthSystem, Evanston, IL, USA

Subhajit Sengupta

649. Van Andel Research Institute, Grand Rapids, MI, USA

Hui Shen & Wanding Zhou

650. Laboratory of Molecular Medicine, Human Genome Center, Institute of Medical Science, University of Tokyo, Tokyo, Japan

Tatsuhiro Shibata, Hirokazu Taniguchi & Tomoko Urushidate

651. Japan Agency for Medical Research and Development, Tokyo, Japan

Kiyo Shimizu & Takashi Yugawa

652. Korea University, Seoul, South Korea

Seung Jun Shin & Stefan G. Stark

653. Murtha Cancer Center, Walter Reed National Military Medical Center, Bethesda, MD, USA

Craig Shriver

654. Human Genetics, University of Kiel, Kiel, Germany

Reiner Siebert

655. Department of Oncologic Pathology, Dana-Farber Cancer Institute, Harvard Medical School, Boston, MA, USA

Sabina Signoretti

656. Oregon Health and Science University, Portland, OR, USA

Jaclyn Smith

657. Center for RNA Interference and Noncoding RNA, The University of Texas MD Anderson Cancer Center, Houston, TX, USA

Anil K. Sood

658. Department of Experimental Therapeutics, The University of Texas MD Anderson Cancer Center, Houston, TX, USA

Anil K. Sood

659. Department of Gynecologic Oncology and Reproductive Medicine, The University of Texas MD Anderson Cancer Center, Houston, TX, USA

Anil K. Sood

660. University Hospitals Coventry and Warwickshire NHS Trust, Coventry, UK

Sharmila Sothi

661. Department of Radiation Oncology, Radboud University Nijmegen Medical Centre, Nijmegen, GA, The Netherlands

Paul N. Span

662. Institute for Genomics and Systems Biology, University of Chicago, Chicago, IL, USA

Jonathan Spring

663. Clinic for Hematology and Oncology, St.-Antonius-Hospital, Eschweiler, Germany

Peter Staib

664. Computational and Systems Biology Program, Memorial Sloan Kettering Cancer Center, New York, NY, USA

Stefan G. Stark

665. University of Iceland, Reykjavik, Iceland

Ólafur Andri Stefánsson

666. Division of Computational Genomics and Systems Genetics, German Cancer Research Center (DKFZ), Heidelberg, Germany

Oliver Stegle

667. Dundee Cancer Centre, Ninewells Hospital, Dundee, UK

Alasdair Stenhouse & Alastair M. Thompson

668. Department for Internal Medicine III, University of Ulm and University Hospital of Ulm, Ulm, Germany

Stephan Stilgenbauer

669. Institut Curie, INSERM Unit 830, Paris, France

Henk G. Stunnenberg & Anne Vincent-Salomon

670. Department of Gastroenterology and Hepatology, Yokohama City University Graduate School of Medicine, Kanagawa, Japan

Akihiro Suzuki

671. Department of Laboratory Medicine, Radboud University Nijmegen Medical Centre, Nijmegen, GA, The Netherlands

Fred Sweep

672. Division of Cancer Genome Research, German Cancer Research Center (DKFZ), Heidelberg, Germany

Holger Sültmann

673. Department of General Surgery, Singapore General Hospital, Singapore, Singapore

Benita Kiat Tee Tan

674. Cancer Science Institute of Singapore, National University of Singapore, Singapore, Singapore

Patrick Tan & Bin Tean Teh

675. Department of Medical and Clinical Genetics, Genome-Scale Biology Research Program, University of Helsinki, Helsinki, Finland

Tomas J. Tanskanen

676. East Anglian Medical Genetics Service, Cambridge University Hospitals NHS Foundation Trust, Cambridge, UK

Patrick Tarpey

677. Irving Institute for Cancer Dynamics, Columbia University, New York, NY, USA

Simon Tavaré

678. Institute of Molecular and Cell Biology, Singapore, Singapore

Bin Tean Teh

679. Laboratory of Cancer Epigenome, Division of Medical Science, National Cancer Centre Singapore, Singapore, Singapore

Bin Tean Teh

680. Universite Lyon, INCa-Synergie, Centre Léon Bérard, Lyon, France

Gilles Thomas

681. Department of Urology, Mayo Clinic, Rochester, MN, USA

R. Houston Thompson

682. Royal National Orthopaedic Hospital - Stanmore, Stanmore, Middlesex, UK

Roberto Tirabosco

683. Department of Biochemistry, Genetics and Immunology, University of Vigo, Vigo, Spain

Marta Tojo

684. Giovanni Paolo II / I.R.C.C.S. Cancer Institute, Bari, BA, Italy

Stefania Tommasi

685. Neuroblastoma Genomics, German Cancer Research Center (DKFZ), Heidelberg, Germany

Umut H. Toprak

686. Fondazione Policlinico Universitario Gemelli IRCCS, Rome, Italy, Rome, Italy

Giampaolo Tortora

687. University of Verona, Verona, Italy

Giampaolo Tortora

688. Centre National de Génotypage, CEA - Institute de Génomique, Evry, France

Jörg Tost

689. CAPHRI Research School, Maastricht University, Maastricht, ER, The Netherlands

David Townend

690. Department of Biopathology, Centre Léon Bérard, Lyon, France

Isabelle Treilleux

691. Université Claude Bernard Lyon 1, Villeurbanne, France

Isabelle Treilleux

692. Core Research for Evolutional Science and Technology (CREST), JST, Tokyo, Japan

Tatsuhiko Tsunoda

693. Department of Biological Sciences, Laboratory for Medical Science Mathematics, Graduate School of Science, University of Tokyo, Yokohama, Japan

Tatsuhiko Tsunoda

694. Department of Medical Science Mathematics, Medical Research Institute, Tokyo Medical and Dental University (TMDU), Tokyo, Japan

Tatsuhiko Tsunoda

695. Cancer Ageing and Somatic Mutation Programme, Wellcome Sanger Institute, Hinxton, UK

Jose M. C. Tubio

696. University Hospitals Birmingham NHS Foundation Trust, Birmingham, UK

Olga Tucker

697. Centre for Cancer Research and Cell Biology, Queen's University, Belfast, UK

Richard Turkington

698. Breast Medical Oncology, The University of Texas MD Anderson Cancer Center, Houston, TX, USA

Naoto T. Ueno

699. Department of Surgery, Johns Hopkins University School of Medicine, Baltimore, MD, USA

Christopher Umbricht

700. Department of Oncology-Pathology, Science for Life Laboratory, Karolinska Institute, Stockholm, Sweden

Husen M. Umer

701. School of Cancer Sciences, Faculty of Medicine, University of Southampton, Southampton, UK

Timothy J. Underwood

702. Department of Gene Technology, Tallinn University of Technology, Tallinn, Estonia

Liis Uusküla-Reimand

703. Genetics and Genome Biology Program, SickKids Research Institute, The Hospital for Sick Children, Toronto, ON, Canada

Liis Uusküla-Reimand

704. Departments of Neurosurgery and Hematology and Medical Oncology, Winship Cancer Institute and School of Medicine, Emory University, Atlanta, GA, USA

Erwin G. Van Meir

705. Department of Clinical and Molecular Medicine, Faculty of Medicine and Health Sciences, Norwegian University of Science and Technology, Trondheim, Norway

Miguel Vazquez

706. Argmix Consulting, North Vancouver, BC, Canada

Shankar Vembu

707. Department of Information Technology, Ghent University, Interuniversitair Micro-Electronica Centrum (IMEC), Ghent, Belgium

Lieven P. C. Verbeke

708. Nuffield Department of Surgical Sciences, John Radcliffe Hospital, University of Oxford, Oxford, UK

Clare Verrill

709. Institute of Mathematics and Computer Science, University of Latvia, Riga, LV, Latvia

Juris Viksna

710. Discipline of Pathology, Sydney Medical School, University of Sydney, Sydney, NSW, Australia

Ricardo E. Vilain

711. Department of Applied Mathematics and Theoretical Physics, Centre for Mathematical Sciences, University of Cambridge, Cambridge, UK

Ignacio Vázquez-García

712. Department of Epidemiology and Biostatistics, Memorial Sloan Kettering Cancer Center, New York, NY, USA

Ignacio Vázquez-García & Venkata D. Yellapantula

713. Department of Statistics, Columbia University, New York, NY, USA

Ignacio Vázquez-García

714. Department of Immunology, Genetics and Pathology, Science for Life Laboratory, Uppsala University, Uppsala, Sweden

Claes Wadelius

715. School of Electronic and Information Engineering, Xi’an Jiaotong University, Xi’an, China

Jiayin Wang & Kai Ye

716. Department of Histopathology, Cambridge University Hospitals NHS Foundation Trust, Cambridge, UK

Anne Y. Warren

717. Oxford NIHR Biomedical Research Centre, University of Oxford, Oxford, UK

David C. Wedge

718. Georgia Regents University Cancer Center, Augusta, GA, USA

Paul Weinberger

719. Wythenshawe Hospital, Manchester, UK

Ian Welch

720. Department of Genetics, Washington University School of Medicine, St.Louis, MO, USA

Michael C. Wendl

721. Department of Biological Oceanography, Leibniz Institute of Baltic Sea Research, Rostock, Germany

Johannes Werner

722. Wellcome Centre for Human Genetics, University of Oxford, Oxford, UK

Justin P. Whalley

723. Department of Molecular and Human Genetics, Baylor College of Medicine, Houston, TX, USA

David A. Wheeler

724. Thoracic Oncology Laboratory, Mayo Clinic, Rochester, MN, USA

Dennis Wigle

725. Institute for Genomic Medicine, Nationwide Children's Hospital, Columbus, OH, USA

Richard K. Wilson

726. Department of Obstetrics and Gynecology, Division of Gynecologic Oncology, Mayo Clinic, Rochester, MN, USA

Boris Winterhoff

727. International Institute for Molecular Oncology, Poznań, Poland

Maciej Wiznerowicz

728. Poznan University of Medical Sciences, Poznań, Poland

Maciej Wiznerowicz

729. Genomics and Proteomics Core Facility High Throughput Sequencing Unit, German Cancer Research Center (DKFZ), Heidelberg, Germany

Stephan Wolf

730. NCCS-VARI Translational Research Laboratory, National Cancer Centre Singapore, Singapore, Singapore

Bernice H. Wong

731. Edison Family Center for Genome Sciences and Systems Biology, Washington University, St. Louis, MO, USA

Winghing Wong

732. MRC-University of Glasgow Centre for Virus Research, Glasgow, UK

Derek W. Wright

733. Department of Medical Informatics and Clinical Epidemiology, Division of Bioinformatics and Computational Biology, OHSU Knight Cancer Institute, Oregon Health and Science University, Portland, OR, USA

Guanming Wu

734. School of Electronic Information and Communications, Huazhong University of Science and Technology, Wuhan, China

Tian Xia

735. Department of Applied Mathematics and Statistics, Johns Hopkins University, Baltimore, MD, USA

Yanxun Xu

736. Department of Cancer Genome Informatics, Graduate School of Medicine, Osaka University, Osaka, Japan

Shinichi Yachida

737. Institute of Computer Science, Heidelberg University, Heidelberg, Germany

Sergei Yakneen

738. School of Mathematics and Statistics, University of Sydney, Sydney, NSW, Australia

Jean Y. Yang

739. Ben May Department for Cancer Research, University of Chicago, Chicago, IL, USA

Lixing Yang

740. Department of Human Genetics, University of Chicago, Chicago, IL, USA

Lixing Yang

741. Tri-Institutional PhD Program in Computational Biology and Medicine, Weill Cornell Medicine, New York, NY, USA

Xiaotong Yao

742. The First Affiliated Hospital, Xi’an Jiaotong University, Xi’an, China

Kai Ye

743. Department of Medicine and Therapeutics, The Chinese University of Hong Kong, Shatin, NT, Hong Kong, China

Jun Yu

744. Department of Biostatistics, The University of Texas MD Anderson Cancer Center, Houston, TX, USA

Kaixian Yu & Hongtu Zhu

745. Duke-NUS Medical School, Singapore, Singapore

Willie Yu

746. Department of Surgery, Ruijin Hospital, Shanghai Jiaotong University School of Medicine, Shanghai, China

Yingyan Yu

747. School of Computing Science, University of Glasgow, Glasgow, UK

Ke Yuan

748. Division of Orthopaedic Surgery, Oslo University Hospital, Oslo, Norway

Olga Zaikova

749. Eastern Clinical School, Monash University, Melbourne, VIC, Australia

Nikolajs Zeps

750. Epworth HealthCare, Richmond, VIC, Australia

Nikolajs Zeps

751. Department of Biostatistics and Computational Biology, Dana-Farber Cancer Institute and Harvard Medical School, Boston, MA, USA

Cheng-Zhong Zhang

752. Department of Biomedical Informatics, College of Medicine, The Ohio State University, Columbus, OH, USA

Yan Zhang

753. The Ohio State University Comprehensive Cancer Center (OSUCCC – James), Columbus, OH, USA

Yan Zhang

754. The University of Texas School of Biomedical Informatics (SBMI) at Houston, Houston, TX, USA

Zhongming Zhao

755. Department of Biostatistics, University of North Carolina at Chapel Hill, Chapel Hill, NC, USA

Hongtu Zhu

756. Department of Biochemistry and Molecular Genetics, Feinberg School of Medicine, Northwestern University, Chicago, IL, USA

Lihua Zou

757. Faculty of Medicine and Health, University of Sydney, Sydney, NSW, Australia

Anna deFazio

758. Department of Pathology, Erasmus Medical Center Rotterdam, Rotterdam, GD, The Netherlands

Carolien H. M. van Deurzen

759. Division of Molecular Carcinogenesis, The Netherlands Cancer Institute, Amsterdam, CX, The Netherlands

L. van't Veer

760. Institute of Molecular Life Sciences and Swiss Institute of Bioinformatics, University of Zurich, Zurich, Switzerland

Christian von Mering

Consortia

PCAWG Transcriptome Core Group

- Claudia Calabrese
- , Natalie R. Davidson
- , Deniz Demircioğlu
- , Nuno A. Fonseca
- , Yao He
- , André Kahles
- , Kjong-Van Lehmann

- , Fenglin Liu
- , Yuichi Shiraishi
- , Cameron M. Soulette
- & Lara Urban

PCAWG Transcriptome Working Group

- Nuno A. Fonseca
- , André Kahles
- , Kjong-Van Lehmann
- , Lara Urban
- , Cameron M. Soulette
- , Yuichi Shiraishi
- , Fenglin Liu
- , Yao He
- , Deniz Demircioğlu
- , Natalie R. Davidson
- , Claudia Calabrese
- , Junjun Zhang
- , Marc D. Perry
- , Qian Xiang
- , Liliana Greger
- , Siliang Li
- , Dongbing Liu
- , Stefan G. Stark
- , Fan Zhang
- , Samirkumar B. Amin
- , Peter Bailey
- , Aurélien Chateigner
- , Isidro Cortés-Ciriano
- , Brian Craft
- , Serap Erkek
- , Milana Frenkel-Morgenstern
- , Mary Goldman
- , Katherine A. Hoadley
- , Yong Hou
- , Matthew R. Huska

- , Ekta Khurana
- , Helena Kilpinen
- , Jan O. Korbel
- , Fabien C. Lamaze
- , Chang Li
- , Xiaobo Li
- , Xinyue Li
- , Xingmin Liu
- , Maximillian G. Marin
- , Julia Markowski
- , Tannistha Nandi
- , Morten M. Nielsen
- , Akinyemi I. Ojesina
- , Qiang Pan-Hammarström
- , Peter J. Park
- , Chandra Sekhar Pedamallu
- , Jakob S. Pedersen
- , Reiner Siebert
- , Hong Su
- , Patrick Tan
- , Bin Tean Teh
- , Jian Wang
- , Sebastian M. Waszak
- , Heng Xiong
- , Sergei Yakneen
- , Chen Ye
- , Christina Yung
- , Xiuqing Zhang
- , Liangtao Zheng
- , Jingchun Zhu
- , Shida Zhu
- , Philip Awadalla
- , Chad J. Creighton
- , Matthew Meyerson
- , B. F. Francis Ouellette
- , Kui Wu
- , Huanming Yang

- , Jonathan Göke
- , Roland F. Schwarz
- , Oliver Stegle
- , Zemin Zhang
- , Alvis Brazma
- , Gunnar Rätsch
- & Angela N. Brooks

PCAWG Consortium

- Lauri A. Aaltonen
- , Federico Abascal
- , Adam Abeshouse
- , Hiroyuki Aburatani
- , David J. Adams
- , Nishant Agrawal
- , Keun Soo Ahn
- , Sung-Min Ahn
- , Hiroshi Aikata
- , Rehan Akbani
- , Kadir C. Akdemir
- , Hikmat Al-Ahmadie
- , Sultan T. Al-Sedairy
- , Fatima Al-Shahrour
- , Malik Alawi
- , Monique Albert
- , Kenneth Aldape
- , Ludmil B. Alexandrov
- , Adrian Ally
- , Kathryn Alsop
- , Eva G. Alvarez
- , Fernanda Amary
- , Samirkumar B. Amin
- , Brice Aminou
- , Ole Ammerpohl
- , Matthew J. Anderson
- , Yeng Ang

- , Davide Antonello
- , Pavana Anur
- , Samuel Aparicio
- , Elizabeth L. Appelbaum
- , Yasuhito Arai
- , Axel Aretz
- , Koji Arihiro
- , Shun-ichi Ariizumi
- , Joshua Armenia
- , Laurent Arnould
- , Sylvia Asa
- , Yassen Assenov
- , Gurnit Atwal
- , Sietse Aukema
- , J. Todd Auman
- , Miriam R. R. Aure
- , Philip Awadalla
- , Marta Aymerich
- , Gary D. Bader
- , Adrian Baez-Ortega
- , Matthew H. Bailey
- , Peter J. Bailey
- , Miruna Balasundaram
- , Saianand Balu
- , Pratiti Bandopadhayay
- , Rosamonde E. Banks
- , Stefano Barbi
- , Andrew P. Barbour
- , Jonathan Barenboim
- , Jill Barnholtz-Sloan
- , Hugh Barr
- , Elisabet Barrera
- , John Bartlett
- , Javier Bartolome
- , Claudio Bassi
- , Oliver F. Bathe
- , Daniel Baumhoer

- , Prashant Bavi
- , Stephen B. Baylin
- , Wojciech Bazant
- , Duncan Beardsmore
- , Timothy A. Beck
- , Sam Behjati
- , Andreas Behren
- , Beifang Niu
- , Cindy Bell
- , Sergi Beltran
- , Christopher Benz
- , Andrew Berchuck
- , Anke K. Bergmann
- , Erik N. Bergstrom
- , Benjamin P. Berman
- , Daniel M. Berney
- , Stephan H. Bernhart
- , Rameen Beroukhim
- , Mario Berrios
- , Samantha Bersani
- , Johanna Bertl
- , Miguel Betancourt
- , Vinayak Bhandari
- , Shriram G. Bhosle
- , Andrew V. Biankin
- , Matthias Bieg
- , Darell Bigner
- , Hans Binder
- , Ewan Birney
- , Michael Birrer
- , Nidhan K. Biswas
- , Bodil Bjerkehagen
- , Tom Bodenheimer
- , Lori Boice
- , Giada Bonizzato
- , Johann S. De Bono
- , Arnoud Boot

- , Moiz S. Bootwalla
- , Ake Borg
- , Arndt Borkhardt
- , Keith A. Boroevich
- , Ivan Borozan
- , Christoph Borst
- , Marcus Bosenberg
- , Mattia Bosio
- , Jacqueline Boultwood
- , Guillaume Bourque
- , Paul C. Boutros
- , G. Steven Bova
- , David T. Bowen
- , Reanne Bowlby
- , David D. L. Bowtell
- , Sandrine Boyault
- , Rich Boyce
- , Jeffrey Boyd
- , Alvis Brazma
- , Paul Brennan
- , Daniel S. Brewer
- , Arie B. Brinkman
- , Robert G. Bristow
- , Russell R. Broaddus
- , Jane E. Brock
- , Malcolm Brock
- , Annegien Broeks
- , Angela N. Brooks
- , Denise Brooks
- , Benedikt Brors
- , Søren Brunak
- , Timothy J. C. Bruxner
- , Alicia L. Bruzos
- , Alex Buchanan
- , Ivo Buchhalter
- , Christiane Buchholz
- , Susan Bullman

- , Hazel Burke
- , Birgit Burkhardt
- , Kathleen H. Burns
- , John Busanovich
- , Carlos D. Bustamante
- , Adam P. Butler
- , Atul J. Butte
- , Niall J. Byrne
- , Anne-Lise Børresen-Dale
- , Samantha J. Caesar-Johnson
- , Andy Cafferkey
- , Declan Cahill
- , Claudia Calabrese
- , Carlos Caldas
- , Fabien Calvo
- , Niedzica Camacho
- , Peter J. Campbell
- , Elias Campo
- , Cinzia Cantù
- , Shaolong Cao
- , Thomas E. Carey
- , Joana Carlevaro-Fita
- , Rebecca Carlsen
- , Ivana Cataldo
- , Mario Cazzola
- , Jonathan Cebon
- , Robert Cerfolio
- , Dianne E. Chadwick
- , Dimple Chakravarty
- , Don Chalmers
- , Calvin Wing Yiu Chan
- , Kin Chan
- , Michelle Chan-Seng-Yue
- , Vishal S. Chandan
- , David K. Chang
- , Stephen J. Chanock
- , Lorraine A. Chantrill

- , Aurélien Chateigner
- , Nilanjan Chatterjee
- , Kazuaki Chayama
- , Hsiao-Wei Chen
- , Jieming Chen
- , Ken Chen
- , Yiwen Chen
- , Zhaohong Chen
- , Andrew D. Cherniack
- , Jeremy Chien
- , Yoke-Eng Chiew
- , Suet-Feung Chin
- , Juok Cho
- , Sunghoon Cho
- , Jung Kyoon Choi
- , Wan Choi
- , Christine Chomienne
- , Zechen Chong
- , Su Pin Choo
- , Angela Chou
- , Angelika N. Christ
- , Elizabeth L. Christie
- , Eric Chuah
- , Carrie Cibulskis
- , Kristian Cibulskis
- , Sara Cingarlini
- , Peter Clapham
- , Alexander Claviez
- , Sean Cleary
- , Nicole Cloonan
- , Marek Cmero
- , Colin C. Collins
- , Ashton A. Connor
- , Susanna L. Cooke
- , Colin S. Cooper
- , Leslie Cope
- , Vincenzo Corbo

- , Matthew G. Cordes
- , Stephen M. Cordner
- , Isidro Cortés-Ciriano
- , Kyle Covington
- , Prue A. Cowin
- , Brian Craft
- , David Craft
- , Chad J. Creighton
- , Yupeng Cun
- , Erin Curley
- , Ioana Cutcutache
- , Karolina Czajka
- , Bogdan Czerniak
- , Rebecca A. Dagg
- , Ludmila Danilova
- , Maria Vittoria Davi
- , Natalie R. Davidson
- , Helen Davies
- , Ian J. Davis
- , Brandi N. Davis-Dusenbery
- , Kevin J. Dawson
- , Francisco M. De La Vega
- , Ricardo De Paoli-Iseppi
- , Timothy Defreitas
- , Angelo P. Dei Tos
- , Olivier Delaneau
- , John A. Demchok
- , Jonas Demeulemeester
- , German M. Demidov
- , Deniz Demircioğlu
- , Nening M. Dennis
- , Robert E. Denroche
- , Stefan C. Dentro
- , Nikita Desai
- , Vikram Deshpande
- , Amit G. Deshwar
- , Christine Desmedt

- , Jordi Deu-Pons
- , Noreen Dhalla
- , Neesha C. Dhani
- , Priyanka Dhingra
- , Rajiv Dhir
- , Anthony DiBiase
- , Klev Diamanti
- , Li Ding
- , Shuai Ding
- , Huy Q. Dinh
- , Luc Dirix
- , HarshaVardhan Doddapaneni
- , Nilgun Donmez
- , Michelle T. Dow
- , Ronny Drapkin
- , Oliver Drechsel
- , Ruben M. Drews
- , Serge Serge
- , Tim Dudderidge
- , Ana Dueso-Barroso
- , Andrew J. Dunford
- , Michael Dunn
- , Lewis Jonathan Dursi
- , Fraser R. Duthie
- , Ken Dutton-Regester
- , Jenna Eagles
- , Douglas F. Easton
- , Stuart Edmonds
- , Paul A. Edwards
- , Sandra E. Edwards
- , Rosalind A. Eeles
- , Anna Ehinger
- , Juergen Eils
- , Roland Eils
- , Adel El-Naggar
- , Matthew Eldridge
- , Kyle Ellrott

- , Serap Erkek
- , Georgia Escaramis
- , Shadrielle M. G. Espiritu
- , Xavier Estivill
- , Dariush Etemadmoghadam
- , Jorunn E. Eyfjord
- , Bishoy M. Faltas
- , Daiming Fan
- , Yu Fan
- , William C. Faquin
- , Claudiu Farcas
- , Matteo Fassan
- , Aquila Fatima
- , Francesco Favero
- , Nodirjon Fayzullaev
- , Ina Felau
- , Sian Fereday
- , Martin L. Ferguson
- , Vincent Ferretti
- , Lars Feuerbach
- , Matthew A. Field
- , J. Lynn Fink
- , Gaetano Finocchiaro
- , Cyril Fisher
- , Matthew W. Fittall
- , Anna Fitzgerald
- , Rebecca C. Fitzgerald
- , Adrienne M. Flanagan
- , Neil E. Fleshner
- , Paul Flicek
- , John A. Foekens
- , Kwun M. Fong
- , Nuno A. Fonseca
- , Christopher S. Foster
- , Natalie S. Fox
- , Michael Fraser
- , Scott Frazer

- , Milana Frenkel-Morgenstern
- , William Friedman
- , Joan Frigola
- , Catrina C. Fronick
- , Akihiro Fujimoto
- , Masashi Fujita
- , Masashi Fukayama
- , Lucinda A. Fulton
- , Robert S. Fulton
- , Mayuko Furuta
- , P. Andrew Futreal
- , Anja Füllgrabe
- , Stacey B. Gabriel
- , Steven Gallinger
- , Carlo Gambacorti-Passerini
- , Jianjiong Gao
- , Shengjie Gao
- , Levi Garraway
- , Øystein Garred
- , Erik Garrison
- , Dale W. Garsed
- , Nils Gehlenborg
- , Josep L. L. Gelpi
- , Joshy George
- , Daniela S. Gerhard
- , Clarissa Gerhauser
- , Jeffrey E. Gershenwald
- , Mark Gerstein
- , Moritz Gerstung
- , Gad Getz
- , Mohammed Ghori
- , Ronald Ghossein
- , Nasra H. Giama
- , Richard A. Gibbs
- , Bob Gibson
- , Anthony J. Gill
- , Pelvender Gill

- , Dilip D. Giri
- , Dominik Glodzik
- , Vincent J. Gnanapragasam
- , Maria Elisabeth Goebler
- , Mary J. Goldman
- , Carmen Gomez
- , Santiago Gonzalez
- , Abel Gonzalez-Perez
- , Dmitry A. Gordenin
- , James Gossage
- , Kunihito Gotoh
- , Ramaswamy Govindan
- , Dorthe Grabau
- , Janet S. Graham
- , Robert C. Grant
- , Anthony R. Green
- , Eric Green
- , Liliana Greger
- , Nicola Grehan
- , Sonia Grimaldi
- , Sean M. Grimmond
- , Robert L. Grossman
- , Adam Grundhoff
- , Gunes Gundem
- , Qianyun Guo
- , Manaswi Gupta
- , Shailja Gupta
- , Ivo G. Gut
- , Marta Gut
- , Jonathan Göke
- , Gavin Ha
- , Andrea Haake
- , David Haan
- , Siegfried Haas
- , Kerstin Haase
- , James E. Haber
- , Nina Habermann

- , Faraz Hach
- , Syed Haider
- , Natsuko Hama
- , Freddie C. Hamdy
- , Anne Hamilton
- , Mark P. Hamilton
- , Leng Han
- , George B. Hanna
- , Martin Hansmann
- , Nicholas J. Haradhvala
- , Olivier Harismendy
- , Ivon Harliwong
- , Arif O. Harmanci
- , Eoghan Harrington
- , Takanori Hasegawa
- , David Haussler
- , Steve Hawkins
- , Shinya Hayami
- , Shuto Hayashi
- , D. Neil Hayes
- , Stephen J. Hayes
- , Nicholas K. Hayward
- , Steven Hazell
- , Yao He
- , Allison P. Heath
- , Simon C. Heath
- , David Hedley
- , Apurva M. Hegde
- , David I. Heiman
- , Michael C. Heinold
- , Zachary Heins
- , Lawrence E. Heisler
- , Eva Hellstrom-Lindberg
- , Mohamed Helmy
- , Seong Gu Heo
- , Austin J. Hepperla
- , José María Heredia-Genestar

- , Carl Herrmann
- , Peter Hersey
- , Julian M. Hess
- , Holmfridur Hilmarsdottir
- , Jonathan Hinton
- , Satoshi Hirano
- , Nobuyoshi Hiraoka
- , Katherine A. Hoadley
- , Asger Hobolth
- , Ermin Hodzic
- , Jessica I. Hoell
- , Steve Hoffmann
- , Oliver Hofmann
- , Andrea Holbrook
- , Aliaksei Z. Holik
- , Michael A. Hollingsworth
- , Oliver Holmes
- , Robert A. Holt
- , Chen Hong
- , Eun Pyo Hong
- , Jongwhi H. Hong
- , Gerrit K. Hooijer
- , Henrik Hornshøj
- , Fumie Hosoda
- , Yong Hou
- , Volker Hovestadt
- , William Howat
- , Alan P. Hoyle
- , Ralph H. Hruban
- , Jianhong Hu
- , Taobo Hu
- , Xing Hua
- , Kuan-lin Huang
- , Mei Huang
- , Mi Ni Huang
- , Vincent Huang
- , Yi Huang

- , Wolfgang Huber
- , Thomas J. Hudson
- , Michael Hummel
- , Jillian A. Hung
- , David Huntsman
- , Ted R. Hupp
- , Jason Huse
- , Matthew R. Huska
- , Barbara Hutter
- , Carolyn M. Hutter
- , Daniel Hübschmann
- , Christine A. Iacobuzio-Donahue
- , Charles David Imbusch
- , Marcin Imielinski
- , Seiya Imoto
- , William B. Isaacs
- , Keren Isaev
- , Shumpei Ishikawa
- , Murat Iskar
- , S. M. Ashiqul Islam
- , Michael Ittmann
- , Sinisa Ivkovic
- , Jose M. G. Izarzugaza
- , Jocelyne Jacquemier
- , Valerie Jakrot
- , Nigel B. Jamieson
- , Gun Ho Jang
- , Se Jin Jang
- , Joy C. Jayaseelan
- , Reyka Jayasinghe
- , Stuart R. Jefferys
- , Karine Jegalian
- , Jennifer L. Jennings
- , Seung-Hyup Jeon
- , Lara Jerman
- , Yuan Ji
- , Wei Jiao

- , Peter A. Johansson
- , Amber L. Johns
- , Jeremy Johns
- , Rory Johnson
- , Todd A. Johnson
- , Clemency Jolly
- , Yann Joly
- , Jon G. Jonasson
- , Corbin D. Jones
- , David R. Jones
- , David T. W. Jones
- , Nic Jones
- , Steven J. M. Jones
- , Jos Jonkers
- , Young Seok Ju
- , Hartmut Juhl
- , Jongsun Jung
- , Malene Juul
- , Randi Istrup Juul
- , Sissel Juul
- , Natalie Jäger
- , Rolf Kabbe
- , Andre Kahles
- , Abdullah Kahraman
- , Vera B. Kaiser
- , Hojabr Kakavand
- , Sangeetha Kalimuthu
- , Christof von Kalle
- , Koo Jeong Kang
- , Katalin Karaszi
- , Beth Karlan
- , Rosa Karlić
- , Dennis Karsch
- , Katayoon Kasaian
- , Karin S. Kassahn
- , Hitoshi Katai
- , Mamoru Kato

- , Hiroto Katoh
- , Yoshiiku Kawakami
- , Jonathan D. Kay
- , Stephen H. Kazakoff
- , Marat D. Kazanov
- , Maria Keays
- , Electron Kebebew
- , Richard F. Kefford
- , Manolis Kellis
- , James G. Kench
- , Catherine J. Kennedy
- , Jules N. A. Kerssemakers
- , David Khoo
- , Vincent Khoo
- , Narong Khuntikeo
- , Ekta Khurana
- , Helena Kilpinen
- , Hark Kyun Kim
- , Hyung-Lae Kim
- , Hyung-Yong Kim
- , Hyunghwan Kim
- , Jaegil Kim
- , Jihoon Kim
- , Jong K. Kim
- , Youngwook Kim
- , Tari A. King
- , Wolfram Klapper
- , Kortine Kleinheinz
- , Leszek J. Klimczak
- , Stian Knappskog
- , Michael Kneba
- , Bartha M. Knoppers
- , Youngil Koh
- , Jan Komorowski
- , Daisuke Komura
- , Mitsuhiro Komura
- , Gu Kong

- , Marcel Kool
- , Jan O. Korbel
- , Viktoriya Korchina
- , Andrey Korshunov
- , Michael Koscher
- , Roelof Koster
- , Zsofia Kote-Jarai
- , Antonios Koures
- , Milena Kovacevic
- , Barbara Kremeyer
- , Helene Kretzmer
- , Markus Kreuz
- , Savitri Krishnamurthy
- , Dieter Kube
- , Kiran Kumar
- , Pardeep Kumar
- , Sushant Kumar
- , Yogesh Kumar
- , Ritika Kundra
- , Kirsten Kübler
- , Ralf Küppers
- , Jesper Lagergren
- , Phillip H. Lai
- , Peter W. Laird
- , Sunil R. Lakhani
- , Christopher M. Lalansingh
- , Emilie Lalonde
- , Fabien C. Lamaze
- , Adam Lambert
- , Eric Lander
- , Pablo Landgraf
- , Luca Landoni
- , Anita Langerød
- , Andrés Lanzós
- , Denis Larsimont
- , Erik Larsson
- , Mark Lathrop

- , Loretta M. S. Lau
- , Chris Lawerenz
- , Rita T. Lawlor
- , Michael S. Lawrence
- , Alexander J. Lazar
- , Ana Mijalkovic Lazic
- , Xuan Le
- , Darlene Lee
- , Donghoon Lee
- , Eunjung Alice Lee
- , Hee Jin Lee
- , Jake June-Koo Lee
- , Jeong-Yeon Lee
- , Juhee Lee
- , Ming Ta Michael Lee
- , Henry Lee-Six
- , Kjong-Van Lehmann
- , Hans Lehrach
- , Dido Lenze
- , Conrad R. Leonard
- , Daniel A. Leongamornlert
- , Ignaty Leshchiner
- , Louis Letourneau
- , Ivica Letunic
- , Douglas A. Levine
- , Lora Lewis
- , Tim Ley
- , Chang Li
- , Constance H. Li
- , Haiyan Irene Li
- , Jun Li
- , Lin Li
- , Shantao Li
- , Siliang Li
- , Xiaobo Li
- , Xiaotong Li
- , Xinyue Li

- , Yilong Li
- , Han Liang
- , Sheng-Ben Liang
- , Peter Lichter
- , Pei Lin
- , Ziao Lin
- , W. M. Linehan
- , Ole Christian Lingjærde
- , Dongbing Liu
- , Eric Minwei Liu
- , Fei-Fei Fei Liu
- , Fenglin Liu
- , Jia Liu
- , Xingmin Liu
- , Julie Livingstone
- , Dimitri Livitz
- , Naomi Livni
- , Lucas Lochovsky
- , Markus Loeffler
- , Georgina V. Long
- , Armando Lopez-Guillermo
- , Shaoke Lou
- , David N. Louis
- , Laurence B. Lovat
- , Yiling Lu
- , Yong-Jie Lu
- , Youyong Lu
- , Claudio Luchini
- , Ilinca Lungu
- , Xuemei Luo
- , Hayley J. Luxton
- , Andy G. Lynch
- , Lisa Lype
- , Cristina López
- , Carlos López-Otín
- , Eric Z. Ma
- , Yussanne Ma

- , Gaetan MacGrogan
- , Shona MacRae
- , Geoff Macintyre
- , Tobias Madsen
- , Kazuhiro Maejima
- , Andrea Mafficini
- , Dennis T. Maglinte
- , Arindam Maitra
- , Partha P. Majumder
- , Luca Malcovati
- , Salem Malikic
- , Giuseppe Malleo
- , Graham J. Mann
- , Luisa Mantovani-Löffler
- , Kathleen Marchal
- , Giovanni Marchegiani
- , Elaine R. Mardis
- , Adam A. Margolin
- , Maximillian G. Marin
- , Florian Markowetz
- , Julia Markowski
- , Jeffrey Marks
- , Tomas Marques-Bonet
- , Marco A. Marra
- , Luke Marsden
- , John W. M. Martens
- , Sancha Martin
- , Jose I. Martin-Subero
- , Iñigo Martincorena
- , Alexander Martinez-Fundichely
- , Yosef E. Maruvka
- , R. Jay Mashl
- , Charlie E. Massie
- , Thomas J. Matthew
- , Lucy Matthews
- , Erik Mayer
- , Simon Mayes

- , Michael Mayo
- , Faridah Mbabaali
- , Karen McCune
- , Ultan McDermott
- , Patrick D. McGillivray
- , Michael D. McLellan
- , John D. McPherson
- , John R. McPherson
- , Treasa A. McPherson
- , Samuel R. Meier
- , Alice Meng
- , Shaowu Meng
- , Andrew Menzies
- , Neil D. Merrett
- , Sue Merson
- , Matthew Meyerson
- , William Meyerson
- , Piotr A. Mieczkowski
- , George L. Mihaiescu
- , Sanja Mijalkovic
- , Tom Mikkelsen
- , Michele Milella
- , Linda Mileshkin
- , Christopher A. Miller
- , David K. Miller
- , Jessica K. Miller
- , Gordon B. Mills
- , Ana Milovanovic
- , Sarah Minner
- , Marco Miotto
- , Gisela Mir Arnau
- , Lisa Mirabello
- , Chris Mitchell
- , Thomas J. Mitchell
- , Satoru Miyano
- , Naoki Miyoshi
- , Shinichi Mizuno

- , Fruzsina Molnár-Gábor
- , Malcolm J. Moore
- , Richard A. Moore
- , Sandro Morganella
- , Quaid D. Morris
- , Carl Morrison
- , Lisle E. Mose
- , Catherine D. Moser
- , Ferran Muiños
- , Loris Mularoni
- , Andrew J. Mungall
- , Karen Mungall
- , Elizabeth A. Musgrove
- , Ville Mustonen
- , David Mutch
- , Francesc Muyas
- , Donna M. Muzny
- , Alfonso Muñoz
- , Jerome Myers
- , Ola Myklebost
- , Peter Möller
- , Genta Nagae
- , Adnan M. Nagrial
- , Hardeep K. Nahal-Bose
- , Hitoshi Nakagama
- , Hidewaki Nakagawa
- , Hiromi Nakamura
- , Toru Nakamura
- , Kaoru Nakano
- , Tannistha Nandi
- , Jyoti Nangalia
- , Mia Nastic
- , Arcadi Navarro
- , Fabio C. P. Navarro
- , David E. Neal
- , Gerd Nettekoven
- , Felicity Newell

- , Steven J. Newhouse
- , Yulia Newton
- , Alvin Wei Tian Ng
- , Anthony Ng
- , Jonathan Nicholson
- , David Nicol
- , Yongzhan Nie
- , G. Petur Nielsen
- , Morten Muhlig Nielsen
- , Serena Nik-Zainal
- , Michael S. Noble
- , Katia Nones
- , Paul A. Northcott
- , Faiyaz Notta
- , Brian D. O'Connor
- , Peter O'Donnell
- , Maria O'Donovan
- , Sarah O'Meara
- , Brian Patrick O'Neill
- , J. Robert O'Neill
- , David Ocana
- , Angelica Ochoa
- , Layla Oesper
- , Christopher Ogden
- , Hideki Ohdan
- , Kazuhiro Ohi
- , Lucila Ohno-Machado
- , Karin A. Oien
- , Akinyemi I. Ojesina
- , Hidenori Ojima
- , Takuji Okusaka
- , Larsson Omberg
- , Choon Kiat Ong
- , Stephan Ossowski
- , German Ott
- , B. F. Francis Ouellette
- , Christine P'ng

- , Marta Paczkowska
- , Salvatore Paiella
- , Chawalit Pairojkul
- , Marina Pajic
- , Qiang Pan-Hammarström
- , Elli Papaemmanuil
- , Irene Papatheodorou
- , Nagarajan Paramasivam
- , Ji Wan Park
- , Joong-Won Park
- , Keunchil Park
- , Kiejung Park
- , Peter J. Park
- , Joel S. Parker
- , Simon L. Parsons
- , Harvey Pass
- , Danielle Pasternack
- , Alessandro Pastore
- , Ann-Marie Patch
- , Iris Pauporté
- , Antonio Pea
- , John V. Pearson
- , Chandra Sekhar Pedamallu
- , Jakob Skou Pedersen
- , Paolo Pederzoli
- , Martin Peifer
- , Nathan A. Pennell
- , Charles M. Perou
- , Marc D. Perry
- , Gloria M. Petersen
- , Myron Peto
- , Nicholas Petrelli
- , Robert Petryszak
- , Stefan M. Pfister
- , Mark Phillips
- , Oriol Pich
- , Hilda A. Pickett

- , Todd D. Pihl
- , Nischalan Pillay
- , Sarah Pinder
- , Mark Pinese
- , Andreia V. Pinho
- , Esa Pitkänen
- , Xavier Pivot
- , Elena Piñeiro-Yáñez
- , Laura Planko
- , Christoph Plass
- , Paz Polak
- , Tirso Pons
- , Irinel Popescu
- , Olga Potapova
- , Aparna Prasad
- , Shaun R. Preston
- , Manuel Prinz
- , Antonia L. Pritchard
- , Stephenie D. Prokopec
- , Elena Provenzano
- , Xose S. Puente
- , Sonia Puig
- , Montserrat Puiggròs
- , Sergio Pulido-Tamayo
- , Gulietta M. Pupo
- , Colin A. Purdie
- , Michael C. Quinn
- , Raquel Rabionet
- , Janet S. Rader
- , Bernhard Radlwimmer
- , Petar Radovic
- , Benjamin Raeder
- , Keiran M. Raine
- , Manasa Ramakrishna
- , Kamna Ramakrishnan
- , Suresh Ramalingam
- , Benjamin J. Raphael

- , W. Kimryn Rathmell
- , Tobias Rausch
- , Guido Reifenberger
- , Jüri Reimand
- , Jorge Reis-Filho
- , Victor Reuter
- , Iker Reyes-Salazar
- , Matthew A. Reyna
- , Sheila M. Reynolds
- , Esther Rheinbay
- , Yasser Riazalhosseini
- , Andrea L. Richardson
- , Julia Richter
- , Matthew Ringel
- , Markus Ringnér
- , Yasushi Rino
- , Karsten Rippe
- , Jeffrey Roach
- , Lewis R. Roberts
- , Nicola D. Roberts
- , Steven A. Roberts
- , A. Gordon Robertson
- , Alan J. Robertson
- , Javier Bartolomé Rodriguez
- , Bernardo Rodriguez-Martin
- , F. Germán Rodríguez-González
- , Michael H. A. Roehrl
- , Marius Rohde
- , Hirofumi Rokutan
- , Gilles Romieu
- , Ilse Rooman
- , Tom Roques
- , Daniel Rosebrock
- , Mara Rosenberg
- , Philip C. Rosenstiel
- , Andreas Rosenwald
- , Edward W. Rowe

- , Romina Royo
- , Steven G. Rozen
- , Yulia Rubanova
- , Mark A. Rubin
- , Carlota Rubio-Perez
- , Vasilisa A. Rudneva
- , Borislav C. Rusev
- , Andrea Ruzzenente
- , Gunnar Rätsch
- , Radhakrishnan Sabarinathan
- , Veronica Y. Sabelnykova
- , Sara Sadeghi
- , S. Cenk Sahinalp
- , Natalie Saini
- , Mihoko Saito-Adachi
- , Gordon Saksena
- , Adriana Salcedo
- , Roberto Salgado
- , Leonidas Salichos
- , Richard Sallari
- , Charles Saller
- , Roberto Salvia
- , Michelle Sam
- , Jaswinder S. Samra
- , Francisco Sanchez-Vega
- , Chris Sander
- , Grant Sanders
- , Rajiv Sarin
- , Iman Sarrafi
- , Aya Sasaki-Oku
- , Torill Sauer
- , Guido Sauter
- , Robyn P. M. Saw
- , Maria Scardoni
- , Christopher J. Scarlett
- , Aldo Scarpa
- , Ghislaine Scelo

- , Dirk Schadendorf
- , Jacqueline E. Schein
- , Markus B. Schilhabel
- , Matthias Schlesner
- , Thorsten Schlomm
- , Heather K. Schmidt
- , Sarah-Jane Schramm
- , Stefan Schreiber
- , Nikolaus Schultz
- , Steven E. Schumacher
- , Roland F. Schwarz
- , Richard A. Scolyer
- , David Scott
- , Ralph Scully
- , Raja Seethala
- , Ayellet V. Segre
- , Iris Selander
- , Colin A. Semple
- , Yasin Senbabaoglu
- , Subhajit Sengupta
- , Elisabetta Sereni
- , Stefano Serra
- , Dennis C. Sgroi
- , Mark Shackleton
- , Nimish C. Shah
- , Sagedeh Shahabi
- , Catherine A. Shang
- , Ping Shang
- , Ofer Shapira
- , Troy Shelton
- , Ciyue Shen
- , Hui Shen
- , Rebecca Shepherd
- , Ruian Shi
- , Yan Shi
- , Yu-Jia Shiah
- , Tatsuhiro Shibata

- , Juliann Shih
- , Eigo Shimizu
- , Kiyo Shimizu
- , Seung Jun Shin
- , Yuichi Shiraishi
- , Tal Shmaya
- , Ilya Shmulevich
- , Solomon I. Shorser
- , Charles Short
- , Raunak Shrestha
- , Suyash S. Shringarpure
- , Craig Shriver
- , Shimin Shuai
- , Nikos Sidiropoulos
- , Reiner Siebert
- , Anieta M. Sieuwerts
- , Lina Sieverling
- , Sabina Signoretti
- , Katarzyna O. Sikora
- , Michele Simbolo
- , Ronald Simon
- , Janae V. Simons
- , Jared T. Simpson
- , Peter T. Simpson
- , Samuel Singer
- , Nasa Sinnott-Armstrong
- , Payal Sipahimalani
- , Tara J. Skelly
- , Marcel Smid
- , Jaclyn Smith
- , Karen Smith-McCune
- , Nicholas D. Socci
- , Heidi J. Sofia
- , Matthew G. Soloway
- , Lei Song
- , Anil K. Sood
- , Sharmila Sothi

- , Christos Sotiriou
- , Cameron M. Soulette
- , Paul N. Span
- , Paul T. Spellman
- , Nicola Sperandio
- , Andrew J. Spillane
- , Oliver Spiro
- , Jonathan Spring
- , Johan Staaf
- , Peter F. Stadler
- , Peter Staib
- , Stefan G. Stark
- , Lucy Stebbings
- , Ólafur Andri Stefánsson
- , Oliver Stegle
- , Lincoln D. Stein
- , Alasdair Stenhouse
- , Chip Stewart
- , Stephan Stilgenbauer
- , Miranda D. Stobbe
- , Michael R. Stratton
- , Jonathan R. Stretch
- , Adam J. Struck
- , Joshua M. Stuart
- , Henk G. Stunnenberg
- , Hong Su
- , Xiaoping Su
- , Ren X. Sun
- , Stephanie Sungalee
- , Hana Susak
- , Akihiro Suzuki
- , Fred Sweep
- , Monika Szczepanowski
- , Holger Sültmann
- , Takashi Yugawa
- , Angela Tam
- , David Tamborero

- , Benita Kiat Tee Tan
- , Donghui Tan
- , Patrick Tan
- , Hiroko Tanaka
- , Hirokazu Taniguchi
- , Tomas J. Tanskanen
- , Maxime Tarabichi
- , Roy Tarnuzzer
- , Patrick Tarpey
- , Morgan L. Taschuk
- , Kenji Tatsuno
- , Simon Tavaré
- , Darrin F. Taylor
- , Amaro Taylor-Weiner
- , Jon W. Teague
- , Bin Tean Teh
- , Varsha Tembe
- , Javier Temes
- , Kevin Thai
- , Sarah P. Thayer
- , Nina Thiessen
- , Gilles Thomas
- , Sarah Thomas
- , Alan Thompson
- , Alastair M. Thompson
- , John F. F. Thompson
- , R. Houston Thompson
- , Heather Thorne
- , Leigh B. Thorne
- , Adrian Thorogood
- , Grace Tiao
- , Nebojsa Tijanic
- , Lee E. Timms
- , Roberto Tirabosco
- , Marta Tojo
- , Stefania Tommasi
- , Christopher W. Toon

- , Umut H. Toprak
- , David Torrents
- , Giampaolo Tortora
- , Jörg Tost
- , Yasushi Totoki
- , David Townend
- , Nadia Traficante
- , Isabelle Treilleux
- , Jean-Rémi Trotta
- , Lorenz H. P. Trümper
- , Ming Tsao
- , Tatsuhiko Tsunoda
- , Jose M. C. Tubio
- , Olga Tucker
- , Richard Turkington
- , Daniel J. Turner
- , Andrew Tutt
- , Masaki Ueno
- , Naoto T. Ueno
- , Christopher Umbricht
- , Husen M. Umer
- , Timothy J. Underwood
- , Lara Urban
- , Tomoko Urushidate
- , Tetsuo Ushiku
- , Liis Uusküla-Reimand
- , Alfonso Valencia
- , David J. Van Den Berg
- , Steven Van Laere
- , Peter Van Loo
- , Erwin G. Van Meir
- , Gert G. Van den Eynden
- , Theodorus Van der Kwast
- , Naveen Vasudev
- , Miguel Vazquez
- , Ravikiran Vedururu
- , Umadevi Veluvolu

- , Shankar Vembu
- , Lieven P. C. Verbeke
- , Peter Vermeulen
- , Clare Verrill
- , Alain Viari
- , David Vicente
- , Caterina Vicentini
- , K. VijayRaghavan
- , Juris Viksna
- , Ricardo E. Vilain
- , Izar Villasante
- , Anne Vincent-Salomon
- , Tapio Visakorpi
- , Douglas Voet
- , Paresh Vyas
- , Ignacio Vázquez-García
- , Nick M. Waddell
- , Nicola Waddell
- , Claes Wadelius
- , Lina Wadi
- , Rabea Wagener
- , Jeremiah A. Wala
- , Jian Wang
- , Jiayin Wang
- , Linghua Wang
- , Qi Wang
- , Wenyi Wang
- , Yumeng Wang
- , Zhining Wang
- , Paul M. Waring
- , Hans-Jörg Warnatz
- , Jonathan Warrell
- , Anne Y. Warren
- , Sebastian M. Waszak
- , David C. Wedge
- , Dieter Weichenhan
- , Paul Weinberger

- , John N. Weinstein
- , Joachim Weischenfeldt
- , Daniel J. Weisenberger
- , Ian Welch
- , Michael C. Wendl
- , Johannes Werner
- , Justin P. Whalley
- , David A. Wheeler
- , Hayley C. Whitaker
- , Dennis Wigle
- , Matthew D. Wilkerson
- , Ashley Williams
- , James S. Wilmott
- , Gavin W. Wilson
- , Julie M. Wilson
- , Richard K. Wilson
- , Boris Winterhoff
- , Jeffrey A. Wintersinger
- , Maciej Wiznerowicz
- , Stephan Wolf
- , Bernice H. Wong
- , Tina Wong
- , Winghing Wong
- , Youngchoon Woo
- , Scott Wood
- , Bradly G. Wouters
- , Adam J. Wright
- , Derek W. Wright
- , Mark H. Wright
- , Chin-Lee Wu
- , Dai-Ying Wu
- , Guanming Wu
- , Jianmin Wu
- , Kui Wu
- , Yang Wu
- , Zhenggang Wu
- , Liu Xi

- , Tian Xia
- , Qian Xiang
- , Xiao Xiao
- , Rui Xing
- , Heng Xiong
- , Qinying Xu
- , Yanxun Xu
- , Hong Xue
- , Shinichi Yachida
- , Sergei Yakneen
- , Rui Yamaguchi
- , Takafumi N. Yamaguchi
- , Masakazu Yamamoto
- , Shogo Yamamoto
- , Hiroki Yamaue
- , Fan Yang
- , Huanming Yang
- , Jean Y. Yang
- , Liming Yang
- , Lixing Yang
- , Shanlin Yang
- , Tsun-Po Yang
- , Yang Yang
- , Xiaotong Yao
- , Marie-Laure Yaspo
- , Lucy Yates
- , Christina Yau
- , Chen Ye
- , Kai Ye
- , Venkata D. Yellapantula
- , Christopher J. Yoon
- , Sung-Soo Yoon
- , Fouad Yousif
- , Jun Yu
- , Kaixian Yu
- , Willie Yu
- , Yingyan Yu

- , Ke Yuan
- , Yuan Yuan
- , Denis Yuen
- , Takashi Yugawa
- , Christina K. Yung
- , Olga Zaikova
- , Jorge Zamora
- , Marc Zapatka
- , Jean C. Zenklusen
- , Thorsten Zenz
- , Nikolajs Zeps
- , Cheng-Zhong Zhang
- , Fan Zhang
- , Hailei Zhang
- , Hongwei Zhang
- , Hongxin Zhang
- , Jiashan Zhang
- , Jing Zhang
- , Junjun Zhang
- , Xiuqing Zhang
- , Xuanping Zhang
- , Yan Zhang
- , Zemin Zhang
- , Zhongming Zhao
- , Liangtao Zheng
- , Xiuqing Zheng
- , Wanding Zhou
- , Yong Zhou
- , Bin Zhu
- , Hongtu Zhu
- , Jingchun Zhu
- , Shida Zhu
- , Lihua Zou
- , Xueqing Zou
- , Anna deFazio
- , Nicholas van As
- , Carolien H. M. van Deurzen

- , Marc J. van de Vijver
- , L. van’t Veer
- & Christian von Mering

Corresponding authors

Correspondence to Alvis Brazma, Angela N. Brooks or Gunnar Rätsch.

Rights and permissions

Open Access This article is licensed under a Creative Commons Attribution 4.0 International License, which permits use, sharing, adaptation, distribution and reproduction in any medium or format, as long as you give appropriate credit to the original author(s) and the source, provide a link to the Creative Commons license, and indicate if changes were made. The images or other third party material in this article are included in the article’s Creative Commons license, unless indicated otherwise in a credit line to the material. If material is not included in the article’s Creative Commons license and your intended use is not permitted by statutory regulation or exceeds the permitted use, you will need to obtain permission directly from the copyright holder. To view a copy of this license, visit http://creativecommons.org/licenses/by/4.0/.

Reprints and Permissions

About this article

Cite this article

PCAWG Transcriptome Core Group., Calabrese, C., Davidson, N.R. *et al.* Author Correction: Genomic basis for RNA alterations in cancer. *Nature* **614**, E37 (2023). https://doi.org/10.1038/s41586-022-05596-y

- Published: 25 January 2023

- Issue Date: 16 February 2023

- DOI: https://doi.org/10.1038/s41586-022-05596-y

Share this article

Anyone you share the following link with will be able to read this content:

Get shareable link

Sorry, a shareable link is not currently available for this article.

Copy to clipboard

Provided by the Springer Nature SharedIt content-sharing initiative

---

This article was downloaded by **calibre** from https://www.nature.com/articles/s41586-022-05596-y

- Author Correction
- Open Access
- Published: 25 January 2023

Author Correction: Patterns of somatic structural variation in human cancer genomes

- Yilong Li,
- Nicola D. Roberts,
- Jeremiah A. Wala,
- Ofer Shapira,
- Steven E. Schumacher,
- Kiran Kumar,
- Ekta Khurana,
- Sebastian Waszak,
- Jan O. Korbel,
- James E. Haber,
- Marcin Imielinski,
- PCAWG Structural Variation Working Group,
- Joachim Weischenfeldt ,
- Rameen Beroukhim ,
- Peter J. Campbell &
- PCAWG Consortium

Show authors

Nature **volume 614**, page E38 (2023)

- 777 Accesses

- 1 Altmetric

- Metrics details

The Original Article was published on 05 February 2020

Correction to: *Nature* https://doi.org/10.1038/s41586-019-1913-9 Published online 5 February 2020

In the published version of this paper, the members of the Pan-Cancer Analysis of Whole Genomes (PCAWG) Consortium were listed in the Supplementary Information; however, these members should have been included in the main paper. The original Article has been corrected to include the members and affiliations of the PCAWG Consortium in the main paper; the corrections have been made to the HTML version of the Article but not the PDF version. Additional minor corrections to affiliations have been made to the PDF and HTML versions of the original Article for consistency of information between the PCAWG list and the main paper.

Author information

Author notes

1. These authors contributed equally: Yilong Li, Nicola D. Roberts, Jeremiah A. Wala, Ofer Shapira

2. A list of members and their affiliations appears at the end of the paper

3. A list of members and their affiliations appears online

Authors and Affiliations

1. Cancer Genome Project, Wellcome Trust Sanger Institute, Hinxton, UK

   Yilong Li, Nicola D. Roberts, Peter J. Campbell, Young Seok Ju, Yilong Li, Iñigo Martincorena, Nicola D. Roberts, Jorge Zamora & Peter J. Campbell

2. Totient Inc, Cambridge, MA, USA

Yilong Li & Yilong Li

3. The Broad Institute of Harvard and MIT, Cambridge, MA, USA

Jeremiah A. Wala, Ofer Shapira, Steven E. Schumacher, Kiran Kumar, Rameen Beroukhim, Andrew J. Dunford, Julian M. Hess, Kiran Kumar, Matthew Meyerson, Steven E. Schumacher, Chip Stewart, Jeremiah A. Wala, Cheng-Zhong Zhang & Rameen Beroukhim

4. Bioinformatics and Integrative Genomics, Harvard University, Cambridge, MA, USA

Jeremiah A. Wala, Ofer Shapira, Steven E. Schumacher, Kiran Kumar, Rameen Beroukhim, Matthew Meyerson, Steven E. Schumacher, Jeremiah A. Wala, Cheng-Zhong Zhang & Rameen Beroukhim

5. Department of Cancer Biology, Dana-Farber Cancer Institute, Boston, MA, USA

Jeremiah A. Wala, Ofer Shapira, Steven E. Schumacher, Kiran Kumar, Rameen Beroukhim, Steven E. Schumacher, Jeremiah A. Wala & Rameen Beroukhim

6. Weill Cornell Medical College, New York, NY, USA

Ekta Khurana & Marcin Imielinski

7. European Molecular Biology Laboratory, Genome Biology Unit, Heidelberg, Germany

Sebastian Waszak, Jan O. Korbel & Jan O. Korbel

8. Department of Molecular Biology, Rosenstiel Basic Medical Sciences Research Center, Brandeis University, Waltham, MA, USA

James E. Haber & James E. Haber

9. New York Genome Center, New York, NY, USA

Marcin Imielinski, Marcin Imielinski & Xiaotong Yao

10. Biotech Research & Innovation Centre (BRIC), The Finsen Laboratory, Rigshospitalet, University of Copenhagen, Copenhagen, Denmark

Nikos Sidiropoulos, Joachim Weischenfeldt & Joachim Weischenfeldt

11. Department of Haematology, University of Cambridge, Cambridge, UK

Peter J. Campbell & Peter J. Campbell

12. University of Texas MD Anderson Cancer Center, Houston, TX, USA

Kadir C. Akdemir & Ken Chen

13. Department of Zoology, Genetics and Physical Anthropology, University of Santiago de Compostela, Santiago de Compostela, Spain

Eva G. Alvarez, Bernardo Rodriguez-Martin, Jose M. C. Tubio & Jorge Zamora

14. Centre for Research in Molecular Medicine and Chronic Diseases (CIMUS), University of Santiago de Compostela, Santiago de Compostela, Spain

Eva G. Alvarez, Bernardo Rodriguez-Martin, Jose M. C. Tubio & Jorge Zamora

15. The Biomedical Research Centre (CINBIO), University of Vigo, Vigo, Spain

Eva G. Alvarez, Bernardo Rodriguez-Martin, Jose M. C. Tubio & Jorge Zamora

16. Transmissible Cancer Group, Department of Veterinary Medicine, University of Cambridge, Cambridge, UK

Adrian Baez-Ortega

17. Computational Biology Program, Ontario Institute for Cancer Research, Toronto, Ontario, Canada

Paul C. Boutros

18. Department of Medical Biophysics, University of Toronto, Toronto, Ontario, Canada

Paul C. Boutros

19. Department of Pharmacology, University of Toronto, Toronto, Ontario, Canada

Paul C. Boutros

20. University of California Los Angeles, Los Angeles, CA, USA

Paul C. Boutros

21. Peter MacCallum Cancer Centre, Melbourne, Victoria, Australia

David D. L. Bowtell, Dariush Etemadmoghadam, Dale W. Garsed & Mark Shackleton

22. Sir Peter MacCallum Department of Oncology, University of Melbourne, Melbourne, Victoria, Australia

David D. L. Bowtell & Mark Shackleton

23. National Center for Tumor Diseases (NCT) Heidelberg, Heidelberg, Germany

Benedikt Brors & Barbara Hutter

24. Division of Applied Bioinformatics, German Cancer Research Center (DKFZ), Heidelberg, Germany

Benedikt Brors, Lars Feuerbach & Lina Sieverling

25. German Cancer Genome Consortium (DKTK), Heidelberg, Germany

Benedikt Brors & Barbara Hutter

26. Johns Hopkins School of Medicine, Baltimore, MD, USA

Kathleen H. Burns

27. Faculty of Medicine, Department of Biochemistry, Microbiology and Immunology, University of Ottawa, Ottawa, Ontario, Canada

Kin Chan

28. Centre for Molecular Science Informatics, Department of Chemistry, University of Cambridge, Cambridge, UK

Isidro Cortés-Ciriano

29. Department of Biomedical Informatics, Harvard Medical School, Boston, MA, USA

Isidro Cortés-Ciriano, Jake June-Koo Lee & Peter J. Park

30. Ludwig Center, Harvard Medical School, Boston, MA, USA

Isidro Cortés-Ciriano, Jake June-Koo Lee & Peter J. Park

31. Barcelona Supercomputing Center (BSC), Barcelona, Spain

Ana Dueso-Barroso, J. Lynn Fink, Montserrat Puiggròs, David Torrents & Izar Villasante

32. Cancer Research UK Cambridge Institute, University of Cambridge, Cambridge, UK

Paul A. Edwards, Andy G. Lynch, Geoff Macintyre & Florian Markowetz

33. University of Cambridge, Cambridge, UK

Paul A. Edwards, Andy G. Lynch, Geoff Macintyre & Florian Markowetz

34. Sidra Medicine, Doha, Qatar

Xavier Estivill

35. Barcelona Supercomputing Center (BSC), Barcelona, Spain

Xavier Estivill

36. Queensland Centre for Medical Genomics, Institute for Molecular Bioscience, The University of Queensland, Brisbane, Queensland, Australia

J. Lynn Fink

37. The Azrieli Faculty of Medicine, Bar-Ilan University, Safed, Israel

Milana Frenkel-Morgenstern

38. Department of Computer Science, Princeton University, Princeton, NJ, USA

Mark Gerstein

39. Department of Computer Science, Yale University, New Haven, CT, USA

Mark Gerstein

40. Program in Computational Biology and Bioinformatics, Yale University, New Haven, CT, USA

Mark Gerstein

41. Genome Integrity and Structural Biology Laboratory, National Institute of Environmental Health Sciences (NIEHS), Durham, NC, USA

Dmitry A. Gordenin

42. Biomolecular Engineering Department, University of California, Santa Cruz, Santa Cruz, CA, USA

David Haan

43. Massachusetts General Hospital Center for Cancer Research, Charlestown, MA, USA

Julian M. Hess

44. Heidelberg Center for Personalized Oncology (DKFZ-HIPO), German Cancer Research Center (DKFZ), Heidelberg, Germany

Barbara Hutter

45. Hopp Children's Cancer Center (KiTZ), Heidelberg, Germany

David T. W. Jones

46. Pediatric Glioma Research Group, German Cancer Research Center (DKFZ), Heidelberg, Germany

David T. W. Jones

47. Korea Advanced Institute of Science and Technology, Daejeon, South Korea

Young Seok Ju

48. Skolkovo Institute of Science and Technology, Moscow, Russia

Marat D. Kazanov

49. A. A. Kharkevich Institute of Information Transmission Problems, Moscow, Russia

Marat D. Kazanov

50. Dmitry Rogachev National Research Center of Pediatric Hematology, Oncology and Immunology, Moscow, Russia

Marat D. Kazanov

51. Integrative Bioinformatics Support Group, National Institute of Environmental Health Sciences (NIEHS), Durham, NC, USA

Leszek J. Klimczak

52. Center For Medical Innovation, Seoul National University Hospital, Seoul, South Korea

Youngil Koh

53. Department of Internal Medicine, Seoul National University Hospital, Seoul, South Korea

Youngil Koh & Sung-Soo Yoon

54. Division of Genetics and Genomics, Harvard Medical School, Boston, MA, USA

Eunjung Alice Lee

55. Boston Children’s Hospital, Boston, MA, USA

Eunjung Alice Lee

56. School of Medicine/School of Mathematics and Statistics, University of St Andrews, St Andrews, UK

Andy G. Lynch

57. Department of Physiology and Biophysics, Weill Cornell Medicine, New York, NY, USA

Alexander Martinez-Fundichely

58. Institute for Computational Biomedicine, Weill Cornell Medicine, New York, NY, USA

Alexander Martinez-Fundichely

59. Englander Institute for Precision Medicine, Weill Cornell Medicine, New York, NY, USA

Alexander Martinez-Fundichely

60. Dana-Farber Cancer Institute, Boston, MA, USA

Matthew Meyerson & Cheng-Zhong Zhang

61. The Institute of Medical Science, The University of Tokyo, Tokyo, Japan

Satoru Miyano

62. RIKEN Center for Integrative Medical Sciences, Yokohama, Japan

Hidewaki Nakagawa

63. Department of Molecular Biophysics and Biochemistry, Yale University, New Haven, CT, USA

Fabio C. P. Navarro

64. Universitat Pompeu Fabra (UPF), Barcelona, Spain

Stephan Ossowski

65. Centre for Genomic Regulation (CRG), The Barcelona Institute of Science and Technology, Barcelona, Spain

Stephan Ossowski

66. Institute of Medical Genetics and Applied Genomics, University of Tübingen, Tübingen, Germany

Stephan Ossowski

67. Department of Genetics and Computational Biology, QIMR Berghofer Medical Research Institute, Brisbane, Queensland, Australia

John V. Pearson & Nicola Waddell

68. Institute for Molecular Bioscience, University of Queensland, Brisbane, Queensland, Australia

John V. Pearson & Nicola Waddell

69. German Cancer Research Center (DKFZ), Heidelberg, Germany

Karsten Rippe

70. School of Molecular Biosciences and Center for Reproductive Biology, Washington State University, Pullman, WA, USA

Steven A. Roberts

71. Cancer Research Institute, Beth Israel Deaconess Medical Center, Boston, MA, USA

Ralph Scully

72. Faculty of Biosciences, Heidelberg University, Heidelberg, Germany

Lina Sieverling

73. Institució Catalana de Recerca i Estudis Avançats (ICREA), Barcelona, Spain

David Torrents

74. Ben May Department for Cancer Research, Department of Human Genetics, The University of Chicago, Chicago, IL, USA

Lixing Yang

75. Tri-institutional PhD Program of Computational Biology and Medicine, Weill Cornell Medicine, New York, NY, USA

Xiaotong Yao

76. Applied Tumor Genomics Research Program, Research Programs Unit, University of Helsinki, Helsinki, Finland

Lauri A. Aaltonen

77. Wellcome Sanger Institute, Wellcome Genome Campus, Hinxton, UK

Federico Abascal, David J. Adams, Ludmil B. Alexandrov, Sam Behjati, Shriram G. Bhosle, David T. Bowen, Adam P. Butler, Peter J. Campbell, Peter Clapham, Helen Davies, Kevin J. Dawson, Stefan C. Dentro, Serge Serge, Erik Garrison, Mohammed Ghori, Dominik Glodzik, Jonathan Hinton, David R. Jones, Young Seok Ju, Stian Knappskog, Barbara Kremeyer, Henry Lee-Six, Daniel A. Leongamornlert, Yilong Li, Sancha Martin, Iñigo Martincorena, Ultan McDermott, Andrew Menzies, Thomas J. Mitchell, Sandro Morganella, Jyoti Nangalia, Jonathan Nicholson, Serena Nik-Zainal, Sarah O'Meara, Elli Papaemmanuil, Keiran M. Raine, Manasa Ramakrishna, Kamna Ramakrishnan, Nicola D. Roberts, Rebecca Shepherd, Lucy Stebbings, Michael R. Stratton, Maxime Tarabichi, Jon W. Teague, Ignacio Vázquez-García, David C. Wedge, Lucy Yates, Jorge Zamora & Xueqing Zou

78. Memorial Sloan Kettering Cancer Center, New York, NY, USA

Adam Abeshouse, Hikmat Al-Ahmadie, Gunes Gundem, Zachary Heins, Jason Huse, Douglas A. Levine, Eric Minwei Liu & Angelica Ochoa

79. Genome Science Division, Research Center for Advanced Science and Technology, University of Tokyo, Tokyo, Japan

Hiroyuki Aburatani, Genta Nagae, Akihiro Suzuki, Kenji Tatsuno & Shogo Yamamoto

80. Department of Surgery, University of Chicago, Chicago, IL, USA

Nishant Agrawal

81. Department of Surgery, Division of Hepatobiliary and Pancreatic Surgery, School of Medicine, Keimyung University Dongsan Medical Center, Daegu, South Korea

Keun Soo Ahn & Koo Jeong Kang

82. Department of Oncology, Gil Medical Center, Gachon University, Incheon, South Korea

Sung-Min Ahn

83. Hiroshima University, Hiroshima, Japan

Hiroshi Aikata, Koji Arihiro, Kazuaki Chayama, Yoshiiku Kawakami & Hideki Ohdan

84. Department of Bioinformatics and Computational Biology, The University of Texas MD Anderson Cancer Center, Houston, TX, USA

Rehan Akbani, Shaolong Cao, Yiwen Chen, Zechen Chong, Yu Fan, Jun Li, Han Liang, Wenyi Wang, Yumeng Wang & Yuan Yuan

85. University of Texas MD Anderson Cancer Center, Houston, TX, USA

Kadir C. Akdemir & Ken Chen

86. King Faisal Specialist Hospital and Research Centre, Al Maather, Riyadh, Saudi Arabia

Sultan T. Al-Sedairy

87. Bioinformatics Unit, Spanish National Cancer Research Centre (CNIO), Madrid, Spain

Fatima Al-Shahrour & Elena Piñeiro-Yáñez

88. Bioinformatics Core Facility, University Medical Center Hamburg, Hamburg, Germany

Malik Alawi

89. Heinrich Pette Institute, Leibniz Institute for Experimental Virology, Hamburg, Germany

Malik Alawi & Adam Grundhoff

90. Ontario Tumour Bank, Ontario Institute for Cancer Research, Toronto, ON, Canada

Monique Albert & John Bartlett

91. Department of Pathology, The University of Texas MD Anderson Cancer Center, Houston, TX, USA

Kenneth Aldape, Russell R. Broaddus, Bogdan Czerniak, Adel El-Naggar, Savitri Krishnamurthy, Alexander J. Lazar & Xiaoping Su

92. Laboratory of Pathology, Center for Cancer Research, National Cancer Institute, Bethesda, MD, USA

Kenneth Aldape

93. Department of Cellular and Molecular Medicine and Department of Bioengineering, University of California San Diego, La Jolla, CA, USA

Ludmil B. Alexandrov & Erik N. Bergstrom

94. UC San Diego Moores Cancer Center, San Diego, CA, USA

Ludmil B. Alexandrov, Erik N. Bergstrom & Olivier Harismendy

95. Canada's Michael Smith Genome Sciences Centre, BC Cancer, Vancouver, BC, Canada

Adrian Ally, Miruna Balasundaram, Reanne Bowlby, Denise Brooks, Rebecca Carlsen, Eric Chuah, Noreen Dhalla, Robert A. Holt, Steven J. M. Jones, Katayoon Kasaian, Darlene Lee, Haiyan Irene Li, Yussanne Ma, Marco A. Marra, Michael Mayo, Richard A. Moore, Andrew J. Mungall, Karen Mungall, A. Gordon Robertson, Sara Sadeghi, Jacqueline E. Schein, Payal Sipahimalani, Angela Tam, Nina Thiessen & Tina Wong

96. Sir Peter MacCallum Department of Oncology, Peter MacCallum Cancer Centre, University of Melbourne, Melbourne, VIC, Australia

Kathryn Alsop, David D. L. Bowtell, Elizabeth L. Christie, Dariush Etemadmoghadam, Sian Fereday, Dale W. Garsed, Linda Mileshkin, Chris Mitchell, Mark Shackleton, Heather Thorne & Nadia Traficante

97. Centre for Research in Molecular Medicine and Chronic Diseases (CiMUS), Universidade de Santiago de Compostela, Santiago de Compostela, Spain

Eva G. Alvarez, Alicia L. Bruzos, Bernardo Rodriguez-Martin, Javier Temes, Jose M. C. Tubio & Jorge Zamora

98. Department of Zoology, Genetics and Physical Anthropology, (CiMUS), Universidade de Santiago de Compostela, Santiago de Compostela, Spain

Eva G. Alvarez, Alicia L. Bruzos, Bernardo Rodriguez-Martin, Javier Temes, Jose M. C. Tubio & Jorge Zamora

99. The Biomedical Research Centre (CINBIO), Universidade de Vigo, Vigo, Spain

Eva G. Alvarez, Alicia L. Bruzos, Bernardo Rodriguez-Martin, Marta Tojo, Jose M. C. Tubio & Jorge Zamora

100. Royal National Orthopaedic Hospital - Bolsover, London, UK

Fernanda Amary

101. Department of Genomic Medicine, The University of Texas MD Anderson Cancer Center, Houston, TX, USA

Samirkumar B. Amin, P. Andrew Futreal & Alexander J. Lazar

102. Quantitative and Computational Biosciences Graduate Program, Baylor College of Medicine, Houston, TX, USA

Samirkumar B. Amin, Han Liang & Yumeng Wang

103. The Jackson Laboratory for Genomic Medicine, Farmington, CT, USA

Samirkumar B. Amin, Joshy George & Lucas Lochovsky

104. Genome Informatics Program, Ontario Institute for Cancer Research, Toronto, ON, Canada

Brice Aminou, Niall J. Byrne, Aurélien Chateigner, Nodirjon Fayzullaev, Vincent Ferretti, George L. Mihaiescu, Hardeep K. Nahal-Bose, Brian D. O'Connor, B. F. Francis Ouellette, Marc D. Perry, Kevin Thai, Qian Xiang, Christina K. Yung & Junjun Zhang

105. Institute of Human Genetics, Christian-Albrechts-University, Kiel, Germany

Ole Ammerpohl, Andrea Haake, Cristina López, Julia Richter & Rabea Wagener

106. Institute of Human Genetics, Ulm University and Ulm University Medical Center, Ulm, Germany

Ole Ammerpohl, Sietse Aukema, Cristina López, Reiner Siebert & Rabea Wagener

107. Queensland Centre for Medical Genomics, Institute for Molecular Bioscience, University of Queensland, St. Lucia, Brisbane, QLD, Australia

Matthew J. Anderson, Timothy J. C. Bruxner, Angelika N. Christ, J. Lynn Fink, Ivon Harliwong, Karin S. Kassahn, David K. Miller, Alan J. Robertson & Darrin F. Taylor

108. Salford Royal NHS Foundation Trust, Salford, UK

Yeng Ang, Hsiao-Wei Chen, Ritika Kundra & Francisco Sanchez-Vega

109. Department of Surgery, Pancreas Institute, University and Hospital Trust of Verona, Verona, Italy

Davide Antonello, Claudio Bassi, Narong Khuntikeo, Luca Landoni, Giuseppe Malleo, Giovanni Marchegiani, Neil D. Merrett, Marco Miotto, Salvatore Paiella, Antonio Pea, Paolo Pederzoli, Roberto Salvia, Jaswinder S. Samra, Elisabetta Sereni & Samuel Singer

110. Molecular and Medical Genetics, OHSU Knight Cancer Institute, Oregon Health and Science University, Portland, OR, USA

Pavana Anur, Myron Peto & Paul T. Spellman

111. Department of Molecular Oncology, BC Cancer Research Centre, Vancouver, BC, Canada

Samuel Aparicio

112. The McDonnell Genome Institute at Washington University, St. Louis, MO, USA

Elizabeth L. Appelbaum, Matthew H. Bailey, Matthew G. Cordes, Li Ding, Catrina C. Fronick, Lucinda A. Fulton, Robert S. Fulton, Kuan-lin Huang, Reyka Jayasinghe, Elaine R. Mardis, R. Jay Mashl, Michael D. McLellan, Christopher A. Miller, Heather K. Schmidt, Jiayin Wang, Michael C. Wendl, Richard K. Wilson & Tina Wong

113. University College London, London, UK

Elizabeth L. Appelbaum, Jonathan D. Kay, Helena Kilpinen, Laurence B. Lovat, Hayley J. Luxton & Hayley C. Whitaker

114. Division of Cancer Genomics, National Cancer Center Research Institute, National Cancer Center, Tokyo, Japan

Yasuhito Arai, Natsuko Hama, Fumie Hosoda, Hiromi Nakamura, Tatsuhiro Shibata, Yasushi Totoki & Shinichi Yachida

115. DLR Project Management Agency, Bonn, Germany

Axel Aretz

116. Tokyo Women's Medical University, Tokyo, Japan

Shun-ichi Ariizumi & Masakazu Yamamoto

117. Center for Molecular Oncology, Memorial Sloan Kettering Cancer Center, New York, NY, USA

Joshua Armenia, Hsiao-Wei Chen, Jianjiong Gao, Ritika Kundra, Francisco Sanchez-Vega, Nikolaus Schultz & Hongxin Zhang

118. Los Alamos National Laboratory, Los Alamos, NM, USA

Laurent Arnould

119. Department of Pathology, University Health Network, Toronto General Hospital, Toronto, ON, Canada

Sylvia Asa, Michael H. A. Roehrl & Theodorus Van der Kwast

120. Nottingham University Hospitals NHS Trust, Nottingham, UK

Sylvia Asa, Simon L. Parsons & Ming Tsao

121. Epigenomics and Cancer Risk Factors, German Cancer Research Center (DKFZ), Heidelberg, Germany

Yassen Assenov

122. Computational Biology Program, Ontario Institute for Cancer Research, Toronto, ON, Canada

Gurnit Atwal, Philip Awadalla, Jonathan Barenboim, Vinayak Bhandari, Ivan Borozan, Paul C. Boutros, Lewis Jonathan Dursi, Shadrielle M. G. Espiritu, Natalie S. Fox, Michael Fraser, Syed Haider, Vincent Huang, Keren Isaev, Wei Jiao, Christopher M. Lalansingh, Emilie Lalonde, Fabien C. Lamaze, Constance H. Li, Julie Livingstone, Christine P'ng, Marta Paczkowska, Stephenie D. Prokopec, Jüri Reimand, Veronica Y. Sabelnykova, Adriana Salcedo, Yu-Jia Shiah, Solomon I. Shorser, Shimin Shuai, Jared T. Simpson, Lincoln D. Stein, Ren X. Sun, Lina Wadi, Gavin W. Wilson, Adam J. Wright, Takafumi N. Yamaguchi, Fouad Yousif & Denis Yuen

123. Department of Molecular Genetics, University of Toronto, Toronto, ON, Canada

Gurnit Atwal, Philip Awadalla, Gary D. Bader, Shimin Shuai & Lincoln D. Stein

124. Vector Institute, Toronto, ON, Canada

Gurnit Atwal, Quaid D. Morris, Yulia Rubanova & Jeffrey A. Wintersinger

125. Hematopathology Section, Institute of Pathology, Christian-Albrechts-University, Kiel, Germany

Sietse Aukema, Wolfram Klapper, Julia Richter & Monika Szczepanowski

126. Department of Pathology and Laboratory Medicine, School of Medicine, University of North Carolina at Chapel Hill, Chapel Hill, NC, USA

J. Todd Auman & Charles M. Perou

127. Department of Cancer Genetics, Institute for Cancer Research, Oslo University Hospital, The Norwegian Radium Hospital, Oslo, Norway

Miriam R. R. Aure, Anne-Lise Børresen-Dale & Anita Langerød

128. Pathology, Hospital Clinic, Institut d'Investigacions Biomèdiques August Pi i Sunyer (IDIBAPS), University of Barcelona, Barcelona, Spain

Marta Aymerich

129. Department of Veterinary Medicine, Transmissible Cancer Group, University of Cambridge, Cambridge, UK

Adrian Baez-Ortega

130. Alvin J. Siteman Cancer Center, Washington University School of Medicine, St. Louis, MO, USA

Matthew H. Bailey, Li Ding, Robert S. Fulton, Ramaswamy Govindan & Michael D. McLellan

131. Wolfson Wohl Cancer Research Centre, Institute of Cancer Sciences, University of Glasgow, Glasgow, UK

Peter J. Bailey, Andrew V. Biankin, David K. Chang, Susanna L. Cooke, Fraser R. Duthie, Janet S. Graham, Nigel B. Jamieson, Elizabeth A. Musgrove & Derek W. Wright

132. Lineberger Comprehensive Cancer Center, University of North Carolina at Chapel Hill, Chapel Hill, NC, USA

Saianand Balu, Tom Bodenheimer, D. Neil Hayes, Austin J. Hepperla, Katherine A. Hoadley, Alan P. Hoyle, Stuart R. Jefferys, Shaowu Meng, Lisle E. Mose, Grant Sanders, Yan Shi, Janae V. Simons & Matthew G. Soloway

133. Broad Institute of MIT and Harvard, Cambridge, MA, USA

Pratiti Bandopadhayay, Rameen Beroukhim, Angela N. Brooks, Susan Bullman, John Busanovich, Andrew D. Cherniack, Juok Cho, Carrie Cibulskis, Kristian Cibulskis, David Craft, Timothy Defreitas, Andrew J. Dunford, Scott Frazer, Stacey B. Gabriel, Nils Gehlenborg, Gad Getz, Manaswi Gupta, Gavin Ha, Nicholas J. Haradhvala, David I. Heiman, Julian M. Hess, Manolis Kellis, Jaegil Kim, Kiran Kumar, Kirsten Kübler, Eric Lander, Michael S. Lawrence, Ignaty Leshchiner, Pei Lin, Ziao Lin, Dimitri Livitz, Yosef E. Maruvka, Samuel R. Meier, Matthew Meyerson, Michael S. Noble, Chandra Sekhar Pedamallu, Paz Polak, Esther Rheinbay, Daniel Rosebrock, Mara Rosenberg, Gordon Saksena, Richard Sallari, Steven E. Schumacher, Ayellet V. Segre, Ofer Shapira, Juliann Shih, Nasa Sinnott-Armstrong, Oliver Spiro, Chip Stewart, Amaro Taylor-Weiner, Grace Tiao, Douglas Voet, Jeremiah A. Wala, Cheng-Zhong Zhang & Hailei Zhang

134. Dana-Farber/Boston Children’s Cancer and Blood Disorders Center, Boston, MA, USA

Pratiti Bandopadhayay

135. Department of Pediatrics, Harvard Medical School, Boston, MA, USA

Pratiti Bandopadhayay

136. Leeds Institute of Medical Research @ St. James’s, University of Leeds, St. James’s University Hospital, Leeds, UK

Rosamonde E. Banks & Naveen Vasudev

137. Department of Pathology and Diagnostics, University and Hospital Trust of Verona, Verona, Italy

Stefano Barbi, Vincenzo Corbo & Michele Simbolo

138. Department of Surgery, Princess Alexandra Hospital, Brisbane, QLD, Australia

Andrew P. Barbour

139. Surgical Oncology Group, Diamantina Institute, University of Queensland, Brisbane, QLD, Australia

Andrew P. Barbour

140. Department of Population and Quantitative Health Sciences, Case Western Reserve University School of Medicine, Cleveland, OH, USA

Jill Barnholtz-Sloan

141. Research Health Analytics and Informatics, University Hospitals Cleveland Medical Center, Cleveland, OH, USA

Jill Barnholtz-Sloan

142. Gloucester Royal Hospital, Gloucester, UK

Hugh Barr

143. European Molecular Biology Laboratory, European Bioinformatics Institute (EMBL-EBI), Cambridge, UK

Elisabet Barrera, Wojciech Bazant, Ewan Birney, Rich Boyce, Alvis Brazma, Andy Cafferkey, Claudia Calabrese, Paul Flicek, Nuno A. Fonseca, Anja Füllgrabe, Moritz Gerstung, Santiago Gonzalez, Liliana Greger, Maria Keays, Jan O. Korbel, Alfonso Muñoz, Steven J. Newhouse, David Ocana, Irene Papatheodorou, Robert

Petryszak, Roland F. Schwarz, Charles Short, Oliver Stegle & Lara Urban

144. Diagnostic Development, Ontario Institute for Cancer Research, Toronto, ON, Canada

John Bartlett & Ilinca Lungu

145. Barcelona Supercomputing Center (BSC), Barcelona, Spain

Javier Bartolome, Mattia Bosio, Ana Dueso-Barroso, J. Lynn Fink, Josep L. L. Gelpi, Ana Milovanovic, Montserrat Puiggròs, Javier Bartolomé Rodriguez, Romina Royo, David Torrents, Alfonso Valencia, Miguel Vazquez, David Vicente & Izar Villasante

146. Arnie Charbonneau Cancer Institute, University of Calgary, Calgary, AB, Canada

Oliver F. Bathe

147. Departments of Surgery and Oncology, University of Calgary, Calgary, AB, Canada

Oliver F. Bathe

148. Department of Pathology, Oslo University Hospital, The Norwegian Radium Hospital, Oslo, Norway

Daniel Baumhoer & Bodil Bjerkehagen

149. PanCuRx Translational Research Initiative, Ontario Institute for Cancer Research, Toronto, ON, Canada

Prashant Bavi, Michelle Chan-Seng-Yue, Sean Cleary, Robert E. Denroche, Steven Gallinger, Robert C. Grant, Gun Ho Jang, Sangeetha Kalimuthu, Ilinca Lungu, John D. McPherson, Faiyaz Notta, Michael H. A. Roehrl, Gavin W. Wilson & Julie M. Wilson

150. Department of Oncology, Sidney Kimmel Comprehensive Cancer Center at Johns Hopkins University School of Medicine, Baltimore, MD, USA

Stephen B. Baylin, Nilanjan Chatterjee, Leslie Cope, Ludmila Danilova & Ralph H. Hruban

151. University Hospital Southampton NHS Foundation Trust, Southampton, UK

Stephen B. Baylin & Tim Dudderidge

152. Royal Stoke University Hospital, Stoke-on-Trent, UK

Duncan Beardsmore & Christopher Umbricht

153. Genome Sequence Informatics, Ontario Institute for Cancer Research, Toronto, ON, Canada

Timothy A. Beck, Bob Gibson, Lawrence E. Heisler, Xuemei Luo & Morgan L. Taschuk

154. Human Longevity Inc, San Diego, CA, USA

Timothy A. Beck

155. Olivia Newton-John Cancer Research Institute, La Trobe University, Heidelberg, VIC, Australia

Andreas Behren & Jonathan Cebon

156. Computer Network Information Center, Chinese Academy of Sciences, Beijing, China

Beifang Niu

157. Genome Canada, Ottawa, ON, Canada

Cindy Bell

158. CNAG-CRG, Centre for Genomic Regulation (CRG), Barcelona Institute of Science and Technology (BIST), Barcelona, Spain

Sergi Beltran, Ivo G. Gut, Marta Gut, Simon C. Heath, Tomas Marques-Bonet, Arcadi Navarro, Miranda D. Stobbe, Jean-Rémi Trotta & Justin P. Whalley

159. Universitat Pompeu Fabra (UPF), Barcelona, Spain

Sergi Beltran, Mattia Bosio, German M. Demidov, Oliver Drechsel, Ivo G. Gut, Marta Gut, Simon C. Heath, Francesc Muyas, Stephan Ossowski, Aparna Prasad, Raquel Rabionet, Miranda D. Stobbe & Hana Susak

160. Buck Institute for Research on Aging, Novato, CA, USA

Christopher Benz & Christina Yau

161. Duke University Medical Center, Durham, NC, USA

Andrew Berchuck

162. Department of Human Genetics, Hannover Medical School, Hannover, Germany

Anke K. Bergmann

163. Center for Bioinformatics and Functional Genomics, Cedars-Sinai Medical Center, Los Angeles, CA, USA

Benjamin P. Berman & Huy Q. Dinh

164. Department of Biomedical Sciences, Cedars-Sinai Medical Center, Los Angeles, CA, USA

Benjamin P. Berman

165. The Hebrew University Faculty of Medicine, Jerusalem, Israel

Benjamin P. Berman

166. Barts Cancer Institute, Barts and the London School of Medicine and Dentistry, Queen Mary University of London, London, UK

Daniel M. Berney & Yong-Jie Lu

167. Department of Computer Science, Bioinformatics Group, University of Leipzig, Leipzig, Germany

Stephan H. Bernhart, Hans Binder, Steve Hoffmann & Peter F. Stadler

168. Interdisciplinary Center for Bioinformatics, University of Leipzig, Leipzig, Germany

Stephan H. Bernhart, Hans Binder, Steve Hoffmann, Helene Kretzmer & Peter F. Stadler

169. Transcriptome Bioinformatics, LIFE Research Center for Civilization Diseases, University of Leipzig, Leipzig, Germany

Stephan H. Bernhart, Steve Hoffmann, Helene Kretzmer & Peter F. Stadler

170. Department of Medical Oncology, Dana-Farber Cancer Institute, Boston, MA, USA

Rameen Beroukhim, Angela N. Brooks, Susan Bullman, Andrew D. Cherniack, Levi Garraway, Matthew Meyerson, Chandra Sekhar Pedamallu, Steven E. Schumacher, Juliann Shih & Jeremiah A. Wala

171. Department of Cancer Biology, Dana-Farber Cancer Institute, Boston, MA, USA

Rameen Beroukhim, Aquila Fatima, Andrea L. Richardson, Steven E. Schumacher, Ofer Shapira, Andrew Tutt & Jeremiah A. Wala

172. Harvard Medical School, Boston, MA, USA

Rameen Beroukhim, Gad Getz, Kirsten Kübler, Matthew Meyerson, Chandra Sekhar Pedamallu, Paz Polak, Esther Rheinbay & Jeremiah A. Wala

173. USC Norris Comprehensive Cancer Center, University of Southern California, Los Angeles, CA, USA

Mario Berrios, Moiz S. Bootwalla, Andrea Holbrook, Phillip H. Lai, Dennis T. Maglinte, David J. Van Den Berg & Daniel J. Weisenberger

174. Department of Diagnostics and Public Health, University and Hospital Trust of Verona, Verona, Italy

Samantha Bersani, Ivana Cataldo, Claudio Luchini & Maria Scardoni

175. Department of Mathematics, Aarhus University, Aarhus, Denmark

Johanna Bertl & Asger Hobolth

176. Department of Molecular Medicine (MOMA), Aarhus University Hospital, Aarhus N, Denmark

Johanna Bertl, Henrik Hornshøj, Malene Juul, Randi Istrup Juul, Tobias Madsen, Morten Muhlig Nielsen & Jakob Skou Pedersen

177. Instituto Carlos Slim de la Salud, Mexico City, Mexico

Miguel Betancourt

178. Department of Medical Biophysics, University of Toronto, Toronto, ON, Canada

Vinayak Bhandari, Paul C. Boutros, Robert G. Bristow, Keren Isaev, Constance H. Li, Jüri Reimand, Michael H. A. Roehrl & Bradly G. Wouters

179. Cancer Division, Garvan Institute of Medical Research, Kinghorn Cancer Centre, University of New South Wales (UNSW Sydney),

Sydney, NSW, Australia

Andrew V. Biankin, David K. Chang, Lorraine A. Chantrill, Angela Chou, Anthony J. Gill, Amber L. Johns, James G. Kench, David K. Miller, Adnan M. Nagrial, Marina Pajic, Mark Pinese, Ilse Rooman, Christopher J. Scarlett, Christopher W. Toon & Jianmin Wu

180. South Western Sydney Clinical School, Faculty of Medicine, University of New South Wales (UNSW Sydney), Liverpool, NSW, Australia

Andrew V. Biankin

181. West of Scotland Pancreatic Unit, Glasgow Royal Infirmary, Glasgow, UK

Andrew V. Biankin & Nigel B. Jamieson

182. Center for Digital Health, Berlin Institute of Health and Charitè - Universitätsmedizin Berlin, Berlin, Germany

Matthias Bieg

183. Heidelberg Center for Personalized Oncology (DKFZ-HIPO), German Cancer Research Center (DKFZ), Heidelberg, Germany

Matthias Bieg, Ivo Buchhalter, Barbara Hutter & Nagarajan Paramasivam

184. The Preston Robert Tisch Brain Tumor Center, Duke University Medical Center, Durham, NC, USA

Darell Bigner

185. Massachusetts General Hospital, Boston, MA, USA

Michael Birrer, Vikram Deshpande, William C. Faquin, Nicholas J. Haradhvala, Kirsten Kübler, Michael S. Lawrence, David N.

Louis, Yosef E. Maruvka, G. Petur Nielsen, Esther Rheinbay, Mara Rosenberg, Dennis C. Sgroi & Chin-Lee Wu

186. National Institute of Biomedical Genomics, Kalyani, West Bengal, India

Nidhan K. Biswas, Arindam Maitra & Partha P. Majumder

187. Institute of Clinical Medicine and Institute of Oral Biology, University of Oslo, Oslo, Norway

Bodil Bjerkehagen

188. University of North Carolina at Chapel Hill, Chapel Hill, NC, USA

Lori Boice, Mei Huang, Sonia Puig & Leigh B. Thorne

189. ARC-Net Centre for Applied Research on Cancer, University and Hospital Trust of Verona, Verona, Italy

Giada Bonizzato, Cinzia Cantù, Ivana Cataldo, Vincenzo Corbo, Sonia Grimaldi, Rita T. Lawlor, Andrea Mafficini, Borislav C. Rusev, Aldo Scarpa, Katarzyna O. Sikora, Nicola Sperandio, Alain Viari & Caterina Vicentini

190. The Institute of Cancer Research, London, UK

Johann S. De Bono, Niedzica Camacho, Colin S. Cooper, Sandra E. Edwards, Rosalind A. Eeles, Zsofia Kote-Jarai, Daniel A. Leongamornlert, Lucy Matthews & Sue Merson

191. Centre for Computational Biology, Duke-NUS Medical School, Singapore, Singapore

Arnoud Boot, Ioana Cutcutache, Mi Ni Huang, John R. McPherson, Steven G. Rozen & Yang Wu

192. Programme in Cancer and Stem Cell Biology, Duke-NUS Medical School, Singapore, Singapore

Arnoud Boot, Ioana Cutcutache, Mi Ni Huang, John R. McPherson, Steven G. Rozen, Patrick Tan, Bin Tean Teh & Yang Wu

193. Division of Oncology and Pathology, Department of Clinical Sciences Lund, Lund University, Lund, Sweden

Ake Borg, Markus Ringnér & Johan Staaf

194. Department of Pediatric Oncology, Hematology and Clinical Immunology, Heinrich-Heine-University, Düsseldorf, Germany

Arndt Borkhardt & Jessica I. Hoell

195. Laboratory for Medical Science Mathematics, RIKEN Center for Integrative Medical Sciences, Yokohama, Japan

Keith A. Boroevich, Todd A. Johnson, Michael S. Lawrence & Tatsuhiko Tsunoda

196. RIKEN Center for Integrative Medical Sciences, Yokohama, Japan

Keith A. Boroevich, Akihiro Fujimoto, Masashi Fujita, Mayuko Furuta, Kazuhiro Maejima, Hidewaki Nakagawa, Kaoru Nakano & Aya Sasaki-Oku

197. Department of Internal Medicine/Hematology, Friedrich-Ebert-Hospital, Neumünster, Germany

Christoph Borst & Siegfried Haas

198. Departments of Dermatology and Pathology, Yale University, New Haven, CT, USA

Marcus Bosenberg

199. Centre for Genomic Regulation (CRG), The Barcelona Institute of Science and Technology, Barcelona, Spain

Mattia Bosio, German M. Demidov, Oliver Drechsel, Georgia Escaramis, Xavier Estivill, Aliaksei Z. Holik, Francesc Muyas, Stephan Ossowski, Raquel Rabionet & Hana Susak

200. Radcliffe Department of Medicine, University of Oxford, Oxford, UK

Jacqueline Boultwood

201. Canadian Center for Computational Genomics, McGill University, Montreal, QC, Canada

Guillaume Bourque

202. Department of Human Genetics, McGill University, Montreal, QC, Canada

Guillaume Bourque, Mark Lathrop & Yasser Riazalhosseini

203. Department of Human Genetics, University of California Los Angeles, Los Angeles, CA, USA

Paul C. Boutros

204. Department of Pharmacology, University of Toronto, Toronto, ON, Canada

Paul C. Boutros

205. Faculty of Medicine and Health Technology, Tampere University and Tays Cancer Center, Tampere University Hospital, Tampere, Finland

G. Steven Bova & Tapio Visakorpi

206. Haematology, Leeds Teaching Hospitals NHS Trust, Leeds, UK

David T. Bowen

207. Translational Research and Innovation, Centre Léon Bérard, Lyon, France

Sandrine Boyault

208. Fox Chase Cancer Center, Philadelphia, PA, USA

Jeffrey Boyd & Elaine R. Mardis

209. International Agency for Research on Cancer, World Health Organization, Lyon, France

Paul Brennan & Ghislaine Scelo

210. Earlham Institute, Norwich, UK

Daniel S. Brewer & Colin S. Cooper

211. Norwich Medical School, University of East Anglia, Norwich, UK

Daniel S. Brewer & Colin S. Cooper

212. Department of Molecular Biology, Faculty of Science, Radboud Institute for Molecular Life Sciences, Radboud University, Nijmegen, HB, The Netherlands

Arie B. Brinkman

213. CRUK Manchester Institute and Centre, Manchester, UK

Robert G. Bristow

214. Department of Radiation Oncology, University of Toronto, Toronto, ON, Canada

Robert G. Bristow

215. Division of Cancer Sciences, Manchester Cancer Research Centre, University of Manchester, Manchester, UK

Robert G. Bristow

216. Radiation Medicine Program, Princess Margaret Cancer Centre, Toronto, ON, Canada

Robert G. Bristow & Fei-Fei Fei Liu

217. Department of Pathology, Brigham and Women's Hospital, Harvard Medical School, Boston, MA, USA

Jane E. Brock & Sabina Signoretti

218. Department of Surgery, Division of Thoracic Surgery, The Johns Hopkins University School of Medicine, Baltimore, MD, USA

Malcolm Brock

219. Division of Molecular Pathology, The Netherlands Cancer Institute, Oncode Institute, Amsterdam, CX, The Netherlands

Annegien Broeks & Jos Jonkers

220. Department of Biomolecular Engineering, University of California Santa Cruz, Santa Cruz, CA, USA

Angela N. Brooks, David Haan, Maximillian G. Marin, Thomas J. Matthew, Yulia Newton, Cameron M. Soulette & Joshua M. Stuart

221. UC Santa Cruz Genomics Institute, University of California Santa Cruz, Santa Cruz, CA, USA

Angela N. Brooks, Brian Craft, Mary J. Goldman, David Haussler, Joshua M. Stuart & Jingchun Zhu

222. Division of Applied Bioinformatics, German Cancer Research Center (DKFZ), Heidelberg, Germany

Benedikt Brors, Lars Feuerbach, Chen Hong, Charles David Imbusch & Lina Sieverling

223. German Cancer Consortium (DKTK), German Cancer Research Center (DKFZ), Heidelberg, Germany

Benedikt Brors, Barbara Hutter, Peter Lichter, Dirk Schadendorf & Holger Sültmann

224. National Center for Tumor Diseases (NCT) Heidelberg, Heidelberg, Germany

Benedikt Brors, Barbara Hutter, Holger Sültmann & Thorsten Zenz

225. Center for Biological Sequence Analysis, Department of Bio and Health Informatics, Technical University of Denmark, Lyngby, Denmark

Søren Brunak

226. Novo Nordisk Foundation Center for Protein Research, University of Copenhagen, Copenhagen, Denmark

Søren Brunak

227. Institute for Molecular Bioscience, University of Queensland, St. Lucia, Brisbane, QLD, Australia

Timothy J. C. Bruxner, Oliver Holmes, Stephen H. Kazakoff, Conrad R. Leonard, Felicity Newell, Katia Nones, Ann-Marie Patch, John V. Pearson, Michael C. Quinn, Nick M. Waddell, Nicola Waddell, Scott Wood & Qinying Xu

228. Biomedical Engineering, Oregon Health and Science University, Portland, OR, USA

Alex Buchanan & Kyle Ellrott

229. Division of Theoretical Bioinformatics, German Cancer Research Center (DKFZ), Heidelberg, Germany

Ivo Buchhalter, Calvin Wing Yiu Chan, Roland Eils, Michael C. Heinold, Carl Herrmann, Natalie Jäger, Rolf Kabbe, Jules N. A. Kerssemakers, Kortine Kleinheinz, Nagarajan Paramasivam, Manuel Prinz, Matthias Schlesner & Johannes Werner

230. Institute of Pharmacy and Molecular Biotechnology and BioQuant, Heidelberg University, Heidelberg, Germany

Ivo Buchhalter, Roland Eils, Michael C. Heinold, Carl Herrmann, Daniel Hübschmann, Kortine Kleinheinz & Umut H. Toprak

231. Federal Ministry of Education and Research, Berlin, Germany

Christiane Buchholz

232. Melanoma Institute Australia, University of Sydney, Sydney, NSW, Australia

Hazel Burke, Ricardo De Paoli-Iseppi, Nicholas K. Hayward, Peter Hersey, Valerie Jakrot, Hojabr Kakavand, Georgina V. Long, Graham J. Mann, Robyn P. M. Saw, Richard A. Scolyer, Ping Shang, Andrew J. Spillane, Jonathan R. Stretch, John F. F. Thompson & James S. Wilmott

233. Pediatric Hematology and Oncology, University Hospital Muenster, Muenster, Germany

Birgit Burkhardt

234. Department of Pathology, Johns Hopkins University School of Medicine, Baltimore, MD, USA

Kathleen H. Burns & Christopher Umbricht

235. McKusick-Nathans Institute of Genetic Medicine, Sidney Kimmel Comprehensive Cancer Center at Johns Hopkins University School of Medicine, Baltimore, MD, USA

Kathleen H. Burns

236. Foundation Medicine, Inc, Cambridge, MA, USA

John Busanovich

237. Department of Biomedical Data Science, Stanford University School of Medicine, Stanford, CA, USA

Carlos D. Bustamante & Francisco M. De La Vega

238. Department of Genetics, Stanford University School of Medicine, Stanford, CA, USA

Carlos D. Bustamante, Francisco M. De La Vega, Suyash S. Shringarpure, Nasa Sinnott-Armstrong & Mark H. Wright

239. Bakar Computational Health Sciences Institute and Department of Pediatrics, University of California, San Francisco, CA, USA

Atul J. Butte & Jieming Chen

240. Institute of Clinical Medicine, Faculty of Medicine, University of Oslo, Oslo, Norway

Anne-Lise Børresen-Dale

241. National Cancer Institute, National Institutes of Health, Bethesda, MD, USA

Samantha J. Caesar-Johnson, John A. Demchok, Ina Felau, Roy Tarnuzzer, Zhining Wang, Liming Yang, Jean C. Zenklusen & Jiashan Zhang

242. Royal Marsden NHS Foundation Trust, London and Sutton, UK

Declan Cahill, Nening M. Dennis, Tim Dudderidge, Rosalind A. Eeles, Cyril Fisher, Steven Hazell, Vincent Khoo, Pardeep Kumar, Naomi Livni, Erik Mayer, David Nicol, Christopher

Ogden, Edward W. Rowe, Sarah Thomas, Alan Thompson & Nicholas van As

243. Genome Biology Unit, European Molecular Biology Laboratory (EMBL), Heidelberg, Germany

Claudia Calabrese, Serap Erkek, Moritz Gerstung, Santiago Gonzalez, Nina Habermann, Wolfgang Huber, Lara Jerman, Jan O. Korbel, Esa Pitkänen, Benjamin Raeder, Tobias Rausch, Vasilisa A. Rudneva, Oliver Stegle, Stephanie Sungalee, Lara Urban, Sebastian M. Waszak, Joachim Weischenfeldt & Sergei Yakneen

244. Department of Oncology, University of Cambridge, Cambridge, UK

Carlos Caldas & Suet-Feung Chin

245. Li Ka Shing Centre, Cancer Research UK Cambridge Institute, University of Cambridge, Cambridge, UK

Carlos Caldas, Suet-Feung Chin, Ruben M. Drews, Paul A. Edwards, Matthew Eldridge, Steve Hawkins, Andy G. Lynch, Geoff Macintyre, Florian Markowetz, Charlie E. Massie, David E. Neal, Simon Tavaré & Ke Yuan

246. Institut Gustave Roussy, Villejuif, France

Fabien Calvo

247. Cambridge University Hospitals NHS Foundation Trust, Cambridge, UK

Peter J. Campbell, Vincent J. Gnanapragasam, William Howat, Thomas J. Mitchell, David E. Neal, Nimish C. Shah & Anne Y. Warren

248. Department of Haematology, University of Cambridge, Cambridge, UK

Peter J. Campbell

249. Anatomia Patológica, Hospital Clinic, Institut d'Investigacions Biomèdiques August Pi i Sunyer (IDIBAPS), University of Barcelona, Barcelona, Spain

Elias Campo

250. Spanish Ministry of Science and Innovation, Madrid, Spain

Elias Campo

251. University of Michigan Comprehensive Cancer Center, Ann Arbor, MI, USA

Thomas E. Carey

252. Department for BioMedical Research, University of Bern, Bern, Switzerland

Joana Carlevaro-Fita

253. Department of Medical Oncology, Inselspital, University Hospital and University of Bern, Bern, Switzerland

Joana Carlevaro-Fita, Rory Johnson & Andrés Lanzós

254. Graduate School for Cellular and Biomedical Sciences, University of Bern, Bern, Switzerland

Joana Carlevaro-Fita & Andrés Lanzós

255. University of Pavia, Pavia, Italy

Mario Cazzola & Luca Malcovati

256. University of Alabama at Birmingham, Birmingham, AL, USA

Robert Cerfolio

257. UHN Program in BioSpecimen Sciences, Toronto General Hospital, Toronto, ON, Canada

Dianne E. Chadwick, Sheng-Ben Liang, Michael H. A. Roehrl & Sagedeh Shahabi

258. Department of Urology, Icahn School of Medicine at Mount Sinai, New York, NY, USA

Dimple Chakravarty

259. Centre for Law and Genetics, University of Tasmania, Sandy Bay Campus, Hobart, TAS, Australia

Don Chalmers

260. Faculty of Biosciences, Heidelberg University, Heidelberg, Germany

Calvin Wing Yiu Chan, Chen Hong & Lina Sieverling

261. Department of Biochemistry, Microbiology and Immunology, Faculty of Medicine, University of Ottawa, Ottawa, ON, Canada

Kin Chan

262. Division of Anatomic Pathology, Mayo Clinic, Rochester, MN, USA

Vishal S. Chandan

263. Division of Cancer Epidemiology and Genetics, National Cancer Institute, National Institutes of Health, Bethesda, MD, USA

Stephen J. Chanock, Xing Hua, Lisa Mirabello, Lei Song & Bin Zhu

264. Illawarra Shoalhaven Local Health District L3 Illawarra Cancer Care Centre, Wollongong Hospital, Wollongong, NSW, Australia

Lorraine A. Chantrill

265. BioForA, French National Institute for Agriculture, Food, and Environment (INRAE), ONF, Orléans, France

Aurélien Chateigner

266. Department of Biostatistics, Bloomberg School of Public Health, Johns Hopkins University, Baltimore, MD, USA

Nilanjan Chatterjee

267. University of California San Diego, San Diego, CA, USA

Zhaohong Chen, Michelle T. Dow, Claudiu Farcas, S. M. Ashiqul Islam, Antonios Koures, Lucila Ohno-Machado, Christos Sotiriou & Ashley Williams

268. Division of Experimental Pathology, Mayo Clinic, Rochester, MN, USA

Jeremy Chien

269. Centre for Cancer Research, The Westmead Institute for Medical Research, University of Sydney, Sydney, NSW, Australia

Yoke-Eng Chiew, Angela Chou, Jillian A. Hung, Catherine J. Kennedy, Graham J. Mann, Gulietta M. Pupo, Sarah-Jane Schramm, Varsha Tembe & Anna deFazio

270. Department of Gynaecological Oncology, Westmead Hospital, Sydney, NSW, Australia

Yoke-Eng Chiew, Jillian A. Hung, Catherine J. Kennedy & Anna deFazio

271. PDXen Biosystems Inc, Seoul, South Korea

Sunghoon Cho

272. Korea Advanced Institute of Science and Technology, Daejeon, South Korea

Jung Kyoon Choi, Young Seok Ju & Christopher J. Yoon

273. Electronics and Telecommunications Research Institute, Daejeon, South Korea

Wan Choi, Seung-Hyup Jeon, Hyunghwan Kim & Youngchoon Woo

274. Institut National du Cancer (INCA), Boulogne-Billancourt, France

Christine Chomienne & Iris Pauporté

275. Department of Genetics, Informatics Institute, University of Alabama at Birmingham, Birmingham, AL, USA

Zechen Chong

276. Division of Medical Oncology, National Cancer Centre, Singapore, Singapore

Su Pin Choo

277. Medical Oncology, University and Hospital Trust of Verona, Verona, Italy

Sara Cingarlini & Michele Milella

278. Department of Pediatrics, University Hospital Schleswig-Holstein, Kiel, Germany

Alexander Claviez

279. Hepatobiliary/Pancreatic Surgical Oncology Program, University Health Network, Toronto, ON, Canada

Sean Cleary, Ashton A. Connor & Steven Gallinger

280. School of Biological Sciences, University of Auckland, Auckland, New Zealand

Nicole Cloonan

281. Department of Surgery, University of Melbourne, Parkville, VIC, Australia

Marek Cmero

282. The Murdoch Children's Research Institute, Royal Children's Hospital, Parkville, VIC, Australia

Marek Cmero

283. Walter and Eliza Hall Institute, Parkville, VIC, Australia

Marek Cmero

284. Vancouver Prostate Centre, Vancouver, Canada

Colin C. Collins, Nilgun Donmez, Faraz Hach, Salem Malikic, S. Cenk Sahinalp, Iman Sarrafi & Raunak Shrestha

285. Lunenfeld-Tanenbaum Research Institute, Mount Sinai Hospital, Toronto, ON, Canada

Ashton A. Connor, Steven Gallinger, Robert C. Grant, Treasa A. McPherson & Iris Selander

286. University of East Anglia, Norwich, UK

Colin S. Cooper

287. Norfolk and Norwich University Hospital NHS Trust, Norwich, UK

Matthew G. Cordes, Catrina C. Fronick & Tom Roques

288. Victorian Institute of Forensic Medicine, Southbank, VIC, Australia

Stephen M. Cordner

289. Department of Biomedical Informatics, Harvard Medical School, Boston, MA, USA

Isidro Cortés-Ciriano, Jake June-Koo Lee & Peter J. Park

290. Department of Chemistry, Centre for Molecular Science Informatics, University of Cambridge, Cambridge, UK

Isidro Cortés-Ciriano

291. Ludwig Center at Harvard Medical School, Boston, MA, USA

Isidro Cortés-Ciriano, Jake June-Koo Lee & Peter J. Park

292. Human Genome Sequencing Center, Baylor College of Medicine, Houston, TX, USA

Kyle Covington, HarshaVardhan Doddapaneni, Richard A. Gibbs, Jianhong Hu, Joy C. Jayaseelan, Viktoriya Korchina, Lora Lewis, Donna M. Muzny, Linghua Wang, David A. Wheeler & Liu Xi

293. Peter MacCallum Cancer Centre, University of Melbourne, Melbourne, VIC, Australia

Prue A. Cowin, Anne Hamilton, Gisela Mir Arnau & Ravikiran Vedururu

294. Physics Division, Optimization and Systems Biology Lab, Massachusetts General Hospital, Boston, MA, USA

David Craft

295. Department of Medicine, Baylor College of Medicine, Houston, TX, USA

Chad J. Creighton

296. University of Cologne, Cologne, Germany

Yupeng Cun, Martin Peifer & Tsun-Po Yang

297. International Genomics Consortium, Phoenix, AZ, USA

Erin Curley & Troy Shelton

298. Genomics Research Program, Ontario Institute for Cancer Research, Toronto, ON, Canada

Karolina Czajka, Jenna Eagles, Thomas J. Hudson, Jeremy Johns, Faridah Mbabaali, John D. McPherson, Jessica K. Miller, Danielle Pasternack, Michelle Sam & Lee E. Timms

299. Barking Havering and Redbridge University Hospitals NHS Trust, Romford, UK

Bogdan Czerniak, Adel El-Naggar & David Khoo

300. Children's Hospital at Westmead, University of Sydney, Sydney, NSW, Australia

Rebecca A. Dagg

301. Department of Medicine, Section of Endocrinology, University and Hospital Trust of Verona, Verona, Italy

Maria Vittoria Davi

302. Computational Biology Center, Memorial Sloan Kettering Cancer Center, New York, NY, USA

Natalie R. Davidson, Andre Kahles, Kjong-Van Lehmann, Alessandro Pastore, Gunnar Rätsch, Chris Sander, Yasin Senbabaoglu & Nicholas D. Socci

303. Department of Biology, ETH Zurich, Zürich, Switzerland

Natalie R. Davidson, Andre Kahles, Kjong-Van Lehmann, Gunnar Rätsch & Stefan G. Stark

304. Department of Computer Science, ETH Zurich, Zurich, Switzerland

Natalie R. Davidson, Andre Kahles, Kjong-Van Lehmann & Gunnar Rätsch

305. SIB Swiss Institute of Bioinformatics, Lausanne, Switzerland

Natalie R. Davidson, Andre Kahles, Kjong-Van Lehmann, Gunnar Rätsch & Stefan G. Stark

306. Weill Cornell Medical College, New York, NY, USA

Natalie R. Davidson, Bishoy M. Faltas & Gunnar Rätsch

307. Academic Department of Medical Genetics, University of Cambridge, Addenbrooke's Hospital, Cambridge, UK

Helen Davies & Serena Nik-Zainal

308. MRC Cancer Unit, University of Cambridge, Cambridge, UK

Helen Davies, Rebecca C. Fitzgerald, Nicola Grehan, Serena Nik-Zainal & Maria O'Donovan

309. Departments of Pediatrics and Genetics, University of North Carolina at Chapel Hill, Chapel Hill, NC, USA

Ian J. Davis

310. Seven Bridges Genomics, Charlestown, MA, USA

Brandi N. Davis-Dusenbery, Sinisa Ivkovic, Milena Kovacevic, Ana Mijalkovic Lazic, Sanja Mijalkovic, Mia Nastic, Petar Radovic & Nebojsa Tijanic

311. Annai Systems, Inc, Carlsbad, CA, USA

Francisco M. De La Vega, Tal Shmaya & Dai-Ying Wu

312. Department of Pathology, General Hospital of Treviso, Department of Medicine, University of Padua, Treviso, Italy

Angelo P. Dei Tos

313. Department of Computational Biology, University of Lausanne, Lausanne, Switzerland

Olivier Delaneau

314. Department of Genetic Medicine and Development, University of Geneva Medical School, Geneva, CH, Switzerland

Olivier Delaneau

315. Swiss Institute of Bioinformatics, University of Geneva, Geneva, CH, Switzerland

Olivier Delaneau

316. The Francis Crick Institute, London, UK

Jonas Demeulemeester, Stefan C. Dentro, Matthew W. Fittall, Kerstin Haase, Clemency Jolly, Maxime Tarabichi & Peter Van Loo

317. University of Leuven, Leuven, Belgium

Jonas Demeulemeester & Peter Van Loo

318. Institute of Medical Genetics and Applied Genomics, University of Tübingen, Tübingen, Germany

German M. Demidov, Francesc Muyas & Stephan Ossowski

319. Computational and Systems Biology, Genome Institute of Singapore, Singapore, Singapore

Deniz Demircioğlu & Jonathan Göke

320. School of Computing, National University of Singapore, Singapore, Singapore

Deniz Demircioğlu

321. Big Data Institute, Li Ka Shing Centre, University of Oxford, Oxford, UK

Stefan C. Dentro & David C. Wedge

322. Biomedical Data Science Laboratory, Francis Crick Institute, London, UK

Nikita Desai

323. Bioinformatics Group, Department of Computer Science, University College London, London, UK

Nikita Desai

324. The Edward S. Rogers Sr. Department of Electrical and Computer Engineering, University of Toronto, Toronto, ON, Canada

Amit G. Deshwar

325. Breast Cancer Translational Research Laboratory JC Heuson, Institut Jules Bordet, Brussels, Belgium

Christine Desmedt

326. Department of Oncology, Laboratory for Translational Breast Cancer Research, KU Leuven, Leuven, Belgium

Christine Desmedt

327. Institute for Research in Biomedicine (IRB Barcelona), The Barcelona Institute of Science and Technology, Barcelona, Spain

Jordi Deu-Pons, Joan Frigola, Abel Gonzalez-Perez, Ferran Muiños, Loris Mularoni, Oriol Pich, Iker Reyes-Salazar, Carlota Rubio-Perez, Radhakrishnan Sabarinathan & David Tamborero

328. Research Program on Biomedical Informatics, Universitat Pompeu Fabra, Barcelona, Spain

Jordi Deu-Pons, Abel Gonzalez-Perez, Ferran Muiños, Loris Mularoni, Oriol Pich, Carlota Rubio-Perez, Radhakrishnan Sabarinathan & David Tamborero

329. Division of Medical Oncology, Princess Margaret Cancer Centre, Toronto, ON, Canada

Neesha C. Dhani, David Hedley & Malcolm J. Moore

330. Department of Physiology and Biophysics, Weill Cornell Medicine, New York, NY, USA

Priyanka Dhingra, Ekta Khurana, Eric Minwei Liu & Alexander Martinez-Fundichely

331. Institute for Computational Biomedicine, Weill Cornell Medicine, New York, NY, USA

Priyanka Dhingra, Ekta Khurana, Eric Minwei Liu & Alexander Martinez-Fundichely

332. Department of Pathology, UPMC Shadyside, Pittsburgh, PA, USA

Rajiv Dhir

333. Independent Consultant, Wellesley, USA

Anthony DiBiase

334. Department of Cell and Molecular Biology, Science for Life Laboratory, Uppsala University, Uppsala, Sweden

Klev Diamanti, Jan Komorowski & Husen M. Umer

335. Department of Medicine and Department of Genetics, Washington University School of Medicine, St. Louis, St. Louis, MO, USA

Li Ding, Robert S. Fulton, Michael D. McLellan, Michael C. Wendl & Venkata D. Yellapantula

336. Hefei University of Technology, Anhui, China

Shuai Ding & Shanlin Yang

337. Translational Cancer Research Unit, GZA Hospitals St.-Augustinus, Center for Oncological Research, Faculty of Medicine and Health Sciences, University of Antwerp, Antwerp, Belgium

Luc Dirix, Steven Van Laere, Gert G. Van den Eynden & Peter Vermeulen

338. Simon Fraser University, Burnaby, BC, Canada

Nilgun Donmez, Ermin Hodzic, Salem Malikic, S. Cenk Sahinalp & Iman Sarrafi

339. University of Pennsylvania, Philadelphia, PA, USA

Ronny Drapkin

340. Faculty of Science and Technology, University of Vic—Central University of Catalonia (UVic-UCC), Vic, Spain

Ana Dueso-Barroso

341. The Wellcome Trust, London, UK

Michael Dunn

342. The Hospital for Sick Children, Toronto, ON, Canada

Lewis Jonathan Dursi

343. Department of Pathology, Queen Elizabeth University Hospital, Glasgow, UK

Fraser R. Duthie

344. Department of Genetics and Computational Biology, QIMR Berghofer Medical Research Institute, Brisbane, QLD, Australia

Ken Dutton-Regester, Nicholas K. Hayward, Oliver Holmes, Peter A. Johansson, Stephen H. Kazakoff, Conrad R. Leonard, Felicity Newell, Katia Nones, Ann-Marie Patch, John V. Pearson, Antonia L. Pritchard, Michael C. Quinn, Paresh Vyas, Nicola Waddell, Scott Wood & Qinying Xu

345. Department of Oncology, Centre for Cancer Genetic Epidemiology, University of Cambridge, Cambridge, UK

Douglas F. Easton

346. Department of Public Health and Primary Care, Centre for Cancer Genetic Epidemiology, University of Cambridge, Cambridge, UK

Douglas F. Easton

347. Prostate Cancer Canada, Toronto, ON, Canada

Stuart Edmonds

348. University of Cambridge, Cambridge, UK

Paul A. Edwards, Anthony R. Green, Andy G. Lynch, Florian Markowetz & Thomas J. Mitchell

349. Department of Laboratory Medicine, Translational Cancer Research, Lund University Cancer Center at Medicon Village, Lund University, Lund, Sweden

Anna Ehinger

350. Heidelberg University, Heidelberg, Germany

Juergen Eils, Roland Eils & Daniel Hübschmann

351. New BIH Digital Health Center, Berlin Institute of Health (BIH) and Charité - Universitätsmedizin Berlin, Berlin, Germany

Juergen Eils, Roland Eils & Chris Lawerenz

352. CIBER Epidemiología y Salud Pública (CIBERESP), Madrid, Spain

Georgia Escaramis

353. Research Group on Statistics, Econometrics and Health (GRECS), UdG, Barcelona, Spain

Georgia Escaramis

354. Quantitative Genomics Laboratories (qGenomics), Barcelona, Spain

Xavier Estivill

355. Icelandic Cancer Registry, Icelandic Cancer Society, Reykjavik, Iceland

Jorunn E. Eyfjord, Holmfridur Hilmarsdottir & Jon G. Jonasson

356. State Key Laboratory of Cancer Biology, and Xijing Hospital of Digestive Diseases, Fourth Military Medical University, Shaanxi, China

Daiming Fan & Yongzhan Nie

357. Department of Medicine (DIMED), Surgical Pathology Unit, University of Padua, Padua, Italy

Matteo Fassan

358. Rigshospitalet, Copenhagen, Denmark

Francesco Favero

359. Center for Cancer Genomics, National Cancer Institute, National Institutes of Health, Bethesda, MD, USA

Martin L. Ferguson

360. Department of Biochemistry and Molecular Medicine, University of Montreal, Montreal, QC, Canada

Vincent Ferretti

361. Australian Institute of Tropical Health and Medicine, James Cook University, Douglas, QLD, Australia

Matthew A. Field

362. Department of Neuro-Oncology, Istituto Neurologico Besta, Milano, Italy

Gaetano Finocchiaro

363. Bioplatforms Australia, North Ryde, NSW, Australia

Anna Fitzgerald & Catherine A. Shang

364. Department of Pathology (Research), University College London Cancer Institute, London, UK

Adrienne M. Flanagan

365. Department of Surgical Oncology, Princess Margaret Cancer Centre, Toronto, ON, Canada

Neil E. Fleshner

366. Department of Medical Oncology, Josephine Nefkens Institute and Cancer Genomics Centre, Erasmus Medical Center, Rotterdam, CN, The Netherlands

John A. Foekens, John W. M. Martens, F. Germán Rodríguez-González, Anieta M. Sieuwerts & Marcel Smid

367. The University of Queensland Thoracic Research Centre, The Prince Charles Hospital, Brisbane, QLD, Australia

Kwun M. Fong

368. CIBIO/InBIO - Research Center in Biodiversity and Genetic Resources, Universidade do Porto, Vairão, Portugal

Nuno A. Fonseca

369. HCA Laboratories, London, UK

Christopher S. Foster

370. University of Liverpool, Liverpool, UK

Christopher S. Foster

371. The Azrieli Faculty of Medicine, Bar-Ilan University, Safed, Israel

Milana Frenkel-Morgenstern

372. Department of Neurosurgery, University of Florida, Gainesville, FL, USA

William Friedman

373. Department of Pathology, Graduate School of Medicine, University of Tokyo, Tokyo, Japan

Masashi Fukayama & Tetsuo Ushiku

374. University of Milano Bicocca, Monza, Italy

Carlo Gambacorti-Passerini

375. BGI-Shenzhen, Shenzhen, China

Shengjie Gao, Yong Hou, Chang Li, Lin Li, Siliang Li, Xiaobo Li, Xinyue Li, Dongbing Liu, Xingmin Liu, Qiang Pan-Hammarström, Hong Su, Jian Wang, Kui Wu, Heng Xiong, Huanming Yang, Chen Ye, Xiuqing Zhang, Yong Zhou & Shida Zhu

376. Department of Pathology, Oslo University Hospital Ulleval, Oslo, Norway

Øystein Garred

377. Center for Biomedical Informatics, Harvard Medical School, Boston, MA, USA

Nils Gehlenborg

378. Department Biochemistry and Molecular Biomedicine, University of Barcelona, Barcelona, Spain

Josep L. L. Gelpi

379. Office of Cancer Genomics, National Cancer Institute, National Institutes of Health, Bethesda, MD, USA

Daniela S. Gerhard

380. Cancer Epigenomics, German Cancer Research Center (DKFZ), Heidelberg, Germany

Clarissa Gerhauser, Christoph Plass & Dieter Weichenhan

381. Department of Cancer Biology, The University of Texas MD Anderson Cancer Center, Houston, TX, USA

Jeffrey E. Gershenwald

382. Department of Surgical Oncology, The University of Texas MD Anderson Cancer Center, Houston, TX, USA

Jeffrey E. Gershenwald

383. Department of Computer Science, Yale University, New Haven, CT, USA

Mark Gerstein & Fabio C. P. Navarro

384. Department of Molecular Biophysics and Biochemistry, Yale University, New Haven, CT, USA

Mark Gerstein, Sushant Kumar, Lucas Lochovsky, Shaoke Lou, Patrick D. McGillivray, Fabio C. P. Navarro, Leonidas Salichos & Jonathan Warrell

385. Program in Computational Biology and Bioinformatics, Yale University, New Haven, CT, USA

Mark Gerstein, Arif O. Harmanci, Sushant Kumar, Donghoon Lee, Shantao Li, Xiaotong Li, Lucas Lochovsky, Shaoke Lou, William Meyerson, Leonidas Salichos, Jonathan Warrell, Jing Zhang & Yan Zhang

386. Center for Cancer Research, Massachusetts General Hospital, Boston, MA, USA

Gad Getz & Paz Polak

387. Department of Pathology, Massachusetts General Hospital, Boston, MA, USA

Gad Getz

388. Department of Pathology, Memorial Sloan Kettering Cancer Center, New York, NY, USA

Ronald Ghossein, Dilip D. Giri, Christine A. Iacobuzio-Donahue, Jorge Reis-Filho & Victor Reuter

389. Division of Gastroenterology and Hepatology, Mayo Clinic, Rochester, MN, USA

Nasra H. Giama, Catherine D. Moser & Lewis R. Roberts

390. University of Sydney, Sydney, NSW, Australia

Anthony J. Gill & James G. Kench

391. University of Oxford, Oxford, UK

Pelvender Gill, Freddie C. Hamdy, Katalin Karaszi, Adam Lambert, Luke Marsden, Clare Verrill & Paresh Vyas

392. Department of Surgery, Academic Urology Group, University of Cambridge, Cambridge, UK

Vincent J. Gnanapragasam

393. Department of Medicine II, University of Würzburg, Wuerzburg, Germany

Maria Elisabeth Goebler

394. Sylvester Comprehensive Cancer Center, University of Miami, Miami, FL, USA

Carmen Gomez

395. Institut Hospital del Mar d'Investigacions Mèdiques (IMIM), Barcelona, Spain

Abel Gonzalez-Perez

396. Genome Integrity and Structural Biology Laboratory, National Institute of Environmental Health Sciences (NIEHS), Durham, NC,

USA

Dmitry A. Gordenin & Natalie Saini

397. St. Thomas’s Hospital, London, UK

James Gossage

398. Osaka International Cancer Center, Osaka, Japan

Kunihito Gotoh

399. Department of Pathology, Skåne University Hospital, Lund University, Lund, Sweden

Dorthe Grabau

400. Department of Medical Oncology, Beatson West of Scotland Cancer Centre, Glasgow, UK

Janet S. Graham

401. National Human Genome Research Institute, National Institutes of Health, Bethesda, MD, USA

Eric Green, Carolyn M. Hutter & Heidi J. Sofia

402. Centre for Cancer Research, Victorian Comprehensive Cancer Centre, University of Melbourne, Melbourne, VIC, Australia

Sean M. Grimmond

403. Department of Medicine, Section of Hematology/Oncology, University of Chicago, Chicago, IL, USA

Robert L. Grossman

404. German Center for Infection Research (DZIF), Partner Site Hamburg-Borstel-Lübeck-Riems, Hamburg, Germany

Adam Grundhoff

405. Bioinformatics Research Centre (BiRC), Aarhus University, Aarhus, Denmark

Qianyun Guo, Asger Hobolth & Jakob Skou Pedersen

406. Department of Biotechnology, Ministry of Science and Technology, Government of India, New Delhi, Delhi, India

Shailja Gupta & K. VijayRaghavan

407. National Cancer Centre Singapore, Singapore, Singapore

Jonathan Göke

408. Brandeis University, Waltham, MA, USA

James E. Haber

409. Department of Urologic Sciences, University of British Columbia, Vancouver, BC, Canada

Faraz Hach

410. Department of Internal Medicine, Stanford University, Stanford, CA, USA

Mark P. Hamilton

411. The University of Texas Health Science Center at Houston, Houston, TX, USA

Leng Han, Yang Yang & Xuanping Zhang

412. Imperial College NHS Trust, Imperial College, London, INY, UK

George B. Hanna

413. Senckenberg Institute of Pathology, University of Frankfurt Medical School, Frankfurt, Germany

Martin Hansmann

414. Department of Medicine, Division of Biomedical Informatics, UC San Diego School of Medicine, San Diego, CA, USA

Olivier Harismendy

415. Center for Precision Health, School of Biomedical Informatics, The University of Texas Health Science Center, Houston, TX, USA

Arif O. Harmanci

416. Oxford Nanopore Technologies, New York, NY, USA

Eoghan Harrington & Sissel Juul

417. Institute of Medical Science, University of Tokyo, Tokyo, Japan

Takanori Hasegawa, Shuto Hayashi, Seiya Imoto, Mitsuhiro Komura, Satoru Miyano, Naoki Miyoshi, Kazuhiro Ohi, Eigo Shimizu, Yuichi Shiraishi, Hiroko Tanaka & Rui Yamaguchi

418. Howard Hughes Medical Institute, University of California Santa Cruz, Santa Cruz, CA, USA

David Haussler

419. Wakayama Medical University, Wakayama, Japan

Shinya Hayami, Masaki Ueno & Hiroki Yamaue

420. Department of Internal Medicine, Division of Medical Oncology, Lineberger Comprehensive Cancer Center, University of North Carolina at Chapel Hill, Chapel Hill, NC, USA

D. Neil Hayes

421. University of Tennessee Health Science Center for Cancer Research, Memphis, TN, USA

D. Neil Hayes

422. Department of Histopathology, Salford Royal NHS Foundation Trust, Salford, UK

Stephen J. Hayes

423. Faculty of Biology, Medicine and Health, University of Manchester, Manchester, UK

Stephen J. Hayes

424. BIOPIC, ICG and College of Life Sciences, Peking University, Beijing, China

Yao He & Zemin Zhang

425. Peking-Tsinghua Center for Life Sciences, Peking University, Beijing, China

Yao He & Zemin Zhang

426. Children's Hospital of Philadelphia, Philadelphia, PA, USA

Allison P. Heath

427. Department of Bioinformatics and Computational Biology and Department of Systems Biology, The University of Texas MD Anderson Cancer Center, Houston, TX, USA

Apurva M. Hegde, Yiling Lu & John N. Weinstein

428. Karolinska Institute, Stockholm, Sweden

Eva Hellstrom-Lindberg & Jesper Lagergren

429. The Donnelly Centre, University of Toronto, Toronto, ON, Canada

Mohamed Helmy & Jeffrey A. Wintersinger

430. Department of Medical Genetics, College of Medicine, Hallym University, Chuncheon, South Korea

Seong Gu Heo, Eun Pyo Hong & Ji Wan Park

431. Department of Experimental and Health Sciences, Institute of Evolutionary Biology (UPF-CSIC), Universitat Pompeu Fabra, Barcelona, Spain

José María Heredia-Genestar, Tomas Marques-Bonet & Arcadi Navarro

432. Health Data Science Unit, University Clinics, Heidelberg, Germany

Carl Herrmann

433. Massachusetts General Hospital Center for Cancer Research, Charlestown, MA, USA

Julian M. Hess & Yosef E. Maruvka

434. Hokkaido University, Sapporo, Japan

Satoshi Hirano & Toru Nakamura

435. Department of Pathology and Clinical Laboratory, National Cancer Center Hospital, Tokyo, Japan

Nobuyoshi Hiraoka

436. Department of Genetics, University of North Carolina at Chapel Hill, Chapel Hill, NC, USA

Katherine A. Hoadley & Tara J. Skelly

437. Computational Biology, Leibniz Institute on Aging - Fritz Lipmann Institute (FLI), Jena, Germany

Steve Hoffmann

438. University of Melbourne Centre for Cancer Research, Melbourne, VIC, Australia

Oliver Hofmann

439. University of Nebraska Medical Center, Omaha, NE, USA

Michael A. Hollingsworth & Sarah P. Thayer

440. Syntekabio Inc, Daejeon, South Korea

Jongwhi H. Hong

441. Department of Pathology, Academic Medical Center, Amsterdam, AZ, The Netherlands

Gerrit K. Hooijer

442. China National GeneBank-Shenzhen, Shenzhen, China

Yong Hou, Chang Li, Siliang Li, Xiaobo Li, Dongbing Liu, Xingmin Liu, Henk G. Stunnenberg, Hong Su, Kui Wu, Heng Xiong, Chen Ye & Shida Zhu

443. Division of Molecular Genetics, German Cancer Research Center (DKFZ), Heidelberg, Germany

Volker Hovestadt, Murat Iskar, Peter Lichter, Bernhard Radlwimmer & Marc Zapatka

444. Division of Life Science and Applied Genomics Center, Hong Kong University of Science and Technology, Clear Water Bay, Hong Kong, China

Taobo Hu, Yogesh Kumar, Eric Z. Ma, Zhenggang Wu & Hong Xue

445. Icahn School of Medicine at Mount Sinai, New York, NY, USA

Kuan-lin Huang

446. Geneplus-Shenzhen, Shenzhen, China

Yi Huang

447. School of Computer Science and Technology, Xi’an Jiaotong University, Xi’an, China

Yi Huang, Jiayin Wang, Xiao Xiao & Xuanping Zhang

448. AbbVie, North Chicago, IL, USA

Thomas J. Hudson

449. Institute of Pathology, Charité – University Medicine Berlin, Berlin, Germany

Michael Hummel & Dido Lenze

450. Centre for Translational and Applied Genomics, British Columbia Cancer Agency, Vancouver, BC, Canada

David Huntsman

451. Edinburgh Royal Infirmary, Edinburgh, UK

Ted R. Hupp

452. Berlin Institute for Medical Systems Biology, Max Delbrück Center for Molecular Medicine, Berlin, Germany

Matthew R. Huska, Julia Markowski & Roland F. Schwarz

453. Department of Pediatric Immunology, Hematology and Oncology, University Hospital, Heidelberg, Germany

Daniel Hübschmann

454. German Cancer Research Center (DKFZ), Heidelberg, Germany

Daniel Hübschmann, Christof von Kalle & Roland F. Schwarz

455. Heidelberg Institute for Stem Cell Technology and Experimental Medicine (HI-STEM), Heidelberg, Germany

Daniel Hübschmann

456. Institute for Computational Biomedicine, Weill Cornell Medical College, New York, NY, USA

Marcin Imielinski

457. New York Genome Center, New York, NY, USA

Marcin Imielinski & Xiaotong Yao

458. Department of Urology, James Buchanan Brady Urological Institute, Johns Hopkins University School of Medicine, Baltimore, MD, USA

William B. Isaacs

459. Department of Preventive Medicine, Graduate School of Medicine, The University of Tokyo, Tokyo, Japan

Shumpei Ishikawa, Hiroto Katoh & Daisuke Komura

460. Department of Molecular and Cellular Biology, Baylor College of Medicine, Houston, TX, USA

Michael Ittmann

461. Department of Pathology and Immunology, Baylor College of Medicine, Houston, TX, USA

Michael Ittmann

462. Michael E. DeBakey Veterans Affairs Medical Center, Houston, TX, USA

Michael Ittmann

463. Technical University of Denmark, Lyngby, Denmark

Jose M. G. Izarzugaza

464. Department of Pathology, College of Medicine, Hanyang University, Seoul, South Korea

Jocelyne Jacquemier, Hyung-Yong Kim & Gu Kong

465. Academic Unit of Surgery, School of Medicine, College of Medical, Veterinary and Life Sciences, University of Glasgow, Glasgow Royal Infirmary, Glasgow, UK

Nigel B. Jamieson

466. Department of Pathology, Asan Medical Center, College of Medicine, Ulsan University, Songpa-gu, Seoul, South Korea

Se Jin Jang & Hee Jin Lee

467. Science Writer, Garrett Park, MD, USA

Karine Jegalian

468. International Cancer Genome Consortium (ICGC)/ICGC Accelerating Research in Genomic Oncology (ARGO) Secretariat, Ontario Institute for Cancer Research, Toronto, ON, Canada

Jennifer L. Jennings

469. University of Ljubljana, Ljubljana, Slovenia

Lara Jerman

470. Department of Public Health Sciences, University of Chicago, Chicago, IL, USA

Yuan Ji

471. Research Institute, NorthShore University HealthSystem, Evanston, IL, USA

Yuan Ji

472. Department for Biomedical Research, University of Bern, Bern, Switzerland

Rory Johnson, Andrés Lanzós & Mark A. Rubin

473. Centre of Genomics and Policy, McGill University and Génome Québec Innovation Centre, Montreal, QC, Canada

Yann Joly, Bartha M. Knoppers, Mark Phillips & Adrian Thorogood

474. Carolina Center for Genome Sciences, University of North Carolina at Chapel Hill, Chapel Hill, NC, USA

Corbin D. Jones

475. Hopp Children's Cancer Center (KiTZ), Heidelberg, Germany

David T. W. Jones, Marcel Kool & Stefan M. Pfister

476. Pediatric Glioma Research Group, German Cancer Research Center (DKFZ), Heidelberg, Germany

David T. W. Jones

477. Cancer Research UK, London, UK

Nic Jones & David Scott

478. Indivumed GmbH, Hamburg, Germany

Hartmut Juhl

479. Genome Integration Data Center, Syntekabio, Inc, Daejeon, South Korea

Jongsun Jung

480. University Hospital Zurich, Zurich, Switzerland

Andre Kahles, Kjong-Van Lehmann & Gunnar Rätsch

481. Clinical Bioinformatics, Swiss Institute of Bioinformatics, Geneva, Switzerland

Abdullah Kahraman

482. Institute for Pathology and Molecular Pathology, University Hospital Zurich, Zurich, Switzerland

Abdullah Kahraman

483. Institute of Molecular Life Sciences, University of Zurich, Zurich, Switzerland

Abdullah Kahraman & Christian von Mering

484. MRC Human Genetics Unit, MRC IGMM, University of Edinburgh, Edinburgh, UK

Vera B. Kaiser & Colin A. Semple

485. Women's Cancer Program at the Samuel Oschin Comprehensive Cancer Institute, Cedars-Sinai Medical Center, Los Angeles, CA, USA

Beth Karlan

486. Department of Biology, Bioinformatics Group, Division of Molecular Biology, Faculty of Science, University of Zagreb, Zagreb, Croatia

Rosa Karlić

487. Department for Internal Medicine II, University Hospital Schleswig-Holstein, Kiel, Germany

Dennis Karsch & Michael Kneba

488. Genetics and Molecular Pathology, SA Pathology, Adelaide, SA, Australia

Karin S. Kassahn

489. Department of Gastric Surgery, National Cancer Center Hospital, Tokyo, Japan

Hitoshi Katai

490. Department of Bioinformatics, Division of Cancer Genomics, National Cancer Center Research Institute, Tokyo, Japan

Mamoru Kato, Hirofumi Rokutan & Mihoko Saito-Adachi

491. A.A. Kharkevich Institute of Information Transmission Problems, Moscow, Russia

Marat D. Kazanov

492. Oncology and Immunology, Dmitry Rogachev National Research Center of Pediatric Hematology, Moscow, Russia

Marat D. Kazanov

493. Skolkovo Institute of Science and Technology, Moscow, Russia

Marat D. Kazanov

494. Department of Surgery, The George Washington University, School of Medicine and Health Science, Washington, DC, USA

Electron Kebebew

495. Endocrine Oncology Branch, Center for Cancer Research, National Cancer Institute, National Institutes of Health, Bethesda, MD, USA

Electron Kebebew

496. Melanoma Institute Australia, Macquarie University, Sydney, NSW, Australia

Richard F. Kefford

497. MIT Computer Science and Artificial Intelligence Laboratory, Massachusetts Institute of Technology, Cambridge, MA, USA

Manolis Kellis

498. Tissue Pathology and Diagnostic Oncology, Royal Prince Alfred Hospital, Sydney, NSW, Australia

James G. Kench & Richard A. Scolyer

499. Cholangiocarcinoma Screening and Care Program and Liver Fluke and Cholangiocarcinoma Research Centre, Faculty of Medicine, Khon Kaen University, Khon Kaen, Thailand

Narong Khuntikeo

500. Controlled Department and Institution, New York, NY, USA

Ekta Khurana

501. Englander Institute for Precision Medicine, Weill Cornell Medicine, New York, NY, USA

Ekta Khurana & Alexander Martinez-Fundichely

502. National Cancer Center, Gyeonggi, South Korea

Hark Kyun Kim

503. Department of Biochemistry, College of Medicine, Ewha Womans University, Seoul, South Korea

Hyung-Lae Kim

504. Health Sciences Department of Biomedical Informatics, University of California San Diego, La Jolla, CA, USA

Jihoon Kim

505. Research Core Center, National Cancer Centre Korea, Goyang-si, South Korea

Jong K. Kim

506. Department of Health Sciences and Technology, Sungkyunkwan University School of Medicine, Seoul, South Korea

Youngwook Kim

507. Samsung Genome Institute, Seoul, South Korea

Youngwook Kim

508. Breast Oncology Program, Dana-Farber/Brigham and Women's Cancer Center, Boston, MA, USA

Tari A. King

509. Department of Surgery, Memorial Sloan Kettering Cancer Center, New York, NY, USA

Tari A. King & Samuel Singer

510. Division of Breast Surgery, Brigham and Women's Hospital, Boston, MA, USA

Tari A. King

511. Integrative Bioinformatics Support Group, National Institute of Environmental Health Sciences (NIEHS), Durham, NC, USA

Leszek J. Klimczak

512. Department of Clinical Science, University of Bergen, Bergen, Norway

Stian Knappskog & Ola Myklebost

513. Center For Medical Innovation, Seoul National University Hospital, Seoul, South Korea

Youngil Koh

514. Department of Internal Medicine, Seoul National University Hospital, Seoul, South Korea

Youngil Koh & Sung-Soo Yoon

515. Institute of Computer Science, Polish Academy of Sciences, Warsawa, Poland

Jan Komorowski

516. Functional and Structural Genomics, German Cancer Research Center (DKFZ), Heidelberg, Germany

Marcel Kool, Andrey Korshunov, Michael Koscher, Stefan M. Pfister & Qi Wang

517. Laboratory of Translational Genomics, Division of Cancer Epidemiology and Genetics, National Cancer Institute, , National Institutes of Health, Bethesda, MD, USA

Roelof Koster

518. Institute for Medical Informatics Statistics and Epidemiology, University of Leipzig, Leipzig, Germany

Markus Kreuz & Markus Loeffler

519. Morgan Welch Inflammatory Breast Cancer Research Program and Clinic, The University of Texas MD Anderson Cancer Center, Houston, TX, USA

Savitri Krishnamurthy

520. Department of Hematology and Oncology, Georg-Augusts-University of Göttingen, Göttingen, Germany

Dieter Kube & Lorenz H. P. Trümper

521. Institute of Cell Biology (Cancer Research), University of Duisburg-Essen, Essen, Germany

Ralf Küppers

522. King’s College London and Guy’s and St. Thomas’ NHS Foundation Trust, London, UK

Jesper Lagergren

523. Center for Epigenetics, Van Andel Research Institute, Grand Rapids, MI, USA

Peter W. Laird

524. The University of Queensland Centre for Clinical Research, Royal Brisbane and Women’s Hospital, Herston, QLD, Australia

Sunil R. Lakhani & Peter T. Simpson

525. Department of Pediatric Oncology and Hematology, University of Cologne, Cologne, Germany

Pablo Landgraf

526. University of Düsseldorf, Düsseldorf, Germany

Pablo Landgraf & Guido Reifenberger

527. Department of Pathology, Institut Jules Bordet, Brussels, Belgium

Denis Larsimont

528. Institute of Biomedicine, Sahlgrenska Academy at University of Gothenburg, Gothenburg, Sweden

Erik Larsson

529. Children's Medical Research Institute, Sydney, NSW, Australia

Loretta M. S. Lau & Hilda A. Pickett

530. ILSbio, LLC Biobank, Chestertown, MD, USA

Xuan Le

531. Division of Genetics and Genomics, Boston Children's Hospital, Harvard Medical School, Boston, MA, USA

Eunjung Alice Lee

532. Institute for Bioengineering and Biopharmaceutical Research (IBBR), Hanyang University, Seoul, South Korea

Jeong-Yeon Lee

533. Department of Statistics, University of California Santa Cruz, Santa Cruz, CA, USA

Juhee Lee

534. National Genotyping Center, Institute of Biomedical Sciences, Academia Sinica, Taipei, Taiwan

Ming Ta Michael Lee

535. Department of Vertebrate Genomics/Otto Warburg Laboratory Gene Regulation and Systems Biology of Cancer, Max Planck Institute for Molecular Genetics, Berlin, Germany

Hans Lehrach, Hans-Jörg Warnatz & Marie-Laure Yaspo

536. McGill University and Genome Quebec Innovation Centre, Montreal, QC, Canada

Louis Letourneau

537. biobyte solutions GmbH, Heidelberg, Germany

Ivica Letunic

538. Gynecologic Oncology, NYU Laura and Isaac Perlmutter Cancer Center, New York University, New York, NY, USA

Douglas A. Levine

539. Division of Oncology, Stem Cell Biology Section, Washington University School of Medicine, St. Louis, MO, USA

Tim Ley

540. Department of Systems Biology, The University of Texas MD Anderson Cancer Center, Houston, TX, USA

Han Liang

541. Harvard University, Cambridge, MA, USA

Ziao Lin

542. Urologic Oncology Branch, Center for Cancer Research, National Cancer Institute, National Institutes of Health, Bethesda, MD, USA

W. M. Linehan

543. University of Oslo, Oslo, Norway

Ole Christian Lingjærde & Torill Sauer

544. University of Toronto, Toronto, ON, Canada

Fei-Fei Fei Liu, Quaid D. Morris, Ruian Shi, Shankar Vembu & Fan Yang

545. Peking University, Beijing, China

Fenglin Liu, Fan Zhang, Liangtao Zheng & Xiuqing Zheng

546. School of Life Sciences, Peking University, Beijing, China

Fenglin Liu

547. Leidos Biomedical Research, Inc, McLean, VA, USA

Jia Liu

548. Hematology, Hospital Clinic, Institut d'Investigacions Biomèdiques August Pi i Sunyer (IDIBAPS), University of Barcelona, Barcelona, Spain

Armando Lopez-Guillermo

549. Second Military Medical University, Shanghai, China

Yong-Jie Lu & Hongwei Zhang

550. Chinese Cancer Genome Consortium, Shenzhen, China

Youyong Lu

551. Department of Medical Oncology, Beijing Hospital, Beijing, China

Youyong Lu

552. Laboratory of Molecular Oncology, Key Laboratory of Carcinogenesis and Translational Research (Ministry of Education), Peking University Cancer Hospital and Institute, Beijing, China

Youyong Lu & Rui Xing

553. School of Medicine/School of Mathematics and Statistics, University of St. Andrews, St, Andrews, Fife, UK

Andy G. Lynch

554. Institute for Systems Biology, Seattle, WA, USA

Lisa Lype, Sheila M. Reynolds & Ilya Shmulevich

555. Department of Biochemistry and Molecular Biology, Faculty of Medicine, University Institute of Oncology-IUOPA, Oviedo, Spain

Carlos López-Otín & Xose S. Puente

556. Institut Bergonié, Bordeaux, France

Gaetan MacGrogan

557. Cancer Unit, MRC University of Cambridge, Cambridge, UK

Shona MacRae

558. Department of Pathology and Laboratory Medicine, Center for Personalized Medicine, Children's Hospital Los Angeles, Los Angeles, CA, USA

Dennis T. Maglinte

559. John Curtin School of Medical Research, Canberra, ACT, Australia

Graham J. Mann

560. MVZ Department of Oncology, PraxisClinic am Johannisplatz, Leipzig, Germany

Luisa Mantovani-Löffler

561. Department of Information Technology, Ghent University, Ghent, Belgium

Kathleen Marchal & Sergio Pulido-Tamayo

562. Department of Plant Biotechnology and Bioinformatics, Ghent University, Ghent, Belgium

Kathleen Marchal, Sergio Pulido-Tamayo & Lieven P. C. Verbeke

563. Institute for Genomic Medicine, Nationwide Children's Hospital, Columbus, OH, USA

Elaine R. Mardis

564. Computational Biology Program, School of Medicine, Oregon Health and Science University, Portland, OR, USA

Adam A. Margolin & Adam J. Struck

565. Department of Surgery, Duke University, Durham, NC, USA

Jeffrey Marks

566. Institució Catalana de Recerca i Estudis Avançats (ICREA), Barcelona, Spain

Tomas Marques-Bonet, Jose I. Martin-Subero, Arcadi Navarro, David Torrents & Alfonso Valencia

567. Institut Català de Paleontologia Miquel Crusafont, Universitat Autònoma de Barcelona, Barcelona, Spain

Tomas Marques-Bonet

568. University of Glasgow, Glasgow, UK

Sancha Martin & Ke Yuan

569. Institut d'Investigacions Biomèdiques August Pi i Sunyer (IDIBAPS), Barcelona, Spain

Jose I. Martin-Subero

570. Division of Oncology, Washington University School of Medicine, St. Louis, MO, USA

R. Jay Mashl

571. Department of Surgery and Cancer, Imperial College, London, INY, UK

Erik Mayer

572. Applications Department, Oxford Nanopore Technologies, Oxford, UK

Simon Mayes & Daniel J. Turner

573. Department of Obstetrics, Gynecology and Reproductive Services, University of California San Francisco, San Francisco, CA, USA

Karen McCune & Karen Smith-McCune

574. Department of Biochemistry and Molecular Medicine, University California at Davis, Sacramento, CA, USA

John D. McPherson

575. STTARR Innovation Facility, Princess Margaret Cancer Centre, Toronto, ON, Canada

Alice Meng

576. Discipline of Surgery, Western Sydney University, Penrith, NSW, Australia

Neil D. Merrett

577. Yale School of Medicine, Yale University, New Haven, CT, USA

William Meyerson

578. Department of Genetics, Lineberger Comprehensive Cancer Center, University of North Carolina at Chapel Hill, Chapel Hill, NC, USA

Piotr A. Mieczkowski, Joel S. Parker, Charles M. Perou, Donghui Tan, Umadevi Veluvolu & Matthew D. Wilkerson

579. Departments of Neurology and Neurosurgery, Henry Ford Hospital, Detroit, MI, USA

Tom Mikkelsen

580. Precision Oncology, OHSU Knight Cancer Institute, Oregon Health and Science University, Portland, OR, USA

Gordon B. Mills

581. Institute of Pathology, University Medical Center Hamburg-Eppendorf, Hamburg, Germany

Sarah Minner, Guido Sauter & Ronald Simon

582. Department of Health Sciences, Faculty of Medical Sciences, Kyushu University, Fukuoka, Japan

Shinichi Mizuno

583. Heidelberg Academy of Sciences and Humanities, Heidelberg, Germany

Fruzsina Molnár-Gábor

584. Department of Clinical Pathology, University of Melbourne, Melbourne, VIC, Australia

Carl Morrison, Karin A. Oien, Chawalit Pairojkul, Paul M. Waring & Marc J. van de Vijver

585. Department of Pathology, Roswell Park Cancer Institute, Buffalo, NY, USA

Carl Morrison

586. Department of Computer Science, University of Helsinki, Helsinki, Finland

Ville Mustonen

587. Institute of Biotechnology, University of Helsinki, Helsinki, Finland

Ville Mustonen

588. Organismal and Evolutionary Biology Research Programme, University of Helsinki, Helsinki, Finland

Ville Mustonen

589. Department of Obstetrics and Gynecology, Division of Gynecologic Oncology, Washington University School of Medicine, St. Louis, MO, USA

David Mutch

590. Penrose St. Francis Health Services, Colorado Springs, CO, USA

Jerome Myers

591. Institute of Pathology, Ulm University and University Hospital of Ulm, Ulm, Germany

Peter Möller

592. National Cancer Center, Tokyo, Japan

Hitoshi Nakagama

593. Genome Institute of Singapore, Singapore, Singapore

Tannistha Nandi & Patrick Tan

594. 32Program in Computational Biology and Bioinformatics, Yale University, New Haven, CT, USA

Fabio C. P. Navarro

595. German Cancer Aid, Bonn, Germany

Gerd Nettekoven & Laura Planko

596. Programme in Cancer and Stem Cell Biology, Centre for Computational Biology, Duke-NUS Medical School, Singapore, Singapore

Alvin Wei Tian Ng

597. The Chinese University of Hong Kong, Shatin, NT, Hong Kong, China

Anthony Ng

598. Fourth Military Medical University, Shaanxi, China

Yongzhan Nie

599. The University of Cambridge School of Clinical Medicine, Cambridge, UK

Serena Nik-Zainal

600. St. Jude Children’s Research Hospital, Memphis, TN, USA

Paul A. Northcott

601. University Health Network, Princess Margaret Cancer Centre, Toronto, ON, Canada

Faiyaz Notta & Ming Tsao

602. Center for Biomolecular Science and Engineering, University of California Santa Cruz, Santa Cruz, CA, USA

Brian D. O’Connor

603. Department of Medicine, University of Chicago, Chicago, IL, USA

Peter O’Donnell

604. Department of Neurology, Mayo Clinic, Rochester, MN, USA

Brian Patrick O’Neill

605. Cambridge Oesophagogastric Centre, Cambridge University Hospitals NHS Foundation Trust, Cambridge, UK

J. Robert O’Neill

606. Department of Computer Science, Carleton College, Northfield, MN, USA

Layla Oesper

607. Institute of Cancer Sciences, College of Medical Veterinary and Life Sciences, University of Glasgow, Glasgow, UK

Karin A. Oien

608. Department of Epidemiology, University of Alabama at Birmingham, Birmingham, AL, USA

Akinyemi I. Ojesina

609. HudsonAlpha Institute for Biotechnology, Huntsville, AL, USA

Akinyemi I. Ojesina

610. O'Neal Comprehensive Cancer Center, University of Alabama at Birmingham, Birmingham, AL, USA

Akinyemi I. Ojesina

611. Department of Pathology, Keio University School of Medicine, Tokyo, Japan

Hidenori Ojima

612. Department of Hepatobiliary and Pancreatic Oncology, National Cancer Center Hospital, Tokyo, Japan

Takuji Okusaka

613. Sage Bionetworks, Seattle, WA, USA

Larsson Omberg

614. Lymphoma Genomic Translational Research Laboratory, National Cancer Centre, Singapore, Singapore

Choon Kiat Ong

615. Department of Clinical Pathology, Robert-Bosch-Hospital, Stuttgart, Germany

German Ott

616. Department of Cell and Systems Biology, University of Toronto, Toronto, ON, Canada

B. F. Francis Ouellette

617. Department of Biosciences and Nutrition, Karolinska Institutet, Stockholm, Sweden

Qiang Pan-Hammarström

618. Center for Liver Cancer, Research Institute and Hospital, National Cancer Center, Gyeonggi, South Korea

Joong-Won Park

619. Division of Hematology-Oncology, Samsung Medical Center, Sungkyunkwan University School of Medicine, Seoul, South Korea

Keunchil Park

620. Samsung Advanced Institute for Health Sciences and Technology, Sungkyunkwan University School of Medicine, Seoul, South Korea

Keunchil Park

621. Cheonan Industry-Academic Collaboration Foundation, Sangmyung University, Cheonan, South Korea

Kiejung Park

622. NYU Langone Medical Center, New York, NY, USA

Harvey Pass

623. Department of Hematology and Medical Oncology, Cleveland Clinic, Cleveland, OH, USA

Nathan A. Pennell

624. Department of Radiation Oncology, University of California San Francisco, San Francisco, CA, USA

Marc D. Perry

625. Department of Health Sciences Research, Mayo Clinic, Rochester, MN, USA

Gloria M. Petersen

626. Helen F. Graham Cancer Center at Christiana Care Health Systems, Newark, DE, USA

Nicholas Petrelli

627. Heidelberg University Hospital, Heidelberg, Germany

Stefan M. Pfister

628. CSRA Incorporated, Fairfax, VA, USA

Todd D. Pihl

629. Research Department of Pathology, University College London Cancer Institute, London, UK

Nischalan Pillay

630. Department of Research Oncology, Guy's Hospital, King's Health Partners AHSC, King's College London School of Medicine, London, UK

Sarah Pinder

631. Faculty of Medicine and Health Sciences, Macquarie University, Sydney, NSW, Australia

Andreia V. Pinho

632. University Hospital of Minjoz, INSERM UMR 1098, Besançon, France

Xavier Pivot

633. Spanish National Cancer Research Centre, Madrid, Spain

Tirso Pons

634. Center of Digestive Diseases and Liver Transplantation, Fundeni Clinical Institute, Bucharest, Romania

Irinel Popescu

635. Cureline, Inc, South San Francisco, CA, USA

Olga Potapova

636. St. Luke's Cancer Centre, Royal Surrey County Hospital NHS Foundation Trust, Guildford, UK

Shaun R. Preston

637. Cambridge Breast Unit, Addenbrooke's Hospital, Cambridge University Hospital NHS Foundation Trust and NIHR Cambridge Biomedical Research Centre, Cambridge, UK

Elena Provenzano

638. East of Scotland Breast Service, Ninewells Hospital, Aberdeen, UK

Colin A. Purdie

639. Department of Genetics, Microbiology and Statistics, University of Barcelona, IRSJD, IBUB, Barcelona, Spain

Raquel Rabionet

640. Department of Obstetrics and Gynecology, Medical College of Wisconsin, Milwaukee, WI, USA

Janet S. Rader

641. Hematology and Medical Oncology, Winship Cancer Institute of Emory University, Atlanta, GA, USA

Suresh Ramalingam

642. Department of Computer Science, Princeton University, Princeton, NJ, USA

Benjamin J. Raphael & Matthew A. Reyna

643. Vanderbilt Ingram Cancer Center, Vanderbilt University, Nashville, TN, USA

W. Kimryn Rathmell

644. Ohio State University College of Medicine and Arthur G. James Comprehensive Cancer Center, Columbus, OH, USA

Matthew Ringel

645. Department of Surgery, Yokohama City University Graduate School of Medicine, Kanagawa, Japan

Yasushi Rino

646. Division of Chromatin Networks, German Cancer Research Center (DKFZ) and BioQuant, Heidelberg, Germany

Karsten Rippe

647. Research Computing Center, University of North Carolina at Chapel Hill, Chapel Hill, NC, USA

Jeffrey Roach

648. School of Molecular Biosciences and Center for Reproductive Biology, Washington State University, Pullman, WA, USA

Steven A. Roberts

649. Finsen Laboratory and Biotech Research and Innovation Centre (BRIC), University of Copenhagen, Copenhagen, Denmark

F. Germán Rodríguez-González, Nikos Sidiropoulos & Joachim Weischenfeldt

650. Department of Laboratory Medicine and Pathobiology, University of Toronto, Toronto, ON, Canada

Michael H. A. Roehrl & Stefano Serra

651. Department of Pathology, Human Oncology and Pathogenesis Program, Memorial Sloan Kettering Cancer Center, New York, NY, USA

Michael H. A. Roehrl

652. University Hospital Giessen, Pediatric Hematology and Oncology, Giessen, Germany

Marius Rohde

653. Oncologie Sénologie, ICM Institut Régional du Cancer, Montpellier, France

Gilles Romieu

654. Institute of Clinical Molecular Biology, Christian-Albrechts-University, Kiel, Germany

Philip C. Rosenstiel & Markus B. Schilhabel

655. Institute of Pathology, University of Wuerzburg, Wuerzburg, Germany

Andreas Rosenwald

656. Department of Urology, North Bristol NHS Trust, Bristol, UK

Edward W. Rowe

657. SingHealth, Duke-NUS Institute of Precision Medicine, National Heart Centre Singapore, Singapore, Singapore

Steven G. Rozen, Patrick Tan & Bin Tean Teh

658. Department of Computer Science, University of Toronto, Toronto, ON, Canada

Yulia Rubanova, Jared T. Simpson & Jeffrey A. Wintersinger

659. Bern Center for Precision Medicine, University Hospital of Bern, University of Bern, Bern, Switzerland

Mark A. Rubin

660. Englander Institute for Precision Medicine, Weill Cornell Medicine and New York Presbyterian Hospital, New York, NY, USA

Mark A. Rubin

661. Meyer Cancer Center, Weill Cornell Medicine, New York, NY, USA

Mark A. Rubin

662. Pathology and Laboratory, Weill Cornell Medical College, New York, NY, USA

Mark A. Rubin

663. Vall d'Hebron Institute of Oncology: VHIO, Barcelona, Spain

Carlota Rubio-Perez

664. General and Hepatobiliary-Biliary Surgery, Pancreas Institute, University and Hospital Trust of Verona, Verona, Italy

Andrea Ruzzenente

665. National Centre for Biological Sciences, Tata Institute of Fundamental Research, Bangalore, India

Radhakrishnan Sabarinathan

666. Indiana University, Bloomington, IN, USA

S. Cenk Sahinalp

667. Department of Pathology, GZA-ZNA Hospitals, Antwerp, Belgium

Roberto Salgado

668. Analytical Biological Services, Inc, Wilmington, DE, USA

Charles Saller

669. Sydney Medical School, University of Sydney, Sydney, NSW, Australia

Jaswinder S. Samra & Richard A. Scolyer

670. cBio Center, Dana-Farber Cancer Institute, Harvard Medical School, Boston, MA, USA

Chris Sander & Ciyue Shen

671. Department of Cell Biology, Harvard Medical School, Boston, MA, USA

Chris Sander & Ciyue Shen

672. Advanced Centre for Treatment Research and Education in Cancer, Tata Memorial Centre, Navi Mumbai, Maharashtra, India

Rajiv Sarin

673. School of Environmental and Life Sciences, Faculty of Science, The University of Newcastle, Ourimbah, NSW, Australia

Christopher J. Scarlett

674. Department of Dermatology, University Hospital of Essen, Essen, Germany

Dirk Schadendorf

675. Bioinformatics and Omics Data Analytics, German Cancer Research Center (DKFZ), Heidelberg, Germany

Matthias Schlesner

676. Department of Urology, Charité Universitätsmedizin Berlin, Berlin, Germany

Thorsten Schlomm & Joachim Weischenfeldt

677. Martini-Clinic, Prostate Cancer Center, University Medical Center Hamburg-Eppendorf, Hamburg, Germany

Thorsten Schlomm

678. Department of General Internal Medicine, University of Kiel, Kiel, Germany

Stefan Schreiber

679. German Cancer Consortium (DKTK), Partner site Berlin, Berlin, Germany

Roland F. Schwarz

680. Cancer Research Institute, Beth Israel Deaconess Medical Center, Boston, MA, USA

Ralph Scully

681. University of Pittsburgh, Pittsburgh, PA, USA

Raja Seethala

682. Department of Ophthalmology and Ocular Genomics Institute, Massachusetts Eye and Ear, Harvard Medical School, Boston, MA, USA

Ayellet V. Segre

683. Center for Psychiatric Genetics, NorthShore University HealthSystem, Evanston, IL, USA

Subhajit Sengupta

684. Van Andel Research Institute, Grand Rapids, MI, USA

Hui Shen & Wanding Zhou

685. Laboratory of Molecular Medicine, Human Genome Center, Institute of Medical Science, University of Tokyo, Tokyo, Japan

Tatsuhiro Shibata, Hirokazu Taniguchi & Tomoko Urushidate

686. Japan Agency for Medical Research and Development, Tokyo, Japan

Kiyo Shimizu & Takashi Yugawa

687. Korea University, Seoul, South Korea

Seung Jun Shin & Stefan G. Stark

688. Murtha Cancer Center, Walter Reed National Military Medical Center, Bethesda, MD, USA

Craig Shriver

689. Human Genetics, University of Kiel, Kiel, Germany

Reiner Siebert

690. Department of Oncologic Pathology, Dana-Farber Cancer Institute, Harvard Medical School, Boston, MA, USA

Sabina Signoretti

691. Oregon Health and Science University, Portland, OR, USA

Jaclyn Smith

692. Center for RNA Interference and Noncoding RNA, The University of Texas MD Anderson Cancer Center, Houston, TX, USA

Anil K. Sood

693. Department of Experimental Therapeutics, The University of Texas MD Anderson Cancer Center, Houston, TX, USA

Anil K. Sood

694. Department of Gynecologic Oncology and Reproductive Medicine, The University of Texas MD Anderson Cancer Center, Houston, TX, USA

Anil K. Sood

695. University Hospitals Coventry and Warwickshire NHS Trust, Coventry, UK

Sharmila Sothi

696. Department of Radiation Oncology, Radboud University Nijmegen Medical Centre, Nijmegen, GA, The Netherlands

Paul N. Span

697. Institute for Genomics and Systems Biology, University of Chicago, Chicago, IL, USA

Jonathan Spring

698. Clinic for Hematology and Oncology, St.-Antonius-Hospital, Eschweiler, Germany

Peter Staib

699. Computational and Systems Biology Program, Memorial Sloan Kettering Cancer Center, New York, NY, USA

Stefan G. Stark

700. University of Iceland, Reykjavik, Iceland

Ólafur Andri Stefánsson

701. Division of Computational Genomics and Systems Genetics, German Cancer Research Center (DKFZ), Heidelberg, Germany

Oliver Stegle

702. Dundee Cancer Centre, Ninewells Hospital, Dundee, UK

Alasdair Stenhouse & Alastair M. Thompson

703. Department for Internal Medicine III, University of Ulm and University Hospital of Ulm, Ulm, Germany

Stephan Stilgenbauer

704. Institut Curie, INSERM Unit 830, Paris, France

Henk G. Stunnenberg & Anne Vincent-Salomon

705. Department of Gastroenterology and Hepatology, Yokohama City University Graduate School of Medicine, Kanagawa, Japan

Akihiro Suzuki

706. Department of Laboratory Medicine, Radboud University Nijmegen Medical Centre, Nijmegen, GA, The Netherlands

Fred Sweep

707. Division of Cancer Genome Research, German Cancer Research Center (DKFZ), Heidelberg, Germany

Holger Sültmann

708. Department of General Surgery, Singapore General Hospital, Singapore, Singapore

Benita Kiat Tee Tan

709. Cancer Science Institute of Singapore, National University of Singapore, Singapore, Singapore

Patrick Tan & Bin Tean Teh

710. Department of Medical and Clinical Genetics, Genome-Scale Biology Research Program, University of Helsinki, Helsinki, Finland

Tomas J. Tanskanen

711. East Anglian Medical Genetics Service, Cambridge University Hospitals NHS Foundation Trust, Cambridge, UK

Patrick Tarpey

712. Irving Institute for Cancer Dynamics, Columbia University, New York, NY, USA

Simon Tavaré

713. Institute of Molecular and Cell Biology, Singapore, Singapore

Bin Tean Teh

714. Laboratory of Cancer Epigenome, Division of Medical Science, National Cancer Centre Singapore, Singapore, Singapore

Bin Tean Teh

715. Universite Lyon, INCa-Synergie, Centre Léon Bérard, Lyon, France

Gilles Thomas

716. Department of Urology, Mayo Clinic, Rochester, MN, USA

R. Houston Thompson

717. Royal National Orthopaedic Hospital - Stanmore, Stanmore, Middlesex, UK

Roberto Tirabosco

718. Department of Biochemistry, Genetics and Immunology, University of Vigo, Vigo, Spain

Marta Tojo

719. Giovanni Paolo II / I.R.C.C.S. Cancer Institute, Bari, BA, Italy

Stefania Tommasi

720. Neuroblastoma Genomics, German Cancer Research Center (DKFZ), Heidelberg, Germany

Umut H. Toprak

721. Fondazione Policlinico Universitario Gemelli IRCCS, Rome, Italy, Rome, Italy

Giampaolo Tortora

722. University of Verona, Verona, Italy

Giampaolo Tortora

723. Centre National de Génotypage, CEA - Institute de Génomique, Evry, France

Jörg Tost

724. CAPHRI Research School, Maastricht University, Maastricht, ER, The Netherlands

David Townend

725. Department of Biopathology, Centre Léon Bérard, Lyon, France

Isabelle Treilleux

726. Université Claude Bernard Lyon 1, Villeurbanne, France

Isabelle Treilleux

727. Core Research for Evolutional Science and Technology (CREST), JST, Tokyo, Japan

Tatsuhiko Tsunoda

728. Department of Biological Sciences, Laboratory for Medical Science Mathematics, Graduate School of Science, University of Tokyo, Yokohama, Japan

Tatsuhiko Tsunoda

729. Department of Medical Science Mathematics, Medical Research Institute, Tokyo Medical and Dental University (TMDU), Tokyo, Japan

Tatsuhiko Tsunoda

730. Cancer Ageing and Somatic Mutation Programme, Wellcome Sanger Institute, Hinxton, UK

Jose M. C. Tubio

731. University Hospitals Birmingham NHS Foundation Trust, Birmingham, UK

Olga Tucker

732. Centre for Cancer Research and Cell Biology, Queen's University, Belfast, UK

Richard Turkington

733. Breast Medical Oncology, The University of Texas MD Anderson Cancer Center, Houston, TX, USA

Naoto T. Ueno

734. Department of Surgery, Johns Hopkins University School of Medicine, Baltimore, MD, USA

Christopher Umbricht

735. Department of Oncology-Pathology, Science for Life Laboratory, Karolinska Institute, Stockholm, Sweden

Husen M. Umer

736. School of Cancer Sciences, Faculty of Medicine, University of Southampton, Southampton, UK

Timothy J. Underwood

737. Department of Gene Technology, Tallinn University of Technology, Tallinn, Estonia

Liis Uusküla-Reimand

738. Genetics and Genome Biology Program, SickKids Research Institute, The Hospital for Sick Children, Toronto, ON, Canada

Liis Uusküla-Reimand

739. Departments of Neurosurgery and Hematology and Medical Oncology, Winship Cancer Institute and School of Medicine, Emory University, Atlanta, GA, USA

Erwin G. Van Meir

740. Department of Clinical and Molecular Medicine, Faculty of Medicine and Health Sciences, Norwegian University of Science and Technology, Trondheim, Norway

Miguel Vazquez

741. Argmix Consulting, North Vancouver, BC, Canada

Shankar Vembu

742. Department of Information Technology, Ghent University, Interuniversitair Micro-Electronica Centrum (IMEC), Ghent, Belgium

Lieven P. C. Verbeke

743. Nuffield Department of Surgical Sciences, John Radcliffe Hospital, University of Oxford, Oxford, UK

Clare Verrill

744. Institute of Mathematics and Computer Science, University of Latvia, Riga, LV, Latvia

Juris Viksna

745. Discipline of Pathology, Sydney Medical School, University of Sydney, Sydney, NSW, Australia

Ricardo E. Vilain

746. Department of Applied Mathematics and Theoretical Physics, Centre for Mathematical Sciences, University of Cambridge, Cambridge, UK

Ignacio Vázquez-García

747. Department of Epidemiology and Biostatistics, Memorial Sloan Kettering Cancer Center, New York, NY, USA

Ignacio Vázquez-García & Venkata D. Yellapantula

748. Department of Statistics, Columbia University, New York, NY, USA

Ignacio Vázquez-García

749. Department of Immunology, Genetics and Pathology, Science for Life Laboratory, Uppsala University, Uppsala, Sweden

Claes Wadelius

750. School of Electronic and Information Engineering, Xi'an Jiaotong University, Xi'an, China

Jiayin Wang & Kai Ye

751. Department of Histopathology, Cambridge University Hospitals NHS Foundation Trust, Cambridge, UK

Anne Y. Warren

752. Oxford NIHR Biomedical Research Centre, University of Oxford, Oxford, UK

David C. Wedge

753. Georgia Regents University Cancer Center, Augusta, GA, USA

Paul Weinberger

754. Wythenshawe Hospital, Manchester, UK

Ian Welch

755. Department of Genetics, Washington University School of Medicine, St.Louis, MO, USA

Michael C. Wendl

756. Department of Biological Oceanography, Leibniz Institute of Baltic Sea Research, Rostock, Germany

Johannes Werner

757. Wellcome Centre for Human Genetics, University of Oxford, Oxford, UK

Justin P. Whalley

758. Department of Molecular and Human Genetics, Baylor College of Medicine, Houston, TX, USA

David A. Wheeler

759. Thoracic Oncology Laboratory, Mayo Clinic, Rochester, MN, USA

Dennis Wigle

760. Institute for Genomic Medicine, Nationwide Children's Hospital, Columbus, OH, USA

Richard K. Wilson

761. Department of Obstetrics and Gynecology, Division of Gynecologic Oncology, Mayo Clinic, Rochester, MN, USA

Boris Winterhoff

762. International Institute for Molecular Oncology, Poznań, Poland

Maciej Wiznerowicz

763. Poznan University of Medical Sciences, Poznań, Poland

Maciej Wiznerowicz

764. Genomics and Proteomics Core Facility High Throughput Sequencing Unit, German Cancer Research Center (DKFZ), Heidelberg, Germany

Stephan Wolf

765. NCCS-VARI Translational Research Laboratory, National Cancer Centre Singapore, Singapore, Singapore

Bernice H. Wong

766. Edison Family Center for Genome Sciences and Systems Biology, Washington University, St. Louis, MO, USA

Winghing Wong

767. MRC-University of Glasgow Centre for Virus Research, Glasgow, UK

Derek W. Wright

768. Department of Medical Informatics and Clinical Epidemiology, Division of Bioinformatics and Computational Biology, OHSU Knight Cancer Institute, Oregon Health and Science University, Portland, OR, USA

Guanming Wu

769. School of Electronic Information and Communications, Huazhong University of Science and Technology, Wuhan, China

Tian Xia

770. Department of Applied Mathematics and Statistics, Johns Hopkins University, Baltimore, MD, USA

Yanxun Xu

771. Department of Cancer Genome Informatics, Graduate School of Medicine, Osaka University, Osaka, Japan

Shinichi Yachida

772. Institute of Computer Science, Heidelberg University, Heidelberg, Germany

Sergei Yakneen

773. School of Mathematics and Statistics, University of Sydney, Sydney, NSW, Australia

Jean Y. Yang

774. Ben May Department for Cancer Research, University of Chicago, Chicago, IL, USA

Lixing Yang

775. Department of Human Genetics, University of Chicago, Chicago, IL, USA

Lixing Yang

776. Tri-Institutional PhD Program in Computational Biology and Medicine, Weill Cornell Medicine, New York, NY, USA

Xiaotong Yao

777. The First Affiliated Hospital, Xi’an Jiaotong University, Xi’an, China

Kai Ye

778. Department of Medicine and Therapeutics, The Chinese University of Hong Kong, Shatin, NT, Hong Kong, China

Jun Yu

779. Department of Biostatistics, The University of Texas MD Anderson Cancer Center, Houston, TX, USA

Kaixian Yu & Hongtu Zhu

780. Duke-NUS Medical School, Singapore, Singapore

Willie Yu

781. Department of Surgery, Ruijin Hospital, Shanghai Jiaotong University School of Medicine, Shanghai, China

Yingyan Yu

782. School of Computing Science, University of Glasgow, Glasgow, UK

Ke Yuan

783. Division of Orthopaedic Surgery, Oslo University Hospital, Oslo, Norway

Olga Zaikova

784. Eastern Clinical School, Monash University, Melbourne, VIC, Australia

Nikolajs Zeps

785. Epworth HealthCare, Richmond, VIC, Australia

Nikolajs Zeps

786. Department of Biostatistics and Computational Biology, Dana-Farber Cancer Institute and Harvard Medical School, Boston, MA, USA

Cheng-Zhong Zhang

787. Department of Biomedical Informatics, College of Medicine, The Ohio State University, Columbus, OH, USA

Yan Zhang

788. The Ohio State University Comprehensive Cancer Center (OSUCCC – James), Columbus, OH, USA

Yan Zhang

789. The University of Texas School of Biomedical Informatics (SBMI) at Houston, Houston, TX, USA

Zhongming Zhao

790. Department of Biostatistics, University of North Carolina at Chapel Hill, Chapel Hill, NC, USA

Hongtu Zhu

791. Department of Biochemistry and Molecular Genetics, Feinberg School of Medicine, Northwestern University, Chicago, IL, USA

Lihua Zou

792. Faculty of Medicine and Health, University of Sydney, Sydney, NSW, Australia

Anna deFazio

793. Department of Pathology, Erasmus Medical Center Rotterdam, Rotterdam, GD, The Netherlands

Carolien H. M. van Deurzen

794. Division of Molecular Carcinogenesis, The Netherlands Cancer Institute, Amsterdam, CX, The Netherlands

L. van't Veer

795. Institute of Molecular Life Sciences and Swiss Institute of Bioinformatics, University of Zurich, Zurich, Switzerland

Christian von Mering

Consortia

PCAWG Structural Variation Working Group

- Kadir C. Akdemir
- , Eva G. Alvarez
- , Adrian Baez-Ortega
- , Rameen Beroukhim
- , Paul C. Boutros
- , David D. L. Bowtell
- , Benedikt Brors
- , Kathleen H. Burns
- , Peter J. Campbell
- , Kin Chan
- , Ken Chen
- , Isidro Cortés-Ciriano
- , Ana Dueso-Barroso
- , Andrew J. Dunford
- , Paul A. Edwards
- , Xavier Estivill
- , Dariush Etemadmoghadam
- , Lars Feuerbach
- , J. Lynn Fink
- , Milana Frenkel-Morgenstern
- , Dale W. Garsed
- , Mark Gerstein
- , Dmitry A. Gordenin
- , David Haan
- , James E. Haber
- , Julian M. Hess
- , Barbara Hutter
- , Marcin Imielinski

- , David T. W. Jones
- , Young Seok Ju
- , Marat D. Kazanov
- , Leszek J. Klimczak
- , Youngil Koh
- , Jan O. Korbel
- , Kiran Kumar
- , Eunjung Alice Lee
- , Jake June-Koo Lee
- , Yilong Li
- , Andy G. Lynch
- , Geoff Macintyre
- , Florian Markowetz
- , Iñigo Martincorena
- , Alexander Martinez-Fundichely
- , Matthew Meyerson
- , Satoru Miyano
- , Hidewaki Nakagawa
- , Fabio C. P. Navarro
- , Stephan Ossowski
- , Peter J. Park
- , John V. Pearson
- , Montserrat Puiggròs
- , Karsten Rippe
- , Nicola D. Roberts
- , Steven A. Roberts
- , Bernardo Rodriguez-Martin
- , Steven E. Schumacher
- , Ralph Scully
- , Mark Shackleton
- , Nikos Sidiropoulos
- , Lina Sieverling
- , Chip Stewart
- , David Torrents
- , Jose M. C. Tubio
- , Izar Villasante
- , Nicola Waddell

- , Jeremiah A. Wala
- , Joachim Weischenfeldt
- , Lixing Yang
- , Xiaotong Yao
- , Sung-Soo Yoon
- , Jorge Zamora
- & Cheng-Zhong Zhang

PCAWG Consortium

- Lauri A. Aaltonen
- , Federico Abascal
- , Adam Abeshouse
- , Hiroyuki Aburatani
- , David J. Adams
- , Nishant Agrawal
- , Keun Soo Ahn
- , Sung-Min Ahn
- , Hiroshi Aikata
- , Rehan Akbani
- , Kadir C. Akdemir
- , Hikmat Al-Ahmadie
- , Sultan T. Al-Sedairy
- , Fatima Al-Shahrour
- , Malik Alawi
- , Monique Albert
- , Kenneth Aldape
- , Ludmil B. Alexandrov
- , Adrian Ally
- , Kathryn Alsop
- , Eva G. Alvarez
- , Fernanda Amary
- , Samirkumar B. Amin
- , Brice Aminou
- , Ole Ammerpohl
- , Matthew J. Anderson
- , Yeng Ang

- , Davide Antonello
- , Pavana Anur
- , Samuel Aparicio
- , Elizabeth L. Appelbaum
- , Yasuhito Arai
- , Axel Aretz
- , Koji Arihiro
- , Shun-ichi Ariizumi
- , Joshua Armenia
- , Laurent Arnould
- , Sylvia Asa
- , Yassen Assenov
- , Gurnit Atwal
- , Sietse Aukema
- , J. Todd Auman
- , Miriam R. R. Aure
- , Philip Awadalla
- , Marta Aymerich
- , Gary D. Bader
- , Adrian Baez-Ortega
- , Matthew H. Bailey
- , Peter J. Bailey
- , Miruna Balasundaram
- , Saianand Balu
- , Pratiti Bandopadhayay
- , Rosamonde E. Banks
- , Stefano Barbi
- , Andrew P. Barbour
- , Jonathan Barenboim
- , Jill Barnholtz-Sloan
- , Hugh Barr
- , Elisabet Barrera
- , John Bartlett
- , Javier Bartolome
- , Claudio Bassi
- , Oliver F. Bathe
- , Daniel Baumhoer

- , Prashant Bavi
- , Stephen B. Baylin
- , Wojciech Bazant
- , Duncan Beardsmore
- , Timothy A. Beck
- , Sam Behjati
- , Andreas Behren
- , Beifang Niu
- , Cindy Bell
- , Sergi Beltran
- , Christopher Benz
- , Andrew Berchuck
- , Anke K. Bergmann
- , Erik N. Bergstrom
- , Benjamin P. Berman
- , Daniel M. Berney
- , Stephan H. Bernhart
- , Rameen Beroukhim
- , Mario Berrios
- , Samantha Bersani
- , Johanna Bertl
- , Miguel Betancourt
- , Vinayak Bhandari
- , Shriram G. Bhosle
- , Andrew V. Biankin
- , Matthias Bieg
- , Darell Bigner
- , Hans Binder
- , Ewan Birney
- , Michael Birrer
- , Nidhan K. Biswas
- , Bodil Bjerkehagen
- , Tom Bodenheimer
- , Lori Boice
- , Giada Bonizzato
- , Johann S. De Bono
- , Arnoud Boot

- , Moiz S. Bootwalla
- , Ake Borg
- , Arndt Borkhardt
- , Keith A. Boroevich
- , Ivan Borozan
- , Christoph Borst
- , Marcus Bosenberg
- , Mattia Bosio
- , Jacqueline Boultwood
- , Guillaume Bourque
- , Paul C. Boutros
- , G. Steven Bova
- , David T. Bowen
- , Reanne Bowlby
- , David D. L. Bowtell
- , Sandrine Boyault
- , Rich Boyce
- , Jeffrey Boyd
- , Alvis Brazma
- , Paul Brennan
- , Daniel S. Brewer
- , Arie B. Brinkman
- , Robert G. Bristow
- , Russell R. Broaddus
- , Jane E. Brock
- , Malcolm Brock
- , Annegien Broeks
- , Angela N. Brooks
- , Denise Brooks
- , Benedikt Brors
- , Søren Brunak
- , Timothy J. C. Bruxner
- , Alicia L. Bruzos
- , Alex Buchanan
- , Ivo Buchhalter
- , Christiane Buchholz
- , Susan Bullman

- , Hazel Burke
- , Birgit Burkhardt
- , Kathleen H. Burns
- , John Busanovich
- , Carlos D. Bustamante
- , Adam P. Butler
- , Atul J. Butte
- , Niall J. Byrne
- , Anne-Lise Børresen-Dale
- , Samantha J. Caesar-Johnson
- , Andy Cafferkey
- , Declan Cahill
- , Claudia Calabrese
- , Carlos Caldas
- , Fabien Calvo
- , Niedzica Camacho
- , Peter J. Campbell
- , Elias Campo
- , Cinzia Cantù
- , Shaolong Cao
- , Thomas E. Carey
- , Joana Carlevaro-Fita
- , Rebecca Carlsen
- , Ivana Cataldo
- , Mario Cazzola
- , Jonathan Cebon
- , Robert Cerfolio
- , Dianne E. Chadwick
- , Dimple Chakravarty
- , Don Chalmers
- , Calvin Wing Yiu Chan
- , Kin Chan
- , Michelle Chan-Seng-Yue
- , Vishal S. Chandan
- , David K. Chang
- , Stephen J. Chanock
- , Lorraine A. Chantrill

- , Aurélien Chateigner
- , Nilanjan Chatterjee
- , Kazuaki Chayama
- , Hsiao-Wei Chen
- , Jieming Chen
- , Ken Chen
- , Yiwen Chen
- , Zhaohong Chen
- , Andrew D. Cherniack
- , Jeremy Chien
- , Yoke-Eng Chiew
- , Suet-Feung Chin
- , Juok Cho
- , Sunghoon Cho
- , Jung Kyoon Choi
- , Wan Choi
- , Christine Chomienne
- , Zechen Chong
- , Su Pin Choo
- , Angela Chou
- , Angelika N. Christ
- , Elizabeth L. Christie
- , Eric Chuah
- , Carrie Cibulskis
- , Kristian Cibulskis
- , Sara Cingarlini
- , Peter Clapham
- , Alexander Claviez
- , Sean Cleary
- , Nicole Cloonan
- , Marek Cmero
- , Colin C. Collins
- , Ashton A. Connor
- , Susanna L. Cooke
- , Colin S. Cooper
- , Leslie Cope
- , Vincenzo Corbo

- , Matthew G. Cordes
- , Stephen M. Cordner
- , Isidro Cortés-Ciriano
- , Kyle Covington
- , Prue A. Cowin
- , Brian Craft
- , David Craft
- , Chad J. Creighton
- , Yupeng Cun
- , Erin Curley
- , Ioana Cutcutache
- , Karolina Czajka
- , Bogdan Czerniak
- , Rebecca A. Dagg
- , Ludmila Danilova
- , Maria Vittoria Davi
- , Natalie R. Davidson
- , Helen Davies
- , Ian J. Davis
- , Brandi N. Davis-Dusenbery
- , Kevin J. Dawson
- , Francisco M. De La Vega
- , Ricardo De Paoli-Iseppi
- , Timothy Defreitas
- , Angelo P. Dei Tos
- , Olivier Delaneau
- , John A. Demchok
- , Jonas Demeulemeester
- , German M. Demidov
- , Deniz Demircioğlu
- , Nening M. Dennis
- , Robert E. Denroche
- , Stefan C. Dentro
- , Nikita Desai
- , Vikram Deshpande
- , Amit G. Deshwar
- , Christine Desmedt

- , Jordi Deu-Pons
- , Noreen Dhalla
- , Neesha C. Dhani
- , Priyanka Dhingra
- , Rajiv Dhir
- , Anthony DiBiase
- , Klev Diamanti
- , Li Ding
- , Shuai Ding
- , Huy Q. Dinh
- , Luc Dirix
- , HarshaVardhan Doddapaneni
- , Nilgun Donmez
- , Michelle T. Dow
- , Ronny Drapkin
- , Oliver Drechsel
- , Ruben M. Drews
- , Serge Serge
- , Tim Dudderidge
- , Ana Dueso-Barroso
- , Andrew J. Dunford
- , Michael Dunn
- , Lewis Jonathan Dursi
- , Fraser R. Duthie
- , Ken Dutton-Regester
- , Jenna Eagles
- , Douglas F. Easton
- , Stuart Edmonds
- , Paul A. Edwards
- , Sandra E. Edwards
- , Rosalind A. Eeles
- , Anna Ehinger
- , Juergen Eils
- , Roland Eils
- , Adel El-Naggar
- , Matthew Eldridge
- , Kyle Ellrott

- , Serap Erkek
- , Georgia Escaramis
- , Shadrielle M. G. Espiritu
- , Xavier Estivill
- , Dariush Etemadmoghadam
- , Jorunn E. Eyfjord
- , Bishoy M. Faltas
- , Daiming Fan
- , Yu Fan
- , William C. Faquin
- , Claudiu Farcas
- , Matteo Fassan
- , Aquila Fatima
- , Francesco Favero
- , Nodirjon Fayzullaev
- , Ina Felau
- , Sian Fereday
- , Martin L. Ferguson
- , Vincent Ferretti
- , Lars Feuerbach
- , Matthew A. Field
- , J. Lynn Fink
- , Gaetano Finocchiaro
- , Cyril Fisher
- , Matthew W. Fittall
- , Anna Fitzgerald
- , Rebecca C. Fitzgerald
- , Adrienne M. Flanagan
- , Neil E. Fleshner
- , Paul Flicek
- , John A. Foekens
- , Kwun M. Fong
- , Nuno A. Fonseca
- , Christopher S. Foster
- , Natalie S. Fox
- , Michael Fraser
- , Scott Frazer

- , Milana Frenkel-Morgenstern
- , William Friedman
- , Joan Frigola
- , Catrina C. Fronick
- , Akihiro Fujimoto
- , Masashi Fujita
- , Masashi Fukayama
- , Lucinda A. Fulton
- , Robert S. Fulton
- , Mayuko Furuta
- , P. Andrew Futreal
- , Anja Füllgrabe
- , Stacey B. Gabriel
- , Steven Gallinger
- , Carlo Gambacorti-Passerini
- , Jianjiong Gao
- , Shengjie Gao
- , Levi Garraway
- , Øystein Garred
- , Erik Garrison
- , Dale W. Garsed
- , Nils Gehlenborg
- , Josep L. L. Gelpi
- , Joshy George
- , Daniela S. Gerhard
- , Clarissa Gerhauser
- , Jeffrey E. Gershenwald
- , Mark Gerstein
- , Moritz Gerstung
- , Gad Getz
- , Mohammed Ghori
- , Ronald Ghossein
- , Nasra H. Giama
- , Richard A. Gibbs
- , Bob Gibson
- , Anthony J. Gill
- , Pelvender Gill

- , Dilip D. Giri
- , Dominik Glodzik
- , Vincent J. Gnanapragasam
- , Maria Elisabeth Goebler
- , Mary J. Goldman
- , Carmen Gomez
- , Santiago Gonzalez
- , Abel Gonzalez-Perez
- , Dmitry A. Gordenin
- , James Gossage
- , Kunihito Gotoh
- , Ramaswamy Govindan
- , Dorthe Grabau
- , Janet S. Graham
- , Robert C. Grant
- , Anthony R. Green
- , Eric Green
- , Liliana Greger
- , Nicola Grehan
- , Sonia Grimaldi
- , Sean M. Grimmond
- , Robert L. Grossman
- , Adam Grundhoff
- , Gunes Gundem
- , Qianyun Guo
- , Manaswi Gupta
- , Shailja Gupta
- , Ivo G. Gut
- , Marta Gut
- , Jonathan Göke
- , Gavin Ha
- , Andrea Haake
- , David Haan
- , Siegfried Haas
- , Kerstin Haase
- , James E. Haber
- , Nina Habermann

- , Faraz Hach
- , Syed Haider
- , Natsuko Hama
- , Freddie C. Hamdy
- , Anne Hamilton
- , Mark P. Hamilton
- , Leng Han
- , George B. Hanna
- , Martin Hansmann
- , Nicholas J. Haradhvala
- , Olivier Harismendy
- , Ivon Harliwong
- , Arif O. Harmanci
- , Eoghan Harrington
- , Takanori Hasegawa
- , David Haussler
- , Steve Hawkins
- , Shinya Hayami
- , Shuto Hayashi
- , D. Neil Hayes
- , Stephen J. Hayes
- , Nicholas K. Hayward
- , Steven Hazell
- , Yao He
- , Allison P. Heath
- , Simon C. Heath
- , David Hedley
- , Apurva M. Hegde
- , David I. Heiman
- , Michael C. Heinold
- , Zachary Heins
- , Lawrence E. Heisler
- , Eva Hellstrom-Lindberg
- , Mohamed Helmy
- , Seong Gu Heo
- , Austin J. Hepperla
- , José María Heredia-Genestar

- , Carl Herrmann
- , Peter Hersey
- , Julian M. Hess
- , Holmfridur Hilmarsdottir
- , Jonathan Hinton
- , Satoshi Hirano
- , Nobuyoshi Hiraoka
- , Katherine A. Hoadley
- , Asger Hobolth
- , Ermin Hodzic
- , Jessica I. Hoell
- , Steve Hoffmann
- , Oliver Hofmann
- , Andrea Holbrook
- , Aliaksei Z. Holik
- , Michael A. Hollingsworth
- , Oliver Holmes
- , Robert A. Holt
- , Chen Hong
- , Eun Pyo Hong
- , Jongwhi H. Hong
- , Gerrit K. Hooijer
- , Henrik Hornshøj
- , Fumie Hosoda
- , Yong Hou
- , Volker Hovestadt
- , William Howat
- , Alan P. Hoyle
- , Ralph H. Hruban
- , Jianhong Hu
- , Taobo Hu
- , Xing Hua
- , Kuan-lin Huang
- , Mei Huang
- , Mi Ni Huang
- , Vincent Huang
- , Yi Huang

- , Wolfgang Huber
- , Thomas J. Hudson
- , Michael Hummel
- , Jillian A. Hung
- , David Huntsman
- , Ted R. Hupp
- , Jason Huse
- , Matthew R. Huska
- , Barbara Hutter
- , Carolyn M. Hutter
- , Daniel Hübschmann
- , Christine A. Iacobuzio-Donahue
- , Charles David Imbusch
- , Marcin Imielinski
- , Seiya Imoto
- , William B. Isaacs
- , Keren Isaev
- , Shumpei Ishikawa
- , Murat Iskar
- , S. M. Ashiqul Islam
- , Michael Ittmann
- , Sinisa Ivkovic
- , Jose M. G. Izarzugaza
- , Jocelyne Jacquemier
- , Valerie Jakrot
- , Nigel B. Jamieson
- , Gun Ho Jang
- , Se Jin Jang
- , Joy C. Jayaseelan
- , Reyka Jayasinghe
- , Stuart R. Jefferys
- , Karine Jegalian
- , Jennifer L. Jennings
- , Seung-Hyup Jeon
- , Lara Jerman
- , Yuan Ji
- , Wei Jiao

- , Peter A. Johansson
- , Amber L. Johns
- , Jeremy Johns
- , Rory Johnson
- , Todd A. Johnson
- , Clemency Jolly
- , Yann Joly
- , Jon G. Jonasson
- , Corbin D. Jones
- , David R. Jones
- , David T. W. Jones
- , Nic Jones
- , Steven J. M. Jones
- , Jos Jonkers
- , Young Seok Ju
- , Hartmut Juhl
- , Jongsun Jung
- , Malene Juul
- , Randi Istrup Juul
- , Sissel Juul
- , Natalie Jäger
- , Rolf Kabbe
- , Andre Kahles
- , Abdullah Kahraman
- , Vera B. Kaiser
- , Hojabr Kakavand
- , Sangeetha Kalimuthu
- , Christof von Kalle
- , Koo Jeong Kang
- , Katalin Karaszi
- , Beth Karlan
- , Rosa Karlić
- , Dennis Karsch
- , Katayoon Kasaian
- , Karin S. Kassahn
- , Hitoshi Katai
- , Mamoru Kato

- , Hiroto Katoh
- , Yoshiiku Kawakami
- , Jonathan D. Kay
- , Stephen H. Kazakoff
- , Marat D. Kazanov
- , Maria Keays
- , Electron Kebebew
- , Richard F. Kefford
- , Manolis Kellis
- , James G. Kench
- , Catherine J. Kennedy
- , Jules N. A. Kerssemakers
- , David Khoo
- , Vincent Khoo
- , Narong Khuntikeo
- , Ekta Khurana
- , Helena Kilpinen
- , Hark Kyun Kim
- , Hyung-Lae Kim
- , Hyung-Yong Kim
- , Hyunghwan Kim
- , Jaegil Kim
- , Jihoon Kim
- , Jong K. Kim
- , Youngwook Kim
- , Tari A. King
- , Wolfram Klapper
- , Kortine Kleinheinz
- , Leszek J. Klimczak
- , Stian Knappskog
- , Michael Kneba
- , Bartha M. Knoppers
- , Youngil Koh
- , Jan Komorowski
- , Daisuke Komura
- , Mitsuhiro Komura
- , Gu Kong

- , Marcel Kool
- , Jan O. Korbel
- , Viktoriya Korchina
- , Andrey Korshunov
- , Michael Koscher
- , Roelof Koster
- , Zsofia Kote-Jarai
- , Antonios Koures
- , Milena Kovacevic
- , Barbara Kremeyer
- , Helene Kretzmer
- , Markus Kreuz
- , Savitri Krishnamurthy
- , Dieter Kube
- , Kiran Kumar
- , Pardeep Kumar
- , Sushant Kumar
- , Yogesh Kumar
- , Ritika Kundra
- , Kirsten Kübler
- , Ralf Küppers
- , Jesper Lagergren
- , Phillip H. Lai
- , Peter W. Laird
- , Sunil R. Lakhani
- , Christopher M. Lalansingh
- , Emilie Lalonde
- , Fabien C. Lamaze
- , Adam Lambert
- , Eric Lander
- , Pablo Landgraf
- , Luca Landoni
- , Anita Langerød
- , Andrés Lanzós
- , Denis Larsimont
- , Erik Larsson
- , Mark Lathrop

- , Loretta M. S. Lau
- , Chris Lawerenz
- , Rita T. Lawlor
- , Michael S. Lawrence
- , Alexander J. Lazar
- , Ana Mijalkovic Lazic
- , Xuan Le
- , Darlene Lee
- , Donghoon Lee
- , Eunjung Alice Lee
- , Hee Jin Lee
- , Jake June-Koo Lee
- , Jeong-Yeon Lee
- , Juhee Lee
- , Ming Ta Michael Lee
- , Henry Lee-Six
- , Kjong-Van Lehmann
- , Hans Lehrach
- , Dido Lenze
- , Conrad R. Leonard
- , Daniel A. Leongamornlert
- , Ignaty Leshchiner
- , Louis Letourneau
- , Ivica Letunic
- , Douglas A. Levine
- , Lora Lewis
- , Tim Ley
- , Chang Li
- , Constance H. Li
- , Haiyan Irene Li
- , Jun Li
- , Lin Li
- , Shantao Li
- , Siliang Li
- , Xiaobo Li
- , Xiaotong Li
- , Xinyue Li

- , Yilong Li
- , Han Liang
- , Sheng-Ben Liang
- , Peter Lichter
- , Pei Lin
- , Ziao Lin
- , W. M. Linehan
- , Ole Christian Lingjærde
- , Dongbing Liu
- , Eric Minwei Liu
- , Fei-Fei Fei Liu
- , Fenglin Liu
- , Jia Liu
- , Xingmin Liu
- , Julie Livingstone
- , Dimitri Livitz
- , Naomi Livni
- , Lucas Lochovsky
- , Markus Loeffler
- , Georgina V. Long
- , Armando Lopez-Guillermo
- , Shaoke Lou
- , David N. Louis
- , Laurence B. Lovat
- , Yiling Lu
- , Yong-Jie Lu
- , Youyong Lu
- , Claudio Luchini
- , Ilinca Lungu
- , Xuemei Luo
- , Hayley J. Luxton
- , Andy G. Lynch
- , Lisa Lype
- , Cristina López
- , Carlos López-Otín
- , Eric Z. Ma
- , Yussanne Ma

- , Gaetan MacGrogan
- , Shona MacRae
- , Geoff Macintyre
- , Tobias Madsen
- , Kazuhiro Maejima
- , Andrea Mafficini
- , Dennis T. Maglinte
- , Arindam Maitra
- , Partha P. Majumder
- , Luca Malcovati
- , Salem Malikic
- , Giuseppe Malleo
- , Graham J. Mann
- , Luisa Mantovani-Löffler
- , Kathleen Marchal
- , Giovanni Marchegiani
- , Elaine R. Mardis
- , Adam A. Margolin
- , Maximillian G. Marin
- , Florian Markowetz
- , Julia Markowski
- , Jeffrey Marks
- , Tomas Marques-Bonet
- , Marco A. Marra
- , Luke Marsden
- , John W. M. Martens
- , Sancha Martin
- , Jose I. Martin-Subero
- , Iñigo Martincorena
- , Alexander Martinez-Fundichely
- , Yosef E. Maruvka
- , R. Jay Mashl
- , Charlie E. Massie
- , Thomas J. Matthew
- , Lucy Matthews
- , Erik Mayer
- , Simon Mayes

- , Michael Mayo
- , Faridah Mbabaali
- , Karen McCune
- , Ultan McDermott
- , Patrick D. McGillivray
- , Michael D. McLellan
- , John D. McPherson
- , John R. McPherson
- , Treasa A. McPherson
- , Samuel R. Meier
- , Alice Meng
- , Shaowu Meng
- , Andrew Menzies
- , Neil D. Merrett
- , Sue Merson
- , Matthew Meyerson
- , William Meyerson
- , Piotr A. Mieczkowski
- , George L. Mihaiescu
- , Sanja Mijalkovic
- , Tom Mikkelsen
- , Michele Milella
- , Linda Mileshkin
- , Christopher A. Miller
- , David K. Miller
- , Jessica K. Miller
- , Gordon B. Mills
- , Ana Milovanovic
- , Sarah Minner
- , Marco Miotto
- , Gisela Mir Arnau
- , Lisa Mirabello
- , Chris Mitchell
- , Thomas J. Mitchell
- , Satoru Miyano
- , Naoki Miyoshi
- , Shinichi Mizuno

- , Fruzsina Molnár-Gábor
- , Malcolm J. Moore
- , Richard A. Moore
- , Sandro Morganella
- , Quaid D. Morris
- , Carl Morrison
- , Lisle E. Mose
- , Catherine D. Moser
- , Ferran Muiños
- , Loris Mularoni
- , Andrew J. Mungall
- , Karen Mungall
- , Elizabeth A. Musgrove
- , Ville Mustonen
- , David Mutch
- , Francesc Muyas
- , Donna M. Muzny
- , Alfonso Muñoz
- , Jerome Myers
- , Ola Myklebost
- , Peter Möller
- , Genta Nagae
- , Adnan M. Nagrial
- , Hardeep K. Nahal-Bose
- , Hitoshi Nakagama
- , Hidewaki Nakagawa
- , Hiromi Nakamura
- , Toru Nakamura
- , Kaoru Nakano
- , Tannistha Nandi
- , Jyoti Nangalia
- , Mia Nastic
- , Arcadi Navarro
- , Fabio C. P. Navarro
- , David E. Neal
- , Gerd Nettekoven
- , Felicity Newell

- , Steven J. Newhouse
- , Yulia Newton
- , Alvin Wei Tian Ng
- , Anthony Ng
- , Jonathan Nicholson
- , David Nicol
- , Yongzhan Nie
- , G. Petur Nielsen
- , Morten Muhlig Nielsen
- , Serena Nik-Zainal
- , Michael S. Noble
- , Katia Nones
- , Paul A. Northcott
- , Faiyaz Notta
- , Brian D. O’Connor
- , Peter O’Donnell
- , Maria O’Donovan
- , Sarah O’Meara
- , Brian Patrick O’Neill
- , J. Robert O’Neill
- , David Ocana
- , Angelica Ochoa
- , Layla Oesper
- , Christopher Ogden
- , Hideki Ohdan
- , Kazuhiro Ohi
- , Lucila Ohno-Machado
- , Karin A. Oien
- , Akinyemi I. Ojesina
- , Hidenori Ojima
- , Takuji Okusaka
- , Larsson Omberg
- , Choon Kiat Ong
- , Stephan Ossowski
- , German Ott
- , B. F. Francis Ouellette
- , Christine P’ng

- , Marta Paczkowska
- , Salvatore Paiella
- , Chawalit Pairojkul
- , Marina Pajic
- , Qiang Pan-Hammarström
- , Elli Papaemmanuil
- , Irene Papatheodorou
- , Nagarajan Paramasivam
- , Ji Wan Park
- , Joong-Won Park
- , Keunchil Park
- , Kiejung Park
- , Peter J. Park
- , Joel S. Parker
- , Simon L. Parsons
- , Harvey Pass
- , Danielle Pasternack
- , Alessandro Pastore
- , Ann-Marie Patch
- , Iris Pauporté
- , Antonio Pea
- , John V. Pearson
- , Chandra Sekhar Pedamallu
- , Jakob Skou Pedersen
- , Paolo Pederzoli
- , Martin Peifer
- , Nathan A. Pennell
- , Charles M. Perou
- , Marc D. Perry
- , Gloria M. Petersen
- , Myron Peto
- , Nicholas Petrelli
- , Robert Petryszak
- , Stefan M. Pfister
- , Mark Phillips
- , Oriol Pich
- , Hilda A. Pickett

- , Todd D. Pihl
- , Nischalan Pillay
- , Sarah Pinder
- , Mark Pinese
- , Andreia V. Pinho
- , Esa Pitkänen
- , Xavier Pivot
- , Elena Piñeiro-Yáñez
- , Laura Planko
- , Christoph Plass
- , Paz Polak
- , Tirso Pons
- , Irinel Popescu
- , Olga Potapova
- , Aparna Prasad
- , Shaun R. Preston
- , Manuel Prinz
- , Antonia L. Pritchard
- , Stephenie D. Prokopec
- , Elena Provenzano
- , Xose S. Puente
- , Sonia Puig
- , Montserrat Puiggròs
- , Sergio Pulido-Tamayo
- , Gulietta M. Pupo
- , Colin A. Purdie
- , Michael C. Quinn
- , Raquel Rabionet
- , Janet S. Rader
- , Bernhard Radlwimmer
- , Petar Radovic
- , Benjamin Raeder
- , Keiran M. Raine
- , Manasa Ramakrishna
- , Kamna Ramakrishnan
- , Suresh Ramalingam
- , Benjamin J. Raphael

- , W. Kimryn Rathmell
- , Tobias Rausch
- , Guido Reifenberger
- , Jüri Reimand
- , Jorge Reis-Filho
- , Victor Reuter
- , Iker Reyes-Salazar
- , Matthew A. Reyna
- , Sheila M. Reynolds
- , Esther Rheinbay
- , Yasser Riazalhosseini
- , Andrea L. Richardson
- , Julia Richter
- , Matthew Ringel
- , Markus Ringnér
- , Yasushi Rino
- , Karsten Rippe
- , Jeffrey Roach
- , Lewis R. Roberts
- , Nicola D. Roberts
- , Steven A. Roberts
- , A. Gordon Robertson
- , Alan J. Robertson
- , Javier Bartolomé Rodriguez
- , Bernardo Rodriguez-Martin
- , F. Germán Rodríguez-González
- , Michael H. A. Roehrl
- , Marius Rohde
- , Hirofumi Rokutan
- , Gilles Romieu
- , Ilse Rooman
- , Tom Roques
- , Daniel Rosebrock
- , Mara Rosenberg
- , Philip C. Rosenstiel
- , Andreas Rosenwald
- , Edward W. Rowe

- , Romina Royo
- , Steven G. Rozen
- , Yulia Rubanova
- , Mark A. Rubin
- , Carlota Rubio-Perez
- , Vasilisa A. Rudneva
- , Borislav C. Rusev
- , Andrea Ruzzenente
- , Gunnar Rätsch
- , Radhakrishnan Sabarinathan
- , Veronica Y. Sabelnykova
- , Sara Sadeghi
- , S. Cenk Sahinalp
- , Natalie Saini
- , Mihoko Saito-Adachi
- , Gordon Saksena
- , Adriana Salcedo
- , Roberto Salgado
- , Leonidas Salichos
- , Richard Sallari
- , Charles Saller
- , Roberto Salvia
- , Michelle Sam
- , Jaswinder S. Samra
- , Francisco Sanchez-Vega
- , Chris Sander
- , Grant Sanders
- , Rajiv Sarin
- , Iman Sarrafi
- , Aya Sasaki-Oku
- , Torill Sauer
- , Guido Sauter
- , Robyn P. M. Saw
- , Maria Scardoni
- , Christopher J. Scarlett
- , Aldo Scarpa
- , Ghislaine Scelo

- , Dirk Schadendorf
- , Jacqueline E. Schein
- , Markus B. Schilhabel
- , Matthias Schlesner
- , Thorsten Schlomm
- , Heather K. Schmidt
- , Sarah-Jane Schramm
- , Stefan Schreiber
- , Nikolaus Schultz
- , Steven E. Schumacher
- , Roland F. Schwarz
- , Richard A. Scolyer
- , David Scott
- , Ralph Scully
- , Raja Seethala
- , Ayellet V. Segre
- , Iris Selander
- , Colin A. Semple
- , Yasin Senbabaoglu
- , Subhajit Sengupta
- , Elisabetta Sereni
- , Stefano Serra
- , Dennis C. Sgroi
- , Mark Shackleton
- , Nimish C. Shah
- , Sagedeh Shahabi
- , Catherine A. Shang
- , Ping Shang
- , Ofer Shapira
- , Troy Shelton
- , Ciyue Shen
- , Hui Shen
- , Rebecca Shepherd
- , Ruian Shi
- , Yan Shi
- , Yu-Jia Shiah
- , Tatsuhiro Shibata

- , Juliann Shih
- , Eigo Shimizu
- , Kiyo Shimizu
- , Seung Jun Shin
- , Yuichi Shiraishi
- , Tal Shmaya
- , Ilya Shmulevich
- , Solomon I. Shorser
- , Charles Short
- , Raunak Shrestha
- , Suyash S. Shringarpure
- , Craig Shriver
- , Shimin Shuai
- , Nikos Sidiropoulos
- , Reiner Siebert
- , Anieta M. Sieuwerts
- , Lina Sieverling
- , Sabina Signoretti
- , Katarzyna O. Sikora
- , Michele Simbolo
- , Ronald Simon
- , Janae V. Simons
- , Jared T. Simpson
- , Peter T. Simpson
- , Samuel Singer
- , Nasa Sinnott-Armstrong
- , Payal Sipahimalani
- , Tara J. Skelly
- , Marcel Smid
- , Jaclyn Smith
- , Karen Smith-McCune
- , Nicholas D. Socci
- , Heidi J. Sofia
- , Matthew G. Soloway
- , Lei Song
- , Anil K. Sood
- , Sharmila Sothi

- , Christos Sotiriou
- , Cameron M. Soulette
- , Paul N. Span
- , Paul T. Spellman
- , Nicola Sperandio
- , Andrew J. Spillane
- , Oliver Spiro
- , Jonathan Spring
- , Johan Staaf
- , Peter F. Stadler
- , Peter Staib
- , Stefan G. Stark
- , Lucy Stebbings
- , Ólafur Andri Stefánsson
- , Oliver Stegle
- , Lincoln D. Stein
- , Alasdair Stenhouse
- , Chip Stewart
- , Stephan Stilgenbauer
- , Miranda D. Stobbe
- , Michael R. Stratton
- , Jonathan R. Stretch
- , Adam J. Struck
- , Joshua M. Stuart
- , Henk G. Stunnenberg
- , Hong Su
- , Xiaoping Su
- , Ren X. Sun
- , Stephanie Sungalee
- , Hana Susak
- , Akihiro Suzuki
- , Fred Sweep
- , Monika Szczepanowski
- , Holger Sültmann
- , Takashi Yugawa
- , Angela Tam
- , David Tamborero

- , Benita Kiat Tee Tan
- , Donghui Tan
- , Patrick Tan
- , Hiroko Tanaka
- , Hirokazu Taniguchi
- , Tomas J. Tanskanen
- , Maxime Tarabichi
- , Roy Tarnuzzer
- , Patrick Tarpey
- , Morgan L. Taschuk
- , Kenji Tatsuno
- , Simon Tavaré
- , Darrin F. Taylor
- , Amaro Taylor-Weiner
- , Jon W. Teague
- , Bin Tean Teh
- , Varsha Tembe
- , Javier Temes
- , Kevin Thai
- , Sarah P. Thayer
- , Nina Thiessen
- , Gilles Thomas
- , Sarah Thomas
- , Alan Thompson
- , Alastair M. Thompson
- , John F. F. Thompson
- , R. Houston Thompson
- , Heather Thorne
- , Leigh B. Thorne
- , Adrian Thorogood
- , Grace Tiao
- , Nebojsa Tijanic
- , Lee E. Timms
- , Roberto Tirabosco
- , Marta Tojo
- , Stefania Tommasi
- , Christopher W. Toon

- , Umut H. Toprak
- , David Torrents
- , Giampaolo Tortora
- , Jörg Tost
- , Yasushi Totoki
- , David Townend
- , Nadia Traficante
- , Isabelle Treilleux
- , Jean-Rémi Trotta
- , Lorenz H. P. Trümper
- , Ming Tsao
- , Tatsuhiko Tsunoda
- , Jose M. C. Tubio
- , Olga Tucker
- , Richard Turkington
- , Daniel J. Turner
- , Andrew Tutt
- , Masaki Ueno
- , Naoto T. Ueno
- , Christopher Umbricht
- , Husen M. Umer
- , Timothy J. Underwood
- , Lara Urban
- , Tomoko Urushidate
- , Tetsuo Ushiku
- , Liis Uusküla-Reimand
- , Alfonso Valencia
- , David J. Van Den Berg
- , Steven Van Laere
- , Peter Van Loo
- , Erwin G. Van Meir
- , Gert G. Van den Eynden
- , Theodorus Van der Kwast
- , Naveen Vasudev
- , Miguel Vazquez
- , Ravikiran Vedururu
- , Umadevi Veluvolu

- , Shankar Vembu
- , Lieven P. C. Verbeke
- , Peter Vermeulen
- , Clare Verrill
- , Alain Viari
- , David Vicente
- , Caterina Vicentini
- , K. VijayRaghavan
- , Juris Viksna
- , Ricardo E. Vilain
- , Izar Villasante
- , Anne Vincent-Salomon
- , Tapio Visakorpi
- , Douglas Voet
- , Paresh Vyas
- , Ignacio Vázquez-García
- , Nick M. Waddell
- , Nicola Waddell
- , Claes Wadelius
- , Lina Wadi
- , Rabea Wagener
- , Jeremiah A. Wala
- , Jian Wang
- , Jiayin Wang
- , Linghua Wang
- , Qi Wang
- , Wenyi Wang
- , Yumeng Wang
- , Zhining Wang
- , Paul M. Waring
- , Hans-Jörg Warnatz
- , Jonathan Warrell
- , Anne Y. Warren
- , Sebastian M. Waszak
- , David C. Wedge
- , Dieter Weichenhan
- , Paul Weinberger

- , John N. Weinstein
- , Joachim Weischenfeldt
- , Daniel J. Weisenberger
- , Ian Welch
- , Michael C. Wendl
- , Johannes Werner
- , Justin P. Whalley
- , David A. Wheeler
- , Hayley C. Whitaker
- , Dennis Wigle
- , Matthew D. Wilkerson
- , Ashley Williams
- , James S. Wilmott
- , Gavin W. Wilson
- , Julie M. Wilson
- , Richard K. Wilson
- , Boris Winterhoff
- , Jeffrey A. Wintersinger
- , Maciej Wiznerowicz
- , Stephan Wolf
- , Bernice H. Wong
- , Tina Wong
- , Winghing Wong
- , Youngchoon Woo
- , Scott Wood
- , Bradly G. Wouters
- , Adam J. Wright
- , Derek W. Wright
- , Mark H. Wright
- , Chin-Lee Wu
- , Dai-Ying Wu
- , Guanming Wu
- , Jianmin Wu
- , Kui Wu
- , Yang Wu
- , Zhenggang Wu
- , Liu Xi

- , Tian Xia
- , Qian Xiang
- , Xiao Xiao
- , Rui Xing
- , Heng Xiong
- , Qinying Xu
- , Yanxun Xu
- , Hong Xue
- , Shinichi Yachida
- , Sergei Yakneen
- , Rui Yamaguchi
- , Takafumi N. Yamaguchi
- , Masakazu Yamamoto
- , Shogo Yamamoto
- , Hiroki Yamaue
- , Fan Yang
- , Huanming Yang
- , Jean Y. Yang
- , Liming Yang
- , Lixing Yang
- , Shanlin Yang
- , Tsun-Po Yang
- , Yang Yang
- , Xiaotong Yao
- , Marie-Laure Yaspo
- , Lucy Yates
- , Christina Yau
- , Chen Ye
- , Kai Ye
- , Venkata D. Yellapantula
- , Christopher J. Yoon
- , Sung-Soo Yoon
- , Fouad Yousif
- , Jun Yu
- , Kaixian Yu
- , Willie Yu
- , Yingyan Yu

- , Ke Yuan
- , Yuan Yuan
- , Denis Yuen
- , Takashi Yugawa
- , Christina K. Yung
- , Olga Zaikova
- , Jorge Zamora
- , Marc Zapatka
- , Jean C. Zenklusen
- , Thorsten Zenz
- , Nikolajs Zeps
- , Cheng-Zhong Zhang
- , Fan Zhang
- , Hailei Zhang
- , Hongwei Zhang
- , Hongxin Zhang
- , Jiashan Zhang
- , Jing Zhang
- , Junjun Zhang
- , Xiuqing Zhang
- , Xuanping Zhang
- , Yan Zhang
- , Zemin Zhang
- , Zhongming Zhao
- , Liangtao Zheng
- , Xiuqing Zheng
- , Wanding Zhou
- , Yong Zhou
- , Bin Zhu
- , Hongtu Zhu
- , Jingchun Zhu
- , Shida Zhu
- , Lihua Zou
- , Xueqing Zou
- , Anna deFazio
- , Nicholas van As
- , Carolien H. M. van Deurzen

- , Marc J. van de Vijver
- , L. van’t Veer
- & Christian von Mering

Corresponding authors

Correspondence to Joachim Weischenfeldt, Rameen Beroukhim or Peter J. Campbell.

Rights and permissions

Open Access This article is licensed under a Creative Commons Attribution 4.0 International License, which permits use, sharing, adaptation, distribution and reproduction in any medium or format, as long as you give appropriate credit to the original author(s) and the source, provide a link to the Creative Commons license, and indicate if changes were made. The images or other third party material in this article are included in the article’s Creative Commons license, unless indicated otherwise in a credit line to the material. If material is not included in the article’s Creative Commons license and your intended use is not permitted by statutory regulation or exceeds the permitted use, you will need to obtain permission directly from the copyright holder. To view a copy of this license, visit http://creativecommons.org/licenses/by/4.0/.

Reprints and Permissions

About this article

Cite this article

Li, Y., Roberts, N.D., Wala, J.A. *et al.* Author Correction: Patterns of somatic structural variation in human cancer genomes. *Nature* **614**, E38 (2023). https://doi.org/10.1038/s41586-022-05597-x

- Published: 25 January 2023

- Issue Date: 16 February 2023
- DOI: https://doi.org/10.1038/s41586-022-05597-x

Share this article

Anyone you share the following link with will be able to read this content:

Get shareable link

Sorry, a shareable link is not currently available for this article.

Copy to clipboard

Provided by the Springer Nature SharedIt content-sharing initiative

---

This article was downloaded by **calibre** from https://www.nature.com/articles/s41586-022-05597-x

- Author Correction
- Open Access
- Published: 25 January 2023

Author Correction: Pan-cancer analysis of whole genomes

- The ICGC/TCGA Pan-Cancer Analysis of Whole Genomes Consortium

Nature **volume 614**, page E39 (2023)

- 1085 Accesses
- Metrics details

The Original Article was published on 05 February 2020

Correction to: *Nature* https://doi.org/10.1038/s41586-020-1969-6 Published online 5 February 2020

In the published version of this paper, the list of members of the Pan-Cancer Analysis of Whole Genomes (PCAWG) Consortium and their affiliations contained minor errors in the affiliations. The original Article has been corrected to include the corrected list.

Author information

Author notes

1. These authors jointly supervised this work: Peter J. Campbell, Gad Getz, Jan O. Korbel, Joshua M. Stuart, Lincoln D. Stein
2. A list of members and their affiliations appears in the online version of the paper and lists of working groups appear in the Supplementary Information

Authors and Affiliations

1. Applied Tumor Genomics Research Program, Research Programs Unit, University of Helsinki, Helsinki, Finland

   Lauri A. Aaltonen

2. Wellcome Sanger Institute, Wellcome Genome Campus, Hinxton, UK

   Federico Abascal, David J. Adams, Ludmil B. Alexandrov, Sam Behjati, Shriram G. Bhosle, David T. Bowen, Adam P. Butler, Peter J. Campbell, Peter Clapham, Helen Davies, Kevin J. Dawson, Stefan C. Dentro, Serge Serge, Erik Garrison, Mohammed Ghori, Dominik Glodzik, Jonathan Hinton, David R. Jones, Young Seok Ju, Stian Knappskog, Barbara Kremeyer, Henry Lee-Six, Daniel A. Leongamornlert, Yilong Li, Sancha Martin, Iñigo Martincorena, Ultan McDermott, Andrew Menzies, Thomas J. Mitchell, Sandro Morganella, Jyoti Nangalia, Jonathan Nicholson, Serena Nik-Zainal, Sarah O'Meara, Elli Papaemmanuil, Keiran M. Raine, Manasa Ramakrishna, Kamna Ramakrishnan, Nicola D. Roberts, Rebecca Shepherd, Lucy Stebbings, Michael R. Stratton, Maxime Tarabichi, Jon W. Teague, Ignacio Vázquez-García, David C. Wedge, Lucy Yates, Jorge Zamora & Xueqing Zou

3. Memorial Sloan Kettering Cancer Center, New York, NY, USA

   Adam Abeshouse, Hikmat Al-Ahmadie, Gunes Gundem, Zachary Heins, Jason Huse, Douglas A. Levine, Eric Minwei Liu & Angelica Ochoa

4. Genome Science Division, Research Center for Advanced Science and Technology, University of Tokyo, Tokyo, Japan

   Hiroyuki Aburatani, Genta Nagae, Akihiro Suzuki, Kenji Tatsuno & Shogo Yamamoto

5. Department of Surgery, University of Chicago, Chicago, IL, USA

   Nishant Agrawal

6. Department of Surgery, Division of Hepatobiliary and Pancreatic Surgery, School of Medicine, Keimyung University Dongsan Medical Center, Daegu, South Korea

   Keun Soo Ahn & Koo Jeong Kang

7. Department of Oncology, Gil Medical Center, Gachon University, Incheon, South Korea

   Sung-Min Ahn

8. Hiroshima University, Hiroshima, Japan

   Hiroshi Aikata, Koji Arihiro, Kazuaki Chayama, Yoshiiku Kawakami & Hideki Ohdan

9. Department of Bioinformatics and Computational Biology, The University of Texas MD Anderson Cancer Center, Houston, TX, USA

   Rehan Akbani, Shaolong Cao, Yiwen Chen, Zechen Chong, Yu Fan, Jun Li, Han Liang, Wenyi Wang, Yumeng Wang & Yuan Yuan

10. University of Texas MD Anderson Cancer Center, Houston, TX, USA

   Kadir C. Akdemir & Ken Chen

11. King Faisal Specialist Hospital and Research Centre, Al Maather, Riyadh, Saudi Arabia

Sultan T. Al-Sedairy

12. Bioinformatics Unit, Spanish National Cancer Research Centre (CNIO), Madrid, Spain

Fatima Al-Shahrour & Elena Piñeiro-Yáñez

13. Bioinformatics Core Facility, University Medical Center Hamburg, Hamburg, Germany

Malik Alawi

14. Heinrich Pette Institute, Leibniz Institute for Experimental Virology, Hamburg, Germany

Malik Alawi & Adam Grundhoff

15. Ontario Tumour Bank, Ontario Institute for Cancer Research, Toronto, ON, Canada

Monique Albert & John Bartlett

16. Department of Pathology, The University of Texas MD Anderson Cancer Center, Houston, TX, USA

Kenneth Aldape, Russell R. Broaddus, Bogdan Czerniak, Adel El-Naggar, Savitri Krishnamurthy, Alexander J. Lazar & Xiaoping Su

17. Laboratory of Pathology, Center for Cancer Research, National Cancer Institute, Bethesda, MD, USA

Kenneth Aldape

18. Department of Cellular and Molecular Medicine and Department of Bioengineering, University of California San Diego, La Jolla, CA, USA

Ludmil B. Alexandrov & Erik N. Bergstrom

19. UC San Diego Moores Cancer Center, San Diego, CA, USA

Ludmil B. Alexandrov, Erik N. Bergstrom & Olivier Harismendy

20. Canada's Michael Smith Genome Sciences Centre, BC Cancer, Vancouver, BC, Canada

Adrian Ally, Miruna Balasundaram, Reanne Bowlby, Denise Brooks, Rebecca Carlsen, Eric Chuah, Noreen Dhalla, Robert A. Holt, Steven J. M. Jones, Katayoon Kasaian, Darlene Lee, Haiyan Irene Li, Yussanne Ma, Marco A. Marra, Michael Mayo, Richard A. Moore, Andrew J. Mungall, Karen Mungall, A. Gordon Robertson, Sara Sadeghi, Jacqueline E. Schein, Payal Sipahimalani, Angela Tam, Nina Thiessen & Tina Wong

21. Sir Peter MacCallum Department of Oncology, Peter MacCallum Cancer Centre, University of Melbourne, Melbourne, VIC, Australia

Kathryn Alsop, David D. L. Bowtell, Elizabeth L. Christie, Dariush Etemadmoghadam, Sian Fereday, Dale W. Garsed, Linda Mileshkin, Chris Mitchell, Mark Shackleton, Heather Thorne & Nadia Traficante

22. Centre for Research in Molecular Medicine and Chronic Diseases (CiMUS), Universidade de Santiago de Compostela, Santiago de Compostela, Spain

Eva G. Alvarez, Alicia L. Bruzos, Bernardo Rodriguez-Martin, Javier Temes, Jose M. C. Tubio & Jorge Zamora

23. Department of Zoology, Genetics and Physical Anthropology, (CiMUS), Universidade de Santiago de Compostela, Santiago de Compostela, Spain

Eva G. Alvarez, Alicia L. Bruzos, Bernardo Rodriguez-Martin, Javier Temes, Jose M. C. Tubio & Jorge Zamora

24. The Biomedical Research Centre (CINBIO), Universidade de Vigo, Vigo, Spain

Eva G. Alvarez, Alicia L. Bruzos, Bernardo Rodriguez-Martin, Marta Tojo, Jose M. C. Tubio & Jorge Zamora

25. Royal National Orthopaedic Hospital - Bolsover, London, UK

Fernanda Amary

26. Department of Genomic Medicine, The University of Texas MD Anderson Cancer Center, Houston, TX, USA

Samirkumar B. Amin, P. Andrew Futreal & Alexander J. Lazar

27. Quantitative and Computational Biosciences Graduate Program, Baylor College of Medicine, Houston, TX, USA

Samirkumar B. Amin, Han Liang & Yumeng Wang

28. The Jackson Laboratory for Genomic Medicine, Farmington, CT, USA

Samirkumar B. Amin, Joshy George & Lucas Lochovsky

29. Genome Informatics Program, Ontario Institute for Cancer Research, Toronto, ON, Canada

Brice Aminou, Niall J. Byrne, Aurélien Chateigner, Nodirjon Fayzullaev, Vincent Ferretti, George L. Mihaiescu, Hardeep K. Nahal-Bose, Brian D. O'Connor, B. F. Francis Ouellette, Marc D. Perry, Kevin Thai, Qian Xiang, Christina K. Yung & Junjun Zhang

30. Institute of Human Genetics, Christian-Albrechts-University, Kiel, Germany

Ole Ammerpohl, Andrea Haake, Cristina López, Julia Richter & Rabea Wagener

31. Institute of Human Genetics, Ulm University and Ulm University Medical Center, Ulm, Germany

Ole Ammerpohl, Sietse Aukema, Cristina López, Reiner Siebert & Rabea Wagener

32. Queensland Centre for Medical Genomics, Institute for Molecular Bioscience, University of Queensland, St. Lucia, Brisbane, QLD, Australia

Matthew J. Anderson, Timothy J. C. Bruxner, Angelika N. Christ, J. Lynn Fink, Ivon Harliwong, Karin S. Kassahn, David K. Miller, Alan J. Robertson & Darrin F. Taylor

33. Salford Royal NHS Foundation Trust, Salford, UK

Yeng Ang, Hsiao-Wei Chen, Ritika Kundra & Francisco Sanchez-Vega

34. Department of Surgery, Pancreas Institute, University and Hospital Trust of Verona, Verona, Italy

Davide Antonello, Claudio Bassi, Narong Khuntikeo, Luca Landoni, Giuseppe Malleo, Giovanni Marchegiani, Neil D. Merrett, Marco Miotto, Salvatore Paiella, Antonio Pea, Paolo Pederzoli, Roberto Salvia, Jaswinder S. Samra, Elisabetta Sereni & Samuel Singer

35. Molecular and Medical Genetics, OHSU Knight Cancer Institute, Oregon Health and Science University, Portland, OR, USA

Pavana Anur, Myron Peto & Paul T. Spellman

36. Department of Molecular Oncology, BC Cancer Research Centre, Vancouver, BC, Canada

Samuel Aparicio

37. The McDonnell Genome Institute at Washington University, St. Louis, MO, USA

Elizabeth L. Appelbaum, Matthew H. Bailey, Matthew G. Cordes, Li Ding, Catrina C. Fronick, Lucinda A. Fulton, Robert S. Fulton, Kuan-lin Huang, Reyka Jayasinghe, Elaine R. Mardis, R. Jay Mashl, Michael D. McLellan, Christopher A. Miller, Heather K. Schmidt, Jiayin Wang, Michael C. Wendl, Richard K. Wilson & Tina Wong

38. University College London, London, UK

Elizabeth L. Appelbaum, Jonathan D. Kay, Helena Kilpinen, Laurence B. Lovat, Hayley J. Luxton & Hayley C. Whitaker

39. Division of Cancer Genomics, National Cancer Center Research Institute, National Cancer Center, Tokyo, Japan

Yasuhito Arai, Natsuko Hama, Fumie Hosoda, Hiromi Nakamura, Tatsuhiro Shibata, Yasushi Totoki & Shinichi Yachida

40. DLR Project Management Agency, Bonn, Germany

Axel Aretz

41. Tokyo Women's Medical University, Tokyo, Japan

Shun-ichi Ariizumi & Masakazu Yamamoto

42. Center for Molecular Oncology, Memorial Sloan Kettering Cancer Center, New York, NY, USA

Joshua Armenia, Hsiao-Wei Chen, Jianjiong Gao, Ritika Kundra, Francisco Sanchez-Vega, Nikolaus Schultz & Hongxin Zhang

43. Los Alamos National Laboratory, Los Alamos, NM, USA

Laurent Arnould

44. Department of Pathology, University Health Network, Toronto General Hospital, Toronto, ON, Canada

Sylvia Asa, Michael H. A. Roehrl & Theodorus Van der Kwast

45. Nottingham University Hospitals NHS Trust, Nottingham, UK

Sylvia Asa, Simon L. Parsons & Ming Tsao

46. Epigenomics and Cancer Risk Factors, German Cancer Research Center (DKFZ), Heidelberg, Germany

Yassen Assenov

47. Computational Biology Program, Ontario Institute for Cancer Research, Toronto, ON, Canada

Gurnit Atwal, Philip Awadalla, Jonathan Barenboim, Vinayak Bhandari, Ivan Borozan, Paul C. Boutros, Lewis Jonathan Dursi, Shadrielle M. G. Espiritu, Natalie S. Fox, Michael Fraser, Syed Haider, Vincent Huang, Keren Isaev, Wei Jiao, Christopher M. Lalansingh, Emilie Lalonde, Fabien C. Lamaze, Constance H. Li, Julie Livingstone, Christine P'ng, Marta Paczkowska, Stephenie D. Prokopec, Jüri Reimand, Veronica Y. Sabelnykova, Adriana Salcedo, Yu-Jia Shiah, Solomon I. Shorser, Shimin Shuai, Jared T. Simpson, Lincoln D. Stein, Ren X. Sun, Lina Wadi, Gavin W. Wilson, Adam J. Wright, Takafumi N. Yamaguchi, Fouad Yousif & Denis Yuen

48. Department of Molecular Genetics, University of Toronto, Toronto, ON, Canada

Gurnit Atwal, Philip Awadalla, Gary D. Bader, Shimin Shuai & Lincoln D. Stein

49. Vector Institute, Toronto, ON, Canada

Gurnit Atwal, Quaid D. Morris, Yulia Rubanova & Jeffrey A. Wintersinger

50. Hematopathology Section, Institute of Pathology, Christian-Albrechts-University, Kiel, Germany

Sietse Aukema, Wolfram Klapper, Julia Richter & Monika Szczepanowski

51. Department of Pathology and Laboratory Medicine, School of Medicine, University of North Carolina at Chapel Hill, Chapel Hill, NC, USA

J. Todd Auman & Charles M. Perou

52. Department of Cancer Genetics, Institute for Cancer Research, Oslo University Hospital, The Norwegian Radium Hospital, Oslo, Norway

Miriam R. R. Aure, Anne-Lise Børresen-Dale & Anita Langerød

53. Pathology, Hospital Clinic, Institut d'Investigacions Biomèdiques August Pi i Sunyer (IDIBAPS), University of Barcelona, Barcelona, Spain

Marta Aymerich

54. Department of Veterinary Medicine, Transmissible Cancer Group, University of Cambridge, Cambridge, UK

Adrian Baez-Ortega

55. Alvin J. Siteman Cancer Center, Washington University School of Medicine, St. Louis, MO, USA

Matthew H. Bailey, Li Ding, Robert S. Fulton, Ramaswamy Govindan & Michael D. McLellan

56. Wolfson Wohl Cancer Research Centre, Institute of Cancer Sciences, University of Glasgow, Glasgow, UK

Peter J. Bailey, Andrew V. Biankin, David K. Chang, Susanna L. Cooke, Fraser R. Duthie, Janet S. Graham, Nigel B. Jamieson, Elizabeth A. Musgrove & Derek W. Wright

57. Lineberger Comprehensive Cancer Center, University of North Carolina at Chapel Hill, Chapel Hill, NC, USA

Saianand Balu, Tom Bodenheimer, D. Neil Hayes, Austin J. Hepperla, Katherine A. Hoadley, Alan P. Hoyle, Stuart R. Jefferys, Shaowu Meng, Lisle E. Mose, Grant Sanders, Yan Shi, Janae V. Simons & Matthew G. Soloway

58. Broad Institute of MIT and Harvard, Cambridge, MA, USA

Pratiti Bandopadhayay, Rameen Beroukhim, Angela N. Brooks, Susan Bullman, John Busanovich, Andrew D. Cherniack, Juok Cho, Carrie Cibulskis, Kristian Cibulskis, David Craft, Timothy Defreitas, Andrew J. Dunford, Scott Frazer, Stacey B. Gabriel, Nils Gehlenborg, Gad Getz, Manaswi Gupta, Gavin Ha, Nicholas J. Haradhvala, David I. Heiman, Julian M. Hess, Manolis Kellis, Jaegil Kim, Kiran Kumar, Kirsten Kübler, Eric Lander, Michael S. Lawrence, Ignaty Leshchiner, Pei Lin, Ziao Lin, Dimitri Livitz, Yosef E. Maruvka, Samuel R. Meier, Matthew Meyerson, Michael S. Noble, Chandra Sekhar Pedamallu, Paz Polak, Esther Rheinbay, Daniel Rosebrock, Mara Rosenberg, Gordon Saksena, Richard Sallari, Steven E. Schumacher, Ayellet V. Segre, Ofer Shapira, Juliann Shih, Nasa Sinnott-Armstrong, Oliver Spiro, Chip Stewart, Amaro Taylor-Weiner, Grace Tiao, Douglas Voet, Jeremiah A. Wala, Cheng-Zhong Zhang & Hailei Zhang

59. Dana-Farber/Boston Children’s Cancer and Blood Disorders Center, Boston, MA, USA

Pratiti Bandopadhayay

60. Department of Pediatrics, Harvard Medical School, Boston, MA, USA

Pratiti Bandopadhayay

61. Leeds Institute of Medical Research @ St. James’s, University of Leeds, St. James’s University Hospital, Leeds, UK

Rosamonde E. Banks & Naveen Vasudev

62. Department of Pathology and Diagnostics, University and Hospital Trust of Verona, Verona, Italy

Stefano Barbi, Vincenzo Corbo & Michele Simbolo

63. Department of Surgery, Princess Alexandra Hospital, Brisbane, QLD, Australia

Andrew P. Barbour

64. Surgical Oncology Group, Diamantina Institute, University of Queensland, Brisbane, QLD, Australia

Andrew P. Barbour

65. Department of Population and Quantitative Health Sciences, Case Western Reserve University School of Medicine, Cleveland, OH, USA

Jill Barnholtz-Sloan

66. Research Health Analytics and Informatics, University Hospitals Cleveland Medical Center, Cleveland, OH, USA

Jill Barnholtz-Sloan

67. Gloucester Royal Hospital, Gloucester, UK

Hugh Barr

68. European Molecular Biology Laboratory, European Bioinformatics Institute (EMBL-EBI), Cambridge, UK

Elisabet Barrera, Wojciech Bazant, Ewan Birney, Rich Boyce, Alvis Brazma, Andy Cafferkey, Claudia Calabrese, Paul Flicek, Nuno A. Fonseca, Anja Füllgrabe, Moritz Gerstung, Santiago Gonzalez, Liliana Greger, Maria Keays, Jan O. Korbel, Alfonso Muñoz, Steven J. Newhouse, David Ocana, Irene Papatheodorou, Robert

Petryszak, Roland F. Schwarz, Charles Short, Oliver Stegle & Lara Urban

69. Diagnostic Development, Ontario Institute for Cancer Research, Toronto, ON, Canada

John Bartlett & Ilinca Lungu

70. Barcelona Supercomputing Center (BSC), Barcelona, Spain

Javier Bartolome, Mattia Bosio, Ana Dueso-Barroso, J. Lynn Fink, Josep L. L. Gelpi, Ana Milovanovic, Montserrat Puiggròs, Javier Bartolomé Rodriguez, Romina Royo, David Torrents, Alfonso Valencia, Miguel Vazquez, David Vicente & Izar Villasante

71. Arnie Charbonneau Cancer Institute, University of Calgary, Calgary, AB, Canada

Oliver F. Bathe

72. Departments of Surgery and Oncology, University of Calgary, Calgary, AB, Canada

Oliver F. Bathe

73. Department of Pathology, Oslo University Hospital, The Norwegian Radium Hospital, Oslo, Norway

Daniel Baumhoer & Bodil Bjerkehagen

74. PanCuRx Translational Research Initiative, Ontario Institute for Cancer Research, Toronto, ON, Canada

Prashant Bavi, Michelle Chan-Seng-Yue, Sean Cleary, Robert E. Denroche, Steven Gallinger, Robert C. Grant, Gun Ho Jang, Sangeetha Kalimuthu, Ilinca Lungu, John D. McPherson, Faiyaz Notta, Michael H. A. Roehrl, Gavin W. Wilson & Julie M. Wilson

75. Department of Oncology, Sidney Kimmel Comprehensive Cancer Center at Johns Hopkins University School of Medicine, Baltimore, MD, USA

Stephen B. Baylin, Nilanjan Chatterjee, Leslie Cope, Ludmila Danilova & Ralph H. Hruban

76. University Hospital Southampton NHS Foundation Trust, Southampton, UK

Stephen B. Baylin & Tim Dudderidge

77. Royal Stoke University Hospital, Stoke-on-Trent, UK

Duncan Beardsmore & Christopher Umbricht

78. Genome Sequence Informatics, Ontario Institute for Cancer Research, Toronto, ON, Canada

Timothy A. Beck, Bob Gibson, Lawrence E. Heisler, Xuemei Luo & Morgan L. Taschuk

79. Human Longevity Inc, San Diego, CA, USA

Timothy A. Beck

80. Olivia Newton-John Cancer Research Institute, La Trobe University, Heidelberg, VIC, Australia

Andreas Behren & Jonathan Cebon

81. Computer Network Information Center, Chinese Academy of Sciences, Beijing, China

Beifang Niu

82. Genome Canada, Ottawa, ON, Canada

Cindy Bell

83. CNAG-CRG, Centre for Genomic Regulation (CRG), Barcelona Institute of Science and Technology (BIST), Barcelona, Spain

Sergi Beltran, Ivo G. Gut, Marta Gut, Simon C. Heath, Tomas Marques-Bonet, Arcadi Navarro, Miranda D. Stobbe, Jean-Rémi Trotta & Justin P. Whalley

84. Universitat Pompeu Fabra (UPF), Barcelona, Spain

Sergi Beltran, Mattia Bosio, German M. Demidov, Oliver Drechsel, Ivo G. Gut, Marta Gut, Simon C. Heath, Francesc Muyas, Stephan Ossowski, Aparna Prasad, Raquel Rabionet, Miranda D. Stobbe & Hana Susak

85. Buck Institute for Research on Aging, Novato, CA, USA

Christopher Benz & Christina Yau

86. Duke University Medical Center, Durham, NC, USA

Andrew Berchuck

87. Department of Human Genetics, Hannover Medical School, Hannover, Germany

Anke K. Bergmann

88. Center for Bioinformatics and Functional Genomics, Cedars-Sinai Medical Center, Los Angeles, CA, USA

Benjamin P. Berman & Huy Q. Dinh

89. Department of Biomedical Sciences, Cedars-Sinai Medical Center, Los Angeles, CA, USA

Benjamin P. Berman

90. The Hebrew University Faculty of Medicine, Jerusalem, Israel

Benjamin P. Berman

91. Barts Cancer Institute, Barts and the London School of Medicine and Dentistry, Queen Mary University of London, London, UK

Daniel M. Berney & Yong-Jie Lu

92. Department of Computer Science, Bioinformatics Group, University of Leipzig, Leipzig, Germany

Stephan H. Bernhart, Hans Binder, Steve Hoffmann & Peter F. Stadler

93. Interdisciplinary Center for Bioinformatics, University of Leipzig, Leipzig, Germany

Stephan H. Bernhart, Hans Binder, Steve Hoffmann, Helene Kretzmer & Peter F. Stadler

94. Transcriptome Bioinformatics, LIFE Research Center for Civilization Diseases, University of Leipzig, Leipzig, Germany

Stephan H. Bernhart, Steve Hoffmann, Helene Kretzmer & Peter F. Stadler

95. Department of Medical Oncology, Dana-Farber Cancer Institute, Boston, MA, USA

Rameen Beroukhim, Angela N. Brooks, Susan Bullman, Andrew D. Cherniack, Levi Garraway, Matthew Meyerson, Chandra Sekhar Pedamallu, Steven E. Schumacher, Juliann Shih & Jeremiah A. Wala

96. Department of Cancer Biology, Dana-Farber Cancer Institute, Boston, MA, USA

Rameen Beroukhim, Aquila Fatima, Andrea L. Richardson, Steven E. Schumacher, Ofer Shapira, Andrew Tutt & Jeremiah A. Wala

97. Harvard Medical School, Boston, MA, USA

Rameen Beroukhim, Gad Getz, Kirsten Kübler, Matthew Meyerson, Chandra Sekhar Pedamallu, Paz Polak, Esther Rheinbay & Jeremiah A. Wala

98. USC Norris Comprehensive Cancer Center, University of Southern California, Los Angeles, CA, USA

Mario Berrios, Moiz S. Bootwalla, Andrea Holbrook, Phillip H. Lai, Dennis T. Maglinte, David J. Van Den Berg & Daniel J. Weisenberger

99. Department of Diagnostics and Public Health, University and Hospital Trust of Verona, Verona, Italy

Samantha Bersani, Ivana Cataldo, Claudio Luchini & Maria Scardoni

100. Department of Mathematics, Aarhus University, Aarhus, Denmark

Johanna Bertl & Asger Hobolth

101. Department of Molecular Medicine (MOMA), Aarhus University Hospital, Aarhus N, Denmark

Johanna Bertl, Henrik Hornshøj, Malene Juul, Randi Istrup Juul, Tobias Madsen, Morten Muhlig Nielsen & Jakob Skou Pedersen

102. Instituto Carlos Slim de la Salud, Mexico City, Mexico

Miguel Betancourt

103. Department of Medical Biophysics, University of Toronto, Toronto, ON, Canada

Vinayak Bhandari, Paul C. Boutros, Robert G. Bristow, Keren Isaev, Constance H. Li, Jüri Reimand, Michael H. A. Roehrl & Bradly G. Wouters

104. Cancer Division, Garvan Institute of Medical Research, Kinghorn Cancer Centre, University of New South Wales (UNSW Sydney),

Sydney, NSW, Australia

Andrew V. Biankin, David K. Chang, Lorraine A. Chantrill, Angela Chou, Anthony J. Gill, Amber L. Johns, James G. Kench, David K. Miller, Adnan M. Nagrial, Marina Pajic, Mark Pinese, Ilse Rooman, Christopher J. Scarlett, Christopher W. Toon & Jianmin Wu

105. South Western Sydney Clinical School, Faculty of Medicine, University of New South Wales (UNSW Sydney), Liverpool, NSW, Australia

Andrew V. Biankin

106. West of Scotland Pancreatic Unit, Glasgow Royal Infirmary, Glasgow, UK

Andrew V. Biankin & Nigel B. Jamieson

107. Center for Digital Health, Berlin Institute of Health and Charitè - Universitätsmedizin Berlin, Berlin, Germany

Matthias Bieg

108. Heidelberg Center for Personalized Oncology (DKFZ-HIPO), German Cancer Research Center (DKFZ), Heidelberg, Germany

Matthias Bieg, Ivo Buchhalter, Barbara Hutter & Nagarajan Paramasivam

109. The Preston Robert Tisch Brain Tumor Center, Duke University Medical Center, Durham, NC, USA

Darell Bigner

110. Massachusetts General Hospital, Boston, MA, USA

Michael Birrer, Vikram Deshpande, William C. Faquin, Nicholas J. Haradhvala, Kirsten Kübler, Michael S. Lawrence, David N.

Louis, Yosef E. Maruvka, G. Petur Nielsen, Esther Rheinbay, Mara Rosenberg, Dennis C. Sgroi & Chin-Lee Wu

111. National Institute of Biomedical Genomics, Kalyani, West Bengal, India

Nidhan K. Biswas, Arindam Maitra & Partha P. Majumder

112. Institute of Clinical Medicine and Institute of Oral Biology, University of Oslo, Oslo, Norway

Bodil Bjerkehagen

113. University of North Carolina at Chapel Hill, Chapel Hill, NC, USA

Lori Boice, Mei Huang, Sonia Puig & Leigh B. Thorne

114. ARC-Net Centre for Applied Research on Cancer, University and Hospital Trust of Verona, Verona, Italy

Giada Bonizzato, Cinzia Cantù, Ivana Cataldo, Vincenzo Corbo, Sonia Grimaldi, Rita T. Lawlor, Andrea Mafficini, Borislav C. Rusev, Aldo Scarpa, Katarzyna O. Sikora, Nicola Sperandio, Alain Viari & Caterina Vicentini

115. The Institute of Cancer Research, London, UK

Johann S. De Bono, Niedzica Camacho, Colin S. Cooper, Sandra E. Edwards, Rosalind A. Eeles, Zsofia Kote-Jarai, Daniel A. Leongamornlert, Lucy Matthews & Sue Merson

116. Centre for Computational Biology, Duke-NUS Medical School, Singapore, Singapore

Arnoud Boot, Ioana Cutcutache, Mi Ni Huang, John R. McPherson, Steven G. Rozen & Yang Wu

117. Programme in Cancer and Stem Cell Biology, Duke-NUS Medical School, Singapore, Singapore

Arnoud Boot, Ioana Cutcutache, Mi Ni Huang, John R. McPherson, Steven G. Rozen, Patrick Tan, Bin Tean Teh & Yang Wu

118. Division of Oncology and Pathology, Department of Clinical Sciences Lund, Lund University, Lund, Sweden

Ake Borg, Markus Ringnér & Johan Staaf

119. Department of Pediatric Oncology, Hematology and Clinical Immunology, Heinrich-Heine-University, Düsseldorf, Germany

Arndt Borkhardt & Jessica I. Hoell

120. Laboratory for Medical Science Mathematics, RIKEN Center for Integrative Medical Sciences, Yokohama, Japan

Keith A. Boroevich, Todd A. Johnson, Michael S. Lawrence & Tatsuhiko Tsunoda

121. RIKEN Center for Integrative Medical Sciences, Yokohama, Japan

Keith A. Boroevich, Akihiro Fujimoto, Masashi Fujita, Mayuko Furuta, Kazuhiro Maejima, Hidewaki Nakagawa, Kaoru Nakano & Aya Sasaki-Oku

122. Department of Internal Medicine/Hematology, Friedrich-Ebert-Hospital, Neumünster, Germany

Christoph Borst & Siegfried Haas

123. Departments of Dermatology and Pathology, Yale University, New Haven, CT, USA

Marcus Bosenberg

124. Centre for Genomic Regulation (CRG), The Barcelona Institute of Science and Technology, Barcelona, Spain

Mattia Bosio, German M. Demidov, Oliver Drechsel, Georgia Escaramis, Xavier Estivill, Aliaksei Z. Holik, Francesc Muyas, Stephan Ossowski, Raquel Rabionet & Hana Susak

125. Radcliffe Department of Medicine, University of Oxford, Oxford, UK

Jacqueline Boultwood

126. Canadian Center for Computational Genomics, McGill University, Montreal, QC, Canada

Guillaume Bourque

127. Department of Human Genetics, McGill University, Montreal, QC, Canada

Guillaume Bourque, Mark Lathrop & Yasser Riazalhosseini

128. Department of Human Genetics, University of California Los Angeles, Los Angeles, CA, USA

Paul C. Boutros

129. Department of Pharmacology, University of Toronto, Toronto, ON, Canada

Paul C. Boutros

130. Faculty of Medicine and Health Technology, Tampere University and Tays Cancer Center, Tampere University Hospital, Tampere, Finland

G. Steven Bova & Tapio Visakorpi

131. Haematology, Leeds Teaching Hospitals NHS Trust, Leeds, UK

David T. Bowen

132. Translational Research and Innovation, Centre Léon Bérard, Lyon, France

Sandrine Boyault

133. Fox Chase Cancer Center, Philadelphia, PA, USA

Jeffrey Boyd & Elaine R. Mardis

134. International Agency for Research on Cancer, World Health Organization, Lyon, France

Paul Brennan & Ghislaine Scelo

135. Earlham Institute, Norwich, UK

Daniel S. Brewer & Colin S. Cooper

136. Norwich Medical School, University of East Anglia, Norwich, UK

Daniel S. Brewer & Colin S. Cooper

137. Department of Molecular Biology, Faculty of Science, Radboud Institute for Molecular Life Sciences, Radboud University, Nijmegen, HB, The Netherlands

Arie B. Brinkman

138. CRUK Manchester Institute and Centre, Manchester, UK

Robert G. Bristow

139. Department of Radiation Oncology, University of Toronto, Toronto, ON, Canada

Robert G. Bristow

140. Division of Cancer Sciences, Manchester Cancer Research Centre, University of Manchester, Manchester, UK

Robert G. Bristow

141. Radiation Medicine Program, Princess Margaret Cancer Centre, Toronto, ON, Canada

Robert G. Bristow & Fei-Fei Fei Liu

142. Department of Pathology, Brigham and Women's Hospital, Harvard Medical School, Boston, MA, USA

Jane E. Brock & Sabina Signoretti

143. Department of Surgery, Division of Thoracic Surgery, The Johns Hopkins University School of Medicine, Baltimore, MD, USA

Malcolm Brock

144. Division of Molecular Pathology, The Netherlands Cancer Institute, Oncode Institute, Amsterdam, CX, The Netherlands

Annegien Broeks & Jos Jonkers

145. Department of Biomolecular Engineering, University of California Santa Cruz, Santa Cruz, CA, USA

Angela N. Brooks, David Haan, Maximillian G. Marin, Thomas J. Matthew, Yulia Newton, Cameron M. Soulette & Joshua M. Stuart

146. UC Santa Cruz Genomics Institute, University of California Santa Cruz, Santa Cruz, CA, USA

Angela N. Brooks, Brian Craft, Mary J. Goldman, David Haussler, Joshua M. Stuart & Jingchun Zhu

147. Division of Applied Bioinformatics, German Cancer Research Center (DKFZ), Heidelberg, Germany

Benedikt Brors, Lars Feuerbach, Chen Hong, Charles David Imbusch & Lina Sieverling

148. German Cancer Consortium (DKTK), German Cancer Research Center (DKFZ), Heidelberg, Germany

Benedikt Brors, Barbara Hutter, Peter Lichter, Dirk Schadendorf & Holger Sültmann

149. National Center for Tumor Diseases (NCT) Heidelberg, Heidelberg, Germany

Benedikt Brors, Barbara Hutter, Holger Sültmann & Thorsten Zenz

150. Center for Biological Sequence Analysis, Department of Bio and Health Informatics, Technical University of Denmark, Lyngby, Denmark

Søren Brunak

151. Novo Nordisk Foundation Center for Protein Research, University of Copenhagen, Copenhagen, Denmark

Søren Brunak

152. Institute for Molecular Bioscience, University of Queensland, St. Lucia, Brisbane, QLD, Australia

Timothy J. C. Bruxner, Oliver Holmes, Stephen H. Kazakoff, Conrad R. Leonard, Felicity Newell, Katia Nones, Ann-Marie Patch, John V. Pearson, Michael C. Quinn, Nick M. Waddell, Nicola Waddell, Scott Wood & Qinying Xu

153. Biomedical Engineering, Oregon Health and Science University, Portland, OR, USA

Alex Buchanan & Kyle Ellrott

154. Division of Theoretical Bioinformatics, German Cancer Research Center (DKFZ), Heidelberg, Germany

Ivo Buchhalter, Calvin Wing Yiu Chan, Roland Eils, Michael C. Heinold, Carl Herrmann, Natalie Jäger, Rolf Kabbe, Jules N. A. Kerssemakers, Kortine Kleinheinz, Nagarajan Paramasivam, Manuel Prinz, Matthias Schlesner & Johannes Werner

155. Institute of Pharmacy and Molecular Biotechnology and BioQuant, Heidelberg University, Heidelberg, Germany

Ivo Buchhalter, Roland Eils, Michael C. Heinold, Carl Herrmann, Daniel Hübschmann, Kortine Kleinheinz & Umut H. Toprak

156. Federal Ministry of Education and Research, Berlin, Germany

Christiane Buchholz

157. Melanoma Institute Australia, University of Sydney, Sydney, NSW, Australia

Hazel Burke, Ricardo De Paoli-Iseppi, Nicholas K. Hayward, Peter Hersey, Valerie Jakrot, Hojabr Kakavand, Georgina V. Long, Graham J. Mann, Robyn P. M. Saw, Richard A. Scolyer, Ping Shang, Andrew J. Spillane, Jonathan R. Stretch, John F. F. Thompson & James S. Wilmott

158. Pediatric Hematology and Oncology, University Hospital Muenster, Muenster, Germany

Birgit Burkhardt

159. Department of Pathology, Johns Hopkins University School of Medicine, Baltimore, MD, USA

Kathleen H. Burns & Christopher Umbricht

160. McKusick-Nathans Institute of Genetic Medicine, Sidney Kimmel Comprehensive Cancer Center at Johns Hopkins University School of Medicine, Baltimore, MD, USA

Kathleen H. Burns

161. Foundation Medicine, Inc, Cambridge, MA, USA

John Busanovich

162. Department of Biomedical Data Science, Stanford University School of Medicine, Stanford, CA, USA

Carlos D. Bustamante & Francisco M. De La Vega

163. Department of Genetics, Stanford University School of Medicine, Stanford, CA, USA

Carlos D. Bustamante, Francisco M. De La Vega, Suyash S. Shringarpure, Nasa Sinnott-Armstrong & Mark H. Wright

164. Bakar Computational Health Sciences Institute and Department of Pediatrics, University of California, San Francisco, CA, USA

Atul J. Butte & Jieming Chen

165. Institute of Clinical Medicine, Faculty of Medicine, University of Oslo, Oslo, Norway

Anne-Lise Børresen-Dale

166. National Cancer Institute, National Institutes of Health, Bethesda, MD, USA

Samantha J. Caesar-Johnson, John A. Demchok, Ina Felau, Roy Tarnuzzer, Zhining Wang, Liming Yang, Jean C. Zenklusen & Jiashan Zhang

167. Royal Marsden NHS Foundation Trust, London and Sutton, UK

Declan Cahill, Nening M. Dennis, Tim Dudderidge, Rosalind A. Eeles, Cyril Fisher, Steven Hazell, Vincent Khoo, Pardeep Kumar, Naomi Livni, Erik Mayer, David Nicol, Christopher

Ogden, Edward W. Rowe, Sarah Thomas, Alan Thompson & Nicholas van As

168. Genome Biology Unit, European Molecular Biology Laboratory (EMBL), Heidelberg, Germany

Claudia Calabrese, Serap Erkek, Moritz Gerstung, Santiago Gonzalez, Nina Habermann, Wolfgang Huber, Lara Jerman, Jan O. Korbel, Esa Pitkänen, Benjamin Raeder, Tobias Rausch, Vasilisa A. Rudneva, Oliver Stegle, Stephanie Sungalee, Lara Urban, Sebastian M. Waszak, Joachim Weischenfeldt & Sergei Yakneen

169. Department of Oncology, University of Cambridge, Cambridge, UK

Carlos Caldas & Suet-Feung Chin

170. Li Ka Shing Centre, Cancer Research UK Cambridge Institute, University of Cambridge, Cambridge, UK

Carlos Caldas, Suet-Feung Chin, Ruben M. Drews, Paul A. Edwards, Matthew Eldridge, Steve Hawkins, Andy G. Lynch, Geoff Macintyre, Florian Markowetz, Charlie E. Massie, David E. Neal, Simon Tavaré & Ke Yuan

171. Institut Gustave Roussy, Villejuif, France

Fabien Calvo

172. Cambridge University Hospitals NHS Foundation Trust, Cambridge, UK

Peter J. Campbell, Vincent J. Gnanapragasam, William Howat, Thomas J. Mitchell, David E. Neal, Nimish C. Shah & Anne Y. Warren

173. Department of Haematology, University of Cambridge, Cambridge, UK

Peter J. Campbell

174. Anatomia Patológica, Hospital Clinic, Institut d'Investigacions Biomèdiques August Pi i Sunyer (IDIBAPS), University of Barcelona, Barcelona, Spain

Elias Campo

175. Spanish Ministry of Science and Innovation, Madrid, Spain

Elias Campo

176. University of Michigan Comprehensive Cancer Center, Ann Arbor, MI, USA

Thomas E. Carey

177. Department for BioMedical Research, University of Bern, Bern, Switzerland

Joana Carlevaro-Fita

178. Department of Medical Oncology, Inselspital, University Hospital and University of Bern, Bern, Switzerland

Joana Carlevaro-Fita, Rory Johnson & Andrés Lanzós

179. Graduate School for Cellular and Biomedical Sciences, University of Bern, Bern, Switzerland

Joana Carlevaro-Fita & Andrés Lanzós

180. University of Pavia, Pavia, Italy

Mario Cazzola & Luca Malcovati

181. University of Alabama at Birmingham, Birmingham, AL, USA

Robert Cerfolio

182. UHN Program in BioSpecimen Sciences, Toronto General Hospital, Toronto, ON, Canada

Dianne E. Chadwick, Sheng-Ben Liang, Michael H. A. Roehrl & Sagedeh Shahabi

183. Department of Urology, Icahn School of Medicine at Mount Sinai, New York, NY, USA

Dimple Chakravarty

184. Centre for Law and Genetics, University of Tasmania, Sandy Bay Campus, Hobart, TAS, Australia

Don Chalmers

185. Faculty of Biosciences, Heidelberg University, Heidelberg, Germany

Calvin Wing Yiu Chan, Chen Hong & Lina Sieverling

186. Department of Biochemistry, Microbiology and Immunology, Faculty of Medicine, University of Ottawa, Ottawa, ON, Canada

Kin Chan

187. Division of Anatomic Pathology, Mayo Clinic, Rochester, MN, USA

Vishal S. Chandan

188. Division of Cancer Epidemiology and Genetics, National Cancer Institute, National Institutes of Health, Bethesda, MD, USA

Stephen J. Chanock, Xing Hua, Lisa Mirabello, Lei Song & Bin Zhu

189. Illawarra Shoalhaven Local Health District L3 Illawarra Cancer Care Centre, Wollongong Hospital, Wollongong, NSW, Australia

Lorraine A. Chantrill

190. BioForA, French National Institute for Agriculture, Food, and Environment (INRAE), ONF, Orléans, France

Aurélien Chateigner

191. Department of Biostatistics, Bloomberg School of Public Health, Johns Hopkins University, Baltimore, MD, USA

Nilanjan Chatterjee

192. University of California San Diego, San Diego, CA, USA

Zhaohong Chen, Michelle T. Dow, Claudiu Farcas, S. M. Ashiqul Islam, Antonios Koures, Lucila Ohno-Machado, Christos Sotiriou & Ashley Williams

193. Division of Experimental Pathology, Mayo Clinic, Rochester, MN, USA

Jeremy Chien

194. Centre for Cancer Research, The Westmead Institute for Medical Research, University of Sydney, Sydney, NSW, Australia

Yoke-Eng Chiew, Angela Chou, Jillian A. Hung, Catherine J. Kennedy, Graham J. Mann, Gulietta M. Pupo, Sarah-Jane Schramm, Varsha Tembe & Anna deFazio

195. Department of Gynaecological Oncology, Westmead Hospital, Sydney, NSW, Australia

Yoke-Eng Chiew, Jillian A. Hung, Catherine J. Kennedy & Anna deFazio

196. PDXen Biosystems Inc, Seoul, South Korea

Sunghoon Cho

197. Korea Advanced Institute of Science and Technology, Daejeon, South Korea

Jung Kyoon Choi, Young Seok Ju & Christopher J. Yoon

198. Electronics and Telecommunications Research Institute, Daejeon, South Korea

Wan Choi, Seung-Hyup Jeon, Hyunghwan Kim & Youngchoon Woo

199. Institut National du Cancer (INCA), Boulogne-Billancourt, France

Christine Chomienne & Iris Pauporté

200. Department of Genetics, Informatics Institute, University of Alabama at Birmingham, Birmingham, AL, USA

Zechen Chong

201. Division of Medical Oncology, National Cancer Centre, Singapore, Singapore

Su Pin Choo

202. Medical Oncology, University and Hospital Trust of Verona, Verona, Italy

Sara Cingarlini & Michele Milella

203. Department of Pediatrics, University Hospital Schleswig-Holstein, Kiel, Germany

Alexander Claviez

204. Hepatobiliary/Pancreatic Surgical Oncology Program, University Health Network, Toronto, ON, Canada

Sean Cleary, Ashton A. Connor & Steven Gallinger

205. School of Biological Sciences, University of Auckland, Auckland, New Zealand

Nicole Cloonan

206. Department of Surgery, University of Melbourne, Parkville, VIC, Australia

Marek Cmero

207. The Murdoch Children's Research Institute, Royal Children's Hospital, Parkville, VIC, Australia

Marek Cmero

208. Walter and Eliza Hall Institute, Parkville, VIC, Australia

Marek Cmero

209. Vancouver Prostate Centre, Vancouver, Canada

Colin C. Collins, Nilgun Donmez, Faraz Hach, Salem Malikic, S. Cenk Sahinalp, Iman Sarrafi & Raunak Shrestha

210. Lunenfeld-Tanenbaum Research Institute, Mount Sinai Hospital, Toronto, ON, Canada

Ashton A. Connor, Steven Gallinger, Robert C. Grant, Treasa A. McPherson & Iris Selander

211. University of East Anglia, Norwich, UK

Colin S. Cooper

212. Norfolk and Norwich University Hospital NHS Trust, Norwich, UK

Matthew G. Cordes, Catrina C. Fronick & Tom Roques

213. Victorian Institute of Forensic Medicine, Southbank, VIC, Australia

Stephen M. Cordner

214. Department of Biomedical Informatics, Harvard Medical School, Boston, MA, USA

Isidro Cortés-Ciriano, Jake June-Koo Lee & Peter J. Park

215. Department of Chemistry, Centre for Molecular Science Informatics, University of Cambridge, Cambridge, UK

Isidro Cortés-Ciriano

216. Ludwig Center at Harvard Medical School, Boston, MA, USA

Isidro Cortés-Ciriano, Jake June-Koo Lee & Peter J. Park

217. Human Genome Sequencing Center, Baylor College of Medicine, Houston, TX, USA

Kyle Covington, HarshaVardhan Doddapaneni, Richard A. Gibbs, Jianhong Hu, Joy C. Jayaseelan, Viktoriya Korchina, Lora Lewis, Donna M. Muzny, Linghua Wang, David A. Wheeler & Liu Xi

218. Peter MacCallum Cancer Centre, University of Melbourne, Melbourne, VIC, Australia

Prue A. Cowin, Anne Hamilton, Gisela Mir Arnau & Ravikiran Vedururu

219. Physics Division, Optimization and Systems Biology Lab, Massachusetts General Hospital, Boston, MA, USA

David Craft

220. Department of Medicine, Baylor College of Medicine, Houston, TX, USA

Chad J. Creighton

221. University of Cologne, Cologne, Germany

Yupeng Cun, Martin Peifer & Tsun-Po Yang

222. International Genomics Consortium, Phoenix, AZ, USA

Erin Curley & Troy Shelton

223. Genomics Research Program, Ontario Institute for Cancer Research, Toronto, ON, Canada

Karolina Czajka, Jenna Eagles, Thomas J. Hudson, Jeremy Johns, Faridah Mbabaali, John D. McPherson, Jessica K. Miller, Danielle Pasternack, Michelle Sam & Lee E. Timms

224. Barking Havering and Redbridge University Hospitals NHS Trust, Romford, UK

Bogdan Czerniak, Adel El-Naggar & David Khoo

225. Children's Hospital at Westmead, University of Sydney, Sydney, NSW, Australia

Rebecca A. Dagg

226. Department of Medicine, Section of Endocrinology, University and Hospital Trust of Verona, Verona, Italy

Maria Vittoria Davi

227. Computational Biology Center, Memorial Sloan Kettering Cancer Center, New York, NY, USA

Natalie R. Davidson, Andre Kahles, Kjong-Van Lehmann, Alessandro Pastore, Gunnar Rätsch, Chris Sander, Yasin Senbabaoglu & Nicholas D. Socci

228. Department of Biology, ETH Zurich, Zürich, Switzerland

Natalie R. Davidson, Andre Kahles, Kjong-Van Lehmann, Gunnar Rätsch & Stefan G. Stark

229. Department of Computer Science, ETH Zurich, Zurich, Switzerland

Natalie R. Davidson, Andre Kahles, Kjong-Van Lehmann & Gunnar Rätsch

230. SIB Swiss Institute of Bioinformatics, Lausanne, Switzerland

Natalie R. Davidson, Andre Kahles, Kjong-Van Lehmann, Gunnar Rätsch & Stefan G. Stark

231. Weill Cornell Medical College, New York, NY, USA

Natalie R. Davidson, Bishoy M. Faltas & Gunnar Rätsch

232. Academic Department of Medical Genetics, University of Cambridge, Addenbrooke's Hospital, Cambridge, UK

Helen Davies & Serena Nik-Zainal

233. MRC Cancer Unit, University of Cambridge, Cambridge, UK

Helen Davies, Rebecca C. Fitzgerald, Nicola Grehan, Serena Nik-Zainal & Maria O'Donovan

234. Departments of Pediatrics and Genetics, University of North Carolina at Chapel Hill, Chapel Hill, NC, USA

Ian J. Davis

235. Seven Bridges Genomics, Charlestown, MA, USA

Brandi N. Davis-Dusenbery, Sinisa Ivkovic, Milena Kovacevic, Ana Mijalkovic Lazic, Sanja Mijalkovic, Mia Nastic, Petar Radovic & Nebojsa Tijanic

236. Annai Systems, Inc, Carlsbad, CA, USA

Francisco M. De La Vega, Tal Shmaya & Dai-Ying Wu

237. Department of Pathology, General Hospital of Treviso, Department of Medicine, University of Padua, Treviso, Italy

Angelo P. Dei Tos

238. Department of Computational Biology, University of Lausanne, Lausanne, Switzerland

Olivier Delaneau

239. Department of Genetic Medicine and Development, University of Geneva Medical School, Geneva, CH, Switzerland

Olivier Delaneau

240. Swiss Institute of Bioinformatics, University of Geneva, Geneva, CH, Switzerland

Olivier Delaneau

241. The Francis Crick Institute, London, UK

Jonas Demeulemeester, Stefan C. Dentro, Matthew W. Fittall, Kerstin Haase, Clemency Jolly, Maxime Tarabichi & Peter Van Loo

242. University of Leuven, Leuven, Belgium

Jonas Demeulemeester & Peter Van Loo

243. Institute of Medical Genetics and Applied Genomics, University of Tübingen, Tübingen, Germany

German M. Demidov, Francesc Muyas & Stephan Ossowski

244. Computational and Systems Biology, Genome Institute of Singapore, Singapore, Singapore

Deniz Demircioğlu & Jonathan Göke

245. School of Computing, National University of Singapore, Singapore, Singapore

Deniz Demircioğlu

246. Big Data Institute, Li Ka Shing Centre, University of Oxford, Oxford, UK

Stefan C. Dentro & David C. Wedge

247. Biomedical Data Science Laboratory, Francis Crick Institute, London, UK

Nikita Desai

248. Bioinformatics Group, Department of Computer Science, University College London, London, UK

Nikita Desai

249. The Edward S. Rogers Sr. Department of Electrical and Computer Engineering, University of Toronto, Toronto, ON, Canada

Amit G. Deshwar

250. Breast Cancer Translational Research Laboratory JC Heuson, Institut Jules Bordet, Brussels, Belgium

Christine Desmedt

251. Department of Oncology, Laboratory for Translational Breast Cancer Research, KU Leuven, Leuven, Belgium

Christine Desmedt

252. Institute for Research in Biomedicine (IRB Barcelona), The Barcelona Institute of Science and Technology, Barcelona, Spain

Jordi Deu-Pons, Joan Frigola, Abel Gonzalez-Perez, Ferran Muiños, Loris Mularoni, Oriol Pich, Iker Reyes-Salazar, Carlota Rubio-Perez, Radhakrishnan Sabarinathan & David Tamborero

253. Research Program on Biomedical Informatics, Universitat Pompeu Fabra, Barcelona, Spain

Jordi Deu-Pons, Abel Gonzalez-Perez, Ferran Muiños, Loris Mularoni, Oriol Pich, Carlota Rubio-Perez, Radhakrishnan Sabarinathan & David Tamborero

254. Division of Medical Oncology, Princess Margaret Cancer Centre, Toronto, ON, Canada

Neesha C. Dhani, David Hedley & Malcolm J. Moore

255. Department of Physiology and Biophysics, Weill Cornell Medicine, New York, NY, USA

Priyanka Dhingra, Ekta Khurana, Eric Minwei Liu & Alexander Martinez-Fundichely

256. Institute for Computational Biomedicine, Weill Cornell Medicine, New York, NY, USA

Priyanka Dhingra, Ekta Khurana, Eric Minwei Liu & Alexander Martinez-Fundichely

257. Department of Pathology, UPMC Shadyside, Pittsburgh, PA, USA

Rajiv Dhir

258. Independent Consultant, Wellesley, USA

Anthony DiBiase

259. Department of Cell and Molecular Biology, Science for Life Laboratory, Uppsala University, Uppsala, Sweden

Klev Diamanti, Jan Komorowski & Husen M. Umer

260. Department of Medicine and Department of Genetics, Washington University School of Medicine, St. Louis, St. Louis, MO, USA

Li Ding, Robert S. Fulton, Michael D. McLellan, Michael C. Wendl & Venkata D. Yellapantula

261. Hefei University of Technology, Anhui, China

Shuai Ding & Shanlin Yang

262. Translational Cancer Research Unit, GZA Hospitals St.-Augustinus, Center for Oncological Research, Faculty of Medicine and Health Sciences, University of Antwerp, Antwerp, Belgium

Luc Dirix, Steven Van Laere, Gert G. Van den Eynden & Peter Vermeulen

263. Simon Fraser University, Burnaby, BC, Canada

Nilgun Donmez, Ermin Hodzic, Salem Malikic, S. Cenk Sahinalp & Iman Sarrafi

264. University of Pennsylvania, Philadelphia, PA, USA

Ronny Drapkin

265. Faculty of Science and Technology, University of Vic—Central University of Catalonia (UVic-UCC), Vic, Spain

Ana Dueso-Barroso

266. The Wellcome Trust, London, UK

Michael Dunn

267. The Hospital for Sick Children, Toronto, ON, Canada

Lewis Jonathan Dursi

268. Department of Pathology, Queen Elizabeth University Hospital, Glasgow, UK

Fraser R. Duthie

269. Department of Genetics and Computational Biology, QIMR Berghofer Medical Research Institute, Brisbane, QLD, Australia

Ken Dutton-Regester, Nicholas K. Hayward, Oliver Holmes, Peter A. Johansson, Stephen H. Kazakoff, Conrad R. Leonard, Felicity Newell, Katia Nones, Ann-Marie Patch, John V. Pearson, Antonia L. Pritchard, Michael C. Quinn, Paresh Vyas, Nicola Waddell, Scott Wood & Qinying Xu

270. Department of Oncology, Centre for Cancer Genetic Epidemiology, University of Cambridge, Cambridge, UK

Douglas F. Easton

271. Department of Public Health and Primary Care, Centre for Cancer Genetic Epidemiology, University of Cambridge, Cambridge, UK

Douglas F. Easton

272. Prostate Cancer Canada, Toronto, ON, Canada

Stuart Edmonds

273. University of Cambridge, Cambridge, UK

Paul A. Edwards, Anthony R. Green, Andy G. Lynch, Florian Markowetz & Thomas J. Mitchell

274. Department of Laboratory Medicine, Translational Cancer Research, Lund University Cancer Center at Medicon Village, Lund University, Lund, Sweden

Anna Ehinger

275. Heidelberg University, Heidelberg, Germany

Juergen Eils, Roland Eils & Daniel Hübschmann

276. New BIH Digital Health Center, Berlin Institute of Health (BIH) and Charité - Universitätsmedizin Berlin, Berlin, Germany

Juergen Eils, Roland Eils & Chris Lawerenz

277. CIBER Epidemiología y Salud Pública (CIBERESP), Madrid, Spain

Georgia Escaramis

278. Research Group on Statistics, Econometrics and Health (GRECS), UdG, Barcelona, Spain

Georgia Escaramis

279. Quantitative Genomics Laboratories (qGenomics), Barcelona, Spain

Xavier Estivill

280. Icelandic Cancer Registry, Icelandic Cancer Society, Reykjavik, Iceland

Jorunn E. Eyfjord, Holmfridur Hilmarsdottir & Jon G. Jonasson

281. State Key Laboratory of Cancer Biology, and Xijing Hospital of Digestive Diseases, Fourth Military Medical University, Shaanxi, China

Daiming Fan & Yongzhan Nie

282. Department of Medicine (DIMED), Surgical Pathology Unit, University of Padua, Padua, Italy

Matteo Fassan

283. Rigshospitalet, Copenhagen, Denmark

Francesco Favero

284. Center for Cancer Genomics, National Cancer Institute, National Institutes of Health, Bethesda, MD, USA

Martin L. Ferguson

285. Department of Biochemistry and Molecular Medicine, University of Montreal, Montreal, QC, Canada

Vincent Ferretti

286. Australian Institute of Tropical Health and Medicine, James Cook University, Douglas, QLD, Australia

Matthew A. Field

287. Department of Neuro-Oncology, Istituto Neurologico Besta, Milano, Italy

Gaetano Finocchiaro

288. Bioplatforms Australia, North Ryde, NSW, Australia

Anna Fitzgerald & Catherine A. Shang

289. Department of Pathology (Research), University College London Cancer Institute, London, UK

Adrienne M. Flanagan

290. Department of Surgical Oncology, Princess Margaret Cancer Centre, Toronto, ON, Canada

Neil E. Fleshner

291. Department of Medical Oncology, Josephine Nefkens Institute and Cancer Genomics Centre, Erasmus Medical Center, Rotterdam, CN, The Netherlands

John A. Foekens, John W. M. Martens, F. Germán Rodríguez-González, Anieta M. Sieuwerts & Marcel Smid

292. The University of Queensland Thoracic Research Centre, The Prince Charles Hospital, Brisbane, QLD, Australia

Kwun M. Fong

293. CIBIO/InBIO - Research Center in Biodiversity and Genetic Resources, Universidade do Porto, Vairão, Portugal

Nuno A. Fonseca

294. HCA Laboratories, London, UK

Christopher S. Foster

295. University of Liverpool, Liverpool, UK

Christopher S. Foster

296. The Azrieli Faculty of Medicine, Bar-Ilan University, Safed, Israel

Milana Frenkel-Morgenstern

297. Department of Neurosurgery, University of Florida, Gainesville, FL, USA

William Friedman

298. Department of Pathology, Graduate School of Medicine, University of Tokyo, Tokyo, Japan

Masashi Fukayama & Tetsuo Ushiku

299. University of Milano Bicocca, Monza, Italy

Carlo Gambacorti-Passerini

300. BGI-Shenzhen, Shenzhen, China

Shengjie Gao, Yong Hou, Chang Li, Lin Li, Siliang Li, Xiaobo Li, Xinyue Li, Dongbing Liu, Xingmin Liu, Qiang Pan-Hammarström, Hong Su, Jian Wang, Kui Wu, Heng Xiong, Huanming Yang, Chen Ye, Xiuqing Zhang, Yong Zhou & Shida Zhu

301. Department of Pathology, Oslo University Hospital Ulleval, Oslo, Norway

Øystein Garred

302. Center for Biomedical Informatics, Harvard Medical School, Boston, MA, USA

Nils Gehlenborg

303. Department Biochemistry and Molecular Biomedicine, University of Barcelona, Barcelona, Spain

Josep L. L. Gelpi

304. Office of Cancer Genomics, National Cancer Institute, National Institutes of Health, Bethesda, MD, USA

Daniela S. Gerhard

305. Cancer Epigenomics, German Cancer Research Center (DKFZ), Heidelberg, Germany

Clarissa Gerhauser, Christoph Plass & Dieter Weichenhan

306. Department of Cancer Biology, The University of Texas MD Anderson Cancer Center, Houston, TX, USA

Jeffrey E. Gershenwald

307. Department of Surgical Oncology, The University of Texas MD Anderson Cancer Center, Houston, TX, USA

Jeffrey E. Gershenwald

308. Department of Computer Science, Yale University, New Haven, CT, USA

Mark Gerstein & Fabio C. P. Navarro

309. Department of Molecular Biophysics and Biochemistry, Yale University, New Haven, CT, USA

Mark Gerstein, Sushant Kumar, Lucas Lochovsky, Shaoke Lou, Patrick D. McGillivray, Fabio C. P. Navarro, Leonidas Salichos & Jonathan Warrell

310. Program in Computational Biology and Bioinformatics, Yale University, New Haven, CT, USA

Mark Gerstein, Arif O. Harmanci, Sushant Kumar, Donghoon Lee, Shantao Li, Xiaotong Li, Lucas Lochovsky, Shaoke Lou, William Meyerson, Leonidas Salichos, Jonathan Warrell, Jing Zhang & Yan Zhang

311. Center for Cancer Research, Massachusetts General Hospital, Boston, MA, USA

Gad Getz & Paz Polak

312. Department of Pathology, Massachusetts General Hospital, Boston, MA, USA

Gad Getz

313. Department of Pathology, Memorial Sloan Kettering Cancer Center, New York, NY, USA

Ronald Ghossein, Dilip D. Giri, Christine A. Iacobuzio-Donahue, Jorge Reis-Filho & Victor Reuter

314. Division of Gastroenterology and Hepatology, Mayo Clinic, Rochester, MN, USA

Nasra H. Giama, Catherine D. Moser & Lewis R. Roberts

315. University of Sydney, Sydney, NSW, Australia

Anthony J. Gill & James G. Kench

316. University of Oxford, Oxford, UK

Pelvender Gill, Freddie C. Hamdy, Katalin Karaszi, Adam Lambert, Luke Marsden, Clare Verrill & Paresh Vyas

317. Department of Surgery, Academic Urology Group, University of Cambridge, Cambridge, UK

Vincent J. Gnanapragasam

318. Department of Medicine II, University of Würzburg, Wuerzburg, Germany

Maria Elisabeth Goebler

319. Sylvester Comprehensive Cancer Center, University of Miami, Miami, FL, USA

Carmen Gomez

320. Institut Hospital del Mar d'Investigacions Mèdiques (IMIM), Barcelona, Spain

Abel Gonzalez-Perez

321. Genome Integrity and Structural Biology Laboratory, National Institute of Environmental Health Sciences (NIEHS), Durham, NC,

USA

Dmitry A. Gordenin & Natalie Saini

322. St. Thomas's Hospital, London, UK

James Gossage

323. Osaka International Cancer Center, Osaka, Japan

Kunihito Gotoh

324. Department of Pathology, Skåne University Hospital, Lund University, Lund, Sweden

Dorthe Grabau

325. Department of Medical Oncology, Beatson West of Scotland Cancer Centre, Glasgow, UK

Janet S. Graham

326. National Human Genome Research Institute, National Institutes of Health, Bethesda, MD, USA

Eric Green, Carolyn M. Hutter & Heidi J. Sofia

327. Centre for Cancer Research, Victorian Comprehensive Cancer Centre, University of Melbourne, Melbourne, VIC, Australia

Sean M. Grimmond

328. Department of Medicine, Section of Hematology/Oncology, University of Chicago, Chicago, IL, USA

Robert L. Grossman

329. German Center for Infection Research (DZIF), Partner Site Hamburg-Borstel-Lübeck-Riems, Hamburg, Germany

Adam Grundhoff

330. Bioinformatics Research Centre (BiRC), Aarhus University, Aarhus, Denmark

Qianyun Guo, Asger Hobolth & Jakob Skou Pedersen

331. Department of Biotechnology, Ministry of Science and Technology, Government of India, New Delhi, Delhi, India

Shailja Gupta & K. VijayRaghavan

332. National Cancer Centre Singapore, Singapore, Singapore

Jonathan Göke

333. Brandeis University, Waltham, MA, USA

James E. Haber

334. Department of Urologic Sciences, University of British Columbia, Vancouver, BC, Canada

Faraz Hach

335. Department of Internal Medicine, Stanford University, Stanford, CA, USA

Mark P. Hamilton

336. The University of Texas Health Science Center at Houston, Houston, TX, USA

Leng Han, Yang Yang & Xuanping Zhang

337. Imperial College NHS Trust, Imperial College, London, INY, UK

George B. Hanna

338. Senckenberg Institute of Pathology, University of Frankfurt Medical School, Frankfurt, Germany

Martin Hansmann

339. Department of Medicine, Division of Biomedical Informatics, UC San Diego School of Medicine, San Diego, CA, USA

Olivier Harismendy

340. Center for Precision Health, School of Biomedical Informatics, The University of Texas Health Science Center, Houston, TX, USA

Arif O. Harmanci

341. Oxford Nanopore Technologies, New York, NY, USA

Eoghan Harrington & Sissel Juul

342. Institute of Medical Science, University of Tokyo, Tokyo, Japan

Takanori Hasegawa, Shuto Hayashi, Seiya Imoto, Mitsuhiro Komura, Satoru Miyano, Naoki Miyoshi, Kazuhiro Ohi, Eigo Shimizu, Yuichi Shiraishi, Hiroko Tanaka & Rui Yamaguchi

343. Howard Hughes Medical Institute, University of California Santa Cruz, Santa Cruz, CA, USA

David Haussler

344. Wakayama Medical University, Wakayama, Japan

Shinya Hayami, Masaki Ueno & Hiroki Yamaue

345. Department of Internal Medicine, Division of Medical Oncology, Lineberger Comprehensive Cancer Center, University of North Carolina at Chapel Hill, Chapel Hill, NC, USA

D. Neil Hayes

346. University of Tennessee Health Science Center for Cancer Research, Memphis, TN, USA

D. Neil Hayes

347. Department of Histopathology, Salford Royal NHS Foundation Trust, Salford, UK

Stephen J. Hayes

348. Faculty of Biology, Medicine and Health, University of Manchester, Manchester, UK

Stephen J. Hayes

349. BIOPIC, ICG and College of Life Sciences, Peking University, Beijing, China

Yao He & Zemin Zhang

350. Peking-Tsinghua Center for Life Sciences, Peking University, Beijing, China

Yao He & Zemin Zhang

351. Children's Hospital of Philadelphia, Philadelphia, PA, USA

Allison P. Heath

352. Department of Bioinformatics and Computational Biology and Department of Systems Biology, The University of Texas MD Anderson Cancer Center, Houston, TX, USA

Apurva M. Hegde, Yiling Lu & John N. Weinstein

353. Karolinska Institute, Stockholm, Sweden

Eva Hellstrom-Lindberg & Jesper Lagergren

354. The Donnelly Centre, University of Toronto, Toronto, ON, Canada

Mohamed Helmy & Jeffrey A. Wintersinger

355. Department of Medical Genetics, College of Medicine, Hallym University, Chuncheon, South Korea

Seong Gu Heo, Eun Pyo Hong & Ji Wan Park

356. Department of Experimental and Health Sciences, Institute of Evolutionary Biology (UPF-CSIC), Universitat Pompeu Fabra, Barcelona, Spain

José María Heredia-Genestar, Tomas Marques-Bonet & Arcadi Navarro

357. Health Data Science Unit, University Clinics, Heidelberg, Germany

Carl Herrmann

358. Massachusetts General Hospital Center for Cancer Research, Charlestown, MA, USA

Julian M. Hess & Yosef E. Maruvka

359. Hokkaido University, Sapporo, Japan

Satoshi Hirano & Toru Nakamura

360. Department of Pathology and Clinical Laboratory, National Cancer Center Hospital, Tokyo, Japan

Nobuyoshi Hiraoka

361. Department of Genetics, University of North Carolina at Chapel Hill, Chapel Hill, NC, USA

Katherine A. Hoadley & Tara J. Skelly

362. Computational Biology, Leibniz Institute on Aging - Fritz Lipmann Institute (FLI), Jena, Germany

Steve Hoffmann

363. University of Melbourne Centre for Cancer Research, Melbourne, VIC, Australia

Oliver Hofmann

364. University of Nebraska Medical Center, Omaha, NE, USA

Michael A. Hollingsworth & Sarah P. Thayer

365. Syntekabio Inc, Daejeon, South Korea

Jongwhi H. Hong

366. Department of Pathology, Academic Medical Center, Amsterdam, AZ, The Netherlands

Gerrit K. Hooijer

367. China National GeneBank-Shenzhen, Shenzhen, China

Yong Hou, Chang Li, Siliang Li, Xiaobo Li, Dongbing Liu, Xingmin Liu, Henk G. Stunnenberg, Hong Su, Kui Wu, Heng Xiong, Chen Ye & Shida Zhu

368. Division of Molecular Genetics, German Cancer Research Center (DKFZ), Heidelberg, Germany

Volker Hovestadt, Murat Iskar, Peter Lichter, Bernhard Radlwimmer & Marc Zapatka

369. Division of Life Science and Applied Genomics Center, Hong Kong University of Science and Technology, Clear Water Bay, Hong Kong, China

Taobo Hu, Yogesh Kumar, Eric Z. Ma, Zhenggang Wu & Hong Xue

370. Icahn School of Medicine at Mount Sinai, New York, NY, USA

Kuan-lin Huang

371. Geneplus-Shenzhen, Shenzhen, China

Yi Huang

372. School of Computer Science and Technology, Xi'an Jiaotong University, Xi'an, China

Yi Huang, Jiayin Wang, Xiao Xiao & Xuanping Zhang

373. AbbVie, North Chicago, IL, USA

Thomas J. Hudson

374. Institute of Pathology, Charité – University Medicine Berlin, Berlin, Germany

Michael Hummel & Dido Lenze

375. Centre for Translational and Applied Genomics, British Columbia Cancer Agency, Vancouver, BC, Canada

David Huntsman

376. Edinburgh Royal Infirmary, Edinburgh, UK

Ted R. Hupp

377. Berlin Institute for Medical Systems Biology, Max Delbrück Center for Molecular Medicine, Berlin, Germany

Matthew R. Huska, Julia Markowski & Roland F. Schwarz

378. Department of Pediatric Immunology, Hematology and Oncology, University Hospital, Heidelberg, Germany

Daniel Hübschmann

379. German Cancer Research Center (DKFZ), Heidelberg, Germany

Daniel Hübschmann, Christof von Kalle & Roland F. Schwarz

380. Heidelberg Institute for Stem Cell Technology and Experimental Medicine (HI-STEM), Heidelberg, Germany

Daniel Hübschmann

381. Institute for Computational Biomedicine, Weill Cornell Medical College, New York, NY, USA

Marcin Imielinski

382. New York Genome Center, New York, NY, USA

Marcin Imielinski & Xiaotong Yao

383. Department of Urology, James Buchanan Brady Urological Institute, Johns Hopkins University School of Medicine, Baltimore, MD, USA

William B. Isaacs

384. Department of Preventive Medicine, Graduate School of Medicine, The University of Tokyo, Tokyo, Japan

Shumpei Ishikawa, Hiroto Katoh & Daisuke Komura

385. Department of Molecular and Cellular Biology, Baylor College of Medicine, Houston, TX, USA

Michael Ittmann

386. Department of Pathology and Immunology, Baylor College of Medicine, Houston, TX, USA

Michael Ittmann

387. Michael E. DeBakey Veterans Affairs Medical Center, Houston, TX, USA

Michael Ittmann

388. Technical University of Denmark, Lyngby, Denmark

Jose M. G. Izarzugaza

389. Department of Pathology, College of Medicine, Hanyang University, Seoul, South Korea

Jocelyne Jacquemier, Hyung-Yong Kim & Gu Kong

390. Academic Unit of Surgery, School of Medicine, College of Medical, Veterinary and Life Sciences, University of Glasgow, Glasgow Royal Infirmary, Glasgow, UK

Nigel B. Jamieson

391. Department of Pathology, Asan Medical Center, College of Medicine, Ulsan University, Songpa-gu, Seoul, South Korea

Se Jin Jang & Hee Jin Lee

392. Science Writer, Garrett Park, MD, USA

Karine Jegalian

393. International Cancer Genome Consortium (ICGC)/ICGC Accelerating Research in Genomic Oncology (ARGO) Secretariat, Ontario Institute for Cancer Research, Toronto, ON, Canada

Jennifer L. Jennings

394. University of Ljubljana, Ljubljana, Slovenia

Lara Jerman

395. Department of Public Health Sciences, University of Chicago, Chicago, IL, USA

Yuan Ji

396. Research Institute, NorthShore University HealthSystem, Evanston, IL, USA

Yuan Ji

397. Department for Biomedical Research, University of Bern, Bern, Switzerland

Rory Johnson, Andrés Lanzós & Mark A. Rubin

398. Centre of Genomics and Policy, McGill University and Génome Québec Innovation Centre, Montreal, QC, Canada

Yann Joly, Bartha M. Knoppers, Mark Phillips & Adrian Thorogood

399. Carolina Center for Genome Sciences, University of North Carolina at Chapel Hill, Chapel Hill, NC, USA

Corbin D. Jones

400. Hopp Children’s Cancer Center (KiTZ), Heidelberg, Germany

David T. W. Jones, Marcel Kool & Stefan M. Pfister

401. Pediatric Glioma Research Group, German Cancer Research Center (DKFZ), Heidelberg, Germany

David T. W. Jones

402. Cancer Research UK, London, UK

Nic Jones & David Scott

403. Indivumed GmbH, Hamburg, Germany

Hartmut Juhl

404. Genome Integration Data Center, Syntekabio, Inc, Daejeon, South Korea

Jongsun Jung

405. University Hospital Zurich, Zurich, Switzerland

Andre Kahles, Kjong-Van Lehmann & Gunnar Rätsch

406. Clinical Bioinformatics, Swiss Institute of Bioinformatics, Geneva, Switzerland

Abdullah Kahraman

407. Institute for Pathology and Molecular Pathology, University Hospital Zurich, Zurich, Switzerland

Abdullah Kahraman

408. Institute of Molecular Life Sciences, University of Zurich, Zurich, Switzerland

Abdullah Kahraman & Christian von Mering

409. MRC Human Genetics Unit, MRC IGMM, University of Edinburgh, Edinburgh, UK

Vera B. Kaiser & Colin A. Semple

410. Women's Cancer Program at the Samuel Oschin Comprehensive Cancer Institute, Cedars-Sinai Medical Center, Los Angeles, CA, USA

Beth Karlan

411. Department of Biology, Bioinformatics Group, Division of Molecular Biology, Faculty of Science, University of Zagreb, Zagreb, Croatia

Rosa Karlić

412. Department for Internal Medicine II, University Hospital Schleswig-Holstein, Kiel, Germany

Dennis Karsch & Michael Kneba

413. Genetics and Molecular Pathology, SA Pathology, Adelaide, SA, Australia

Karin S. Kassahn

414. Department of Gastric Surgery, National Cancer Center Hospital, Tokyo, Japan

Hitoshi Katai

415. Department of Bioinformatics, Division of Cancer Genomics, National Cancer Center Research Institute, Tokyo, Japan

Mamoru Kato, Hirofumi Rokutan & Mihoko Saito-Adachi

416. A.A. Kharkevich Institute of Information Transmission Problems, Moscow, Russia

Marat D. Kazanov

417. Oncology and Immunology, Dmitry Rogachev National Research Center of Pediatric Hematology, Moscow, Russia

Marat D. Kazanov

418. Skolkovo Institute of Science and Technology, Moscow, Russia

Marat D. Kazanov

419. Department of Surgery, The George Washington University, School of Medicine and Health Science, Washington, DC, USA

Electron Kebebew

420. Endocrine Oncology Branch, Center for Cancer Research, National Cancer Institute, National Institutes of Health, Bethesda, MD, USA

Electron Kebebew

421. Melanoma Institute Australia, Macquarie University, Sydney, NSW, Australia

Richard F. Kefford

422. MIT Computer Science and Artificial Intelligence Laboratory, Massachusetts Institute of Technology, Cambridge, MA, USA

Manolis Kellis

423. Tissue Pathology and Diagnostic Oncology, Royal Prince Alfred Hospital, Sydney, NSW, Australia

James G. Kench & Richard A. Scolyer

424. Cholangiocarcinoma Screening and Care Program and Liver Fluke and Cholangiocarcinoma Research Centre, Faculty of Medicine, Khon Kaen University, Khon Kaen, Thailand

Narong Khuntikeo

425. Controlled Department and Institution, New York, NY, USA

Ekta Khurana

426. Englander Institute for Precision Medicine, Weill Cornell Medicine, New York, NY, USA

Ekta Khurana & Alexander Martinez-Fundichely

427. National Cancer Center, Gyeonggi, South Korea

Hark Kyun Kim

428. Department of Biochemistry, College of Medicine, Ewha Womans University, Seoul, South Korea

Hyung-Lae Kim

429. Health Sciences Department of Biomedical Informatics, University of California San Diego, La Jolla, CA, USA

Jihoon Kim

430. Research Core Center, National Cancer Centre Korea, Goyang-si, South Korea

Jong K. Kim

431. Department of Health Sciences and Technology, Sungkyunkwan University School of Medicine, Seoul, South Korea

Youngwook Kim

432. Samsung Genome Institute, Seoul, South Korea

Youngwook Kim

433. Breast Oncology Program, Dana-Farber/Brigham and Women's Cancer Center, Boston, MA, USA

Tari A. King

434. Department of Surgery, Memorial Sloan Kettering Cancer Center, New York, NY, USA

Tari A. King & Samuel Singer

435. Division of Breast Surgery, Brigham and Women's Hospital, Boston, MA, USA

Tari A. King

436. Integrative Bioinformatics Support Group, National Institute of Environmental Health Sciences (NIEHS), Durham, NC, USA

Leszek J. Klimczak

437. Department of Clinical Science, University of Bergen, Bergen, Norway

Stian Knappskog & Ola Myklebost

438. Center For Medical Innovation, Seoul National University Hospital, Seoul, South Korea

Youngil Koh

439. Department of Internal Medicine, Seoul National University Hospital, Seoul, South Korea

Youngil Koh & Sung-Soo Yoon

440. Institute of Computer Science, Polish Academy of Sciences, Warsawa, Poland

Jan Komorowski

441. Functional and Structural Genomics, German Cancer Research Center (DKFZ), Heidelberg, Germany

Marcel Kool, Andrey Korshunov, Michael Koscher, Stefan M. Pfister & Qi Wang

442. Laboratory of Translational Genomics, Division of Cancer Epidemiology and Genetics, National Cancer Institute, , National Institutes of Health, Bethesda, MD, USA

Roelof Koster

443. Institute for Medical Informatics Statistics and Epidemiology, University of Leipzig, Leipzig, Germany

Markus Kreuz & Markus Loeffler

444. Morgan Welch Inflammatory Breast Cancer Research Program and Clinic, The University of Texas MD Anderson Cancer Center, Houston, TX, USA

Savitri Krishnamurthy

445. Department of Hematology and Oncology, Georg-Augusts-University of Göttingen, Göttingen, Germany

Dieter Kube & Lorenz H. P. Trümper

446. Institute of Cell Biology (Cancer Research), University of Duisburg-Essen, Essen, Germany

Ralf Küppers

447. King's College London and Guy's and St. Thomas' NHS Foundation Trust, London, UK

Jesper Lagergren

448. Center for Epigenetics, Van Andel Research Institute, Grand Rapids, MI, USA

Peter W. Laird

449. The University of Queensland Centre for Clinical Research, Royal Brisbane and Women's Hospital, Herston, QLD, Australia

Sunil R. Lakhani & Peter T. Simpson

450. Department of Pediatric Oncology and Hematology, University of Cologne, Cologne, Germany

Pablo Landgraf

451. University of Düsseldorf, Düsseldorf, Germany

Pablo Landgraf & Guido Reifenberger

452. Department of Pathology, Institut Jules Bordet, Brussels, Belgium

Denis Larsimont

453. Institute of Biomedicine, Sahlgrenska Academy at University of Gothenburg, Gothenburg, Sweden

Erik Larsson

454. Children’s Medical Research Institute, Sydney, NSW, Australia

Loretta M. S. Lau & Hilda A. Pickett

455. ILSbio, LLC Biobank, Chestertown, MD, USA

Xuan Le

456. Division of Genetics and Genomics, Boston Children’s Hospital, Harvard Medical School, Boston, MA, USA

Eunjung Alice Lee

457. Institute for Bioengineering and Biopharmaceutical Research (IBBR), Hanyang University, Seoul, South Korea

Jeong-Yeon Lee

458. Department of Statistics, University of California Santa Cruz, Santa Cruz, CA, USA

Juhee Lee

459. National Genotyping Center, Institute of Biomedical Sciences, Academia Sinica, Taipei, Taiwan

Ming Ta Michael Lee

460. Department of Vertebrate Genomics/Otto Warburg Laboratory Gene Regulation and Systems Biology of Cancer, Max Planck Institute for Molecular Genetics, Berlin, Germany

Hans Lehrach, Hans-Jörg Warnatz & Marie-Laure Yaspo

461. McGill University and Genome Quebec Innovation Centre, Montreal, QC, Canada

Louis Letourneau

462. biobyte solutions GmbH, Heidelberg, Germany

Ivica Letunic

463. Gynecologic Oncology, NYU Laura and Isaac Perlmutter Cancer Center, New York University, New York, NY, USA

Douglas A. Levine

464. Division of Oncology, Stem Cell Biology Section, Washington University School of Medicine, St. Louis, MO, USA

Tim Ley

465. Department of Systems Biology, The University of Texas MD Anderson Cancer Center, Houston, TX, USA

Han Liang

466. Harvard University, Cambridge, MA, USA

Ziao Lin

467. Urologic Oncology Branch, Center for Cancer Research, National Cancer Institute, National Institutes of Health, Bethesda, MD, USA

W. M. Linehan

468. University of Oslo, Oslo, Norway

Ole Christian Lingjærde & Torill Sauer

469. University of Toronto, Toronto, ON, Canada

Fei-Fei Fei Liu, Quaid D. Morris, Ruian Shi, Shankar Vembu & Fan Yang

470. Peking University, Beijing, China

Fenglin Liu, Fan Zhang, Liangtao Zheng & Xiuqing Zheng

471. School of Life Sciences, Peking University, Beijing, China

Fenglin Liu

472. Leidos Biomedical Research, Inc, McLean, VA, USA

Jia Liu

473. Hematology, Hospital Clinic, Institut d'Investigacions Biomèdiques August Pi i Sunyer (IDIBAPS), University of Barcelona, Barcelona, Spain

Armando Lopez-Guillermo

474. Second Military Medical University, Shanghai, China

Yong-Jie Lu & Hongwei Zhang

475. Chinese Cancer Genome Consortium, Shenzhen, China

Youyong Lu

476. Department of Medical Oncology, Beijing Hospital, Beijing, China

Youyong Lu

477. Laboratory of Molecular Oncology, Key Laboratory of Carcinogenesis and Translational Research (Ministry of Education), Peking University Cancer Hospital and Institute, Beijing, China

Youyong Lu & Rui Xing

478. School of Medicine/School of Mathematics and Statistics, University of St. Andrews, St, Andrews, Fife, UK

Andy G. Lynch

479. Institute for Systems Biology, Seattle, WA, USA

Lisa Lype, Sheila M. Reynolds & Ilya Shmulevich

480. Department of Biochemistry and Molecular Biology, Faculty of Medicine, University Institute of Oncology-IUOPA, Oviedo, Spain

Carlos López-Otín & Xose S. Puente

481. Institut Bergonié, Bordeaux, France

Gaetan MacGrogan

482. Cancer Unit, MRC University of Cambridge, Cambridge, UK

Shona MacRae

483. Department of Pathology and Laboratory Medicine, Center for Personalized Medicine, Children's Hospital Los Angeles, Los Angeles, CA, USA

Dennis T. Maglinte

484. John Curtin School of Medical Research, Canberra, ACT, Australia

Graham J. Mann

485. MVZ Department of Oncology, PraxisClinic am Johannisplatz, Leipzig, Germany

Luisa Mantovani-Löffler

486. Department of Information Technology, Ghent University, Ghent, Belgium

Kathleen Marchal & Sergio Pulido-Tamayo

487. Department of Plant Biotechnology and Bioinformatics, Ghent University, Ghent, Belgium

Kathleen Marchal, Sergio Pulido-Tamayo & Lieven P. C. Verbeke

488. Institute for Genomic Medicine, Nationwide Children's Hospital, Columbus, OH, USA

Elaine R. Mardis

489. Computational Biology Program, School of Medicine, Oregon Health and Science University, Portland, OR, USA

Adam A. Margolin & Adam J. Struck

490. Department of Surgery, Duke University, Durham, NC, USA

Jeffrey Marks

491. Institució Catalana de Recerca i Estudis Avançats (ICREA), Barcelona, Spain

Tomas Marques-Bonet, Jose I. Martin-Subero, Arcadi Navarro, David Torrents & Alfonso Valencia

492. Institut Català de Paleontologia Miquel Crusafont, Universitat Autònoma de Barcelona, Barcelona, Spain

Tomas Marques-Bonet

493. University of Glasgow, Glasgow, UK

Sancha Martin & Ke Yuan

494. Institut d'Investigacions Biomèdiques August Pi i Sunyer (IDIBAPS), Barcelona, Spain

Jose I. Martin-Subero

495. Division of Oncology, Washington University School of Medicine, St. Louis, MO, USA

R. Jay Mashl

496. Department of Surgery and Cancer, Imperial College, London, INY, UK

Erik Mayer

497. Applications Department, Oxford Nanopore Technologies, Oxford, UK

Simon Mayes & Daniel J. Turner

498. Department of Obstetrics, Gynecology and Reproductive Services, University of California San Francisco, San Francisco, CA, USA

Karen McCune & Karen Smith-McCune

499. Department of Biochemistry and Molecular Medicine, University California at Davis, Sacramento, CA, USA

John D. McPherson

500. STTARR Innovation Facility, Princess Margaret Cancer Centre, Toronto, ON, Canada

Alice Meng

501. Discipline of Surgery, Western Sydney University, Penrith, NSW, Australia

Neil D. Merrett

502. Yale School of Medicine, Yale University, New Haven, CT, USA

William Meyerson

503. Department of Genetics, Lineberger Comprehensive Cancer Center, University of North Carolina at Chapel Hill, Chapel Hill, NC, USA

Piotr A. Mieczkowski, Joel S. Parker, Charles M. Perou, Donghui Tan, Umadevi Veluvolu & Matthew D. Wilkerson

504. Departments of Neurology and Neurosurgery, Henry Ford Hospital, Detroit, MI, USA

Tom Mikkelsen

505. Precision Oncology, OHSU Knight Cancer Institute, Oregon Health and Science University, Portland, OR, USA

Gordon B. Mills

506. Institute of Pathology, University Medical Center Hamburg-Eppendorf, Hamburg, Germany

Sarah Minner, Guido Sauter & Ronald Simon

507. Department of Health Sciences, Faculty of Medical Sciences, Kyushu University, Fukuoka, Japan

Shinichi Mizuno

508. Heidelberg Academy of Sciences and Humanities, Heidelberg, Germany

Fruzsina Molnár-Gábor

509. Department of Clinical Pathology, University of Melbourne, Melbourne, VIC, Australia

Carl Morrison, Karin A. Oien, Chawalit Pairojkul, Paul M. Waring & Marc J. van de Vijver

510. Department of Pathology, Roswell Park Cancer Institute, Buffalo, NY, USA

Carl Morrison

511. Department of Computer Science, University of Helsinki, Helsinki, Finland

Ville Mustonen

512. Institute of Biotechnology, University of Helsinki, Helsinki, Finland

Ville Mustonen

513. Organismal and Evolutionary Biology Research Programme, University of Helsinki, Helsinki, Finland

Ville Mustonen

514. Department of Obstetrics and Gynecology, Division of Gynecologic Oncology, Washington University School of Medicine, St. Louis, MO, USA

David Mutch

515. Penrose St. Francis Health Services, Colorado Springs, CO, USA

Jerome Myers

516. Institute of Pathology, Ulm University and University Hospital of Ulm, Ulm, Germany

Peter Möller

517. National Cancer Center, Tokyo, Japan

Hitoshi Nakagama

518. Genome Institute of Singapore, Singapore, Singapore

Tannistha Nandi & Patrick Tan

519. 32Program in Computational Biology and Bioinformatics, Yale University, New Haven, CT, USA

Fabio C. P. Navarro

520. German Cancer Aid, Bonn, Germany

Gerd Nettekoven & Laura Planko

521. Programme in Cancer and Stem Cell Biology, Centre for Computational Biology, Duke-NUS Medical School, Singapore, Singapore

Alvin Wei Tian Ng

522. The Chinese University of Hong Kong, Shatin, NT, Hong Kong, China

Anthony Ng

523. Fourth Military Medical University, Shaanxi, China

Yongzhan Nie

524. The University of Cambridge School of Clinical Medicine, Cambridge, UK

Serena Nik-Zainal

525. St. Jude Children's Research Hospital, Memphis, TN, USA

Paul A. Northcott

526. University Health Network, Princess Margaret Cancer Centre, Toronto, ON, Canada

Faiyaz Notta & Ming Tsao

527. Center for Biomolecular Science and Engineering, University of California Santa Cruz, Santa Cruz, CA, USA

Brian D. O'Connor

528. Department of Medicine, University of Chicago, Chicago, IL, USA

Peter O'Donnell

529. Department of Neurology, Mayo Clinic, Rochester, MN, USA

Brian Patrick O'Neill

530. Cambridge Oesophagogastric Centre, Cambridge University Hospitals NHS Foundation Trust, Cambridge, UK

J. Robert O'Neill

531. Department of Computer Science, Carleton College, Northfield, MN, USA

Layla Oesper

532. Institute of Cancer Sciences, College of Medical Veterinary and Life Sciences, University of Glasgow, Glasgow, UK

Karin A. Oien

533. Department of Epidemiology, University of Alabama at Birmingham, Birmingham, AL, USA

Akinyemi I. Ojesina

534. HudsonAlpha Institute for Biotechnology, Huntsville, AL, USA

Akinyemi I. Ojesina

535. O’Neal Comprehensive Cancer Center, University of Alabama at Birmingham, Birmingham, AL, USA

Akinyemi I. Ojesina

536. Department of Pathology, Keio University School of Medicine, Tokyo, Japan

Hidenori Ojima

537. Department of Hepatobiliary and Pancreatic Oncology, National Cancer Center Hospital, Tokyo, Japan

Takuji Okusaka

538. Sage Bionetworks, Seattle, WA, USA

Larsson Omberg

539. Lymphoma Genomic Translational Research Laboratory, National Cancer Centre, Singapore, Singapore

Choon Kiat Ong

540. Department of Clinical Pathology, Robert-Bosch-Hospital, Stuttgart, Germany

German Ott

541. Department of Cell and Systems Biology, University of Toronto, Toronto, ON, Canada

B. F. Francis Ouellette

542. Department of Biosciences and Nutrition, Karolinska Institutet, Stockholm, Sweden

Qiang Pan-Hammarström

543. Center for Liver Cancer, Research Institute and Hospital, National Cancer Center, Gyeonggi, South Korea

Joong-Won Park

544. Division of Hematology-Oncology, Samsung Medical Center, Sungkyunkwan University School of Medicine, Seoul, South Korea

Keunchil Park

545. Samsung Advanced Institute for Health Sciences and Technology, Sungkyunkwan University School of Medicine, Seoul, South Korea

Keunchil Park

546. Cheonan Industry-Academic Collaboration Foundation, Sangmyung University, Cheonan, South Korea

Kiejung Park

547. NYU Langone Medical Center, New York, NY, USA

Harvey Pass

548. Department of Hematology and Medical Oncology, Cleveland Clinic, Cleveland, OH, USA

Nathan A. Pennell

549. Department of Radiation Oncology, University of California San Francisco, San Francisco, CA, USA

Marc D. Perry

550. Department of Health Sciences Research, Mayo Clinic, Rochester, MN, USA

Gloria M. Petersen

551. Helen F. Graham Cancer Center at Christiana Care Health Systems, Newark, DE, USA

Nicholas Petrelli

552. Heidelberg University Hospital, Heidelberg, Germany

Stefan M. Pfister

553. CSRA Incorporated, Fairfax, VA, USA

Todd D. Pihl

554. Research Department of Pathology, University College London Cancer Institute, London, UK

Nischalan Pillay

555. Department of Research Oncology, Guy's Hospital, King's Health Partners AHSC, King's College London School of Medicine, London, UK

Sarah Pinder

556. Faculty of Medicine and Health Sciences, Macquarie University, Sydney, NSW, Australia

Andreia V. Pinho

557. University Hospital of Minjoz, INSERM UMR 1098, Besançon, France

Xavier Pivot

558. Spanish National Cancer Research Centre, Madrid, Spain

Tirso Pons

559. Center of Digestive Diseases and Liver Transplantation, Fundeni Clinical Institute, Bucharest, Romania

Irinel Popescu

560. Cureline, Inc, South San Francisco, CA, USA

Olga Potapova

561. St. Luke's Cancer Centre, Royal Surrey County Hospital NHS Foundation Trust, Guildford, UK

Shaun R. Preston

562. Cambridge Breast Unit, Addenbrooke's Hospital, Cambridge University Hospital NHS Foundation Trust and NIHR Cambridge Biomedical Research Centre, Cambridge, UK

Elena Provenzano

563. East of Scotland Breast Service, Ninewells Hospital, Aberdeen, UK

Colin A. Purdie

564. Department of Genetics, Microbiology and Statistics, University of Barcelona, IRSJD, IBUB, Barcelona, Spain

Raquel Rabionet

565. Department of Obstetrics and Gynecology, Medical College of Wisconsin, Milwaukee, WI, USA

Janet S. Rader

566. Hematology and Medical Oncology, Winship Cancer Institute of Emory University, Atlanta, GA, USA

Suresh Ramalingam

567. Department of Computer Science, Princeton University, Princeton, NJ, USA

Benjamin J. Raphael & Matthew A. Reyna

568. Vanderbilt Ingram Cancer Center, Vanderbilt University, Nashville, TN, USA

W. Kimryn Rathmell

569. Ohio State University College of Medicine and Arthur G. James Comprehensive Cancer Center, Columbus, OH, USA

Matthew Ringel

570. Department of Surgery, Yokohama City University Graduate School of Medicine, Kanagawa, Japan

Yasushi Rino

571. Division of Chromatin Networks, German Cancer Research Center (DKFZ) and BioQuant, Heidelberg, Germany

Karsten Rippe

572. Research Computing Center, University of North Carolina at Chapel Hill, Chapel Hill, NC, USA

Jeffrey Roach

573. School of Molecular Biosciences and Center for Reproductive Biology, Washington State University, Pullman, WA, USA

Steven A. Roberts

574. Finsen Laboratory and Biotech Research and Innovation Centre (BRIC), University of Copenhagen, Copenhagen, Denmark

F. Germán Rodríguez-González, Nikos Sidiropoulos & Joachim Weischenfeldt

575. Department of Laboratory Medicine and Pathobiology, University of Toronto, Toronto, ON, Canada

Michael H. A. Roehrl & Stefano Serra

576. Department of Pathology, Human Oncology and Pathogenesis Program, Memorial Sloan Kettering Cancer Center, New York, NY, USA

Michael H. A. Roehrl

577. University Hospital Giessen, Pediatric Hematology and Oncology, Giessen, Germany

Marius Rohde

578. Oncologie Sénologie, ICM Institut Régional du Cancer, Montpellier, France

Gilles Romieu

579. Institute of Clinical Molecular Biology, Christian-Albrechts-University, Kiel, Germany

Philip C. Rosenstiel & Markus B. Schilhabel

580. Institute of Pathology, University of Wuerzburg, Wuerzburg, Germany

Andreas Rosenwald

581. Department of Urology, North Bristol NHS Trust, Bristol, UK

Edward W. Rowe

582. SingHealth, Duke-NUS Institute of Precision Medicine, National Heart Centre Singapore, Singapore, Singapore

Steven G. Rozen, Patrick Tan & Bin Tean Teh

583. Department of Computer Science, University of Toronto, Toronto, ON, Canada

Yulia Rubanova, Jared T. Simpson & Jeffrey A. Wintersinger

584. Bern Center for Precision Medicine, University Hospital of Bern, University of Bern, Bern, Switzerland

Mark A. Rubin

585. Englander Institute for Precision Medicine, Weill Cornell Medicine and New York Presbyterian Hospital, New York, NY, USA

Mark A. Rubin

586. Meyer Cancer Center, Weill Cornell Medicine, New York, NY, USA

Mark A. Rubin

587. Pathology and Laboratory, Weill Cornell Medical College, New York, NY, USA

Mark A. Rubin

588. Vall d’Hebron Institute of Oncology: VHIO, Barcelona, Spain

Carlota Rubio-Perez

589. General and Hepatobiliary-Biliary Surgery, Pancreas Institute, University and Hospital Trust of Verona, Verona, Italy

Andrea Ruzzenente

590. National Centre for Biological Sciences, Tata Institute of Fundamental Research, Bangalore, India

Radhakrishnan Sabarinathan

591. Indiana University, Bloomington, IN, USA

S. Cenk Sahinalp

592. Department of Pathology, GZA-ZNA Hospitals, Antwerp, Belgium

Roberto Salgado

593. Analytical Biological Services, Inc, Wilmington, DE, USA

Charles Saller

594. Sydney Medical School, University of Sydney, Sydney, NSW, Australia

Jaswinder S. Samra & Richard A. Scolyer

595. cBio Center, Dana-Farber Cancer Institute, Harvard Medical School, Boston, MA, USA

Chris Sander & Ciyue Shen

596. Department of Cell Biology, Harvard Medical School, Boston, MA, USA

Chris Sander & Ciyue Shen

597. Advanced Centre for Treatment Research and Education in Cancer, Tata Memorial Centre, Navi Mumbai, Maharashtra, India

Rajiv Sarin

598. School of Environmental and Life Sciences, Faculty of Science, The University of Newcastle, Ourimbah, NSW, Australia

Christopher J. Scarlett

599. Department of Dermatology, University Hospital of Essen, Essen, Germany

Dirk Schadendorf

600. Bioinformatics and Omics Data Analytics, German Cancer Research Center (DKFZ), Heidelberg, Germany

Matthias Schlesner

601. Department of Urology, Charité Universitätsmedizin Berlin, Berlin, Germany

Thorsten Schlomm & Joachim Weischenfeldt

602. Martini-Clinic, Prostate Cancer Center, University Medical Center Hamburg-Eppendorf, Hamburg, Germany

Thorsten Schlomm

603. Department of General Internal Medicine, University of Kiel, Kiel, Germany

Stefan Schreiber

604. German Cancer Consortium (DKTK), Partner site Berlin, Berlin, Germany

Roland F. Schwarz

605. Cancer Research Institute, Beth Israel Deaconess Medical Center, Boston, MA, USA

Ralph Scully

606. University of Pittsburgh, Pittsburgh, PA, USA

Raja Seethala

607. Department of Ophthalmology and Ocular Genomics Institute, Massachusetts Eye and Ear, Harvard Medical School, Boston, MA, USA

Ayellet V. Segre

608. Center for Psychiatric Genetics, NorthShore University HealthSystem, Evanston, IL, USA

Subhajit Sengupta

609. Van Andel Research Institute, Grand Rapids, MI, USA

Hui Shen & Wanding Zhou

610. Laboratory of Molecular Medicine, Human Genome Center, Institute of Medical Science, University of Tokyo, Tokyo, Japan

Tatsuhiro Shibata, Hirokazu Taniguchi & Tomoko Urushidate

611. Japan Agency for Medical Research and Development, Tokyo, Japan

Kiyo Shimizu & Takashi Yugawa

612. Korea University, Seoul, South Korea

Seung Jun Shin & Stefan G. Stark

613. Murtha Cancer Center, Walter Reed National Military Medical Center, Bethesda, MD, USA

Craig Shriver

614. Human Genetics, University of Kiel, Kiel, Germany

Reiner Siebert

615. Department of Oncologic Pathology, Dana-Farber Cancer Institute, Harvard Medical School, Boston, MA, USA

Sabina Signoretti

616. Oregon Health and Science University, Portland, OR, USA

Jaclyn Smith

617. Center for RNA Interference and Noncoding RNA, The University of Texas MD Anderson Cancer Center, Houston, TX, USA

Anil K. Sood

618. Department of Experimental Therapeutics, The University of Texas MD Anderson Cancer Center, Houston, TX, USA

Anil K. Sood

619. Department of Gynecologic Oncology and Reproductive Medicine, The University of Texas MD Anderson Cancer Center, Houston, TX, USA

Anil K. Sood

620. University Hospitals Coventry and Warwickshire NHS Trust, Coventry, UK

Sharmila Sothi

621. Department of Radiation Oncology, Radboud University Nijmegen Medical Centre, Nijmegen, GA, The Netherlands

Paul N. Span

622. Institute for Genomics and Systems Biology, University of Chicago, Chicago, IL, USA

Jonathan Spring

623. Clinic for Hematology and Oncology, St.-Antonius-Hospital, Eschweiler, Germany

Peter Staib

624. Computational and Systems Biology Program, Memorial Sloan Kettering Cancer Center, New York, NY, USA

Stefan G. Stark

625. University of Iceland, Reykjavik, Iceland

Ólafur Andri Stefánsson

626. Division of Computational Genomics and Systems Genetics, German Cancer Research Center (DKFZ), Heidelberg, Germany

Oliver Stegle

627. Dundee Cancer Centre, Ninewells Hospital, Dundee, UK

Alasdair Stenhouse & Alastair M. Thompson

628. Department for Internal Medicine III, University of Ulm and University Hospital of Ulm, Ulm, Germany

Stephan Stilgenbauer

629. Institut Curie, INSERM Unit 830, Paris, France

Henk G. Stunnenberg & Anne Vincent-Salomon

630. Department of Gastroenterology and Hepatology, Yokohama City University Graduate School of Medicine, Kanagawa, Japan

Akihiro Suzuki

631. Department of Laboratory Medicine, Radboud University Nijmegen Medical Centre, Nijmegen, GA, The Netherlands

Fred Sweep

632. Division of Cancer Genome Research, German Cancer Research Center (DKFZ), Heidelberg, Germany

Holger Sültmann

633. Department of General Surgery, Singapore General Hospital, Singapore, Singapore

Benita Kiat Tee Tan

634. Cancer Science Institute of Singapore, National University of Singapore, Singapore, Singapore

Patrick Tan & Bin Tean Teh

635. Department of Medical and Clinical Genetics, Genome-Scale Biology Research Program, University of Helsinki, Helsinki, Finland

Tomas J. Tanskanen

636. East Anglian Medical Genetics Service, Cambridge University Hospitals NHS Foundation Trust, Cambridge, UK

Patrick Tarpey

637. Irving Institute for Cancer Dynamics, Columbia University, New York, NY, USA

Simon Tavaré

638. Institute of Molecular and Cell Biology, Singapore, Singapore

Bin Tean Teh

639. Laboratory of Cancer Epigenome, Division of Medical Science, National Cancer Centre Singapore, Singapore, Singapore

Bin Tean Teh

640. Universite Lyon, INCa-Synergie, Centre Léon Bérard, Lyon, France

Gilles Thomas

641. Department of Urology, Mayo Clinic, Rochester, MN, USA

R. Houston Thompson

642. Royal National Orthopaedic Hospital - Stanmore, Stanmore, Middlesex, UK

Roberto Tirabosco

643. Department of Biochemistry, Genetics and Immunology, University of Vigo, Vigo, Spain

Marta Tojo

644. Giovanni Paolo II / I.R.C.C.S. Cancer Institute, Bari, BA, Italy

Stefania Tommasi

645. Neuroblastoma Genomics, German Cancer Research Center (DKFZ), Heidelberg, Germany

Umut H. Toprak

646. Fondazione Policlinico Universitario Gemelli IRCCS, Rome, Italy, Rome, Italy

Giampaolo Tortora

647. University of Verona, Verona, Italy

Giampaolo Tortora

648. Centre National de Génotypage, CEA - Institute de Génomique, Evry, France

Jörg Tost

649. CAPHRI Research School, Maastricht University, Maastricht, ER, The Netherlands

David Townend

650. Department of Biopathology, Centre Léon Bérard, Lyon, France

Isabelle Treilleux

651. Université Claude Bernard Lyon 1, Villeurbanne, France

Isabelle Treilleux

652. Core Research for Evolutional Science and Technology (CREST), JST, Tokyo, Japan

Tatsuhiko Tsunoda

653. Department of Biological Sciences, Laboratory for Medical Science Mathematics, Graduate School of Science, University of Tokyo, Yokohama, Japan

Tatsuhiko Tsunoda

654. Department of Medical Science Mathematics, Medical Research Institute, Tokyo Medical and Dental University (TMDU), Tokyo, Japan

Tatsuhiko Tsunoda

655. Cancer Ageing and Somatic Mutation Programme, Wellcome Sanger Institute, Hinxton, UK

Jose M. C. Tubio

656. University Hospitals Birmingham NHS Foundation Trust, Birmingham, UK

Olga Tucker

657. Centre for Cancer Research and Cell Biology, Queen's University, Belfast, UK

Richard Turkington

658. Breast Medical Oncology, The University of Texas MD Anderson Cancer Center, Houston, TX, USA

Naoto T. Ueno

659. Department of Surgery, Johns Hopkins University School of Medicine, Baltimore, MD, USA

Christopher Umbricht

660. Department of Oncology-Pathology, Science for Life Laboratory, Karolinska Institute, Stockholm, Sweden

Husen M. Umer

661. School of Cancer Sciences, Faculty of Medicine, University of Southampton, Southampton, UK

Timothy J. Underwood

662. Department of Gene Technology, Tallinn University of Technology, Tallinn, Estonia

Liis Uusküla-Reimand

663. Genetics and Genome Biology Program, SickKids Research Institute, The Hospital for Sick Children, Toronto, ON, Canada

Liis Uusküla-Reimand

664. Departments of Neurosurgery and Hematology and Medical Oncology, Winship Cancer Institute and School of Medicine, Emory University, Atlanta, GA, USA

Erwin G. Van Meir

665. Department of Clinical and Molecular Medicine, Faculty of Medicine and Health Sciences, Norwegian University of Science and Technology, Trondheim, Norway

Miguel Vazquez

666. Argmix Consulting, North Vancouver, BC, Canada

Shankar Vembu

667. Department of Information Technology, Ghent University, Interuniversitair Micro-Electronica Centrum (IMEC), Ghent, Belgium

Lieven P. C. Verbeke

668. Nuffield Department of Surgical Sciences, John Radcliffe Hospital, University of Oxford, Oxford, UK

Clare Verrill

669. Institute of Mathematics and Computer Science, University of Latvia, Riga, LV, Latvia

Juris Viksna

670. Discipline of Pathology, Sydney Medical School, University of Sydney, Sydney, NSW, Australia

Ricardo E. Vilain

671. Department of Applied Mathematics and Theoretical Physics, Centre for Mathematical Sciences, University of Cambridge, Cambridge, UK

Ignacio Vázquez-García

672. Department of Epidemiology and Biostatistics, Memorial Sloan Kettering Cancer Center, New York, NY, USA

Ignacio Vázquez-García & Venkata D. Yellapantula

673. Department of Statistics, Columbia University, New York, NY, USA

Ignacio Vázquez-García

674. Department of Immunology, Genetics and Pathology, Science for Life Laboratory, Uppsala University, Uppsala, Sweden

Claes Wadelius

675. School of Electronic and Information Engineering, Xi’an Jiaotong University, Xi’an, China

Jiayin Wang & Kai Ye

676. Department of Histopathology, Cambridge University Hospitals NHS Foundation Trust, Cambridge, UK

Anne Y. Warren

677. Oxford NIHR Biomedical Research Centre, University of Oxford, Oxford, UK

David C. Wedge

678. Georgia Regents University Cancer Center, Augusta, GA, USA

Paul Weinberger

679. Wythenshawe Hospital, Manchester, UK

Ian Welch

680. Department of Genetics, Washington University School of Medicine, St.Louis, MO, USA

Michael C. Wendl

681. Department of Biological Oceanography, Leibniz Institute of Baltic Sea Research, Rostock, Germany

Johannes Werner

682. Wellcome Centre for Human Genetics, University of Oxford, Oxford, UK

Justin P. Whalley

683. Department of Molecular and Human Genetics, Baylor College of Medicine, Houston, TX, USA

David A. Wheeler

684. Thoracic Oncology Laboratory, Mayo Clinic, Rochester, MN, USA

Dennis Wigle

685. Institute for Genomic Medicine, Nationwide Children's Hospital, Columbus, OH, USA

Richard K. Wilson

686. Department of Obstetrics and Gynecology, Division of Gynecologic Oncology, Mayo Clinic, Rochester, MN, USA

Boris Winterhoff

687. International Institute for Molecular Oncology, Poznań, Poland

Maciej Wiznerowicz

688. Poznan University of Medical Sciences, Poznań, Poland

Maciej Wiznerowicz

689. Genomics and Proteomics Core Facility High Throughput Sequencing Unit, German Cancer Research Center (DKFZ), Heidelberg, Germany

Stephan Wolf

690. NCCS-VARI Translational Research Laboratory, National Cancer Centre Singapore, Singapore, Singapore

Bernice H. Wong

691. Edison Family Center for Genome Sciences and Systems Biology, Washington University, St. Louis, MO, USA

Winghing Wong

692. MRC-University of Glasgow Centre for Virus Research, Glasgow, UK

Derek W. Wright

693. Department of Medical Informatics and Clinical Epidemiology, Division of Bioinformatics and Computational Biology, OHSU Knight Cancer Institute, Oregon Health and Science University, Portland, OR, USA

Guanming Wu

694. School of Electronic Information and Communications, Huazhong University of Science and Technology, Wuhan, China

Tian Xia

695. Department of Applied Mathematics and Statistics, Johns Hopkins University, Baltimore, MD, USA

Yanxun Xu

696. Department of Cancer Genome Informatics, Graduate School of Medicine, Osaka University, Osaka, Japan

Shinichi Yachida

697. Institute of Computer Science, Heidelberg University, Heidelberg, Germany

Sergei Yakneen

698. School of Mathematics and Statistics, University of Sydney, Sydney, NSW, Australia

Jean Y. Yang

699. Ben May Department for Cancer Research, University of Chicago, Chicago, IL, USA

Lixing Yang

700. Department of Human Genetics, University of Chicago, Chicago, IL, USA

Lixing Yang

701. Tri-Institutional PhD Program in Computational Biology and Medicine, Weill Cornell Medicine, New York, NY, USA

Xiaotong Yao

702. The First Affiliated Hospital, Xi’an Jiaotong University, Xi’an, China

Kai Ye

703. Department of Medicine and Therapeutics, The Chinese University of Hong Kong, Shatin, NT, Hong Kong, China

Jun Yu

704. Department of Biostatistics, The University of Texas MD Anderson Cancer Center, Houston, TX, USA

Kaixian Yu & Hongtu Zhu

705. Duke-NUS Medical School, Singapore, Singapore

Willie Yu

706. Department of Surgery, Ruijin Hospital, Shanghai Jiaotong University School of Medicine, Shanghai, China

Yingyan Yu

707. School of Computing Science, University of Glasgow, Glasgow, UK

Ke Yuan

708. Division of Orthopaedic Surgery, Oslo University Hospital, Oslo, Norway

Olga Zaikova

709. Eastern Clinical School, Monash University, Melbourne, VIC, Australia

Nikolajs Zeps

710. Epworth HealthCare, Richmond, VIC, Australia

Nikolajs Zeps

711. Department of Biostatistics and Computational Biology, Dana-Farber Cancer Institute and Harvard Medical School, Boston, MA, USA

Cheng-Zhong Zhang

712. Department of Biomedical Informatics, College of Medicine, The Ohio State University, Columbus, OH, USA

Yan Zhang

713. The Ohio State University Comprehensive Cancer Center (OSUCCC – James), Columbus, OH, USA

Yan Zhang

714. The University of Texas School of Biomedical Informatics (SBMI) at Houston, Houston, TX, USA

Zhongming Zhao

715. Department of Biostatistics, University of North Carolina at Chapel Hill, Chapel Hill, NC, USA

Hongtu Zhu

716. Department of Biochemistry and Molecular Genetics, Feinberg School of Medicine, Northwestern University, Chicago, IL, USA

Lihua Zou

717. Faculty of Medicine and Health, University of Sydney, Sydney, NSW, Australia

Anna deFazio

718. Department of Pathology, Erasmus Medical Center Rotterdam, Rotterdam, GD, The Netherlands

Carolien H. M. van Deurzen

719. Division of Molecular Carcinogenesis, The Netherlands Cancer Institute, Amsterdam, CX, The Netherlands

L. van't Veer

720. Institute of Molecular Life Sciences and Swiss Institute of Bioinformatics, University of Zurich, Zurich, Switzerland

Christian von Mering

Consortia

The ICGC/TCGA Pan-Cancer Analysis of Whole Genomes Consortium

- Lauri A. Aaltonen
- , Federico Abascal
- , Adam Abeshouse
- , Hiroyuki Aburatani
- , David J. Adams
- , Nishant Agrawal
- , Keun Soo Ahn
- , Sung-Min Ahn
- , Hiroshi Aikata
- , Rehan Akbani
- , Kadir C. Akdemir
- , Hikmat Al-Ahmadie
- , Sultan T. Al-Sedairy
- , Fatima Al-Shahrour
- , Malik Alawi
- , Monique Albert
- , Kenneth Aldape
- , Ludmil B. Alexandrov
- , Adrian Ally
- , Kathryn Alsop
- , Eva G. Alvarez
- , Fernanda Amary
- , Samirkumar B. Amin
- , Brice Aminou
- , Ole Ammerpohl
- , Matthew J. Anderson
- , Yeng Ang

- , Davide Antonello
- , Pavana Anur
- , Samuel Aparicio
- , Elizabeth L. Appelbaum
- , Yasuhito Arai
- , Axel Aretz
- , Koji Arihiro
- , Shun-ichi Ariizumi
- , Joshua Armenia
- , Laurent Arnould
- , Sylvia Asa
- , Yassen Assenov
- , Gurnit Atwal
- , Sietse Aukema
- , J. Todd Auman
- , Miriam R. R. Aure
- , Philip Awadalla
- , Marta Aymerich
- , Gary D. Bader
- , Adrian Baez-Ortega
- , Matthew H. Bailey
- , Peter J. Bailey
- , Miruna Balasundaram
- , Saianand Balu
- , Pratiti Bandopadhayay
- , Rosamonde E. Banks
- , Stefano Barbi
- , Andrew P. Barbour
- , Jonathan Barenboim
- , Jill Barnholtz-Sloan
- , Hugh Barr
- , Elisabet Barrera
- , John Bartlett
- , Javier Bartolome
- , Claudio Bassi
- , Oliver F. Bathe
- , Daniel Baumhoer

- , Prashant Bavi
- , Stephen B. Baylin
- , Wojciech Bazant
- , Duncan Beardsmore
- , Timothy A. Beck
- , Sam Behjati
- , Andreas Behren
- , Beifang Niu
- , Cindy Bell
- , Sergi Beltran
- , Christopher Benz
- , Andrew Berchuck
- , Anke K. Bergmann
- , Erik N. Bergstrom
- , Benjamin P. Berman
- , Daniel M. Berney
- , Stephan H. Bernhart
- , Rameen Beroukhim
- , Mario Berrios
- , Samantha Bersani
- , Johanna Bertl
- , Miguel Betancourt
- , Vinayak Bhandari
- , Shriram G. Bhosle
- , Andrew V. Biankin
- , Matthias Bieg
- , Darell Bigner
- , Hans Binder
- , Ewan Birney
- , Michael Birrer
- , Nidhan K. Biswas
- , Bodil Bjerkehagen
- , Tom Bodenheimer
- , Lori Boice
- , Giada Bonizzato
- , Johann S. De Bono
- , Arnoud Boot

- , Moiz S. Bootwalla
- , Ake Borg
- , Arndt Borkhardt
- , Keith A. Boroevich
- , Ivan Borozan
- , Christoph Borst
- , Marcus Bosenberg
- , Mattia Bosio
- , Jacqueline Boultwood
- , Guillaume Bourque
- , Paul C. Boutros
- , G. Steven Bova
- , David T. Bowen
- , Reanne Bowlby
- , David D. L. Bowtell
- , Sandrine Boyault
- , Rich Boyce
- , Jeffrey Boyd
- , Alvis Brazma
- , Paul Brennan
- , Daniel S. Brewer
- , Arie B. Brinkman
- , Robert G. Bristow
- , Russell R. Broaddus
- , Jane E. Brock
- , Malcolm Brock
- , Annegien Broeks
- , Angela N. Brooks
- , Denise Brooks
- , Benedikt Brors
- , Søren Brunak
- , Timothy J. C. Bruxner
- , Alicia L. Bruzos
- , Alex Buchanan
- , Ivo Buchhalter
- , Christiane Buchholz
- , Susan Bullman

- , Hazel Burke
- , Birgit Burkhardt
- , Kathleen H. Burns
- , John Busanovich
- , Carlos D. Bustamante
- , Adam P. Butler
- , Atul J. Butte
- , Niall J. Byrne
- , Anne-Lise Børresen-Dale
- , Samantha J. Caesar-Johnson
- , Andy Cafferkey
- , Declan Cahill
- , Claudia Calabrese
- , Carlos Caldas
- , Fabien Calvo
- , Niedzica Camacho
- , Peter J. Campbell
- , Elias Campo
- , Cinzia Cantù
- , Shaolong Cao
- , Thomas E. Carey
- , Joana Carlevaro-Fita
- , Rebecca Carlsen
- , Ivana Cataldo
- , Mario Cazzola
- , Jonathan Cebon
- , Robert Cerfolio
- , Dianne E. Chadwick
- , Dimple Chakravarty
- , Don Chalmers
- , Calvin Wing Yiu Chan
- , Kin Chan
- , Michelle Chan-Seng-Yue
- , Vishal S. Chandan
- , David K. Chang
- , Stephen J. Chanock
- , Lorraine A. Chantrill

- , Aurélien Chateigner
- , Nilanjan Chatterjee
- , Kazuaki Chayama
- , Hsiao-Wei Chen
- , Jieming Chen
- , Ken Chen
- , Yiwen Chen
- , Zhaohong Chen
- , Andrew D. Cherniack
- , Jeremy Chien
- , Yoke-Eng Chiew
- , Suet-Feung Chin
- , Juok Cho
- , Sunghoon Cho
- , Jung Kyoon Choi
- , Wan Choi
- , Christine Chomienne
- , Zechen Chong
- , Su Pin Choo
- , Angela Chou
- , Angelika N. Christ
- , Elizabeth L. Christie
- , Eric Chuah
- , Carrie Cibulskis
- , Kristian Cibulskis
- , Sara Cingarlini
- , Peter Clapham
- , Alexander Claviez
- , Sean Cleary
- , Nicole Cloonan
- , Marek Cmero
- , Colin C. Collins
- , Ashton A. Connor
- , Susanna L. Cooke
- , Colin S. Cooper
- , Leslie Cope
- , Vincenzo Corbo

- , Matthew G. Cordes
- , Stephen M. Cordner
- , Isidro Cortés-Ciriano
- , Kyle Covington
- , Prue A. Cowin
- , Brian Craft
- , David Craft
- , Chad J. Creighton
- , Yupeng Cun
- , Erin Curley
- , Ioana Cutcutache
- , Karolina Czajka
- , Bogdan Czerniak
- , Rebecca A. Dagg
- , Ludmila Danilova
- , Maria Vittoria Davi
- , Natalie R. Davidson
- , Helen Davies
- , Ian J. Davis
- , Brandi N. Davis-Dusenbery
- , Kevin J. Dawson
- , Francisco M. De La Vega
- , Ricardo De Paoli-Iseppi
- , Timothy Defreitas
- , Angelo P. Dei Tos
- , Olivier Delaneau
- , John A. Demchok
- , Jonas Demeulemeester
- , German M. Demidov
- , Deniz Demircioğlu
- , Nening M. Dennis
- , Robert E. Denroche
- , Stefan C. Dentro
- , Nikita Desai
- , Vikram Deshpande
- , Amit G. Deshwar
- , Christine Desmedt

- , Jordi Deu-Pons
- , Noreen Dhalla
- , Neesha C. Dhani
- , Priyanka Dhingra
- , Rajiv Dhir
- , Anthony DiBiase
- , Klev Diamanti
- , Li Ding
- , Shuai Ding
- , Huy Q. Dinh
- , Luc Dirix
- , HarshaVardhan Doddapaneni
- , Nilgun Donmez
- , Michelle T. Dow
- , Ronny Drapkin
- , Oliver Drechsel
- , Ruben M. Drews
- , Serge Serge
- , Tim Dudderidge
- , Ana Dueso-Barroso
- , Andrew J. Dunford
- , Michael Dunn
- , Lewis Jonathan Dursi
- , Fraser R. Duthie
- , Ken Dutton-Regester
- , Jenna Eagles
- , Douglas F. Easton
- , Stuart Edmonds
- , Paul A. Edwards
- , Sandra E. Edwards
- , Rosalind A. Eeles
- , Anna Ehinger
- , Juergen Eils
- , Roland Eils
- , Adel El-Naggar
- , Matthew Eldridge
- , Kyle Ellrott

- , Serap Erkek
- , Georgia Escaramis
- , Shadrielle M. G. Espiritu
- , Xavier Estivill
- , Dariush Etemadmoghadam
- , Jorunn E. Eyfjord
- , Bishoy M. Faltas
- , Daiming Fan
- , Yu Fan
- , William C. Faquin
- , Claudiu Farcas
- , Matteo Fassan
- , Aquila Fatima
- , Francesco Favero
- , Nodirjon Fayzullaev
- , Ina Felau
- , Sian Fereday
- , Martin L. Ferguson
- , Vincent Ferretti
- , Lars Feuerbach
- , Matthew A. Field
- , J. Lynn Fink
- , Gaetano Finocchiaro
- , Cyril Fisher
- , Matthew W. Fittall
- , Anna Fitzgerald
- , Rebecca C. Fitzgerald
- , Adrienne M. Flanagan
- , Neil E. Fleshner
- , Paul Flicek
- , John A. Foekens
- , Kwun M. Fong
- , Nuno A. Fonseca
- , Christopher S. Foster
- , Natalie S. Fox
- , Michael Fraser
- , Scott Frazer

- , Milana Frenkel-Morgenstern
- , William Friedman
- , Joan Frigola
- , Catrina C. Fronick
- , Akihiro Fujimoto
- , Masashi Fujita
- , Masashi Fukayama
- , Lucinda A. Fulton
- , Robert S. Fulton
- , Mayuko Furuta
- , P. Andrew Futreal
- , Anja Füllgrabe
- , Stacey B. Gabriel
- , Steven Gallinger
- , Carlo Gambacorti-Passerini
- , Jianjiong Gao
- , Shengjie Gao
- , Levi Garraway
- , Øystein Garred
- , Erik Garrison
- , Dale W. Garsed
- , Nils Gehlenborg
- , Josep L. L. Gelpi
- , Joshy George
- , Daniela S. Gerhard
- , Clarissa Gerhauser
- , Jeffrey E. Gershenwald
- , Mark Gerstein
- , Moritz Gerstung
- , Gad Getz
- , Mohammed Ghori
- , Ronald Ghossein
- , Nasra H. Giama
- , Richard A. Gibbs
- , Bob Gibson
- , Anthony J. Gill
- , Pelvender Gill

- , Dilip D. Giri
- , Dominik Glodzik
- , Vincent J. Gnanapragasam
- , Maria Elisabeth Goebler
- , Mary J. Goldman
- , Carmen Gomez
- , Santiago Gonzalez
- , Abel Gonzalez-Perez
- , Dmitry A. Gordenin
- , James Gossage
- , Kunihito Gotoh
- , Ramaswamy Govindan
- , Dorthe Grabau
- , Janet S. Graham
- , Robert C. Grant
- , Anthony R. Green
- , Eric Green
- , Liliana Greger
- , Nicola Grehan
- , Sonia Grimaldi
- , Sean M. Grimmond
- , Robert L. Grossman
- , Adam Grundhoff
- , Gunes Gundem
- , Qianyun Guo
- , Manaswi Gupta
- , Shailja Gupta
- , Ivo G. Gut
- , Marta Gut
- , Jonathan Göke
- , Gavin Ha
- , Andrea Haake
- , David Haan
- , Siegfried Haas
- , Kerstin Haase
- , James E. Haber
- , Nina Habermann

- , Faraz Hach
- , Syed Haider
- , Natsuko Hama
- , Freddie C. Hamdy
- , Anne Hamilton
- , Mark P. Hamilton
- , Leng Han
- , George B. Hanna
- , Martin Hansmann
- , Nicholas J. Haradhvala
- , Olivier Harismendy
- , Ivon Harliwong
- , Arif O. Harmanci
- , Eoghan Harrington
- , Takanori Hasegawa
- , David Haussler
- , Steve Hawkins
- , Shinya Hayami
- , Shuto Hayashi
- , D. Neil Hayes
- , Stephen J. Hayes
- , Nicholas K. Hayward
- , Steven Hazell
- , Yao He
- , Allison P. Heath
- , Simon C. Heath
- , David Hedley
- , Apurva M. Hegde
- , David I. Heiman
- , Michael C. Heinold
- , Zachary Heins
- , Lawrence E. Heisler
- , Eva Hellstrom-Lindberg
- , Mohamed Helmy
- , Seong Gu Heo
- , Austin J. Hepperla
- , José María Heredia-Genestar

- , Carl Herrmann
- , Peter Hersey
- , Julian M. Hess
- , Holmfridur Hilmarsdottir
- , Jonathan Hinton
- , Satoshi Hirano
- , Nobuyoshi Hiraoka
- , Katherine A. Hoadley
- , Asger Hobolth
- , Ermin Hodzic
- , Jessica I. Hoell
- , Steve Hoffmann
- , Oliver Hofmann
- , Andrea Holbrook
- , Aliaksei Z. Holik
- , Michael A. Hollingsworth
- , Oliver Holmes
- , Robert A. Holt
- , Chen Hong
- , Eun Pyo Hong
- , Jongwhi H. Hong
- , Gerrit K. Hooijer
- , Henrik Hornshøj
- , Fumie Hosoda
- , Yong Hou
- , Volker Hovestadt
- , William Howat
- , Alan P. Hoyle
- , Ralph H. Hruban
- , Jianhong Hu
- , Taobo Hu
- , Xing Hua
- , Kuan-lin Huang
- , Mei Huang
- , Mi Ni Huang
- , Vincent Huang
- , Yi Huang

- , Wolfgang Huber
- , Thomas J. Hudson
- , Michael Hummel
- , Jillian A. Hung
- , David Huntsman
- , Ted R. Hupp
- , Jason Huse
- , Matthew R. Huska
- , Barbara Hutter
- , Carolyn M. Hutter
- , Daniel Hübschmann
- , Christine A. Iacobuzio-Donahue
- , Charles David Imbusch
- , Marcin Imielinski
- , Seiya Imoto
- , William B. Isaacs
- , Keren Isaev
- , Shumpei Ishikawa
- , Murat Iskar
- , S. M. Ashiqul Islam
- , Michael Ittmann
- , Sinisa Ivkovic
- , Jose M. G. Izarzugaza
- , Jocelyne Jacquemier
- , Valerie Jakrot
- , Nigel B. Jamieson
- , Gun Ho Jang
- , Se Jin Jang
- , Joy C. Jayaseelan
- , Reyka Jayasinghe
- , Stuart R. Jefferys
- , Karine Jegalian
- , Jennifer L. Jennings
- , Seung-Hyup Jeon
- , Lara Jerman
- , Yuan Ji
- , Wei Jiao

- , Peter A. Johansson
- , Amber L. Johns
- , Jeremy Johns
- , Rory Johnson
- , Todd A. Johnson
- , Clemency Jolly
- , Yann Joly
- , Jon G. Jonasson
- , Corbin D. Jones
- , David R. Jones
- , David T. W. Jones
- , Nic Jones
- , Steven J. M. Jones
- , Jos Jonkers
- , Young Seok Ju
- , Hartmut Juhl
- , Jongsun Jung
- , Malene Juul
- , Randi Istrup Juul
- , Sissel Juul
- , Natalie Jäger
- , Rolf Kabbe
- , Andre Kahles
- , Abdullah Kahraman
- , Vera B. Kaiser
- , Hojabr Kakavand
- , Sangeetha Kalimuthu
- , Christof von Kalle
- , Koo Jeong Kang
- , Katalin Karaszi
- , Beth Karlan
- , Rosa Karlić
- , Dennis Karsch
- , Katayoon Kasaian
- , Karin S. Kassahn
- , Hitoshi Katai
- , Mamoru Kato

- , Hiroto Katoh
- , Yoshiiku Kawakami
- , Jonathan D. Kay
- , Stephen H. Kazakoff
- , Marat D. Kazanov
- , Maria Keays
- , Electron Kebebew
- , Richard F. Kefford
- , Manolis Kellis
- , James G. Kench
- , Catherine J. Kennedy
- , Jules N. A. Kerssemakers
- , David Khoo
- , Vincent Khoo
- , Narong Khuntikeo
- , Ekta Khurana
- , Helena Kilpinen
- , Hark Kyun Kim
- , Hyung-Lae Kim
- , Hyung-Yong Kim
- , Hyunghwan Kim
- , Jaegil Kim
- , Jihoon Kim
- , Jong K. Kim
- , Youngwook Kim
- , Tari A. King
- , Wolfram Klapper
- , Kortine Kleinheinz
- , Leszek J. Klimczak
- , Stian Knappskog
- , Michael Kneba
- , Bartha M. Knoppers
- , Youngil Koh
- , Jan Komorowski
- , Daisuke Komura
- , Mitsuhiro Komura
- , Gu Kong

- , Marcel Kool
- , Jan O. Korbel
- , Viktoriya Korchina
- , Andrey Korshunov
- , Michael Koscher
- , Roelof Koster
- , Zsofia Kote-Jarai
- , Antonios Koures
- , Milena Kovacevic
- , Barbara Kremeyer
- , Helene Kretzmer
- , Markus Kreuz
- , Savitri Krishnamurthy
- , Dieter Kube
- , Kiran Kumar
- , Pardeep Kumar
- , Sushant Kumar
- , Yogesh Kumar
- , Ritika Kundra
- , Kirsten Kübler
- , Ralf Küppers
- , Jesper Lagergren
- , Phillip H. Lai
- , Peter W. Laird
- , Sunil R. Lakhani
- , Christopher M. Lalansingh
- , Emilie Lalonde
- , Fabien C. Lamaze
- , Adam Lambert
- , Eric Lander
- , Pablo Landgraf
- , Luca Landoni
- , Anita Langerød
- , Andrés Lanzós
- , Denis Larsimont
- , Erik Larsson
- , Mark Lathrop

- , Loretta M. S. Lau
- , Chris Lawerenz
- , Rita T. Lawlor
- , Michael S. Lawrence
- , Alexander J. Lazar
- , Ana Mijalkovic Lazic
- , Xuan Le
- , Darlene Lee
- , Donghoon Lee
- , Eunjung Alice Lee
- , Hee Jin Lee
- , Jake June-Koo Lee
- , Jeong-Yeon Lee
- , Juhee Lee
- , Ming Ta Michael Lee
- , Henry Lee-Six
- , Kjong-Van Lehmann
- , Hans Lehrach
- , Dido Lenze
- , Conrad R. Leonard
- , Daniel A. Leongamornlert
- , Ignaty Leshchiner
- , Louis Letourneau
- , Ivica Letunic
- , Douglas A. Levine
- , Lora Lewis
- , Tim Ley
- , Chang Li
- , Constance H. Li
- , Haiyan Irene Li
- , Jun Li
- , Lin Li
- , Shantao Li
- , Siliang Li
- , Xiaobo Li
- , Xiaotong Li
- , Xinyue Li

- , Yilong Li
- , Han Liang
- , Sheng-Ben Liang
- , Peter Lichter
- , Pei Lin
- , Ziao Lin
- , W. M. Linehan
- , Ole Christian Lingjærde
- , Dongbing Liu
- , Eric Minwei Liu
- , Fei-Fei Fei Liu
- , Fenglin Liu
- , Jia Liu
- , Xingmin Liu
- , Julie Livingstone
- , Dimitri Livitz
- , Naomi Livni
- , Lucas Lochovsky
- , Markus Loeffler
- , Georgina V. Long
- , Armando Lopez-Guillermo
- , Shaoke Lou
- , David N. Louis
- , Laurence B. Lovat
- , Yiling Lu
- , Yong-Jie Lu
- , Youyong Lu
- , Claudio Luchini
- , Ilinca Lungu
- , Xuemei Luo
- , Hayley J. Luxton
- , Andy G. Lynch
- , Lisa Lype
- , Cristina López
- , Carlos López-Otín
- , Eric Z. Ma
- , Yussanne Ma

- , Gaetan MacGrogan
- , Shona MacRae
- , Geoff Macintyre
- , Tobias Madsen
- , Kazuhiro Maejima
- , Andrea Mafficini
- , Dennis T. Maglinte
- , Arindam Maitra
- , Partha P. Majumder
- , Luca Malcovati
- , Salem Malikic
- , Giuseppe Malleo
- , Graham J. Mann
- , Luisa Mantovani-Löffler
- , Kathleen Marchal
- , Giovanni Marchegiani
- , Elaine R. Mardis
- , Adam A. Margolin
- , Maximillian G. Marin
- , Florian Markowetz
- , Julia Markowski
- , Jeffrey Marks
- , Tomas Marques-Bonet
- , Marco A. Marra
- , Luke Marsden
- , John W. M. Martens
- , Sancha Martin
- , Jose I. Martin-Subero
- , Iñigo Martincorena
- , Alexander Martinez-Fundichely
- , Yosef E. Maruvka
- , R. Jay Mashl
- , Charlie E. Massie
- , Thomas J. Matthew
- , Lucy Matthews
- , Erik Mayer
- , Simon Mayes

- , Michael Mayo
- , Faridah Mbabaali
- , Karen McCune
- , Ultan McDermott
- , Patrick D. McGillivray
- , Michael D. McLellan
- , John D. McPherson
- , John R. McPherson
- , Treasa A. McPherson
- , Samuel R. Meier
- , Alice Meng
- , Shaowu Meng
- , Andrew Menzies
- , Neil D. Merrett
- , Sue Merson
- , Matthew Meyerson
- , William Meyerson
- , Piotr A. Mieczkowski
- , George L. Mihaiescu
- , Sanja Mijalkovic
- , Tom Mikkelsen
- , Michele Milella
- , Linda Mileshkin
- , Christopher A. Miller
- , David K. Miller
- , Jessica K. Miller
- , Gordon B. Mills
- , Ana Milovanovic
- , Sarah Minner
- , Marco Miotto
- , Gisela Mir Arnau
- , Lisa Mirabello
- , Chris Mitchell
- , Thomas J. Mitchell
- , Satoru Miyano
- , Naoki Miyoshi
- , Shinichi Mizuno

- , Fruzsina Molnár-Gábor
- , Malcolm J. Moore
- , Richard A. Moore
- , Sandro Morganella
- , Quaid D. Morris
- , Carl Morrison
- , Lisle E. Mose
- , Catherine D. Moser
- , Ferran Muiños
- , Loris Mularoni
- , Andrew J. Mungall
- , Karen Mungall
- , Elizabeth A. Musgrove
- , Ville Mustonen
- , David Mutch
- , Francesc Muyas
- , Donna M. Muzny
- , Alfonso Muñoz
- , Jerome Myers
- , Ola Myklebost
- , Peter Möller
- , Genta Nagae
- , Adnan M. Nagrial
- , Hardeep K. Nahal-Bose
- , Hitoshi Nakagama
- , Hidewaki Nakagawa
- , Hiromi Nakamura
- , Toru Nakamura
- , Kaoru Nakano
- , Tannistha Nandi
- , Jyoti Nangalia
- , Mia Nastic
- , Arcadi Navarro
- , Fabio C. P. Navarro
- , David E. Neal
- , Gerd Nettekoven
- , Felicity Newell

- , Steven J. Newhouse
- , Yulia Newton
- , Alvin Wei Tian Ng
- , Anthony Ng
- , Jonathan Nicholson
- , David Nicol
- , Yongzhan Nie
- , G. Petur Nielsen
- , Morten Muhlig Nielsen
- , Serena Nik-Zainal
- , Michael S. Noble
- , Katia Nones
- , Paul A. Northcott
- , Faiyaz Notta
- , Brian D. O’Connor
- , Peter O’Donnell
- , Maria O’Donovan
- , Sarah O’Meara
- , Brian Patrick O’Neill
- , J. Robert O’Neill
- , David Ocana
- , Angelica Ochoa
- , Layla Oesper
- , Christopher Ogden
- , Hideki Ohdan
- , Kazuhiro Ohi
- , Lucila Ohno-Machado
- , Karin A. Oien
- , Akinyemi I. Ojesina
- , Hidenori Ojima
- , Takuji Okusaka
- , Larsson Omberg
- , Choon Kiat Ong
- , Stephan Ossowski
- , German Ott
- , B. F. Francis Ouellette
- , Christine P’ng

- , Marta Paczkowska
- , Salvatore Paiella
- , Chawalit Pairojkul
- , Marina Pajic
- , Qiang Pan-Hammarström
- , Elli Papaemmanuil
- , Irene Papatheodorou
- , Nagarajan Paramasivam
- , Ji Wan Park
- , Joong-Won Park
- , Keunchil Park
- , Kiejung Park
- , Peter J. Park
- , Joel S. Parker
- , Simon L. Parsons
- , Harvey Pass
- , Danielle Pasternack
- , Alessandro Pastore
- , Ann-Marie Patch
- , Iris Pauporté
- , Antonio Pea
- , John V. Pearson
- , Chandra Sekhar Pedamallu
- , Jakob Skou Pedersen
- , Paolo Pederzoli
- , Martin Peifer
- , Nathan A. Pennell
- , Charles M. Perou
- , Marc D. Perry
- , Gloria M. Petersen
- , Myron Peto
- , Nicholas Petrelli
- , Robert Petryszak
- , Stefan M. Pfister
- , Mark Phillips
- , Oriol Pich
- , Hilda A. Pickett

- , Todd D. Pihl
- , Nischalan Pillay
- , Sarah Pinder
- , Mark Pinese
- , Andreia V. Pinho
- , Esa Pitkänen
- , Xavier Pivot
- , Elena Piñeiro-Yáñez
- , Laura Planko
- , Christoph Plass
- , Paz Polak
- , Tirso Pons
- , Irinel Popescu
- , Olga Potapova
- , Aparna Prasad
- , Shaun R. Preston
- , Manuel Prinz
- , Antonia L. Pritchard
- , Stephenie D. Prokopec
- , Elena Provenzano
- , Xose S. Puente
- , Sonia Puig
- , Montserrat Puiggròs
- , Sergio Pulido-Tamayo
- , Gulietta M. Pupo
- , Colin A. Purdie
- , Michael C. Quinn
- , Raquel Rabionet
- , Janet S. Rader
- , Bernhard Radlwimmer
- , Petar Radovic
- , Benjamin Raeder
- , Keiran M. Raine
- , Manasa Ramakrishna
- , Kamna Ramakrishnan
- , Suresh Ramalingam
- , Benjamin J. Raphael

- , W. Kimryn Rathmell
- , Tobias Rausch
- , Guido Reifenberger
- , Jüri Reimand
- , Jorge Reis-Filho
- , Victor Reuter
- , Iker Reyes-Salazar
- , Matthew A. Reyna
- , Sheila M. Reynolds
- , Esther Rheinbay
- , Yasser Riazalhosseini
- , Andrea L. Richardson
- , Julia Richter
- , Matthew Ringel
- , Markus Ringnér
- , Yasushi Rino
- , Karsten Rippe
- , Jeffrey Roach
- , Lewis R. Roberts
- , Nicola D. Roberts
- , Steven A. Roberts
- , A. Gordon Robertson
- , Alan J. Robertson
- , Javier Bartolomé Rodriguez
- , Bernardo Rodriguez-Martin
- , F. Germán Rodríguez-González
- , Michael H. A. Roehrl
- , Marius Rohde
- , Hirofumi Rokutan
- , Gilles Romieu
- , Ilse Rooman
- , Tom Roques
- , Daniel Rosebrock
- , Mara Rosenberg
- , Philip C. Rosenstiel
- , Andreas Rosenwald
- , Edward W. Rowe

- , Romina Royo
- , Steven G. Rozen
- , Yulia Rubanova
- , Mark A. Rubin
- , Carlota Rubio-Perez
- , Vasilisa A. Rudneva
- , Borislav C. Rusev
- , Andrea Ruzzenente
- , Gunnar Rätsch
- , Radhakrishnan Sabarinathan
- , Veronica Y. Sabelnykova
- , Sara Sadeghi
- , S. Cenk Sahinalp
- , Natalie Saini
- , Mihoko Saito-Adachi
- , Gordon Saksena
- , Adriana Salcedo
- , Roberto Salgado
- , Leonidas Salichos
- , Richard Sallari
- , Charles Saller
- , Roberto Salvia
- , Michelle Sam
- , Jaswinder S. Samra
- , Francisco Sanchez-Vega
- , Chris Sander
- , Grant Sanders
- , Rajiv Sarin
- , Iman Sarrafi
- , Aya Sasaki-Oku
- , Torill Sauer
- , Guido Sauter
- , Robyn P. M. Saw
- , Maria Scardoni
- , Christopher J. Scarlett
- , Aldo Scarpa
- , Ghislaine Scelo

- , Dirk Schadendorf
- , Jacqueline E. Schein
- , Markus B. Schilhabel
- , Matthias Schlesner
- , Thorsten Schlomm
- , Heather K. Schmidt
- , Sarah-Jane Schramm
- , Stefan Schreiber
- , Nikolaus Schultz
- , Steven E. Schumacher
- , Roland F. Schwarz
- , Richard A. Scolyer
- , David Scott
- , Ralph Scully
- , Raja Seethala
- , Ayellet V. Segre
- , Iris Selander
- , Colin A. Semple
- , Yasin Senbabaoglu
- , Subhajit Sengupta
- , Elisabetta Sereni
- , Stefano Serra
- , Dennis C. Sgroi
- , Mark Shackleton
- , Nimish C. Shah
- , Sagedeh Shahabi
- , Catherine A. Shang
- , Ping Shang
- , Ofer Shapira
- , Troy Shelton
- , Ciyue Shen
- , Hui Shen
- , Rebecca Shepherd
- , Ruian Shi
- , Yan Shi
- , Yu-Jia Shiah
- , Tatsuhiro Shibata

- , Juliann Shih
- , Eigo Shimizu
- , Kiyo Shimizu
- , Seung Jun Shin
- , Yuichi Shiraishi
- , Tal Shmaya
- , Ilya Shmulevich
- , Solomon I. Shorser
- , Charles Short
- , Raunak Shrestha
- , Suyash S. Shringarpure
- , Craig Shriver
- , Shimin Shuai
- , Nikos Sidiropoulos
- , Reiner Siebert
- , Anieta M. Sieuwerts
- , Lina Sieverling
- , Sabina Signoretti
- , Katarzyna O. Sikora
- , Michele Simbolo
- , Ronald Simon
- , Janae V. Simons
- , Jared T. Simpson
- , Peter T. Simpson
- , Samuel Singer
- , Nasa Sinnott-Armstrong
- , Payal Sipahimalani
- , Tara J. Skelly
- , Marcel Smid
- , Jaclyn Smith
- , Karen Smith-McCune
- , Nicholas D. Socci
- , Heidi J. Sofia
- , Matthew G. Soloway
- , Lei Song
- , Anil K. Sood
- , Sharmila Sothi

- , Christos Sotiriou
- , Cameron M. Soulette
- , Paul N. Span
- , Paul T. Spellman
- , Nicola Sperandio
- , Andrew J. Spillane
- , Oliver Spiro
- , Jonathan Spring
- , Johan Staaf
- , Peter F. Stadler
- , Peter Staib
- , Stefan G. Stark
- , Lucy Stebbings
- , Ólafur Andri Stefánsson
- , Oliver Stegle
- , Lincoln D. Stein
- , Alasdair Stenhouse
- , Chip Stewart
- , Stephan Stilgenbauer
- , Miranda D. Stobbe
- , Michael R. Stratton
- , Jonathan R. Stretch
- , Adam J. Struck
- , Joshua M. Stuart
- , Henk G. Stunnenberg
- , Hong Su
- , Xiaoping Su
- , Ren X. Sun
- , Stephanie Sungalee
- , Hana Susak
- , Akihiro Suzuki
- , Fred Sweep
- , Monika Szczepanowski
- , Holger Sültmann
- , Takashi Yugawa
- , Angela Tam
- , David Tamborero

- , Benita Kiat Tee Tan
- , Donghui Tan
- , Patrick Tan
- , Hiroko Tanaka
- , Hirokazu Taniguchi
- , Tomas J. Tanskanen
- , Maxime Tarabichi
- , Roy Tarnuzzer
- , Patrick Tarpey
- , Morgan L. Taschuk
- , Kenji Tatsuno
- , Simon Tavaré
- , Darrin F. Taylor
- , Amaro Taylor-Weiner
- , Jon W. Teague
- , Bin Tean Teh
- , Varsha Tembe
- , Javier Temes
- , Kevin Thai
- , Sarah P. Thayer
- , Nina Thiessen
- , Gilles Thomas
- , Sarah Thomas
- , Alan Thompson
- , Alastair M. Thompson
- , John F. F. Thompson
- , R. Houston Thompson
- , Heather Thorne
- , Leigh B. Thorne
- , Adrian Thorogood
- , Grace Tiao
- , Nebojsa Tijanic
- , Lee E. Timms
- , Roberto Tirabosco
- , Marta Tojo
- , Stefania Tommasi
- , Christopher W. Toon

- , Umut H. Toprak
- , David Torrents
- , Giampaolo Tortora
- , Jörg Tost
- , Yasushi Totoki
- , David Townend
- , Nadia Traficante
- , Isabelle Treilleux
- , Jean-Rémi Trotta
- , Lorenz H. P. Trümper
- , Ming Tsao
- , Tatsuhiko Tsunoda
- , Jose M. C. Tubio
- , Olga Tucker
- , Richard Turkington
- , Daniel J. Turner
- , Andrew Tutt
- , Masaki Ueno
- , Naoto T. Ueno
- , Christopher Umbricht
- , Husen M. Umer
- , Timothy J. Underwood
- , Lara Urban
- , Tomoko Urushidate
- , Tetsuo Ushiku
- , Liis Uusküla-Reimand
- , Alfonso Valencia
- , David J. Van Den Berg
- , Steven Van Laere
- , Peter Van Loo
- , Erwin G. Van Meir
- , Gert G. Van den Eynden
- , Theodorus Van der Kwast
- , Naveen Vasudev
- , Miguel Vazquez
- , Ravikiran Vedururu
- , Umadevi Veluvolu

- , Shankar Vembu
- , Lieven P. C. Verbeke
- , Peter Vermeulen
- , Clare Verrill
- , Alain Viari
- , David Vicente
- , Caterina Vicentini
- , K. VijayRaghavan
- , Juris Viksna
- , Ricardo E. Vilain
- , Izar Villasante
- , Anne Vincent-Salomon
- , Tapio Visakorpi
- , Douglas Voet
- , Paresh Vyas
- , Ignacio Vázquez-García
- , Nick M. Waddell
- , Nicola Waddell
- , Claes Wadelius
- , Lina Wadi
- , Rabea Wagener
- , Jeremiah A. Wala
- , Jian Wang
- , Jiayin Wang
- , Linghua Wang
- , Qi Wang
- , Wenyi Wang
- , Yumeng Wang
- , Zhining Wang
- , Paul M. Waring
- , Hans-Jörg Warnatz
- , Jonathan Warrell
- , Anne Y. Warren
- , Sebastian M. Waszak
- , David C. Wedge
- , Dieter Weichenhan
- , Paul Weinberger

- , John N. Weinstein
- , Joachim Weischenfeldt
- , Daniel J. Weisenberger
- , Ian Welch
- , Michael C. Wendl
- , Johannes Werner
- , Justin P. Whalley
- , David A. Wheeler
- , Hayley C. Whitaker
- , Dennis Wigle
- , Matthew D. Wilkerson
- , Ashley Williams
- , James S. Wilmott
- , Gavin W. Wilson
- , Julie M. Wilson
- , Richard K. Wilson
- , Boris Winterhoff
- , Jeffrey A. Wintersinger
- , Maciej Wiznerowicz
- , Stephan Wolf
- , Bernice H. Wong
- , Tina Wong
- , Winghing Wong
- , Youngchoon Woo
- , Scott Wood
- , Bradly G. Wouters
- , Adam J. Wright
- , Derek W. Wright
- , Mark H. Wright
- , Chin-Lee Wu
- , Dai-Ying Wu
- , Guanming Wu
- , Jianmin Wu
- , Kui Wu
- , Yang Wu
- , Zhenggang Wu
- , Liu Xi

- , Tian Xia
- , Qian Xiang
- , Xiao Xiao
- , Rui Xing
- , Heng Xiong
- , Qinying Xu
- , Yanxun Xu
- , Hong Xue
- , Shinichi Yachida
- , Sergei Yakneen
- , Rui Yamaguchi
- , Takafumi N. Yamaguchi
- , Masakazu Yamamoto
- , Shogo Yamamoto
- , Hiroki Yamaue
- , Fan Yang
- , Huanming Yang
- , Jean Y. Yang
- , Liming Yang
- , Lixing Yang
- , Shanlin Yang
- , Tsun-Po Yang
- , Yang Yang
- , Xiaotong Yao
- , Marie-Laure Yaspo
- , Lucy Yates
- , Christina Yau
- , Chen Ye
- , Kai Ye
- , Venkata D. Yellapantula
- , Christopher J. Yoon
- , Sung-Soo Yoon
- , Fouad Yousif
- , Jun Yu
- , Kaixian Yu
- , Willie Yu
- , Yingyan Yu

- , Ke Yuan
- , Yuan Yuan
- , Denis Yuen
- , Qinying Xu
- , Christina K. Yung
- , Olga Zaikova
- , Jorge Zamora
- , Marc Zapatka
- , Jean C. Zenklusen
- , Thorsten Zenz
- , Nikolajs Zeps
- , Cheng-Zhong Zhang
- , Fan Zhang
- , Hailei Zhang
- , Hongwei Zhang
- , Hongxin Zhang
- , Jiashan Zhang
- , Jing Zhang
- , Junjun Zhang
- , Xiuqing Zhang
- , Xuanping Zhang
- , Yan Zhang
- , Zemin Zhang
- , Zhongming Zhao
- , Liangtao Zheng
- , Xiuqing Zheng
- , Wanding Zhou
- , Yong Zhou
- , Bin Zhu
- , Hongtu Zhu
- , Jingchun Zhu
- , Shida Zhu
- , Lihua Zou
- , Xueqing Zou
- , Anna deFazio
- , Nicholas van As
- , Carolien H. M. van Deurzen

- , Marc J. van de Vijver
- , L. van’t Veer
- & Christian von Mering

Corresponding authors

Correspondence to Peter J. Campbell, Gad Getz, Jan O. Korbel, Lincoln D. Stein or Joshua M. Stuart.

Rights and permissions

Open Access This article is licensed under a Creative Commons Attribution 4.0 International License, which permits use, sharing, adaptation, distribution and reproduction in any medium or format, as long as you give appropriate credit to the original author(s) and the source, provide a link to the Creative Commons license, and indicate if changes were made. The images or other third party material in this article are included in the article’s Creative Commons license, unless indicated otherwise in a credit line to the material. If material is not included in the article’s Creative Commons license and your intended use is not permitted by statutory regulation or exceeds the permitted use, you will need to obtain permission directly from the copyright holder. To view a copy of this license, visit http://creativecommons.org/licenses/by/4.0/.

Reprints and Permissions

About this article

Cite this article

The ICGC/TCGA Pan-Cancer Analysis of Whole Genomes Consortium. Author Correction: Pan-cancer analysis of whole genomes. *Nature* **614**, E39 (2023). https://doi.org/10.1038/s41586-022-05598-w

- Published: 25 January 2023

- Issue Date: 16 February 2023
- DOI: https://doi.org/10.1038/s41586-022-05598-w

Share this article

Anyone you share the following link with will be able to read this content:

Get shareable link

Sorry, a shareable link is not currently available for this article.

Copy to clipboard

Provided by the Springer Nature SharedIt content-sharing initiative

---

This article was downloaded by **calibre** from https://www.nature.com/articles/s41586-022-05598-w

- Author Correction
- Open Access
- Published: 25 January 2023

Author Correction: Analyses of non-coding somatic drivers in 2,658 cancer whole genomes

- Esther Rheinbay,
- Morten Muhlig Nielsen,
- Federico Abascal,
- Jeremiah A. Wala,
- Ofer Shapira,
- Grace Tiao,
- Henrik Hornshøj,
- Julian M. Hess,
- Randi Istrup Juul,
- Ziao Lin,
- Lars Feuerbach,
- Radhakrishnan Sabarinathan,
- Tobias Madsen,
- Jaegil Kim,
- Loris Mularoni,
- Shimin Shuai,
- Andrés Lanzós,
- Carl Herrmann,
- Yosef E. Maruvka,
- Ciyue Shen,
- Samirkumar B. Amin,
- Pratiti Bandopadhayay,
- Johanna Bertl,
- Keith A. Boroevich,

- John Busanovich,
- Joana Carlevaro-Fita,
- Dimple Chakravarty,
- Calvin Wing Yiu Chan,
- David Craft,
- Priyanka Dhingra,
- Klev Diamanti,
- Nuno A. Fonseca,
- Abel Gonzalez-Perez,
- Qianyun Guo,
- Mark P. Hamilton,
- Nicholas J. Haradhvala,
- Chen Hong,
- Keren Isaev,
- Todd A. Johnson,
- Malene Juul,
- Andre Kahles,
- Abdullah Kahraman,
- Youngwook Kim,
- Jan Komorowski,
- Kiran Kumar,
- Sushant Kumar,
- Donghoon Lee,
- Kjong-Van Lehmann,
- Yilong Li,
- Eric Minwei Liu,
- Lucas Lochovsky,
- Keunchil Park,
- Oriol Pich,
- Nicola D. Roberts,
- Gordon Saksena,
- Steven E. Schumacher,
- Nikos Sidiropoulos,
- Lina Sieverling,
- Nasa Sinnott-Armstrong,
- Chip Stewart,
- David Tamborero,

- Jose M. C. Tubio,
- Husen M. Umer,
- Liis Uusküla-Reimand,
- Claes Wadelius,
- Lina Wadi,
- Xiaotong Yao,
- Cheng-Zhong Zhang,
- Jing Zhang,
- James E. Haber,
- Asger Hobolth,
- Marcin Imielinski,
- Manolis Kellis,
- Michael S. Lawrence,
- Christian von Mering,
- Hidewaki Nakagawa,
- Benjamin J. Raphael,
- Mark A. Rubin,
- Chris Sander,
- Lincoln D. Stein,
- Joshua M. Stuart,
- Tatsuhiko Tsunoda,
- David A. Wheeler,
- Rory Johnson,
- Jüri Reimand,
- Mark Gerstein,
- Ekta Khurana,
- Peter J. Campbell,
- Núria López-Bigas,
- PCAWG Drivers and Functional Interpretation Working Group,
- PCAWG Structural Variation Working Group,
- Joachim Weischenfeldt ,
- Rameen Beroukhim ,
- Iñigo Martincorena ,
- Jakob Skou Pedersen ,
- Gad Getz &
- PCAWG Consortium

Show authors

Nature **volume 614**, page E40 (2023)

- 1112 Accesses
- 2 Altmetric
- Metrics details

The Original Article was published on 05 February 2020

Correction to: *Nature* https://doi.org/10.1038/s41586-020-1965-x Published online 5 February 2020

In the published version of this paper, the members of the Pan-Cancer Analysis of Whole Genomes (PCAWG) Consortium were listed in the Supplementary Information; however, these members should have been included in the main paper. The original Article has been corrected to include the members and affiliations of the PCAWG Consortium in the main paper; the corrections have been made to the HTML version of the Article but not the PDF version. Additional minor corrections to affiliations have been made to the PDF and HTML versions of the original Article for consistency of information between the PCAWG list and the main paper. An additional affiliation has been added for Husen M. Umer (Department of Oncology-Pathology, Science for Life Laboratory, Karolinska Institute, Stockholm, Sweden). The affiliation for Erik Larsson has been changed from Computational Biology Center, Memorial Sloan Kettering Cancer Center, New York, NY, USA to Institute of Biomedicine, Sahlgrenska Academy at University of Gothenburg, Gothenburg, Sweden.

Author information

Author notes

1. These authors contributed equally: Esther Rheinbay, Morten Muhlig Nielsen, Federico Abascal, Jeremiah A. Wala, Ofer Shapira

2. These authors jointly supervised this work: Joachim Weischenfeldt, Rameen Beroukhim, Iñigo Martincorena, Jakob Skou Pedersen, Gad Getz

3. A list of members and their affiliations appears in the online version of the paper

4. A list of members and their affiliations appears online

Authors and Affiliations

1. The Broad Institute of MIT and Harvard, Cambridge, MA, USA

   Esther Rheinbay, Jeremiah A. Wala, Ofer Shapira, Grace Tiao, Julian M. Hess, Ziao Lin, Jaegil Kim, Yosef E. Maruvka, Pratiti Bandopadhayay, John Busanovich, Nicholas J. Haradhvala, Kiran Kumar, Gordon Saksena, Steven E. Schumacher, Chip Stewart, Manolis Kellis, Michael S. Lawrence, Pratiti Bandopadhayay, Rameen Beroukhim, Gad Getz, Nicholas J. Haradhvala, Julian M. Hess, Manolis Kellis, Jaegil Kim, Michael S. Lawrence, Ziao Lin, Yosef E. Maruvka, Esther Rheinbay, Gordon Saksena, Steven E. Schumacher, Ofer Shapira, Grace Tiao, Rameen Beroukhim, John Busanovich, Julian M. Hess, Kiran Kumar, Steven E. Schumacher, Chip Stewart, Jeremiah A. Wala, Rameen Beroukhim & Gad Getz

2. Center for Cancer Research, Massachusetts General Hospital, Charlestown, MA, USA

   Esther Rheinbay, Yosef E. Maruvka, Nicholas J. Haradhvala, Michael S. Lawrence, Gad Getz, Nicholas J. Haradhvala, Michael S. Lawrence, Yosef E. Maruvka, Esther Rheinbay & Gad Getz

3. Harvard Medical School, Boston, MA, USA

Esther Rheinbay, Gad Getz, Esther Rheinbay & Gad Getz

4. Department of Molecular Medicine (MOMA), Aarhus University Hospital, Aarhus, Denmark

Morten Muhlig Nielsen, Henrik Hornshøj, Randi Istrup Juul, Tobias Madsen, Johanna Bertl, Malene Juul, Johanna Bertl, Henrik Hornshøj, Malene Juul, Randi Istrup Juul, Tobias Madsen, Morten Muhlig Nielsen, Jakob Skou Pedersen & Jakob Skou Pedersen

5. Wellcome Trust Sanger Institute, Hinxton, UK

Federico Abascal, Peter J. Campbell, Federico Abascal, Peter J. Campbell, Iñigo Martincorena, Peter J. Campbell, Iñigo Martincorena & Iñigo Martincorena

6. Bioinformatics and Integrative Genomics, Harvard University, Cambridge, MA, USA

Jeremiah A. Wala, Rameen Beroukhim, Rameen Beroukhim, Jeremiah A. Wala & Rameen Beroukhim

7. Department of Cancer Biology, Dana-Farber Cancer Institute, Boston, MA, USA

Ofer Shapira, Pratiti Bandopadhayay, John Busanovich, Kiran Kumar, Steven E. Schumacher, Pratiti Bandopadhayay, Steven E. Schumacher, Ofer Shapira, John Busanovich, Kiran Kumar & Steven E. Schumacher

8. Harvard University, Cambridge, MA, USA

Ziao Lin & Ziao Lin

9. Division of Applied Bioinformatics, German Cancer Research Center (DKFZ), Heidelberg, Germany

Lars Feuerbach, Chen Hong, Lina Sieverling, Lars Feuerbach, Chen Hong, Lina Sieverling, Lars Feuerbach & Lina Sieverling

10. Institute for Research in Biomedicine (IRB Barcelona), The Barcelona Institute of Science and Technology, Barcelona, Spain

Radhakrishnan Sabarinathan, Loris Mularoni, Abel Gonzalez-Perez, Oriol Pich, David Tamborero, Núria López-Bigas, Loris Mularoni & David Tamborero

11. Research Program on Biomedical Informatics, Universitat Pompeu Fabra, Barcelona, Spain

Radhakrishnan Sabarinathan, Loris Mularoni, Abel Gonzalez-Perez, Oriol Pich, David Tamborero, Núria López-Bigas, Loris Mularoni & David Tamborero

12. Computational Biology Program, Ontario Institute for Cancer Research, Toronto, Ontario, Canada

Shimin Shuai, Keren Isaev, Lina Wadi, Lincoln D. Stein, Jüri Reimand, Keren Isaev, Jüri Reimand, Shimin Shuai, Lincoln D. Stein & Lina Wadi

13. Ontario Institute for Cancer Research, Toronto, Ontario, Canada

Shimin Shuai, Lincoln D. Stein, Shimin Shuai & Lincoln D. Stein

14. Department for BioMedical Research, University of Bern, Bern, Switzerland

Andrés Lanzós, Joana Carlevaro-Fita, Rory Johnson, Joana Carlevaro-Fita, Rory Johnson & Andrés Lanzós

15. Graduate School of Cellular and Biomedical Sciences, University of Bern, Bern, Switzerland

Andrés Lanzós, Joana Carlevaro-Fita, Joana Carlevaro-Fita & Andrés Lanzós

16. Department of Medical Oncology, Bern University Hospital, University of Bern, Bern, Switzerland

Andrés Lanzós, Joana Carlevaro-Fita, Rory Johnson, Joana Carlevaro-Fita, Rory Johnson & Andrés Lanzós

17. Division of Theoretical Bioinformatics, German Cancer Research Center (DKFZ), Heidelberg, Germany

    Carl Herrmann, Calvin Wing Yiu Chan, Calvin Wing Yiu Chan & Carl Herrmann

18. Bioquant Center, Institute of Pharmacy and Molecular Biotechnology, University of Heidelberg, Heidelberg, Germany

    Carl Herrmann & Carl Herrmann

19. Department of Cell Biology, Harvard Medical School, Boston, MA, USA

    Ciyue Shen, Chris Sander, Chris Sander & Ciyue Shen

20. cBio Center, Dana-Farber Cancer Institute, Harvard Medical School, Boston, MA, USA

    Ciyue Shen, Chris Sander, Chris Sander & Ciyue Shen

21. Department of Genomic Medicine, University of Texas MD Anderson Cancer Center, Houston, TX, USA

    Samirkumar B. Amin & Samirkumar B. Amin

22. Graduate Program in Structural and Computational Biology and Molecular Biophysics, Baylor College of Medicine, Houston, TX, USA

    Samirkumar B. Amin & Samirkumar B. Amin

23. Laboratory for Medical Science Mathematics, RIKEN Center for Integrative Medical Sciences, Yokohama, Japan

Keith A. Boroevich, Todd A. Johnson, Tatsuhiko Tsunoda, Keith A. Boroevich, Todd A. Johnson & Tatsuhiko Tsunoda

24. Department of Genitourinary Medical Oncology - Research, Division of Cancer Medicine, University of Texas MD Anderson Cancer Center, Houston, TX, USA

Dimple Chakravarty & Dimple Chakravarty

25. Department of Urology, Icahn school of Medicine at Mount Sinai, New York, NY, USA

Dimple Chakravarty & Dimple Chakravarty

26. Faculty of Biosciences, Heidelberg University, Heidelberg, Germany

Calvin Wing Yiu Chan, Chen Hong, Lina Sieverling, Calvin Wing Yiu Chan, Chen Hong, Lina Sieverling & Lina Sieverling

27. Department of Radiation Oncology, Harvard Medical School, Massachusetts General Hospital, Boston, MA, USA

David Craft

28. Department of Physiology and Biophysics, Weill Cornell Medicine, New York, NY, USA

Priyanka Dhingra, Eric Minwei Liu, Ekta Khurana, Priyanka Dhingra, Ekta Khurana & Eric Minwei Liu

29. Institute for Computational Biomedicine, Weill Cornell Medicine, New York, NY, USA

Priyanka Dhingra, Eric Minwei Liu, Ekta Khurana, Priyanka Dhingra, Ekta Khurana & Eric Minwei Liu

30. Science for Life Laboratory, Department of Cell and Molecular Biology, Uppsala University, Uppsala, Sweden

Klev Diamanti, Jan Komorowski, Husen M. Umer, Klev Diamanti, Jan Komorowski & Husen M. Umer

31. European Bioinformatics Institute, European Molecular Biology Laboratory, Hinxton, UK

Nuno A. Fonseca & Nuno A. Fonseca

32. Bioinformatics Research Centre (BiRC), Aarhus University, Aarhus, Denmark

Qianyun Guo, Asger Hobolth, Qianyun Guo, Asger Hobolth, Jakob Skou Pedersen & Jakob Skou Pedersen

33. Department of Molecular and Cellular Biology, Baylor College of Medicine, Houston, TX, USA

Mark P. Hamilton & Mark P. Hamilton

34. Department of Medical Biophysics, University of Toronto, Toronto, Ontario, Canada

Keren Isaev, Jüri Reimand, Keren Isaev & Jüri Reimand

35. Division of Computational Biology, Memorial Sloan Kettering Cancer Center, New York, NY, USA

Andre Kahles, Kjong-Van Lehmann, Andre Kahles & Kjong-Van Lehmann

36. Institute of Molecular Life Sciences and Swiss Institute of Bioinformatics, University of Zurich, Zurich, Switzerland

Abdullah Kahraman, Christian von Mering, Abdullah Kahraman & Christian von Mering

37. Samsung Medical Center, Sungkyunkwan University School of Medicine, Seoul, South Korea

Youngwook Kim, Keunchil Park, Youngwook Kim & Keunchil Park

38. Institute of Computer Science, Polish Academy of Sciences, Warsaw, Poland

Jan Komorowski & Jan Komorowski

39. Program in Computational Biology and Bioinformatics, Yale University, New Haven, CT, USA

Sushant Kumar, Donghoon Lee, Jing Zhang, Mark Gerstein, Mark Gerstein, Sushant Kumar, Donghoon Lee, Jing Zhang & Mark Gerstein

40. SBGD Inc, Cambridge, MA, USA

Yilong Li & Yilong Li

41. Department of Haematology, University of Cambridge, Cambridge, UK

Yilong Li, Nicola D. Roberts, Peter J. Campbell, Peter J. Campbell, Peter J. Campbell, Yilong Li & Nicola D. Roberts

42. Department of Molecular Biophysics and Biochemistry, Yale University, New Haven, CT, USA

Lucas Lochovsky, Mark Gerstein, Mark Gerstein, Lucas Lochovsky & Mark Gerstein

43. Biotech Research & Innovation Centre (BRIC), The Finsen Laboratory, Rigshospitalet, University of Copenhagen, Copenhagen, Denmark

Nikos Sidiropoulos, Nikos Sidiropoulos, Joachim Weischenfeldt, Nikos Sidiropoulos, Joachim Weischenfeldt & Joachim Weischenfeldt

44. Department of Genetics, Stanford University School of Medicine, Stanford, CA, USA

Nasa Sinnott-Armstrong & Nasa Sinnott-Armstrong

45. Department of Zoology, Genetics and Physical Anthropology, Universidade de Santiago de Compostela, Santiago de Compostela, Spain

Jose M. C. Tubio & Jose M. C. Tubio

46. Centre for Research in Molecular Medicine and Chronic Diseases (CIMUS), Universidade de Santiago de Compostela, Santiago de Compostela, Spain

Jose M. C. Tubio & Jose M. C. Tubio

47. The Biomedical Research Centre (CINBIO), Universidade de Vigo, Vigo, Spain

Jose M. C. Tubio & Jose M. C. Tubio

48. Department of Oncology-Pathology, Science for Life Laboratory, Karolinska Institute, Stockholm, Sweden

Husen M. Umer

49. Genetics and Genome Biology Program, SickKids Research Institute, Toronto, Ontario, Canada

Liis Uusküla-Reimand & Liis Uusküla-Reimand

50. Department of Gene Technology, Tallinn University of Technology, Tallinn, Estonia

Liis Uusküla-Reimand & Liis Uusküla-Reimand

51. Science for Life Laboratory, Department of Immunology, Genetics and Pathology, Uppsala University, Uppsala, Sweden

Claes Wadelius & Claes Wadelius

52. New York Genome Center, New York, NY, USA

    Xiaotong Yao, Marcin Imielinski, Marcin Imielinski & Xiaotong Yao

53. Department of Biostatistics and Computational Biology, Dana-Farber Cancer Institute, Boston, MA, USA

    Cheng-Zhong Zhang & Cheng-Zhong Zhang

54. Department of Biomedical Informatics, Harvard Medical School, Boston, MA, USA

    Cheng-Zhong Zhang & Cheng-Zhong Zhang

55. Department of Biology and Rosenstiel Basic Medical Sciences Research Center, Brandeis University, Waltham, MA, USA

    James E. Haber & James E. Haber

56. Department of Pathology and Laboratory Medicine, and Englander Institute for Precision Medicine, and Institute for Computational Biomedicine, and Meyer Cancer Center, Weill Cornell Medicine, New York, NY, USA

    Marcin Imielinski & Marcin Imielinski

57. MIT Computer Science and Artificial Intelligence Laboratory, Cambridge, MA, USA

    Manolis Kellis & Manolis Kellis

58. Laboratory for Cancer Genomics, RIKEN Center for Integrative Medical Sciences, Tokyo, Japan

    Hidewaki Nakagawa, Hidewaki Nakagawa & Hidewaki Nakagawa

59. Department of Computer Science, Princeton University, Princeton, NJ, USA

Benjamin J. Raphael & Benjamin J. Raphael

60. Department of Pathology and Laboratory Medicine, Weill Cornell Medicine, New York, NY, USA

Mark A. Rubin & Mark A. Rubin

61. Englander Institute for Precision Medicine, Weill Cornell Medicine, New York, NY, USA

Mark A. Rubin, Ekta Khurana, Ekta Khurana & Mark A. Rubin

62. Meyer Cancer Center, Weill Cornell Medicine, New York, NY, USA

Mark A. Rubin, Ekta Khurana, Ekta Khurana & Mark A. Rubin

63. Center for Biomolecular Science and Engineering, University of California at Santa Cruz, Santa Cruz, CA, USA

Joshua M. Stuart & Joshua M. Stuart

64. Department of Medical Science Mathematics, Medical Research Institute, Tokyo Medical and Dental University, Tokyo, Japan

Tatsuhiko Tsunoda & Tatsuhiko Tsunoda

65. Laboratory for Medical Science Mathematics, Department of Biological Sciences, Graduate School of Science, The University of Tokyo, Tokyo, Japan

Tatsuhiko Tsunoda & Tatsuhiko Tsunoda

66. Human Genome Sequencing Center, Baylor College of Medicine, Houston, TX, USA

David A. Wheeler & David A. Wheeler

67. Department of Computer Science, Yale University, New Haven, CT, USA

Mark Gerstein, Mark Gerstein & Mark Gerstein

68. Catalan Institution for Research and Advanced Studies (ICREA), Barcelona, Spain

Núria López-Bigas

69. Genome Biology Unit, European Molecular Biology Laboratory (EMBL), Heidelberg, Germany

Joachim Weischenfeldt, Joachim Weischenfeldt & Joachim Weischenfeldt

70. Department of Medical Oncology, Dana-Farber Cancer Institute, Boston, MA, USA

Rameen Beroukhim, Rameen Beroukhim & Rameen Beroukhim

71. Department of Pathology, Massachusetts General Hospital, Boston, MA, USA

Gad Getz & Gad Getz

72. Department of Molecular Genetics, University of Toronto, Toronto, Ontario, Canada

Gary D. Bader

73. Computational Biology Program, Ontario Institute for Cancer Research, Toronto, Ontario, Canada

Jonathan Barenboim, Marta Paczkowska & Paul C. Boutros

74. Technical University of Denmark, Lyngby, Denmark

Søren Brunak & Jose M. G. Izarzugaza

75. University of Copenhagen, Copenhagen, Denmark

Søren Brunak

76. University of Texas MD Anderson Cancer Center, Houston, TX, USA

Ken Chen, Kadir C. Akdemir & Ken Chen

77. Korea Advanced Institute of Science and Technology, Daejeon, South Korea

Jung Kyoon Choi & Young Seok Ju

78. Institute for Research in Biomedicine (IRB Barcelona), The Barcelona Institute of Science and Technology, Barcelona, Spain

Jordi Deu-Pons & Joan Frigola

79. Research Program on Biomedical Informatics, Universitat Pompeu Fabra, Barcelona, Spain

Jordi Deu-Pons, Ferran Muiños & Carlota Rubio-Perez

80. Barcelona Supercomputing Center (BSC), Barcelona, Spain

J. Lynn Fink, Alfonso Valencia, Miguel Vazquez, Ana Dueso-Barroso, J. Lynn Fink, Montserrat Puiggròs, David Torrents & Izar Villasante

81. Queensland Centre for Medical Genomics, Institute for Molecular Bioscience, The University of Queensland, St Lucia, Queensland, Australia

J. Lynn Fink & J. Lynn Fink

82. University of Milano Bicocca, Monza, Italy

Carlo Gambacorti-Passerini

83. Peter MacCallum Cancer Centre, Melbourne, Victoria, Australia

Dale W. Garsed, David D. L. Bowtell, Dariush Etemadmoghadam & Dale W. Garsed

84. Sir Peter MacCallum Department of Oncology, The University of Melbourne, Melbourne, Victoria, Australia

Dale W. Garsed, Mark Shackleton, Dariush Etemadmoghadam, Dale W. Garsed & Mark Shackleton

85. CNAG-CRG, Centre for Genomic Regulation (CRG), Barcelona Institute of Science and Technology (BIST), Barcelona, Spain

Ivo G. Gut

86. Universitat Pompeu Fabra, Barcelona, Spain

Ivo G. Gut & Stephan Ossowski

87. Biomolecular Engineering Department, University of California, Santa Cruz, Santa Cruz, CA, USA

David Haan & David Haan

88. Program in Computational Biology and Bioinformatics, Yale University, New Haven, CT, USA

Arif O. Harmanci, Shantao Li, Xiaotong Li, Shaoke Lou, William Meyerson, Leonidas Salichos, Jonathan Warrell & Yan Zhang

89. Center for Precision Health, School of Biomedical Informatics, University of Texas Health Science Center, Houston, TX, USA

Arif O. Harmanci

90. The Donnelly Centre, University of Toronto, Toronto, Ontario, Canada

Mohamed Helmy

91. Simon Fraser University, Burnaby, British Columbia, Canada

Ermin Hodzic & S. Cenk Sahinalp

92. Research Core Center, National Cancer Centre Korea, Goyang-si, South Korea

Jong K. Kim

93. European Molecular Biology Laboratory, European Bioinformatics Institute (EMBL-EBI), Hinxton, Cambridge, UK

Jan O. Korbel & Jan O. Korbel

94. Genome Biology Unit, European Molecular Biology Laboratory (EMBL), Heidelberg, Germany

Jan O. Korbel, Sebastian M. Waszak & Jan O. Korbel

95. Institute of Biomedicine, Sahlgrenska Academy at University of Gothenburg, Gothenburg, Sweden

Erik Larsson

96. Department of Molecular Biophysics and Biochemistry, Yale University, New Haven, CT, USA

Shaoke Lou, Patrick D. McGillivray, Leonidas Salichos, Jonathan Warrell & Fabio C. P. Navarro

97. Department of Information Technology, Ghent University, Ghent, Belgium

Kathleen Marchal & Sergio Pulido-Tamayo

98. Department of Plant Biotechnology and Bioinformatics, Ghent University, Ghent, Belgium

Kathleen Marchal, Sergio Pulido-Tamayo & Lieven P. C. Verbeke

99. Department of Physiology and Biophysics, Weill Cornell Medicine, New York, NY, USA

Alexander Martinez-Fundichely & Alexander Martinez-Fundichely

100. Institute for Computational Biomedicine, Weill Cornell Medicine, New York, NY, USA

Alexander Martinez-Fundichely & Alexander Martinez-Fundichely

101. Englander Institute for Precision Medicine, Weill Cornell Medicine, New York, NY, USA

Alexander Martinez-Fundichely & Alexander Martinez-Fundichely

102. Yale School of Medicine, Yale University, New Haven, CT, USA

William Meyerson

103. Institute for Research in Biomedicine (IRB Barcelona), The Barcelona Institute of Science and Technology, Barcelona, Spain

Ferran Muiños, Iker Reyes-Salazar & Carlota Rubio-Perez

104. Cheonan Industry-Academic Collaboration Foundation, Sangmyung University, Cheonan, South Korea

Kiejung Park

105. Spanish National Cancer Research Centre, Madrid, Spain

Tirso Pons

106. Department of Computer Science, Princeton University, Princeton, NJ, USA

Matthew A. Reyna

107. Vall d'Hebron Institute of Oncology (VHIO), Barcelona, Spain

Carlota Rubio-Perez

108. Vancouver Prostate Centre, Vancouver, British Columbia, Canada

S. Cenk Sahinalp & Raunak Shrestha

109. Indiana University, Bloomington, IN, USA

S. Cenk Sahinalp

110. Peter MacCallum Cancer Centre, University of Melbourne, Melbourne, Victoria, Australia

Mark Shackleton & Mark Shackleton

111. Institució Catalana de Recerca i Estudis Avançats (ICREA), Barcelona, Spain

Alfonso Valencia & David Torrents

112. Department of Clinical and Molecular Medicine, Faculty of Medicine and Health Sciences, Norwegian University of Science and Technology, Trondheim, Norway

Miguel Vazquez

113. Department of Information Technology, Interuniversitair Micro-Electronica Centrum (IMEC), Ghent University, Ghent, Belgium

Lieven P. C. Verbeke

114. The McDonnell Genome Institute, Washington University, St Louis, MO, USA

Jiayin Wang

115. School of Computer Science and Technology, Xian Jiaotong University, Xian, China

Jiayin Wang & Xuanping Zhang

116. School of Electronic and Information Engineering, Xian Jiaotong University, Xian, China

Jiayin Wang

117. Oregon Health & Sciences University, Portland, OR, USA

Guanming Wu

118. Department of Medicine and Therapeutics, The Chinese University of Hong Kong, Shatin, Hong Kong, China

Jun Yu

119. The University of Texas Health Science Center at Houston, Houston, TX, USA

Xuanping Zhang

120. Department of Biomedical Informatics, College of Medicine, The Ohio State University, Columbus, OH, USA

Yan Zhang

121. The Ohio State University Comprehensive Cancer Center (OSUCCC – James), Columbus, OH, USA

Yan Zhang

122. School of Biomedical Informatics, The University of Texas Health Science Center at Houston, Houston, TX, USA

Zhongming Zhao

123. Department of Biochemistry and Molecular Genetics, Feinberg School of Medicine, Northwestern University, Chicago, IL, USA

Lihua Zou

124. Department of Zoology, Genetics and Physical Anthropology, Universidade de Santiago de Compostela, Santiago de Compostela, Spain

Eva G. Alvarez, Bernardo Rodriguez-Martin & Jorge Zamora

125. Centre for Research in Molecular Medicine and Chronic Diseases (CIMUS), Universidade de Santiago de Compostela, Santiago de Compostela, Spain

Eva G. Alvarez, Bernardo Rodriguez-Martin & Jorge Zamora

126. The Biomedical Research Centre (CINBIO), Universidade de Vigo, Vigo, Spain

Eva G. Alvarez, Bernardo Rodriguez-Martin & Jorge Zamora

127. Transmissible Cancer Group, Department of Veterinary Medicine, University of Cambridge, Cambridge, UK

Adrian Baez-Ortega

128. Department of Medical Biophysics, University of Toronto, Toronto, Ontario, Canada

Paul C. Boutros

129. Department of Pharmacology, University of Toronto, Toronto, Ontario, Canada

Paul C. Boutros

130. University of California Los Angeles, Los Angeles, CA, USA

Paul C. Boutros

131. Sir Peter MacCallum Department of Oncology, University of Melbourne, Melbourne, Victoria, Australia

David D. L. Bowtell

132. National Center for Tumor Diseases (NCT) Heidelberg, Heidelberg, Germany

Benedikt Brors & Barbara Hutter

133. Division of Applied Bioinformatics, German Cancer Research Center (DKFZ), Heidelberg, Germany

Benedikt Brors

134. German Cancer Genome Consortium (DKTK), Heidelberg, Germany

Benedikt Brors

135. Johns Hopkins School of Medicine, Baltimore, MD, USA

Kathleen H. Burns

136. Department of Biochemistry, Microbiology and Immunology, Faculty of Medicine, University of Ottawa, Ottawa, Ontario, Canada

Kin Chan

137. Centre for Molecular Science Informatics, Department of Chemistry, University of Cambridge, Cambridge, UK

Isidro Cortés-Ciriano

138. Department of Biomedical Informatics, Harvard Medical School, Boston, MA, USA

Isidro Cortés-Ciriano, Jake June-Koo Lee & Peter J. Park

139. Ludwig Center, Harvard Medical School, Boston, MA, USA

Isidro Cortés-Ciriano

140. Broad Institute of MIT and Harvard, Cambridge, MA, USA

Andrew J. Dunford & Matthew Meyerson

141. Cancer Research UK Cambridge Institute, University of Cambridge, Cambridge, UK

Paul A. Edwards, Andy G. Lynch, Geoff Macintyre & Florian Markowetz

142. University of Cambridge, Cambridge, UK

Paul A. Edwards, Andy G. Lynch & Florian Markowetz

143. Centre for Genomic Regulation (CRG), The Barcelona Institute of Science and Technology, Barcelona, Spain

Xavier Estivill & Stephan Ossowski

144. Quantitative Genomics Laboratories (qGenomics), Barcelona, Spain

Xavier Estivill

145. The Azrieli Faculty of Medicine, Bar-Ilan University, Safed, Israel

Milana Frenkel-Morgenstern

146. Genome Integrity and Structural Biology Laboratory, National Institute of Environmental Health Sciences (NIEHS), Durham, NC, USA

Dmitry A. Gordenin

147. German Cancer Consortium (DKTK), Heidelberg, Germany

Barbara Hutter

148. Heidelberg Center for Personalized Oncology (DKFZ-HIPO), German Cancer Research Center (DKFZ), Heidelberg, Germany

Barbara Hutter

149. Hopp Childrens Cancer Center (KiTZ), Heidelberg, Germany

David T. W. Jones

150. Pediatric Glioma Research Group, German Cancer Research Center (DKFZ), Heidelberg, Germany

David T. W. Jones

151. Wellcome Sanger Institute, Hinxton, UK

Young Seok Ju & Jorge Zamora

152. Skolkovo Institute of Science and Technology, Moscow, Russia

Marat D. Kazanov

153. A. A. Kharkevich Institute of Information Transmission Problems, Moscow, Russia

Marat D. Kazanov

154. Dmitry Rogachev National Research Center of Pediatric Hematology, Oncology and Immunology, Moscow, Russia

Marat D. Kazanov

155. Integrative Bioinformatics Support Group, National Institute of Environmental Health Sciences (NIEHS), Durham, NC, USA

Leszek J. Klimczak

156. Center For Medical Innovation, Seoul National University Hospital, Seoul, South Korea

Youngil Koh

157. Department of Internal Medicine, Seoul National University Hospital, Seoul, South Korea

Youngil Koh & Sung-Soo Yoon

158. Division of Genetics and Genomics, Boston Children's Hospital and Harvard Medical School, Boston, MA, USA

Eunjung Alice Lee

159. Ludwig Center at Harvard, Boston, MA, USA

Jake June-Koo Lee & Peter J. Park

160. School of Medicine and School of Mathematics and Statistics, University of St Andrews, St Andrews, UK

Andy G. Lynch

161. Harvard Medical School, Boston, MA, USA

Matthew Meyerson

162. Dana-Farber Cancer Institute, Boston, MA, USA

Matthew Meyerson

163. Department of Medical Oncology, University Hospital, University of Bern, Bern, Switzerland

Matthew Meyerson

164. Department of Pathology, The University of Melbourne, Melbourne, Victoria, Australia

Matthew Meyerson

165. The Institute of Medical Science, The University of Tokyo, Tokyo, Japan

Satoru Miyano

166. Institute of Medical Genetics and Applied Genomics, University of Tübingen, Tübingen, Germany

Stephan Ossowski

167. Department of Genetics and Computational Biology, QIMR Berghofer Medical Research Institute, Brisbane, Queensland, Australia

John V. Pearson & Nicola Waddell

168. Institute for Molecular Bioscience, University of Queensland, St Lucia, Brisbane, Queensland, Australia

John V. Pearson & Nicola Waddell

169. German Cancer Research Center (DKFZ), Heidelberg, Germany

Karsten Rippe

170. Center for Reproductive Biology, School of Molecular Biosciences, Washington State University, Pullman, WA, USA

Steven A. Roberts

171. Cancer Research Institute, Beth Israel Deaconess Medical Center, Boston, MA, USA

Ralph Scully

172. Ben May Department for Cancer Research, Department of Human Genetics, The University of Chicago, Chicago, IL, USA

Lixing Yang

173. Applied Tumor Genomics Research Program, Research Programs Unit, University of Helsinki, Helsinki, Finland

Lauri A. Aaltonen

174. Wellcome Sanger Institute, Wellcome Genome Campus, Hinxton, UK

Federico Abascal, David J. Adams, Ludmil B. Alexandrov, Sam Behjati, Shriram G. Bhosle, David T. Bowen, Adam P. Butler, Peter J. Campbell, Peter Clapham, Helen Davies, Kevin J. Dawson, Stefan C. Dentro, Serge Serge, Erik Garrison, Mohammed Ghori, Dominik Glodzik, Jonathan Hinton, David R. Jones, Young Seok Ju, Stian Knappskog, Barbara Kremeyer, Henry Lee-Six, Daniel A. Leongamornlert, Yilong Li, Sancha Martin, Iñigo Martincorena, Ultan McDermott, Andrew Menzies, Thomas J. Mitchell, Sandro Morganella, Jyoti Nangalia, Jonathan Nicholson, Serena Nik-Zainal, Sarah O'Meara, Elli Papaemmanuil, Keiran M. Raine, Manasa Ramakrishna, Kamna Ramakrishnan, Nicola D. Roberts, Rebecca Shepherd, Lucy Stebbings, Michael R. Stratton, Maxime Tarabichi, Jon W. Teague, Ignacio Vázquez-García, David C. Wedge, Lucy Yates, Jorge Zamora & Xueqing Zou

175. Memorial Sloan Kettering Cancer Center, New York, NY, USA

Adam Abeshouse, Hikmat Al-Ahmadie, Gunes Gundem, Zachary Heins, Jason Huse, Douglas A. Levine, Eric Minwei Liu & Angelica Ochoa

176. Genome Science Division, Research Center for Advanced Science and Technology, University of Tokyo, Tokyo, Japan

Hiroyuki Aburatani, Genta Nagae, Akihiro Suzuki, Kenji Tatsuno & Shogo Yamamoto

177. Department of Surgery, University of Chicago, Chicago, IL, USA

Nishant Agrawal

178. Department of Surgery, Division of Hepatobiliary and Pancreatic Surgery, School of Medicine, Keimyung University Dongsan Medical Center, Daegu, South Korea

Keun Soo Ahn & Koo Jeong Kang

179. Department of Oncology, Gil Medical Center, Gachon University, Incheon, South Korea

Sung-Min Ahn

180. Hiroshima University, Hiroshima, Japan

Hiroshi Aikata, Koji Arihiro, Kazuaki Chayama, Yoshiiku Kawakami & Hideki Ohdan

181. Department of Bioinformatics and Computational Biology, The University of Texas MD Anderson Cancer Center, Houston, TX, USA

Rehan Akbani, Shaolong Cao, Yiwen Chen, Zechen Chong, Yu Fan, Jun Li, Han Liang, Wenyi Wang, Yumeng Wang & Yuan Yuan

182. University of Texas MD Anderson Cancer Center, Houston, TX, USA

Kadir C. Akdemir & Ken Chen

183. King Faisal Specialist Hospital and Research Centre, Al Maather, Riyadh, Saudi Arabia

Sultan T. Al-Sedairy

184. Bioinformatics Unit, Spanish National Cancer Research Centre (CNIO), Madrid, Spain

Fatima Al-Shahrour & Elena Piñeiro-Yáñez

185. Bioinformatics Core Facility, University Medical Center Hamburg, Hamburg, Germany

Malik Alawi

186. Heinrich Pette Institute, Leibniz Institute for Experimental Virology, Hamburg, Germany

Malik Alawi & Adam Grundhoff

187. Ontario Tumour Bank, Ontario Institute for Cancer Research, Toronto, ON, Canada

Monique Albert & John Bartlett

188. Department of Pathology, The University of Texas MD Anderson Cancer Center, Houston, TX, USA

Kenneth Aldape, Russell R. Broaddus, Bogdan Czerniak, Adel El-Naggar, Savitri Krishnamurthy, Alexander J. Lazar & Xiaoping Su

189. Laboratory of Pathology, Center for Cancer Research, National Cancer Institute, Bethesda, MD, USA

Kenneth Aldape

190. Department of Cellular and Molecular Medicine and Department of Bioengineering, University of California San Diego, La Jolla, CA, USA

Ludmil B. Alexandrov & Erik N. Bergstrom

191. UC San Diego Moores Cancer Center, San Diego, CA, USA

Ludmil B. Alexandrov, Erik N. Bergstrom & Olivier Harismendy

192. Canada's Michael Smith Genome Sciences Centre, BC Cancer, Vancouver, BC, Canada

Adrian Ally, Miruna Balasundaram, Reanne Bowlby, Denise Brooks, Rebecca Carlsen, Eric Chuah, Noreen Dhalla, Robert A. Holt, Steven J. M. Jones, Katayoon Kasaian, Darlene Lee, Haiyan

Irene Li, Yussanne Ma, Marco A. Marra, Michael Mayo, Richard A. Moore, Andrew J. Mungall, Karen Mungall, A. Gordon Robertson, Sara Sadeghi, Jacqueline E. Schein, Payal Sipahimalani, Angela Tam, Nina Thiessen & Tina Wong

193. Sir Peter MacCallum Department of Oncology, Peter MacCallum Cancer Centre, University of Melbourne, Melbourne, VIC, Australia

Kathryn Alsop, David D. L. Bowtell, Elizabeth L. Christie, Dariush Etemadmoghadam, Sian Fereday, Dale W. Garsed, Linda Mileshkin, Chris Mitchell, Mark Shackleton, Heather Thorne & Nadia Traficante

194. Centre for Research in Molecular Medicine and Chronic Diseases (CiMUS), Universidade de Santiago de Compostela, Santiago de Compostela, Spain

Eva G. Alvarez, Alicia L. Bruzos, Bernardo Rodriguez-Martin, Javier Temes, Jose M. C. Tubio & Jorge Zamora

195. Department of Zoology, Genetics and Physical Anthropology, (CiMUS), Universidade de Santiago de Compostela, Santiago de Compostela, Spain

Eva G. Alvarez, Alicia L. Bruzos, Bernardo Rodriguez-Martin, Javier Temes, Jose M. C. Tubio & Jorge Zamora

196. The Biomedical Research Centre (CINBIO), Universidade de Vigo, Vigo, Spain

Eva G. Alvarez, Alicia L. Bruzos, Bernardo Rodriguez-Martin, Marta Tojo, Jose M. C. Tubio & Jorge Zamora

197. Royal National Orthopaedic Hospital - Bolsover, London, UK

Fernanda Amary

198. Department of Genomic Medicine, The University of Texas MD Anderson Cancer Center, Houston, TX, USA

Samirkumar B. Amin, P. Andrew Futreal & Alexander J. Lazar

199. Quantitative and Computational Biosciences Graduate Program, Baylor College of Medicine, Houston, TX, USA

Samirkumar B. Amin, Han Liang & Yumeng Wang

200. The Jackson Laboratory for Genomic Medicine, Farmington, CT, USA

Samirkumar B. Amin, Joshy George & Lucas Lochovsky

201. Genome Informatics Program, Ontario Institute for Cancer Research, Toronto, ON, Canada

Brice Aminou, Niall J. Byrne, Aurélien Chateigner, Nodirjon Fayzullaev, Vincent Ferretti, George L. Mihaiescu, Hardeep K. Nahal-Bose, Brian D. O'Connor, B. F. Francis Ouellette, Marc D. Perry, Kevin Thai, Qian Xiang, Christina K. Yung & Junjun Zhang

202. Institute of Human Genetics, Christian-Albrechts-University, Kiel, Germany

Ole Ammerpohl, Andrea Haake, Cristina López, Julia Richter & Rabea Wagener

203. Institute of Human Genetics, Ulm University and Ulm University Medical Center, Ulm, Germany

Ole Ammerpohl, Sietse Aukema, Cristina López, Reiner Siebert & Rabea Wagener

204. Queensland Centre for Medical Genomics, Institute for Molecular Bioscience, University of Queensland, St. Lucia, Brisbane, QLD, Australia

Matthew J. Anderson, Timothy J. C. Bruxner, Angelika N. Christ, J. Lynn Fink, Ivon Harliwong, Karin S. Kassahn, David K. Miller, Alan J. Robertson & Darrin F. Taylor

205. Salford Royal NHS Foundation Trust, Salford, UK

Yeng Ang, Hsiao-Wei Chen, Ritika Kundra & Francisco Sanchez-Vega

206. Department of Surgery, Pancreas Institute, University and Hospital Trust of Verona, Verona, Italy

Davide Antonello, Claudio Bassi, Narong Khuntikeo, Luca Landoni, Giuseppe Malleo, Giovanni Marchegiani, Neil D. Merrett, Marco Miotto, Salvatore Paiella, Antonio Pea, Paolo Pederzoli, Roberto Salvia, Jaswinder S. Samra, Elisabetta Sereni & Samuel Singer

207. Molecular and Medical Genetics, OHSU Knight Cancer Institute, Oregon Health and Science University, Portland, OR, USA

Pavana Anur, Myron Peto & Paul T. Spellman

208. Department of Molecular Oncology, BC Cancer Research Centre, Vancouver, BC, Canada

Samuel Aparicio

209. The McDonnell Genome Institute at Washington University, St. Louis, MO, USA

Elizabeth L. Appelbaum, Matthew H. Bailey, Matthew G. Cordes, Li Ding, Catrina C. Fronick, Lucinda A. Fulton, Robert S. Fulton, Kuan-lin Huang, Reyka Jayasinghe, Elaine R. Mardis, R. Jay Mashl, Michael D. McLellan, Christopher A. Miller, Heather K. Schmidt, Jiayin Wang, Michael C. Wendl, Richard K. Wilson & Tina Wong

210. University College London, London, UK

Elizabeth L. Appelbaum, Jonathan D. Kay, Helena Kilpinen, Laurence B. Lovat, Hayley J. Luxton & Hayley C. Whitaker

211. Division of Cancer Genomics, National Cancer Center Research Institute, National Cancer Center, Tokyo, Japan

Yasuhito Arai, Natsuko Hama, Fumie Hosoda, Hiromi Nakamura, Tatsuhiro Shibata, Yasushi Totoki & Shinichi Yachida

212. DLR Project Management Agency, Bonn, Germany

Axel Aretz

213. Tokyo Women's Medical University, Tokyo, Japan

Shun-ichi Ariizumi & Masakazu Yamamoto

214. Center for Molecular Oncology, Memorial Sloan Kettering Cancer Center, New York, NY, USA

Joshua Armenia, Hsiao-Wei Chen, Jianjiong Gao, Ritika Kundra, Francisco Sanchez-Vega, Nikolaus Schultz & Hongxin Zhang

215. Los Alamos National Laboratory, Los Alamos, NM, USA

Laurent Arnould

216. Department of Pathology, University Health Network, Toronto General Hospital, Toronto, ON, Canada

Sylvia Asa, Michael H. A. Roehrl & Theodorus Van der Kwast

217. Nottingham University Hospitals NHS Trust, Nottingham, UK

Sylvia Asa, Simon L. Parsons & Ming Tsao

218. Epigenomics and Cancer Risk Factors, German Cancer Research Center (DKFZ), Heidelberg, Germany

Yassen Assenov

219. Computational Biology Program, Ontario Institute for Cancer Research, Toronto, ON, Canada

Gurnit Atwal, Philip Awadalla, Jonathan Barenboim, Vinayak Bhandari, Ivan Borozan, Paul C. Boutros, Lewis Jonathan Dursi, Shadrielle M. G. Espiritu, Natalie S. Fox, Michael Fraser, Syed Haider, Vincent Huang, Keren Isaev, Wei Jiao, Christopher M. Lalansingh, Emilie Lalonde, Fabien C. Lamaze, Constance H. Li, Julie Livingstone, Christine P'ng, Marta Paczkowska, Stephenie D. Prokopec, Jüri Reimand, Veronica Y. Sabelnykova, Adriana Salcedo, Yu-Jia Shiah, Solomon I. Shorser, Shimin Shuai, Jared T. Simpson, Lincoln D. Stein, Ren X. Sun, Lina Wadi, Gavin W. Wilson, Adam J. Wright, Takafumi N. Yamaguchi, Fouad Yousif & Denis Yuen

220. Department of Molecular Genetics, University of Toronto, Toronto, ON, Canada

Gurnit Atwal, Philip Awadalla, Gary D. Bader, Shimin Shuai & Lincoln D. Stein

221. Vector Institute, Toronto, ON, Canada

Gurnit Atwal, Quaid D. Morris, Yulia Rubanova & Jeffrey A. Wintersinger

222. Hematopathology Section, Institute of Pathology, Christian-Albrechts-University, Kiel, Germany

Sietse Aukema, Wolfram Klapper, Julia Richter & Monika Szczepanowski

223. Department of Pathology and Laboratory Medicine, School of Medicine, University of North Carolina at Chapel Hill, Chapel Hill, NC, USA

J. Todd Auman & Charles M. Perou

224. Department of Cancer Genetics, Institute for Cancer Research, Oslo University Hospital, The Norwegian Radium Hospital, Oslo, Norway

Miriam R. R. Aure, Anne-Lise Børresen-Dale & Anita Langerød

225. Pathology, Hospital Clinic, Institut d'Investigacions Biomèdiques August Pi i Sunyer (IDIBAPS), University of Barcelona, Barcelona, Spain

Marta Aymerich

226. Department of Veterinary Medicine, Transmissible Cancer Group, University of Cambridge, Cambridge, UK

Adrian Baez-Ortega

227. Alvin J. Siteman Cancer Center, Washington University School of Medicine, St. Louis, MO, USA

Matthew H. Bailey, Li Ding, Robert S. Fulton, Ramaswamy Govindan & Michael D. McLellan

228. Wolfson Wohl Cancer Research Centre, Institute of Cancer Sciences, University of Glasgow, Glasgow, UK

Peter J. Bailey, Andrew V. Biankin, David K. Chang, Susanna L. Cooke, Fraser R. Duthie, Janet S. Graham, Nigel B. Jamieson, Elizabeth A. Musgrove & Derek W. Wright

229. Lineberger Comprehensive Cancer Center, University of North Carolina at Chapel Hill, Chapel Hill, NC, USA

Saianand Balu, Tom Bodenheimer, D. Neil Hayes, Austin J. Hepperla, Katherine A. Hoadley, Alan P. Hoyle, Stuart R. Jefferys, Shaowu Meng, Lisle E. Mose, Grant Sanders, Yan Shi, Janae V. Simons & Matthew G. Soloway

230. Broad Institute of MIT and Harvard, Cambridge, MA, USA

Pratiti Bandopadhayay, Rameen Beroukhim, Angela N. Brooks, Susan Bullman, John Busanovich, Andrew D. Cherniack, Juok Cho, Carrie Cibulskis, Kristian Cibulskis, David Craft, Timothy Defreitas, Andrew

J. Dunford, Scott Frazer, Stacey B. Gabriel, Nils Gehlenborg, Gad Getz, Manaswi Gupta, Gavin Ha, Nicholas J. Haradhvala, David I. Heiman, Julian M. Hess, Manolis Kellis, Jaegil Kim, Kiran Kumar, Kirsten Kübler, Eric Lander, Michael S. Lawrence, Ignaty Leshchiner, Pei Lin, Ziao Lin, Dimitri Livitz, Yosef E. Maruvka, Samuel R. Meier, Matthew Meyerson, Michael S. Noble, Chandra Sekhar Pedamallu, Paz Polak, Esther Rheinbay, Daniel Rosebrock, Mara Rosenberg, Gordon Saksena, Richard Sallari, Steven E. Schumacher, Ayellet V. Segre, Ofer Shapira, Juliann Shih, Nasa Sinnott-Armstrong, Oliver Spiro, Chip Stewart, Amaro Taylor-Weiner, Grace Tiao, Douglas Voet, Jeremiah A. Wala, Cheng-Zhong Zhang & Hailei Zhang

231. Dana-Farber/Boston Children's Cancer and Blood Disorders Center, Boston, MA, USA

Pratiti Bandopadhayay

232. Department of Pediatrics, Harvard Medical School, Boston, MA, USA

Pratiti Bandopadhayay

233. Leeds Institute of Medical Research @ St. James's, University of Leeds, St. James's University Hospital, Leeds, UK

Rosamonde E. Banks & Naveen Vasudev

234. Department of Pathology and Diagnostics, University and Hospital Trust of Verona, Verona, Italy

Stefano Barbi, Vincenzo Corbo & Michele Simbolo

235. Department of Surgery, Princess Alexandra Hospital, Brisbane, QLD, Australia

Andrew P. Barbour

236. Surgical Oncology Group, Diamantina Institute, University of Queensland, Brisbane, QLD, Australia

Andrew P. Barbour

237. Department of Population and Quantitative Health Sciences, Case Western Reserve University School of Medicine, Cleveland, OH, USA

Jill Barnholtz-Sloan

238. Research Health Analytics and Informatics, University Hospitals Cleveland Medical Center, Cleveland, OH, USA

Jill Barnholtz-Sloan

239. Gloucester Royal Hospital, Gloucester, UK

Hugh Barr

240. European Molecular Biology Laboratory, European Bioinformatics Institute (EMBL-EBI), Cambridge, UK

Elisabet Barrera, Wojciech Bazant, Ewan Birney, Rich Boyce, Alvis Brazma, Andy Cafferkey, Claudia Calabrese, Paul Flicek, Nuno A. Fonseca, Anja Füllgrabe, Moritz Gerstung, Santiago Gonzalez, Liliana Greger, Maria Keays, Jan O. Korbel, Alfonso Muñoz, Steven J. Newhouse, David Ocana, Irene Papatheodorou, Robert Petryszak, Roland F. Schwarz, Charles Short, Oliver Stegle & Lara Urban

241. Diagnostic Development, Ontario Institute for Cancer Research, Toronto, ON, Canada

John Bartlett & Ilinca Lungu

242. Barcelona Supercomputing Center (BSC), Barcelona, Spain

Javier Bartolome, Mattia Bosio, Ana Dueso-Barroso, J. Lynn Fink, Josep L. L. Gelpi, Ana Milovanovic, Montserrat Puiggròs, Javier Bartolomé Rodriguez, Romina Royo, David Torrents, Alfonso Valencia, Miguel Vazquez, David Vicente & Izar Villasante

243. Arnie Charbonneau Cancer Institute, University of Calgary, Calgary, AB, Canada

Oliver F. Bathe

244. Departments of Surgery and Oncology, University of Calgary, Calgary, AB, Canada

Oliver F. Bathe

245. Department of Pathology, Oslo University Hospital, The Norwegian Radium Hospital, Oslo, Norway

Daniel Baumhoer & Bodil Bjerkehagen

246. PanCuRx Translational Research Initiative, Ontario Institute for Cancer Research, Toronto, ON, Canada

Prashant Bavi, Michelle Chan-Seng-Yue, Sean Cleary, Robert E. Denroche, Steven Gallinger, Robert C. Grant, Gun Ho Jang, Sangeetha Kalimuthu, Ilinca Lungu, John D. McPherson, Faiyaz Notta, Michael H. A. Roehrl, Gavin W. Wilson & Julie M. Wilson

247. Department of Oncology, Sidney Kimmel Comprehensive Cancer Center at Johns Hopkins University School of Medicine, Baltimore, MD, USA

Stephen B. Baylin, Nilanjan Chatterjee, Leslie Cope, Ludmila Danilova & Ralph H. Hruban

248. University Hospital Southampton NHS Foundation Trust, Southampton, UK

Stephen B. Baylin & Tim Dudderidge

249. Royal Stoke University Hospital, Stoke-on-Trent, UK

Duncan Beardsmore & Christopher Umbricht

250. Genome Sequence Informatics, Ontario Institute for Cancer Research, Toronto, ON, Canada

Timothy A. Beck, Bob Gibson, Lawrence E. Heisler, Xuemei Luo & Morgan L. Taschuk

251. Human Longevity Inc, San Diego, CA, USA

Timothy A. Beck

252. Olivia Newton-John Cancer Research Institute, La Trobe University, Heidelberg, VIC, Australia

Andreas Behren & Jonathan Cebon

253. Computer Network Information Center, Chinese Academy of Sciences, Beijing, China

Beifang Niu

254. Genome Canada, Ottawa, ON, Canada

Cindy Bell

255. CNAG-CRG, Centre for Genomic Regulation (CRG), Barcelona Institute of Science and Technology (BIST), Barcelona, Spain

Sergi Beltran, Ivo G. Gut, Marta Gut, Simon C. Heath, Tomas Marques-Bonet, Arcadi Navarro, Miranda D. Stobbe, Jean-Rémi Trotta & Justin P. Whalley

256. Universitat Pompeu Fabra (UPF), Barcelona, Spain

Sergi Beltran, Mattia Bosio, German M. Demidov, Oliver Drechsel, Ivo G. Gut, Marta Gut, Simon C. Heath, Francesc Muyas, Stephan Ossowski, Aparna Prasad, Raquel Rabionet, Miranda D. Stobbe & Hana Susak

257. Buck Institute for Research on Aging, Novato, CA, USA

Christopher Benz & Christina Yau

258. Duke University Medical Center, Durham, NC, USA

Andrew Berchuck

259. Department of Human Genetics, Hannover Medical School, Hannover, Germany

Anke K. Bergmann

260. Center for Bioinformatics and Functional Genomics, Cedars-Sinai Medical Center, Los Angeles, CA, USA

Benjamin P. Berman & Huy Q. Dinh

261. Department of Biomedical Sciences, Cedars-Sinai Medical Center, Los Angeles, CA, USA

Benjamin P. Berman

262. The Hebrew University Faculty of Medicine, Jerusalem, Israel

Benjamin P. Berman

263. Barts Cancer Institute, Barts and the London School of Medicine and Dentistry, Queen Mary University of London, London, UK

Daniel M. Berney & Yong-Jie Lu

264. Department of Computer Science, Bioinformatics Group, University of Leipzig, Leipzig, Germany

Stephan H. Bernhart, Hans Binder, Steve Hoffmann & Peter F. Stadler

265. Interdisciplinary Center for Bioinformatics, University of Leipzig, Leipzig, Germany

Stephan H. Bernhart, Hans Binder, Steve Hoffmann, Helene Kretzmer & Peter F. Stadler

266. Transcriptome Bioinformatics, LIFE Research Center for Civilization Diseases, University of Leipzig, Leipzig, Germany

Stephan H. Bernhart, Steve Hoffmann, Helene Kretzmer & Peter F. Stadler

267. Department of Medical Oncology, Dana-Farber Cancer Institute, Boston, MA, USA

Rameen Beroukhim, Angela N. Brooks, Susan Bullman, Andrew D. Cherniack, Levi Garraway, Matthew Meyerson, Chandra Sekhar Pedamallu, Steven E. Schumacher, Juliann Shih & Jeremiah A. Wala

268. Department of Cancer Biology, Dana-Farber Cancer Institute, Boston, MA, USA

Rameen Beroukhim, Aquila Fatima, Andrea L. Richardson, Steven E. Schumacher, Ofer Shapira, Andrew Tutt & Jeremiah A. Wala

269. Harvard Medical School, Boston, MA, USA

Rameen Beroukhim, Gad Getz, Kirsten Kübler, Matthew Meyerson, Chandra Sekhar Pedamallu, Paz Polak, Esther Rheinbay & Jeremiah A. Wala

270. USC Norris Comprehensive Cancer Center, University of Southern California, Los Angeles, CA, USA

Mario Berrios, Moiz S. Bootwalla, Andrea Holbrook, Phillip H. Lai, Dennis T. Maglinte, David J. Van Den Berg & Daniel J. Weisenberger

271. Department of Diagnostics and Public Health, University and Hospital Trust of Verona, Verona, Italy

Samantha Bersani, Ivana Cataldo, Claudio Luchini & Maria Scardoni

272. Department of Mathematics, Aarhus University, Aarhus, Denmark

Johanna Bertl & Asger Hobolth

273. Department of Molecular Medicine (MOMA), Aarhus University Hospital, Aarhus N, Denmark

Johanna Bertl, Henrik Hornshøj, Malene Juul, Randi Istrup Juul, Tobias Madsen, Morten Muhlig Nielsen & Jakob Skou Pedersen

274. Instituto Carlos Slim de la Salud, Mexico City, Mexico

Miguel Betancourt

275. Department of Medical Biophysics, University of Toronto, Toronto, ON, Canada

Vinayak Bhandari, Paul C. Boutros, Robert G. Bristow, Keren Isaev, Constance H. Li, Jüri Reimand, Michael H. A. Roehrl & Bradly G. Wouters

276. Cancer Division, Garvan Institute of Medical Research, Kinghorn Cancer Centre, University of New South Wales (UNSW Sydney), Sydney, NSW, Australia

Andrew V. Biankin, David K. Chang, Lorraine A. Chantrill, Angela Chou, Anthony J. Gill, Amber L. Johns, James G. Kench, David K. Miller, Adnan M. Nagrial, Marina Pajic, Mark Pinese, Ilse Rooman, Christopher J. Scarlett, Christopher W. Toon & Jianmin Wu

277. South Western Sydney Clinical School, Faculty of Medicine, University of New South Wales (UNSW Sydney), Liverpool, NSW, Australia

Andrew V. Biankin

278. West of Scotland Pancreatic Unit, Glasgow Royal Infirmary, Glasgow, UK

Andrew V. Biankin & Nigel B. Jamieson

279. Center for Digital Health, Berlin Institute of Health and Charitè - Universitätsmedizin Berlin, Berlin, Germany

Matthias Bieg

280. Heidelberg Center for Personalized Oncology (DKFZ-HIPO), German Cancer Research Center (DKFZ), Heidelberg, Germany

Matthias Bieg, Ivo Buchhalter, Barbara Hutter & Nagarajan Paramasivam

281. The Preston Robert Tisch Brain Tumor Center, Duke University Medical Center, Durham, NC, USA

Darell Bigner

282. Massachusetts General Hospital, Boston, MA, USA

Michael Birrer, Vikram Deshpande, William C. Faquin, Nicholas J. Haradhvala, Kirsten Kübler, Michael S. Lawrence, David N. Louis, Yosef E. Maruvka, G. Petur Nielsen, Esther Rheinbay, Mara Rosenberg, Dennis C. Sgroi & Chin-Lee Wu

283. National Institute of Biomedical Genomics, Kalyani, West Bengal, India

Nidhan K. Biswas, Arindam Maitra & Partha P. Majumder

284. Institute of Clinical Medicine and Institute of Oral Biology, University of Oslo, Oslo, Norway

Bodil Bjerkehagen

285. University of North Carolina at Chapel Hill, Chapel Hill, NC, USA

Lori Boice, Mei Huang, Sonia Puig & Leigh B. Thorne

286. ARC-Net Centre for Applied Research on Cancer, University and Hospital Trust of Verona, Verona, Italy

Giada Bonizzato, Cinzia Cantù, Ivana Cataldo, Vincenzo Corbo, Sonia Grimaldi, Rita T. Lawlor, Andrea Mafficini, Borislav C. Rusev, Aldo Scarpa, Katarzyna O. Sikora, Nicola Sperandio, Alain Viari & Caterina Vicentini

287. The Institute of Cancer Research, London, UK

Johann S. De Bono, Niedzica Camacho, Colin S. Cooper, Sandra E. Edwards, Rosalind A. Eeles, Zsofia Kote-Jarai, Daniel A. Leongamornlert, Lucy Matthews & Sue Merson

288. Centre for Computational Biology, Duke-NUS Medical School, Singapore, Singapore

Arnoud Boot, Ioana Cutcutache, Mi Ni Huang, John R. McPherson, Steven G. Rozen & Yang Wu

289. Programme in Cancer and Stem Cell Biology, Duke-NUS Medical School, Singapore, Singapore

Arnoud Boot, Ioana Cutcutache, Mi Ni Huang, John R. McPherson, Steven G. Rozen, Patrick Tan, Bin Tean Teh & Yang Wu

290. Division of Oncology and Pathology, Department of Clinical Sciences Lund, Lund University, Lund, Sweden

Ake Borg, Markus Ringnér & Johan Staaf

291. Department of Pediatric Oncology, Hematology and Clinical Immunology, Heinrich-Heine-University, Düsseldorf, Germany

Arndt Borkhardt & Jessica I. Hoell

292. Laboratory for Medical Science Mathematics, RIKEN Center for Integrative Medical Sciences, Yokohama, Japan

Keith A. Boroevich, Todd A. Johnson, Michael S. Lawrence & Tatsuhiko Tsunoda

293. RIKEN Center for Integrative Medical Sciences, Yokohama, Japan

Keith A. Boroevich, Akihiro Fujimoto, Masashi Fujita, Mayuko Furuta, Kazuhiro Maejima, Hidewaki Nakagawa, Kaoru Nakano & Aya Sasaki-Oku

294. Department of Internal Medicine/Hematology, Friedrich-Ebert-Hospital, Neumünster, Germany

Christoph Borst & Siegfried Haas

295. Departments of Dermatology and Pathology, Yale University, New Haven, CT, USA

Marcus Bosenberg

296. Centre for Genomic Regulation (CRG), The Barcelona Institute of Science and Technology, Barcelona, Spain

Mattia Bosio, German M. Demidov, Oliver Drechsel, Georgia Escaramis, Xavier Estivill, Aliaksei Z. Holik, Francesc Muyas, Stephan Ossowski, Raquel Rabionet & Hana Susak

297. Radcliffe Department of Medicine, University of Oxford, Oxford, UK

Jacqueline Boultwood

298. Canadian Center for Computational Genomics, McGill University, Montreal, QC, Canada

Guillaume Bourque

299. Department of Human Genetics, McGill University, Montreal, QC, Canada

Guillaume Bourque, Mark Lathrop & Yasser Riazalhosseini

300. Department of Human Genetics, University of California Los Angeles, Los Angeles, CA, USA

Paul C. Boutros

301. Department of Pharmacology, University of Toronto, Toronto, ON, Canada

Paul C. Boutros

302. Faculty of Medicine and Health Technology, Tampere University and Tays Cancer Center, Tampere University Hospital, Tampere, Finland

G. Steven Bova & Tapio Visakorpi

303. Haematology, Leeds Teaching Hospitals NHS Trust, Leeds, UK

David T. Bowen

304. Translational Research and Innovation, Centre Léon Bérard, Lyon, France

Sandrine Boyault

305. Fox Chase Cancer Center, Philadelphia, PA, USA

Jeffrey Boyd & Elaine R. Mardis

306. International Agency for Research on Cancer, World Health Organization, Lyon, France

Paul Brennan & Ghislaine Scelo

307. Earlham Institute, Norwich, UK

Daniel S. Brewer & Colin S. Cooper

308. Norwich Medical School, University of East Anglia, Norwich, UK

Daniel S. Brewer & Colin S. Cooper

309. Department of Molecular Biology, Faculty of Science, Radboud Institute for Molecular Life Sciences, Radboud University, Nijmegen, HB, The Netherlands

Arie B. Brinkman

310. CRUK Manchester Institute and Centre, Manchester, UK

Robert G. Bristow

311. Department of Radiation Oncology, University of Toronto, Toronto, ON, Canada

Robert G. Bristow

312. Division of Cancer Sciences, Manchester Cancer Research Centre, University of Manchester, Manchester, UK

Robert G. Bristow

313. Radiation Medicine Program, Princess Margaret Cancer Centre, Toronto, ON, Canada

Robert G. Bristow & Fei-Fei Fei Liu

314. Department of Pathology, Brigham and Women's Hospital, Harvard Medical School, Boston, MA, USA

Jane E. Brock & Sabina Signoretti

315. Department of Surgery, Division of Thoracic Surgery, The Johns Hopkins University School of Medicine, Baltimore, MD, USA

Malcolm Brock

316. Division of Molecular Pathology, The Netherlands Cancer Institute, Oncode Institute, Amsterdam, CX, The Netherlands

Annegien Broeks & Jos Jonkers

317. Department of Biomolecular Engineering, University of California Santa Cruz, Santa Cruz, CA, USA

Angela N. Brooks, David Haan, Maximillian G. Marin, Thomas J. Matthew, Yulia Newton, Cameron M. Soulette & Joshua M. Stuart

318. UC Santa Cruz Genomics Institute, University of California Santa Cruz, Santa Cruz, CA, USA

Angela N. Brooks, Brian Craft, Mary J. Goldman, David Haussler, Joshua M. Stuart & Jingchun Zhu

319. Division of Applied Bioinformatics, German Cancer Research Center (DKFZ), Heidelberg, Germany

Benedikt Brors, Lars Feuerbach, Chen Hong, Charles David Imbusch & Lina Sieverling

320. German Cancer Consortium (DKTK), German Cancer Research Center (DKFZ), Heidelberg, Germany

Benedikt Brors, Barbara Hutter, Peter Lichter, Dirk Schadendorf & Holger Sültmann

321. National Center for Tumor Diseases (NCT) Heidelberg, Heidelberg, Germany

Benedikt Brors, Barbara Hutter, Holger Sültmann & Thorsten Zenz

322. Center for Biological Sequence Analysis, Department of Bio and Health Informatics, Technical University of Denmark, Lyngby, Denmark

Søren Brunak

323. Novo Nordisk Foundation Center for Protein Research, University of Copenhagen, Copenhagen, Denmark

Søren Brunak

324. Institute for Molecular Bioscience, University of Queensland, St. Lucia, Brisbane, QLD, Australia

Timothy J. C. Bruxner, Oliver Holmes, Stephen H. Kazakoff, Conrad R. Leonard, Felicity Newell, Katia Nones, Ann-Marie Patch, John V. Pearson, Michael C. Quinn, Nick M. Waddell, Nicola Waddell, Scott Wood & Qinying Xu

325. Biomedical Engineering, Oregon Health and Science University, Portland, OR, USA

Alex Buchanan & Kyle Ellrott

326. Division of Theoretical Bioinformatics, German Cancer Research Center (DKFZ), Heidelberg, Germany

Ivo Buchhalter, Calvin Wing Yiu Chan, Roland Eils, Michael C. Heinold, Carl Herrmann, Natalie Jäger, Rolf Kabbe, Jules N. A. Kerssemakers, Kortine Kleinheinz, Nagarajan Paramasivam, Manuel Prinz, Matthias Schlesner & Johannes Werner

327. Institute of Pharmacy and Molecular Biotechnology and BioQuant, Heidelberg University, Heidelberg, Germany

Ivo Buchhalter, Roland Eils, Michael C. Heinold, Carl Herrmann, Daniel Hübschmann, Kortine Kleinheinz & Umut H. Toprak

328. Federal Ministry of Education and Research, Berlin, Germany

Christiane Buchholz

329. Melanoma Institute Australia, University of Sydney, Sydney, NSW, Australia

Hazel Burke, Ricardo De Paoli-Iseppi, Nicholas K. Hayward, Peter Hersey, Valerie Jakrot, Hojabr Kakavand, Georgina V. Long, Graham

J. Mann, Robyn P. M. Saw, Richard A. Scolyer, Ping Shang, Andrew J. Spillane, Jonathan R. Stretch, John F. F. Thompson & James S. Wilmott

330. Pediatric Hematology and Oncology, University Hospital Muenster, Muenster, Germany

Birgit Burkhardt

331. Department of Pathology, Johns Hopkins University School of Medicine, Baltimore, MD, USA

Kathleen H. Burns & Christopher Umbricht

332. McKusick-Nathans Institute of Genetic Medicine, Sidney Kimmel Comprehensive Cancer Center at Johns Hopkins University School of Medicine, Baltimore, MD, USA

Kathleen H. Burns

333. Foundation Medicine, Inc, Cambridge, MA, USA

John Busanovich

334. Department of Biomedical Data Science, Stanford University School of Medicine, Stanford, CA, USA

Carlos D. Bustamante & Francisco M. De La Vega

335. Department of Genetics, Stanford University School of Medicine, Stanford, CA, USA

Carlos D. Bustamante, Francisco M. De La Vega, Suyash S. Shringarpure, Nasa Sinnott-Armstrong & Mark H. Wright

336. Bakar Computational Health Sciences Institute and Department of Pediatrics, University of California, San Francisco, CA, USA

Atul J. Butte & Jieming Chen

337. Institute of Clinical Medicine, Faculty of Medicine, University of Oslo, Oslo, Norway

Anne-Lise Børresen-Dale

338. National Cancer Institute, National Institutes of Health, Bethesda, MD, USA

Samantha J. Caesar-Johnson, John A. Demchok, Ina Felau, Roy Tarnuzzer, Zhining Wang, Liming Yang, Jean C. Zenklusen & Jiashan Zhang

339. Royal Marsden NHS Foundation Trust, London and Sutton, UK

Declan Cahill, Nening M. Dennis, Tim Dudderidge, Rosalind A. Eeles, Cyril Fisher, Steven Hazell, Vincent Khoo, Pardeep Kumar, Naomi Livni, Erik Mayer, David Nicol, Christopher Ogden, Edward W. Rowe, Sarah Thomas, Alan Thompson & Nicholas van As

340. Genome Biology Unit, European Molecular Biology Laboratory (EMBL), Heidelberg, Germany

Claudia Calabrese, Serap Erkek, Moritz Gerstung, Santiago Gonzalez, Nina Habermann, Wolfgang Huber, Lara Jerman, Jan O. Korbel, Esa Pitkänen, Benjamin Raeder, Tobias Rausch, Vasilisa A. Rudneva, Oliver Stegle, Stephanie Sungalee, Lara Urban, Sebastian M. Waszak, Joachim Weischenfeldt & Sergei Yakneen

341. Department of Oncology, University of Cambridge, Cambridge, UK

Carlos Caldas & Suet-Feung Chin

342. Li Ka Shing Centre, Cancer Research UK Cambridge Institute, University of Cambridge, Cambridge, UK

Carlos Caldas, Suet-Feung Chin, Ruben M. Drews, Paul A. Edwards, Matthew Eldridge, Steve Hawkins, Andy G. Lynch, Geoff

Macintyre, Florian Markowetz, Charlie E. Massie, David E. Neal, Simon Tavaré & Ke Yuan

343. Institut Gustave Roussy, Villejuif, France

Fabien Calvo

344. Cambridge University Hospitals NHS Foundation Trust, Cambridge, UK

Peter J. Campbell, Vincent J. Gnanapragasam, William Howat, Thomas J. Mitchell, David E. Neal, Nimish C. Shah & Anne Y. Warren

345. Department of Haematology, University of Cambridge, Cambridge, UK

Peter J. Campbell

346. Anatomia Patológica, Hospital Clinic, Institut d’Investigacions Biomèdiques August Pi i Sunyer (IDIBAPS), University of Barcelona, Barcelona, Spain

Elias Campo

347. Spanish Ministry of Science and Innovation, Madrid, Spain

Elias Campo

348. University of Michigan Comprehensive Cancer Center, Ann Arbor, MI, USA

Thomas E. Carey

349. Department for BioMedical Research, University of Bern, Bern, Switzerland

Joana Carlevaro-Fita

350. Department of Medical Oncology, Inselspital, University Hospital and University of Bern, Bern, Switzerland

Joana Carlevaro-Fita, Rory Johnson & Andrés Lanzós

351. Graduate School for Cellular and Biomedical Sciences, University of Bern, Bern, Switzerland

Joana Carlevaro-Fita & Andrés Lanzós

352. University of Pavia, Pavia, Italy

Mario Cazzola & Luca Malcovati

353. University of Alabama at Birmingham, Birmingham, AL, USA

Robert Cerfolio

354. UHN Program in BioSpecimen Sciences, Toronto General Hospital, Toronto, ON, Canada

Dianne E. Chadwick, Sheng-Ben Liang, Michael H. A. Roehrl & Sagedeh Shahabi

355. Department of Urology, Icahn School of Medicine at Mount Sinai, New York, NY, USA

Dimple Chakravarty

356. Centre for Law and Genetics, University of Tasmania, Sandy Bay Campus, Hobart, TAS, Australia

Don Chalmers

357. Faculty of Biosciences, Heidelberg University, Heidelberg, Germany

Calvin Wing Yiu Chan, Chen Hong & Lina Sieverling

358. Department of Biochemistry, Microbiology and Immunology, Faculty of Medicine, University of Ottawa, Ottawa, ON, Canada

Kin Chan

359. Division of Anatomic Pathology, Mayo Clinic, Rochester, MN, USA

Vishal S. Chandan

360. Division of Cancer Epidemiology and Genetics, National Cancer Institute, National Institutes of Health, Bethesda, MD, USA

Stephen J. Chanock, Xing Hua, Lisa Mirabello, Lei Song & Bin Zhu

361. Illawarra Shoalhaven Local Health District L3 Illawarra Cancer Care Centre, Wollongong Hospital, Wollongong, NSW, Australia

Lorraine A. Chantrill

362. BioForA, French National Institute for Agriculture, Food, and Environment (INRAE), ONF, Orléans, France

Aurélien Chateigner

363. Department of Biostatistics, Bloomberg School of Public Health, Johns Hopkins University, Baltimore, MD, USA

Nilanjan Chatterjee

364. University of California San Diego, San Diego, CA, USA

Zhaohong Chen, Michelle T. Dow, Claudiu Farcas, S. M. Ashiqul Islam, Antonios Koures, Lucila Ohno-Machado, Christos Sotiriou & Ashley Williams

365. Division of Experimental Pathology, Mayo Clinic, Rochester, MN, USA

Jeremy Chien

366. Centre for Cancer Research, The Westmead Institute for Medical Research, University of Sydney, Sydney, NSW, Australia

Yoke-Eng Chiew, Angela Chou, Jillian A. Hung, Catherine J. Kennedy, Graham J. Mann, Gulietta M. Pupo, Sarah-Jane Schramm, Varsha Tembe & Anna deFazio

367. Department of Gynaecological Oncology, Westmead Hospital, Sydney, NSW, Australia

Yoke-Eng Chiew, Jillian A. Hung, Catherine J. Kennedy & Anna deFazio

368. PDXen Biosystems Inc, Seoul, South Korea

Sunghoon Cho

369. Korea Advanced Institute of Science and Technology, Daejeon, South Korea

Jung Kyoon Choi, Young Seok Ju & Christopher J. Yoon

370. Electronics and Telecommunications Research Institute, Daejeon, South Korea

Wan Choi, Seung-Hyup Jeon, Hyunghwan Kim & Youngchoon Woo

371. Institut National du Cancer (INCA), Boulogne-Billancourt, France

Christine Chomienne & Iris Pauporté

372. Department of Genetics, Informatics Institute, University of Alabama at Birmingham, Birmingham, AL, USA

Zechen Chong

373. Division of Medical Oncology, National Cancer Centre, Singapore, Singapore

Su Pin Choo

374. Medical Oncology, University and Hospital Trust of Verona, Verona, Italy

Sara Cingarlini & Michele Milella

375. Department of Pediatrics, University Hospital Schleswig-Holstein, Kiel, Germany

Alexander Claviez

376. Hepatobiliary/Pancreatic Surgical Oncology Program, University Health Network, Toronto, ON, Canada

Sean Cleary, Ashton A. Connor & Steven Gallinger

377. School of Biological Sciences, University of Auckland, Auckland, New Zealand

Nicole Cloonan

378. Department of Surgery, University of Melbourne, Parkville, VIC, Australia

Marek Cmero

379. The Murdoch Children's Research Institute, Royal Children's Hospital, Parkville, VIC, Australia

Marek Cmero

380. Walter and Eliza Hall Institute, Parkville, VIC, Australia

Marek Cmero

381. Vancouver Prostate Centre, Vancouver, Canada

Colin C. Collins, Nilgun Donmez, Faraz Hach, Salem Malikic, S. Cenk Sahinalp, Iman Sarrafi & Raunak Shrestha

382. Lunenfeld-Tanenbaum Research Institute, Mount Sinai Hospital, Toronto, ON, Canada

Ashton A. Connor, Steven Gallinger, Robert C. Grant, Treasa A. McPherson & Iris Selander

383. University of East Anglia, Norwich, UK

Colin S. Cooper

384. Norfolk and Norwich University Hospital NHS Trust, Norwich, UK

Matthew G. Cordes, Catrina C. Fronick & Tom Roques

385. Victorian Institute of Forensic Medicine, Southbank, VIC, Australia

Stephen M. Cordner

386. Department of Biomedical Informatics, Harvard Medical School, Boston, MA, USA

Isidro Cortés-Ciriano, Jake June-Koo Lee & Peter J. Park

387. Department of Chemistry, Centre for Molecular Science Informatics, University of Cambridge, Cambridge, UK

Isidro Cortés-Ciriano

388. Ludwig Center at Harvard Medical School, Boston, MA, USA

Isidro Cortés-Ciriano, Jake June-Koo Lee & Peter J. Park

389. Human Genome Sequencing Center, Baylor College of Medicine, Houston, TX, USA

Kyle Covington, HarshaVardhan Doddapaneni, Richard A. Gibbs, Jianhong Hu, Joy C. Jayaseelan, Viktoriya Korchina, Lora Lewis, Donna M. Muzny, Linghua Wang, David A. Wheeler & Liu Xi

390. Peter MacCallum Cancer Centre, University of Melbourne, Melbourne, VIC, Australia

Prue A. Cowin, Anne Hamilton, Gisela Mir Arnau & Ravikiran Vedururu

391. Physics Division, Optimization and Systems Biology Lab, Massachusetts General Hospital, Boston, MA, USA

David Craft

392. Department of Medicine, Baylor College of Medicine, Houston, TX, USA

Chad J. Creighton

393. University of Cologne, Cologne, Germany

Yupeng Cun, Martin Peifer & Tsun-Po Yang

394. International Genomics Consortium, Phoenix, AZ, USA

Erin Curley & Troy Shelton

395. Genomics Research Program, Ontario Institute for Cancer Research, Toronto, ON, Canada

Karolina Czajka, Jenna Eagles, Thomas J. Hudson, Jeremy Johns, Faridah Mbabaali, John D. McPherson, Jessica K. Miller, Danielle Pasternack, Michelle Sam & Lee E. Timms

396. Barking Havering and Redbridge University Hospitals NHS Trust, Romford, UK

Bogdan Czerniak, Adel El-Naggar & David Khoo

397. Children's Hospital at Westmead, University of Sydney, Sydney, NSW, Australia

Rebecca A. Dagg

398. Department of Medicine, Section of Endocrinology, University and Hospital Trust of Verona, Verona, Italy

Maria Vittoria Davi

399. Computational Biology Center, Memorial Sloan Kettering Cancer Center, New York, NY, USA

Natalie R. Davidson, Andre Kahles, Kjong-Van Lehmann, Alessandro Pastore, Gunnar Rätsch, Chris Sander, Yasin Senbabaoglu & Nicholas D. Socci

400. Department of Biology, ETH Zurich, Zürich, Switzerland

Natalie R. Davidson, Andre Kahles, Kjong-Van Lehmann, Gunnar Rätsch & Stefan G. Stark

401. Department of Computer Science, ETH Zurich, Zurich, Switzerland

Natalie R. Davidson, Andre Kahles, Kjong-Van Lehmann & Gunnar Rätsch

402. SIB Swiss Institute of Bioinformatics, Lausanne, Switzerland

Natalie R. Davidson, Andre Kahles, Kjong-Van Lehmann, Gunnar Rätsch & Stefan G. Stark

403. Weill Cornell Medical College, New York, NY, USA

Natalie R. Davidson, Bishoy M. Faltas & Gunnar Rätsch

404. Academic Department of Medical Genetics, University of Cambridge, Addenbrooke's Hospital, Cambridge, UK

Helen Davies & Serena Nik-Zainal

405. MRC Cancer Unit, University of Cambridge, Cambridge, UK

Helen Davies, Rebecca C. Fitzgerald, Nicola Grehan, Serena Nik-Zainal & Maria O'Donovan

406. Departments of Pediatrics and Genetics, University of North Carolina at Chapel Hill, Chapel Hill, NC, USA

Ian J. Davis

407. Seven Bridges Genomics, Charlestown, MA, USA

Brandi N. Davis-Dusenbery, Sinisa Ivkovic, Milena Kovacevic, Ana Mijalkovic Lazic, Sanja Mijalkovic, Mia Nastic, Petar Radovic & Nebojsa Tijanic

408. Annai Systems, Inc, Carlsbad, CA, USA

Francisco M. De La Vega, Tal Shmaya & Dai-Ying Wu

409. Department of Pathology, General Hospital of Treviso, Department of Medicine, University of Padua, Treviso, Italy

Angelo P. Dei Tos

410. Department of Computational Biology, University of Lausanne, Lausanne, Switzerland

Olivier Delaneau

411. Department of Genetic Medicine and Development, University of Geneva Medical School, Geneva, CH, Switzerland

Olivier Delaneau

412. Swiss Institute of Bioinformatics, University of Geneva, Geneva, CH, Switzerland

Olivier Delaneau

413. The Francis Crick Institute, London, UK

Jonas Demeulemeester, Stefan C. Dentro, Matthew W. Fittall, Kerstin Haase, Clemency Jolly, Maxime Tarabichi & Peter Van Loo

414. University of Leuven, Leuven, Belgium

Jonas Demeulemeester & Peter Van Loo

415. Institute of Medical Genetics and Applied Genomics, University of Tübingen, Tübingen, Germany

German M. Demidov, Francesc Muyas & Stephan Ossowski

416. Computational and Systems Biology, Genome Institute of Singapore, Singapore, Singapore

Deniz Demircioğlu & Jonathan Göke

417. School of Computing, National University of Singapore, Singapore, Singapore

Deniz Demircioğlu

418. Big Data Institute, Li Ka Shing Centre, University of Oxford, Oxford, UK

Stefan C. Dentro & David C. Wedge

419. Biomedical Data Science Laboratory, Francis Crick Institute, London, UK

Nikita Desai

420. Bioinformatics Group, Department of Computer Science, University College London, London, UK

Nikita Desai

421. The Edward S. Rogers Sr. Department of Electrical and Computer Engineering, University of Toronto, Toronto, ON, Canada

Amit G. Deshwar

422. Breast Cancer Translational Research Laboratory JC Heuson, Institut Jules Bordet, Brussels, Belgium

Christine Desmedt

423. Department of Oncology, Laboratory for Translational Breast Cancer Research, KU Leuven, Leuven, Belgium

Christine Desmedt

424. Institute for Research in Biomedicine (IRB Barcelona), The Barcelona Institute of Science and Technology, Barcelona, Spain

Jordi Deu-Pons, Joan Frigola, Abel Gonzalez-Perez, Ferran Muiños, Loris Mularoni, Oriol Pich, Iker Reyes-Salazar, Carlota Rubio-Perez, Radhakrishnan Sabarinathan & David Tamborero

425. Research Program on Biomedical Informatics, Universitat Pompeu Fabra, Barcelona, Spain

Jordi Deu-Pons, Abel Gonzalez-Perez, Ferran Muiños, Loris Mularoni, Oriol Pich, Carlota Rubio-Perez, Radhakrishnan Sabarinathan & David Tamborero

426. Division of Medical Oncology, Princess Margaret Cancer Centre, Toronto, ON, Canada

Neesha C. Dhani, David Hedley & Malcolm J. Moore

427. Department of Physiology and Biophysics, Weill Cornell Medicine, New York, NY, USA

Priyanka Dhingra, Ekta Khurana, Eric Minwei Liu & Alexander Martinez-Fundichely

428. Institute for Computational Biomedicine, Weill Cornell Medicine, New York, NY, USA

Priyanka Dhingra, Ekta Khurana, Eric Minwei Liu & Alexander Martinez-Fundichely

429. Department of Pathology, UPMC Shadyside, Pittsburgh, PA, USA

Rajiv Dhir

430. Independent Consultant, Wellesley, USA

Anthony DiBiase

431. Department of Cell and Molecular Biology, Science for Life Laboratory, Uppsala University, Uppsala, Sweden

Klev Diamanti, Jan Komorowski & Husen M. Umer

432. Department of Medicine and Department of Genetics, Washington University School of Medicine, St. Louis, St. Louis, MO, USA

Li Ding, Robert S. Fulton, Michael D. McLellan, Michael C. Wendl & Venkata D. Yellapantula

433. Hefei University of Technology, Anhui, China

Shuai Ding & Shanlin Yang

434. Translational Cancer Research Unit, GZA Hospitals St.-Augustinus, Center for Oncological Research, Faculty of Medicine and Health Sciences, University of Antwerp, Antwerp, Belgium

Luc Dirix, Steven Van Laere, Gert G. Van den Eynden & Peter Vermeulen

435. Simon Fraser University, Burnaby, BC, Canada

Nilgun Donmez, Ermin Hodzic, Salem Malikic, S. Cenk Sahinalp & Iman Sarrafi

436. University of Pennsylvania, Philadelphia, PA, USA

Ronny Drapkin

437. Faculty of Science and Technology, University of Vic—Central University of Catalonia (UVic-UCC), Vic, Spain

Ana Dueso-Barroso

438. The Wellcome Trust, London, UK

Michael Dunn

439. The Hospital for Sick Children, Toronto, ON, Canada

Lewis Jonathan Dursi

440. Department of Pathology, Queen Elizabeth University Hospital, Glasgow, UK

Fraser R. Duthie

441. Department of Genetics and Computational Biology, QIMR Berghofer Medical Research Institute, Brisbane, QLD, Australia

Ken Dutton-Regester, Nicholas K. Hayward, Oliver Holmes, Peter A. Johansson, Stephen H. Kazakoff, Conrad R. Leonard, Felicity Newell, Katia Nones, Ann-Marie Patch, John V. Pearson, Antonia L. Pritchard, Michael C. Quinn, Paresh Vyas, Nicola Waddell, Scott Wood & Qinying Xu

442. Department of Oncology, Centre for Cancer Genetic Epidemiology, University of Cambridge, Cambridge, UK

Douglas F. Easton

443. Department of Public Health and Primary Care, Centre for Cancer Genetic Epidemiology, University of Cambridge, Cambridge, UK

Douglas F. Easton

444. Prostate Cancer Canada, Toronto, ON, Canada

Stuart Edmonds

445. University of Cambridge, Cambridge, UK

Paul A. Edwards, Anthony R. Green, Andy G. Lynch, Florian Markowetz & Thomas J. Mitchell

446. Department of Laboratory Medicine, Translational Cancer Research, Lund University Cancer Center at Medicon Village, Lund University, Lund, Sweden

Anna Ehinger

447. Heidelberg University, Heidelberg, Germany

Juergen Eils, Roland Eils & Daniel Hübschmann

448. New BIH Digital Health Center, Berlin Institute of Health (BIH) and Charité - Universitätsmedizin Berlin, Berlin, Germany

Juergen Eils, Roland Eils & Chris Lawerenz

449. CIBER Epidemiología y Salud Pública (CIBERESP), Madrid, Spain

Georgia Escaramis

450. Research Group on Statistics, Econometrics and Health (GRECS), UdG, Barcelona, Spain

Georgia Escaramis

451. Quantitative Genomics Laboratories (qGenomics), Barcelona, Spain

Xavier Estivill

452. Icelandic Cancer Registry, Icelandic Cancer Society, Reykjavik, Iceland

Jorunn E. Eyfjord, Holmfridur Hilmarsdottir & Jon G. Jonasson

453. State Key Laboratory of Cancer Biology, and Xijing Hospital of Digestive Diseases, Fourth Military Medical University, Shaanxi, China

Daiming Fan & Yongzhan Nie

454. Department of Medicine (DIMED), Surgical Pathology Unit, University of Padua, Padua, Italy

Matteo Fassan

455. Rigshospitalet, Copenhagen, Denmark

Francesco Favero

456. Center for Cancer Genomics, National Cancer Institute, National Institutes of Health, Bethesda, MD, USA

Martin L. Ferguson

457. Department of Biochemistry and Molecular Medicine, University of Montreal, Montreal, QC, Canada

Vincent Ferretti

458. Australian Institute of Tropical Health and Medicine, James Cook University, Douglas, QLD, Australia

Matthew A. Field

459. Department of Neuro-Oncology, Istituto Neurologico Besta, Milano, Italy

Gaetano Finocchiaro

460. Bioplatforms Australia, North Ryde, NSW, Australia

Anna Fitzgerald & Catherine A. Shang

461. Department of Pathology (Research), University College London Cancer Institute, London, UK

Adrienne M. Flanagan

462. Department of Surgical Oncology, Princess Margaret Cancer Centre, Toronto, ON, Canada

Neil E. Fleshner

463. Department of Medical Oncology, Josephine Nefkens Institute and Cancer Genomics Centre, Erasmus Medical Center, Rotterdam, CN, The Netherlands

John A. Foekens, John W. M. Martens, F. Germán Rodríguez-González, Anieta M. Sieuwerts & Marcel Smid

464. The University of Queensland Thoracic Research Centre, The Prince Charles Hospital, Brisbane, QLD, Australia

Kwun M. Fong

465. CIBIO/InBIO - Research Center in Biodiversity and Genetic Resources, Universidade do Porto, Vairão, Portugal

Nuno A. Fonseca

466. HCA Laboratories, London, UK

Christopher S. Foster

467. University of Liverpool, Liverpool, UK

Christopher S. Foster

468. The Azrieli Faculty of Medicine, Bar-Ilan University, Safed, Israel

Milana Frenkel-Morgenstern

469. Department of Neurosurgery, University of Florida, Gainesville, FL, USA

William Friedman

470. Department of Pathology, Graduate School of Medicine, University of Tokyo, Tokyo, Japan

Masashi Fukayama & Tetsuo Ushiku

471. University of Milano Bicocca, Monza, Italy

Carlo Gambacorti-Passerini

472. BGI-Shenzhen, Shenzhen, China

Shengjie Gao, Yong Hou, Chang Li, Lin Li, Siliang Li, Xiaobo Li, Xinyue Li, Dongbing Liu, Xingmin Liu, Qiang Pan-Hammarström, Hong Su, Jian Wang, Kui Wu, Heng Xiong, Huanming Yang, Chen Ye, Xiuqing Zhang, Yong Zhou & Shida Zhu

473. Department of Pathology, Oslo University Hospital Ulleval, Oslo, Norway

Øystein Garred

474. Center for Biomedical Informatics, Harvard Medical School, Boston, MA, USA

Nils Gehlenborg

475. Department Biochemistry and Molecular Biomedicine, University of Barcelona, Barcelona, Spain

Josep L. L. Gelpi

476. Office of Cancer Genomics, National Cancer Institute, National Institutes of Health, Bethesda, MD, USA

Daniela S. Gerhard

477. Cancer Epigenomics, German Cancer Research Center (DKFZ), Heidelberg, Germany

Clarissa Gerhauser, Christoph Plass & Dieter Weichenhan

478. Department of Cancer Biology, The University of Texas MD Anderson Cancer Center, Houston, TX, USA

Jeffrey E. Gershenwald

479. Department of Surgical Oncology, The University of Texas MD Anderson Cancer Center, Houston, TX, USA

Jeffrey E. Gershenwald

480. Department of Computer Science, Yale University, New Haven, CT, USA

Mark Gerstein & Fabio C. P. Navarro

481. Department of Molecular Biophysics and Biochemistry, Yale University, New Haven, CT, USA

Mark Gerstein, Sushant Kumar, Lucas Lochovsky, Shaoke Lou, Patrick D. McGillivray, Fabio C. P. Navarro, Leonidas Salichos & Jonathan Warrell

482. Program in Computational Biology and Bioinformatics, Yale University, New Haven, CT, USA

Mark Gerstein, Arif O. Harmanci, Sushant Kumar, Donghoon Lee, Shantao Li, Xiaotong Li, Lucas Lochovsky, Shaoke Lou, William Meyerson, Leonidas Salichos, Jonathan Warrell, Jing Zhang & Yan Zhang

483. Center for Cancer Research, Massachusetts General Hospital, Boston, MA, USA

Gad Getz & Paz Polak

484. Department of Pathology, Massachusetts General Hospital, Boston, MA, USA

Gad Getz

485. Department of Pathology, Memorial Sloan Kettering Cancer Center, New York, NY, USA

Ronald Ghossein, Dilip D. Giri, Christine A. Iacobuzio-Donahue, Jorge Reis-Filho & Victor Reuter

486. Division of Gastroenterology and Hepatology, Mayo Clinic, Rochester, MN, USA

Nasra H. Giama, Catherine D. Moser & Lewis R. Roberts

487. University of Sydney, Sydney, NSW, Australia

Anthony J. Gill & James G. Kench

488. University of Oxford, Oxford, UK

Pelvender Gill, Freddie C. Hamdy, Katalin Karaszi, Adam Lambert, Luke Marsden, Clare Verrill & Paresh Vyas

489. Department of Surgery, Academic Urology Group, University of Cambridge, Cambridge, UK

Vincent J. Gnanapragasam

490. Department of Medicine II, University of Würzburg, Wuerzburg, Germany

Maria Elisabeth Goebler

491. Sylvester Comprehensive Cancer Center, University of Miami, Miami, FL, USA

Carmen Gomez

492. Institut Hospital del Mar d'Investigacions Mèdiques (IMIM), Barcelona, Spain

Abel Gonzalez-Perez

493. Genome Integrity and Structural Biology Laboratory, National Institute of Environmental Health Sciences (NIEHS), Durham, NC, USA

Dmitry A. Gordenin & Natalie Saini

494. St. Thomas's Hospital, London, UK

James Gossage

495. Osaka International Cancer Center, Osaka, Japan

Kunihito Gotoh

496. Department of Pathology, Skåne University Hospital, Lund University, Lund, Sweden

Dorthe Grabau

497. Department of Medical Oncology, Beatson West of Scotland Cancer Centre, Glasgow, UK

Janet S. Graham

498. National Human Genome Research Institute, National Institutes of Health, Bethesda, MD, USA

Eric Green, Carolyn M. Hutter & Heidi J. Sofia

499. Centre for Cancer Research, Victorian Comprehensive Cancer Centre, University of Melbourne, Melbourne, VIC, Australia

Sean M. Grimmond

500. Department of Medicine, Section of Hematology/Oncology, University of Chicago, Chicago, IL, USA

Robert L. Grossman

501. German Center for Infection Research (DZIF), Partner Site Hamburg-Borstel-Lübeck-Riems, Hamburg, Germany

Adam Grundhoff

502. Bioinformatics Research Centre (BiRC), Aarhus University, Aarhus, Denmark

Qianyun Guo, Asger Hobolth & Jakob Skou Pedersen

503. Department of Biotechnology, Ministry of Science and Technology, Government of India, New Delhi, Delhi, India

Shailja Gupta & K. VijayRaghavan

504. National Cancer Centre Singapore, Singapore, Singapore

Jonathan Göke

505. Brandeis University, Waltham, MA, USA

James E. Haber

506. Department of Urologic Sciences, University of British Columbia, Vancouver, BC, Canada

Faraz Hach

507. Department of Internal Medicine, Stanford University, Stanford, CA, USA

Mark P. Hamilton

508. The University of Texas Health Science Center at Houston, Houston, TX, USA

Leng Han, Yang Yang & Xuanping Zhang

509. Imperial College NHS Trust, Imperial College, London, INY, UK

George B. Hanna

510. Senckenberg Institute of Pathology, University of Frankfurt Medical School, Frankfurt, Germany

Martin Hansmann

511. Department of Medicine, Division of Biomedical Informatics, UC San Diego School of Medicine, San Diego, CA, USA

Olivier Harismendy

512. Center for Precision Health, School of Biomedical Informatics, The University of Texas Health Science Center, Houston, TX, USA

Arif O. Harmanci

513. Oxford Nanopore Technologies, New York, NY, USA

Eoghan Harrington & Sissel Juul

514. Institute of Medical Science, University of Tokyo, Tokyo, Japan

Takanori Hasegawa, Shuto Hayashi, Seiya Imoto, Mitsuhiro Komura, Satoru Miyano, Naoki Miyoshi, Kazuhiro Ohi, Eigo Shimizu, Yuichi Shiraishi, Hiroko Tanaka & Rui Yamaguchi

515. Howard Hughes Medical Institute, University of California Santa Cruz, Santa Cruz, CA, USA

David Haussler

516. Wakayama Medical University, Wakayama, Japan

Shinya Hayami, Masaki Ueno & Hiroki Yamaue

517. Department of Internal Medicine, Division of Medical Oncology, Lineberger Comprehensive Cancer Center, University of North Carolina at Chapel Hill, Chapel Hill, NC, USA

D. Neil Hayes

518. University of Tennessee Health Science Center for Cancer Research, Memphis, TN, USA

D. Neil Hayes

519. Department of Histopathology, Salford Royal NHS Foundation Trust, Salford, UK

Stephen J. Hayes

520. Faculty of Biology, Medicine and Health, University of Manchester, Manchester, UK

Stephen J. Hayes

521. BIOPIC, ICG and College of Life Sciences, Peking University, Beijing, China

Yao He & Zemin Zhang

522. Peking-Tsinghua Center for Life Sciences, Peking University, Beijing, China

Yao He & Zemin Zhang

523. Children’s Hospital of Philadelphia, Philadelphia, PA, USA

Allison P. Heath

524. Department of Bioinformatics and Computational Biology and Department of Systems Biology, The University of Texas MD Anderson Cancer Center, Houston, TX, USA

Apurva M. Hegde, Yiling Lu & John N. Weinstein

525. Karolinska Institute, Stockholm, Sweden

Eva Hellstrom-Lindberg & Jesper Lagergren

526. The Donnelly Centre, University of Toronto, Toronto, ON, Canada

Mohamed Helmy & Jeffrey A. Wintersinger

527. Department of Medical Genetics, College of Medicine, Hallym University, Chuncheon, South Korea

Seong Gu Heo, Eun Pyo Hong & Ji Wan Park

528. Department of Experimental and Health Sciences, Institute of Evolutionary Biology (UPF-CSIC), Universitat Pompeu Fabra, Barcelona, Spain

José María Heredia-Genestar, Tomas Marques-Bonet & Arcadi Navarro

529. Health Data Science Unit, University Clinics, Heidelberg, Germany

Carl Herrmann

530. Massachusetts General Hospital Center for Cancer Research, Charlestown, MA, USA

Julian M. Hess & Yosef E. Maruvka

531. Hokkaido University, Sapporo, Japan

Satoshi Hirano & Toru Nakamura

532. Department of Pathology and Clinical Laboratory, National Cancer Center Hospital, Tokyo, Japan

Nobuyoshi Hiraoka

533. Department of Genetics, University of North Carolina at Chapel Hill, Chapel Hill, NC, USA

Katherine A. Hoadley & Tara J. Skelly

534. Computational Biology, Leibniz Institute on Aging - Fritz Lipmann Institute (FLI), Jena, Germany

Steve Hoffmann

535. University of Melbourne Centre for Cancer Research, Melbourne, VIC, Australia

Oliver Hofmann

536. University of Nebraska Medical Center, Omaha, NE, USA

Michael A. Hollingsworth & Sarah P. Thayer

537. Syntekabio Inc, Daejeon, South Korea

Jongwhi H. Hong

538. Department of Pathology, Academic Medical Center, Amsterdam, AZ, The Netherlands

Gerrit K. Hooijer

539. China National GeneBank-Shenzhen, Shenzhen, China

Yong Hou, Chang Li, Siliang Li, Xiaobo Li, Dongbing Liu, Xingmin Liu, Henk G. Stunnenberg, Hong Su, Kui Wu, Heng Xiong, Chen Ye & Shida Zhu

540. Division of Molecular Genetics, German Cancer Research Center (DKFZ), Heidelberg, Germany

Volker Hovestadt, Murat Iskar, Peter Lichter, Bernhard Radlwimmer & Marc Zapatka

541. Division of Life Science and Applied Genomics Center, Hong Kong University of Science and Technology, Clear Water Bay, Hong Kong, China

Taobo Hu, Yogesh Kumar, Eric Z. Ma, Zhenggang Wu & Hong Xue

542. Icahn School of Medicine at Mount Sinai, New York, NY, USA

Kuan-lin Huang

543. Geneplus-Shenzhen, Shenzhen, China

Yi Huang

544. School of Computer Science and Technology, Xi'an Jiaotong University, Xi'an, China

Yi Huang, Jiayin Wang, Xiao Xiao & Xuanping Zhang

545. AbbVie, North Chicago, IL, USA

Thomas J. Hudson

546. Institute of Pathology, Charité – University Medicine Berlin, Berlin, Germany

Michael Hummel & Dido Lenze

547. Centre for Translational and Applied Genomics, British Columbia Cancer Agency, Vancouver, BC, Canada

David Huntsman

548. Edinburgh Royal Infirmary, Edinburgh, UK

Ted R. Hupp

549. Berlin Institute for Medical Systems Biology, Max Delbrück Center for Molecular Medicine, Berlin, Germany

Matthew R. Huska, Julia Markowski & Roland F. Schwarz

550. Department of Pediatric Immunology, Hematology and Oncology, University Hospital, Heidelberg, Germany

Daniel Hübschmann

551. German Cancer Research Center (DKFZ), Heidelberg, Germany

Daniel Hübschmann, Christof von Kalle & Roland F. Schwarz

552. Heidelberg Institute for Stem Cell Technology and Experimental Medicine (HI-STEM), Heidelberg, Germany

Daniel Hübschmann

553. Institute for Computational Biomedicine, Weill Cornell Medical College, New York, NY, USA

Marcin Imielinski

554. New York Genome Center, New York, NY, USA

Marcin Imielinski & Xiaotong Yao

555. Department of Urology, James Buchanan Brady Urological Institute, Johns Hopkins University School of Medicine, Baltimore, MD, USA

William B. Isaacs

556. Department of Preventive Medicine, Graduate School of Medicine, The University of Tokyo, Tokyo, Japan

Shumpei Ishikawa, Hiroto Katoh & Daisuke Komura

557. Department of Molecular and Cellular Biology, Baylor College of Medicine, Houston, TX, USA

Michael Ittmann

558. Department of Pathology and Immunology, Baylor College of Medicine, Houston, TX, USA

Michael Ittmann

559. Michael E. DeBakey Veterans Affairs Medical Center, Houston, TX, USA

Michael Ittmann

560. Technical University of Denmark, Lyngby, Denmark

Jose M. G. Izarzugaza

561. Department of Pathology, College of Medicine, Hanyang University, Seoul, South Korea

Jocelyne Jacquemier, Hyung-Yong Kim & Gu Kong

562. Academic Unit of Surgery, School of Medicine, College of Medical, Veterinary and Life Sciences, University of Glasgow, Glasgow Royal Infirmary, Glasgow, UK

Nigel B. Jamieson

563. Department of Pathology, Asan Medical Center, College of Medicine, Ulsan University, Songpa-gu, Seoul, South Korea

Se Jin Jang & Hee Jin Lee

564. Science Writer, Garrett Park, MD, USA

Karine Jegalian

565. International Cancer Genome Consortium (ICGC)/ICGC Accelerating Research in Genomic Oncology (ARGO) Secretariat, Ontario Institute for Cancer Research, Toronto, ON, Canada

Jennifer L. Jennings

566. University of Ljubljana, Ljubljana, Slovenia

Lara Jerman

567. Department of Public Health Sciences, University of Chicago, Chicago, IL, USA

Yuan Ji

568. Research Institute, NorthShore University HealthSystem, Evanston, IL, USA

Yuan Ji

569. Department for Biomedical Research, University of Bern, Bern, Switzerland

Rory Johnson, Andrés Lanzós & Mark A. Rubin

570. Centre of Genomics and Policy, McGill University and Génome Québec Innovation Centre, Montreal, QC, Canada

Yann Joly, Bartha M. Knoppers, Mark Phillips & Adrian Thorogood

571. Carolina Center for Genome Sciences, University of North Carolina at Chapel Hill, Chapel Hill, NC, USA

Corbin D. Jones

572. Hopp Children's Cancer Center (KiTZ), Heidelberg, Germany

David T. W. Jones, Marcel Kool & Stefan M. Pfister

573. Pediatric Glioma Research Group, German Cancer Research Center (DKFZ), Heidelberg, Germany

David T. W. Jones

574. Cancer Research UK, London, UK

Nic Jones & David Scott

575. Indivumed GmbH, Hamburg, Germany

Hartmut Juhl

576. Genome Integration Data Center, Syntekabio, Inc, Daejeon, South Korea

Jongsun Jung

577. University Hospital Zurich, Zurich, Switzerland

Andre Kahles, Kjong-Van Lehmann & Gunnar Rätsch

578. Clinical Bioinformatics, Swiss Institute of Bioinformatics, Geneva, Switzerland

Abdullah Kahraman

579. Institute for Pathology and Molecular Pathology, University Hospital Zurich, Zurich, Switzerland

Abdullah Kahraman

580. Institute of Molecular Life Sciences, University of Zurich, Zurich, Switzerland

Abdullah Kahraman & Christian von Mering

581. MRC Human Genetics Unit, MRC IGMM, University of Edinburgh, Edinburgh, UK

Vera B. Kaiser & Colin A. Semple

582. Women's Cancer Program at the Samuel Oschin Comprehensive Cancer Institute, Cedars-Sinai Medical Center, Los Angeles, CA, USA

Beth Karlan

583. Department of Biology, Bioinformatics Group, Division of Molecular Biology, Faculty of Science, University of Zagreb, Zagreb, Croatia

Rosa Karlić

584. Department for Internal Medicine II, University Hospital Schleswig-Holstein, Kiel, Germany

Dennis Karsch & Michael Kneba

585. Genetics and Molecular Pathology, SA Pathology, Adelaide, SA, Australia

Karin S. Kassahn

586. Department of Gastric Surgery, National Cancer Center Hospital, Tokyo, Japan

Hitoshi Katai

587. Department of Bioinformatics, Division of Cancer Genomics, National Cancer Center Research Institute, Tokyo, Japan

Mamoru Kato, Hirofumi Rokutan & Mihoko Saito-Adachi

588. A.A. Kharkevich Institute of Information Transmission Problems, Moscow, Russia

Marat D. Kazanov

589. Oncology and Immunology, Dmitry Rogachev National Research Center of Pediatric Hematology, Moscow, Russia

Marat D. Kazanov

590. Skolkovo Institute of Science and Technology, Moscow, Russia

Marat D. Kazanov

591. Department of Surgery, The George Washington University, School of Medicine and Health Science, Washington, DC, USA

Electron Kebebew

592. Endocrine Oncology Branch, Center for Cancer Research, National Cancer Institute, National Institutes of Health, Bethesda, MD, USA

Electron Kebebew

593. Melanoma Institute Australia, Macquarie University, Sydney, NSW, Australia

Richard F. Kefford

594. MIT Computer Science and Artificial Intelligence Laboratory, Massachusetts Institute of Technology, Cambridge, MA, USA

Manolis Kellis

595. Tissue Pathology and Diagnostic Oncology, Royal Prince Alfred Hospital, Sydney, NSW, Australia

James G. Kench & Richard A. Scolyer

596. Cholangiocarcinoma Screening and Care Program and Liver Fluke and Cholangiocarcinoma Research Centre, Faculty of Medicine, Khon Kaen University, Khon Kaen, Thailand

Narong Khuntikeo

597. Controlled Department and Institution, New York, NY, USA

Ekta Khurana

598. Englander Institute for Precision Medicine, Weill Cornell Medicine, New York, NY, USA

Ekta Khurana & Alexander Martinez-Fundichely

599. National Cancer Center, Gyeonggi, South Korea

Hark Kyun Kim

600. Department of Biochemistry, College of Medicine, Ewha Womans University, Seoul, South Korea

Hyung-Lae Kim

601. Health Sciences Department of Biomedical Informatics, University of California San Diego, La Jolla, CA, USA

Jihoon Kim

602. Research Core Center, National Cancer Centre Korea, Goyang-si, South Korea

Jong K. Kim

603. Department of Health Sciences and Technology, Sungkyunkwan University School of Medicine, Seoul, South Korea

Youngwook Kim

604. Samsung Genome Institute, Seoul, South Korea

Youngwook Kim

605. Breast Oncology Program, Dana-Farber/Brigham and Women's Cancer Center, Boston, MA, USA

Tari A. King

606. Department of Surgery, Memorial Sloan Kettering Cancer Center, New York, NY, USA

Tari A. King & Samuel Singer

607. Division of Breast Surgery, Brigham and Women's Hospital, Boston, MA, USA

Tari A. King

608. Integrative Bioinformatics Support Group, National Institute of Environmental Health Sciences (NIEHS), Durham, NC, USA

Leszek J. Klimczak

609. Department of Clinical Science, University of Bergen, Bergen, Norway

Stian Knappskog & Ola Myklebost

610. Center For Medical Innovation, Seoul National University Hospital, Seoul, South Korea

Youngil Koh

611. Department of Internal Medicine, Seoul National University Hospital, Seoul, South Korea

Youngil Koh & Sung-Soo Yoon

612. Institute of Computer Science, Polish Academy of Sciences, Warsawa, Poland

Jan Komorowski

613. Functional and Structural Genomics, German Cancer Research Center (DKFZ), Heidelberg, Germany

Marcel Kool, Andrey Korshunov, Michael Koscher, Stefan M. Pfister & Qi Wang

614. Laboratory of Translational Genomics, Division of Cancer Epidemiology and Genetics, National Cancer Institute, , National Institutes of Health, Bethesda, MD, USA

Roelof Koster

615. Institute for Medical Informatics Statistics and Epidemiology, University of Leipzig, Leipzig, Germany

Markus Kreuz & Markus Loeffler

616. Morgan Welch Inflammatory Breast Cancer Research Program and Clinic, The University of Texas MD Anderson Cancer Center, Houston, TX, USA

Savitri Krishnamurthy

617. Department of Hematology and Oncology, Georg-Augusts-University of Göttingen, Göttingen, Germany

Dieter Kube & Lorenz H. P. Trümper

618. Institute of Cell Biology (Cancer Research), University of Duisburg-Essen, Essen, Germany

Ralf Küppers

619. King’s College London and Guy’s and St. Thomas’ NHS Foundation Trust, London, UK

Jesper Lagergren

620. Center for Epigenetics, Van Andel Research Institute, Grand Rapids, MI, USA

Peter W. Laird

621. The University of Queensland Centre for Clinical Research, Royal Brisbane and Women’s Hospital, Herston, QLD, Australia

Sunil R. Lakhani & Peter T. Simpson

622. Department of Pediatric Oncology and Hematology, University of Cologne, Cologne, Germany

Pablo Landgraf

623. University of Düsseldorf, Düsseldorf, Germany

Pablo Landgraf & Guido Reifenberger

624. Department of Pathology, Institut Jules Bordet, Brussels, Belgium

Denis Larsimont

625. Institute of Biomedicine, Sahlgrenska Academy at University of Gothenburg, Gothenburg, Sweden

Erik Larsson

626. Children’s Medical Research Institute, Sydney, NSW, Australia

Loretta M. S. Lau & Hilda A. Pickett

627. ILSbio, LLC Biobank, Chestertown, MD, USA

Xuan Le

628. Division of Genetics and Genomics, Boston Children's Hospital, Harvard Medical School, Boston, MA, USA

Eunjung Alice Lee

629. Institute for Bioengineering and Biopharmaceutical Research (IBBR), Hanyang University, Seoul, South Korea

Jeong-Yeon Lee

630. Department of Statistics, University of California Santa Cruz, Santa Cruz, CA, USA

Juhee Lee

631. National Genotyping Center, Institute of Biomedical Sciences, Academia Sinica, Taipei, Taiwan

Ming Ta Michael Lee

632. Department of Vertebrate Genomics/Otto Warburg Laboratory Gene Regulation and Systems Biology of Cancer, Max Planck Institute for Molecular Genetics, Berlin, Germany

Hans Lehrach, Hans-Jörg Warnatz & Marie-Laure Yaspo

633. McGill University and Genome Quebec Innovation Centre, Montreal, QC, Canada

Louis Letourneau

634. biobyte solutions GmbH, Heidelberg, Germany

Ivica Letunic

635. Gynecologic Oncology, NYU Laura and Isaac Perlmutter Cancer Center, New York University, New York, NY, USA

Douglas A. Levine

636. Division of Oncology, Stem Cell Biology Section, Washington University School of Medicine, St. Louis, MO, USA

Tim Ley

637. Department of Systems Biology, The University of Texas MD Anderson Cancer Center, Houston, TX, USA

Han Liang

638. Harvard University, Cambridge, MA, USA

Ziao Lin

639. Urologic Oncology Branch, Center for Cancer Research, National Cancer Institute, National Institutes of Health, Bethesda, MD, USA

W. M. Linehan

640. University of Oslo, Oslo, Norway

Ole Christian Lingjærde & Torill Sauer

641. University of Toronto, Toronto, ON, Canada

Fei-Fei Fei Liu, Quaid D. Morris, Ruian Shi, Shankar Vembu & Fan Yang

642. Peking University, Beijing, China

Fenglin Liu, Fan Zhang, Liangtao Zheng & Xiuqing Zheng

643. School of Life Sciences, Peking University, Beijing, China

Fenglin Liu

644. Leidos Biomedical Research, Inc, McLean, VA, USA

Jia Liu

645. Hematology, Hospital Clinic, Institut d'Investigacions Biomèdiques August Pi i Sunyer (IDIBAPS), University of Barcelona, Barcelona, Spain

Armando Lopez-Guillermo

646. Second Military Medical University, Shanghai, China

Yong-Jie Lu & Hongwei Zhang

647. Chinese Cancer Genome Consortium, Shenzhen, China

Youyong Lu

648. Department of Medical Oncology, Beijing Hospital, Beijing, China

Youyong Lu

649. Laboratory of Molecular Oncology, Key Laboratory of Carcinogenesis and Translational Research (Ministry of Education), Peking University Cancer Hospital and Institute, Beijing, China

Youyong Lu & Rui Xing

650. School of Medicine/School of Mathematics and Statistics, University of St. Andrews, St, Andrews, Fife, UK

Andy G. Lynch

651. Institute for Systems Biology, Seattle, WA, USA

Lisa Lype, Sheila M. Reynolds & Ilya Shmulevich

652. Department of Biochemistry and Molecular Biology, Faculty of Medicine, University Institute of Oncology-IUOPA, Oviedo, Spain

Carlos López-Otín & Xose S. Puente

653. Institut Bergonié, Bordeaux, France

Gaetan MacGrogan

654. Cancer Unit, MRC University of Cambridge, Cambridge, UK

Shona MacRae

655. Department of Pathology and Laboratory Medicine, Center for Personalized Medicine, Children's Hospital Los Angeles, Los Angeles, CA, USA

Dennis T. Maglinte

656. John Curtin School of Medical Research, Canberra, ACT, Australia

Graham J. Mann

657. MVZ Department of Oncology, PraxisClinic am Johannisplatz, Leipzig, Germany

Luisa Mantovani-Löffler

658. Department of Information Technology, Ghent University, Ghent, Belgium

Kathleen Marchal & Sergio Pulido-Tamayo

659. Department of Plant Biotechnology and Bioinformatics, Ghent University, Ghent, Belgium

Kathleen Marchal, Sergio Pulido-Tamayo & Lieven P. C. Verbeke

660. Institute for Genomic Medicine, Nationwide Children's Hospital, Columbus, OH, USA

Elaine R. Mardis

661. Computational Biology Program, School of Medicine, Oregon Health and Science University, Portland, OR, USA

Adam A. Margolin & Adam J. Struck

662. Department of Surgery, Duke University, Durham, NC, USA

Jeffrey Marks

663. Institució Catalana de Recerca i Estudis Avançats (ICREA), Barcelona, Spain

Tomas Marques-Bonet, Jose I. Martin-Subero, Arcadi Navarro, David Torrents & Alfonso Valencia

664. Institut Català de Paleontologia Miquel Crusafont, Universitat Autònoma de Barcelona, Barcelona, Spain

Tomas Marques-Bonet

665. University of Glasgow, Glasgow, UK

Sancha Martin & Ke Yuan

666. Institut d'Investigacions Biomèdiques August Pi i Sunyer (IDIBAPS), Barcelona, Spain

Jose I. Martin-Subero

667. Division of Oncology, Washington University School of Medicine, St. Louis, MO, USA

R. Jay Mashl

668. Department of Surgery and Cancer, Imperial College, London, INY, UK

Erik Mayer

669. Applications Department, Oxford Nanopore Technologies, Oxford, UK

Simon Mayes & Daniel J. Turner

670. Department of Obstetrics, Gynecology and Reproductive Services, University of California San Francisco, San Francisco, CA, USA

Karen McCune & Karen Smith-McCune

671. Department of Biochemistry and Molecular Medicine, University California at Davis, Sacramento, CA, USA

John D. McPherson

672. STTARR Innovation Facility, Princess Margaret Cancer Centre, Toronto, ON, Canada

Alice Meng

673. Discipline of Surgery, Western Sydney University, Penrith, NSW, Australia

Neil D. Merrett

674. Yale School of Medicine, Yale University, New Haven, CT, USA

William Meyerson

675. Department of Genetics, Lineberger Comprehensive Cancer Center, University of North Carolina at Chapel Hill, Chapel Hill, NC, USA

Piotr A. Mieczkowski, Joel S. Parker, Charles M. Perou, Donghui Tan, Umadevi Veluvolu & Matthew D. Wilkerson

676. Departments of Neurology and Neurosurgery, Henry Ford Hospital, Detroit, MI, USA

Tom Mikkelsen

677. Precision Oncology, OHSU Knight Cancer Institute, Oregon Health and Science University, Portland, OR, USA

Gordon B. Mills

678. Institute of Pathology, University Medical Center Hamburg-Eppendorf, Hamburg, Germany

Sarah Minner, Guido Sauter & Ronald Simon

679. Department of Health Sciences, Faculty of Medical Sciences, Kyushu University, Fukuoka, Japan

Shinichi Mizuno

680. Heidelberg Academy of Sciences and Humanities, Heidelberg, Germany

Fruzsina Molnár-Gábor

681. Department of Clinical Pathology, University of Melbourne, Melbourne, VIC, Australia

Carl Morrison, Karin A. Oien, Chawalit Pairojkul, Paul M. Waring & Marc J. van de Vijver

682. Department of Pathology, Roswell Park Cancer Institute, Buffalo, NY, USA

Carl Morrison

683. Department of Computer Science, University of Helsinki, Helsinki, Finland

Ville Mustonen

684. Institute of Biotechnology, University of Helsinki, Helsinki, Finland

Ville Mustonen

685. Organismal and Evolutionary Biology Research Programme, University of Helsinki, Helsinki, Finland

Ville Mustonen

686. Department of Obstetrics and Gynecology, Division of Gynecologic Oncology, Washington University School of Medicine, St. Louis, MO, USA

David Mutch

687. Penrose St. Francis Health Services, Colorado Springs, CO, USA

Jerome Myers

688. Institute of Pathology, Ulm University and University Hospital of Ulm, Ulm, Germany

Peter Möller

689. National Cancer Center, Tokyo, Japan

Hitoshi Nakagama

690. Genome Institute of Singapore, Singapore, Singapore

Tannistha Nandi & Patrick Tan

691. 32Program in Computational Biology and Bioinformatics, Yale University, New Haven, CT, USA

Fabio C. P. Navarro

692. German Cancer Aid, Bonn, Germany

Gerd Nettekoven & Laura Planko

693. Programme in Cancer and Stem Cell Biology, Centre for Computational Biology, Duke-NUS Medical School, Singapore,

Singapore

Alvin Wei Tian Ng

694. The Chinese University of Hong Kong, Shatin, NT, Hong Kong, China

Anthony Ng

695. Fourth Military Medical University, Shaanxi, China

Yongzhan Nie

696. The University of Cambridge School of Clinical Medicine, Cambridge, UK

Serena Nik-Zainal

697. St. Jude Children's Research Hospital, Memphis, TN, USA

Paul A. Northcott

698. University Health Network, Princess Margaret Cancer Centre, Toronto, ON, Canada

Faiyaz Notta & Ming Tsao

699. Center for Biomolecular Science and Engineering, University of California Santa Cruz, Santa Cruz, CA, USA

Brian D. O'Connor

700. Department of Medicine, University of Chicago, Chicago, IL, USA

Peter O'Donnell

701. Department of Neurology, Mayo Clinic, Rochester, MN, USA

Brian Patrick O'Neill

702. Cambridge Oesophagogastric Centre, Cambridge University Hospitals NHS Foundation Trust, Cambridge, UK

J. Robert O'Neill

703. Department of Computer Science, Carleton College, Northfield, MN, USA

Layla Oesper

704. Institute of Cancer Sciences, College of Medical Veterinary and Life Sciences, University of Glasgow, Glasgow, UK

Karin A. Oien

705. Department of Epidemiology, University of Alabama at Birmingham, Birmingham, AL, USA

Akinyemi I. Ojesina

706. HudsonAlpha Institute for Biotechnology, Huntsville, AL, USA

Akinyemi I. Ojesina

707. O'Neal Comprehensive Cancer Center, University of Alabama at Birmingham, Birmingham, AL, USA

Akinyemi I. Ojesina

708. Department of Pathology, Keio University School of Medicine, Tokyo, Japan

Hidenori Ojima

709. Department of Hepatobiliary and Pancreatic Oncology, National Cancer Center Hospital, Tokyo, Japan

Takuji Okusaka

710. Sage Bionetworks, Seattle, WA, USA

Larsson Omberg

711. Lymphoma Genomic Translational Research Laboratory, National Cancer Centre, Singapore, Singapore

Choon Kiat Ong

712. Department of Clinical Pathology, Robert-Bosch-Hospital, Stuttgart, Germany

German Ott

713. Department of Cell and Systems Biology, University of Toronto, Toronto, ON, Canada

B. F. Francis Ouellette

714. Department of Biosciences and Nutrition, Karolinska Institutet, Stockholm, Sweden

Qiang Pan-Hammarström

715. Center for Liver Cancer, Research Institute and Hospital, National Cancer Center, Gyeonggi, South Korea

Joong-Won Park

716. Division of Hematology-Oncology, Samsung Medical Center, Sungkyunkwan University School of Medicine, Seoul, South Korea

Keunchil Park

717. Samsung Advanced Institute for Health Sciences and Technology, Sungkyunkwan University School of Medicine, Seoul, South Korea

Keunchil Park

718. Cheonan Industry-Academic Collaboration Foundation, Sangmyung University, Cheonan, South Korea

Kiejung Park

719. NYU Langone Medical Center, New York, NY, USA

Harvey Pass

720. Department of Hematology and Medical Oncology, Cleveland Clinic, Cleveland, OH, USA

Nathan A. Pennell

721. Department of Radiation Oncology, University of California San Francisco, San Francisco, CA, USA

Marc D. Perry

722. Department of Health Sciences Research, Mayo Clinic, Rochester, MN, USA

Gloria M. Petersen

723. Helen F. Graham Cancer Center at Christiana Care Health Systems, Newark, DE, USA

Nicholas Petrelli

724. Heidelberg University Hospital, Heidelberg, Germany

Stefan M. Pfister

725. CSRA Incorporated, Fairfax, VA, USA

Todd D. Pihl

726. Research Department of Pathology, University College London Cancer Institute, London, UK

Nischalan Pillay

727. Department of Research Oncology, Guy's Hospital, King's Health Partners AHSC, King's College London School of Medicine, London, UK

Sarah Pinder

728. Faculty of Medicine and Health Sciences, Macquarie University, Sydney, NSW, Australia

Andreia V. Pinho

729. University Hospital of Minjoz, INSERM UMR 1098, Besançon, France

Xavier Pivot

730. Spanish National Cancer Research Centre, Madrid, Spain

Tirso Pons

731. Center of Digestive Diseases and Liver Transplantation, Fundeni Clinical Institute, Bucharest, Romania

Irinel Popescu

732. Cureline, Inc, South San Francisco, CA, USA

Olga Potapova

733. St. Luke's Cancer Centre, Royal Surrey County Hospital NHS Foundation Trust, Guildford, UK

Shaun R. Preston

734. Cambridge Breast Unit, Addenbrooke's Hospital, Cambridge University Hospital NHS Foundation Trust and NIHR Cambridge Biomedical Research Centre, Cambridge, UK

Elena Provenzano

735. East of Scotland Breast Service, Ninewells Hospital, Aberdeen, UK

Colin A. Purdie

736. Department of Genetics, Microbiology and Statistics, University of Barcelona, IRSJD, IBUB, Barcelona, Spain

Raquel Rabionet

737. Department of Obstetrics and Gynecology, Medical College of Wisconsin, Milwaukee, WI, USA

Janet S. Rader

738. Hematology and Medical Oncology, Winship Cancer Institute of Emory University, Atlanta, GA, USA

Suresh Ramalingam

739. Department of Computer Science, Princeton University, Princeton, NJ, USA

Benjamin J. Raphael & Matthew A. Reyna

740. Vanderbilt Ingram Cancer Center, Vanderbilt University, Nashville, TN, USA

W. Kimryn Rathmell

741. Ohio State University College of Medicine and Arthur G. James Comprehensive Cancer Center, Columbus, OH, USA

Matthew Ringel

742. Department of Surgery, Yokohama City University Graduate School of Medicine, Kanagawa, Japan

Yasushi Rino

743. Division of Chromatin Networks, German Cancer Research Center (DKFZ) and BioQuant, Heidelberg, Germany

Karsten Rippe

744. Research Computing Center, University of North Carolina at Chapel Hill, Chapel Hill, NC, USA

Jeffrey Roach

745. School of Molecular Biosciences and Center for Reproductive Biology, Washington State University, Pullman, WA, USA

Steven A. Roberts

746. Finsen Laboratory and Biotech Research and Innovation Centre (BRIC), University of Copenhagen, Copenhagen, Denmark

F. Germán Rodríguez-González, Nikos Sidiropoulos & Joachim Weischenfeldt

747. Department of Laboratory Medicine and Pathobiology, University of Toronto, Toronto, ON, Canada

Michael H. A. Roehrl & Stefano Serra

748. Department of Pathology, Human Oncology and Pathogenesis Program, Memorial Sloan Kettering Cancer Center, New York, NY, USA

Michael H. A. Roehrl

749. University Hospital Giessen, Pediatric Hematology and Oncology, Giessen, Germany

Marius Rohde

750. Oncologie Sénologie, ICM Institut Régional du Cancer, Montpellier, France

Gilles Romieu

751. Institute of Clinical Molecular Biology, Christian-Albrechts-University, Kiel, Germany

Philip C. Rosenstiel & Markus B. Schilhabel

752. Institute of Pathology, University of Wuerzburg, Wuerzburg, Germany

Andreas Rosenwald

753. Department of Urology, North Bristol NHS Trust, Bristol, UK

Edward W. Rowe

754. SingHealth, Duke-NUS Institute of Precision Medicine, National Heart Centre Singapore, Singapore, Singapore

Steven G. Rozen, Patrick Tan & Bin Tean Teh

755. Department of Computer Science, University of Toronto, Toronto, ON, Canada

Yulia Rubanova, Jared T. Simpson & Jeffrey A. Wintersinger

756. Bern Center for Precision Medicine, University Hospital of Bern, University of Bern, Bern, Switzerland

Mark A. Rubin

757. Englander Institute for Precision Medicine, Weill Cornell Medicine and New York Presbyterian Hospital, New York, NY, USA

Mark A. Rubin

758. Meyer Cancer Center, Weill Cornell Medicine, New York, NY, USA

Mark A. Rubin

759. Pathology and Laboratory, Weill Cornell Medical College, New York, NY, USA

Mark A. Rubin

760. Vall d'Hebron Institute of Oncology: VHIO, Barcelona, Spain

Carlota Rubio-Perez

761. General and Hepatobiliary-Biliary Surgery, Pancreas Institute, University and Hospital Trust of Verona, Verona, Italy

Andrea Ruzzenente

762. National Centre for Biological Sciences, Tata Institute of Fundamental Research, Bangalore, India

Radhakrishnan Sabarinathan

763. Indiana University, Bloomington, IN, USA

S. Cenk Sahinalp

764. Department of Pathology, GZA-ZNA Hospitals, Antwerp, Belgium

Roberto Salgado

765. Analytical Biological Services, Inc, Wilmington, DE, USA

Charles Saller

766. Sydney Medical School, University of Sydney, Sydney, NSW, Australia

Jaswinder S. Samra & Richard A. Scolyer

767. cBio Center, Dana-Farber Cancer Institute, Harvard Medical School, Boston, MA, USA

Chris Sander & Ciyue Shen

768. Department of Cell Biology, Harvard Medical School, Boston, MA, USA

Chris Sander & Ciyue Shen

769. Advanced Centre for Treatment Research and Education in Cancer, Tata Memorial Centre, Navi Mumbai, Maharashtra, India

Rajiv Sarin

770. School of Environmental and Life Sciences, Faculty of Science, The University of Newcastle, Ourimbah, NSW, Australia

Christopher J. Scarlett

771. Department of Dermatology, University Hospital of Essen, Essen, Germany

Dirk Schadendorf

772. Bioinformatics and Omics Data Analytics, German Cancer Research Center (DKFZ), Heidelberg, Germany

Matthias Schlesner

773. Department of Urology, Charité Universitätsmedizin Berlin, Berlin, Germany

Thorsten Schlomm & Joachim Weischenfeldt

774. Martini-Clinic, Prostate Cancer Center, University Medical Center Hamburg-Eppendorf, Hamburg, Germany

Thorsten Schlomm

775. Department of General Internal Medicine, University of Kiel, Kiel, Germany

Stefan Schreiber

776. German Cancer Consortium (DKTK), Partner site Berlin, Berlin, Germany

Roland F. Schwarz

777. Cancer Research Institute, Beth Israel Deaconess Medical Center, Boston, MA, USA

Ralph Scully

778. University of Pittsburgh, Pittsburgh, PA, USA

Raja Seethala

779. Department of Ophthalmology and Ocular Genomics Institute, Massachusetts Eye and Ear, Harvard Medical School, Boston, MA, USA

Ayellet V. Segre

780. Center for Psychiatric Genetics, NorthShore University HealthSystem, Evanston, IL, USA

Subhajit Sengupta

781. Van Andel Research Institute, Grand Rapids, MI, USA

Hui Shen & Wanding Zhou

782. Laboratory of Molecular Medicine, Human Genome Center, Institute of Medical Science, University of Tokyo, Tokyo, Japan

Tatsuhiro Shibata, Hirokazu Taniguchi & Tomoko Urushidate

783. Japan Agency for Medical Research and Development, Tokyo, Japan

Kiyo Shimizu & Takashi Yugawa

784. Korea University, Seoul, South Korea

Seung Jun Shin & Stefan G. Stark

785. Murtha Cancer Center, Walter Reed National Military Medical Center, Bethesda, MD, USA

Craig Shriver

786. Human Genetics, University of Kiel, Kiel, Germany

Reiner Siebert

787. Department of Oncologic Pathology, Dana-Farber Cancer Institute, Harvard Medical School, Boston, MA, USA

Sabina Signoretti

788. Oregon Health and Science University, Portland, OR, USA

Jaclyn Smith

789. Center for RNA Interference and Noncoding RNA, The University of Texas MD Anderson Cancer Center, Houston, TX, USA

Anil K. Sood

790. Department of Experimental Therapeutics, The University of Texas MD Anderson Cancer Center, Houston, TX, USA

Anil K. Sood

791. Department of Gynecologic Oncology and Reproductive Medicine, The University of Texas MD Anderson Cancer Center, Houston, TX, USA

Anil K. Sood

792. University Hospitals Coventry and Warwickshire NHS Trust, Coventry, UK

Sharmila Sothi

793. Department of Radiation Oncology, Radboud University Nijmegen Medical Centre, Nijmegen, GA, The Netherlands

Paul N. Span

794. Institute for Genomics and Systems Biology, University of Chicago, Chicago, IL, USA

Jonathan Spring

795. Clinic for Hematology and Oncology, St.-Antonius-Hospital, Eschweiler, Germany

Peter Staib

796. Computational and Systems Biology Program, Memorial Sloan Kettering Cancer Center, New York, NY, USA

Stefan G. Stark

797. University of Iceland, Reykjavik, Iceland

Ólafur Andri Stefánsson

798. Division of Computational Genomics and Systems Genetics, German Cancer Research Center (DKFZ), Heidelberg, Germany

Oliver Stegle

799. Dundee Cancer Centre, Ninewells Hospital, Dundee, UK

Alasdair Stenhouse & Alastair M. Thompson

800. Department for Internal Medicine III, University of Ulm and University Hospital of Ulm, Ulm, Germany

Stephan Stilgenbauer

801. Institut Curie, INSERM Unit 830, Paris, France

Henk G. Stunnenberg & Anne Vincent-Salomon

802. Department of Gastroenterology and Hepatology, Yokohama City University Graduate School of Medicine, Kanagawa, Japan

Akihiro Suzuki

803. Department of Laboratory Medicine, Radboud University Nijmegen Medical Centre, Nijmegen, GA, The Netherlands

Fred Sweep

804. Division of Cancer Genome Research, German Cancer Research Center (DKFZ), Heidelberg, Germany

Holger Sültmann

805. Department of General Surgery, Singapore General Hospital, Singapore, Singapore

Benita Kiat Tee Tan

806. Cancer Science Institute of Singapore, National University of Singapore, Singapore, Singapore

Patrick Tan & Bin Tean Teh

807. Department of Medical and Clinical Genetics, Genome-Scale Biology Research Program, University of Helsinki, Helsinki, Finland

Tomas J. Tanskanen

808. East Anglian Medical Genetics Service, Cambridge University Hospitals NHS Foundation Trust, Cambridge, UK

Patrick Tarpey

809. Irving Institute for Cancer Dynamics, Columbia University, New York, NY, USA

Simon Tavaré

810. Institute of Molecular and Cell Biology, Singapore, Singapore

Bin Tean Teh

811. Laboratory of Cancer Epigenome, Division of Medical Science, National Cancer Centre Singapore, Singapore, Singapore

Bin Tean Teh

812. Universite Lyon, INCa-Synergie, Centre Léon Bérard, Lyon, France

Gilles Thomas

813. Department of Urology, Mayo Clinic, Rochester, MN, USA

R. Houston Thompson

814. Royal National Orthopaedic Hospital - Stanmore, Stanmore, Middlesex, UK

Roberto Tirabosco

815. Department of Biochemistry, Genetics and Immunology, University of Vigo, Vigo, Spain

Marta Tojo

816. Giovanni Paolo II / I.R.C.C.S. Cancer Institute, Bari, BA, Italy

Stefania Tommasi

817. Neuroblastoma Genomics, German Cancer Research Center (DKFZ), Heidelberg, Germany

Umut H. Toprak

818. Fondazione Policlinico Universitario Gemelli IRCCS, Rome, Italy, Rome, Italy

Giampaolo Tortora

819. University of Verona, Verona, Italy

Giampaolo Tortora

820. Centre National de Génotypage, CEA - Institute de Génomique, Evry, France

Jörg Tost

821. CAPHRI Research School, Maastricht University, Maastricht, ER, The Netherlands

David Townend

822. Department of Biopathology, Centre Léon Bérard, Lyon, France

Isabelle Treilleux

823. Université Claude Bernard Lyon 1, Villeurbanne, France

Isabelle Treilleux

824. Core Research for Evolutional Science and Technology (CREST), JST, Tokyo, Japan

Tatsuhiko Tsunoda

825. Department of Biological Sciences, Laboratory for Medical Science Mathematics, Graduate School of Science, University of Tokyo, Yokohama, Japan

Tatsuhiko Tsunoda

826. Department of Medical Science Mathematics, Medical Research Institute, Tokyo Medical and Dental University (TMDU), Tokyo, Japan

Tatsuhiko Tsunoda

827. Cancer Ageing and Somatic Mutation Programme, Wellcome Sanger Institute, Hinxton, UK

Jose M. C. Tubio

828. University Hospitals Birmingham NHS Foundation Trust, Birmingham, UK

Olga Tucker

829. Centre for Cancer Research and Cell Biology, Queen's University, Belfast, UK

Richard Turkington

830. Breast Medical Oncology, The University of Texas MD Anderson Cancer Center, Houston, TX, USA

Naoto T. Ueno

831. Department of Surgery, Johns Hopkins University School of Medicine, Baltimore, MD, USA

Christopher Umbricht

832. Department of Oncology-Pathology, Science for Life Laboratory, Karolinska Institute, Stockholm, Sweden

Husen M. Umer

833. School of Cancer Sciences, Faculty of Medicine, University of Southampton, Southampton, UK

Timothy J. Underwood

834. Department of Gene Technology, Tallinn University of Technology, Tallinn, Estonia

Liis Uusküla-Reimand

835. Genetics and Genome Biology Program, SickKids Research Institute, The Hospital for Sick Children, Toronto, ON, Canada

Liis Uusküla-Reimand

836. Departments of Neurosurgery and Hematology and Medical Oncology, Winship Cancer Institute and School of Medicine, Emory University, Atlanta, GA, USA

Erwin G. Van Meir

837. Department of Clinical and Molecular Medicine, Faculty of Medicine and Health Sciences, Norwegian University of Science and Technology, Trondheim, Norway

Miguel Vazquez

838. Argmix Consulting, North Vancouver, BC, Canada

Shankar Vembu

839. Department of Information Technology, Ghent University, Interuniversitair Micro-Electronica Centrum (IMEC), Ghent, Belgium

Lieven P. C. Verbeke

840. Nuffield Department of Surgical Sciences, John Radcliffe Hospital, University of Oxford, Oxford, UK

Clare Verrill

841. Institute of Mathematics and Computer Science, University of Latvia, Riga, LV, Latvia

Juris Viksna

842. Discipline of Pathology, Sydney Medical School, University of Sydney, Sydney, NSW, Australia

Ricardo E. Vilain

843. Department of Applied Mathematics and Theoretical Physics, Centre for Mathematical Sciences, University of Cambridge, Cambridge, UK

Ignacio Vázquez-García

844. Department of Epidemiology and Biostatistics, Memorial Sloan Kettering Cancer Center, New York, NY, USA

Ignacio Vázquez-García & Venkata D. Yellapantula

845. Department of Statistics, Columbia University, New York, NY, USA

Ignacio Vázquez-García

846. Department of Immunology, Genetics and Pathology, Science for Life Laboratory, Uppsala University, Uppsala, Sweden

Claes Wadelius

847. School of Electronic and Information Engineering, Xi’an Jiaotong University, Xi’an, China

Jiayin Wang & Kai Ye

848. Department of Histopathology, Cambridge University Hospitals NHS Foundation Trust, Cambridge, UK

Anne Y. Warren

849. Oxford NIHR Biomedical Research Centre, University of Oxford, Oxford, UK

David C. Wedge

850. Georgia Regents University Cancer Center, Augusta, GA, USA

Paul Weinberger

851. Wythenshawe Hospital, Manchester, UK

Ian Welch

852. Department of Genetics, Washington University School of Medicine, St.Louis, MO, USA

Michael C. Wendl

853. Department of Biological Oceanography, Leibniz Institute of Baltic Sea Research, Rostock, Germany

Johannes Werner

854. Wellcome Centre for Human Genetics, University of Oxford, Oxford, UK

Justin P. Whalley

855. Department of Molecular and Human Genetics, Baylor College of Medicine, Houston, TX, USA

David A. Wheeler

856. Thoracic Oncology Laboratory, Mayo Clinic, Rochester, MN, USA

Dennis Wigle

857. Institute for Genomic Medicine, Nationwide Children's Hospital, Columbus, OH, USA

Richard K. Wilson

858. Department of Obstetrics and Gynecology, Division of Gynecologic Oncology, Mayo Clinic, Rochester, MN, USA

Boris Winterhoff

859. International Institute for Molecular Oncology, Poznań, Poland

Maciej Wiznerowicz

860. Poznan University of Medical Sciences, Poznań, Poland

Maciej Wiznerowicz

861. Genomics and Proteomics Core Facility High Throughput Sequencing Unit, German Cancer Research Center (DKFZ), Heidelberg, Germany

Stephan Wolf

862. NCCS-VARI Translational Research Laboratory, National Cancer Centre Singapore, Singapore, Singapore

Bernice H. Wong

863. Edison Family Center for Genome Sciences and Systems Biology, Washington University, St. Louis, MO, USA

Winghing Wong

864. MRC-University of Glasgow Centre for Virus Research, Glasgow, UK

Derek W. Wright

865. Department of Medical Informatics and Clinical Epidemiology, Division of Bioinformatics and Computational Biology, OHSU Knight Cancer Institute, Oregon Health and Science University, Portland, OR, USA

Guanming Wu

866. School of Electronic Information and Communications, Huazhong University of Science and Technology, Wuhan, China

Tian Xia

867. Department of Applied Mathematics and Statistics, Johns Hopkins University, Baltimore, MD, USA

Yanxun Xu

868. Department of Cancer Genome Informatics, Graduate School of Medicine, Osaka University, Osaka, Japan

Shinichi Yachida

869. Institute of Computer Science, Heidelberg University, Heidelberg, Germany

Sergei Yakneen

870. School of Mathematics and Statistics, University of Sydney, Sydney, NSW, Australia

Jean Y. Yang

871. Ben May Department for Cancer Research, University of Chicago, Chicago, IL, USA

Lixing Yang

872. Department of Human Genetics, University of Chicago, Chicago, IL, USA

Lixing Yang

873. Tri-Institutional PhD Program in Computational Biology and Medicine, Weill Cornell Medicine, New York, NY, USA

Xiaotong Yao

874. The First Affiliated Hospital, Xi’an Jiaotong University, Xi’an, China

Kai Ye

875. Department of Medicine and Therapeutics, The Chinese University of Hong Kong, Shatin, NT, Hong Kong, China

Jun Yu

876. Department of Biostatistics, The University of Texas MD Anderson Cancer Center, Houston, TX, USA

Kaixian Yu & Hongtu Zhu

877. Duke-NUS Medical School, Singapore, Singapore

Willie Yu

878. Department of Surgery, Ruijin Hospital, Shanghai Jiaotong University School of Medicine, Shanghai, China

Yingyan Yu

879. School of Computing Science, University of Glasgow, Glasgow, UK

Ke Yuan

880. Division of Orthopaedic Surgery, Oslo University Hospital, Oslo, Norway

Olga Zaikova

881. Eastern Clinical School, Monash University, Melbourne, VIC, Australia

Nikolajs Zeps

882. Epworth HealthCare, Richmond, VIC, Australia

Nikolajs Zeps

883. Department of Biostatistics and Computational Biology, Dana-Farber Cancer Institute and Harvard Medical School, Boston, MA, USA

Cheng-Zhong Zhang

884. Department of Biomedical Informatics, College of Medicine, The Ohio State University, Columbus, OH, USA

Yan Zhang

885. The Ohio State University Comprehensive Cancer Center (OSUCCC – James), Columbus, OH, USA

Yan Zhang

886. The University of Texas School of Biomedical Informatics (SBMI) at Houston, Houston, TX, USA

Zhongming Zhao

887. Department of Biostatistics, University of North Carolina at Chapel Hill, Chapel Hill, NC, USA

Hongtu Zhu

888. Department of Biochemistry and Molecular Genetics, Feinberg School of Medicine, Northwestern University, Chicago, IL, USA

Lihua Zou

889. Faculty of Medicine and Health, University of Sydney, Sydney, NSW, Australia

Anna deFazio

890. Department of Pathology, Erasmus Medical Center Rotterdam, Rotterdam, GD, The Netherlands

Carolien H. M. van Deurzen

891. Division of Molecular Carcinogenesis, The Netherlands Cancer Institute, Amsterdam, CX, The Netherlands

L. van't Veer

892. Institute of Molecular Life Sciences and Swiss Institute of Bioinformatics, University of Zurich, Zurich, Switzerland

Christian von Mering

Consortia

PCAWG Drivers and Functional Interpretation Working Group

- Federico Abascal
- , Samirkumar B. Amin
- , Gary D. Bader
- , Pratiti Bandopadhayay
- , Jonathan Barenboim
- , Rameen Beroukhim
- , Johanna Bertl
- , Keith A. Boroevich
- , Søren Brunak
- , Peter J. Campbell
- , Joana Carlevaro-Fita
- , Dimple Chakravarty
- , Calvin Wing Yiu Chan

- , Ken Chen
- , Jung Kyoon Choi
- , Jordi Deu-Pons
- , Priyanka Dhingra
- , Klev Diamanti
- , Lars Feuerbach
- , J. Lynn Fink
- , Nuno A. Fonseca
- , Joan Frigola
- , Carlo Gambacorti-Passerini
- , Dale W. Garsed
- , Mark Gerstein
- , Gad Getz
- , Qianyun Guo
- , Ivo G. Gut
- , David Haan
- , Mark P. Hamilton
- , Nicholas J. Haradhvala
- , Arif O. Harmanci
- , Mohamed Helmy
- , Carl Herrmann
- , Julian M. Hess
- , Asger Hobolth
- , Ermin Hodzic
- , Chen Hong
- , Henrik Hornshøj
- , Keren Isaev
- , Jose M. G. Izarzugaza
- , Rory Johnson
- , Todd A. Johnson
- , Malene Juul
- , Randi Istrup Juul
- , Andre Kahles
- , Abdullah Kahraman
- , Manolis Kellis
- , Ekta Khurana
- , Jaegil Kim

- , Jong K. Kim
- , Youngwook Kim
- , Jan Komorowski
- , Jan O. Korbel
- , Sushant Kumar
- , Andrés Lanzós
- , Erik Larsson
- , Michael S. Lawrence
- , Donghoon Lee
- , Kjong-Van Lehmann
- , Shantao Li
- , Xiaotong Li
- , Ziao Lin
- , Eric Minwei Liu
- , Lucas Lochovsky
- , Shaoke Lou
- , Tobias Madsen
- , Kathleen Marchal
- , Iñigo Martincorena
- , Alexander Martinez-Fundichely
- , Yosef E. Maruvka
- , Patrick D. McGillivray
- , William Meyerson
- , Ferran Muiños
- , Loris Mularoni
- , Hidewaki Nakagawa
- , Morten Muhlig Nielsen
- , Marta Paczkowska
- , Keunchil Park
- , Kiejung Park
- , Jakob Skou Pedersen
- , Tirso Pons
- , Sergio Pulido-Tamayo
- , Benjamin J. Raphael
- , Jüri Reimand
- , Iker Reyes-Salazar
- , Matthew A. Reyna

- , Esther Rheinbay
- , Mark A. Rubin
- , Carlota Rubio-Perez
- , S. Cenk Sahinalp
- , Gordon Saksena
- , Leonidas Salichos
- , Chris Sander
- , Steven E. Schumacher
- , Mark Shackleton
- , Ofer Shapira
- , Ciyue Shen
- , Raunak Shrestha
- , Shimin Shuai
- , Nikos Sidiropoulos
- , Lina Sieverling
- , Nasa Sinnott-Armstrong
- , Lincoln D. Stein
- , Joshua M. Stuart
- , David Tamborero
- , Grace Tiao
- , Tatsuhiko Tsunoda
- , Husen M. Umer
- , Liis Uusküla-Reimand
- , Alfonso Valencia
- , Miguel Vazquez
- , Lieven P. C. Verbeke
- , Claes Wadelius
- , Lina Wadi
- , Jiayin Wang
- , Jonathan Warrell
- , Sebastian M. Waszak
- , Joachim Weischenfeldt
- , David A. Wheeler
- , Guanming Wu
- , Jun Yu
- , Jing Zhang
- , Xuanping Zhang

- , Yan Zhang
- , Zhongming Zhao
- , Lihua Zou
- & Christian von Mering

PCAWG Structural Variation Working Group

- Kadir C. Akdemir
- , Eva G. Alvarez
- , Adrian Baez-Ortega
- , Rameen Beroukhim
- , Paul C. Boutros
- , David D. L. Bowtell
- , Benedikt Brors
- , Kathleen H. Burns
- , John Busanovich
- , Peter J. Campbell
- , Kin Chan
- , Ken Chen
- , Isidro Cortés-Ciriano
- , Ana Dueso-Barroso
- , Andrew J. Dunford
- , Paul A. Edwards
- , Xavier Estivill
- , Dariush Etemadmoghadam
- , Lars Feuerbach
- , J. Lynn Fink
- , Milana Frenkel-Morgenstern
- , Dale W. Garsed
- , Mark Gerstein
- , Dmitry A. Gordenin
- , David Haan
- , James E. Haber
- , Julian M. Hess
- , Barbara Hutter
- , Marcin Imielinski
- , David T. W. Jones

- , Young Seok Ju
- , Marat D. Kazanov
- , Leszek J. Klimczak
- , Youngil Koh
- , Jan O. Korbel
- , Kiran Kumar
- , Eunjung Alice Lee
- , Jake June-Koo Lee
- , Yilong Li
- , Andy G. Lynch
- , Geoff Macintyre
- , Florian Markowetz
- , Iñigo Martincorena
- , Alexander Martinez-Fundichely
- , Matthew Meyerson
- , Satoru Miyano
- , Hidewaki Nakagawa
- , Fabio C. P. Navarro
- , Stephan Ossowski
- , Peter J. Park
- , John V. Pearson
- , Montserrat Puiggròs
- , Karsten Rippe
- , Nicola D. Roberts
- , Steven A. Roberts
- , Bernardo Rodriguez-Martin
- , Steven E. Schumacher
- , Ralph Scully
- , Mark Shackleton
- , Nikos Sidiropoulos
- , Lina Sieverling
- , Chip Stewart
- , David Torrents
- , Jose M. C. Tubio
- , Izar Villasante
- , Nicola Waddell
- , Jeremiah A. Wala

- , Joachim Weischenfeldt
- , Lixing Yang
- , Xiaotong Yao
- , Sung-Soo Yoon
- , Jorge Zamora
- & Cheng-Zhong Zhang

PCAWG Consortium

- Lauri A. Aaltonen
- , Federico Abascal
- , Adam Abeshouse
- , Hiroyuki Aburatani
- , David J. Adams
- , Nishant Agrawal
- , Keun Soo Ahn
- , Sung-Min Ahn
- , Hiroshi Aikata
- , Rehan Akbani
- , Kadir C. Akdemir
- , Hikmat Al-Ahmadie
- , Sultan T. Al-Sedairy
- , Fatima Al-Shahrour
- , Malik Alawi
- , Monique Albert
- , Kenneth Aldape
- , Ludmil B. Alexandrov
- , Adrian Ally
- , Kathryn Alsop
- , Eva G. Alvarez
- , Fernanda Amary
- , Samirkumar B. Amin
- , Brice Aminou
- , Ole Ammerpohl
- , Matthew J. Anderson
- , Yeng Ang
- , Davide Antonello
- , Pavana Anur
- , Samuel Aparicio
- , Elizabeth L. Appelbaum
- , Yasuhito Arai
- , Axel Aretz
- , Koji Arihiro

- , Shun-ichi Ariizumi
- , Joshua Armenia
- , Laurent Arnould
- , Sylvia Asa
- , Yassen Assenov
- , Gurnit Atwal
- , Sietse Aukema
- , J. Todd Auman
- , Miriam R. R. Aure
- , Philip Awadalla
- , Marta Aymerich
- , Gary D. Bader
- , Adrian Baez-Ortega
- , Matthew H. Bailey
- , Peter J. Bailey
- , Miruna Balasundaram
- , Saianand Balu
- , Pratiti Bandopadhayay
- , Rosamonde E. Banks
- , Stefano Barbi
- , Andrew P. Barbour
- , Jonathan Barenboim
- , Jill Barnholtz-Sloan
- , Hugh Barr
- , Elisabet Barrera
- , John Bartlett
- , Javier Bartolome
- , Claudio Bassi
- , Oliver F. Bathe
- , Daniel Baumhoer
- , Prashant Bavi
- , Stephen B. Baylin
- , Wojciech Bazant
- , Duncan Beardsmore
- , Timothy A. Beck
- , Sam Behjati
- , Andreas Behren

- , Beifang Niu
- , Cindy Bell
- , Sergi Beltran
- , Christopher Benz
- , Andrew Berchuck
- , Anke K. Bergmann
- , Erik N. Bergstrom
- , Benjamin P. Berman
- , Daniel M. Berney
- , Stephan H. Bernhart
- , Rameen Beroukhim
- , Mario Berrios
- , Samantha Bersani
- , Johanna Bertl
- , Miguel Betancourt
- , Vinayak Bhandari
- , Shriram G. Bhosle
- , Andrew V. Biankin
- , Matthias Bieg
- , Darell Bigner
- , Hans Binder
- , Ewan Birney
- , Michael Birrer
- , Nidhan K. Biswas
- , Bodil Bjerkehagen
- , Tom Bodenheimer
- , Lori Boice
- , Giada Bonizzato
- , Johann S. De Bono
- , Arnoud Boot
- , Moiz S. Bootwalla
- , Ake Borg
- , Arndt Borkhardt
- , Keith A. Boroevich
- , Ivan Borozan
- , Christoph Borst
- , Marcus Bosenberg

- , Mattia Bosio
- , Jacqueline Boultwood
- , Guillaume Bourque
- , Paul C. Boutros
- , G. Steven Bova
- , David T. Bowen
- , Reanne Bowlby
- , David D. L. Bowtell
- , Sandrine Boyault
- , Rich Boyce
- , Jeffrey Boyd
- , Alvis Brazma
- , Paul Brennan
- , Daniel S. Brewer
- , Arie B. Brinkman
- , Robert G. Bristow
- , Russell R. Broaddus
- , Jane E. Brock
- , Malcolm Brock
- , Annegien Broeks
- , Angela N. Brooks
- , Denise Brooks
- , Benedikt Brors
- , Søren Brunak
- , Timothy J. C. Bruxner
- , Alicia L. Bruzos
- , Alex Buchanan
- , Ivo Buchhalter
- , Christiane Buchholz
- , Susan Bullman
- , Hazel Burke
- , Birgit Burkhardt
- , Kathleen H. Burns
- , John Busanovich
- , Carlos D. Bustamante
- , Adam P. Butler
- , Atul J. Butte

- , Niall J. Byrne
- , Anne-Lise Børresen-Dale
- , Samantha J. Caesar-Johnson
- , Andy Cafferkey
- , Declan Cahill
- , Claudia Calabrese
- , Carlos Caldas
- , Fabien Calvo
- , Niedzica Camacho
- , Peter J. Campbell
- , Elias Campo
- , Cinzia Cantù
- , Shaolong Cao
- , Thomas E. Carey
- , Joana Carlevaro-Fita
- , Rebecca Carlsen
- , Ivana Cataldo
- , Mario Cazzola
- , Jonathan Cebon
- , Robert Cerfolio
- , Dianne E. Chadwick
- , Dimple Chakravarty
- , Don Chalmers
- , Calvin Wing Yiu Chan
- , Kin Chan
- , Michelle Chan-Seng-Yue
- , Vishal S. Chandan
- , David K. Chang
- , Stephen J. Chanock
- , Lorraine A. Chantrill
- , Aurélien Chateigner
- , Nilanjan Chatterjee
- , Kazuaki Chayama
- , Hsiao-Wei Chen
- , Jieming Chen
- , Ken Chen
- , Yiwen Chen

- , Zhaohong Chen
- , Andrew D. Cherniack
- , Jeremy Chien
- , Yoke-Eng Chiew
- , Suet-Feung Chin
- , Juok Cho
- , Sunghoon Cho
- , Jung Kyoon Choi
- , Wan Choi
- , Christine Chomienne
- , Zechen Chong
- , Su Pin Choo
- , Angela Chou
- , Angelika N. Christ
- , Elizabeth L. Christie
- , Eric Chuah
- , Carrie Cibulskis
- , Kristian Cibulskis
- , Sara Cingarlini
- , Peter Clapham
- , Alexander Claviez
- , Sean Cleary
- , Nicole Cloonan
- , Marek Cmero
- , Colin C. Collins
- , Ashton A. Connor
- , Susanna L. Cooke
- , Colin S. Cooper
- , Leslie Cope
- , Vincenzo Corbo
- , Matthew G. Cordes
- , Stephen M. Cordner
- , Isidro Cortés-Ciriano
- , Kyle Covington
- , Prue A. Cowin
- , Brian Craft
- , David Craft

- , Chad J. Creighton
- , Yupeng Cun
- , Erin Curley
- , Ioana Cutcutache
- , Karolina Czajka
- , Bogdan Czerniak
- , Rebecca A. Dagg
- , Ludmila Danilova
- , Maria Vittoria Davi
- , Natalie R. Davidson
- , Helen Davies
- , Ian J. Davis
- , Brandi N. Davis-Dusenbery
- , Kevin J. Dawson
- , Francisco M. De La Vega
- , Ricardo De Paoli-Iseppi
- , Timothy Defreitas
- , Angelo P. Dei Tos
- , Olivier Delaneau
- , John A. Demchok
- , Jonas Demeulemeester
- , German M. Demidov
- , Deniz Demircioğlu
- , Nening M. Dennis
- , Robert E. Denroche
- , Stefan C. Dentro
- , Nikita Desai
- , Vikram Deshpande
- , Amit G. Deshwar
- , Christine Desmedt
- , Jordi Deu-Pons
- , Noreen Dhalla
- , Neesha C. Dhani
- , Priyanka Dhingra
- , Rajiv Dhir
- , Anthony DiBiase
- , Klev Diamanti

- , Li Ding
- , Shuai Ding
- , Huy Q. Dinh
- , Luc Dirix
- , HarshaVardhan Doddapaneni
- , Nilgun Donmez
- , Michelle T. Dow
- , Ronny Drapkin
- , Oliver Drechsel
- , Ruben M. Drews
- , Serge Serge
- , Tim Dudderidge
- , Ana Dueso-Barroso
- , Andrew J. Dunford
- , Michael Dunn
- , Lewis Jonathan Dursi
- , Fraser R. Duthie
- , Ken Dutton-Regester
- , Jenna Eagles
- , Douglas F. Easton
- , Stuart Edmonds
- , Paul A. Edwards
- , Sandra E. Edwards
- , Rosalind A. Eeles
- , Anna Ehinger
- , Juergen Eils
- , Roland Eils
- , Adel El-Naggar
- , Matthew Eldridge
- , Kyle Ellrott
- , Serap Erkek
- , Georgia Escaramis
- , Shadrielle M. G. Espiritu
- , Xavier Estivill
- , Dariush Etemadmoghadam
- , Jorunn E. Eyfjord
- , Bishoy M. Faltas

- , Daiming Fan
- , Yu Fan
- , William C. Faquin
- , Claudiu Farcas
- , Matteo Fassan
- , Aquila Fatima
- , Francesco Favero
- , Nodirjon Fayzullaev
- , Ina Felau
- , Sian Fereday
- , Martin L. Ferguson
- , Vincent Ferretti
- , Lars Feuerbach
- , Matthew A. Field
- , J. Lynn Fink
- , Gaetano Finocchiaro
- , Cyril Fisher
- , Matthew W. Fittall
- , Anna Fitzgerald
- , Rebecca C. Fitzgerald
- , Adrienne M. Flanagan
- , Neil E. Fleshner
- , Paul Flicek
- , John A. Foekens
- , Kwun M. Fong
- , Nuno A. Fonseca
- , Christopher S. Foster
- , Natalie S. Fox
- , Michael Fraser
- , Scott Frazer
- , Milana Frenkel-Morgenstern
- , William Friedman
- , Joan Frigola
- , Catrina C. Fronick
- , Akihiro Fujimoto
- , Masashi Fujita
- , Masashi Fukayama

- , Lucinda A. Fulton
- , Robert S. Fulton
- , Mayuko Furuta
- , P. Andrew Futreal
- , Anja Füllgrabe
- , Stacey B. Gabriel
- , Steven Gallinger
- , Carlo Gambacorti-Passerini
- , Jianjiong Gao
- , Shengjie Gao
- , Levi Garraway
- , Øystein Garred
- , Erik Garrison
- , Dale W. Garsed
- , Nils Gehlenborg
- , Josep L. L. Gelpi
- , Joshy George
- , Daniela S. Gerhard
- , Clarissa Gerhauser
- , Jeffrey E. Gershenwald
- , Mark Gerstein
- , Moritz Gerstung
- , Gad Getz
- , Mohammed Ghori
- , Ronald Ghossein
- , Nasra H. Giama
- , Richard A. Gibbs
- , Bob Gibson
- , Anthony J. Gill
- , Pelvender Gill
- , Dilip D. Giri
- , Dominik Glodzik
- , Vincent J. Gnanapragasam
- , Maria Elisabeth Goebler
- , Mary J. Goldman
- , Carmen Gomez
- , Santiago Gonzalez

- , Abel Gonzalez-Perez
- , Dmitry A. Gordenin
- , James Gossage
- , Kunihito Gotoh
- , Ramaswamy Govindan
- , Dorthe Grabau
- , Janet S. Graham
- , Robert C. Grant
- , Anthony R. Green
- , Eric Green
- , Liliana Greger
- , Nicola Grehan
- , Sonia Grimaldi
- , Sean M. Grimmond
- , Robert L. Grossman
- , Adam Grundhoff
- , Gunes Gundem
- , Qianyun Guo
- , Manaswi Gupta
- , Shailja Gupta
- , Ivo G. Gut
- , Marta Gut
- , Jonathan Göke
- , Gavin Ha
- , Andrea Haake
- , David Haan
- , Siegfried Haas
- , Kerstin Haase
- , James E. Haber
- , Nina Habermann
- , Faraz Hach
- , Syed Haider
- , Natsuko Hama
- , Freddie C. Hamdy
- , Anne Hamilton
- , Mark P. Hamilton
- , Leng Han

- , George B. Hanna
- , Martin Hansmann
- , Nicholas J. Haradhvala
- , Olivier Harismendy
- , Ivon Harliwong
- , Arif O. Harmanci
- , Eoghan Harrington
- , Takanori Hasegawa
- , David Haussler
- , Steve Hawkins
- , Shinya Hayami
- , Shuto Hayashi
- , D. Neil Hayes
- , Stephen J. Hayes
- , Nicholas K. Hayward
- , Steven Hazell
- , Yao He
- , Allison P. Heath
- , Simon C. Heath
- , David Hedley
- , Apurva M. Hegde
- , David I. Heiman
- , Michael C. Heinold
- , Zachary Heins
- , Lawrence E. Heisler
- , Eva Hellstrom-Lindberg
- , Mohamed Helmy
- , Seong Gu Heo
- , Austin J. Hepperla
- , José María Heredia-Genestar
- , Carl Herrmann
- , Peter Hersey
- , Julian M. Hess
- , Holmfridur Hilmarsdottir
- , Jonathan Hinton
- , Satoshi Hirano
- , Nobuyoshi Hiraoka

- , Katherine A. Hoadley
- , Asger Hobolth
- , Ermin Hodzic
- , Jessica I. Hoell
- , Steve Hoffmann
- , Oliver Hofmann
- , Andrea Holbrook
- , Aliaksei Z. Holik
- , Michael A. Hollingsworth
- , Oliver Holmes
- , Robert A. Holt
- , Chen Hong
- , Eun Pyo Hong
- , Jongwhi H. Hong
- , Gerrit K. Hooijer
- , Henrik Hornshøj
- , Fumie Hosoda
- , Yong Hou
- , Volker Hovestadt
- , William Howat
- , Alan P. Hoyle
- , Ralph H. Hruban
- , Jianhong Hu
- , Taobo Hu
- , Xing Hua
- , Kuan-lin Huang
- , Mei Huang
- , Mi Ni Huang
- , Vincent Huang
- , Yi Huang
- , Wolfgang Huber
- , Thomas J. Hudson
- , Michael Hummel
- , Jillian A. Hung
- , David Huntsman
- , Ted R. Hupp
- , Jason Huse

- , Matthew R. Huska
- , Barbara Hutter
- , Carolyn M. Hutter
- , Daniel Hübschmann
- , Christine A. Iacobuzio-Donahue
- , Charles David Imbusch
- , Marcin Imielinski
- , Seiya Imoto
- , William B. Isaacs
- , Keren Isaev
- , Shumpei Ishikawa
- , Murat Iskar
- , S. M. Ashiqul Islam
- , Michael Ittmann
- , Sinisa Ivkovic
- , Jose M. G. Izarzugaza
- , Jocelyne Jacquemier
- , Valerie Jakrot
- , Nigel B. Jamieson
- , Gun Ho Jang
- , Se Jin Jang
- , Joy C. Jayaseelan
- , Reyka Jayasinghe
- , Stuart R. Jefferys
- , Karine Jegalian
- , Jennifer L. Jennings
- , Seung-Hyup Jeon
- , Lara Jerman
- , Yuan Ji
- , Wei Jiao
- , Peter A. Johansson
- , Amber L. Johns
- , Jeremy Johns
- , Rory Johnson
- , Todd A. Johnson
- , Clemency Jolly
- , Yann Joly

- , Jon G. Jonasson
- , Corbin D. Jones
- , David R. Jones
- , David T. W. Jones
- , Nic Jones
- , Steven J. M. Jones
- , Jos Jonkers
- , Young Seok Ju
- , Hartmut Juhl
- , Jongsun Jung
- , Malene Juul
- , Randi Istrup Juul
- , Sissel Juul
- , Natalie Jäger
- , Rolf Kabbe
- , Andre Kahles
- , Abdullah Kahraman
- , Vera B. Kaiser
- , Hojabr Kakavand
- , Sangeetha Kalimuthu
- , Christof von Kalle
- , Koo Jeong Kang
- , Katalin Karaszi
- , Beth Karlan
- , Rosa Karlić
- , Dennis Karsch
- , Katayoon Kasaian
- , Karin S. Kassahn
- , Hitoshi Katai
- , Mamoru Kato
- , Hiroto Katoh
- , Yoshiiku Kawakami
- , Jonathan D. Kay
- , Stephen H. Kazakoff
- , Marat D. Kazanov
- , Maria Keays
- , Electron Kebebew

- , Richard F. Kefford
- , Manolis Kellis
- , James G. Kench
- , Catherine J. Kennedy
- , Jules N. A. Kerssemakers
- , David Khoo
- , Vincent Khoo
- , Narong Khuntikeo
- , Ekta Khurana
- , Helena Kilpinen
- , Hark Kyun Kim
- , Hyung-Lae Kim
- , Hyung-Yong Kim
- , Hyunghwan Kim
- , Jaegil Kim
- , Jihoon Kim
- , Jong K. Kim
- , Youngwook Kim
- , Tari A. King
- , Wolfram Klapper
- , Kortine Kleinheinz
- , Leszek J. Klimczak
- , Stian Knappskog
- , Michael Kneba
- , Bartha M. Knoppers
- , Youngil Koh
- , Jan Komorowski
- , Daisuke Komura
- , Mitsuhiro Komura
- , Gu Kong
- , Marcel Kool
- , Jan O. Korbel
- , Viktoriya Korchina
- , Andrey Korshunov
- , Michael Koscher
- , Roelof Koster
- , Zsofia Kote-Jarai

- , Antonios Koures
- , Milena Kovacevic
- , Barbara Kremeyer
- , Helene Kretzmer
- , Markus Kreuz
- , Savitri Krishnamurthy
- , Dieter Kube
- , Kiran Kumar
- , Pardeep Kumar
- , Sushant Kumar
- , Yogesh Kumar
- , Ritika Kundra
- , Kirsten Kübler
- , Ralf Küppers
- , Jesper Lagergren
- , Phillip H. Lai
- , Peter W. Laird
- , Sunil R. Lakhani
- , Christopher M. Lalansingh
- , Emilie Lalonde
- , Fabien C. Lamaze
- , Adam Lambert
- , Eric Lander
- , Pablo Landgraf
- , Luca Landoni
- , Anita Langerød
- , Andrés Lanzós
- , Denis Larsimont
- , Erik Larsson
- , Mark Lathrop
- , Loretta M. S. Lau
- , Chris Lawerenz
- , Rita T. Lawlor
- , Michael S. Lawrence
- , Alexander J. Lazar
- , Ana Mijalkovic Lazic
- , Xuan Le

- , Darlene Lee
- , Donghoon Lee
- , Eunjung Alice Lee
- , Hee Jin Lee
- , Jake June-Koo Lee
- , Jeong-Yeon Lee
- , Juhee Lee
- , Ming Ta Michael Lee
- , Henry Lee-Six
- , Kjong-Van Lehmann
- , Hans Lehrach
- , Dido Lenze
- , Conrad R. Leonard
- , Daniel A. Leongamornlert
- , Ignaty Leshchiner
- , Louis Letourneau
- , Ivica Letunic
- , Douglas A. Levine
- , Lora Lewis
- , Tim Ley
- , Chang Li
- , Constance H. Li
- , Haiyan Irene Li
- , Jun Li
- , Lin Li
- , Shantao Li
- , Siliang Li
- , Xiaobo Li
- , Xiaotong Li
- , Xinyue Li
- , Yilong Li
- , Han Liang
- , Sheng-Ben Liang
- , Peter Lichter
- , Pei Lin
- , Ziao Lin
- , W. M. Linehan

- , Ole Christian Lingjærde
- , Dongbing Liu
- , Eric Minwei Liu
- , Fei-Fei Fei Liu
- , Fenglin Liu
- , Jia Liu
- , Xingmin Liu
- , Julie Livingstone
- , Dimitri Livitz
- , Naomi Livni
- , Lucas Lochovsky
- , Markus Loeffler
- , Georgina V. Long
- , Armando Lopez-Guillermo
- , Shaoke Lou
- , David N. Louis
- , Laurence B. Lovat
- , Yiling Lu
- , Yong-Jie Lu
- , Youyong Lu
- , Claudio Luchini
- , Ilinca Lungu
- , Xuemei Luo
- , Hayley J. Luxton
- , Andy G. Lynch
- , Lisa Lype
- , Cristina López
- , Carlos López-Otín
- , Eric Z. Ma
- , Yussanne Ma
- , Gaetan MacGrogan
- , Shona MacRae
- , Geoff Macintyre
- , Tobias Madsen
- , Kazuhiro Maejima
- , Andrea Mafficini
- , Dennis T. Maglinte

- , Arindam Maitra
- , Partha P. Majumder
- , Luca Malcovati
- , Salem Malikic
- , Giuseppe Malleo
- , Graham J. Mann
- , Luisa Mantovani-Löffler
- , Kathleen Marchal
- , Giovanni Marchegiani
- , Elaine R. Mardis
- , Adam A. Margolin
- , Maximillian G. Marin
- , Florian Markowetz
- , Julia Markowski
- , Jeffrey Marks
- , Tomas Marques-Bonet
- , Marco A. Marra
- , Luke Marsden
- , John W. M. Martens
- , Sancha Martin
- , Jose I. Martin-Subero
- , Iñigo Martincorena
- , Alexander Martinez-Fundichely
- , Yosef E. Maruvka
- , R. Jay Mashl
- , Charlie E. Massie
- , Thomas J. Matthew
- , Lucy Matthews
- , Erik Mayer
- , Simon Mayes
- , Michael Mayo
- , Faridah Mbabaali
- , Karen McCune
- , Ultan McDermott
- , Patrick D. McGillivray
- , Michael D. McLellan
- , John D. McPherson

- , John R. McPherson
- , Treasa A. McPherson
- , Samuel R. Meier
- , Alice Meng
- , Shaowu Meng
- , Andrew Menzies
- , Neil D. Merrett
- , Sue Merson
- , Matthew Meyerson
- , William Meyerson
- , Piotr A. Mieczkowski
- , George L. Mihaiescu
- , Sanja Mijalkovic
- , Tom Mikkelsen
- , Michele Milella
- , Linda Mileshkin
- , Christopher A. Miller
- , David K. Miller
- , Jessica K. Miller
- , Gordon B. Mills
- , Ana Milovanovic
- , Sarah Minner
- , Marco Miotto
- , Gisela Mir Arnau
- , Lisa Mirabello
- , Chris Mitchell
- , Thomas J. Mitchell
- , Satoru Miyano
- , Naoki Miyoshi
- , Shinichi Mizuno
- , Fruzsina Molnár-Gábor
- , Malcolm J. Moore
- , Richard A. Moore
- , Sandro Morganella
- , Quaid D. Morris
- , Carl Morrison
- , Lisle E. Mose

- , Catherine D. Moser
- , Ferran Muiños
- , Loris Mularoni
- , Andrew J. Mungall
- , Karen Mungall
- , Elizabeth A. Musgrove
- , Ville Mustonen
- , David Mutch
- , Francesc Muyas
- , Donna M. Muzny
- , Alfonso Muñoz
- , Jerome Myers
- , Ola Myklebost
- , Peter Möller
- , Genta Nagae
- , Adnan M. Nagrial
- , Hardeep K. Nahal-Bose
- , Hitoshi Nakagama
- , Hidewaki Nakagawa
- , Hiromi Nakamura
- , Toru Nakamura
- , Kaoru Nakano
- , Tannistha Nandi
- , Jyoti Nangalia
- , Mia Nastic
- , Arcadi Navarro
- , Fabio C. P. Navarro
- , David E. Neal
- , Gerd Nettekoven
- , Felicity Newell
- , Steven J. Newhouse
- , Yulia Newton
- , Alvin Wei Tian Ng
- , Anthony Ng
- , Jonathan Nicholson
- , David Nicol
- , Yongzhan Nie

- , G. Petur Nielsen
- , Morten Muhlig Nielsen
- , Serena Nik-Zainal
- , Michael S. Noble
- , Katia Nones
- , Paul A. Northcott
- , Faiyaz Notta
- , Brian D. O'Connor
- , Peter O'Donnell
- , Maria O'Donovan
- , Sarah O'Meara
- , Brian Patrick O'Neill
- , J. Robert O'Neill
- , David Ocana
- , Angelica Ochoa
- , Layla Oesper
- , Christopher Ogden
- , Hideki Ohdan
- , Kazuhiro Ohi
- , Lucila Ohno-Machado
- , Karin A. Oien
- , Akinyemi I. Ojesina
- , Hidenori Ojima
- , Takuji Okusaka
- , Larsson Omberg
- , Choon Kiat Ong
- , Stephan Ossowski
- , German Ott
- , B. F. Francis Ouellette
- , Christine P'ng
- , Marta Paczkowska
- , Salvatore Paiella
- , Chawalit Pairojkul
- , Marina Pajic
- , Qiang Pan-Hammarström
- , Elli Papaemmanuil
- , Irene Papatheodorou

- , Nagarajan Paramasivam
- , Ji Wan Park
- , Joong-Won Park
- , Keunchil Park
- , Kiejung Park
- , Peter J. Park
- , Joel S. Parker
- , Simon L. Parsons
- , Harvey Pass
- , Danielle Pasternack
- , Alessandro Pastore
- , Ann-Marie Patch
- , Iris Pauporté
- , Antonio Pea
- , John V. Pearson
- , Chandra Sekhar Pedamallu
- , Jakob Skou Pedersen
- , Paolo Pederzoli
- , Martin Peifer
- , Nathan A. Pennell
- , Charles M. Perou
- , Marc D. Perry
- , Gloria M. Petersen
- , Myron Peto
- , Nicholas Petrelli
- , Robert Petryszak
- , Stefan M. Pfister
- , Mark Phillips
- , Oriol Pich
- , Hilda A. Pickett
- , Todd D. Pihl
- , Nischalan Pillay
- , Sarah Pinder
- , Mark Pinese
- , Andreia V. Pinho
- , Esa Pitkänen
- , Xavier Pivot

- , Elena Piñeiro-Yáñez
- , Laura Planko
- , Christoph Plass
- , Paz Polak
- , Tirso Pons
- , Irinel Popescu
- , Olga Potapova
- , Aparna Prasad
- , Shaun R. Preston
- , Manuel Prinz
- , Antonia L. Pritchard
- , Stephenie D. Prokopec
- , Elena Provenzano
- , Xose S. Puente
- , Sonia Puig
- , Montserrat Puiggròs
- , Sergio Pulido-Tamayo
- , Gulietta M. Pupo
- , Colin A. Purdie
- , Michael C. Quinn
- , Raquel Rabionet
- , Janet S. Rader
- , Bernhard Radlwimmer
- , Petar Radovic
- , Benjamin Raeder
- , Keiran M. Raine
- , Manasa Ramakrishna
- , Kamna Ramakrishnan
- , Suresh Ramalingam
- , Benjamin J. Raphael
- , W. Kimryn Rathmell
- , Tobias Rausch
- , Guido Reifenberger
- , Jüri Reimand
- , Jorge Reis-Filho
- , Victor Reuter
- , Iker Reyes-Salazar

- , Matthew A. Reyna
- , Sheila M. Reynolds
- , Esther Rheinbay
- , Yasser Riazalhosseini
- , Andrea L. Richardson
- , Julia Richter
- , Matthew Ringel
- , Markus Ringnér
- , Yasushi Rino
- , Karsten Rippe
- , Jeffrey Roach
- , Lewis R. Roberts
- , Nicola D. Roberts
- , Steven A. Roberts
- , A. Gordon Robertson
- , Alan J. Robertson
- , Javier Bartolomé Rodriguez
- , Bernardo Rodriguez-Martin
- , F. Germán Rodríguez-González
- , Michael H. A. Roehrl
- , Marius Rohde
- , Hirofumi Rokutan
- , Gilles Romieu
- , Ilse Rooman
- , Tom Roques
- , Daniel Rosebrock
- , Mara Rosenberg
- , Philip C. Rosenstiel
- , Andreas Rosenwald
- , Edward W. Rowe
- , Romina Royo
- , Steven G. Rozen
- , Yulia Rubanova
- , Mark A. Rubin
- , Carlota Rubio-Perez
- , Vasilisa A. Rudneva
- , Borislav C. Rusev

- , Andrea Ruzzenente
- , Gunnar Rätsch
- , Radhakrishnan Sabarinathan
- , Veronica Y. Sabelnykova
- , Sara Sadeghi
- , S. Cenk Sahinalp
- , Natalie Saini
- , Mihoko Saito-Adachi
- , Gordon Saksena
- , Adriana Salcedo
- , Roberto Salgado
- , Leonidas Salichos
- , Richard Sallari
- , Charles Saller
- , Roberto Salvia
- , Michelle Sam
- , Jaswinder S. Samra
- , Francisco Sanchez-Vega
- , Chris Sander
- , Grant Sanders
- , Rajiv Sarin
- , Iman Sarrafi
- , Aya Sasaki-Oku
- , Torill Sauer
- , Guido Sauter
- , Robyn P. M. Saw
- , Maria Scardoni
- , Christopher J. Scarlett
- , Aldo Scarpa
- , Ghislaine Scelo
- , Dirk Schadendorf
- , Jacqueline E. Schein
- , Markus B. Schilhabel
- , Matthias Schlesner
- , Thorsten Schlomm
- , Heather K. Schmidt
- , Sarah-Jane Schramm

- , Stefan Schreiber
- , Nikolaus Schultz
- , Steven E. Schumacher
- , Roland F. Schwarz
- , Richard A. Scolyer
- , David Scott
- , Ralph Scully
- , Raja Seethala
- , Ayellet V. Segre
- , Iris Selander
- , Colin A. Semple
- , Yasin Senbabaoglu
- , Subhajit Sengupta
- , Elisabetta Sereni
- , Stefano Serra
- , Dennis C. Sgroi
- , Mark Shackleton
- , Nimish C. Shah
- , Sagedeh Shahabi
- , Catherine A. Shang
- , Ping Shang
- , Ofer Shapira
- , Troy Shelton
- , Ciyue Shen
- , Hui Shen
- , Rebecca Shepherd
- , Ruian Shi
- , Yan Shi
- , Yu-Jia Shiah
- , Tatsuhiro Shibata
- , Juliann Shih
- , Eigo Shimizu
- , Kiyo Shimizu
- , Seung Jun Shin
- , Yuichi Shiraishi
- , Tal Shmaya
- , Ilya Shmulevich

- , Solomon I. Shorser
- , Charles Short
- , Raunak Shrestha
- , Suyash S. Shringarpure
- , Craig Shriver
- , Shimin Shuai
- , Nikos Sidiropoulos
- , Reiner Siebert
- , Anieta M. Sieuwerts
- , Lina Sieverling
- , Sabina Signoretti
- , Katarzyna O. Sikora
- , Michele Simbolo
- , Ronald Simon
- , Janae V. Simons
- , Jared T. Simpson
- , Peter T. Simpson
- , Samuel Singer
- , Nasa Sinnott-Armstrong
- , Payal Sipahimalani
- , Tara J. Skelly
- , Marcel Smid
- , Jaclyn Smith
- , Karen Smith-McCune
- , Nicholas D. Socci
- , Heidi J. Sofia
- , Matthew G. Soloway
- , Lei Song
- , Anil K. Sood
- , Sharmila Sothi
- , Christos Sotiriou
- , Cameron M. Soulette
- , Paul N. Span
- , Paul T. Spellman
- , Nicola Sperandio
- , Andrew J. Spillane
- , Oliver Spiro

- , Jonathan Spring
- , Johan Staaf
- , Peter F. Stadler
- , Peter Staib
- , Stefan G. Stark
- , Lucy Stebbings
- , Ólafur Andri Stefánsson
- , Oliver Stegle
- , Lincoln D. Stein
- , Alasdair Stenhouse
- , Chip Stewart
- , Stephan Stilgenbauer
- , Miranda D. Stobbe
- , Michael R. Stratton
- , Jonathan R. Stretch
- , Adam J. Struck
- , Joshua M. Stuart
- , Henk G. Stunnenberg
- , Hong Su
- , Xiaoping Su
- , Ren X. Sun
- , Stephanie Sungalee
- , Hana Susak
- , Akihiro Suzuki
- , Fred Sweep
- , Monika Szczepanowski
- , Holger Sültmann
- , Takashi Yugawa
- , Angela Tam
- , David Tamborero
- , Benita Kiat Tee Tan
- , Donghui Tan
- , Patrick Tan
- , Hiroko Tanaka
- , Hirokazu Taniguchi
- , Tomas J. Tanskanen
- , Maxime Tarabichi

- , Roy Tarnuzzer
- , Patrick Tarpey
- , Morgan L. Taschuk
- , Kenji Tatsuno
- , Simon Tavaré
- , Darrin F. Taylor
- , Amaro Taylor-Weiner
- , Jon W. Teague
- , Bin Tean Teh
- , Varsha Tembe
- , Javier Temes
- , Kevin Thai
- , Sarah P. Thayer
- , Nina Thiessen
- , Gilles Thomas
- , Sarah Thomas
- , Alan Thompson
- , Alastair M. Thompson
- , John F. F. Thompson
- , R. Houston Thompson
- , Heather Thorne
- , Leigh B. Thorne
- , Adrian Thorogood
- , Grace Tiao
- , Nebojsa Tijanic
- , Lee E. Timms
- , Roberto Tirabosco
- , Marta Tojo
- , Stefania Tommasi
- , Christopher W. Toon
- , Umut H. Toprak
- , David Torrents
- , Giampaolo Tortora
- , Jörg Tost
- , Yasushi Totoki
- , David Townend
- , Nadia Traficante

- , Isabelle Treilleux
- , Jean-Rémi Trotta
- , Lorenz H. P. Trümper
- , Ming Tsao
- , Tatsuhiko Tsunoda
- , Jose M. C. Tubio
- , Olga Tucker
- , Richard Turkington
- , Daniel J. Turner
- , Andrew Tutt
- , Masaki Ueno
- , Naoto T. Ueno
- , Christopher Umbricht
- , Husen M. Umer
- , Timothy J. Underwood
- , Lara Urban
- , Tomoko Urushidate
- , Tetsuo Ushiku
- , Liis Uusküla-Reimand
- , Alfonso Valencia
- , David J. Van Den Berg
- , Steven Van Laere
- , Peter Van Loo
- , Erwin G. Van Meir
- , Gert G. Van den Eynden
- , Theodorus Van der Kwast
- , Naveen Vasudev
- , Miguel Vazquez
- , Ravikiran Vedururu
- , Umadevi Veluvolu
- , Shankar Vembu
- , Lieven P. C. Verbeke
- , Peter Vermeulen
- , Clare Verrill
- , Alain Viari
- , David Vicente
- , Caterina Vicentini

- , K. VijayRaghavan
- , Juris Viksna
- , Ricardo E. Vilain
- , Izar Villasante
- , Anne Vincent-Salomon
- , Tapio Visakorpi
- , Douglas Voet
- , Paresh Vyas
- , Ignacio Vázquez-García
- , Nick M. Waddell
- , Nicola Waddell
- , Claes Wadelius
- , Lina Wadi
- , Rabea Wagener
- , Jeremiah A. Wala
- , Jian Wang
- , Jiayin Wang
- , Linghua Wang
- , Qi Wang
- , Wenyi Wang
- , Yumeng Wang
- , Zhining Wang
- , Paul M. Waring
- , Hans-Jörg Warnatz
- , Jonathan Warrell
- , Anne Y. Warren
- , Sebastian M. Waszak
- , David C. Wedge
- , Dieter Weichenhan
- , Paul Weinberger
- , John N. Weinstein
- , Joachim Weischenfeldt
- , Daniel J. Weisenberger
- , Ian Welch
- , Michael C. Wendl
- , Johannes Werner
- , Justin P. Whalley

- , David A. Wheeler
- , Hayley C. Whitaker
- , Dennis Wigle
- , Matthew D. Wilkerson
- , Ashley Williams
- , James S. Wilmott
- , Gavin W. Wilson
- , Julie M. Wilson
- , Richard K. Wilson
- , Boris Winterhoff
- , Jeffrey A. Wintersinger
- , Maciej Wiznerowicz
- , Stephan Wolf
- , Bernice H. Wong
- , Tina Wong
- , Winghing Wong
- , Youngchoon Woo
- , Scott Wood
- , Bradly G. Wouters
- , Adam J. Wright
- , Derek W. Wright
- , Mark H. Wright
- , Chin-Lee Wu
- , Dai-Ying Wu
- , Guanming Wu
- , Jianmin Wu
- , Kui Wu
- , Yang Wu
- , Zhenggang Wu
- , Liu Xi
- , Tian Xia
- , Qian Xiang
- , Xiao Xiao
- , Rui Xing
- , Heng Xiong
- , Qinying Xu
- , Yanxun Xu

- , Hong Xue
- , Shinichi Yachida
- , Sergei Yakneen
- , Rui Yamaguchi
- , Takafumi N. Yamaguchi
- , Masakazu Yamamoto
- , Shogo Yamamoto
- , Hiroki Yamaue
- , Fan Yang
- , Huanming Yang
- , Jean Y. Yang
- , Liming Yang
- , Lixing Yang
- , Shanlin Yang
- , Tsun-Po Yang
- , Yang Yang
- , Xiaotong Yao
- , Marie-Laure Yaspo
- , Lucy Yates
- , Christina Yau
- , Chen Ye
- , Kai Ye
- , Venkata D. Yellapantula
- , Christopher J. Yoon
- , Sung-Soo Yoon
- , Fouad Yousif
- , Jun Yu
- , Kaixian Yu
- , Willie Yu
- , Yingyan Yu
- , Ke Yuan
- , Yuan Yuan
- , Denis Yuen
- , Takashi Yugawa
- , Christina K. Yung
- , Olga Zaikova
- , Jorge Zamora

- , Marc Zapatka
- , Jean C. Zenklusen
- , Thorsten Zenz
- , Nikolajs Zeps
- , Cheng-Zhong Zhang
- , Fan Zhang
- , Hailei Zhang
- , Hongwei Zhang
- , Hongxin Zhang
- , Jiashan Zhang
- , Jing Zhang
- , Junjun Zhang
- , Xiuqing Zhang
- , Xuanping Zhang
- , Yan Zhang
- , Zemin Zhang
- , Zhongming Zhao
- , Liangtao Zheng
- , Xiuqing Zheng
- , Wanding Zhou
- , Yong Zhou
- , Bin Zhu
- , Hongtu Zhu
- , Jingchun Zhu
- , Shida Zhu
- , Lihua Zou
- , Xueqing Zou
- , Anna deFazio
- , Nicholas van As
- , Carolien H. M. van Deurzen
- , Marc J. van de Vijver
- , L. van’t Veer
- & Christian von Mering

Corresponding authors

Correspondence to Joachim Weischenfeldt, Rameen Beroukhim, Iñigo Martincorena, Jakob Skou Pedersen or Gad Getz.

Rights and permissions

Open Access This article is licensed under a Creative Commons Attribution 4.0 International License, which permits use, sharing, adaptation, distribution and reproduction in any medium or format, as long as you give appropriate credit to the original author(s) and the source, provide a link to the Creative Commons license, and indicate if changes were made. The images or other third party material in this article are included in the article's Creative Commons license, unless indicated otherwise in a credit line to the material. If material is not included in the article's Creative Commons license and your intended use is not permitted by statutory regulation or exceeds the permitted use, you will need to obtain permission directly from the copyright holder. To view a copy of this license, visit http://creativecommons.org/licenses/by/4.0/.

Reprints and Permissions

About this article

Cite this article

Rheinbay, E., Nielsen, M.M., Abascal, F. *et al.* Author Correction: Analyses of non-coding somatic drivers in 2,658 cancer whole genomes. *Nature* **614**, E40 (2023). https://doi.org/10.1038/s41586-022-05599-9

- Published: 25 January 2023
- Issue Date: 16 February 2023
- DOI: https://doi.org/10.1038/s41586-022-05599-9

Share this article

Anyone you share the following link with will be able to read this content:

Get shareable link

Sorry, a shareable link is not currently available for this article.

Copy to clipboard

Provided by the Springer Nature SharedIt content-sharing initiative

---

This article was downloaded by **calibre** from https://www.nature.com/articles/s41586-022-05599-9

- Author Correction
- Open Access
- Published: 25 January 2023

Author Correction: The repertoire of mutational signatures in human cancer

- Ludmil B. Alexandrov,
- Jaegil Kim,
- Nicholas J. Haradhvala,
- Mi Ni Huang,
- Alvin Wei Tian Ng,
- Yang Wu,
- Arnoud Boot,
- Kyle R. Covington,
- Dmitry A. Gordenin,
- Erik N. Bergstrom,
- S. M. Ashiqul Islam,
- Nuria Lopez-Bigas,
- Leszek J. Klimczak,
- John R. McPherson,
- Sandro Morganella,
- Radhakrishnan Sabarinathan,
- David A. Wheeler,
- Ville Mustonen,
- PCAWG Mutational Signatures Working Group,
- Gad Getz,
- Steven G. Rozen ,
- Michael R. Stratton &
- PCAWG Consortium

Show authors

Nature **volume 614**, page E41 (2023)

- 1092 Accesses
- 1 Altmetric
- Metrics details

The Original Article was published on 05 February 2020

Correction to: *Nature* https://doi.org/10.1038/s41586-020-1943-3 Published online 5 February 2020

In the published version of this paper, the members of the Pan-Cancer Analysis of Whole Genomes (PCAWG) Consortium were listed in the Supplementary Information; however, these members should have been included in the main paper. The original Article has been corrected to include the members and affiliations of the PCAWG Consortium in the main paper; the corrections have been made to the HTML version of the Article but not the PDF version. Additional minor corrections to affiliations have been made to the PDF and HTML versions of the original Article for consistency of information between the PCAWG list and the main paper.

Author information

Author notes

1. These authors contributed equally: Ludmil B. Alexandrov, Jaegil Kim, Nicholas J. Haradhvala, Mi Ni Huang
2. These authors jointly supervised this work: Gad Getz, Steven G. Rozen, Michael R. Stratton
3. A list of members and their affiliations appears at the end of the paper

4. A list of members and their affiliations appears online

Authors and Affiliations

1. Department of Cellular and Molecular Medicine, Department of Bioengineering, Moores Cancer Center, University of California, San Diego, CA, USA

   Ludmil B. Alexandrov, Erik N. Bergstrom, S. M. Ashiqul Islam, Ludmil B. Alexandrov, Erik N. Bergstrom & S. M. Ashiqul Islam

2. Broad Institute of MIT and Harvard, Cambridge, MA, USA

   Jaegil Kim, Nicholas J. Haradhvala, Gad Getz, Nicholas J. Haradhvala, Jaegil Kim, Michael Lawrence, Paz Polak, Fouad Yousif & Gad Getz

3. Center for Cancer Research, Massachusetts General Hospital, Boston, MA, USA

   Nicholas J. Haradhvala, Gad Getz, Nicholas J. Haradhvala, Paz Polak & Gad Getz

4. Programme in Cancer & Stem Cell Biology, Duke-NUS Medical School, Singapore, Singapore

   Mi Ni Huang, Alvin Wei Tian Ng, Yang Wu, Arnoud Boot, John R. McPherson, Arnoud Boot, Mi Ni Huang, John R. McPherson, Alvin Wei Tian Ng, Steven G. Rozen, Bin Tean Teh, Yang Wu, Willie Yu & Steven G. Rozen

5. Centre for Computational Biology, Duke-NUS Medical School, Singapore, Singapore

   Mi Ni Huang, Alvin Wei Tian Ng, Yang Wu, Arnoud Boot, John R. McPherson, Arnoud Boot, Mi Ni Huang, John R. McPherson, Alvin

Wei Tian Ng, Steven G. Rozen, Yang Wu, Willie Yu & Steven G. Rozen

6. Human Genome Sequencing Center, Baylor College of Medicine, Houston, TX, USA

   Kyle R. Covington, David A. Wheeler, Kyle R. Covington & David A. Wheeler

7. Dan L. Duncan Cancer Center, Baylor College of Medicine, Houston, TX, USA

   Kyle R. Covington & Kyle R. Covington

8. Genome Integrity and Structural Biology Laboratory, National Institute of Environmental Health Sciences (NIEHS), Durham, NC, USA

   Dmitry A. Gordenin, Dmitry A. Gordenin & Natalie Saini

9. Institute for Research in Biomedicine (IRB Barcelona), The Barcelona Institute of Science and Technology, Barcelona, Spain

   Nuria Lopez-Bigas & Nuria Lopez-Bigas

10. Research Program on Biomedical Informatics, Universitat Pompeu Fabra, Barcelona, Spain

    Nuria Lopez-Bigas, Radhakrishnan Sabarinathan, Nuria Lopez-Bigas & Radhakrishnan Sabarinathan

11. Institució Catalana de Recerca i Estudis Avançats (ICREA), Barcelona, Spain

    Nuria Lopez-Bigas & Nuria Lopez-Bigas

12. Integrative Bioinformatics Support Group, National Institute of Environmental Health Sciences (NIEHS), Durham, NC, USA

Leszek J. Klimczak & Leszek J. Klimczak

13. Wellcome Sanger Institute, Hinxton, UK

Sandro Morganella, Iñigo Martincorena, Sandro Morganella, Michael R. Stratton, Ignacio Vázquez-García & Michael R. Stratton

14. National Centre for Biological Sciences, Tata Institute of Fundamental Research, Bangalore, India

Radhakrishnan Sabarinathan & Radhakrishnan Sabarinathan

15. Institute for Research in Biomedicine (IRB Barcelona), The Barcelona Institute of Science and Technology, Barcelona, Spain

Radhakrishnan Sabarinathan & Radhakrishnan Sabarinathan

16. Department of Molecular and Human Genetics, Baylor College of Medicine, Houston, TX, USA

David A. Wheeler & David A. Wheeler

17. Department of Computer Science, University of Helsinki, Helsinki, Finland

Ville Mustonen & Ville Mustonen

18. Organismal and Evolutionary Biology Research Programme, University of Helsinki, Helsinki, Finland

Ville Mustonen & Ville Mustonen

19. Institute of Biotechnology, University of Helsinki, Helsinki, Finland

Ville Mustonen & Ville Mustonen

20. Department of Pathology, Massachusetts General Hospital, Boston, MA, USA

Gad Getz & Gad Getz

21. Harvard Medical School, Boston, MA, USA

Gad Getz, Paz Polak & Gad Getz

22. SingHealth, Duke-NUS Institute of Precision Medicine, National Heart Centre Singapore, Singapore, Singapore

Steven G. Rozen, Bin Tean Teh & Steven G. Rozen

23. Department of Medical Biophysics, University of Toronto, Toronto, Ontario, Canada

Paul Boutros

24. University of California Los Angeles, Los Angeles, CA, USA

Paul Boutros

25. Computational Biology Program, Ontario Institute for Cancer Research, Toronto, Ontario, Canada

Paul Boutros & Stephenie Prokopec

26. Department of Pharmacology, University of Toronto, Toronto, Ontario, Canada

Paul Boutros

27. Department of Biochemistry, Microbiology and Immunology, Faculty of Medicine, University of Ottawa, Ottawa, Ontario, Canada

Kin Chan

28. RIKEN Center for Integrative Medical Sciences, Yokohama, Japan

Akihiro Fujimoto & Hidewaki Nakagawa

29. A. A. Kharkevich Institute of Information Transmission Problems, Moscow, Russia

Marat Kazanov

30. Dmitry Rogachev National Research Center of Pediatric Hematology, Oncology and Immunology, Moscow, Russia

Marat Kazanov

31. Skolkovo Institute of Science and Technology, Moscow, Russia

Marat Kazanov

32. Laboratory for Medical Science Mathematics, RIKEN Center for Integrative Medical Sciences, Yokohama, Japan

Michael Lawrence

33. Massachusetts General Hospital, Boston, MA, USA

Michael Lawrence

34. School of Molecular Biosciences, Washington State University, Pullman, WA, USA

Steven A. Roberts

35. Center for Reproductive Biology, Washington State University, Pullman, WA, USA

Steven A. Roberts

36. Laboratory of Molecular Medicine, Human Genome Center, The Institute of Medical Science, The University of Tokyo, Tokyo, Japan

Tatsuhiro Shibata

37. Division of Cancer Genomics, National Cancer Center Research Institute, Tokyo, Japan

Tatsuhiro Shibata

38. The Institute of Medical Science, The University of Tokyo, Tokyo, Japan

Yuichi Shiraishi

39. Cancer Science Institute of Singapore, National University of Singapore, Singapore, Singapore

Bin Tean Teh

40. Institute of Molecular and Cell Biology, Singapore, Singapore

Bin Tean Teh

41. Laboratory of Cancer Epigenome, Division of Medical Science, National Cancer Centre Singapore, Singapore, Singapore

Bin Tean Teh

42. Department of Epidemiology and Biostatistics, Memorial Sloan Kettering Cancer Center, New York, NY, USA

Ignacio Vázquez-García

43. Department of Statistics, Columbia University, New York, NY, USA

Ignacio Vázquez-García

44. Department of Applied Mathematics and Theoretical Physics, Centre for Mathematical Sciences, University of Cambridge, Cambridge, UK

Ignacio Vázquez-García

45. Applied Tumor Genomics Research Program, Research Programs Unit, University of Helsinki, Helsinki, Finland

Lauri A. Aaltonen

46. Wellcome Sanger Institute, Wellcome Genome Campus, Hinxton, UK

Federico Abascal, David J. Adams, Ludmil B. Alexandrov, Sam Behjati, Shriram G. Bhosle, David T. Bowen, Adam P. Butler, Peter J. Campbell, Peter Clapham, Helen Davies, Kevin J. Dawson, Stefan C. Dentro, Serge Serge, Erik Garrison, Mohammed Ghori, Dominik Glodzik, Jonathan Hinton, David R. Jones, Young Seok Ju, Stian Knappskog, Barbara Kremeyer, Henry Lee-Six, Daniel A. Leongamornlert, Yilong Li, Sancha Martin, Iñigo Martincorena, Ultan McDermott, Andrew Menzies, Thomas J. Mitchell, Sandro Morganella, Jyoti Nangalia, Jonathan Nicholson, Serena Nik-Zainal, Sarah O'Meara, Elli Papaemmanuil, Keiran M. Raine, Manasa Ramakrishna, Kamna Ramakrishnan, Nicola D. Roberts, Rebecca Shepherd, Lucy Stebbings, Michael R. Stratton, Maxime Tarabichi, Jon W. Teague, Ignacio Vázquez-García, David C. Wedge, Lucy Yates, Jorge Zamora & Xueqing Zou

47. Memorial Sloan Kettering Cancer Center, New York, NY, USA

Adam Abeshouse, Hikmat Al-Ahmadie, Gunes Gundem, Zachary Heins, Jason Huse, Douglas A. Levine, Eric Minwei Liu & Angelica Ochoa

48. Genome Science Division, Research Center for Advanced Science and Technology, University of Tokyo, Tokyo, Japan

Hiroyuki Aburatani, Genta Nagae, Akihiro Suzuki, Kenji Tatsuno & Shogo Yamamoto

49. Department of Surgery, University of Chicago, Chicago, IL, USA

Nishant Agrawal

50. Department of Surgery, Division of Hepatobiliary and Pancreatic Surgery, School of Medicine, Keimyung University Dongsan Medical Center, Daegu, South Korea

Keun Soo Ahn & Koo Jeong Kang

51. Department of Oncology, Gil Medical Center, Gachon University, Incheon, South Korea

Sung-Min Ahn

52. Hiroshima University, Hiroshima, Japan

Hiroshi Aikata, Koji Arihiro, Kazuaki Chayama, Yoshiiku Kawakami & Hideki Ohdan

53. Department of Bioinformatics and Computational Biology, The University of Texas MD Anderson Cancer Center, Houston, TX, USA

Rehan Akbani, Shaolong Cao, Yiwen Chen, Zechen Chong, Yu Fan, Jun Li, Han Liang, Wenyi Wang, Yumeng Wang & Yuan Yuan

54. University of Texas MD Anderson Cancer Center, Houston, TX, USA

Kadir C. Akdemir & Ken Chen

55. King Faisal Specialist Hospital and Research Centre, Al Maather, Riyadh, Saudi Arabia

Sultan T. Al-Sedairy

56. Bioinformatics Unit, Spanish National Cancer Research Centre (CNIO), Madrid, Spain

Fatima Al-Shahrour & Elena Piñeiro-Yáñez

57. Bioinformatics Core Facility, University Medical Center Hamburg, Hamburg, Germany

Malik Alawi

58. Heinrich Pette Institute, Leibniz Institute for Experimental Virology, Hamburg, Germany

Malik Alawi & Adam Grundhoff

59. Ontario Tumour Bank, Ontario Institute for Cancer Research, Toronto, ON, Canada

Monique Albert & John Bartlett

60. Department of Pathology, The University of Texas MD Anderson Cancer Center, Houston, TX, USA

Kenneth Aldape, Russell R. Broaddus, Bogdan Czerniak, Adel El-Naggar, Savitri Krishnamurthy, Alexander J. Lazar & Xiaoping Su

61. Laboratory of Pathology, Center for Cancer Research, National Cancer Institute, Bethesda, MD, USA

Kenneth Aldape

62. Department of Cellular and Molecular Medicine and Department of Bioengineering, University of California San Diego, La Jolla, CA, USA

Ludmil B. Alexandrov & Erik N. Bergstrom

63. UC San Diego Moores Cancer Center, San Diego, CA, USA

Ludmil B. Alexandrov, Erik N. Bergstrom & Olivier Harismendy

64. Canada's Michael Smith Genome Sciences Centre, BC Cancer, Vancouver, BC, Canada

Adrian Ally, Miruna Balasundaram, Reanne Bowlby, Denise Brooks, Rebecca Carlsen, Eric Chuah, Noreen Dhalla, Robert A. Holt, Steven J. M. Jones, Katayoon Kasaian, Darlene Lee, Haiyan

Irene Li, Yussanne Ma, Marco A. Marra, Michael Mayo, Richard A. Moore, Andrew J. Mungall, Karen Mungall, A. Gordon Robertson, Sara Sadeghi, Jacqueline E. Schein, Payal Sipahimalani, Angela Tam, Nina Thiessen & Tina Wong

65. Sir Peter MacCallum Department of Oncology, Peter MacCallum Cancer Centre, University of Melbourne, Melbourne, VIC, Australia

Kathryn Alsop, David D. L. Bowtell, Elizabeth L. Christie, Dariush Etemadmoghadam, Sian Fereday, Dale W. Garsed, Linda Mileshkin, Chris Mitchell, Mark Shackleton, Heather Thorne & Nadia Traficante

66. Centre for Research in Molecular Medicine and Chronic Diseases (CiMUS), Universidade de Santiago de Compostela, Santiago de Compostela, Spain

Eva G. Alvarez, Alicia L. Bruzos, Bernardo Rodriguez-Martin, Javier Temes, Jose M. C. Tubio & Jorge Zamora

67. Department of Zoology, Genetics and Physical Anthropology, (CiMUS), Universidade de Santiago de Compostela, Santiago de Compostela, Spain

Eva G. Alvarez, Alicia L. Bruzos, Bernardo Rodriguez-Martin, Javier Temes, Jose M. C. Tubio & Jorge Zamora

68. The Biomedical Research Centre (CINBIO), Universidade de Vigo, Vigo, Spain

Eva G. Alvarez, Alicia L. Bruzos, Bernardo Rodriguez-Martin, Marta Tojo, Jose M. C. Tubio & Jorge Zamora

69. Royal National Orthopaedic Hospital - Bolsover, London, UK

Fernanda Amary

70. Department of Genomic Medicine, The University of Texas MD Anderson Cancer Center, Houston, TX, USA

Samirkumar B. Amin, P. Andrew Futreal & Alexander J. Lazar

71. Quantitative and Computational Biosciences Graduate Program, Baylor College of Medicine, Houston, TX, USA

Samirkumar B. Amin, Han Liang & Yumeng Wang

72. The Jackson Laboratory for Genomic Medicine, Farmington, CT, USA

Samirkumar B. Amin, Joshy George & Lucas Lochovsky

73. Genome Informatics Program, Ontario Institute for Cancer Research, Toronto, ON, Canada

Brice Aminou, Niall J. Byrne, Aurélien Chateigner, Nodirjon Fayzullaev, Vincent Ferretti, George L. Mihaiescu, Hardeep K. Nahal-Bose, Brian D. O’Connor, B. F. Francis Ouellette, Marc D. Perry, Kevin Thai, Qian Xiang, Christina K. Yung & Junjun Zhang

74. Institute of Human Genetics, Christian-Albrechts-University, Kiel, Germany

Ole Ammerpohl, Andrea Haake, Cristina López, Julia Richter & Rabea Wagener

75. Institute of Human Genetics, Ulm University and Ulm University Medical Center, Ulm, Germany

Ole Ammerpohl, Sietse Aukema, Cristina López, Reiner Siebert & Rabea Wagener

76. Queensland Centre for Medical Genomics, Institute for Molecular Bioscience, University of Queensland, St. Lucia, Brisbane, QLD, Australia

Matthew J. Anderson, Timothy J. C. Bruxner, Angelika N. Christ, J. Lynn Fink, Ivon Harliwong, Karin S. Kassahn, David K. Miller, Alan J. Robertson & Darrin F. Taylor

77. Salford Royal NHS Foundation Trust, Salford, UK

Yeng Ang, Hsiao-Wei Chen, Ritika Kundra & Francisco Sanchez-Vega

78. Department of Surgery, Pancreas Institute, University and Hospital Trust of Verona, Verona, Italy

Davide Antonello, Claudio Bassi, Narong Khuntikeo, Luca Landoni, Giuseppe Malleo, Giovanni Marchegiani, Neil D. Merrett, Marco Miotto, Salvatore Paiella, Antonio Pea, Paolo Pederzoli, Roberto Salvia, Jaswinder S. Samra, Elisabetta Sereni & Samuel Singer

79. Molecular and Medical Genetics, OHSU Knight Cancer Institute, Oregon Health and Science University, Portland, OR, USA

Pavana Anur, Myron Peto & Paul T. Spellman

80. Department of Molecular Oncology, BC Cancer Research Centre, Vancouver, BC, Canada

Samuel Aparicio

81. The McDonnell Genome Institute at Washington University, St. Louis, MO, USA

Elizabeth L. Appelbaum, Matthew H. Bailey, Matthew G. Cordes, Li Ding, Catrina C. Fronick, Lucinda A. Fulton, Robert S. Fulton, Kuan-lin Huang, Reyka Jayasinghe, Elaine R. Mardis, R. Jay Mashl, Michael D. McLellan, Christopher A. Miller, Heather K. Schmidt, Jiayin Wang, Michael C. Wendl, Richard K. Wilson & Tina Wong

82. University College London, London, UK

Elizabeth L. Appelbaum, Jonathan D. Kay, Helena Kilpinen, Laurence B. Lovat, Hayley J. Luxton & Hayley C. Whitaker

83. Division of Cancer Genomics, National Cancer Center Research Institute, National Cancer Center, Tokyo, Japan

Yasuhito Arai, Natsuko Hama, Fumie Hosoda, Hiromi Nakamura, Tatsuhiro Shibata, Yasushi Totoki & Shinichi Yachida

84. DLR Project Management Agency, Bonn, Germany

Axel Aretz

85. Tokyo Women's Medical University, Tokyo, Japan

Shun-ichi Ariizumi & Masakazu Yamamoto

86. Center for Molecular Oncology, Memorial Sloan Kettering Cancer Center, New York, NY, USA

Joshua Armenia, Hsiao-Wei Chen, Jianjiong Gao, Ritika Kundra, Francisco Sanchez-Vega, Nikolaus Schultz & Hongxin Zhang

87. Los Alamos National Laboratory, Los Alamos, NM, USA

Laurent Arnould

88. Department of Pathology, University Health Network, Toronto General Hospital, Toronto, ON, Canada

Sylvia Asa, Michael H. A. Roehrl & Theodorus Van der Kwast

89. Nottingham University Hospitals NHS Trust, Nottingham, UK

Sylvia Asa, Simon L. Parsons & Ming Tsao

90. Epigenomics and Cancer Risk Factors, German Cancer Research Center (DKFZ), Heidelberg, Germany

Yassen Assenov

91. Computational Biology Program, Ontario Institute for Cancer Research, Toronto, ON, Canada

Gurnit Atwal, Philip Awadalla, Jonathan Barenboim, Vinayak Bhandari, Ivan Borozan, Paul C. Boutros, Lewis Jonathan Dursi, Shadrielle M. G. Espiritu, Natalie S. Fox, Michael Fraser, Syed Haider, Vincent Huang, Keren Isaev, Wei Jiao, Christopher M. Lalansingh, Emilie Lalonde, Fabien C. Lamaze, Constance H. Li, Julie Livingstone, Christine P'ng, Marta Paczkowska, Stephenie D. Prokopec, Jüri Reimand, Veronica Y. Sabelnykova, Adriana Salcedo, Yu-Jia Shiah, Solomon I. Shorser, Shimin Shuai, Jared T. Simpson, Lincoln D. Stein, Ren X. Sun, Lina Wadi, Gavin W. Wilson, Adam J. Wright, Takafumi N. Yamaguchi, Fouad Yousif & Denis Yuen

92. Department of Molecular Genetics, University of Toronto, Toronto, ON, Canada

Gurnit Atwal, Philip Awadalla, Gary D. Bader, Shimin Shuai & Lincoln D. Stein

93. Vector Institute, Toronto, ON, Canada

Gurnit Atwal, Quaid D. Morris, Yulia Rubanova & Jeffrey A. Wintersinger

94. Hematopathology Section, Institute of Pathology, Christian-Albrechts-University, Kiel, Germany

Sietse Aukema, Wolfram Klapper, Julia Richter & Monika Szczepanowski

95. Department of Pathology and Laboratory Medicine, School of Medicine, University of North Carolina at Chapel Hill, Chapel Hill, NC, USA

J. Todd Auman & Charles M. Perou

96. Department of Cancer Genetics, Institute for Cancer Research, Oslo University Hospital, The Norwegian Radium Hospital, Oslo, Norway

Miriam R. R. Aure, Anne-Lise Børresen-Dale & Anita Langerød

97. Pathology, Hospital Clinic, Institut d'Investigacions Biomèdiques August Pi i Sunyer (IDIBAPS), University of Barcelona, Barcelona, Spain

Marta Aymerich

98. Department of Veterinary Medicine, Transmissible Cancer Group, University of Cambridge, Cambridge, UK

Adrian Baez-Ortega

99. Alvin J. Siteman Cancer Center, Washington University School of Medicine, St. Louis, MO, USA

Matthew H. Bailey, Li Ding, Robert S. Fulton, Ramaswamy Govindan & Michael D. McLellan

100. Wolfson Wohl Cancer Research Centre, Institute of Cancer Sciences, University of Glasgow, Glasgow, UK

Peter J. Bailey, Andrew V. Biankin, David K. Chang, Susanna L. Cooke, Fraser R. Duthie, Janet S. Graham, Nigel B. Jamieson, Elizabeth A. Musgrove & Derek W. Wright

101. Lineberger Comprehensive Cancer Center, University of North Carolina at Chapel Hill, Chapel Hill, NC, USA

Saianand Balu, Tom Bodenheimer, D. Neil Hayes, Austin J. Hepperla, Katherine A. Hoadley, Alan P. Hoyle, Stuart R. Jefferys, Shaowu Meng, Lisle E. Mose, Grant Sanders, Yan Shi, Janae V. Simons & Matthew G. Soloway

102. Broad Institute of MIT and Harvard, Cambridge, MA, USA

Pratiti Bandopadhayay, Rameen Beroukhim, Angela N. Brooks, Susan Bullman, John Busanovich, Andrew D. Cherniack, Juok Cho, Carrie Cibulskis, Kristian Cibulskis, David Craft, Timothy Defreitas, Andrew

J. Dunford, Scott Frazer, Stacey B. Gabriel, Nils Gehlenborg, Gad Getz, Manaswi Gupta, Gavin Ha, Nicholas J. Haradhvala, David I. Heiman, Julian M. Hess, Manolis Kellis, Jaegil Kim, Kiran Kumar, Kirsten Kübler, Eric Lander, Michael S. Lawrence, Ignaty Leshchiner, Pei Lin, Ziao Lin, Dimitri Livitz, Yosef E. Maruvka, Samuel R. Meier, Matthew Meyerson, Michael S. Noble, Chandra Sekhar Pedamallu, Paz Polak, Esther Rheinbay, Daniel Rosebrock, Mara Rosenberg, Gordon Saksena, Richard Sallari, Steven E. Schumacher, Ayellet V. Segre, Ofer Shapira, Juliann Shih, Nasa Sinnott-Armstrong, Oliver Spiro, Chip Stewart, Amaro Taylor-Weiner, Grace Tiao, Douglas Voet, Jeremiah A. Wala, Cheng-Zhong Zhang & Hailei Zhang

103. Dana-Farber/Boston Children's Cancer and Blood Disorders Center, Boston, MA, USA

Pratiti Bandopadhayay

104. Department of Pediatrics, Harvard Medical School, Boston, MA, USA

Pratiti Bandopadhayay

105. Leeds Institute of Medical Research @ St. James's, University of Leeds, St. James's University Hospital, Leeds, UK

Rosamonde E. Banks & Naveen Vasudev

106. Department of Pathology and Diagnostics, University and Hospital Trust of Verona, Verona, Italy

Stefano Barbi, Vincenzo Corbo & Michele Simbolo

107. Department of Surgery, Princess Alexandra Hospital, Brisbane, QLD, Australia

Andrew P. Barbour

108. Surgical Oncology Group, Diamantina Institute, University of Queensland, Brisbane, QLD, Australia

Andrew P. Barbour

109. Department of Population and Quantitative Health Sciences, Case Western Reserve University School of Medicine, Cleveland, OH, USA

Jill Barnholtz-Sloan

110. Research Health Analytics and Informatics, University Hospitals Cleveland Medical Center, Cleveland, OH, USA

Jill Barnholtz-Sloan

111. Gloucester Royal Hospital, Gloucester, UK

Hugh Barr

112. European Molecular Biology Laboratory, European Bioinformatics Institute (EMBL-EBI), Cambridge, UK

Elisabet Barrera, Wojciech Bazant, Ewan Birney, Rich Boyce, Alvis Brazma, Andy Cafferkey, Claudia Calabrese, Paul Flicek, Nuno A. Fonseca, Anja Füllgrabe, Moritz Gerstung, Santiago Gonzalez, Liliana Greger, Maria Keays, Jan O. Korbel, Alfonso Muñoz, Steven J. Newhouse, David Ocana, Irene Papatheodorou, Robert Petryszak, Roland F. Schwarz, Charles Short, Oliver Stegle & Lara Urban

113. Diagnostic Development, Ontario Institute for Cancer Research, Toronto, ON, Canada

John Bartlett & Ilinca Lungu

114. Barcelona Supercomputing Center (BSC), Barcelona, Spain

Javier Bartolome, Mattia Bosio, Ana Dueso-Barroso, J. Lynn Fink, Josep L. L. Gelpi, Ana Milovanovic, Montserrat Puiggròs, Javier Bartolomé Rodriguez, Romina Royo, David Torrents, Alfonso Valencia, Miguel Vazquez, David Vicente & Izar Villasante

115. Arnie Charbonneau Cancer Institute, University of Calgary, Calgary, AB, Canada

Oliver F. Bathe

116. Departments of Surgery and Oncology, University of Calgary, Calgary, AB, Canada

Oliver F. Bathe

117. Department of Pathology, Oslo University Hospital, The Norwegian Radium Hospital, Oslo, Norway

Daniel Baumhoer & Bodil Bjerkehagen

118. PanCuRx Translational Research Initiative, Ontario Institute for Cancer Research, Toronto, ON, Canada

Prashant Bavi, Michelle Chan-Seng-Yue, Sean Cleary, Robert E. Denroche, Steven Gallinger, Robert C. Grant, Gun Ho Jang, Sangeetha Kalimuthu, Ilinca Lungu, John D. McPherson, Faiyaz Notta, Michael H. A. Roehrl, Gavin W. Wilson & Julie M. Wilson

119. Department of Oncology, Sidney Kimmel Comprehensive Cancer Center at Johns Hopkins University School of Medicine, Baltimore, MD, USA

Stephen B. Baylin, Nilanjan Chatterjee, Leslie Cope, Ludmila Danilova & Ralph H. Hruban

120. University Hospital Southampton NHS Foundation Trust, Southampton, UK

Stephen B. Baylin & Tim Dudderidge

121. Royal Stoke University Hospital, Stoke-on-Trent, UK

Duncan Beardsmore & Christopher Umbricht

122. Genome Sequence Informatics, Ontario Institute for Cancer Research, Toronto, ON, Canada

Timothy A. Beck, Bob Gibson, Lawrence E. Heisler, Xuemei Luo & Morgan L. Taschuk

123. Human Longevity Inc, San Diego, CA, USA

Timothy A. Beck

124. Olivia Newton-John Cancer Research Institute, La Trobe University, Heidelberg, VIC, Australia

Andreas Behren & Jonathan Cebon

125. Computer Network Information Center, Chinese Academy of Sciences, Beijing, China

Beifang Niu

126. Genome Canada, Ottawa, ON, Canada

Cindy Bell

127. CNAG-CRG, Centre for Genomic Regulation (CRG), Barcelona Institute of Science and Technology (BIST), Barcelona, Spain

Sergi Beltran, Ivo G. Gut, Marta Gut, Simon C. Heath, Tomas Marques-Bonet, Arcadi Navarro, Miranda D. Stobbe, Jean-Rémi Trotta & Justin P. Whalley

128. Universitat Pompeu Fabra (UPF), Barcelona, Spain

Sergi Beltran, Mattia Bosio, German M. Demidov, Oliver Drechsel, Ivo G. Gut, Marta Gut, Simon C. Heath, Francesc Muyas, Stephan Ossowski, Aparna Prasad, Raquel Rabionet, Miranda D. Stobbe & Hana Susak

129. Buck Institute for Research on Aging, Novato, CA, USA

Christopher Benz & Christina Yau

130. Duke University Medical Center, Durham, NC, USA

Andrew Berchuck

131. Department of Human Genetics, Hannover Medical School, Hannover, Germany

Anke K. Bergmann

132. Center for Bioinformatics and Functional Genomics, Cedars-Sinai Medical Center, Los Angeles, CA, USA

Benjamin P. Berman & Huy Q. Dinh

133. Department of Biomedical Sciences, Cedars-Sinai Medical Center, Los Angeles, CA, USA

Benjamin P. Berman

134. The Hebrew University Faculty of Medicine, Jerusalem, Israel

Benjamin P. Berman

135. Barts Cancer Institute, Barts and the London School of Medicine and Dentistry, Queen Mary University of London, London, UK

Daniel M. Berney & Yong-Jie Lu

136. Department of Computer Science, Bioinformatics Group, University of Leipzig, Leipzig, Germany

Stephan H. Bernhart, Hans Binder, Steve Hoffmann & Peter F. Stadler

137. Interdisciplinary Center for Bioinformatics, University of Leipzig, Leipzig, Germany

Stephan H. Bernhart, Hans Binder, Steve Hoffmann, Helene Kretzmer & Peter F. Stadler

138. Transcriptome Bioinformatics, LIFE Research Center for Civilization Diseases, University of Leipzig, Leipzig, Germany

Stephan H. Bernhart, Steve Hoffmann, Helene Kretzmer & Peter F. Stadler

139. Department of Medical Oncology, Dana-Farber Cancer Institute, Boston, MA, USA

Rameen Beroukhim, Angela N. Brooks, Susan Bullman, Andrew D. Cherniack, Levi Garraway, Matthew Meyerson, Chandra Sekhar Pedamallu, Steven E. Schumacher, Juliann Shih & Jeremiah A. Wala

140. Department of Cancer Biology, Dana-Farber Cancer Institute, Boston, MA, USA

Rameen Beroukhim, Aquila Fatima, Andrea L. Richardson, Steven E. Schumacher, Ofer Shapira, Andrew Tutt & Jeremiah A. Wala

141. Harvard Medical School, Boston, MA, USA

Rameen Beroukhim, Gad Getz, Kirsten Kübler, Matthew Meyerson, Chandra Sekhar Pedamallu, Paz Polak, Esther Rheinbay & Jeremiah A. Wala

142. USC Norris Comprehensive Cancer Center, University of Southern California, Los Angeles, CA, USA

Mario Berrios, Moiz S. Bootwalla, Andrea Holbrook, Phillip H. Lai, Dennis T. Maglinte, David J. Van Den Berg & Daniel J. Weisenberger

143. Department of Diagnostics and Public Health, University and Hospital Trust of Verona, Verona, Italy

Samantha Bersani, Ivana Cataldo, Claudio Luchini & Maria Scardoni

144. Department of Mathematics, Aarhus University, Aarhus, Denmark

Johanna Bertl & Asger Hobolth

145. Department of Molecular Medicine (MOMA), Aarhus University Hospital, Aarhus N, Denmark

Johanna Bertl, Henrik Hornshøj, Malene Juul, Randi Istrup Juul, Tobias Madsen, Morten Muhlig Nielsen & Jakob Skou Pedersen

146. Instituto Carlos Slim de la Salud, Mexico City, Mexico

Miguel Betancourt

147. Department of Medical Biophysics, University of Toronto, Toronto, ON, Canada

Vinayak Bhandari, Paul C. Boutros, Robert G. Bristow, Keren Isaev, Constance H. Li, Jüri Reimand, Michael H. A. Roehrl & Bradly G. Wouters

148. Cancer Division, Garvan Institute of Medical Research, Kinghorn Cancer Centre, University of New South Wales (UNSW Sydney), Sydney, NSW, Australia

Andrew V. Biankin, David K. Chang, Lorraine A. Chantrill, Angela Chou, Anthony J. Gill, Amber L. Johns, James G. Kench, David K. Miller, Adnan M. Nagrial, Marina Pajic, Mark Pinese, Ilse Rooman, Christopher J. Scarlett, Christopher W. Toon & Jianmin Wu

149. South Western Sydney Clinical School, Faculty of Medicine, University of New South Wales (UNSW Sydney), Liverpool, NSW, Australia

Andrew V. Biankin

150. West of Scotland Pancreatic Unit, Glasgow Royal Infirmary, Glasgow, UK

Andrew V. Biankin & Nigel B. Jamieson

151. Center for Digital Health, Berlin Institute of Health and Charitè - Universitätsmedizin Berlin, Berlin, Germany

Matthias Bieg

152. Heidelberg Center for Personalized Oncology (DKFZ-HIPO), German Cancer Research Center (DKFZ), Heidelberg, Germany

Matthias Bieg, Ivo Buchhalter, Barbara Hutter & Nagarajan Paramasivam

153. The Preston Robert Tisch Brain Tumor Center, Duke University Medical Center, Durham, NC, USA

Darell Bigner

154. Massachusetts General Hospital, Boston, MA, USA

Michael Birrer, Vikram Deshpande, William C. Faquin, Nicholas J. Haradhvala, Kirsten Kübler, Michael S. Lawrence, David N. Louis, Yosef E. Maruvka, G. Petur Nielsen, Esther Rheinbay, Mara Rosenberg, Dennis C. Sgroi & Chin-Lee Wu

155. National Institute of Biomedical Genomics, Kalyani, West Bengal, India

Nidhan K. Biswas, Arindam Maitra & Partha P. Majumder

156. Institute of Clinical Medicine and Institute of Oral Biology, University of Oslo, Oslo, Norway

Bodil Bjerkehagen

157. University of North Carolina at Chapel Hill, Chapel Hill, NC, USA

Lori Boice, Mei Huang, Sonia Puig & Leigh B. Thorne

158. ARC-Net Centre for Applied Research on Cancer, University and Hospital Trust of Verona, Verona, Italy

Giada Bonizzato, Cinzia Cantù, Ivana Cataldo, Vincenzo Corbo, Sonia Grimaldi, Rita T. Lawlor, Andrea Mafficini, Borislav C. Rusev, Aldo Scarpa, Katarzyna O. Sikora, Nicola Sperandio, Alain Viari & Caterina Vicentini

159. The Institute of Cancer Research, London, UK

Johann S. De Bono, Niedzica Camacho, Colin S. Cooper, Sandra E. Edwards, Rosalind A. Eeles, Zsofia Kote-Jarai, Daniel A. Leongamornlert, Lucy Matthews & Sue Merson

160. Centre for Computational Biology, Duke-NUS Medical School, Singapore, Singapore

Arnoud Boot, Ioana Cutcutache, Mi Ni Huang, John R. McPherson, Steven G. Rozen & Yang Wu

161. Programme in Cancer and Stem Cell Biology, Duke-NUS Medical School, Singapore, Singapore

Arnoud Boot, Ioana Cutcutache, Mi Ni Huang, John R. McPherson, Steven G. Rozen, Patrick Tan, Bin Tean Teh & Yang Wu

162. Division of Oncology and Pathology, Department of Clinical Sciences Lund, Lund University, Lund, Sweden

Ake Borg, Markus Ringnér & Johan Staaf

163. Department of Pediatric Oncology, Hematology and Clinical Immunology, Heinrich-Heine-University, Düsseldorf, Germany

Arndt Borkhardt & Jessica I. Hoell

164. Laboratory for Medical Science Mathematics, RIKEN Center for Integrative Medical Sciences, Yokohama, Japan

Keith A. Boroevich, Todd A. Johnson, Michael S. Lawrence & Tatsuhiko Tsunoda

165. RIKEN Center for Integrative Medical Sciences, Yokohama, Japan

Keith A. Boroevich, Akihiro Fujimoto, Masashi Fujita, Mayuko Furuta, Kazuhiro Maejima, Hidewaki Nakagawa, Kaoru Nakano & Aya Sasaki-Oku

166. Department of Internal Medicine/Hematology, Friedrich-Ebert-Hospital, Neumünster, Germany

Christoph Borst & Siegfried Haas

167. Departments of Dermatology and Pathology, Yale University, New Haven, CT, USA

Marcus Bosenberg

168. Centre for Genomic Regulation (CRG), The Barcelona Institute of Science and Technology, Barcelona, Spain

Mattia Bosio, German M. Demidov, Oliver Drechsel, Georgia Escaramis, Xavier Estivill, Aliaksei Z. Holik, Francesc Muyas, Stephan Ossowski, Raquel Rabionet & Hana Susak

169. Radcliffe Department of Medicine, University of Oxford, Oxford, UK

Jacqueline Boultwood

170. Canadian Center for Computational Genomics, McGill University, Montreal, QC, Canada

Guillaume Bourque

171. Department of Human Genetics, McGill University, Montreal, QC, Canada

Guillaume Bourque, Mark Lathrop & Yasser Riazalhosseini

172. Department of Human Genetics, University of California Los Angeles, Los Angeles, CA, USA

Paul C. Boutros

173. Department of Pharmacology, University of Toronto, Toronto, ON, Canada

Paul C. Boutros

174. Faculty of Medicine and Health Technology, Tampere University and Tays Cancer Center, Tampere University Hospital, Tampere, Finland

G. Steven Bova & Tapio Visakorpi

175. Haematology, Leeds Teaching Hospitals NHS Trust, Leeds, UK

David T. Bowen

176. Translational Research and Innovation, Centre Léon Bérard, Lyon, France

Sandrine Boyault

177. Fox Chase Cancer Center, Philadelphia, PA, USA

Jeffrey Boyd & Elaine R. Mardis

178. International Agency for Research on Cancer, World Health Organization, Lyon, France

Paul Brennan & Ghislaine Scelo

179. Earlham Institute, Norwich, UK

Daniel S. Brewer & Colin S. Cooper

180. Norwich Medical School, University of East Anglia, Norwich, UK

Daniel S. Brewer & Colin S. Cooper

181. Department of Molecular Biology, Faculty of Science, Radboud Institute for Molecular Life Sciences, Radboud University, Nijmegen, HB, The Netherlands

Arie B. Brinkman

182. CRUK Manchester Institute and Centre, Manchester, UK

Robert G. Bristow

183. Department of Radiation Oncology, University of Toronto, Toronto, ON, Canada

Robert G. Bristow

184. Division of Cancer Sciences, Manchester Cancer Research Centre, University of Manchester, Manchester, UK

Robert G. Bristow

185. Radiation Medicine Program, Princess Margaret Cancer Centre, Toronto, ON, Canada

Robert G. Bristow & Fei-Fei Fei Liu

186. Department of Pathology, Brigham and Women's Hospital, Harvard Medical School, Boston, MA, USA

Jane E. Brock & Sabina Signoretti

187. Department of Surgery, Division of Thoracic Surgery, The Johns Hopkins University School of Medicine, Baltimore, MD, USA

Malcolm Brock

188. Division of Molecular Pathology, The Netherlands Cancer Institute, Oncode Institute, Amsterdam, CX, The Netherlands

Annegien Broeks & Jos Jonkers

189. Department of Biomolecular Engineering, University of California Santa Cruz, Santa Cruz, CA, USA

Angela N. Brooks, David Haan, Maximillian G. Marin, Thomas J. Matthew, Yulia Newton, Cameron M. Soulette & Joshua M. Stuart

190. UC Santa Cruz Genomics Institute, University of California Santa Cruz, Santa Cruz, CA, USA

Angela N. Brooks, Brian Craft, Mary J. Goldman, David Haussler, Joshua M. Stuart & Jingchun Zhu

191. Division of Applied Bioinformatics, German Cancer Research Center (DKFZ), Heidelberg, Germany

Benedikt Brors, Lars Feuerbach, Chen Hong, Charles David Imbusch & Lina Sieverling

192. German Cancer Consortium (DKTK), German Cancer Research Center (DKFZ), Heidelberg, Germany

Benedikt Brors, Barbara Hutter, Peter Lichter, Dirk Schadendorf & Holger Sültmann

193. National Center for Tumor Diseases (NCT) Heidelberg, Heidelberg, Germany

Benedikt Brors, Barbara Hutter, Holger Sültmann & Thorsten Zenz

194. Center for Biological Sequence Analysis, Department of Bio and Health Informatics, Technical University of Denmark, Lyngby, Denmark

Søren Brunak

195. Novo Nordisk Foundation Center for Protein Research, University of Copenhagen, Copenhagen, Denmark

Søren Brunak

196. Institute for Molecular Bioscience, University of Queensland, St. Lucia, Brisbane, QLD, Australia

Timothy J. C. Bruxner, Oliver Holmes, Stephen H. Kazakoff, Conrad R. Leonard, Felicity Newell, Katia Nones, Ann-Marie Patch, John V. Pearson, Michael C. Quinn, Nick M. Waddell, Nicola Waddell, Scott Wood & Qinying Xu

197. Biomedical Engineering, Oregon Health and Science University, Portland, OR, USA

Alex Buchanan & Kyle Ellrott

198. Division of Theoretical Bioinformatics, German Cancer Research Center (DKFZ), Heidelberg, Germany

Ivo Buchhalter, Calvin Wing Yiu Chan, Roland Eils, Michael C. Heinold, Carl Herrmann, Natalie Jäger, Rolf Kabbe, Jules N. A. Kerssemakers, Kortine Kleinheinz, Nagarajan Paramasivam, Manuel Prinz, Matthias Schlesner & Johannes Werner

199. Institute of Pharmacy and Molecular Biotechnology and BioQuant, Heidelberg University, Heidelberg, Germany

Ivo Buchhalter, Roland Eils, Michael C. Heinold, Carl Herrmann, Daniel Hübschmann, Kortine Kleinheinz & Umut H. Toprak

200. Federal Ministry of Education and Research, Berlin, Germany

Christiane Buchholz

201. Melanoma Institute Australia, University of Sydney, Sydney, NSW, Australia

Hazel Burke, Ricardo De Paoli-Iseppi, Nicholas K. Hayward, Peter Hersey, Valerie Jakrot, Hojabr Kakavand, Georgina V. Long, Graham

J. Mann, Robyn P. M. Saw, Richard A. Scolyer, Ping Shang, Andrew J. Spillane, Jonathan R. Stretch, John F. F. Thompson & James S. Wilmott

202. Pediatric Hematology and Oncology, University Hospital Muenster, Muenster, Germany

Birgit Burkhardt

203. Department of Pathology, Johns Hopkins University School of Medicine, Baltimore, MD, USA

Kathleen H. Burns & Christopher Umbricht

204. McKusick-Nathans Institute of Genetic Medicine, Sidney Kimmel Comprehensive Cancer Center at Johns Hopkins University School of Medicine, Baltimore, MD, USA

Kathleen H. Burns

205. Foundation Medicine, Inc, Cambridge, MA, USA

John Busanovich

206. Department of Biomedical Data Science, Stanford University School of Medicine, Stanford, CA, USA

Carlos D. Bustamante & Francisco M. De La Vega

207. Department of Genetics, Stanford University School of Medicine, Stanford, CA, USA

Carlos D. Bustamante, Francisco M. De La Vega, Suyash S. Shringarpure, Nasa Sinnott-Armstrong & Mark H. Wright

208. Bakar Computational Health Sciences Institute and Department of Pediatrics, University of California, San Francisco, CA, USA

Atul J. Butte & Jieming Chen

209. Institute of Clinical Medicine, Faculty of Medicine, University of Oslo, Oslo, Norway

Anne-Lise Børresen-Dale

210. National Cancer Institute, National Institutes of Health, Bethesda, MD, USA

Samantha J. Caesar-Johnson, John A. Demchok, Ina Felau, Roy Tarnuzzer, Zhining Wang, Liming Yang, Jean C. Zenklusen & Jiashan Zhang

211. Royal Marsden NHS Foundation Trust, London and Sutton, UK

Declan Cahill, Nening M. Dennis, Tim Dudderidge, Rosalind A. Eeles, Cyril Fisher, Steven Hazell, Vincent Khoo, Pardeep Kumar, Naomi Livni, Erik Mayer, David Nicol, Christopher Ogden, Edward W. Rowe, Sarah Thomas, Alan Thompson & Nicholas van As

212. Genome Biology Unit, European Molecular Biology Laboratory (EMBL), Heidelberg, Germany

Claudia Calabrese, Serap Erkek, Moritz Gerstung, Santiago Gonzalez, Nina Habermann, Wolfgang Huber, Lara Jerman, Jan O. Korbel, Esa Pitkänen, Benjamin Raeder, Tobias Rausch, Vasilisa A. Rudneva, Oliver Stegle, Stephanie Sungalee, Lara Urban, Sebastian M. Waszak, Joachim Weischenfeldt & Sergei Yakneen

213. Department of Oncology, University of Cambridge, Cambridge, UK

Carlos Caldas & Suet-Feung Chin

214. Li Ka Shing Centre, Cancer Research UK Cambridge Institute, University of Cambridge, Cambridge, UK

Carlos Caldas, Suet-Feung Chin, Ruben M. Drews, Paul A. Edwards, Matthew Eldridge, Steve Hawkins, Andy G. Lynch, Geoff

Macintyre, Florian Markowetz, Charlie E. Massie, David E. Neal, Simon Tavaré & Ke Yuan

215. Institut Gustave Roussy, Villejuif, France

Fabien Calvo

216. Cambridge University Hospitals NHS Foundation Trust, Cambridge, UK

Peter J. Campbell, Vincent J. Gnanapragasam, William Howat, Thomas J. Mitchell, David E. Neal, Nimish C. Shah & Anne Y. Warren

217. Department of Haematology, University of Cambridge, Cambridge, UK

Peter J. Campbell

218. Anatomia Patológica, Hospital Clinic, Institut d'Investigacions Biomèdiques August Pi i Sunyer (IDIBAPS), University of Barcelona, Barcelona, Spain

Elias Campo

219. Spanish Ministry of Science and Innovation, Madrid, Spain

Elias Campo

220. University of Michigan Comprehensive Cancer Center, Ann Arbor, MI, USA

Thomas E. Carey

221. Department for BioMedical Research, University of Bern, Bern, Switzerland

Joana Carlevaro-Fita

222. Department of Medical Oncology, Inselspital, University Hospital and University of Bern, Bern, Switzerland

Joana Carlevaro-Fita, Rory Johnson & Andrés Lanzós

223. Graduate School for Cellular and Biomedical Sciences, University of Bern, Bern, Switzerland

Joana Carlevaro-Fita & Andrés Lanzós

224. University of Pavia, Pavia, Italy

Mario Cazzola & Luca Malcovati

225. University of Alabama at Birmingham, Birmingham, AL, USA

Robert Cerfolio

226. UHN Program in BioSpecimen Sciences, Toronto General Hospital, Toronto, ON, Canada

Dianne E. Chadwick, Sheng-Ben Liang, Michael H. A. Roehrl & Sagedeh Shahabi

227. Department of Urology, Icahn School of Medicine at Mount Sinai, New York, NY, USA

Dimple Chakravarty

228. Centre for Law and Genetics, University of Tasmania, Sandy Bay Campus, Hobart, TAS, Australia

Don Chalmers

229. Faculty of Biosciences, Heidelberg University, Heidelberg, Germany

Calvin Wing Yiu Chan, Chen Hong & Lina Sieverling

230. Department of Biochemistry, Microbiology and Immunology, Faculty of Medicine, University of Ottawa, Ottawa, ON, Canada

Kin Chan

231. Division of Anatomic Pathology, Mayo Clinic, Rochester, MN, USA

Vishal S. Chandan

232. Division of Cancer Epidemiology and Genetics, National Cancer Institute, National Institutes of Health, Bethesda, MD, USA

Stephen J. Chanock, Xing Hua, Lisa Mirabello, Lei Song & Bin Zhu

233. Illawarra Shoalhaven Local Health District L3 Illawarra Cancer Care Centre, Wollongong Hospital, Wollongong, NSW, Australia

Lorraine A. Chantrill

234. BioForA, French National Institute for Agriculture, Food, and Environment (INRAE), ONF, Orléans, France

Aurélien Chateigner

235. Department of Biostatistics, Bloomberg School of Public Health, Johns Hopkins University, Baltimore, MD, USA

Nilanjan Chatterjee

236. University of California San Diego, San Diego, CA, USA

Zhaohong Chen, Michelle T. Dow, Claudiu Farcas, S. M. Ashiqul Islam, Antonios Koures, Lucila Ohno-Machado, Christos Sotiriou & Ashley Williams

237. Division of Experimental Pathology, Mayo Clinic, Rochester, MN, USA

Jeremy Chien

238. Centre for Cancer Research, The Westmead Institute for Medical Research, University of Sydney, Sydney, NSW, Australia

Yoke-Eng Chiew, Angela Chou, Jillian A. Hung, Catherine J. Kennedy, Graham J. Mann, Gulietta M. Pupo, Sarah-Jane Schramm, Varsha Tembe & Anna deFazio

239. Department of Gynaecological Oncology, Westmead Hospital, Sydney, NSW, Australia

Yoke-Eng Chiew, Jillian A. Hung, Catherine J. Kennedy & Anna deFazio

240. PDXen Biosystems Inc, Seoul, South Korea

Sunghoon Cho

241. Korea Advanced Institute of Science and Technology, Daejeon, South Korea

Jung Kyoon Choi, Young Seok Ju & Christopher J. Yoon

242. Electronics and Telecommunications Research Institute, Daejeon, South Korea

Wan Choi, Seung-Hyup Jeon, Hyunghwan Kim & Youngchoon Woo

243. Institut National du Cancer (INCA), Boulogne-Billancourt, France

Christine Chomienne & Iris Pauporté

244. Department of Genetics, Informatics Institute, University of Alabama at Birmingham, Birmingham, AL, USA

Zechen Chong

245. Division of Medical Oncology, National Cancer Centre, Singapore, Singapore

Su Pin Choo

246. Medical Oncology, University and Hospital Trust of Verona, Verona, Italy

Sara Cingarlini & Michele Milella

247. Department of Pediatrics, University Hospital Schleswig-Holstein, Kiel, Germany

Alexander Claviez

248. Hepatobiliary/Pancreatic Surgical Oncology Program, University Health Network, Toronto, ON, Canada

Sean Cleary, Ashton A. Connor & Steven Gallinger

249. School of Biological Sciences, University of Auckland, Auckland, New Zealand

Nicole Cloonan

250. Department of Surgery, University of Melbourne, Parkville, VIC, Australia

Marek Cmero

251. The Murdoch Children's Research Institute, Royal Children's Hospital, Parkville, VIC, Australia

Marek Cmero

252. Walter and Eliza Hall Institute, Parkville, VIC, Australia

Marek Cmero

253. Vancouver Prostate Centre, Vancouver, Canada

Colin C. Collins, Nilgun Donmez, Faraz Hach, Salem Malikic, S. Cenk Sahinalp, Iman Sarrafi & Raunak Shrestha

254. Lunenfeld-Tanenbaum Research Institute, Mount Sinai Hospital, Toronto, ON, Canada

Ashton A. Connor, Steven Gallinger, Robert C. Grant, Treasa A. McPherson & Iris Selander

255. University of East Anglia, Norwich, UK

Colin S. Cooper

256. Norfolk and Norwich University Hospital NHS Trust, Norwich, UK

Matthew G. Cordes, Catrina C. Fronick & Tom Roques

257. Victorian Institute of Forensic Medicine, Southbank, VIC, Australia

Stephen M. Cordner

258. Department of Biomedical Informatics, Harvard Medical School, Boston, MA, USA

Isidro Cortés-Ciriano, Jake June-Koo Lee & Peter J. Park

259. Department of Chemistry, Centre for Molecular Science Informatics, University of Cambridge, Cambridge, UK

Isidro Cortés-Ciriano

260. Ludwig Center at Harvard Medical School, Boston, MA, USA

Isidro Cortés-Ciriano, Jake June-Koo Lee & Peter J. Park

261. Human Genome Sequencing Center, Baylor College of Medicine, Houston, TX, USA

Kyle Covington, HarshaVardhan Doddapaneni, Richard A. Gibbs, Jianhong Hu, Joy C. Jayaseelan, Viktoriya Korchina, Lora Lewis, Donna M. Muzny, Linghua Wang, David A. Wheeler & Liu Xi

262. Peter MacCallum Cancer Centre, University of Melbourne, Melbourne, VIC, Australia

Prue A. Cowin, Anne Hamilton, Gisela Mir Arnau & Ravikiran Vedururu

263. Physics Division, Optimization and Systems Biology Lab, Massachusetts General Hospital, Boston, MA, USA

David Craft

264. Department of Medicine, Baylor College of Medicine, Houston, TX, USA

Chad J. Creighton

265. University of Cologne, Cologne, Germany

Yupeng Cun, Martin Peifer & Tsun-Po Yang

266. International Genomics Consortium, Phoenix, AZ, USA

Erin Curley & Troy Shelton

267. Genomics Research Program, Ontario Institute for Cancer Research, Toronto, ON, Canada

Karolina Czajka, Jenna Eagles, Thomas J. Hudson, Jeremy Johns, Faridah Mbabaali, John D. McPherson, Jessica K. Miller, Danielle Pasternack, Michelle Sam & Lee E. Timms

268. Barking Havering and Redbridge University Hospitals NHS Trust, Romford, UK

Bogdan Czerniak, Adel El-Naggar & David Khoo

269. Children’s Hospital at Westmead, University of Sydney, Sydney, NSW, Australia

Rebecca A. Dagg

270. Department of Medicine, Section of Endocrinology, University and Hospital Trust of Verona, Verona, Italy

Maria Vittoria Davi

271. Computational Biology Center, Memorial Sloan Kettering Cancer Center, New York, NY, USA

Natalie R. Davidson, Andre Kahles, Kjong-Van Lehmann, Alessandro Pastore, Gunnar Rätsch, Chris Sander, Yasin Senbabaoglu & Nicholas D. Socci

272. Department of Biology, ETH Zurich, Zürich, Switzerland

Natalie R. Davidson, Andre Kahles, Kjong-Van Lehmann, Gunnar Rätsch & Stefan G. Stark

273. Department of Computer Science, ETH Zurich, Zurich, Switzerland

Natalie R. Davidson, Andre Kahles, Kjong-Van Lehmann & Gunnar Rätsch

274. SIB Swiss Institute of Bioinformatics, Lausanne, Switzerland

Natalie R. Davidson, Andre Kahles, Kjong-Van Lehmann, Gunnar Rätsch & Stefan G. Stark

275. Weill Cornell Medical College, New York, NY, USA

Natalie R. Davidson, Bishoy M. Faltas & Gunnar Rätsch

276. Academic Department of Medical Genetics, University of Cambridge, Addenbrooke’s Hospital, Cambridge, UK

Helen Davies & Serena Nik-Zainal

277. MRC Cancer Unit, University of Cambridge, Cambridge, UK

Helen Davies, Rebecca C. Fitzgerald, Nicola Grehan, Serena Nik-Zainal & Maria O'Donovan

278. Departments of Pediatrics and Genetics, University of North Carolina at Chapel Hill, Chapel Hill, NC, USA

Ian J. Davis

279. Seven Bridges Genomics, Charlestown, MA, USA

Brandi N. Davis-Dusenbery, Sinisa Ivkovic, Milena Kovacevic, Ana Mijalkovic Lazic, Sanja Mijalkovic, Mia Nastic, Petar Radovic & Nebojsa Tijanic

280. Annai Systems, Inc, Carlsbad, CA, USA

Francisco M. De La Vega, Tal Shmaya & Dai-Ying Wu

281. Department of Pathology, General Hospital of Treviso, Department of Medicine, University of Padua, Treviso, Italy

Angelo P. Dei Tos

282. Department of Computational Biology, University of Lausanne, Lausanne, Switzerland

Olivier Delaneau

283. Department of Genetic Medicine and Development, University of Geneva Medical School, Geneva, CH, Switzerland

Olivier Delaneau

284. Swiss Institute of Bioinformatics, University of Geneva, Geneva, CH, Switzerland

Olivier Delaneau

285. The Francis Crick Institute, London, UK

Jonas Demeulemeester, Stefan C. Dentro, Matthew W. Fittall, Kerstin Haase, Clemency Jolly, Maxime Tarabichi & Peter Van Loo

286. University of Leuven, Leuven, Belgium

Jonas Demeulemeester & Peter Van Loo

287. Institute of Medical Genetics and Applied Genomics, University of Tübingen, Tübingen, Germany

German M. Demidov, Francesc Muyas & Stephan Ossowski

288. Computational and Systems Biology, Genome Institute of Singapore, Singapore, Singapore

Deniz Demircioğlu & Jonathan Göke

289. School of Computing, National University of Singapore, Singapore, Singapore

Deniz Demircioğlu

290. Big Data Institute, Li Ka Shing Centre, University of Oxford, Oxford, UK

Stefan C. Dentro & David C. Wedge

291. Biomedical Data Science Laboratory, Francis Crick Institute, London, UK

Nikita Desai

292. Bioinformatics Group, Department of Computer Science, University College London, London, UK

Nikita Desai

293. The Edward S. Rogers Sr. Department of Electrical and Computer Engineering, University of Toronto, Toronto, ON, Canada

Amit G. Deshwar

294. Breast Cancer Translational Research Laboratory JC Heuson, Institut Jules Bordet, Brussels, Belgium

Christine Desmedt

295. Department of Oncology, Laboratory for Translational Breast Cancer Research, KU Leuven, Leuven, Belgium

Christine Desmedt

296. Institute for Research in Biomedicine (IRB Barcelona), The Barcelona Institute of Science and Technology, Barcelona, Spain

Jordi Deu-Pons, Joan Frigola, Abel Gonzalez-Perez, Ferran Muiños, Loris Mularoni, Oriol Pich, Iker Reyes-Salazar, Carlota Rubio-Perez, Radhakrishnan Sabarinathan & David Tamborero

297. Research Program on Biomedical Informatics, Universitat Pompeu Fabra, Barcelona, Spain

Jordi Deu-Pons, Abel Gonzalez-Perez, Ferran Muiños, Loris Mularoni, Oriol Pich, Carlota Rubio-Perez, Radhakrishnan Sabarinathan & David Tamborero

298. Division of Medical Oncology, Princess Margaret Cancer Centre, Toronto, ON, Canada

Neesha C. Dhani, David Hedley & Malcolm J. Moore

299. Department of Physiology and Biophysics, Weill Cornell Medicine, New York, NY, USA

Priyanka Dhingra, Ekta Khurana, Eric Minwei Liu & Alexander Martinez-Fundichely

300. Institute for Computational Biomedicine, Weill Cornell Medicine, New York, NY, USA

Priyanka Dhingra, Ekta Khurana, Eric Minwei Liu & Alexander Martinez-Fundichely

301. Department of Pathology, UPMC Shadyside, Pittsburgh, PA, USA

Rajiv Dhir

302. Independent Consultant, Wellesley, USA

Anthony DiBiase

303. Department of Cell and Molecular Biology, Science for Life Laboratory, Uppsala University, Uppsala, Sweden

Klev Diamanti, Jan Komorowski & Husen M. Umer

304. Department of Medicine and Department of Genetics, Washington University School of Medicine, St. Louis, St. Louis, MO, USA

Li Ding, Robert S. Fulton, Michael D. McLellan, Michael C. Wendl & Venkata D. Yellapantula

305. Hefei University of Technology, Anhui, China

Shuai Ding & Shanlin Yang

306. Translational Cancer Research Unit, GZA Hospitals St.-Augustinus, Center for Oncological Research, Faculty of Medicine and Health Sciences, University of Antwerp, Antwerp, Belgium

Luc Dirix, Steven Van Laere, Gert G. Van den Eynden & Peter Vermeulen

307. Simon Fraser University, Burnaby, BC, Canada

Nilgun Donmez, Ermin Hodzic, Salem Malikic, S. Cenk Sahinalp & Iman Sarrafi

308. University of Pennsylvania, Philadelphia, PA, USA

Ronny Drapkin

309. Faculty of Science and Technology, University of Vic—Central University of Catalonia (UVic-UCC), Vic, Spain

Ana Dueso-Barroso

310. The Wellcome Trust, London, UK

Michael Dunn

311. The Hospital for Sick Children, Toronto, ON, Canada

Lewis Jonathan Dursi

312. Department of Pathology, Queen Elizabeth University Hospital, Glasgow, UK

Fraser R. Duthie

313. Department of Genetics and Computational Biology, QIMR Berghofer Medical Research Institute, Brisbane, QLD, Australia

Ken Dutton-Regester, Nicholas K. Hayward, Oliver Holmes, Peter A. Johansson, Stephen H. Kazakoff, Conrad R. Leonard, Felicity Newell, Katia Nones, Ann-Marie Patch, John V. Pearson, Antonia L. Pritchard, Michael C. Quinn, Paresh Vyas, Nicola Waddell, Scott Wood & Qinying Xu

314. Department of Oncology, Centre for Cancer Genetic Epidemiology, University of Cambridge, Cambridge, UK

Douglas F. Easton

315. Department of Public Health and Primary Care, Centre for Cancer Genetic Epidemiology, University of Cambridge, Cambridge, UK

Douglas F. Easton

316. Prostate Cancer Canada, Toronto, ON, Canada

Stuart Edmonds

317. University of Cambridge, Cambridge, UK

Paul A. Edwards, Anthony R. Green, Andy G. Lynch, Florian Markowetz & Thomas J. Mitchell

318. Department of Laboratory Medicine, Translational Cancer Research, Lund University Cancer Center at Medicon Village, Lund University, Lund, Sweden

Anna Ehinger

319. Heidelberg University, Heidelberg, Germany

Juergen Eils, Roland Eils & Daniel Hübschmann

320. New BIH Digital Health Center, Berlin Institute of Health (BIH) and Charité - Universitätsmedizin Berlin, Berlin, Germany

Juergen Eils, Roland Eils & Chris Lawerenz

321. CIBER Epidemiología y Salud Pública (CIBERESP), Madrid, Spain

Georgia Escaramis

322. Research Group on Statistics, Econometrics and Health (GRECS), UdG, Barcelona, Spain

Georgia Escaramis

323. Quantitative Genomics Laboratories (qGenomics), Barcelona, Spain

Xavier Estivill

324. Icelandic Cancer Registry, Icelandic Cancer Society, Reykjavik, Iceland

Jorunn E. Eyfjord, Holmfridur Hilmarsdottir & Jon G. Jonasson

325. State Key Laboratory of Cancer Biology, and Xijing Hospital of Digestive Diseases, Fourth Military Medical University, Shaanxi, China

Daiming Fan & Yongzhan Nie

326. Department of Medicine (DIMED), Surgical Pathology Unit, University of Padua, Padua, Italy

Matteo Fassan

327. Rigshospitalet, Copenhagen, Denmark

Francesco Favero

328. Center for Cancer Genomics, National Cancer Institute, National Institutes of Health, Bethesda, MD, USA

Martin L. Ferguson

329. Department of Biochemistry and Molecular Medicine, University of Montreal, Montreal, QC, Canada

Vincent Ferretti

330. Australian Institute of Tropical Health and Medicine, James Cook University, Douglas, QLD, Australia

Matthew A. Field

331. Department of Neuro-Oncology, Istituto Neurologico Besta, Milano, Italy

Gaetano Finocchiaro

332. Bioplatforms Australia, North Ryde, NSW, Australia

Anna Fitzgerald & Catherine A. Shang

333. Department of Pathology (Research), University College London Cancer Institute, London, UK

Adrienne M. Flanagan

334. Department of Surgical Oncology, Princess Margaret Cancer Centre, Toronto, ON, Canada

Neil E. Fleshner

335. Department of Medical Oncology, Josephine Nefkens Institute and Cancer Genomics Centre, Erasmus Medical Center, Rotterdam, CN, The Netherlands

John A. Foekens, John W. M. Martens, F. Germán Rodríguez-González, Anieta M. Sieuwerts & Marcel Smid

336. The University of Queensland Thoracic Research Centre, The Prince Charles Hospital, Brisbane, QLD, Australia

Kwun M. Fong

337. CIBIO/InBIO - Research Center in Biodiversity and Genetic Resources, Universidade do Porto, Vairão, Portugal

Nuno A. Fonseca

338. HCA Laboratories, London, UK

Christopher S. Foster

339. University of Liverpool, Liverpool, UK

Christopher S. Foster

340. The Azrieli Faculty of Medicine, Bar-Ilan University, Safed, Israel

Milana Frenkel-Morgenstern

341. Department of Neurosurgery, University of Florida, Gainesville, FL, USA

William Friedman

342. Department of Pathology, Graduate School of Medicine, University of Tokyo, Tokyo, Japan

Masashi Fukayama & Tetsuo Ushiku

343. University of Milano Bicocca, Monza, Italy

Carlo Gambacorti-Passerini

344. BGI-Shenzhen, Shenzhen, China

Shengjie Gao, Yong Hou, Chang Li, Lin Li, Siliang Li, Xiaobo Li, Xinyue Li, Dongbing Liu, Xingmin Liu, Qiang Pan-Hammarström, Hong Su, Jian Wang, Kui Wu, Heng Xiong, Huanming Yang, Chen Ye, Xiuqing Zhang, Yong Zhou & Shida Zhu

345. Department of Pathology, Oslo University Hospital Ulleval, Oslo, Norway

Øystein Garred

346. Center for Biomedical Informatics, Harvard Medical School, Boston, MA, USA

Nils Gehlenborg

347. Department Biochemistry and Molecular Biomedicine, University of Barcelona, Barcelona, Spain

Josep L. L. Gelpi

348. Office of Cancer Genomics, National Cancer Institute, National Institutes of Health, Bethesda, MD, USA

Daniela S. Gerhard

349. Cancer Epigenomics, German Cancer Research Center (DKFZ), Heidelberg, Germany

Clarissa Gerhauser, Christoph Plass & Dieter Weichenhan

350. Department of Cancer Biology, The University of Texas MD Anderson Cancer Center, Houston, TX, USA

Jeffrey E. Gershenwald

351. Department of Surgical Oncology, The University of Texas MD Anderson Cancer Center, Houston, TX, USA

Jeffrey E. Gershenwald

352. Department of Computer Science, Yale University, New Haven, CT, USA

Mark Gerstein & Fabio C. P. Navarro

353. Department of Molecular Biophysics and Biochemistry, Yale University, New Haven, CT, USA

Mark Gerstein, Sushant Kumar, Lucas Lochovsky, Shaoke Lou, Patrick D. McGillivray, Fabio C. P. Navarro, Leonidas Salichos & Jonathan Warrell

354. Program in Computational Biology and Bioinformatics, Yale University, New Haven, CT, USA

Mark Gerstein, Arif O. Harmanci, Sushant Kumar, Donghoon Lee, Shantao Li, Xiaotong Li, Lucas Lochovsky, Shaoke Lou, William Meyerson, Leonidas Salichos, Jonathan Warrell, Jing Zhang & Yan Zhang

355. Center for Cancer Research, Massachusetts General Hospital, Boston, MA, USA

Gad Getz & Paz Polak

356. Department of Pathology, Massachusetts General Hospital, Boston, MA, USA

Gad Getz

357. Department of Pathology, Memorial Sloan Kettering Cancer Center, New York, NY, USA

Ronald Ghossein, Dilip D. Giri, Christine A. Iacobuzio-Donahue, Jorge Reis-Filho & Victor Reuter

358. Division of Gastroenterology and Hepatology, Mayo Clinic, Rochester, MN, USA

Nasra H. Giama, Catherine D. Moser & Lewis R. Roberts

359. University of Sydney, Sydney, NSW, Australia

Anthony J. Gill & James G. Kench

360. University of Oxford, Oxford, UK

Pelvender Gill, Freddie C. Hamdy, Katalin Karaszi, Adam Lambert, Luke Marsden, Clare Verrill & Paresh Vyas

361. Department of Surgery, Academic Urology Group, University of Cambridge, Cambridge, UK

Vincent J. Gnanapragasam

362. Department of Medicine II, University of Würzburg, Wuerzburg, Germany

Maria Elisabeth Goebler

363. Sylvester Comprehensive Cancer Center, University of Miami, Miami, FL, USA

Carmen Gomez

364. Institut Hospital del Mar d'Investigacions Mèdiques (IMIM), Barcelona, Spain

Abel Gonzalez-Perez

365. Genome Integrity and Structural Biology Laboratory, National Institute of Environmental Health Sciences (NIEHS), Durham, NC, USA

Dmitry A. Gordenin & Natalie Saini

366. St. Thomas's Hospital, London, UK

James Gossage

367. Osaka International Cancer Center, Osaka, Japan

Kunihito Gotoh

368. Department of Pathology, Skåne University Hospital, Lund University, Lund, Sweden

Dorthe Grabau

369. Department of Medical Oncology, Beatson West of Scotland Cancer Centre, Glasgow, UK

Janet S. Graham

370. National Human Genome Research Institute, National Institutes of Health, Bethesda, MD, USA

Eric Green, Carolyn M. Hutter & Heidi J. Sofia

371. Centre for Cancer Research, Victorian Comprehensive Cancer Centre, University of Melbourne, Melbourne, VIC, Australia

Sean M. Grimmond

372. Department of Medicine, Section of Hematology/Oncology, University of Chicago, Chicago, IL, USA

Robert L. Grossman

373. German Center for Infection Research (DZIF), Partner Site Hamburg-Borstel-Lübeck-Riems, Hamburg, Germany

Adam Grundhoff

374. Bioinformatics Research Centre (BiRC), Aarhus University, Aarhus, Denmark

Qianyun Guo, Asger Hobolth & Jakob Skou Pedersen

375. Department of Biotechnology, Ministry of Science and Technology, Government of India, New Delhi, Delhi, India

Shailja Gupta & K. VijayRaghavan

376. National Cancer Centre Singapore, Singapore, Singapore

Jonathan Göke

377. Brandeis University, Waltham, MA, USA

James E. Haber

378. Department of Urologic Sciences, University of British Columbia, Vancouver, BC, Canada

Faraz Hach

379. Department of Internal Medicine, Stanford University, Stanford, CA, USA

Mark P. Hamilton

380. The University of Texas Health Science Center at Houston, Houston, TX, USA

Leng Han, Yang Yang & Xuanping Zhang

381. Imperial College NHS Trust, Imperial College, London, INY, UK

George B. Hanna

382. Senckenberg Institute of Pathology, University of Frankfurt Medical School, Frankfurt, Germany

Martin Hansmann

383. Department of Medicine, Division of Biomedical Informatics, UC San Diego School of Medicine, San Diego, CA, USA

Olivier Harismendy

384. Center for Precision Health, School of Biomedical Informatics, The University of Texas Health Science Center, Houston, TX, USA

Arif O. Harmanci

385. Oxford Nanopore Technologies, New York, NY, USA

Eoghan Harrington & Sissel Juul

386. Institute of Medical Science, University of Tokyo, Tokyo, Japan

Takanori Hasegawa, Shuto Hayashi, Seiya Imoto, Mitsuhiro Komura, Satoru Miyano, Naoki Miyoshi, Kazuhiro Ohi, Eigo Shimizu, Yuichi Shiraishi, Hiroko Tanaka & Rui Yamaguchi

387. Howard Hughes Medical Institute, University of California Santa Cruz, Santa Cruz, CA, USA

David Haussler

388. Wakayama Medical University, Wakayama, Japan

Shinya Hayami, Masaki Ueno & Hiroki Yamaue

389. Department of Internal Medicine, Division of Medical Oncology, Lineberger Comprehensive Cancer Center, University of North Carolina at Chapel Hill, Chapel Hill, NC, USA

D. Neil Hayes

390. University of Tennessee Health Science Center for Cancer Research, Memphis, TN, USA

D. Neil Hayes

391. Department of Histopathology, Salford Royal NHS Foundation Trust, Salford, UK

Stephen J. Hayes

392. Faculty of Biology, Medicine and Health, University of Manchester, Manchester, UK

Stephen J. Hayes

393. BIOPIC, ICG and College of Life Sciences, Peking University, Beijing, China

Yao He & Zemin Zhang

394. Peking-Tsinghua Center for Life Sciences, Peking University, Beijing, China

Yao He & Zemin Zhang

395. Children's Hospital of Philadelphia, Philadelphia, PA, USA

Allison P. Heath

396. Department of Bioinformatics and Computational Biology and Department of Systems Biology, The University of Texas MD Anderson Cancer Center, Houston, TX, USA

Apurva M. Hegde, Yiling Lu & John N. Weinstein

397. Karolinska Institute, Stockholm, Sweden

Eva Hellstrom-Lindberg & Jesper Lagergren

398. The Donnelly Centre, University of Toronto, Toronto, ON, Canada

Mohamed Helmy & Jeffrey A. Wintersinger

399. Department of Medical Genetics, College of Medicine, Hallym University, Chuncheon, South Korea

Seong Gu Heo, Eun Pyo Hong & Ji Wan Park

400. Department of Experimental and Health Sciences, Institute of Evolutionary Biology (UPF-CSIC), Universitat Pompeu Fabra, Barcelona, Spain

José María Heredia-Genestar, Tomas Marques-Bonet & Arcadi Navarro

401. Health Data Science Unit, University Clinics, Heidelberg, Germany

Carl Herrmann

402. Massachusetts General Hospital Center for Cancer Research, Charlestown, MA, USA

Julian M. Hess & Yosef E. Maruvka

403. Hokkaido University, Sapporo, Japan

Satoshi Hirano & Toru Nakamura

404. Department of Pathology and Clinical Laboratory, National Cancer Center Hospital, Tokyo, Japan

Nobuyoshi Hiraoka

405. Department of Genetics, University of North Carolina at Chapel Hill, Chapel Hill, NC, USA

Katherine A. Hoadley & Tara J. Skelly

406. Computational Biology, Leibniz Institute on Aging - Fritz Lipmann Institute (FLI), Jena, Germany

Steve Hoffmann

407. University of Melbourne Centre for Cancer Research, Melbourne, VIC, Australia

Oliver Hofmann

408. University of Nebraska Medical Center, Omaha, NE, USA

Michael A. Hollingsworth & Sarah P. Thayer

409. Syntekabio Inc, Daejeon, South Korea

Jongwhi H. Hong

410. Department of Pathology, Academic Medical Center, Amsterdam, AZ, The Netherlands

Gerrit K. Hooijer

411. China National GeneBank-Shenzhen, Shenzhen, China

Yong Hou, Chang Li, Siliang Li, Xiaobo Li, Dongbing Liu, Xingmin Liu, Henk G. Stunnenberg, Hong Su, Kui Wu, Heng Xiong, Chen Ye & Shida Zhu

412. Division of Molecular Genetics, German Cancer Research Center (DKFZ), Heidelberg, Germany

Volker Hovestadt, Murat Iskar, Peter Lichter, Bernhard Radlwimmer & Marc Zapatka

413. Division of Life Science and Applied Genomics Center, Hong Kong University of Science and Technology, Clear Water Bay, Hong Kong, China

Taobo Hu, Yogesh Kumar, Eric Z. Ma, Zhenggang Wu & Hong Xue

414. Icahn School of Medicine at Mount Sinai, New York, NY, USA

Kuan-lin Huang

415. Geneplus-Shenzhen, Shenzhen, China

Yi Huang

416. School of Computer Science and Technology, Xi’an Jiaotong University, Xi’an, China

Yi Huang, Jiayin Wang, Xiao Xiao & Xuanping Zhang

417. AbbVie, North Chicago, IL, USA

Thomas J. Hudson

418. Institute of Pathology, Charité – University Medicine Berlin, Berlin, Germany

Michael Hummel & Dido Lenze

419. Centre for Translational and Applied Genomics, British Columbia Cancer Agency, Vancouver, BC, Canada

David Huntsman

420. Edinburgh Royal Infirmary, Edinburgh, UK

Ted R. Hupp

421. Berlin Institute for Medical Systems Biology, Max Delbrück Center for Molecular Medicine, Berlin, Germany

Matthew R. Huska, Julia Markowski & Roland F. Schwarz

422. Department of Pediatric Immunology, Hematology and Oncology, University Hospital, Heidelberg, Germany

Daniel Hübschmann

423. German Cancer Research Center (DKFZ), Heidelberg, Germany

Daniel Hübschmann, Christof von Kalle & Roland F. Schwarz

424. Heidelberg Institute for Stem Cell Technology and Experimental Medicine (HI-STEM), Heidelberg, Germany

Daniel Hübschmann

425. Institute for Computational Biomedicine, Weill Cornell Medical College, New York, NY, USA

Marcin Imielinski

426. New York Genome Center, New York, NY, USA

Marcin Imielinski & Xiaotong Yao

427. Department of Urology, James Buchanan Brady Urological Institute, Johns Hopkins University School of Medicine, Baltimore, MD, USA

William B. Isaacs

428. Department of Preventive Medicine, Graduate School of Medicine, The University of Tokyo, Tokyo, Japan

Shumpei Ishikawa, Hiroto Katoh & Daisuke Komura

429. Department of Molecular and Cellular Biology, Baylor College of Medicine, Houston, TX, USA

Michael Ittmann

430. Department of Pathology and Immunology, Baylor College of Medicine, Houston, TX, USA

Michael Ittmann

431. Michael E. DeBakey Veterans Affairs Medical Center, Houston, TX, USA

Michael Ittmann

432. Technical University of Denmark, Lyngby, Denmark

Jose M. G. Izarzugaza

433. Department of Pathology, College of Medicine, Hanyang University, Seoul, South Korea

Jocelyne Jacquemier, Hyung-Yong Kim & Gu Kong

434. Academic Unit of Surgery, School of Medicine, College of Medical, Veterinary and Life Sciences, University of Glasgow, Glasgow Royal Infirmary, Glasgow, UK

Nigel B. Jamieson

435. Department of Pathology, Asan Medical Center, College of Medicine, Ulsan University, Songpa-gu, Seoul, South Korea

Se Jin Jang & Hee Jin Lee

436. Science Writer, Garrett Park, MD, USA

Karine Jegalian

437. International Cancer Genome Consortium (ICGC)/ICGC Accelerating Research in Genomic Oncology (ARGO) Secretariat, Ontario Institute for Cancer Research, Toronto, ON, Canada

Jennifer L. Jennings

438. University of Ljubljana, Ljubljana, Slovenia

Lara Jerman

439. Department of Public Health Sciences, University of Chicago, Chicago, IL, USA

Yuan Ji

440. Research Institute, NorthShore University HealthSystem, Evanston, IL, USA

Yuan Ji

441. Department for Biomedical Research, University of Bern, Bern, Switzerland

Rory Johnson, Andrés Lanzós & Mark A. Rubin

442. Centre of Genomics and Policy, McGill University and Génome Québec Innovation Centre, Montreal, QC, Canada

Yann Joly, Bartha M. Knoppers, Mark Phillips & Adrian Thorogood

443. Carolina Center for Genome Sciences, University of North Carolina at Chapel Hill, Chapel Hill, NC, USA

Corbin D. Jones

444. Hopp Children's Cancer Center (KiTZ), Heidelberg, Germany

David T. W. Jones, Marcel Kool & Stefan M. Pfister

445. Pediatric Glioma Research Group, German Cancer Research Center (DKFZ), Heidelberg, Germany

David T. W. Jones

446. Cancer Research UK, London, UK

Nic Jones & David Scott

447. Indivumed GmbH, Hamburg, Germany

Hartmut Juhl

448. Genome Integration Data Center, Syntekabio, Inc, Daejeon, South Korea

Jongsun Jung

449. University Hospital Zurich, Zurich, Switzerland

Andre Kahles, Kjong-Van Lehmann & Gunnar Rätsch

450. Clinical Bioinformatics, Swiss Institute of Bioinformatics, Geneva, Switzerland

Abdullah Kahraman

451. Institute for Pathology and Molecular Pathology, University Hospital Zurich, Zurich, Switzerland

Abdullah Kahraman

452. Institute of Molecular Life Sciences, University of Zurich, Zurich, Switzerland

Abdullah Kahraman & Christian von Mering

453. MRC Human Genetics Unit, MRC IGMM, University of Edinburgh, Edinburgh, UK

Vera B. Kaiser & Colin A. Semple

454. Women's Cancer Program at the Samuel Oschin Comprehensive Cancer Institute, Cedars-Sinai Medical Center, Los Angeles, CA, USA

Beth Karlan

455. Department of Biology, Bioinformatics Group, Division of Molecular Biology, Faculty of Science, University of Zagreb, Zagreb, Croatia

Rosa Karlić

456. Department for Internal Medicine II, University Hospital Schleswig-Holstein, Kiel, Germany

Dennis Karsch & Michael Kneba

457. Genetics and Molecular Pathology, SA Pathology, Adelaide, SA, Australia

Karin S. Kassahn

458. Department of Gastric Surgery, National Cancer Center Hospital, Tokyo, Japan

Hitoshi Katai

459. Department of Bioinformatics, Division of Cancer Genomics, National Cancer Center Research Institute, Tokyo, Japan

Mamoru Kato, Hirofumi Rokutan & Mihoko Saito-Adachi

460. A.A. Kharkevich Institute of Information Transmission Problems, Moscow, Russia

Marat D. Kazanov

461. Oncology and Immunology, Dmitry Rogachev National Research Center of Pediatric Hematology, Moscow, Russia

Marat D. Kazanov

462. Skolkovo Institute of Science and Technology, Moscow, Russia

Marat D. Kazanov

463. Department of Surgery, The George Washington University, School of Medicine and Health Science, Washington, DC, USA

Electron Kebebew

464. Endocrine Oncology Branch, Center for Cancer Research, National Cancer Institute, National Institutes of Health, Bethesda, MD, USA

Electron Kebebew

465. Melanoma Institute Australia, Macquarie University, Sydney, NSW, Australia

Richard F. Kefford

466. MIT Computer Science and Artificial Intelligence Laboratory, Massachusetts Institute of Technology, Cambridge, MA, USA

Manolis Kellis

467. Tissue Pathology and Diagnostic Oncology, Royal Prince Alfred Hospital, Sydney, NSW, Australia

James G. Kench & Richard A. Scolyer

468. Cholangiocarcinoma Screening and Care Program and Liver Fluke and Cholangiocarcinoma Research Centre, Faculty of Medicine, Khon Kaen University, Khon Kaen, Thailand

Narong Khuntikeo

469. Controlled Department and Institution, New York, NY, USA

Ekta Khurana

470. Englander Institute for Precision Medicine, Weill Cornell Medicine, New York, NY, USA

Ekta Khurana & Alexander Martinez-Fundichely

471. National Cancer Center, Gyeonggi, South Korea

Hark Kyun Kim

472. Department of Biochemistry, College of Medicine, Ewha Womans University, Seoul, South Korea

Hyung-Lae Kim

473. Health Sciences Department of Biomedical Informatics, University of California San Diego, La Jolla, CA, USA

Jihoon Kim

474. Research Core Center, National Cancer Centre Korea, Goyang-si, South Korea

Jong K. Kim

475. Department of Health Sciences and Technology, Sungkyunkwan University School of Medicine, Seoul, South Korea

Youngwook Kim

476. Samsung Genome Institute, Seoul, South Korea

Youngwook Kim

477. Breast Oncology Program, Dana-Farber/Brigham and Women's Cancer Center, Boston, MA, USA

Tari A. King

478. Department of Surgery, Memorial Sloan Kettering Cancer Center, New York, NY, USA

Tari A. King & Samuel Singer

479. Division of Breast Surgery, Brigham and Women's Hospital, Boston, MA, USA

Tari A. King

480. Integrative Bioinformatics Support Group, National Institute of Environmental Health Sciences (NIEHS), Durham, NC, USA

Leszek J. Klimczak

481. Department of Clinical Science, University of Bergen, Bergen, Norway

Stian Knappskog & Ola Myklebost

482. Center For Medical Innovation, Seoul National University Hospital, Seoul, South Korea

Youngil Koh

483. Department of Internal Medicine, Seoul National University Hospital, Seoul, South Korea

Youngil Koh & Sung-Soo Yoon

484. Institute of Computer Science, Polish Academy of Sciences, Warsawa, Poland

Jan Komorowski

485. Functional and Structural Genomics, German Cancer Research Center (DKFZ), Heidelberg, Germany

Marcel Kool, Andrey Korshunov, Michael Koscher, Stefan M. Pfister & Qi Wang

486. Laboratory of Translational Genomics, Division of Cancer Epidemiology and Genetics, National Cancer Institute, , National Institutes of Health, Bethesda, MD, USA

Roelof Koster

487. Institute for Medical Informatics Statistics and Epidemiology, University of Leipzig, Leipzig, Germany

Markus Kreuz & Markus Loeffler

488. Morgan Welch Inflammatory Breast Cancer Research Program and Clinic, The University of Texas MD Anderson Cancer Center, Houston, TX, USA

Savitri Krishnamurthy

489. Department of Hematology and Oncology, Georg-Augusts-University of Göttingen, Göttingen, Germany

Dieter Kube & Lorenz H. P. Trümper

490. Institute of Cell Biology (Cancer Research), University of Duisburg-Essen, Essen, Germany

Ralf Küppers

491. King’s College London and Guy’s and St. Thomas’ NHS Foundation Trust, London, UK

Jesper Lagergren

492. Center for Epigenetics, Van Andel Research Institute, Grand Rapids, MI, USA

Peter W. Laird

493. The University of Queensland Centre for Clinical Research, Royal Brisbane and Women’s Hospital, Herston, QLD, Australia

Sunil R. Lakhani & Peter T. Simpson

494. Department of Pediatric Oncology and Hematology, University of Cologne, Cologne, Germany

Pablo Landgraf

495. University of Düsseldorf, Düsseldorf, Germany

Pablo Landgraf & Guido Reifenberger

496. Department of Pathology, Institut Jules Bordet, Brussels, Belgium

Denis Larsimont

497. Institute of Biomedicine, Sahlgrenska Academy at University of Gothenburg, Gothenburg, Sweden

Erik Larsson

498. Children’s Medical Research Institute, Sydney, NSW, Australia

Loretta M. S. Lau & Hilda A. Pickett

499. ILSbio, LLC Biobank, Chestertown, MD, USA

Xuan Le

500. Division of Genetics and Genomics, Boston Children's Hospital, Harvard Medical School, Boston, MA, USA

Eunjung Alice Lee

501. Institute for Bioengineering and Biopharmaceutical Research (IBBR), Hanyang University, Seoul, South Korea

Jeong-Yeon Lee

502. Department of Statistics, University of California Santa Cruz, Santa Cruz, CA, USA

Juhee Lee

503. National Genotyping Center, Institute of Biomedical Sciences, Academia Sinica, Taipei, Taiwan

Ming Ta Michael Lee

504. Department of Vertebrate Genomics/Otto Warburg Laboratory Gene Regulation and Systems Biology of Cancer, Max Planck Institute for Molecular Genetics, Berlin, Germany

Hans Lehrach, Hans-Jörg Warnatz & Marie-Laure Yaspo

505. McGill University and Genome Quebec Innovation Centre, Montreal, QC, Canada

Louis Letourneau

506. biobyte solutions GmbH, Heidelberg, Germany

Ivica Letunic

507. Gynecologic Oncology, NYU Laura and Isaac Perlmutter Cancer Center, New York University, New York, NY, USA

Douglas A. Levine

508. Division of Oncology, Stem Cell Biology Section, Washington University School of Medicine, St. Louis, MO, USA

Tim Ley

509. Department of Systems Biology, The University of Texas MD Anderson Cancer Center, Houston, TX, USA

Han Liang

510. Harvard University, Cambridge, MA, USA

Ziao Lin

511. Urologic Oncology Branch, Center for Cancer Research, National Cancer Institute, National Institutes of Health, Bethesda, MD, USA

W. M. Linehan

512. University of Oslo, Oslo, Norway

Ole Christian Lingjærde & Torill Sauer

513. University of Toronto, Toronto, ON, Canada

Fei-Fei Fei Liu, Quaid D. Morris, Ruian Shi, Shankar Vembu & Fan Yang

514. Peking University, Beijing, China

Fenglin Liu, Fan Zhang, Liangtao Zheng & Xiuqing Zheng

515. School of Life Sciences, Peking University, Beijing, China

Fenglin Liu

516. Leidos Biomedical Research, Inc, McLean, VA, USA

Jia Liu

517. Hematology, Hospital Clinic, Institut d'Investigacions Biomèdiques August Pi i Sunyer (IDIBAPS), University of Barcelona, Barcelona, Spain

Armando Lopez-Guillermo

518. Second Military Medical University, Shanghai, China

Yong-Jie Lu & Hongwei Zhang

519. Chinese Cancer Genome Consortium, Shenzhen, China

Youyong Lu

520. Department of Medical Oncology, Beijing Hospital, Beijing, China

Youyong Lu

521. Laboratory of Molecular Oncology, Key Laboratory of Carcinogenesis and Translational Research (Ministry of Education), Peking University Cancer Hospital and Institute, Beijing, China

Youyong Lu & Rui Xing

522. School of Medicine/School of Mathematics and Statistics, University of St. Andrews, St, Andrews, Fife, UK

Andy G. Lynch

523. Institute for Systems Biology, Seattle, WA, USA

Lisa Lype, Sheila M. Reynolds & Ilya Shmulevich

524. Department of Biochemistry and Molecular Biology, Faculty of Medicine, University Institute of Oncology-IUOPA, Oviedo, Spain

Carlos López-Otín & Xose S. Puente

525. Institut Bergonié, Bordeaux, France

Gaetan MacGrogan

526. Cancer Unit, MRC University of Cambridge, Cambridge, UK

Shona MacRae

527. Department of Pathology and Laboratory Medicine, Center for Personalized Medicine, Children's Hospital Los Angeles, Los Angeles, CA, USA

Dennis T. Maglinte

528. John Curtin School of Medical Research, Canberra, ACT, Australia

Graham J. Mann

529. MVZ Department of Oncology, PraxisClinic am Johannisplatz, Leipzig, Germany

Luisa Mantovani-Löffler

530. Department of Information Technology, Ghent University, Ghent, Belgium

Kathleen Marchal & Sergio Pulido-Tamayo

531. Department of Plant Biotechnology and Bioinformatics, Ghent University, Ghent, Belgium

Kathleen Marchal, Sergio Pulido-Tamayo & Lieven P. C. Verbeke

532. Institute for Genomic Medicine, Nationwide Children's Hospital, Columbus, OH, USA

Elaine R. Mardis

533. Computational Biology Program, School of Medicine, Oregon Health and Science University, Portland, OR, USA

Adam A. Margolin & Adam J. Struck

534. Department of Surgery, Duke University, Durham, NC, USA

Jeffrey Marks

535. Institució Catalana de Recerca i Estudis Avançats (ICREA), Barcelona, Spain

Tomas Marques-Bonet, Jose I. Martin-Subero, Arcadi Navarro, David Torrents & Alfonso Valencia

536. Institut Català de Paleontologia Miquel Crusafont, Universitat Autònoma de Barcelona, Barcelona, Spain

Tomas Marques-Bonet

537. University of Glasgow, Glasgow, UK

Sancha Martin & Ke Yuan

538. Institut d'Investigacions Biomèdiques August Pi i Sunyer (IDIBAPS), Barcelona, Spain

Jose I. Martin-Subero

539. Division of Oncology, Washington University School of Medicine, St. Louis, MO, USA

R. Jay Mashl

540. Department of Surgery and Cancer, Imperial College, London, INY, UK

Erik Mayer

541. Applications Department, Oxford Nanopore Technologies, Oxford, UK

Simon Mayes & Daniel J. Turner

542. Department of Obstetrics, Gynecology and Reproductive Services, University of California San Francisco, San Francisco, CA, USA

Karen McCune & Karen Smith-McCune

543. Department of Biochemistry and Molecular Medicine, University California at Davis, Sacramento, CA, USA

John D. McPherson

544. STTARR Innovation Facility, Princess Margaret Cancer Centre, Toronto, ON, Canada

Alice Meng

545. Discipline of Surgery, Western Sydney University, Penrith, NSW, Australia

Neil D. Merrett

546. Yale School of Medicine, Yale University, New Haven, CT, USA

William Meyerson

547. Department of Genetics, Lineberger Comprehensive Cancer Center, University of North Carolina at Chapel Hill, Chapel Hill, NC, USA

Piotr A. Mieczkowski, Joel S. Parker, Charles M. Perou, Donghui Tan, Umadevi Veluvolu & Matthew D. Wilkerson

548. Departments of Neurology and Neurosurgery, Henry Ford Hospital, Detroit, MI, USA

Tom Mikkelsen

549. Precision Oncology, OHSU Knight Cancer Institute, Oregon Health and Science University, Portland, OR, USA

Gordon B. Mills

550. Institute of Pathology, University Medical Center Hamburg-Eppendorf, Hamburg, Germany

Sarah Minner, Guido Sauter & Ronald Simon

551. Department of Health Sciences, Faculty of Medical Sciences, Kyushu University, Fukuoka, Japan

Shinichi Mizuno

552. Heidelberg Academy of Sciences and Humanities, Heidelberg, Germany

Fruzsina Molnár-Gábor

553. Department of Clinical Pathology, University of Melbourne, Melbourne, VIC, Australia

Carl Morrison, Karin A. Oien, Chawalit Pairojkul, Paul M. Waring & Marc J. van de Vijver

554. Department of Pathology, Roswell Park Cancer Institute, Buffalo, NY, USA

Carl Morrison

555. Department of Computer Science, University of Helsinki, Helsinki, Finland

Ville Mustonen

556. Institute of Biotechnology, University of Helsinki, Helsinki, Finland

Ville Mustonen

557. Organismal and Evolutionary Biology Research Programme, University of Helsinki, Helsinki, Finland

Ville Mustonen

558. Department of Obstetrics and Gynecology, Division of Gynecologic Oncology, Washington University School of Medicine, St. Louis, MO, USA

David Mutch

559. Penrose St. Francis Health Services, Colorado Springs, CO, USA

Jerome Myers

560. Institute of Pathology, Ulm University and University Hospital of Ulm, Ulm, Germany

Peter Möller

561. National Cancer Center, Tokyo, Japan

Hitoshi Nakagama

562. Genome Institute of Singapore, Singapore, Singapore

Tannistha Nandi & Patrick Tan

563. 32Program in Computational Biology and Bioinformatics, Yale University, New Haven, CT, USA

Fabio C. P. Navarro

564. German Cancer Aid, Bonn, Germany

Gerd Nettekoven & Laura Planko

565. Programme in Cancer and Stem Cell Biology, Centre for Computational Biology, Duke-NUS Medical School, Singapore,

Singapore

Alvin Wei Tian Ng

566. The Chinese University of Hong Kong, Shatin, NT, Hong Kong, China

Anthony Ng

567. Fourth Military Medical University, Shaanxi, China

Yongzhan Nie

568. The University of Cambridge School of Clinical Medicine, Cambridge, UK

Serena Nik-Zainal

569. St. Jude Children's Research Hospital, Memphis, TN, USA

Paul A. Northcott

570. University Health Network, Princess Margaret Cancer Centre, Toronto, ON, Canada

Faiyaz Notta & Ming Tsao

571. Center for Biomolecular Science and Engineering, University of California Santa Cruz, Santa Cruz, CA, USA

Brian D. O'Connor

572. Department of Medicine, University of Chicago, Chicago, IL, USA

Peter O'Donnell

573. Department of Neurology, Mayo Clinic, Rochester, MN, USA

Brian Patrick O'Neill

574. Cambridge Oesophagogastric Centre, Cambridge University Hospitals NHS Foundation Trust, Cambridge, UK

J. Robert O'Neill

575. Department of Computer Science, Carleton College, Northfield, MN, USA

Layla Oesper

576. Institute of Cancer Sciences, College of Medical Veterinary and Life Sciences, University of Glasgow, Glasgow, UK

Karin A. Oien

577. Department of Epidemiology, University of Alabama at Birmingham, Birmingham, AL, USA

Akinyemi I. Ojesina

578. HudsonAlpha Institute for Biotechnology, Huntsville, AL, USA

Akinyemi I. Ojesina

579. O'Neal Comprehensive Cancer Center, University of Alabama at Birmingham, Birmingham, AL, USA

Akinyemi I. Ojesina

580. Department of Pathology, Keio University School of Medicine, Tokyo, Japan

Hidenori Ojima

581. Department of Hepatobiliary and Pancreatic Oncology, National Cancer Center Hospital, Tokyo, Japan

Takuji Okusaka

582. Sage Bionetworks, Seattle, WA, USA

Larsson Omberg

583. Lymphoma Genomic Translational Research Laboratory, National Cancer Centre, Singapore, Singapore

Choon Kiat Ong

584. Department of Clinical Pathology, Robert-Bosch-Hospital, Stuttgart, Germany

German Ott

585. Department of Cell and Systems Biology, University of Toronto, Toronto, ON, Canada

B. F. Francis Ouellette

586. Department of Biosciences and Nutrition, Karolinska Institutet, Stockholm, Sweden

Qiang Pan-Hammarström

587. Center for Liver Cancer, Research Institute and Hospital, National Cancer Center, Gyeonggi, South Korea

Joong-Won Park

588. Division of Hematology-Oncology, Samsung Medical Center, Sungkyunkwan University School of Medicine, Seoul, South Korea

Keunchil Park

589. Samsung Advanced Institute for Health Sciences and Technology, Sungkyunkwan University School of Medicine, Seoul, South Korea

Keunchil Park

590. Cheonan Industry-Academic Collaboration Foundation, Sangmyung University, Cheonan, South Korea

Kiejung Park

591. NYU Langone Medical Center, New York, NY, USA

Harvey Pass

592. Department of Hematology and Medical Oncology, Cleveland Clinic, Cleveland, OH, USA

Nathan A. Pennell

593. Department of Radiation Oncology, University of California San Francisco, San Francisco, CA, USA

Marc D. Perry

594. Department of Health Sciences Research, Mayo Clinic, Rochester, MN, USA

Gloria M. Petersen

595. Helen F. Graham Cancer Center at Christiana Care Health Systems, Newark, DE, USA

Nicholas Petrelli

596. Heidelberg University Hospital, Heidelberg, Germany

Stefan M. Pfister

597. CSRA Incorporated, Fairfax, VA, USA

Todd D. Pihl

598. Research Department of Pathology, University College London Cancer Institute, London, UK

Nischalan Pillay

599. Department of Research Oncology, Guy's Hospital, King's Health Partners AHSC, King's College London School of Medicine, London, UK

Sarah Pinder

600. Faculty of Medicine and Health Sciences, Macquarie University, Sydney, NSW, Australia

Andreia V. Pinho

601. University Hospital of Minjoz, INSERM UMR 1098, Besançon, France

Xavier Pivot

602. Spanish National Cancer Research Centre, Madrid, Spain

Tirso Pons

603. Center of Digestive Diseases and Liver Transplantation, Fundeni Clinical Institute, Bucharest, Romania

Irinel Popescu

604. Cureline, Inc, South San Francisco, CA, USA

Olga Potapova

605. St. Luke's Cancer Centre, Royal Surrey County Hospital NHS Foundation Trust, Guildford, UK

Shaun R. Preston

606. Cambridge Breast Unit, Addenbrooke's Hospital, Cambridge University Hospital NHS Foundation Trust and NIHR Cambridge Biomedical Research Centre, Cambridge, UK

Elena Provenzano

607. East of Scotland Breast Service, Ninewells Hospital, Aberdeen, UK

Colin A. Purdie

608. Department of Genetics, Microbiology and Statistics, University of Barcelona, IRSJD, IBUB, Barcelona, Spain

Raquel Rabionet

609. Department of Obstetrics and Gynecology, Medical College of Wisconsin, Milwaukee, WI, USA

Janet S. Rader

610. Hematology and Medical Oncology, Winship Cancer Institute of Emory University, Atlanta, GA, USA

Suresh Ramalingam

611. Department of Computer Science, Princeton University, Princeton, NJ, USA

Benjamin J. Raphael & Matthew A. Reyna

612. Vanderbilt Ingram Cancer Center, Vanderbilt University, Nashville, TN, USA

W. Kimryn Rathmell

613. Ohio State University College of Medicine and Arthur G. James Comprehensive Cancer Center, Columbus, OH, USA

Matthew Ringel

614. Department of Surgery, Yokohama City University Graduate School of Medicine, Kanagawa, Japan

Yasushi Rino

615. Division of Chromatin Networks, German Cancer Research Center (DKFZ) and BioQuant, Heidelberg, Germany

Karsten Rippe

616. Research Computing Center, University of North Carolina at Chapel Hill, Chapel Hill, NC, USA

Jeffrey Roach

617. School of Molecular Biosciences and Center for Reproductive Biology, Washington State University, Pullman, WA, USA

Steven A. Roberts

618. Finsen Laboratory and Biotech Research and Innovation Centre (BRIC), University of Copenhagen, Copenhagen, Denmark

F. Germán Rodríguez-González, Nikos Sidiropoulos & Joachim Weischenfeldt

619. Department of Laboratory Medicine and Pathobiology, University of Toronto, Toronto, ON, Canada

Michael H. A. Roehrl & Stefano Serra

620. Department of Pathology, Human Oncology and Pathogenesis Program, Memorial Sloan Kettering Cancer Center, New York, NY, USA

Michael H. A. Roehrl

621. University Hospital Giessen, Pediatric Hematology and Oncology, Giessen, Germany

Marius Rohde

622. Oncologie Sénologie, ICM Institut Régional du Cancer, Montpellier, France

Gilles Romieu

623. Institute of Clinical Molecular Biology, Christian-Albrechts-University, Kiel, Germany

Philip C. Rosenstiel & Markus B. Schilhabel

624. Institute of Pathology, University of Wuerzburg, Wuerzburg, Germany

Andreas Rosenwald

625. Department of Urology, North Bristol NHS Trust, Bristol, UK

Edward W. Rowe

626. SingHealth, Duke-NUS Institute of Precision Medicine, National Heart Centre Singapore, Singapore, Singapore

Steven G. Rozen, Patrick Tan & Bin Tean Teh

627. Department of Computer Science, University of Toronto, Toronto, ON, Canada

Yulia Rubanova, Jared T. Simpson & Jeffrey A. Wintersinger

628. Bern Center for Precision Medicine, University Hospital of Bern, University of Bern, Bern, Switzerland

Mark A. Rubin

629. Englander Institute for Precision Medicine, Weill Cornell Medicine and New York Presbyterian Hospital, New York, NY, USA

Mark A. Rubin

630. Meyer Cancer Center, Weill Cornell Medicine, New York, NY, USA

Mark A. Rubin

631. Pathology and Laboratory, Weill Cornell Medical College, New York, NY, USA

Mark A. Rubin

632. Vall d'Hebron Institute of Oncology: VHIO, Barcelona, Spain

Carlota Rubio-Perez

633. General and Hepatobiliary-Biliary Surgery, Pancreas Institute, University and Hospital Trust of Verona, Verona, Italy

Andrea Ruzzenente

634. National Centre for Biological Sciences, Tata Institute of Fundamental Research, Bangalore, India

Radhakrishnan Sabarinathan

635. Indiana University, Bloomington, IN, USA

S. Cenk Sahinalp

636. Department of Pathology, GZA-ZNA Hospitals, Antwerp, Belgium

Roberto Salgado

637. Analytical Biological Services, Inc, Wilmington, DE, USA

Charles Saller

638. Sydney Medical School, University of Sydney, Sydney, NSW, Australia

Jaswinder S. Samra & Richard A. Scolyer

639. cBio Center, Dana-Farber Cancer Institute, Harvard Medical School, Boston, MA, USA

Chris Sander & Ciyue Shen

640. Department of Cell Biology, Harvard Medical School, Boston, MA, USA

Chris Sander & Ciyue Shen

641. Advanced Centre for Treatment Research and Education in Cancer, Tata Memorial Centre, Navi Mumbai, Maharashtra, India

Rajiv Sarin

642. School of Environmental and Life Sciences, Faculty of Science, The University of Newcastle, Ourimbah, NSW, Australia

Christopher J. Scarlett

643. Department of Dermatology, University Hospital of Essen, Essen, Germany

Dirk Schadendorf

644. Bioinformatics and Omics Data Analytics, German Cancer Research Center (DKFZ), Heidelberg, Germany

Matthias Schlesner

645. Department of Urology, Charité Universitätsmedizin Berlin, Berlin, Germany

Thorsten Schlomm & Joachim Weischenfeldt

646. Martini-Clinic, Prostate Cancer Center, University Medical Center Hamburg-Eppendorf, Hamburg, Germany

Thorsten Schlomm

647. Department of General Internal Medicine, University of Kiel, Kiel, Germany

Stefan Schreiber

648. German Cancer Consortium (DKTK), Partner site Berlin, Berlin, Germany

Roland F. Schwarz

649. Cancer Research Institute, Beth Israel Deaconess Medical Center, Boston, MA, USA

Ralph Scully

650. University of Pittsburgh, Pittsburgh, PA, USA

Raja Seethala

651. Department of Ophthalmology and Ocular Genomics Institute, Massachusetts Eye and Ear, Harvard Medical School, Boston, MA, USA

Ayellet V. Segre

652. Center for Psychiatric Genetics, NorthShore University HealthSystem, Evanston, IL, USA

Subhajit Sengupta

653. Van Andel Research Institute, Grand Rapids, MI, USA

Hui Shen & Wanding Zhou

654. Laboratory of Molecular Medicine, Human Genome Center, Institute of Medical Science, University of Tokyo, Tokyo, Japan

Tatsuhiro Shibata, Hirokazu Taniguchi & Tomoko Urushidate

655. Japan Agency for Medical Research and Development, Tokyo, Japan

Kiyo Shimizu & Takashi Yugawa

656. Korea University, Seoul, South Korea

Seung Jun Shin & Stefan G. Stark

657. Murtha Cancer Center, Walter Reed National Military Medical Center, Bethesda, MD, USA

Craig Shriver

658. Human Genetics, University of Kiel, Kiel, Germany

Reiner Siebert

659. Department of Oncologic Pathology, Dana-Farber Cancer Institute, Harvard Medical School, Boston, MA, USA

Sabina Signoretti

660. Oregon Health and Science University, Portland, OR, USA

Jaclyn Smith

661. Center for RNA Interference and Noncoding RNA, The University of Texas MD Anderson Cancer Center, Houston, TX, USA

Anil K. Sood

662. Department of Experimental Therapeutics, The University of Texas MD Anderson Cancer Center, Houston, TX, USA

Anil K. Sood

663. Department of Gynecologic Oncology and Reproductive Medicine, The University of Texas MD Anderson Cancer Center, Houston, TX, USA

Anil K. Sood

664. University Hospitals Coventry and Warwickshire NHS Trust, Coventry, UK

Sharmila Sothi

665. Department of Radiation Oncology, Radboud University Nijmegen Medical Centre, Nijmegen, GA, The Netherlands

Paul N. Span

666. Institute for Genomics and Systems Biology, University of Chicago, Chicago, IL, USA

Jonathan Spring

667. Clinic for Hematology and Oncology, St.-Antonius-Hospital, Eschweiler, Germany

Peter Staib

668. Computational and Systems Biology Program, Memorial Sloan Kettering Cancer Center, New York, NY, USA

Stefan G. Stark

669. University of Iceland, Reykjavik, Iceland

Ólafur Andri Stefánsson

670. Division of Computational Genomics and Systems Genetics, German Cancer Research Center (DKFZ), Heidelberg, Germany

Oliver Stegle

671. Dundee Cancer Centre, Ninewells Hospital, Dundee, UK

Alasdair Stenhouse & Alastair M. Thompson

672. Department for Internal Medicine III, University of Ulm and University Hospital of Ulm, Ulm, Germany

Stephan Stilgenbauer

673. Institut Curie, INSERM Unit 830, Paris, France

Henk G. Stunnenberg & Anne Vincent-Salomon

674. Department of Gastroenterology and Hepatology, Yokohama City University Graduate School of Medicine, Kanagawa, Japan

Akihiro Suzuki

675. Department of Laboratory Medicine, Radboud University Nijmegen Medical Centre, Nijmegen, GA, The Netherlands

Fred Sweep

676. Division of Cancer Genome Research, German Cancer Research Center (DKFZ), Heidelberg, Germany

Holger Sültmann

677. Department of General Surgery, Singapore General Hospital, Singapore, Singapore

Benita Kiat Tee Tan

678. Cancer Science Institute of Singapore, National University of Singapore, Singapore, Singapore

Patrick Tan & Bin Tean Teh

679. Department of Medical and Clinical Genetics, Genome-Scale Biology Research Program, University of Helsinki, Helsinki, Finland

Tomas J. Tanskanen

680. East Anglian Medical Genetics Service, Cambridge University Hospitals NHS Foundation Trust, Cambridge, UK

Patrick Tarpey

681. Irving Institute for Cancer Dynamics, Columbia University, New York, NY, USA

Simon Tavaré

682. Institute of Molecular and Cell Biology, Singapore, Singapore

Bin Tean Teh

683. Laboratory of Cancer Epigenome, Division of Medical Science, National Cancer Centre Singapore, Singapore, Singapore

Bin Tean Teh

684. Universite Lyon, INCa-Synergie, Centre Léon Bérard, Lyon, France

Gilles Thomas

685. Department of Urology, Mayo Clinic, Rochester, MN, USA

R. Houston Thompson

686. Royal National Orthopaedic Hospital - Stanmore, Stanmore, Middlesex, UK

Roberto Tirabosco

687. Department of Biochemistry, Genetics and Immunology, University of Vigo, Vigo, Spain

Marta Tojo

688. Giovanni Paolo II / I.R.C.C.S. Cancer Institute, Bari, BA, Italy

Stefania Tommasi

689. Neuroblastoma Genomics, German Cancer Research Center (DKFZ), Heidelberg, Germany

Umut H. Toprak

690. Fondazione Policlinico Universitario Gemelli IRCCS, Rome, Italy, Rome, Italy

Giampaolo Tortora

691. University of Verona, Verona, Italy

Giampaolo Tortora

692. Centre National de Génotypage, CEA - Institute de Génomique, Evry, France

Jörg Tost

693. CAPHRI Research School, Maastricht University, Maastricht, ER, The Netherlands

David Townend

694. Department of Biopathology, Centre Léon Bérard, Lyon, France

Isabelle Treilleux

695. Université Claude Bernard Lyon 1, Villeurbanne, France

Isabelle Treilleux

696. Core Research for Evolutional Science and Technology (CREST), JST, Tokyo, Japan

Tatsuhiko Tsunoda

697. Department of Biological Sciences, Laboratory for Medical Science Mathematics, Graduate School of Science, University of Tokyo, Yokohama, Japan

Tatsuhiko Tsunoda

698. Department of Medical Science Mathematics, Medical Research Institute, Tokyo Medical and Dental University (TMDU), Tokyo, Japan

Tatsuhiko Tsunoda

699. Cancer Ageing and Somatic Mutation Programme, Wellcome Sanger Institute, Hinxton, UK

Jose M. C. Tubio

700. University Hospitals Birmingham NHS Foundation Trust, Birmingham, UK

Olga Tucker

701. Centre for Cancer Research and Cell Biology, Queen's University, Belfast, UK

Richard Turkington

702. Breast Medical Oncology, The University of Texas MD Anderson Cancer Center, Houston, TX, USA

Naoto T. Ueno

703. Department of Surgery, Johns Hopkins University School of Medicine, Baltimore, MD, USA

Christopher Umbricht

704. Department of Oncology-Pathology, Science for Life Laboratory, Karolinska Institute, Stockholm, Sweden

Husen M. Umer

705. School of Cancer Sciences, Faculty of Medicine, University of Southampton, Southampton, UK

Timothy J. Underwood

706. Department of Gene Technology, Tallinn University of Technology, Tallinn, Estonia

Liis Uusküla-Reimand

707. Genetics and Genome Biology Program, SickKids Research Institute, The Hospital for Sick Children, Toronto, ON, Canada

Liis Uusküla-Reimand

708. Departments of Neurosurgery and Hematology and Medical Oncology, Winship Cancer Institute and School of Medicine, Emory University, Atlanta, GA, USA

Erwin G. Van Meir

709. Department of Clinical and Molecular Medicine, Faculty of Medicine and Health Sciences, Norwegian University of Science and Technology, Trondheim, Norway

Miguel Vazquez

710. Argmix Consulting, North Vancouver, BC, Canada

Shankar Vembu

711. Department of Information Technology, Ghent University, Interuniversitair Micro-Electronica Centrum (IMEC), Ghent, Belgium

Lieven P. C. Verbeke

712. Nuffield Department of Surgical Sciences, John Radcliffe Hospital, University of Oxford, Oxford, UK

Clare Verrill

713. Institute of Mathematics and Computer Science, University of Latvia, Riga, LV, Latvia

Juris Viksna

714. Discipline of Pathology, Sydney Medical School, University of Sydney, Sydney, NSW, Australia

Ricardo E. Vilain

715. Department of Applied Mathematics and Theoretical Physics, Centre for Mathematical Sciences, University of Cambridge, Cambridge, UK

Ignacio Vázquez-García

716. Department of Epidemiology and Biostatistics, Memorial Sloan Kettering Cancer Center, New York, NY, USA

Ignacio Vázquez-García & Venkata D. Yellapantula

717. Department of Statistics, Columbia University, New York, NY, USA

Ignacio Vázquez-García

718. Department of Immunology, Genetics and Pathology, Science for Life Laboratory, Uppsala University, Uppsala, Sweden

Claes Wadelius

719. School of Electronic and Information Engineering, Xi’an Jiaotong University, Xi’an, China

Jiayin Wang & Kai Ye

720. Department of Histopathology, Cambridge University Hospitals NHS Foundation Trust, Cambridge, UK

Anne Y. Warren

721. Oxford NIHR Biomedical Research Centre, University of Oxford, Oxford, UK

David C. Wedge

722. Georgia Regents University Cancer Center, Augusta, GA, USA

Paul Weinberger

723. Wythenshawe Hospital, Manchester, UK

Ian Welch

724. Department of Genetics, Washington University School of Medicine, St.Louis, MO, USA

Michael C. Wendl

725. Department of Biological Oceanography, Leibniz Institute of Baltic Sea Research, Rostock, Germany

Johannes Werner

726. Wellcome Centre for Human Genetics, University of Oxford, Oxford, UK

Justin P. Whalley

727. Department of Molecular and Human Genetics, Baylor College of Medicine, Houston, TX, USA

David A. Wheeler

728. Thoracic Oncology Laboratory, Mayo Clinic, Rochester, MN, USA

Dennis Wigle

729. Institute for Genomic Medicine, Nationwide Children’s Hospital, Columbus, OH, USA

Richard K. Wilson

730. Department of Obstetrics and Gynecology, Division of Gynecologic Oncology, Mayo Clinic, Rochester, MN, USA

Boris Winterhoff

731. International Institute for Molecular Oncology, Poznań, Poland

Maciej Wiznerowicz

732. Poznan University of Medical Sciences, Poznań, Poland

Maciej Wiznerowicz

733. Genomics and Proteomics Core Facility High Throughput Sequencing Unit, German Cancer Research Center (DKFZ), Heidelberg, Germany

Stephan Wolf

734. NCCS-VARI Translational Research Laboratory, National Cancer Centre Singapore, Singapore, Singapore

Bernice H. Wong

735. Edison Family Center for Genome Sciences and Systems Biology, Washington University, St. Louis, MO, USA

Winghing Wong

736. MRC-University of Glasgow Centre for Virus Research, Glasgow, UK

Derek W. Wright

737. Department of Medical Informatics and Clinical Epidemiology, Division of Bioinformatics and Computational Biology, OHSU Knight Cancer Institute, Oregon Health and Science University, Portland, OR, USA

Guanming Wu

738. School of Electronic Information and Communications, Huazhong University of Science and Technology, Wuhan, China

Tian Xia

739. Department of Applied Mathematics and Statistics, Johns Hopkins University, Baltimore, MD, USA

Yanxun Xu

740. Department of Cancer Genome Informatics, Graduate School of Medicine, Osaka University, Osaka, Japan

Shinichi Yachida

741. Institute of Computer Science, Heidelberg University, Heidelberg, Germany

Sergei Yakneen

742. School of Mathematics and Statistics, University of Sydney, Sydney, NSW, Australia

Jean Y. Yang

743. Ben May Department for Cancer Research, University of Chicago, Chicago, IL, USA

Lixing Yang

744. Department of Human Genetics, University of Chicago, Chicago, IL, USA

Lixing Yang

745. Tri-Institutional PhD Program in Computational Biology and Medicine, Weill Cornell Medicine, New York, NY, USA

Xiaotong Yao

746. The First Affiliated Hospital, Xi'an Jiaotong University, Xi'an, China

Kai Ye

747. Department of Medicine and Therapeutics, The Chinese University of Hong Kong, Shatin, NT, Hong Kong, China

Jun Yu

748. Department of Biostatistics, The University of Texas MD Anderson Cancer Center, Houston, TX, USA

Kaixian Yu & Hongtu Zhu

749. Duke-NUS Medical School, Singapore, Singapore

Willie Yu

750. Department of Surgery, Ruijin Hospital, Shanghai Jiaotong University School of Medicine, Shanghai, China

Yingyan Yu

751. School of Computing Science, University of Glasgow, Glasgow, UK

Ke Yuan

752. Division of Orthopaedic Surgery, Oslo University Hospital, Oslo, Norway

Olga Zaikova

753. Eastern Clinical School, Monash University, Melbourne, VIC, Australia

Nikolajs Zeps

754. Epworth HealthCare, Richmond, VIC, Australia

Nikolajs Zeps

755. Department of Biostatistics and Computational Biology, Dana-Farber Cancer Institute and Harvard Medical School, Boston, MA, USA

Cheng-Zhong Zhang

756. Department of Biomedical Informatics, College of Medicine, The Ohio State University, Columbus, OH, USA

Yan Zhang

757. The Ohio State University Comprehensive Cancer Center (OSUCCC – James), Columbus, OH, USA

Yan Zhang

758. The University of Texas School of Biomedical Informatics (SBMI) at Houston, Houston, TX, USA

Zhongming Zhao

759. Department of Biostatistics, University of North Carolina at Chapel Hill, Chapel Hill, NC, USA

Hongtu Zhu

760. Department of Biochemistry and Molecular Genetics, Feinberg School of Medicine, Northwestern University, Chicago, IL, USA

Lihua Zou

761. Faculty of Medicine and Health, University of Sydney, Sydney, NSW, Australia

Anna deFazio

762. Department of Pathology, Erasmus Medical Center Rotterdam, Rotterdam, GD, The Netherlands

Carolien H. M. van Deurzen

763. Division of Molecular Carcinogenesis, The Netherlands Cancer Institute, Amsterdam, CX, The Netherlands

L. van’t Veer

764. Institute of Molecular Life Sciences and Swiss Institute of Bioinformatics, University of Zurich, Zurich, Switzerland

Christian von Mering

Consortia

PCAWG Mutational Signatures Working Group

- Ludmil B. Alexandrov
- , Erik N. Bergstrom
- , Arnoud Boot
- , Paul Boutros
- , Kin Chan
- , Kyle R. Covington
- , Akihiro Fujimoto
- , Gad Getz
- , Dmitry A. Gordenin
- , Nicholas J. Haradhvala
- , Mi Ni Huang
- , S. M. Ashiqul Islam
- , Marat Kazanov
- , Jaegil Kim

- , Leszek J. Klimczak
- , Nuria Lopez-Bigas
- , Michael Lawrence
- , Iñigo Martincorena
- , John R. McPherson
- , Sandro Morganella
- , Ville Mustonen
- , Hidewaki Nakagawa
- , Alvin Wei Tian Ng
- , Paz Polak
- , Stephenie Prokopec
- , Steven A. Roberts
- , Steven G. Rozen
- , Radhakrishnan Sabarinathan
- , Natalie Saini
- , Tatsuhiro Shibata
- , Yuichi Shiraishi
- , Michael R. Stratton
- , Bin Tean Teh
- , Ignacio Vázquez-García
- , David A. Wheeler
- , Yang Wu
- , Fouad Yousif
- & Willie Yu

PCAWG Consortium

- Lauri A. Aaltonen
- , Federico Abascal
- , Adam Abeshouse
- , Hiroyuki Aburatani
- , David J. Adams
- , Nishant Agrawal
- , Keun Soo Ahn
- , Sung-Min Ahn
- , Hiroshi Aikata
- , Rehan Akbani

- , Kadir C. Akdemir
- , Hikmat Al-Ahmadie
- , Sultan T. Al-Sedairy
- , Fatima Al-Shahrour
- , Malik Alawi
- , Monique Albert
- , Kenneth Aldape
- , Ludmil B. Alexandrov
- , Adrian Ally
- , Kathryn Alsop
- , Eva G. Alvarez
- , Fernanda Amary
- , Samirkumar B. Amin
- , Brice Aminou
- , Ole Ammerpohl
- , Matthew J. Anderson
- , Yeng Ang
- , Davide Antonello
- , Pavana Anur
- , Samuel Aparicio
- , Elizabeth L. Appelbaum
- , Yasuhito Arai
- , Axel Aretz
- , Koji Arihiro
- , Shun-ichi Ariizumi
- , Joshua Armenia
- , Laurent Arnould
- , Sylvia Asa
- , Yassen Assenov
- , Gurnit Atwal
- , Sietse Aukema
- , J. Todd Auman
- , Miriam R. R. Aure
- , Philip Awadalla
- , Marta Aymerich
- , Gary D. Bader
- , Adrian Baez-Ortega

- , Matthew H. Bailey
- , Peter J. Bailey
- , Miruna Balasundaram
- , Saianand Balu
- , Pratiti Bandopadhayay
- , Rosamonde E. Banks
- , Stefano Barbi
- , Andrew P. Barbour
- , Jonathan Barenboim
- , Jill Barnholtz-Sloan
- , Hugh Barr
- , Elisabet Barrera
- , John Bartlett
- , Javier Bartolome
- , Claudio Bassi
- , Oliver F. Bathe
- , Daniel Baumhoer
- , Prashant Bavi
- , Stephen B. Baylin
- , Wojciech Bazant
- , Duncan Beardsmore
- , Timothy A. Beck
- , Sam Behjati
- , Andreas Behren
- , Beifang Niu
- , Cindy Bell
- , Sergi Beltran
- , Christopher Benz
- , Andrew Berchuck
- , Anke K. Bergmann
- , Erik N. Bergstrom
- , Benjamin P. Berman
- , Daniel M. Berney
- , Stephan H. Bernhart
- , Rameen Beroukhim
- , Mario Berrios
- , Samantha Bersani

- , Johanna Bertl
- , Miguel Betancourt
- , Vinayak Bhandari
- , Shriram G. Bhosle
- , Andrew V. Biankin
- , Matthias Bieg
- , Darell Bigner
- , Hans Binder
- , Ewan Birney
- , Michael Birrer
- , Nidhan K. Biswas
- , Bodil Bjerkehagen
- , Tom Bodenheimer
- , Lori Boice
- , Giada Bonizzato
- , Johann S. De Bono
- , Arnoud Boot
- , Moiz S. Bootwalla
- , Ake Borg
- , Arndt Borkhardt
- , Keith A. Boroevich
- , Ivan Borozan
- , Christoph Borst
- , Marcus Bosenberg
- , Mattia Bosio
- , Jacqueline Boultwood
- , Guillaume Bourque
- , Paul C. Boutros
- , G. Steven Bova
- , David T. Bowen
- , Reanne Bowlby
- , David D. L. Bowtell
- , Sandrine Boyault
- , Rich Boyce
- , Jeffrey Boyd
- , Alvis Brazma
- , Paul Brennan

- , Daniel S. Brewer
- , Arie B. Brinkman
- , Robert G. Bristow
- , Russell R. Broaddus
- , Jane E. Brock
- , Malcolm Brock
- , Annegien Broeks
- , Angela N. Brooks
- , Denise Brooks
- , Benedikt Brors
- , Søren Brunak
- , Timothy J. C. Bruxner
- , Alicia L. Bruzos
- , Alex Buchanan
- , Ivo Buchhalter
- , Christiane Buchholz
- , Susan Bullman
- , Hazel Burke
- , Birgit Burkhardt
- , Kathleen H. Burns
- , John Busanovich
- , Carlos D. Bustamante
- , Adam P. Butler
- , Atul J. Butte
- , Niall J. Byrne
- , Anne-Lise Børresen-Dale
- , Samantha J. Caesar-Johnson
- , Andy Cafferkey
- , Declan Cahill
- , Claudia Calabrese
- , Carlos Caldas
- , Fabien Calvo
- , Niedzica Camacho
- , Peter J. Campbell
- , Elias Campo
- , Cinzia Cantù
- , Shaolong Cao

- , Thomas E. Carey
- , Joana Carlevaro-Fita
- , Rebecca Carlsen
- , Ivana Cataldo
- , Mario Cazzola
- , Jonathan Cebon
- , Robert Cerfolio
- , Dianne E. Chadwick
- , Dimple Chakravarty
- , Don Chalmers
- , Calvin Wing Yiu Chan
- , Kin Chan
- , Michelle Chan-Seng-Yue
- , Vishal S. Chandan
- , David K. Chang
- , Stephen J. Chanock
- , Lorraine A. Chantrill
- , Aurélien Chateigner
- , Nilanjan Chatterjee
- , Kazuaki Chayama
- , Hsiao-Wei Chen
- , Jieming Chen
- , Ken Chen
- , Yiwen Chen
- , Zhaohong Chen
- , Andrew D. Cherniack
- , Jeremy Chien
- , Yoke-Eng Chiew
- , Suet-Feung Chin
- , Juok Cho
- , Sunghoon Cho
- , Jung Kyoon Choi
- , Wan Choi
- , Christine Chomienne
- , Zechen Chong
- , Su Pin Choo
- , Angela Chou

- , Angelika N. Christ
- , Elizabeth L. Christie
- , Eric Chuah
- , Carrie Cibulskis
- , Kristian Cibulskis
- , Sara Cingarlini
- , Peter Clapham
- , Alexander Claviez
- , Sean Cleary
- , Nicole Cloonan
- , Marek Cmero
- , Colin C. Collins
- , Ashton A. Connor
- , Susanna L. Cooke
- , Colin S. Cooper
- , Leslie Cope
- , Vincenzo Corbo
- , Matthew G. Cordes
- , Stephen M. Cordner
- , Isidro Cortés-Ciriano
- , Kyle Covington
- , Prue A. Cowin
- , Brian Craft
- , David Craft
- , Chad J. Creighton
- , Yupeng Cun
- , Erin Curley
- , Ioana Cutcutache
- , Karolina Czajka
- , Bogdan Czerniak
- , Rebecca A. Dagg
- , Ludmila Danilova
- , Maria Vittoria Davi
- , Natalie R. Davidson
- , Helen Davies
- , Ian J. Davis
- , Brandi N. Davis-Dusenbery

- , Kevin J. Dawson
- , Francisco M. De La Vega
- , Ricardo De Paoli-Iseppi
- , Timothy Defreitas
- , Angelo P. Dei Tos
- , Olivier Delaneau
- , John A. Demchok
- , Jonas Demeulemeester
- , German M. Demidov
- , Deniz Demircioğlu
- , Nening M. Dennis
- , Robert E. Denroche
- , Stefan C. Dentro
- , Nikita Desai
- , Vikram Deshpande
- , Amit G. Deshwar
- , Christine Desmedt
- , Jordi Deu-Pons
- , Noreen Dhalla
- , Neesha C. Dhani
- , Priyanka Dhingra
- , Rajiv Dhir
- , Anthony DiBiase
- , Klev Diamanti
- , Li Ding
- , Shuai Ding
- , Huy Q. Dinh
- , Luc Dirix
- , HarshaVardhan Doddapaneni
- , Nilgun Donmez
- , Michelle T. Dow
- , Ronny Drapkin
- , Oliver Drechsel
- , Ruben M. Drews
- , Serge Serge
- , Tim Dudderidge
- , Ana Dueso-Barroso

- , Andrew J. Dunford
- , Michael Dunn
- , Lewis Jonathan Dursi
- , Fraser R. Duthie
- , Ken Dutton-Regester
- , Jenna Eagles
- , Douglas F. Easton
- , Stuart Edmonds
- , Paul A. Edwards
- , Sandra E. Edwards
- , Rosalind A. Eeles
- , Anna Ehinger
- , Juergen Eils
- , Roland Eils
- , Adel El-Naggar
- , Matthew Eldridge
- , Kyle Ellrott
- , Serap Erkek
- , Georgia Escaramis
- , Shadrielle M. G. Espiritu
- , Xavier Estivill
- , Dariush Etemadmoghadam
- , Jorunn E. Eyfjord
- , Bishoy M. Faltas
- , Daiming Fan
- , Yu Fan
- , William C. Faquin
- , Claudiu Farcas
- , Matteo Fassan
- , Aquila Fatima
- , Francesco Favero
- , Nodirjon Fayzullaev
- , Ina Felau
- , Sian Fereday
- , Martin L. Ferguson
- , Vincent Ferretti
- , Lars Feuerbach

- , Matthew A. Field
- , J. Lynn Fink
- , Gaetano Finocchiaro
- , Cyril Fisher
- , Matthew W. Fittall
- , Anna Fitzgerald
- , Rebecca C. Fitzgerald
- , Adrienne M. Flanagan
- , Neil E. Fleshner
- , Paul Flicek
- , John A. Foekens
- , Kwun M. Fong
- , Nuno A. Fonseca
- , Christopher S. Foster
- , Natalie S. Fox
- , Michael Fraser
- , Scott Frazer
- , Milana Frenkel-Morgenstern
- , William Friedman
- , Joan Frigola
- , Catrina C. Fronick
- , Akihiro Fujimoto
- , Masashi Fujita
- , Masashi Fukayama
- , Lucinda A. Fulton
- , Robert S. Fulton
- , Mayuko Furuta
- , P. Andrew Futreal
- , Anja Füllgrabe
- , Stacey B. Gabriel
- , Steven Gallinger
- , Carlo Gambacorti-Passerini
- , Jianjiong Gao
- , Shengjie Gao
- , Levi Garraway
- , Øystein Garred
- , Erik Garrison

- , Dale W. Garsed
- , Nils Gehlenborg
- , Josep L. L. Gelpi
- , Joshy George
- , Daniela S. Gerhard
- , Clarissa Gerhauser
- , Jeffrey E. Gershenwald
- , Mark Gerstein
- , Moritz Gerstung
- , Gad Getz
- , Mohammed Ghori
- , Ronald Ghossein
- , Nasra H. Giama
- , Richard A. Gibbs
- , Bob Gibson
- , Anthony J. Gill
- , Pelvender Gill
- , Dilip D. Giri
- , Dominik Glodzik
- , Vincent J. Gnanapragasam
- , Maria Elisabeth Goebler
- , Mary J. Goldman
- , Carmen Gomez
- , Santiago Gonzalez
- , Abel Gonzalez-Perez
- , Dmitry A. Gordenin
- , James Gossage
- , Kunihito Gotoh
- , Ramaswamy Govindan
- , Dorthe Grabau
- , Janet S. Graham
- , Robert C. Grant
- , Anthony R. Green
- , Eric Green
- , Liliana Greger
- , Nicola Grehan
- , Sonia Grimaldi

- , Sean M. Grimmond
- , Robert L. Grossman
- , Adam Grundhoff
- , Gunes Gundem
- , Qianyun Guo
- , Manaswi Gupta
- , Shailja Gupta
- , Ivo G. Gut
- , Marta Gut
- , Jonathan Göke
- , Gavin Ha
- , Andrea Haake
- , David Haan
- , Siegfried Haas
- , Kerstin Haase
- , James E. Haber
- , Nina Habermann
- , Faraz Hach
- , Syed Haider
- , Natsuko Hama
- , Freddie C. Hamdy
- , Anne Hamilton
- , Mark P. Hamilton
- , Leng Han
- , George B. Hanna
- , Martin Hansmann
- , Nicholas J. Haradhvala
- , Olivier Harismendy
- , Ivon Harliwong
- , Arif O. Harmanci
- , Eoghan Harrington
- , Takanori Hasegawa
- , David Haussler
- , Steve Hawkins
- , Shinya Hayami
- , Shuto Hayashi
- , D. Neil Hayes

- , Stephen J. Hayes
- , Nicholas K. Hayward
- , Steven Hazell
- , Yao He
- , Allison P. Heath
- , Simon C. Heath
- , David Hedley
- , Apurva M. Hegde
- , David I. Heiman
- , Michael C. Heinold
- , Zachary Heins
- , Lawrence E. Heisler
- , Eva Hellstrom-Lindberg
- , Mohamed Helmy
- , Seong Gu Heo
- , Austin J. Hepperla
- , José María Heredia-Genestar
- , Carl Herrmann
- , Peter Hersey
- , Julian M. Hess
- , Holmfridur Hilmarsdottir
- , Jonathan Hinton
- , Satoshi Hirano
- , Nobuyoshi Hiraoka
- , Katherine A. Hoadley
- , Asger Hobolth
- , Ermin Hodzic
- , Jessica I. Hoell
- , Steve Hoffmann
- , Oliver Hofmann
- , Andrea Holbrook
- , Aliaksei Z. Holik
- , Michael A. Hollingsworth
- , Oliver Holmes
- , Robert A. Holt
- , Chen Hong
- , Eun Pyo Hong

- , Jongwhi H. Hong
- , Gerrit K. Hooijer
- , Henrik Hornshøj
- , Fumie Hosoda
- , Yong Hou
- , Volker Hovestadt
- , William Howat
- , Alan P. Hoyle
- , Ralph H. Hruban
- , Jianhong Hu
- , Taobo Hu
- , Xing Hua
- , Kuan-lin Huang
- , Mei Huang
- , Mi Ni Huang
- , Vincent Huang
- , Yi Huang
- , Wolfgang Huber
- , Thomas J. Hudson
- , Michael Hummel
- , Jillian A. Hung
- , David Huntsman
- , Ted R. Hupp
- , Jason Huse
- , Matthew R. Huska
- , Barbara Hutter
- , Carolyn M. Hutter
- , Daniel Hübschmann
- , Christine A. Iacobuzio-Donahue
- , Charles David Imbusch
- , Marcin Imielinski
- , Seiya Imoto
- , William B. Isaacs
- , Keren Isaev
- , Shumpei Ishikawa
- , Murat Iskar
- , S. M. Ashiqul Islam

- , Michael Ittmann
- , Sinisa Ivkovic
- , Jose M. G. Izarzugaza
- , Jocelyne Jacquemier
- , Valerie Jakrot
- , Nigel B. Jamieson
- , Gun Ho Jang
- , Se Jin Jang
- , Joy C. Jayaseelan
- , Reyka Jayasinghe
- , Stuart R. Jefferys
- , Karine Jegalian
- , Jennifer L. Jennings
- , Seung-Hyup Jeon
- , Lara Jerman
- , Yuan Ji
- , Wei Jiao
- , Peter A. Johansson
- , Amber L. Johns
- , Jeremy Johns
- , Rory Johnson
- , Todd A. Johnson
- , Clemency Jolly
- , Yann Joly
- , Jon G. Jonasson
- , Corbin D. Jones
- , David R. Jones
- , David T. W. Jones
- , Nic Jones
- , Steven J. M. Jones
- , Jos Jonkers
- , Young Seok Ju
- , Hartmut Juhl
- , Jongsun Jung
- , Malene Juul
- , Randi Istrup Juul
- , Sissel Juul

- , Natalie Jäger
- , Rolf Kabbe
- , Andre Kahles
- , Abdullah Kahraman
- , Vera B. Kaiser
- , Hojabr Kakavand
- , Sangeetha Kalimuthu
- , Christof von Kalle
- , Koo Jeong Kang
- , Katalin Karaszi
- , Beth Karlan
- , Rosa Karlić
- , Dennis Karsch
- , Katayoon Kasaian
- , Karin S. Kassahn
- , Hitoshi Katai
- , Mamoru Kato
- , Hiroto Katoh
- , Yoshiiku Kawakami
- , Jonathan D. Kay
- , Stephen H. Kazakoff
- , Marat D. Kazanov
- , Maria Keays
- , Electron Kebebew
- , Richard F. Kefford
- , Manolis Kellis
- , James G. Kench
- , Catherine J. Kennedy
- , Jules N. A. Kerssemakers
- , David Khoo
- , Vincent Khoo
- , Narong Khuntikeo
- , Ekta Khurana
- , Helena Kilpinen
- , Hark Kyun Kim
- , Hyung-Lae Kim
- , Hyung-Yong Kim

- , Hyunghwan Kim
- , Jaegil Kim
- , Jihoon Kim
- , Jong K. Kim
- , Youngwook Kim
- , Tari A. King
- , Wolfram Klapper
- , Kortine Kleinheinz
- , Leszek J. Klimczak
- , Stian Knappskog
- , Michael Kneba
- , Bartha M. Knoppers
- , Youngil Koh
- , Jan Komorowski
- , Daisuke Komura
- , Mitsuhiro Komura
- , Gu Kong
- , Marcel Kool
- , Jan O. Korbel
- , Viktoriya Korchina
- , Andrey Korshunov
- , Michael Koscher
- , Roelof Koster
- , Zsofia Kote-Jarai
- , Antonios Koures
- , Milena Kovacevic
- , Barbara Kremeyer
- , Helene Kretzmer
- , Markus Kreuz
- , Savitri Krishnamurthy
- , Dieter Kube
- , Kiran Kumar
- , Pardeep Kumar
- , Sushant Kumar
- , Yogesh Kumar
- , Ritika Kundra
- , Kirsten Kübler

- , Ralf Küppers
- , Jesper Lagergren
- , Phillip H. Lai
- , Peter W. Laird
- , Sunil R. Lakhani
- , Christopher M. Lalansingh
- , Emilie Lalonde
- , Fabien C. Lamaze
- , Adam Lambert
- , Eric Lander
- , Pablo Landgraf
- , Luca Landoni
- , Anita Langerød
- , Andrés Lanzós
- , Denis Larsimont
- , Erik Larsson
- , Mark Lathrop
- , Loretta M. S. Lau
- , Chris Lawerenz
- , Rita T. Lawlor
- , Michael S. Lawrence
- , Alexander J. Lazar
- , Ana Mijalkovic Lazic
- , Xuan Le
- , Darlene Lee
- , Donghoon Lee
- , Eunjung Alice Lee
- , Hee Jin Lee
- , Jake June-Koo Lee
- , Jeong-Yeon Lee
- , Juhee Lee
- , Ming Ta Michael Lee
- , Henry Lee-Six
- , Kjong-Van Lehmann
- , Hans Lehrach
- , Dido Lenze
- , Conrad R. Leonard

- , Daniel A. Leongamornlert
- , Ignaty Leshchiner
- , Louis Letourneau
- , Ivica Letunic
- , Douglas A. Levine
- , Lora Lewis
- , Tim Ley
- , Chang Li
- , Constance H. Li
- , Haiyan Irene Li
- , Jun Li
- , Lin Li
- , Shantao Li
- , Siliang Li
- , Xiaobo Li
- , Xiaotong Li
- , Xinyue Li
- , Yilong Li
- , Han Liang
- , Sheng-Ben Liang
- , Peter Lichter
- , Pei Lin
- , Ziao Lin
- , W. M. Linehan
- , Ole Christian Lingjærde
- , Dongbing Liu
- , Eric Minwei Liu
- , Fei-Fei Fei Liu
- , Fenglin Liu
- , Jia Liu
- , Xingmin Liu
- , Julie Livingstone
- , Dimitri Livitz
- , Naomi Livni
- , Lucas Lochovsky
- , Markus Loeffler
- , Georgina V. Long

- , Armando Lopez-Guillermo
- , Shaoke Lou
- , David N. Louis
- , Laurence B. Lovat
- , Yiling Lu
- , Yong-Jie Lu
- , Youyong Lu
- , Claudio Luchini
- , Ilinca Lungu
- , Xuemei Luo
- , Hayley J. Luxton
- , Andy G. Lynch
- , Lisa Lype
- , Cristina López
- , Carlos López-Otín
- , Eric Z. Ma
- , Yussanne Ma
- , Gaetan MacGrogan
- , Shona MacRae
- , Geoff Macintyre
- , Tobias Madsen
- , Kazuhiro Maejima
- , Andrea Mafficini
- , Dennis T. Maglinte
- , Arindam Maitra
- , Partha P. Majumder
- , Luca Malcovati
- , Salem Malikic
- , Giuseppe Malleo
- , Graham J. Mann
- , Luisa Mantovani-Löffler
- , Kathleen Marchal
- , Giovanni Marchegiani
- , Elaine R. Mardis
- , Adam A. Margolin
- , Maximillian G. Marin
- , Florian Markowetz

- , Julia Markowski
- , Jeffrey Marks
- , Tomas Marques-Bonet
- , Marco A. Marra
- , Luke Marsden
- , John W. M. Martens
- , Sancha Martin
- , Jose I. Martin-Subero
- , Iñigo Martincorena
- , Alexander Martinez-Fundichely
- , Yosef E. Maruvka
- , R. Jay Mashl
- , Charlie E. Massie
- , Thomas J. Matthew
- , Lucy Matthews
- , Erik Mayer
- , Simon Mayes
- , Michael Mayo
- , Faridah Mbabaali
- , Karen McCune
- , Ultan McDermott
- , Patrick D. McGillivray
- , Michael D. McLellan
- , John D. McPherson
- , John R. McPherson
- , Treasa A. McPherson
- , Samuel R. Meier
- , Alice Meng
- , Shaowu Meng
- , Andrew Menzies
- , Neil D. Merrett
- , Sue Merson
- , Matthew Meyerson
- , William Meyerson
- , Piotr A. Mieczkowski
- , George L. Mihaiescu
- , Sanja Mijalkovic

- , Tom Mikkelsen
- , Michele Milella
- , Linda Mileshkin
- , Christopher A. Miller
- , David K. Miller
- , Jessica K. Miller
- , Gordon B. Mills
- , Ana Milovanovic
- , Sarah Minner
- , Marco Miotto
- , Gisela Mir Arnau
- , Lisa Mirabello
- , Chris Mitchell
- , Thomas J. Mitchell
- , Satoru Miyano
- , Naoki Miyoshi
- , Shinichi Mizuno
- , Fruzsina Molnár-Gábor
- , Malcolm J. Moore
- , Richard A. Moore
- , Sandro Morganella
- , Quaid D. Morris
- , Carl Morrison
- , Lisle E. Mose
- , Catherine D. Moser
- , Ferran Muiños
- , Loris Mularoni
- , Andrew J. Mungall
- , Karen Mungall
- , Elizabeth A. Musgrove
- , Ville Mustonen
- , David Mutch
- , Francesc Muyas
- , Donna M. Muzny
- , Alfonso Muñoz
- , Jerome Myers
- , Ola Myklebost

- , Peter Möller
- , Genta Nagae
- , Adnan M. Nagrial
- , Hardeep K. Nahal-Bose
- , Hitoshi Nakagama
- , Hidewaki Nakagawa
- , Hiromi Nakamura
- , Toru Nakamura
- , Kaoru Nakano
- , Tannistha Nandi
- , Jyoti Nangalia
- , Mia Nastic
- , Arcadi Navarro
- , Fabio C. P. Navarro
- , David E. Neal
- , Gerd Nettekoven
- , Felicity Newell
- , Steven J. Newhouse
- , Yulia Newton
- , Alvin Wei Tian Ng
- , Anthony Ng
- , Jonathan Nicholson
- , David Nicol
- , Yongzhan Nie
- , G. Petur Nielsen
- , Morten Muhlig Nielsen
- , Serena Nik-Zainal
- , Michael S. Noble
- , Katia Nones
- , Paul A. Northcott
- , Faiyaz Notta
- , Brian D. O’Connor
- , Peter O’Donnell
- , Maria O’Donovan
- , Sarah O’Meara
- , Brian Patrick O’Neill
- , J. Robert O’Neill

- , David Ocana
- , Angelica Ochoa
- , Layla Oesper
- , Christopher Ogden
- , Hideki Ohdan
- , Kazuhiro Ohi
- , Lucila Ohno-Machado
- , Karin A. Oien
- , Akinyemi I. Ojesina
- , Hidenori Ojima
- , Takuji Okusaka
- , Larsson Omberg
- , Choon Kiat Ong
- , Stephan Ossowski
- , German Ott
- , B. F. Francis Ouellette
- , Christine P’ng
- , Marta Paczkowska
- , Salvatore Paiella
- , Chawalit Pairojkul
- , Marina Pajic
- , Qiang Pan-Hammarström
- , Elli Papaemmanuil
- , Irene Papatheodorou
- , Nagarajan Paramasivam
- , Ji Wan Park
- , Joong-Won Park
- , Keunchil Park
- , Kiejung Park
- , Peter J. Park
- , Joel S. Parker
- , Simon L. Parsons
- , Harvey Pass
- , Danielle Pasternack
- , Alessandro Pastore
- , Ann-Marie Patch
- , Iris Pauporté

- , Antonio Pea
- , John V. Pearson
- , Chandra Sekhar Pedamallu
- , Jakob Skou Pedersen
- , Paolo Pederzoli
- , Martin Peifer
- , Nathan A. Pennell
- , Charles M. Perou
- , Marc D. Perry
- , Gloria M. Petersen
- , Myron Peto
- , Nicholas Petrelli
- , Robert Petryszak
- , Stefan M. Pfister
- , Mark Phillips
- , Oriol Pich
- , Hilda A. Pickett
- , Todd D. Pihl
- , Nischalan Pillay
- , Sarah Pinder
- , Mark Pinese
- , Andreia V. Pinho
- , Esa Pitkänen
- , Xavier Pivot
- , Elena Piñeiro-Yáñez
- , Laura Planko
- , Christoph Plass
- , Paz Polak
- , Tirso Pons
- , Irinel Popescu
- , Olga Potapova
- , Aparna Prasad
- , Shaun R. Preston
- , Manuel Prinz
- , Antonia L. Pritchard
- , Stephenie D. Prokopec
- , Elena Provenzano

- , Xose S. Puente
- , Sonia Puig
- , Montserrat Puiggròs
- , Sergio Pulido-Tamayo
- , Gulietta M. Pupo
- , Colin A. Purdie
- , Michael C. Quinn
- , Raquel Rabionet
- , Janet S. Rader
- , Bernhard Radlwimmer
- , Petar Radovic
- , Benjamin Raeder
- , Keiran M. Raine
- , Manasa Ramakrishna
- , Kamna Ramakrishnan
- , Suresh Ramalingam
- , Benjamin J. Raphael
- , W. Kimryn Rathmell
- , Tobias Rausch
- , Guido Reifenberger
- , Jüri Reimand
- , Jorge Reis-Filho
- , Victor Reuter
- , Iker Reyes-Salazar
- , Matthew A. Reyna
- , Sheila M. Reynolds
- , Esther Rheinbay
- , Yasser Riazalhosseini
- , Andrea L. Richardson
- , Julia Richter
- , Matthew Ringel
- , Markus Ringnér
- , Yasushi Rino
- , Karsten Rippe
- , Jeffrey Roach
- , Lewis R. Roberts
- , Nicola D. Roberts

- , Steven A. Roberts
- , A. Gordon Robertson
- , Alan J. Robertson
- , Javier Bartolomé Rodriguez
- , Bernardo Rodriguez-Martin
- , F. Germán Rodríguez-González
- , Michael H. A. Roehrl
- , Marius Rohde
- , Hirofumi Rokutan
- , Gilles Romieu
- , Ilse Rooman
- , Tom Roques
- , Daniel Rosebrock
- , Mara Rosenberg
- , Philip C. Rosenstiel
- , Andreas Rosenwald
- , Edward W. Rowe
- , Romina Royo
- , Steven G. Rozen
- , Yulia Rubanova
- , Mark A. Rubin
- , Carlota Rubio-Perez
- , Vasilisa A. Rudneva
- , Borislav C. Rusev
- , Andrea Ruzzenente
- , Gunnar Rätsch
- , Radhakrishnan Sabarinathan
- , Veronica Y. Sabelnykova
- , Sara Sadeghi
- , S. Cenk Sahinalp
- , Natalie Saini
- , Mihoko Saito-Adachi
- , Gordon Saksena
- , Adriana Salcedo
- , Roberto Salgado
- , Leonidas Salichos
- , Richard Sallari

- , Charles Saller
- , Roberto Salvia
- , Michelle Sam
- , Jaswinder S. Samra
- , Francisco Sanchez-Vega
- , Chris Sander
- , Grant Sanders
- , Rajiv Sarin
- , Iman Sarrafi
- , Aya Sasaki-Oku
- , Torill Sauer
- , Guido Sauter
- , Robyn P. M. Saw
- , Maria Scardoni
- , Christopher J. Scarlett
- , Aldo Scarpa
- , Ghislaine Scelo
- , Dirk Schadendorf
- , Jacqueline E. Schein
- , Markus B. Schilhabel
- , Matthias Schlesner
- , Thorsten Schlomm
- , Heather K. Schmidt
- , Sarah-Jane Schramm
- , Stefan Schreiber
- , Nikolaus Schultz
- , Steven E. Schumacher
- , Roland F. Schwarz
- , Richard A. Scolyer
- , David Scott
- , Ralph Scully
- , Raja Seethala
- , Ayellet V. Segre
- , Iris Selander
- , Colin A. Semple
- , Yasin Senbabaoglu
- , Subhajit Sengupta

- , Elisabetta Sereni
- , Stefano Serra
- , Dennis C. Sgroi
- , Mark Shackleton
- , Nimish C. Shah
- , Sagedeh Shahabi
- , Catherine A. Shang
- , Ping Shang
- , Ofer Shapira
- , Troy Shelton
- , Ciyue Shen
- , Hui Shen
- , Rebecca Shepherd
- , Ruian Shi
- , Yan Shi
- , Yu-Jia Shiah
- , Tatsuhiro Shibata
- , Juliann Shih
- , Eigo Shimizu
- , Kiyo Shimizu
- , Seung Jun Shin
- , Yuichi Shiraishi
- , Tal Shmaya
- , Ilya Shmulevich
- , Solomon I. Shorser
- , Charles Short
- , Raunak Shrestha
- , Suyash S. Shringarpure
- , Craig Shriver
- , Shimin Shuai
- , Nikos Sidiropoulos
- , Reiner Siebert
- , Anieta M. Sieuwerts
- , Lina Sieverling
- , Sabina Signoretti
- , Katarzyna O. Sikora
- , Michele Simbolo

- , Ronald Simon
- , Janae V. Simons
- , Jared T. Simpson
- , Peter T. Simpson
- , Samuel Singer
- , Nasa Sinnott-Armstrong
- , Payal Sipahimalani
- , Tara J. Skelly
- , Marcel Smid
- , Jaclyn Smith
- , Karen Smith-McCune
- , Nicholas D. Socci
- , Heidi J. Sofia
- , Matthew G. Soloway
- , Lei Song
- , Anil K. Sood
- , Sharmila Sothi
- , Christos Sotiriou
- , Cameron M. Soulette
- , Paul N. Span
- , Paul T. Spellman
- , Nicola Sperandio
- , Andrew J. Spillane
- , Oliver Spiro
- , Jonathan Spring
- , Johan Staaf
- , Peter F. Stadler
- , Peter Staib
- , Stefan G. Stark
- , Lucy Stebbings
- , Ólafur Andri Stefánsson
- , Oliver Stegle
- , Lincoln D. Stein
- , Alasdair Stenhouse
- , Chip Stewart
- , Stephan Stilgenbauer
- , Miranda D. Stobbe

- , Michael R. Stratton
- , Jonathan R. Stretch
- , Adam J. Struck
- , Joshua M. Stuart
- , Henk G. Stunnenberg
- , Hong Su
- , Xiaoping Su
- , Ren X. Sun
- , Stephanie Sungalee
- , Hana Susak
- , Akihiro Suzuki
- , Fred Sweep
- , Monika Szczepanowski
- , Holger Sültmann
- , Takashi Yugawa
- , Angela Tam
- , David Tamborero
- , Benita Kiat Tee Tan
- , Donghui Tan
- , Patrick Tan
- , Hiroko Tanaka
- , Hirokazu Taniguchi
- , Tomas J. Tanskanen
- , Maxime Tarabichi
- , Roy Tarnuzzer
- , Patrick Tarpey
- , Morgan L. Taschuk
- , Kenji Tatsuno
- , Simon Tavaré
- , Darrin F. Taylor
- , Amaro Taylor-Weiner
- , Jon W. Teague
- , Bin Tean Teh
- , Varsha Tembe
- , Javier Temes
- , Kevin Thai
- , Sarah P. Thayer

- , Nina Thiessen
- , Gilles Thomas
- , Sarah Thomas
- , Alan Thompson
- , Alastair M. Thompson
- , John F. F. Thompson
- , R. Houston Thompson
- , Heather Thorne
- , Leigh B. Thorne
- , Adrian Thorogood
- , Grace Tiao
- , Nebojsa Tijanic
- , Lee E. Timms
- , Roberto Tirabosco
- , Marta Tojo
- , Stefania Tommasi
- , Christopher W. Toon
- , Umut H. Toprak
- , David Torrents
- , Giampaolo Tortora
- , Jörg Tost
- , Yasushi Totoki
- , David Townend
- , Nadia Traficante
- , Isabelle Treilleux
- , Jean-Rémi Trotta
- , Lorenz H. P. Trümper
- , Ming Tsao
- , Tatsuhiko Tsunoda
- , Jose M. C. Tubio
- , Olga Tucker
- , Richard Turkington
- , Daniel J. Turner
- , Andrew Tutt
- , Masaki Ueno
- , Naoto T. Ueno
- , Christopher Umbricht

- , Husen M. Umer
- , Timothy J. Underwood
- , Lara Urban
- , Tomoko Urushidate
- , Tetsuo Ushiku
- , Liis Uusküla-Reimand
- , Alfonso Valencia
- , David J. Van Den Berg
- , Steven Van Laere
- , Peter Van Loo
- , Erwin G. Van Meir
- , Gert G. Van den Eynden
- , Theodorus Van der Kwast
- , Naveen Vasudev
- , Miguel Vazquez
- , Ravikiran Vedururu
- , Umadevi Veluvolu
- , Shankar Vembu
- , Lieven P. C. Verbeke
- , Peter Vermeulen
- , Clare Verrill
- , Alain Viari
- , David Vicente
- , Caterina Vicentini
- , K. VijayRaghavan
- , Juris Viksna
- , Ricardo E. Vilain
- , Izar Villasante
- , Anne Vincent-Salomon
- , Tapio Visakorpi
- , Douglas Voet
- , Paresh Vyas
- , Ignacio Vázquez-García
- , Nick M. Waddell
- , Nicola Waddell
- , Claes Wadelius
- , Lina Wadi

- , Rabea Wagener
- , Jeremiah A. Wala
- , Jian Wang
- , Jiayin Wang
- , Linghua Wang
- , Qi Wang
- , Wenyi Wang
- , Yumeng Wang
- , Zhining Wang
- , Paul M. Waring
- , Hans-Jörg Warnatz
- , Jonathan Warrell
- , Anne Y. Warren
- , Sebastian M. Waszak
- , David C. Wedge
- , Dieter Weichenhan
- , Paul Weinberger
- , John N. Weinstein
- , Joachim Weischenfeldt
- , Daniel J. Weisenberger
- , Ian Welch
- , Michael C. Wendl
- , Johannes Werner
- , Justin P. Whalley
- , David A. Wheeler
- , Hayley C. Whitaker
- , Dennis Wigle
- , Matthew D. Wilkerson
- , Ashley Williams
- , James S. Wilmott
- , Gavin W. Wilson
- , Julie M. Wilson
- , Richard K. Wilson
- , Boris Winterhoff
- , Jeffrey A. Wintersinger
- , Maciej Wiznerowicz
- , Stephan Wolf

- , Bernice H. Wong
- , Tina Wong
- , Winghing Wong
- , Youngchoon Woo
- , Scott Wood
- , Bradly G. Wouters
- , Adam J. Wright
- , Derek W. Wright
- , Mark H. Wright
- , Chin-Lee Wu
- , Dai-Ying Wu
- , Guanming Wu
- , Jianmin Wu
- , Kui Wu
- , Yang Wu
- , Zhenggang Wu
- , Liu Xi
- , Tian Xia
- , Qian Xiang
- , Xiao Xiao
- , Rui Xing
- , Heng Xiong
- , Qinying Xu
- , Yanxun Xu
- , Hong Xue
- , Shinichi Yachida
- , Sergei Yakneen
- , Rui Yamaguchi
- , Takafumi N. Yamaguchi
- , Masakazu Yamamoto
- , Shogo Yamamoto
- , Hiroki Yamaue
- , Fan Yang
- , Huanming Yang
- , Jean Y. Yang
- , Liming Yang
- , Lixing Yang

- , Shanlin Yang
- , Tsun-Po Yang
- , Yang Yang
- , Xiaotong Yao
- , Marie-Laure Yaspo
- , Lucy Yates
- , Christina Yau
- , Chen Ye
- , Kai Ye
- , Venkata D. Yellapantula
- , Christopher J. Yoon
- , Sung-Soo Yoon
- , Fouad Yousif
- , Jun Yu
- , Kaixian Yu
- , Willie Yu
- , Yingyan Yu
- , Ke Yuan
- , Yuan Yuan
- , Denis Yuen
- , Takashi Yugawa
- , Christina K. Yung
- , Olga Zaikova
- , Jorge Zamora
- , Marc Zapatka
- , Jean C. Zenklusen
- , Thorsten Zenz
- , Nikolajs Zeps
- , Cheng-Zhong Zhang
- , Fan Zhang
- , Hailei Zhang
- , Hongwei Zhang
- , Hongxin Zhang
- , Jiashan Zhang
- , Jing Zhang
- , Junjun Zhang
- , Xiuqing Zhang

- , Xuanping Zhang
- , Yan Zhang
- , Zemin Zhang
- , Zhongming Zhao
- , Liangtao Zheng
- , Xiuqing Zheng
- , Wanding Zhou
- , Yong Zhou
- , Bin Zhu
- , Hongtu Zhu
- , Jingchun Zhu
- , Shida Zhu
- , Lihua Zou
- , Xueqing Zou
- , Anna deFazio
- , Nicholas van As
- , Carolien H. M. van Deurzen
- , Marc J. van de Vijver
- , L. van't Veer
- & Christian von Mering

Corresponding authors

Correspondence to Steven G. Rozen or Michael R. Stratton.

Rights and permissions

Open Access This article is licensed under a Creative Commons Attribution 4.0 International License, which permits use, sharing, adaptation, distribution and reproduction in any medium or format, as long as you give appropriate credit to the original author(s) and the source, provide a link to the Creative Commons license, and indicate if changes were made. The images or other third party material in this article are included in the article's Creative Commons license, unless indicated otherwise in a credit line to the material. If material is not included in the article's Creative Commons license and your intended use is not permitted

by statutory regulation or exceeds the permitted use, you will need to obtain permission directly from the copyright holder. To view a copy of this license, visit http://creativecommons.org/licenses/by/4.0/.

Reprints and Permissions

About this article

Cite this article

Alexandrov, L.B., Kim, J., Haradhvala, N.J. *et al.* Author Correction: The repertoire of mutational signatures in human cancer. *Nature* **614**, E41 (2023). https://doi.org/10.1038/s41586-022-05600-5

- Published: 25 January 2023
- Issue Date: 16 February 2023
- DOI: https://doi.org/10.1038/s41586-022-05600-5

Share this article

Anyone you share the following link with will be able to read this content:

Get shareable link

Sorry, a shareable link is not currently available for this article.

Copy to clipboard

Provided by the Springer Nature SharedIt content-sharing initiative

---

This article was downloaded by **calibre** from https://www.nature.com/articles/s41586-022-05600-5

- Author Correction
- Open Access
- Published: 25 January 2023

Author Correction: The evolutionary history of 2,658 cancers

- Moritz Gerstung ,
- Clemency Jolly,
- Ignaty Leshchiner,
- Stefan C. Dentro,
- Santiago Gonzalez,
- Daniel Rosebrock,
- Thomas J. Mitchell,
- Yulia Rubanova,
- Pavana Anur,
- Kaixian Yu,
- Maxime Tarabichi,
- Amit Deshwar,
- Jeff Wintersinger,
- Kortine Kleinheinz,
- Ignacio Vázquez-García,
- Kerstin Haase,
- Lara Jerman,
- Subhajit Sengupta,
- Geoff Macintyre,
- Salem Malikic,
- Nilgun Donmez,
- Dimitri G. Livitz,
- Marek Cmero,
- Jonas Demeulemeester,

- Steven Schumacher,
- Yu Fan,
- Xiaotong Yao,
- Juhee Lee,
- Matthias Schlesner,
- Paul C. Boutros,
- David D. Bowtell,
- Hongtu Zhu,
- Gad Getz,
- Marcin Imielinski,
- Rameen Beroukhim,
- S. Cenk Sahinalp,
- Yuan Ji,
- Martin Peifer,
- Florian Markowetz,
- Ville Mustonen,
- Ke Yuan,
- Wenyi Wang,
- Quaid D. Morris,
- PCAWG Evolution & Heterogeneity Working Group,
- Paul T. Spellman,
- David C. Wedge,
- Peter Van Loo &
- PCAWG Consortium

Show authors

Nature **volume 614**, page E42 (2023)

- 974 Accesses
- 1 Altmetric
- Metrics details

The Original Article was published on 05 February 2020

Correction to: *Nature* https://doi.org/10.1038/s41586-019-1907-7 Published online 5 February 2020

In the published version of this paper, the members of the Pan-Cancer Analysis of Whole Genomes (PCAWG) Consortium were listed in the Supplementary Information; however, these members should have been included in the main paper. The original Article has been corrected to include the members and affiliations of the PCAWG Consortium in the main paper; the corrections have been made to the HTML version of the Article but not the PDF version. Additional minor corrections to affiliations have been made to the PDF and HTML versions of the original Article for consistency of information between the PCAWG list and the main paper.

Author information

Author notes

1. These authors contributed equally: Moritz Gerstung, Clemency Jolly, Ignaty Leshchiner, Stefan C. Dentro, Santiago Gonzalez

2. These authors jointly supervised this work: Paul T. Spellman, David C. Wedge, Peter Van Loo

3. A list of members and their affiliations appears at the end of the paper

4. A list of members and their affiliations appears online

Authors and Affiliations

1. European Molecular Biology Laboratory, European Bioinformatics Institute (EMBL-EBI), Cambridge, UK

   Moritz Gerstung, Santiago Gonzalez, Lara Jerman, Moritz Gerstung, Santiago Gonzalez & Lara Jerman

2. European Molecular Biology Laboratory, Genome Biology Unit, Heidelberg, Germany

Moritz Gerstung & Moritz Gerstung

3. Wellcome Sanger Institute, Cambridge, UK

Moritz Gerstung, Stefan C. Dentro, Thomas J. Mitchell, Maxime Tarabichi, Ignacio Vázquez-García, Stefan C. Dentro, Moritz Gerstung, Maxime Tarabichi, David J. Adams, Peter J. Campbell, Kevin J. Dawson, Henry Lee-Six, Inigo Martincorena, Thomas J. Mitchell & Ignacio Vázquez-García

4. The Francis Crick Institute, London, UK

Clemency Jolly, Stefan C. Dentro, Maxime Tarabichi, Kerstin Haase, Jonas Demeulemeester, Stefan C. Dentro, Clemency Jolly, Kerstin Haase, Maxime Tarabichi, Jonas Demeulemeester, Matthew Fittall, Peter Van Loo & Peter Van Loo

5. Broad Institute of MIT and Harvard, Cambridge, MA, USA

Ignaty Leshchiner, Daniel Rosebrock, Dimitri G. Livitz, Steven Schumacher, Gad Getz, Rameen Beroukhim, Ignaty Leshchiner, Rameen Beroukhim, Gad Getz, Gavin Ha, Dimitri G. Livitz, Daniel Rosebrock, Steven Schumacher & Oliver Spiro

6. Big Data Institute, University of Oxford, Oxford, UK

Stefan C. Dentro, Stefan C. Dentro, David C. Wedge & David C. Wedge

7. University of Cambridge, Cambridge, UK

Thomas J. Mitchell, Ignacio Vázquez-García, Thomas J. Mitchell & Ignacio Vázquez-García

8. University of Toronto, Toronto, Ontario, Canada

Yulia Rubanova, Amit Deshwar, Jeff Wintersinger, Paul C. Boutros, Quaid D. Morris, Jeff Wintersinger, Amit G. Deshwar, Yulia

Rubanova, Paul C. Boutros, Ruian Shi, Shankar Vembu & Quaid D. Morris

9. Vector Institute, Toronto, Ontario, Canada

Yulia Rubanova, Amit Deshwar, Jeff Wintersinger, Quaid D. Morris, Jeff Wintersinger, Amit G. Deshwar, Yulia Rubanova & Quaid D. Morris

10. Molecular and Medical Genetics, Oregon Health & Science University, Portland, OR, USA

Pavana Anur, Pavana Anur, Myron Peto, Paul T. Spellman & Paul T. Spellman

11. The University of Texas MD Anderson Cancer Center, Houston, TX, USA

Kaixian Yu, Yu Fan, Hongtu Zhu, Wenyi Wang, Kaixian Yu, Shaolong Cao, Yu Fan, Seung Jun Shin, Hongtu Zhu & Wenyi Wang

12. German Cancer Research Center (DKFZ), Heidelberg, Germany

Kortine Kleinheinz, Matthias Schlesner, Roland Eils, Kortine Kleinheinz & Matthias Schlesner

13. Heidelberg University, Heidelberg, Germany

Kortine Kleinheinz, Roland Eils & Kortine Kleinheinz

14. University of Ljubljana, Ljubljana, Slovenia

Lara Jerman & Lara Jerman

15. NorthShore University HealthSystem, Evanston, IL, USA

Subhajit Sengupta, Yuan Ji, Yuan Ji & Subhajit Sengupta

16. Cancer Research UK Cambridge Institute, University of Cambridge, Cambridge, UK

Geoff Macintyre, Florian Markowetz, Ke Yuan, Geoff Macintyre, Ruben M. Drews, Florian Markowetz & Ke Yuan

17. Simon Fraser University, Burnaby, British Columbia, Canada

Salem Malikic, Nilgun Donmez, Nilgun Donmez & Salem Malikic

18. Vancouver Prostate Centre, Vancouver, British Columbia, Canada

Salem Malikic, Nilgun Donmez, S. Cenk Sahinalp, Nilgun Donmez, Salem Malikic & S. Cenk Sahinalp

19. University of Melbourne, Melbourne, Victoria, Australia

Marek Cmero, Elizabeth L. Christie, Marek Cmero & Dale W. Garsed

20. Walter and Eliza Hall Institute, Melbourne, Victoria, Australia

Marek Cmero & Marek Cmero

21. University of Leuven, Leuven, Belgium

Jonas Demeulemeester, Jonas Demeulemeester, Peter Van Loo & Peter Van Loo

22. Weill Cornell Medicine, New York, NY, USA

Xiaotong Yao, Marcin Imielinski, Marcin Imielinski & Xiaotong Yao

23. New York Genome Center, New York, NY, USA

Xiaotong Yao, Marcin Imielinski, Marcin Imielinski & Xiaotong Yao

24. University of California Santa Cruz, Santa Cruz, CA, USA

Juhee Lee & Juhee Lee

25. Ontario Institute for Cancer Research, Toronto, Ontario, Canada

Paul C. Boutros, Paul C. Boutros, Adriana Salcedo & Lincoln D. Stein

26. University of California, Los Angeles, CA, USA

Paul C. Boutros & Paul C. Boutros

27. Peter MacCallum Cancer Centre, Melbourne, Victoria, Australia

David D. Bowtell, David D. Bowtell, Elizabeth L. Christie & Dale W. Garsed

28. Center for Cancer Research, Massachusetts General Hospital, Charlestown, MA, USA

Gad Getz & Gad Getz

29. Department of Pathology, Massachusetts General Hospital, Boston, MA, USA

Gad Getz & Gad Getz

30. Harvard Medical School, Boston, MA, USA

Gad Getz & Gad Getz

31. Dana-Farber Cancer Institute, Boston, MA, USA

Rameen Beroukhim & Rameen Beroukhim

32. Indiana University, Bloomington, IN, USA

S. Cenk Sahinalp & S. Cenk Sahinalp

33. The University of Chicago, Chicago, IL, USA

Yuan Ji & Yuan Ji

34. University of Cologne, Cologne, Germany

Martin Peifer, Yupeng Cun, Martin Peifer & Tsun-Po Yang

35. University of Helsinki, Helsinki, Finland

Ville Mustonen & Ville Mustonen

36. University of Glasgow, Glasgow, UK

Ke Yuan & Ke Yuan

37. Oxford NIHR Biomedical Research Centre, Oxford, UK

David C. Wedge & David C. Wedge

38. Department of Computer Science, Carleton College, Northfield, MN, USA

Layla Oesper

39. Department of Computer Science, Princeton University, Princeton, NJ, USA

Benjamin J. Raphael

40. Korea University, Seoul, South Korea

Seung Jun Shin

41. Human Genome Sequencing Center, Baylor College of Medicine, Houston, TX, USA

David A. Wheeler

42. Applied Tumor Genomics Research Program, Research Programs Unit, University of Helsinki, Helsinki, Finland

Lauri A. Aaltonen

43. Wellcome Sanger Institute, Wellcome Genome Campus, Hinxton, UK

Federico Abascal, David J. Adams, Ludmil B. Alexandrov, Sam Behjati, Shriram G. Bhosle, David T. Bowen, Adam P. Butler, Peter J. Campbell, Peter Clapham, Helen Davies, Kevin J. Dawson, Stefan C. Dentro, Serge Serge, Erik Garrison, Mohammed Ghori, Dominik Glodzik, Jonathan Hinton, David R. Jones, Young Seok Ju, Stian Knappskog, Barbara Kremeyer, Henry Lee-Six, Daniel A. Leongamornlert, Yilong Li, Sancha Martin, Iñigo Martincorena, Ultan McDermott, Andrew Menzies, Thomas J. Mitchell, Sandro Morganella, Jyoti Nangalia, Jonathan Nicholson, Serena Nik-Zainal, Sarah O'Meara, Elli Papaemmanuil, Keiran M. Raine, Manasa Ramakrishna, Kamna Ramakrishnan, Nicola D. Roberts, Rebecca Shepherd, Lucy Stebbings, Michael R. Stratton, Maxime Tarabichi, Jon W. Teague, Ignacio Vázquez-García, David C. Wedge, Lucy Yates, Jorge Zamora & Xueqing Zou

44. Memorial Sloan Kettering Cancer Center, New York, NY, USA

Adam Abeshouse, Hikmat Al-Ahmadie, Gunes Gundem, Zachary Heins, Jason Huse, Douglas A. Levine, Eric Minwei Liu & Angelica Ochoa

45. Genome Science Division, Research Center for Advanced Science and Technology, University of Tokyo, Tokyo, Japan

Hiroyuki Aburatani, Genta Nagae, Akihiro Suzuki, Kenji Tatsuno & Shogo Yamamoto

46. Department of Surgery, University of Chicago, Chicago, IL, USA

Nishant Agrawal

47. Department of Surgery, Division of Hepatobiliary and Pancreatic Surgery, School of Medicine, Keimyung University Dongsan Medical Center, Daegu, South Korea

Keun Soo Ahn & Koo Jeong Kang

48. Department of Oncology, Gil Medical Center, Gachon University, Incheon, South Korea

Sung-Min Ahn

49. Hiroshima University, Hiroshima, Japan

Hiroshi Aikata, Koji Arihiro, Kazuaki Chayama, Yoshiiku Kawakami & Hideki Ohdan

50. Department of Bioinformatics and Computational Biology, The University of Texas MD Anderson Cancer Center, Houston, TX, USA

Rehan Akbani, Shaolong Cao, Yiwen Chen, Zechen Chong, Yu Fan, Jun Li, Han Liang, Wenyi Wang, Yumeng Wang & Yuan Yuan

51. University of Texas MD Anderson Cancer Center, Houston, TX, USA

Kadir C. Akdemir & Ken Chen

52. King Faisal Specialist Hospital and Research Centre, Al Maather, Riyadh, Saudi Arabia

Sultan T. Al-Sedairy

53. Bioinformatics Unit, Spanish National Cancer Research Centre (CNIO), Madrid, Spain

Fatima Al-Shahrour & Elena Piñeiro-Yáñez

54. Bioinformatics Core Facility, University Medical Center Hamburg, Hamburg, Germany

Malik Alawi

55. Heinrich Pette Institute, Leibniz Institute for Experimental Virology, Hamburg, Germany

Malik Alawi & Adam Grundhoff

56. Ontario Tumour Bank, Ontario Institute for Cancer Research, Toronto, ON, Canada

Monique Albert & John Bartlett

57. Department of Pathology, The University of Texas MD Anderson Cancer Center, Houston, TX, USA

Kenneth Aldape, Russell R. Broaddus, Bogdan Czerniak, Adel El-Naggar, Savitri Krishnamurthy, Alexander J. Lazar & Xiaoping Su

58. Laboratory of Pathology, Center for Cancer Research, National Cancer Institute, Bethesda, MD, USA

Kenneth Aldape

59. Department of Cellular and Molecular Medicine and Department of Bioengineering, University of California San Diego, La Jolla, CA, USA

Ludmil B. Alexandrov & Erik N. Bergstrom

60. UC San Diego Moores Cancer Center, San Diego, CA, USA

Ludmil B. Alexandrov, Erik N. Bergstrom & Olivier Harismendy

61. Canada’s Michael Smith Genome Sciences Centre, BC Cancer, Vancouver, BC, Canada

Adrian Ally, Miruna Balasundaram, Reanne Bowlby, Denise Brooks, Rebecca Carlsen, Eric Chuah, Noreen Dhalla, Robert A. Holt, Steven J. M. Jones, Katayoon Kasaian, Darlene Lee, Haiyan Irene Li, Yussanne Ma, Marco A. Marra, Michael Mayo, Richard A. Moore, Andrew J. Mungall, Karen Mungall, A. Gordon Robertson, Sara Sadeghi, Jacqueline E. Schein, Payal Sipahimalani, Angela Tam, Nina Thiessen & Tina Wong

62. Sir Peter MacCallum Department of Oncology, Peter MacCallum Cancer Centre, University of Melbourne, Melbourne, VIC, Australia

Kathryn Alsop, David D. L. Bowtell, Elizabeth L. Christie, Dariush Etemadmoghadam, Sian Fereday, Dale W. Garsed, Linda Mileshkin, Chris Mitchell, Mark Shackleton, Heather Thorne & Nadia Traficante

63. Centre for Research in Molecular Medicine and Chronic Diseases (CiMUS), Universidade de Santiago de Compostela, Santiago de Compostela, Spain

Eva G. Alvarez, Alicia L. Bruzos, Bernardo Rodriguez-Martin, Javier Temes, Jose M. C. Tubio & Jorge Zamora

64. Department of Zoology, Genetics and Physical Anthropology, (CiMUS), Universidade de Santiago de Compostela, Santiago de Compostela, Spain

Eva G. Alvarez, Alicia L. Bruzos, Bernardo Rodriguez-Martin, Javier Temes, Jose M. C. Tubio & Jorge Zamora

65. The Biomedical Research Centre (CINBIO), Universidade de Vigo, Vigo, Spain

Eva G. Alvarez, Alicia L. Bruzos, Bernardo Rodriguez-Martin, Marta Tojo, Jose M. C. Tubio & Jorge Zamora

66. Royal National Orthopaedic Hospital - Bolsover, London, UK

Fernanda Amary

67. Department of Genomic Medicine, The University of Texas MD Anderson Cancer Center, Houston, TX, USA

Samirkumar B. Amin, P. Andrew Futreal & Alexander J. Lazar

68. Quantitative and Computational Biosciences Graduate Program, Baylor College of Medicine, Houston, TX, USA

Samirkumar B. Amin, Han Liang & Yumeng Wang

69. The Jackson Laboratory for Genomic Medicine, Farmington, CT, USA

Samirkumar B. Amin, Joshy George & Lucas Lochovsky

70. Genome Informatics Program, Ontario Institute for Cancer Research, Toronto, ON, Canada

Brice Aminou, Niall J. Byrne, Aurélien Chateigner, Nodirjon Fayzullaev, Vincent Ferretti, George L. Mihaiescu, Hardeep K. Nahal-Bose, Brian D. O'Connor, B. F. Francis Ouellette, Marc D. Perry, Kevin Thai, Qian Xiang, Christina K. Yung & Junjun Zhang

71. Institute of Human Genetics, Christian-Albrechts-University, Kiel, Germany

Ole Ammerpohl, Andrea Haake, Cristina López, Julia Richter & Rabea Wagener

72. Institute of Human Genetics, Ulm University and Ulm University Medical Center, Ulm, Germany

Ole Ammerpohl, Sietse Aukema, Cristina López, Reiner Siebert & Rabea Wagener

73. Queensland Centre for Medical Genomics, Institute for Molecular Bioscience, University of Queensland, St. Lucia, Brisbane, QLD, Australia

Matthew J. Anderson, Timothy J. C. Bruxner, Angelika N. Christ, J. Lynn Fink, Ivon Harliwong, Karin S. Kassahn, David K. Miller, Alan J. Robertson & Darrin F. Taylor

74. Salford Royal NHS Foundation Trust, Salford, UK

Yeng Ang, Hsiao-Wei Chen, Ritika Kundra & Francisco Sanchez-Vega

75. Department of Surgery, Pancreas Institute, University and Hospital Trust of Verona, Verona, Italy

Davide Antonello, Claudio Bassi, Narong Khuntikeo, Luca Landoni, Giuseppe Malleo, Giovanni Marchegiani, Neil D. Merrett, Marco Miotto, Salvatore Paiella, Antonio Pea, Paolo Pederzoli, Roberto Salvia, Jaswinder S. Samra, Elisabetta Sereni & Samuel Singer

76. Molecular and Medical Genetics, OHSU Knight Cancer Institute, Oregon Health and Science University, Portland, OR, USA

Pavana Anur, Myron Peto & Paul T. Spellman

77. Department of Molecular Oncology, BC Cancer Research Centre, Vancouver, BC, Canada

Samuel Aparicio

78. The McDonnell Genome Institute at Washington University, St. Louis, MO, USA

Elizabeth L. Appelbaum, Matthew H. Bailey, Matthew G. Cordes, Li Ding, Catrina C. Fronick, Lucinda A. Fulton, Robert S. Fulton, Kuan-lin Huang, Reyka Jayasinghe, Elaine R. Mardis, R. Jay Mashl, Michael D. McLellan, Christopher A. Miller, Heather K. Schmidt, Jiayin Wang, Michael C. Wendl, Richard K. Wilson & Tina Wong

79. University College London, London, UK

Elizabeth L. Appelbaum, Jonathan D. Kay, Helena Kilpinen, Laurence B. Lovat, Hayley J. Luxton & Hayley C. Whitaker

80. Division of Cancer Genomics, National Cancer Center Research Institute, National Cancer Center, Tokyo, Japan

Yasuhito Arai, Natsuko Hama, Fumie Hosoda, Hiromi Nakamura, Tatsuhiro Shibata, Yasushi Totoki & Shinichi Yachida

81. DLR Project Management Agency, Bonn, Germany

Axel Aretz

82. Tokyo Women's Medical University, Tokyo, Japan

Shun-ichi Ariizumi & Masakazu Yamamoto

83. Center for Molecular Oncology, Memorial Sloan Kettering Cancer Center, New York, NY, USA

Joshua Armenia, Hsiao-Wei Chen, Jianjiong Gao, Ritika Kundra, Francisco Sanchez-Vega, Nikolaus Schultz & Hongxin Zhang

84. Los Alamos National Laboratory, Los Alamos, NM, USA

Laurent Arnould

85. Department of Pathology, University Health Network, Toronto General Hospital, Toronto, ON, Canada

Sylvia Asa, Michael H. A. Roehrl & Theodorus Van der Kwast

86. Nottingham University Hospitals NHS Trust, Nottingham, UK

Sylvia Asa, Simon L. Parsons & Ming Tsao

87. Epigenomics and Cancer Risk Factors, German Cancer Research Center (DKFZ), Heidelberg, Germany

Yassen Assenov

88. Computational Biology Program, Ontario Institute for Cancer Research, Toronto, ON, Canada

Gurnit Atwal, Philip Awadalla, Jonathan Barenboim, Vinayak Bhandari, Ivan Borozan, Paul C. Boutros, Lewis Jonathan Dursi, Shadrielle M. G. Espiritu, Natalie S. Fox, Michael Fraser, Syed Haider, Vincent Huang, Keren Isaev, Wei Jiao, Christopher M. Lalansingh, Emilie Lalonde, Fabien C. Lamaze, Constance H. Li, Julie Livingstone, Christine P'ng, Marta Paczkowska, Stephenie D. Prokopec, Jüri Reimand, Veronica Y. Sabelnykova, Adriana Salcedo, Yu-Jia Shiah, Solomon I. Shorser, Shimin Shuai, Jared T.

Simpson, Lincoln D. Stein, Ren X. Sun, Lina Wadi, Gavin W. Wilson, Adam J. Wright, Takafumi N. Yamaguchi, Fouad Yousif & Denis Yuen

89. Department of Molecular Genetics, University of Toronto, Toronto, ON, Canada

Gurnit Atwal, Philip Awadalla, Gary D. Bader, Shimin Shuai & Lincoln D. Stein

90. Vector Institute, Toronto, ON, Canada

Gurnit Atwal, Quaid D. Morris, Yulia Rubanova & Jeffrey A. Wintersinger

91. Hematopathology Section, Institute of Pathology, Christian-Albrechts-University, Kiel, Germany

Sietse Aukema, Wolfram Klapper, Julia Richter & Monika Szczepanowski

92. Department of Pathology and Laboratory Medicine, School of Medicine, University of North Carolina at Chapel Hill, Chapel Hill, NC, USA

J. Todd Auman & Charles M. Perou

93. Department of Cancer Genetics, Institute for Cancer Research, Oslo University Hospital, The Norwegian Radium Hospital, Oslo, Norway

Miriam R. R. Aure, Anne-Lise Børresen-Dale & Anita Langerød

94. Pathology, Hospital Clinic, Institut d’Investigacions Biomèdiques August Pi i Sunyer (IDIBAPS), University of Barcelona, Barcelona, Spain

Marta Aymerich

95. Department of Veterinary Medicine, Transmissible Cancer Group, University of Cambridge, Cambridge, UK

Adrian Baez-Ortega

96. Alvin J. Siteman Cancer Center, Washington University School of Medicine, St. Louis, MO, USA

Matthew H. Bailey, Li Ding, Robert S. Fulton, Ramaswamy Govindan & Michael D. McLellan

97. Wolfson Wohl Cancer Research Centre, Institute of Cancer Sciences, University of Glasgow, Glasgow, UK

Peter J. Bailey, Andrew V. Biankin, David K. Chang, Susanna L. Cooke, Fraser R. Duthie, Janet S. Graham, Nigel B. Jamieson, Elizabeth A. Musgrove & Derek W. Wright

98. Lineberger Comprehensive Cancer Center, University of North Carolina at Chapel Hill, Chapel Hill, NC, USA

Saianand Balu, Tom Bodenheimer, D. Neil Hayes, Austin J. Hepperla, Katherine A. Hoadley, Alan P. Hoyle, Stuart R. Jefferys, Shaowu Meng, Lisle E. Mose, Grant Sanders, Yan Shi, Janae V. Simons & Matthew G. Soloway

99. Broad Institute of MIT and Harvard, Cambridge, MA, USA

Pratiti Bandopadhayay, Rameen Beroukhim, Angela N. Brooks, Susan Bullman, John Busanovich, Andrew D. Cherniack, Juok Cho, Carrie Cibulskis, Kristian Cibulskis, David Craft, Timothy Defreitas, Andrew J. Dunford, Scott Frazer, Stacey B. Gabriel, Nils Gehlenborg, Gad Getz, Manaswi Gupta, Gavin Ha, Nicholas J. Haradhvala, David I. Heiman, Julian M. Hess, Manolis Kellis, Jaegil Kim, Kiran Kumar, Kirsten Kübler, Eric Lander, Michael S. Lawrence, Ignaty Leshchiner, Pei Lin, Ziao Lin, Dimitri Livitz, Yosef E. Maruvka, Samuel R. Meier, Matthew Meyerson, Michael S. Noble, Chandra Sekhar Pedamallu, Paz Polak, Esther

Rheinbay, Daniel Rosebrock, Mara Rosenberg, Gordon Saksena, Richard Sallari, Steven E. Schumacher, Ayellet V. Segre, Ofer Shapira, Juliann Shih, Nasa Sinnott-Armstrong, Oliver Spiro, Chip Stewart, Amaro Taylor-Weiner, Grace Tiao, Douglas Voet, Jeremiah A. Wala, Cheng-Zhong Zhang & Hailei Zhang

100. Dana-Farber/Boston Children's Cancer and Blood Disorders Center, Boston, MA, USA

Pratiti Bandopadhayay

101. Department of Pediatrics, Harvard Medical School, Boston, MA, USA

Pratiti Bandopadhayay

102. Leeds Institute of Medical Research @ St. James's, University of Leeds, St. James's University Hospital, Leeds, UK

Rosamonde E. Banks & Naveen Vasudev

103. Department of Pathology and Diagnostics, University and Hospital Trust of Verona, Verona, Italy

Stefano Barbi, Vincenzo Corbo & Michele Simbolo

104. Department of Surgery, Princess Alexandra Hospital, Brisbane, QLD, Australia

Andrew P. Barbour

105. Surgical Oncology Group, Diamantina Institute, University of Queensland, Brisbane, QLD, Australia

Andrew P. Barbour

106. Department of Population and Quantitative Health Sciences, Case Western Reserve University School of Medicine, Cleveland, OH, USA

Jill Barnholtz-Sloan

107. Research Health Analytics and Informatics, University Hospitals Cleveland Medical Center, Cleveland, OH, USA

Jill Barnholtz-Sloan

108. Gloucester Royal Hospital, Gloucester, UK

Hugh Barr

109. European Molecular Biology Laboratory, European Bioinformatics Institute (EMBL-EBI), Cambridge, UK

Elisabet Barrera, Wojciech Bazant, Ewan Birney, Rich Boyce, Alvis Brazma, Andy Cafferkey, Claudia Calabrese, Paul Flicek, Nuno A. Fonseca, Anja Füllgrabe, Moritz Gerstung, Santiago Gonzalez, Liliana Greger, Maria Keays, Jan O. Korbel, Alfonso Muñoz, Steven J. Newhouse, David Ocana, Irene Papatheodorou, Robert Petryszak, Roland F. Schwarz, Charles Short, Oliver Stegle & Lara Urban

110. Diagnostic Development, Ontario Institute for Cancer Research, Toronto, ON, Canada

John Bartlett & Ilinca Lungu

111. Barcelona Supercomputing Center (BSC), Barcelona, Spain

Javier Bartolome, Mattia Bosio, Ana Dueso-Barroso, J. Lynn Fink, Josep L. L. Gelpi, Ana Milovanovic, Montserrat Puiggròs, Javier Bartolomé Rodriguez, Romina Royo, David Torrents, Alfonso Valencia, Miguel Vazquez, David Vicente & Izar Villasante

112. Arnie Charbonneau Cancer Institute, University of Calgary, Calgary, AB, Canada

Oliver F. Bathe

113. Departments of Surgery and Oncology, University of Calgary, Calgary, AB, Canada

Oliver F. Bathe

114. Department of Pathology, Oslo University Hospital, The Norwegian Radium Hospital, Oslo, Norway

Daniel Baumhoer & Bodil Bjerkehagen

115. PanCuRx Translational Research Initiative, Ontario Institute for Cancer Research, Toronto, ON, Canada

Prashant Bavi, Michelle Chan-Seng-Yue, Sean Cleary, Robert E. Denroche, Steven Gallinger, Robert C. Grant, Gun Ho Jang, Sangeetha Kalimuthu, Ilinca Lungu, John D. McPherson, Faiyaz Notta, Michael H. A. Roehrl, Gavin W. Wilson & Julie M. Wilson

116. Department of Oncology, Sidney Kimmel Comprehensive Cancer Center at Johns Hopkins University School of Medicine, Baltimore, MD, USA

Stephen B. Baylin, Nilanjan Chatterjee, Leslie Cope, Ludmila Danilova & Ralph H. Hruban

117. University Hospital Southampton NHS Foundation Trust, Southampton, UK

Stephen B. Baylin & Tim Dudderidge

118. Royal Stoke University Hospital, Stoke-on-Trent, UK

Duncan Beardsmore & Christopher Umbricht

119. Genome Sequence Informatics, Ontario Institute for Cancer Research, Toronto, ON, Canada

Timothy A. Beck, Bob Gibson, Lawrence E. Heisler, Xuemei Luo & Morgan L. Taschuk

120. Human Longevity Inc, San Diego, CA, USA

Timothy A. Beck

121. Olivia Newton-John Cancer Research Institute, La Trobe University, Heidelberg, VIC, Australia

Andreas Behren & Jonathan Cebon

122. Computer Network Information Center, Chinese Academy of Sciences, Beijing, China

Beifang Niu

123. Genome Canada, Ottawa, ON, Canada

Cindy Bell

124. CNAG-CRG, Centre for Genomic Regulation (CRG), Barcelona Institute of Science and Technology (BIST), Barcelona, Spain

Sergi Beltran, Ivo G. Gut, Marta Gut, Simon C. Heath, Tomas Marques-Bonet, Arcadi Navarro, Miranda D. Stobbe, Jean-Rémi Trotta & Justin P. Whalley

125. Universitat Pompeu Fabra (UPF), Barcelona, Spain

Sergi Beltran, Mattia Bosio, German M. Demidov, Oliver Drechsel, Ivo G. Gut, Marta Gut, Simon C. Heath, Francesc Muyas, Stephan Ossowski, Aparna Prasad, Raquel Rabionet, Miranda D. Stobbe & Hana Susak

126. Buck Institute for Research on Aging, Novato, CA, USA

Christopher Benz & Christina Yau

127. Duke University Medical Center, Durham, NC, USA

Andrew Berchuck

128. Department of Human Genetics, Hannover Medical School, Hannover, Germany

Anke K. Bergmann

129. Center for Bioinformatics and Functional Genomics, Cedars-Sinai Medical Center, Los Angeles, CA, USA

Benjamin P. Berman & Huy Q. Dinh

130. Department of Biomedical Sciences, Cedars-Sinai Medical Center, Los Angeles, CA, USA

Benjamin P. Berman

131. The Hebrew University Faculty of Medicine, Jerusalem, Israel

Benjamin P. Berman

132. Barts Cancer Institute, Barts and the London School of Medicine and Dentistry, Queen Mary University of London, London, UK

Daniel M. Berney & Yong-Jie Lu

133. Department of Computer Science, Bioinformatics Group, University of Leipzig, Leipzig, Germany

Stephan H. Bernhart, Hans Binder, Steve Hoffmann & Peter F. Stadler

134. Interdisciplinary Center for Bioinformatics, University of Leipzig, Leipzig, Germany

Stephan H. Bernhart, Hans Binder, Steve Hoffmann, Helene Kretzmer & Peter F. Stadler

135. Transcriptome Bioinformatics, LIFE Research Center for Civilization Diseases, University of Leipzig, Leipzig, Germany

Stephan H. Bernhart, Steve Hoffmann, Helene Kretzmer & Peter F. Stadler

136. Department of Medical Oncology, Dana-Farber Cancer Institute, Boston, MA, USA

Rameen Beroukhim, Angela N. Brooks, Susan Bullman, Andrew D. Cherniack, Levi Garraway, Matthew Meyerson, Chandra Sekhar Pedamallu, Steven E. Schumacher, Juliann Shih & Jeremiah A. Wala

137. Department of Cancer Biology, Dana-Farber Cancer Institute, Boston, MA, USA

Rameen Beroukhim, Aquila Fatima, Andrea L. Richardson, Steven E. Schumacher, Ofer Shapira, Andrew Tutt & Jeremiah A. Wala

138. Harvard Medical School, Boston, MA, USA

Rameen Beroukhim, Gad Getz, Kirsten Kübler, Matthew Meyerson, Chandra Sekhar Pedamallu, Paz Polak, Esther Rheinbay & Jeremiah A. Wala

139. USC Norris Comprehensive Cancer Center, University of Southern California, Los Angeles, CA, USA

Mario Berrios, Moiz S. Bootwalla, Andrea Holbrook, Phillip H. Lai, Dennis T. Maglinte, David J. Van Den Berg & Daniel J. Weisenberger

140. Department of Diagnostics and Public Health, University and Hospital Trust of Verona, Verona, Italy

Samantha Bersani, Ivana Cataldo, Claudio Luchini & Maria Scardoni

141. Department of Mathematics, Aarhus University, Aarhus, Denmark

Johanna Bertl & Asger Hobolth

142. Department of Molecular Medicine (MOMA), Aarhus University Hospital, Aarhus N, Denmark

Johanna Bertl, Henrik Hornshøj, Malene Juul, Randi Istrup Juul, Tobias Madsen, Morten Muhlig Nielsen & Jakob Skou Pedersen

143. Instituto Carlos Slim de la Salud, Mexico City, Mexico

Miguel Betancourt

144. Department of Medical Biophysics, University of Toronto, Toronto, ON, Canada

Vinayak Bhandari, Paul C. Boutros, Robert G. Bristow, Keren Isaev, Constance H. Li, Jüri Reimand, Michael H. A. Roehrl & Bradly G. Wouters

145. Cancer Division, Garvan Institute of Medical Research, Kinghorn Cancer Centre, University of New South Wales (UNSW Sydney), Sydney, NSW, Australia

Andrew V. Biankin, David K. Chang, Lorraine A. Chantrill, Angela Chou, Anthony J. Gill, Amber L. Johns, James G. Kench, David K. Miller, Adnan M. Nagrial, Marina Pajic, Mark Pinese, Ilse Rooman, Christopher J. Scarlett, Christopher W. Toon & Jianmin Wu

146. South Western Sydney Clinical School, Faculty of Medicine, University of New South Wales (UNSW Sydney), Liverpool, NSW, Australia

Andrew V. Biankin

147. West of Scotland Pancreatic Unit, Glasgow Royal Infirmary, Glasgow, UK

Andrew V. Biankin & Nigel B. Jamieson

148. Center for Digital Health, Berlin Institute of Health and Charitè - Universitätsmedizin Berlin, Berlin, Germany

Matthias Bieg

149. Heidelberg Center for Personalized Oncology (DKFZ-HIPO), German Cancer Research Center (DKFZ), Heidelberg, Germany

Matthias Bieg, Ivo Buchhalter, Barbara Hutter & Nagarajan Paramasivam

150. The Preston Robert Tisch Brain Tumor Center, Duke University Medical Center, Durham, NC, USA

Darell Bigner

151. Massachusetts General Hospital, Boston, MA, USA

Michael Birrer, Vikram Deshpande, William C. Faquin, Nicholas J. Haradhvala, Kirsten Kübler, Michael S. Lawrence, David N. Louis, Yosef E. Maruvka, G. Petur Nielsen, Esther Rheinbay, Mara Rosenberg, Dennis C. Sgroi & Chin-Lee Wu

152. National Institute of Biomedical Genomics, Kalyani, West Bengal, India

Nidhan K. Biswas, Arindam Maitra & Partha P. Majumder

153. Institute of Clinical Medicine and Institute of Oral Biology, University of Oslo, Oslo, Norway

Bodil Bjerkehagen

154. University of North Carolina at Chapel Hill, Chapel Hill, NC, USA

Lori Boice, Mei Huang, Sonia Puig & Leigh B. Thorne

155. ARC-Net Centre for Applied Research on Cancer, University and Hospital Trust of Verona, Verona, Italy

Giada Bonizzato, Cinzia Cantù, Ivana Cataldo, Vincenzo Corbo, Sonia Grimaldi, Rita T. Lawlor, Andrea Mafficini, Borislav C. Rusev, Aldo

Scarpa, Katarzyna O. Sikora, Nicola Sperandio, Alain Viari & Caterina Vicentini

156. The Institute of Cancer Research, London, UK

Johann S. De Bono, Niedzica Camacho, Colin S. Cooper, Sandra E. Edwards, Rosalind A. Eeles, Zsofia Kote-Jarai, Daniel A. Leongamornlert, Lucy Matthews & Sue Merson

157. Centre for Computational Biology, Duke-NUS Medical School, Singapore, Singapore

Arnoud Boot, Ioana Cutcutache, Mi Ni Huang, John R. McPherson, Steven G. Rozen & Yang Wu

158. Programme in Cancer and Stem Cell Biology, Duke-NUS Medical School, Singapore, Singapore

Arnoud Boot, Ioana Cutcutache, Mi Ni Huang, John R. McPherson, Steven G. Rozen, Patrick Tan, Bin Tean Teh & Yang Wu

159. Division of Oncology and Pathology, Department of Clinical Sciences Lund, Lund University, Lund, Sweden

Ake Borg, Markus Ringnér & Johan Staaf

160. Department of Pediatric Oncology, Hematology and Clinical Immunology, Heinrich-Heine-University, Düsseldorf, Germany

Arndt Borkhardt & Jessica I. Hoell

161. Laboratory for Medical Science Mathematics, RIKEN Center for Integrative Medical Sciences, Yokohama, Japan

Keith A. Boroevich, Todd A. Johnson, Michael S. Lawrence & Tatsuhiko Tsunoda

162. RIKEN Center for Integrative Medical Sciences, Yokohama, Japan

Keith A. Boroevich, Akihiro Fujimoto, Masashi Fujita, Mayuko Furuta, Kazuhiro Maejima, Hidewaki Nakagawa, Kaoru Nakano & Aya Sasaki-Oku

163. Department of Internal Medicine/Hematology, Friedrich-Ebert-Hospital, Neumünster, Germany

Christoph Borst & Siegfried Haas

164. Departments of Dermatology and Pathology, Yale University, New Haven, CT, USA

Marcus Bosenberg

165. Centre for Genomic Regulation (CRG), The Barcelona Institute of Science and Technology, Barcelona, Spain

Mattia Bosio, German M. Demidov, Oliver Drechsel, Georgia Escaramis, Xavier Estivill, Aliaksei Z. Holik, Francesc Muyas, Stephan Ossowski, Raquel Rabionet & Hana Susak

166. Radcliffe Department of Medicine, University of Oxford, Oxford, UK

Jacqueline Boultwood

167. Canadian Center for Computational Genomics, McGill University, Montreal, QC, Canada

Guillaume Bourque

168. Department of Human Genetics, McGill University, Montreal, QC, Canada

Guillaume Bourque, Mark Lathrop & Yasser Riazalhosseini

169. Department of Human Genetics, University of California Los Angeles, Los Angeles, CA, USA

Paul C. Boutros

170. Department of Pharmacology, University of Toronto, Toronto, ON, Canada

Paul C. Boutros

171. Faculty of Medicine and Health Technology, Tampere University and Tays Cancer Center, Tampere University Hospital, Tampere, Finland

G. Steven Bova & Tapio Visakorpi

172. Haematology, Leeds Teaching Hospitals NHS Trust, Leeds, UK

David T. Bowen

173. Translational Research and Innovation, Centre Léon Bérard, Lyon, France

Sandrine Boyault

174. Fox Chase Cancer Center, Philadelphia, PA, USA

Jeffrey Boyd & Elaine R. Mardis

175. International Agency for Research on Cancer, World Health Organization, Lyon, France

Paul Brennan & Ghislaine Scelo

176. Earlham Institute, Norwich, UK

Daniel S. Brewer & Colin S. Cooper

177. Norwich Medical School, University of East Anglia, Norwich, UK

Daniel S. Brewer & Colin S. Cooper

178. Department of Molecular Biology, Faculty of Science, Radboud Institute for Molecular Life Sciences, Radboud University, Nijmegen, HB, The Netherlands

Arie B. Brinkman

179. CRUK Manchester Institute and Centre, Manchester, UK

Robert G. Bristow

180. Department of Radiation Oncology, University of Toronto, Toronto, ON, Canada

Robert G. Bristow

181. Division of Cancer Sciences, Manchester Cancer Research Centre, University of Manchester, Manchester, UK

Robert G. Bristow

182. Radiation Medicine Program, Princess Margaret Cancer Centre, Toronto, ON, Canada

Robert G. Bristow & Fei-Fei Fei Liu

183. Department of Pathology, Brigham and Women's Hospital, Harvard Medical School, Boston, MA, USA

Jane E. Brock & Sabina Signoretti

184. Department of Surgery, Division of Thoracic Surgery, The Johns Hopkins University School of Medicine, Baltimore, MD, USA

Malcolm Brock

185. Division of Molecular Pathology, The Netherlands Cancer Institute, Oncode Institute, Amsterdam, CX, The Netherlands

Annegien Broeks & Jos Jonkers

186. Department of Biomolecular Engineering, University of California Santa Cruz, Santa Cruz, CA, USA

Angela N. Brooks, David Haan, Maximillian G. Marin, Thomas J. Matthew, Yulia Newton, Cameron M. Soulette & Joshua M. Stuart

187. UC Santa Cruz Genomics Institute, University of California Santa Cruz, Santa Cruz, CA, USA

Angela N. Brooks, Brian Craft, Mary J. Goldman, David Haussler, Joshua M. Stuart & Jingchun Zhu

188. Division of Applied Bioinformatics, German Cancer Research Center (DKFZ), Heidelberg, Germany

Benedikt Brors, Lars Feuerbach, Chen Hong, Charles David Imbusch & Lina Sieverling

189. German Cancer Consortium (DKTK), German Cancer Research Center (DKFZ), Heidelberg, Germany

Benedikt Brors, Barbara Hutter, Peter Lichter, Dirk Schadendorf & Holger Sültmann

190. National Center for Tumor Diseases (NCT) Heidelberg, Heidelberg, Germany

Benedikt Brors, Barbara Hutter, Holger Sültmann & Thorsten Zenz

191. Center for Biological Sequence Analysis, Department of Bio and Health Informatics, Technical University of Denmark, Lyngby, Denmark

Søren Brunak

192. Novo Nordisk Foundation Center for Protein Research, University of Copenhagen, Copenhagen, Denmark

Søren Brunak

193. Institute for Molecular Bioscience, University of Queensland, St. Lucia, Brisbane, QLD, Australia

Timothy J. C. Bruxner, Oliver Holmes, Stephen H. Kazakoff, Conrad R. Leonard, Felicity Newell, Katia Nones, Ann-Marie Patch, John V. Pearson, Michael C. Quinn, Nick M. Waddell, Nicola Waddell, Scott Wood & Qinying Xu

194. Biomedical Engineering, Oregon Health and Science University, Portland, OR, USA

Alex Buchanan & Kyle Ellrott

195. Division of Theoretical Bioinformatics, German Cancer Research Center (DKFZ), Heidelberg, Germany

Ivo Buchhalter, Calvin Wing Yiu Chan, Roland Eils, Michael C. Heinold, Carl Herrmann, Natalie Jäger, Rolf Kabbe, Jules N. A. Kerssemakers, Kortine Kleinheinz, Nagarajan Paramasivam, Manuel Prinz, Matthias Schlesner & Johannes Werner

196. Institute of Pharmacy and Molecular Biotechnology and BioQuant, Heidelberg University, Heidelberg, Germany

Ivo Buchhalter, Roland Eils, Michael C. Heinold, Carl Herrmann, Daniel Hübschmann, Kortine Kleinheinz & Umut H. Toprak

197. Federal Ministry of Education and Research, Berlin, Germany

Christiane Buchholz

198. Melanoma Institute Australia, University of Sydney, Sydney, NSW, Australia

Hazel Burke, Ricardo De Paoli-Iseppi, Nicholas K. Hayward, Peter Hersey, Valerie Jakrot, Hojabr Kakavand, Georgina V. Long, Graham J. Mann, Robyn P. M. Saw, Richard A. Scolyer, Ping Shang, Andrew J. Spillane, Jonathan R. Stretch, John F. F. Thompson & James S. Wilmott

199. Pediatric Hematology and Oncology, University Hospital Muenster, Muenster, Germany

Birgit Burkhardt

200. Department of Pathology, Johns Hopkins University School of Medicine, Baltimore, MD, USA

Kathleen H. Burns & Christopher Umbricht

201. McKusick-Nathans Institute of Genetic Medicine, Sidney Kimmel Comprehensive Cancer Center at Johns Hopkins University School of Medicine, Baltimore, MD, USA

Kathleen H. Burns

202. Foundation Medicine, Inc, Cambridge, MA, USA

John Busanovich

203. Department of Biomedical Data Science, Stanford University School of Medicine, Stanford, CA, USA

Carlos D. Bustamante & Francisco M. De La Vega

204. Department of Genetics, Stanford University School of Medicine, Stanford, CA, USA

Carlos D. Bustamante, Francisco M. De La Vega, Suyash S. Shringarpure, Nasa Sinnott-Armstrong & Mark H. Wright

205. Bakar Computational Health Sciences Institute and Department of Pediatrics, University of California, San Francisco, CA, USA

Atul J. Butte & Jieming Chen

206. Institute of Clinical Medicine, Faculty of Medicine, University of Oslo, Oslo, Norway

Anne-Lise Børresen-Dale

207. National Cancer Institute, National Institutes of Health, Bethesda, MD, USA

Samantha J. Caesar-Johnson, John A. Demchok, Ina Felau, Roy Tarnuzzer, Zhining Wang, Liming Yang, Jean C. Zenklusen & Jiashan Zhang

208. Royal Marsden NHS Foundation Trust, London and Sutton, UK

Declan Cahill, Nening M. Dennis, Tim Dudderidge, Rosalind A. Eeles, Cyril Fisher, Steven Hazell, Vincent Khoo, Pardeep Kumar, Naomi Livni, Erik Mayer, David Nicol, Christopher Ogden, Edward W. Rowe, Sarah Thomas, Alan Thompson & Nicholas van As

209. Genome Biology Unit, European Molecular Biology Laboratory (EMBL), Heidelberg, Germany

Claudia Calabrese, Serap Erkek, Moritz Gerstung, Santiago Gonzalez, Nina Habermann, Wolfgang Huber, Lara Jerman, Jan O. Korbel, Esa Pitkänen, Benjamin Raeder, Tobias Rausch, Vasilisa A. Rudneva, Oliver Stegle, Stephanie Sungalee, Lara Urban, Sebastian M. Waszak, Joachim Weischenfeldt & Sergei Yakneen

210. Department of Oncology, University of Cambridge, Cambridge, UK

Carlos Caldas & Suet-Feung Chin

211. Li Ka Shing Centre, Cancer Research UK Cambridge Institute, University of Cambridge, Cambridge, UK

Carlos Caldas, Suet-Feung Chin, Ruben M. Drews, Paul A. Edwards, Matthew Eldridge, Steve Hawkins, Andy G. Lynch, Geoff Macintyre, Florian Markowetz, Charlie E. Massie, David E. Neal, Simon Tavaré & Ke Yuan

212. Institut Gustave Roussy, Villejuif, France

Fabien Calvo

213. Cambridge University Hospitals NHS Foundation Trust, Cambridge, UK

Peter J. Campbell, Vincent J. Gnanapragasam, William Howat, Thomas J. Mitchell, David E. Neal, Nimish C. Shah & Anne Y. Warren

214. Department of Haematology, University of Cambridge, Cambridge, UK

Peter J. Campbell

215. Anatomia Patológica, Hospital Clinic, Institut d'Investigacions Biomèdiques August Pi i Sunyer (IDIBAPS), University of Barcelona, Barcelona, Spain

Elias Campo

216. Spanish Ministry of Science and Innovation, Madrid, Spain

Elias Campo

217. University of Michigan Comprehensive Cancer Center, Ann Arbor, MI, USA

Thomas E. Carey

218. Department for BioMedical Research, University of Bern, Bern, Switzerland

Joana Carlevaro-Fita

219. Department of Medical Oncology, Inselspital, University Hospital and University of Bern, Bern, Switzerland

Joana Carlevaro-Fita, Rory Johnson & Andrés Lanzós

220. Graduate School for Cellular and Biomedical Sciences, University of Bern, Bern, Switzerland

Joana Carlevaro-Fita & Andrés Lanzós

221. University of Pavia, Pavia, Italy

Mario Cazzola & Luca Malcovati

222. University of Alabama at Birmingham, Birmingham, AL, USA

Robert Cerfolio

223. UHN Program in BioSpecimen Sciences, Toronto General Hospital, Toronto, ON, Canada

Dianne E. Chadwick, Sheng-Ben Liang, Michael H. A. Roehrl & Sagedeh Shahabi

224. Department of Urology, Icahn School of Medicine at Mount Sinai, New York, NY, USA

Dimple Chakravarty

225. Centre for Law and Genetics, University of Tasmania, Sandy Bay Campus, Hobart, TAS, Australia

Don Chalmers

226. Faculty of Biosciences, Heidelberg University, Heidelberg, Germany

Calvin Wing Yiu Chan, Chen Hong & Lina Sieverling

227. Department of Biochemistry, Microbiology and Immunology, Faculty of Medicine, University of Ottawa, Ottawa, ON, Canada

Kin Chan

228. Division of Anatomic Pathology, Mayo Clinic, Rochester, MN, USA

Vishal S. Chandan

229. Division of Cancer Epidemiology and Genetics, National Cancer Institute, National Institutes of Health, Bethesda, MD, USA

Stephen J. Chanock, Xing Hua, Lisa Mirabello, Lei Song & Bin Zhu

230. Illawarra Shoalhaven Local Health District L3 Illawarra Cancer Care Centre, Wollongong Hospital, Wollongong, NSW, Australia

Lorraine A. Chantrill

231. BioForA, French National Institute for Agriculture, Food, and Environment (INRAE), ONF, Orléans, France

Aurélien Chateigner

232. Department of Biostatistics, Bloomberg School of Public Health, Johns Hopkins University, Baltimore, MD, USA

Nilanjan Chatterjee

233. University of California San Diego, San Diego, CA, USA

Zhaohong Chen, Michelle T. Dow, Claudiu Farcas, S. M. Ashiqul Islam, Antonios Koures, Lucila Ohno-Machado, Christos Sotiriou & Ashley Williams

234. Division of Experimental Pathology, Mayo Clinic, Rochester, MN, USA

Jeremy Chien

235. Centre for Cancer Research, The Westmead Institute for Medical Research, University of Sydney, Sydney, NSW, Australia

Yoke-Eng Chiew, Angela Chou, Jillian A. Hung, Catherine J. Kennedy, Graham J. Mann, Gulietta M. Pupo, Sarah-Jane Schramm, Varsha Tembe & Anna deFazio

236. Department of Gynaecological Oncology, Westmead Hospital, Sydney, NSW, Australia

Yoke-Eng Chiew, Jillian A. Hung, Catherine J. Kennedy & Anna deFazio

237. PDXen Biosystems Inc, Seoul, South Korea

Sunghoon Cho

238. Korea Advanced Institute of Science and Technology, Daejeon, South Korea

Jung Kyoon Choi, Young Seok Ju & Christopher J. Yoon

239. Electronics and Telecommunications Research Institute, Daejeon, South Korea

Wan Choi, Seung-Hyup Jeon, Hyunghwan Kim & Youngchoon Woo

240. Institut National du Cancer (INCA), Boulogne-Billancourt, France

Christine Chomienne & Iris Pauporté

241. Department of Genetics, Informatics Institute, University of Alabama at Birmingham, Birmingham, AL, USA

Zechen Chong

242. Division of Medical Oncology, National Cancer Centre, Singapore, Singapore

Su Pin Choo

243. Medical Oncology, University and Hospital Trust of Verona, Verona, Italy

Sara Cingarlini & Michele Milella

244. Department of Pediatrics, University Hospital Schleswig-Holstein, Kiel, Germany

Alexander Claviez

245. Hepatobiliary/Pancreatic Surgical Oncology Program, University Health Network, Toronto, ON, Canada

Sean Cleary, Ashton A. Connor & Steven Gallinger

246. School of Biological Sciences, University of Auckland, Auckland, New Zealand

Nicole Cloonan

247. Department of Surgery, University of Melbourne, Parkville, VIC, Australia

Marek Cmero

248. The Murdoch Children's Research Institute, Royal Children's Hospital, Parkville, VIC, Australia

Marek Cmero

249. Walter and Eliza Hall Institute, Parkville, VIC, Australia

Marek Cmero

250. Vancouver Prostate Centre, Vancouver, Canada

Colin C. Collins, Nilgun Donmez, Faraz Hach, Salem Malikic, S. Cenk Sahinalp, Iman Sarrafi & Raunak Shrestha

251. Lunenfeld-Tanenbaum Research Institute, Mount Sinai Hospital, Toronto, ON, Canada

Ashton A. Connor, Steven Gallinger, Robert C. Grant, Treasa A. McPherson & Iris Selander

252. University of East Anglia, Norwich, UK

Colin S. Cooper

253. Norfolk and Norwich University Hospital NHS Trust, Norwich, UK

Matthew G. Cordes, Catrina C. Fronick & Tom Roques

254. Victorian Institute of Forensic Medicine, Southbank, VIC, Australia

Stephen M. Cordner

255. Department of Biomedical Informatics, Harvard Medical School, Boston, MA, USA

Isidro Cortés-Ciriano, Jake June-Koo Lee & Peter J. Park

256. Department of Chemistry, Centre for Molecular Science Informatics, University of Cambridge, Cambridge, UK

Isidro Cortés-Ciriano

257. Ludwig Center at Harvard Medical School, Boston, MA, USA

Isidro Cortés-Ciriano, Jake June-Koo Lee & Peter J. Park

258. Human Genome Sequencing Center, Baylor College of Medicine, Houston, TX, USA

Kyle Covington, HarshaVardhan Doddapaneni, Richard A. Gibbs, Jianhong Hu, Joy C. Jayaseelan, Viktoriya Korchina, Lora Lewis, Donna M. Muzny, Linghua Wang, David A. Wheeler & Liu Xi

259. Peter MacCallum Cancer Centre, University of Melbourne, Melbourne, VIC, Australia

Prue A. Cowin, Anne Hamilton, Gisela Mir Arnau & Ravikiran Vedururu

260. Physics Division, Optimization and Systems Biology Lab, Massachusetts General Hospital, Boston, MA, USA

David Craft

261. Department of Medicine, Baylor College of Medicine, Houston, TX, USA

Chad J. Creighton

262. University of Cologne, Cologne, Germany

Yupeng Cun, Martin Peifer & Tsun-Po Yang

263. International Genomics Consortium, Phoenix, AZ, USA

Erin Curley & Troy Shelton

264. Genomics Research Program, Ontario Institute for Cancer Research, Toronto, ON, Canada

Karolina Czajka, Jenna Eagles, Thomas J. Hudson, Jeremy Johns, Faridah Mbabaali, John D. McPherson, Jessica K. Miller, Danielle Pasternack, Michelle Sam & Lee E. Timms

265. Barking Havering and Redbridge University Hospitals NHS Trust, Romford, UK

Bogdan Czerniak, Adel El-Naggar & David Khoo

266. Children's Hospital at Westmead, University of Sydney, Sydney, NSW, Australia

Rebecca A. Dagg

267. Department of Medicine, Section of Endocrinology, University and Hospital Trust of Verona, Verona, Italy

Maria Vittoria Davi

268. Computational Biology Center, Memorial Sloan Kettering Cancer Center, New York, NY, USA

Natalie R. Davidson, Andre Kahles, Kjong-Van Lehmann, Alessandro Pastore, Gunnar Rätsch, Chris Sander, Yasin Senbabaoglu & Nicholas D. Socci

269. Department of Biology, ETH Zurich, Zürich, Switzerland

Natalie R. Davidson, Andre Kahles, Kjong-Van Lehmann, Gunnar Rätsch & Stefan G. Stark

270. Department of Computer Science, ETH Zurich, Zurich, Switzerland

Natalie R. Davidson, Andre Kahles, Kjong-Van Lehmann & Gunnar Rätsch

271. SIB Swiss Institute of Bioinformatics, Lausanne, Switzerland

Natalie R. Davidson, Andre Kahles, Kjong-Van Lehmann, Gunnar Rätsch & Stefan G. Stark

272. Weill Cornell Medical College, New York, NY, USA

Natalie R. Davidson, Bishoy M. Faltas & Gunnar Rätsch

273. Academic Department of Medical Genetics, University of Cambridge, Addenbrooke's Hospital, Cambridge, UK

Helen Davies & Serena Nik-Zainal

274. MRC Cancer Unit, University of Cambridge, Cambridge, UK

Helen Davies, Rebecca C. Fitzgerald, Nicola Grehan, Serena Nik-Zainal & Maria O'Donovan

275. Departments of Pediatrics and Genetics, University of North Carolina at Chapel Hill, Chapel Hill, NC, USA

Ian J. Davis

276. Seven Bridges Genomics, Charlestown, MA, USA

Brandi N. Davis-Dusenbery, Sinisa Ivkovic, Milena Kovacevic, Ana Mijalkovic Lazic, Sanja Mijalkovic, Mia Nastic, Petar Radovic & Nebojsa Tijanic

277. Annai Systems, Inc, Carlsbad, CA, USA

Francisco M. De La Vega, Tal Shmaya & Dai-Ying Wu

278. Department of Pathology, General Hospital of Treviso, Department of Medicine, University of Padua, Treviso, Italy

Angelo P. Dei Tos

279. Department of Computational Biology, University of Lausanne, Lausanne, Switzerland

Olivier Delaneau

280. Department of Genetic Medicine and Development, University of Geneva Medical School, Geneva, CH, Switzerland

Olivier Delaneau

281. Swiss Institute of Bioinformatics, University of Geneva, Geneva, CH, Switzerland

Olivier Delaneau

282. The Francis Crick Institute, London, UK

Jonas Demeulemeester, Stefan C. Dentro, Matthew W. Fittall, Kerstin Haase, Clemency Jolly, Maxime Tarabichi & Peter Van Loo

283. University of Leuven, Leuven, Belgium

Jonas Demeulemeester & Peter Van Loo

284. Institute of Medical Genetics and Applied Genomics, University of Tübingen, Tübingen, Germany

German M. Demidov, Francesc Muyas & Stephan Ossowski

285. Computational and Systems Biology, Genome Institute of Singapore, Singapore, Singapore

Deniz Demircioğlu & Jonathan Göke

286. School of Computing, National University of Singapore, Singapore, Singapore

Deniz Demircioğlu

287. Big Data Institute, Li Ka Shing Centre, University of Oxford, Oxford, UK

Stefan C. Dentro & David C. Wedge

288. Biomedical Data Science Laboratory, Francis Crick Institute, London, UK

Nikita Desai

289. Bioinformatics Group, Department of Computer Science, University College London, London, UK

Nikita Desai

290. The Edward S. Rogers Sr. Department of Electrical and Computer Engineering, University of Toronto, Toronto, ON, Canada

Amit G. Deshwar

291. Breast Cancer Translational Research Laboratory JC Heuson, Institut Jules Bordet, Brussels, Belgium

Christine Desmedt

292. Department of Oncology, Laboratory for Translational Breast Cancer Research, KU Leuven, Leuven, Belgium

Christine Desmedt

293. Institute for Research in Biomedicine (IRB Barcelona), The Barcelona Institute of Science and Technology, Barcelona, Spain

Jordi Deu-Pons, Joan Frigola, Abel Gonzalez-Perez, Ferran Muiños, Loris Mularoni, Oriol Pich, Iker Reyes-Salazar, Carlota Rubio-Perez, Radhakrishnan Sabarinathan & David Tamborero

294. Research Program on Biomedical Informatics, Universitat Pompeu Fabra, Barcelona, Spain

Jordi Deu-Pons, Abel Gonzalez-Perez, Ferran Muiños, Loris Mularoni, Oriol Pich, Carlota Rubio-Perez, Radhakrishnan Sabarinathan & David Tamborero

295. Division of Medical Oncology, Princess Margaret Cancer Centre, Toronto, ON, Canada

Neesha C. Dhani, David Hedley & Malcolm J. Moore

296. Department of Physiology and Biophysics, Weill Cornell Medicine, New York, NY, USA

Priyanka Dhingra, Ekta Khurana, Eric Minwei Liu & Alexander Martinez-Fundichely

297. Institute for Computational Biomedicine, Weill Cornell Medicine, New York, NY, USA

Priyanka Dhingra, Ekta Khurana, Eric Minwei Liu & Alexander Martinez-Fundichely

298. Department of Pathology, UPMC Shadyside, Pittsburgh, PA, USA

Rajiv Dhir

299. Independent Consultant, Wellesley, USA

Anthony DiBiase

300. Department of Cell and Molecular Biology, Science for Life Laboratory, Uppsala University, Uppsala, Sweden

Klev Diamanti, Jan Komorowski & Husen M. Umer

301. Department of Medicine and Department of Genetics, Washington University School of Medicine, St. Louis, St. Louis, MO, USA

Li Ding, Robert S. Fulton, Michael D. McLellan, Michael C. Wendl & Venkata D. Yellapantula

302. Hefei University of Technology, Anhui, China

Shuai Ding & Shanlin Yang

303. Translational Cancer Research Unit, GZA Hospitals St.-Augustinus, Center for Oncological Research, Faculty of Medicine and Health Sciences, University of Antwerp, Antwerp, Belgium

Luc Dirix, Steven Van Laere, Gert G. Van den Eynden & Peter Vermeulen

304. Simon Fraser University, Burnaby, BC, Canada

Nilgun Donmez, Ermin Hodzic, Salem Malikic, S. Cenk Sahinalp & Iman Sarrafi

305. University of Pennsylvania, Philadelphia, PA, USA

Ronny Drapkin

306. Faculty of Science and Technology, University of Vic—Central University of Catalonia (UVic-UCC), Vic, Spain

Ana Dueso-Barroso

307. The Wellcome Trust, London, UK

Michael Dunn

308. The Hospital for Sick Children, Toronto, ON, Canada

Lewis Jonathan Dursi

309. Department of Pathology, Queen Elizabeth University Hospital, Glasgow, UK

Fraser R. Duthie

310. Department of Genetics and Computational Biology, QIMR Berghofer Medical Research Institute, Brisbane, QLD, Australia

Ken Dutton-Regester, Nicholas K. Hayward, Oliver Holmes, Peter A. Johansson, Stephen H. Kazakoff, Conrad R. Leonard, Felicity Newell, Katia Nones, Ann-Marie Patch, John V. Pearson, Antonia L. Pritchard, Michael C. Quinn, Paresh Vyas, Nicola Waddell, Scott Wood & Qinying Xu

311. Department of Oncology, Centre for Cancer Genetic Epidemiology, University of Cambridge, Cambridge, UK

Douglas F. Easton

312. Department of Public Health and Primary Care, Centre for Cancer Genetic Epidemiology, University of Cambridge, Cambridge, UK

Douglas F. Easton

313. Prostate Cancer Canada, Toronto, ON, Canada

Stuart Edmonds

314. University of Cambridge, Cambridge, UK

Paul A. Edwards, Anthony R. Green, Andy G. Lynch, Florian Markowetz & Thomas J. Mitchell

315. Department of Laboratory Medicine, Translational Cancer Research, Lund University Cancer Center at Medicon Village, Lund University, Lund, Sweden

Anna Ehinger

316. Heidelberg University, Heidelberg, Germany

Juergen Eils, Roland Eils & Daniel Hübschmann

317. New BIH Digital Health Center, Berlin Institute of Health (BIH) and Charité - Universitätsmedizin Berlin, Berlin, Germany

Juergen Eils, Roland Eils & Chris Lawerenz

318. CIBER Epidemiología y Salud Pública (CIBERESP), Madrid, Spain

Georgia Escaramis

319. Research Group on Statistics, Econometrics and Health (GRECS), UdG, Barcelona, Spain

Georgia Escaramis

320. Quantitative Genomics Laboratories (qGenomics), Barcelona, Spain

Xavier Estivill

321. Icelandic Cancer Registry, Icelandic Cancer Society, Reykjavik, Iceland

Jorunn E. Eyfjord, Holmfridur Hilmarsdottir & Jon G. Jonasson

322. State Key Laboratory of Cancer Biology, and Xijing Hospital of Digestive Diseases, Fourth Military Medical University, Shaanxi, China

Daiming Fan & Yongzhan Nie

323. Department of Medicine (DIMED), Surgical Pathology Unit, University of Padua, Padua, Italy

Matteo Fassan

324. Rigshospitalet, Copenhagen, Denmark

Francesco Favero

325. Center for Cancer Genomics, National Cancer Institute, National Institutes of Health, Bethesda, MD, USA

Martin L. Ferguson

326. Department of Biochemistry and Molecular Medicine, University of Montreal, Montreal, QC, Canada

Vincent Ferretti

327. Australian Institute of Tropical Health and Medicine, James Cook University, Douglas, QLD, Australia

Matthew A. Field

328. Department of Neuro-Oncology, Istituto Neurologico Besta, Milano, Italy

Gaetano Finocchiaro

329. Bioplatforms Australia, North Ryde, NSW, Australia

Anna Fitzgerald & Catherine A. Shang

330. Department of Pathology (Research), University College London Cancer Institute, London, UK

Adrienne M. Flanagan

331. Department of Surgical Oncology, Princess Margaret Cancer Centre, Toronto, ON, Canada

Neil E. Fleshner

332. Department of Medical Oncology, Josephine Nefkens Institute and Cancer Genomics Centre, Erasmus Medical Center, Rotterdam, CN, The Netherlands

John A. Foekens, John W. M. Martens, F. Germán Rodríguez-González, Anieta M. Sieuwerts & Marcel Smid

333. The University of Queensland Thoracic Research Centre, The Prince Charles Hospital, Brisbane, QLD, Australia

Kwun M. Fong

334. CIBIO/InBIO - Research Center in Biodiversity and Genetic Resources, Universidade do Porto, Vairão, Portugal

Nuno A. Fonseca

335. HCA Laboratories, London, UK

Christopher S. Foster

336. University of Liverpool, Liverpool, UK

Christopher S. Foster

337. The Azrieli Faculty of Medicine, Bar-Ilan University, Safed, Israel

Milana Frenkel-Morgenstern

338. Department of Neurosurgery, University of Florida, Gainesville, FL, USA

William Friedman

339. Department of Pathology, Graduate School of Medicine, University of Tokyo, Tokyo, Japan

Masashi Fukayama & Tetsuo Ushiku

340. University of Milano Bicocca, Monza, Italy

Carlo Gambacorti-Passerini

341. BGI-Shenzhen, Shenzhen, China

Shengjie Gao, Yong Hou, Chang Li, Lin Li, Siliang Li, Xiaobo Li, Xinyue Li, Dongbing Liu, Xingmin Liu, Qiang Pan-Hammarström, Hong Su, Jian Wang, Kui Wu, Heng Xiong, Huanming Yang, Chen Ye, Xiuqing Zhang, Yong Zhou & Shida Zhu

342. Department of Pathology, Oslo University Hospital Ulleval, Oslo, Norway

Øystein Garred

343. Center for Biomedical Informatics, Harvard Medical School, Boston, MA, USA

Nils Gehlenborg

344. Department Biochemistry and Molecular Biomedicine, University of Barcelona, Barcelona, Spain

Josep L. L. Gelpi

345. Office of Cancer Genomics, National Cancer Institute, National Institutes of Health, Bethesda, MD, USA

Daniela S. Gerhard

346. Cancer Epigenomics, German Cancer Research Center (DKFZ), Heidelberg, Germany

Clarissa Gerhauser, Christoph Plass & Dieter Weichenhan

347. Department of Cancer Biology, The University of Texas MD Anderson Cancer Center, Houston, TX, USA

Jeffrey E. Gershenwald

348. Department of Surgical Oncology, The University of Texas MD Anderson Cancer Center, Houston, TX, USA

Jeffrey E. Gershenwald

349. Department of Computer Science, Yale University, New Haven, CT, USA

Mark Gerstein & Fabio C. P. Navarro

350. Department of Molecular Biophysics and Biochemistry, Yale University, New Haven, CT, USA

Mark Gerstein, Sushant Kumar, Lucas Lochovsky, Shaoke Lou, Patrick D. McGillivray, Fabio C. P. Navarro, Leonidas Salichos & Jonathan Warrell

351. Program in Computational Biology and Bioinformatics, Yale University, New Haven, CT, USA

Mark Gerstein, Arif O. Harmanci, Sushant Kumar, Donghoon Lee, Shantao Li, Xiaotong Li, Lucas Lochovsky, Shaoke Lou, William Meyerson, Leonidas Salichos, Jonathan Warrell, Jing Zhang & Yan Zhang

352. Center for Cancer Research, Massachusetts General Hospital, Boston, MA, USA

Gad Getz & Paz Polak

353. Department of Pathology, Massachusetts General Hospital, Boston, MA, USA

Gad Getz

354. Department of Pathology, Memorial Sloan Kettering Cancer Center, New York, NY, USA

Ronald Ghossein, Dilip D. Giri, Christine A. Iacobuzio-Donahue, Jorge Reis-Filho & Victor Reuter

355. Division of Gastroenterology and Hepatology, Mayo Clinic, Rochester, MN, USA

Nasra H. Giama, Catherine D. Moser & Lewis R. Roberts

356. University of Sydney, Sydney, NSW, Australia

Anthony J. Gill & James G. Kench

357. University of Oxford, Oxford, UK

Pelvender Gill, Freddie C. Hamdy, Katalin Karaszi, Adam Lambert, Luke Marsden, Clare Verrill & Paresh Vyas

358. Department of Surgery, Academic Urology Group, University of Cambridge, Cambridge, UK

Vincent J. Gnanapragasam

359. Department of Medicine II, University of Würzburg, Wuerzburg, Germany

Maria Elisabeth Goebler

360. Sylvester Comprehensive Cancer Center, University of Miami, Miami, FL, USA

Carmen Gomez

361. Institut Hospital del Mar d’Investigacions Mèdiques (IMIM), Barcelona, Spain

Abel Gonzalez-Perez

362. Genome Integrity and Structural Biology Laboratory, National Institute of Environmental Health Sciences (NIEHS), Durham, NC, USA

Dmitry A. Gordenin & Natalie Saini

363. St. Thomas's Hospital, London, UK

James Gossage

364. Osaka International Cancer Center, Osaka, Japan

Kunihito Gotoh

365. Department of Pathology, Skåne University Hospital, Lund University, Lund, Sweden

Dorthe Grabau

366. Department of Medical Oncology, Beatson West of Scotland Cancer Centre, Glasgow, UK

Janet S. Graham

367. National Human Genome Research Institute, National Institutes of Health, Bethesda, MD, USA

Eric Green, Carolyn M. Hutter & Heidi J. Sofia

368. Centre for Cancer Research, Victorian Comprehensive Cancer Centre, University of Melbourne, Melbourne, VIC, Australia

Sean M. Grimmond

369. Department of Medicine, Section of Hematology/Oncology, University of Chicago, Chicago, IL, USA

Robert L. Grossman

370. German Center for Infection Research (DZIF), Partner Site Hamburg-Borstel-Lübeck-Riems, Hamburg, Germany

Adam Grundhoff

371. Bioinformatics Research Centre (BiRC), Aarhus University, Aarhus, Denmark

Qianyun Guo, Asger Hobolth & Jakob Skou Pedersen

372. Department of Biotechnology, Ministry of Science and Technology, Government of India, New Delhi, Delhi, India

Shailja Gupta & K. VijayRaghavan

373. National Cancer Centre Singapore, Singapore, Singapore

Jonathan Göke

374. Brandeis University, Waltham, MA, USA

James E. Haber

375. Department of Urologic Sciences, University of British Columbia, Vancouver, BC, Canada

Faraz Hach

376. Department of Internal Medicine, Stanford University, Stanford, CA, USA

Mark P. Hamilton

377. The University of Texas Health Science Center at Houston, Houston, TX, USA

Leng Han, Yang Yang & Xuanping Zhang

378. Imperial College NHS Trust, Imperial College, London, INY, UK

George B. Hanna

379. Senckenberg Institute of Pathology, University of Frankfurt Medical School, Frankfurt, Germany

Martin Hansmann

380. Department of Medicine, Division of Biomedical Informatics, UC San Diego School of Medicine, San Diego, CA, USA

Olivier Harismendy

381. Center for Precision Health, School of Biomedical Informatics, The University of Texas Health Science Center, Houston, TX, USA

Arif O. Harmanci

382. Oxford Nanopore Technologies, New York, NY, USA

Eoghan Harrington & Sissel Juul

383. Institute of Medical Science, University of Tokyo, Tokyo, Japan

Takanori Hasegawa, Shuto Hayashi, Seiya Imoto, Mitsuhiro Komura, Satoru Miyano, Naoki Miyoshi, Kazuhiro Ohi, Eigo Shimizu, Yuichi Shiraishi, Hiroko Tanaka & Rui Yamaguchi

384. Howard Hughes Medical Institute, University of California Santa Cruz, Santa Cruz, CA, USA

David Haussler

385. Wakayama Medical University, Wakayama, Japan

Shinya Hayami, Masaki Ueno & Hiroki Yamaue

386. Department of Internal Medicine, Division of Medical Oncology, Lineberger Comprehensive Cancer Center, University of North Carolina at Chapel Hill, Chapel Hill, NC, USA

D. Neil Hayes

387. University of Tennessee Health Science Center for Cancer Research, Memphis, TN, USA

D. Neil Hayes

388. Department of Histopathology, Salford Royal NHS Foundation Trust, Salford, UK

Stephen J. Hayes

389. Faculty of Biology, Medicine and Health, University of Manchester, Manchester, UK

Stephen J. Hayes

390. BIOPIC, ICG and College of Life Sciences, Peking University, Beijing, China

Yao He & Zemin Zhang

391. Peking-Tsinghua Center for Life Sciences, Peking University, Beijing, China

Yao He & Zemin Zhang

392. Children's Hospital of Philadelphia, Philadelphia, PA, USA

Allison P. Heath

393. Department of Bioinformatics and Computational Biology and Department of Systems Biology, The University of Texas MD Anderson Cancer Center, Houston, TX, USA

Apurva M. Hegde, Yiling Lu & John N. Weinstein

394. Karolinska Institute, Stockholm, Sweden

Eva Hellstrom-Lindberg & Jesper Lagergren

395. The Donnelly Centre, University of Toronto, Toronto, ON, Canada

Mohamed Helmy & Jeffrey A. Wintersinger

396. Department of Medical Genetics, College of Medicine, Hallym University, Chuncheon, South Korea

Seong Gu Heo, Eun Pyo Hong & Ji Wan Park

397. Department of Experimental and Health Sciences, Institute of Evolutionary Biology (UPF-CSIC), Universitat Pompeu Fabra, Barcelona, Spain

José María Heredia-Genestar, Tomas Marques-Bonet & Arcadi Navarro

398. Health Data Science Unit, University Clinics, Heidelberg, Germany

Carl Herrmann

399. Massachusetts General Hospital Center for Cancer Research, Charlestown, MA, USA

Julian M. Hess & Yosef E. Maruvka

400. Hokkaido University, Sapporo, Japan

Satoshi Hirano & Toru Nakamura

401. Department of Pathology and Clinical Laboratory, National Cancer Center Hospital, Tokyo, Japan

Nobuyoshi Hiraoka

402. Department of Genetics, University of North Carolina at Chapel Hill, Chapel Hill, NC, USA

Katherine A. Hoadley & Tara J. Skelly

403. Computational Biology, Leibniz Institute on Aging - Fritz Lipmann Institute (FLI), Jena, Germany

Steve Hoffmann

404. University of Melbourne Centre for Cancer Research, Melbourne, VIC, Australia

Oliver Hofmann

405. University of Nebraska Medical Center, Omaha, NE, USA

Michael A. Hollingsworth & Sarah P. Thayer

406. Syntekabio Inc, Daejeon, South Korea

Jongwhi H. Hong

407. Department of Pathology, Academic Medical Center, Amsterdam, AZ, The Netherlands

Gerrit K. Hooijer

408. China National GeneBank-Shenzhen, Shenzhen, China

Yong Hou, Chang Li, Siliang Li, Xiaobo Li, Dongbing Liu, Xingmin Liu, Henk G. Stunnenberg, Hong Su, Kui Wu, Heng Xiong, Chen Ye & Shida Zhu

409. Division of Molecular Genetics, German Cancer Research Center (DKFZ), Heidelberg, Germany

Volker Hovestadt, Murat Iskar, Peter Lichter, Bernhard Radlwimmer & Marc Zapatka

410. Division of Life Science and Applied Genomics Center, Hong Kong University of Science and Technology, Clear Water Bay, Hong Kong, China

Taobo Hu, Yogesh Kumar, Eric Z. Ma, Zhenggang Wu & Hong Xue

411. Icahn School of Medicine at Mount Sinai, New York, NY, USA

Kuan-lin Huang

412. Geneplus-Shenzhen, Shenzhen, China

Yi Huang

413. School of Computer Science and Technology, Xi'an Jiaotong University, Xi'an, China

Yi Huang, Jiayin Wang, Xiao Xiao & Xuanping Zhang

414. AbbVie, North Chicago, IL, USA

Thomas J. Hudson

415. Institute of Pathology, Charité – University Medicine Berlin, Berlin, Germany

Michael Hummel & Dido Lenze

416. Centre for Translational and Applied Genomics, British Columbia Cancer Agency, Vancouver, BC, Canada

David Huntsman

417. Edinburgh Royal Infirmary, Edinburgh, UK

Ted R. Hupp

418. Berlin Institute for Medical Systems Biology, Max Delbrück Center for Molecular Medicine, Berlin, Germany

Matthew R. Huska, Julia Markowski & Roland F. Schwarz

419. Department of Pediatric Immunology, Hematology and Oncology, University Hospital, Heidelberg, Germany

Daniel Hübschmann

420. German Cancer Research Center (DKFZ), Heidelberg, Germany

Daniel Hübschmann, Christof von Kalle & Roland F. Schwarz

421. Heidelberg Institute for Stem Cell Technology and Experimental Medicine (HI-STEM), Heidelberg, Germany

Daniel Hübschmann

422. Institute for Computational Biomedicine, Weill Cornell Medical College, New York, NY, USA

Marcin Imielinski

423. New York Genome Center, New York, NY, USA

Marcin Imielinski & Xiaotong Yao

424. Department of Urology, James Buchanan Brady Urological Institute, Johns Hopkins University School of Medicine, Baltimore, MD, USA

William B. Isaacs

425. Department of Preventive Medicine, Graduate School of Medicine, The University of Tokyo, Tokyo, Japan

Shumpei Ishikawa, Hiroto Katoh & Daisuke Komura

426. Department of Molecular and Cellular Biology, Baylor College of Medicine, Houston, TX, USA

Michael Ittmann

427. Department of Pathology and Immunology, Baylor College of Medicine, Houston, TX, USA

Michael Ittmann

428. Michael E. DeBakey Veterans Affairs Medical Center, Houston, TX, USA

Michael Ittmann

429. Technical University of Denmark, Lyngby, Denmark

Jose M. G. Izarzugaza

430. Department of Pathology, College of Medicine, Hanyang University, Seoul, South Korea

Jocelyne Jacquemier, Hyung-Yong Kim & Gu Kong

431. Academic Unit of Surgery, School of Medicine, College of Medical, Veterinary and Life Sciences, University of Glasgow, Glasgow Royal Infirmary, Glasgow, UK

Nigel B. Jamieson

432. Department of Pathology, Asan Medical Center, College of Medicine, Ulsan University, Songpa-gu, Seoul, South Korea

Se Jin Jang & Hee Jin Lee

433. Science Writer, Garrett Park, MD, USA

Karine Jegalian

434. International Cancer Genome Consortium (ICGC)/ICGC Accelerating Research in Genomic Oncology (ARGO) Secretariat, Ontario Institute for Cancer Research, Toronto, ON, Canada

Jennifer L. Jennings

435. University of Ljubljana, Ljubljana, Slovenia

Lara Jerman

436. Department of Public Health Sciences, University of Chicago, Chicago, IL, USA

Yuan Ji

437. Research Institute, NorthShore University HealthSystem, Evanston, IL, USA

Yuan Ji

438. Department for Biomedical Research, University of Bern, Bern, Switzerland

Rory Johnson, Andrés Lanzós & Mark A. Rubin

439. Centre of Genomics and Policy, McGill University and Génome Québec Innovation Centre, Montreal, QC, Canada

Yann Joly, Bartha M. Knoppers, Mark Phillips & Adrian Thorogood

440. Carolina Center for Genome Sciences, University of North Carolina at Chapel Hill, Chapel Hill, NC, USA

Corbin D. Jones

441. Hopp Children's Cancer Center (KiTZ), Heidelberg, Germany

David T. W. Jones, Marcel Kool & Stefan M. Pfister

442. Pediatric Glioma Research Group, German Cancer Research Center (DKFZ), Heidelberg, Germany

David T. W. Jones

443. Cancer Research UK, London, UK

Nic Jones & David Scott

444. Indivumed GmbH, Hamburg, Germany

Hartmut Juhl

445. Genome Integration Data Center, Syntekabio, Inc, Daejeon, South Korea

Jongsun Jung

446. University Hospital Zurich, Zurich, Switzerland

Andre Kahles, Kjong-Van Lehmann & Gunnar Rätsch

447. Clinical Bioinformatics, Swiss Institute of Bioinformatics, Geneva, Switzerland

Abdullah Kahraman

448. Institute for Pathology and Molecular Pathology, University Hospital Zurich, Zurich, Switzerland

Abdullah Kahraman

449. Institute of Molecular Life Sciences, University of Zurich, Zurich, Switzerland

Abdullah Kahraman & Christian von Mering

450. MRC Human Genetics Unit, MRC IGMM, University of Edinburgh, Edinburgh, UK

Vera B. Kaiser & Colin A. Semple

451. Women's Cancer Program at the Samuel Oschin Comprehensive Cancer Institute, Cedars-Sinai Medical Center, Los Angeles, CA, USA

Beth Karlan

452. Department of Biology, Bioinformatics Group, Division of Molecular Biology, Faculty of Science, University of Zagreb, Zagreb, Croatia

Rosa Karlić

453. Department for Internal Medicine II, University Hospital Schleswig-Holstein, Kiel, Germany

Dennis Karsch & Michael Kneba

454. Genetics and Molecular Pathology, SA Pathology, Adelaide, SA, Australia

Karin S. Kassahn

455. Department of Gastric Surgery, National Cancer Center Hospital, Tokyo, Japan

Hitoshi Katai

456. Department of Bioinformatics, Division of Cancer Genomics, National Cancer Center Research Institute, Tokyo, Japan

Mamoru Kato, Hirofumi Rokutan & Mihoko Saito-Adachi

457. A.A. Kharkevich Institute of Information Transmission Problems, Moscow, Russia

Marat D. Kazanov

458. Oncology and Immunology, Dmitry Rogachev National Research Center of Pediatric Hematology, Moscow, Russia

Marat D. Kazanov

459. Skolkovo Institute of Science and Technology, Moscow, Russia

Marat D. Kazanov

460. Department of Surgery, The George Washington University, School of Medicine and Health Science, Washington, DC, USA

Electron Kebebew

461. Endocrine Oncology Branch, Center for Cancer Research, National Cancer Institute, National Institutes of Health, Bethesda, MD, USA

Electron Kebebew

462. Melanoma Institute Australia, Macquarie University, Sydney, NSW, Australia

Richard F. Kefford

463. MIT Computer Science and Artificial Intelligence Laboratory, Massachusetts Institute of Technology, Cambridge, MA, USA

Manolis Kellis

464. Tissue Pathology and Diagnostic Oncology, Royal Prince Alfred Hospital, Sydney, NSW, Australia

James G. Kench & Richard A. Scolyer

465. Cholangiocarcinoma Screening and Care Program and Liver Fluke and Cholangiocarcinoma Research Centre, Faculty of Medicine, Khon Kaen University, Khon Kaen, Thailand

Narong Khuntikeo

466. Controlled Department and Institution, New York, NY, USA

Ekta Khurana

467. Englander Institute for Precision Medicine, Weill Cornell Medicine, New York, NY, USA

Ekta Khurana & Alexander Martinez-Fundichely

468. National Cancer Center, Gyeonggi, South Korea

Hark Kyun Kim

469. Department of Biochemistry, College of Medicine, Ewha Womans University, Seoul, South Korea

Hyung-Lae Kim

470. Health Sciences Department of Biomedical Informatics, University of California San Diego, La Jolla, CA, USA

Jihoon Kim

471. Research Core Center, National Cancer Centre Korea, Goyang-si, South Korea

Jong K. Kim

472. Department of Health Sciences and Technology, Sungkyunkwan University School of Medicine, Seoul, South Korea

Youngwook Kim

473. Samsung Genome Institute, Seoul, South Korea

Youngwook Kim

474. Breast Oncology Program, Dana-Farber/Brigham and Women's Cancer Center, Boston, MA, USA

Tari A. King

475. Department of Surgery, Memorial Sloan Kettering Cancer Center, New York, NY, USA

Tari A. King & Samuel Singer

476. Division of Breast Surgery, Brigham and Women's Hospital, Boston, MA, USA

Tari A. King

477. Integrative Bioinformatics Support Group, National Institute of Environmental Health Sciences (NIEHS), Durham, NC, USA

Leszek J. Klimczak

478. Department of Clinical Science, University of Bergen, Bergen, Norway

Stian Knappskog & Ola Myklebost

479. Center For Medical Innovation, Seoul National University Hospital, Seoul, South Korea

Youngil Koh

480. Department of Internal Medicine, Seoul National University Hospital, Seoul, South Korea

Youngil Koh & Sung-Soo Yoon

481. Institute of Computer Science, Polish Academy of Sciences, Warsawa, Poland

Jan Komorowski

482. Functional and Structural Genomics, German Cancer Research Center (DKFZ), Heidelberg, Germany

Marcel Kool, Andrey Korshunov, Michael Koscher, Stefan M. Pfister & Qi Wang

483. Laboratory of Translational Genomics, Division of Cancer Epidemiology and Genetics, National Cancer Institute, , National Institutes of Health, Bethesda, MD, USA

Roelof Koster

484. Institute for Medical Informatics Statistics and Epidemiology, University of Leipzig, Leipzig, Germany

Markus Kreuz & Markus Loeffler

485. Morgan Welch Inflammatory Breast Cancer Research Program and Clinic, The University of Texas MD Anderson Cancer Center, Houston, TX, USA

Savitri Krishnamurthy

486. Department of Hematology and Oncology, Georg-Augusts-University of Göttingen, Göttingen, Germany

Dieter Kube & Lorenz H. P. Trümper

487. Institute of Cell Biology (Cancer Research), University of Duisburg-Essen, Essen, Germany

Ralf Küppers

488. King’s College London and Guy’s and St. Thomas’ NHS Foundation Trust, London, UK

Jesper Lagergren

489. Center for Epigenetics, Van Andel Research Institute, Grand Rapids, MI, USA

Peter W. Laird

490. The University of Queensland Centre for Clinical Research, Royal Brisbane and Women’s Hospital, Herston, QLD, Australia

Sunil R. Lakhani & Peter T. Simpson

491. Department of Pediatric Oncology and Hematology, University of Cologne, Cologne, Germany

Pablo Landgraf

492. University of Düsseldorf, Düsseldorf, Germany

Pablo Landgraf & Guido Reifenberger

493. Department of Pathology, Institut Jules Bordet, Brussels, Belgium

Denis Larsimont

494. Institute of Biomedicine, Sahlgrenska Academy at University of Gothenburg, Gothenburg, Sweden

Erik Larsson

495. Children's Medical Research Institute, Sydney, NSW, Australia

Loretta M. S. Lau & Hilda A. Pickett

496. ILSbio, LLC Biobank, Chestertown, MD, USA

Xuan Le

497. Division of Genetics and Genomics, Boston Children's Hospital, Harvard Medical School, Boston, MA, USA

Eunjung Alice Lee

498. Institute for Bioengineering and Biopharmaceutical Research (IBBR), Hanyang University, Seoul, South Korea

Jeong-Yeon Lee

499. Department of Statistics, University of California Santa Cruz, Santa Cruz, CA, USA

Juhee Lee

500. National Genotyping Center, Institute of Biomedical Sciences, Academia Sinica, Taipei, Taiwan

Ming Ta Michael Lee

501. Department of Vertebrate Genomics/Otto Warburg Laboratory Gene Regulation and Systems Biology of Cancer, Max Planck Institute for Molecular Genetics, Berlin, Germany

Hans Lehrach, Hans-Jörg Warnatz & Marie-Laure Yaspo

502. McGill University and Genome Quebec Innovation Centre, Montreal, QC, Canada

Louis Letourneau

503. biobyte solutions GmbH, Heidelberg, Germany

Ivica Letunic

504. Gynecologic Oncology, NYU Laura and Isaac Perlmutter Cancer Center, New York University, New York, NY, USA

Douglas A. Levine

505. Division of Oncology, Stem Cell Biology Section, Washington University School of Medicine, St. Louis, MO, USA

Tim Ley

506. Department of Systems Biology, The University of Texas MD Anderson Cancer Center, Houston, TX, USA

Han Liang

507. Harvard University, Cambridge, MA, USA

Ziao Lin

508. Urologic Oncology Branch, Center for Cancer Research, National Cancer Institute, National Institutes of Health, Bethesda, MD, USA

W. M. Linehan

509. University of Oslo, Oslo, Norway

Ole Christian Lingjærde & Torill Sauer

510. University of Toronto, Toronto, ON, Canada

Fei-Fei Fei Liu, Quaid D. Morris, Ruian Shi, Shankar Vembu & Fan Yang

511. Peking University, Beijing, China

Fenglin Liu, Fan Zhang, Liangtao Zheng & Xiuqing Zheng

512. School of Life Sciences, Peking University, Beijing, China

Fenglin Liu

513. Leidos Biomedical Research, Inc, McLean, VA, USA

Jia Liu

514. Hematology, Hospital Clinic, Institut d'Investigacions Biomèdiques August Pi i Sunyer (IDIBAPS), University of Barcelona, Barcelona, Spain

Armando Lopez-Guillermo

515. Second Military Medical University, Shanghai, China

Yong-Jie Lu & Hongwei Zhang

516. Chinese Cancer Genome Consortium, Shenzhen, China

Youyong Lu

517. Department of Medical Oncology, Beijing Hospital, Beijing, China

Youyong Lu

518. Laboratory of Molecular Oncology, Key Laboratory of Carcinogenesis and Translational Research (Ministry of Education), Peking University Cancer Hospital and Institute, Beijing, China

Youyong Lu & Rui Xing

519. School of Medicine/School of Mathematics and Statistics, University of St. Andrews, St, Andrews, Fife, UK

Andy G. Lynch

520. Institute for Systems Biology, Seattle, WA, USA

Lisa Lype, Sheila M. Reynolds & Ilya Shmulevich

521. Department of Biochemistry and Molecular Biology, Faculty of Medicine, University Institute of Oncology-IUOPA, Oviedo, Spain

Carlos López-Otín & Xose S. Puente

522. Institut Bergonié, Bordeaux, France

Gaetan MacGrogan

523. Cancer Unit, MRC University of Cambridge, Cambridge, UK

Shona MacRae

524. Department of Pathology and Laboratory Medicine, Center for Personalized Medicine, Children's Hospital Los Angeles, Los Angeles, CA, USA

Dennis T. Maglinte

525. John Curtin School of Medical Research, Canberra, ACT, Australia

Graham J. Mann

526. MVZ Department of Oncology, PraxisClinic am Johannisplatz, Leipzig, Germany

Luisa Mantovani-Löffler

527. Department of Information Technology, Ghent University, Ghent, Belgium

Kathleen Marchal & Sergio Pulido-Tamayo

528. Department of Plant Biotechnology and Bioinformatics, Ghent University, Ghent, Belgium

Kathleen Marchal, Sergio Pulido-Tamayo & Lieven P. C. Verbeke

529. Institute for Genomic Medicine, Nationwide Children's Hospital, Columbus, OH, USA

Elaine R. Mardis

530. Computational Biology Program, School of Medicine, Oregon Health and Science University, Portland, OR, USA

Adam A. Margolin & Adam J. Struck

531. Department of Surgery, Duke University, Durham, NC, USA

Jeffrey Marks

532. Institució Catalana de Recerca i Estudis Avançats (ICREA), Barcelona, Spain

Tomas Marques-Bonet, Jose I. Martin-Subero, Arcadi Navarro, David Torrents & Alfonso Valencia

533. Institut Català de Paleontologia Miquel Crusafont, Universitat Autònoma de Barcelona, Barcelona, Spain

Tomas Marques-Bonet

534. University of Glasgow, Glasgow, UK

Sancha Martin & Ke Yuan

535. Institut d'Investigacions Biomèdiques August Pi i Sunyer (IDIBAPS), Barcelona, Spain

Jose I. Martin-Subero

536. Division of Oncology, Washington University School of Medicine, St. Louis, MO, USA

R. Jay Mashl

537. Department of Surgery and Cancer, Imperial College, London, INY, UK

Erik Mayer

538. Applications Department, Oxford Nanopore Technologies, Oxford, UK

Simon Mayes & Daniel J. Turner

539. Department of Obstetrics, Gynecology and Reproductive Services, University of California San Francisco, San Francisco, CA, USA

Karen McCune & Karen Smith-McCune

540. Department of Biochemistry and Molecular Medicine, University California at Davis, Sacramento, CA, USA

John D. McPherson

541. STTARR Innovation Facility, Princess Margaret Cancer Centre, Toronto, ON, Canada

Alice Meng

542. Discipline of Surgery, Western Sydney University, Penrith, NSW, Australia

Neil D. Merrett

543. Yale School of Medicine, Yale University, New Haven, CT, USA

William Meyerson

544. Department of Genetics, Lineberger Comprehensive Cancer Center, University of North Carolina at Chapel Hill, Chapel Hill, NC, USA

Piotr A. Mieczkowski, Joel S. Parker, Charles M. Perou, Donghui Tan, Umadevi Veluvolu & Matthew D. Wilkerson

545. Departments of Neurology and Neurosurgery, Henry Ford Hospital, Detroit, MI, USA

Tom Mikkelsen

546. Precision Oncology, OHSU Knight Cancer Institute, Oregon Health and Science University, Portland, OR, USA

Gordon B. Mills

547. Institute of Pathology, University Medical Center Hamburg-Eppendorf, Hamburg, Germany

Sarah Minner, Guido Sauter & Ronald Simon

548. Department of Health Sciences, Faculty of Medical Sciences, Kyushu University, Fukuoka, Japan

Shinichi Mizuno

549. Heidelberg Academy of Sciences and Humanities, Heidelberg, Germany

Fruzsina Molnár-Gábor

550. Department of Clinical Pathology, University of Melbourne, Melbourne, VIC, Australia

Carl Morrison, Karin A. Oien, Chawalit Pairojkul, Paul M. Waring & Marc J. van de Vijver

551. Department of Pathology, Roswell Park Cancer Institute, Buffalo, NY, USA

Carl Morrison

552. Department of Computer Science, University of Helsinki, Helsinki, Finland

Ville Mustonen

553. Institute of Biotechnology, University of Helsinki, Helsinki, Finland

Ville Mustonen

554. Organismal and Evolutionary Biology Research Programme, University of Helsinki, Helsinki, Finland

Ville Mustonen

555. Department of Obstetrics and Gynecology, Division of Gynecologic Oncology, Washington University School of Medicine, St. Louis, MO, USA

David Mutch

556. Penrose St. Francis Health Services, Colorado Springs, CO, USA

Jerome Myers

557. Institute of Pathology, Ulm University and University Hospital of Ulm, Ulm, Germany

Peter Möller

558. National Cancer Center, Tokyo, Japan

Hitoshi Nakagama

559. Genome Institute of Singapore, Singapore, Singapore

Tannistha Nandi & Patrick Tan

560. 32Program in Computational Biology and Bioinformatics, Yale University, New Haven, CT, USA

Fabio C. P. Navarro

561. German Cancer Aid, Bonn, Germany

Gerd Nettekoven & Laura Planko

562. Programme in Cancer and Stem Cell Biology, Centre for Computational Biology, Duke-NUS Medical School, Singapore, Singapore

Alvin Wei Tian Ng

563. The Chinese University of Hong Kong, Shatin, NT, Hong Kong, China

Anthony Ng

564. Fourth Military Medical University, Shaanxi, China

Yongzhan Nie

565. The University of Cambridge School of Clinical Medicine, Cambridge, UK

Serena Nik-Zainal

566. St. Jude Children’s Research Hospital, Memphis, TN, USA

Paul A. Northcott

567. University Health Network, Princess Margaret Cancer Centre, Toronto, ON, Canada

Faiyaz Notta & Ming Tsao

568. Center for Biomolecular Science and Engineering, University of California Santa Cruz, Santa Cruz, CA, USA

Brian D. O’Connor

569. Department of Medicine, University of Chicago, Chicago, IL, USA

Peter O’Donnell

570. Department of Neurology, Mayo Clinic, Rochester, MN, USA

Brian Patrick O’Neill

571. Cambridge Oesophagogastric Centre, Cambridge University Hospitals NHS Foundation Trust, Cambridge, UK

J. Robert O’Neill

572. Department of Computer Science, Carleton College, Northfield, MN, USA

Layla Oesper

573. Institute of Cancer Sciences, College of Medical Veterinary and Life Sciences, University of Glasgow, Glasgow, UK

Karin A. Oien

574. Department of Epidemiology, University of Alabama at Birmingham, Birmingham, AL, USA

Akinyemi I. Ojesina

575. HudsonAlpha Institute for Biotechnology, Huntsville, AL, USA

Akinyemi I. Ojesina

576. O'Neal Comprehensive Cancer Center, University of Alabama at Birmingham, Birmingham, AL, USA

Akinyemi I. Ojesina

577. Department of Pathology, Keio University School of Medicine, Tokyo, Japan

Hidenori Ojima

578. Department of Hepatobiliary and Pancreatic Oncology, National Cancer Center Hospital, Tokyo, Japan

Takuji Okusaka

579. Sage Bionetworks, Seattle, WA, USA

Larsson Omberg

580. Lymphoma Genomic Translational Research Laboratory, National Cancer Centre, Singapore, Singapore

Choon Kiat Ong

581. Department of Clinical Pathology, Robert-Bosch-Hospital, Stuttgart, Germany

German Ott

582. Department of Cell and Systems Biology, University of Toronto, Toronto, ON, Canada

B. F. Francis Ouellette

583. Department of Biosciences and Nutrition, Karolinska Institutet, Stockholm, Sweden

Qiang Pan-Hammarström

584. Center for Liver Cancer, Research Institute and Hospital, National Cancer Center, Gyeonggi, South Korea

Joong-Won Park

585. Division of Hematology-Oncology, Samsung Medical Center, Sungkyunkwan University School of Medicine, Seoul, South Korea

Keunchil Park

586. Samsung Advanced Institute for Health Sciences and Technology, Sungkyunkwan University School of Medicine, Seoul, South Korea

Keunchil Park

587. Cheonan Industry-Academic Collaboration Foundation, Sangmyung University, Cheonan, South Korea

Kiejung Park

588. NYU Langone Medical Center, New York, NY, USA

Harvey Pass

589. Department of Hematology and Medical Oncology, Cleveland Clinic, Cleveland, OH, USA

Nathan A. Pennell

590. Department of Radiation Oncology, University of California San Francisco, San Francisco, CA, USA

Marc D. Perry

591. Department of Health Sciences Research, Mayo Clinic, Rochester, MN, USA

Gloria M. Petersen

592. Helen F. Graham Cancer Center at Christiana Care Health Systems, Newark, DE, USA

Nicholas Petrelli

593. Heidelberg University Hospital, Heidelberg, Germany

Stefan M. Pfister

594. CSRA Incorporated, Fairfax, VA, USA

Todd D. Pihl

595. Research Department of Pathology, University College London Cancer Institute, London, UK

Nischalan Pillay

596. Department of Research Oncology, Guy's Hospital, King's Health Partners AHSC, King's College London School of Medicine, London, UK

Sarah Pinder

597. Faculty of Medicine and Health Sciences, Macquarie University, Sydney, NSW, Australia

Andreia V. Pinho

598. University Hospital of Minjoz, INSERM UMR 1098, Besançon, France

Xavier Pivot

599. Spanish National Cancer Research Centre, Madrid, Spain

Tirso Pons

600. Center of Digestive Diseases and Liver Transplantation, Fundeni Clinical Institute, Bucharest, Romania

Irinel Popescu

601. Cureline, Inc, South San Francisco, CA, USA

Olga Potapova

602. St. Luke's Cancer Centre, Royal Surrey County Hospital NHS Foundation Trust, Guildford, UK

Shaun R. Preston

603. Cambridge Breast Unit, Addenbrooke's Hospital, Cambridge University Hospital NHS Foundation Trust and NIHR Cambridge Biomedical Research Centre, Cambridge, UK

Elena Provenzano

604. East of Scotland Breast Service, Ninewells Hospital, Aberdeen, UK

Colin A. Purdie

605. Department of Genetics, Microbiology and Statistics, University of Barcelona, IRSJD, IBUB, Barcelona, Spain

Raquel Rabionet

606. Department of Obstetrics and Gynecology, Medical College of Wisconsin, Milwaukee, WI, USA

Janet S. Rader

607. Hematology and Medical Oncology, Winship Cancer Institute of Emory University, Atlanta, GA, USA

Suresh Ramalingam

608. Department of Computer Science, Princeton University, Princeton, NJ, USA

Benjamin J. Raphael & Matthew A. Reyna

609. Vanderbilt Ingram Cancer Center, Vanderbilt University, Nashville, TN, USA

W. Kimryn Rathmell

610. Ohio State University College of Medicine and Arthur G. James Comprehensive Cancer Center, Columbus, OH, USA

Matthew Ringel

611. Department of Surgery, Yokohama City University Graduate School of Medicine, Kanagawa, Japan

Yasushi Rino

612. Division of Chromatin Networks, German Cancer Research Center (DKFZ) and BioQuant, Heidelberg, Germany

Karsten Rippe

613. Research Computing Center, University of North Carolina at Chapel Hill, Chapel Hill, NC, USA

Jeffrey Roach

614. School of Molecular Biosciences and Center for Reproductive Biology, Washington State University, Pullman, WA, USA

Steven A. Roberts

615. Finsen Laboratory and Biotech Research and Innovation Centre (BRIC), University of Copenhagen, Copenhagen, Denmark

F. Germán Rodríguez-González, Nikos Sidiropoulos & Joachim Weischenfeldt

616. Department of Laboratory Medicine and Pathobiology, University of Toronto, Toronto, ON, Canada

Michael H. A. Roehrl & Stefano Serra

617. Department of Pathology, Human Oncology and Pathogenesis Program, Memorial Sloan Kettering Cancer Center, New York, NY, USA

Michael H. A. Roehrl

618. University Hospital Giessen, Pediatric Hematology and Oncology, Giessen, Germany

Marius Rohde

619. Oncologie Sénologie, ICM Institut Régional du Cancer, Montpellier, France

Gilles Romieu

620. Institute of Clinical Molecular Biology, Christian-Albrechts-University, Kiel, Germany

Philip C. Rosenstiel & Markus B. Schilhabel

621. Institute of Pathology, University of Wuerzburg, Wuerzburg, Germany

Andreas Rosenwald

622. Department of Urology, North Bristol NHS Trust, Bristol, UK

Edward W. Rowe

623. SingHealth, Duke-NUS Institute of Precision Medicine, National Heart Centre Singapore, Singapore, Singapore

Steven G. Rozen, Patrick Tan & Bin Tean Teh

624. Department of Computer Science, University of Toronto, Toronto, ON, Canada

Yulia Rubanova, Jared T. Simpson & Jeffrey A. Wintersinger

625. Bern Center for Precision Medicine, University Hospital of Bern, University of Bern, Bern, Switzerland

Mark A. Rubin

626. Englander Institute for Precision Medicine, Weill Cornell Medicine and New York Presbyterian Hospital, New York, NY, USA

Mark A. Rubin

627. Meyer Cancer Center, Weill Cornell Medicine, New York, NY, USA

Mark A. Rubin

628. Pathology and Laboratory, Weill Cornell Medical College, New York, NY, USA

Mark A. Rubin

629. Vall d'Hebron Institute of Oncology: VHIO, Barcelona, Spain

Carlota Rubio-Perez

630. General and Hepatobiliary-Biliary Surgery, Pancreas Institute, University and Hospital Trust of Verona, Verona, Italy

Andrea Ruzzenente

631. National Centre for Biological Sciences, Tata Institute of Fundamental Research, Bangalore, India

Radhakrishnan Sabarinathan

632. Indiana University, Bloomington, IN, USA

S. Cenk Sahinalp

633. Department of Pathology, GZA-ZNA Hospitals, Antwerp, Belgium

Roberto Salgado

634. Analytical Biological Services, Inc, Wilmington, DE, USA

Charles Saller

635. Sydney Medical School, University of Sydney, Sydney, NSW, Australia

Jaswinder S. Samra & Richard A. Scolyer

636. cBio Center, Dana-Farber Cancer Institute, Harvard Medical School, Boston, MA, USA

Chris Sander & Ciyue Shen

637. Department of Cell Biology, Harvard Medical School, Boston, MA, USA

Chris Sander & Ciyue Shen

638. Advanced Centre for Treatment Research and Education in Cancer, Tata Memorial Centre, Navi Mumbai, Maharashtra, India

Rajiv Sarin

639. School of Environmental and Life Sciences, Faculty of Science, The University of Newcastle, Ourimbah, NSW, Australia

Christopher J. Scarlett

640. Department of Dermatology, University Hospital of Essen, Essen, Germany

Dirk Schadendorf

641. Bioinformatics and Omics Data Analytics, German Cancer Research Center (DKFZ), Heidelberg, Germany

Matthias Schlesner

642. Department of Urology, Charité Universitätsmedizin Berlin, Berlin, Germany

Thorsten Schlomm & Joachim Weischenfeldt

643. Martini-Clinic, Prostate Cancer Center, University Medical Center Hamburg-Eppendorf, Hamburg, Germany

Thorsten Schlomm

644. Department of General Internal Medicine, University of Kiel, Kiel, Germany

Stefan Schreiber

645. German Cancer Consortium (DKTK), Partner site Berlin, Berlin, Germany

Roland F. Schwarz

646. Cancer Research Institute, Beth Israel Deaconess Medical Center, Boston, MA, USA

Ralph Scully

647. University of Pittsburgh, Pittsburgh, PA, USA

Raja Seethala

648. Department of Ophthalmology and Ocular Genomics Institute, Massachusetts Eye and Ear, Harvard Medical School, Boston, MA, USA

Ayellet V. Segre

649. Center for Psychiatric Genetics, NorthShore University HealthSystem, Evanston, IL, USA

Subhajit Sengupta

650. Van Andel Research Institute, Grand Rapids, MI, USA

Hui Shen & Wanding Zhou

651. Laboratory of Molecular Medicine, Human Genome Center, Institute of Medical Science, University of Tokyo, Tokyo, Japan

Tatsuhiro Shibata, Hirokazu Taniguchi & Tomoko Urushidate

652. Japan Agency for Medical Research and Development, Tokyo, Japan

Kiyo Shimizu & Takashi Yugawa

653. Korea University, Seoul, South Korea

Seung Jun Shin & Stefan G. Stark

654. Murtha Cancer Center, Walter Reed National Military Medical Center, Bethesda, MD, USA

Craig Shriver

655. Human Genetics, University of Kiel, Kiel, Germany

Reiner Siebert

656. Department of Oncologic Pathology, Dana-Farber Cancer Institute, Harvard Medical School, Boston, MA, USA

Sabina Signoretti

657. Oregon Health and Science University, Portland, OR, USA

Jaclyn Smith

658. Center for RNA Interference and Noncoding RNA, The University of Texas MD Anderson Cancer Center, Houston, TX, USA

Anil K. Sood

659. Department of Experimental Therapeutics, The University of Texas MD Anderson Cancer Center, Houston, TX, USA

Anil K. Sood

660. Department of Gynecologic Oncology and Reproductive Medicine, The University of Texas MD Anderson Cancer Center, Houston, TX, USA

Anil K. Sood

661. University Hospitals Coventry and Warwickshire NHS Trust, Coventry, UK

Sharmila Sothi

662. Department of Radiation Oncology, Radboud University Nijmegen Medical Centre, Nijmegen, GA, The Netherlands

Paul N. Span

663. Institute for Genomics and Systems Biology, University of Chicago, Chicago, IL, USA

Jonathan Spring

664. Clinic for Hematology and Oncology, St.-Antonius-Hospital, Eschweiler, Germany

Peter Staib

665. Computational and Systems Biology Program, Memorial Sloan Kettering Cancer Center, New York, NY, USA

Stefan G. Stark

666. University of Iceland, Reykjavik, Iceland

Ólafur Andri Stefánsson

667. Division of Computational Genomics and Systems Genetics, German Cancer Research Center (DKFZ), Heidelberg, Germany

Oliver Stegle

668. Dundee Cancer Centre, Ninewells Hospital, Dundee, UK

Alasdair Stenhouse & Alastair M. Thompson

669. Department for Internal Medicine III, University of Ulm and University Hospital of Ulm, Ulm, Germany

Stephan Stilgenbauer

670. Institut Curie, INSERM Unit 830, Paris, France

Henk G. Stunnenberg & Anne Vincent-Salomon

671. Department of Gastroenterology and Hepatology, Yokohama City University Graduate School of Medicine, Kanagawa, Japan

Akihiro Suzuki

672. Department of Laboratory Medicine, Radboud University Nijmegen Medical Centre, Nijmegen, GA, The Netherlands

Fred Sweep

673. Division of Cancer Genome Research, German Cancer Research Center (DKFZ), Heidelberg, Germany

Holger Sültmann

674. Department of General Surgery, Singapore General Hospital, Singapore, Singapore

Benita Kiat Tee Tan

675. Cancer Science Institute of Singapore, National University of Singapore, Singapore, Singapore

Patrick Tan & Bin Tean Teh

676. Department of Medical and Clinical Genetics, Genome-Scale Biology Research Program, University of Helsinki, Helsinki, Finland

Tomas J. Tanskanen

677. East Anglian Medical Genetics Service, Cambridge University Hospitals NHS Foundation Trust, Cambridge, UK

Patrick Tarpey

678. Irving Institute for Cancer Dynamics, Columbia University, New York, NY, USA

Simon Tavaré

679. Institute of Molecular and Cell Biology, Singapore, Singapore

Bin Tean Teh

680. Laboratory of Cancer Epigenome, Division of Medical Science, National Cancer Centre Singapore, Singapore, Singapore

Bin Tean Teh

681. Universite Lyon, INCa-Synergie, Centre Léon Bérard, Lyon, France

Gilles Thomas

682. Department of Urology, Mayo Clinic, Rochester, MN, USA

R. Houston Thompson

683. Royal National Orthopaedic Hospital - Stanmore, Stanmore, Middlesex, UK

Roberto Tirabosco

684. Department of Biochemistry, Genetics and Immunology, University of Vigo, Vigo, Spain

Marta Tojo

685. Giovanni Paolo II / I.R.C.C.S. Cancer Institute, Bari, BA, Italy

Stefania Tommasi

686. Neuroblastoma Genomics, German Cancer Research Center (DKFZ), Heidelberg, Germany

Umut H. Toprak

687. Fondazione Policlinico Universitario Gemelli IRCCS, Rome, Italy, Rome, Italy

Giampaolo Tortora

688. University of Verona, Verona, Italy

Giampaolo Tortora

689. Centre National de Génotypage, CEA - Institute de Génomique, Evry, France

Jörg Tost

690. CAPHRI Research School, Maastricht University, Maastricht, ER, The Netherlands

David Townend

691. Department of Biopathology, Centre Léon Bérard, Lyon, France

Isabelle Treilleux

692. Université Claude Bernard Lyon 1, Villeurbanne, France

Isabelle Treilleux

693. Core Research for Evolutional Science and Technology (CREST), JST, Tokyo, Japan

Tatsuhiko Tsunoda

694. Department of Biological Sciences, Laboratory for Medical Science Mathematics, Graduate School of Science, University of Tokyo, Yokohama, Japan

Tatsuhiko Tsunoda

695. Department of Medical Science Mathematics, Medical Research Institute, Tokyo Medical and Dental University (TMDU), Tokyo, Japan

Tatsuhiko Tsunoda

696. Cancer Ageing and Somatic Mutation Programme, Wellcome Sanger Institute, Hinxton, UK

Jose M. C. Tubio

697. University Hospitals Birmingham NHS Foundation Trust, Birmingham, UK

Olga Tucker

698. Centre for Cancer Research and Cell Biology, Queen's University, Belfast, UK

Richard Turkington

699. Breast Medical Oncology, The University of Texas MD Anderson Cancer Center, Houston, TX, USA

Naoto T. Ueno

700. Department of Surgery, Johns Hopkins University School of Medicine, Baltimore, MD, USA

Christopher Umbricht

701. Department of Oncology-Pathology, Science for Life Laboratory, Karolinska Institute, Stockholm, Sweden

Husen M. Umer

702. School of Cancer Sciences, Faculty of Medicine, University of Southampton, Southampton, UK

Timothy J. Underwood

703. Department of Gene Technology, Tallinn University of Technology, Tallinn, Estonia

Liis Uusküla-Reimand

704. Genetics and Genome Biology Program, SickKids Research Institute, The Hospital for Sick Children, Toronto, ON, Canada

Liis Uusküla-Reimand

705. Departments of Neurosurgery and Hematology and Medical Oncology, Winship Cancer Institute and School of Medicine, Emory University, Atlanta, GA, USA

Erwin G. Van Meir

706. Department of Clinical and Molecular Medicine, Faculty of Medicine and Health Sciences, Norwegian University of Science and Technology, Trondheim, Norway

Miguel Vazquez

707. Argmix Consulting, North Vancouver, BC, Canada

Shankar Vembu

708. Department of Information Technology, Ghent University, Interuniversitair Micro-Electronica Centrum (IMEC), Ghent, Belgium

Lieven P. C. Verbeke

709. Nuffield Department of Surgical Sciences, John Radcliffe Hospital, University of Oxford, Oxford, UK

Clare Verrill

710. Institute of Mathematics and Computer Science, University of Latvia, Riga, LV, Latvia

Juris Viksna

711. Discipline of Pathology, Sydney Medical School, University of Sydney, Sydney, NSW, Australia

Ricardo E. Vilain

712. Department of Applied Mathematics and Theoretical Physics, Centre for Mathematical Sciences, University of Cambridge, Cambridge, UK

Ignacio Vázquez-García

713. Department of Epidemiology and Biostatistics, Memorial Sloan Kettering Cancer Center, New York, NY, USA

Ignacio Vázquez-García & Venkata D. Yellapantula

714. Department of Statistics, Columbia University, New York, NY, USA

Ignacio Vázquez-García

715. Department of Immunology, Genetics and Pathology, Science for Life Laboratory, Uppsala University, Uppsala, Sweden

Claes Wadelius

716. School of Electronic and Information Engineering, Xi’an Jiaotong University, Xi’an, China

Jiayin Wang & Kai Ye

717. Department of Histopathology, Cambridge University Hospitals NHS Foundation Trust, Cambridge, UK

Anne Y. Warren

718. Oxford NIHR Biomedical Research Centre, University of Oxford, Oxford, UK

David C. Wedge

719. Georgia Regents University Cancer Center, Augusta, GA, USA

Paul Weinberger

720. Wythenshawe Hospital, Manchester, UK

Ian Welch

721. Department of Genetics, Washington University School of Medicine, St.Louis, MO, USA

Michael C. Wendl

722. Department of Biological Oceanography, Leibniz Institute of Baltic Sea Research, Rostock, Germany

Johannes Werner

723. Wellcome Centre for Human Genetics, University of Oxford, Oxford, UK

Justin P. Whalley

724. Department of Molecular and Human Genetics, Baylor College of Medicine, Houston, TX, USA

David A. Wheeler

725. Thoracic Oncology Laboratory, Mayo Clinic, Rochester, MN, USA

Dennis Wigle

726. Institute for Genomic Medicine, Nationwide Children's Hospital, Columbus, OH, USA

Richard K. Wilson

727. Department of Obstetrics and Gynecology, Division of Gynecologic Oncology, Mayo Clinic, Rochester, MN, USA

Boris Winterhoff

728. International Institute for Molecular Oncology, Poznań, Poland

Maciej Wiznerowicz

729. Poznan University of Medical Sciences, Poznań, Poland

Maciej Wiznerowicz

730. Genomics and Proteomics Core Facility High Throughput Sequencing Unit, German Cancer Research Center (DKFZ), Heidelberg, Germany

Stephan Wolf

731. NCCS-VARI Translational Research Laboratory, National Cancer Centre Singapore, Singapore, Singapore

Bernice H. Wong

732. Edison Family Center for Genome Sciences and Systems Biology, Washington University, St. Louis, MO, USA

Winghing Wong

733. MRC-University of Glasgow Centre for Virus Research, Glasgow, UK

Derek W. Wright

734. Department of Medical Informatics and Clinical Epidemiology, Division of Bioinformatics and Computational Biology, OHSU Knight Cancer Institute, Oregon Health and Science University, Portland, OR, USA

Guanming Wu

735. School of Electronic Information and Communications, Huazhong University of Science and Technology, Wuhan, China

Tian Xia

736. Department of Applied Mathematics and Statistics, Johns Hopkins University, Baltimore, MD, USA

Yanxun Xu

737. Department of Cancer Genome Informatics, Graduate School of Medicine, Osaka University, Osaka, Japan

Shinichi Yachida

738. Institute of Computer Science, Heidelberg University, Heidelberg, Germany

Sergei Yakneen

739. School of Mathematics and Statistics, University of Sydney, Sydney, NSW, Australia

Jean Y. Yang

740. Ben May Department for Cancer Research, University of Chicago, Chicago, IL, USA

Lixing Yang

741. Department of Human Genetics, University of Chicago, Chicago, IL, USA

Lixing Yang

742. Tri-Institutional PhD Program in Computational Biology and Medicine, Weill Cornell Medicine, New York, NY, USA

Xiaotong Yao

743. The First Affiliated Hospital, Xi’an Jiaotong University, Xi’an, China

Kai Ye

744. Department of Medicine and Therapeutics, The Chinese University of Hong Kong, Shatin, NT, Hong Kong, China

Jun Yu

745. Department of Biostatistics, The University of Texas MD Anderson Cancer Center, Houston, TX, USA

Kaixian Yu & Hongtu Zhu

746. Duke-NUS Medical School, Singapore, Singapore

Willie Yu

747. Department of Surgery, Ruijin Hospital, Shanghai Jiaotong University School of Medicine, Shanghai, China

Yingyan Yu

748. School of Computing Science, University of Glasgow, Glasgow, UK

Ke Yuan

749. Division of Orthopaedic Surgery, Oslo University Hospital, Oslo, Norway

Olga Zaikova

750. Eastern Clinical School, Monash University, Melbourne, VIC, Australia

Nikolajs Zeps

751. Epworth HealthCare, Richmond, VIC, Australia

Nikolajs Zeps

752. Department of Biostatistics and Computational Biology, Dana-Farber Cancer Institute and Harvard Medical School, Boston, MA, USA

Cheng-Zhong Zhang

753. Department of Biomedical Informatics, College of Medicine, The Ohio State University, Columbus, OH, USA

Yan Zhang

754. The Ohio State University Comprehensive Cancer Center (OSUCCC – James), Columbus, OH, USA

Yan Zhang

755. The University of Texas School of Biomedical Informatics (SBMI) at Houston, Houston, TX, USA

Zhongming Zhao

756. Department of Biostatistics, University of North Carolina at Chapel Hill, Chapel Hill, NC, USA

Hongtu Zhu

757. Department of Biochemistry and Molecular Genetics, Feinberg School of Medicine, Northwestern University, Chicago, IL, USA

Lihua Zou

758. Faculty of Medicine and Health, University of Sydney, Sydney, NSW, Australia

Anna deFazio

759. Department of Pathology, Erasmus Medical Center Rotterdam, Rotterdam, GD, The Netherlands

Carolien H. M. van Deurzen

760. Division of Molecular Carcinogenesis, The Netherlands Cancer Institute, Amsterdam, CX, The Netherlands

L. van't Veer

761. Institute of Molecular Life Sciences and Swiss Institute of Bioinformatics, University of Zurich, Zurich, Switzerland

Christian von Mering

Consortia

PCAWG Evolution & Heterogeneity Working Group

- Stefan C. Dentro
- , Ignaty Leshchiner
- , Moritz Gerstung
- , Clemency Jolly
- , Kerstin Haase
- , Maxime Tarabichi
- , Jeff Wintersinger
- , Amit G. Deshwar
- , Kaixian Yu
- , Santiago Gonzalez
- , Yulia Rubanova
- , Geoff Macintyre
- , David J. Adams
- , Pavana Anur
- , Rameen Beroukhim
- , Paul C. Boutros
- , David D. Bowtell
- , Peter J. Campbell
- , Shaolong Cao
- , Elizabeth L. Christie
- , Marek Cmero
- , Yupeng Cun
- , Kevin J. Dawson
- , Jonas Demeulemeester
- , Nilgun Donmez
- , Ruben M. Drews
- , Roland Eils
- , Yu Fan

- , Matthew Fittall
- , Dale W. Garsed
- , Gad Getz
- , Gavin Ha
- , Marcin Imielinski
- , Lara Jerman
- , Yuan Ji
- , Kortine Kleinheinz
- , Juhee Lee
- , Henry Lee-Six
- , Dimitri G. Livitz
- , Salem Malikic
- , Florian Markowetz
- , Inigo Martincorena
- , Thomas J. Mitchell
- , Ville Mustonen
- , Layla Oesper
- , Martin Peifer
- , Myron Peto
- , Benjamin J. Raphael
- , Daniel Rosebrock
- , S. Cenk Sahinalp
- , Adriana Salcedo
- , Matthias Schlesner
- , Steven Schumacher
- , Subhajit Sengupta
- , Ruian Shi
- , Seung Jun Shin
- , Oliver Spiro
- , Lincoln D. Stein
- , Ignacio Vázquez-García
- , Shankar Vembu
- , David A. Wheeler
- , Tsun-Po Yang
- , Xiaotong Yao
- , Ke Yuan
- , Hongtu Zhu

- , Wenyi Wang
- , Quaid D. Morris
- , Paul T. Spellman
- , David C. Wedge
- & Peter Van Loo

PCAWG Consortium

- Lauri A. Aaltonen
- , Federico Abascal
- , Adam Abeshouse
- , Hiroyuki Aburatani
- , David J. Adams
- , Nishant Agrawal
- , Keun Soo Ahn
- , Sung-Min Ahn
- , Hiroshi Aikata
- , Rehan Akbani
- , Kadir C. Akdemir
- , Hikmat Al-Ahmadie
- , Sultan T. Al-Sedairy
- , Fatima Al-Shahrour
- , Malik Alawi
- , Monique Albert
- , Kenneth Aldape
- , Ludmil B. Alexandrov
- , Adrian Ally
- , Kathryn Alsop
- , Eva G. Alvarez
- , Fernanda Amary
- , Samirkumar B. Amin
- , Brice Aminou
- , Ole Ammerpohl
- , Matthew J. Anderson
- , Yeng Ang
- , Davide Antonello
- , Pavana Anur

- , Samuel Aparicio
- , Elizabeth L. Appelbaum
- , Yasuhito Arai
- , Axel Aretz
- , Koji Arihiro
- , Shun-ichi Ariizumi
- , Joshua Armenia
- , Laurent Arnould
- , Sylvia Asa
- , Yassen Assenov
- , Gurnit Atwal
- , Sietse Aukema
- , J. Todd Auman
- , Miriam R. R. Aure
- , Philip Awadalla
- , Marta Aymerich
- , Gary D. Bader
- , Adrian Baez-Ortega
- , Matthew H. Bailey
- , Peter J. Bailey
- , Miruna Balasundaram
- , Saianand Balu
- , Pratiti Bandopadhayay
- , Rosamonde E. Banks
- , Stefano Barbi
- , Andrew P. Barbour
- , Jonathan Barenboim
- , Jill Barnholtz-Sloan
- , Hugh Barr
- , Elisabet Barrera
- , John Bartlett
- , Javier Bartolome
- , Claudio Bassi
- , Oliver F. Bathe
- , Daniel Baumhoer
- , Prashant Bavi
- , Stephen B. Baylin

- , Wojciech Bazant
- , Duncan Beardsmore
- , Timothy A. Beck
- , Sam Behjati
- , Andreas Behren
- , Beifang Niu
- , Cindy Bell
- , Sergi Beltran
- , Christopher Benz
- , Andrew Berchuck
- , Anke K. Bergmann
- , Erik N. Bergstrom
- , Benjamin P. Berman
- , Daniel M. Berney
- , Stephan H. Bernhart
- , Rameen Beroukhim
- , Mario Berrios
- , Samantha Bersani
- , Johanna Bertl
- , Miguel Betancourt
- , Vinayak Bhandari
- , Shriram G. Bhosle
- , Andrew V. Biankin
- , Matthias Bieg
- , Darell Bigner
- , Hans Binder
- , Ewan Birney
- , Michael Birrer
- , Nidhan K. Biswas
- , Bodil Bjerkehagen
- , Tom Bodenheimer
- , Lori Boice
- , Giada Bonizzato
- , Johann S. De Bono
- , Arnoud Boot
- , Moiz S. Bootwalla
- , Ake Borg

- , Arndt Borkhardt
- , Keith A. Boroevich
- , Ivan Borozan
- , Christoph Borst
- , Marcus Bosenberg
- , Mattia Bosio
- , Jacqueline Boultwood
- , Guillaume Bourque
- , Paul C. Boutros
- , G. Steven Bova
- , David T. Bowen
- , Reanne Bowlby
- , David D. L. Bowtell
- , Sandrine Boyault
- , Rich Boyce
- , Jeffrey Boyd
- , Alvis Brazma
- , Paul Brennan
- , Daniel S. Brewer
- , Arie B. Brinkman
- , Robert G. Bristow
- , Russell R. Broaddus
- , Jane E. Brock
- , Malcolm Brock
- , Annegien Broeks
- , Angela N. Brooks
- , Denise Brooks
- , Benedikt Brors
- , Søren Brunak
- , Timothy J. C. Bruxner
- , Alicia L. Bruzos
- , Alex Buchanan
- , Ivo Buchhalter
- , Christiane Buchholz
- , Susan Bullman
- , Hazel Burke
- , Birgit Burkhardt

- , Kathleen H. Burns
- , John Busanovich
- , Carlos D. Bustamante
- , Adam P. Butler
- , Atul J. Butte
- , Niall J. Byrne
- , Anne-Lise Børresen-Dale
- , Samantha J. Caesar-Johnson
- , Andy Cafferkey
- , Declan Cahill
- , Claudia Calabrese
- , Carlos Caldas
- , Fabien Calvo
- , Niedzica Camacho
- , Peter J. Campbell
- , Elias Campo
- , Cinzia Cantù
- , Shaolong Cao
- , Thomas E. Carey
- , Joana Carlevaro-Fita
- , Rebecca Carlsen
- , Ivana Cataldo
- , Mario Cazzola
- , Jonathan Cebon
- , Robert Cerfolio
- , Dianne E. Chadwick
- , Dimple Chakravarty
- , Don Chalmers
- , Calvin Wing Yiu Chan
- , Kin Chan
- , Michelle Chan-Seng-Yue
- , Vishal S. Chandan
- , David K. Chang
- , Stephen J. Chanock
- , Lorraine A. Chantrill
- , Aurélien Chateigner
- , Nilanjan Chatterjee

- , Kazuaki Chayama
- , Hsiao-Wei Chen
- , Jieming Chen
- , Ken Chen
- , Yiwen Chen
- , Zhaohong Chen
- , Andrew D. Cherniack
- , Jeremy Chien
- , Yoke-Eng Chiew
- , Suet-Feung Chin
- , Juok Cho
- , Sunghoon Cho
- , Jung Kyoon Choi
- , Wan Choi
- , Christine Chomienne
- , Zechen Chong
- , Su Pin Choo
- , Angela Chou
- , Angelika N. Christ
- , Elizabeth L. Christie
- , Eric Chuah
- , Carrie Cibulskis
- , Kristian Cibulskis
- , Sara Cingarlini
- , Peter Clapham
- , Alexander Claviez
- , Sean Cleary
- , Nicole Cloonan
- , Marek Cmero
- , Colin C. Collins
- , Ashton A. Connor
- , Susanna L. Cooke
- , Colin S. Cooper
- , Leslie Cope
- , Vincenzo Corbo
- , Matthew G. Cordes
- , Stephen M. Cordner

- , Isidro Cortés-Ciriano
- , Kyle Covington
- , Prue A. Cowin
- , Brian Craft
- , David Craft
- , Chad J. Creighton
- , Yupeng Cun
- , Erin Curley
- , Ioana Cutcutache
- , Karolina Czajka
- , Bogdan Czerniak
- , Rebecca A. Dagg
- , Ludmila Danilova
- , Maria Vittoria Davi
- , Natalie R. Davidson
- , Helen Davies
- , Ian J. Davis
- , Brandi N. Davis-Dusenbery
- , Kevin J. Dawson
- , Francisco M. De La Vega
- , Ricardo De Paoli-Iseppi
- , Timothy Defreitas
- , Angelo P. Dei Tos
- , Olivier Delaneau
- , John A. Demchok
- , Jonas Demeulemeester
- , German M. Demidov
- , Deniz Demircioğlu
- , Nening M. Dennis
- , Robert E. Denroche
- , Stefan C. Dentro
- , Nikita Desai
- , Vikram Deshpande
- , Amit G. Deshwar
- , Christine Desmedt
- , Jordi Deu-Pons
- , Noreen Dhalla

- , Neesha C. Dhani
- , Priyanka Dhingra
- , Rajiv Dhir
- , Anthony DiBiase
- , Klev Diamanti
- , Li Ding
- , Shuai Ding
- , Huy Q. Dinh
- , Luc Dirix
- , HarshaVardhan Doddapaneni
- , Nilgun Donmez
- , Michelle T. Dow
- , Ronny Drapkin
- , Oliver Drechsel
- , Ruben M. Drews
- , Serge Serge
- , Tim Dudderidge
- , Ana Dueso-Barroso
- , Andrew J. Dunford
- , Michael Dunn
- , Lewis Jonathan Dursi
- , Fraser R. Duthie
- , Ken Dutton-Regester
- , Jenna Eagles
- , Douglas F. Easton
- , Stuart Edmonds
- , Paul A. Edwards
- , Sandra E. Edwards
- , Rosalind A. Eeles
- , Anna Ehinger
- , Juergen Eils
- , Roland Eils
- , Adel El-Naggar
- , Matthew Eldridge
- , Kyle Ellrott
- , Serap Erkek
- , Georgia Escaramis

- , Shadrielle M. G. Espiritu
- , Xavier Estivill
- , Dariush Etemadmoghadam
- , Jorunn E. Eyfjord
- , Bishoy M. Faltas
- , Daiming Fan
- , Yu Fan
- , William C. Faquin
- , Claudiu Farcas
- , Matteo Fassan
- , Aquila Fatima
- , Francesco Favero
- , Nodirjon Fayzullaev
- , Ina Felau
- , Sian Fereday
- , Martin L. Ferguson
- , Vincent Ferretti
- , Lars Feuerbach
- , Matthew A. Field
- , J. Lynn Fink
- , Gaetano Finocchiaro
- , Cyril Fisher
- , Matthew W. Fittall
- , Anna Fitzgerald
- , Rebecca C. Fitzgerald
- , Adrienne M. Flanagan
- , Neil E. Fleshner
- , Paul Flicek
- , John A. Foekens
- , Kwun M. Fong
- , Nuno A. Fonseca
- , Christopher S. Foster
- , Natalie S. Fox
- , Michael Fraser
- , Scott Frazer
- , Milana Frenkel-Morgenstern
- , William Friedman

- , Joan Frigola
- , Catrina C. Fronick
- , Akihiro Fujimoto
- , Masashi Fujita
- , Masashi Fukayama
- , Lucinda A. Fulton
- , Robert S. Fulton
- , Mayuko Furuta
- , P. Andrew Futreal
- , Anja Füllgrabe
- , Stacey B. Gabriel
- , Steven Gallinger
- , Carlo Gambacorti-Passerini
- , Jianjiong Gao
- , Shengjie Gao
- , Levi Garraway
- , Øystein Garred
- , Erik Garrison
- , Dale W. Garsed
- , Nils Gehlenborg
- , Josep L. L. Gelpi
- , Joshy George
- , Daniela S. Gerhard
- , Clarissa Gerhauser
- , Jeffrey E. Gershenwald
- , Mark Gerstein
- , Moritz Gerstung
- , Gad Getz
- , Mohammed Ghori
- , Ronald Ghossein
- , Nasra H. Giama
- , Richard A. Gibbs
- , Bob Gibson
- , Anthony J. Gill
- , Pelvender Gill
- , Dilip D. Giri
- , Dominik Glodzik

- , Vincent J. Gnanapragasam
- , Maria Elisabeth Goebler
- , Mary J. Goldman
- , Carmen Gomez
- , Santiago Gonzalez
- , Abel Gonzalez-Perez
- , Dmitry A. Gordenin
- , James Gossage
- , Kunihito Gotoh
- , Ramaswamy Govindan
- , Dorthe Grabau
- , Janet S. Graham
- , Robert C. Grant
- , Anthony R. Green
- , Eric Green
- , Liliana Greger
- , Nicola Grehan
- , Sonia Grimaldi
- , Sean M. Grimmond
- , Robert L. Grossman
- , Adam Grundhoff
- , Gunes Gundem
- , Qianyun Guo
- , Manaswi Gupta
- , Shailja Gupta
- , Ivo G. Gut
- , Marta Gut
- , Jonathan Göke
- , Gavin Ha
- , Andrea Haake
- , David Haan
- , Siegfried Haas
- , Kerstin Haase
- , James E. Haber
- , Nina Habermann
- , Faraz Hach
- , Syed Haider

- , Natsuko Hama
- , Freddie C. Hamdy
- , Anne Hamilton
- , Mark P. Hamilton
- , Leng Han
- , George B. Hanna
- , Martin Hansmann
- , Nicholas J. Haradhvala
- , Olivier Harismendy
- , Ivon Harliwong
- , Arif O. Harmanci
- , Eoghan Harrington
- , Takanori Hasegawa
- , David Haussler
- , Steve Hawkins
- , Shinya Hayami
- , Shuto Hayashi
- , D. Neil Hayes
- , Stephen J. Hayes
- , Nicholas K. Hayward
- , Steven Hazell
- , Yao He
- , Allison P. Heath
- , Simon C. Heath
- , David Hedley
- , Apurva M. Hegde
- , David I. Heiman
- , Michael C. Heinold
- , Zachary Heins
- , Lawrence E. Heisler
- , Eva Hellstrom-Lindberg
- , Mohamed Helmy
- , Seong Gu Heo
- , Austin J. Hepperla
- , José María Heredia-Genestar
- , Carl Herrmann
- , Peter Hersey

- , Julian M. Hess
- , Holmfridur Hilmarsdottir
- , Jonathan Hinton
- , Satoshi Hirano
- , Nobuyoshi Hiraoka
- , Katherine A. Hoadley
- , Asger Hobolth
- , Ermin Hodzic
- , Jessica I. Hoell
- , Steve Hoffmann
- , Oliver Hofmann
- , Andrea Holbrook
- , Aliaksei Z. Holik
- , Michael A. Hollingsworth
- , Oliver Holmes
- , Robert A. Holt
- , Chen Hong
- , Eun Pyo Hong
- , Jongwhi H. Hong
- , Gerrit K. Hooijer
- , Henrik Hornshøj
- , Fumie Hosoda
- , Yong Hou
- , Volker Hovestadt
- , William Howat
- , Alan P. Hoyle
- , Ralph H. Hruban
- , Jianhong Hu
- , Taobo Hu
- , Xing Hua
- , Kuan-lin Huang
- , Mei Huang
- , Mi Ni Huang
- , Vincent Huang
- , Yi Huang
- , Wolfgang Huber
- , Thomas J. Hudson

- , Michael Hummel
- , Jillian A. Hung
- , David Huntsman
- , Ted R. Hupp
- , Jason Huse
- , Matthew R. Huska
- , Barbara Hutter
- , Carolyn M. Hutter
- , Daniel Hübschmann
- , Christine A. Iacobuzio-Donahue
- , Charles David Imbusch
- , Marcin Imielinski
- , Seiya Imoto
- , William B. Isaacs
- , Keren Isaev
- , Shumpei Ishikawa
- , Murat Iskar
- , S. M. Ashiqul Islam
- , Michael Ittmann
- , Sinisa Ivkovic
- , Jose M. G. Izarzugaza
- , Jocelyne Jacquemier
- , Valerie Jakrot
- , Nigel B. Jamieson
- , Gun Ho Jang
- , Se Jin Jang
- , Joy C. Jayaseelan
- , Reyka Jayasinghe
- , Stuart R. Jefferys
- , Karine Jegalian
- , Jennifer L. Jennings
- , Seung-Hyup Jeon
- , Lara Jerman
- , Yuan Ji
- , Wei Jiao
- , Peter A. Johansson
- , Amber L. Johns

- , Jeremy Johns
- , Rory Johnson
- , Todd A. Johnson
- , Clemency Jolly
- , Yann Joly
- , Jon G. Jonasson
- , Corbin D. Jones
- , David R. Jones
- , David T. W. Jones
- , Nic Jones
- , Steven J. M. Jones
- , Jos Jonkers
- , Young Seok Ju
- , Hartmut Juhl
- , Jongsun Jung
- , Malene Juul
- , Randi Istrup Juul
- , Sissel Juul
- , Natalie Jäger
- , Rolf Kabbe
- , Andre Kahles
- , Abdullah Kahraman
- , Vera B. Kaiser
- , Hojabr Kakavand
- , Sangeetha Kalimuthu
- , Christof von Kalle
- , Koo Jeong Kang
- , Katalin Karaszi
- , Beth Karlan
- , Rosa Karlić
- , Dennis Karsch
- , Katayoon Kasaian
- , Karin S. Kassahn
- , Hitoshi Katai
- , Mamoru Kato
- , Hiroto Katoh
- , Yoshiiku Kawakami

- , Jonathan D. Kay
- , Stephen H. Kazakoff
- , Marat D. Kazanov
- , Maria Keays
- , Electron Kebebew
- , Richard F. Kefford
- , Manolis Kellis
- , James G. Kench
- , Catherine J. Kennedy
- , Jules N. A. Kerssemakers
- , David Khoo
- , Vincent Khoo
- , Narong Khuntikeo
- , Ekta Khurana
- , Helena Kilpinen
- , Hark Kyun Kim
- , Hyung-Lae Kim
- , Hyung-Yong Kim
- , Hyunghwan Kim
- , Jaegil Kim
- , Jihoon Kim
- , Jong K. Kim
- , Youngwook Kim
- , Tari A. King
- , Wolfram Klapper
- , Kortine Kleinheinz
- , Leszek J. Klimczak
- , Stian Knappskog
- , Michael Kneba
- , Bartha M. Knoppers
- , Youngil Koh
- , Jan Komorowski
- , Daisuke Komura
- , Mitsuhiro Komura
- , Gu Kong
- , Marcel Kool
- , Jan O. Korbel

- , Viktoriya Korchina
- , Andrey Korshunov
- , Michael Koscher
- , Roelof Koster
- , Zsofia Kote-Jarai
- , Antonios Koures
- , Milena Kovacevic
- , Barbara Kremeyer
- , Helene Kretzmer
- , Markus Kreuz
- , Savitri Krishnamurthy
- , Dieter Kube
- , Kiran Kumar
- , Pardeep Kumar
- , Sushant Kumar
- , Yogesh Kumar
- , Ritika Kundra
- , Kirsten Kübler
- , Ralf Küppers
- , Jesper Lagergren
- , Phillip H. Lai
- , Peter W. Laird
- , Sunil R. Lakhani
- , Christopher M. Lalansingh
- , Emilie Lalonde
- , Fabien C. Lamaze
- , Adam Lambert
- , Eric Lander
- , Pablo Landgraf
- , Luca Landoni
- , Anita Langerød
- , Andrés Lanzós
- , Denis Larsimont
- , Erik Larsson
- , Mark Lathrop
- , Loretta M. S. Lau
- , Chris Lawerenz

- , Rita T. Lawlor
- , Michael S. Lawrence
- , Alexander J. Lazar
- , Ana Mijalkovic Lazic
- , Xuan Le
- , Darlene Lee
- , Donghoon Lee
- , Eunjung Alice Lee
- , Hee Jin Lee
- , Jake June-Koo Lee
- , Jeong-Yeon Lee
- , Juhee Lee
- , Ming Ta Michael Lee
- , Henry Lee-Six
- , Kjong-Van Lehmann
- , Hans Lehrach
- , Dido Lenze
- , Conrad R. Leonard
- , Daniel A. Leongamornlert
- , Ignaty Leshchiner
- , Louis Letourneau
- , Ivica Letunic
- , Douglas A. Levine
- , Lora Lewis
- , Tim Ley
- , Chang Li
- , Constance H. Li
- , Haiyan Irene Li
- , Jun Li
- , Lin Li
- , Shantao Li
- , Siliang Li
- , Xiaobo Li
- , Xiaotong Li
- , Xinyue Li
- , Yilong Li
- , Han Liang

- , Sheng-Ben Liang
- , Peter Lichter
- , Pei Lin
- , Ziao Lin
- , W. M. Linehan
- , Ole Christian Lingjærde
- , Dongbing Liu
- , Eric Minwei Liu
- , Fei-Fei Fei Liu
- , Fenglin Liu
- , Jia Liu
- , Xingmin Liu
- , Julie Livingstone
- , Dimitri Livitz
- , Naomi Livni
- , Lucas Lochovsky
- , Markus Loeffler
- , Georgina V. Long
- , Armando Lopez-Guillermo
- , Shaoke Lou
- , David N. Louis
- , Laurence B. Lovat
- , Yiling Lu
- , Yong-Jie Lu
- , Youyong Lu
- , Claudio Luchini
- , Ilinca Lungu
- , Xuemei Luo
- , Hayley J. Luxton
- , Andy G. Lynch
- , Lisa Lype
- , Cristina López
- , Carlos López-Otín
- , Eric Z. Ma
- , Yussanne Ma
- , Gaetan MacGrogan
- , Shona MacRae

- , Geoff Macintyre
- , Tobias Madsen
- , Kazuhiro Maejima
- , Andrea Mafficini
- , Dennis T. Maglinte
- , Arindam Maitra
- , Partha P. Majumder
- , Luca Malcovati
- , Salem Malikic
- , Giuseppe Malleo
- , Graham J. Mann
- , Luisa Mantovani-Löffler
- , Kathleen Marchal
- , Giovanni Marchegiani
- , Elaine R. Mardis
- , Adam A. Margolin
- , Maximillian G. Marin
- , Florian Markowetz
- , Julia Markowski
- , Jeffrey Marks
- , Tomas Marques-Bonet
- , Marco A. Marra
- , Luke Marsden
- , John W. M. Martens
- , Sancha Martin
- , Jose I. Martin-Subero
- , Iñigo Martincorena
- , Alexander Martinez-Fundichely
- , Yosef E. Maruvka
- , R. Jay Mashl
- , Charlie E. Massie
- , Thomas J. Matthew
- , Lucy Matthews
- , Erik Mayer
- , Simon Mayes
- , Michael Mayo
- , Faridah Mbabaali

- , Karen McCune
- , Ultan McDermott
- , Patrick D. McGillivray
- , Michael D. McLellan
- , John D. McPherson
- , John R. McPherson
- , Treasa A. McPherson
- , Samuel R. Meier
- , Alice Meng
- , Shaowu Meng
- , Andrew Menzies
- , Neil D. Merrett
- , Sue Merson
- , Matthew Meyerson
- , William Meyerson
- , Piotr A. Mieczkowski
- , George L. Mihaiescu
- , Sanja Mijalkovic
- , Tom Mikkelsen
- , Michele Milella
- , Linda Mileshkin
- , Christopher A. Miller
- , David K. Miller
- , Jessica K. Miller
- , Gordon B. Mills
- , Ana Milovanovic
- , Sarah Minner
- , Marco Miotto
- , Gisela Mir Arnau
- , Lisa Mirabello
- , Chris Mitchell
- , Thomas J. Mitchell
- , Satoru Miyano
- , Naoki Miyoshi
- , Shinichi Mizuno
- , Fruzsina Molnár-Gábor
- , Malcolm J. Moore

- , Richard A. Moore
- , Sandro Morganella
- , Quaid D. Morris
- , Carl Morrison
- , Lisle E. Mose
- , Catherine D. Moser
- , Ferran Muiños
- , Loris Mularoni
- , Andrew J. Mungall
- , Karen Mungall
- , Elizabeth A. Musgrove
- , Ville Mustonen
- , David Mutch
- , Francesc Muyas
- , Donna M. Muzny
- , Alfonso Muñoz
- , Jerome Myers
- , Ola Myklebost
- , Peter Möller
- , Genta Nagae
- , Adnan M. Nagrial
- , Hardeep K. Nahal-Bose
- , Hitoshi Nakagama
- , Hidewaki Nakagawa
- , Hiromi Nakamura
- , Toru Nakamura
- , Kaoru Nakano
- , Tannistha Nandi
- , Jyoti Nangalia
- , Mia Nastic
- , Arcadi Navarro
- , Fabio C. P. Navarro
- , David E. Neal
- , Gerd Nettekoven
- , Felicity Newell
- , Steven J. Newhouse
- , Yulia Newton

- , Alvin Wei Tian Ng
- , Anthony Ng
- , Jonathan Nicholson
- , David Nicol
- , Yongzhan Nie
- , G. Petur Nielsen
- , Morten Muhlig Nielsen
- , Serena Nik-Zainal
- , Michael S. Noble
- , Katia Nones
- , Paul A. Northcott
- , Faiyaz Notta
- , Brian D. O'Connor
- , Peter O'Donnell
- , Maria O'Donovan
- , Sarah O'Meara
- , Brian Patrick O'Neill
- , J. Robert O'Neill
- , David Ocana
- , Angelica Ochoa
- , Layla Oesper
- , Christopher Ogden
- , Hideki Ohdan
- , Kazuhiro Ohi
- , Lucila Ohno-Machado
- , Karin A. Oien
- , Akinyemi I. Ojesina
- , Hidenori Ojima
- , Takuji Okusaka
- , Larsson Omberg
- , Choon Kiat Ong
- , Stephan Ossowski
- , German Ott
- , B. F. Francis Ouellette
- , Christine P'ng
- , Marta Paczkowska
- , Salvatore Paiella

- , Chawalit Pairojkul
- , Marina Pajic
- , Qiang Pan-Hammarström
- , Elli Papaemmanuil
- , Irene Papatheodorou
- , Nagarajan Paramasivam
- , Ji Wan Park
- , Joong-Won Park
- , Keunchil Park
- , Kiejung Park
- , Peter J. Park
- , Joel S. Parker
- , Simon L. Parsons
- , Harvey Pass
- , Danielle Pasternack
- , Alessandro Pastore
- , Ann-Marie Patch
- , Iris Pauporté
- , Antonio Pea
- , John V. Pearson
- , Chandra Sekhar Pedamallu
- , Jakob Skou Pedersen
- , Paolo Pederzoli
- , Martin Peifer
- , Nathan A. Pennell
- , Charles M. Perou
- , Marc D. Perry
- , Gloria M. Petersen
- , Myron Peto
- , Nicholas Petrelli
- , Robert Petryszak
- , Stefan M. Pfister
- , Mark Phillips
- , Oriol Pich
- , Hilda A. Pickett
- , Todd D. Pihl
- , Nischalan Pillay

- , Sarah Pinder
- , Mark Pinese
- , Andreia V. Pinho
- , Esa Pitkänen
- , Xavier Pivot
- , Elena Piñeiro-Yáñez
- , Laura Planko
- , Christoph Plass
- , Paz Polak
- , Tirso Pons
- , Irinel Popescu
- , Olga Potapova
- , Aparna Prasad
- , Shaun R. Preston
- , Manuel Prinz
- , Antonia L. Pritchard
- , Stephenie D. Prokopec
- , Elena Provenzano
- , Xose S. Puente
- , Sonia Puig
- , Montserrat Puiggròs
- , Sergio Pulido-Tamayo
- , Gulietta M. Pupo
- , Colin A. Purdie
- , Michael C. Quinn
- , Raquel Rabionet
- , Janet S. Rader
- , Bernhard Radlwimmer
- , Petar Radovic
- , Benjamin Raeder
- , Keiran M. Raine
- , Manasa Ramakrishna
- , Kamna Ramakrishnan
- , Suresh Ramalingam
- , Benjamin J. Raphael
- , W. Kimryn Rathmell
- , Tobias Rausch

- , Guido Reifenberger
- , Jüri Reimand
- , Jorge Reis-Filho
- , Victor Reuter
- , Iker Reyes-Salazar
- , Matthew A. Reyna
- , Sheila M. Reynolds
- , Esther Rheinbay
- , Yasser Riazalhosseini
- , Andrea L. Richardson
- , Julia Richter
- , Matthew Ringel
- , Markus Ringnér
- , Yasushi Rino
- , Karsten Rippe
- , Jeffrey Roach
- , Lewis R. Roberts
- , Nicola D. Roberts
- , Steven A. Roberts
- , A. Gordon Robertson
- , Alan J. Robertson
- , Javier Bartolomé Rodriguez
- , Bernardo Rodriguez-Martin
- , F. Germán Rodríguez-González
- , Michael H. A. Roehrl
- , Marius Rohde
- , Hirofumi Rokutan
- , Gilles Romieu
- , Ilse Rooman
- , Tom Roques
- , Daniel Rosebrock
- , Mara Rosenberg
- , Philip C. Rosenstiel
- , Andreas Rosenwald
- , Edward W. Rowe
- , Romina Royo
- , Steven G. Rozen

- , Yulia Rubanova
- , Mark A. Rubin
- , Carlota Rubio-Perez
- , Vasilisa A. Rudneva
- , Borislav C. Rusev
- , Andrea Ruzzenente
- , Gunnar Rätsch
- , Radhakrishnan Sabarinathan
- , Veronica Y. Sabelnykova
- , Sara Sadeghi
- , S. Cenk Sahinalp
- , Natalie Saini
- , Mihoko Saito-Adachi
- , Gordon Saksena
- , Adriana Salcedo
- , Roberto Salgado
- , Leonidas Salichos
- , Richard Sallari
- , Charles Saller
- , Roberto Salvia
- , Michelle Sam
- , Jaswinder S. Samra
- , Francisco Sanchez-Vega
- , Chris Sander
- , Grant Sanders
- , Rajiv Sarin
- , Iman Sarrafi
- , Aya Sasaki-Oku
- , Torill Sauer
- , Guido Sauter
- , Robyn P. M. Saw
- , Maria Scardoni
- , Christopher J. Scarlett
- , Aldo Scarpa
- , Ghislaine Scelo
- , Dirk Schadendorf
- , Jacqueline E. Schein

- , Markus B. Schilhabel
- , Matthias Schlesner
- , Thorsten Schlomm
- , Heather K. Schmidt
- , Sarah-Jane Schramm
- , Stefan Schreiber
- , Nikolaus Schultz
- , Steven E. Schumacher
- , Roland F. Schwarz
- , Richard A. Scolyer
- , David Scott
- , Ralph Scully
- , Raja Seethala
- , Ayellet V. Segre
- , Iris Selander
- , Colin A. Semple
- , Yasin Senbabaoglu
- , Subhajit Sengupta
- , Elisabetta Sereni
- , Stefano Serra
- , Dennis C. Sgroi
- , Mark Shackleton
- , Nimish C. Shah
- , Sagedeh Shahabi
- , Catherine A. Shang
- , Ping Shang
- , Ofer Shapira
- , Troy Shelton
- , Ciyue Shen
- , Hui Shen
- , Rebecca Shepherd
- , Ruian Shi
- , Yan Shi
- , Yu-Jia Shiah
- , Tatsuhiro Shibata
- , Juliann Shih
- , Eigo Shimizu

- , Kiyo Shimizu
- , Seung Jun Shin
- , Yuichi Shiraishi
- , Tal Shmaya
- , Ilya Shmulevich
- , Solomon I. Shorser
- , Charles Short
- , Raunak Shrestha
- , Suyash S. Shringarpure
- , Craig Shriver
- , Shimin Shuai
- , Nikos Sidiropoulos
- , Reiner Siebert
- , Anieta M. Sieuwerts
- , Lina Sieverling
- , Sabina Signoretti
- , Katarzyna O. Sikora
- , Michele Simbolo
- , Ronald Simon
- , Janae V. Simons
- , Jared T. Simpson
- , Peter T. Simpson
- , Samuel Singer
- , Nasa Sinnott-Armstrong
- , Payal Sipahimalani
- , Tara J. Skelly
- , Marcel Smid
- , Jaclyn Smith
- , Karen Smith-McCune
- , Nicholas D. Socci
- , Heidi J. Sofia
- , Matthew G. Soloway
- , Lei Song
- , Anil K. Sood
- , Sharmila Sothi
- , Christos Sotiriou
- , Cameron M. Soulette

- , Paul N. Span
- , Paul T. Spellman
- , Nicola Sperandio
- , Andrew J. Spillane
- , Oliver Spiro
- , Jonathan Spring
- , Johan Staaf
- , Peter F. Stadler
- , Peter Staib
- , Stefan G. Stark
- , Lucy Stebbings
- , Ólafur Andri Stefánsson
- , Oliver Stegle
- , Lincoln D. Stein
- , Alasdair Stenhouse
- , Chip Stewart
- , Stephan Stilgenbauer
- , Miranda D. Stobbe
- , Michael R. Stratton
- , Jonathan R. Stretch
- , Adam J. Struck
- , Joshua M. Stuart
- , Henk G. Stunnenberg
- , Hong Su
- , Xiaoping Su
- , Ren X. Sun
- , Stephanie Sungalee
- , Hana Susak
- , Akihiro Suzuki
- , Fred Sweep
- , Monika Szczepanowski
- , Holger Sültmann
- , Takashi Yugawa
- , Angela Tam
- , David Tamborero
- , Benita Kiat Tee Tan
- , Donghui Tan

- , Patrick Tan
- , Hiroko Tanaka
- , Hirokazu Taniguchi
- , Tomas J. Tanskanen
- , Maxime Tarabichi
- , Roy Tarnuzzer
- , Patrick Tarpey
- , Morgan L. Taschuk
- , Kenji Tatsuno
- , Simon Tavaré
- , Darrin F. Taylor
- , Amaro Taylor-Weiner
- , Jon W. Teague
- , Bin Tean Teh
- , Varsha Tembe
- , Javier Temes
- , Kevin Thai
- , Sarah P. Thayer
- , Nina Thiessen
- , Gilles Thomas
- , Sarah Thomas
- , Alan Thompson
- , Alastair M. Thompson
- , John F. F. Thompson
- , R. Houston Thompson
- , Heather Thorne
- , Leigh B. Thorne
- , Adrian Thorogood
- , Grace Tiao
- , Nebojsa Tijanic
- , Lee E. Timms
- , Roberto Tirabosco
- , Marta Tojo
- , Stefania Tommasi
- , Christopher W. Toon
- , Umut H. Toprak
- , David Torrents

- , Giampaolo Tortora
- , Jörg Tost
- , Yasushi Totoki
- , David Townend
- , Nadia Traficante
- , Isabelle Treilleux
- , Jean-Rémi Trotta
- , Lorenz H. P. Trümper
- , Ming Tsao
- , Tatsuhiko Tsunoda
- , Jose M. C. Tubio
- , Olga Tucker
- , Richard Turkington
- , Daniel J. Turner
- , Andrew Tutt
- , Masaki Ueno
- , Naoto T. Ueno
- , Christopher Umbricht
- , Husen M. Umer
- , Timothy J. Underwood
- , Lara Urban
- , Tomoko Urushidate
- , Tetsuo Ushiku
- , Liis Uusküla-Reimand
- , Alfonso Valencia
- , David J. Van Den Berg
- , Steven Van Laere
- , Peter Van Loo
- , Erwin G. Van Meir
- , Gert G. Van den Eynden
- , Theodorus Van der Kwast
- , Naveen Vasudev
- , Miguel Vazquez
- , Ravikiran Vedururu
- , Umadevi Veluvolu
- , Shankar Vembu
- , Lieven P. C. Verbeke

- , Peter Vermeulen
- , Clare Verrill
- , Alain Viari
- , David Vicente
- , Caterina Vicentini
- , K. VijayRaghavan
- , Juris Viksna
- , Ricardo E. Vilain
- , Izar Villasante
- , Anne Vincent-Salomon
- , Tapio Visakorpi
- , Douglas Voet
- , Paresh Vyas
- , Ignacio Vázquez-García
- , Nick M. Waddell
- , Nicola Waddell
- , Claes Wadelius
- , Lina Wadi
- , Rabea Wagener
- , Jeremiah A. Wala
- , Jian Wang
- , Jiayin Wang
- , Linghua Wang
- , Qi Wang
- , Wenyi Wang
- , Yumeng Wang
- , Zhining Wang
- , Paul M. Waring
- , Hans-Jörg Warnatz
- , Jonathan Warrell
- , Anne Y. Warren
- , Sebastian M. Waszak
- , David C. Wedge
- , Dieter Weichenhan
- , Paul Weinberger
- , John N. Weinstein
- , Joachim Weischenfeldt

- , Daniel J. Weisenberger
- , Ian Welch
- , Michael C. Wendl
- , Johannes Werner
- , Justin P. Whalley
- , David A. Wheeler
- , Hayley C. Whitaker
- , Dennis Wigle
- , Matthew D. Wilkerson
- , Ashley Williams
- , James S. Wilmott
- , Gavin W. Wilson
- , Julie M. Wilson
- , Richard K. Wilson
- , Boris Winterhoff
- , Jeffrey A. Wintersinger
- , Maciej Wiznerowicz
- , Stephan Wolf
- , Bernice H. Wong
- , Tina Wong
- , Winghing Wong
- , Youngchoon Woo
- , Scott Wood
- , Bradly G. Wouters
- , Adam J. Wright
- , Derek W. Wright
- , Mark H. Wright
- , Chin-Lee Wu
- , Dai-Ying Wu
- , Guanming Wu
- , Jianmin Wu
- , Kui Wu
- , Yang Wu
- , Zhenggang Wu
- , Liu Xi
- , Tian Xia
- , Qian Xiang

- , Xiao Xiao
- , Rui Xing
- , Heng Xiong
- , Qinying Xu
- , Yanxun Xu
- , Hong Xue
- , Shinichi Yachida
- , Sergei Yakneen
- , Rui Yamaguchi
- , Takafumi N. Yamaguchi
- , Masakazu Yamamoto
- , Shogo Yamamoto
- , Hiroki Yamaue
- , Fan Yang
- , Huanming Yang
- , Jean Y. Yang
- , Liming Yang
- , Lixing Yang
- , Shanlin Yang
- , Tsun-Po Yang
- , Yang Yang
- , Xiaotong Yao
- , Marie-Laure Yaspo
- , Lucy Yates
- , Christina Yau
- , Chen Ye
- , Kai Ye
- , Venkata D. Yellapantula
- , Christopher J. Yoon
- , Sung-Soo Yoon
- , Fouad Yousif
- , Jun Yu
- , Kaixian Yu
- , Willie Yu
- , Yingyan Yu
- , Ke Yuan
- , Yuan Yuan

- , Denis Yuen
- , Takashi Yugawa
- , Christina K. Yung
- , Olga Zaikova
- , Jorge Zamora
- , Marc Zapatka
- , Jean C. Zenklusen
- , Thorsten Zenz
- , Nikolajs Zeps
- , Cheng-Zhong Zhang
- , Fan Zhang
- , Hailei Zhang
- , Hongwei Zhang
- , Hongxin Zhang
- , Jiashan Zhang
- , Jing Zhang
- , Junjun Zhang
- , Xiuqing Zhang
- , Xuanping Zhang
- , Yan Zhang
- , Zemin Zhang
- , Zhongming Zhao
- , Liangtao Zheng
- , Xiuqing Zheng
- , Wanding Zhou
- , Yong Zhou
- , Bin Zhu
- , Hongtu Zhu
- , Jingchun Zhu
- , Shida Zhu
- , Lihua Zou
- , Xueqing Zou
- , Anna deFazio
- , Nicholas van As
- , Carolien H. M. van Deurzen
- , Marc J. van de Vijver
- , L. van’t Veer

- & Christian von Mering

Corresponding authors

Correspondence to Moritz Gerstung or Peter Van Loo.

Rights and permissions

Open Access This article is licensed under a Creative Commons Attribution 4.0 International License, which permits use, sharing, adaptation, distribution and reproduction in any medium or format, as long as you give appropriate credit to the original author(s) and the source, provide a link to the Creative Commons license, and indicate if changes were made. The images or other third party material in this article are included in the article's Creative Commons license, unless indicated otherwise in a credit line to the material. If material is not included in the article's Creative Commons license and your intended use is not permitted by statutory regulation or exceeds the permitted use, you will need to obtain permission directly from the copyright holder. To view a copy of this license, visit http://creativecommons.org/licenses/by/4.0/.

Reprints and Permissions

About this article

Cite this article

Gerstung, M., Jolly, C., Leshchiner, I. *et al.* Author Correction: The evolutionary history of 2,658 cancers. *Nature* **614**, E42 (2023). https://doi.org/10.1038/s41586-022-05601-4

- Published: 25 January 2023
- Issue Date: 16 February 2023
- DOI: https://doi.org/10.1038/s41586-022-05601-4

Share this article

Anyone you share the following link with will be able to read this content:

Get shareable link

Sorry, a shareable link is not currently available for this article.

Copy to clipboard

Provided by the Springer Nature SharedIt content-sharing initiative

This article was downloaded by **calibre** from https://www.nature.com/articles/s41586-022-05601-4